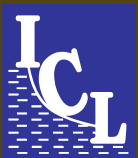




Kyoji Sassa
Kazuo Konagai
Binod Tiwari
Željko Arbanas
Shinji Sassa
Editors

Progress in Landslide Research and Technology, Volume 1 Issue 1, 2022



OPEN ACCESS

Progress in Landslide Research and Technology

The Open Access book series of the International Consortium on Landslides (ICL) aims to be the common platform for the publication of recent progress in landslide research and technology for practical applications and the benefit of society contributing to the Kyoto Landslide Commitment 2020, which is expected to continue up to 2030 and even beyond for the global promotion of understanding and reducing landslide disaster risk as well as the 2030 Agenda Sustainable Development Goals. The contributions include original and review articles, case studies, activity reports and teaching tools for the promotion of understanding and reducing landslide disaster risks.

Kyoji Sassa • Kazuo Konagai •
Binod Tiwari • Željko Arbanas •
Shinji Sassa
Editors

Progress in Landslide
Research and Technology,
Volume 1 Issue 1, 2022

Editors

Kyoji Sassa
International Consortium on Landslides
Kyoto, Japan

Kazuo Konagai
International Consortium on Landslides
Kyoto, Japan

Binod Tiwari
Department of Civil and Environmental
Engineering
California State University, Fullerton
Fullerton, CA, USA

Željko Arbanas
Faculty of Civil Engineering
University of Rijeka
Rijeka, Croatia

Shinji Sassa
National Institute of Maritime, Port
and Aviation Technology
Port and Airport Research Institute
Yokosuka, Japan

This work contains media enhancements, which are displayed with a “play” icon. Material in the print book can be viewed on a mobile device by downloading the Springer Nature “More Media” app available in the major app stores. The media enhancements in the online version of the work can be accessed directly by authorized users.



ISSN 2731-3794 ISSN 2731-3808 (electronic)
Progress in Landslide Research and Technology
ISBN 978-3-031-16897-0 ISBN 978-3-031-16898-7 (eBook)
<https://doi.org/10.1007/978-3-031-16898-7>

© International Consortium on Landslides 2023. This book is an open access publication.

Open Access This book is licensed under the terms of the Creative Commons Attribution 4.0 International License (<http://creativecommons.org/licenses/by/4.0/>), which permits use, sharing, adaptation, distribution and reproduction in any medium or format, as long as you give appropriate credit to the original author(s) and the source, provide a link to the Creative Commons license and indicate if changes were made.

The images or other third party material in this book are included in the book’s Creative Commons license, unless indicated otherwise in a credit line to the material. If material is not included in the book’s Creative Commons license and your intended use is not permitted by statutory regulation or exceeds the permitted use, you will need to obtain permission directly from the copyright holder.

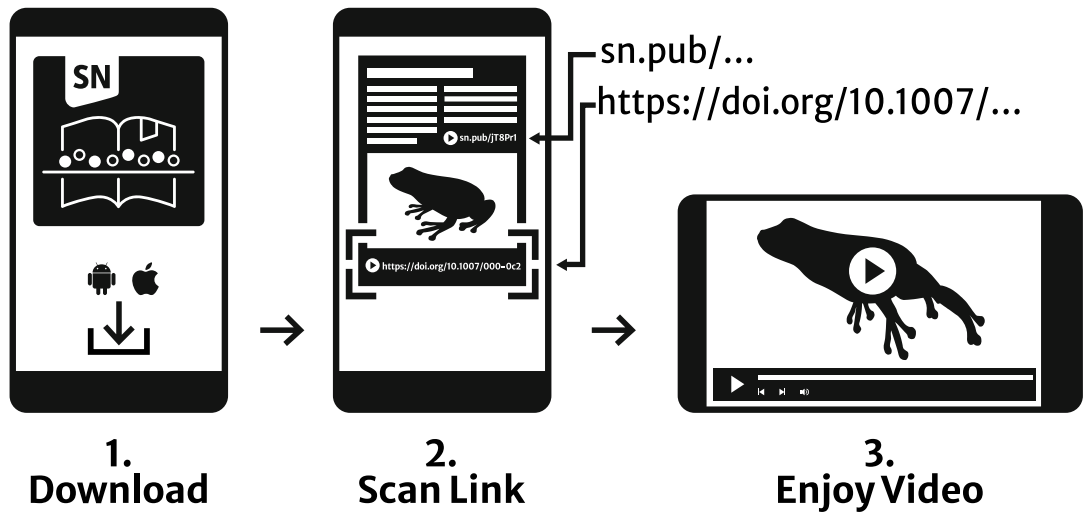
The use of general descriptive names, registered names, trademarks, service marks, etc. in this publication does not imply, even in the absence of a specific statement, that such names are exempt from the relevant protective laws and regulations and therefore free for general use.

The publisher, the authors, and the editors are safe to assume that the advice and information in this book are believed to be true and accurate at the date of publication. Neither the publisher nor the authors or the editors give a warranty, expressed or implied, with respect to the material contained herein or for any errors or omissions that may have been made. The publisher remains neutral with regard to jurisdictional claims in published maps and institutional affiliations.

Cover illustration: Aranyaka landslide in Kagelle District, Sri Lanka. It occurred in May 2016, after a long rainfall. It killed 127 persons and destroyed 75 houses (Technical Cooperation for Landslide Mitigation Project by JICA. All rights reserved)

This Springer imprint is published by the registered company Springer Nature Switzerland AG
The registered company address is: Gewerbestrasse 11, 6330 Cham, Switzerland

Springer Nature More Media App



Support: customerservice@springernature.com

Progress in Landslide Research and Technology— Book Series of the International Consortium on Landslides

Progress in Landslide Research and Technology is the Open Access Book Series of the International Consortium on Landslides (ICL). The series provides a common platform for the publication of recent progress in landslide research and technology for practical applications and the benefit for the society contributing to the Kyoto Landslide Commitment 2020, which is expected to continue up to 2030 and even beyond to globally promote the understanding and reduction of landslide disaster risk, as well as to address the 2030 Agenda Sustainable Development Goals. The contributions include the following eight categories:

1. Original articles reporting progress of landslide research and technology.
2. Review articles (minimum 8 pages): Review of landslide research and technology in a thematic area of landslides. A review article integrating a series of research and technology of the author or its group.
3. ICL landslide lessons (minimum 10 pages): Lessons by global and emerging experts with distinguished achievements in one of specific aspects in understanding and reducing landslide disaster risk.
4. IPL/WCoE/Kyoto Commitment activities (minimum 8 pages): Progress or achievements of the projects of the International Programme on Landslides (IPL), the World Centres of Excellence on Landslide Risk Reduction (WCoEs) and Kyoto Landslide Commitment.
5. Teaching tools with online extras (minimum 8 pages): User-friendly teaching tools with extras (i.e. photos, illustration, videos, guidelines, and manuals) online to fill the gap between the available level of science and technologies and the practical use in the society.
6. Technical note and case studies (minimum 4 pages): Technical note and case studies on landslides and landslide disaster risk reduction practice.
7. World Landslide Reports (2-4 pages): Landslide reports from landslide-prone developing countries and urbanizing areas of the developed countries from around the world. No processing charge, but limited to approximately 10 reports per issue.
8. Introduction of KLC2020 official promoters (1–3 pages): KLC2020 official promoters are eligible for this category. The introduction of the official promoters is published in all issues throughout the year.

Editorial Office

Secretariat of the Kyoto Landslide Commitment 2020

International Consortium on Landslides (ICL)

138-1 Tanaka-Asukai cho, Sakyo-ku, Kyoto 606-8226, Japan

E-mail: klc2020@iclhq.org

Editorial Board of the Book Series

Editor-in-Chief

Kyoji Sassa, International Consortium on Landslides, Japan

Assistant Editor-in-Chief

Kazuo Konagai, International Consortium on Landslides, Japan

Binod Tiwari, California State University, Fullerton, USA

Željko Arbanas, University of Rijeka, Croatia

Editors

Beena Ajmera, Iowa State University, USA

Irasema Alcántara-Ayala, National Autonomous University of Mexico, Mexico

Sabatino Cuomo, University of Salerno, Italy

Yasser Elshayeb, Cairo University, Egypt

Xuanmei Fan, Chengdu University of Technology, China

Faisal Fathani, University of Gadjah Mada, Indonesia

Louis Ge, National Taiwan University, Chinese Taipei

Ivan Gratchev, Griffith University, Australia

David Huntley, Geological Survey of Canada, Canada

Snježana Mihalić-Arbanas, University of Zagreb, Croatia

Matjaž Mikoš, University of Ljubljana, Slovenia

Yoshihisa Miyata, National Defense Academy of Japan, Japan

Maneesha Ramesh, Amrita University, India

Paola Reichenbach, Research Institute for Geo-Hydrological Protection, CNR, Italy

Shinji Sassa, Port and Airport Research Institute, Japan

Josef Stemberk, Institute of Rock Structure and Mechanics, CAS, Czech Republic

Alexander Strom, Geodynamic Research Center, Russia

Huiming Tang, China University of Geosciences, Wuhan, China

David Tappin, British Geological Survey, UK

Veronica Tofani, University of Florence, Italy

Vít Vilímek, Charles University, Czech Republic

Fawu Wang, Tongji University, China

Wei Shan, Northeast Forestry University, China

KLC2020 Managing Committee

Kyoji Sassa (Chairman), Secretary-General, Secretariat of the Kyoto Landslide Commitment 2020

Kaoru Takara, Managing Director, Secretariat of the Kyoto Landslide Commitment 2020

Matjaž Mikoš, Chair of the Global Promotion Committee of the International Programme on Landslides and Kyoto Landslide Commitment 2020

Qunli Han, Co-Chair of the Global Promotion Committee of the International Programme on Landslides and Kyoto Landslide Commitment 2020

Nicola Casagli, President of the International Consortium on Landslides

Peter Bobrowsky, Immediate Past-president of the International Consortium on Landslides

Advisory Members for KLC2020

Abou Amani, Director, Division of Water Sciences, Secretary, Intergovernmental Hydrological Programme (IHP), UNESCO

Soichiro Yasukawa, Programme Specialist, Coordinator for Disaster Risk Reduction and Resilience, UNESCO

Daniel Lebel, Director-General, Geological Survey of Canada, Natural Resources Canada, Canada

John Ludden, President of the International Union of Geological Sciences (IUGS)

John LaBrecque, Chair of IUGG GeoRisk Commission, Center for Space Research, U.Texas Austin, USA.

Rafiq Azzam, President of the International Association for the Engineering Geology and the Environment (IAEG)

Paolo Canuti, Past President of the International Consortium on Landslides (ICL), Italy

Sálvano Briceño, First Chair of the Global Promotion Committee of the International Programme on Landslides

Badaoui Rouhban, Chair of the KLC2020 Launching Session and Moderator of ISDR-ICL Sendai Landslide Partnerships 2015–2025 Session of 3rd WCDRR in 2015

KLC2020 Official Promoters

Host organization

International Consortium on Landslides (ICL)/Nicola Casagli

Public sectors: KLC2020 Official Promoters—public

International Unions/Associations, Governmental Organizations, Universities, and Research Institutes

- The International Union of Geological Sciences (IUGS)/John Ludden
- The International Union of Geodesy and Geophysics (IUGG)/Kathy Whaler
- The International Association for the Engineering Geology and the Environment/Rafiq Azzam
- International Geosynthetics Society (IGS/John Kraus)
- Geological Survey of Canada, Natural Resources Canada, Canada/Daniel Lebel
- Faculty of Civil and Geodetic Engineering, University of Ljubljana, Slovenia/Matjaž Mikoš
- China University of Geosciences, Wuhan, China/Huiming Tang
- Department of Civil Engineering, National Taiwan University, Chinese Taipei/Shang-Hsien Hsien
- Institute of Rock Structure and Mechanics, the Czech Academy of Sciences/Josef Stemberk
- Institute of Cold Regions Science and Engineering, Northeast Forestry University, China/Wei Shan

Private sectors: KLC2020 official promoters—private

Companies and corporation

- Marui & Co. Ltd., Japan
- Nippon Koei Co., Ltd., Japan
- Ellegi Srl, Italy
- IDS GeoRadar s.r.l., Italy
- Chuo Kaihatsu Corporation, Japan

- Godai Corporation, Japan
- Kiso-Jiban Consultants Co., Ltd., Japan
- Kokusai Kogyo Co., Ltd., Japan
- OSASI Technos, Inc., Japan

Standing Editors for KLC2020 Book Series

Kyoji Sassa, International Consortium on Landslides, Kyoto, Japan

Kazuo Konagai, International Consortium on Landslides, Kyoto, Japan

Binod Tiwari, California State University, Fullerton, USA

Željko Arbanas, University of Rijeka, Croatia

Paola Reichenbach, Research Institute for Geo-Hydrological Protection, CNR, Italy

Shinji Sassa, Port and Airport Research Institute, Yokosuka, Japan

Fawu Wang, Tongji University, Shanghai, China

Khang Dang, VNU University of Science, Vietnam National University, Vietnam

Beena Ajmera, Iowa State University, USA

Global Promotion Committee of the International Programme on Landslides and Kyoto Landslide Commitment 2020

A Commitment to the Sendai Framework and the Sustainable Development Goals

Chair: Matjaž Mikoš (Faculty of Civil and Geodetic Engineering, University of Ljubljana)

Co-Chairs: Qunli Han (Integrated Research on Disaster Risk, IRDR), Soichiro Yasukawa (Programme Specialist on Disaster Risk Reduction, UNESCO, Paris), Hiroshi Kitazato (Treasurer of IUGS), and John LaBrecque (Chair of IUGG GeoRisk Commission)

Secretary: Kyoji Sassa (IPL World Centre, Director)

Members of the IPL-KLC Global Promotion Committee

ICL full members

Geotechnical Engineering Office, Hong Kong, China; UNESCO Chair for the Prevention and the Sustainable Management of Geo-hydrological Hazards—University of Florence, Italy; Korea Institute of Geoscience and Mineral Resources (KIGAM), Korea; Faculty of Civil and Geodetic Engineering, University of Ljubljana (ULFGG), Slovenia, and other members (total 59 members from 29 countries/regions).

ICL supporting organizations

UNESCO, UNDRR, WMO, FAO, UNU, ISC, WFEO, IUGS, IUGG, Government of Japan (CAO, MEXT, MAFF, MLIT)

KLC2020 Official Promoters

Host organization

International Consortium on Landslides (ICL)/Nicola Casagli

Public sectors: KLC2020 official promoters—public

- The International Union of Geological Sciences (IUGS)/John Ludden
- The International Union of Geodesy and Geophysics (IUGG)/Kathy Whaler
- The International Association for the Engineering Geology and the Environment (IAEG)/Rafiq Azzam
- International Geosynthetics Society (IGS)/John Kraus
- Geological Survey of Canada, Natural Resources Canada, Canada/Daniel Lebel

- Faculty of Civil and Geodetic Engineering, University of Ljubljana, Slovenia/Matjaž Mikoš
- China University of Geosciences, Wuhan, China/Huiming Tang
- Department of Civil Engineering, National Taiwan University, Chinese Taipei/Shang-Hsien Hsien
- Institute of Rock Structure and Mechanics, the Czech Academy of Sciences/Josef Stemberk
- Institute of Cold Regions Science and Engineering, Northeast Forestry University, China/Wei Shan

Private sectors: KLC2020 official promoters—private

- Marui & Co. Ltd., Japan
- Nippon Koei Co., Ltd., Japan
- Ellegi Srl, Italy
- IDS GeoRadar s.r.l., Italy
- Chuo Kaihatsu Corporation, Japan
- Godai Corporation, Japan
- Kiso-Jiban Consultants Co., Ltd., Japan
- Kokusai Kogyo Co., Ltd., Japan
- OSASI Technos, Inc., Japan

IPL World Centre

IPL World Centre (IWC) was established in 2006 by the Tokyo Action Plan to serve, as it does, as the secretariat of IPL, GPC/IPL as well as of UNITWIN UNESCO-KU-ICL Programme. IWC also serves as the secretariat of KLC2020. IWC is a part of the legal body (NPO-ICL registered in Kyoto, Japan) of ICL. The Council of the IWC consists of advisors from Ministry of Education, Sports, Science and Technology, Ministry of Agriculture, Forestry and Fisheries, Ministry of Land, Infrastructure and Tourism of the Government of Japan, UNESCO, and of members from ICL Headquarters, chairs of GPC/IPL-KLC, presidents and officers of ICL.

Secretariat of GPC/IPL-KLC

Secretary: Kyoji Sassa
 International Consortium on Landslides
 138-1 Tanaka-Asukai cho, Sakyo-ku
 Kyoto 606-8226, Japan
 Tel: +81 (75) 723 0640, Fax: +81(75) 950 0910
 UNITWIN UNESCO-KU-ICL Programme
 UNITWIN Headquarters Building
 Kyoto University Uji Campus
 Uji, Kyoto 611-0011, Japan, unitwin@iclhq.org
 E-mail: klc2020@iclhq.org, secretariat@iclhq.org
 URL: <http://www.iplhq.org/>, <http://icl.iplhq.org/>

Foreword by Nicola Casagli

The International Consortium on Landslides (ICL) is an international non-governmental and non-profit scientific organization, established in 2002 as a result of several international initiatives by specialists in the field of landslides. The principal objectives are to (i) promote landslide research; (ii) integrate geosciences and technology; (iii) combine and coordinate international expertise; and (iv) promote a global, multidisciplinary programme on landslides, the International Programme on Landslides (IPL). ICL has now more than 80 members from 34 countries worldwide.

In 2020, ICL has proposed the Kyoto 2020 commitment for global promotion of understanding and reducing landslide disaster risk, as a commitment to the Sendai Landslide Partnerships 2015–2025.

The KLC2020 supports the implementation, follow-up, and review of the Sendai Framework, the 2030 UN Agenda for Sustainable Development, the New Urban Agenda, and the Paris Climate Agreement as it addresses the adverse effects of climate change.

The KLC2020 has been signed by about 90 institutions among governmental and international organizations, ICL supporting organizations, full members, associate members, and supporters from 23 countries in three continents. All KLC2020 partners are organizations who strongly contribute to understand and reduce landslide disaster risk and who will share their expertise and knowledge to build a common platform for sharing ideas, good practices, and policies with key actors and stakeholders concerned with landslide risk at the global level.

The International Consortium on Landslides organizes every three year the World Landslide Forums. They are major events for discussion open to scientists, engineers, practitioners, and policy makers who are involved in landslide disaster risk reduction for presenting their latest progress.

The 5th World Landslide Forum (WLF5) (<https://wlf5.iplhq.org>) was organized on November 2–6, 2021, in Kyoto, Japan, in a hybrid mode. WLF5 was initially planned to be organized on November 2–6, 2020. Due to the COVID-19 pandemic, WLF5 was postponed by one year to November 2021. WLF5 has been successfully organized since 525 participants from 46 countries attended, despite the COVID-19 pandemic.

The 6th World Landslide Forum (WLF6) (<http://wlf6.org>) will be organized from November 14 to 17, 2023, in Florence, Italy. WLF6 is focused on landslide science for sustainable development, as a contribution to the Kyoto 2020 Commitment for global promotion of understanding and reducing landslide disaster risk.

The aim of the Forum is to achieve a fruitful cooperation among landslide researchers to define shared priority actions for landslide risk reduction on a global scale. The Forum will deal with the main aspects related to landslide analysis, landslide monitoring and early warning, landslide modelling, landslide hazard and risk assessment, mitigation techniques, landslide triggering mechanism, and climate change.

In line with the 2030 Agenda and the Sustainable Development Goals, the Forum will be a sustainable event. The Forum is hosted in Florence City Center, with everything at walking distance and no printed material. The Forum programme and proceedings will be distributed to the participants in electronic format.

The ICL Journal, Landslides, (<https://www.springer.com/journal/10346>) has reached in 2020 an impact factor of 6.578, thanks to the extensive contribution of the landslide community in promoting research at global level through significant publications in the journal and thanks to Editor-in Chief, Kyoji Sassa, and Assistant Editor-in-Chief, Željko Arbanas, with the support from the associate editors and screening editors.

In order to promote the KLC2020, ICL has proposed an Open Access Book Series “Progress in Landslide Research and Technology (P-LRT)”. The series is conceived for the publication of recent progress in landslide research and technology for practical applications and for the benefit of the society, contributing to the Kyoto Landslide Commitment 2020, which is expected to continue up to 2030 and even beyond to globally promote the understanding and reduction of landslide disaster risk, as well as to address the UN Sustainable Development Goals. P-LRT was launched during the high-level panel discussion “Review of KLC2020 and the way forward” during the 5th World Landslide Forum in Kyoto, Japan, on November 3, 2021.

All the above-mentioned achievements and activities reflect the steady and significant increase in importance and visibility of the consortium within the global community of landslide researchers, practitioners, and stakeholders, and this thanks to the dedication and hard work of the officers and members of the ICL that contribute to the consortium activities initiatives and outputs of the ICL and IPL.

ICL partner members and potential new ones are invited to continue this effort, to further promote the ICL-IPL activities, and to contribute to the Landslides journal and the ICL Open Access Book Series P-LRT. The final aim is to pursue the KCL2020 priority actions and to have strong cooperation among landslide researchers to define a common platform for landslide risk reduction on a global scale.



Nicola Casagli
President of the International Consortium on Landslides
UNESCO Chair on Prevention and Sustainable
Management of Geo-hydrological Hazards
University of Florence
Florence, Italy

Video link: https://us06web.zoom.us/rec/play/_HdjSVdclIjHujalsUkm7-QI9ezxJNmV2WyMNi39FHE0GK5nyo4FgIXbkB76Bf6R2l6mLTO8eP7v1D8.MwH1tc9EIBuFrvhK?autoplay=true&startTime=1649823637000

Foreword by John Ludden

It is my great pleasure to contribute to the 5th World Landslide Forum as President of the International Union of Geological Sciences (IUGS). This conference and publication on “Progress in landslide research and technology” is timely given the climate change drivers that are affecting our planet and notwithstanding the ever-present risk of earthquakes and poor building conditions.

I am pleased to see the creation of the ICL Open Access Book Series “Progress in Landslide Research and Technology” for the Kyoto Landslide Commitment 2020 was adopted by the high-level panel discussion “Review of KLC2020 and the way forward” following the opening session of the 5th World Landslide Forum.

The IUGS role is to provide underpinning geological standards for geological correlation and nomenclature across the globe. These are increasingly important in a world stressed by the extremes of climate change. Some of the current drivers for geoscience are as follows:

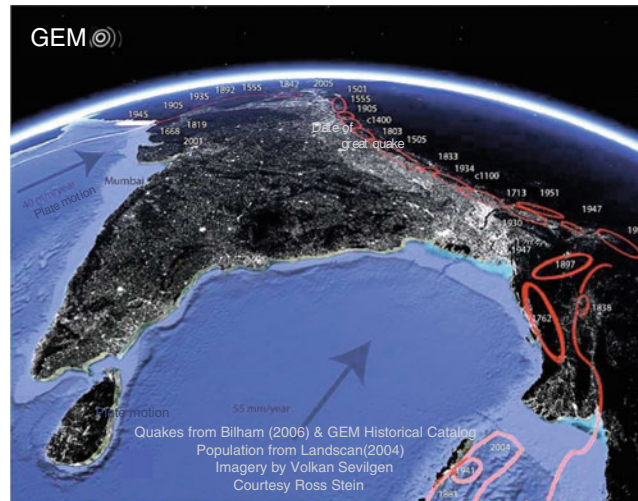
- Diversification of energy supplies and decarbonization
- Reducing global emissions
- Understanding geological risk rather than hazard
- Global population change
- Open and big data and information sciences
- Tougher environmental regulations
- Greater public scrutiny.

All of these are linked in some way to landslide research and the risks proposed by landslides. The energy and climate linked drivers are of course linked to rainfall, drought, and flooding, all conditions that prepare landslides, which might then be triggered by tectonic events.

The need for geoscience is we know it is changing and we need to ask ourselves if we are prepared for change. Are we sure that we are preparing our students for work, communicating with the public on key issues, living up to governments expectations, and promoting global science and education?

Why Geoscience Matters

- Understanding the dynamic Earth
- Creating a safe and healthy planet
- Driving sustainable growth
- Reducing global inequalities



I include this slide which was taken from my presentation. It is taken from the global earthquake model @GEM <https://www.globalquakemodel.org/> as it neatly defines the fundamental research that is still needed on geology and geophysics to understand the processes that shape the Earth, but also how populations are affected by earthquakes and are potentially exposed to geological risk. This underpins the need for integrated research in the geosciences, engineering, and socioeconomic sciences in future. The work of the WLF on landslides and their identification, management, and ultimately mitigation is essential.



John Ludden
 Professor of Lyell Centre
 President of the International Union
 of Geological Sciences,
 Heriot-Watt University
 Edinburgh, UK

Video link: https://us06web.zoom.us/rec/play/tAY4VmeWk-ekqexGybZ2SQu-9j9H_-kQ7jC-N3NqiJhtGQiGzk0uHtJyKx9BOAqbtehWKsSHZKhhjW8B.uJkwU2PAA7LJa4ak?autoplay=true&startTime=1646279698000

Foreword by Kathy Whaler

Landslides are an ever-present hazard in many parts of the globe, resulting in enormous losses of life, infrastructure, and livelihoods. Their causes are both natural, such as earthquakes, and anthropogenic, including deforestation and construction. Landslides may be part of a multi-hazard or cascading hazard event. Additionally, the impact of naturally occurring landslides can be exacerbated by anthropogenic activity. The incidence of and exposure to landslides are increasing with climate change and population growth. Hence, a variety of methods are required to understand, forecast, mitigate, and communicate the risk associated with landslides, involving scientists and social scientists from many different disciplines. The International Union of Geodesy and Geophysics (IUGG) has eight associations specializing in particular branches of geodesy and geophysics. Five of them, addressing the sciences of seismology, volcanology, hydrology, the cryosphere, and the atmosphere, are concerned with processes that may result in landslides, and geodesy, a sixth association, investigates changes in the shape of the Earth and its associated gravitational field such as can result from landslides. In addition, IUGG has a number of cross-cutting commissions, including one on geophysical risk and sustainability. Thus, IUGG is highly interested in branches of science that can be responsible for landslides. However, landslides tend to be understudied in comparison with the underlying geophysical processes that may cause them. Hence, initiatives such as the Kyoto Landslides Commitment 2020 are extremely important, and IUGG is pleased to be a supporter.

As I write this (mid-April 2022), over 100 people are reported to have lost their lives after a tropical storm caused flooding and landslides in the Philippines, with scores of people missing and over 100,000 people affected, and heavy rain has triggered mudslides which have trapped people beneath buildings and washed away dozens of homes in South Africa, with at least 13,000 homes affected and a death toll approaching 400. The toll from these disasters is expected to rise over the coming days. Their devastating consequences demonstrate the pressing need to tackle the issue of landslides.

I am confident that this Open Access Book Series will advance the science and understanding of landslides and provide a valuable resource for specialists concerned with addressing the risk that they pose. The scope of this first volume is vast, covering many aspects of landslide science, engineering, hazard and resilience, inventories, standards, and establishing and monitoring best practice, natural hazard observatories and observations, experimental modelling, and early warning systems. It contains original and review articles, technical notes, and teaching and training tools. It is particularly welcome that it is accessible without charge to all researchers and practitioners, especially as the impacts of landslides are

widely felt in the world's less developed nations. I congratulate the KLC2020 team for bringing this ambitious project to completion and look forward to seeing the other volumes in the series.



Kathy Whaler
Professor of Geophysics
University of Edinburgh
Edinburgh, UK

IUGG President
Prevention and Sustainable Management
of Geo-hydrological Hazards
Florence, Italy

Video link: https://us06web.zoom.us/rec/play/N37E4kxkCxdK6WAW0EKz1KxYorsvlODG0gDy84512lvTV3M1pghqqJ_jmhgKzwiX4r_7MgpZt88W9Q.hTSNArH9gDXxIDKp?autoplay=true&startTime=1652058810000

Greetings by Mami Mizutori for Opening Session of the 5th World Landslide Forum

Thank you for this opportunity to speak to you at the opening session of the 5th World Landslide Forum.

At the outset allow me to say that it is unfortunate that there is still not a greater public understanding and awareness of landslide risk and the way it interacts with other drivers of disaster risk such as land use, the loss of protective drainage systems from deforestation, and the use of marginal lands on unstable hillsides to house poor people.

This is in spite of the fact that global warming has led to a dramatic increase in extreme weather events over the last twenty years which in turn increases the likelihood of landslides in hazard-prone populated areas.

The tragic result is many people losing their lives and their homes every year underlines the importance of including landslide risk in the national and local strategies for disaster risk reduction of all countries.

I would like to assure you that this is certainly an area that the UN Office for Disaster Risk Reduction will look at as we review the existing 121 national strategies that have been developed by UN Member States as we embark on the mid-term review of the Sendai Framework for Disaster Risk Reduction which will culminate in 2023.

As all of you are well aware of, the Sendai Framework is the global plan to reduce disaster losses adopted by UN Member States in 2015 which stresses the importance of scientific and technological work to facilitate effective decision-making in disaster risk reduction.

This is why, we are deeply appreciative of this large and important gathering of the science community working on landslide issues.

On November 5, every year, we mark the World Tsunami Awareness Day. While 80% of tsunami events are caused by earthquakes, we also know that landslides can contribute to tsunami occurrence.

In countries and regions including Indonesia and the Caribbean, tsunamis due to landslides and volcanic eruptions are more likely, and given their deadly nature, there is a great importance in managing this risk.

The work of the Sendai Landslide Partnership 2015–2025 facilitated by the International Consortium on Landslides is a significant contribution to reducing disaster risk and provides practical solutions and tools, education, and capacity building, to reduce landslide risks.

Although the 5th World Landslide Forum was postponed by a year due to COVID-19, it was most encouraging to see that the Kyoto 2020 Commitment for Global Promotion of Understanding and Reducing Landslide Disaster Risk was launched last year.

I am very grateful for this tremendous effort and all the good work that the International Consortium continues to take forward.

I wish you a very successful meeting and look forward to the outcome.

Thank you very much.



Mami Mizutori
United Nations Special Representative
of the Secretary-General for Disaster Risk Reduction

Greetings by David Malone for Opening Session of the 5th World Landslide Forum

Greetings. My name is David Malone. I'm Rector and Head of the UN University in Tokyo, Japan, were a global organization, one of the UN agencies created about 50 years ago to fill a gap in the UN's agency world.

It's lovely being in Tokyo, and of course, living in Japan makes me acutely aware of the relevance of the landslide issue globally. When I was a boy, I grew up in Iran for five years, and Iran was subjected in its mountainous areas to very dangerous landslides, which took lives years, year after year. All it took in some narrow gorges was for a truck to blow its horn or even a smaller car to blow its horn and that would dislodge rocks and an avalanche. In effect, a landslide would then occur often killing a number of individuals.

The landslide issue is part of course of a wider Disaster Reduction Programme of the UN. It's led by a very competent and valued Japanese colleague, Mami Mizutori, who I hope will hear from this year during this conference, or if not, we definitely should hear from next year because she's an expert. And I'm not such an expert.

I'm merely somebody who has lived in countries that experience quite a lot of natural disasters. Now, when we think of landslides, we tend to think of them as acts of God, which we can't really prepare for. That's actually dead wrong. Landslides can be planned for, and the proof of this is two earthquakes, which occurred in 2010.

Eleven years ago, one of them in in Haiti, which took 300,000 lives. It registered a 7.3 magnitude earthquake on the Richter scale. And it triggered many landslides in the mountainous areas of Haiti—much of Haiti is mountainous. Three hundred thousand lives were lost in a relatively low-intensity earthquake! In the same hemisphere, in the country of Chile, two months later, there was an earthquake of huge magnitude—8.8 on the Richter scale—and only 435 lives were lost.

Why? Because, on the one hand, Chile as a more prosperous country than Haiti can invest in Disaster Reduction technologies, in high-quality training of its civilian rescue personnel, and also in training its armed forces to help in search and rescue, whereas Haiti is a very poor country, with very limited administrative capacity—although receiving quite a lot of international support. In spite of this, Haiti remains a country with very few means to counter the risk and frequent reality of natural disasters, including landslides.

Hence, the importance of the programme that Mami needs for the UN. And hence, also, the importance of this consortium on the important problem of landslides. Japan is an advanced economy country. Two years ago in Hiroshima, there were torrential rains, these torrential rains brought about landslides, which caused houses on steep hills, just above the city to collapse and a number of people—150 or so, if I remember correctly—dying from those causes.

Landslides can be managed. Major catastrophes caused by landslides can be managed constructively, in terms of damage to human lives and to economies through better

infrastructure, the careful zoning of housing, and many other measures. This is why I want to congratulate Kyoji and his colleagues, and say how honoured I've been to join with you today. Thank you very much for your attention.



David Malone
Under-Secretary-General of the United Nations
Rector of United Nations University
Tokyo, Japan

Video link: https://us06web.zoom.us/rec/play/9hePF-MHCgPjoGJX6YkdAbEG0JmQT3_RY4lAZwpGtyeqyo2xKfZb1GLpZVvM4lDOVsjFBXpxT5ana_M8.2hG6-2GxXT2CGXnm?autoplay=true&startTime=1646360227000

Greetings by Shamila Nair-Bedouelle for Opening Session of the 5th World Landslide Forum

Dear Excellences, Ladies and Gentlemen, Distinguished Guests,

It is my great pleasure to address you all at the 5th World Landslide Forum, a unique space that gathers the international network of scientists, practitioners, and decision-makers dedicated to disaster risk reduction, in particular concerning landslides.

In many parts of the world, landslides are a major threat to the people and the environment. They occur at relatively small scales, are very complex to predict, and are able to create considerable damage and losses. Currently, with no doubts the risk of landslide hazards is rising. Climate change, urban pressure, and the lack of disaster preparedness intensify the occurrence and magnitude of external perturbations. Therefore, landslide risk reduction constitutes an essential part of global DRR agendas such as the Sendai Framework.

While the Sendai Framework for Disaster Risk Reduction is the roadmap for DRR, other global agendas including the Sustainable Development Goals, the Paris Climate Agreement, and the New Urban Agenda have complementary targets with the latter. Therefore, in shaping its contribution to those global agendas, UNESCO commits to greater integration in its approach to support its Member States, between its different mandates and disciplines and with partners such as the International Consortium on Landslides (ICL).

UNESCO and ICL have a long history of cooperation and partnership since ICL was established in 2002. From that year onwards, UNESCO has been accompanying ICL in its journey on advocacy and research. I am very glad to see that the commitment of both institutions converged into a fruitful and mutually benefitting collaboration.

The adaption of the Kyoto 2020 Commitment for global promotion of understanding and reducing landslide disaster risk (KLC2020), which was signed last year, will raise global awareness on the landslide risk, mobilizing wider partnerships to bring together stakeholders from all levels of society, across different regions, sectors, and disciplines. During the upcoming days of the 5th World Landslide Forum in Kyoto, the world landslide community will commit to implement the KLC2020 through landslide sciences and good practices.

During this Forum, our organization is proud to organize a session on Landslides at UNESCO-designated sites, as many natural World Heritage sites, Biosphere Reserves, and UNESCO Global Geoparks are exposed to landslide hazards and need a proper protection.

I am sure that the coming discussions will bring major scientific and practical outcomes to further advance in landslide risk reduction, mitigation, and planning. You can count on UNESCO's full commitment to continue to support ICL members in future activities and undertakings.

Thank you



Shamila Nair-Bedouelle
Assistant Director-General for Natural Sciences
UNESCO

Video link: https://us06web.zoom.us/rec/play/RUsYHuB4O8d4Ber-H-dUns1vLFD_VxPccKP99dG_yhmtswnekwaJ0SN4taYh6f3a2PHVWJ7j76RIbkDC.UJt9n3UomTlNwv1V?autoplay=true&startTime=1650065352000

Contents

Introduction: Aim and Outline of the Book Series “Progress in Landslide Research and Technology”	1
Kyoji Sassa and Matjaž Mikoš	
International Consortium on Landslides and International Programme on Landslides	
International Consortium on Landslides: From IDNDR, IGCP, UNITWIN, WCDRR 2 & 3 to Kyoto Landslide Commitment 2020	11
Kyoji Sassa, Paolo Canuti, Peter Bobrowsky, and Nicola Casagli	
International Programme on Landslides—A Short Overview of Its Historical Development	45
Matjaž Mikoš, Kyoji Sassa, and Qunli Han	
Original Articles	
Understanding and Reducing the Disaster Risk of Landslide-Induced Tsunamis: Outcome of the Panel Discussion and the World Tsunami Awareness Day Special Event of the Fifth World Landslide Forum	65
Shinji Sassa, Stephan T. Grilli, David R. Tappin, Kyoji Sassa, Dwikorita Karnawati, Viacheslav K. Gusiakov, and Finn Løvholt	
Natural-Hazard-Related Web Observatory as a Sustainable Development Tool	83
Matjaž Mikoš, Nejc Bezak, Joao Pita Costa, M. Beshar Massri, Inna Novalija, Mitja Jermol, and Marko Grobelnik	
Mapping Post-fire Monthly Erosion Rates at the Catchment Scale Using Empirical Models Implemented in GIS. A Case Study in Northern Italy	99
Damiano Vacha, Giuseppe Mandrone, Donato Morresi, and Matteo Garbarino	
Mechanisms of Shallow Rainfall-Induced Landslides from Australia: Insights into Field and Laboratory Investigations	113
Ivan Gratchev, Sinnappoo Ravindran, Dong Hyun Kim, Chen Cui, and Qianhao Tang	
Design Protection Barriers Against Flow-Like Landslides	123
Sabatino Cuomo, Angela Di Perna, and Mario Martinelli	
Landslide Warning Systems in Low-And Lower-Middle-Income Countries: Future Challenges and Societal Impact	137
Irasema Alcántara-Ayala and Ricardo J. Garnica-Peña	
The Role of Translational Landslides in the Evolution of Cuesta Topography ...	149
Shinro Abe, Daisuke Higaki, and Kazunori Hayashi	

Application of Spectral Element Method (SEM) in Slope Instability Analysis	163
Ram Chandra Tiwari and Netra Prakash Bhandary	
Climate Change-Induced Regional Landslide Hazard and Exposure Assessment for Aiding Climate Resilient Road Infrastructure Planning: A Case Study in Bagmati and Madhesh Provinces, Nepal	175
I Putu Krishna Wijaya, Peeranan Towashiraporn, Anish Joshi, Susantha Jayasinghe, Anggraini Dewi, and Md. Nurul Alam	
Using Experimental Models to Calibrate Numerical Models for Slope Stability and Deformation Analysis	185
Binod Tiwari and Duc Tran	
Sustainability of Geosynthetics-Based Landslide Stabilization Solutions	197
Ivan P. Damians, Yoshihisa Miyata, Pietro Rimoldi, Nathalie Touze, and John Kraus	
Review Articles	
Establishment of the Disaster Risk Reduction Unit in UNESCO and UNESCO's Contribution to Global Resilience	209
Lesly Mercedes Barriga Delgado, Irina Pavlova, Soichiro Yasukawa, and Sergio Esperancinha	
IPL Projects, World Centres of Excellence on Landslide Risk Reduction, and Kyoto Landslide Commitment 2020	
Early Warning System Against Rainfall-Induced Landslide in Sri Lanka	217
Kazuo Konagai, Asiri Karunawardena, Kithsiri N. Bandara, Kyoji Sassa, Ryo Onishi, Ryosuke Uzuoka, Shiho Asano, Katsuo Sasahara, Sanchitha Jayakody, and Imaya Ariyaratna	
Real-Time High-Resolution Prediction of Orographic Rainfall for Early Warning of Landslides	237
Ryo Onishi, Joe Hirai, Dmitry Kolomenskiy, and Yuki Yasuda	
IPL Project 202: Landslide Monitoring Best Practices for Climate-Resilient Railway Transportation Corridors in Southwestern British Columbia, Canada	249
David Huntley, Peter Bobrowsky, Roger MacLeod, Drew Rotheram-Clarke, Robert Cocking, Jamel Joseph, Jessica Holmes, Kevin Sattler, Jonathan Chambers, Philip Meldrum, Paul Wilkinson, Shane Donohue, and David Elwood	
Advanced Technologies for Landslides—ATLaS (WCoE 2020–2023)	267
Nicola Casagli, Veronica Tofani, Sandro Moretti, Riccardo Fanti, Giovanni Gigli, Silvia Bianchini, Samuele Segoni, William Frodella, and Tommaso Carlà	
Strengthening the Resilience by Implementing a Standard for Landslide Early Warning System	277
Teuku Faisal Fathani, Dwikorita Karnawati, Wahyu Wilopo, and HENDY Setiawan	
Central Asia Rockslides Inventory: Compilation, Analysis and Training—Progress of the IPL WCoE	285
Alexander Strom	
A Global Database of Giant Landslides on Volcanic Islands	295
Matt Rowberry, Jan Klimeš, Jan Blahůt, Jan Balek, and Michal Kusák	

Landslide Disasters Caused by the 2018 Eastern Iburi Earthquake in Hokkaido Japan and the Countermeasures to Completely Prevent the Similar Disasters in the Future	305
Fawu Wang and Kounghoon Nam	
Landslide Travel Distances in Colombia from National Landslide Database Analysis	315
Steven Moncayo and Guillermo Ávila	
Landform Geometry for Restoration of Mountain Roads and Landslide Hazard Resilience	327
A. A. Virajh Dias, H. M. J. M. K. Herath, and L. K. N. S. Kulathilake	
ICL Landslide Teaching Tools	
LS-RAPID Manual with Video Tutorials	343
Beena Ajmera, Hossein Emami Ahari, Doan Huy Loi, Hendy Setiawan, Khang Dang, and Kyoji Sassa	
Technical Notes and Case Studies	
Challenges in Defining Frequentist Rainfall Thresholds to Be Implemented in a Landslide Early Warning System in India	409
Stefano Luigi Gariano, Massimo Melillo, Maria Teresa Brunetti, Sumit Kumar, Rajkumar Mathiyalagan, and Silvia Peruccacci	
KLC2020 Official Promoters	417
The International Geosynthetics Society	419
Geological Survey of Canada, Natural Resources Canada	421
Faculty of Civil and Geodetic Engineering, University of Ljubljana	425
China University of Geosciences, Wuhan	429
Department of Civil Engineering, National Taiwan University	433
Institute of Rock Structure and Mechanics, The Czech Academy of Sciences	437
Institute of Cold Regions Science and Engineering, Northeast Forestry University	441
Marui & Co. Ltd.	443
Nippon Koei Co., Ltd., Geohazard Management Division	447
Ellegi Srl	451
IDS GeoRadar s.r.l.	453
Chuo Kaihatsu Corporation	459
Godai Corporation	459

Kiso-Jiban Consultants Co. Ltd	463
Kokusai Kogyo Co. Ltd	465
OSASI Technos, Inc.	467
List of ICL Members	469
Author Index	473



Introduction: Aim and Outline of the Book Series “Progress in Landslide Research and Technology”

Kyoji Sassa and Matjaž Mikoš

Abstract

The Kyoto 2020 Commitment for Global Promotion of Understanding and Reducing Landslide Disaster Risk (Kyoto Landslide Commitment 2020: KLC2020) was launched on 5 November 2020 by the adoption of 2020 Kyoto Declaration in the end of the launching session of the Kyoto Landslide Commitment 2020. The KLC2020 was signed by 90 worldwide partners. On 3 November 2021, during the 5th World Landslide Forum (WLF5) held in a hybrid mode (onsite, online-virtual, and pre-recorded modes) in Kyoto, Japan, the ICL and the KLC2020 partners launched the new open-access book series “Progress in Landslide Research and Technology” to promote the Kyoto Landslide Commitment 2020 for global promotion of understanding and reducing landslide disaster risk. This article introduces the aim and outline of the new book series “Progress in Landslide Research and Technology.”

Keywords

Kyoto Landslide Commitment 2020 • 5th World Landslide Forum • Open Access Book Series

1 Aim

The Kyoto 2020 Commitment for Global Promotion of Understanding and Reducing Landslide Disaster Risk (Kyoto Landslide Commitment 2020: KLC2020): A

K. Sassa (✉)
International Consortium on Landslides, Secretariat, Kyoto,
606-8226, Japan
e-mail: sassa@iclhq.org

M. Mikoš
University of Ljubljana, UNESCO Chair on Water-related
Disaster Risk Reduction & Faculty of Civil and Geodetic
Engineering, 1000 Ljubljana, Slovenia
e-mail: matjaz.mikos@fgg.uni-lj.si

Commitment to the ISDR-ICL Sendai Partnerships 2015–2025, the Sendai Framework for Disaster Risk Reduction 2015–2030, the 2030 United Nations Agenda Sustainable Development Goals, the New Urban Agenda and the Paris Climate Agreement was launched on 5 November 2020 by the adoption of 2020 Kyoto Declaration in the end of the launching session of the Kyoto Landslide Commitment 2020.

Figure 1 shows the logos of the International Consortium on Landslides (ICL) and the KLC2020. KLC2020 was proposed by the ICL based on the 2006 Tokyo Action Plan. The Memorandum of Understanding to promote the Action Plan was exchanged between the ICL and each of the ICL supporting organizations (United Nations Educational, Scientific and Cultural Organization (UNESCO), World Meteorological Organization (WMO), Food and Agriculture Organization of the United Nations (FAO), United Nations Office for Disaster Risk Reduction (UNDRR), United Nations University (UNU), International Science Council (ISC), World Federation of Engineering Organizations (WFEO)) in 2006. IPL and KLC2020 will continue to 2030 and beyond, symbolized by an arrow.

Following the launching of the Kyoto Landslide Commitment 2020 and the establishment of the Secretariat of the KLC2020 on 5 November 2020, the Secretariat examined and prepared a mechanism for the further development of the KLC2020 to 2030 and beyond. It was then proposed to launch an open-access book series as a platform for KLC2020 partners, practitioners, and stakeholders. The open-access book series shall contribute to greater applications of the advanced scientific knowledge, with a multi-hazard approach, and in raising awareness at all levels worldwide.

On 3 November 2021, during the 5th World Landslide Forum (WLF5) held in a hybrid mode (onsite, online-virtual, and pre-recorded modes) in Kyoto, Japan, the ICL and the KLC2020 partners have launched the new open-access book series “Progress in Landslide Research and Technology” for

Fig. 1 Logos of the ICL and the Kyoto landslide commitment 2020



the Kyoto Landslide Commitment 2020 for global promotion of understanding and reducing landslide disaster risk. The ICL has published 3–7 volumes of books for triennial WLF (WLF2 in 2011, WLF3 in 2014, WLF4 in 2017, and WLF5 in 2021) to report the progress of research and technology for the past three years. Biannual publication of the new open access book series “Progress in Landslide Research and Technology” shall replace the role of triennial WLF book publication. Thus, ICL has decided not to publish books for WLF6 in 2023 and later.

The ICL was founded in January 2002 and started issuing a new full color scientific journal “*Landslides*” in 2003, and published the founding issue in April 2004. *Landslides* has grown up from a quarterly journal to a monthly journal with 3977 published pages in 2021 and the 2020 Impact Factor of 6.578. ICL and its valuable network of scientists has readily available sufficient scientific material for *understanding landslide disaster risk as mentioned* in the concluding remarks by Sálvano Briceño in the high-level panel discussion of the WLF5.

At the opportunity of the 20th anniversary of ICL in 2022, the ICL and KLC2020 partners, with the financial and technical support from the KLC2020 official promoters, has published the founding issue of the open-access book series “Progress in Landslide Research and Technology” for global promotion of reducing landslide disaster risk.

Table 1 presents different aim and scope between the ICL New Book Series and the ICL Journal.

The target readers of journal papers are scientists. Articles consist of original/new findings for landslide research. Readers are those who have necessary background knowledge, have access to the referred journals and can read the cited references.

The target readers of the open access book series are practitioners and other stakeholders who apply in practice the most advanced knowledge of science and technology for landslide disaster risk reduction. Articles must be written in a simplified way that is easily understandable by these practitioners and stakeholders.

2 Outline

The ICL and the Global Promotion Committee of the International Programme on Landslides including the ICL supporting organizations (UNESCO, WMO, FAO, UNDRR, UNU, ISC, WFEO, International Union of Geological Sciences (IUGS), and International Union of Geodesy and Geophysics (IUGG) have organized World Landslide Forums every three years in 2008, 2011, 2014, 2017 and planned WLF5 in Nov. 2020. Due to COVID-19, the WLF5 in 2020 was postponed to 2–6 Nov. 2021. However, due to Covid-19 restrictions, foreign participants were not allowed to attend WLF5 in Kyoto, Japan in-person. The WLF5 was organized in a hybrid system, namely, by including onsite, online, and the pre-recorded presentations.

Table 1 Differences in the aim and scope between ICL book series and ICL journal

	ICL new book series “ <i>P-LRT</i> ” since 2022	ICL journal “ <i>Landslides</i> ” since 2004
Aim	Promotion of reducing landslide disaster risk	Promotion of understanding landslide disaster risk
Scope	Original articles for practice and society	Original research for landslide science
Online access	Open access (Free)	Charged access
Publication fee	Book processing charge: 50 USD/page (0–25 USD/page until 10 pages/year for ICL members and KLC official promoters)	Free
Pages/issue	400–500 pages	250–350 pages
No of issue	2 books/year	12 issues/year
Publication style	Electronic and print	Electronic and print
	210 mm × 280 mm	210 mm × 280 mm
	2 column format	2 column format

Table 2 Participants (onsite, online and pre-recorded) of WLF5 held on 2–6 November 2021 in Kyoto, Japan

No	Country/Region	Participants	No	Country/Region	Participants
1	Australia	2	30	Nigeria	1
2	Bangladesh	1	31	Norway	9
3	Belgium	3	32	Philippines	1
4	Bhutan	1	33	Poland	2
5	Brazil	2	34	Republic of Korea	7
6	Canada	7	35	Romania	1
7	Chile	3	36	Russia	8
8	China	45	37	Serbia	2
9	Colombia	2	38	Slovenia	9
10	Croatia	3	39	Spain	3
11	Czech Republic	16	40	Sri Lanka	2
12	El Salvador	2	41	Switzerland	4
13	Ethiopia	1	42	Chinese Taipei	10
14	France	3	43	Turkey	2
15	Germany	7	44	UK	10
16	Greece	3	45	USA	21
17	Honduras	2	46	Vietnam	4
18	India	10			
19	Indonesia	10		International Organizations	
20	IRAN	1		IUGG	2
21	Italy	47		IUGS	2
22	Japan	215		WFE0	1
23	Malaysia	5		United Nations Organizations	
24	Mauritius	1		FAO	1
25	Mexico	6		UNDRR	3
26	Morocco	1		UNESCO	3
27	Nepal	3		UNU	1
28	Netherlands	7		WMO	1
29	New Zealand	5		Total	525

The total number of participants of WLF5 was 525, in which 215 from Japan, 47 from Italy, 45 from China, 21 from USA, more than 10 are from Czech Republic, UK, India, Indonesia and Chinese Taipei, 5 from United Nations organizations, and 3 from international organizations (Table 2).

On the morning of 3 November 2021, an opening greeting session from ICL and ICL supporting organizations and a high-level panel discussion session “Review of KLC2020 and the way forward” were organized at Room A of the National Kyoto International Conference Center in Kyoto, Japan. At the end of the two plenary sessions, the Launching Declaration of the ICL Open Access Book Series “Progress in Landslide Research and Technology” for the Kyoto Landslide Commitment 2020 was adopted by all panelists and participants attending in-person and virtually.

The Opening Greeting session was chaired by Kyoji Sassa (WLF5 Forum Chair) and Qunli Han (Chair of Global Promotion Committee of IPL/Executive Director of Integrated Research on Disaster Risk). It consisted of the following:

Opening address from the primary organizer:

- Nicola Casagli (President of the International Consortium on Landslides).

Greetings from United Nations organizations:

- David Malone (Under-Secretary-General of the United Nations/Rector of the United Nations University)
- Mami Mizutori (United Nations Special Representative of the Secretary-General for Disaster Risk Reduction)

- Petteri Taalas (Secretary-General of the World Meteorological Organization: WMO)
- Maria Helena Semedo (Deputy Director-General of the Food and Agriculture Organizations: FAO)
- Shamila Nair-Bedouelle (Assistant Director-General for Natural Sciences, the United Nations Educational, Scientific and Cultural Organization: UNESCO).

Greetings from scientific organizations:

- José M.P. Vieira (President of the World Federation of Engineering Organizations: WFEO)
- Kathryn Whaler (President of the International Union of Geodesy and Geophysics: IUGG)
- John Ludden (President of the International Union of Geological Sciences: IUGS).

Welcome messages from host organizations:

- Hiroaki Tsunakawa, Director for Sabo Planning Coordination, Ministry of Land Infrastructure, Transport and Tourism, Japan
- Akira Murakami, Executive Vice-President of Kyoto University.

Prof. Akira Murakami, Executive Vice-President of Kyoto University came to the Kyoto International Conference Center and presented welcome message on site. He joined this group photo (front and center) in Fig. 2.

High-level Panel Discussion “Review of KLC2020 and the way forward”

Opening Greetings from Forum Chairs:

- Peter Bobrowsky (Geological Survey of Canada, Canada)
- Kaoru Takara (Kyoto University, Japan)

Chairs: Matjaž Mikoš (Co-Chair, Global Promotion Committee of IPL/Chair of WLF4, Ljubljana, 2017).

Kazuo Konagai (Chair of Science Committee of the KLC2020 Secretariat, Kyoto, Japan)

Keynote speech:

- Kyoji Sassa (Secretary General of KLC2020 Secretariat): Review of KLC2020 and a new Open Access Book Series for KLC2020

Sassa presented a short history of KLC2020 beginning from the 2005 Letter of Intent which was proposed by the ICL and agreed in a thematic session in the Second World Conference on Disaster Reduction in Kobe, Japan in January 2005.

- The Letter of Intent was signed by UNESCO, WMO, FAO, UNISDR (UNDRR), UNU, ICSU (ISC) and WFEO within 2005.
- The ISDR-ICL Sendai Landslide Partnerships 2015–2025 was established in March 2015.
- The KLC2020 was approved and signed by ninety signatory organizations and launched in November 2020.

Fig. 2 Group photo of the WLF5 onsite participants in room A of the Kyoto international conference center and on the online zoom platform on 3 November 2021



Finally, he proposed a new open access book series titled, “Progress in Landslide Research and Technology” as a platform in order to promote the Kyoto Landslide Commitment 2020.

Speeches were delivered by nine panelists from KLC2020 signatory organizations.

ICL supporting organizations:

- Paola Albrito (Chief of Branch, Intergovernmental processes, Interagency cooperation and Partnerships, UNDRR)
- Soichiro Yasukawa (Programme Specialist on Disaster Risk Reduction, UNESCO)
- José M.P. Vieira (President of the World Federation of Engineering Organizations: WFEO)
- Hiroshi Kitazato (Treasurer of IUGS, Tokyo University of Marine Science and Technology, Japan)
- John LaBrecque (Chair of IUGG GeoRisk Commission, Center for Space Research, University of Texas, Austin, USA).

ICL full members:

- Binod Tiwari (ICL Vice President for America, California State University, Fullerton, USA)
- Paola Reichenbach (Director of Research, IRPI, Italian National Research Council, Italy)
- Maneesha Ramesh (Dean, School for Sustainable Development and International Programs, Amrita University, India).

ICL supporter:

- Hiroaki Tauchi (General Manager, International Geohazard Management Department, Nippon Koei, Co., Ltd., Tokyo, Japan)

Discussion (panelists and floor)

Concluding remarks

- Sálvano Briceño (First Chairperson of the Global Promotion Committee of IPL (2007–2014), Former Director of UNISDR (2001–2011).

Dr. Sálvano Briceño is the Former Director of UNISDR (2001–2011). During this period, he continued to support the activities of ICL. He contributed to the establishment of the 2006 Tokyo Action Plan which created the International Programme on Landslides (IPL) and the Global Promotion Committee of the International Programme on Landslides. He worked as the first chairperson of the Global Promotion

Committee of the International Programme on Landslides (2007–2014). Currently, he is a senior advisor of the ICL.

In the concluding remarks, he firstly stressed the significance of the intergovernmental network on landslide risk reduction, and the importance of cooperating with relevant intergovernmental processes, such as the Intergovernmental Panel on Climate Change (IPCC). In the main policy areas of mitigation and adaptation of the IPCC, preventing, mitigating and preparing for landslide disasters should become a main objective of climate change policies and research, given their heavy impact on development, and their expected increase due to global warming, and to the expansion of vulnerability due to urban growth and urban density.

Secondly, he called for “a greater application of scientific knowledge, with a multi-hazard approach, in raising awareness at all levels worldwide,” stating that understanding the origin and causes as well as the impacts of landslides, floods, cyclones, earthquakes, volcanic eruptions, droughts and land degradation, needs to become the current knowledge of citizens and communities around the world. The ICL and its valuable network of specialists has sufficient scientific material readily available to contribute to such a task, but the task requires a substantive increase in academic participation in the media, in various forms, interviews, presentations, debates, briefs for guidance to journalists, press releases, etc.

The high-level panel discussion concluded with the **Adoption of the Launching Declaration of the ICL Open Access Book Series for KLC2020** by all panelists and participants attending in-person and virtually, as shown below.

Launching Declaration of the ICL Open Access Book Series “Progress in Landslide Research and Technology” for the Kyoto Landslide Commitment 2020

The Kyoto 2020 Commitment for Global Promotion of Understanding and Reducing Landslide Disaster Risk (Kyoto Landslide Commitment 2020)—A Commitment to the Sendai Landslide Partnerships 2015–2025, the Sendai Framework for Disaster Risk Reduction 2015–2030, the 2030 Agenda Sustainable Development Goals, the New Urban Agenda and the Paris Climate Agreement was launched on 5 November 2020 together with 90 signatories. The KLC2020 established a Secretariat of the Kyoto Landslide Commitment within the ICL Secretariat in Kyoto, Japan at the same time.

In order to promote “Kyoto 2020 Commitment until 2030 and beyond, a new stable and global platform is essential for the information dissemination and

collaboration within KLC2020 partners and the Society. Therefore, the establishment of an Open Access book series of the International Consortium on Landslides (ICL) “Progress in Landslide Research and Technology” was planned and proposed by the KLC2020 Secretariat. This book series can be downloaded free of charge by all, both in developing and developed countries suffering from landslide disasters and also the policy makers involved in landslide disaster risk reduction.

Until today, twenty international/national and public/private organizations in the world have accepted the role of the KLC2020 official promoters who promote the Kyoto Landslide Commitment 2020 and provide financial support for the implementation of the KLC2020 activities. Many experts have accepted the role of voluntary editors and advisory members. Both financial and personal resources have been secured for this new publication series.

On 3 November 2021 during the Fifth World Landslide Forum in Kyoto, Japan, at the high-level panel discussion “Review of KLC2020 and the way forward”, all panelists and participants agreed on, and declared the launching of the ICL Open Access Book Series “Progress in Landslide Research and Technology” for the Kyoto Landslide Commitment 2020.

Date: 3 November 2021.

Place: Kyoto, Japan.

3 Call for KLC2020 Official Promoters

The Secretariat of the Kyoto Landslide Commitment 2020 has expended efforts to create a new Open Access Book Series “the Progress of Landslide Research and Technology” as the key tool for the implementation of the KLC2020. The detailed information is uploaded in the ICL webpage <<https://icl.iplhq.org/book-series-of-klc2020/>>.

The KLC2020 Secretariat requests organizations to cooperate for promoting the KLC2020 activities including this new book series “Progress of Landslide Research and Technology” as the KLC2020 official promoters. KLC2020 official promoters are public and private organizations who promote the Kyoto Landslide Commitment 2020 and provide financial support for the implementation of the KLC2020 activities including publication of the Open Access Book Series. So far, the following twenty organizations have accepted the role of KLC2020 Official Promoters.

KLC2020 Official Promoters

Host organization

International Consortium on Landslides (ICL)/Nicola Casagli

Public sectors: KLC2020 Official Promoters-public

International Unions/Associations, Governmental organizations, Universities and Research institutes

- The International Union of Geological Sciences (IUGS)/John Ludden
- The International Union of Geodesy and Geophysics (IUGG)/Kathy Whaler
- The International Association for the Engineering Geology and the Environment/Rafiq Azzam
- International Geosynthetics Society (IGS)/John Kraus
- Geological Survey of Canada, Natural Resources Canada, Canada/Daniel Lebel
- Faculty of Civil and Geodetic Engineering, University of Ljubljana, Slovenia/Matjaž Mikoš
- China University of Geosciences, Wuhan, China/Huiming Tang
- Department of Civil Engineering, National Taiwan University, Chinese Taipei/Shang-Hsien Hsien
- Institute of Rock Structure and Mechanics, the Czech Academy of Sciences/Josef Semberk
- Institute of Cold Regions Science and Engineering, Northeast Forestry University, China/Wei Shan.

Private sectors: KLC2020 Official Promoters-private

Companies and corporation

- Marui & Co. Ltd, Japan
- Nippon Koei Co., Ltd, Japan
- Ellegi srl, Italy
- IDS GeoRadar s.r.l., Italy
- Chuo Kaihatsu Corporation, Japan
- Godai Corporation, Japan
- Kiso-Jiban Consultants Co., Ltd, Japan
- Kokusai Kogyo Co., Ltd., Japan
- OSASI Technos, Inc., Japan.

Advisory members for KLC2020

Abou Amani, Director, Division of Water Sciences, Secretary, Intergovernmental Hydrological Programme (IHP), UNESCO

Soichiro Yasukawa, Programme Specialist, Coordinator for Disaster Risk Reduction and Resilience, UNESCO

Daniel Lebel, Director General, Geological Survey of Canada, Natural Resources Canada, Canada.

John Ludden, President of the International Union of Geological Sciences (IUGS).

John LaBrecque, Chair of IUGG GeoRisk Commission, Center for Space Research, U. Texas Austin, USA.

Rafiq Azzam, President of the International Association for the Engineering Geology and the Environment (IAEG).

Paolo Canuti, Past President of the International Consortium on Landslides (ICL), Italy.

Sálvano Briceño, First Chair of the Global Promotion Committee of the International Programme on Landslides.

Badaoui Rouhban, Chair of the KLC2020 Launching Session and Moderator of ISDR-ICL Sendai Landslide Partnerships 2015–2025 Session of 3rd WCDRR in 2015.

4 Call for Articles

The target users of book series are practitioners and other stakeholders who apply the most advanced knowledge of science and technology for landslide disaster risk reduction. Articles must be written in a simplified way easily understandable by practitioners and other stakeholders, including requiring minimum necessary extraneous information. Application/explanation of new modelling, new technology or new concept already published in journals are effective for landslide disaster risk reduction. Teaching tools including video and illustration are useful for landslide disaster risk reduction. Reports of the IPL Projects, WCoE activities, and activities of Kyoto Landslide Commitment 2020 that contribute to the landslide disaster risk reduction are also appropriate.

Categories of ICL Book Series “P-LRT”

1. Original articles (minimum 8 pages): Original articles reporting progress of landslide research and technology.
2. Review articles (minimum 8 pages): Review of landslide research and technology in a thematic area of landslides. A review article integrating a series of research and technology of the author or its group.
3. ICL landslide lessons (minimum 20 pages): Lessons by global and emerging experts with distinguished achievements in one of specific aspects in understanding and reducing landslide disaster risk.

4. IPL/WCoE/Kyoto Commitment activities (minimum 8 pages): Progress or achievements of the projects of the International Programme on Landslides (IPL) and the World Centres of Excellence on Landslide Risk Reduction (WCoEs), and Kyoto Landslide Commitment.
5. Teaching tools with online extras (minimum 8 pages): User-friendly teaching tools with extras (i.e., photos, illustration, videos, guidelines & manuals) online to fill the gap between the available level of science and technologies and the practical use in the society.
6. Technical note & Case studies (minimum 4 pages): Technical note and case studies on landslides and landslide disaster risk reduction practice.
7. World Landslide Reports: Landslide reports from landslide-prone developing countries and urbanizing areas of the developed countries from around the world. No processing charge, but limited to 40 pages per issue.
8. Introduction of KLC2020 Official Promoters (1–3 pages): KLC2020 Official Promoters are eligible for this category. The introduction of the official promoters is published in all issues (normally 2) throughout the year.

This book series are planned to be published two times per year, in April–May and October–November. Submission-review- publication will take 6 months. The length of an issue will be 400–500 pages. To make a good publication plan together with authors participating to promote the Kyoto Landslide Commitment 2020, the Editorial office requests potential authors to inform their plans for article submission to each issue to the KLC2020 Secretariat <KLC2020@iclhq.org>.



Video link

<https://us06web.zoom.us/rec/play/5djycamTN2UUbdp9d8-wAT-taQFN-IkTURujGp0GzRnXuQsRjPqGooNiGWoKvFCBZoq5one6ZPE899Oc.xBIr3J4Vq9MFXSDX?autoplay=true&startTime=1661758164000>

Contact for publication in P-LRT

Kyoji Sassa

Editor-in-Chief of *Progress in Landslide Research and Technology*

Secretariat of the Kyoto Landslide Commitment 2020
International Consortium on Landslides

138-1 Tanaka-Asukai-cho, Sakyo-ku, Kyoto 606-8226,
Japan

Email: KLC2020 Secretariat <KLC2020@iclhq.org>



Kyoji Sassa
Secretary-General of the Kyoto
Landslide Commitment 2020



Matjaž Mikoš
Chair of the Global
Promotion
Committee of the
IPL and the Kyoto
Landslide
Commitment 2020

Open Access This chapter is licensed under the terms of the Creative Commons Attribution 4.0 International License (<http://creativecommons.org/licenses/by/4.0/>), which permits use, sharing, adaptation, distribution and reproduction in any medium or format, as long as you give appropriate credit to the original author(s) and the source, provide a link to the Creative Commons license and indicate if changes were made.

The images or other third party material in this chapter are included in the chapter's Creative Commons license, unless indicated otherwise in a credit line to the material. If material is not included in the chapter's Creative Commons license and your intended use is not permitted by statutory regulation or exceeds the permitted use, you will need to obtain permission directly from the copyright holder.



**International Consortium on Landslides
and International Programme on Landslides**



International Consortium on Landslides: From IDNDR, IGCP, UNITWIN, WCDRR 2 & 3 to Kyoto Landslide Commitment 2020

Kyoji Sassa, Paolo Canuti, Peter Bobrowsky, and Nicola Casagli

Abstract

The International Consortium on Landslides (ICL) was proposed and established in January 2002, based on the Japan–China international joint research activities (1991–1999) in a part of IDNDR (International Decade for Natural Disaster Reduction) and the UNESCO-IUGS Joint programme IGCP-425: Landslide Hazard Assessment and Cultural Heritage (1998–2003). The ICL has developed through the UNESCO-KU-ICL UNITWIN Cooperation Programme from 2003, the second World Conference on Disaster Reduction in Kobe in 2005, the 2006 Tokyo Action Plan, the third World Conference on Disaster Risk Reduction in Sendai in 2015, and the ISDR-ICL Sendai Landslide Partnerships 2015–2025. On 5 November 2020, the Kyoto Landslide Commitment 2020 for global promotion of understanding and reducing landslide disaster risk was launched by 90 signatory organizations consisting of the ICL, ICL supporting organizations and other stakeholders. The ICL history is reviewed focusing on the link with United Nations Programmes, UN World Conferences by the founding, the second, the immediate past, and the current Presidents of the ICL.

Keywords

IDNDR • IGCP • Tokyo action plan • Sendai landslide partnerships • KLC2020

1 IDNDR (1991–1999)

As a part of the Japanese contribution to the IDNDR (International Decade for Natural Disaster Reduction) in the last decade of the twentieth century, the Ministry of Education, Culture, Sports, Science and Technology of the Government of Japan (MEXT) funded international joint research projects. The projects included a Japan–China Joint Project “Assessment of Landslide Hazards in Lishan (Yang-Que-Fe Palace), Xian, China,” which was proposed by Kyoji Sassa, Disaster Prevention Research Institute, Kyoto University. The goal of the project was to investigate the landslide risk to the Lishan Resort Palace of the Tang Dynasty (a.d. 618–907) (Fig. 1a and b). The rear slope of Lishan Palace has been stable since the Tang Dynasty. The base rock is Precambrian gneiss (hard rock). In the initial stage of this project, there were split opinions among Japanese and Chinese landslide researchers on the possibility of large-scale landslides. Everyone agreed that the slope is affected by slope deformation. One opinion was that the deformation is limited within top loess soil layer, while another opinion was the deformation can be affected by deep seated mass movement within the Precambrian gneiss (hard rock). Both agreed that precise investigation and extensive monitoring are needed to clarify the mechanism of the slope deformation, namely whether the current slow deformation is a precursor stage of large-scale rockslide or not.

The Palace is one of the most important Cultural Heritage sites in China attracting more than three million visitors per year. Social, cultural and economical losses by its destruction by large-scale landslides could be very large. A Japan–China Joint project was, then, conducted by Chinese and Japanese budgets and scientists. This special project by MEXT continued for eight years from 1991 to 1999.

Based on the investigation results from 1991 to 1996, the project group organized the International Symposium on Landslide Hazard Assessment, Xian, China, in July 1997 as the Committee for Prediction of Rapid Landslide Motion of

K. Sassa (✉) · P. Canuti · P. Bobrowsky · N. Casagli
Presidents of the International Consortium on Landslides, Kyoto,
Japan
e-mail: secretariat@iclhq.org

the IUGS Working Group on Landslides (WGL/RLM). The symposium received support from the United Nations Educational, Scientific and Cultural Organization (UNESCO), the International Union of Forest Research Organizations (IUFRO), the State Planning Commission of the Government of China, the Embassy of Japan, the Japan Landslide Society and others. The report on the investigation clearly presented evidence of the risk of a large-scale rockslide, based on detailed monitoring and observation of investigation tunnels.

Figure 1a presents a front view of Lishan slope which is a large-scale fault scarp. Hot ground water came up from the deep ground to the ground as hot springs. Those hot springs are used for the Lishan Resort Palace of the Tang Dynasty (a.d. 618–907). Active faults in Xian caused many earthquakes of Magnitude M4–8 in the past. Precambrian gneiss could be broken even though they are hard.

Figure 1b shows the Lishan Palace and the center of Lintong town. Those areas may be destroyed by landslide debris if a high-speed long travelling landslide occurred. Figure 1c is an investigation map including estimated potential landslide blocks from slight deformation and topography (green). The two red colored lines are lines of long-span extensometers. Two black lines are investigation tunnels where shear bands within the gneiss bedrock were found. Figure 1d shows the sign of the precursor movement of deep-seated landslides (Block 1 and Block 2). Two weeks after rainfall, Extensometer A7 showed extension indicating relative downslope movement of Block 1. One week after the second rainfall, Extensometer A1 recorded compression which means the movement of Block 1 onto Huaqing Palace (Yang-Que-Fe Palace). Very slight extension of B1 means that Block 2 slightly moved due to the larger movement of Block 1. Slight movement in gneiss rocks should weaken the shear band within the rock mass. A shear band was found in the investigation tunnels. Then, strength of rock should have been decreased, and failure more likely.

When a rockslide is initiated along a shear band, the shear strength of rock should drop and rapid slope movement should occur onto the alluvial deposit on which the Palace and the town are constructed. Using samples taken from the saturated alluvial deposit within the Palace, the apparent friction angle during the undrained loading was determined by the dynamic loading ring shear apparatus. The result was shown in Fig. 1f. The mobilized apparent friction angle was 5.4 degrees. The capacity of normal stress in this apparatus was 400 kPa. From a real landslide on this slope, the apparent friction angle was estimated to be 3.3 degrees. Apparent friction angle in gneiss rock cannot be measured. Then, the travel distance was estimated assuming 25, 30, and 35 degrees. This gave the travel distances of 930 m, 1530 m, and 2430 m. The Palace and the Lintong Town would be destroyed in any case.

Mr. Qiyuan An, the honorary chairman of the symposium and also the Secretary-General of the Communist Party of the Shaanxi Provincial Government, understood the landslide risk at the Lishan Palace (Huaqing Palace). Mr. An took a key role in initiation of landslide prevention works, based on landslide risk analysis, by investing about three million U.S. dollars from the municipal, regional, and national governments of China. This is probably the first case in the world of the initiation of extensive landslide remedial measures at a Cultural Heritage site for mitigation of potential landslides at the precursor stage. This investigation of landslides at the precursor stage was evaluated as a contribution of geoscientists to protection of Cultural Heritage.

Products of the Symposium

1. Participants released the 1997 Xian Appeal “1997 Xian Appeal for Protection of the Cultural Heritage (Huaqing Palace) in Xian and Promotion of Worldwide Landslide Hazard Assessment and Risk Mitigation” under the authorship of symposium panelists.
2. Proceedings of the International Symposium on Landslide Hazard Assessment (ISBN4-9900618-0-2 C3051), 421 pages (edited by Sassa 1997).
3. Special Programme and Video “For the Protection of Huaqing Palace in Xian” produced by Xian Television (1997) (Chinese, English, and Japanese versions, 20 min).
4. Invitation by Prof. Edward Derbyshire (one of participants and the Chairman of the Scientific Board of IGCP) to propose a new International Geological Correlation Programme (IGCP) project to promote this research.

2 IGCP 425 (1998–2003)

The IGCP-425 “Landslide Hazard Assessment and Mitigation for Cultural Heritage Sites and Other Locations of High Societal Value” project was initiated from 1998 until 2003. The International Consortium (ICL) was established during the IGCP symposium. The ICL founded the International Programme on Landslides (IPL) at the first Board of Representative meeting at UNESCO Headquarters, in Paris, France in November 2002. The Machu Picchu project was conducted by IPL C101-1 Landslide investigation and capacity building in Machu Picchu-Aguas Calientes area from 2002. Activities in 2002 and 2003 were conducted as IGCP-425 and also IPL C101-1. This project is very important project for the ICL together with IPL C100 Landslides: Journal of the International Consortium on Landslides.

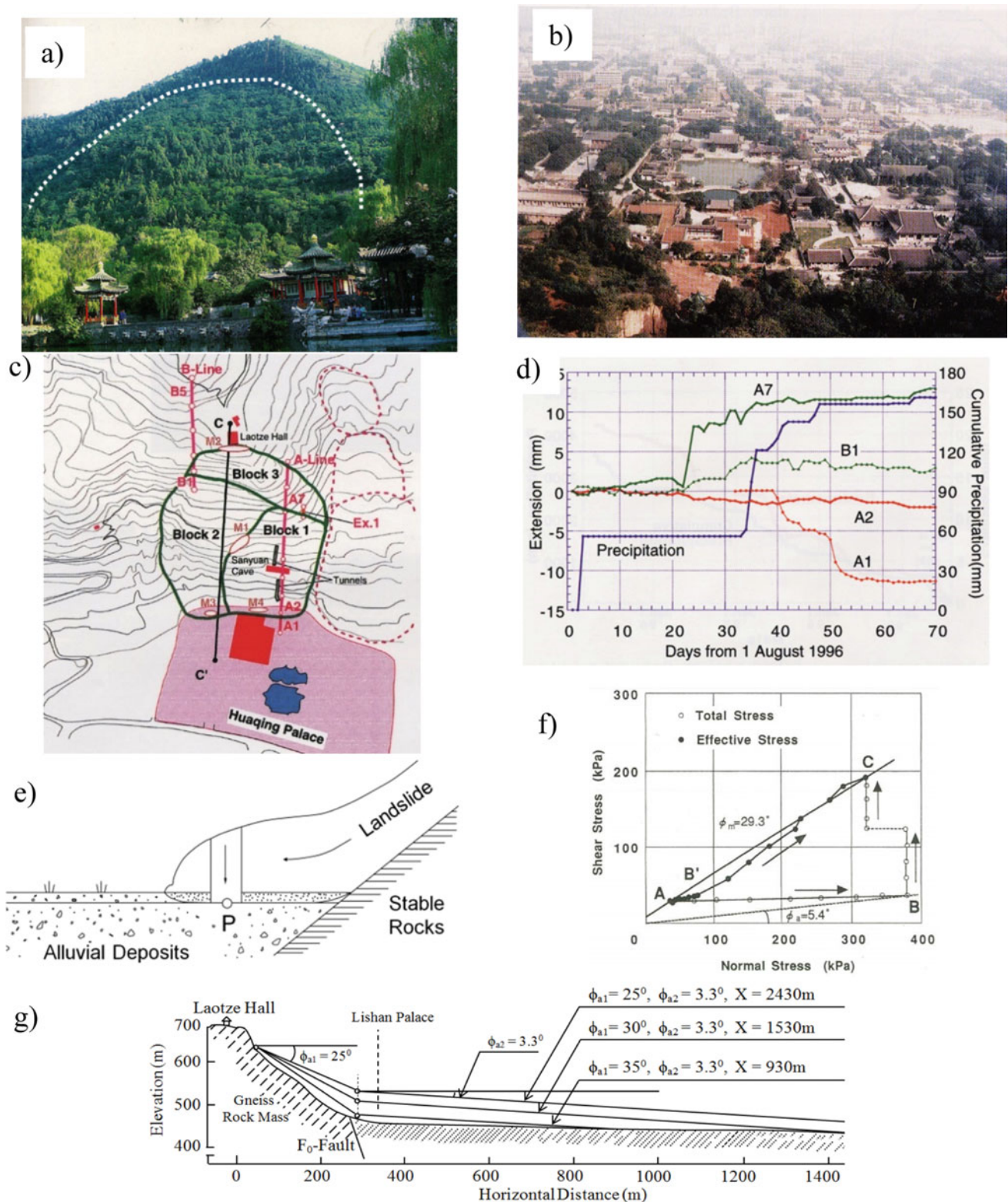


Fig. 1 Landslide disaster risk investigation at Lishan resort palace (Tang Dynasty) in Xian, China. **a** Creeping slope in the back of the Lishan Palace. **b** View from the slope to the Lishan palace and the center of Lintong town. **c** Potential landslide blocks and extensometer lines. **d** Monitoring results showing the movement of the blocks.

e Illustration of undrained loading of landslide mass onto the saturated alluvial deposits. **f** Result of the undrained loading ring-shear test on the saturated sample taken from the alluvial deposit. **g** Estimated travel distance from the apparent friction angle of the alluvial deposit and assumed apparent friction angle of rock slope (25–35 degrees)

Figures 2, 3, 4, 5 and 6 presents the outline of “Landslide disaster risk investigation in Machu Picchu, World Heritage, in Cusco, Peru”. Figure 2a is a photo taken by K. Sassa from the chartered helicopter to observe the Machu Picchu slope in 2000. The Machu Picchu citadel was constructed on the planer mountain ridge. The ground surface seems to be parallel to the bedding (shear band). Many fault systems seem to control the topography. A step in “A” which seems to be the outcrop of a shear band was found. Figure 2b presents the close-up photo of the step “A” taken from Urbanba River on the back side. Two parallel shear bands are clear and some displacement was found at these shear bands. The border of landslide block (red dotted line) seems to pass the flat area (Plaza) in the center of Machu Picchu citadel. Figure 2c is a group photo at one of long-span extensometers and GPS on the top of extensometer box in Machu Picchu. Figure 3 contains the estimated landslide

blocks No. 1 (red color area: active), No. 2 (less active) and No. 3 (green colored area: not active at present). Three section lines are taken (A-line, B-line and C-line).

Figure 6 shows the hypothesis of landslide evolution in Machu Picchu slope. Ancient landslides occurred along the current ground surface and all materials were moved out forming the current ground surface seen in Fig. 2a. The toe of the slope has already failed as seen in Fig. 2a and also shown as the yellow landslide debris in Fig. 3. Stage 2 in which landslides failed from the toe along the Urbanba River as a result of river side erosion, is ongoing in Block 2. However, in Block 1, the slope is covered by landslide debris. The whole block are reactivated type landslides, which are moving slowly. The bottom figure of Fig. 6 contains the cross section. The shear band (sliding surface) of Block 1 is located one step lower than the current ground surface of Block 2.

Fig. 2 Photos in Machu Picchu Citadel **a** Photo of the Machu Picchu Citadel and creeping shear band from a chartered helicopter taken by K. Sassa in 2000. **b** Photos of the creeping shear band A from the backside ground. **c** A group photo of installation of long-span extensometers and GPS in the Citadel

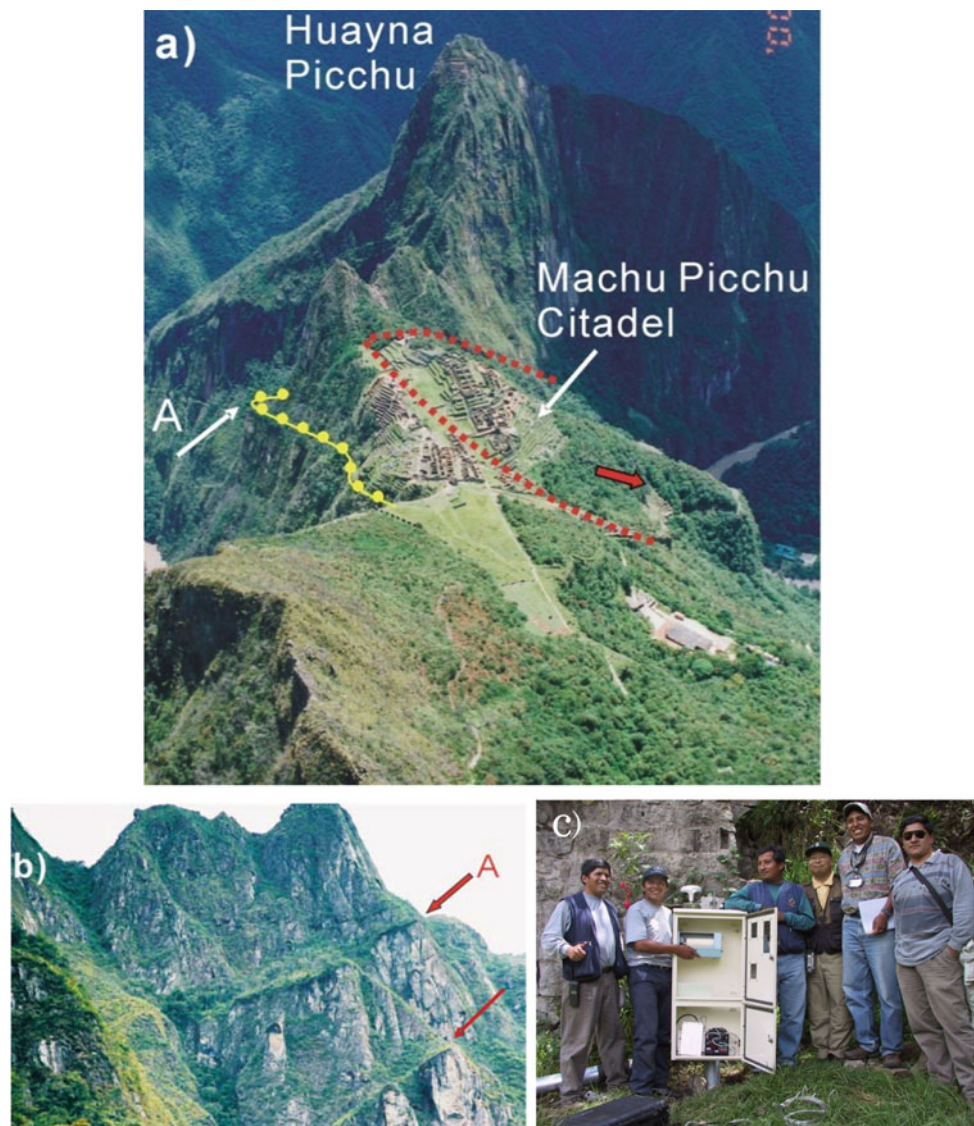


Fig. 3 Landslide block (1-3) and two section lines crossing block 1 and 2 (red: active, green: inactive, yellow: landslide debris, red: Inca Citadel, Blue: Urubamba River)

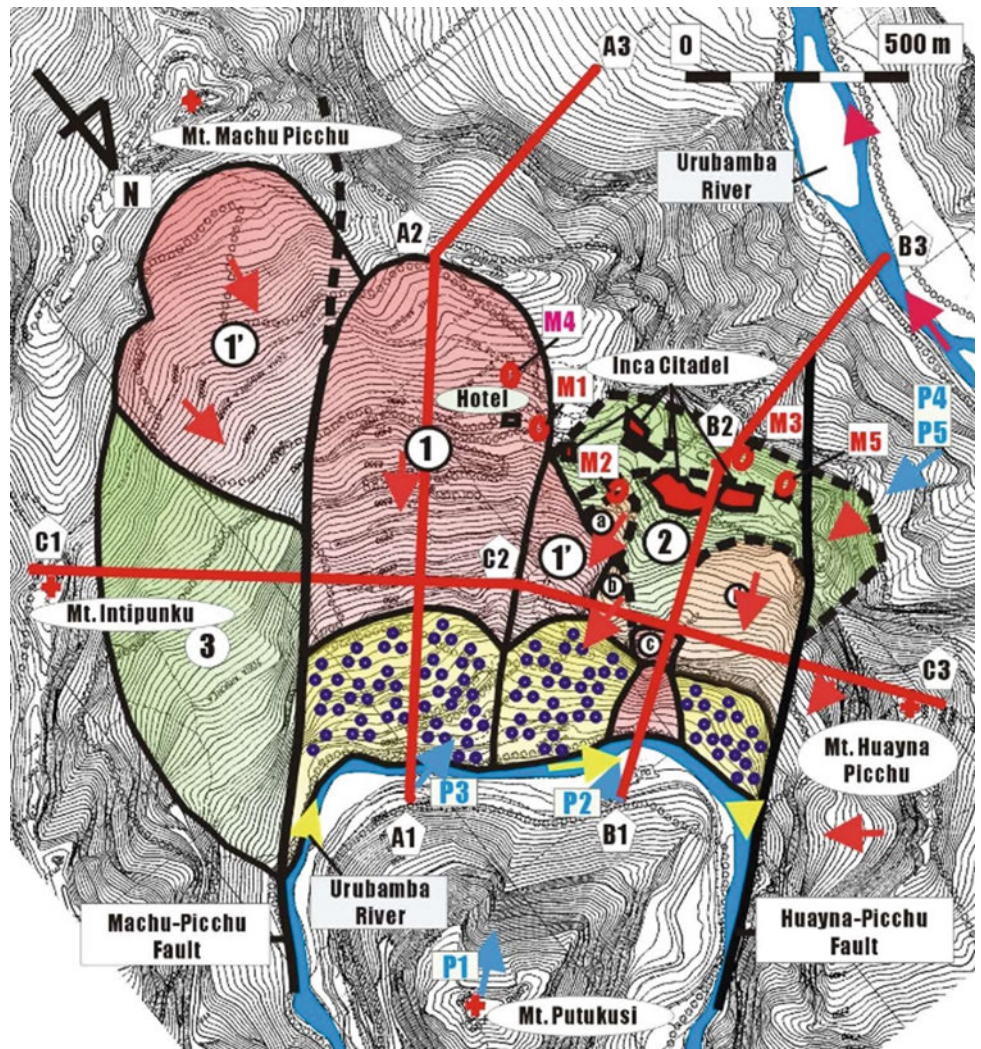


Fig. 4 Monitored movement of the long span extensometer and the location of the extensometer (Cafeteria) along the section of Landslide block 1

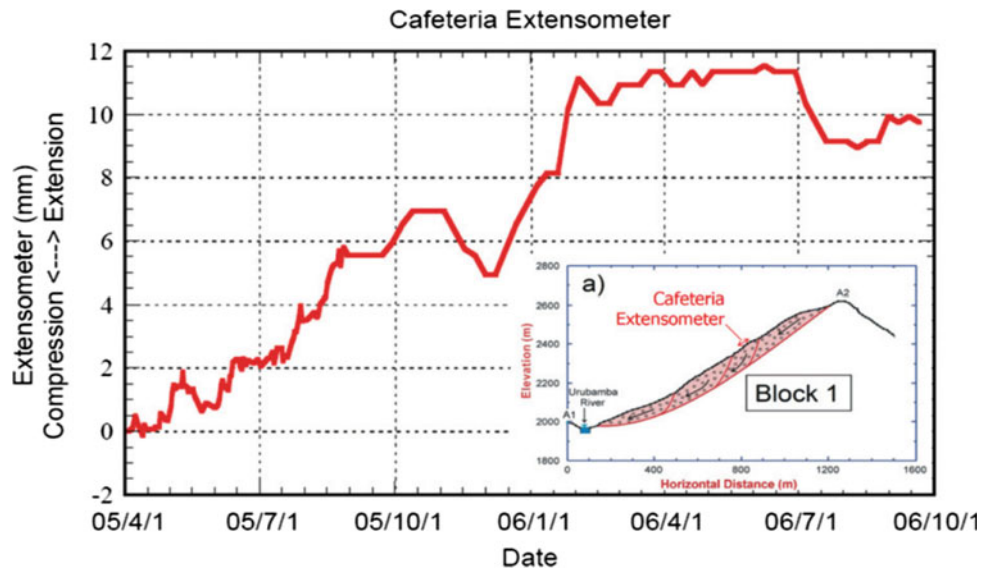


Fig. 5 Monitored movement of the long span extensometer and the location of the extensometer (IntiMachay) along the section of Landslide block 2

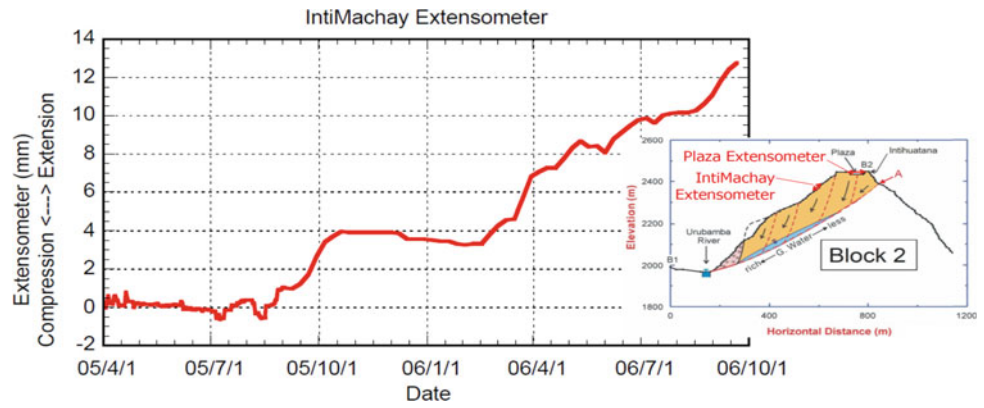
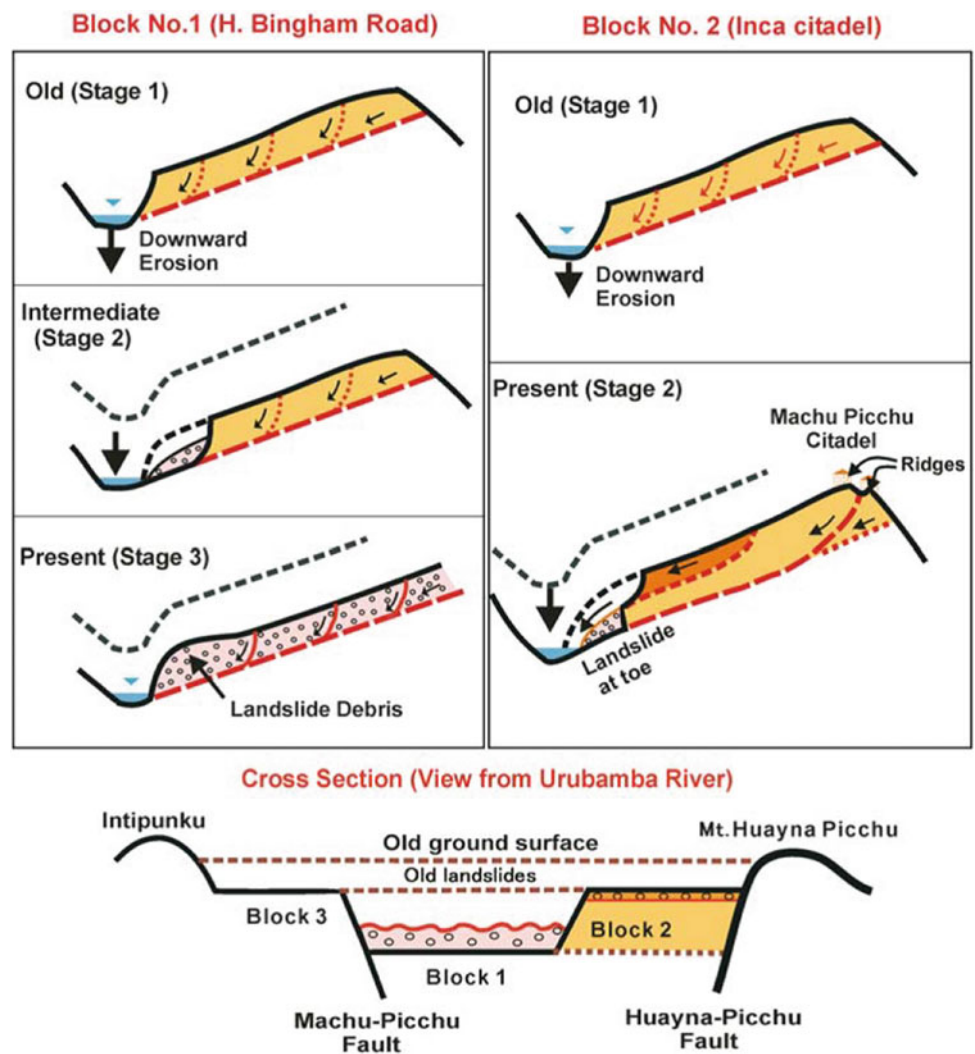


Fig. 6 Hypothesis of the landslide evolution in Machu Picchu slope (Section from Mountain ridge to the river in block 1 and block 2), and the cross section of block 1, block 2 and block 3



In order to detect the precursors of landslide movement in Machu Picchu slope, many of extensometers (both long and short span) and GPS were installed and monitored. Landslide monitoring was very sensitive for the society because a feasible stabilization method was not found, even if movement was

detected. The monitoring started in 2001, and was interrupted, then re-started in 2005–2006 before stopping again. Figures 4 and 5 show the monitoring results in Block No. 1 and Block No. 2, respectively. Both extensometers recorded the extensions of 10–12 mm. (Sassa et al. 2005).

3 International Consortium on Landslides: Founded in 2002, Kyoto, Japan

The UNESCO/IGCP Symposium on Landslide Risk Mitigation and Protection of Cultural and Natural Heritage was jointly organized by UNESCO, the IGCP-425 group, the International Union of Geological Sciences (IUGS), the Instituto Nacional de Cultura, Peru (INC), the Instituto Nacional de Recursos Naturales (INRENA), Peru, and the IGCP National Committee of the Science Council of Japan at the headquarters of the Science Council of Japan, in Tokyo on 15–19 January 2001. Participants, including three representatives (Wolfgang Eder, Hideo Noguchi, and Christian Manhart) from the Divisions of Earth Sciences and Cultural Heritage of UNESCO, the National Director of INC (Luis Enrique Tord), the President of the IUGS (Ed de Mulder), Paolo Canuti, Peter Borowsky, Nicola Casagli and other IGCP-425 colleagues (Fig. 7a), agreed on and issued the 2001 Tokyo Declaration “Geoscientists tame landslides” to propose the establishment of the International Consortium on Landslides. Participants were the IGCP-425 group member (ongoing 24 subproject members and 7 new project members) as well as UNESCO, IUGS and INC (cultural agency), Peru.

On 21–25 January 2002, The UNESCO-Kyoto University joint symposium “Landslide Risk Mitigation and Protection of Cultural and Natural Heritage” was organized in Kyoto. The symposium was cosponsored by the Ministry of Foreign Affairs and the National Commission for UNESCO of Japan, IUGS, the Japan Landside Society, and others. Six representatives of UNESCO (Divisions of Water Sciences,

Earth Sciences, and Cultural Heritage, Section of Engineering Sciences and Technology), one from the World Meteorological Organization (WMO), one from the UN Secretariat for the International Strategy for Disaster Risk Reduction (UN/ISDR) came together with many IGCP-425 members and Kyoto University (Fig. 7b).

On the first day of the symposium, the founding meeting of the International Consortium on Landslides (ICL) was organized. It was chaired by Andras Szollosi-Nagy (Director of Water Sciences of UNESCO) on behalf of Walter Erdelen, Assistant Director-General of UNESCO (Fig. 7b). At the meeting, the Statutes of the ICL were examined and adopted, and the first President (Kyoji Sassa) and interim steering committee members were nominated by the participants. Through the release of the 2002 Kyoto Appeal “Establishment of a New International Consortium on Landslides,” the International Consortium on Landslides (ICL) was inaugurated on 21 January 2002, as an international non-governmental and non-profit scientific organization.

4 UNESCO-KU-ICL UNITWIN Programme Founded in 2003

The UNITWIN programme is explained on the UNITWIN-UNESCO-Chair Programme website at: <https://www.unesco.org/en/education/unitwin> as follows: “UNITWIN” is the abbreviation for the university twinning and networking scheme. This UNESCO programme was established in 1992, in accordance with a resolution adopted by the

Fig. 7 Group photos of the IGCP-425 symposium. **a** A group photo of the UNESCO-Kyoto university joint symposium “landslide risk mitigation and protection of cultural and natural heritage organized on 21–25 January 2002 in Kyoto, Japan. **b** A group photo of the UNESCO/IGCP symposium on landslide risk mitigation and protection of cultural and natural heritage organized at the Science Council of Japan in Tokyo on 15–19 January 2001



General Conference of UNESCO at its 26th session in 1991. The UNITWIN/UNESCO Chairs Programme consists of the establishment of UNESCO Chairs and UNITWIN Networks in higher education institutions.

Participants from UNESCO in the ICL foundation meeting on 21–25 January 2002 suggested to place the planned International Programme on Landslides (IPL) as an official UNESCO Programme, namely UNITWIN Cooperation Programme. The ICL, then, submitted the application document to UNESCO to an UNITWIN Cooperation Programme between UNESCO, Kyoto University and the ICL. The title was changed from Landslide Risk Mitigation for Society and the Environment to Landslide and Water Related Disaster Management, and then to Landslide, Earthquake, and Water-related Disaster Risk Management. The current logo is shown in Fig. 8.

The progress of UNESCO-KU-ICL UNITWIN Cooperation programme was introduced by a series of photos in Fig. 9. Figure 9a presents the initial title of the UNITWIN Cooperation Programme. Figure 9b is a photo of the signature by Makoto Nagao, President of Kyoto University and by Kyoji Sassa, President of the ICL on 18 March 2003 at the Kyoto University. The agreement document was previously signed by Koïchiro Matsuura, Director-General of UNESCO on 10 March 2003 in Paris. UNITWIN Headquarter building including three rooms was constructed using funds from Kyoto University and the ICL at the Uji Campus of Kyoto University in September 2004. Figure 9c is a photo of the opening ceremony within the building on 3 September 2004 with Kyoto University President (K. Oike), three officials from UNESCO and three from Gov. of Japan.

In Fig. 9d, UNESCO (Sonia Bahri), Kyoto University (Norio Okada, Director of DPRI/KU), and ICL (Paolo Canuti, President of the ICL) signed the agreement to extend and amend the programme from “Landslide Risk Mitigation” to “Landslide and Water-Related Disaster Risk Management” on 16 November 2010 at UNESCO in Paris.

Figure 9f show a picture of the 2018 ICL-IPL Kyoto Conference organized at the Kyoto International Conference Center and the Uji campus of Kyoto University. On the final day, participants took a group photo of ICL members and ICL supporting members including S. Yasukawa

(UNESCO), T. Oki (UNU), Q. Han (IRDR), and four participants from Government of Japan (Cabinet office, MEXT, MAFF, MLIT) in front of the UNESCO/KU/ICL UNTWIN Headquarters Building.

5 2nd WCDR in 2005, Kobe, Japan

The World Conference on Disaster Reduction (WCDR) was held on 18–22 January in Kobe, Japan. Before the WCDR, the fourth International Symposium on Landslide Risk Mitigation and Protection of Cultural and Natural Heritage and the ICL Secretariat Meeting were organized at Kyoto University. Participants from the ICL and Hans van Ginkel (Rector of UNU) and Wolfgang Eder (Director, Division of Earth Sciences of UNESCO), discussed management and proposal of ICL in the thematic conference Session 3.8 on Floods (IFI) and *Landslides* (IPL).

A thematic session titled “New International Initiatives for Research and Risk Mitigation of Floods (IFI) and Landslides (IPL)” was held on January 19, 2005. Joint organizers of this session were ICL and the International Association of Hydrological Sciences (IAHS) together with UNESCO, WMO, FAO, UNU, MEX, Kyoto University, and the Public Works Research Institute (PWRI) of Japan. Figure 10 presents a joint photo before the session. The opening addresses of this session were presented by UNESCO Director-General Koichiro Matsuura, by WMO Secretary-General Michel Jarraud, Salvano Briceno Director of UN/ISDR and others. The discussion was chaired by Hans van Ginkel (Rector of UNU) with Andras Szollosi-Nagy (Director, Division of Water Science of UNESCO) as Moderator.

During this session, the ICL proposed and received approval on a “**Letter of Intent**” aiming to provide a platform for a holistic approach in research and learning on “Integrated earth system risk analysis and sustainable disaster management.” Immediately after the session, Hans van Ginkel representing the United Nations University and Sálvano Briceno representing UN International Strategy for Disaster Risk Reduction signed this Letter of Intent. After WCDRR, by the end of July 2005, other five United Nations and two

Fig. 8 Logo of UNESCO-KU-ICL UNITWIN cooperation programme



Fig. 9 Photos of UNESCO/Kyoto university/international consortium on landslides UNITWIN cooperation programme



Fig. 10 Group photo during the thematic session 3.8 “New international initiative for research and risk mitigation of floods (IFI) and landslides (IPL) during the world conference on disaster reduction on 18–22 January 2005



international organizations (UNESCO, WMO, FAO, UN/ISDR, UNU, and ICSU (ISC) and WFEO) signed it. The Letter of Intent is much lighter than bilateral Agreement and Memorandum of Understanding. Figure 11 presents the version which electronically integrated seven "Letter of Intents" signed by each organization into one page figure.

The ICL and the signed organizations jointly organized a Round Table Discussion to implement the "Letter of Intent" at the United Nations University in Tokyo, Japan in 2006.

Fig. 11 Letter of Intent which was agreed at the second United Nations world conference on disaster risk reduction in Kobe, Japan, and signed by seven global stakeholders in 2005

6 Round Table Discussion at UNU, Tokyo, Japan and the Tokyo Action Plan in 2006

To implement on an activity related to the 2005 Letter of Intent, a Round Table Discussion on Strengthening Research and Learning on Earth System Risk Analysis and Sustainable Disaster Management within UN-ISDR as Regards "Land-slides" was jointly organized at the United Nations University, Tokyo by the ICL, UNESCO, WMO, FAO, UN/ISDR, UNEP, UNU and Kyoto University in January 2006. The

LETTER OF INTENT			
"United Nations World Conference on Disaster Reduction (WCDR)", Kobe, Japan, 18-22 January 2005			
This 'Letter of intent' aims to provide a platform for a holistic approach in research and learning on 'Integrated Earth system risk analysis and sustainable disaster management'.			
Rationale			
<ul style="list-style-type: none"> • Understanding that any discussion about global sustainable development without addressing the issue of Disaster Risk Reduction is incomplete; • Acknowledging that risk-prevention policies including warning systems related to Natural Hazards must be improved or established; • Underlining that disasters affect poor people and developing countries disproportionately; • Stressing that after years of under-investment in preventive scientific, technical and communicational infrastructure activities it is time to change course and develop all activities needed to better understand natural hazards and to reduce the vulnerability notably of developing countries to natural hazards, and • Acknowledging that a harmful deficiency in coordination and communication measurements related to Disaster Risk Reduction exists. 			
Proposal			
Representatives of United Nations Organisations, as well as the Scientific (ICSU) and Engineering (WFEO) Communities propose to promote further joint global activities in disaster reduction and risk prevention through			
Strengthening research and learning on 'Earth System Risk Analysis and Sustainable Disaster Management' within the framework of the 'United Nations International Strategy for Disaster Risk Reduction' (ISDR).			
More specifically it is proposed,			
based on the existing structural framework of the ISDR and plan of action of the UN-WCDR, as well as other relevant networks and institutional and international expertise,			
to establish specific, goal-oriented 'Memoranda of Understanding' (MoUs) between international stakeholders targeting Disaster Risk Reduction, for example focusing on landslide risk reduction, and other natural hazards.			
Invitation			
Global, regional and national competent institutions are invited to support this initiative by joining any of the specific MoUs following this letter through participation in clearly defined projects related to the issues and objectives of any of the MoUs.			
Signatories:			
			
Mr. Koichiro Matsuura Director-General United Nations Educational, Scientific and Cultural Organization	Mr. Michel Jarraud Secretary-General World Meteorological Organization	Mr. Jacques Diouf Director-General Food and Agriculture Organization of the United Nations	Mr. Sálvino Briceño Director UN International Strategy for Disaster Risk Reduction
4 MAR 2005	22. 3. 2005	21. VI. 2005	19. 01. 05
Date	Date	Date	Date
			
Mr. Hans van Ginkel Rector United Nations University	Ms. Jaine Lubchenco President International Council for Science	Ms. Françoise Come Executive Director World Federation of Engineering Organizations	
19. 01. 05.	21. 04. 05	24/ 2/ 2005	
Date	Date	Date	
The International Consortium on Landslides (ICL) proposed the "Letter of Intent" at the thematic session 3.8 "New International Initiatives for Research and Risk Mitigation of Floods (IFI) and Landslides (IPL)" of the United Nations World Conference on Disaster Reduction held on 19 January 2005 in Kobe, Japan. This is the Letter of Intent, which was electronically combined based on the original Letters of Intent, formally approved and signed by all parties. All of the original Letters of Intent with signatures are deposited in the secretariat of the International Consortium on Landslides which is located in the Research Centre on Landslides of the Disaster Prevention Research Institute, Kyoto University.			
 International Consortium on Landslides			
Secretariat : Research Centre on Landslides, Disaster Prevention Research Institute, Kyoto University, Kyoto, Japan Web: http://ICL.dpri.kyoto-u.ac.jp , E-mail: imuj@landslide.dpri.kyoto-u.ac.jp , Tel: +81-774-38-4110, Fax: +81-774-32-5597			

Fig. 12 A group photo of the participants during the round table discussion on strengthening research and learning on earth system risk analysis and sustainable disaster management within UN-ISDR in regards to “Landslides” was organized at the United Nations university, Tokyo, Japan on 18–20 January 2006



discussion was cosponsored by the Governments of Japan (CAO, MOFA, MEXT, MAFF, MLIT), Italy (Ministry of Foreign Affairs, Civil Protection), Slovak Republic (Ministry of Environment), Czech Republic (Ministry of Environment), Korea (National Emergency Agency) and others. Figure 12 presents a group photo of participants at Elizabeth Rose Hall of the United Nations University, Tokyo, Japan on 18 January 2006.

On the final day of the round table discussion on 20 January 2006, participants adopted the 2006 Tokyo Action Plan which provided the solid base for the current International Programme on Landslides (IPL) leading to the Sendai Landslide Partnerships 2015–2025 and Kyoto Landslide Commitment 2020 continuing to 2025 and beyond.

The full text of the 2006 Tokyo Action Plan is provided below.

“2006 Tokyo Action Plan” Strengthening Research and Learning on Landslides and Related Earth System Disasters for Global Risk

The 2006 Tokyo Round Table Discussion “Strengthening Research and Learning on Earth System Risk Analysis and Sustainable Disaster Management within UN-ISDR as Regards Landslides”—towards a dynamic global network of the International Programme on Landslides (IPL) was held at the United Nations University, Tokyo, from 18th to 20th January, 2006 to formulate a framework for cooperation and to identify focus areas to reduce landslide risk worldwide. The following action plan was adopted as a summary of the meeting, to be implemented within the scope of the Hyogo Framework for Action 2005–2015, “Building

the Resilience of Nations and Communities to Disasters”, declared at the United Nations World Conference on Disaster Reduction held in Kobe, Japan in 2005.

Preamble

Large and small landslides occur almost every year in nearly all regions of the world. Figure 13 shows the example for casualties in Japan for 1967–2004. Landslide disasters in Japan have occurred every year; the total number of deaths due to landslides is about one half of those caused by earthquakes, including the catastrophic 1995 Kobe earthquake.

“Landslides” are a complex-disaster phenomenon that can be caused by earthquakes, volcanic eruptions, heavy rainfall (typhoons, hurricanes), sustained rainfall, heavy snowmelt, unregulated anthropogenic developments, mining, and others (Fig. 14a). Large-scale coastal or marine landslides are known to cause tsunami waves that kill many people; an example was the 1792 UNZEN-Mayuyama landslide, which caused a devastating tsunami that resulted in 16,000 fatalities from the landslides and the tsunami in Japan. Also, large-scale landslides on volcanoes can dislocate the mountain tops and trigger volcanic eruptions; such was the case for the 1980 eruption of Mount St. Helens in the USA and presumably for Mt. Bandai in Japan. Landslides also may occur without earthquakes, heavy rains, volcanic eruptions, or human activities due to progress of natural weathering; therefore, they occur almost everywhere in the world. Landslides most commonly impact residents living on and around slopes.

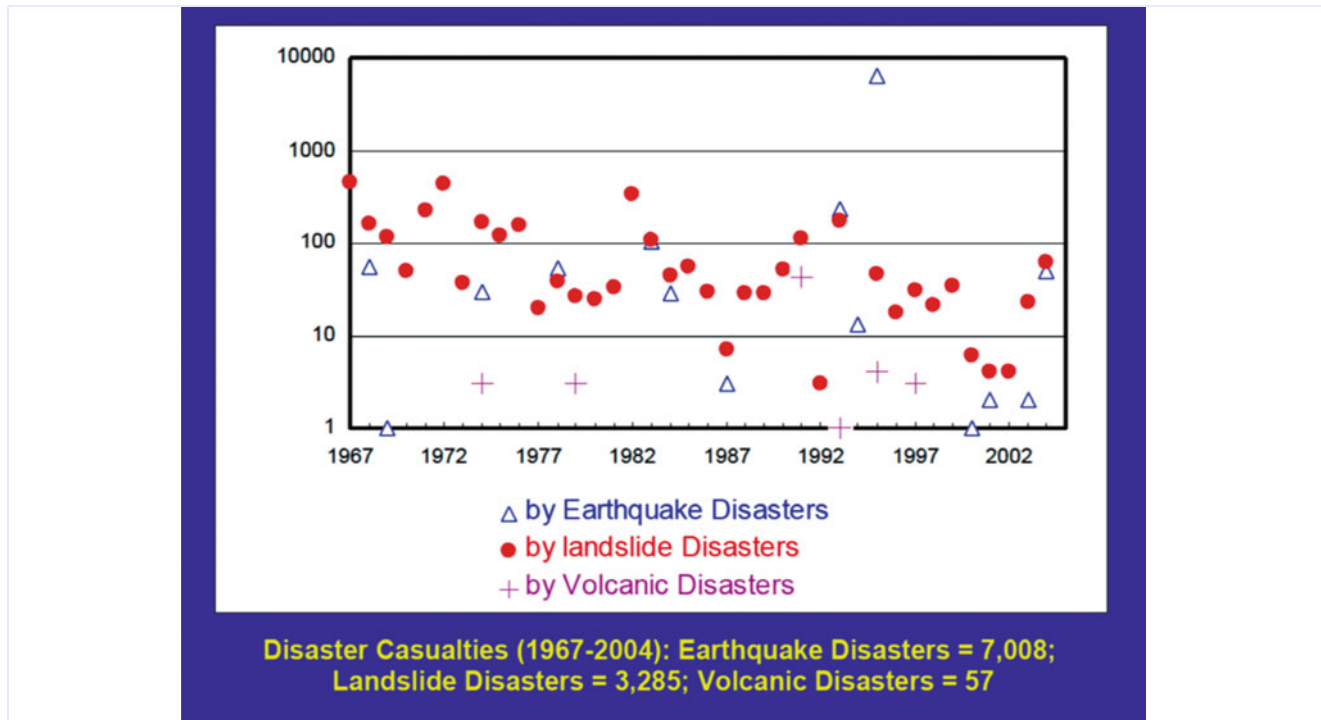


Fig. 13 Comparison of the numbers of victims in Japan from 1967 to 2004 due to landslide disasters, earthquake disasters including deaths by earthquake-induced-landslides, and volcanic disasters including

deaths due to volcanic gas (The statistic of victims by landslide disasters since 1967 was published by the Sabo technical center)

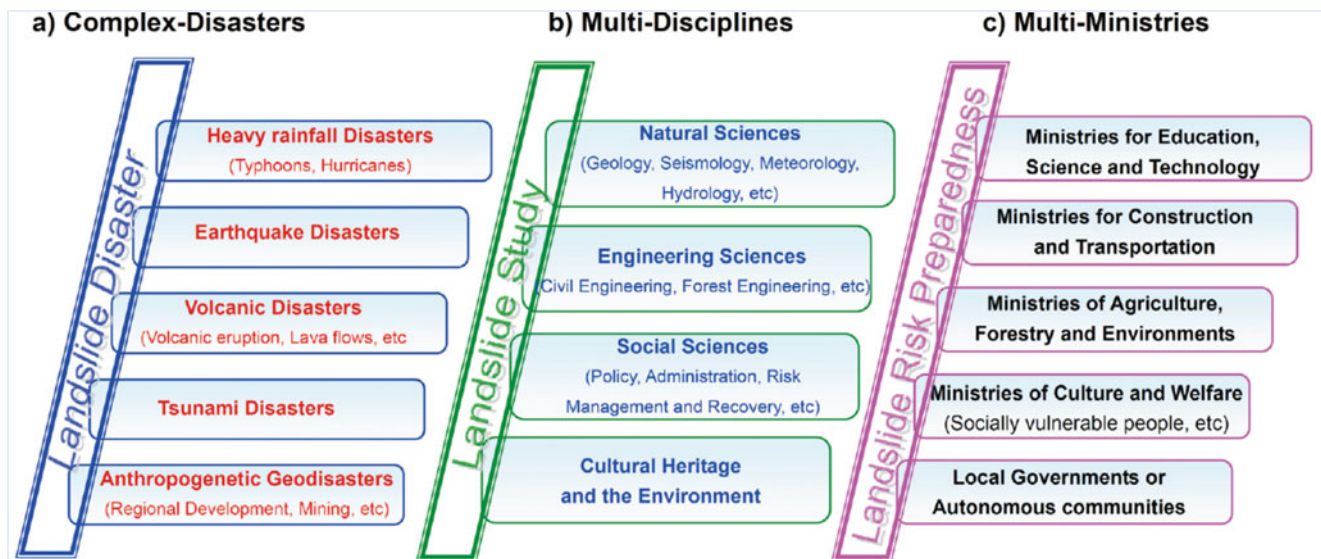


Fig. 14 Characteristics of landslide disasters

Landslides are a natural phenomenon which can only be effectively studied in an integrated, multi-disciplinary fashion, including contribution from different natural and engineering sciences (earth and water sciences), and different social sciences. This is also the case because landslides are strongly related to

cultural heritage and the environment (Fig. 14b). Landslides should be jointly managed by cooperation of different ministries and departments of government including some representing education, science and technology, construction and transportation, agriculture, forestry, and the environment, culture and

vulnerable groups (the poor, aged, handicapped, or children). As landslides are highly localized phenomena it is crucial to seek the contribution of local governments or autonomous communities (Fig. 14c).

The disasters caused by landslides are of very complex nature wherever they occur around the world. Research on landslides should be integrated into a new multi-disciplinary science field of landslide study. Landslide risk preparedness is to be managed by multi-ministries.

Action Plan

Global cooperation in landslide-risk reduction research and learning will be carried out encompassing related disasters affecting the earth-system, such as heavy rainfall, earthquakes, volcanic eruptions, tsunamis, and disasters of anthropogenic origin. Establishment of a Dynamic Global Network of the International Programme on Landslides” and its operation will effectively function for landslide and related risk reduction through the implementation of the following Action Items adopting a multi-hazard, multi-sectoral approach;

Actions

1. Establishment of the IPL Framework

(1) Establishment of the IPL Global Promotion Committee

The IPL Global Promotion Committee shall be established by ICL members and ICL supporting organizations, as illustrated in Figure 15. The committee will meet annually, on the occasion of ICL Board of Representative meetings, or possibly at other occasions and locations. The committee will conceive a strategy to promote the 2006 Tokyo Action Plan, and will discuss the management of IPL global cooperation fields, and their possible modification, selection, and termination.

(2) Establishment of IPL World Centre

The IPL World Centre will be established to coordinate and support implementation of the global cooperating fields of the International Programme on Landslides (IPL), which works as the secretariat of the IPL Global Promotion Committee and the International Programme on Landslides (IPL). The Centre will be hosted by the Headquarter of the UNESCO-KU-ICL UNITWIN Cooperation Programme “Landslide Risk Mitigation for Society and

the Environment” in the Research Centre on Landslides, Disaster Prevention Research Institute, Kyoto University, Kyoto, Japan, where the secretariat of the International Programme on Landslides has been located since its foundation in 2002.

2. Promotion of the Global Cooperating Fields of the International Programme on Landslides (IPL)

(1) Technology Development

A. Monitoring and Early Warning

- Use of various on-site, in-situ technologies, as well as satellite observations in monitoring landslide effects and contributing factors for early-warning purposes
- Development of automated monitoring methods covering large spatial extent and real-time data communication, as well as low-cost monitoring devices
- Development of early-warning methodologies, in particular for rain-induced landslides
- Applications linking meteorological, hydrological and landslide models.

B. Hazard Mapping, Vulnerability and Risk Assessment

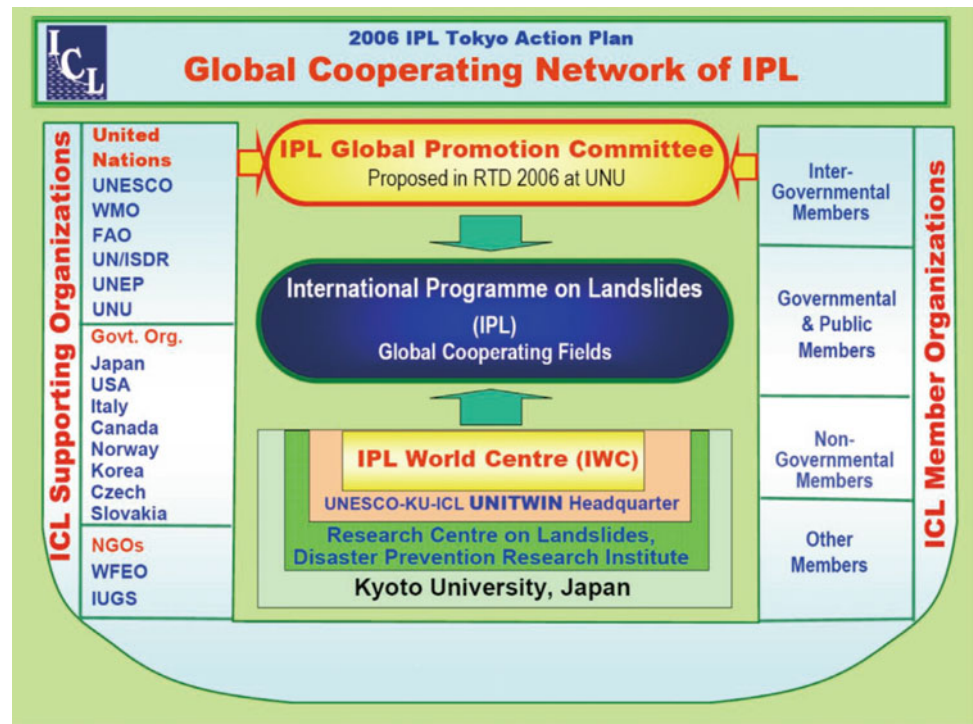
- Hazard Mapping at local and global scales
- Vulnerability assessment, considering human life, land resources, structures, infrastructure, and cultural heritage
- Risk assessment and communicating risk in an easily understood manner.

(2) Targeted Landslides: Mechanisms and Impacts

A. Catastrophic Landslides

- Catastrophic landslides induced by natural and anthropogenic factors such as rainfall, earthquakes, volcanic activity, river erosion, and human activities, and their combinations
- Landslides threatening human lives and high societal values
- Gigantic coastal landslides and marine landslides causing tsunamis.

Fig. 15 Structure of the IPL global-cooperation framework



B. Landslides Threatening Heritage Sites

- Studies for protection of cultural heritage, cultural landscape, and the natural heritage from landslides using non-invasive technologies and appropriate mitigation strategies (e.g. Machu Picchu, Bamiyan, Lishan, Cordillera Blanca).

(3) Capacity Building

A. Enhancing Human and Institutional Capacities

- Building human capacities and expertise in landslide management
- Institution building at national and local levels through Centers of Excellence
- Enhancing implementation and action at local level.

B. Collating and Disseminating Information/Knowledge

- Developing a culture of awareness on landslide risks
- Developing model policy frameworks, standards, guidelines/checklists, and training modules.

(4) Mitigation, Preparedness and Recovery

A. Preparedness

- Strengthening disaster preparedness of all stakeholders
- Strengthening capacities of communities and local institutions to cope with landslide hazards
- Forecasting and providing early warning of adverse conditions likely to lead to landslide activity
- Preparing contingency recovery plans, including pre-positioning of technical and material resources for likely landslide events.

B. Mitigation

- Development of innovative, low-cost, and ecologically appropriate landslide mitigation techniques.
- Mountain conservation methods, including soil conservation, forest and watershed management, and appropriate land-use techniques
- Appropriate civil engineering works, including construction and urban and coastal development;

- Restricting inappropriate development in landslide prone areas
- Development of appropriate policy and planning mechanisms, such as land-use management (including zoning)
- Promotion and strengthening of monitoring and warning systems.

C. Recovery

- Post-landslide recovery and rebuilding efforts should integrate landslide mitigation measures
- Prevention of secondary risks of landslides resulting from inappropriate re-building efforts in response to any disaster (for example, earthquakes, volcanic eruptions, extreme weather events, etc.)
- Implementation of landslide recovery efforts and programs (including psycho-social and health aspects) with the participation of affected communities and local authorities
- Providing long-term support to ensure sustainable recovery.

3. Promotional Activities

(a) World Landslides Forum

Capitalizing on the competence, international experience and established organizational network of ICL-IPL, it is proposed to create a global information platform for future joint activities of the world-wide landslide community, named the ‘World Landslide Forum’ that shall be convened every 3 years.

The first World Landslides Forum—organized by the ICL—can be planned to take place in January 2009, bringing together academics, practitioners, politicians, et al. to a global, multidisciplinary, problem-focused platform. This forum will provide an opportunity for the first identification of a WCoE. Linkages to ISDR activities, as well as other global events, including the World Water Forum, the International Year of Planet Earth, etc., will be established.

(b) Identification and Promotion of World Centres of Excellence on Landslide Risk Reduction

The IPL Global Promotion Committee will identify and promote World Centres of Excellence (WCoE) every 3 years within eligible organizations, such as universities, institutes, NGOs, government ministries and local

governments, contributing to “Risk Reduction for Landslides and Related Earth System Disasters”. Linkages to CoE at the national level will be used to promote cooperation with the ICL and dissemination of knowledge and information. An independent Panel of Experts, set up by the Global Promotion Committee of IPL, may be appointed to endorse the CoEs.

(c) Contributions to Global Landslide Issues

The IPL will mobilize global cooperation for strengthening research and learning on risk reduction for landslides and related earth system disasters at sites identified as of great concern to the global community, such as Macchu-Picchu, the Kashmir, Central Asia high mountainous area, and Bamiyan.

(d) Partnerships

Mutually beneficial partnerships with other global initiatives, such as the International Hydrological Program (IHP), the International Geoscience Program (IGCP), and The Mountain Partnership will be developed.

In order to promote the 2006 Tokyo Action Plan, the ICL exchanged a Memorandum of Understanding to each UNESCO, WMO, FAO, UNU, UN/ISDR (UNDRR), ICSU (ISC) and WFEO. The Tokyo Action Plan established a new International Programme on Landslides with the Global Promotion Committee of IPL. The current logo of IPL was made based on the Tokyo Action Plan and the resulting MOU with 7 global stakeholders.

Figure 16 presents the signing ceremony between UNESCO and ICL to promote the 2006 Tokyo Action Plan



Fig. 16 Koichiro Matsuura, Director-General of UNESCO and Kyoji Sassa, President of the ICL exchanged a MoU to promote the 2006 Tokyo action plan on 22 August in Tokyo, 2006



Fig. 17 Logo of the international programme on landslides including seven global stakeholders which agreed and signed an MoU with ICL to promote the Tokyo action plan

at a hotel in Tokyo with participants from ICL members, Vice President of Kyoto University, representatives from ICL supporting organizations in the Government of Japan. Figure 17 is the logo of a new International Programme on Landslides (IPL) supported by the seven global stakeholders.

7 The First World Landslide Forum in 2008 in Tokyo, Japan

The 2006 Tokyo Action Plan proposed “World Landslide Forum” as one of the promotional activities. It *capitalized on the competence, international experience and established organizational network of ICL-IPL to create a global information platform for future joint activities of the world-wide landslide community. The ‘World Landslide Forum’ was planned to be convened every 3 years.*

The 2006 Tokyo Action Plan proposed the establishment of the IPL Global Promotion Committee. The first session of the IPL Global Promotion Committee and IPL Symposium 2007 were organized at Elizabeth Rose Hall, United Nations University, Tokyo, Japan on 22–25 January 2007. In this meeting, chairpersons of IPL Global Promotion Committee were selected. Specifically, as chairperson: Salvano Briceno (UN/ISDR), and as Deputy chairpersons: Badaoui Rouhban (UNESCO), Kyoji Sassa (ICL-Headquarters) and Paolo Canuti (ICL-Europe). The IPL World Centre was defined as the secretariat for IPL and the IPL Global Promotion Committee. The IPL World Centre is a part of the legal body of ICL. The organizations and the programme of the First World Landslide Forum was examined in this meeting.

Following the 2006 Tokyo Action Plan, the First World Landslide Forum was organized at the United Nations University, Tokyo, Japan by the following organizers and cosponsors.

Organizers: International Consortium on Landslides, United Nations Educational, Scientific and Cultural Organization (UNESCO), World Meteorological Organization (WMO), Food and Agriculture Organization of the United Nations (FAO), United Nations International Strategy for Disaster Risk Reduction (UN/ISDR), United Nations University (UNU), United Nations Environment Programme (UNEP), World Bank (IBRD), United Nations Development Programme (UNDP), International Council for Science (ICSU), World Federation of Engineering Organizations (WFEO), Kyoto University, and Japan Landslide Society.

Cosponsors: Cabinet Office of Japan, Ministry of Foreign Affairs, Japan, Ministry of Education, Culture, Sports, Science and Technology, Japan, Ministry of Agriculture, Forestry and Fisheries of Japan, Ministry of Land Infrastructure and Transport, Japan, Japan Meteorological Agency, Science Council of Japan, Japan International Cooperation Agency, Public Works Research Institute, Japan, Asian Disaster Reduction Center, Japan, Ministry for Research and University, Italy, Ministry of Foreign Affairs, Italy, Ministry of the Environment, Italy, Department of Civil Protection of the Presidency of the Council of Ministers, Italy, International Union of Geological Sciences, International Union of Geodesy and Geophysics, International Flood Initiative, International Year of Planet Earth, and Academy of Forest, Wood and Environment, Japan.

As a result of the national and international support, the First World Landslide Forum (WLF1) attracted many people and organizations from 48 countries. The participants are pictured in Fig. 18.

The 2006 Tokyo Action Plan proposed the establishment of the **IPL Global Promotion Committee (GPC/IPL)**. The first session of the IPL Global Promotion Committee was organized at Elizabeth Rose Hall, United Nations University, Tokyo, Japan on 22–25 January 2007. The management of GPC/IPL was decided. In this meeting, Salvano Briceno (Director of UN/ISDR) was selected to be as the first chairperson of GPC/IPL. The second GPC/IPL was organized on 21–25 January 2008 and the third GPC/IPL was organized on 17 November 2008, one day before the First World Landslide Forum. Thereafter, GPC/IPL has been organized every year at the same time of the annual Board of Representative Meeting of ICL (BOR/ICL).

The 2006 Tokyo Action Plan proposed the identification and promotion of **World Centers of Excellence on Landslide Risk Reduction (WCOE)** to be identified every three years. The ICL identified the first twelve WCOEs (2008–2011) at WLF1 as follows:

Fig. 18 Group photo of participants on the first day of the first world landslide forum



1. China: China Geological Survey
2. Czech Republic: Faculty of Science, Charles University in Prague
3. Italy: Department of Earth Science, University of Florence
4. Italy: Research Center on Prediction Prevention and Control of Georisks of Rome University "La Sapienza"
5. Japan: The Japan Landslide Society
6. Malaysia: Slope Engineering Branch, Public Works Department of Malaysia
7. Norway: International Center for Geohazards (ICG) at NGI
8. Russia and Kyrgyz: Institute of Geospheres Dynamics of Russian Academy of Science (IDG RAS) and Kyrgyz Institute of Seismology (KIS)
9. Slovenia: University of Ljubljana, Faculty of Civil and Geodetic Engineering (UL FGG)
10. South Africa: Engineering Geoscience Unit, Council for Geoscience
11. Thailand: Asian Disaster Preparedness Center
12. USA: U.S. Geological Survey.

Thereafter, more than ten WCOEs have been identified at every WLF.

After the First World Landslide Forum in Tokyo in 2008, the Second World Landslide Forum was in Rome, Italy in 2011, the Third World Landslide Forum in Beijing, China in 2014, the Fourth World Landslide Forum in Ljubljana, Slovenia in 2017 and the Fifth World Landslide Forum in Kyoto, Japan in 2021 (postponed by one year due to COVID-19).

8 3rd WCDRR in 2015, Sendai, Japan

The Third World Landslide Forum was organized in Beijing, China on 2–6 May 2014. On 3 May, a high-level panel discussion on an initiative to create a safer geoenvironment toward WCDRR 2015 and forward was moderated by Hans van Ginkel, Chair of Independent Panel of Experts for World Centers of Excellence (WCoE).

From the high-level panel discussion, the Beijing Declaration-Landslide Risk Mitigation Toward a Safer Geo-environment was adopted. This declaration included that participants endorse plans to organize an ICL-IPL Conference as part of the Third World Conference on Disaster Risk Reduction (3rd WCDRR) to take place in Sendai, Japan in March 2015. They urged the ICL-IPL Sendai Conference to define and adopt concrete actions, which will be carried out by international networks and partnerships, of public and private institutions, in science and technology creating the *ICL-IPL Sendai Partnerships* to help achieve the ISDR goals.

The high-level panel discussion in Beijing, China on 3 May 2014 was a very important step for the ISDR-ICL Sendai Partnerships 2015–2025. A group photo after the high-level panel discussion is shown in Fig. 19, which includes Director-General of UNESCO, Irina Bokova, Rector of United Nations University, Han van Ginkel, Representatives from UNISDR, WMO, and IRDR as well as President, Vice President and other key persons of ICL and key persons from the Government of China as the host.



Fig. 19 A group photo of participants after the high-level panel discussion on 3 May 2014 which proposed the establishment of the *ICL-IPL Sendai Partnerships* at 2nd WCDRR in Sendai, Japan in

March 2015. Irina Bokova, Director-General of UNESCO (in the center of this photo) delivered a certificate to each leader of twelve WCoEs immediately after the high-level panel discussion

Establishment of the ISDR-ICL Sendai Partnerships 2015–2025

After the 2014 Beijing Declaration, the ICL made efforts to organize a session in the Third UN World Conference on Disaster Risk Reduction (3rd WCDRR) in Sendai, Japan in March 2015. ICL succeeded in being a co-organizer of the Working Session No. 4 (WS 4) “Underlying Risk Factors” (Priority No. 4 of the Hyogo Framework for Action) of 3rd WCDRR together with MLIT, UNESCO, and other organizations under the initiative of ISDR. During the preparatory stages, the titles of planned partnership were changed twice during the discussion.

- (1) ICL-IPL Sendai Partnerships 2015–2024 Landslide disaster risk reduction for a safer geoenvironment.
- (2) ISDR-ICL: SENDAI PARTNERSHIPS 2015–2024 for Global Promotion of Understanding and Reducing Landslide, Flood, and Tsunami Disaster Risk.
- (3) ISDR-ICL Sendai Partnerships 2015–2025 for global promotion of understanding and reducing landslide disaster risk.

The last version of partnerships was reported, and its implementation plan was examined in the ICL-IPL Sendai Partnership Conference on 11–15 March 2015. These Sendai Partnerships were then proposed to the Working Session No. 4 “Underlying Risk Factors” held at 10:00–11:30 AM JST in Hagi Hall of the Sendai International Center on 16 March 2015. The chairperson of the session was Kamal Kishore and the moderator was Badaoui Rouhban. Kyoji Sassa proposed these Sendai Partnerships in the final part of the session which

was devoted to make statements of commitments on addressing the Underlying Risk Factors in the post-2015 framework for disaster risk reduction. As a result, the launch of the Sendai Partnerships was announced in the session.

Signing ceremony and the Sendai Partnerships

The signing ceremony of the ISDR-ICL Sendai Partnerships was organized in a Japanese Restaurant “JUNSEN” in Sendai, Japan from 12:00–13:30 JST on 16 March 2015. Sixteen intergovernmental, international, and national organizations signed the Sendai Partnerships. Some of the heads of several organizations attended and signed in-person, while some organizations nominated an officer in-charge of disaster reduction to sign the documents. Other organizations signed the Sendai Partnerships in advance and sent a representative to bring the signed partnership to the ceremony.

A photo of the signing ceremony is shown in Fig. 20. The list of signed organizations of the ISDR-ICL Sendai Landslide Partnerships 2015–2025 and the signed document are presented in the following pages. Six new partners signed the partnerships in 2016 and 2017.

1. International Consortium on Landslides (ICL)
2. United Nations Office for Disaster Risk Reduction (UNISDR)
3. United Nations Educational, Scientific and Cultural Organization (UNESCO)
4. Food and Agriculture Organization of the United Nations (FAO)
5. United Nations University (UNU)



Fig. 20 Signing ceremony of ISDR-ICL Sendai Partnerships 2015–2025. Front (left to right) Sorrenti Ambra (for Franco Gabrielli, Italian civil protection), Irasema Alcantara-Ayala (for Gordon Mcbean, ICSU), Srikantha Herath (for Kazuhiko Takeuchi, UNU), Roland Oberhansli (IUGS), Kaoru Saito (Cabinet Office, Japan), Giuseppe Arduino (for Qunli Han, UNESCO), Kyoji Sassa (ICL), Margareta Wahlström (UNISDR), Dominique Burgeon (FAO), Robert Mikac (for Croatia Civil Protection), Takashi Onishi (Science Council of Japan), Alik

Ismail-Zedeh (IUGG), and Kaoru Takara (for Kayo Inaba, Kyoto University). Back (left to right) Hiroshi Fukuoka (ICL), Nicola Casagli (ICL), Yuki Matsuoka (UNISDR), Alexandros Makarigakis (UNESCO), Toshimitsu Komatsu (WFEO), Satoru Nishikawa (Water Agency, Japan), Badaoui Rouhban (IPL-ICL), Paolo Canuti (ICL), Yueping Yin (ICL), and Matjaz Mikos (ICL). Left bottom Qunli Han (UNESCO) and Franco Gabrielli (Italian civil protection)

6. International Council for Science (ICSU)
7. World Federation of Engineering Organizations (WFEO)
8. International Union of Geological Sciences (IUGS)
9. International Union of Geodesy and Geophysics (IUGG)
10. Cabinet Office, Government of Japan (CAO)
11. Ministry of Education, Culture, Sports, Science and Technology, Government of Japan (MEXT)
12. Kyoto University
13. Science Council of Japan
14. National Civil Protection Department, Italian Presidency of the Council of Ministers, Government of Italy
15. National Protection and Rescue Directorate, Republic of Croatia
16. Global Risk Forum (GRF) Davos
17. World Meteorological Organization (WMO)
18. Euro Geo Surveys
19. Indonesian National agency for Disaster Management
20. Science Committee of the Integrated Research on Disaster Reduction (IRDR)
21. Administration of the Republic of Slovenia for Civil Protection and Disaster Relief (URSZR)
22. Ministry of Natural Resources and Environment the Socialist Republic of Vietnam.

The ISDR-ICL Sendai Partnerships 2015–2025 with signatures are provided below.

Voluntary commitment to the World Conference on Disaster Risk Reduction
Sendai, Japan, 2015

**ISDR-ICL SENDAI PARTNERSHIPS 2015-2025
FOR GLOBAL PROMOTION OF UNDERSTANDING AND REDUCING
LANDSLIDE DISASTER RISK**

*Tools for Implementing and Monitoring the Post-2015 Framework for Disaster Risk
Reduction and the Sustainable Development Goals*

At the 2nd United Nations World Conference on Disaster Reduction, which was held in Kobe, Japan, on 18-22 January 2005, the International Consortium on Landslides (ICL) co-organized a session which resulted in a global partnership and platform taking a holistic approach to research and learning on Integrated Earth system risk analysis and sustainable disaster management. This partnership was forged through a 'Letter of Intent', that was signed by UNESCO, UNISDR, WMO, FAO, UNU, ICSU, and WFP. It further led to the adoption and implementation of the 2006 Tokyo Action Plan, thus creating a global partnership on Landslides, i.e. the current International Programme on Landslides (IPL) of ICL.

At the 3rd World Conference on Disaster Risk Reduction (WCDRR), which was convened by the United Nations and hosted by Japan in Sendai from 14 to 18 March 2015, the ICL and its IPL contributed further to the UN International Strategy for Disaster Reduction (ISDR) and co-organized the Working Session 'Underlying Risk Factors' together with UNESCO, the Japanese Ministry of Land, Infrastructure, Transport and Tourism (MLIT) and other pertinent organizations.

At the Working Session, the causes that create risk and their cumulative effects, as well as the relevant achievements of the Hyogo Framework for Action 2005-2015, were reviewed. Steps to address the principal drivers of vulnerability and exposure and to support hazard and risk assessment were suggested. In addition, the participating scientific and academic institutions and governmental and non-governmental organizations proposed that the *Sendai Partnerships 2015-2025 for Global Promotion of Understanding and Reducing Landslide Disaster Risk* be established. This sound global platform will be mobilized in the coming decade to pursue prevention, to provide practical solutions, education, communication, and public outreach to reduce landslide disaster risk. These Partnerships will engage all significant stakeholders concerned with the challenge of understanding and reducing disaster risk, including relevant international, national, local, governmental, and non-governmental institutions, programmes and initiatives. The Partnerships will focus on delivering tangible and practical results that are directly related to the implementation of the goals and targets of the post-2015 Framework for Disaster Risk Reduction.

The *Sendai Partnerships 2015-2025 for Global Promotion of Understanding and Reducing Landslide Disaster Risk* are hereby established. They represent Tools for Implementing and Monitoring the Post-2015 Framework for Disaster Risk Reduction and the Sustainable Development Goals.

Partners in the 'Partnerships' adopt the following Resolution:

We acknowledge that:

- Landslide disasters are caused by exposure to hazardous motions of soil and rock that threaten vulnerable human settlements in mountains, cities, coasts, and

Voluntary commitment to the World Conference on Disaster Risk Reduction
Sendai, Japan, 2015

- islands.
- Climate change will intensify the risk of landslides in some landslide prone areas through an increase in the frequency and/or magnitude of heavy rainfall, and shifts in the location and periodicity of heavy rainfall.
- Developments in mountains and coastal areas, including construction of roads and railways and expansion of urban areas due to population shifts, increase exposure to hazards of landslides.
- Although they are not frequent, strong earthquakes have potential to trigger rapid and long runout landslides and liquefaction. Earthquake-induced coastal or submarine large-scale landslides or megaslides (with depths on the order of hundreds of meters to one thousand meters) in the ocean floor can trigger large tsunami waves. These hazardous motions of soil and water impacting on exposed and vulnerable population can result into very damaging effects.
- The combined effects of triggering factors, including rainfall, earthquakes, and volcanic eruptions, can lead to greater impacts through disastrous landslides such as lahars, debris flows, rock falls, and megaslides.
- Understanding landslide disaster risk requires a multi-hazard approach and a focus on social and institutional vulnerability. The study of social and institutional as well as physical vulnerability is needed to assess the extent and magnitude of landslide disasters and to guide formulation of effective policy response.
- Human intervention can make a greater impact on exposure and vulnerability through, among other factors, land use and urban planning, building codes, risk assessments, early warning systems, legal and policy development, integrated research, insurance, and, above all, substantive educational and awareness-raising efforts by relevant stakeholders.
- The understanding of landslide disaster risk, including risk identification, vulnerability assessment, time prediction, and disaster assessment, using the most up-to-date and advanced knowledge, is a challenging task. The effectiveness of landslide disaster risk reduction measures depends on scientific and technological developments for understanding disaster risk (natural hazards or events and social vulnerability), political 'buy-in', and on increased public awareness and education.
- At a higher level, social and financial investment is vital for understanding and reducing landslide disaster risk, in particular social and institutional vulnerability through coordination of policies, planning, research, capacity development, and the production of publications and tools that are accessible, available free of charge and are easy to use for everyone in both developing and developed countries.





We agree on the following initial fields of cooperation in research and capacity building, coupled with social and financial investment:































- Development of people-centered early warning technology for landslides with increased precision and reliable prediction both in time and location, especially in a changing climate context.
- Development of hazard and vulnerability mapping, vulnerability and risk assessment with increased precision, and reliability as part of multi-hazard risk identification and management.
- Development of improved technologies for monitoring, testing, analyzing, simulating, and effective early warning for landslides.
- Development of international teaching tools that are always updated and may be used free of charge by national and local leaders and practitioners, in developed and developing countries through the Sendai Partnerships 2015-2025.
- Open communication with society through integrated research, capacity building, knowledge transfer, awareness-raising, training, and educational activities to enable societies to develop effective policies and strategies for reducing landslide disaster

Voluntary commitment to the World Conference on Disaster Risk Reduction
Sendai, Japan, 2015

 Mr. Kouru Saito Director Disaster Preparedness and International Cooperation Division Disaster Management Bureau Cabinet Office, Government of Japan 16/03/2015 Date	 Mr. Hideo Maruyama Director Office for Disaster Reduction Research Ministry of Education, Culture, Sports, Science and Technology, Japan 16. 03. 2015 Date
 Mr. Takashi Onishi President Science Council of Japan March 16, 2015 Date	 Ms. Kayo Inaba Executive Vice President for Gender Equality, International Affairs, and Public Relations Kyoto University 16. 03. 15 Date
 Mr. Profetto Fréno Gabrielli Head National Civil Protection Department Italian Presidency of the Council of Ministers Government of Italy 16. 03. 2015 Date	 Mr. Jadran Perić Director General National Protection and Rescue Directorate Republic of Croatia 16.03.2015 Date
 Mr. Walter Ammann President/CEO Global Risk Forum GRF Davos 16 March 2015 Date	 Laura Demicheli Secretary General of EuroGeoSurveys 31/03/15 Date

Voluntary commitment to the World Conference on Disaster Risk Reduction
Sendai, Japan, 2015

Signatory  Rudi Prudhamanto Deputy Minister of the Indonesian National Agency for Disaster Management 31 May 2017 Date	 Shushu Lwasa Chair of the Science Committee of the Integrated Research on Disaster Reduction (IRDRI) 31 May 2017 Date
 Darko But Director General of the Administration of the Republic of Slovenia for Civil Protection and Disaster Relief (URSRR) 31 May 2017 Date	 Nguyen Linh Ngon Deputy Minister, Ministry of Natural Resources and Environment the Socialist Republic of Vietnam 31 May 2017 Date

Voluntary commitment to the World Conference on Disaster Risk Reduction Sendai, Japan, 2015												
<p>risk, to strengthen their capacities for preventing hazards to develop into major disasters, and to enhance the effectiveness and efficiency of relief programs.</p> <p>Development of new initiatives to study research frontiers in understanding landslide-disaster risk, such as the effect of climate change on large-scale landslides and debris flows, the effective prediction of localized rainfall to provide earlier warning and evacuation especially in developing countries, the mechanism and dynamics of submarine landslides during earthquakes that may cause or enhance tsunamis, and geotechnical studies of catastrophic megafaults for prediction and hazard assessment.</p> <p>We further agree to advocate that activities should be balanced at regional, national, and community levels in order to empower and engage more professionals, practitioners and decision-makers in formulating policies and establishing programmes for the benefit of disaster risk reduction efforts.</p> <p>We further agree that progress made in the contribution of the <i>Sendai Partnerships 2015-2025 for Global Promotion of Understanding and Reducing Landslide Disaster Risk</i> toward the implementation of the Post-2015 Framework for Disaster Risk Reduction will be reported and emerging challenges will be discussed every two years at the Global Platform for Disaster Risk Reduction in Geneva.</p> <p>A Call for joining the Partnerships Competes global, regional, national, and local institutions participating in the 3rd WCDRR and in the implementation of the Post-2015 Framework for Disaster Risk Reduction are invited to support this initiative by joining and signing these Partnerships through participation in clearly defined projects related to the issues and objectives of these Partnerships. The potential partners are requested to be in contact with the secretariat of the host organization.</p> <p>Host Organization and Secretariat The International Consortium on Landslides (ICL) hosts the Sendai Partnerships 2015-2025 as a voluntary commitment to the United Nations World Conference on Disaster Risk Reduction, Sendai, Japan. The ICL Secretariat in Kyoto, Japan, serves as the Secretariat of the Sendai Partnerships.</p> <p>Signatories:</p> <table border="0"> <tr> <td>  Mr. Kyuji Sasao Executive Director International Consortium on Landslides Host organization of the Partnerships 16/03/15 Date </td> <td>  Ms. Margareta Wahlström Special Representative of the UN Secretary General for Disaster Risk Reduction Chief of UNISDR 16 March 2015 in Sendai Date </td> </tr> </table>		 Mr. Kyuji Sasao Executive Director International Consortium on Landslides Host organization of the Partnerships 16/03/15 Date	 Ms. Margareta Wahlström Special Representative of the UN Secretary General for Disaster Risk Reduction Chief of UNISDR 16 March 2015 in Sendai Date	<table border="0"> <tr> <td>  Mr. Qunli Han Director Division of Ecological and Earth Sciences United Nations Educational, Scientific and Cultural Organization 16 March 2015 Date </td> <td>  Mr. Dominique Burgon Resilience Coordinator, Director Emergency and Rehabilitation Division Food and Agriculture Organization of the United Nations 16 March 2015 Date </td> </tr> <tr> <td>  Mr. Kazuhiko Takemura Senior Vice-Rector United Nations University 16 March 2015 Date </td> <td>  Mr. Petteri Taalas Secretary-General World Meteorological Organization 15.4.16 Date </td> </tr> <tr> <td>  Mr. Gordon Milne President International Council for Science 16/03/2015 Date </td> <td>  Mr. Toshimasa Komatsu Vice President World Federation of Engineering Organizations March 16, 2015 Date </td> </tr> <tr> <td>  Mr. Roland Oberhänsli President International Union of Geological Sciences 16/03/2015 Date </td> <td>  Mr. Alik Ismail Zadeh Secretary-General International Union of Geodesy and Geophysics 16 MARCH 2015, SENDAI, JAPAN Date </td> </tr> </table>	 Mr. Qunli Han Director Division of Ecological and Earth Sciences United Nations Educational, Scientific and Cultural Organization 16 March 2015 Date	 Mr. Dominique Burgon Resilience Coordinator, Director Emergency and Rehabilitation Division Food and Agriculture Organization of the United Nations 16 March 2015 Date	 Mr. Kazuhiko Takemura Senior Vice-Rector United Nations University 16 March 2015 Date	 Mr. Petteri Taalas Secretary-General World Meteorological Organization 15.4.16 Date	 Mr. Gordon Milne President International Council for Science 16/03/2015 Date	 Mr. Toshimasa Komatsu Vice President World Federation of Engineering Organizations March 16, 2015 Date	 Mr. Roland Oberhänsli President International Union of Geological Sciences 16/03/2015 Date	 Mr. Alik Ismail Zadeh Secretary-General International Union of Geodesy and Geophysics 16 MARCH 2015, SENDAI, JAPAN Date
 Mr. Kyuji Sasao Executive Director International Consortium on Landslides Host organization of the Partnerships 16/03/15 Date	 Ms. Margareta Wahlström Special Representative of the UN Secretary General for Disaster Risk Reduction Chief of UNISDR 16 March 2015 in Sendai Date											
 Mr. Qunli Han Director Division of Ecological and Earth Sciences United Nations Educational, Scientific and Cultural Organization 16 March 2015 Date	 Mr. Dominique Burgon Resilience Coordinator, Director Emergency and Rehabilitation Division Food and Agriculture Organization of the United Nations 16 March 2015 Date											
 Mr. Kazuhiko Takemura Senior Vice-Rector United Nations University 16 March 2015 Date	 Mr. Petteri Taalas Secretary-General World Meteorological Organization 15.4.16 Date											
 Mr. Gordon Milne President International Council for Science 16/03/2015 Date	 Mr. Toshimasa Komatsu Vice President World Federation of Engineering Organizations March 16, 2015 Date											
 Mr. Roland Oberhänsli President International Union of Geological Sciences 16/03/2015 Date	 Mr. Alik Ismail Zadeh Secretary-General International Union of Geodesy and Geophysics 16 MARCH 2015, SENDAI, JAPAN Date											

9 KLC2020: Launched in Kyoto, Japan

ISDR-ICL Sendai Partnerships 2015–2025 (Sendai Landslide Partnerships 2015–2025) has been very successful in promoting the understanding and reduction of landslide disaster risk since 2015. The Sendai Partnerships will terminate in 2025. However, the landslide risk to human settlements in mountainous and coastal areas in many countries will likely continue to rise including after the latter-half of the Sendai Landslide Partnerships 2015–2025. The ICL and partners of the Sendai Landslide Partnerships wish to establish a stable and long-term framework to mobilize a global alliance which will accelerate and incentivize action for landslide disaster risk reduction.

The Fourth World Landslide Forum (WLF4) was organized in Ljubljana, Slovenia from 30 May to 2 June 2017. Five volumes of books were published under the title of “Advancing Culture of Living with Landslides.” Volume 1 was devoted to the ISDR-ICL Sendai Partnerships 2015–2025 and published in an open access format.

On the first day (30 May 2017) of WLF4, the High-Level panel discussion on “Strengthening Intergovernmental Network and the International Programme on Landslides (IPL) for ISDR-ICL Sendai Partnerships 2015–2025 for

global promotion of understanding and reducing landslide disaster risk” was organized. The panelists were from the signatory organizations of Sendai Partnerships (ICL, UNESCO, WMO, FAO, UNU, ISC, WFEO, IUGS, IUGG, Cabinet Office of Japan, Italian Civil Protection, and Global Risk Forum, Davos) and new signatory organizations (Indonesian National Agency for Disaster Management, Administration of the Republic of Slovenia for Civil Protection and Disaster Relief, Ministry of Natural Resources and Environment, Vietnam, IRDR Science Committee, and EuroGeoSurveys).

Participants of the high-level panel discussion in WLF4 considered and further endorsed the first outline of the Kyoto Landslide Commitment 2020 as a stable framework to mobilize in the medium and long term to accelerate and incentivize action for landslide disaster risk reduction to 2025, 2030 and beyond.

The Kyoto Landslide Commitment 2020 (KLC2020) is a framework aimed at providing key actors and stakeholders concerned with landslide risk at all levels and sectors with the tools, information, platforms, technical expertise and incentives to promote landslide risk reduction at a global scale. It supports the implementation, follow-up and review of the Sendai Framework, the 2030 Agenda for Sustainable

Development, the New Urban Agenda and the Paris Climate Agreement as it addresses the adverse effects of climate change.

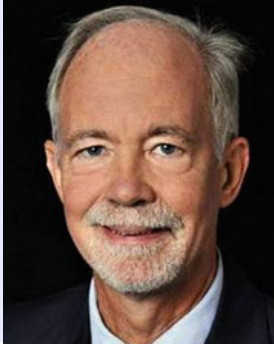

The concept of the Kyoto 2020 Commitment was approved by the 2017 Ljubljana Declaration (Sassa et al. 2017) with the zero-draft of KC2020 made during the 2017 ICL-IPL UNESCO Conference. The zero-draft was continuously revised throughout 2018 to the final draft which was approved by 2018 ICL-IPL Kyoto Conference on 1–4 December 2018 (Sassa 2019a).

The 19th session of the Board of Representatives of the International Consortium on Landslides (BOR/ICL), the 14th session of the Global Promotion Committee of the International Programme on Landslides (GPC/IPL), the meeting of the organizing committee of the Fifth World Landslide Forum, and the IPL Symposium on Landslides were held at Room IX, Fontenoy Building, UNESCO Headquarters in Paris, France, on 16–19 September 2019. On 18 September 2019 during this meeting, 57 global, international and national organizations signed the Kyoto Landslide Commitment as the first signatories (Sassa 2019b).





The ICL and all partners of KLC2020 expected to launch this Kyoto Landslide Commitment at the Fifth World Landslide Forum in November 2020 in Kyoto, Japan. However, due to the COVID-19 Pandemic, the Fifth World Landslide Forum was postponed to 2–6 November 2021 in Kyoto, Japan. The Kyoto Landslide Commitment 2020 had been prepared since 2017 and was already signed by 57 organizations. Since the effective date of the Commitment could not be extended, it was decided to organize the launching session of the Kyoto Landslide Commitment on 5 November 2020 during the 2020 ICL-IPL Online/Virtual Conference in Kyoto, Japan. (Sassa 2021).

Representatives from ninety total signatory organizations and observers attended this launching session. Photos were requested from the participating representatives of the ninety signatory organizations. The photos of chairs of the session, greeting persons from ICL supporting organizations, and panelists of the session are shown below.









Launching Session of Kyoto Landslide Commitment 2020

		
<p>Co-chair: David Malone Under-secretary-general of the United Nations</p>	<p>Co-chair: Qunli Han Executive director of integrated research on disaster reduction</p>	<p>Secretary-General: Kyoji Sassa KLC2020 Secretariat Keynote speech</p>

Greeting Messages: Signatories from ICL Supporting Organizations

	Mami Mizutori United Nations special representative of the secretary-general for disaster risk reduction		Junichi Kanbara Sabo planning coordinator, ministry of land, infrastructure, transport and tourism, government of Japan		Qiuming Cheng Former President, international union of geological sciences
	Petteri Taalas Secretary general of WMO		Miguel Clusener-Godt Director, division of ecological and earth sciences of UNESCO		Kathryn Whaler President, international union of geodesy and geophysics
	Hiroto Mitsugi Assistant director-general of FAO		Gong Ke President, world federation of engineering organizations		Kaoru Takara Dean, Graduate school of advanced integrated studies in human survivability, Kyoto University
	Daya Reddy President, international science council				

Panel Discussion: Chairs, Panelists, and closure

			
<p>Chair: Matjaž Mikoš Co-Chair, global promotion committee of IPL/Chair of WLF4, 2017</p>	<p>Moderator: Badaoui Rouhban Advisor, the international programme on landslides (IPL)</p>	<p>Paola Albrito Chief of Branch, intergovernmental processes, interagency cooperation and partnerships, UNDRR</p>	<p>Soichiro Yasukawa Programme specialist on disaster risk reduction, UNESCO</p>
			
<p>Peter Bobrowsky ICL President, geological survey of Canada</p>	<p>Dwikorita Karnawati Head of the agency for meteorology, climatology and geophysics of the Republic of Indonesia</p>	<p>Beena Ajmera North Dakota State University, the youngest signatory of KLC2020</p>	<p>Nicola Casagli Closing remark Incoming ICL President</p>

10 Ninety Signatories of Kyoto Landslide Commitment 2020

The list of the ninety signatories of Kyoto Landslide Commitment, their positions/organizations, and countries/regions/ international organizations (int. org.) and date of signature are presented in Table 1.

11 Signed Version of the Kyoto Landslide Commitment 2020

The full text of the Kyoto Landslide Commitment 2020 is attached below. As noted in Table 1, ninety organizations signed the attached document and joined the partners of the Kyoto Landslide Commitment 2020. KLC2020 does not

Table 1 List of signatories of the Kyoto landslide commitment from 2019 and 2020

No	Signatories	Position/Organization	Countries/Regions/Intr. Org	Date of signature
<i>Management of Kyoto landslide commitment 2020</i>				
1	David Malone	Chair, KLC2020 general Conference	UNU	05/09/2020
2	Kyoji Sassa	Secretary-general, KLC2020 secretariat	ICL	05/09/2020
<i>Host organization</i>				
1	Peter Bobrowsky	President, international consortium on landslides	ICL	18/09/2019
<i>ICL supporting organizations and other partners from governmental and international organizations</i>				
1	Petteri Taalas	Secretary-general, WMO	WMO	04/11/2020
2	Miguel Clusener-Godt	Director, division of ecological and earth sciences, UNESCO	UNESCO	10/09/2019
3	Paola Albrito	Chief of branch, intergovernmental processes, interagency cooperation and partnerships, United Nations office for disaster risk reduction (UNDRR)	UNDRR	07/09/2020
4	Taikan Oki	Senior Vice-Rector, United Nations university	UNU	05/09/2019
5	Jacques de Méreuil	Executive Director, world federation of engineering organizations	WFEO	18/09/2019
6	Qunli Han	Executive Director, integrated research on disaster risk	IRDR	18/09/2019
7	Qiuming Cheng	President, international union of geological sciences	IUGS	02/02/2020
8	Kathy Whaler	President, international union of geodesy and geophysics	IUGG	18/08/2020
9	Daya Reddy	President, international science council	ISC	01/09/2020
10	Juichi Yamagiwa	President, Kyoto University	Japan	18/09/2019
11	Akifumi Nakao	Director, international cooperation division, disaster management bureau, cabinet office, government of Japan	Japan	15/01/2020
12	Masaru Kunitomo	Director, Sabo planning coordination, Sabo planning division, ministry of land infrastructure, transport and tourism	Japan	18/09/2019
13	Tomohiro Saeki	Head, forest disaster prevention and restoration office, forestry agency, ministry of agriculture, forestry and fisheries	Japan	18/03/2020
14	Kenichiro Saito	Director, office for disaster reduction research ministry of education, culture, sports, science and technology	Japan	01/08/2020
15	Angelo Borrelli	Head, national civil protection department, Italian presidency of the council of ministers	Italy	18/09/2019
16	Darko But	Director general, administration for civil protection and disaster relief of the Republic of Slovenia	Slovenia	18/09/2019
17	Walter J. Ammann	CEO & President, global risk forum GRF Davos	GRF Davos	18/09/2019
18	Rafiq Azzam	President, international association for engineering geology and the environment	IAEG	01/10/2019
19	Nathalie Touze	Vice-President, international geosynthetics society	IGS	18/09/2019
<i>ICL supporting organizations as well as ICL full members</i>				
1	Julian SH Kwan	Geotechnical engineering office, civil engineering and development department, the government of Hong Kong SAR	Hong Kong SAR, China	18/09/2019
2	Nicola Casagli	UNESCO chair for the prevention and the sustainable management of geo-hydrological hazards, University of Firenze (UNIFI)	Italy	18/09/2019
3	Young-Suk SONG	Head, geo-environmental hazard research center, Korea institute of geoscience and mineral resources	Korea, Rep	20/08/2020
4	Matjaž Mikoš	University of Ljubljana, faculty of civil and geodetic engineering	Slovenia	18/09/2019

(continued)

Table 1 (continued)

No	Signatories	Position/Organization	Countries/Regions/Intr. Org	Date of signature
<i>ICL full members</i>				
1	Sabid Zekan	Vice-President, geotechnical society of Bosnia and Herzegovina	Bosnia and Herzegovina	10/08/2020
2	Renato Eugenio de Lima	Director, center for scientific support on disasters—Federal University of Paraná—Brazil (CENACID-UFPR)	Brazil	18/09/2019
3	Daniel Lebel	Director general, geological survey of Canada	Canada	18/09/2019
4	Michael T. Hendry	Associate Professor, university of Alberta	Canada	18/09/2019
5	Wei Shan	Dean of cold regions science and engineering, northeast forestry university	China	18/09/2019
6	Chang-Dong Li	China university of geosciences (Wuhan)	China	18/09/2019
7	Lijun Su	Institute of mountain hazards & environment, CAS	China	18/09/2019
8	Charles Wang Wai Ng	Associate Vice-President for research and development, CLP Holdings Professor of sustainability, chair professor of civil and environmental engineering, The Hong Kong university of science and technology	Hong Kong SAR, China	08/07/2020
9	Clarence E. Choi	Assistant Professor, department of civil engineering, the university of Hong Kong	Hong Kong SAR, China	24/08/2020
10	Aiguo Xing	Shanghai Jiao Tong University	China	04/08/2020
11	Snježana Mihalić Arbanas and Željko Arbanas	Croatian Landslide Group	Croatia	18/09/2019
12	Guillermo Ávila	National University of Colombia	Colombia	18/09/2019
13	Vít Vilímek	Charles University	Czech Republic	18/09/2019
14	Josef Stemberk	Director, institute of rock structure and mechanics, the Czech academy of sciences	Czech Republic	18/09/2019
15	Hauke Zachert	Head, institute and laboratory of geotechnics, technical university Darmstadt	Germany	18/09/2019
16	Andro Aslanishvili	Head of LEPL national environmental agency of Georgia, ministry of environment protection and agriculture	Georgia	18/09/2019
17	Lidia Elizabeth Torres Bernhard	Director, Instituto Hondureño de Ciencias de la Tierra, IHCIT/Universidad Nacional Autónoma de Honduras UNAH	Honduras	02/09/2020
18	Maneesha V Ramesh	Amrita Vishwa Vidyapeetham	India	18/09/2019
19	Dwikorita Karnawati	Head, agency for meteorology, climatology, and geophysics of the Republic of Indonesia (BMKG Indonesia)	Indonesia	18/09/2019
20	Teuku Faisal Fathani	Director, center for disaster mitigation and technological innovation (GAMA-InaTEK), Universitas Gadjah Mada, Indonesia	Indonesia	18/09/2019
22	Paulus P. Rahardjo	Head of geotechnical engineering research center, Universitas Katolik Parahyangan	Indonesia	10/08/2020
23	Mohammad Shekarchizadeh	President, building & housing research center	Iran	14/04/2019
24	Daniele Spizzichino	ISPRA-Italian institute for environmental protection and research	Italy	18/09/2019
25	Carlo Esposito	Centro di Ricerca CERI—Sapienza Università di Roma	Italy	18/09/2019
26	Giuseppe Mandrone	Dept. Earth Science, University of Torino	Italy	18/09/2019
27	Andrea Segalini	University of Parma, Dept. of engineering and architecture	Italy	18/09/2019
28	Giovanna Capparelli	Camilab—Dimes Dept. university of Calabria	Italy	18/09/2019
29	Paola Reichenbach	Senior researcher, research institute for geo-hydrological protection, Italian national research council (IRPI-CNR)	Italy	22/06/2020

(continued)

Table 1 (continued)

No	Signatories	Position/Organization	Countries/Regions/Intr. Org	Date of signature
30	Lorenzo Petronio	Chief technology officer, national institute of oceanography and applied geophysics (OGS)	Italy	24/08/2020
31	Hiroshi Yagi	President, Japan landslide society	Japan	18/09/2019
32	Fawu Wang	Director-general, international consortium on geo-disaster reduction	Japan	18/09/2019
33	Irasema Alcántara-Ayala	Institute of geography, national autonomous university of Mexico (UNAM)	Mexico	29/07/2020
34	Zoran Gligorić	Dean, faculty of mining and geology, university of Belgrade	Serbia	18/09/2019
35	Tomislav Popit	University of Ljubljana, faculty of natural sciences and engineering	Slovenia	18/09/2019
36	Miloš Bavec	Director, geological survey of Slovenia	Slovenia	18/09/2019
37	A A Virajh Dias	Central engineering consultancy Bureau	Sri Lanka	18/09/2019
38	Asiri Karunawardena	Director general, national building research organisation	Sri Lanka	15/06/2020
39	Ray-Shyan Wu	Distinguished professor, national central university	Chinese Taipei	12/03/2020
40	Louis Ge	Department of civil engineering, national Taiwan university	Chinese Taipei	18/09/2019
41	Hans Guttman	Executive director, Asian disaster preparedness center	Thailand	18/09/2019
42	Benjaporn Chakranon	Director general, land development department, ministry of agriculture and cooperatives	Thailand	11/08/2020
43	Oleksandr M. Trofymchuk	Institute of telecommunications and global information space, national academy of science of Ukraine	Ukraine	18/09/2019
44	Binod Tiwari	Associate vice president, office of research and sponsored projects, division of academic affairs, California state university, Fullerton	USA	18/09/2019
45	Nguyen Xuan Khang	Director general, institute of transport science and technology	Vietnam	18/09/2019
46	Tran Tan Van	Director, Vietnam institute of geosciences and mineral resources (VIGMR)	Vietnam	18/09/2019
<i>ICL associate members</i>				
1	Qiang Xu	Executive deputy director, state key laboratory of Geohazard prevention and geoenvironment protection, Chengdu university of technology	China	18/09/2019
2	Zdenek Venera	Director, Czech geological survey	Czech Republic	30/07/2020
3	Mario Parise	Department of earth and environmental sciences, university Aldo Moro, Bari	Italy	18/09/2019
4	Michele Calvello	Geotechnical engineering group (GEG), university of Salerno	Italy	18/09/2019
5	Andrea Stefano Di Giulio	Head, department of earth and environmental sciences, university of Pavia	Italy	15/07/2020
6	Ryo Moriwaki	Director, center for disaster management informatics research, Ehime university	Japan	18/09/2019
7	Michel Jaboyedoff	Directeur ISTE—institute of earth sciences, risk-group, university of Lausanne	Switzerland	14/08/2020
8	Nejan Huvaj	Middle east technical university (METU)	Turkey	18/09/2019
9	Beena Ajmera	North Dakota state university	USA	18/09/2019
<i>ICL supporters</i>				
1	Matthias Twardzik	Business development manager—monitoring organization: IDS GeoRadar	Italy	11/08/2020
2	Shinro Abe	Adviser, Okuyama Boring Co., Ltd	Japan	18/09/2019
3	Nobuyuki Shibasaki	General manager, land conservation division, Nippon Koei Co., Ltd	Japan	18/09/2019
4	Ryosuke Tsunaki	Executive engineer, Sabo & landslide technical center	Japan	18/09/2019

(continued)

Table 1 (continued)

No	Signatories	Position/Organization	Countries/Regions/Intr. Org	Date of signature
5	Maki Yano	President, OSASI Technos, Inc	Japan	18/09/2019
6	Masaru Narita	President, Oyo cooperation	Japan	22/04/2020
7	Taketoshi Marui	President, Marui & Co., Ltd	Japan	05/06/2020
8	Yamazaki Tsutomu	Director and general manager of technical headquarters, Japan conservation engineer & Co. Ltd	Japan	16/06/2020
9	Yuji Sato	Director and general manager of technical headquarters, Godai Kaihatsu Co., Ltd	Japan	24/08/2020
10	Satoshi Hijikata	President, Kokusai Kogyo Co., Ltd	Japan	05/09/2020

require any additional works or responsibilities from the partners other than their own intrinsic works/mandates. The current KLC2020 partners are ICL members (full members, associate members, and supporters), partners of Sendai Landslide Partnerships (ISDR-ICL Sendai Partnerships) 2015–2025, governments of nations of ICL members, and international societies that contribute to the World Landslide Forums and KLC2020. All partners are organizations with some activities related to understanding and reducing landslide disaster risk as part of their intrinsic missions. The current signatories call on wide-ranging further signatories for the success of the Kyoto Landslide Commitment 2020 continuing to 2030 and beyond.

Any reader of the following full text of the Kyoto Landslide Commitment 2020 wishing to join the KLC2020 should contact the secretary of KLC 2020 at klc2020@iclhq.org.

KYOTO 2020 Commitment for global promotion of understanding and reducing landslide disaster risk

A Commitment to the Sendai Landslide Partnerships 2015–2025, the Sendai Framework for Disaster Risk Reduction 2015–2030, the 2030 Agenda Sustainable Development Goals, the New Urban Agenda and the Paris Climate Agreement

Preamble

Landslide disasters are the result of impacts of hazardous movement of soil and rocks that threaten vulnerable human settlements and infrastructure in mountains, cities, on coasts, and islands. An increase in the frequency and/or magnitude of heavy rainfall and shifts in the location, timing and periodicity of rainfall and permafrost/glacier degradation due to changing climate and global warming may significantly intensify the risk of landslides in many landslide prone areas.

Developments in mountains and coastal areas, including infrastructure construction such as roads, railways, energy and communication corridors, expansion of urban areas, including deforestation due to population growth and movement increase exposure to the hazards of landslides. Landslide disaster risk reduction is a globally important objective in all countries/regions where people living near mountains and on slopes are exposed to landslides.

The International Consortium on Landslides (ICL) proposed the ‘ISDR-ICL Sendai Partnerships 2015–2025 for Global Promotion of Understanding and Reducing Landslide Disaster Risk’ in the Working Session “Underlying Risk Factors” during the 3rd World Conference on Disaster Risk Reduction (WCDRR) in Sendai, Japan, 2015. The Sendai Partnerships was adopted and signed by 17 United Nations, international and national stakeholders. Joint efforts thereafter have been made and resulted in significant outcomes and materials including the edition and publication of the open access full color book “ISDR-ICL Sendai Partnerships 2015–2025”, Vol. 1 of the Fourth World Landslide Forum (Ljubljana, 2017), the edition of “Landslide Dynamics: ISDR-ICL Landslide Interactive Teaching Tools”, as well as the enhanced publication of the monthly full-color journal *Landslides: Journal of the International Consortium on Landslides*.

The landslide risk to human settlements in mountainous and coastal areas in many countries will likely continue to rise including after the latter-half period of the Sendai Landslide Partnerships 2015–2025. In September 2015, the United Nations General Assembly adopted the 2030 Agenda for Sustainable Development and its 17 Sustainable Development Goals (SDG) including SDG 11 ‘Make cities and human settlements inclusive, safe, resilient and sustainable’ and SDG 13 ‘Take urgent action to combat climate

change and its impacts'. As a voluntary commitment to the 2030 Agenda, to the Sendai Framework for Disaster Risk Reduction 2015–2030 and to the Paris Agreement on Climate Change as well as to the Sendai Landslide Partnerships itself, participants in the Fourth World Landslide Forum considered and further endorsed the first outline of a commitment, the Kyoto Landslide Commitment 2020, as a stable framework to mobilize in the medium and long term a global alliance which will accelerate and incentivize action for landslide disaster risk reduction.

The High-Level panel discussion on “Strengthening Intergovernmental Network and the International Programme on Landslides (IPL) for ISDR-ICL Sendai Partnerships 2015–2025 for global promotion of understanding and reducing landslide disaster risk” was organized during the Fourth World Landslide Forum. The panelists were from the signatory organizations of Sendai Partnerships (ICL, UNESCO, WMO, FAO, UNU, ISC, WFE0, IUGS, IUGG, Cabinet Office of Japan, Italian Civil Protection, Global Risk Forum, Davos) and new signatory organizations (the Indonesian National Agency for Disaster Management, the Administration of the Republic of Slovenia for Civil Protection and Disaster Relief, Ministry of Natural Resources and Environment, Vietnam, IRDR Science Committee, EuroGeoSurveys) as well as experts in this field.

The outcome of this High-Level panel discussion was reviewed by the Round Table Discussion to promote the Sendai Partnerships and the participants approved the 2017 Ljubljana Declaration on Landslide Risk Reduction. The Declaration endorsed the plan for the organization of the Fifth World Landslide Forum in Kyoto, Japan in November 2020 and the preparation of the Kyoto Landslide Commitment 2020 of a global alliance which aims, in the medium and long term, to accelerate and incentivize action for landslide disaster risk reduction to 2025, 2030 and beyond.

The Kyoto Landslide Commitment 2020 (KLC2020) is a framework aimed at providing key actors and stakeholders concerned with landslide risk at all levels and sectors with the tools, information, platforms, technical expertise and incentives to promote landslide risk reduction on a global scale. It supports the implementation, follow-up and review of the Sendai Framework, the 2030 Agenda for Sustainable Development, the New Urban Agenda and the Paris Climate Agreement as it addresses the adverse effects of climate change.

KLC2020 reaffirms the following resolution of the Sendai Landslide Partnerships, acknowledging that:

- *Landslide disasters are caused by exposure to hazardous motions of soil and rock that threaten vulnerable human settlements in mountains, cities, on coasts, and islands.*
- *Climate change will intensify the risk of landslides in some landslide prone areas through an increase in the frequency and/or magnitude of heavy rainfall, and shifts in the location and periodicity of heavy rainfall.*
- *Global warming will intensify the risk of landslides in permafrost area and glacial lake outburst floods through snow and ice melting.*
- *Developments in mountains and coastal areas, including construction of roads and railways and expansion of urban areas due to population shifts, increase exposure to hazards of landslides.*
- *Although they are not frequent, strong earthquakes have potential to trigger rapid and long runout landslides and liquefaction. Earthquake-induced coastal or submarine large-scale landslides or megaslides (with depths on the order of hundreds of meters to one thousand meters) in the ocean floor can trigger large tsunami waves. These hazardous motions of soil and water impacting on exposed and vulnerable population can result into very damaging effects.*
- *The combined effects of triggering factors, including rainfall, earthquakes, and volcanic eruptions, can lead to greater impacts through disastrous landslides such as lahars, debris flows, rock falls, and megaslides.*
- *Understanding landslide disaster risk requires a multi-hazard approach and a focus on social and institutional vulnerability. The study of social and institutional as well as physical vulnerability is needed to assess the extent and magnitude of landslide disasters and to guide formulation of effective policy responses.*
- *Human intervention can make a greater impact on exposure and vulnerability through, among other factors, land use and urban planning, building codes, risk assessments, early warning systems, legal and policy development, integrated research, insurance, and, above all, substantive educational and awareness-raising efforts by relevant stakeholders.*
- *The understanding of landslide disaster risk, including risk identification, vulnerability*

assessment, time prediction, and disaster assessment, using the most up-to-date and advanced knowledge, is a challenging task. The effectiveness of landslide disaster risk reduction measures depends on scientific and technological developments for understanding disaster risk (natural hazards or events and social vulnerability), political “buy-in”, and on increased public awareness and education.

- *At a higher level, social and financial investment is vital for understanding and reducing landslide disaster risk, in particular social and institutional vulnerability through coordination of policies, planning, research, capacity development, and the production of publications and tools that are accessible, available free of charge and are easy to use for everyone in both developing and developed countries.*

We agree on the following priority actions of Kyoto 2020 Commitment for Global Promotion of Understanding and Reducing Landslide Disaster Risk in research and capacity building, coupled with social and financial investment:

Action 1 Promote the development of people-centered early warning technology for landslides with increased precision and reliable prediction both in time and location, especially in a changing climate context.

Action 2 Advance hazard and vulnerability mapping, including vulnerability and risk assessment with increased precision, as well as reliability as part of multi-hazard risk identification and management.

Action 3 Improve the technologies for monitoring, testing, analyzing, simulating, and effective early warning for landslides suitable for specific regions considering natural, cultural and financial aspects.

Action 4 Apply the ISDR-ICL Landslide Interactive Teaching Tools for landslide risk reduction in landslide prone areas and improve them with feedbacks from users in developed and less developed countries.

Action 5 Promote open communication with local governments and society through integrated research, capacity building, knowledge transfer, awareness-raising, training, and educational activities, to enable societies and local communities to develop effective policies and strategies for reducing landslide disaster risk, to strengthen their capacities for preventing hazards from developing into major disasters, and to enhance the effectiveness and efficiency of relief programs.

Action 6 Investigate the effect of climate change on rainfall-induced landslides and promote the development of effective rainfall forecasting models to provide earlier warning and evacuation especially in developing countries.

Action 7 Investigate the mechanism and dynamics of submarine landslides during earthquakes that may cause or enhance tsunamis, as well as develop and upgrade its hazard assessment and mitigation measures.

Action 8 Promote geotechnical studies of catastrophic megaslides and develop their prediction and hazard assessment.

Action 9 Foster new initiatives to study research frontiers in understanding and reducing landslide disaster risk by promoting joint efforts by researchers, policy makers and funding agencies.

Action 10 Facilitate and encourage monitoring, reporting on, and assessing progress made, through the organization of progress report meetings at the regional and national level, to take place in respective countries, in order to show delivery and performance on progress made towards achieving the Kyoto Landslide Commitment priority actions No. 1–9. Participating parties and relevant stakeholders reporting on deliveries and achievements at these meetings are invited to report on this progress in the monthly full color journal “*Landslides*” so as to allow viewing progress in addressing landslide risk reduction. They are also encouraged to cooperate, as feasible and appropriate, with countries, the United Nations family, regional organizations, and all other partners and stakeholders concerned with landslide risk in their contribution to the Sendai Monitor System and the Voluntary National Reviews, and in their reporting on relevant key SDGs, notably on resilient and sustainable cities and climate action and on the Paris Agreement follow-up.

We submit that the above priority actions contribute to the four priority areas of the Sendai Framework and to the achievement of its seven global targets, in line with the “Words into Action” guidelines for Sendai Framework implementation, as well as of the SDG related targets. These actions also support landslide risk actors involved in building urban resilience so as to achieve coherence with the New Urban Agenda. Furthermore, they contribute to the discussion within the Global Platforms for Disaster Risk Reduction. Finally, they support the implementation of the Strategic Framework 2016–2021 of the United Nations Office for Disaster Risk Reduction (UNDRR).

We consider KLC2020 as a framework to enhance cooperation in landslide risk reduction internationally, but also as a platform aimed at providing support to regional, national and local efforts, triggering exchanges on good practices and twinning and building the capacity of institutions and professionals at the national and local levels.

Commitments by all participating parties are periodically reviewed and updated at the Triennial World Landslide Forum in which parties of KLC2020 are called upon to participate.

Fundamental Coordinating Commitments by the International Consortium on Landslides (ICL) and the Global Promotion Committee of the International Programme on Landslides (IPL) and others providing the common platform for the Kyoto Landslide Commitment 2020 include the following:

1. The Triennial Conference “World Landslide Forum” will be organized and the progress of Kyoto Landslide Commitment by all participating parties will be reported and examined for further development.
2. Landslides: Journal of International Consortium on Landslides will continue to be published monthly in full color and distributed to all participating parties.
3. Contribution fee and full color printing fee will continue to be waived to promote contribution from less developed countries and young researchers.
4. ICL provides that all parties of the Kyoto Landslide Commitment 2020 have the right to submit and publish news and reports of their activities in the “Landslides” journal. All parties will receive the digital access rights (tokens) to all issues of the journal (2002-present).
5. ICL will publish and update Landslide Dynamics: Landslide Interactive Teaching Tools (LITT) as a core activity for public education at each Forum. In early 2018, the first LITT (Vol.1 Fundamentals, Mapping and Monitoring, Vol.2 Testing, Risk Management and Country Practices) have been edited and published including PPT for lessons and PDF for reference in digital format.
6. ICL and the Global Promotion Committee of the International Programme on Landslides (GPC/IPL) will organize the annual IPL symposium and publish a series of books with ISBN numbers together with Research, Administrative and Strategic Review meetings at relevant venues such as UNESCO or elsewhere including the biennial Global Platform for Disaster Risk Reduction.

7. Other commitments by ICL and IPL groups will include:

- Landslide experts are called upon to gain trust and confidence from the local authorities and the communities facing the risk of landslides in order to effectively communicate the risk and urge local actions to help reduce the risk. Thus, ICL and IPL groups will promote a good dialogue at local levels throughout the activities of the Kyoto Landslide Commitment 2020.
- To promote cooperation between policy makers, national government authorities working on landslide risk reduction and landslide scientists and engineers, a joint round table discussion between ICL members and high-level Ministerial members will be organized at each triennial Forum.
- Community safeguard policy for the countries/ areas which are affected by rain-induced rapid and long-travel landslides, earthquake-induced megaslides as well as coastal and submarine landslides will be examined in specific sessions at each Forum.
- To identify, whenever possible and appropriate, focal points at the national/regional level in as many countries/regions as possible for engagement with the Kyoto Landslide Commitment 2020 and for ensuring contact and coordination with the Secretariat.

We are conscious that KLC2020 will build and capitalize on the work and achievements of ICL and IPL notably the 2006 Tokyo Action Plan, the 2015 Sendai Partnerships and the outcomes of the World Landslide Fora.

We are committed to working together with Member States of the UN system, the UN family, regional organizations, and all other partners and stakeholders concerned with landslide risk, including civil society, academic, scientific and research entities, business, professional associates and private sector financial institutions, and the media.

We firmly believe that sustained cooperation and exchange between countries at a governmental level is needed if we are to promote in a sustainable way landslide risk reduction for resilience. Therefore, the timeliness and opportunity of having in place a platform or a mechanism at an intergovernmental level which would work to advise, strengthen and support decisions and initiatives on landslide risk reduction must be considered. This mechanism will enhance

synergetic and concerted efforts not only among governmental entities but also between them and other sectors including the private sector and the civil society. We call upon KLC2020 partners and stakeholders concerned to consider developing an Inter-governmental Panel on Landslide Risk Reduction in the framework of KLC2020 within the International Programme on Landslides (IPL) so as to raise the level of interest in this area and maintain it through support to a long term global alliance that will continue to 2025, 2030 and beyond. The Panel will help mobilize strong political interest and commitment of the international community as well as further scientific knowledge and technological know-how. It will advise on translating the objectives of ICL into meaningful programmes at the country level. The functions, form, governance and operation of the Panel will hopefully defined by relevant intergovernmental bodies.

A Call for joining the Commitment

Competent global, regional, national, local institutions and entities participating in the Fifth World Landslide Forum are invited to support this initiative by joining and signing this Commitment through participation in clearly defined commitments for understanding and reducing landslide disaster risk. The potential parties are requested to make contact with the Secretariat of the host organization. Furthermore, ICL and competent national, regional and international institutions are encouraged to enter into bilateral arrangements including through a dedicated Agreement of Cooperation which will provide a framework of cooperation and facilitate collaboration in areas of common interest and which enable both parties to mutually benefit and develop their cooperation, for the benefit of landslide hazard-prone communities in the country concerned and worldwide.

Host Organization and Secretariat

The International Consortium on Landslides (ICL) hosts the Kyoto Landslide Commitment 2020 as a voluntary commitment to the Sendai Landslide Partnerships 2015–2025, the Sendai Framework for Disaster Risk Reduction 2015–2030 and the 2030 Agenda Sustainable Development Goals. The ICL Secretariat in Kyoto, Japan, serves as the Secretariat of the Kyoto Landslide Commitment 2020.

Signatories:

Signature
Name
Position
Organization
date/month/year
Date

12 The Fifth World Landslide Forum and the Open Access Book Series “Progress in Landslide Research and Technology”

The Fifth World Landslide Forum was organized on 2–6 November 2021 in the hybrid mode with onsite, online, and pre-recorded presentations. The high-level panel discussion “Review of KLC2020 and the way forward” was organized on 3 November 2021 at the National Kyoto International Conference Center in Kyoto, Japan. The high-level panel discussion proposed the Launching Declaration of the ICL Open Access Book Series “Progress in Landslide Research and Technology” for the Kyoto Landslide Commitment 2020. This book series provides a new stable and global platform essential for the dissemination of information and collaboration within KLC2020 partners and the Society. It can be downloaded free of charge by anyone, both in developing and developed countries suffering from landslide disasters and also the policy makers involved in landslide disaster risk reduction.

The ICL book series “*Progress in Landslide Research and Technology*” is aimed to promote the reduction of landslide disaster risk. The target readers of the book series are practitioners and other stakeholders who apply the most advanced knowledge of science and technology for landslide disaster risk reduction in their practice. Articles must be written in a simplified way that easily understandable by practitioners and stakeholders. On the contrary, the target readers of ICL Journal “*Landslides*” are scientists. Both ICL publications are complementarity in contributing to understanding and reducing landslide disaster risk.

Acknowledgements The International Consortium on Landslides extends sincere thanks for ICL supporting organizations and advisors from UNESCO, UNDRR, UNU, WMO, FAO, ISC, WFEO, IUGS, IUGG and Government of Japan (Cabinet office, MEXT, MAFF, MLIT) and Kyoto University for their continued support to the ICL-IPL

activities, the Sendai Landslide Partnerships 2015–2025 and the current Kyoto Landslide Commitment 2020.

The International Consortium on Landslides thanks for ICL supporters which have provided funds to ICL and IPL activities, especially publishing the ICL monthly journal *Landslides* since its foundation. The Kyoto Landslide Commitment 2020 and the ICL extend their deep appreciation to the KLC2020 official promoters which are jointly implementing the KLC2020 and provide financial contribution to its activities. The International Consortium on Landslides and the Kyoto Landslide Commitment secretariat make the following two calls for KLC2020.

Call for contribution to this new open access book series for Vol. 1, No. 2 in 2022, Vol. 2, No. 1 and No. 2 in 2023. Articles for Vol.1, No.1 are provided in this issue.

Call for the KLC2020 official promoters which are public and private organizations who promote the Kyoto Landslide Commitment 2020 and provide financial support for the implementation of the KLC2020 activities including the Open Access Book Series “Progress in Landslide Research and Technology”.

Inquiries to ICL and KLC2020 can be made to:

ICL secretariat at secretariat@iclhq.org or

KLC2020 secretariat at klc2020@iclhq.org.

References

- Sassa K (ed) (1997) Proceedings of the international symposium on landslide hazard assessment (ISBN4-9900618-0-2 C3051), p 421
- Sassa K (2005) ICL history and activities. In: Sassa K, Fukuoka H, Wang F, Wang G (eds) *Landslides in risk analysis and sustainable disaster management*, pp 3–21
- Sassa K (2009) Report of the 2008 first world forum on 18–21 November 2008 at UNU, Tokyo. *Landslides* 6–3:167–179
- Sassa K (2015) ISDR-ICL Sendai partnerships 2015–2025 for global promotion of understanding and reducing landslide disaster risk. *Landslides* 12–4:631–640
- Sassa K (2019a) The fifth world landslide forum and the final draft of the Kyoto 2020 commitment. *Landslides* 16–2:201–211
- Sassa K (2019b) The Kyoto landslide commitment 2020: first signatories. *Landslides* 16–11:2053–2057
- Sassa K (2021) The Kyoto landslide commitment 2020: launched. *Landslides* 18–1:5–20
- Sassa K (2022) The fifth world landslide forum and progress of the open access book series for Kyoto landslide commitment 2020. *Landslides* 19–1:1–5
- Sassa K, Fukuoka H, Wang G, Wang F, Benavente E, Ugarte D, Astete F (2005) Landslide Investigation in Machu Picchu world heritage, Cusco, Peru (C101-1). In: Sassa K, Fukuoka H, Wang F, Wang G (eds) *Landslides in risk analysis and sustainable disaster management*, pp 25–38
- Sassa K, Yin Y, Canuti P (eds) (2015) The third world landslide forum, Beijing, 2014. *Landslides* 12–1:177–192
- Sassa K, Mikoš M, Yin Y (eds) (2017) *Advancing culture of living with landslides, volume 1: ISDR-ICL Sendai partnerships 2015–2025 (open access)*. Springer International Publishing AG, Switzerland, p 586
- Television X (1997) For the protection of Huaqing palace in Xian. Special programme of Xian TV, China

Open Access This chapter is licensed under the terms of the Creative Commons Attribution 4.0 International License (<http://creativecommons.org/licenses/by/4.0/>), which permits use, sharing, adaptation, distribution and reproduction in any medium or format, as long as you give appropriate credit to the original author(s) and the source, provide a link to the Creative Commons license and indicate if changes were made.

The images or other third party material in this chapter are included in the chapter’s Creative Commons license, unless indicated otherwise in a credit line to the material. If material is not included in the chapter’s Creative Commons license and your intended use is not permitted by statutory regulation or exceeds the permitted use, you will need to obtain permission directly from the copyright holder.





International Programme on Landslides—A Short Overview of Its Historical Development

Matjaž Mikoš, Kyoji Sassa, and Qunli Han

Abstract

The International Programme on Landslides (IPL) was launched in 2002 by the International Consortium on Landslides (ICL) to reduce landslide disaster risk, and in 2006 developed into a global cooperation programme by international organizations supporting ICL activities. Ever since, it is successfully managed by the Global Promotion Committee, consisting of the International Consortium on Landslides (ICL) members and representatives from the ICL supporting organizations. The article reviews the main IPL activities, i.e. IPL projects, triennial World Landslide Forums (WLF), World Centres of Excellence (WCoE) on Landslide Risk Reduction, and more. The article ends with an updated list of WCoEs 2008–2023 and IPL projects since 2002.

Keywords

International collaboration • International consortium on landslides • International programme on landslides • Landslide practice • Landslide research • Resilience • Sustainability

1 International Programme on Landslides—IPL

The International Consortium on Landslides (ICL) was established in January 2002 as a non-profit scientific organization. The ICL was approved to be a NGO having operational relations with UNESCO in April 2007. The International Programme on Landslides (IPL) was launched at the first meeting of the Board of Representatives of ICL (BOR/ICL) at United Nations Educational, Scientific and Cultural Organization (UNESCO) Headquarters, Paris, in November 2002.

The International Programme on Landslides (IPL) as a global cooperation programme was further developed during a special thematic session of the United Nations World Conference on Disaster Reduction (WCDR) held in Kobe, Hyogo, Japan in January 2005, as a new international disaster science and capacity building initiative. The thematic session was organized by UNESCO, WMO, UNU, Ministry of Education, Culture, Sports, Science and Technology (MEXT) of the Government of Japan, and ICL.

The current second stage of IPL was defined and established by the 2006 Tokyo Action Plan “Strengthening Research and Learning on Landslides and Related Earth System Disasters for Global Risk Preparedness” (Sassa 2006). In 2006, the International Consortium on Landslides exchanged Memorandum of Understandings to promote IPL with each of ICL supporting organizations: United Nations Educational, Scientific and Cultural Organization (UNESCO), World Meteorological Organization (WMO), Food and Agriculture Organization of the United Nations (FAO), United Nations International Strategy for Disaster Risk Reduction (UNISDR), United Nations University (UNU), International Council for Science (ICSU), and the World Federation of Engineering Organizations (WFEO).

IPL as an international programme is managed by IPL Global Promotion Committee consisting of ICL and ICL supporting organizations (UNESCO, UNISDR and others).

M. Mikoš (✉)

Chair On Water-Related Disaster Risk Reduction and Faculty of Civil and Geodetic Engineering, University of Ljubljana, UNESCO, 1000 Ljubljana, Slovenia
e-mail: matjaz.mikos@fgg.uni-lj.si

K. Sassa

International Consortium On Landslides (ICL), Kyoto, 606-8226, Japan

Q. Han

Integrated Research On Disaster Risk (IRDR), Beijing, China

For more information on the International Consortium on Landslides (ICL), see a review paper in this volume, prepared by Sassa (2022c) or visit the new ICL web pages (ICL 2022).

In recent years, several review papers about the history, objectives and activities of IPL were published (e.g. Sassa 2004c; 2009a; Casagli et al. 2009; Sassa 2013; Mikoš and Mihalić Arbanas 2014; Han et al. 2017, 2020). This is an updated review paper on IPL history, objectives and its main activities: IPL projects, World Landslide Forums, World Centres of Excellence in Landslide Risk Reduction, and other IPL activities.

2 Global Promotion Committee (GPC)

2.1 Global Promotion Committee of the International Programme on Landslides (GPC/IPL)

Until the end of 2021, the International Programme on Landslides (IPL) was managed by the Global Promotion Committee (GPC), with ICL and ICL supporting organization selecting GPC/IPL Chair and several co-chairs. The first GPC Chair (2008–2013) was Salvano Briceño, former Director of UNISDR, and the second Chair (2014–2021) was Qunli Han, Director of Ecological and Earth Sciences, UNESCO.

The IPL World Centre (IWC) was established in 2006 by the Tokyo Action Plan to serve as the Secretariat of IPL and GPC/IPL. Members of the GPC/IPL were ICL Full Members and ICL Supporting Organizations (ICL 2018b).

2.2 Global Promotion Committee of the International Programme on Landslides and Kyoto Landslide Commitment 2020 (GPC/IPL-KLC)

ICL launched in 2020 a new voluntary commitment to the Sendai Framework for Disaster Risk Reduction 2015–2030, and to United Nations Agenda 2030 and its Sustainable

Development Goals, namely the Kyoto Landslide Commitment 2020 (Sassa 2021a), a successor of the ISDR-ICL Sendai Partnerships for global promotion of understanding and reducing of landslide disaster risk 2015–2025 (Sassa 2015, 2016) (Fig. 1). For an overview of Sendai Voluntary Commitments, see the paper by Matsuoka and Gonzales Rocha (2020).

Through this development, GPC/IPL was transformed into the Global Promotion Committee of the International Programme on Landslides and Kyoto Landslide Commitment 2020 (GPC/IPL-KLC). Its Chair is selected from ICL and its Co-chairs from ICL supporting organizations. Since January 2022, the Chair of the GPC is Matjaž Mikoš, UNESCO Chair on Water-related Disaster Risk Reduction, University of Ljubljana, and Co-Chairs are Qunli Han, Executive Director of International Programme Office of Integrated Research on Disaster Risk (IRDR), Soichiro Yasukawa, Programme Specialist on Disaster Risk Reduction, UNESCO, Paris, Hiroshi Kitazato, Treasurer of IUGS, and John LaBrecque, Chair of IUGG GeoRisk Commission—Secretary to GPC is Kyoji Sassa, Director of IPL World Centre. Members of the newly established GPC/IPL-KLC are ICL Full Members, ICL Supporting Organizations, and KLC2020 Official Promoters.

3 IPL Projects

3.1 The Initial Stage of IPL Projects (2002–2008)

The initial stage of IPL projects which was managed by ICL, started in 2002 at the same time of ICL's foundation. The projects were divided into two categories: coordinating projects (called C-project) planned by several ICL members, and single member projects (called M-project) (Sassa et al. 2005). An overview of these initial IPL projects is given in Appendices Table 2. The first IPL project C-100 was publication of *Landslides: Journal of the International Consortium on Landslides*. This initial IPL project is still active, and the journal was a success from its launching and is nowadays effectively one of few leading journals in the field of landslide science and research (Mikoš et al. 2021).

Fig. 1 Logos of the ICL and Kyoto landslide commitment 2020



3.2 The IPL Projects (Since 2008)

Annually, all ICL members have the right to propose an IPL project using a structured application form (Sassa 2013). All submitted proposals are evaluated from formal point of view for their completeness by the ICL Secretariat in Kyoto, Japan, and then evaluated from their technical merit point of view by the IPL Evaluation Committee. In the last years, all proposals are evaluated on their objectives (35%), implementation capabilities (40%), and expected outputs (25%). All proposing institutions are asked to present their projects at annual ICL meetings, and they have a chance to improve their applications according to suggestions and comments received by the audience, and by written comments from the IPL Evaluation Committee. The project proposals are evaluated and ranked by at least ten landslide experts. Proposals with scores over the threshold of 70% are normally supported and approved by the Global Promotion Committee of IPL. All projects are declared on-going after their approval as long as they submit reports on an annual basis to the IPL Secretariat using structured report forms, and submit research articles on the project results to the journal *Landslides*, World Landslide Forums, or give presentations at annual IPL conferences. A full overview of all completed and on-going IPL projects is given in the Appendices Table 2.

Altogether 165 IPL projects (including subprojects) have been approved since 2002 in 36 countries, many have been completed or terminated after years of activities, and some are still on-going. On average, close to 10 projects are approved annually, running then for several years—at least for two years to be evaluated and approved. A short statistic with regard to IPL projects reveals the following (see Appendices Table 2 for details):

- the vast majority of projects are national projects, only a few are bilateral projects among two countries (Canada, China, Italy, Japan, Russian Federation, Sri Lanka, Vietnam)—the last such project is IPL-249 by Japan and Sri Lanka, approved in 2019.
- the highest number of IPL projects were approved in the following 12 countries: Italy (28), Japan (23), China (14), Russian Federation (11), Czech Republic (8), India (7), Indonesia (7), Malaysia (7), Sri Lanka (7), Canada (5), Malaysia (5), Slovenia (5), and the remaining 24 countries have 4 or fewer IPL projects.

3.3 The IPL Award for Success

The IPL Award for Success is selected by the IPL Award Committee and is given to a maximum three best successful projects implemented within IPL at the occasion of each

World Landslide Forum following a rigorous evaluation of outputs, activities and impacts of all IPL projects during the previous 3-year cycle of activities. The achievements of awarded IPL projects are directly influenced by the finances and infrastructure of the developed or developing countries. The IPL Awards is not meant for best but rather the most successful IPL projects. The awarded IPL projects in the past are shown in italic fonts in Appendices Table 2. A list of all recipients is also published on the IPL web page: <https://iplhq.org/category/iplhq/award-and-honors/ipl-award-for-success/>.

4 World Landslide Forum (WLF)

The World Landslide Forums as triannual events were established by the 2006 Tokyo Action Plan as a special way of IPL promotional activities (ISDR-ICL 2008). Initially, WLF was proposed to be created as a global information platform for future joint activities of the world-wide landslide community. WLF should bring together academics, practitioners, politicians and other stakeholders to a global, multidisciplinary and problem-based platform. WLF was also seen as the place to recognize World Centres of Excellence (WCoE) in Landslide Risk Reduction and to support other ICL and IPL related promotional activities to global landslide community. Overview of World Landslide Forums since the first one WLF1 in Tokyo, Japan in 2008 (Fig. 3) with location, country, and forum motto is given in Table 1. All six logos of WLFs are given in Fig. 2.

World Landslide Forums can be evaluated as a case of good practice in the fields of landslide practice, research, science, and risk reduction. Normally, it attracts 500 + participants from all over the world, and the wealth of knowledge exchange among the participants was widely available to all stakeholders as published contributions in the WLF Proceedings. The outreach of these publications can be evaluated as solid if measured with bibliometric indices (Mikoš 2018). The last WLF5 in Kyoto, Japan published its reviewed contributions in the ICL Contribution to Landslide Disaster Risk Reduction book series in six volumes under the title “Understanding and Reducing Landslide Disaster Risk”. This book series was now replaced by the book series “Progress in Landslide Research and Technology (P-LRT) to be published twice a year by Springer Nature (Sassa 2021b).

5 World Centre of Excellence (WCoE) in Landslide Risk Reduction

The World Centres of Excellence on Landslide Risk Reduction were established by the 2006 Tokyo Action Plan.

Table 1 World landslide forums since 2008

Year	Forum	Location, Country	Forum motto	References
2008	WLF 1	Tokyo, Japan	Strengthening research and learning on earth system risk analysis and sustainable disaster management within UN-ISDR as regards “landslides”	Sassa (2009a, b)
2011	WLF 2	Rome, Italy	Putting science into practice	Margottini et al. (2010); Sassa et al. (2012)
2014	WLF 3	Beijing, China	Landslide science for a safer geoenvironment	Sassa et al. (2015)
2017	WLF 4	Ljubljana, Slovenia	Advancing culture of living with landslides	Mikoš et al. (2017)
2020*	WLF 5	Kyoto, Japan	Implementing and monitoring the Sendai landslide partnerships 2015–2025	Sassa (2022a, 2022b)
2023	WLF 6	Florence, Italy	Landslide science for sustainable development	ICL (2022)

* Postponed to 2021 due to COVID pandemic

**Fig. 2** Logos of six world landslide forums (2008–2023)

WCoE candidates are governmental and non-governmental entities such as universities, agencies, and other institutions, and their subsidiary entities (faculties, departments, centres, divisions or others) that are (i) contributing to risk reduction

for landslides and related earth system disasters and (ii) are willing to support IPL intellectually, practically and financially by either joining ICL or contributing to GPC/IPL and promote landslide research and risk reduction on a regional and /or global scale in a mutually beneficial manner (Sassa 2013).

5.1 WCoE Guidelines and Evaluation Procedure

All WCoE candidates must submit their application form in a prescribed format to IPL Secretariat. Their applications are first evaluated by the IPL Evaluation Committee (10 + landslide experts from around the world) on the basis of their past achievements, current activities (e.g. scientific, technical and educational capacities, training courses, publications, dissemination of knowledge and information), and planned activities as WCoE to support IPL. Evaluation results are submitted to the Independent Panel of Experts nominated by the GPC/IPL. Their recommendations are finally approved by the GPC/IPL and identified at WLFs for the period of three years (Fig. 4). WCoEs must submit annual reports each year while active and may apply for a prolongation at the next WLF under the same rules as new candidates (Sassa 2013).

Since the first WLF1 in 2008 in Tokyo, triennially, out of all evaluated proposals, altogether 81 WCoEs from 23 countries and the European Commission (Joint Research Center in ISPRA Italy for 2011–2014) were recognized by the GPC/IPL.

5.2 WCoEs From 2008 till 2023

Triennially, out of all evaluated proposals, altogether 81 WCoEs from 23 countries and the European Commission



Fig. 3 Joint Photo of WLF1 participants at U-Thant hall of UNU in Tokyo on 18 November 2008 (Fig. 2 in Sassa 2009b)



Fig. 4 Twenty organizations were awarded the title of WCoE in landslide risk reduction at WLF4 in Ljubljana, 2017 (Fig. 1 from Mikoš et al. 2017)

(Joint Research Center in ISPRA Italy for 2011–2014) were announced at WLFs: twelve WCoEs at WLF1 in 2008, fifteen WCoEs at WLF2 in 2011 and WLF3 in 2014, twenty WCoEs at WLF4 in 2017, and nineteen WCoEs at WLF5 in 2021 (postponed by a year due to COVID-19 pandemic). An overview of all WCoEs is given in Appendices Table 3. The next selection of WCoEs will be completed for WLF6 in Florence, Italy in 2023.

Nearly all WCoEs were from (an) institution(s) of only one country, and the exceptions are WCoEs in Russian Federation & Kyrgyz Republic (2008–2011, 2011–2014, 2014–2017) and Japan & Sri Lanka (2020–2023). In each 3-year period, not more than two WCoEs were recognized in one country, such countries with two WCoEs in one term are: China (2014–2017, 2017–2020), India (2020–2023), Italy (2008–2011, 2020–2023), Japan (2011–2014,

2014–2017), Slovenia (2017–2020), and Sri Lanka (2017–2020).

The highest number of WCoEs for a 3-year period were recognized in the following countries: Italy (8), China (7), Slovenia (6), Czech Republic (5), Japan (5), India (4), Indonesia (4), Malaysia (4), Sri Lanka (4), and Thailand (4). Only two institutions were recognized as WCoE in all five periods: University of Florence, Italy (Casagli and Tofani 2019) and University of Ljubljana, Slovenia (Mikoš and Petkovišek 2019).

6 ICL-IPL Conference

ICL is holding its BOR annually, before COVID pandemic. This was associated with an annual conference called the IPL Symposium on Landslides (ICL 2018a). The proceedings of the recent conferences in years 2017, 2018, and 2019 are available in the pdf format on the web (Sassa and Dang 2017, 2018, 2019). The event is an occasion for ICL members to:

- report on their latest research results, including results of on-going IPL projects and from WCoEs activities as an additional research output to their published articles in the journal *Landslides*; and
- present their proposals for new IPL projects and new WCoEs as a part of the evaluation process.

The last IPL-KLC Hybrid Conference was in Kyoto, Japan, 14–16 March 2022. IPL was also organizing an International Forum entitled “Urbanization and Landslide Disaster” in Kyoto, Japan, dedicated to the Hiroshima Landslide Disaster of August, 2014 (Sassa et al. 2014).

Abbreviations

In this article, the following abbreviations were used:

BOR/ICL	Board of Representative Meeting of ICL.
DRR	Disaster Risk Reduction.
FAO	Food and Agriculture Organization of the United Nations.
GPC/IPL	Global Promotion Committee of the International Programme on Landslides.
GPC/IPL-KLC	Global Promotion Committee of the International Programme on Landslides and Kyoto Landslide Commitment.
IBRD	World Bank.
ICSU	International Council for Science.
ICL	International Consortium on Landslides.
IPL	International Program on Landslides.
IUGS	International Union of Geological Sciences.
JLS	Japan Landslide Society.
KLC2020	Kyoto Landslide Commitment 2020.
KU	Kyoto University.
SDG	Sustainable Development Goal of the 2030 United Nations Agenda.
SFDRR 2015-2030	Sendai Framework for Disaster Risk Reduction 2015–2030.
UNDP	United Nations Development Program.
UNEP	United Nations Environment Program.
UNESCO	United Nations Educational, Scientific and Cultural Organization.
UN-ISDR	United Nations International Strategy for Disaster Risk Reduction.

UNITWIN	University Twinning and Networking Scheme.
UNU	United Nations University.
WCDR	United Nations World Conference on Disaster Reduction.
WCoEs	World Centers of Excellence on Landslide Risk Reduction.
WFEO	World Federation of Engineering Organizations.
WMO	World Meteorological Organization.
WLF	World Landslide Forum.

Acknowledgements The author would like to acknowledge financial support from Slovenian Research Agency, core funding P2-0180 “Water Science and Technology and Geotechnical Engineering”, and University of Ljubljana, Development Fund support for the activities of the UNESCO WRDDR Chair. Furthermore, the authors would like to thank members of the IPL Evaluation Committee for their valuable assessment of the submitted IPL proposals and the WCoE proposals in the past period, especially to (in alphabetical order): Biljana Abolmasov, Željko Arbanas, Irasema Alcántara-Ayala, Peter Bobrowsky, Giovanna Capparelli, Nicola Casagli, Franz Wolfgang Eder, Teuku Faisal Fathani, Hiroshi Fukuoka, Dwikorita Karnawati, Jan Klimeš, Hideaki Marui, Snježana Mihaljić Arbanas, Alexander Strom, Binod Tiwari, Veronica Tofani, Timotej Verbošek, Vit Vilímek, Jan Vlcko, and Fawu Wang. Sincere thanks for the continuous technical support go also to the ICL and IPL Secretariat in Kyoto, and especially to Professor Emeritus Kyoji Sassa, Secretary of IPL World Centre 2 and of GPC/IPL-KLC for his continuous support.

Appendices

See Tables 2 and 3.

Table 2 Chronological overview of the IPL projects since 2002 (Sassa et al. 2005; ICL 2012; Han et al. 2017, 2020; Bobrowsky and Sassa 2022; IPL web page archive at <https://iplhq.org/>)

IPL	Project title	Project leader	Country	Year
C100	Landslides: journal of the international consortium on landslides	Kyoji Sassa	Japan	2002
C101	Landslide risk evaluation and mitigation in cultural and natural heritage sites	Kyoji Sassa Paolo Canuti	Japan	2002
C101-1	Landslide investigation and capacity building in Machu Pichu-Aguas Calientes area	Kyoji Sassa	Japan	2002
C101-1-1	Low environmental impact technologies for slope monitoring by radar interferometry: application to Machu Picchu site	Claudio Margottini	Italy	2002
C101-1-2	Expressions of risky geomorphologic processes as well as paleogeographical evolution of the area of Machu Picchu	Vit Vilímek Jiří Zvelebil	Czech Republic	2002
C101-1-3	Shallow geophysics and terrain stability mapping techniques applied to the Urubamba Valley, Peru: landslide hazard evaluation	Romulo Mucho Peter Bobrowsky	Peru	2004
C101-1-4	A proposal for an integrated geophysical study of the Cuzco region	Daniel Nieto Yabar	Italy	2004
C101-1-5	UNESCO-Italian-ESA satellite monitoring of Machu Picchu	Paolo Canuti Claudio Margottini	Italy	2004
C101-2	Landslides monitoring and slope stability at selected historic sites in Slovakia	Jan Vlcko	Slovakia	2002

(continued)

Table 2 (continued)

IPL	Project title	Project leader	Country	Year
C101-3	<i>The geomorphological instability of the Buddha niches and surrounding cliff in Bamiyan valley (Central Afghanistan)</i>	<i>Claudio Margottini</i>	Italy	2002
C101-4	Stability assessment and prevention measurement of Lishan Landslide, Xian, China	Qing Jin Yang	China	2002
C101-5	Environment protection and disaster mitigation of rock avalanches landslides and debris flow in Tianchi Lake region and natural preservation area of Changbai Mountains, Northeast China	Binglan Cao	China	2002
C101-6	Conservation of Masouleh Town	S. H. Tabatabaei	Iran	2002
C101-7	Cultural and natural heritage threatened by landslides in the region of Iassy, Romania	Nicolae Botu	Romania	2005
C102 IPL-102	<i>Assessment of global high-risk landslide disaster hotspots</i>	<i>Farrokh Nadim</i>	Norway	2002
C103	Global landslide observation strategy	Kaoru Takara Nicola Casagli	Japan & Italy	2004
C104	World landslide database	Hiroshi Fukuoka Nicola Casagli	Japan & Italy	2006
C105	Early warning of landslides	Kyoji Sassa	Japan	2007
C106	Capacity building and outreach	Claudio Margottini Alexander Strom	Italy & Russian Federation	2008
C106-1	<i>Landslide museum in Civita di Bagnoregio</i>	<i>Claudio Margottini</i>	Italy	2006
C106-2	International summer school on rockslides and related phenomena in the Kokomeren river valley, Tien Shan, Kyrgyzstan	Alexander Strom	Russian Federation	2006
M101	Areal prediction of earthquake and rain induced rapid and long-travelling flow phenomena (APERITIF)	Kyoji Sassa Hiroshi Fukuoka	Japan	2002
M102	Disaster evaluation and mitigation of the giant Jinnosuke-dani Landslide in the Tedoru water reservoir area, Japan	Tatsunori Matsumoto	Japan	2002
M103	Capacity building on management of risks caused by landslides in central American countries	Farrokh Nadim	Norway	2002
M104	A global literature study on the use of critical rainfall intensity for warning against landslide disasters	Haakon Heyerdal	Norway	2004
M105	Hurricane-flood-landslide continuum: a forecast system	Randall Updike	USA	2002
M106	<i>A best practices handbook for landslide hazard mitigation</i>	<i>Lynn Highland, Peter Bobrowsky</i>	Canada	2002
M107	Landslide risk assessment in landslide prone regions of Slovakia—modelling of climatic changes impact	Rudolf Holzer	Slovakia	2002
M108	Disaster evaluation and mitigation of landslides in the Three-Gorge water reservoir area, China	Renjie Ding	China	2002
M109	Recognition, mitigation and control of landslides of flow type in Greater Kingston and adjoining parishes in Eastern Jamaica, including public education on landslide hazard	Rafi Ahmad	Jamaica	2002
M110	Capacity building in landslide hazard management and control for mountainous developing countries in Asia	Hideaki Marui	Japan	2002
M111	Detail study of the internal structure of large rockslide dams in the Tien Shan and international field mission: Internal structure of dissected rockslide dams in Kyrgyzstan	Alexander Strom	Russian Federation	2002
M112/IPL-112	Landslide mapping and risk mitigation planning in Thailand	Saowanee Prachansri	Thailand	2002 2008
M113	Zone risk map: towards harmonized, intercomparable landslide risk assessment and risk maps	Yasser Elshayeb	Egypt	2002
M114	Landslide hazard assessment along Tehran-Caspian seaside corridors	Zieaoddin Shoaei	Iran	2002

(continued)

Table 2 (continued)

IPL	Project title	Project leader	Country	Year
M115	Establishment of a regional network for disaster mitigation, disaster education, and disaster database system in Asia	Ryuichi Yatabe	Japan	2003
M116	Standardization of terminology, integration of information and the development of decision support software in the area of landslide hazards	Catherine Hickson	Canada	2003
M117	Geomorphic Hazards from landslide dams	Oliver Korup	Switzerland	2003
M118	Development of an expert DSS for assessing landscape impact mitigation works for cultural heritage at risk	Giuseppe Delmonaco	Italy	2003
M119	Slope instability phenomena in Korinthos county	Nikos Nikolaou	Greece	2002
M120	Landslide hazard zonation in Garwal using GIS and geological attributes	Ashok Kumar Pachauri	India	2003
M121	Integrated system of a new generation for monitoring of dynamics of unstable rock slopes and rock fall early warning	Jiří Zvelebil Vit Vilímek	Czech Republik	2003
M122	Inka cultural heritage and landslides: detailed studies in Cusco and Sacred Valleys, Peru	Raul Carreno	Peru	2004
M123	Cusco regional landslide hazard mapping and preliminary assessment	Raul Carreno	Peru	2004
M124	The influence of clay mineralogy and ground water chemistry on the mechanism of landslides	Viktor Osipov	Russian Federation	2004
M125	Landslide mechanisms on volcanic soils	Carlos Eduardo Rodriguez	Colombia	2004
M126	Compilation of landslide/rockslide inventory of the Tien Shan mountain system	Alexander Strom	Russian Federation	2004
M127	Development of low-cost detector of slope instability for individual use	Ikuo Towhata	Japan	2004
M128	Development of sounding methodology for a root-reinforced landslide mass	Kazuo Konagai	Japan	2004
M129	Evaluation of natural hazards associated with rapid glacial retreat in Cordillera Blanca (Peru)	Vit Vilimek	Czech Republic	2005
M131	Technology development for landslide monitoring in China	Yueping Yin Peter Bobrowsky	China & Canada	2006
M132	<i>Research on vegetation protection system for highway soil slope in seasonal frozen regions</i>	<i>Wei Shan Fawu Wang</i>	<i>China, Japan</i>	2006
M133	Establishment of rainfall-soil chart for erosion induced landslide prediction	Roslan Abidin	Malaysia	2006
M134	Large-scale rockslides in coarse-bedded carbonate rocks in the Apennines (Italy), Caucasus (Russia) and Zagros (Iran): evaluation of possible triggers and hazard assessment	Alexander Strom	Russian Federation	2007
M135	Landslide hazard assessment in Changunarayan hill of Kathmandu, Nepal—geotechnical investigation and preventive plan	Ryuichi Yatabe	Japan	2008
M136	Shear behaviour and mechanics of Megaslides and their nearby faults in Hittian Balla, Pakistan and Shaolin, Taiwan	Kazuo Konagai Kyoji Sassa	Japan	2008
M137	Italian landslide inventory (IFFI Project)	Alessandro Triglia	Italy	2008
M138	Long run out and catastrophic landslides study: Yigong Landslide, Tibet China	Yin Yueping	China	2008
M139	Development of low-cost early warning system of slope instability for civilian use	Ikuo Towhata Taro Uchimura	Japan	2008
M140	Landslide and multi-geohazards mapping for community empowerment in Indonesia	Dwikorita Karnawati	Indonesia	2008
M141	Geo-risks management for third world countries—mapping and assessment of risky geo-factors for land use (e.g. in Ethiopia)	Jiří Zvelebil	Czech Republic	2008
IPL-142	Seismic landslide hazards mapping in Sichuan	Yuepin Yin	China	2009
IPL-143	Evaluation of sensitivity of the combined hydrological model (dynamic) for landslide susceptibility risk mapping in Sri Lanka	A. A. Virajh Dias	Sri Lanka	2008
IPL-144	<i>SafeLand—living with landslide risk in Europe: assessment, effects of global change, and risk management strategies</i>	<i>Bjørn Kalsnes</i>	<i>Norway</i>	2009

(continued)

Table 2 (continued)

IPL	Project title	Project leader	Country	Year
IPL-145	Preparation of landslide risk map in Taleghan Area-Iran	S. H. Tabatabaei	Iran	2009
IPL-146	Spatial monitoring of joint influence of an atmospheric precipitation and seismic motions on formation of landslides in Uzbekistan (Central Asia)	Rustam Niyazov	Uzbekistan	2009
IPL-147	Study on debris flow controlling factors and triggering mechanism in Peninsular Malaysia	Che Hassandi Abdullah	Malaysia	2009
IPL-148	Geo-evaluation of the stability of slopes around crater lakes in Cameroon: the cases of lakes Nyos, Barombi, Mbo and Awing	Ntasin Edwin Bongsiysi	Cameroon	2009
IPL-149	Canadian landslide best practice manual	Peter Bobrowsky	Canada	2009
<i>IPL-150</i>	<i>Capacity building and the impact of climate-driven changes on regional landslide distribution, frequency and scale of catastrophe</i>	<i>Ogbonnaya Igwe</i>	<i>Nigeria</i>	<i>2009</i>
IPL-151	Soil matrix suction in active landslides in flysch—the Slano Blato landslide case	Bojan Majes	Slovenia	2009
IPL-152	Assessment of coastal landslides risk by innovative remote sensing techniques	Gabriele Scarascia Mugnozza	Italy	2009
IPL-153	Landslide hazard zonation in Kharkov region of Ukraine using GIS	Oleksandr M Trofymchuk	Ukraine	2009
IPL-154	Development of a methodology for risk assessment of the earthquake-induced landslides	D. Higaki S. Tsuchiya	Japan	2009
<i>IPL-155</i>	<i>Determination of soil parameters of subsurface to be used in slope stability analysis in two different precipitation zones of Sri Lanka</i>	<i>A. A. Virajh Dias</i>	<i>Sri Lanka</i>	<i>2009</i>
IPL-156	Best practices for early warning of landslides in a changing climate scenarios	N. M. S. I. Arambepola	Thailand	2009
IPL-157	Dynamics of subaerial and submarine megaslides	Kyoji Sassa	Japan	2009
<i>IPL-158</i>	<i>Development of community-based landslide early warning system</i>	<i>Teuku Faisal Fathani</i>	<i>Indonesia</i>	<i>2009</i>
<i>IPL-159</i>	<i>Development of education program for sustainable development in landslide vulnerable area through student community service</i>	<i>Dwikorita Karnawati</i>	<i>Indonesia</i>	<i>2009</i>
IPL-160	Landslides and floods under extreme weather condition and resilient society	Hiroshi Fukuoka	Japan	2009
IPL-161	Risk identification and land-use planning for disaster mitigation of landslides and floods in Croatia	Hideaki Marui	Japan	2009
IPL-162	Tier-based harmonized approach for landslide susceptibility mapping over Europe	Javier Hervás	Italy	2009
IPL-163	Mechanical-mathematical modeling and monitoring for landslide processes	Svalova Valentina	Russian Federation	2009
IPL-165	Development of community-based landslide hazard mapping for landslide risk reduction at the village scale in Java, Indonesia	Dwikorita Karnawati	Indonesia	2010
<i>IPL-167</i>	<i>The effect of freezing–thawing on the stability of ancient landslide of North-Black highway</i>	<i>Wei Shan</i>	<i>China</i>	<i>2010</i>
IPL-168	Engaging U.S. citizens in landslide science through the website, “Did You See It? Report a Landslide”	Rex Baum	USA	2010
IPL-169	Landslide hazard and risk assessment in Geyser Valley (Kamchatka)	Oleg V. Zerkal	Russian Federation	2010
IPL-170	Landslide susceptibility and landslide hazard zonation in volcanic terrains using geographic information system (GIS): a case study in the Río Chiquitobarranca Del Muerto watershed; Pico de Orizaba volcano, México	Gabriel Legorreta Paulín	Mexico	2010
IPL-171	Study of the geotechnical characteristics of an unstable urban area of Barranquilla (Colombia) severely affected for slope instabilities and soil volume changes	Guillermo Ávila	Colombia	2010
IPL-172	Documentation, training and capacity building for landslides risk management	Surya Parkash	India	2011
IPL-173	Croatian virtual landslide data center	Snježana Mihalić Arbanas	Croatia	2011

(continued)

Table 2 (continued)

IPL	Project title	Project leader	Country	Year
IPL-175	Development of landslide risk assessment technology and education in Vietnam and other areas in the Greater Mekong sub-region	Kyoji Sassa Nguen Xuan Khang	Japan, Vietnam	2011
IPL-176	Slope data acquisition along highways in Sabah state for hazard assessment and mapping	Che Hassandi Abdullah	Malaysia	2012
IPL-177	Study on geological disasters focusing on landslides in and around Tegucigalpa City, Honduras	Anábal Godoy	Honduras	2012
IPL-179	Database of glacial lake outburst floods (GLOFs)	Adam Emmer Vit Vilímek	Czech Republic	2012
IPL-180	Introducing community-based early warning system for landslide hazard management in Cox's bazaar municipality, Bangladesh	N. M. S. I. Arambepola	Thailand	2011
IPL-181	Study of slow moving landslide Umka near Belgrade, Serbia	Biljana Abolmasov	Serbia	2012
IPL-182	Characterization of landslides mechanisms and impacts as a tool to fast risk analysis of landslides related disasters in Brazil	Renato Eugenio de Lima	Brazil	2012
<i>IPL-183</i>	<i>Landslides in West Africa: impacts, mechanism and management</i>	<i>Igwe Ogonnaya</i>	<i>Nigeria</i>	<i>2012</i>
IPL-184	Study of landslides in flysch deposits of North Istria, Croatia: sliding mechanisms, geotechnical properties, landslide modeling and landslide susceptibility	Željko Arbanas	Croatia	2012
IPL-185	Landslide hazards assessment and modeling sediment yield of landslides using geographic information system (GIS): a case study in the Rio El Estado on the SW flank of Pico de Orizaba volcano, Puebla-Veracruz, Mexico	Gabriel Legorreta Paulín	Mexico	2013
<i>IPL-186</i>	<i>Rock-fall hazard assessment and monitoring in the archaeological site of Petra, Jordan</i>	<i>Claudio Margottini</i>	<i>Italy</i>	<i>2013</i>
IPL-187	Design and validation of an early warning system for landslides—DeVEL	Rolf Katzenbach	Germany	2013
IPL-188	Study of slow-moving landslide Potoška planina (Karavanke Mountain, NW Slovenia)	Marko Komac	Slovenia	2013
IPL-190	Landslide risk identification and resilience study in tectonically active mountains and sea floors	Hiroshi Fukuoka	Japan	2013
IPL-191	Landslide hazard zonation in Carpathian region of Ukraine using GIS	Yakovliev Yevhenii Oleksandr M. Trofymchuk	Ukraine	2015
IPL-192	Development of post-earthquake rainfall induced landslide (PERIL) hazard mitigation framework	Binod Tiwari	USA	2015
IPL-193	Integrated systems for landslides monitoring, early warning and risk mitigation along motorways	Pasquale Versace	Italy	2015
IPL-194	Public awareness and education programme for landslides management in Malaysia	Che Hassandi Abdullah	Malaysia	2015
IPL-195	Study for mitigation and recovery of mud eruption disaster in East Java and modeling for risk reduction mudflow hazards	Paulus P. Rahardjo	Indonesia	2015
IPL-196	Development and applications of a multi-sensors drone for geohazards monitoring and mapping	Veronica Tofani	Italy	2015
IPL-197	Low frequency, high damaging potential landslide events in “low risk” regions—challenges for hazard and risk management	Jan Klimeš	Czech Republic	2015
IPL-198	Multi-scale rainfall triggering models for Early Warning of Landslides (MUSE)	Filippo Catani	Italy	2015
<i>IPL-199</i>	<i>The effect of root systems in natural slope erosion protection in the hill country of Sri Lanka</i>	<i>Pvip Perera</i>	<i>Sri Lanka</i>	<i>2015</i>
<i>IPL-200</i>	<i>An assessment of the rock fall susceptibility based on cut slopes adjacent to highways and railways</i>	<i>H. M. J. M. K. Herath</i>	<i>Sri Lanka</i>	<i>2015</i>
IPL-201	Landslide inventory and susceptibility map in durrës and Kavaja region	Hasan Kuliçi	Albania	2016
IPL-202	Ripley landslide monitoring project (Ashcroft, BC, Canada)	Peter Bobrowsky	Canada	2016

(continued)

Table 2 (continued)

IPL	Project title	Project leader	Country	Year
IPL-203	Analysis and identify of landslides based on species distribution and surface temperature difference	Ying Guo	China	2016
IPL-204	A study on socio-economic and environmental impacts of landslides	Surya Prakash	India	2016
IPL-205	Integrated systems for landslides monitoring, early warning and risk mitigation along motorways	Pasquale Versace Giovanna Capparelli	Italy	2016
IPL-206	Towards improved landslide mapping and forecasting	Fausto Guzzetti Mario Parise	Italy	2016
IPL-207	Evaluation on social research approach in determining “acceptable risk” and “tolerable risk” in landslide risk areas in Malaysia	Che Hassandi Bin Abdullah	Malaysia	2016
IPL-208	<i>Landslide disaster risk communication in mountain areas</i>	<i>Irasema Alcántara-Ayala</i>	<i>Mexico</i>	<i>2016</i>
IPL-209	Landslides and related sediment disaster project covering the entire South–East Nigeria, West Africa	Igwe Ogbonnaya	Nigeria	2016
IPL-210	Massive landsliding in Serbia following Cyclone Tamara in May 2014	Biljana Abolmasov	Serbia	2016
IPL-211	Development of wireless sensor network for monitoring and earlier warning of shallow and deep landslides (WISE-LAND)	Adrin Tohari	Indonesia	2016
IPL-212	The construction of a global database of giant landslides on oceanic island volcanoes	Matt Rowberry	Czech Republic	2016
IPL-213	Real-time landslide monitoring and early warning system in western ghats & Himalayas, India	Maneesha Vinodini Ramesh	India	2016
IPL-215	The development of paleo-landslides in the middle part of the Moskva river valley within the limits of the Moscow City	Oleg Zerkal	Russian Federation	2016
IPL-216	Diversity and hydrogeology of mass movements in the Vipava valley, SW Slovenia	Timotej Verbovšek	Slovenia	2016
IPL-217	<i>PROTHEGO—PROTection of European cultural HERitage from GeO–hazards</i>	<i>Daniele Spizzichino Claudio Margottini</i>	<i>Italy</i>	<i>2017</i>
IPL-218	Landslide rapid mapping from remote sensing	Ping Lu	China	2017
IPL-219	Rockfall hazard identification and rockfall protection in the coastal zone of Croatia	Željko Arbanas	Croatia	2017
IPL-220	Kostanjek landslide monitoring project (Zagreb, Croatia)	Martin Krkač	Croatia	2017
IPL-221	PS continuous streaming for landslide monitoring and mapping	Federico Raspi Silvia Bianchini, Andrea Ciampalini	Italy	2017
IPL-222	Landslide risk analysis and mitigation in the ancient rock-cut city of Vardzia (Georgia)	Claudio Margottini	Italy	2017
IPL-223	Landslides in Africa: understanding catastrophic failures and effective preventive measures in vulnerable regions of the continent	Igwe Ogbonnaya	Nigeria	2017
IPL-224	Combination of radar and optical remote sensing for hazard assessment of the potentially river-damming landslides: the cases of the Vakhsh and the and Brakmaputra Rivers	Alexander Strom	Russian Federation	2017
IPL-225	Recognition of potentially hazardous torrential fans using geomorphometric methods and simulating fan formation	Matjaž Mikoš	Slovenia	2017
IPL-226	Studying landslide movements from source areas to zone of deposition using a deterministic approach	Mateja Jemec Auflič	Slovenia	2017
IPL-227	Development of a web based landslide information system for the landslides in Sri Lanka	K. M. Weerasinghe	Sri Lanka	2017
IPL-228	BLISM (Bosnian landslide investigation and stabilization method)	Sabid Zekan	Bosnia and Herzegovina	2017
IPL-230	Evolution-based key technology of landslide prevention in Three Gorges Reservoir region, China	Huiming Tang	China	2018
IPL-231	Landslide mechanism considering soil–water–vegetation coupling effects	Su Lijun	China	2018

(continued)

Table 2 (continued)

IPL	Project title	Project leader	Country	Year
IPL-232	Investigations on landslides in Nilgiris, Tamil Nadu, India	S. S. Chandrasekaran	India	2018
IPL-233	Archival records and documentation of some socio-economically significant landslides in India	Surya Parkash	India	2018
IPL-234	Development of landslide detection system based on rainfall prediction and seismic aspect in Banjarnegara Region, Centre of Java, Indonesia	Munawar	Indonesia	2018
IPL-235	EO4GEO—towards an innovative strategy for skills development and capacity building in the space geo-information sector supporting Copernicus user uptake	Luca Guerrieri Daniele Spizzichino	Italy	2018
IPL-236	A multiparametric field laboratory for the investigation on the relationship between material behavior and morphodynamic of landslides	Andrea Segalini	Italy	2018
IPL-237	The role of time-dependent rock mass deformations and landscape evolution rates as predisposing factors for massive rock slope failures	Carlo Esposito	Italy	2018
IPL-238	Landslides threatening Russian cultural heritage sites	D. N. Gobotsov	Russian Federation	2018
IPL-239	Detailed interpretation and evaluation of dynamic model behavior of Pothupitiya landslide potential area (combined ground water and slope stability dynamic model under PC raster environment)	A A Virajh Dias	Sri Lanka	2018
IPL-240	Global lecture series—recent advances on landslide analysis and remediation	Binod Tiwari	USA	2018
IPL-242	Studies of disasters related to natural and anthropogenic landslides in Brazil—characterization of landslides triggers and impacts as a tool to rapid risk analysis	Renato Eugenio de Lima	Brazil	2019
IPL-243	Wildfire-related landslides in Italy: triggering mechanisms and propagation processes	Giuseppe Mandrone	Italy	2019
IPL-244	Evolution mechanism and control of landslides induced by sudden rainstorm	Huiming Tang	China	2019
IPL-245	Laboratory physical modeling of rainfall, slope deformation and landslides triggering	Giovanna Capparelli	Italy	2019
IPL-246	Classification and spatial distribution of landslides on dumps in brown coal basin in the Czech Republic	Martin Veselý	Czech Republic	2019
IPL-248	Innovation in slow-moving landslide risk assessment of roads and urban sites by combining multi-sensor multi-source monitoring data	Dario Peduto	Italy	2019
IPL-249	Development of early warning technology of rain-induced rapid and long-travelling landslides in Sri Lanka	Kazuo Konagai Asiri Karunawardena	Japan, Sri Lanka	2019
IPL-250	Investigation of ecohydrological processes on soil-root mechanical properties and landslide susceptibility in the steep terrain regions, Eastern Tibetan Plateau	Peng Cui	China	2020
IPL-251	Advancing landslide early warning systems using machine learning & artificial intelligence techniques	Maneesha Vinodini Ramesh	India	2020
IPL-252	Landslide monitoring with cost-effective GNSS devices and development of a new equipment (LZERO) for real-time applications	David Zuliani	Italy	2020
IPL-253	Integrated landslide disaster risk research in Mexico	Irasema Alcantara-Ayala	Mexico	2020
IPL-254	Ukraine cultural heritage objects within landslide hazardous sites	Oleksandr M. Trofymchuk	Ukraine	2020

The initial stage of the International Programme on Landslides (IPL: 2002–2008) was under support from UNESCO Coordinating projects (C by multiple members) and Member projects (M by a single member). IPL projects receiving IPL Award of Success are given in italic

Table 3 All recognized world centres of excellence for landslide risk reduction since 2008 in the chronological order (Han et al. 2017, 2020; Bobrowsky and Sassa 2022)

No	Title	Leader	Country	Organization
World centre of excellence 2008–2011				
1	Scientific research for mitigation, preparedness and risk assessment of landslides	Yuepin Yin	China	China geological survey
2	Landslide field research and capacity building through international collaboration	Vit Vlímek	Czech Republic	Faculty of science, Charles university in Prague
3	Earth observation advanced technologies for landslide monitoring, management and mitigation	Nicola Casagli	Italy	Department of earth science, University of Florence
4	Research and development of advanced technology for landslide hazard analysis	Alberto Presitininzi Gabriele Scarascia-Mugnozza	Italy	Research centre on prediction prevention and control of georisks of Rome University “La Sapienza”
5	Development of methodology for risk assessment of the earthquake-induced landslides	Hideaki Marui	Japan	The Japan Landslide Society (JLS)
6	Implementation of national slope master plan	Ashaari Mohamad Che Hassandi bin Abdullah	Malaysia	Slope engineering branch, public works department of Malaysia
7	Research on mitigation of landslide risk and training of specialists	Farrokh Nadim	Norway	International centre for Geohazards (ICG) at NGI
8	International summer school on rockslides and related phenomena in the Kokomeren river basin, Kyrgyzstan	Alexander Strom	Russian Federation & Kyrgyz Republic	Institute of geospheres dynamics of Russian academy of science (IDG RAS) & Kyrgyz institute of seismology (KIS)
9	Mechanisms of landslides in over-consolidated clays and flysch	Bojan Majes Matjaž Mikoš	Slovenia	University of Ljubljana, faculty of civil and geodetic engineering (UL FGG)
10	Landslide inventorization and susceptibility mapping in South Africa	S. Diop SG Chiliza	South Africa	Engineering geoscience unit, council for geoscience
11	Promoting knowledge sharing, innovations and institutions with south–south focus network on landslide risk reduction in Asia	N. S. M. I. Arambepola	Thailand	Asian disaster preparedness center
12	Conduct landslide hazard assessments and develop early warning systems	Peter Lyttle	USA	U.S. geological survey
World centre of excellence 2011–2014				
1	Canadian landslide loss risk reduction strategy and implementation	Peter T. Bobrowsky	Canada	Geological survey of Canada
2	Risk assessment and disaster mitigation code for long run-out landslides	Yueping Yin	China	China geological survey
3	Scientific research for landslide risk analysis and international education for mitigation and preparedness	Vit Vilímek	Czech Republic	Charles university, faculty of science
4	Research on landslide risk management harmonisation in support to European union policy making	Javier Hervás	European commission	Joint research centre, European commission
5	Training, research and documentation on landslides risk management	Surya Parkash	India	National institute of disaster management
6	Development of community-based and most adaptive technology for landslide risk reduction	Dwikorita Karnawati	Indonesia	Universitas Gadjah Mada
7	Advanced technologies for landslides	Nicola Casagli Filippo Catani	Italy	Department of earth science, university of Florence
8	Development of a methodology for risk reduction of earthquake-induced landslides	Daisuke Higaki	Japan	The Japan landslide society (JLS)
9	Risk identification and land-use planning for disaster mitigation of landslides	Hideaki Marui	Japan	Niigata university, institute for natural hazards and disaster recovery

(continued)

Table 3 (continued)

No	Title	Leader	Country	Organization
10	Landslide monitoring and community based early warning systems	Irasema Alcántara-Ayala	Mexico	National autonomous university of Mexico
11	Research on mitigation of landslide risk and training of specialists	Farrokh Nadim	Norway	International centre for geohazards at NGI
12	Annual Summer school on rockslides and related phenomena in Kyrgyzstan	Alexander Strom	Russian Federation & Kyrgyz Republic	Inst. of geospheres dynamics of Russian academy of sciences & Kyrgyz institute of seismology
13	Mechanisms of landslides in over-consolidated clays and flysch	Bojan Majes	Slovenia	University of Ljubljana, faculty of civil and geodetic engineering (UL FGG)
14	Promoting knowledge, innovations and institutions with south-south focus through a regional network of landslide risk reduction	N. S. M. I. Arambepola	Thailand	Asian disaster preparedness center
15	Scientific research for landslide hazard analysis, U. S. geological survey	Peter Lyttle	USA	U.S. geological survey landslide programme
World centre of excellence 2014–2017				
1	Formation mechanism research, disaster warning and universal education of cold regions landslide	Wei Shan	China	Research center of cold regions landslide
2	Scientific research for mitigation, preparedness and risk assessment of landslides	Wang Min	China	China geological survey
3	Scientific research for landslide risk analysis, modeling, mitigation and education	Liang-Jenq Leu	Chinese Taipei	Department of civil engineering, national Taiwan university
4	Landslide risk reduction in the Adriatic-Balkan region through the regional cooperation	Željko Arbanas Snježana Mihalčić Arbanas	Croatia	Croatian landslide group
5	Landslide risk assessment and development guidelines for effective risk reduction	Josef Stemberk	Czech Republic	Institute of rock structure and mechanics Czech academy of sciences & charles university, faculty of science
6	Development of community-based and most adaptive technology for landslide risk reduction	Dwikorita Karnawati	Indonesia	Universitas Gadjah Mada, Yogyakarta
7	Advanced technologies for landslides (ATLaS)	Nicola Casagli	Italy	Department of earth science, university of Florence
8	Emergency response support system for large-scale landslide disasters	Satoshi Tsuchiya	Japan	The Japan landslide society (JLS)
9	Risk identification and land-use planning for disaster mitigation of landslides	Hiroshi Fukuoka	Japan	Niigata university, institute for natural hazards and disaster recovery
10	Implementation of national slope master plan	Che Hassandi Abdullah	Malaysia	Slopes engineering branch, public works department of Malaysia
11	Building human capacities and expertise in landslide disaster risk managements	Ogbonnaya Igwe	Nigeria	Department of geology, university of Nigeria, Nsukka, Nigeria
12	International summer school on rockslides and related phenomena in the Kokomeren river valley, Tien Shan, Kyrgyzstan	Alexander Strom	Russian Federation & Kyrgyz Republic	Geodynamics research center—branch of JSC “Hydroproject institute” & institute of seismology of national academy of sciences of Kyrgyz Republic
13	Mechanisms of landslides and creep in over-consolidated clays and flysch	Ana Petkovšek	Slovenia	University of Ljubljana, faculty of civil and geodetic engineering (UL FGG)
14	Developing model policy frameworks, standards and guidelines	Nihal Rupasinghe A. A. Virajh Dias	Sri Lanka	Central engineering consultancy Bureau, Colombo
15	Promoting knowledge, innovations and institutions with south-south focus through a regional network of landslide risk reduction in changing climate scenario in Asia	N. M. S. I. Arambepola	Thailand	Asian disaster preparedness center (ADPC)

(continued)

Table 3 (continued)

No	Title	Leader	Country	Organization
World centre of excellence 2017–2020				
1	Landslide monitoring and critical infrastructure	Peter T. Bobrowsky	Canada	Geological survey of Canada
2	Scientific research for mitigation, preparedness and risk assessment of landslides	Yueping Yin	China	China geological survey
3	Formation mechanism research, disaster warning, and universal education of landslides in permafrost regions	Wei Shan	China	Institute of cold regions science and engineering, Northeast forestry University
4	Center for applied landslide research (CALaR)	Snjezana Mihalić Arbanas, Željko Arbanas	Croatia	Croatian landslide group from university of Zagreb and university of Rijeka
5	Landslide risk assessment and development guidelines for effective risk reduction—continuation	Vit Vilimek	Czech Republic	Charles University, Faculty of Science & Institute of Rock Structure and Mechanics Czech Academy of Sciences
6	Enhancement of the existing real-time landslide monitoring and early warning system in western ghats & Himalayas, India	Maneesha V Ramesh	India	Amrita university
7	Development of community-based and most adaptive technology for landslide risk reduction	Dwikorita Karnawati	Indonesia	University of Gadjah Mada
8	ATLaS: advanced technologies for landslides	Nicola Casagli	Italy	Department of Earth Sciences, University of Florence
9	Methods and tools for landslide forecasting and risk mitigation and adaptation strategies	Fausto Guzzetti	Italy	Istituto di Ricerca per la Protezione Idrogeologica (IRPI), of the Italian national research council (CNR)
10	Landslide hazards mitigation programs in the Korean demilitarized zone	Sangjun Im	Korea	Korean society of forest engineering
11	Landslide quantitative risk analysis study for Malaysia	Che Hassandi Abdullah	Malaysia	Slope engineering branch, public works department of Malaysia
12	Landslides integrated research for disaster risk reduction	Irasema Alcántara Ayala	Mexico	National autonomous university of Mexico (UNAM)
13	Characterizing past and planned activities: Klima 2050—innovational methods for risk reduction associated to hydro-meteorologically induced landslides	José Cepeda	Norway	Norwegian geotechnical institute (NGI)
14	Central Asia rockslide inventory. Compilation and analysis	Alexander Strom	Russian Federation	JSC “Hydroproject institute”
15	Harmonization of landslide data and local communities capacity building for landslide risk reduction	Biljana Abolmasov	Serbia	University of Belgrade, faculty of mining and geology
16	Landslides in weathered flysch: from activation to deposition	Ana Petkovšek	Slovenia	University of Ljubljana, faculty of civil and geodetic engineering (UL FGG)
17	Landslide risk reduction in Slovenia	Mateja Jemec Auflič	Slovenia	Geological survey of Slovenia
18	Model policy frameworks, standards, and guidelines on landslide disaster risk reduction	A. A. Virajh Dias	Sri Lanka	Central engineering consultancy Bureau (CECB)
19	Characterizing past and planned activities: NBRO is the national focal point for landslide disaster risk management	Asiri Karunawardena	Sri Lanka	National building research organization
20	Implementation of national slope master plan	Oleksander Trofymchuk	Ukraine	The institute of telecommunication and global information space (ITIGS) of the national academy of science of Ukraine (NASU)

(continued)

Table 3 (continued)

No	Title	Leader	Country	Organization
World centre of excellence 2020–2023				
1	Slow moving translational landslides in argillaceous soils and weak rocks	Michael T. Hendry	Canada	University of Alberta
2	Formation mechanism research, disaster warning, and universal education of cold regions landslide	Wei Shan	China	Research center of cold regions landslide
3	Landslide modeling: from physical to phenomenological models	Željko Arbanas Snježana Mihaljić Arbanas	Croatia	Croatian landslide group
4	Community centered landslide disaster risk reduction in changing climate, continuation	Josef Stemberk	Czech Republic	Institute of rock structure and mechanics Czech academy of sciences & Charles university, faculty of science
5	Documentation, training and capacity enhancement on landslides risk reduction and resilience	Surya Parkash	India	National institute of disaster management (NIDM), Ministry of home affairs, government of India, New Delhi
6	Internet of things (IoT) for landslide disaster risk reduction	Maneesha V Ramesh	India	Amrita Vishwa Vidyapeetham, Amritapuri campus
7	Development of risk reduction strategy and technological innovation for landslide mitigation	Teuku Faisal Fathani	Indonesia	Universitas Gadjah Mada
8	Development of multidisciplinary and integrated methodologies for mitigating geological risks	Francesca Bozzano	Italy	CERI—Centro di Ricerca Previsione, Prevenzione e Controllo dei Rischi Geologici (Research centre on geological risks)—Sapienza Università di Roma
9	Advanced technologies for landslides (ATLaS)	Nicoa Casagli	Italy	UNESCO chair for the prevention and the sustainable management of geo-hydrological hazards, university of Florence
10	Integrated research on landslide disaster risk	Irasema Alcántara-Ayala	Mexico	Institute of geography, national autonomous university of Mexico (UNAM)
11	Landslides in weathered heterogeneous sedimentary rock masses such as Flysch	Matjaž Mikoš	Slovenia	University of Ljubljana, faculty of civil and geodetic engineering (UL FGG)
12	International training course on slope land disaster reduction	Louis Ge	Chinese Taipei	Department of civil engineering, national Taiwan university
13	National Slope Master Plan, method of certification heritage objects in hazardous landslide sites	Oleksandr Trofymchuk	Ukraine	The institute of telecommunication and global information space (ITIGS) of the national academy of science of Ukraine (NASU), research institute of building constructions (RIBC)
14	Developing model policy frameworks, standards, and guidelines on landslide disaster reduction	S. S. I. Kodagoda	Sri Lanka	Central engineering consultancy Bureau
15	Research on landslide initiation mechanism based on physical model	Katsuo Sasahara & Asiri Karunawardena	Japan & Sri Lanka	The Japan landslide society & national building research organisation
16	Bridging science, policies, and partnership for landslide risk management	Hans Guttman	Thailand	Asian disaster preparedness center (ADPC)
17	Central Asia rockslide inventory. compilation, analysis and training	Alexander Strom	Russian Federation	JSC “Hydroproject institute”
18	Harmonization of landslides data and national authorities capacity building for landslide risk reduction—continuation	Biljana Abolmasov	Serbia	University of Belgrade, Faculty of Mining and Geology
19	Landslide susceptibility map assessment base on climatological changes using geographic information systems	Ir. Hj. Zulkifly Bin A. Ghani	Malaysia	Slope engineering branch, public work department Malaysia

References

- Bobrowsky P, Sassa K (2022) Awards and certificates at the fifth world landslide forum. *Landslides* 19(1):249–262. <https://doi.org/10.1007/s10346-021-01822-2>
- Casagli N, Falorni G, Tofani V (2009) Projects of international programme on landslides. In: Sassa K, Canuti P (eds) *Landslides—disaster risk reduction*. Springer, Berlin, Heidelberg. pp 15–28. https://doi.org/10.1007/978-3-540-69970-5_2
- Casagli N, Tofani V (2019) Department of earth sciences, university of Florence. *Landslides* 16(9):1809–1813. <https://doi.org/10.1007/s10346-019-01226-3>
- Han Q (2020) Foreword by Han Qunli. *Landslides* 17(10):2247. <https://doi.org/10.1007/s10346-020-01517-0>
- Han Q, Sassa K, Kan FM, Margottini C (2017) International programme on landslides (IPL): objectives, history and list of world centres of excellence and IPL projects. In: Sassa K, Mikoš M, Yin Y (eds) *Advancing culture of living with landslides, vol 1 ISDR-ICL Sendai partnerships 2015–2025*. Springer Open, Cham, Switzerland. (ISBN 978-3-319-53500-5), pp 229–246. https://doi.org/10.1007/978-3-319-59469-9_19
- Han Q, Sassa K, Mikoš M (2020) International programme on landslides (IPL): a programme of the ICL for landslide disaster risk reduction. In: Sassa K, Mikoš M, Sassa S, Bobrowsky PT, Takara K, Dang K (eds) *Understanding and reducing landslide disaster risk, vol 1 Sendai partnerships and Kyoto landslide commitment*. Springer Nature, Switzerland. (ISBN 978-3-030-60195-9). https://doi.org/10.1007/978-3-030-60196-6_11
- ICL (2018a) Announcement of 2018 ICL-IPL conference in Kyoto, Japan—planning of the fifth world landslide forum (WLF5) and the Kyoto 2020 commitment (KC2020). *Landslides* 15(7):1449–1451. <https://doi.org/10.1007/s10346-018-1016-y>
- ICL (2018b) The global promotion committee of the international programme on landslides (IPL) and IPL world centre. *Landslides* 15(7):1453–1455. <https://doi.org/10.1007/s10346-018-1012-2>
- ICL (2022) The international consortium on landslides. <http://wlf6.org>. Accessed 18 Feb 2022
- ISDR-ICL (2008) The first world landslide forum—implementing the 2006 Tokyo action plan on the international programme on landslides (IPL). *Landslides* 5(2):243–249. <https://doi.org/10.1007/s10346-008-0124-5>
- Margottini C, Canuti P, Sassa K (2010) Putting science into practice: the second world landslide forum, Rome, 3–9 October 2011. *Landslides* 7(3):367–373. <https://doi.org/10.1007/s10346-010-0235-7>
- Matsuoka Y, Gonzales Rocha E (2020) Sendai voluntary commitments: landslide stakeholders and the all-of-society approach enhanced by UNDRR. *Landslides* 17(10):2253–2269. <https://doi.org/10.1007/s10346-020-01519-y>
- Mikoš M (2018) The bibliometric impact of books published by the international consortium on landslides. *Landslides* 15(8):1459–1482. <https://doi.org/10.1007/s10346-018-1019-8>
- Mikoš M, Petkovšek A (2019) Faculty of civil and geodetic engineering, university of Ljubljana. *Landslides* 16(9):1815–1819. <https://doi.org/10.1007/s10346-019-01231-6>
- Mikoš M, Yin Y, Sassa K (2017) The fourth world landslide forum, Ljubljana, 2017. *Landslides* 14(5):1843–1854. <https://doi.org/10.1007/s10346-017-0889-5>
- Mikoš M, Mihalić Arbanas S (2014) Activities of the international programme on landslides (IPL): IPL projects and world centres of excellence on landslide risk reduction (WCoE). In: Sassa K, Canuti P, Yin Y (eds) *Landslide science for a safer geoenvironment, vol 1 the international programme on landslides (IPL)*. Springer, Switzerland. pp xvii–1 (ISBN 978-331904998-4). <https://doi.org/10.1007/978-3-319-04999-1>
- Mikoš M, Sassa K, Arbanas Ž (2021) The ICL journal landslides—16 years of capacity development for landslide risk reduction. In: Sassa K, Mikoš M, Sassa S, Bobrowsky PT, Takara K, Dank K (eds) *Understanding and reducing landslide disaster risk, vol 1 Sendai landslide partnerships and Kyoto landslide commitment*. Springer, Cham. pp 163–177 (ISBN 978-3-030-60195-9). https://doi.org/10.1007/978-3-030-60196-6_9
- Sassa K (2004a) Preface. *Landslides* 1(1):1–5. <https://doi.org/10.1007/s10346-004-0011-7>
- Sassa K (2004b) The international consortium on landslides. *Landslides* 1(1):91–94. <https://doi.org/10.1007/s10346-004-0012-6>
- Sassa K (2004c) The international programme on landslides (IPL). *Landslides* 1(2):95–99. <https://doi.org/10.1007/s10346-004-0016-2>
- Sassa K (2004d) Opening ceremony of the UNESCO-Kyoto university-ICL UNITWIN programme headquarters building. *Landslides* 1(3):315–323. <https://doi.org/10.1007/s10346-004-0037-x>
- Sassa K (2006) “2006 Tokyo action plan”—strengthening research and learning on landslides and related earth system disasters for global risk preparedness. *Landslides* 3(4):361–369. <https://doi.org/10.1007/s10346-006-0065-9>
- Sassa K (2009a) Progress of the international programme on landslides (IPL)—objectives of the IPL and the world landslide forum. In: Sassa K, Canuti P (eds) *Landslides—disaster risk reduction*. Springer, Berlin, Heidelberg, pp 3–14. https://doi.org/10.1007/978-3-540-69970-5_1
- Sassa K (2009b) Report of the 2008 first world landslide forum on 18–21 November 2008 at UNU, Tokyo. *Landslides* 6(3):167–179. <https://doi.org/10.1007/s10346-009-0161-8>
- Sassa K (2013) International programme on landslides. In: Sassa K, Rouhban B, Briceño S, McSaveney M, He B (eds) *Landslides: global risk preparedness*. Springer, Berlin, Heidelberg, pp 3–24. https://doi.org/10.1007/978-3-642-22087-6_1
- Sassa K (2015) ISDR-ICL Sendai partnerships 2015–2025 for global promotion of understanding and reducing landslide disaster risk. *Landslides* 12(4):631–640. <https://doi.org/10.1007/s10346-015-0586-1>
- Sassa K (2016) Implementation of the ISDR-ICL Sendai partnerships 2015–2025 for global promotion of understanding and reducing landslide disaster risk. *Landslides* 13(2):211–214. <https://doi.org/10.1007/s10346-016-0690-x>
- Sassa K (2017a) The fifth world landslide forum—implementing and monitoring the ISDR-ICL Sendai partnerships 2015–2025. *Landslides* 14(3):1282–1288. <https://doi.org/10.1007/s10346-017-0828-5>
- Sassa K (2017b) The 2017 Ljubljana declaration on landslide risk reduction and the Kyoto 2020 commitment for global promotion of understanding and reducing landslide disaster risk. *Landslides* 14(4):1289–1296. <https://doi.org/10.1007/s10346-017-0857-0>
- Sassa K (2017c) The fifth world landslide forum. *Landslides* 14(5):1857–1859. <https://doi.org/10.1007/s10346-017-0859-y>
- Sassa K (2021a) The Kyoto landslide commitment 2020: launched. *Landslides* 18(1):5–20. <https://doi.org/10.1007/s10346-020-01575-4>
- Sassa K (2021b) New open access book series “Progress in landslide research and technology.” *Landslides* 18(11):3509–3512. <https://doi.org/10.1007/s10346-021-01759-6>
- Sassa K (2022a) The fifth world landslide forum and progress of the open access book series for Kyoto landslide commitment 2020. *Landslides* 19(1):1–5. <https://doi.org/10.1007/s10346-021-01820-4>
- Sassa K (2022b) Speakers and titles of oral presentation in WLF5. *Landslides* 19(1):225–247. <https://doi.org/10.1007/s10346-021-01821-3>
- Sassa K (2022c) The international consortium on landslides. This volume
- Sassa K, Dang K (eds) (2017) *Proceedings of 2017 IPL symposium on landslides, 29 November 2017. Paris, France, p. 148*. (ISBN

- 978-4-9903382-4-4). <http://iplhq.org/icl/wp-content/uploads/2017/12/2017-IPL-Symposium-Proceedings.pdf>
- Sassa K, Dang K (eds) (2018) Proceedings of 2018 IPL symposium on landslides, 3 December 2018. Kyoto, Japan, p. 289. (ISBN 978-4-9903382-0-6). <http://icl.iplhq.org/icl/wp-content/uploads/2019/02/2018-IPL-Symposium-on-Landslides-Proceedings.pdf>
- Sassa K, Dang K (eds) (2019) Proceedings of 2019 IPL symposium on landslides, 16–19 September 2019. Paris, France, p. 374. (ISBN 978-4-9903382-5-1). <http://iplhq.org/icl/wp-content/uploads/2019/10/Proceedings-2019-IPL-Symposium-on-Landslides-ISBN-978-4-9903382-5-1-2019.10.04.pdf>
- Sassa K, Canuti P, Margottini C, Yin Y (2012) The second world landslide forum, Rome, 2011 and the third world landslide forum, Beijing, 2014. *Landslides* 9(2):285–297. <https://doi.org/10.1007/s10346-012-0328-6>
- Sassa K, Fukuoka H, Wang F, Wang G (eds) (2005) *Landslides—risk analysis and sustainable disaster management*. Springer, Berlin, p 385. (ISBN 978-3-540-28664-6)
- Sassa K, Fukuoka H, Dang K (eds) (2014) Proceedings of the international forum “Urbanization and landslides disaster”, 8 October 2014. Kyoto, Japan, p. 121. <http://icl.iplhq.org/icl/wp-content/uploads/2016/03/Hiroshima-Proceedings.pdf>
- Sassa K, Yin Y, Canuti P (2015) The third world landslide forum, Beijing, 2014. *Landslides* 12(1):177–192. <https://doi.org/10.1007/s10346-015-0555-8>

Open Access This chapter is licensed under the terms of the Creative Commons Attribution 4.0 International License (<http://creativecommons.org/licenses/by/4.0/>), which permits use, sharing, adaptation, distribution and reproduction in any medium or format, as long as you give appropriate credit to the original author(s) and the source, provide a link to the Creative Commons license and indicate if changes were made.

The images or other third party material in this chapter are included in the chapter’s Creative Commons license, unless indicated otherwise in a credit line to the material. If material is not included in the chapter’s Creative Commons license and your intended use is not permitted by statutory regulation or exceeds the permitted use, you will need to obtain permission directly from the copyright holder.



Original Articles



Understanding and Reducing the Disaster Risk of Landslide-Induced Tsunamis: Outcome of the Panel Discussion and the World Tsunami Awareness Day Special Event of the Fifth World Landslide Forum

Shinji Sassa, Stephan T. Grilli, David R. Tappin, Kyoji Sassa, Dwikorita Karnawati, Viacheslav K. Gusiakov, and Finn Løvholt

Abstract

Landslide-induced tsunamis are one of the most important cascading multi-hazard risks in light of landslide disasters. During the Fifth World Landslide Forum, a World Tsunami Awareness Day Special Event was held in hybrid mode on 5 November 2021. This article presents the outcome of the panel discussion organized across America, Europe, and Asia, as well as a review of the special event for understanding and reducing the disaster risk of landslide-induced tsunamis.

Keywords

Landslide-induced tsunami • Hazard mapping • Early warning • Multi-phased physics • Multiple mechanisms

S. Sassa (✉)

Port and Airport Research Institute, National Institute of Maritime, Port and Aviation Technology, Yokosuka, Japan
e-mail: sassa@p.mpat.go.jp

S. T. Grilli

Department of Ocean Engineering, University of Rhode Island, Narragansett, RI, USA
e-mail: grilli@uri.edu

D. R. Tappin

British Geological Survey, Keyworth, Nottingham, UK
e-mail: drta@bgs.ac.uk

K. Sassa

International Consortium on Landslides, Kyoto, Japan

D. Karnawati

Agency for Meteorology, Climatology and Geophysics of the Republic of Indonesia, Jakarta, Indonesia
e-mail: dwiko@bmgk.go.id

V. K. Gusiakov

Institute of Computational Mathematics and Mathematical Geophysics, Russian Academy of Sciences, Novosibirsk, Russia
e-mail: gvk@sscc.ru

F. Løvholt

Norwegian Geotechnical Institute, Oslo, Norway
e-mail: Finn.Lovholt@ngi.no

1 Introduction

During the Fifth World Landslide Forum (WLF5), in Kyoto, Japan, a World Tsunami Awareness Day Special Event was organized on November 5th, 2021, following a Landslide-induced Tsunami session held on November 4th, 2021. A total of twenty-three relevant papers from thirteen countries/regions were presented and included in the four types of publications for WLF5: Thematic Issue of Journal Landslides (3; 2020), Full Color Book (11; Sassa et al. 2020), Electronic Proceedings (3; 2020) and One-Page Abstract Volume (6; 2021). The key topics ranged from numerical modelling and analysis of landslide-generated waves in rivers, to tsunami uncertainty due to landslide dynamics, using statistics to understand submarine landslide processes and hazard, tsunamis from submarine landslides triggered on islands, simulations of tsunami waves induced by coastal and submarine landslides, tsunami generation by volcanic flank collapse, underestimated tsunami hazard from submarine landslides, landslide-induced icy tsunamis in a reservoir, tsunami early warning system, and tsunami disaster caused by earthquake-induced submarine landslides.

In the World Tsunami Awareness Day Special Event of WLF5, a panel discussion was held across America, Europe, and Asia, for better understanding and reducing the disaster risk of landslide-induced tsunamis, consistent with the Kyoto Landslide Commitment 2020 (KLC2020). Shinji Sassa (S. S.) served as the coordinator of the World Tsunami Awareness Day Special Event during WLF5, and organized the Panel Discussion. The panelists were Stephan T. Grilli (USA), David R. Tappin (UK), Kyoji Sassa (Japan), Dwikorita Karnawati (Indonesia), Viacheslav K. Gusiakov (Russia), and Finn Løvholt (Norway) (S. G., D. T., K. S., D. K., V. G., F. L., respectively). This article presents the outcome of the panel discussion as well as a review of the World Tsunami Awareness Day Special Event of WLF5.

2 Review of the World Tsunami Awareness Day Special Event

The World Tsunami Awareness Day Special Event of WLF5 featured a total of eleven relevant presentations concerning landslide-induced tsunamis, which will be reviewed as below.

F. Løvholt addressed landslide tsunami uncertainty and presented a probabilistic tsunami hazard analysis (LPTHA) framework for analysing uncertainties emerging from the landslide source processes. An example is presented for the Lyngen fjord in Norway. The statistics of the fall height (H) to run-out length (L) ratio as a function of the volume for large rockslides in Norway is shown in Fig. 1. Comparing

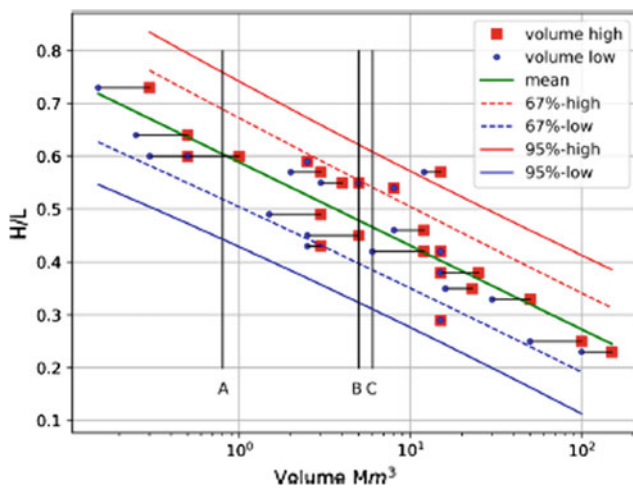


Fig. 1 Regression analysis of the run-out statistics of rock slides in Norway: H is the fall height, L is the total horizontal run out distance. The vertical lines A, B and C indicate the volumes of 0.8, 5 and 6 Mm^3 , respectively (Fig. 7 in Løvholt et al. 2020)

tsunami inundation maps considering three different levels of magnitude frequency distributions (MFDs, Fig. 2) displays that the tsunami run-up height is highly sensitive to these uncertain landslide parameters pertaining to landslide dynamics.

D. Minh Duc analysed a landslide-induced tsunami-like wave in the Truong river in Vietnam. A heavy rainfall induced a landslide along bedrock of weathered granite that caused an impulsive wave across the river, affecting houses in a residential area (Fig. 3). The results of the numerical analysis combined with the observations of the landslide scarp, deposit and tsunami traces indicate that a rapid landslide motion with a maximum speed of 16.4 m/s generated a maximum wave height of 5 m (Fig. 4).

J. Blahút reported an attempt to model a tsunami genesis and propagation from an incipient volcano slope failure termed San Andres Landslide on Canary Islands, Spain. The scenario comprised a subaerial failure of a block more than 2.5 km long and 7.5 km wide (Fig. 5). The landslide-induced initial wave could reach 80 m with its propagation through Atlantic Ocean. The results show that a more accurate landslide dynamic modelling is crucial to obtain realistic behaviour of the sliding mass to assess possible tsunami scenarios.

K. Ikehara showed the linkage between upper-slope submarine landslides and mass transport deposits in the hadal environment. There are many submarine landslides distributed along the upper slope of the Hidaka Trough, Japan (Fig. 6). The results of the investigations on the sediment cores in the Japan Trench indicate that the upper slope is the origin of mass transport deposits (MTD), and therefore an area of large sediment movements, which should be considered in the context of tsunami hazard mitigation.

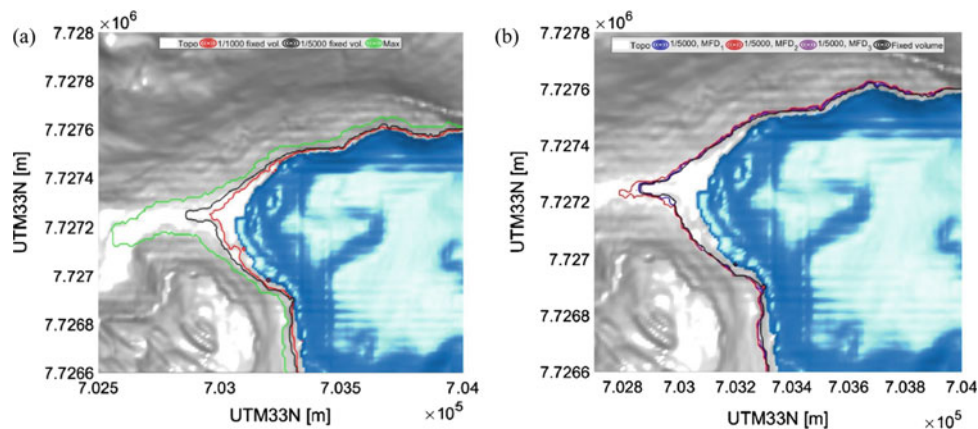


Fig. 2 **a** Inundation height exceedance probabilities for the Lyngen site using the fixed volume approach. Three different levels of MFDs are considered: 1/1000 $year^{-1}$ (red line), 1/5000 $year^{-1}$ (black line) and

the maximum inundated area overall simulations (green line). **b** Case of 1/5000 $year^{-1}$ with synthetic MFDs (Figs. 5 and 9 in Løvholt et al. 2020)

Fig. 3 3D view of the landslide in the Truong river, Vietnam (Fig. 1b in Minh Duc et al. 2020)

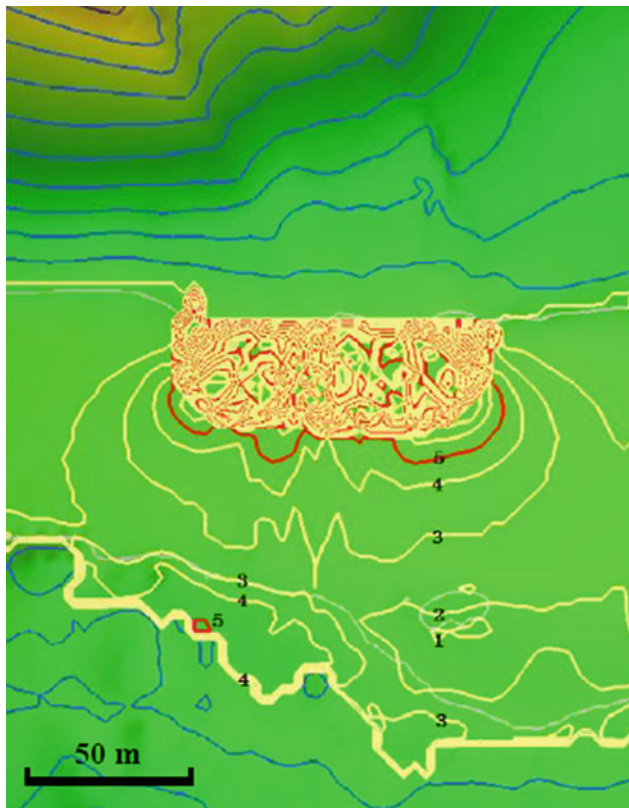
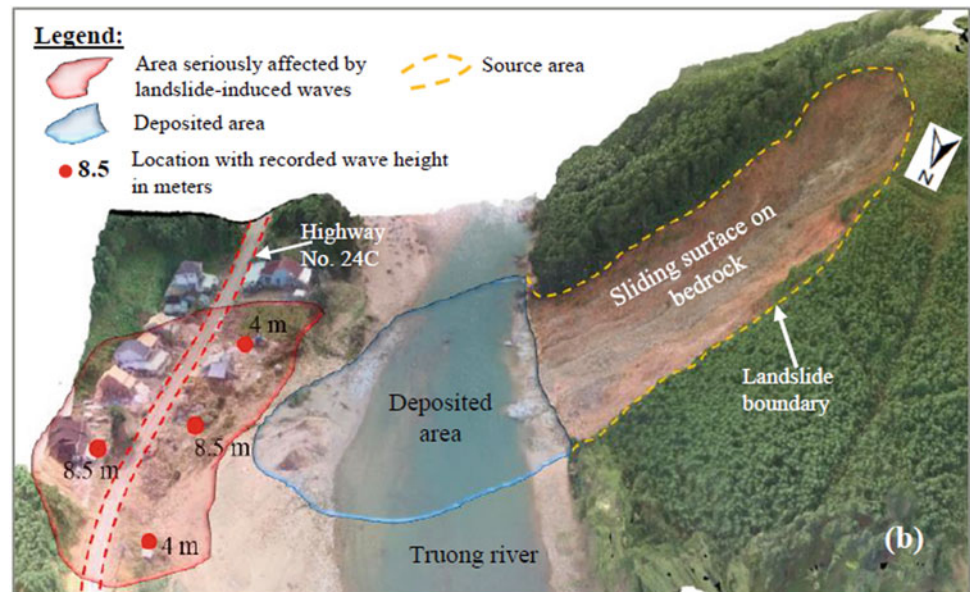


Fig. 4 Contour of the maximum tsunami height simulated. The reaching out line is shown in bold yellow where the tsunami wave moved up to the land with the maximum height of 5 m. (Fig. 11 in Minh Duc et al. 2020)

S. Sassa summarized the landslide-induced tsunami papers for the Fifth World Landslide Forum, and presented a review of large-scale coastal mass movements and their

impacts worldwide, showing the importance of liquefied flows in tsunami generation. The dynamics of liquefied gravity flows is governed by the multi-phased physics (Fig. 7). The cascading mechanisms of the 2018 Indonesia Sulawesi earthquake and tsunami disasters are highlighted in light of the concurrent processes involving liquefaction, coastal and submarine landslides, and multiple tsunamis (Fig. 8).

N. Casagli presented monitoring and early warning of landslides with special reference to Stromboli landslide-induced tsunami. The Stromboli island volcanic activity has induced mass flows causing tsunamis with an average of 1 tsunami every 20 years (Fig. 9). The integration of space-borne and ground-based Synthetic Aperture Radar displacement data with the analysis of change detection (Fig. 10) allowed the identification of the evolution of the slope instability phenomena and hence could be an effective tool for early warning of eruptions, landslides and tsunami.

K. Sassa presented the history of development of the undrained dynamic-loading ring-shear apparatus and the integrated simulation model for the evaluation of the initiation and motion of landslides as well as a new landslide-induced tsunami model based on the aforementioned landslide dynamics. The validity has been confirmed with the world's largest well-documented landslide tsunami disaster with 15,153 deaths in Unzen, Japan in 1972. The application to potential retrogressive Senoumi landslides in Suruga bay shows tsunami inundation depths of 20–50 m in Yaizu city (Fig. 11).

S. Grilli presented a series of studies on tsunami generation by the 2018 volcanic flank collapse of Anak Krakatau in the Sunda Straits of Indonesia. New numerical

Fig. 5 **a** Location of the study area within Canary Islands. **b** Oblique Google earth image of the tsunami source landslide. **c**: Detailed map of El Hierro with historically known slope failures. The tsunami source landslide is highlighted in red (Fig. 1 in Blahút and Luna 2020)

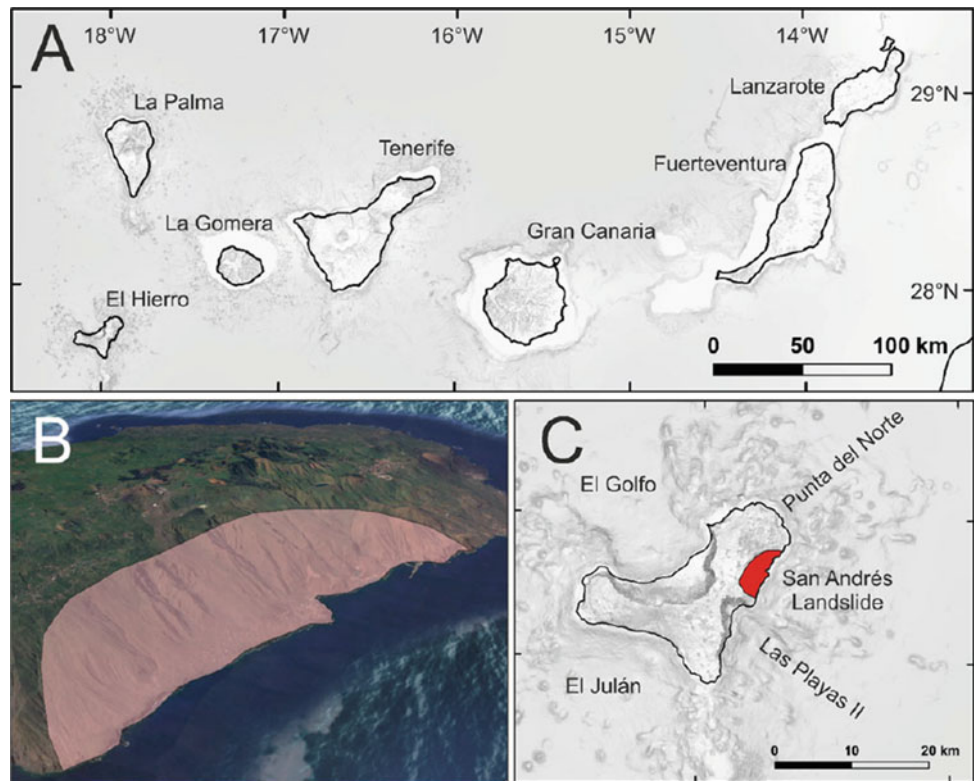


Fig. 6 Bathymetry of the study area and location of the cores. The areas of the upper slope of the Hidaka Trough marked in yellow are the youngest submarine landslides studied by Noda and Katayama (2013) (Fig. 1 in Usami et al. 2020)

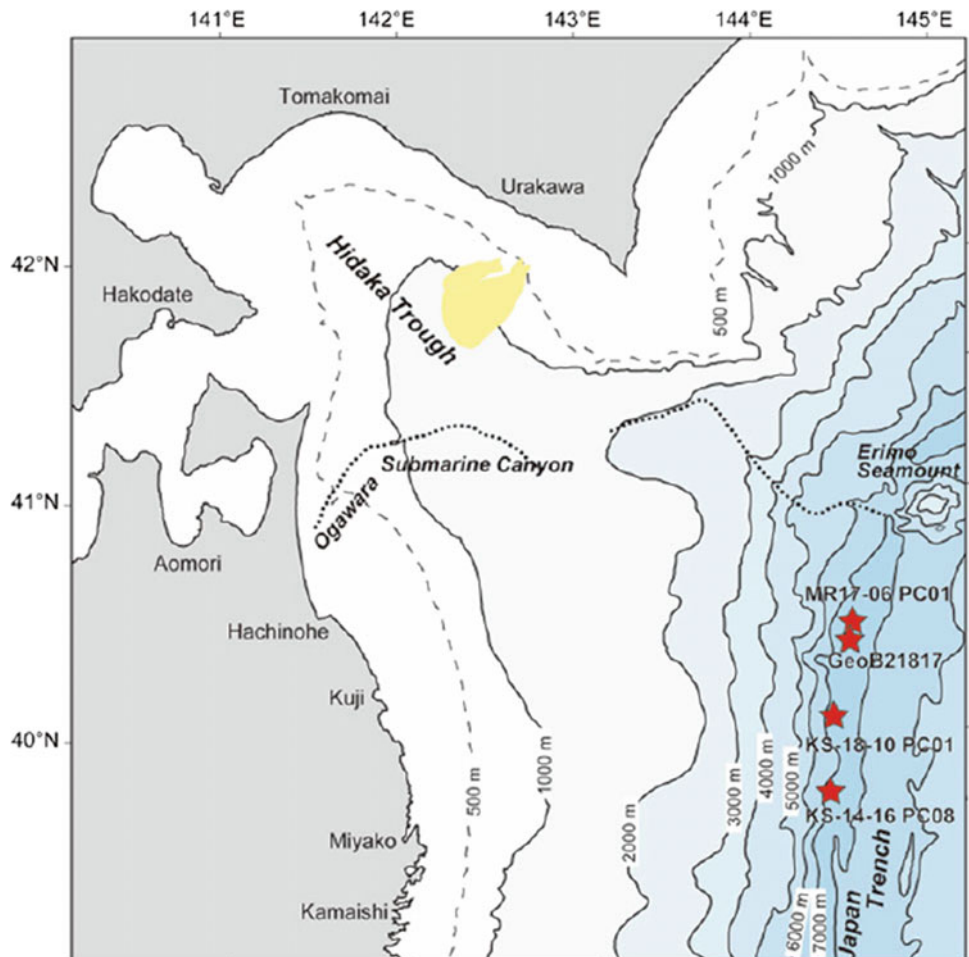


Fig. 9 Volcanic activity and tsunamis at Stromboli volcano (Fig. 3 in Traglia et al. 2020)

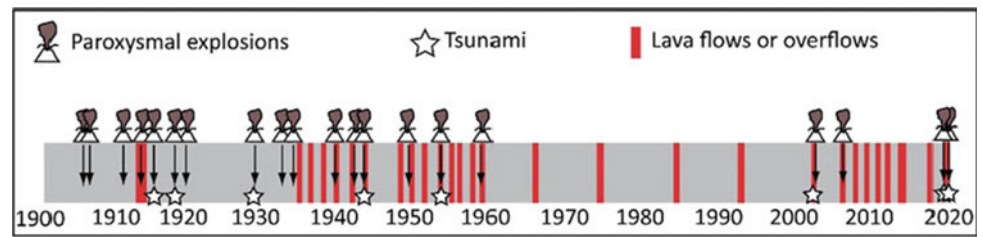
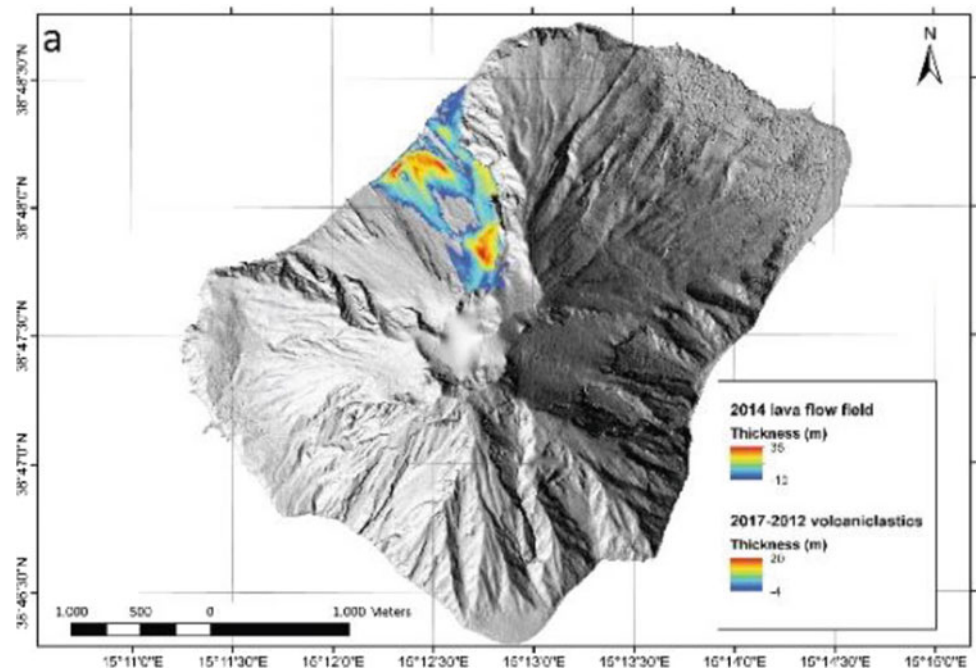


Fig. 10 Change detection from a topographic data (2012–2017) (Fig. 5a in Traglia et al. 2020)



various researchers. An improved modeling of catastrophic events, such as AK 2018, can help us better prepare for and mitigate hazard posed by future similar events.

D. Tappin highlighted the continuing underestimated tsunami hazard from submarine landslides. Recognition of the tsunami hazard from submarine landslides has been possible mainly because of the recent development of advanced technology such as multibeam echosounders. Accordingly, submarine landslide tsunamis are now seen from all geological environments: passive, convergent and strike-slip margins as well as volcanoes (examples are shown for the 1908 Messina tsunami in Fig. 13 and for the 2011 Tohoku tsunami in Fig. 14). Despite these new advances in understanding, however, recognition of the tsunami hazard from submarine landslides is still limited.

V. Gusiakov reported the December 11, 2018 landslide and the landslide-induced icy tsunami in the Bureya water reservoir, Russia. The landslide with an estimated volume of up to 25 million cubic meters generated a destructive tsunami-like wave whose impact on the shore was emphasized by a thick (up to 20 cm) ice cover (Fig. 15). The maximum run-up height turned out to be equal to 90 m

above the initial water level. The event has demonstrated the potential threat of the slope instability and the landslide-induced waves for the safety of hydropower plant (HPP) dams in a mountain region.

D. Karnawati presented an innovation in tsunami early warning system in Indonesia. The system aims at a timely detection of earthquake event and provides tsunami warning within 5 minutes after the earthquake takes place. The end-to-end system adopted for tsunami early warning is shown in Fig. 16. It facilitates an appropriate response from the community to reduce and minimize the impact of tsunami disasters. The 2018 catastrophic events highlighted the impact of volcanic flank collapse- and landslide-induced tsunamis, showing the importance of multi-hazard risks.

3 Outcome of the Panel Discussion

This section presents an outcome of the panel discussion. The essential content from each panelist will first be presented, followed by a summary of the general discussion moderated by the coordinator.

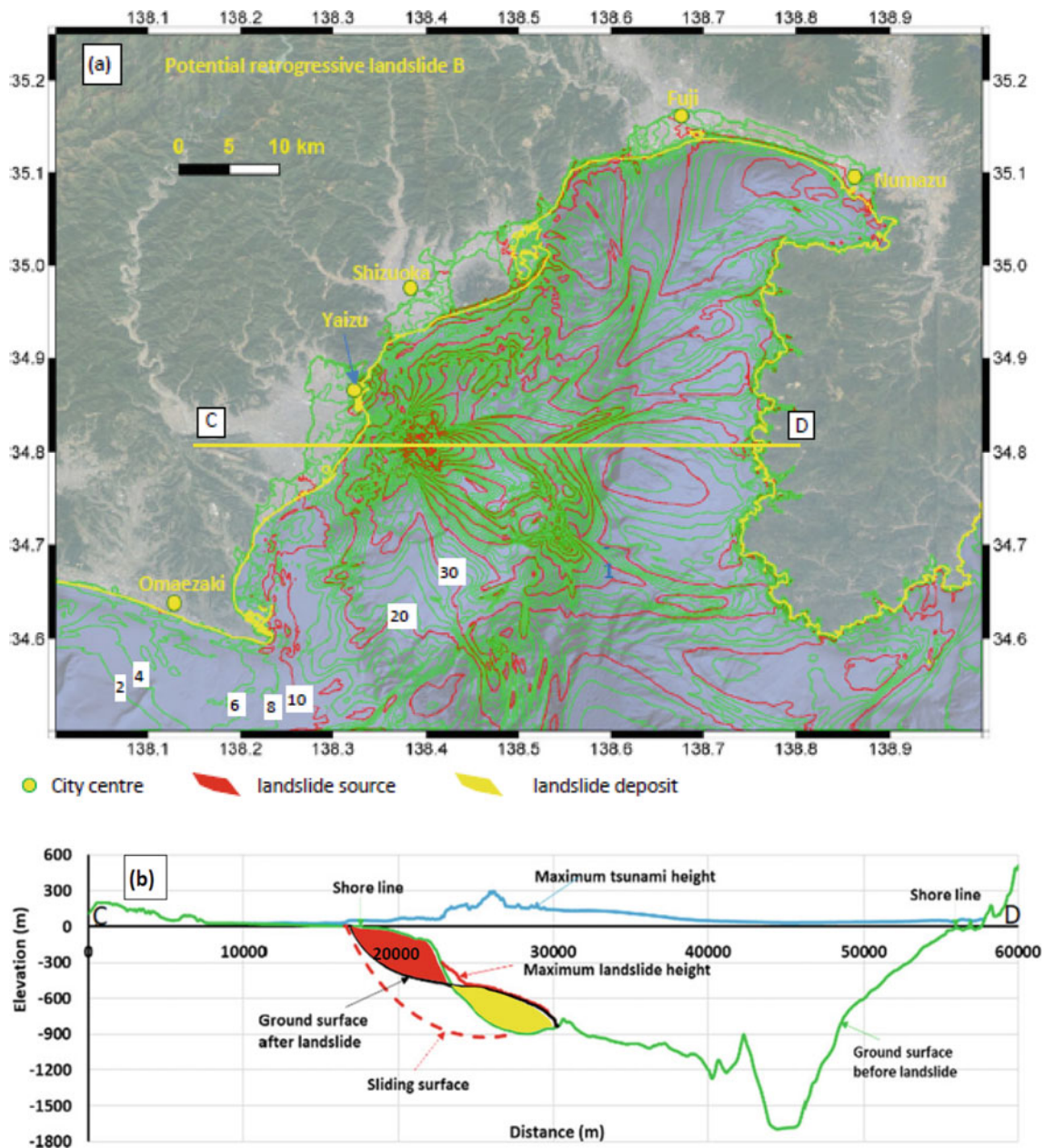


Fig. 11 **a** Contour of the maximum tsunami height caused by a potential retrogressive landslide in Neogene sand triggered by $0.7 \times$ Tohoku earthquake record (MYG004). Tsunami heights are in meters above sea level with 2 m contours in green and 10 m contours in blue. **b** Profile of the maximum tsunami height at each mesh along section C–D (Fig. 32 in Loi et al. 2020)

3.1 Essential Content from each Panelist

S. G. presented three fundamental and important issues, namely: 1. Triggering: when, where, how?; 2. Tsunami generation and propagation: magnitude, where, how?; 3. Landslide tsunami detection: magnitude/where?. These are described as below:

1. Triggering \Rightarrow when, where, how

For subaerial/submarine mass failures (SMF), simulating slide triggering requires topography/bathymetry and soil properties (physical, cohesiveness/rheology etc.) as well as statistics/probability of peak ground acceleration (PGA). A question here is whether predictive slope stability analyses

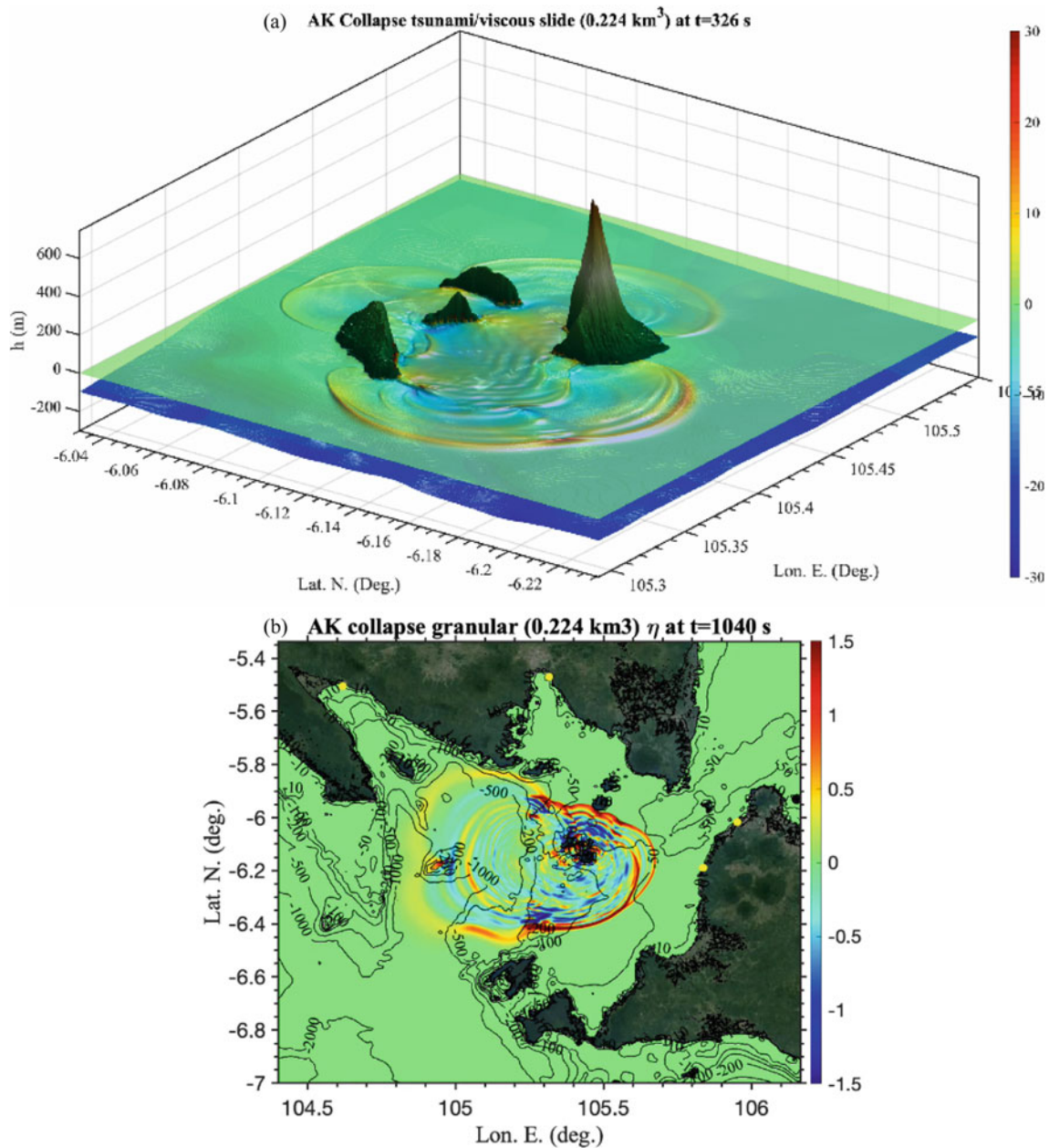


Fig. 12 Tsunami generations from the 2018 volcanic flank collapse of Anak Krakatau for **a** viscous slides and **b** granular slides. (Snapshots from S. Grilli's presentation based on Grilli et al. (2019, 2021))

could be performed together with an estimate of the factor of safety. For tsunami, coupled modeling of slide motion/tsunami generation is necessary. For volcanic tsunamis caused by pyroclastic flows (PF), pyroclastic density currents (PDC) and flank/caldera collapse, assessing triggering requires topography/bathymetry, volcano material/PF/PDC properties (physical, cohesiveness/rheology etc.), and estimates of PF/PDC flow rates and total volume. Monitoring of volcanic physical triggers (e.g., internal pressure, PGA) is also required. For tsunami, coupled modeling of collapse/PF/PDC motion/tsunami generation is necessary.

2. Tsunami generation propagation \Rightarrow magnitude, where, how

Models of tsunami generation (near-field) must feature relevant physics to simulate both slide and tsunami, and their coupling, including strong nonlinearity (in both geometry and flow), dispersion (vertical acceleration) in deep water, and three-dimensionality. Models of tsunami propagation (near-to-far-field) must include dispersion and sufficient nonlinearity. Depth-integrated/averaged models are adequate. The necessary slide/wave models exist for the most

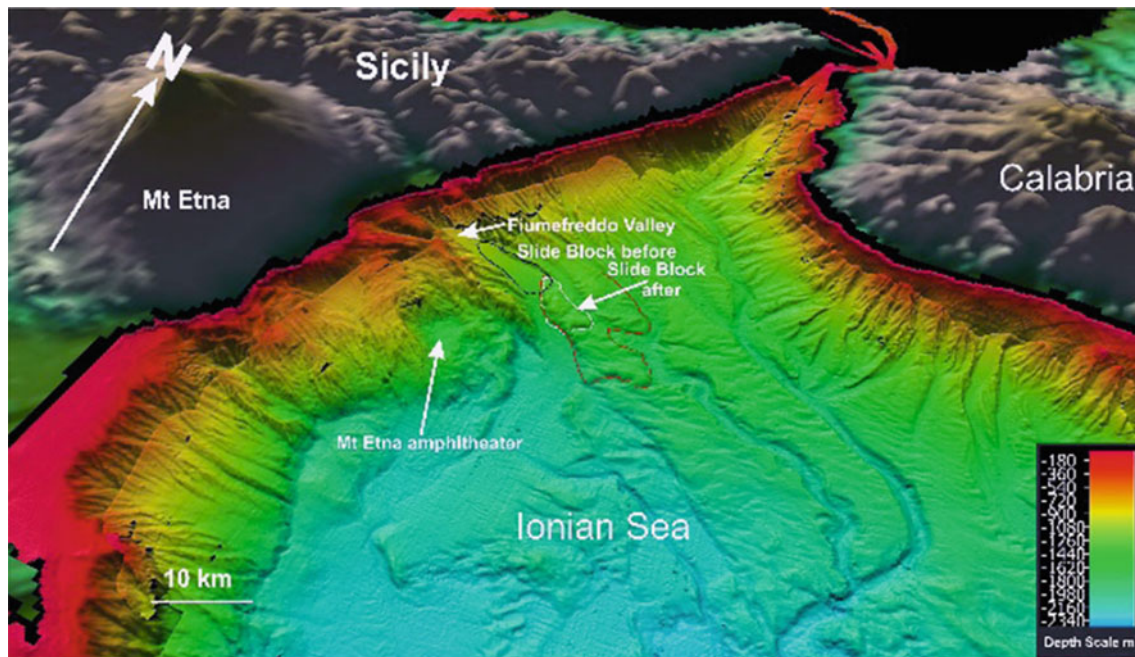


Fig. 13 3D image of the landslide block that contributed to the 1908 Messina tsunami (reproduced from Schambach et al. 2020) (Fig. 5 in Tappin and Grilli 2020)

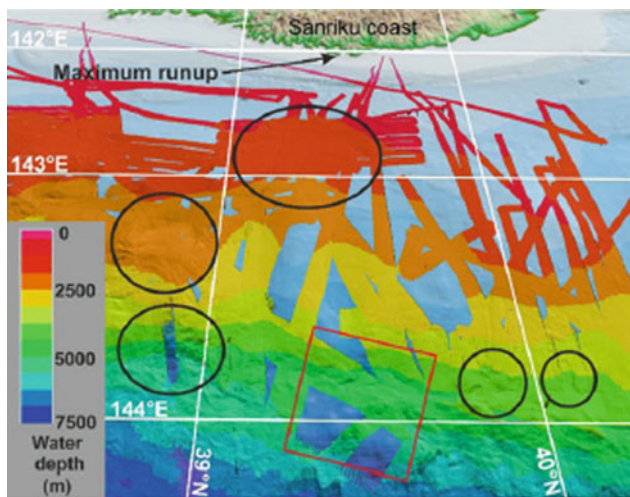


Fig. 14 Mutibeam bathymetry of the east coast of Japan, showing submarine landslides (SLs). Black ellipses/circle are SLs: Red square is the location of the SMF triggered by the March 2011 earthquake (reproduced from Tappin et al. 2014) (Fig. 6 in Tappin and Grilli 2020)

part: such as in near-field, multi-material Navier–Stokes and various multi-layer non-hydrostatic models, including various rheologies, Newtonian and non-Newtonian such as Boussinesq wave model in the near-to-far-field. These models have been applied and validated on many field case studies, e.g., Storegga, Grand Bank 1929, PNG 1998, Messina 1908, Palu 2018 etc.

3. Landslide tsunami detection/warning \Rightarrow magnitude/where

There may not be an earthquake trigger or even a volcanic eruption. Simulations of potential landslide tsunami scenarios and their induced hazard need to be completed in advance for areas deemed at risk that will be monitored. Non-standard detection methods must be implemented, such as High Frequency (HF) radar remote sensing combined with relevant tsunami detection algorithms.

D. T. presented a global map of submarine landslide tsunami locations (Fig. 17), noting that a broad global understanding of the hazard and mapping is required. A learning curve for submarine landslide tsunamis can be described as follows: Most (80%) of tsunamis from earthquakes, but also from seabed slumps, landslides, dual mechanisms and volcanic collapse. Landslide tsunamis over past few decades improve our understanding of their tsunami hazard. Each new event provides data from new technology such as multibeam bathymetry and new numerical tsunami models, however, there are still too few data to provide a broad global understanding of the hazard. Mitigation and warning are only confined to earthquake events, with 20% of oceans mapped, so major mapping programmes are required. Recent events flag non-seismic mechanisms, and form basis for improved mitigation and warning.

K. S. presented simulations of coastal and submarine landslide-induced tsunamis and highlighted the important



Fig. 15 General view of the landslide scar on the southern bank of the Bureya water reservoir and the body of the landslide with a passage, initially made on 1 February 2019 and then extended by the spring flood in April–May 2019. The top left panel shows damaged stumps

and exposed tree roots on the gentle coastal slope directly opposite the landslide on the northern bank of the Bureya river (Figs.3 and 9 in Gusiakov and Makhinov 2020)

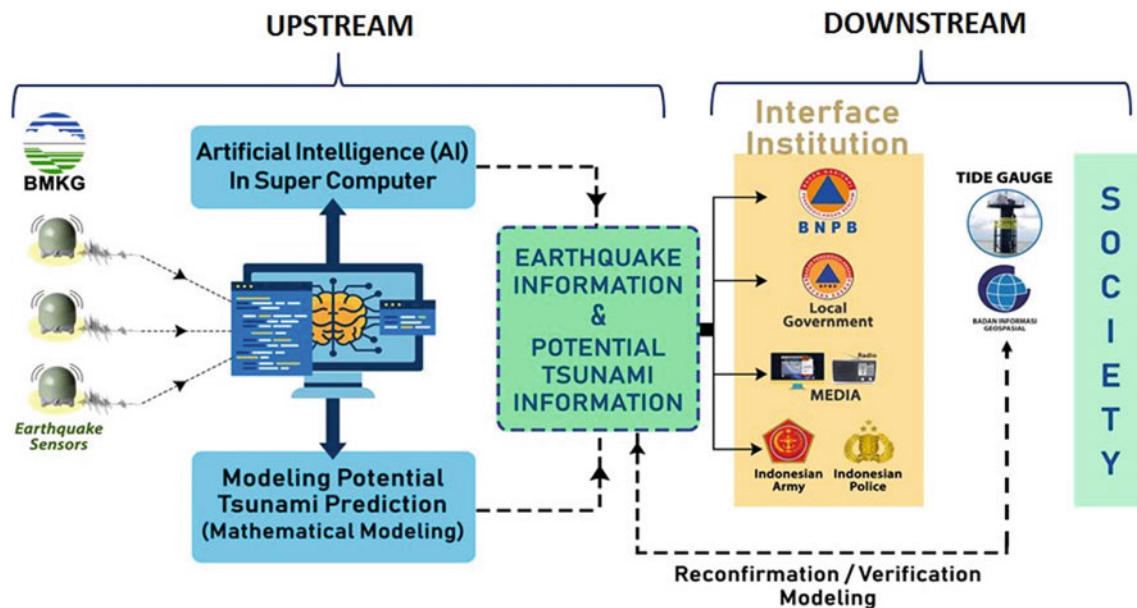


Fig. 16 End-to-end system for tsunami early warning in Indonesia (Karnawati 2020)

role of landslide motion in tsunami generation. A hazard assessment of landslide-induced tsunamis along Suruga bay in Japan was presented for a hypothetical Senoumi landslide and potential retrogressive landslides arising from a future mega earthquake along Nankai Trough together with their hazard map (Fig. 18). How to prepare for possible landslide causing tsunamis was highlighted. Namely, retrogressive

landslides are common in many landslides. However, to investigate the possibility of potential retrogressive landslides at Senoumi, a set of 800 m deep drillings and geophysical exploration are needed. Hence, we have to discuss how to promote the understanding and reducing landslide disaster risk including both landslide causing tsunami and landslide-induced tsunami for KLC2020.

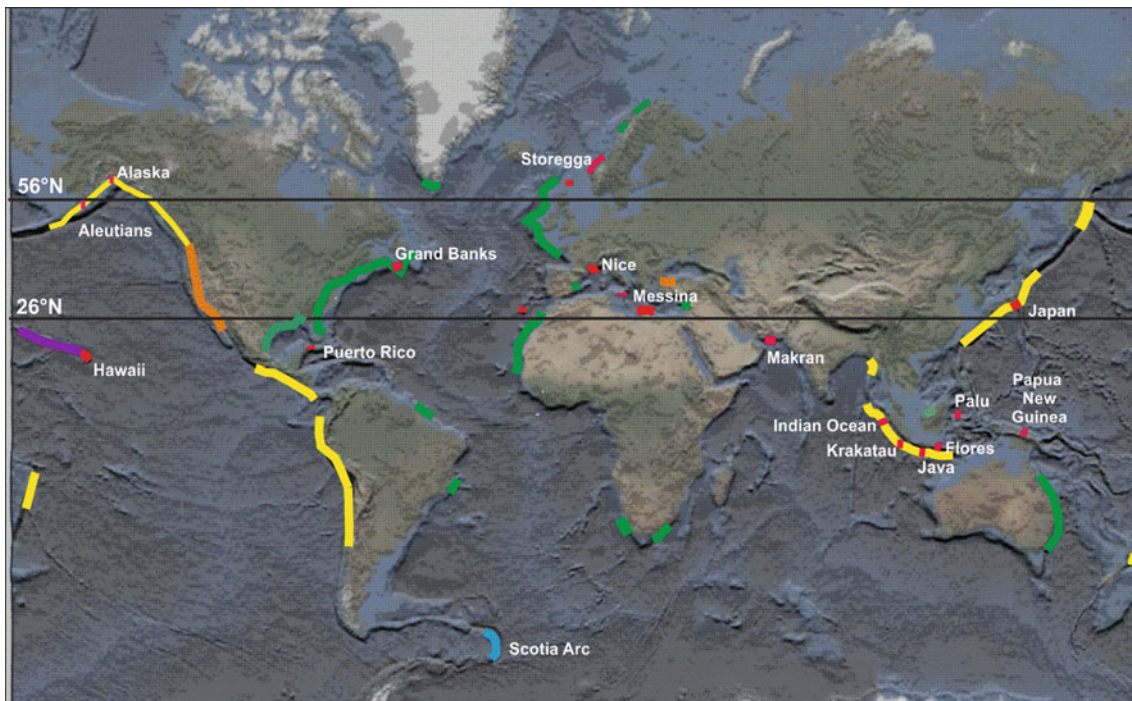


Fig. 17 Global distribution of mapped submarine landslides (SLs): green, SLs on passive margins; yellow, SLs located along convergent margins; orange, SLs on strike slip margins; purple, volcanoes; red, tsunamis associated with SLs (Tappin and Grilli 2020). Submarine

landslide tsunamis (in red) are mainly located along convergent margins, but also along passive and strike slip margins and on flanks of volcanoes

D. K. first illustrated some case examples of Palu earthquake and tsunami with liquefaction and submarine landslide, Sunda Straits tsunami due to volcanic eruption, and historical earthquakes and tsunamis in Ambon, Indonesia. Controlling factors and characteristics of areas typically prone to landslides were presented with reference to geology and bathymetry such as a fault distribution in coastal or near shore areas and position of alluvial fan. Triggering sources involve earthquake and volcanic eruption. A mitigation strategy based on hazard maps and evacuation plans was then provided with six levels of field verification and fact finding in order to (a) verify the hazard levels and zones (tsunami hazard map), (b) select and check the most appropriate evacuation route (shortest and fastest) with appropriate signage, (c) empower the local capacity to take rapid or spontaneous actions in response to any ground shaking, coastal subsidence and landslides, by following the determined evacuation route toward the higher/safer areas, (d) promote public education and regular drills on self-evacuation (integrate the local wisdom and knowledge), (e) establish appropriate land use management based on appropriate hazard map and (f) relocate the people from hazard areas. A list of 12 indicators from UNESCO-IOC tsunami community program was presented (Fig. 19).

V. G. demonstrated the close relationship between oceanic sedimentation zones and landslide-triggered

tsunamigenic potential, which could directly contribute to improving tsunami early warning and long-term risk assessment. Specifically, the main zones of lithogenesis in the Pacific Ocean (1—equatorial humid zone, 2—northern and southern humid zones, 3—zone of effusive-sedimentary lithogenesis, 4—northern and southern arid zones), and the classification and locations of “red”, “green” and “blue” Pacific tsunamigenic earthquakes were presented (Fig. 20). This demonstrates that there is a close relationship between oceanic sedimentation zones and tsunamigenic potential of submarine earthquakes. In spite of greater efforts in recent years to study the slumping mechanism of tsunami generation, this factor is almost completely overlooked in the early tsunami warning and in the long-term tsunami risk assessment (coastal tsunami zoning). Conditions of oceanic sedimentation are of extreme importance in understanding the tsunami generation mechanism, and that slumping has contributed significantly to at least 33% of the historical tsunami events rather than the 7% indicated in the historical tsunami catalogs for the Pacific. The contribution of underwater slumping to the tsunami generation mechanism was recognized long ago. However, little attention was given so far to the relationship of tsunami generation to conditions of oceanic sedimentation in the main tsunamigenic zones of the Pacific. Taking this into account can essentially change the strategy for improving the operational tsunami warnings and

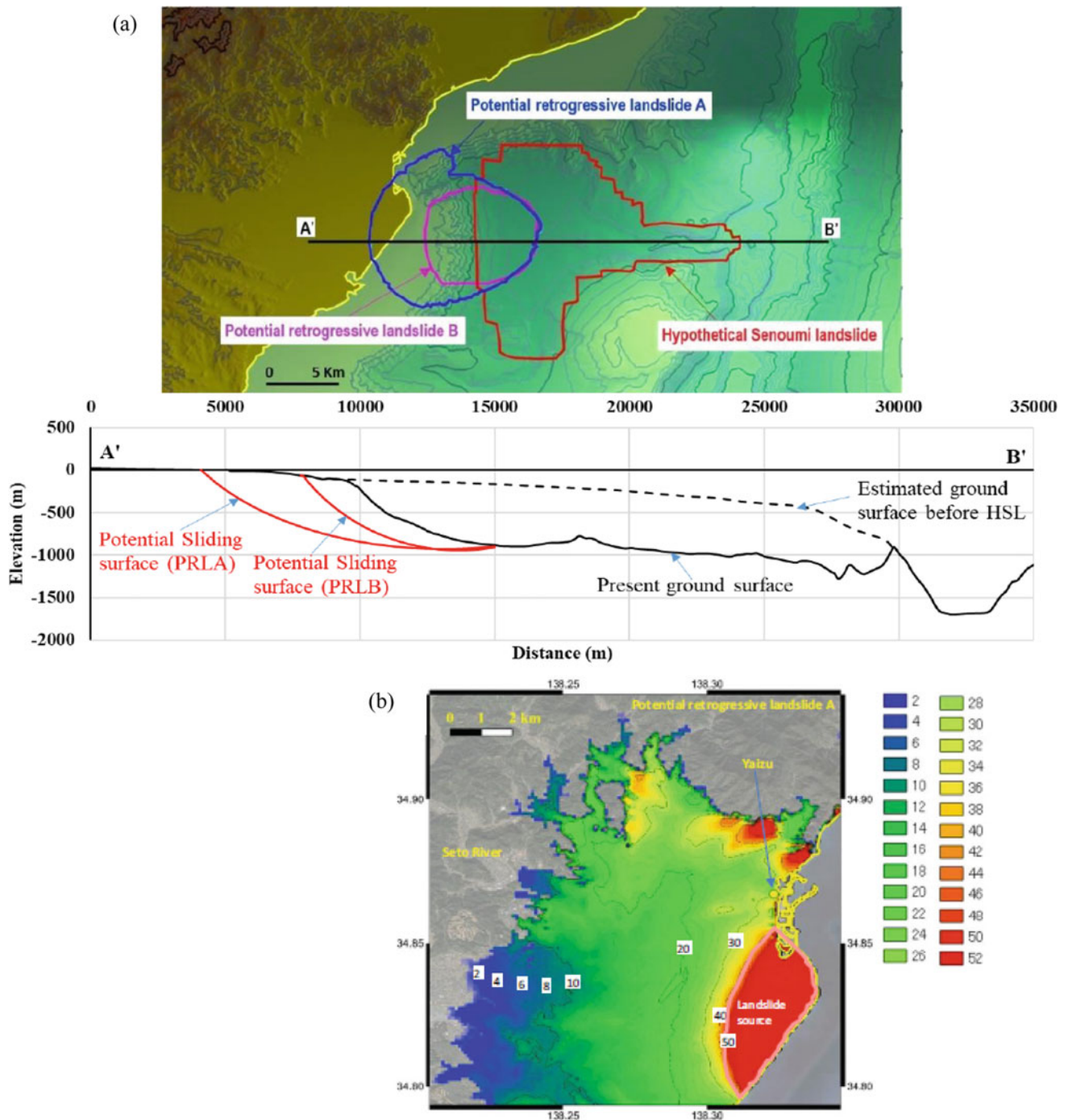


Fig. 18 a Shapes and cross sections of hypothetical Senoumi landslide (HSL) and potential retrogressive landslides A and B (PRLA and PRLB, respectively) b Inundation map at Yaizu City center caused by

PRLA. Inundation depth (color scale in meter) = maximum tsunami height—ground elevation (Figs. 31 and 34(a) in Loi et al. 2020)

the long-term tsunami risk assessment. Specifically, the magnitude criterion for operational warning can be made variable, depending on the earthquake location within the basic zones of oceanic sedimentation (shallow water bays, marginal seas, island arc regions, remote deep-water trenches, middle ocean ridges). In estimating the long-term

tsunami risk, it can be very important to consider the potential of submarine slumping in the tsunami-prone areas.

F. L. stressed the lack of data for landslide volume probability, resulting from limited seafloor sub-bottom mapping, and highlighted the uncertainty in landslide dynamics leading to tsunami genesis. Although physics of

Fig. 19 A list of 12 indicators from UNESCO-IOC tsunami ready community program (excerpt from D. Karnawati's presentation)

I	MITIGATION (MIT)
1	MIT-1. Tsunami hazard zones are mapped and designated
2	MIT-2. The number of people at risk in the tsunami hazard zone is estimated
3	MIT-3. Available economic, infrastructural, political, and social resources are identified
4	MIT-4. Tsunami information is publicly displayed.
II	PREPAREDNESS (PREP)
5	PREP-1. Easily understood tsunami evacuation maps are developed.
6	PREP-2. Outreach and public awareness and education resources are available and distributed.
7	PREP-3. Outreach or educational activities are held at least 3 times a year.
8	PREP-4. A Tsunami community exercise is conducted at least every two years
III	RESPONSE (RESP)
9	RESP-1. A community tsunami emergency operations plan (EOP) has been prepared
10	RESP-2. The capacity to manage emergency response operations during a tsunami has been established.
11	RESP-3. Redundant and reliable means to timely receive 24-hour official tsunami alerts have been identified.
12	RESP-4. Redundant and reliable means to timely disseminate 24-hour official tsunami alerts to the public have been identified.

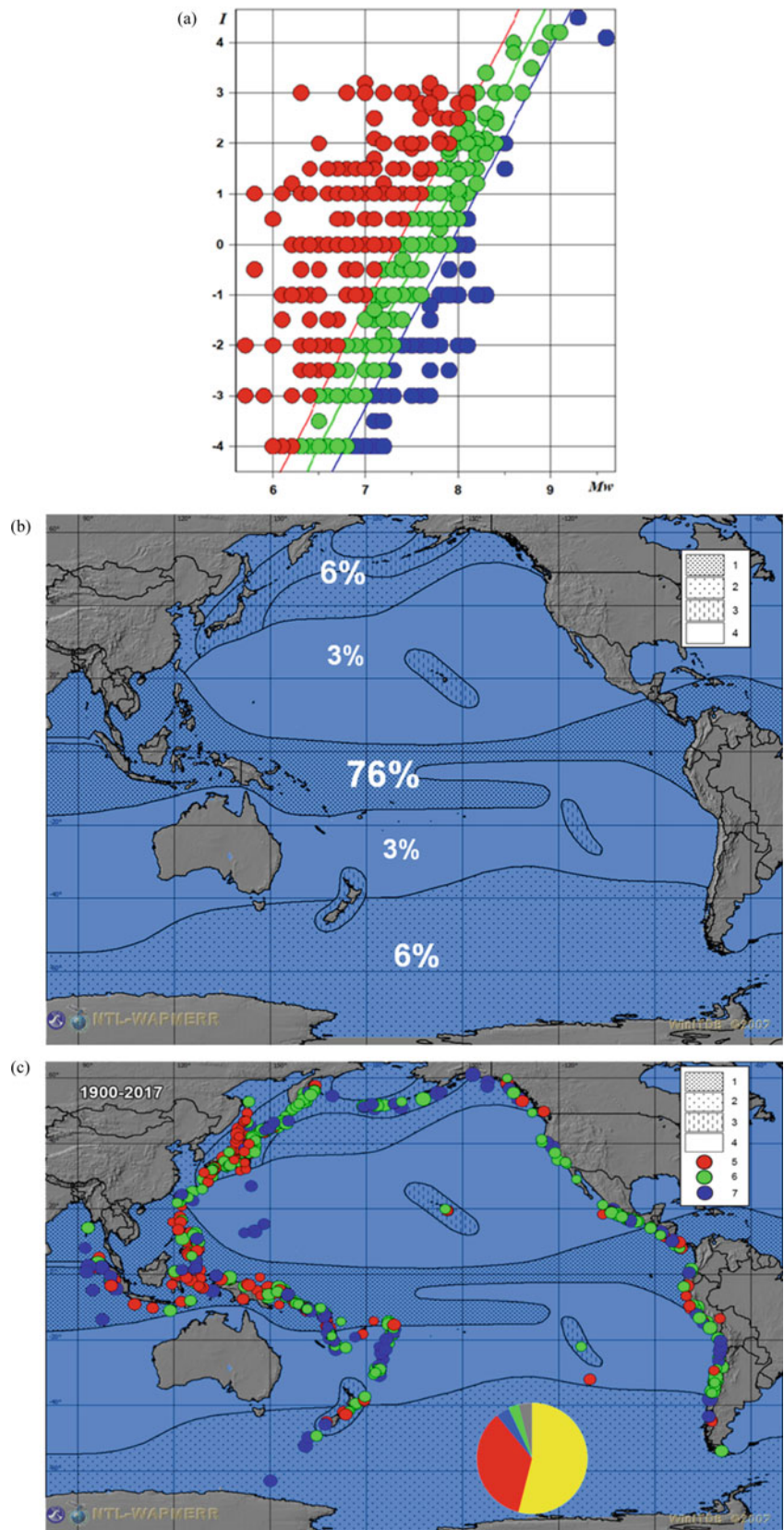
tsunami propagation and inundation are well established and sensitivity to the kinematics of the landslide (i.e., the motion and path) is relatively well known, several cases thoroughly hindcasted represent mainly subaerial landslides. Accordingly, in most places around the world, we lack data for quantifying temporal landslide volume probability with limited and often non-existing mapping of substrata conditions, thickness of sediments, fractures, geotechnical parameters etc. Landslide friction tends to be reduced with landslide volume, but we do not know to which extent this influences tsunami hazard. Landslide dynamics controls tsunami-generation, but this dynamics is uncertain when we attempt to forecast future events. Both material parameters and landslide water interaction are poorly constrained. Past landslide run-out distance observations constrain tsunami-generation poorly and therefore calibration against past cases are associated with large uncertainties. In fact, there is a limited amount of well documented fully subaqueous landslide tsunami events. Transition from landslide failure to flow controls acceleration and rate of failure (retrogression), and how they can contribute to tsunami-generation is crucial. In comparison with earthquake tsunami hazards, temporal landslide vs volume statistics is usually much less well constrained. Paleo-observations are important, dating necessary, but cannot always be linked to the source origin. Longer time scales for hazard involves more uncertainty. Landslides can occur “everywhere”—while earthquakes are constrained to major faults and subduction zones. Greater variability lies in different tsunami generation mechanisms for different types of landslides: Subaerial versus submarine; Landslide dynamics; Slumping, Translation, Turbidity currents with different repeatability characteristics (sediment

escape versus faults and plate motion). The outstanding questions and gaps from the European tsunami community are shown in Fig. 21.

3.2 Summary of the Panel Discussion

During the general Panel Discussion, each of the key items summarized in Fig. 22 was critically discussed among the panelists and the coordinator. The content of this Panel Discussion is summarized in Sassa et al. (2022) and the key discussion points are briefly reviewed in this section. Triggering and source mechanisms need to be well constrained and one needs to better understand how both of these affect tsunami generation, in order to more accurately predict/model landslide-induced tsunamis. There is still a lot to learn for better understanding and mitigating the disaster risk of landslide-induced tsunamis, regarding hazard mapping (Fig. 17) and improving warning. Dual and multiple mechanisms must be considered to achieve improved mitigation. However, our limited understanding and characterization of the past landslide events where tsunami data are unavailable makes it difficult to well constrain landslide dynamics (Fig. 21). Landslide dynamics controls tsunami generation (genesis) but is inherently uncertain; hence, a better integrated understanding of landslide dynamics as well as multi-phased physics of landslide-water interactions are crucial to reducing landslide tsunami disaster risk. Landslide dynamics itself features complex physics, such as liquefaction and evolutions of pore water pressures involving phase change processes (Fig. 7), and the in-depth understanding of such phenomena is important for improving landslide

Fig. 20 **a** Classification of “red”, “green” and “blue” Pacific tsunamigenic earthquakes in the tsunami intensity I —moment magnitude M_w relationship according to Gusiakov (2001)
b The main zones of lithogenesis in the Pacific Ocean (1—equatorial humid zone, 2—northern and southern humid zones, 3—zone of effusive-sedimentary lithogenesis, 4—northern and southern arid zones). The digits show a fraction of sediment volume in each zone in the total volume of marine sediments by Lisitsyn (1974)
c Locations of the “red”, “green” and “blue” tsunamigenic earthquakes. The insert figure shows the fractions of landslide-generated tsunamis (red color) in the total number of Pacific tsunamis (excerpts from V. Gusiakov’s presentation)



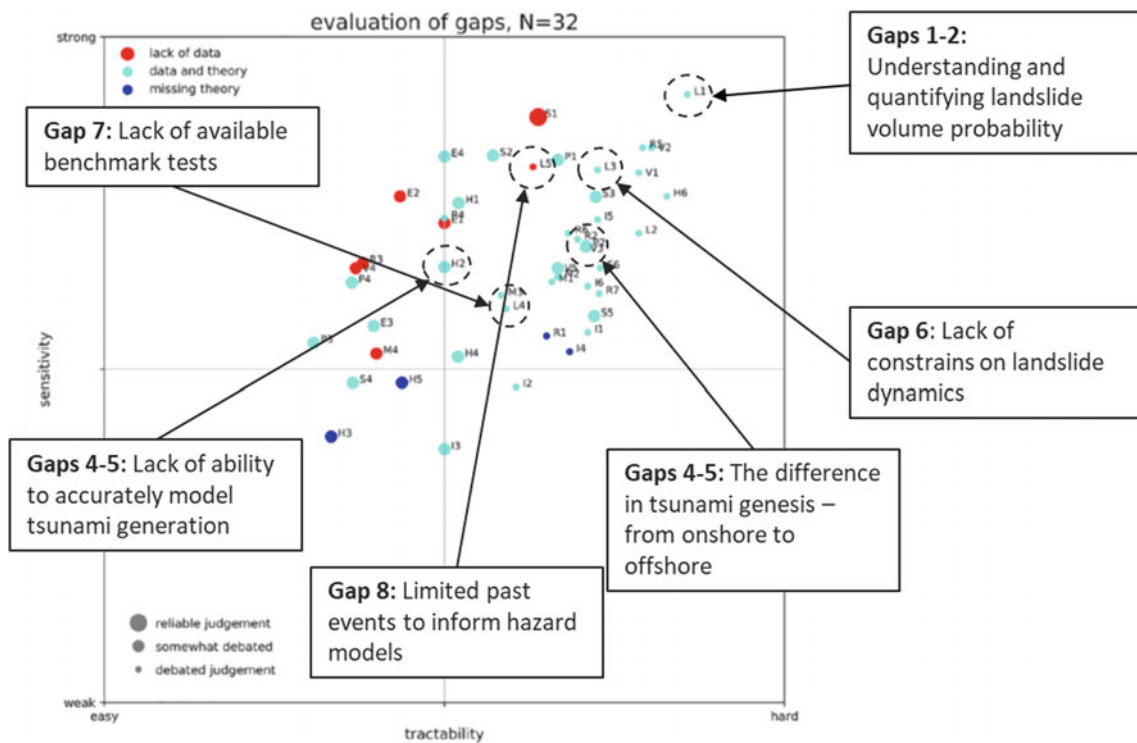


Fig. 21 Outstanding questions and gaps—the European tsunami community response (revised from F. Løvholt’s presentation based on Behrens et al. (2021) to highlight landslide tsunami research questions)

Fig. 22 The framework, essential content, and a short summary of the panel discussion in the World Tsunami Awareness Day Special Event of the Fifth World Landslide Forum (Sassa et al. 2022)

Essentials for understanding and reducing the disaster risk of Landslide-induced Tsunamis
S. Sassa

<p>S. Grilli</p> <ol style="list-style-type: none"> 1. Triggering => when, where, how 2. Tsunami generation propagation => magnitude, where, how 3. Landslide tsunami detection/warning => magnitude/where <p>K. Sassa</p> <ul style="list-style-type: none"> • Coastal and submarine landslide-induced tsunami • Role of landslide motion in tsunami generation • Toward improved landslide tsunami hazard assessment technology <p>V. Gusiakov</p> <ul style="list-style-type: none"> • Oceanic sedimentation zones and tsunamigenic potential • Overlooked tsunami generation mechanism • Toward improved warnings and long-term risk assessment 	<p>D. Tappin</p> <ul style="list-style-type: none"> • Submarine landslide tsunami locations • Broad global understanding of the hazard and mapping required • Dual and multiple mechanisms form basis for improved mitigation and warning <p>D. Karnawati</p> <ul style="list-style-type: none"> • Controlling factors and characteristic of typical prone areas • Multiple triggering sources • Mitigation strategy with hazard map and evacuation <p>F. Løvholt</p> <ul style="list-style-type: none"> • Lack of data for landslide volume probability with limited mapping • Uncertainty in landslide dynamics leading to tsunami genesis • Toward well-developed early warning systems
--	--

**Better understanding of multiple mechanisms and multi-phased physics of Landslide Tsunami Hazard
Hazard Mapping/ Improved Early Warning**

tsunami hazard assessment technologies. A closer investigation of landslides that have caused or potentially cause tsunamis (Fig. 18) is, thus, very important. In this respect, multiple triggering sources of tsunamis such as landslides caused by earthquakes and volcanic eruptions must be better understood. Large volcanic flank collapses have induced large tsunamis, e.g., recently Anak Krakatau 2018 (Fig. 12). Hence, sites of potential future events should be closely

monitored and new instruments, allowing for early detection and warning, deployed. In contrast, some landslide-induced tsunamis may impact shores very rapidly, such as in the cases of coastal and submarine landslides-induced tsunamis, e.g., recently Palu 2018 (Fig. 8). Therefore, in order to prepare for such fast arriving tsunamis, hazard mapping is critically important. Accordingly, both hazard maps and 24-h warning are vital as mitigation strategies (Fig. 19). In

light of multiple mechanisms, oceanic sedimentation conditions and zones have been overlooked as having high submarine landslide tsunami generation potential (Fig. 20). These can play a significant role in improving early warning and hazard maps. However, more data is needed to better constrain geological and geotechnical conditions for hazard mapping. Landslide-water interactions are currently poorly constrained and their better understanding, together with that of the complex multi-phased physics this entails, are crucial towards developing early warning systems. Overall, developing a better understanding of the multiple mechanisms and multi-phased physics governing landslide tsunami hazard is important and necessary for improving landslide tsunami hazard mapping and early warning.

4 Conclusion

This article has presented some recent advances, the current state and challenges in understanding and reducing the disaster risk of landslide-induced tsunamis. A worldwide perspective has been presented by showing the outcomes of the panel discussion held across America, Europe, and Asia and a review of the World Tsunami Awareness Day Special Event of the Fifth World Landslide Forum. Hazard mapping and improved early warning are essential for better understanding and reducing the disaster risk of landslide-induced tsunamis, and this will require developing a better understanding of the multiple mechanisms and multi-phased physics of landslide tsunami hazard. An international collaborative network and platform would be important for such a multi-hazard risk reduction. It is therefore hoped that the content presented here will further promote understanding and reducing the disaster risk of landslide-induced tsunamis at both the regional and global scales.

References

- Behrens J, Løvholt F, Jalayer F, Lorito S, Salgado-Gálvez MA, Sørensen M, Abadie S, Aguirre-Ayerbe I, Aniel-Quiroga I, Babeyko A, Baigüera M, Basili R, Belliazzi S, Grezio A, Johnson K, Murphy S, Paris R, Rafliana I, De Risi R, Rossetto T, Armigliato A, Bureš V, Cech P, Cecioni C, Christodoulides P, Davies G, Dias F, Bayraktar HB, González M, Gritsevich M, Guillas S, Harbitz CB, Kánoğlu U, Macías J, Papadopoulos GA, Polet J, Romano F, Slamon A, Scala A, Stepinac M, Tappin DR, Thio HK, Tonini R, Triantafyllou I, Ulrich T, Varini E, Volpe M, Vyhmeister E (2021) Probabilistic tsunami hazard and risk analysis: a review of research gaps. *Front Earth Sci* 9:628772
- Blahůt J, Luna BQ (2020) Tsunami from the San Andrés landslide on El Hierro, Canary Islands: first attempt using simple scenario. In: Sassa K, Mikoš M, Sassa S, Bobrowsky PT, Takara K, Dang K (eds) Understanding and reducing landslide disaster risk: volume 1 Sendai Landslide Partnerships and Kyoto Landslide Commitment. Part III Landslide-induced Tsunamis. Springer Nature, pp 369–376
- Electronic Proceedings of the Fifth World Landslide Forum (2020) pp 280–306
- Grilli ST, Tappin DR, Carey S, Watt SFL, Ward SN, Grilli AR, Engwell SL, Zhang C, Kirby JT, Schambach L, Muin M (2019) Modelling of the tsunami from the December 22, 2018 lateral collapse of Anak Krakatau volcano in the Sunda Straits, Indonesia. *Sci Rep* 9:11946
- Grilli ST, Zhang C, Kirby JT, Grilli AR, Tappin DR, Watt SFL, Hunt JE, Novellino A, Engwell SL, Nurshal ME, Abdurrachman M, Cassidy M, Madden-Nadeau AL, Day S (2021) Modeling of the December 22nd 2018 Anak Krakatau volcano lateral collapse and tsunami based on recent field surveys: comparison with observed tsunami impact. *Mar Geol* 440:106566
- Gusiakov VK, Makhinov A (2020) December 11, 2018 landslide and 90-m icy tsunami in the Bureya water reservoir. In: Sassa K, Mikoš M, Sassa S, Bobrowsky PT, Takara K, Dang K (eds) Understanding and reducing landslide disaster risk: volume 1 Sendai Landslide Partnerships and Kyoto Landslide Commitment. Part III Landslide-induced Tsunamis. Springer Nature, pp 351–360
- Gusiakov VK (2001) “Red”, “Green” and “Blue” Tsunamigenic earthquakes and their relation with conditions of oceanic sedimentation in the Pacific. In: Hebenstreit GT (ed) Tsunami research at the end of a critical decade. Kluwer Academic Publishers, pp 17–32
- Karnawati D (2020) Innovation in tsunami early warning system in Indonesia. *Electronic Proceedings of the Fifth World Landslide Forum*, pp 291–305
- Lisitsyn AP (1974) Sedimentation in the ocean. Moscow, Nauka, p 425. (in Russian)
- Loi DH, Sassa K, Dang K, Miyagi T (2020) Simulation of tsunami waves induced by coastal and submarine landslides in Japan. In: Sassa K, Mikoš M, Sassa S, Bobrowsky PT, Takara K, Dang K (eds) Understanding and reducing landslide disaster risk: volume 1 Sendai Landslide Partnerships and Kyoto Landslide Commitment. Part III Landslide-induced Tsunamis. Springer Nature, pp 295–327
- Løvholt F, Glimsdal S, Harbitz CB (2020) On the landslide tsunami uncertainty and hazard. *Landslides* 17(10):2301–2315
- Minh Duc D, Khang DQ, Minh Duc D, Minh Ngoc D, Thi Quynh D, Thi Thuy D, Hoang Giang NK, Van Tien P, Huu Ha N (2020) Analysis and modeling of a landslide-induced tsunami-like wave across the Truong river in Quang Nam province, Vietnam. *Landslides* 17(10):2329–2341
- Noda A, Katayama H (2013) Sedimentological map of Hidaka trough. Marine geology map series, no. 81(CD), Geological Survey of Japan, AIST
- One-Page Abstract Volume of the Fifth World Landslide Forum (2021). pp 28–33, pp 411–423
- Sassa S, Takagawa T (2019) Liquefied gravity flow-induced tsunami: first evidence and comparison from the 2018 Indonesia Sulawesi earthquake and tsunami disasters. *Landslides* 16(1):195–200
- Sassa S, Grilli ST, Tappin DR, Sassa K, Karnawati D, Gusiakov VK, Løvholt F (2022) Understanding and reducing the disaster risk of landslide-induced tsunamis: a short summary of the panel discussion in the World Tsunami Awareness Day Special Event of the Fifth World Landslide Forum. *Landslides* 19(2):533–535
- Sassa K, Mikoš M, Sassa S, Bobrowsky PT, Takara K, Dang K (2020) Understanding and reducing landslide disaster risk: volume 1 Sendai Landslide Partnerships and Kyoto Landslide Commitment, Part III Landslide-induced Tsunamis. Springer Nature, pp 295–412
- Schambach L, Grilli ST, Tappin DR, Gangemi MD, Barbaro G (2020) New simulations and understanding of the 1908 Messina tsunami for a dual seismic and deep submarine mass failure source. *Mar Geol* 421:106093
- Tappin DR, Grilli ST, Harris JC, Geller RJ, Masterlark T, Kirby JT, Shi F, Ma G, Thingbaijam KKS, Mai PM (2014) Did a submarine

- landslide contribute to the 2011 Tohoku tsunami? *Mar Geol* 357:344–361
- Tappin DR, Grilli ST (2020) The continuing underestimated tsunami hazard from submarine landslides. In: Sassa K, Mikoš M, Sassa S, Bobrowsky PT, Takara K, Dang K (eds) *Understanding and reducing landslide disaster risk: volume 1 Sendai Landslide Partnerships and Kyoto Landslide Commitment. Part III Landslide-induced Tsunamis*. Springer Nature, pp 343–350
- Thematic issue: Sendai Landslide Partnerships 2015–2025 (2020) *Landslides* 17(10):2301–2341
- Traglia FD, Nolesini T, Casagli N (2020) Dealing with mass-induced tsunamis at Stromboli volcano: monitoring strategies through multi-platform remote sensing. In: Sassa K, Mikoš M, Sassa S, Bobrowsky PT, Takara K, Dang K (eds) *Understanding and reducing landslide disaster risk: volume 1 Sendai Landslide Partnerships and Kyoto Landslide Commitment. Part III Landslide-induced Tsunamis*. Springer Nature, pp 397–404
- Usami K, Ikehara K, Kanamatsu T, Kioka A, Schwestermann T, Strasser M (2020) The link between upper-slope submarine landslides and mass transport deposits in the hadal tranchs. In: Sassa K, Mikoš M, Sassa S, Bobrowsky PT, Takara K, Dang K (eds) *Understanding and reducing landslide disaster risk: volume 1 Sendai Landslide Partnerships and Kyoto Landslide Commitment. Part III Landslide-induced Tsunamis*. Springer Nature, pp 361–367

Open Access This chapter is licensed under the terms of the Creative Commons Attribution 4.0 International License (<http://creativecommons.org/licenses/by/4.0/>), which permits use, sharing, adaptation, distribution and reproduction in any medium or format, as long as you give appropriate credit to the original author(s) and the source, provide a link to the Creative Commons license and indicate if changes were made.

The images or other third party material in this chapter are included in the chapter's Creative Commons license, unless indicated otherwise in a credit line to the material. If material is not included in the chapter's Creative Commons license and your intended use is not permitted by statutory regulation or exceeds the permitted use, you will need to obtain permission directly from the copyright holder.





Natural-Hazard-Related Web Observatory as a Sustainable Development Tool

Matjaž Mikoš, Nejc Bezak, Joao Pita Costa, M. Beshar Massri, Inna Novalija, Mitja Jermol, and Marko Grobelnik

Abstract

Using the Internet and wealth of data and knowledge available on the Web, so-called web observatories have been developed in the last decade—in very different fields of use. The article discusses the use of such observatories to support the implementation of sustainable development at different scales. The focus is on landslides as risk to society, and since they are related to water and soil, a web-based observatory on natural hazards, including landslides, can draw upon water- and soil-related observatories that are used worldwide as a sustainable development tool. A new landslide observatory may support major global initiatives to adapt to climate change. The Observatory's vision, structure and use can be built upon the experiences gathered by developing a global water

observatory for smart water management, using Artificial Intelligence tools. UNESCO Chair on Water-related Disaster Risk Reduction of the University of Ljubljana, Slovenia, and the UNESCO International Research Institute on Artificial Intelligence at the Institute Jožef Stefan, Slovenia, have joined efforts and knowledge to develop a new global web observatory (tentatively first as the Landslide Observatory) to be used by different stakeholders when implementing global climate adaptation policies and relevant European Union strategies. The information gathered on the internet is structured, and shown using geolocators for different regions and/or countries. For interpretation of world-wide web data, landslide expert knowledge is used.

Keywords

Artificial intelligence • Earth observations • International consortium on landslides • International programme on landslides • Sendai framework on disaster risk reduction • Sustainable development goals • World wide web

M. Mikoš (✉)

UNESCO Chair On Water-Related Disaster Risk Reduction, c/o UL FGG, University of Ljubljana, Jamova c. 2, 1000 Ljubljana, Slovenia

e-mail: matjaz.mikos@fgg.uni-lj.si

N. Bezak

Faculty of Civil and Geodetic Engineering, University of Ljubljana, Jamova c. 2, 1000 Ljubljana, Slovenia

J. P. Costa · M. Jermol · M. Grobelnik

Institute Jožef Stefan and UNESCO International Research Centre for Artificial Intelligence IRCAI, Jamova c. 39, 1000 Ljubljana, Slovenia

e-mail: joao.pitacosta@quintelligence.com

M. Jermol

e-mail: mitja.jermol@ijs.si

M. Grobelnik

e-mail: marko.grobelnik@ijs.si

M. B. Massri

Institute Jožef Stefan and UNESCO International Research Centre for Artificial Intelligence IRCAI, Jožef Stefan International Postgraduate School, Jamova c. 39, 1000 Ljubljana, Slovenia

e-mail: beshar.massri@ijs.si

I. Novalija

Institute Jožef Stefan, Jamova c. 39, 1000 Ljubljana, Slovenia

e-mail: inna.kovali@ijs.si

1 Introduction

Landslides are frequent natural hazards globally, and their understanding and research are needed for landslide risk reduction. In many ways understanding is achieved by observing natural phenomena such as land sliding in all its variety of forms (Hung et al. 2014). For intense and focused observations scientists are using observatories, according to the Miriam-Webster Dictionary i.e. a building (as in astronomy) or a place given over to or equipped for observation of natural phenomena. Diverse in-situ (field) observatories have been developed and are running over years to monitor and understand landslide dynamics and/or develop early warning systems. Using the internet and wealth of data and knowledge available on the Web, new types of so-called

web observatories have been developed in the last decade—with very diverse purposes in mind. They are based on Open Data and Big Data, and any other Web data, and by crawling prepare a raw data collection from the Web, then by mapping of data do the pre-processing, converting, indexing, tagging, and integrating, to finally do the visualization and analysis of collected data (Aljohani et al. 2019). A proposed web Landslide Observatory is not a replacement of existing on-site landslide observatories and/or landslide-related Earth Observatories, but rather a web platform to provide structured data, tools, and knowledge to help stakeholders better understand landsliding as natural and social phenomena and their consequences and impacts on the environment and humankind, support sustainable development, and stimulate risk dialogue and increasing society resilience.

Landslides are mentioned in the Operational Implementation Plan for the UNESCO Intergovernmental Hydrological Programme Phase IX (IHP-IX OIP). In its February 2022 draft for the Priority Area 1: Scientific Research and Innovation, rainfall-induced landslides are mentioned in the proposed activity on Research and knowledge generation on the scientific advances in addressing and timely forecasting of water-related disasters and on additional impacts of synchronous and/or cascading water-related hazards.

The Kyoto Landslide 2020 Commitment for Global Promotion of Understanding and Reducing Landslide Disaster Risk (KLC2020) was launched on 5 November 2020 by the International Consortium on Landslides (Sassa 2021a). Earlier, the 2017 Ljubljana Declaration on Landslide Risk Reduction (Sassa 2017) endorsed a plan for the preparation of the KLC2020 as a global alliance which aims, in the medium- and long-term, to accelerate and incentivize actions for landslide disaster risk reduction to 2030 and beyond. The KLC2020 is thus a framework aimed at providing key actors and diverse stakeholders concerned with landslide risk at all levels and in all sectors with tools, information, platforms, technical expertise and incentives to globally promote landslide risk reduction.

KLC2020 supports the implementation, any follow-up and review of several global initiatives: the Sendai Framework for Disaster Risk Reduction 2015–2030 (SFDRR 2015), the 2030 United Nations Agenda for Sustainable Development (UN 2022a) and its 17 Sustainable Development Goals, the New Urban Agenda, and the Paris Climate Agreement. The KLC2020 is also a contribution to the ISDR-ICL Sendai Partnerships 2015–2025 for global promotion of understanding and reducing landslide disaster risk with a subtitle “Tools for Implementing and Monitoring the Post-2015 Framework for Disaster Risk Reduction and the Sustainable Development Goals” (Sassa 2015). The ISDR-ICL Sendai Partnerships 2015–2025 was a voluntary commitment to the United Nations World Conference on

Disaster Risk Reduction, Sendai, Japan, 2015. Today, there are many Voluntary Commitments to SFDRR, not all at global scale (UNDRR 2022).

KLC2020 accounts for ten priority actions in research and capacity building, coupled with social and financial investment, among them, the following priority actions are of interest for discussion in this paper:

- Action 5: Promote open communication with local governments and society through integrated research, capacity building, knowledge transfer, awareness-raising, training, and educational activities, to enable societies and local communities to develop effective policies and strategies for reducing landslide disaster risk, to strengthen their capacities for preventing hazards from developing into major disasters, and to enhance the effectiveness and efficiency of relief programs.
- Action 9: Foster new initiatives to study research frontiers in understanding and reducing landslide disaster risk by promoting joint efforts by researchers, policy makers and funding agencies.

The basic idea behind this paper is to discuss a state-of-the-art on diverse global observatories related to sustainable development and its goals, and how this knowledge can be used to develop a natural-hazard-related web observatory that would help to strengthen the discourse among relevant stakeholders focused on risk dialogue in order to increase resilience and support the implementation of sustainable development goals (SDGs) related to natural hazards. Water has an important role in the 2030 Agenda for Sustainable Development (Casale and Cordeiro Ortigara 2019), as it is directly or indirectly related to all SDGs (Fig. 1).

The University of Ljubljana (UL) Faculty of Civil and Geodetic Engineering (FGG) is a full member of the ICL since 2008, and has actively contributed to different ICL and IPL activities in the years there after (Mikoš and Petkovšek 2019), most notably by organizing the 4th World Landslide Forum in Ljubljana in 2017 (Mikoš et al. 2017).

UL FGG has been since 2008 consecutively recognized five times as the World Centre of Excellence on Landslide Risk Reduction, and is hosting UNESCO Chair on Water-related Disaster Risk Reduction (WRDRR), established at University in Ljubljana in 2016. UL FGG and UNESCO WRDRR Chair are supporting KLC2020, and its two Priority Actions: #5 and #9. In this sense, ULFGG proposed in 2022 a new IPL project entitled “World-wide-web-based Landslide Observatory (W3bLO)”. The project, if approved by the Global Promotion Committee of the International Programme on Landslides and the Kyoto Landslide Commitment 2020 (GPC/IPL-KLC), will be executed in collaboration with the UNESCO International

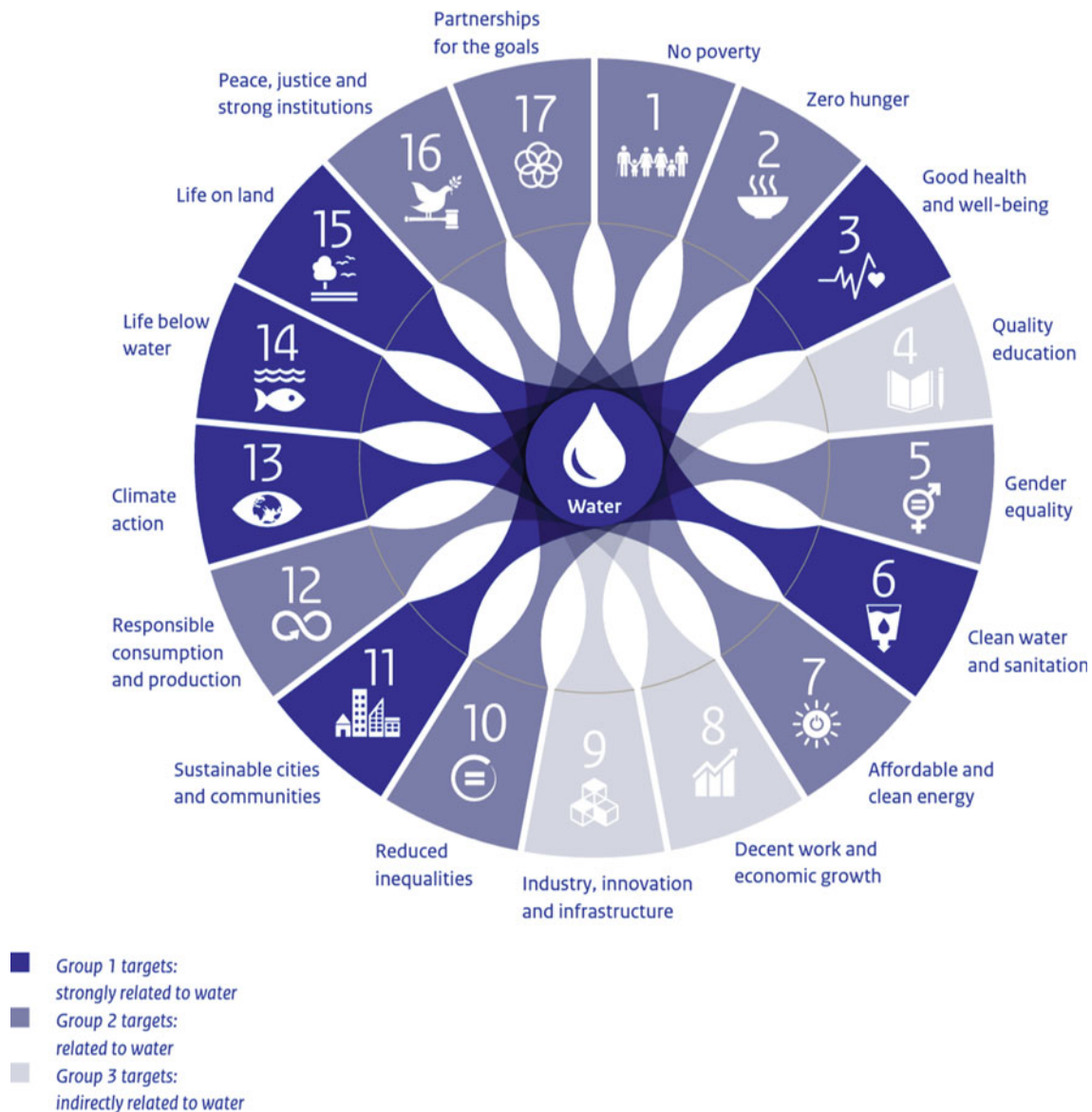


Fig. 1 Importance of Water in 2030 (from PBL 2018, source Casale and Cordeiro Ortigara 2019, Fig. 4)

Research Institute on Artificial Intelligence (IRCAI), hosted by Institute Jožef Stefan, Ljubljana. The IRCAI was inaugurated and virtually launched in March 2021, and is regarded as a coordination point, founding route and exploitation accelerator for approaches to the UN SDGs that make use of Artificial Intelligence. Due to the proximity of the both institutions, located in the City of Ljubljana, Slovenia, and excellent experiences in the past in the field of the joint research cooperation, it was quite natural to try to combine the expertise in the two fields: Artificial Intelligence (IRCAI) and landslide research and risk reduction (ULFGG), for the implementation of sustainable development. The joint idea was to start developing a web-based

observatory to be applied in the field of disaster risk reduction.

The first phase of the project work will be based on the experiences of the IRCAI team while developing a web-based water observatory for smart water management for sustainable development. Before a more focused and in-depth description of a water observatory under construction for smart water management, a short overview of already developed natural-hazard-related observatories will be shown to see what information they offer. A confrontation of the two, and having in mind the SFDRR 2015–2030 targets, a way further in preparing a web-based Landslide Observatory will be paved.

Landslides and mass movements were also recognized as one of the main threats to soil health in the EU Soil Thematic Strategy (Montanarella and Panagos 2021), thus being relevant for target SDG 15.3 for achieving land degradation neutrality. Landslides are related to the EU Biodiversity Strategy for 2030 (European Commission 2022a) that was published on 20 May 2020, and EU Soil Strategy for 2030 (European Commission 2022b), adopted by the European Commission on 17 November 2021. As a tool for the implementation of the latter strategy, the EU Soil Observatory was launched on 4 December 2021 (ESO 2022). Its vision, mission, operational principles, organization, functions and activities are laid down in a concept note (European Commission JRC 2021). Sustainable soil management and the restoration of degraded land is critical if biodiversity protection targets are to be achieved. The reader can easily understand how landslides are involved in water and soil issues concerning sustainable development at all scales. Potentially, a web-based Landslide Observatory will help to implement different international strategies and policies, foremost several SDGs.

Different institutions/entities are offering tools or data for water-, soil-, and natural-hazard-related observatories. For example, Copernicus Emergency Management Service (EMS) Early Warning and Monitoring offers critical geospatial information on emergency response and disaster

risk management at European and global level through continuous observation and forecasts for floods, droughts and forest fires (Table 1).

The Dartmouth Flood Observatory was founded in 1993 by Dartmouth College, Hanover, New Hampshire, USA, and moved in 2010 to University of Colorado, USA. It offers diverse space-based data, images, maps, and tools for surface waters, including floods (Kettner et al. 2021).

The NASA Earth Observatory (NASA 2022a) is bringing together images, global maps, articles, blogs, stories, and discoveries on a variety of natural events, including flooding and landslides. For landslides as for other natural disasters it is important to develop robust inventories of events. NASA has developed Global Landslide Catalog (GLC) and expanded it by Landslide Reporter Catalog (LRC) to the so-called Cooperative Open Online Landslide Repository (COOLR) (NASA 2022b). The COOLR project contains *Landslide Reporter*, the first global citizen science project for landslides, and *Landslide Viewer*, a portal to visualize data from COOLR and other satellite and model products (Juang et al. 2019). In the first 13 month of the project, 162 landslide events were added to the inventory (NASA 2022c)—a good start.

In 2010, the International Consortium on Landslides (ICL) started its ICL World Report on Landslides (ICL 2022), a platform for a global repository on landslides for

Table 1 A selection of natural-hazard-related observatories

Observatory	Information	References
AGU–Blogsphere	A community of earth and space science blogs, hosted by the American Geophysical Union, including The Landslide Blog	AGU (2022)
DFO–Dartmouth flood observatory	Space-based measurement, mapping, and modeling of surface water for research, humanitarian, and water resources applications	DFO (2022)
EDO–European drought observatory	Drought-relevant information and early-warning for Europe	EDO (2022)
EFAS–European flood awareness systems	Complementary regional and national flood forecast and monitoring information	EFAS (2022)
EFFIS–European forest fire information system	Forest fire activity in near-real time. Useful for wildfire management at national and regional level	EFFIS (2022)
EUSO–European union soil observatory	Collecting high-resolution, harmonized and quality-assured soil information (showing status and trends) to track and assess progress by the EU in the sustainable management of soils and restoration of degraded soils	EUSO (2022)
GDACS—Global disaster alert and coordination system	GDACS is a cooperation framework between the United Nations, the European Commission and disaster managers worldwide to improve alerts, information exchange and coordination in the first phase after major sudden-onset disasters. The system covers earthquakes, tropical cyclones, floods, volcanoes, droughts, and forest fires	GDACS (2022)
GDO–global drought observatory	Drought-relevant information and early-warnings globally	GDO (2022)
GloFAS–global flood awareness systems	Complementary global flood forecast and monitoring information	GloFAS (2022)
NASA earth observatory	Images, global maps, articles, blogs, stories, discoveries on natural events such as floods, landslides, fires, drought and other natural events	NASA (2022a)

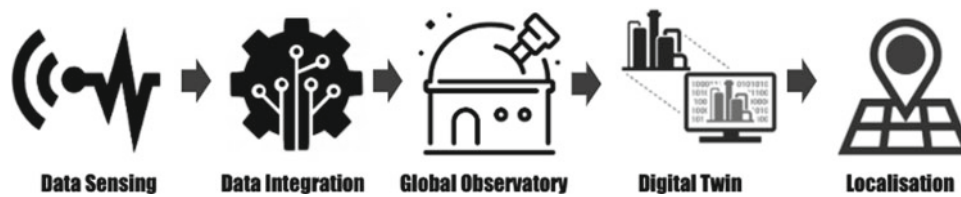


Fig. 2 The approach used leading from data sensing to the digital twin and its approximation to local priorities

landslide experts, researchers and practitioners alike. Later, detailed instructions were prepared on the web site with a ranking system depending on the details submitted to the Report. In 2017, forty reports were submitted (Abolmasov et al. 2017). In early 2022 it is sadly only added a few more.

2 A Data-Driven Global Observatory

The world's globalization phenomena unveiled the awareness of world-wide problems, such as the climate crisis and its consequences, but also the common efforts to find solutions to water-related problems (e.g. floods) through collaborative actions. There are many obstacles still today on such global strategies to which innovative technology and data-driven solutions can help. In this section, we describe a novel concept of a global observatory based on text mining algorithms that is able to answer the wide range questions that are core to global solutions, using Big Data analytic methods over the layered information it is ingesting in real-time.

The main perspectives of this global observatory fall on: (i) the monitoring and exploration of news articles and social media feeds; (ii) the analysis of combinations of indicators through time and what stories can they tell; and (iii) the exploration of published scientific knowledge and patented innovation; and (iv) the exploration of historical data on natural resources and weather, allowing to forecast tendencies in a medium/long-term time horizon of ten years. All of these perspectives can be combined to provide complementary answers to main landslide-related topics.

2.1 Methodology

Observing events both at global and local scales requires firstly the sensing capability and then the interoperability between the knowledge that was sensed. That sensing is translated by the acquisition of heterogeneous data that can provide us with a multitude of perspectives over what is being observed.

As illustrated by the schema in Fig. 2, we consider the construction of the Global Water Observatory into phases going from lower to higher complexity. We start by putting

together data sources that are meaningful to a range of stakeholders that are targeted, from engaged citizens to decision makers that can leverage the information provided to established evidence-based policies.

At the data collection phase, we must be concerned with properly addressing the challenges in the heterogeneous nature of Big Data in all of its Vs dimensions (Song and Zhu 2016), their different frequency and size, as well as the levels of access to it established by data providers. These parameters take into consideration to ensure the appropriate data ingestion into the system. The selection of data sources is done manually, but their ingestion is automated, when the frequency of the update is high (e.g. weather).

In the case of yearly updates, the data is ingested manually (e.g. MEDLINE or statistical aggregated data feeding indicators). This Observatory collects data from many different data sources (e.g., the Worldwide news, the Microsoft Academic Graph, the Word Bank, the United Nations Sustainable Development Goals) in their global scope, according to their relation to the focus topics and priorities (see Table 2). Complementary to this, the local installation of the Observatory is also ingesting local data originated mostly from national open data initiatives, national statistics agencies or open datasets produced in the context of projects that relate to the priorities that are being observed (collected from global repositories, e.g., Schweizerische Eidgenossenschaft 2022).

The next stage is the data cleaning, data processing and data integration prior ingestion. This step is very important to allow for the data quality that is needed in order to obtain useful insights from it. In this step, we include the data curation, where the most meaningful datasets are selected and parsed. The Observatory also includes exploratory data analysis and some data visualization for the purpose of prototyping the data visualization modules that are then available at the Observatory.

The Observatory phase is then possible when the curated data streams of a selection of dynamic data sources are live in the system and can be used to obtain insight on particular topics of interest, monitor Key Performance Indicators associated with business priorities, and allow for a global and local perspective on related topics. These include interactive data visualizations of indicators and statistical data, the dynamic view of the news sources over priorities,

Table 2 Data sources feeding the observatory

Name	Source	Short description
Worldwide news	Event registry	News articles with timestamp, title and URL
Facebook impact	Event registry	Number of posts in Facebook mentioning a certain article
UN open dataset	UN portal	Global indicators on water resource management
World Bank open data	World Bank	Global indicators on the access to clean and drinkable water
SDG	SDG6 web portal	Global indicators of progress on the achievement of SDG6
JRC	Global surface water	The volume of available water by GIS coordinates over time
Statistical water data	Eurostat	Different statistical time series on water-related aspects
European water data	EU open data portal	A range of water-related topics described by time series
Twitter feed	Twitter	The historical data of a part of the global Twitter feed
Weather data	ECMWF	The current data and forecasts on the weather conditions
MEDLINE	USA national library of medicine	The 26 + million biomedical research article abstracts and titles
Microsoft academic graph	Microsoft academic	Published research articles and patents (including MEDLINE)

or the user query over a scientific research topic. This allows for insight on topics in analysis (such as water topics like water scarcity and water quality, and public health topics like Ebola or the new coronavirus) that will be put into the context of local data when sourced from the shared interest of users.

The path ahead is a novel concept of a meaningful Digital Twin (i.e., a dynamical model which given a current state of an observed system, is capable of a digital partial reconstruction of such a system) that builds over the Global Water Observatory to rise above data complexity towards data interoperability. This is usually difficult to achieve in full due to the heterogeneity of the data, the different characteristics of the data sourced (frequency, data types, etc.) and the domain knowledge needed to identify new challenges covering a wide range of business intelligence priorities. Nevertheless, useful aspects of it can be achieved, some of which are already evident from the implementation available at (NAIADES Water Observatory 2022) and discussed in the following sections. An example of this is to track a topic in the news, its impact in the social media, and explore the range of the problem in the published scientific research, as well as extract good practices to deal with this problem.

A final stage to this diagram, and usually forgotten in a theoretical framework, is the adaptation of the system to the needs and priorities on the user's side. Here, we consider the ingestion of local data, the customization of news streams, the availability of exploratory dashboards, the shareable instances for policy makers, and the APIs for 3rd party integration.

Altogether these five phases run simultaneously to have the Observatory running as a live system that can support real-time decision-making. A typical example of the aimed outcome of such an intelligent system is the following sequence of events:

- (i) a new technology is identified in scientific research;
- (ii) the patents around it multiply, alerting its importance;
- (iii) new mentions of its usage arise in the market landscape;
- (iv) companies relating to it are now able to guarantee new investment; and
- (v) news media is more and more aware of the importance of the technology (unknown in (i)).

The system that is able to access the data sources that relate to the items above, is also able to track the term throughout the several phases of popularization. It is also able to show the current status of a particular topic of interest, and optimally alert for potentially trendy topics in the future.

The analysis of indicators in pair with other data-driven perspectives can put the problem into a global context. In the visualization of Fig. 3 we consider five dimensions—x-axis, y-axis, bubble size, bubble color, and time—to represent the many aspects of the representation of the information. The explorations based on this analysis lead us to aspects of the causality inherent to the problem itself, in the sense that some of the answers to the problem in analysis lie in the analysis of the causes of that problem.

2.2 An Observatory for Water Events

Water is fundamental to all human activity and ecosystem health, and is a topic of rising awareness in the context of the recent discussions on climate change. Water resource management is central to those concerns, with the industry accounting for over 19% of global water withdrawal, and agricultural supply chains are responsible for 70% of water stress (Our World in Data 2020). In 2015 the UN established



Fig. 3 Animated visualization of indicators and their relation

“clean water and sanitation for all” as one of the seventeen Sustainable Development Goals, aiming for eight targets to be achieved by 2030 (UN 2022b). The UN secretary-general points out in April 2020 that SDG 6 is “badly off track” compromising the progress on the 2030 Agenda (UN 2020). As noted by the Organization for Economic Co-operation and Development (OECD), the ‘water crisis’ has often proven to be a crisis of governance (OECD 2011), where water scarcity is largely caused by mismanagement of resources, leading to a global prioritization (Akhmouch et al. 2018).

Added to this, climate change is a global problem that in recent years has been in the focus of European and Worldwide strategies. The priorities in the European Union are rapidly changing towards sustainability and environmental efficiency, covering most domains of action. The European Commission’s Green Deal (European Commission 2019a) aiming for a climate neutral Europe in 2050, and boosting the economy through green technology provides a new framework to understand and position water resource management in the context of the challenges of tomorrow (European Commission 2019b).

In this context, the NAIADES project (NAIADES 2022) aims to improve the water resource management in a global context, including European regions where water scarcity is predicted, also dealing with concerns such as saline intrusion and groundwater contamination. The current implementation of the Water Observatory in the context of the European Commission’s-funded Horizon 2020 project NAIADES on “Smart Water Management for Sustainable Development

Goals” (Pita Costa et al. 2021) allows users to have a global perspective on water-related events (e.g. floods), but also to address specific conditions and priorities. It is ingesting water-related data both from global agencies (e.g. UN and World Bank) and local entities (e.g. Swiss open government data opendata.swiss (Schweizerische Eidgenossenschaft 2022)) to activate an intelligent system distributed through the following “views”:

- Indicators: adding to the global indicators fed on statistical data provided by the United Nations, the world bank and other trustworthy agencies, the local installation of the observatory is ingesting curated open datasets that have regional information about water topics of interest to the stakeholder.
- Media: each location has its own news and social media streams configured to priorities and aspects of the news that stakeholders define as topics of interest (e.g., floods).
- Research: similar to the media sources, the research topics allow for some customization to better fit to the needs of the local user.
- Resources: the natural resources information provided for exploration is geolocated to the regions of interest to the user of the platform.

These views change when a new location is selected to better reflect the priorities of its users. This observatory allows the user to achieve a multitude of perspectives aligned with objectives fed by data sources of different nature, as follows:

- Explore the details of the best practices identified in global and local news on water-related topics, with a worldwide coverage through multilingual capability configured to the user priorities;
- Assess the impact of the events of interest from the reshares on social media (Facebook), as well as explore the real-time feed of social media itself (e.g., Twitter);
- Observe the evolution in time of local and global indicators related to the usage of water resources to understand the relations and possible implications in own business;
- Explore the global information of water contamination from trusted scientific sources and news articles, complemented by the social media input, and the good practices to deal with local similar problems in focus;
- Reuse open datasets on weather and water levels to have an assessment on the impact of climate change in available resources in a window of ten years;
- Align with the input of the observatory with the data provided by other data platforms and the proprietary data, enriching the business intelligence.

The NAIADES Global Water Observatory does not only contribute to the improvement of European sustainability in water-related matters, but will also provide the local actors on the water resource management an active role in that. The typical three main groups with different workflows that can be users of this technology belong to supported by the developed technology:

- water resource management: using the provided information in the resolution of problems related to weather events, to understand how their actions are perceived by the consumers, and to explore successful scenarios in similar cases.
- local government: to help evidence-based decision-making using open data, better sync to the Sustainable Development Goals and other guidelines, and evaluate commitments in time.
- general public: for water education with a local context, in aspects that matter to the local population, based on parts of the Water Observatory that can be open to the public.

The intention to globally monitor water resources is not new, and by the late 1960s (Freeze and Harlan 1969) the first spatially-distributed water resources model appeared, with first operational uses of satellite observations in water resources developed in the early 1980s (Ramamoorthi 1983). The reliable management of water resources is only possible under the condition of availability of adequate qualitative and quantitative information about the state of the water body at any moment of time.

Taking advantage of the recent technological progress enabling much innovation that was unthinkable a few years ago, the concept of the Digital Twin is increasingly entering the water sector as an innovation driver. Due to the rapidly growing awareness of the sustainability challenges that we are facing in Europe and worldwide in the context of water resource management, there has been much work done to develop systems that are able to collect information about the available water and even simulate and forecast that in the near future. These are usually geolocation-based systems ingesting water-related data to enable real-time monitoring of resources and usage (Idrica 2018). The other typical approach is the systems focused on workflows in the water sector, including the management of water distribution networks, hydraulic efficiency or leak/fraud detection, better suited to those companies that already have their infrastructure in place and know well what they want to monitor (Idrica 2019).

The approach proposed in this section is novel in many ways. It brings a dimension of media and social media to the analysis of global water events, made possible by the recent advances in text mining and machine learning to capture appropriate insight from the data collected worldwide.

As shown in Fig. 3, the user can select over a variety of indicators each of which represents a time-series of ingested statistical data that can describe progress on a certain topic over the years. Moreover, the analysis of the open data ingested allows us to identify causality relationships between those indicators (Neuman and Grobelnik 2022) and to compare regions and countries on resources and measures to build evidence-based policy-making over data that is often freely accessible but is not always easy to explore.

The media is also a rich dataset that can be used to monitor the water-related events in real-time. NAIADES is using the Event Registry News Engine (Leban et al. 2014) to analyze more than 300 thousand new articles per day over more than 60 languages. The NAIADES Water Observatory is monitoring flood and water contamination events at a worldwide scale (in Fig. 4, we show the news dashboard exhibiting the most recent topics on a selected specific focus in media every second), allowing us to use advanced text mining capabilities to explore the main concepts and categories when addressing water-related events (in Fig. 5, we show the distribution of news categories on a certain water-related topic over a time window).

This news monitoring perspective is also including a Twitter observatory that adds a social media perspective covering the main discussions taking place in related topics, or the sentiment of those social media posts over time that can help us to achieve another perspective on the water event. The current implementation is based on an easily configured dashboard feeding on the collected data that can

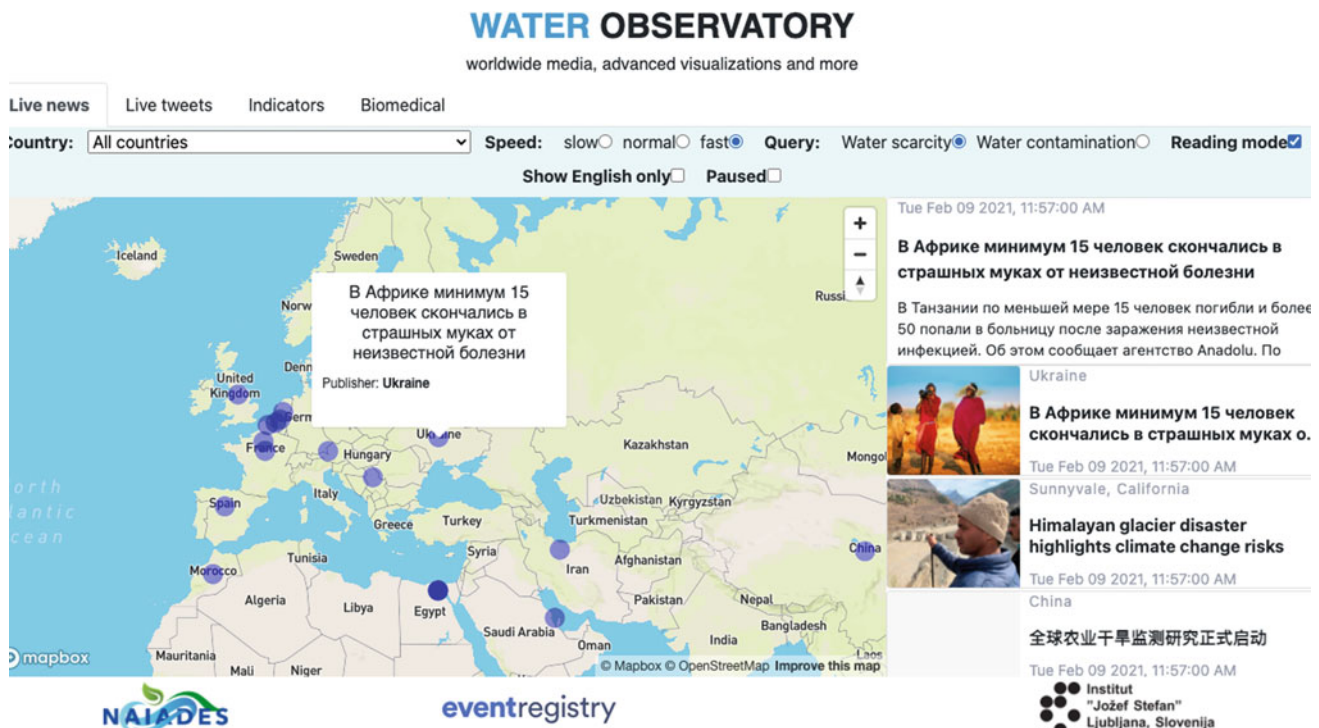
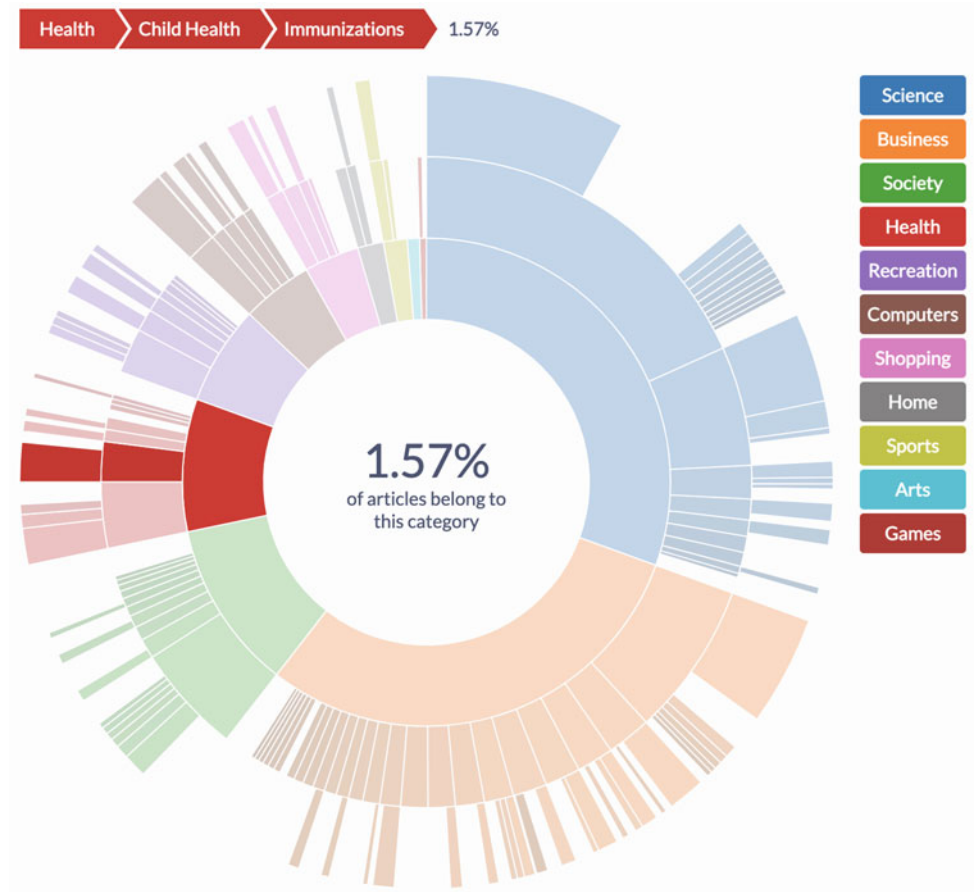


Fig. 4 SDG 6-focused NAIADES water observatory collecting worldwide news on water-related events

Fig. 5 Weight of news categories in the context of “wastewater” during 2021



also serve as a prototype tool to explore potential and build useful data visualization dashboards.

One of the valuable aspects of the usage of social media data is the possibility of using it in order to nowcast public opinion about the actions taken in a certain water-event, or to establish customized alerts to monitor those events. The latter is a much more difficult task due to the noise and low frequency/amount of data. For those, we can use data from collected news on similar events covering the main features to take into consideration.

The important role of scientific research in this context is revealed by the trends and findings on certain water-related topics (e.g. water contamination or wastewater) and the best practices that can be extracted from this data. The observatory is also using other text mining and data analytics algorithms to analyze simultaneously multiple time-series providing interactive exploration tools to understand trends in research over time and how concepts are related with each other over time (see Fig. 6).

The localization of this global system entails the customization of its functionality in news monitoring, ingestion of local indicators and exploration of scientific research on observed problems in, e.g., groundwater contamination. In that, the observatory is synchronizing with the priorities of regional water providers. These agencies (e.g. Aguas de Alicante) are collecting data on their water resource management services to improve the customer satisfaction and optimize their system.

2.3 Addressing Other Landslides Problems

The development of a Landslide Observatory, refocusing some of the technologies used in the earlier described NAIADES Water Observatory, are mostly due to the acquisition of appropriate data and to the definition of monitoring priorities. When analyzing the worldwide news and social media, the usage of appropriate terms, and eventually the ingestion of news venues that are not yet considered is fundamental to cover well the topics of interest and better capture the dynamic perspective they provide. The Observatory is using Wikipedia terms to activate its multi-lingual potential (e.g., “Landslide” is an existing term in Wikipedia covered by 81 languages, while “Mudslide” does not exist having to be substituted by “Mudflow” as noted by Wikipedia).

Following the unfortunate mudslide disaster event in the Shizuoka Prefecture in Japan on July 7, 2021, the news monitors ingested 2165 related news articles covering the event and its consequences. Figure 7 shows the entities and concepts extracted from the sample of news based on the query defined by the user that will activate other data analytics algorithms and data visualization modules (as above in Fig. 5).

When learning over historical data collected on a topic, the Observatory can leverage text mining methods to automatically classify news records based on labeled text, and identify related events that the user can recur to in order to

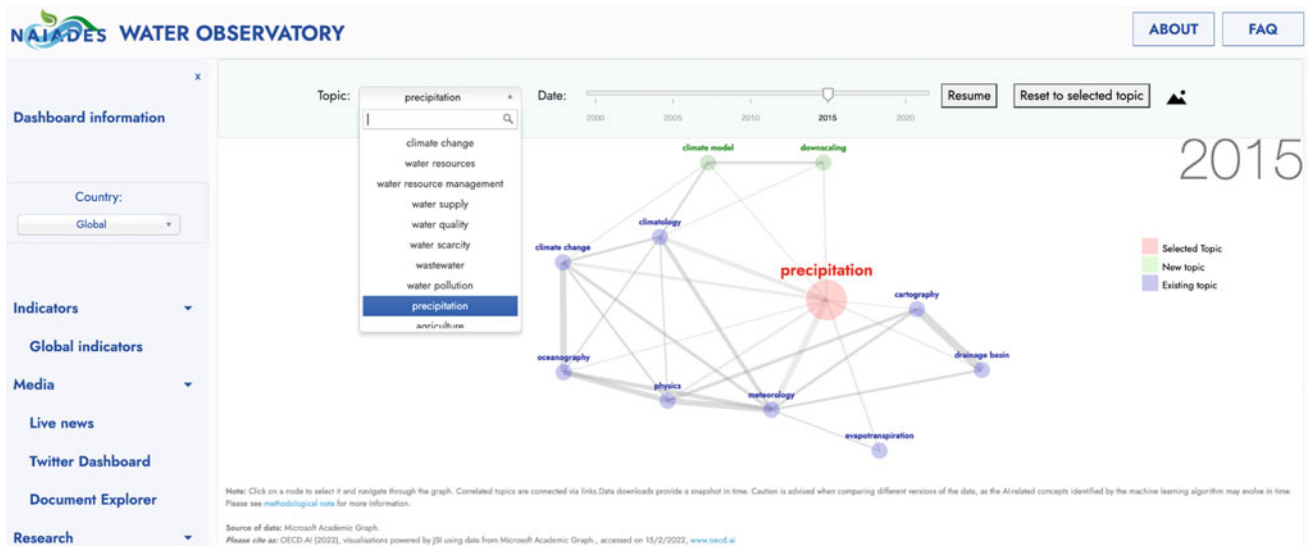


Fig. 6 Main topics in research relating to “precipitation” across time

explore a certain event. By ingesting a stream of Twitter data, we are also able to reuse some of these extracted entities in monitoring similar events in social media, and relating the frequency of mentions with the intensity of the media coverage on such events.

Moreover, with the computation of the news sentiment, they can grasp the perspective of the media on, e.g., the governmental actions to the event. Figure 8 shows the news sentiment overview on news regarding the current mudslide disaster in Ecuador, in a suburb of Quito on January 31, 2022. Although most of the sentiment is negative as expected due to the nature of the event, part of it is positive showing some appreciation for, e.g., the reevaluation of scientists and engineers in the water distribution in Ecuador, or the reopening of public discussions on the bargain power of indigenous groups in mining and drilling disputes (New York Times 2022).

The existing observatory identifies 927,847 articles collected over eight years on the topic of “Landslides” (see Fig. 9). It allows the user to explore the phases of each event

based on the available news articles and explore constructive scenarios from other experiences and methodologies, leveraging the capabilities of text mining technologies made available by the Jožef Stefan Institute (e.g. NewsFeed and Wikifier (Leban et al. 2014)) allowing the use of Wikipedia terms to perform complex queries across languages, and that can better acquire detail and reasoning.

Allied with the exploration in media and social media, the user of the Observatory can explore published research and patented innovation through a complex data visualization technology that makes it easier to perform literature review over a certain topic, allowing for powerful Lucene-based queries over the article’s metadata aiming to refine search by moving a pointer over clusters of related topics (see Fig. 10). Considering that the MEDLINE dataset ingested into the system includes “Landslides” as one of its descriptor categories (USA National Library of Medicine 2019), the exploration of scientific articles covering landslide-related topics can be explored using the following Lucene query: *MeshHeadingList.desc: “Landslides”*.

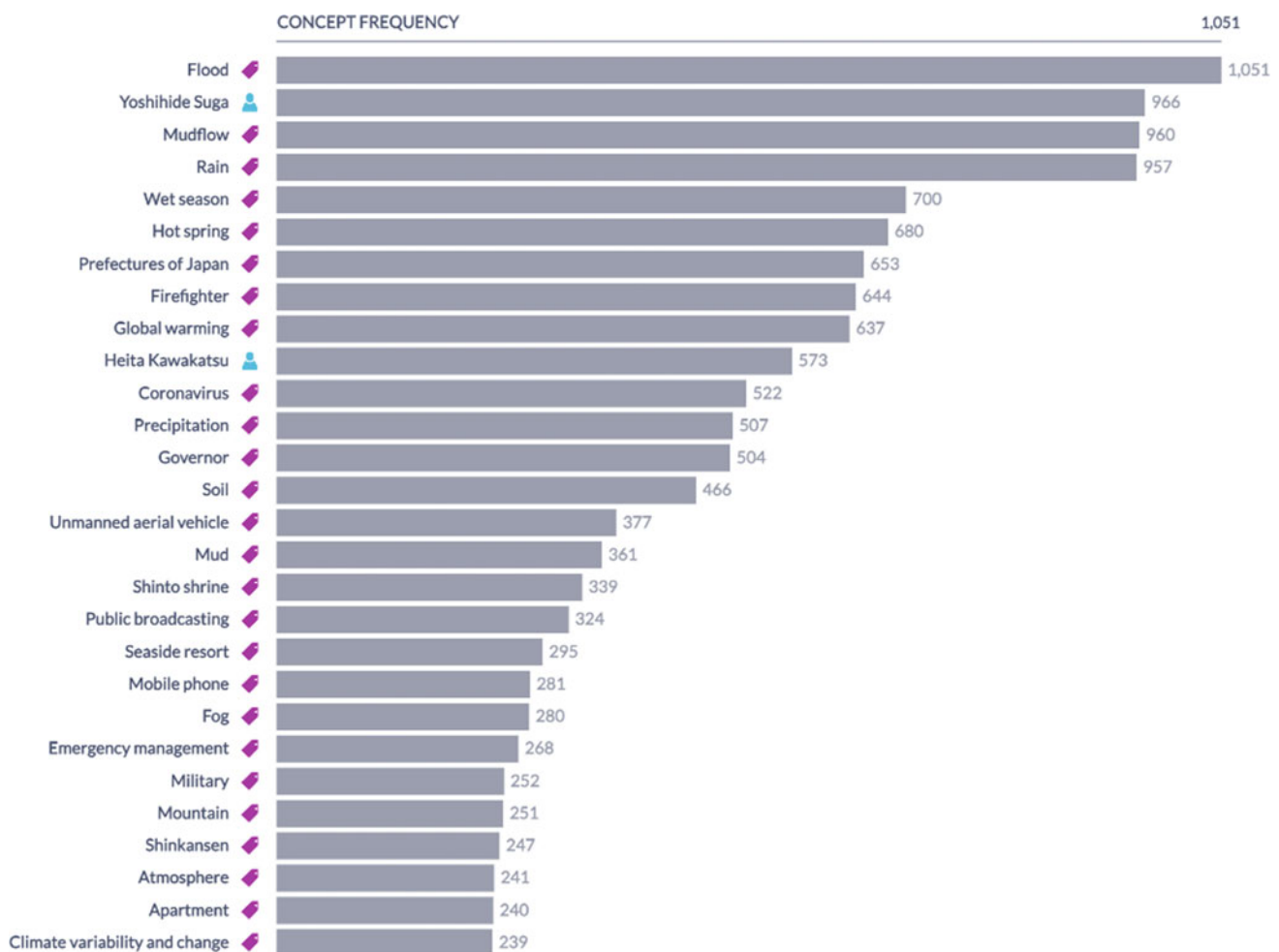


Fig. 7 Main concepts related to the mudslide disaster in Japan on July 15, 2022

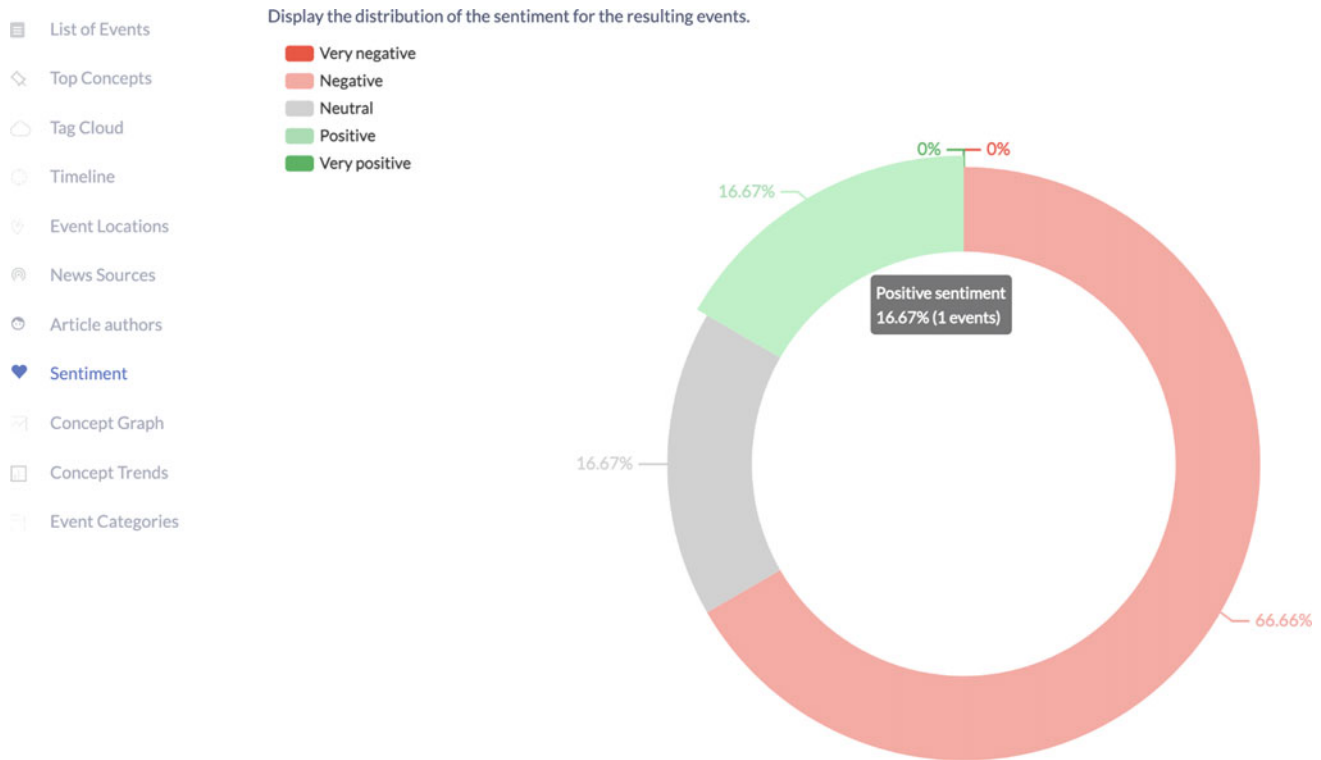


Fig. 8 News sentiment captured from the mudslide

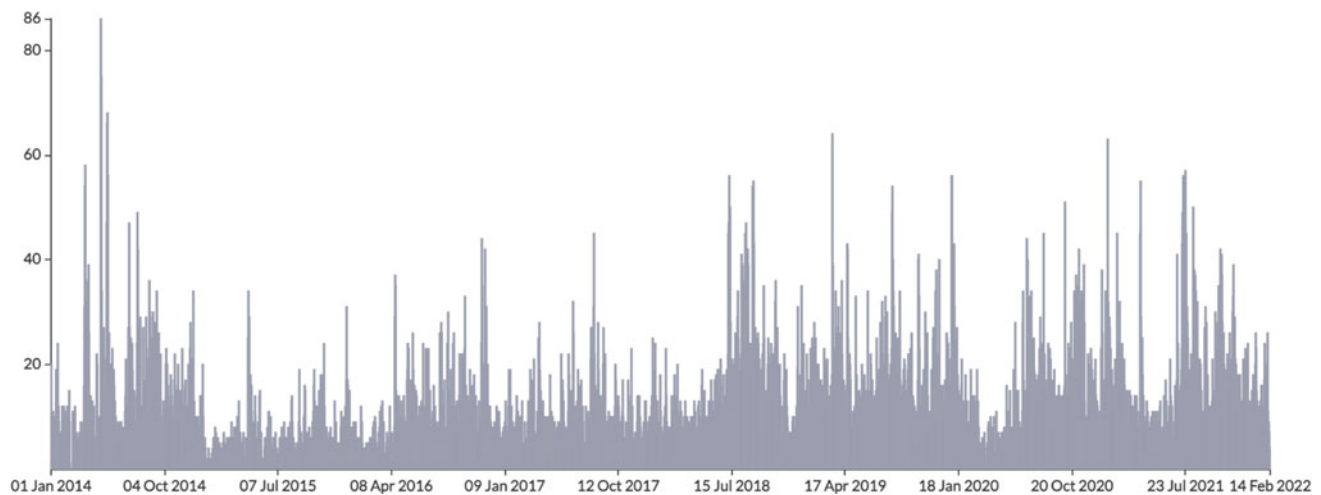


Fig. 9 Exploring a timeline of worldwide news on landslide events throughout 927,847 articles in eight years of collected data

Finally, the access to the indicators view as a data visualization tool to make sense of the ingested statistical data, complements this analysis workflow allowing the user to investigate on different aspects related to landslides, from the “water stress level” to the “water exploitation index”, to name a few of the time series already cleaned and ingested.

3 Conclusions and Further Work

The results discussed in this article show the potential impact of the proposed data-driven global observatory in contexts like water resources and climate change preparedness (already including a focus on floods as water-related events),

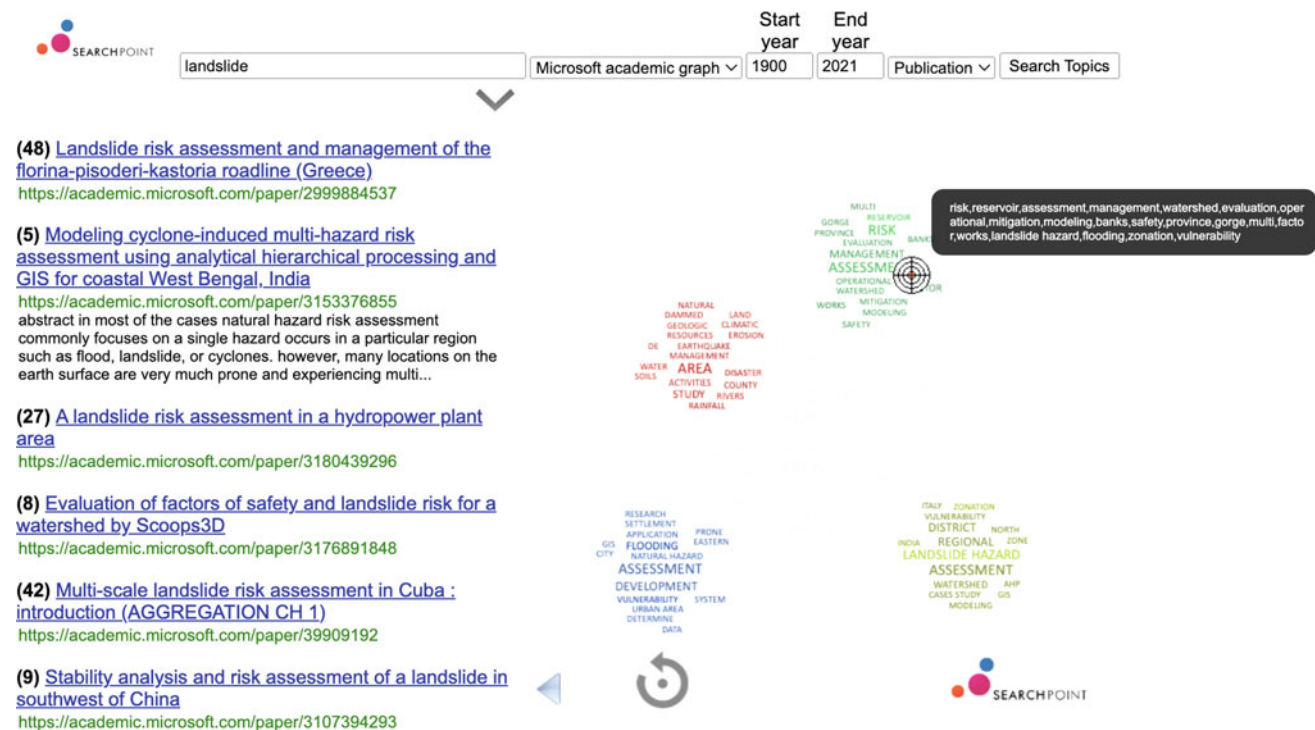


Fig. 10 Exploring scientific research on landslide assessment and management

and the scaling potential to address landslides, as already demonstrated with the results shown. This integrated system is capable of monitoring in real-time worldwide news and social media, statistics, published science, weather and many other data streams that are identified as useful and can provide complementary value to those considered already. The scaling capability of this intelligent system allows it to be deployed in the context of other global problems where there is enough data to provide useful and meaningful contribution, either in other aspects of the climate crisis to better plan response, in addressing other epidemiological concerns to serve as early warning, or in addressing a new focus in the context of data science for social good.

We are now working on extending this system to further integrate the information retrieved with the focus on landslide-related topics. The user will be able to explore a wide range of indicators and compare trends on a global and local level throughout a meaningful timeline. We will also be reusing EC-funded open datasets and initiatives in order to ingest this information as European-level indicators to complement the analysis.

Moreover, we are investigating the optimal long-term forecasting and data visualization that can contribute to climate change preparedness, integrating the knowledge obtained from the appropriate application of text mining methods to indicators, research and news, and elaborating on

the impact of that change in landscape monitoring-specific problems.

Furthermore, we will be further investigating the validity of the localization of this Observatory, integrating some of the local data that can be provided by the user, and customizing news sources to their own priorities, as well as making available data exploration dashboards that allow for further insight and evidence-based policy.

The gained expertise on how to build a web observatory in the field of water management in order to support the implementation of the SDG6 “Clean water and sanitation” will be used to develop a web landslide observatory that may be used for the implementation of the SDG13 Climate Change and other SDGs, where landslides are seen as threatening factor, and other international strategies and policies, including the Kyoto Landslide Commitment 2020 for Global Promotion of Understanding and Reducing Landslide Disaster Risk. The observatory development can also be seen as a contribution to UNESCO Intergovernmental Hydrological Programme Phase IX (IHP-IX OIP).

Acknowledgements The authors would like to acknowledge the financial support of Slovenian Research Agency by core funding P2-0180, the University of Ljubljana by Development Fund for UNESCO Chair, and European Research Council (ERC) under the European Union’s Horizon 2020 research and innovation programme (grant agreement No 820985).

References

- Abolmasov B, Fathani TF, Liu KF, Sassa K (2017) Progress of the world report on landslides. In: Sassa K, Mikoš M, Yin Y (eds) *Advancing culture of living with landslides*. WLF 2017. Springer, Cham, pp 219–226. https://doi.org/10.1007/978-3-319-59469-9_18
- AGU (2022) Blogosphere. American geophysical society. <https://blogs.agu.org/>. Accessed 14 Feb 2022
- Akhmouch A, Clavreul D, Glas P (2018) Introducing the OECD principles on water governance. *Water Int* 43(1):5–12. <https://doi.org/10.1080/02508060.2017.1407561>
- Aljohani NR, Abbasi RA, Bawakid FMS, Saleem F, Ullah Z, Daud A, Aslam MA, Alowibdi JS, Hassan S-U (2019) Web observatory insights: past, present, and future. *Int J Semant Web Inf Syst* 15(4):4. <https://doi.org/10.4018/IJSWIS.2019100104>
- Casale G, Cordeiro Ortigara AR (eds) (2019) *Water in the 2030 agenda for sustainable development: how can Europe act?* Water Europe, Brussels. (ISBN 978-90-8277064-3) p. 36. <https://unesdoc.unesco.org/ark:/48223/pf0000372496>
- DFO (2022) Flood observatory. <https://floodobservatory.colorado.edu/>. Accessed 13 Feb 2022
- EDO (2022) European drought observatory. <https://edo.jrc.ec.europa.eu/edov2/php/index.php?id=1000>. Accessed 13 Feb 2022
- EFAS (2022) European flood awareness systems. <https://www.efas.eu/en>. Accessed 13 Feb 2022
- EFFIS (2022) European forest fire information system. <https://effis.jrc.ec.europa.eu/>. Accessed 13 Feb 2022
- EU (2019) Delivering the European green deal. https://ec.europa.eu/info/strategy/priorities-2019-2024/european-green-deal/delivering-european-green-deal_en. Accessed 13 Feb 2022
- European Commission JRC (2021) Concept note for the EU soil observatory. European commission, Joint Research Centre, Ispra, Italy, p 6. https://ec.europa.eu/jrc/sites/default/files/concept_note_euso_final_sep2021.pdf. Accessed 13 Feb 2022
- European Commission (2019a) The European green deal. European commission, Brussels, Belgium. COM(2019a) 640 final
- European Commission (2019b) European green deal. https://ec.europa.eu/info/strategy/priorities-2019b-2024/european-green-deal_en. Accessed 15 Feb 2022
- European Commission (2019c) Water scarcity and droughts in the European Union. https://ec.europa.eu/environment/water/quantity/scarcity_en.htm. Accessed 15 Feb 2022
- European Commission (2021) EU soil strategy for 2030—reaping the benefits of healthy soils for people, food, nature and climate. COM/2021/699 final. Brussels, Belgium, p 52. <https://eur-lex.europa.eu/legal-content/EN/TXT/?uri=CELEX%3A52021DC0699>
- European Commission (2022a). Biodiversity strategy for 2030. European commission. Environment. Brussels, Belgium. https://ec.europa.eu/environment/strategy/biodiversity-strategy-2030_en. Accessed 13 Feb 2022a
- European Commission (2022b) Soil strategy for 2030. European commission. Environment. Brussels, Belgium. https://ec.europa.eu/environment/strategy/soil-strategy_en. Accessed 13 Feb 2022b
- EUSO (2022) EU soil observatory. <https://ec.europa.eu/jrc/en/eu-soil-observatory>. Accessed 13 Feb 2022
- Freeze RA, Harlan RL (1969) Blueprint for a physically-based, digitally-simulated hydrologic response model. *J Hydrol* 9(3):237–258. [https://doi.org/10.1016/0022-1694\(69\)90020-1](https://doi.org/10.1016/0022-1694(69)90020-1)
- GDACS (2022) Global disaster alert and coordination system. <https://www.gdacs.org/>. Accessed 14 Feb 2022
- GDO (2022) Global drought observatory. <https://edo.jrc.ec.europa.eu/gdo/php/index.php?id=2000>. Accessed 13 Feb 2022
- GloFAS (2022) Global flood awareness systems. <https://www.globalfloods.eu/>. Accessed 13 Feb 2022
- Hungri O, Leroueil S, Picarelli L (2014) The varnes classification of landslide types, an update. *Landslides* 11(2):167–194. <https://doi.org/10.1007/s10346-013-0436-y>
- ICL (2022) ICL world report on landslides. <https://iplhq.org/ls-world-report-on-landslide/>. Accessed 13 Feb 2022
- Idrica (2018) Blue dot observatory. <https://www.blue-dot-observatory.com/>. Accessed: 15 Feb 2022
- Idrica (2019) GoAigua—smart water for a better world. <https://www.idrica.com/goaigua/>. Accessed 15 Feb 2022
- Juang CS, Stanley TA, Kirschbaum DB (2019) Using citizen science to expand the global map of landslides: introducing the cooperative open online landslide repository (COOLR). *PLoS ONE* 14(7): e0218657. <https://doi.org/10.1371/journal.pone.0218657>
- Kettner AJ, Brakenridge GR, Schumann GJ-P, Shen X (2021) DFO—flood observatory. In: *Earth observation for flood applications—progress and perspectives*. Elsevier, Amsterdam. Chapter 7, pp 147–164. (ISBN: 978-0-12-819412-6) <https://doi.org/10.1016/B978-0-12-819412-6.00007-9>
- Leban G, Fortuna B, Brank J, Grobelnik M (2014) Event registry: learning about world events from news. In: *Proceedings of the 23rd international conference on world wide web*, pp 107–110. <https://doi.org/10.1145/2567948.2577024>
- Mikoš M, Petkovišek A (2019) Faculty of civil and geodetic engineering, university of Ljubljana. *Landslides* 16(9):1815–1819. <https://doi.org/10.1007/s10346-019-01231-6>
- Mikoš M, Yin Y, Sassa K (2017) The fourth world landslide forum, Ljubljana, 2017. *Landslides* 14(5):1843–1854. <https://doi.org/10.1007/s10346-017-0889-5>
- Montanarella L, Panagos P (2021) The relevance of sustainable soil management within the European green deal. *Land Use Policy* 100:104950. <https://doi.org/10.1016/j.landusepol.2020.104950>
- NAIADES Water Observatory (2022) Monitoring water related events to explore relevant water issues. <http://naiades.ijs.si/>. Accessed 13 Feb 2022
- NAIADES (2022) <https://naiades-project.eu/>. Accessed 13 Feb 2022
- NASA (2022a) NASA earth observatory. <https://earthobservatory.nasa.gov/>. Accessed 13 Feb 2022a
- NASA (2022b) Landslides @ NASA. <https://landslides.nasa.gov/>. Accessed 13 Feb 2022b
- NASA (2022c) Citizen scientists find undocumented landslides. <https://earthobservatory.nasa.gov/images/145299/citizen-scientists-find-undocumented-landslides>. Accessed 18 Feb 2022c
- Neuman M, Grobelnik M (2022) Causal relationships among global indicators. In *Proceedings of the Slovenian KDD conference*.
- New York Times (2022) Ecuador court gives indigenous groups a boost in mining and drilling disputes. <https://www.nytimes.com/2022/02/04/climate/ecuador-indigenous-constitutional-court.html>. Accessed 15 Feb 2022
- OECD (2011) *Water governance in OECD countries: a multi-level approach*. OECD studies on water, OECD publishing, Paris, France, p 244. <https://doi.org/10.1787/9789264119284-en>
- Our World in Data (2020) Water use and stress. <https://ourworldindata.org/water-use-stress>. Accessed 13 Feb 2022
- PBL (2018) *The geography of future water challenges*. PBL Netherlands environmental assessment agency. The Hague, Netherlands, p 103. http://www.pbl.nl/sites/default/files/downloads/pbl-2018-the-geography-of-future-water-challenges-2920_2.pdf. Accessed 13 Feb 2022
- Pita Costa J et al. (2021) Observing water-related events for evidence-based decision-making. In: *Proceedings of the Slovenian KDD conference*, p 4. <https://ailab.ijs.si/dunja/SiKDD2021/Papers/PitaCostaetal.pdf>. Accessed 15 Feb 2022
- Ramamoorthi A (1983) Snow-melt run-off studies using remote sensing data. *Sadhana—Acad Proc Eng Sci*. 6(3):279–286. <https://www.ias.ac.in/article/fulltext/sadh/006/03/0279-0286>

- Sassa K (2015) ISDR-ICL Sendai partnerships 2015–2025 for global promotion of understanding and reducing landslide disaster risk. *Landslides* 12(4):631–640. <https://doi.org/10.1007/s10346-015-0586-1>
- Sassa K (2017) The 2017 Ljubljana declaration on landslide risk reduction and the Kyoto 2020 commitment for global promotion of understanding and reducing landslide disaster risk. *Landslides* 14(4):1289–1296. <https://doi.org/10.1007/s10346-017-0857-0>
- Sassa K (2021a) The Kyoto landslide commitment 2020: launched. *Landslides* 18(1):5–20. <https://doi.org/10.1007/s10346-020-01575-4>
- Sassa K (2021b) New open access book series “Progress in landslide research and technology.” *Landslides* 18(11):5–20. <https://doi.org/10.1007/s10346-021-01759-6>
- Schweizerische Eidgenossenschaft (2022) Find Swiss open government data. <https://opendata.swiss/en>. Accessed 18 Feb 2022
- SFDRR (2015) Sendai framework for disaster risk reduction 2015–2030. United Nations office for disaster risk reduction. Geneva, Switzerland, p 32. https://www.preventionweb.net/files/43291_sendaiframeworkfordrren.pdf. Accessed 13 Feb 2022
- Song I-Y, Zhu Y (2016) Big data and data science: what should we teach? *Expert Syst* 33(4):364–373. <https://doi.org/10.1111/exsy.12130>
- UN (2020) United Nations launches framework to speed up progress on water and sanitation goal. United Nations UN water. <https://www.unwater.org/un-water-launch-the-sdg-6-global-acceleration-framework/>. Accessed 14 Feb 2022
- UN (2022a) United Nations department of economic and social affairs—sustainable development. <https://sdgs.un.org/>. Accessed 13 Feb 2022a
- UN (2022b) United Nations development programme: goal 6—clean water and sanitation. <https://www.undp.org/sustainable-development-goals#clean-water-and-sanitation>. Accessed 14 Feb 2022b
- UNDRR (2022) Voluntary commitments Sendai framework for disaster risk reduction 2015–2030. <https://sendaicommitments.undrr.org/commitments>. Accessed 13 Feb 2022
- USA National Library of Medicine (2021) Landslides—MeSH descriptor data 2021. <https://meshb-prev.nlm.nih.gov/record/ui?ui=D055876>. Accessed 15 Feb 2022

Open Access This chapter is licensed under the terms of the Creative Commons Attribution 4.0 International License (<http://creativecommons.org/licenses/by/4.0/>), which permits use, sharing, adaptation, distribution and reproduction in any medium or format, as long as you give appropriate credit to the original author(s) and the source, provide a link to the Creative Commons license and indicate if changes were made.

The images or other third party material in this chapter are included in the chapter’s Creative Commons license, unless indicated otherwise in a credit line to the material. If material is not included in the chapter’s Creative Commons license and your intended use is not permitted by statutory regulation or exceeds the permitted use, you will need to obtain permission directly from the copyright holder.





Mapping Post-fire Monthly Erosion Rates at the Catchment Scale Using Empirical Models Implemented in GIS. A Case Study in Northern Italy

Damiano Vacha, Giuseppe Mandrone, Donato Morresi, and Matteo Garbarino

Abstract

Post-wildfire geological hazards are an emerging problem for a number of different environments, including areas not typically associated with these events such as the Alpine Region. The risk connected with post-fire processes such as debris-flows and flood-type events threatens people, infrastructures, services and economical activities. Apart from a few examples, such as in the USA and Australia, there is a lack of models available to quantify the increase in susceptibility of the aforementioned phenomena as a result of the modification induced by the wildfires. In this work we test the application of a modified version of the RUSLE, on GIS, to quantify the post-fire erosive phenomena for a case study in the north-western Italian Alps. The results of its application, taking advantage of high-resolution rainfall series and data deriving from field surveys, highlight the marked increase (more than 20 times) in erosion rates, quantified by expressing both the EI (erodibility index), the A (monthly soil loss) and the SL (monthly sediment loss) rise. The months of April, May and June represent the larger share of the total quantities. This is a consequence of the noticeable increase of the EI, which for the post-fire scenario is more than one order of magnitude higher than the pre-fire one.

Keywords

Wildfires • Erosion • Slope stability • Hazard • Western Alps

1 Introduction

Climate change is having far-reaching effects ranging from unprecedented forest fires, heatwaves, droughts and extreme rainfall events (IPCC 2014a, b). Natural disturbances are thought to experience a further increase in frequency and severity, progressively affecting areas not endangered in the past also due to land use change (Maringer et al. 2016; Mantero et al. 2020). They can occur alone or in combination with each other and cause and/or be followed by secondary hazards, constituting a complex chain of multi-hazards processes also called cascading effect. As an example, forest fires lead to new avalanche-prone slopes, and to a higher risk of rockfall, debris-flow, mudslides, soil erosion and water quality problems. Recent estimates for the Alpine region, forecasting an increased impact of the climate change effects, suggest wildfires and post-wildfire geological hazards to represent a looming issue in the near future (Zumbrunnen et al. 2009; Moreira et al. 2011; Wastl et al. 2012; Arndt et al. 2013, Dupire et al. 2019, Barbero et al. 2019).

Amongst other hydrological hazards, debris-flow and flood-type events represent the most serious concern, as can be seen in the reports and the scientific literature of the regions (USA, Australia) which are facing the problem nowadays (De Graff 2014). The modification of the hydrological properties, due to litter and vegetation removal, ash deposition, alteration of the physical properties of soil and rocks results in an increase of the availability of easily erodible materials on hillslopes and of runoff rates (Moody and Martin 2001; Parise and Cannon 2008, 2012; Staley et al 2017). In fact, rainsplash, sheetflow and rill erosion

D. Vacha · G. Mandrone (✉)

Interuniversity Department of Regional and Urban Studies and Planning (DIST), University of Turin, 10125 Turin, Italy
e-mail: giuseppe.mandrone@unito.it

D. Vacha

e-mail: damiano.vacha@unito.it

D. Morresi · M. Garbarino

Department of Agricultural, Forest and Food Sciences (DISAFA), University of Turin, 10095 Grugliasco, TO, Italy
e-mail: donato.morresi@unito.it

M. Garbarino

e-mail: matteo.garbarino@unito.it

© The Author(s) 2023

K. Sassa et al. (eds.), *Progress in Landslide Research and Technology, Volume 1 Issue 1, 2022*, Progress in Landslide Research and Technology, https://doi.org/10.1007/978-3-031-16898-7_6

increases due to the diminished capacity of rainfall interception by the tree canopies, shrubs and grass. Very soon the surface runoff may concentrate in hollows and low order channels carrying the eroded sediment and entraining the materials deposited in the waterways, eventually exerting a strong erosive action at the expense of the riverbed sediments and causing their “in mass” failure. All of these processes can lead to sediment concentration to levels associated with debris flows (Tang et al. 2019).

Currently, very few models are available for the estimate of the hazard and risk of these phenomena. The USGS preliminary hazard assessment relies on empirical models to assess the likelihood, volume and combined hazard of debris flows for selected watersheds in response to a design storm. These models rely on historical debris–flow occurrence and magnitude data, rainfall storm conditions, terrain and soils information, and burn–severity maps (Staley et al. 2016, 2017). In Australia, the Victorian Department of Sustainability and Environment (DSE) developed an empirical rapid risk assessment procedure for post-fire hydrologic risks, namely debris flows risk, water quality risk and flooding risk. The model, in the early stages of development, is based on available datasets and combines information for terrain, vegetation, rainfall erosivity, burn severity maps and stream network (Sheridan et al. 2009). In other countries, such as the Mediterranean ones, despite an increasing number of hazardous events (Parise and Cannon 2008; Tiranti et al. 2006; Carabella et al. 2019; Esposito et al. 2013, 2017, 2019), no model for the hydro-geomorphic events susceptibility assessment has been implemented or validated extensively. Very few examples of model application can be found in Italy, Greece, Portugal and Spain (Terranova et al. 2009; Fernandez et al. 2010, 2018; Coschignano et al. 2019; Esteves et al. 2013; Rulli et al. 2013; Lanorte et al. 2019; Depountis 2020, Efthimiou 2020). The need to quantify the influence of fires on the propensity for hazardous processes clashes with the fact that, in many regions outside the United States, the scientific community has faced the problem in a consistent way only in recent years and thus the available post-fire event statistics does not allow for a data driven approach. In this study, we focused on the application and validation of a modified version of the RUSLE model (Revised Universal Soil Loss Equation—Wischmeier and Smith 1978) to quantify the post-fire erosive phenomena for a case study in the north-western Italian Alps. In this area, during October 2017, ten wildfires occurred, burning a total area of 10,000 hectares of which 7000 were forests; this value far exceeds the average regional forest burned area (600 ha/year between 2005 and 2013) (Morresi et al. 2022). Season fires in 2017 were favored by the exceptionally dry conditions, high temperatures and the occurrence of several days with hot and dry winds (Arpa Piemonte 2017; Bo et al. 2020). The largest and most severe fire—almost 4000 ha—

occurred in the Susa Valley, where fourteen catchments on the left of the Dora Riparia River were involved. Starting from late April 2018 until the early June, several flow events originated from the burned catchments. The larger damages were recorded at the outlet of the Comba delle Foglie, a small drainage basin overhanging the Bussoleno municipality (Vacha et al. 2021). Ground evidence highlighted a remarkable increase in erosion rates exerted by the surface runoff in many sectors within the fire perimeter, in agreement with literature findings (Moody and Martin 2001; Parise and Cannon 2008, 2012; Staley et al. 2017). Based on the assumption that these processes represent the key aspect governing the availability of sediments to be entrained during rainfalls, and taking into account the available spatial data, the structure of the RUSLE model proved to be the most suitable framework to be adopted. In fact, the approach used is deliberately simple, replicable, improvable and easy to implement in a GIS environment. It is also possible to automate it in order to make it available for the rapid production of thematic maps to support authorities and for civil protection purposes. Moreover, it relies mostly on the available open source spatialized data provided by regional authorities and other public bodies, which makes it easy to replicate the conceptual scheme in other areas. The model has been applied and validated on the Comba delle Foglie catchment, for which a detailed temporal reconstruction of the processes and quantification of the volume of mobilized material has been carried out in a previous work (Vacha et al. 2021).

2 Study Area

The study area is located in the Susa Valley, an east–west Alpine valley, located in the western part of Piedmont (starting ~ 20 km West of Turin). It was affected by the largest and more severe of the ten wildfires that occurred in the region in 2017 (The Bussoleno and Mompantero Wildfire) which burned 4000 ha on the left of the Dora Riparia River, going up the valley from east to west and affecting the slope almost to the divide (Fig. 1). The fire started on October 22, 2017 and lasted until November 1, 2017. It interested an area dominated by European Beech (*Fagus sylvatica* L.) and Scots Pine (*Pinus sylvestris* L.), the forest cover being the 37.1% and the 26.7% for the Broadleaved and the Coniferous species, respectively, with 36.2% of the wildfire surface being represented by non-forested areas (Morresi et al. 2022). Comba delle Foglie is one of the catchments affected by this exceptional wildfire. It is located towards the eastern side of the wildfire area and is a steep, elongated watershed ranging between 480 and 1747 m a.s.l., characterized by an average slope of 35° and an area of approximately 1.37 km² (Vacha et al. 2021). The bedrock

of the catchment is represented by polymetamorphic rocks and in particular by Micaschists and gneiss belonging to the Dora Maira pre-triassic basement (DMb), by calcschists, marbles and dolomitic marbles belonging to the Dora Maira Mesozoic cover (DMc) and by calcschists, serpentinites, serpentinoschists and chloritoschist belonging to the Lower Piedmont Zone (PZ) (Carraro et al. 2002; Gasco et al. 2011). The geomorphological setting of the study is both influenced by its geologic history and by quaternary geomorphic events. The main valley is dominated by erosional and depositional landforms of glacial origin, mainly glacial terraces, suspended-tributary valleys and lodgement and ablation till. The post-glacial remodeling action exerted by gravitative and fluvial processes strongly influenced the landscape. In particular, the left side of the Susa Valley hosts a series of ravine and canyon-like features in correspondence of morphological steps at the outlet of suspended valleys into the main valley. As a result, the quaternary deposits mantle the study area heterogeneously: the main valley floor is filled by alluvial deposits, while the slope are patched by glacial, fluvial and gravity related deposits, often reworked (Cadoppi et al. 2007).

The vegetative cover of the catchment before the fire was low with respect to other sectors of the burned area due to previous wildfires (Ascoli et al. 2011), and it was mostly dominated by young trees of *Populus tremula* and *Salix caprea*. The most relevant parameters describing the watershed are given in Table 1, in which the major morphometric descriptors can be found.

3 Materials and Methods

3.1 Burn Severity

The burn severity map of the Bussoleno and Mompantero Wildfire (Morresi et al. 2022) was adopted in this work. This map was produced through satellite imagery and field surveys, following a methodology based on US FIREMON framework (Key and Benson 2006). The analysis of spectral changes caused by the 2017 wildfires was carried out using multispectral images acquired by the MultiSpectral Instrument (MSI) onboard Sentinel-2 A/B satellites (European Space Agency). In particular, the burn severity obtained by using the uncalibrated RdNBR bi-temporal index (Miller and Thode 2007, Eq. 1) calculated from reflectance composites was adopted here. It was generated using all the clear observations available in the period spanning from 20 May to 10 September for both 2017 and 2018; the validation of the map and the classification in severity categories followed Miller et al. (2009), Miller and Thode (2007) and Parks et al. (2014). This product was chosen because among all the other indices calculated by the authors, it was the one with the best overall accuracy.

$$RdNBR = \frac{dNBR}{\sqrt{|NBR_{prefire}|}} \quad (1)$$

RdNBR is based on the definition of the Normalized Burn Ratio (NBR) (Eq. 2) which is calculated by contrasting the

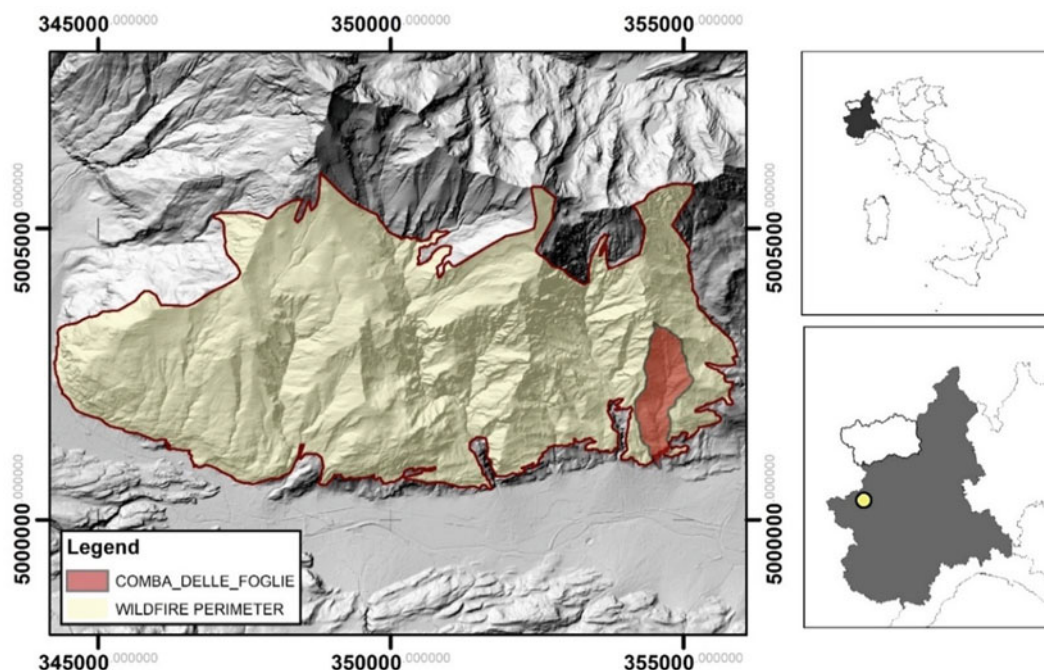


Fig. 1 Perimeter of the Susa valley wildfire and location of the Comba delle Foglie watershed. The base map is the regional DTM

Table 1 Morphometrical and hydrological descriptors of the Comba delle Foglie watershed; area A_w [km²], perimeter P [km], watershed length L_b [km], minimum elevation E_{min} [m s.l.m.], maximum elevation E_{max} [m s.l.m.], mean elevation E_{mean} [m s.l.m.], minimum slope S_{min} [°], maximum slope S_{max} [°], mean slope S_{mean} [°], main channel length L_p [km], average main channel slope L_pS [°], total streams length L [km], Fan to watershed area ratio A_f/A_w [–], Form factor F_f [–] (Horton 1932), Circularity ratio R_c [–] (Miller 1953; Strahler 1964), Elongation ratio R_e [–] (Schumm 1956), Melton Index M_e [–] (Melton 1965), Drainage density D_d [km/km²] (Strahler 1964), Time of concentration T_c [h] (Kirpich 1940)

Index	Unit	Value	Index	Unit	Value	Index	Unit	Value
A_w	[km ²]	1.37	S_{max}	[°]	74.82	A_f/A_w	[–]	8.14
P	[km]	6.1	S_{mean}	[°]	35.01	F_f	[–]	0.22
L_b	[km]	2.59	L_p	[km]	2.44	R_c	[–]	0.44
E_{min}	[m a.s.l.]	480	L_pS	[°]	32.22	R_e	[–]	0.53
E_{max}	[m a.s.l.]	1747	L	[km]	4.14	M_e	[–]	1.02
E_{mean}	[m a.s.l.]	1035				D_d	[km/km ²]	3.19
S_{min}	[°]	1.5				T_c	[h]	0.18

reflectance in the near infrared (NIR) and in the shortwave infrared (SWIR); the delta Normalized Burn Ratio (Key and Benson 2006) is calculated through Eq. (3).

$$NBR = [(NIR - SWIR)/(NIR + SWIR)] \quad (2)$$

$$dNBR = (NBR_{prefire} - NBR_{postfire}) \times 1000 \quad (3)$$

RUSLE—Monthly erosion calculation

Sediment erosion has been assessed implementing the RUSLE model at a monthly scale through the following equation:

$$A_{month} = R_{month} * K * L * S * C * P \quad (4)$$

where A = mean soil loss per month [Mg ha⁻¹ m⁻¹], R = rainfall erosivity factor [MJ mm h⁻¹ ha⁻¹ m⁻¹], K = soil erodibility factor [Mg MJ⁻¹ mm⁻¹ h], L = topographic factor or slope length factor [dimensionless], C = soil coverage [dimensionless], and P = erosion control practices factor [dimensionless]. The value of the sediment loss (SL) is obtained by multiplying the value of A for the drainage surface. The R factor quantifies the mechanical impact energy exerted by a given precipitation and depends on duration and intensity of the rainfall. Remaining parameters in the equation give a measure of the environmental resistance to erosive phenomena. The K , L and C factors are assumed to change in areas affected by wildfires as a result of fire effect on soil erodibility, vegetative cover and shift in rill to interrill soil erodibility ratio (Terranova et al. 2009). RUSLE model is intended to quantify soil losses in the long term, so that processes such as gully and channel erosion and sediment transport cannot be modelled. Prediction accuracy for individual storm is very low, as controversial is the application on large spatial scale. Despite this,

the model can be used as a solid framework to quantify high-risk erodible areas (Efthimiou et al. 2020). With this regard, the product of K , L and C factor is used to compare post-fire to pre-fire condition; thus, EI [Mg MJ⁻¹ mm⁻¹ h] is introduced to describe the erosion susceptibility:

$$EI = C * K * L * S \quad (5)$$

P factor has been considered equal to 1, because there are no support practices for the erosion reduction in the study area.

Rainfall erosivity factor—R

The rainfall erosivity factor (R) factor has been estimated at a monthly scale by calculating the summation of the parameter EI_{30} of every single erosive event (k) for each considered month.

$$R_{month} = \sum_{k=1}^n EI_{30k} \quad (6)$$

Following Brown and Foster (1987), EI_{30} for a single rainstorm event is defined as the product of the kinetic energy of rainfall events (E) and its maximum 30-min intensity (I_{30}):

$$EI_{30} = \left(\sum_{r=1}^m e_r v_r \right) I_{30} \quad (7)$$

where e_r = unit rainfall energy [MJ ha⁻¹ mm⁻¹], v_r = rainfall volume [mm] during the r -th period of a storm which divided into m parts and I_{30} is the maximum 30-min rainfall intensity [mm h⁻¹]. The unit rainfall energy e_r is calculated for each time interval using Eq. (8) (Brown and Foster, 1987):

$$e_r = 0.29 \left[1 - 0.72e^{(-0.05i_r)} \right] \quad (8)$$

Table 2 Location of the three rain gauges of Prarotto, Borgone and Malciaussia

Name	Elevation (m s.l.m.)	WGS84-UTM32N X (m)	WGS84-UTM32N Y (m)	Basin
Prarotto	1440	361,493	5,000,737	Dora riparia
Borgone	400	361,958	4,997,582	Dora riparia
Malciaussia	1800	354,590	5,007,700	Stura di Ianzo

where i_r is the rainfall intensity during the time interval [mm h^{-1}]. High resolution rainfall data (10 min time resolution) were downloaded from Arpa Piemonte database for three rain gauges located in the surrounding of the watershed, namely Prarotto, Borgone and Malciaussia (Table 2 and Fig. 2). Rainfall series covers a period of time ranging from September 1, 2017 to August 3, 2018. The identification of the erosive rainfall (n) events for each station record followed three criteria given by Renard et al. (1997): the cumulative rainfall of an event is greater than 12.7 mm, or the event has at least one peak that is greater than 6.35 mm during a period of 15 min. Individual storms are separated if a rainfall accumulation is less than 1.27 mm during a period of 6 h. Those criteria have been developed for the USA countries, but are also widely accepted in other areas (Panagos et al. 2015a). The Rainfall Intensity Summarisation Tool (RIST) software (USDA 2014) was used to calculate the R-factor based on the single station annual series. After that, the single monthly R factors related to each rain gauge were averaged to get the final value representative of the watershed. The obtained results were compared with the average monthly rainfall erosivity calculated by Ballabio et al. (2017) at European scale analyzing > 17 years of rainfall data and downloaded from ESDAC repository (European Soil Data Centre, European Commission, Joint Research Centre).

Soil erodibility factor—K

The soil erodibility (K) factor has been determined based on soil textural data. Homogeneous lithological units have been individuated by grouping the geological units derived from 1:50,000 geological map (Carraro et al. 2002). Soil samples have been then collected and processed in laboratory for determining grain size distribution following standard ASTM procedures. Afterwards, the K factor for each unit has been then calculated based on the following formulae (Renard et al. 1997):

$$K = 0.0034 + 0.0405 * \exp \left[-0.5 \left(\frac{\log D_g + 1.659}{0.7101} \right)^2 \right] \quad (9)$$

$$D_g = \exp \left[\sum f_i \ln \left(\frac{d_i + d_{i-1}}{2} \right) \right] \quad (10)$$

where D_g = geometric mean particle size for each particle size class (clay, silt, sand), d_i = maximum diameter (mm), d_{i-1} = minimum diameter and f_i is the corresponding mass fraction.

Cover factor—C

The C factor has been assessed based on Forestry/Land Cover Map and by assigning C values according to Panagos et al. (2015b). Tabulated values for each land cover class are given in Table 3, whilst land cover classes areal distribution is given in Table 4.

Length/Slope Factor LS

The LS factor in the original RUSLE model describes the interaction between standard parcel length (L) and slope (S). In this study, it is substituted by the unit contributing area L_s , which takes into account the flow convergence (Mitasova et al. 1996; Terranova et al. 2009). L_s is computed for each 5 m wide DTM cell as follows:

$$L_s = (\mu + 1)(a/a_0)^\mu (\sin b/b_0)^\eta \quad (11)$$

where a [m] = the upslope contributing area for each cell (result of the ArcGIS “flowacc” and “resolution” functions), b [%] = slope, a_0 [m] = 21.1 m (the standard USLE plot length), and b_0 [%] = 9% (the standard USLE plot slope). The parameter μ is calculated as a function of β , which is the ratio of rill to interrill erosion (Miller et al. 2003; Foster et al. 2003):

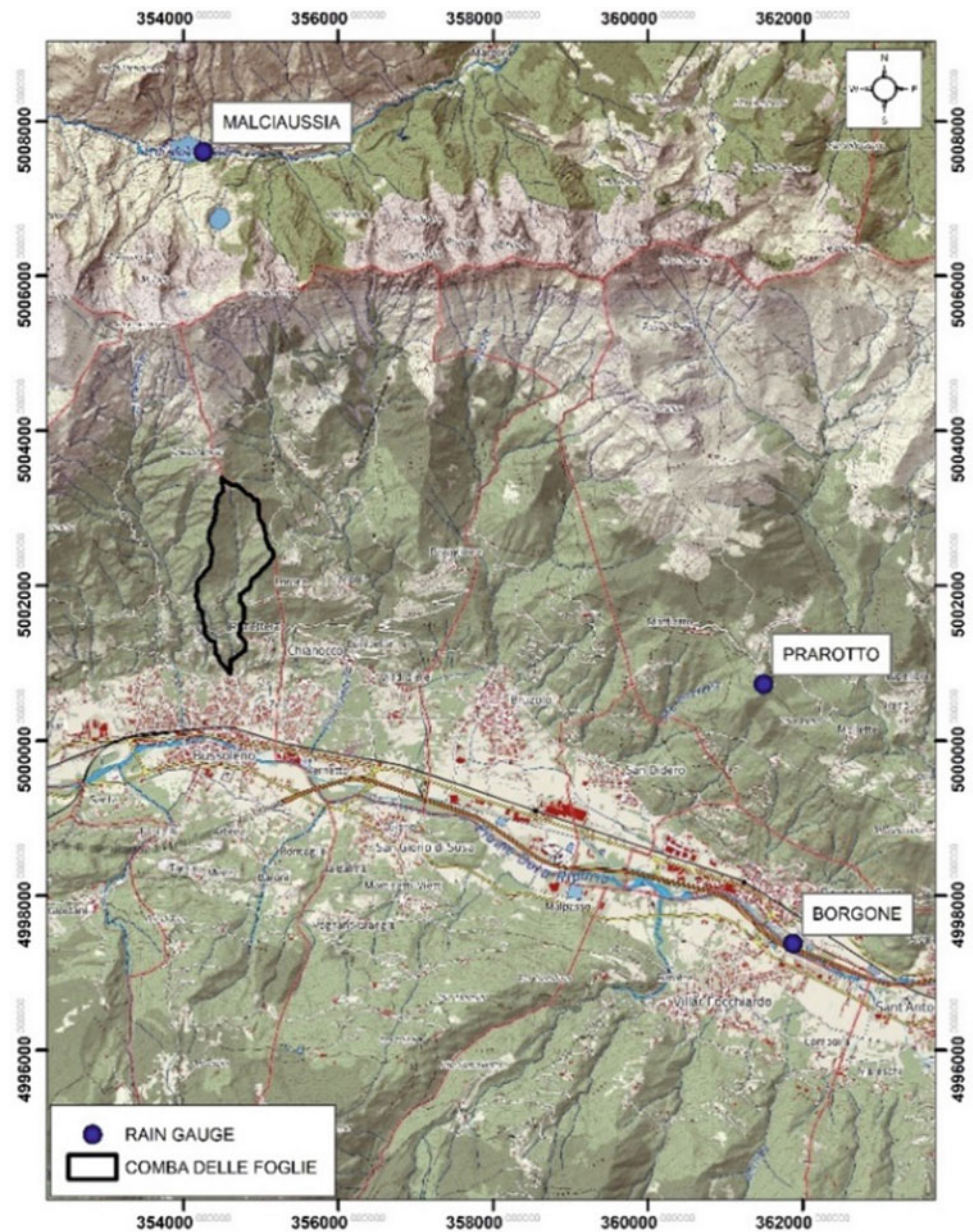
$$\mu = \beta / ((1 + \beta)) \quad (12)$$

Based on literature, β can be set equal to 0.5 for unburned areas and equal to 1 for burned areas with high severity. The parameter η is considered equal to 1.2 following Terranova et al. (2009) and Coschignano et al. (2020). The cell values in a buffer of 10 m around the stream network has been excluded from the calculation since the RUSLE model does not provide estimates for streamflow erosion. For them, a default value of 0 has been assigned.

Model implementation

Pre-fire monthly mean soil loss (A_{pre}) and erodibility index (EI_{pre}) were calculated based on the previous equations on a 5 m resolution raster grid based on DTM cells position.

Fig. 2 Location of the three rain gauges of Prarotto, Borgone and Malciaussia with respect to the Comba delle Foglie watershed position



Then the spatially weighted average of A_{w_pre} was calculated over the entire watershed surface.

Finally, the value of the monthly sediment loss (SL_{pre}) [$Mg\ y^{-1}$] for the watershed was calculated multiplying the value of A_{w_pre} times the watershed area. Post-fire condition was modeled by calculating mean soil loss per month (A_{post}) and erodibility index (EI_{post}) following Eqs. (3) and (4). The single factors of the RUSLE model were adjusted as a function of fire severity (unburned, low, moderate or high) following with some modifications the procedures described in Terranova et al. (2009) and Lanorte et al. (2019). The metrics used in this work are given in Table 5. For both scenarios (pre- vs post-fire), A and EI raster cell values have

been subsequently averaged for each watershed giving A_{w_post} and SL_{post} value.

4 Results

The fire severity class distribution over the watershed (Fig. 3) highlight a predominancy (77.10%) of moderate fire severity, while unburned/low and high severity cover the 21.98%, and 0.92% of the watershed area, respectively. Given the fact that the area experienced another fire in 2003, the burn severity map may underestimate the 2017 situation, even if a relativized index such as RdNBR has been used.

Table 3 RUSLE cover factor proposed for each land cover class (after Panagos et al. 2015b)

CLC class	Class name	C-factor values	CLC class	Class name	C-factor values
112	Discontinuous urban fabric	0	313	Mixed forest	0.0013
131	Mineral extraction sites	0	313b	Mixed forest < 20%	0.003
211	Non-irrigated arable land	0.23	3211	Natural grassland prevailingly without trees and shrubs	0.04
221	Vineyards	0.34	3212	Natural grassland with trees and shrubs	0.03
222	Fruit trees and berry plantations	0.1	322	Moors and heathland	0.055
231	Pastures	0.09	322b	Moors and heathland	0.055
242	Complex cultivation patterns	0.147	324	Transitional woodland-shrub	0.024
243	Land principally used for agriculture, with significant areas of natural vegetation	0.124	332	Bare rocks	0
311	Broad-leaved forest	0.0013	333	Sparsely vegetated areas	0.25
311b	Broad-leaved forest < 20%	0.003	0	Bare Soil	1
312	Coniferous forest	0.0013			
312b	Coniferous forest < 20%	0.003			

Table 4 Land cover classes areal distribution over the Comba delle Foglie watershed

Land principally used for agriculture	Broad-leaved forest	Mixed forest	Transitional woodland-shrub	Broad-leaved forest < 20%	Mixed forest < 20%	Natural grassland with trees and shrubs
%	%	%	%	%	%	%
5.5	24.5	38.2	4.2	0.6	26.1	0.9

Table 5 Adjusted cover factors (C), erodibility factors (K) and β value (used for LS factor calculation) (β) for different fire severity classes

Burn Severity class	RUSLE parameters		
	C	K	β
Unburned/Low	C_{pre}	K_{pre}	0.5
Moderate	$C_{pre} + 0.1$	$1.8 * K_{pre}$	1
High	$C_{pre} + 0.25$	$2 * K_{pre}$	1

Monthly R factors for each rain gauge from September 2017 to August 2018 have been quantified by calculating the summation of the parameter EI_{30} of every single erosive event for each considered month. The R factor obtained for each station has been then averaged for assessing the representative rainfall erosive power at the watershed scale. For the Prarotto, Borgone and Malciaussia rain gauges 22, 24 and 22 erosive events, respectively, have been identified. For the Prarotto rain gauge, the selected storms are characterized by a mean precipitation value of 30.94 mm, duration of 23.23 h and EI_{30} of 95.99 MJ mm ha⁻¹ h⁻¹. For the Borgone rain gauge mean precipitation, duration and EI_{30} values are 27.67 mm, 20.19 h and 73.06 MJ mm ha⁻¹ h⁻¹. At the Malciaussia station, mean value recorded are 29.20 mm, 16.02 h and 55.40 MJ mm ha⁻¹ h⁻¹, for precipitation,

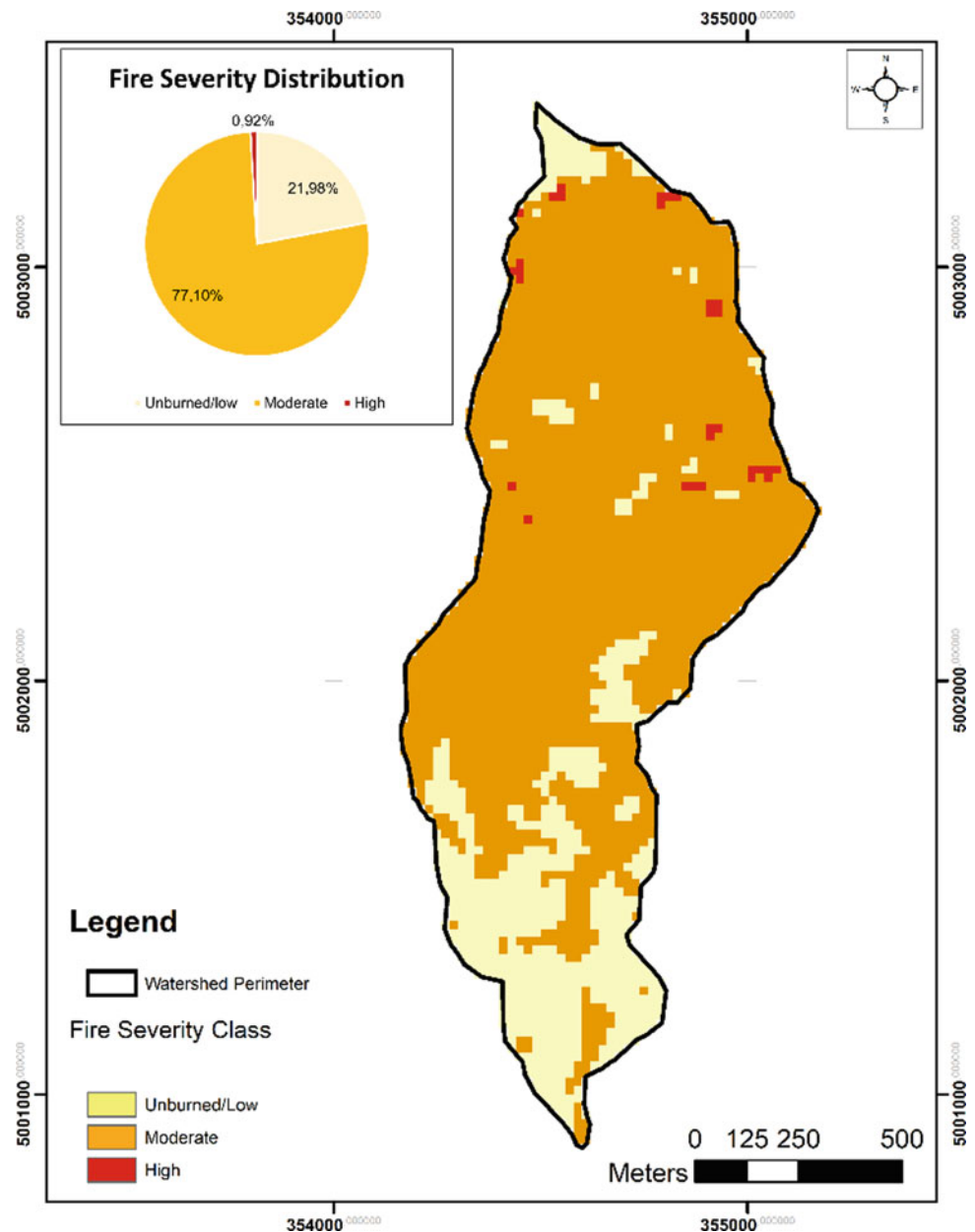
duration and EI_{30} . The maximum values of R factor are reached in May, April and March 2018, and are, on the contrary, equal to zero for September and October 2017.

R factor distribution over time is consistent with Piedmont meteorological data (Arpa Piemonte 2018a, b, 2019), reporting an extremely dry end of 2017 and very wet month of January, April and May 2018. In fact, erosive events registered in these months represents approximately the 75% of the entire annual R factor, and in particular the month of May reaching almost the 40%. Erodiability K factor representative of the pre-fire condition has been determined based on soil textural data collected during the field surveys.

The pre-fire K values have been calculated following Eqs. (9) and (10). The post-fire adjusted K values have been then calculated by applying the correction procedure described in Table 5. Pre-fire and post-fire K values are reported in Fig. 4 (a, b). Pre-fire c factor (Fig. 4c) has been calculated following the procedure described above, by using the values reported in Table 3; post-fire c factor (Fig. 4d) has been then calculated as given in Table 5. Pre-fire LS factor has been calculated through Eqs. (11) and (12), while post-fire LS values have been calculated through Eq. 12 and Table 5. Results are reported in Fig. 4e, f. P value has been set equal to 1.

Erodiability index values for the pre-fire and post-fire situation (Table 6) has been calculated following Eq. (5), and

Fig. 3 Fire severity classes distribution for the Comba delle Foglie catchment



finally monthly mean soil loss A [$\text{Mg ha}^{-1} \text{m}^{-1}$] and averaged monthly sediment loss SL [Mg m^{-1}] for the entire watershed have been computed for both the burned and unburned condition. The post-fire mean erodibility index is more than one order of magnitude higher than the pre-fire one, having a pre-fire value of $4.63\text{E-}04 \text{ Mg MJ}^{-1} \text{ mm}^{-1} \text{ h}$ and a post fire value of $1.21\text{E-}02 \text{ Mg MJ}^{-1} \text{ mm}^{-1} \text{ h}$. Also, the maximum values show a rise of about the same order.

Monthly mean soil loss A [$\text{Mg ha}^{-1} \text{m}^{-1}$] and averaged monthly sediment loss SL [Mg m^{-1}] comparison for the pre- and post-fire conditions (Fig. 5, Table 7) results in a post-fire increase of both the indicators of more than 20 times with respect to pre-fire. Maximum pre-fire values occur in May,

being $0.307 \text{ Mg ha}^{-1} \text{m}^{-1}$ and 39.86 Mg m^{-1} for monthly mean soil loss and monthly sediment loss, respectively; for the post-fire, these parameters reach values of $8.066 \text{ Mg ha}^{-1} \text{m}^{-1}$ and $1050.400 \text{ Mg m}^{-1}$, respectively.

5 Discussion

The sediment erosion has been assessed for the Comba delle Foglie watershed by implementing the RUSLE model at a monthly scale, including model inputs of a detailed erodibility map, the forestry/land cover map, the LS factor map derived from GIS elaboration and a R factor value calculated

Fig. 4 RUSLE factors distribution over the catchment: pre-fire erodibility factor **a**, post-fire erodibility **b**, pre-fire cover factor **c**, post-fire cover factor **d**, pre-fire LS factor **e** and post-fire LS factor **f**

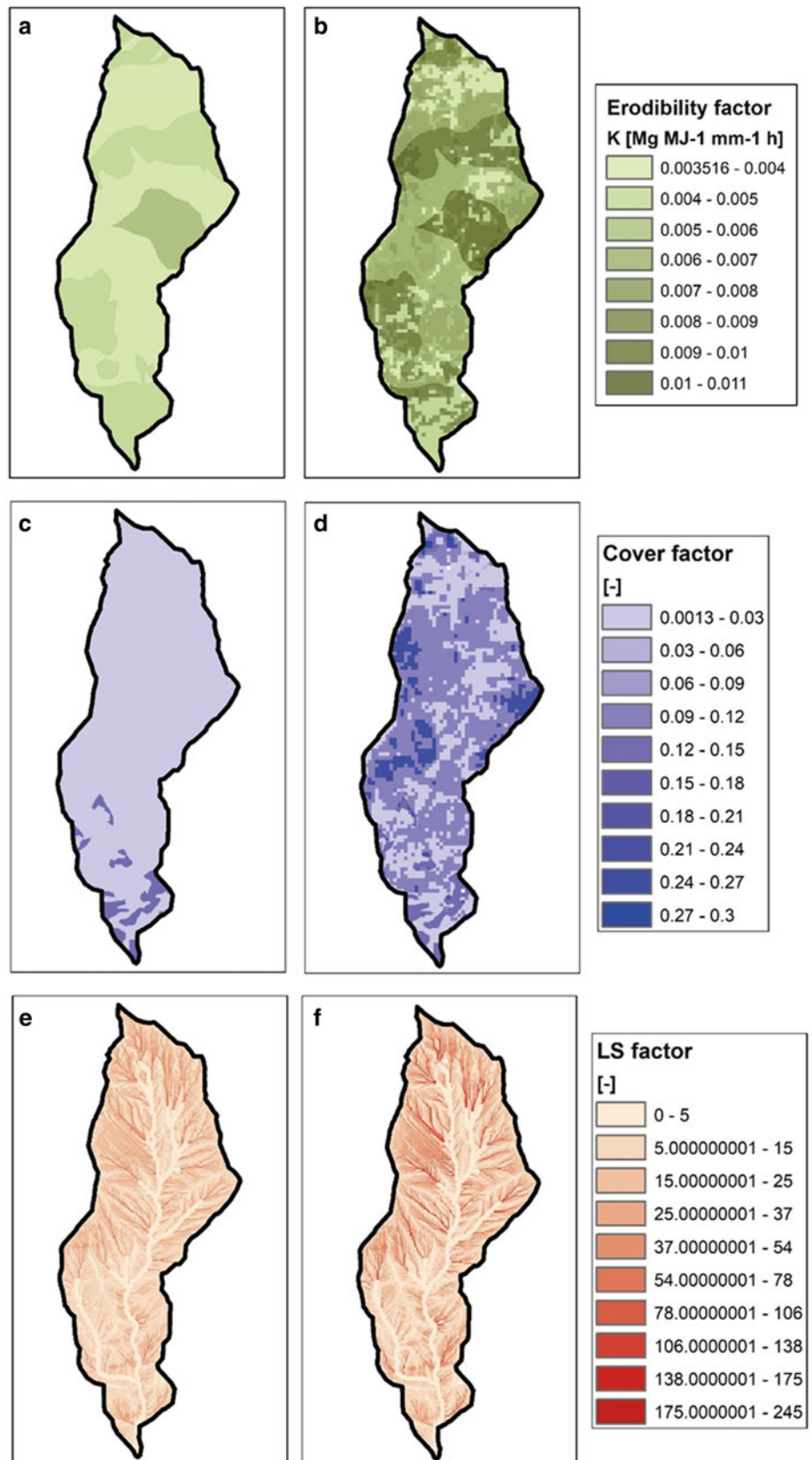


Table 6 Post-fire versus pre-fire erodibility index values over the Comba delle Foglie watershed

EI [$\text{Mg MJ}^{-1} \text{mm}^{-1} \text{h}$]	Pre-fire	Post-fire
MIN	0.00E + 00	0.00E + 00
MAX	2.83E - 02	3.54E - 01
MEAN	4.63E - 04	1.22E - 02
STD	1.65E - 03	2.16E - 02

by retrieving the erosive power of every significant rainfall event. Monthly mean soil loss [$\text{Mg ha}^{-1} \text{m}^{-1}$] and averaged monthly sediment loss [Mg m^{-1}] are the result of the remarkably R values recorded in the months of January, April and May; these three months in fact contribute for about 75% to the annual erosion recorded in the watershed.

Comparing the calculated R factors to average monthly R factor by Ballabio et al (2017) (Fig. 6) is evident a concentration of the erosive events in the post-fire time window, while the precipitations remained well below the average values from September to December 2017, barely reaching the 6% of the cumulated average value. The months of January, April and May show values eleven, eight and four times greater, respectively, than the long time series data. The RUSLE model estimates a SL of approximately 2430 Mg from the extinction of the fire to June (included), when the most significant event occurred. To validate this result, the only available information is related to the characterization of the 7 June event: in that case, the maximum deposit thickness of the debris-flow reconstructed via photogrammetric modelling was approximately 2 m and the invasion area covered about 26,000 m^2 . The total mobilized volume for only the coarser fraction of the deposit, was about 4300 m^3 , of which about 1500 m^3 consisting of materials entrained just at the fan apex. The volume of the coarser sediments coming from the watershed was estimated to be 1300 m^3 . By applying a simple rule of thumb, considering a bulk density of 1500 kg/m^3 , the 7 June flow mass can be estimated in 1950 Mg. Considering the fact that other four minor events (one debris/mud flow in April and three floods in May) happened before the 7 June, it is reasonable to presume that the remnant part of the total sediment loss estimated by the model could be related to those events. Some non-negligible aspects undermine the model robustness and accuracy: in fact, the 7 June event volume estimated via photogrammetrical modeling contrast with the one suggested by Arpa Piemonte (2018b), which after expeditive surveys estimates the total event volume to be about 20,000 m^3 . Another aspect which should be taken into account when dealing with the model validation is the remarkable erosion exerted by the debris-flows along all their paths, which may have increased their volumes considerably. The results of the model are not suitable to predict

streamflow erosion, so when the estimated value is compared to the available surveyed data, this aspect may also increase the uncertainty. Finally, the current model does not take into account the ash and combustion residues which, for sure, contribute to the overall sediment availability to be entrained. Ash and combustion residues are expected to constitute a large part of the removable material especially immediately after the fire, and that they will then be gradually washed away by the runoff as the rainy events occur. Despite all the model limitations and the uncertainties related to its validation, the presented procedure can be considered a reasonable estimator of the amount of material ready to be eroded during the rainstorm events and conveyed in the riverbeds. In fact, it is backed up by ground evidence, the assumption that the considerable amount of sediment mobilized from the date of the fire have been progressively delivered towards the bottom of the slopes and inside the stream network on the repeated rainfalls. In occasion of some smaller mud-flows and hyper-concentrated flows have originated. Then, when the progressive increase of sediments reached a critical threshold in conjunction with a rainy event of a sustained intensity, the most destructive debris-flow on 7 June occurred. During the field inspections prior to 7 June a considerable amount of sediments and combustion residues had been observed inside the channels, especially in the terminal part of the watershed and at the apex of the fan. The investigations carried out following the event revealed evident traces of areal and channeled erosion, starting from the upper part of the slopes and into the lower-order channels. It is clear how all this mass of sediments, both coming from open slopes and being deposited in the drainage network, has constituted the load of the debris-flow during its transit, simultaneously increasing its energy.

6 Conclusions

The Piedmont region, and in particular the western Italian Alps, experienced an unusually severe wildfire season in 2017. The fires occurred in the late autumn and, after a snowy winter, were followed by spring rains. In particular, some of the catchments burned in the Susa Valley wildfire were interested in May and June 2018 by debris/mud-flows and flood type events. The major debris-flow happened at the outlet of Comba delle Foglie and struck the Bussoleno municipality. Based on field evidence, it was found that the flows mobilized materials and sediments, which were eroded from the burned hillslopes and subsequently deposited in the channels. This is consistent with the literature which reported the main cause of the post-fire debris-flows to be the generation of increased erosion due to excess runoff rather than a discrete landslide failure. On the back of these findings, a modified version of the RUSLE model was applied in

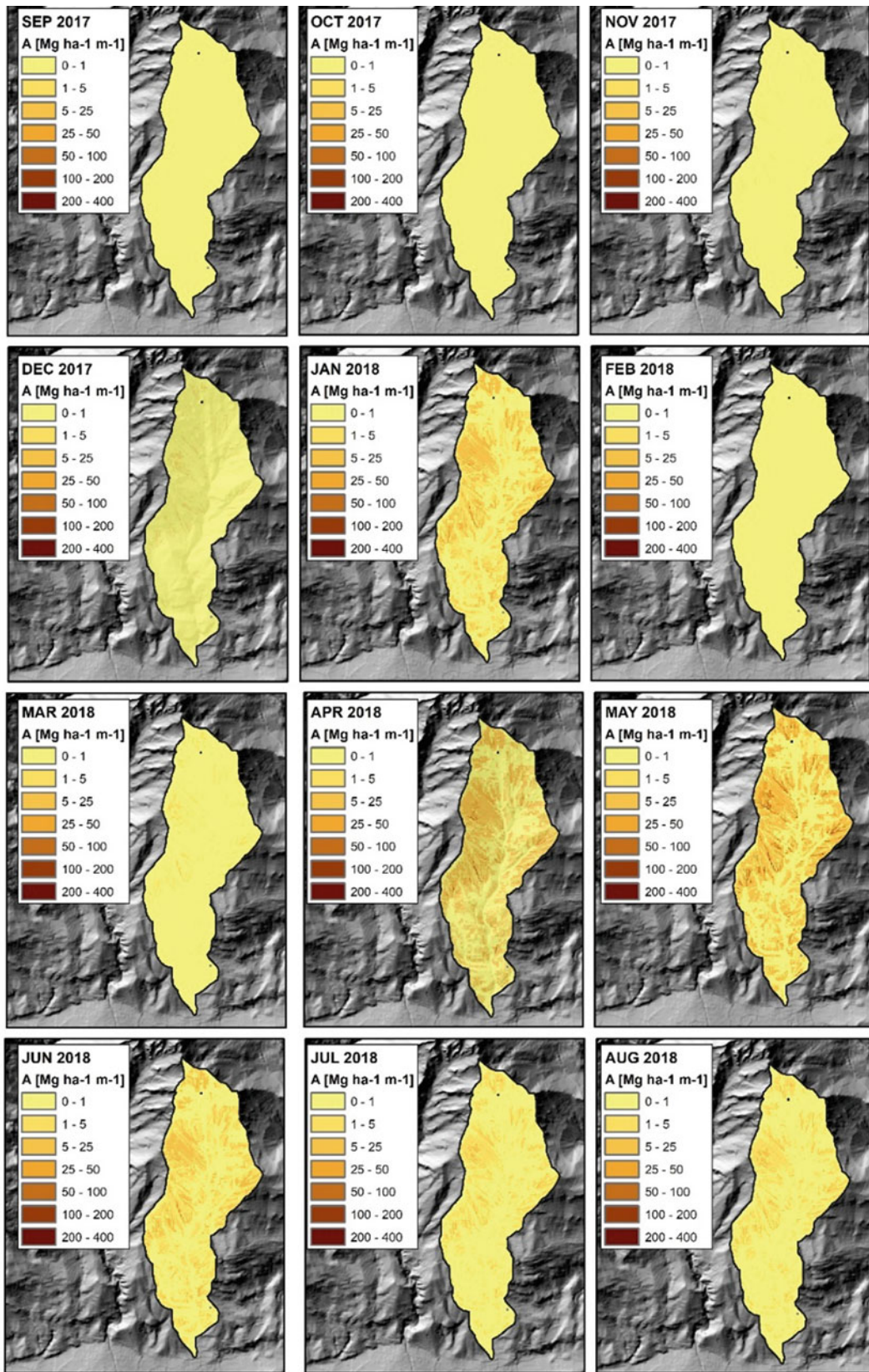
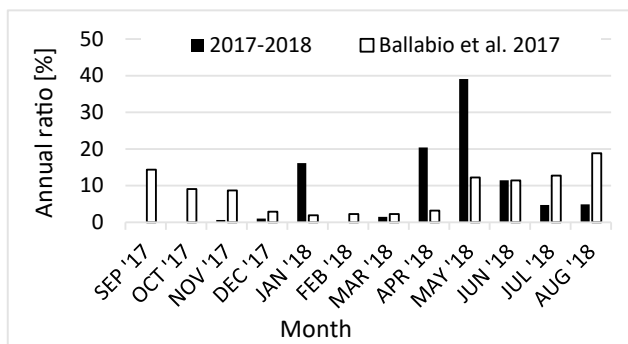


Fig. 5 Monthly mean soil loss

Table 7 Spatially averaged mean soil loss (A) and averaged monthly sediment loss (SL) comparison for the burned and unburned situation

Month	Burned		Unburned	
	A	SL	A	SL
	[Mg/ha*m]	[Mg/m]	[Mg/ha*m]	[Mg/m]
9–17	0.000	0.00	0.000	0.00
10–17	0.000	0.00	0.000	0.00
11–17	0.133	17.32	0.005	0.66
12–17	0.208	27.07	0.008	1.03
1–18	3.342	434.36	0.127	16.48
2–18	0.014	1.82	0.001	0.07
3–18	0.310	40.28	0.012	1.53
4–18	4.223	548.87	0.160	20.83
5–18	8.081	1050.28	0.307	39.86
6–18	2.371	308.14	0.090	11.69
7–18	0.981	127.55	0.037	4.84
8–18	1.014	131.75	0.038	5.00
TOT	20.677	2687.45	0.785	101.98

**Fig. 6** Comparison between calculated and long term inter annual R-factor (Ballabio et al. 2017)

the area of Comba delle Foglie to quantify the erosive processes on a monthly scale. The results of its application, incorporating high resolution rainfall series and data deriving from field surveys, made it possible to reproduce and highlight the marked increase in erosion rates, quantified by expressing both the EI (erodibility index), the A (monthly soil loss) and the SL (monthly sediment loss) rise. In particular, overall A and SL increased more than twenty times in the post-fire scenario, the months of April, May and June representing the larger share of the total quantities. This is a consequence of the noticeable increase of t EI, which for the post-fire scenario is more than one order of magnitude higher than the pre-fire one. The intrinsic uncertainties of the model are related to the fact that it does not consider the stream-flow erosion in the channels, it does not account for the material eroded by the debris-flow during its passage and it does not incorporate the eroded volume of ash and

combustion residues. Some uncertainties are then linked to the fact that the estimates regarding the actual volumes of the flows are limited to a single case (the major one, 7th June) and also do not agree with each other. Despite these uncertainties, the proposed procedure can be considered a reasonable estimator of the amount of material ready to be eroded, especially if it is used to compare different catchments in a relative way; in this case, it can provide useful guidance to rank the post-fire debris-flow susceptibility and to establish intervention priorities. It can be applied everywhere on the regional territory because the model make use on open-source spatialized data and thanks to its structure, it can be easily implemented into a GIS for thematic map production.

Acknowledgements This study is conducted within the ICL IPL project No. 4938. Many thanks to Arpa Piemonte for rainfall data. Field survey were conducted in the framework of the Institutional Technical Table on Wildfire Emergency of the Piedmont Region.

References

- Arndt N, Vacik H, Koch V, Arpacı A, Gossow H (2013) Modeling human-caused forest fire ignition for assessing forest fire danger in Austria. *Iforest* 6:315–325
- Arpa Piemonte (2017) Rapporto tecnico sulla qualità dell'aria e sulle attività dell'agenzia a supporto dell'emergenza per gli incendi boschivi in Piemonte nel mese di ottobre 2017
- Arpa Piemonte (2018a) Rapporto evento del 07/06/2018, Colata detritica nel comune di Bussoleno
- Arpa Piemonte (2018b) Il Clima in Piemonte 2017. Available online at <https://www.arpa.piemonte.it>

- Arpa Piemonte (2019) Il Clima in Piemonte 2018. Available online at <https://www.arpa.piemonte.it>
- Ascoli D, Valsecchi C, Bovio G and Conedera M (2011) Wildfires and beech forests of Southern Alps during the summer 2003 climate anomaly: fire effects and post-fire management. The 5th international wildland fire conference, Sun City, South Africa, 9–13 May 2011
- Ballabio C, Borrelli P, Spinoni J, Meusburger K, Michaelides S, Begueria S, Klik A, Petan S, Janecek M, Olsen P, Aalto J, Lakatos M, Rymaszewicz A, Dumitrescu A, Tadić MP, Nazzareno D, Kostalova J, Rousseva S, Banasik KL, Alewell C, Panagos P (2017) Mapping monthly rainfall erosivity in Europe. *Sci Total Environ* 579:1298–1315
- Barbero R, Curt T, Ganteaume A, Maillé E, Jappiot M, Bellet A (2019) Simulating the effects of weather and climate on large wildfires in France. *Nat Hazards Earth Syst Sci* 19:441–454
- Bo M, Mercalli L, Pognant F, Cat Berro D, Clerico M (2020) Urban air pollution, climate change and wildfires: the case study of an extended forest fire episode in northern Italy favoured by drought and warm weather conditions. *Energy Rep* 6:781–786
- Brown LC, Foster GR (1987) Storm erosivity using idealized intensity distributions. *Trans Am Soc Agric Eng* 30:379–386
- Cadoppi P, Giardino M, Perrone G, Tallone SD (2007) Litho-structural control, morphotectonics, and deep-seated gravitational deformations in the evolution of Alpine relief: a case study in the lower Susa Valley (Italian Western Alps). *Quatern Int* 171:143–159
- Carabella C, Miccadei E, Paglia G, Sciarra N (2019) Post-wildfire landslide hazard assessment: the case of the 2017 montagna del morrone fire (central apennines, Italy). *Geosciences* 9:175
- Carraro F, Cadoppi P, Baggio P, Bellino L, Castelletto M, Giraud V, Mensio L (2002) Foglio 154 – Susa – Carta Geologica d'Italia, scala 1:50.000. Carta Geol—Serv Geol D'Italia Coord CARRARO F 126
- Coschignano G, Nicolaci A, Ferrari E, Cruscomagno F and Iovino F (2019) Evaluation of hydrological and erosive effects at the basin scale in relation to the severity of forest fires. *iForest* 12:427–434
- De Graff JV (2014) Improvement in quantifying debris flow risk for post-wildfire emergency response. *Geoenviron Disasters* 1:5
- Depountis N, Michalopoulou M, Kavoura K, Nikolakopoulos K, Sabatakakis N (2020) Estimating soil erosion rate changes in areas affected by wildfires. *ISPRS Int J Geo-Inf* 9:562
- Dupire S, Curt T, Bigot S, Fréjaville T (2019) Vulnerability of forest ecosystems to fire in the French Alps. *Eur J For Res* 138:813–830
- Efthimiou N, Psomiadis E, Panagos P (2020) Fire severity and soil erosion susceptibility mapping using multi-temporal earth observation data: the case of Mati fatal wildfire in Eastern Attica, Greece. *Catena* 187(2020):104320
- Esposito G, Esposito E, Matano F, Molisso F, Sacchi M, Porfido S (2013) Effects of a wildfire on rocks and soils in the Sarno Mountains, Campania, Southern Apennines. *Rend Online Soc Geol Ital* 24:119–121
- Esposito G, Matano F, Molisso F, Ruoppolo G, Di Benedetto A, Sacchi M (2017) Post-fire erosion response in a watershed mantled by volcanoclastic deposits, Sarno Mountains, Southern Italy. *CATENA* 152:227–241
- Esposito G, Parodi A, Lagasio M, Masi R, Nanni G, Russo F, Alfano S, Giannatiempo G (2019) Characterizing consecutive flooding events after the 2017 Mt. Salto Wildfires (Southern Italy): Hazard and emergency management implications. *Water* 11:2663
- Estevés TCJ, Kirkby MJ, Shakesby RA, Ferreira AJD, Soares J, Irvine B, Ferreira CSS, Coehlo COA, Bento CPM, Carreira M (2012) Mitigating land degradation caused by wildfire: application of the PESERA model to fire-affected sites in central Portugal. *Geoderma* 191:40–50
- Fernandez C, Vega JA (2018) Evaluation of the RUSLE and disturbed wepp erosion models for predicting soil loss in the first year after wildfire in NW Spain. *Environ Res* 165:279–285
- Fernandez C, Vega JA, Vieira DCS (2010) Assessing soil erosion after fire and rehabilitation treatments in NW Spain: performance of RUSLE and revised Morgan–Morgan–Finney models. *Land Degrad Dev* 21:58–67
- Foster GR, Toy TJ, Renard KG (2003) Comparison of the USLE, RUSLE1.06c, and RUSLE2 for application to highly disturbed lands. Proceedings of the first interagency conference on research in the watersheds. USDA—Agricultural Research Service, Washington, DC, pp 154–160
- Gasco I, Gattiglio M, Borghi A (2011) Lithostratigraphic setting and P-T metamorphic evolution for the Dora Maira Massif along the Piedmont Zone boundary (middle Susa Valley, NW Alps). *Int J Earth Sci* 100:1065–1085
- Horton RE (1932) Drainage-basin characteristics. *EOS Trans Am Geophys Union* 13:350–361
- IPCC (2014a) Synthesis report. In: Core Writing Team, Pachauri RK, Meyer LA (eds) *Climate change 2014. Contribution of working groups I, II and III to the fifth assessment report of the intergovernmental panel on climate change*. IPCC, Geneva
- IPCC (2014b) *Climate change 2014: impacts adaptation and vulnerability. Part A. Global and sectoral aspects*. In: Field CB, Barros VR, Dokken DJ, Mach KJ, and others (eds) *Contribution of working group II to the fifth assessment report of the intergovernmental panel on climate change*. Cambridge University Press, Cambridge
- Key CH, Benson NC (2006) *Landscape assessment (LA): sampling and analysis methods*. In: Lutes DC, Keane RE, Caratti JF, Key CH, Benson NC, Sutherland S, Gangi L (eds) *Firemon: fire effects monitoring and inventory system*. RMRS-GTR-164. Rocky Mountain Research Station, General technical report, US Department of Agriculture, Forest Service: Fort Collins, CO, USA pp LA-1–LA-51
- Kirpich ZP (1940) Time of concentration of small agricultural watersheds. *Civ Eng* 10(6):362
- Lanorte A, Cillis G, Calamita G, Nolè G, Pilogallo A, Tucci B, Santis F (2019) Integrated approach of RUSLE, GIS and ESA Sentinel-2 satellite data for post-fire soil erosion assessment in Basilicata region (Southern Italy). *Geomat Nat Haz Risk* 10(1):1563–1595
- Mantero G, Morresi D, Marzano R, Motta R, Mladenoff DJ, Garbarino M (2020) The influence of land abandonment on forest disturbance regimes: a global review. *Landscape Ecol* 35:2723–2744. <https://doi.org/10.1007/s10980-020-01147-w>
- Maringer J, Ascoli D, Dorren L, Bebi P, Conedera M (2016) Temporal trends in the protective capacity of burnt beech forests (*Fagus sylvatica* L.) against rockfall. *Eur J For Res* 135(4):657–673
- Melton MA (1965) The geomorphic and paleoclimatic significance of alluvial deposits in Southern Arizona. *J Geol* 73:1–38
- Miller JD, Thode AE (2007) Quantifying burn severity in a heterogeneous landscape with a relative version of the delta normalized burn ratio (dNBR). *Remote Sens Environ* 109:66–80
- Miller JD, Nyhan JW, Yool SR (2003) Modeling potential erosion due to the Cerro Grande fire with a GIS-based implementation of the revised universal soil loss equation. *Int J Wildland Fire* 12:85–100
- Miller VCA (1953) Quantitative geomorphic study of drainage basin characteristics in the Clinch Mountain area Virginia and tennessee. Columbia University Technology Report No. 3, Contract N6 ONR, pp 271–30
- Mitasova H, Hofierka J, Zlocha M, Iverson LR (1996) Modeling topographic potential for erosion and deposition using GIS. *Int J Geogr Inf Sci* 10(5):629–641
- Moody JA, Martin PA (2001) Initial hydrologic and geomorphic response following a wildfire in the Colorado front range. *Earth Surf Proc Land* 26:1049–1070

- Moreira F, Viedma O, Arianoutsou M, Curt T, Koutsias N, Rigolot E, Barbati A, Corona P, Vaz P, Xanthopoulos G, Mouillot F, Bilgili E (2011) Landscape - wildfire interactions in southern Europe: implications for landscape management. *J Environ Manage* 92:2389–2402
- Morresi D, Marzano R, Lingua E, Motta R, Garbarino M (2022) Mapping burn severity in the western Italian Alps through phenologically coherent reflectance composites derived from Sentinel-2 imagery. *Remote Sens Environ* 269:112800
- Panagos P, Ballabio C, Borrelli P, Meusburger K, Klik A, Rousseva S, Tadic MP, Michaelides S, Hrabalíková M, Olsen P, Aalto J, Lakatos M, Rymaszewicz A, Dumitrescu A, Beguería S, Alewell C (2015a) Rainfall erosivity in Europe. *Sci Total Environ* 511:801–814
- Panagos P, Borrelli P, Meusburger K, Alewell C, Lugato E, Montanarella L (2015b) Estimating the soil erosion cover-management factor at the European scale. *Land Use Policy* 48(2015):38–50
- Parise M, Cannon SH (2008) The effects of wildfires on erosion and debris-flow generation in Mediterranean climatic areas: a first database. *Proceedings of 1st world landslide forum*. Tokyo, Japan, pp 465–468
- Parise M, Cannon SH (2012) Wildfire impacts on the processes that generate debris flows in Burned Watersheds: *Natural Hazards*, vol 61
- Parks SA, Dillon GK, Miller C (2014) A new metric for quantifying burn severity: the relativized burn ratio. *Remote Sens* 6:1827–1844
- Renard KG, Foster GR, Weesies GA, McCool DK, Yoder DC (1997) Predicting soil erosion by water: a guide to conservation planning with the revised universal soil loss equation (RUSLE) (*Agricultural handbook* 703). US Department of Agriculture, Washington, DC, p 404
- Rulli MC, Offeddu L, Santini M (2013) Modeling post-fire water erosion mitigation strategies. *Hydrol Earth Syst Sci* 17:2323–2337
- Schumm SA (1956) Evolution of drainage systems and slopes in badlands at Perth Amboy. *New Jersey, Geol Soc Am Bull* 67:597–646
- Sheridan GJ, Lane PN, Smith H, Nyman P (2009) A rapid risk assessment procedure for post-fire hydrologic hazards; 2009/10 fire season. Technical report produced for the department of sustainability and environment. The Department of Forest and Ecosystem Science, The University of Melbourne, Australia, p 19. ISBN 9780734041470
- Staley DM, Negri JA, Kean JW, Laber JL, Tillery AC, Youberg AM (2017) Prediction of spatially explicit rainfall intensity–duration thresholds for post-fire debris-flow generation in the Western United States. *Geomorphology* 278:149–162
- Staley DM, Negri JA, Kean JW, Tillery AC, Youberg AM (2016) Updated logistic regression equations for the calculation of post-fire debris-flow likelihood in the western United States: U.S. Geological Survey Open-File Report 2016–1106, p 13
- Strahler AN (1964) Quantitative geomorphology of drainage basin and channel networks. *Handbook of applied hydrology*
- Tang H, McGuire LA, Rengers FK, Kean JW, Staley DM, Smith JB (2019) Evolution of debris-flow initiation mechanisms and sediment sources during a sequence of postwildfire rainstorms. *J Geophys Res Earth Surf* 124:1572–1595
- Terranova O, Antronico L, Coscarelli R, Iaquina P (2009) Soil erosion risk scenarios in the Mediterranean environment using RUSLE and GIS: an application model for Calabria (southern Italy). *Geomorphology* 112(2009):228–245
- Tiranti D, Moscariello A, Giudici I, Rabuffetti D, Cremonini R, Campana V, Bosco F, Giardino M (2006) Post-fire rainfall events influence on debris-flows trigger mechanisms, evolution and sedimentary processes: the Rio Casella case study in the North-western Italian Alps. *Geophys Res Abstr* 8:03479
- USDA (2014) United States department of agriculture. Rainfall Intensity Summarization Tool (RIST). Accessed from, <http://www.ars.usda.gov>
- Vacha D, Mandrone G, Garbarino M, Morresi D (2021) First consideration about post 2017 wildfire erosion response and debris flow in Susa Valley (NW Italy). In: Tiwari B, Sassa K, Bobrowsky PT, Takara K (eds) *Understanding and reducing landslide disaster risk*. WLF 2020. ICL contribution to landslide disaster risk reduction. Springer, Cham
- Wastl C, Schunk C, Leuchner M, Pezzatti B, Menzel A (2012) Recent climate change: long-term trends in meteorological forest fire danger in the Alps. *Agric for Meteorol* 162–163:1–13
- Wischmeier WH, Smith DD (1978) Predicting rainfall erosion losses: a guide to conservation planning. *Agriculture Handbook* no. 537, USDA, Washington DC, USA, pp 13–27
- Zumbrunnen T, Bugmann H, Conedera M, Bürgi M (2009) Linking forest fire regimes and climate—a historical analysis in a dry inner Alpine valley. *Ecosystems* 12:73–86

Open Access This chapter is licensed under the terms of the Creative Commons Attribution 4.0 International License (<http://creativecommons.org/licenses/by/4.0/>), which permits use, sharing, adaptation, distribution and reproduction in any medium or format, as long as you give appropriate credit to the original author(s) and the source, provide a link to the Creative Commons license and indicate if changes were made.

The images or other third party material in this chapter are included in the chapter's Creative Commons license, unless indicated otherwise in a credit line to the material. If material is not included in the chapter's Creative Commons license and your intended use is not permitted by statutory regulation or exceeds the permitted use, you will need to obtain permission directly from the copyright holder.





Mechanisms of Shallow Rainfall-Induced Landslides from Australia: Insights into Field and Laboratory Investigations

Ivan Gratchev, Sinnappoo Ravindran, Dong Hyun Kim, Chen Cui, and Qianhao Tang

Abstract

This paper presents and discusses the mechanisms of rainfall-induced shallow landslides that commonly occur in South East Queensland (SEQ) and northern New South Wales (NSW), Australia. The major factors causing the formation of landslide mass such as geology, weathering, and rainfall patterns were discussed. Results from field surveys and laboratory testing of rock/soil material from landslide masses were presented, and relationships between the material strength and landslide occurrence were drawn. It was found that most of shallow slides were related to sandstone deposits. Those failures occurred on natural slopes and road cuts with the inclination of the failure plane being in the range of 35–45°. For natural slopes where the landslide mass mostly consisted of coarse-grained soil, the relationship between the soil strength and water content was established. In addition, the relationship between rainfall patterns such as intensity and duration, and the landslide occurrence was presented. Based on the data from field work and laboratory results including a series of flume tests, the mechanism of shallow landslides triggered by rainfall events was identified and discussed.

Keywords

Shallow landslides • Rainfall-induced landslides • Soil strength • Suction • Geology • Weathering

1 Rainfall-Induced Landslides in Australia

Rainfall-induced landslides are a common natural disaster that occur in all states and territories of Australia, leading to environmental degradation as well as millions of dollars in damage to infrastructure and land. Although large catastrophic landslides such as the 1997 Thredbo landslide (18 fatalities and \$25 million damage) always draw national attention (Middelmann and Mazengarb 2007), it is the overwhelming number of relatively shallow (1–3 m deep) landslides occurring annually which has led the National Research Council (2004) to declare that landslides are responsible for considerably greater socioeconomic losses than generally recognized. For example, Geoscience Australia recorded 963 landslides nationwide within 20 years between 1990 and 2010, yet this number is believed to be largely underestimated as several local landslides may not be captured by the national database. Although it seems rather difficult to estimate the landslide cost across the whole country, a study on landslide risk in New South Wales (Osuchowski and Roberts 2011) indicated that the cost of landslide remediation may vary from \$1 to 3.5 million, and it can greatly increase by several times when landslides happen to affect important transportation infrastructure. National recognition of the landslide problem resulted in several guidelines for landslide susceptibility, hazard and risk management published by Australian Geomechanics Society (2007a, b) and Australian Building Codes Board (2015). These guidelines were adopted by City Councils across the country to evaluate landslide hazards, identify areas with a high landslide risk, and develop strategies for landslide hazard management. These strategies are mostly oriented at

I. Gratchev (✉) · S. Ravindran · C. Cui · Q. Tang
School of Engineering and Built Environment, Griffith University,
Southport, 4222, Australia
e-mail: i.gratchev@griffith.edu.au

S. Ravindran
e-mail: ravi.ravindran@alumni.griffithuni.edu.au

C. Cui
e-mail: chen.cui@griffithuni.edu.au

Q. Tang
e-mail: qianhao.tang@griffithuni.edu.au

D. H. Kim
CEO of Aiclops Inc, Goyangdae-Ro, Ilsanseo-Gu, Gyeonggi-Do
10223, Goyang-Si, 283, Korea
e-mail: dhkim@aiclops.com

avoiding dangerous sites and stabilizing unstable slopes; however, with the development of civil and mining infrastructure, slope stability is expected to become a larger issue for the safety of local communities, and thus more advanced methods will be required to deal with this natural disaster. Unfortunately, there are many uncertainties in forecasting the time and rate of landslide movements, and for this reason, it cannot be performed reliably at present. Better understanding of landslide mechanisms is required to develop more reliable hazard assessment and risk management strategies and achieve more accurate forecasting of landslide movements.

The literature contains several well-documented world case-studies (for example, Wang et al. 2003; Gratchev and Towhata 2011; Gratchev et al. 2011); however, most of them investigated the mechanisms of large-sized catastrophic failures associated with a number of fatalities and considerable economic loss. The mechanisms of such landslides were found to be rather complex, involving the process of soil–water interaction, including changes in soil strength as landslide mass becomes saturated during rainfall. In comparison, limited research into the mechanism of relatively shallow rainfall-induced slides (1–3 m deep) in Australia has been conducted to date. The available data (Abeykoon et al. 2018; Cogan et al. 2018; Cogan and Gratchev 2019; Ravindran et al. 2019) indicate that the mechanism of shallow slides is associated with the behaviour of unsaturated soils, three-phase (soil, water, and air) interaction, and soil suction.

Unfortunately, experimental data on the properties of unsaturated soils remains limited as such studies are costly, time-consuming, and difficult to conduct.

In the past several years, a research group from Griffith University, Australia, has conducted extensive studies on shallow landslides that occurred in South East Queensland (SEQ) and northern New South Wales (NSW) (Fig. 1). This included field surveys of landslide sites and lab testing of landslide material. This generated important data on landslide characteristics, mechanisms, factors affecting it, and properties of rock and soil from the landslide mass. The large study area has also provided a variety of geology, geomorphology, and soil conditions which were found to be the key factors causing the formation of landslides. This work provides a detailed account of major findings which will be of interest to the international reader as well. This paper first discusses the geological settings of typical landslide sites and the effect of geology and geological structures on the landslide occurrence. The influence of rock mass discontinuities and weathering are shown through the analysis of test results obtained for fresh, weathered, and jointed rocks. This paper also provides data on rainfall patterns prior to landslides and describes the rainfall intensity threshold that can be used for landslide hazard assessment. The mechanisms of shallow landslides are analyzed using



Fig. 1 Location of the study area: South East Queensland (SEQ), and northern New South Wales (NSW)

experimental data on properties of soil from landslide masses, with the focus on relationships between the shear strength and water content. In addition, insights from a series of flume tests conducted to simulate the soil mass behavior under different rainfall patterns are presented and discussed.

2 Factors Causing Landslides

2.1 General Characteristics of Landslides

Several shallow rainfall-induced slope failures were studied in SEQ and northern NSW in the past several years. Despite the different locations, those landslides had several similarities that can be described as follows:

1. There were two common types of failures such as slides in jointed rock mass and failures of heavily weathered rock material.
2. Many slope failures in rock mass were associated with geological features such as bedding planes and folds. The rock mass in such structures was affected by sets of discontinuities that created pockets of weathering and accumulation of water which significantly undermined the strength of natural slopes and road cuts (Shokouhi et al. 2013; Kim et al. 2015a). Figure 2a gives an example of slope failure that occurred in the layered formation of sandstone alternated with argillite/shale. Steep inclinations of the bedding planes also had an adverse effect on slope stability.

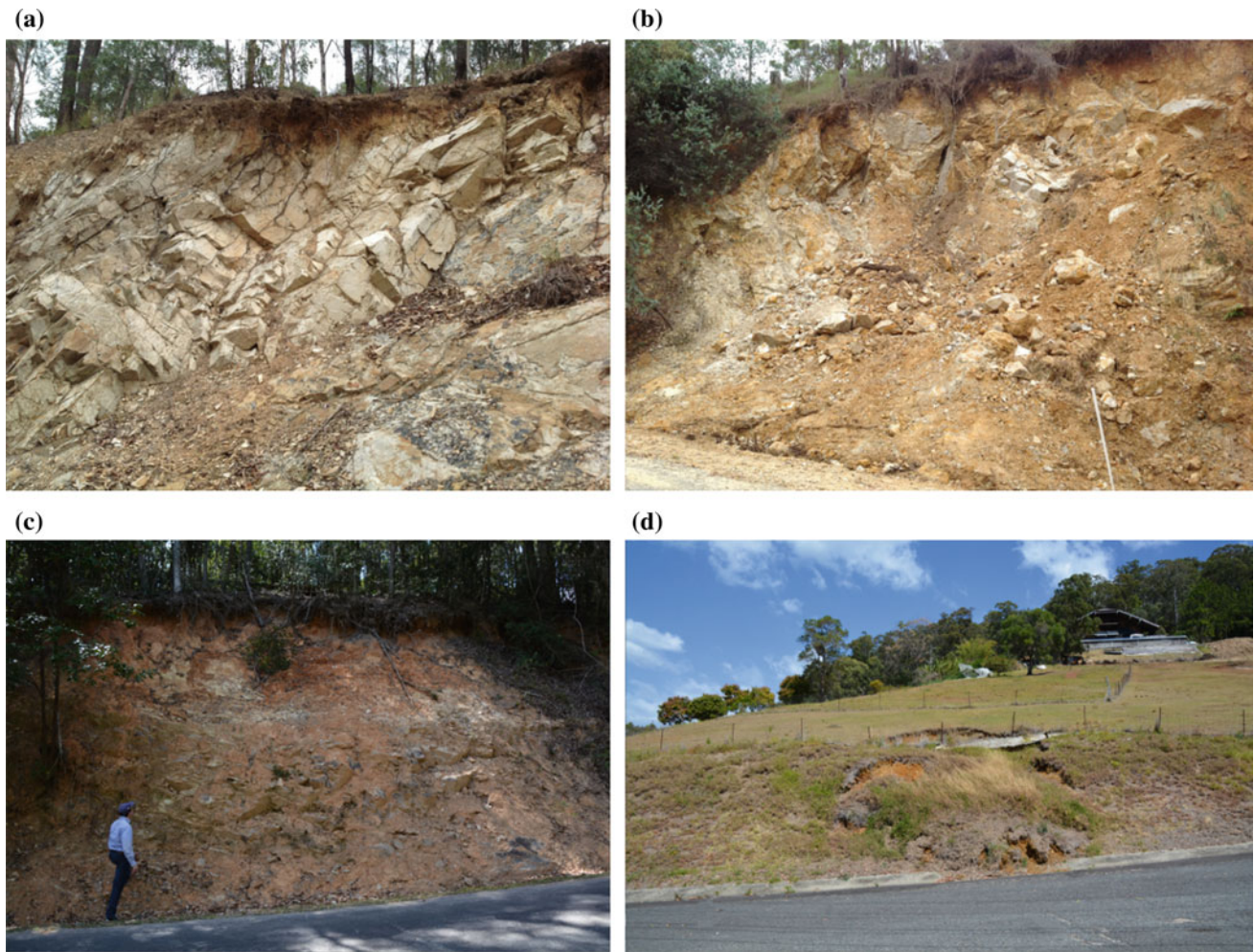


Fig. 2 Examples of rainfall-induced landslides: **a** failure in rock mass of the Neranleigh–Fernvale Beds formation. The bedding planes of sandstone and argillite are steeply inclined, producing an adverse effect

on rock mass stability, **b** landslide in heavily weathered volcanic deposits, **c** shallow slide of heavily weathered material caused by the Cyclone Debbie in 2017, **d** shallow landslide in weathered material

3. On several occasions, the landslide mass was the product of weathering of sedimentary rocks such as sandstone or slightly metamorphized sedimentary rocks such as greywacke and argillite. Kim et al. (2013, 2015b) reported that, despite the different location, most of landslides had similar geological features such as the relatively soft weathered material overlaying relatively hard bedrocks (Fig. 2c). In addition, the bedrock was also deeply weathered while the bedding structure associated with the sets of discontinuities was significant factor contributing to the failure.
4. A few slope failures occurred in weathered igneous rocks as shown in Fig. 2b, where the landslide mass formed in heavily weathered volcanic deposits.
5. The failure plane inclination was found to be in the range of 35 to 45°. This was related to slope cuts along roads and the bedrock inclination. As shown in Fig. 2c, d, the shallow landslide mass (about 1 m deep) was a heavily weathered material, which formed on the slope cut next to a road. The strength of rock/soil has deteriorated over time under environmental conditions.
6. Landslide mass consisted mostly of coarse-grained material such as sand or gravely sand, only few landslides occurred in low plasticity fine-grained soils.
7. The mechanism of such shallow landslides is related to suction. While being stable during dry periods, natural slopes may experience stability issues during a rainfall event as the shear strength of soil tends to decrease with decreasing soil suction (Ravindran and Gratchev 2020, 2021). In several cases, a significant decrease in soil strength was observed as the moisture content of soil greatly increased.

2.2 Geology and Rock Weathering

Geology plays an important role in slope stability as it determines the strength properties of rock. Rock slopes are considered stable when rock strength is high, which is mostly the case for fresh and slightly weathered material. Figure 3 presents a geological map of the Gold Coast area as an example that would relatively well represent the geological conditions in SEQ. Several landslides formed in the Neranleigh–Fernvale Beds formations (Willmott 2010; Gratchev et al. 2013; Shokouhi et al. 2013), which are widely spread in SEQ and northern NSW. The Neranleigh–Fernvale Beds composed of metasediments which are commonly presented as layered argillite (shale) and greywacke (sandstone). Argillite, which is hardened and slightly recrystallized shale, is fined-grained rock, bedding, and fractured in many surface exposures. Greywacke is a typically dark color, low grade metamorphic rock containing fragments that formed a detrital matrix. In some areas, greywacke is replaced with sandstone which is mostly coarse-grained sediment with dark brown color (Kim et al. 2015a, b, c). In many road cuts and natural slopes, where these rocks are exposed on the surface, they are found to be heavily weathered, folded, and steeply inclined.

Towards the continent's inland, there is a large area of sedimentary rocks formed at the end of the Triassic period (Bundamba group, Marburg subgroup). This group consists primarily of planar to cross-bedded, medium to coarse, quartz sandstones interbedded with grey shales and/or siltstones (Willmott 1981).

Volcanic rocks such as basalt, rhyolite, and tuff are found in the mountainous part of the area, and they are remnants of Cainozoic volcanic lava flow deposits. With a relatively high

strength when fresh, these rocks become relatively weak when heavily weathered.

Figure 4 shows the results of unconfined compression tests on fresh samples of basalt, argillite, and sandstone from the Gold Coast area. Rock specimens with a height of 100 mm and diameter of 50 mm were tested in unconfined compression, following the relevant Australian Testing Standard. It is evident from this figure that basalt has the greatest strength compared to different types of sandstone. Four types of sandstone (S1–S4) of the Marburg subgroup were collected at different depths from borehole explorations. It was observed that the strength of sandstone specimens (S1–S4) depended on their porosity. Figure 5 plots the average values of porosity and unconfined compressive strength (USC) for all four types. It is clear that the strength tends to decrease with increasing porosity.

Analysis of over 100 landslides that occurred in northern NSW from 2009–2017 showed that the majority of slides originated in weathered sedimentary rocks (mostly sandstone); however, several slides also occurred in weathered igneous rocks (Ravindran et al. 2019). The reason is that sedimentary or slightly metamorphized sedimentary rocks are widely spread in the northern NSW, and when compared to igneous rocks (for example, basalt), they have relatively low strength.

Weathering. Weathering significantly contributes to the formation of landslides in the study areas. When rock is exposed to environmental conditions, its strength deteriorates over time, resulting in a relatively thick (1–2 m) mass of weathered rocks. A study on the strength of common rock types from SEQ at different levels of weathering was conducted by Gratchev and Kim (2016) and Gratchev et al. (2019). Table 1 summarizes that data from point load tests

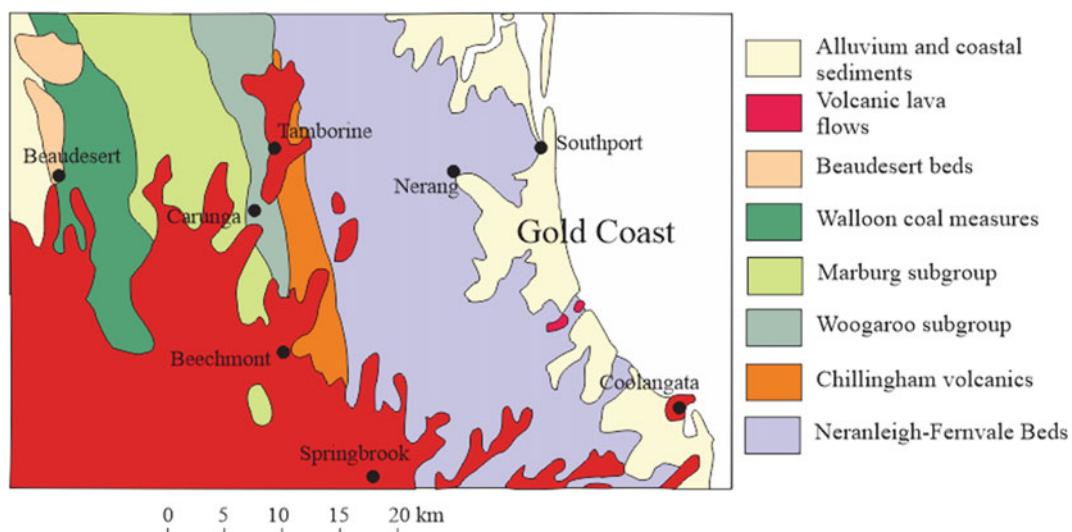


Fig. 3 Geological map of the Gold Coast area (part of SEQ) showing the major geological units

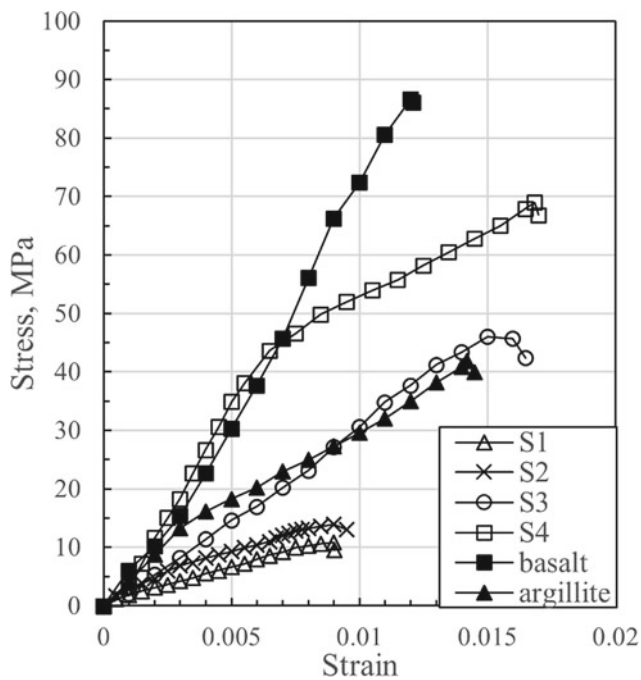


Fig. 4 Results of unconfined compression tests on common types of rock from the Gold Coast area. S1–S4 denote four different types of sandstone from the Marburg subgroup

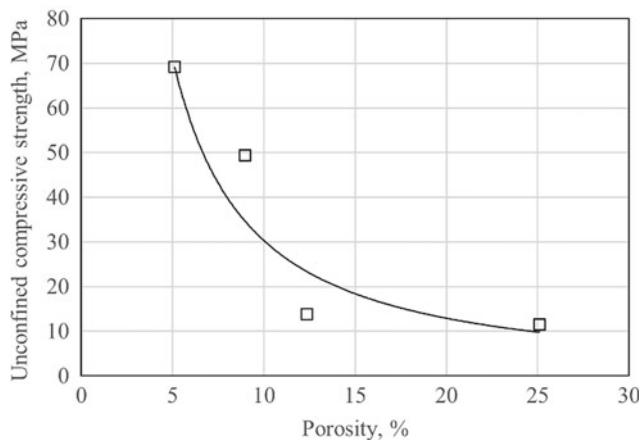


Fig. 5 Results of unconfined compression tests on four different types of sandstone plotted as the unconfined compressive strength (UCS) against rock porosity

conducted on six different rock types, which gives an idea about changes in the rock strength caused by weathering. Visual examination of rock samples was conducted according to the ISRM (1981) guidelines to determine the weathered grade.

It can be inferred from this table that the strength of sedimentary rocks (sandstone and shale) is relatively low compared to the metamorphic greywacke and argillite and

igneous rocks. Also, for all rock types, there is a significant difference between the strength of fresh specimens and heavily weathered ones.

In summary, the relatively low strength of sandstone, compared to other geological units, and its wide distribution in the study area seem to be the major factors for the large number of landslides that occurred in sandstone or sandstone-related material.

2.3 Rock Mass Discontinuities and Strength of Jointed Rock

Another important factor that must be considered in slope stability assessment is joints and discontinuities that affect the stability of rock mass (Gratchev 2019). Rock mass often contains sets of discontinuities that generally undermine the overall strength and create planes of weakness (potential failure zones), and it is thus important to estimate the strength of jointed rock mass (Cui and Gratchev 2020). As several slope failures were associated with sandstone, a series of shear box tests were conducted on jointed and intact core samples of sandstone (Cui et al. 2019) to study the effect of joints on rock strength. For the jointed rock specimens, the surface roughness described by the joint roughness coefficient (JRC) before and after each test was recorded and compared.

Figure 6 shows typical results from those tests that indicate the effect of joints and joint surface roughness on rock shear strength. The intact rock pieces exhibited much greater strength (almost twofold) compared to the jointed specimens. It is interesting that the specimens with a rougher surface (JRC of 10–12) exhibited greater shear strength compared to the specimens with a relatively low JRC of 6–8. The importance of JRC on the strength of jointed rock mass was discussed by Kim et al (2013, 2015b) who showed, through a series of numerical analysis, that when the JRC increased, the slope stability safety factor also increased.

2.4 Rainfall Patterns Prior to Landslides

Bordoni et al. (2015) noted that landslide occurrence can be related to rainfall characteristics such as rainfall duration and intensity. There have been a few studies where the rainfall threshold associated with landslides has been reported by researchers for different areas. Similar type of analysis was conducted by Ravindran et al. (2019) for the mountain passes in northern NSW where the rainfall data prior to landslides in the period of 2009–2017 was collected and analyzed. Figure 7 presents an example of the rainfall data

Table 1 Change in rock strength with weathering grade (WG). F–fresh, SW–slightly weathered, MW–moderately weathered, HW–highly weathered

Rock	WG	Point load index $I_s(50)$, MPa				
		Test no	Min	Max	Mean	SD
Sandstone	F	4	1.25	2.50	1.72	0.54
	SW	10	1.10	2.20	1.53	0.42
	MW	12	0.60	1.40	1.01	0.24
	HW	8	0.30	0.80	0.58	0.17
Shale	F	2	1.57	2.26	1.92	0.49
	SW	3	1.20	1.67	1.37	0.26
	MW	3	0.86	1.20	0.99	0.19
	HW	5	0.21	0.95	0.63	0.28
Greywacke	F	5	3.47	6.10	4.73	0.99
	SW	8	3.52	4.20	3.83	0.23
	MW	6	2.90	3.50	3.21	0.22
	HW	6	1.80	2.50	2.21	0.26
Argillite	F	4	4.10	5.40	4.54	0.51
	SW	7	2.50	3.42	2.95	0.33
	MW	18	1.22	4.00	2.12	0.77
	HW	6	0.20	0.80	0.48	0.21
Basalt	F	5	7.50	9.10	8.38	0.62
	SW	7	5.00	6.40	5.32	0.49
	MW	8	3.10	4.60	4.00	0.45
	HW	9	1.13	2.50	1.79	0.46
Tuff	F	1	–	2.40	–	–
	SW	2	1.40	2.04	1.72	0.45
	MW	–	–	–	–	–
	HW	3	0.28	0.85	0.64	0.32

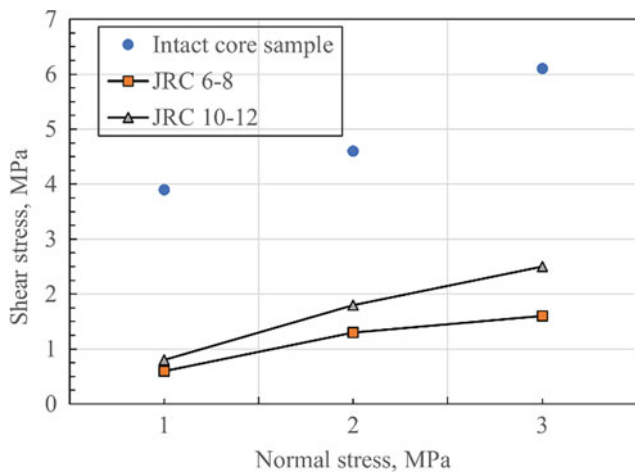


Fig. 6 Results of shear box tests on intact and jointed specimens of sandstone. The core samples with a diameter of 50 cm were used. Note that JRC is the joint roughness coefficient

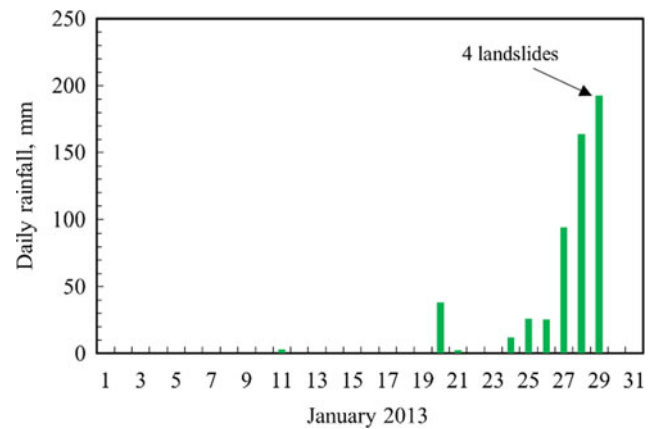


Fig. 7 Rainfall data prior to the occurrence of 4 landslides in the Gibraltar range area in NSW

obtained before the occurrence of four landslides in the Gibraltar range area of NSW in 2013. Analysis of several rainfall events revealed that most of landslides (about 88%) occurred when the cumulative rainfall was between 100 to 600 mm, and it was then suggested the cumulative rainfall amount greater than 300–500 mm would be sufficient to trigger landslides in northern NSW (Ravindran et al. 2019).

Further analysis of the rainfall threshold revealed the relationship between the rainfall intensity and duration as given in Eq. 1.

$$I = 22.6D^{-0.554} (48 < D < 432 \text{ hrs}) \quad (1)$$

where, I is the rainfall intensity (mm/hrs), D is the duration of rainfall (hrs).

Through analysis of flume test results that simulated different slope and rainfall conditions, combined with the analysis of published data on the rainfall intensity and duration prior to the landslide occurrence in tropical regions, Cogan and Gratchev (2019) suggested the rainfall-intensity threshold that can be used for SEQ Australia conditions as given in Eq. 2

$$I = 80.065D^{(-0.596)} \quad (2)$$

It is noted that although these relationships provide useful tools for landslide hazard assessment, they are considered as general estimations, and thus engineering judgement must be exercised while using them.

2.5 Characteristics of Soils from Landslide Sites

Soil samples were collected from several landslide sites to study the index properties and strength of soil material. As reported by Ravindran and Gratchev (2020), most of soil samples were classified as coarse-grained material, predominantly sand. Only small amount of fines (usually less than 5%) were present in the tested soil samples.

Several triaxial tests on saturated soil specimens were conducted to estimate the undrained strength of soil under loads (Ravindran and Gratchev 2021). In addition, a series of shear box tests on soil specimens at different values of water content were carried out to investigate the effect of moisture on soil strength.

Figure 8 presents the results of undrained triaxial tests conducted on coarse-grained soil specimens plotted as the effective stress path. It is clear from these graphs that the excess pore water pressure generated in the specimens under loads (i.e., a decrease in p'); however, the amount of excess pore water pressure wasn't sufficient to cause liquefaction (note that the liquefaction conditions would likely occur when p' drops to almost 0). These typical results suggest that the failure in shallow landslides may not be triggered by the

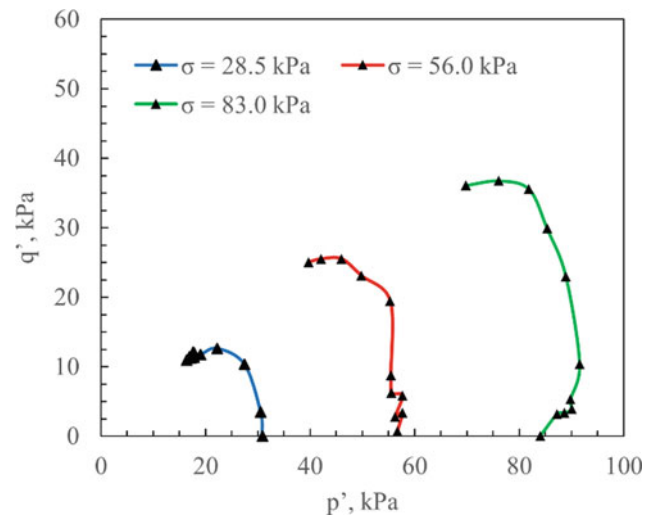


Fig. 8 Results of undrained triaxial tests on coarse-grained soil from a landslide site presented as the effective stress path for different confining pressures

extremely large values of pore water pressure. In fact, as suggested by Krahn et al (1989), shallow slope failures generally occur during rainfall due to the loss of suction.

The test results from a series of shear box tests on 15 different soils from several landslide sites in northern NSW showed that the shear strength of soil decreased as the initial water content of the shear box specimens increased (Fig. 9). It was found that although the friction angle of soil remained almost the same in spite of the increasing amount of moisture in the soil, the apparent cohesion drastically decreased. The experimental data in Fig. 10 indicated that for the range of water content used, there was a pronounced decrease in the apparent cohesion with an increase in water content. This change in the apparent cohesion was mainly attributed to soil

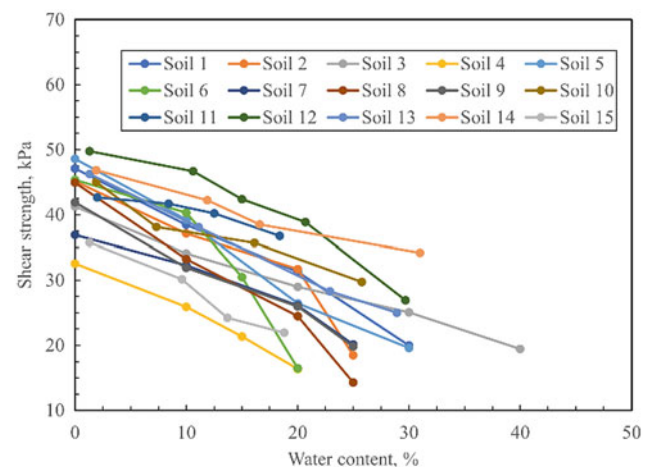


Fig. 9 Results from shear box tests on soils from landslide sites in the northern NSW plotted as the shear strength against the initial water content

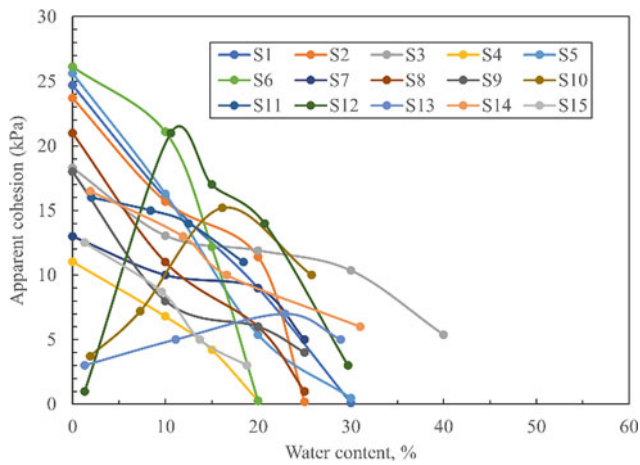


Fig. 10 Results from a series of shear box tests plotted as the apparent cohesion against the initial water content

suction, which was the greatest at a low range of water content and then dropped to zero when the soil specimens became saturated (or very close to saturation) (Fig. 11).

This data has been utilized to draw a relationship between the values of apparent cohesion and water content (Eq. 3) which can be used to estimate changes in strength for similar soil types. Note that Eq. 3 was obtained for the range of water content of 0–30%, and the effective vertical stress of 28.5 kPa.

$$c/c_o = 1.1 - 4.7\theta + 5.9\theta^2 \quad (3)$$

where, c is the apparent cohesion at any water content between 0 and 30%; c_o is the cohesion at zero water content; and θ is the water content.

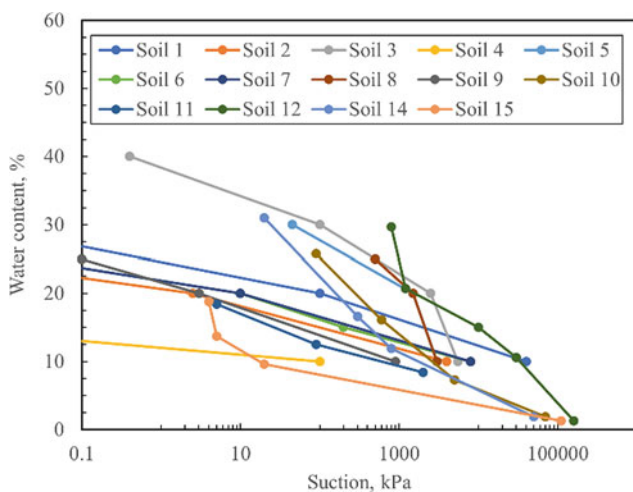


Fig. 11 Results from a series of suction tests showing the relationship between the water content of soil specimens and suction

3 Mechanisms of Shallow Rainfall-Induced Landslides

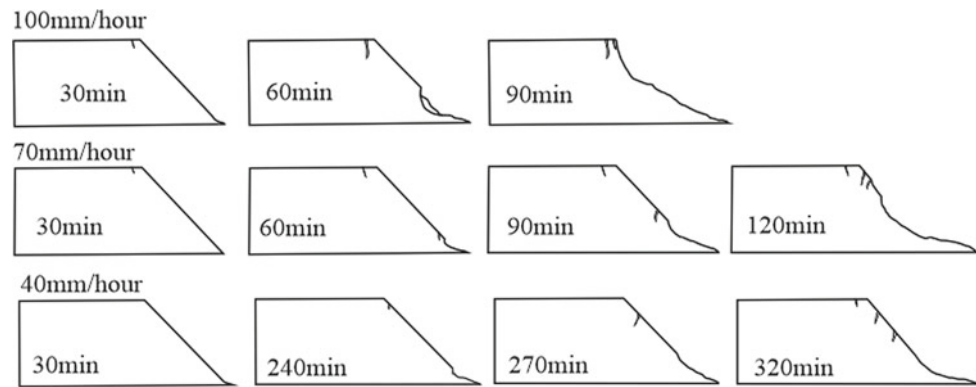
Flume tests provide great opportunities to study the mechanism of rainfall-induced shallow landslides by controlling important factors that contribute to failure. In such tests, it is possible to vary soil types, initial soil conditions, slope geometry, and rainfall intensity. Cogan and Gratchev (2019) conducted a series of flume experiments on sandy slopes with various surface inclinations and rainfall rates, and provided insights into the mechanism of landslide initiation and development. Those tests were equipped with a range of sensors that allowed changes in soil water content, suction, pore water pressure, and displacements to be accurately measured and monitored. It has been found that at a relatively high rainfall intensity, the wetting front formed at the base of the flume. The soil suction decreased as the water content of soil mass increased, resulting in the development of excess pore water pressures through the slope. The pore water pressures then gradually increased until failure. According to visual observations reported by Cogan and Gratchev (2019), at high pore water pressures, the excess water began to wash out the soil particles at the toe, which gradually caused larger collapses to occur.

Rainfall intensity plays an important role in slope stability. It was experimentally observed that an increase in rainfall intensity could lead to more rapid failure. Figure 12 shows the behaviour of a sand slope under different rainfall rates. For 100 mm/hour, failure at the toe occurred about 60 min from the beginning of the experiment while a somewhat similar outcome occurred in the slope after 90 min when the rainfall rate decreased to 70 mm/hour. At a rate of 40 mm/hour, no failure occurred, even after 320 min (with the exception of some minor soil particle erosion at the toe). At this relatively low rainfall intensity, the drainage of water along the slope surface was sufficient to keep the excess pore water pressure at a low value, at which no failure could occur.

3.1 Discussion

Analysis of experimental data from shear box and flume tests reveals the strong influence of water content on soil strength. At a low range of water content, the shear strength of soil appears to be relatively high, and thus sufficient to keep the soil mass stable. Soil suction developed in the soil mass, as evident from the suction and shear box tests, seems to provide the additional strength component in terms of the apparent cohesion. As the water content increases during a rain event, the apparent cohesion along with the total shear

Fig. 12 Changes in the slope geometry over time for different rainfall intensities observed in a series of flume tests



strength of soil begin to decrease. If the rainfall intensity is relatively high, greater amounts of water will permeate the slope and cause the development of a wetting (moisture) front. As the wetting front expands across the soil mass, generating excess pore water pressures, the stability of soil mass will decrease. A relatively low rainfall intensity may not be sufficient for this purpose as the water drainage on the slope surface may exceed the water influx in the slope. In the former case, the slope may become unstable, resulting in the occurrence of landslide. In the latter case, the slope mass can still retain its strength and no slope failure will occur.

4 Concluding Remarks

The paper has summarized and discussed the major findings obtained by the authors in relation to the mechanisms of common landslides in SEQ and northern NSW, Australia, and factors that affect them. The following major conclusions can be drawn:

- Geological factors such as rock type, bedding planes and their inclination, discontinuities of rock mass, and weathering play an important role in the formation of landslides in the study area. It was found that most of the slides were related to jointed, bedded, and weathered sandstone deposits.
- The rainfall intensity and duration have significant effects on slope stability. Cumulative rainfall of greater than 500 mm might be associated with the landslide occurrence. The rainfall threshold described in this study can provide engineers and decision makers with an important tool for more accurate landslide hazard assessment.
- The strength of soil from the landslide mass depends on water content. The apparent cohesion existing in the soil at a low range of water content due to suction tends to disappear when the water content increases towards soil saturation. This correlates with a drop in shear strength of soil, a process that leads to slope instability.

- Considering the results from flume tests, the mechanism of shallow rainfall-induced landslides can be attributed to the formation of wetting (moisture) front, increases in water content, and the excess pore water pressure generation.

References

- Abeykoon A, Gallage C, Dareeju B, Trofimovs J (2018) Real-time monitoring and wireless data transmission to predict rain-induced landslides in critical slopes. *Aust Geomech J* 53(3):61–76
- Australian Building Codes Board (2015) Landslide hazards: handbook. Australian Government and States and Territories of Australia, p 41
- Australian , Geomechanics, Society (2007a) A national landslide risk management framework for Australia. *Aust Geomech* 42(1):1–12
- Australian , Geomechanics, Society (2007b) Guideline for landslide susceptibility, hazard and risk zoning for land use planning. *Aust Geomech* 42(1):13–36
- Bordoni M, Meisina C, Valentino R, Lu N, Bittelli M, Chersich S (2015) Hydrological factors affecting rainfall-induced shallow landslides: from the field monitoring to a simplified slope stability analysis. *Eng Geol* 193:19–37
- Cogan J, Gratchev I (2019) A study on the effect of rainfall and slope characteristics on landslide initiation by means of flume tests. *Landslides* 16(12):2369–2379
- Cogan J, Gratchev I, Wang G (2018) Rainfall-induced shallow landslides caused by ex-tropical cyclone Debbie, 31st March 2017. *Landslides* 15(6):1215–1221
- Cui C, Gratchev I (2020) Effects of pre-existing cracks and infillings on strength of natural rocks—cases of sandstone, argillite and basalt. *J Rock Mech Geotech Eng* 12(6):1333–1338
- Cui C, Gratchev I, Chung M, Kim DH (2019) Changes in joint surface roughness of two natural rocks during shearing. *GEOMATE J* 17 (63):181–186
- Gratchev I (2019) *Rock mechanics through project-based learning*. CRC Press
- Gratchev I, Irsyam M, Towhata I, Muin B, Nawir H (2011) Geotechnical aspects of the Sumatra earthquake of September 30, 2009, Indonesia. *Soils Found* 51(2):333–343
- Gratchev I, Kim DH (2016) On the reliability of the strength retention ratio for estimating the strength of weathered rocks. *Eng Geol* 201:1–5

- Gratchev I, Pathiranagei SV, Kim DH (2019) Strength properties of fresh and weathered rocks subjected to wetting–drying cycles. *Geomech Geophys GeoEnergy GeoResour* 5(3):211–221
- Gratchev I, Shokouhi A, Kim D, Stead D, Wolter A (2013) Assessment of rock slope stability using remote sensing technique in the Gold Coast area, Australia. In: *Proceedings of the 18th Southeast Asian geotechnical and inaugural AGSSEA conference*, pp 729–734
- Gratchev I, Towhata I (2011) Analysis of the mechanisms of slope failures triggered by the 2007 Chuetsu Oki earthquake. *Geotech Geol Eng* 29(5):695–708
- ISRM (1981) Basic geotechnical description of rock masses. *Int J Rock Mech Min Sci Geomech Abs* 18:85–110
- Kim D, Gratchev I, Balasubramaniam A (2013) Determination of joint roughness coefficient (JRC) for slope stability analysis: a case study from the Gold Coast area, Australia. *Landslides* 10(5):657–664
- Kim DH, Gratchev I, Balasubramaniam A (2015a) A photogrammetric approach for stability analysis of weathered rock slopes. *Geotech Geol Eng* 33(3):443–454
- Kim D, Gratchev I, Balasubramaniam A (2015b) Back analysis of a natural jointed rock slope based on the photogrammetry method. *Landslides* 12:147–154
- Kim DH, Gratchev I, Berends J, Balasubramaniam A (2015c) Calibration of restitution coefficients using rockfall simulations based on 3D photogrammetry model: a case study. *Nat Hazards* 78(3):1931–1946
- Krahn J, Fredlund DG, Klassen MJ (1989) Effect of soil suction on slope stability at Notch Hill. *Can Geotech J* 26(2):269–278
- Middelmann MH, Mazengarb C (2007) *Natural hazards in Australia: Identifying risk analysis requirements*. Geoscience Australia. Australian Government, Canberra
- National Research Council (2004) *Partnerships for reducing landslide risk: assessment of the national landslide hazard mitigation strategy*. National Academic Press, Washington, USA
- Osuchowski M, Roberts J (2011) *Landslide costs in the Wollongong Region*. *Geosci Aust Rec* 2011(32):53
- Ravindran S, Gratchev I (2020) Estimation of shear strength of gravelly and sandy soils from shallow landslides. *GEOMATE J* 18(70):130–137
- Ravindran S, Gratchev I (2021) Prediction of shallow rainfall-induced landslides using shear strength of unsaturated soil. *Indian Geotech. J* 51(4):661–672
- Ravindran S, Gratchev I, Jeng DS (2019) Analysis of rainfall-induced landslides in northern New South Wales, Australia. *Australian Geomechanics* 54(4):85–99
- Shokouhi A, Gratchev I, Kim D (2013) Rock slope stability problems in gold coast area. *Aust Int J Geomate* 4(1):501–504
- Wang G, Sassa K, Fukuoka H (2003) Downslope volume enlargement of a debris slide–debris flow in the 1999 Hiroshima, Japan, rainstorm. *Eng Geol* 69(3–4):309–330
- Willmott WF (2010) *Rocks and landscape of the gold coast hinterland*. Geological Society of Australia, Queensland Division
- Willmott WF (1981) *Slope stability and its constraints on closer settlement on tamborine mountain, Southeast Queensland*. Department of Mines and Energy

Open Access This chapter is licensed under the terms of the Creative Commons Attribution 4.0 International License (<http://creativecommons.org/licenses/by/4.0/>), which permits use, sharing, adaptation, distribution and reproduction in any medium or format, as long as you give appropriate credit to the original author(s) and the source, provide a link to the Creative Commons license and indicate if changes were made.



The images or other third party material in this chapter are included in the chapter's Creative Commons license, unless indicated otherwise in a credit line to the material. If material is not included in the chapter's Creative Commons license and your intended use is not permitted by statutory regulation or exceeds the permitted use, you will need to obtain permission directly from the copyright holder.



Design Protection Barriers Against Flow-Like Landslides

Sabatino Cuomo, Angela Di Perna, and Mario Martinelli

Abstract

The interaction of flow-like landslides with protection barriers is analyzed for their design. Three recent analysis approaches are briefly presented and applied to different landslide geometries. Approach no. 1 (empirical) allows estimating the impact force and flow kinetic energy over the time. Approach no. 2 (analytical) additionally provides the displacement of the barrier due to the impact. Approach no. 3 (numerical) fully simulates the Landslide-Structure-Interaction (LSI) also including the estimate of the amount of landslide volume overtopping the barrier. The required input parameters and the results achievable through the three approaches are illustrated and compared.

Keywords

Protection • Design • Approach • Impact • Performance

1 Introduction

The analysis of the Landslide-Structure-Interaction (LSI) is a difficult yet crucial task, especially in the case of a flow-like landslide impacting a protection barrier.

The first fundamental step is the landslide triggering and propagation analysis in the mountain catchment. This issue was recently reviewed by Cuomo (2020), where the readers can find the details about the engineering analysis methods

applicable to detect the potential landslide source areas and the following propagation zones.

In other words, to study the LSI, we need as an input the “reference landslide” (a single landslide or a set of landslides).

The latter must be characterized in terms of velocity, thickness, shape and length. It is worth noting that all those features are extrapolated (using the expert judgement) from the results of the landslide propagation analysis. For instance, soil velocity will be not same all over the landslide body and we will refer to a representative value for the whole landslide just before the LSI starts. The same applies to the landslide thickness and so on.

If the landslide input data are given such as velocity, thickness, unit weight, length, shape and volume, then we can apply one of the empirical methods in the literature to estimate the peak pressure (or force) expected at the impact against the barrier.

Some (hydro-static) methods require only the flow unit weight and thickness (Scotton and Deganutti 1997; Scheidl et al. 2013); other (hydro-dynamic) methods use as inputs the flow density and the squared velocity of the flow (Bugnion et al. 2012; Canelli et al. 2012); other (mixed) methods consider both the static and the dynamic components of the flow (Arattano and Franzi 2003; Cui et al. 2015). However, none of them allow assessing the evolution of the impact force over the time.

Recent research tried to overcome these limitations. Di Perna et al. (2022) proposed an enhanced empirical method, first calibrated via numerical analyses and then validated referring to a large dataset of real debris flows. This method allows estimating the impact duration (not only the peak impact pressure), which regulates the deformation of the protection barrier. Cuomo et al. (2022) casted an analytical method to simulate the inelastic collision of the impacting landslide and the protection barrier. From there, the landslide energy release and the deformation plus the eventual displacement of the barrier are determined. Finally, Cuomo

S. Cuomo (✉) · A. Di Perna
Department of Civil Engineering, Geotechnical Engineering
Group (GEG), University of Salerno, Fisciano, SA, Italy
e-mail: scuomo@unisa.it

A. Di Perna
e-mail: adiperna@unisa.it

M. Martinelli
Deltares, Delft, Netherlands
e-mail: mario.martinelli@deltares.nl

et al. (2021a, 2022) applied an advanced numerical code based on Material Point Method (MPM), i.e., the Anura 3D code (and related developments done by Deltares), to entirely reproduce the LSI including the mutual actions between the landslide and the barrier as well as the landslide propagation during the LSI, i.e., the eventual barrier overtopping by some landslide volume.

This paper intends to provide a practical framework to be used in a contest of landslide risk mitigation, consistent with the aims of the Kyoto Landslide Commitment 2020 (Sassa 2021).

2 Methodological Approach

We assume that a flow-like landslide mass impacts against a rigid barrier, fixed or unfixed to the base ground (Fig. 1), as proposed by Cuomo et al. (2020a).

The landslide body has unitary width, length L_1 , depth h , density of the mixture ρ_m , initial uniform velocity v_0 , pore-water pressure p_L and base friction coefficient $\tan \varphi_b$. The barrier has a bottom base B , top base b , height H , inclination of the impacted side β .

The LSI develops from the initial configuration ($t = t_0$), then landslide propagation ($t_0 < t < t_{imp}$) leads to the impact of the landslide front ($t = t_{imp}$) and to the peak impact force ($t = T_1$) until the end of the LSI ($t = t_f$).

Before the landslide reaches the barrier ($t_0 < t < t_{imp}$), i.e., during the propagation stage, the LSI problem is governed by the basal frictional force F_1 , which acts along the bottom of the flow (L_1) and controls the reduction in flow velocity, resulting in a decrease of the impact force.

Once the flow starts to interact with the barrier ($t_{imp} < t < T_2$), additional stresses (mostly orthogonal to the impacted surface, hence horizontal in many applications) are produced on the impacted side of the barrier. Many studies (e.g., Cui et al. 2015; Song et al. 2017) demonstrated that the impact force–time history can be simplified as a triangular force impulse, usually with a rise time ($t = T_1$) much shorter than the decay time ($T_2 - T_1$).

For the action-reaction principle, the mutual impact forces between the landslide and the barrier are equal and opposite. Such mutual stress causes: (i) the flow to decelerate and (ii) the barrier to slip along the base, if unfixed. The evaluation of the impact forces applied on the inclined side of the barrier (L_2) is fundamental to design the structural characteristics of the barrier.

It is also worth noting that the flow may overtop the barrier during the impact, generating an additional force F_3 on the structure, mainly dependent on the flow-barrier frictional contact ($\tan \delta$).

After the impulsive stage of the LSI ($T_2 < t < t_f$), the problem is mostly governed by the inertial resistance force F_4 , which depends on the amount of friction mobilized along the base (b) of the barrier ($\tan \delta_b$). The displacement Δx of the barrier at the end of LSI (Δx_f) depends on both the amount of energy transferred to the barrier and that dissipated by shear friction along the base.

3 Alternatives for Design

3.1 Design Approach No. 1: Empirical

In a simplified approach, the barrier is assumed as fixed to the base ground and high enough to retain all the landslide volume behind the barrier (Fig. 2).

The landslide is schematized as rectangular with mass m_1 , length L_1 , depth h , unitary width, density ρ_m , initial velocity v_0 and it is supposed that the landslide is completely stopped by the barrier (i.e., $v(T_2) = 0$).

Once the Froude number (Eq. 1) is computed, as representative of the landslide kinematics, we compute the coefficient α from Eq. 2. Then, based on previous studies (Hung et al. 1984; Scotton and Deganutti 1997; Kwan 2012), the peak lateral force F_{peak} (Eq. 3) exerted by the flow on the barrier is calculated by the sum of a dynamic component $F_{peak,dyn}$ (Fig. 2a) and a height-dependent static component $F_{peak,stat}$ (Fig. 2b), as in Eqs. (4–5).

Fig. 1 General conceptual scheme for Landslide Structure Interaction (LSI)

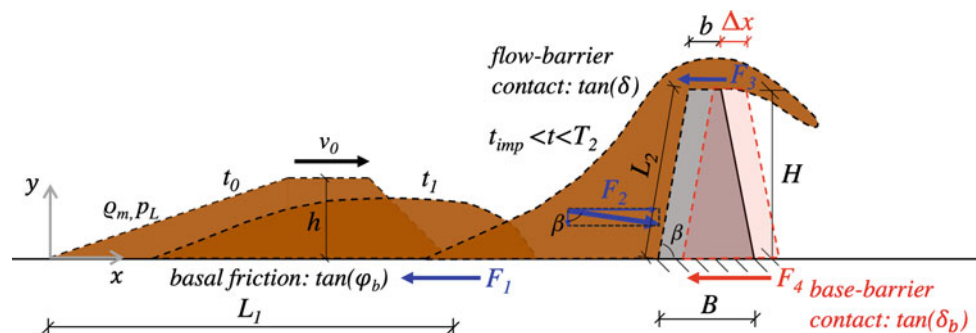
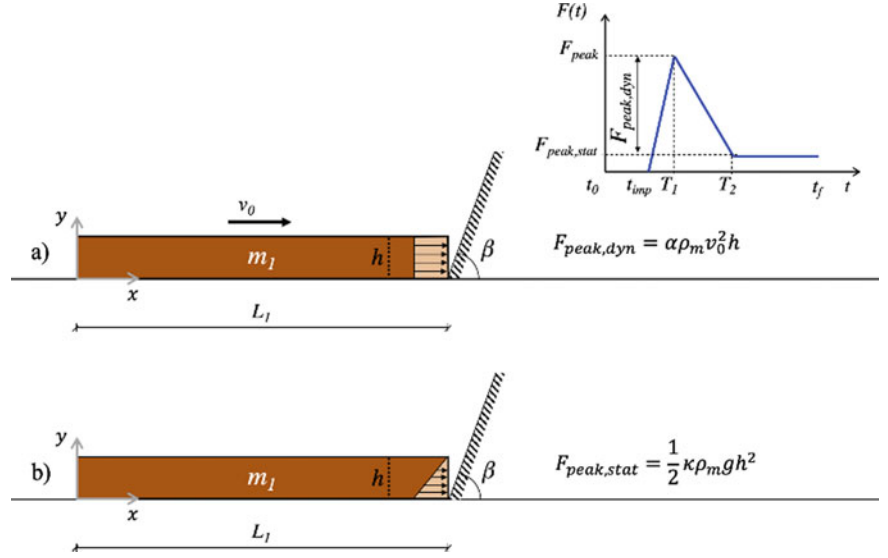


Fig. 2 Scheme in the empirical method

$$Fr = v_0 / \sqrt{gh} \quad (1)$$

$$\alpha = a_1 Fr^{a_2} \quad (2)$$

$$F_{\text{peak}} = F_{\text{peak,dyn}} + F_{\text{peak,stat}} \quad (3)$$

$$F_{\text{peak,dyn}} = \alpha \rho_m v_0^2 h \quad (4)$$

$$F_{\text{peak,stat}} = \frac{1}{2} \kappa \rho_m g h^2 \quad (5)$$

The impact period T_2 is obtained by using the impulse theorem, since the integral over time of the impact force (i.e., the impact impulse) is equal to the variation of linear momentum of the landslide (Eq. 6). The landslide mass is supposed to be constant during the impact. Once T_2 is known through Eq. 6, for $t_{\text{imp}} = 0$, T_1 can be achieved in Eq. 7, by fixing the ratio $\tau = T_1/T_2$ (for example from experimental evidence). The description of the impact dynamics is now complete. In fact, the reduction in landslide velocity $\Delta v(t)$ is obtained from Eq. 8, and the flow velocity over time $v(t)$ from Eq. 9. The corresponding kinetic energy $E_{k,1}(t)$ (Eq. 10) can be computed.

$$T_2 = 2m_1 v_0 / (F_{\text{peak}} + F_{\text{peak,stat}} - \tau F_{\text{peak,stat}}) \quad (6)$$

$$T_1 = \tau T_2 \quad (7)$$

$$\Delta v(t) = \begin{cases} \frac{F_{\text{peak}}}{2m_1 T_1} t^2 & t_{\text{imp}} < t < T_1 \\ \frac{F_{\text{peak}}}{m_1} t - \frac{F_{\text{peak,dyn}}}{2m_1(T_2 - T_1)} t^2 & T_1 < t < T_2 \end{cases} \quad (8)$$

$$v(t) = v_0 - \Delta v(t) \quad (9)$$

$$E_{k,1}(t) = \frac{1}{2} m_1 v^2(t) \quad (10)$$

All the details of this approach are reported in Di Perna et al. (2022), and a suggested set of model parameters are: $a_1 = 1.781$, $a_2 = -0.515$, $\tau = 0.14$, $\kappa = 0$. The main advantage of this method is the simple applicability and the reduced number of parameters. The main limitation is the inability to give information about the dynamics of the barrier if the latter is left free to shift along its base. In some cases, in fact, it could be convenient to introduce an additional energy dissipation mechanism related to the barrier movement and deformation.

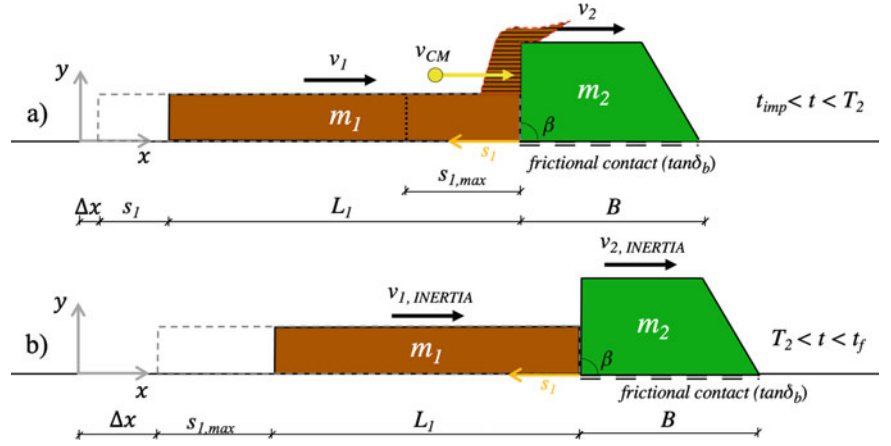
3.2 Design Approach No. 2: Analytical

A more elaborated analytical model is set up where the landslide and the barrier are considered as two colliding bodies. The approaching flow has a volume V_1 , mass m_1 , length $L_{1,0}$, depth h , unitary width, density ρ_m , and initial velocity $v_{1,0}$.

The barrier is rigid, with its own mass m_2 and it is free to slide along the base. The frictional contact at the base is equal to $\tan(\delta_b)$, which can be set as the 80% of the strength properties of the subsoil base material (Cuomo et al. 2020a). As a special case, a barrier fixed to the base ground can be also considered, by setting the mass of the barrier to a very high value compared to that of the flow (i.e., $m_2/m_1 \rightarrow \infty$).

The landslide-barrier interaction (*impact* stage in Fig. 3a) is schematized by an inelastic collision. After the impact, the two bodies reach the same velocity v_{CM} , applied in the centre of mass (CM) of the system.

Fig. 3 Conceptualization in the analytical method: **a** during impact, **b** after impact



The impact force F is a spatio-temporal function since the approaching volume of the landslide increases with time until T_1 and then diminishes due to the dissipation of flow energy. The quantity s_1 represents the change (shortening) of the landslide body after the impact and it is computed as positive in the direction opposite to the flow movement. Since the impacting mass is saturated, the expected behaviour is that a part of the landslide mass will overtop the barrier and the remaining volume will interact with the barrier.

The mathematical steps are reported in Cuomo et al. (2022), while the main equations are written below. The maximum value $s_{1,max}$ is reached when the impact force is equal to the peak value. This means that only a part of the total volume of the landslide contributes to the interaction with the barrier. This concept is relevant. The quantity $K_1 = \left(\frac{m_1 m_2}{m_1 + m_2}\right) \cdot \left(\frac{v_{1,0}}{s_{1,max}}\right)$ is a model parameter referred to the body 1 (landslide), while the quantities q_1 (Eq. 11) and T_2 (Eq. 12) are the primary model unknowns. For $t_{imp} = 0$, once both T_2 and T_1 (Eq. 7) are known, which can be achieved by fixing the ratio $\tau = T_1/T_2$ (e.g., from experimental evidence), the impact dynamics description is complete.

$$q_1 = \frac{3}{4} \frac{K_1 v_{1,0}}{\sqrt{s_{1,max}}} \quad (11)$$

$$T_2 = \frac{8 s_{1,max}}{3 v_{1,0}} \quad (12)$$

$$F(t) = \frac{1}{2} \frac{q_1^2}{K_1} \left(\frac{t}{\tau}\right) \quad 0 < t \leq T_1 \quad (13)$$

$$F(t) = \frac{1}{2} \frac{q_1^2}{K_1} \left(\frac{T_2 - t}{1 - \tau}\right) \quad T_1 \leq t < T_2 \quad (14)$$

The kinematics of the landslide during the impact is described by the velocity of its centre of mass $v_1(t)$ (Eq. 15) and kinetic energy $E_{k,1}(t)$ (Eq. 16).

$$v_1(t) = \begin{cases} v_{1,0} - \frac{q_1^2}{4K_1 m_1} \left(\frac{t^2}{\tau}\right) & 0 < t < T_1 \\ v_{1,0} + \frac{q_1^2}{4K_1 m_1} \left(\frac{t^2 - 2T_2 t + T_1 T_2}{1 - \tau}\right) & T_1 < t < T_2 \end{cases} \quad (15)$$

$$E_{k,1}(t) = \frac{1}{2} m_1 v_1^2(t) \quad (16)$$

Similar equations are derived for body 2 (i.e., the barrier). Here, the frictional contact along the base of the barrier causes its deceleration and therefore, it must be considered in the velocity formulation. The deceleration is equal to the ratio between the frictional contact force and the mass of the barrier and remains constant during the interaction with the flow. It implies that the velocity $v_2(t)$, displacement $\Delta x(t)$ and kinetic energy $E_{k,1}(t)$ of the barrier can be approximately computed (if landslide shear stresses along the impacted side of the barrier are neglected) as:

$$v_2(t) = v_2(t) \begin{cases} \frac{q_1^2}{4K_1 m_1} (\sin \beta + \cos \beta \tan \delta_b) \left(\frac{t^2 - t^{*2}}{\tau}\right) - g \tan \gamma_b (t - t^*) & t^* < t < T_1 \\ \frac{q_1^2}{4K_1 m_1} (\sin \beta + \cos \beta \tan \delta_b) \left(\frac{t^2 - 2T_2 t + T_1 T_2}{1 - \tau}\right) - g \tan \gamma_b (t - t^*) & T_1 < t < T_2 \\ t^* = \frac{2K_1 m_2 \tau g \tan \delta_b}{q_1^2 (\sin \beta + \cos \beta \tan \delta_b)} & \end{cases} \quad (17)$$

$$v_2(t) = \Delta x_f = \begin{cases} \frac{q_1^2}{12K_1m_2} (\sin \beta + \cos \beta \tan \delta_b) \\ \quad \left(\frac{t^3 - 3t^{*2}t + 2t^{*3}}{\tau} \right) \\ -\frac{g}{2} \tan \delta_b (t - t^*)^2 \quad t^* < t \leq T_1 \\ \frac{q_1^2}{12K_1m_2} (\sin \beta + \cos \beta \tan \delta_b) \\ \quad \left(\frac{(T_1 - t)^2 (3T_2 - 2T_1 - t)}{1 - \tau} \right) \\ -\frac{g}{2} \tan \delta_b (T_1 - t)^2 - v_2(T_1)(T_1 - t) \\ \quad + \Delta x(T_1) \quad T_1 < t \leq T_2 \end{cases} \quad (18)$$

$$E_{k,2}(t) = \frac{1}{2} m_2 v_2^2(t) \quad (19)$$

After the impact, the landslide-structure-interaction between the two bodies can be neglected since the motion is mostly governed by shear friction along the base. In this stage, the change in velocity over time can be calculated referring to the uniformly decelerating motion equations. The final displacement Δx_f of the barrier is reported in Eq. (20).

$$\Delta x_f = \frac{q_1^2}{12K_1m_2} (\sin \beta + \cos \beta \tan \delta_b) \left[\frac{(T_1 - t^*)^2 (T_1 + 2t^*)}{\tau} + \frac{2(T_2 - T_1)^3}{1 - \tau} \right] - \frac{g}{2} \tan(\delta_b) \left[(T_1 - t^*)^2 + (T_2 - T_1)^2 \right] \quad (20)$$

In this analytical model, two quantities $s_{1,\max}$ and τ must be evaluated. From numerical calibrations performed by Cuomo et al. (2022) for a set of cases, it emerges that the

ratio $\lambda = s_{1,\max}/L_{1,0}$ was equal to 0.72 for barriers fixed to the base ground and 0.41 for unfixed barriers. Suggested values for τ are 0.17 (fixed) and 0.25 (unfixed).

The proposed analytical model reproduces the global behaviour of the landslide body in the LSI process and implicitly disregards some local mechanisms, such as the formation (behind the barrier) of a dead zone, over which the rear part of the landslide body propagates (Ng et al. 2018). This is one of the limitations of the model.

3.3 Design Approach No. 3: Numerical

Among the many numerical techniques applicable to the complex problem of LSI, the Material Point Method is a particularly suitable tool. In fact, MPM is an appropriate modelling alternative for large deformation problems.

The Lagrangian points (named Material Points) are free to move across a fixed mesh (an example is shown in Fig. 4), which schematizes the domain where the materials are at the start and where they will move during the deformation process. At each time step, the governing equations are solved on the mesh, but then all the stress-strain variables are saved in the MPs.

To schematize the LSI problem in a more realistic way than in the previous methods, the build-up of pore water pressure in the flow material during the impact is considered as well as the hydro-mechanical coupled behaviour and the yielding of the flow material.

For a saturated porous material, each MP reproduces a volume of the mixture V , given by the sum of the solid V_S and liquid V_L phases volumes. Each MP stores the information about both the solid and liquid phases. This is called two-phase single-point formulation (Jassim et al. 2013; Ceccato et al. 2018). The primary unknowns are the solid (\mathbf{a}_S) and the liquid acceleration (\mathbf{a}_L). From there, the velocities of the solid and liquid phases are obtained. The MPs are

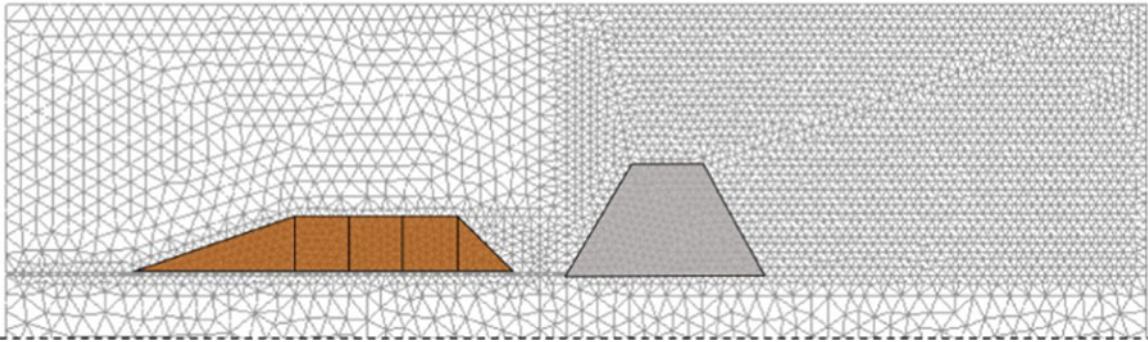


Fig. 4 Example of geometrical schematization in MPM

moved with the kinematics of the solid skeleton during the computation. Instead, the so-called “one-phase single-point” formulation can be opportunely adopted for dry materials, that is the case of the rigid barrier.

The governing equations are the conservation of mass (Eq. (21), with ρ being the density), automatically satisfied as the solid mass is constant in each MP during deformation, the conservation of linear momentum (Eq. 22), and the stress ($\boldsymbol{\sigma}$)–strain ($\boldsymbol{\varepsilon}$) dependency (Eq. (23)). The latter is simulated through the Jaumann stress rate ($\dot{\boldsymbol{\sigma}}$) that can handle large deformations, unlike the Cauchy tensor for small strain rates.

$$\frac{d\rho}{dt} + \rho \nabla \cdot \mathbf{v} = 0 \quad (21)$$

$$\rho \frac{d\mathbf{v}}{dt} = \nabla \boldsymbol{\sigma}^T + \rho \mathbf{g} \quad (22)$$

$$d\dot{\boldsymbol{\sigma}} = \mathbf{D} \cdot d\hat{\boldsymbol{\varepsilon}} \quad (23)$$

The time integration scheme is explicit, since most of the dynamic problems, including wave or shock propagation, cannot be treated properly by an implicit integration which tends to smooth the solution (Fern et al. 2019). Hence, there is a critical time step Δt_{cr} during which a wave with speed c crosses the smallest element length d (Eq. 24 with E being the soil stiffness). The critical time step defines the biggest time increment which can be used for a stable calculation, but often it cannot be estimated in the case of non-linear problems. For this reason, the critical time step is multiplied by an additional factor C_{NB} (namely Courant number) to reach stability. The Courant number has values between 0 and 1. Generally, the smaller the Courant number and the smaller the time step, improving the accuracy of the numerical results.

$$\Delta t_{cr} = \frac{d}{c} = \frac{d}{\sqrt{E/\rho}} \quad (24)$$

The interaction force between solid and liquid phases is governed by Darcy’s law. Numerically, these equations are solved at grid nodes considering the Galerkin method (Luo et al. 2008) with standard nodal shape functions and their solutions are used to update MPs velocities and momentum of each phase. The strain rate $\dot{\boldsymbol{\varepsilon}}$ of the MPs is computed from the nodal velocities obtained from the nodal momentum.

In the two-phase single-point formulation the liquid mass, and consequently the mass of the mixture, is not constant in each material point but can vary depending on porosity changes. Fluxes due to spatial variations of the liquid mass are neglected and Darcy’s law is used to model solid–liquid interaction forces. For this reason, this formulation is generally used in problems with small gradients of porosity, and laminar and stationary flow in slow velocity regime. However, this

formulation proves to be suitable for studying flow–structure–interaction (Cuomo et al. 2021a). The water is assumed to be linearly compressible via the bulk modulus of the fluid \mathbf{K}_L and shear stresses in the liquid phase are neglected.

With reference to the critical time step, the influence of permeability and liquid bulk modulus must be considered as well (Mieremet et al. 2016). In particular, the time step required for numerical stability is smaller in soil with lower permeability (Eq. 25).

$$\Delta t_{cr} = \min \left(\frac{d}{\sqrt{(E + \mathbf{K}_L/n)/\rho_m}}; \frac{2(\rho_m + (1/n - 2)\rho_L)k_{sat}}{\rho_L \mathbf{g}} \right) \quad (25)$$

The sliding model of the flowing mass on the rigid material is handled by a frictional Mohr–Coulomb strength criterion. The contact formulation is used to ensure that no interpenetration occurs, and that the tangential forces are compatible with the shear strength along the contact. The reaction force acting on the structure at node j is calculated as in Eq. 26.

$$F_j(t) = m_{j,S} \Delta a_{S,\text{contact}} + m_{j,L} \Delta a_{L,\text{contact}} \quad (26)$$

The terms $\Delta a_{S,\text{contact}}$ and $\Delta a_{L,\text{contact}}$ are the change in acceleration induced by the contact formulation, for both solid and liquid phase, and $m_{i,S}$ and $m_{i,L}$ are the corresponding nodal masses, respectively. The total reaction force is the integral of the nodal reaction forces along the barrier. Details of the contact formulation are described in Martinelli and Galavi (2022).

4 Design Examples

4.1 Landslide and Barrier Schemes

The initial landslide configuration is meant to represent the shape of the flow at a certain time during propagation (Fig. 5), but it strongly depends on the site-specific flow–path topography and geomorphological conditions.

However, shear friction along the ground topography often results in a stronger, higher front, a weaker, lower body and a tail of the flow mixture (Iverson 1997; Pudasaini and Fischer 2020; Thouret et al. 2020).

Here, we consider a 45°–inclined front and a tail of length equal to three times the flow height. For varying the flow volumes, i number of squares are placed between the head and tail portions.

Given this shape, the landslide has the same volume of an equivalent paralepidid with the same height h , unitary width and a length $L_m = (2 + i) \cdot h$ (Fig. 2).

Fig. 5 Geometric schematization for the LSI numerical simulations with a rigid barrier

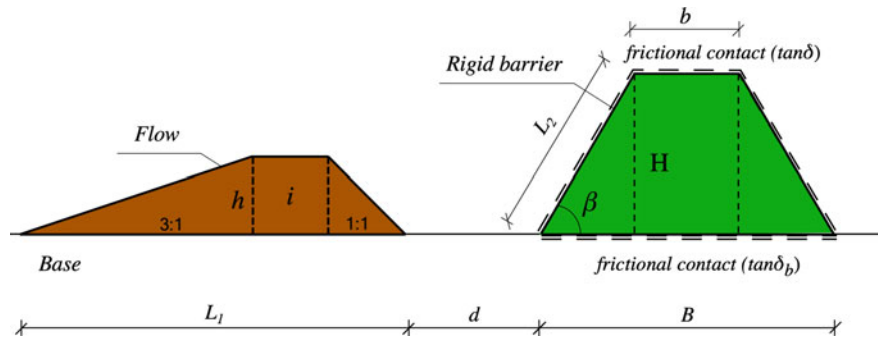


Table 1 Landslide cases

	L_1 (m)	(-)	h (m)	L_m (m)	V_1 (m ³ /m)	m_1 (kg)	$v_{0,1}$ (m/s)	$E_{k1,0}$ (kJ)
L1	21	3	3	15	45	81,000	10	4050
L2	21	3	3	15	45	81,000	5	1013
L3	20	1	4	12	48	86,400	10	4320
L4	15	1	3	9	27	48,600	10	2430
L5	27	5	3	21	63	113,400	10	5670
L6	47	43	1	45	45	81,000	19	4050
L7	21	3	3	15	45	95,400	10	4770

The landslide is assumed to approach the barrier with a fixed geometric configuration and constant velocity, until the LSI starts. For the sake of simplicity, the flow basal frictional force F_1 (Fig. 1) is assumed equal to zero in all the cases, by means of a smooth contact. Although simplified, the landslide scheme resembles its main characteristics such as velocity, impact height, non-zero interstitial pressures and elasto-plastic behavior. The distribution of pore water pressure is simplified as hydrostatic along the vertical at the beginning of LSI. Then, pore water pressures change because of LSI.

The mechanical parameters of the landslide material are: ρ_m (density of the mixture) = 1800 kg/m³; n (porosity) = 0.5; φ' (effective friction angle) = 20°; c' (effective cohesion) = 0; E' (Young modulus) = 2 MPa; ν (Poisson's ratio) = 0.25; k (hydraulic conductivity) = 10⁻⁴ m/s; μ_L (liquid viscosity) = 10⁻⁶ kPa s; and K_L (liquid bulk modulus) = 30 MPa. These properties are used as inputs in the MPM model, whereas for the analytical and empirical approaches only the density of the mixture is considered.

Some landslide typologies (impact scenarios) are chosen as examples for the design of the protection structure.

Table 1 reports the geometric features, the different values of $v_{1,0}$ and h , and even some of the related quantities V_1 , m_1 and $E_{k1,0}$. In the engineering practice, all these quantities are accurately estimated through specific analyses of landslide triggering and propagation (Cuomo et al. 2019, 2021b).

For the barrier it is assumed: non-porous material, base fixed to the ground (empirical approach) or free to sliding (analytical and numerical approaches) with rigid behaviour. This last hypothesis relates to the construction mode typically used for such barriers (Cuomo et al. 2020a, b).

Table 2 outlines the features of some barrier options considered in the following sections to apply the three methods for LSI analysis.

4.2 The (Empirical) Method No. 1: Results

The time trend of the impact force $F(t)$ is computed for the landslide cases L1, L2 and L3 reported in Table 1 and assuming a different steepness (β) of the impacted side of the barrier. In this novel, yet simplified method, (Di Perna et al. 2022), the impact action is mainly related to the landslide

Table 2 Examples of protection barriers

	H (m)	b (m)	B (m)	β (°)	m_2 (kg)
B1	6	4	11	57	90,000
B2	7.5	3.63	8.38	72	90,075
B3	6	6.5	8.50	80	90,000

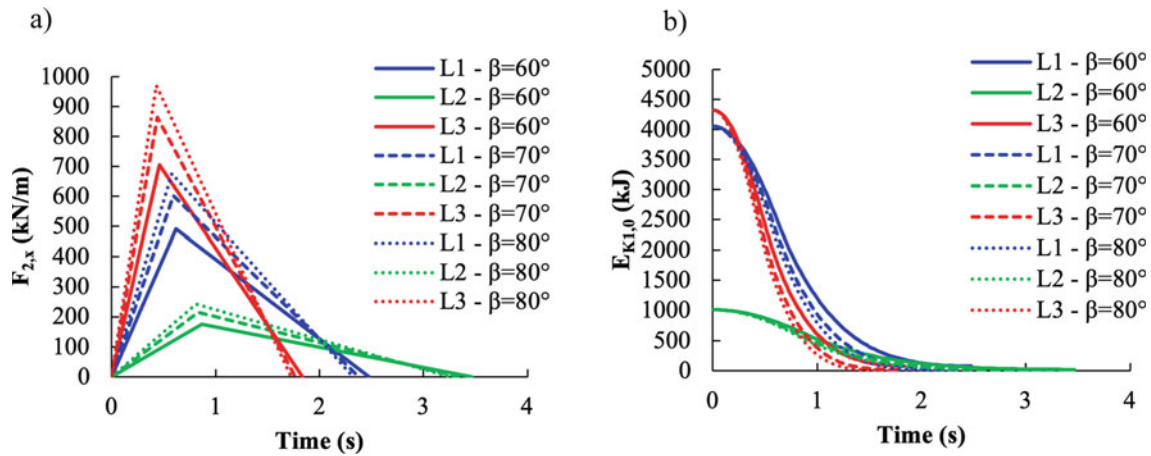


Fig. 6 Empirical model results: **a** time trend of the impact force; **b** kinetic energy of the landslide over the time

features. Indeed, the effect of the steepness (β) of the impacted side of the barrier is also considered, with the “reference velocity” for the impact computed as the component of landslide velocity orthogonal to the barrier facing.

It is evident that the landslide case L3 causes the highest peak impact force (Fig. 6a) due to the largest initial landslide kinetic energy (Fig. 6b). However, this is also the case with the shortest duration due to the most rapid release of kinetic energy $E_k(t)$. For L3, a differently steeped barrier facing also plays a role toward the impact force reducing from 1000 kN/m ($\beta = 80^\circ$) to 700 kN/m ($\beta = 60^\circ$).

Once the plot of Fig. 6a has been computed, then the design of the barrier can be pursued.

A first step is to preliminarily individuate the geometry features (Fig. 1) of the barrier, i.e., the top base (b), the bottom base (B) and the height (H).

Then, the barrier safety analyses for shifting and tilting can be performed based on a simple dynamic model of a rigid block with a base frictional contact (e.g., Newmark model). Alternatively, a complete stress–strain analysis can be performed via Finite Element Method (see for instance,

Cuomo et al. 2020a) or Finite Difference Method (refer to Cuomo et al. 2020b), thus individuating any Ultimate Limit State (ULS) of the barrier (i.e., shifting, global/local deformation, combination of the previous ULSs).

4.3 The (Analytical) Method No. 2: Results

The temporal evolution of the impact force (F) and landslide kinetic energy (E_k) are computed for landslide cases L1, L2 and L3 of Table 1 and for the three barriers of Table 2. Comparing the results of Fig. 7 (analytical) to those in Fig. 6 (empirical method) is useful.

The empirical method provides an overestimation of the impact forces obtained by the analytical method, especially for the landslides with large kinetic energy. The latter decays more rapidly according to the empirical method than for the analytical one. Hence, the analytical method provides similar or lower impact force with a similar or longer time for the landslide energy decay. These differences were expected because the effects of the landslide-structure interaction are

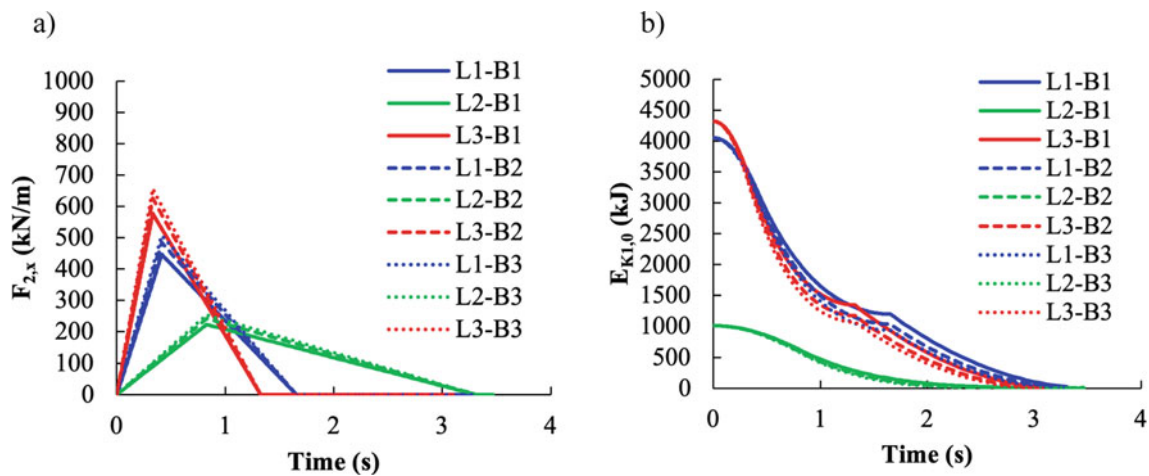


Fig. 7 Analytical model results: **a** time trend of the impact force; **b** kinetic energy of the flow over time

Table 3 Analytical results: final displacement of the barrier

ID	Landslide	Barrier	m_1 (kg)	m_2 (kg)	β (°)	Δx_f (m)
1	L1	B1	81,000	90,000	60	0.64
8	L2	B1	81,000	90,000	60	0
7	L3	B1	86,400	90,000	60	1.17
5	L1	B2	81,000	90,075	70	1.10
4	L1	B3	81,000	90,000	80	1.24

Table 4 Mass (m_2) to limit the final displacement to 0.5 m

Landslide	m_1 (kg)	β (°)	Δx_f	m_2 (kg)
L1	81,000	70	0.5	135,363
L2	81,000	70	0.5	39,015
L3	86,400	70	0.5	190,752

included in the analytical method, but not in the empirical method.

In addition to this assessment, the displacement (Δx_f) of the barrier is computed over time during the LSI. The final displacements of the selected cases are reported in Table 3. It is worth noting that in the scenario no. 8, the displacement is about nil, while in the other cases, the barrier is displaced of few meters during the landslide impact. However, such performance is insufficient in some circumstances.

In fact, if the site-specific field conditions ensure limited space for the barrier or in presence of buildings just behind the barrier, then a requirement for the barrier is to allow low/moderate displacement during the LSI.

In those cases, an inverse use of the analytical method is suggested. Hence, given the landslide features (e.g., Table 4), once the steepness of the impacted side (depending on the construction mode and materials used), and the maximum tolerable barrier displacement (e.g., 0.5 m in Table 4) is established, then the minimum required mass (m_2) for the barrier can be computed. From that value, different design options correspond to different sets of H , B and

b . In this design procedure, the barrier is assumed to be rigid, which is generally a safe assumption. Once the impact action and geometry of the barrier is known, then barrier safety analyses can be done as for method no. 2.

4.4 The (Numerical) Method No. 3: Results

What is the main limitation of the previous approaches? It is that any possible landslide overtopping cannot be assessed. The latter is not a secondary LSI mechanism in the case of flow-like landslides. Moreover, the barrier was not considered as deformable. Both these limitations are overcome by the MPM numerical method. Here, the barrier is still considered as rigid to better compare the results of the three approaches.

Some landslide and barrier cases are considered in Fig. 8, which shows the peak forces are similar (Fig. 8a) to those achieved by the analytical method. Such general agreement among those results is encouraging. This is also reflected by the similar barrier displacements computed analytically

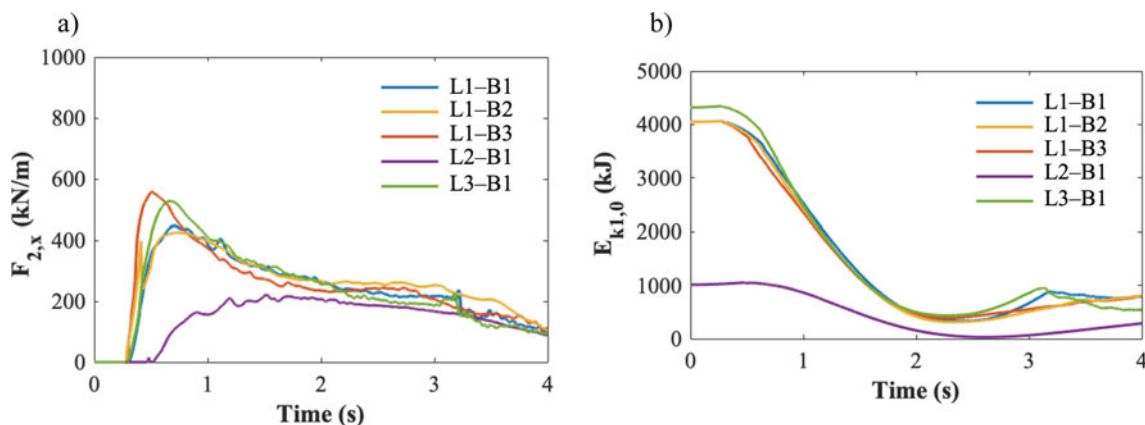
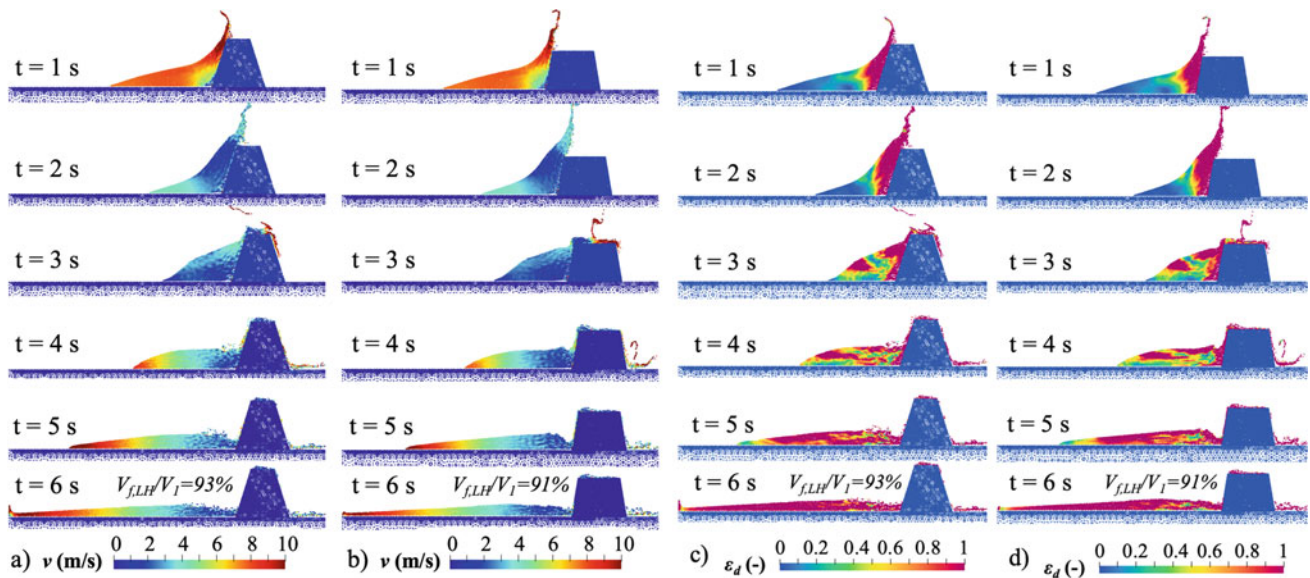


Fig. 8 MPM numerical results: **a** time trend of the impact force; **b** kinetic energy of the flow over time

Table 5 MPM numerical results: barrier final displacement

ID	Landslide	Barrier	m_1 (kg)	m_2 (kg)	β ($^\circ$)	H (m)	B (m)	Δx_f (m)
1	L1	B1	81000	90000	60	6	11	2.06
8	L2	B1	81000	90000	60	6	11	0
7	L3	B1	86400	90000	60	6	11	3.15
5	L1	B2	81000	90075	72	7.5	8.38	4.28
4	L1	B3	81000	90000	80	6	8.50	4.74

**Fig. 9** Velocity during the impact for L1-B2 (a) and L1-B3 (b), Deviatoric strain for L1-B2 (c) and L1-B3 (d)

(Table 3) or numerically (Table 5). However, a slightly slower decay of $F(t)$ and a slower energy release (Fig. 8b) are simulated with respect to the analytical trends. In addition, in the cases no. 5 (L1-B2) and 4 (L1-B3) the analytical and numerical results differ much more. This means that a combined use of multiple methods is always recommended.

The spatio-temporal distribution of the soil velocity and deviatoric (shear) deformation inside the landslide body is plotted in Fig. 9. The above-mentioned complexity of the LSI is outlined and it is clearly shown that velocity and deformation are not uniform in the landslide body during the LSI, because the barrier is displaced away.

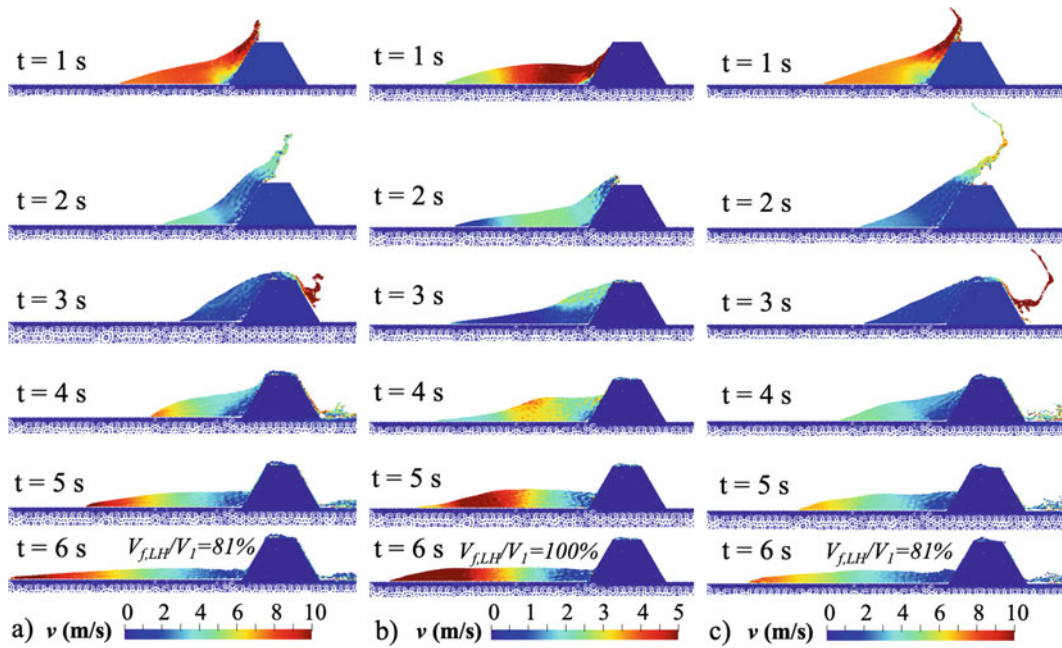


Fig. 10 Velocity distribution during the impact for L1-B1 (a), L2-B1 (b), L3-B1 (c)

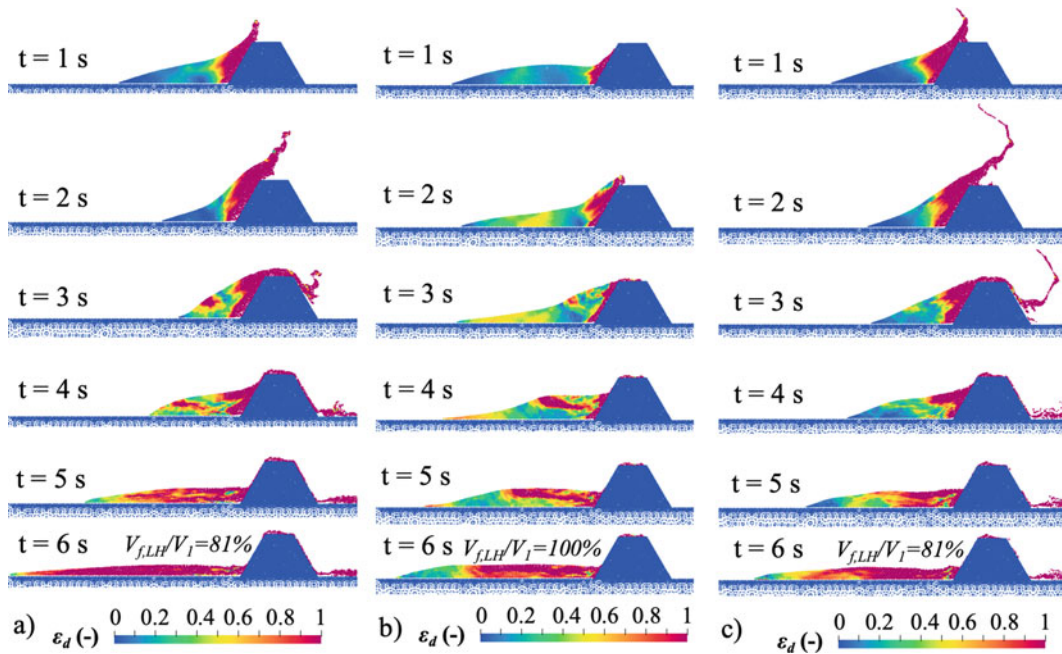


Fig. 11 Deviatoric strain distribution during the impact for L1-B1 (a), L2-B1 (b), L3-B1 (c)

Table 6 LSI examples analysed through different methods

ID	1	2	3	4	5	6	7	8	9
<i>Landslide</i>	<i>L1</i>	<i>L4</i>	<i>L5</i>	<i>L1</i>	<i>L1</i>	<i>L6</i>	<i>L3</i>	<i>L2</i>	<i>L7</i>
L_1 (m)	21	15	27	21	21	47	20	21	21
i (–)	3	1	5	3	3	43	1	3	3
h (m)	3	3	3	3	3	1	4	3	3
Lm (m)	15	9	21	15	15	45	12	15	15
V_1 (m ³ /m)	45	27	63	45	45	45	48	45	45
ρ (kg/m ³)	1800	1800	1800	1800	1800	1800	1800	1800	2120
m_1 (kg)	81000	48600	113400	81000	81000	81000	86400	81000	95400
$v_{0,1}$ (m/s)	10	10	10	10	10	10	10	5	10
$E_{k1,0}$ (kJ)	4050	2430	5670	4050	4050	4050	4320	1012.5	4770
<i>Barrier</i>	<i>B1</i>	<i>B1</i>	<i>B1</i>	<i>B3</i>	<i>B2</i>	<i>B1</i>	<i>B1</i>	<i>B1</i>	<i>B1</i>
B (m)	11	11	11	8.5	8.38	11	11	11	11
b (m)	4	4	4	6.5	3.63	4	4	4	4
H (m)	6	6	6	6	7.5	6	6	6	6
β (°)	60	60	60	80	72	60	60	60	60
L_2 (m)	6.95	6.95	6.95	6.08	7.87	6.95	6.95	6.95	6.95
m_2 (kg)	90000	90000	90000	90000	90075	90000	90000	90000	90000
<i>Results</i>									
$F_{2x,emp}$ (kN/m)	491	491	491	676	620	123	705	175	578
$F_{2x,analyt}$ (kN/m)	387	477	325	500	467	129	500	193	420
$F_{2x,MPM}$ (kN/m)	444	402	444	526	425	333	528	221	513
$T_{2,emp}$ (s)	2.47	1.48	3.46	2.04	2.15	9.85	1.84	3.46	2.47
$T_{2,analyt}$ (s)	1.65	0.99	2.31	1.65	1.65	4.96	1.32	1.64	1.65
$T_{2,MPM}$ (s)	2.59	2.1	3.00	2.19	2.59	4.50	2.643	4.00	3.00

Further insights come from the results shown in Figs. 10 and 11. Soil deformations are relevant in the proximity of the impacted barrier side, pointing out the marginal role of the tail during the impact.

5 Comparison and Discussion

For the nine examples proposed in Table 6, a substantial agreement of at least two out of the three methods is shown for the peak impact force and for the impact duration (Table 6 and Fig. 12). This is important for design purposes.

For the final displacement of the barrier, the empirical method alone does not give information, while the other two methods are in many cases in very good agreement. However, some discrepancies are also possible (e.g., cases 3, 4 and 5) when LSI is very complex.

The numerical method considers the elasto-plastic soil behavior and the hydro-mechanical coupling between the solid skeleton and soil porosity water. These features are not present in the two other methods. It is worth noting that the increment of pore water pressure at the impact is recognized as an important factor of LSI (Cuomo et al. 2021a). That increment in pore water pressure is also the possible overtopping mechanism and the final amount of landslide retained behind the barrier.

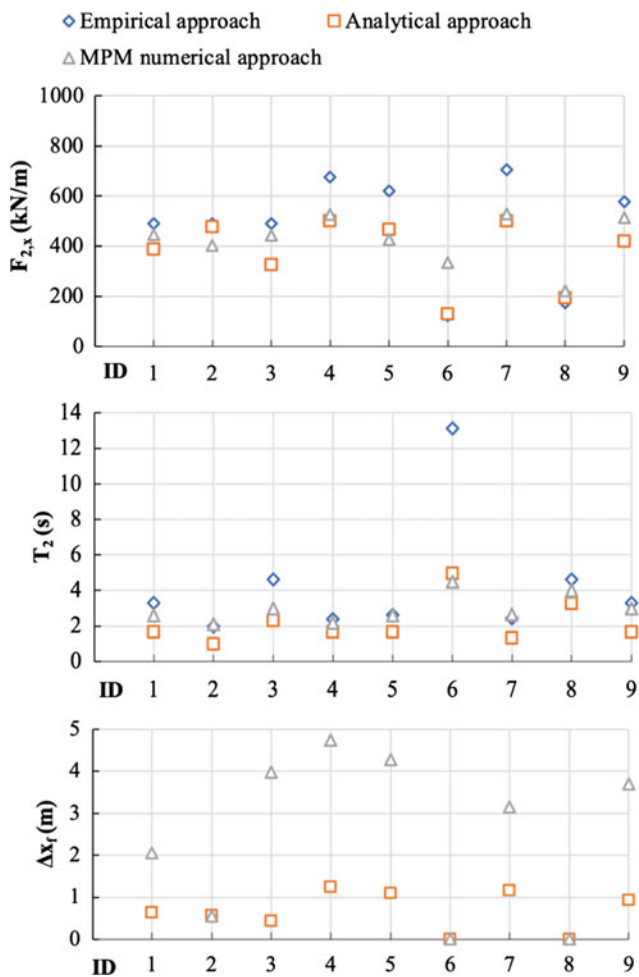


Fig. 12 Comparing the proposed approaches for peak impact force, impact period and barrier final displacement

6 Conclusions

A general conceptual scheme and three different methods have been presented in this paper for the analysis of LSI (Landslide-Structure Interaction).

The results of the distinct methods are generally in good agreement, because they are all adequate to reproduce the physical processes of the LSI. Hence, different tools and options to design a protection barrier have been provided. The combined use of multiple methods is fully encouraged.

Acknowledgements The research was developed within the framework of Industrial Partnership PhD Course (POR Campania FSE 2014/2020). All the MPM simulations were performed using a version of the Anura3D code developed by Deltares.

References

- Arattano M, Franzi L, JNH (2003) On the evaluation of debris flows dynamics by means of mathematical models. *Nat Hazard* 3(6):539–544
- Bugnion L, McArdeell BW, Bartelt P, Wendeler C (2012) Measurements of hillslope debris flow impact pressure on obstacles. *Landslides* 9(2):179–187
- Canelli L, Ferrero AM, Migliazza M, Segalini A (2012) Debris flow risk mitigation by the means of rigid and flexible barriers—experimental tests and impact analysis. *Nat Hazard* 12(5):1693–1699
- Ceccato F, Yerro A, Martinelli M (2018) Modelling soil-water interaction with the material point method. Evaluation of single-point and double-point formulation. *Numer Methods Geotech Eng IX*, pp.351–357.
- Cui P, Zeng C, Lei Y (2015) Experimental analysis on the impact force of viscous debris flow. *Earth Surf Process Land* 40(12):1644–1655
- Cuomo S, Moretti S, Aversa S (2019) Effects of artificial barriers on the propagation of debris avalanches. *Landslides*, 16(6):1077–1087
- Cuomo S (2020) Modelling of flowslides and debris avalanches in natural and engineered slopes: a review. *Geoenviron Disasters* 7 (1):1–25
- Cuomo S, Moretti S, D’Amico A, Frigo L, Aversa S (2020a) Modelling of geosynthetic-reinforced barriers under dynamic impact of debris avalanche. *Geosynth Int* 27(1):65–78
- Cuomo S, Moretti S, Frigo L, Aversa S (2020b) Deformation mechanisms of deformable geosynthetics-reinforced barriers (DGRB) impacted by debris avalanches. *Bull Eng Geol Env* 79 (2):659–672
- Cuomo S, Di Perna A, Martinelli M (2021a) MPM hydro-mechanical modelling of flows impacting rigid walls. *Can Geotech J* 58 (11):1730–1743
- Cuomo S, Masi EB, Tofani V, Moscariello M, Rossi G, Matano F (2021b) Multiseasonal probabilistic slope stability analysis of a large area of unsaturated pyroclastic soils. *Landslides* 18(4):1259–1274
- Cuomo S, Di Perna A, Martinelli M (2022) Analytical and numerical models of debris flow impact. *Eng Geol* (under review)
- Di Perna A, Cuomo S, Martinelli M (2022) Empirical formulation for debris flow impact and energy release. *Geoenviron Disaster* (under review)
- Fern E, Rohe A, Soga K, Alonso E (2019) The material point method for geotechnical engineering: a practical guide. CRC Press
- Hungr O, Morgan GC, Kellershals R (1984) Quantitative analysis of debris torrent hazards for design of remedial measures. *Can Geotech J* 21(4):663–677
- Iverson RM (1997) The physics of debris flows. *Rev Geophys* 35 (3):245–296
- Jassim I, Stolle D, Vermeer P (2013) Two-phase dynamic analysis by material point method. *Int J Numer Anal Meth Geomech* 37 (15):2502–2522
- Kwan JSH (2012) Supplementary technical guidance on design of rigid debris-resisting barriers. GEO report no. 270, Geotechnical Engineering Office, Civil Engineering and Development Department, Hong Kong SAR Government
- Luo H, Baum JD, Löhner R (2008) A discontinuous Galerkin method based on a Taylor basis for the compressible flows on arbitrary grids. *J Comput Phys* 227(20):8875–8893
- Martinelli M, Galavi V (2022) An explicit coupled MPM formulation to simulate penetration problems in soils using quadrilateral elements. *Comput Geotech*. <https://doi.org/10.1016/j.compgeo.2022.104697>

- Mieremet MMJ, Stolle DF, Ceccato F, Vuik C (2016) Numerical stability for modelling of dynamic two-phase interaction. *Int J Numer Anal Meth Geomech* 40(9):1284–1294
- Ng CWW, Choi CE, Koo R, Goodwin GR, Song D, Kwan JS (2018) Dry granular flow interaction with dual-barrier systems. *Géotech* 68(5):386–399
- Pudasaini SP, Fischer JT (2020) A mechanical model for phase separation in debris flow. *Int J Multiph Flow* 129:103292
- Sassa K (2021) The Kyoto landslide commitment 2020: launched. *Landslides* 18(1):5–20
- Scheidl C, Chiari M, Kaitna R, Müllegger M, Krawtschuk A, Zimmermann T, Proske D (2013) Analysing debris-flow impact models, based on a small scale modelling approach. *Surv Geophys* 34(1):121–140
- Scotton P, Deganutti AM (1997) Phreatic line and dynamic impact in laboratory debris flow experiments. In: *Debris-flow hazards mitigation: mechanics, prediction, and assessment*. ASCE, pp 777–786
- Song D, Ng CWW, Choi CE, Zhou GG, Kwan JS, Koo RCH (2017) Influence of debris flow solid fraction on rigid barrier impact. *Can Geotech J* 54(10):1421–1434
- Thouret JC, Antoine S, Magill C, Ollier C (2020) Lahars and debris flows: characteristics and impacts. *Earth Sci Rev* 201:103003

Open Access This chapter is licensed under the terms of the Creative Commons Attribution 4.0 International License (<http://creativecommons.org/licenses/by/4.0/>), which permits use, sharing, adaptation, distribution and reproduction in any medium or format, as long as you give appropriate credit to the original author(s) and the source, provide a link to the Creative Commons license and indicate if changes were made.

The images or other third party material in this chapter are included in the chapter's Creative Commons license, unless indicated otherwise in a credit line to the material. If material is not included in the chapter's Creative Commons license and your intended use is not permitted by statutory regulation or exceeds the permitted use, you will need to obtain permission directly from the copyright holder.





Landslide Warning Systems in Low-And Lower-Middle-Income Countries: Future Challenges and Societal Impact

Irasema Alcántara-Ayala and Ricardo J. Garnica-Peña

Abstract

There is a growing body of literature that recognises the importance of warning systems to reduce landslide disaster risk and avoid the occurrence of disasters. Recent developments in landslide disasters around the world have heightened the need for the implementation of Landslide Early Warning Systems (LEWSs) particularly in low-and lower-middle-income countries (LICs and MICs), where levels of vulnerability and exposure are very high. However, no previous study has systematically evaluated the use of LEWSs in LICs and MICs. By means of a systematic review on the scientific literature this chapter explores the ways in which LEWSs have been implemented in LICs and MICs. This research seeks to address the spatial distribution of LEWSs in the world, specifically in LICs and MICs. Special attention is given to reviewing the development of LEWSs in terms of their inclusion in integrated disaster risk reduction (DRR) strategies or as standalone initiatives, and the type of approaches followed, either as top-down or bottom-up. The chapter has three key components: (1) to prepare a search and inclusion criteria strategy for systematic literature review to collect a set of articles on LEWSs using the ISI Web of Science database; (2) to organize the literature review set to extract and analyse quantitative and qualitative data and information on LEWSs in LICs and MICs; and (3) to provide insights on a future LEWSs research agenda concerning critical issues and gaps in the literature and identifying main challenges with high societal impact. A noteworthy remark about this review is that only 12.4% of the total publications that met the specified criteria are from LICs and MICs. These papers

address diverse dimensions of LEWSs in different degrees, but despite that, the actual use or implementation of LEWSs was addressed only by five papers. This suggests a potential disadvantage in the development and successful systematic implementation of LEWSs in these countries.

Keywords

Landslide early warning systems • Low-and lower-middle-income countries • Implementation • Community-based approaches • Challenges • Societal impact

1 Introduction

In the international sphere, the establishment of the Sendai Framework for Disaster Risk Reduction 2015–2025 (UNISDR 2015) and the call for science and technology to support its implementation (UNISDR 2019) have helped science-evidence policy making and practice to be visualised as a high priority, but also, have opened up opportunities to improve science and to promote wider interaction among all disaster risk relevant stakeholders. Particularly, in the field of landslide research, initiatives such as the Sendai Landslide Partnerships 2015–2025 (Sassa 2015, 2016) and the Kyoto Landslide Commitment 2020 (KLC 2020) (Alcántara-Ayala and Sassa 2021) have created and set in motion solid and effective projects to promote landslide research in benefit of society, and foster relations between institutions and landslide research networks from different regions of the world. These developments have helped some countries make progress towards informed decision making and practice.

Among other significant actions, the KCL (2020) promotes greater awareness of the importance of people-centred early warning. Therefore, and in order to secure some positive progress in aspects relating to the development of

I. Alcántara-Ayala (✉) · R. J. Garnica-Peña
Institute of Geography, National Autonomous University of Mexico (UNAM), 04510 Mexico City, Mexico
e-mail: ialcantara@geografia.unam.mx

R. J. Garnica-Peña
e-mail: garnica@geografia.unam.mx

people-centred early warning systems, this new initiative calls for an increased precision and reliable prediction technology for landslides in both time and space, especially in a changing climate context (Sassa 2019, 2020).

Landslide early warning systems (LEWSs) is a major area of interest within the field of landslide research and one of the most critical key elements for disaster risk reduction (DRR). In the light of such circumstances, there is increasing concern that some low-and lower-middle-income countries (LICs and MICs), are being disadvantaged in the development and successful systematic implementation of LEWSs. Accounting specifically for the varying experiences these countries have at different scales is unknown.

Recent evidence suggests that owing to their complex and operational landslide forecasting character, LEWSs remain a difficult and uncertain task, which require conceptual developments and technological improvements along with open standards for the design, implementation, management, and verification (Guzzetti et al. 2020). This is of uttermost relevance in LICs and MICs where obstacles for science for action should not be underestimated.

Drawing upon a systematic literature review, this study attempts to provide insights on the development and implementation of LEWSs in LICs and MICs from 2000 to 2021. Especially important is to identify whether those reported cases are included into a comprehensive disaster risk reduction strategy, or they are standalone initiatives. Furthermore, finding out if they follow a top-down or a bottom-up approach will be particularly valuable.

The remaining part of the chapter includes a brief section on Early Warning Systems (EWSs), the methodology, and results. Finally, recommendations derived from this systematic literature review are presented.

2 Early Warning Systems (EWSs)

Building on the work of Smith (1996), Twigg (2002) argued that in addition to the three known inter-related stages of EWSs, which comprised evaluation and forecasting; warning and dissemination; and response, the significance of appropriate communication of timely and accurate hazard warnings, based on the comprehensive understanding of perceptions and needs of communities at risk, is key for the success of an EW system.

Accordingly, in an effort to implement people-centred early warning systems, four elements of effective EWSs were established (Fig. 1), and EWSs defined as “the provision of timely and effective information, through identified institutions, that allow individuals exposed to hazards take action to avoid or reduce their risk and prepare for effective response” (UNISDR 2006). After a decade, its meaning was

redefined, but hardly changed in practice, in terms of “an integrated system of hazard monitoring, forecasting and prediction, disaster risk assessment, communication and preparedness activities systems and processes that enables individuals, communities, governments, businesses and others to take timely action to reduce disaster risks in advance of hazardous events” (UNISDR 2016).

Alcántara-Ayala and Oliver-Smith (2017) claimed that despite the evolution of definitions through time, EWSs are not yet articulated or integrated systems, but segments of the capacity-building process required to achieve DRR through DRM. One of the main reasons for this is a lack of disaster risk understanding as a social construct, which implies that not only hazard occurrence, but the spatial and temporal scales of the dimensions of vulnerability and exposure must be considered.

It is beyond the scope of this study to identify and analyse the strengths and serious weaknesses of both EWSs and LEWSs. However, it is important not to forget that despite the fact that, due to uncertainty, determining the occurrence of hazards in space and time is technically challenging, the performance of EWSs is often constrained by a lack of integrated transdisciplinary approaches, sustainability of financial and human resources, sound strategies of risk communication and most importantly, due to disarticulated institutional arrangements and weak disaster risk governance (Alcántara-Ayala 2021). These issues are of great concern to the international community and have important implications for LICs and MICs.



Fig. 1 Four elements of people-centred Early Warning Systems (Source adapted from ISDR-PPEW 2005)

3 Methodology

This study employed a systematic review methodology, which involved definition of the review scope, literature search, literature analysis and synthesis, and perspectives on challenges and societal impact of LEWSs. The central area of interest of the review scope was focused in categorising the spatial extent of the research institutions that have been involved in the development of LEWSs and to identify, when possible, whether these have been included into a comprehensive disaster risk reduction strategy, or they were built as standalone initiatives, following either top-down or a bottom-up approaches.

With respect to the literature search, most suitable keywords and search criteria were chosen in order to extract the required set to be analysed from the ISI Web of Science database. The search was conducted between January and February 2022. The system was requested to search the words “landslide”, “warning system”, and “early warning” in the title and abstract of the articles. In this way, the search results included a total of 1709 papers. Results were sorted by year of publication within 1990–2021 range, to avoid the inclusion of the work in progress in 2022. During the evaluation phase, following filtering to include papers which did not have the full abstract available, search results were reduced to 1691 papers. Additional filtering excluded all works which were not published in English language, and number of papers was reduced to 1669. Additional filtering aimed at eliminating papers which were not suitable for the review scope as well as data papers, retracted publications, editorial material, and letters. The use of these criteria involved the exclusion of 540 papers. Number of papers was cut to 1129. Final filtering involved the classification of papers based on countries of publication. Categories of Low, Lower middle, Upper middle and High income were considered. Final selection was concentrated on Low and Lower middle-income countries. Therefore, number of papers examined for this study was 141 (Fig. 2).

Literature analysis and synthesis involved geographic analysis, time, institutions, areas of research, methodological typology, and approaches. After articles were selected, two researchers review them and further discussed differences to ensure relevance. Data management and analysis were performed using Excel and HistCite. Perspectives on challenges and societal impact of LEWSs in LICs and MICs were building on the relevant experiences included in the analysed set of papers and based on the practical knowledge of the authors.

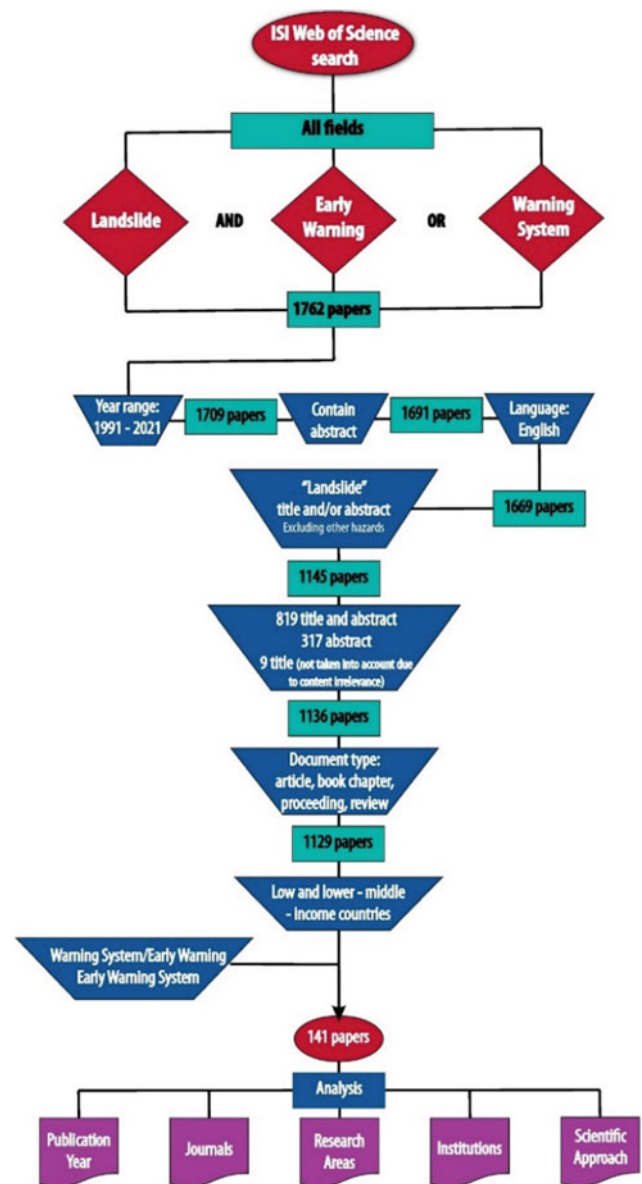


Fig. 2 Search strategy for systematic review

4 Results

A noteworthy remark about this study is that 141 articles, the equivalent of only 12.4% of the total publications that met the specified criteria, were published by researchers working in institutions situated in LICs ($N = 3$) and MICs ($N = 20$). LICs included Malawi, Uganda and Rwanda, whereas MICs involved Bangladesh, Bhutan, Egypt, El Salvador, Ghana, India, Indonesia, Iran, Kenya, Nepal, Nicaragua, Nigeria,

Pakistan, Philippines, Sri Lanka, Tanzania, Ukraine, Uzbekistan, Vietnam and Zambia.

Although the first publication addressing LEWSs worldwide was issued in 1991, only from 2000 LICs and MICs countries researchers started publishing their work on this topic. Therefore, the range of years analysed was established as 2000–2021 (Fig. 3).

During the first seven years, only one publication was produced annually. The largest percentage of publications (52.4%) was concentrated in 2019, 2017 and 2020, with 29, 25 and 20 publications, respectively. During the last two years of the analysis, a clear decrease in number of publications was identified.

Types of documents in which research on LEWSs was published comprised articles ($N = 81$), conference proceedings ($N = 56$), book chapters ($N = 2$) and reviews ($N = 2$). These were included in publications from a wide and diverse range of research fields in the many subject areas relevant to landslides. However, a major concentration of publications, equivalent to 43% of the total, was identified in the fields of engineering, engineering geology and geology (Fig. 4). Only one publication was issued in a social science journal. This indeed mirrors the predominance of technical approaches.

Articles on these themes were published, to a major extent, in the *Landslides Journal* ($N = 14$), followed by *Natural Hazards* ($N = 6$) and *Water* ($N = 6$) journals. Additional publications were included in *Advancing Culture of Living with Landslides, Vol 3* ($N = 4$), *Geomatics, Natural Hazards & Risk* ($N = 4$), *Journal of Mountain Science* ($N = 3$), *International Journal of Disaster Risk Reduction* ($N = 3$) and the *International Journal of Geomate* ($N = 3$) (Fig. 5).

Researchers from 179 institutions, from LICs, MICs and other income countries participated as contributors in the

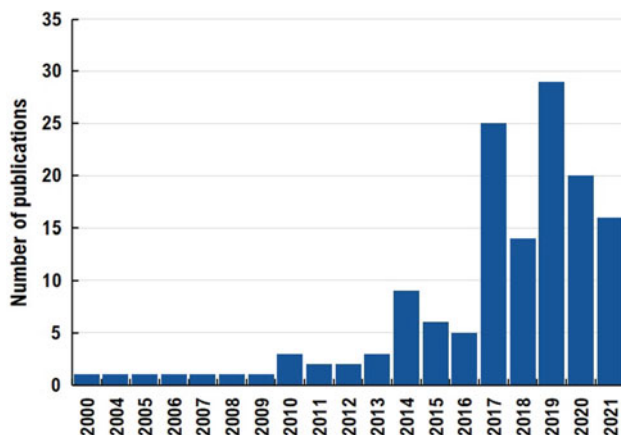


Fig. 3 Time analysis: number of publications analysed concerning LEWSs in LICs and MICs

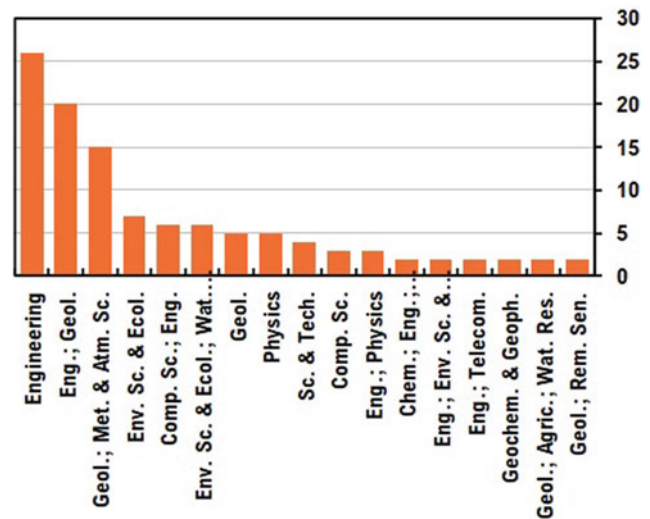


Fig. 4 Research areas concerning the publications analysed on LEWSs in LICs and MICs

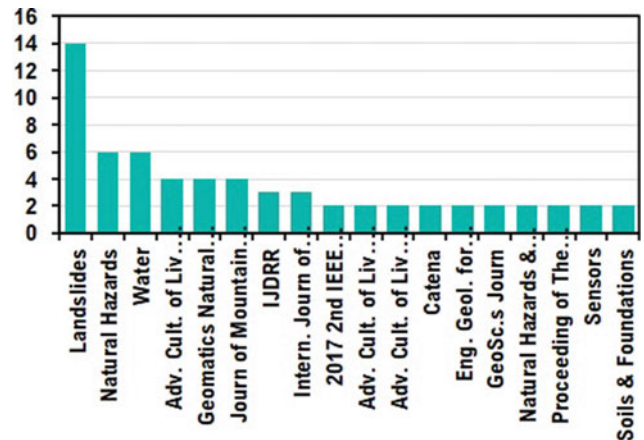


Fig. 5 Journals of publications regarding LEWSs in LICs and MICs

analysed publications. Top institutions in terms of participation in highest number of publications included Amrita Vishwa Vidyapeetham University ($N = 15$), the Indian Institute of Technology Indore ($N = 14$), the Indian Institute of Technology Roorkee ($N = 12$), and the University of Technology Sydney ($N = 11$). They were followed by Sejong University ($N = 7$), the University of Tokyo ($N = 7$) and the Chinese Academy of Sciences ($N = 6$) (Fig. 6).

The review suggested that research associated with LEWSs in LICs, and MICs is built around three main lines of work, the first focused on studies of hazard analysis for LEWSs ($N = 53$, 37.5%), the second, on technological developments for potential LEWSs ($N = 49$, 34.7%), and the third, concerning the design, development, calibration and validation of models and prototypes for LEWSs ($N = 21$, 14.8%) (Fig. 7).

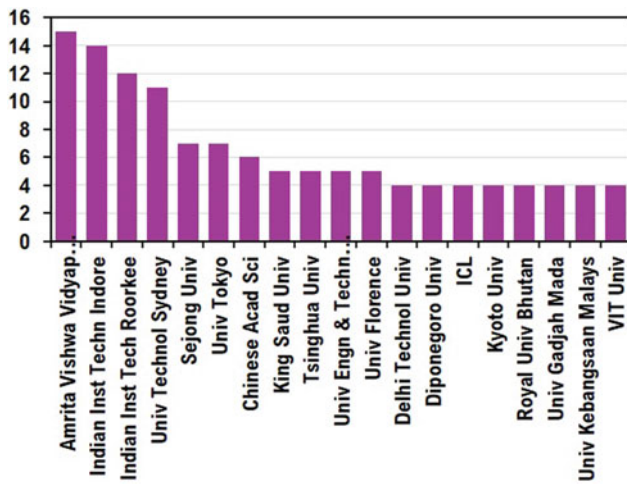


Fig. 6 Research and academic institutions to which the authors of the analysed publications are affiliated

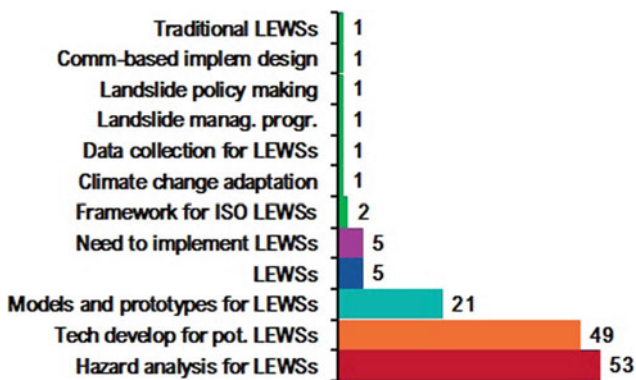


Fig. 7 Thematic lines of research associated with LEWSs in LICs and MICs, based on the systematic literature review

Regardless of the information provided in the title and abstract, out of the total number of papers analysed produced in LICs and MICs (Fig. 8) and represented through a series of study cases (Fig. 9), only five publications included the implementation of an actual LEWS (5, 3.5%) as a main development in the text. Other publications were focused on different aspects to stress the need of implementing LEWSs in different countries (5, 3.5%) (see Fig. 7).

In a lower proportion, other articles focused on various areas, from the proposal of a standard for community-based landslide early warning systems (Fathani et al. 2016, 2017) (2, 1.4%), to addressing the significance of indigenous knowledge for climate change adaptation and warning systems as communities are experiencing the consequences of climate change through the occurrence of landslides and other hazards (Nelson et al. 2019) (1, 0.7%) (see Fig. 7).

In the reviewed publications, other topics of interest from a technical approach, included the establishment of a national system for data collection (1, 0.7%) (Devoli et al. 2007) (see Fig. 7).

From a social science perspective, a publication emphasised and exemplified the architecture of landslide management programmes, which should include social vulnerability ($N = 1$, 0.7%) (Karnawati et al. 2009). Likewise, based on a survey, an assessment on the extent to which landslide disaster risk reduction policy measures have been implemented in Uganda was carried out (1, 0.7%) (Masaba et al. 2017). By means of stakeholder mapping, focus group discussions and key informant interviews, insights derived from the assessment of capacities and vulnerabilities of communities were provided for the design of community-based early warning system for deep-seated landslides ($N = 1$, 0.7%) (Gumiran et al. 2019). Furthermore, a traditional notion of LEWSs was developed by introducing the concept of non-structural mitigation measures through mitigation mapping; this described in terms of the definition of the landslide high-risk area and community evacuation plan based on place-centered mapping in order to promote community participation ($N = 1$, 0.7%) (Hidayati and Noviana 2018) (see Fig. 7).

4.1 Description of Operational LEWSs from Publications

Colleagues from Amrita Vishwa Vidyapeetham University designed and developed an integrated wireless sensor network system for real-time monitoring and early warning of landslides, which includes three levels of warning. Results obtained from the deployment of the LEWS in Western Ghats and North-Eastern Himalayas in India were satisfactory. This beneficial contribution increased the emphasis on the necessity of implementing LEWSs nationwide. Therefore, the Government of India considered its adoption, and a starting step of the strategy was a second LEWS deployment to the North-eastern Himalayas (Ramesh et al. 2017).

Along the side of the installation of a LEWS in Ledoksari Village in Indonesia, Karnawati et al. (2011) reinforced the preparedness of the communities at risk. A partnership between the University and the key person from the Village, under the coordination of the local reGENCY authority was sought as a main mechanism of interaction for the effective implementation of the developed LEWS. Inputs for hazard mapping included landslide susceptibility derived from the assessment of conditions of slope inclination, types and engineering properties of existing lithologies and soil, along with the incorporation of land-use types.

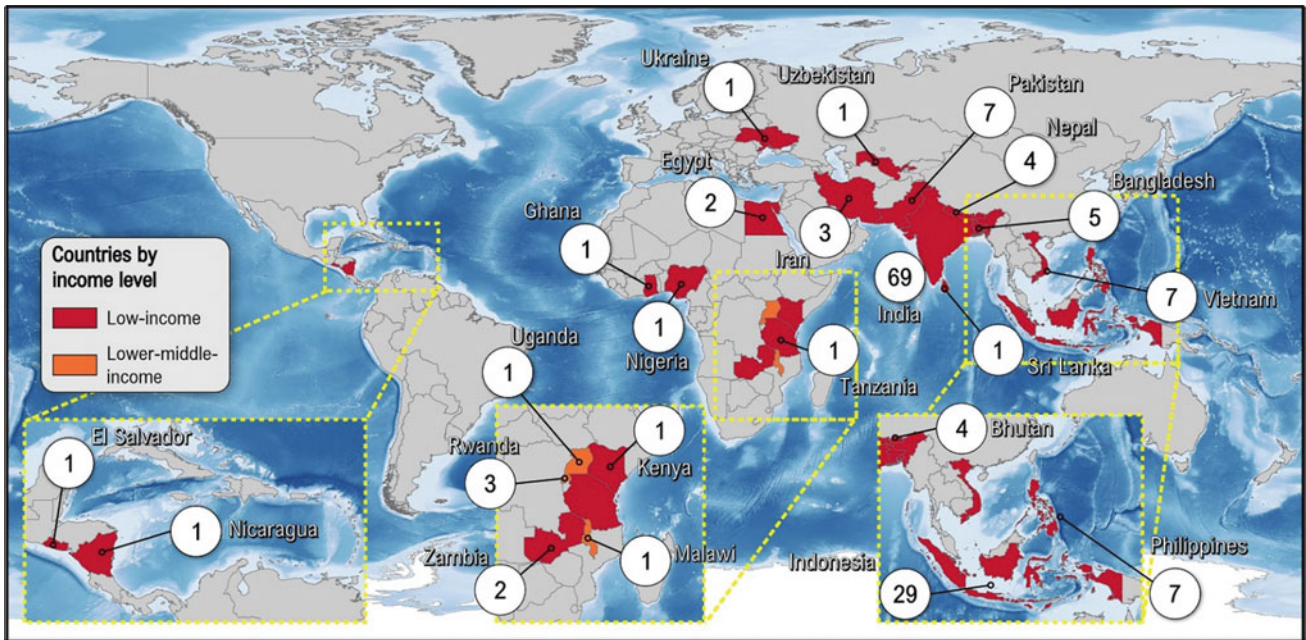


Fig. 8 Countries of the research and academic institutions to which the authors of the analysed publications are affiliated. The number inside the circle represents the number of publications per country

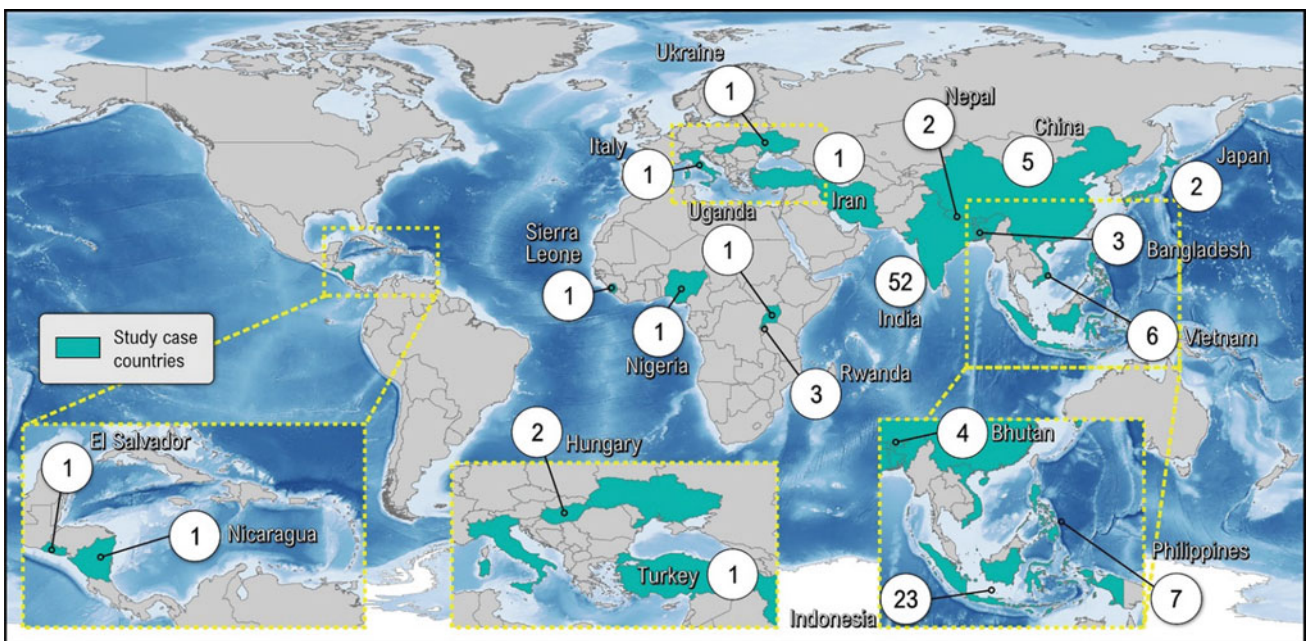


Fig. 9 Study case countries reported in the analysed publications. The number inside the circle represents the number of study cases per country, including those which are not categorised as LICs and MICs

In a comprehensive study, Thapa and Adhikari (2019) led to the development of a LEWS in the central Nepal Himalaya region. This comprised extensometers, soil moisture sensors, rain gauge stations, and solar panels. The protocol involves transmission of data generated through a Global System for Mobile Communications (GSM) network to

responsible organizations in real-time to issue the warning to local residents. Successful experiences with the implementation of the LEWS included saving 495 people from 117 households in August 2018. However, they also found out that landslide monitoring, and dissemination of warnings remains a complex process where a convergence of technical

and communications skills is required to guarantee successful practise.

In the context of the Development and Deployment of Early Warning System for deployment of the monitoring system in ten different sites across the Philippine Deep-Seated Catastrophic Landslides and Slope Failures (DEWS-L) program of the University of the Philippines and the Philippines Institute of Volcanology and Seismology (PHIVOLCS), Marciano and colleagues (2014) set up a series of enhancements in the design of an alternative instrumentation for monitoring deep-seated landslides using tilt and soil moisture sensors.

Experiences derived from the deployment of the LEWS in ten different sites across the Philippines highlighted the need to creating awareness in the community and fostering active community involvement in understanding the risks of landslides. For this reason, engaging the community and other stakeholders was identified as one of the main challenges of effective community and technology based LEWSs. Training members of communities at risk was conducted to establish a Local Landslide Monitoring Committee (LLMC). Integrated by volunteers, the LLMC acquired basic knowledge and skills to accurately monitor, map and survey the visual indicators of ground movement, and to maintain the continuous operation of the sensor columns (Marciano et al. 2014).

The SATREPS project is an example of a regional cooperation project between Japanese and Vietnamese researchers which was developed in a way that can be considered as key stepping stone towards disaster prevention and reduction in Vietnam in the future. Major contributions included development of human resources, research equipment and development of a standard system of landslide investigation, monitoring, forecast and LEWS, which was implemented based on real-time landslide monitoring in the Hai Van Station landslide (Tien et al. 2017).

4.2 Hazard Analysis for LEWSs

Examining the content of the analysed publications, it emerged that although the title and abstract reference LEWSs, 53% of the publications focused on diverse perspectives of hazard analysis that were considered significant for posterior development of warning systems. This category included papers regarding the following topics: landslide field monitoring, laboratory strength tests and experiments, determination of landslide rainfall thresholds, development of landslide susceptibility maps, numerical simulations, modelling, geological and geomorphological approaches, characterization of exposed buildings, artificial neural networks, and neuro-fuzzy approaches for prediction of

landslides. Additional strategies involved the use of slope mass rating, hydrological-geotechnical and factor of safety modelling, satellite-based rainfall estimation, soil moisture changes and deformations in slope surface by means of elastic wave propagation in soil, high resolution SPOT panchromatic and airborne images for landslide recognition and digital terrain modelling in GIS platforms.

4.3 Technical Developments for Potential LEWSs

To summarize the evidence emerging from the literature review about the reported technical developments for the potential developments of LEWSs, the following insights can be listed: learning adaptive neuro-fuzzy inference systems, application of sliding force remote monitoring systems as a diagnostic tool for a rapid assessment of open pit slope stability and prediction of landslides, electrical resistivity techniques, cellular mobile infrastructure for using geo-spatial data, monitoring based on micro-electromechanical systems, landslide detection system based on flat coil and coil sensors, coupling of landslide simulation models and a hydrological models, and very importantly, utilisation of hazard and risk information for spatial planning and zoning, indicating areas where landslide hazard is too high for planning future developments.

4.4 Models and Prototypes for LEWSs

Indeed, from the systematic literature review concerning LEWSs, it was observed that the spread of models and prototypes in LICs and MICs have some shared features. These included the efforts to develop cheap LEWS, applications for smartphone devices, dynamic web-based alert systems, machine learning algorithms for wireless sensor networks, the use of Wireless Sensor Networks, electrical resistivity tomography techniques, field monitoring data and risk evaluation model using fibre-optic based transducers, tools for improving connectivity. Additionally, great significance was given to the promotion of proven and innovative techniques and technologies of early warning systems based on monitoring ground surface deformation using Synthetic Aperture Radar, artificial neural networks based on rainfall forecasting models, simple monitoring systems and using micro electromechanical systems concerning tilt and volumetric water content sensors. What is more, the extensive use of social media users as potential contributors to landslide hazard monitoring and as providers of additional support for landslide prediction and decision making was also considered.

4.5 Implementation of LEWSs: An Urgent Task

The need to implement LEWSs has been regarded as an urgent endeavour. To this regard, five of the examined publications were concerned with diverse perspectives on this matter. In Bangladesh, for instance, interviews on the methods local-level institutions follow to mitigate landslide hazards in terms of structural and non-structural measures were sought. Since structural measures are insufficient due to the financial constraints, mechanisms of sustainable hillslope management and LEWSs were suggested (Sultana and Tan 2021). Likewise, based on a quantitative estimation of elements at risk to landslides, the implementation of LEWSs in India was put forward (Sajinkumar et al. 2014). Similarly in Indonesia, a series of interviews were focused on analysing awareness and preparedness of primary stakeholders (i.e., government and non-departmental government institutions) to mitigate landslide disaster risk and disasters (Susanto et al. 2018). In a similar manner, in Japan, attention has been given to LEWSs as the major non-structural measures which are based on judgment and action of local people. The latter being highly influenced by information provided by mass media (Fujita and Shaw 2014).

4.6 Scientific Collaborations

It can be said that there needs to be more integrated action leading to successful practice concerning the implementation of the Sendai framework, which includes “to promote and improve dialogue and cooperation among scientific and technological communities, other relevant stakeholders and policymakers in order to facilitate a science policy interface for effective decision-making in disaster risk management” and “to enhance the scientific and technical work on disaster risk reduction and its mobilization through the coordination of existing networks and scientific research institutions at all levels and in all regions” (UNISDR 2015).

In the same spirit, through the systematic review of literature it was possible to identify that international scientific cooperation enabled numerous collaborations between LICs and MICs and other countries to understand and manage landslide disaster risk, and most importantly to advance the research on LEWSs and their potential implementation (Fig. 10). Such collaborative efforts can build trust and facilitate progress in landslide disaster risk reduction.

Therefore, indicators of future progress on landslide disaster research, should include number of LICs and MICs with implemented LEWSs, number of long-term scientific collaborations, and number of people at risk who benefited from their use.

5 Discussion

The analysed publications provided an overview of the existing literature on the different dimensions of LEWSs in LICs and MICs. This was useful to highlight the key gaps in the published studies and allowed the possibility to offer suggestions for future research.

In the international arena, scientific cooperation has enabled numerous collaborations in different fields among LICs and MICs and other countries. One of the thirteen guiding principles of the Sendai Framework for DRR has pointed out that (the so-called) “developing countries, in particular the least developed countries, small island developing States, landlocked developing countries and African countries, as well as middle-income and other countries facing specific disaster risk challenges, need adequate, sustainable and timely provision of support, including through finance, technology transfer and capacity building from developed countries and partners tailored to their needs and priorities, as identified by them” (UNISDR 2015). However, in the area of LEWSs, attempts have not been largely focussed yet on such endeavour.

The majority of efforts continue to be centred in hazard perspectives. This was clearly demonstrated by the large number of publications on hazard analysis, technical developments and models and prototypes for the potential implementation of LEWSs. Contrastingly, only five articles reported the actual successful implementation of LEWSs in LICs and MICs, and very few considered the diverse dimensions of community participation as a key element.

Consequently, as one of the main challenges ahead argued here is that LEWSs should not focus on people’s response to purely technical systems in terms of hazards, but rather rely on the participation of communities as a fundamental component of Early Warning Articulated Systems (EWAS). This of course requires an understanding of landslide disaster risk by the communities themselves and by the other relevant DRR stakeholders. A more substantial approach to the significance of EWAS can be found in Alcántara-Ayala and Oliver-Smith (2017, 2019).

A full discussion of the existing obstacles for the establishment and operationalisation of LEWSs in LICs and MICs at different scales lies beyond the scope of this study. However, it would be a vital consideration in any future regional and/or international comprehensive strategies or frameworks, to consider difficulties such as high prices of most devices; loss of property, and loss of valuable data derived from vandalism and insecurity conditions; inaccessibility of remote mountain sites; frequent power interruptions; absence of interest of local authorities to collaborate with the scientific community; bureaucratic procedures to

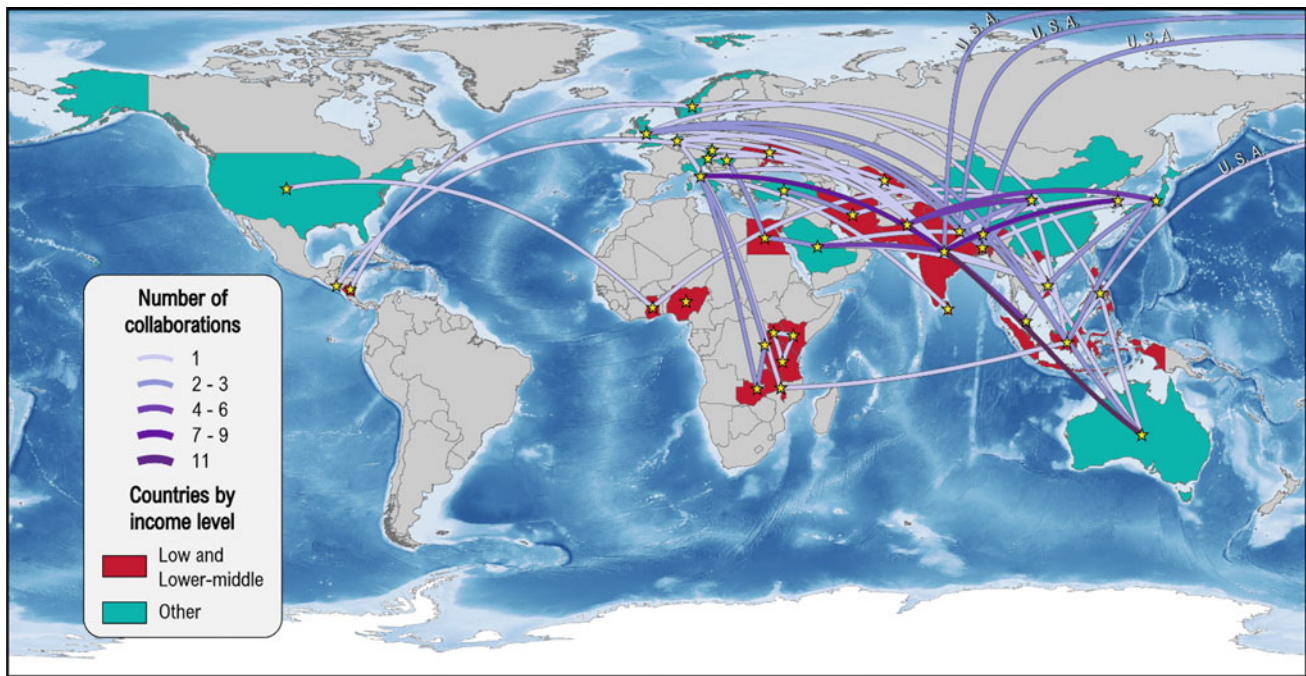


Fig. 10 Regional and international collaborations among LICs and MICs and other countries

obtain permits; lack of information databases regarding hazards, vulnerability and exposure; limited or non-existent technical capacities at national and local scales; lack of sustained financial resources for the design, development, implementation and maintenance of LEWSs; lack of political will and sustained political support; and high expectations and failure to provide the required means.

Certainly, lack of human and financial resources poses special challenges to science, DRR and particularly to the implementation of LEWSs in LICs and MICs. Tackling these challenges effectively requires modern, innovative, and integrated approaches based on sharing financial resources in the best possible way to bridge the gap between science, policy making and practice.

Last, but not least, the setting up of LEWSs aimed at reducing disaster risk in LICs and MICs requires actions from the entire society to support the development of adequate strategies of disaster risk communication, a challenge that should provide some orientations to design appropriate and effective integrated measures in favour of the communities at risk.

6 Concluding Remarks

Derived from the impact of large disasters, especially after the tsunami of Southeast Asia in 2004, particular attention has been given to the establishment and/or evaluation of EWS at international and national levels.

Since 1991, a considerable amount of literature has been published on LEWSs, and although studies have recognised the significance of LEWSs around the world (Guzzetti et al. 2020), these studies have been concentrated to a major extent on Upper middle- and High-income countries.

This systematic literature analysis provided an important opportunity to advance the understanding of the use of LEWSs in LICs and MICs and it is also hoped that the findings could make an important contribution to the field of policy formulation and practice on landslide disaster risk reduction.

The literature to date provides interesting insights into the way that research on LEWSs has been gradually evolved through time from engineered perspectives into more community-based approaches that can be used for solving pressing societal issues. However, such advancement in LICs and MICs has either taken place at a very slow rate or has not properly been reflected in peer reviewed literature. Beyond analytical lenses, what is clear is that landslide disasters continue to occur around the globe and consequences are of greater adverse impact in countries of lower income.

Up to now, the use of LEWSs in LICs and MICs has been limited due to diverse restraints. Prominent among these is the high costs of equipment, their limited usability in the long-term associated with vandalism and insecurity, and lack of sustained financial and human resources. The absence of human resources also suggests that there are no structured strategies for capacity building in the medium and long terms.

Over and above all, the role of communities at risk has been often neglected in the implementation of LEWSs. This aspect is not less important than technical challenges, but a core ingredient in the design and implementation of efficient LEWSs.

The demand for effective regional and international collaborations with the DRR scientific community in terms of LEWSs advancement is out there, and it is growing. Certainly, this is a critical time to focus on the implementation of LEWSs in LICs and MICs.

Acknowledgements Our sincere gratitude to DGAPA-UNAM, who kindly provided financial support to carry out landslide risk research through Project PAPIIT IN300823. Thanks, are also due to Prof. Veronica Tofani from the University of Florence for her valuable review of this manuscript.

References

- Alcántara-Ayala I (2021) Integrated landslide disaster risk management (ILDRiM): the challenge to avoid the construction of new disaster risk. *Environ Hazards* 20(3):1–22. <https://doi.org/10.1080/17477891.2020.1810609>
- Alcántara-Ayala I, Oliver-Smith A (2019) Early warning systems: lost in translation or late by definition? A forin approach. *Int J Disaster Risk Sci* 10:317–331. <https://doi.org/10.1007/s13753-019-00231-3>
- Alcántara-Ayala I, Sassa K (2021) Contribution of the international consortium on landslides to the implementation of the Sendai framework for disaster risk reduction: engraining to the science and technology roadmap. *Landslides* 18:21–29. <https://doi.org/10.1007/s10346-020-01539-8>
- Alcántara-Ayala I, Oliver-Smith A (2017) Linking sustainable development, disaster risk reduction, climate change adaptation and migration. In: Sudmeier-Rieux K, Fernandez M, Penna I, Jaboyedoff M, Gaillard J C (eds), p 281. Springer, Cham. https://doi.org/10.1007/978-3-319-33880-4_7. ISBN 978–3–319–33878–1
- Devoli G, Strauch W, Chávez G, Høeg K (2007) A landslide database for Nicaragua: a tool for landslide-hazard management. *Landslides* 4(2):163–176. <https://doi.org/10.1007/s10346-006-0074-8>
- Fathani TF, Karnawati D, Wilopo W (2016) An integrated methodology to develop a standard for landslide early warning systems. *Nat Hazards Earth Syst Sci* 16:2123–2135. <https://doi.org/10.5194/nhess-16-2123-2016>
- Fathani TF, Karnawati D, Wilopo W (2017) Advancing culture of living with landslides, vol 1. ISDR-ICL Sendai Partnerships 2015–2025. In: Sassa K, Mikoš M, Yin Y (eds), p 586. Springer. https://doi.org/10.1007/978-3-319-59469-9_30. ISBN 978–3–319–53500–5
- Fujita K, Shaw R (2014) Community practices for disaster risk reduction in japan. In: Shaw R (ed), p 239. Springer, Tokyo. https://doi.org/10.1007/978-4-431-54246-9_10. ISBN 978–4–431–54245–2
- Gumiran B, Moncada FM, Gasmen HJ, Boyles-Panting NR, Solidum RU (2019) Participatory capacities and vulnerabilities assessment: towards the realisation of community-based early warning system for deep-seated landslides. *Jamba (potchefstroom, South Africa)*. 11(1):a555. <https://doi.org/10.4102/jamba.v11i1.555>
- Guzzetti F, Gariano SL, Peruccacci S, Brunetti MT, Marchesini I, Rossi M, Melillo M (2020) Geographical landslide early warning systems. *Earth Sci Rev* 200:102973. <https://doi.org/10.1016/j.earscirev.2019.102973>
- Hidayati Z, Noviana M (2018) Non-structural measures for landslide (creeping type) in Selili Hill Samarinda. In: Proceedings of the 4th international conference on engineering, technology, and industrial application (ICETIA) 2017. AIP Conf Proc 1977:040006
- ISDR-PPEW (2005) International early warning programme (IEWP). Brochure. In: ISDR platform for the promotion of early warning (PPEW), Bonn, p 4
- Karnawati D, Fathani TF, Ignatius S, Andayani B, Legono D, Burton PW (2011) Landslide hazard and community-based risk reduction effort in Karanganyar and the surrounding area, Central Java, Indonesia. *J Mt Sci* 8(2):149–153. <https://doi.org/10.1007/s11629-011-2107-6>
- Karnawati D, Fathani TF, Andayani B, Burton PW, Sudarno I (2009) Disaster management and human health risk. In: Duncan K, Brebbia CA (eds) WIT transactions on the built environment, WIT Press, Southampton, UK, p 416. <https://doi.org/10.2495/DMAN090121>. ISBN 978–1–84564–202–0
- Marciano JS, Hilario CG, Zabanal MA, Mendoza EV, Gumiran BL, Flores BF, Peña MO, Razon KH (2014) Monitoring system for deep-seated landslides using locally-developed tilt and moisture sensors: system improvements and experiences from real world deployment. In: IEEE global humanitarian technology conference (GHTC 2014), San Jose, CA, pp 263–270
- Masaba S, Mungai DN, Isabirye M, Nsubuga H (2017) Implementation of landslide disaster risk reduction policy in Uganda. *Int J Disaster Risk Reduction* 24:326–331. <https://doi.org/10.1016/j.ijdrr.2017.01.019>
- Nelson GL, Zamora O, deGuzman LE, Tatlonghari R, Espaldon MV, Brillion J (2019) The indigenous practices and climate change responses of ati and suludnon farmers in Iloilo, Philippines. *J Environ Sci Manag* 22(1):87–98. https://doi.org/10.47125/jesam/2019_1/06
- Ramesh MV, Pullarkatt D, Geethu TH, Rangan PV (2017) Advancing culture of living with landslides, vol 3. Advances in landslide technology. In: Mikoš M, Arbanas Z, Yin Y, Sassa K (eds), p 621. Springer Cham. https://doi.org/10.1007/978-3-319-53487-9_4. ISBN 978–3–319–53486–2
- Sajinkumar KS, Anbazhagan S, Rani VR, Muraleedharan C (2014) A paradigm quantitative approach for a regional risk assessment and management in a few landslide prone hamlets along the windward slope of Western Ghats, India. *Int J Disaster Risk Reduction*. 7:142–153. <https://doi.org/10.1016/j.ijdrr.2013.10.004>
- Sassa K (2015) ISDR-ICL Sendai partnerships 2015–2025 for global promotion of understanding and reducing landslide. *Landslides* 12(4):631–640. <https://doi.org/10.1007/s10346-015-0586-1>
- Sassa K (2016) Implementation of the ISDR-ICL Sendai partnerships 2015–2025 for global promotion of understanding and reducing landslide disaster risk. *Landslides* 13(2):211–214
- Sassa K (2019) The fifth world landslide forum and the final draft of the Kyoto 2020 commitment. *Landslides* 16(2):201–211. <https://doi.org/10.1007/s10346-018-01133-z>
- Sassa K (2020) Launching session of the Kyoto landslide commitment 2020. *Landslides* 17(8):1743–1744. <https://doi.org/10.1007/s10346-020-01467-7>
- Smith K (1996) Environmental hazards: assessing risk and reducing disaster. Routledge, London, p 504. <https://doi.org/10.4324/9780203805305>. ISBN 9780415681063
- Sultana N, Tan S (2021) Landslide mitigation strategies in southeast Bangladesh: lessons learned from the institutional responses. *Int J Disaster Risk Reduction*. 62:102402
- Susanto N, Prastawa H, Putranto TT, Zakina OA, (2018) Improving the awareness index of government and non-departmental government institutions for landslide cases in Semarang city. In: The 9th international conference on global resource conservation (ICGRC) and AJI from Ritsumeikan University

- Thapa PS, Adhikari BR (2019) Development of community-based landslide early warning system in the earthquake-affected areas of Nepal Himalaya. *J Mt Sci* 16(12):2701–2713. <https://doi.org/10.1007/s11629-019-5586-5>
- Tien DV, Khang NX, Sassa K, Miyagi T, Ochiai H, Vinh HD, Quang LH, Dang K, Asano S (2017) Advancing culture of living with landslides, vol 1. ISDR-ICL Sendai Partnerships 2015–2025. In: Sassa K, Mikoš M, Yin Y (eds), p 586. Springer. https://doi.org/10.1007/978-3-319-59469-9_36. ISBN 978–3–319–53500–5
- Twigg J (2002) Early warning systems for natural disaster reduction. In: Zschau J, Küppers AN (eds), p 834. Springer, Berlin. https://doi.org/10.1007/978-3-642-55903-7_4. ISBN: 978–3–540–67962–2
- UNISDR (United Nations International Strategy for Disaster Reduction) (2015) Sendai framework for disaster risk reduction 2015–2030. UNISDR, Geneva
- UNISDR (United Nations International Strategy for Disaster Reduction) (2019) The science and technology roadmap to support the implementation of the Sendai framework for disaster risk reduction 2015–2030. UNISDR, Geneva
- UNISDR (United Nations International Strategy for Disaster Reduction) (2006) Global survey of early warning systems. An assessment of capacities, gaps and opportunities towards building a comprehensive global early warning system for all natural hazards. Geneva, Switzerland: United Nations Office for Disaster Risk reduction, UNISDR, Geneva
- UNISDR (United Nations International Strategy for Disaster Reduction) (2016) Report of the open-ended intergovernmental expert working group on indicators and terminology relating to disaster risk reduction. United Nations International Strategy for Disaster Reduction, UNISDR, Geneva

Open Access This chapter is licensed under the terms of the Creative Commons Attribution 4.0 International License (<http://creativecommons.org/licenses/by/4.0/>), which permits use, sharing, adaptation, distribution and reproduction in any medium or format, as long as you give appropriate credit to the original author(s) and the source, provide a link to the Creative Commons license and indicate if changes were made.

The images or other third party material in this chapter are included in the chapter's Creative Commons license, unless indicated otherwise in a credit line to the material. If material is not included in the chapter's Creative Commons license and your intended use is not permitted by statutory regulation or exceeds the permitted use, you will need to obtain permission directly from the copyright holder.





The Role of Translational Landslides in the Evolution of Cuesta Topography

Shinro Abe, Daisuke Higaki, and Kazunori Hayashi

Abstract

In recent years, large-scale earthquakes such as the 2004 Mid-Niigata Prefecture Earthquake in Japan and the 1999 Chi-Chi Earthquake in Taiwan have caused rockslides on the back slopes of cuestas. These rockslides in cuestas appear not only in earthquakes but also during rainfalls. This study focuses on the rockslides on cuesta's back slopes. From field surveys in Japan, Taiwan, Switzerland, and Nepal, we extracted geological, structural, and morphological features common to them. We examined the relationships between these features and triggers, such as pore pressure increases and earthquakes. The majority of landslides initially occur as primary landslides; the forms of these masses then change gradually over a long period. However, our results show that landslides on cuesta's back slopes slide over and over along the same laminar rock joints and thus hardly change their landscape essence. We demonstrate that rockslides on cuesta's back slopes play a vital role in the evolution of cuesta landscapes.

Keywords

Cuesta • Rockslide • Earthquake-induced landslides • Rock cracks

S. Abe (✉) · K. Hayashi
Okuyama Boring Co., Ltd., 10-39, Shinmei-cho, Yokote, Akita,
Japan
e-mail: abeshinro@gmail.com

K. Hayashi
e-mail: k.hayashi@okuyama.co.jp

D. Higaki
Nippon Koei Co., Ltd., 5-4 Kojimachi, Chiyoda ku, Tokyo, Japan
e-mail: a9024@n-koei.co.jp

1 Introduction

Landforms with differential geometries, such as cuestas and hogbacks, are susceptible to frequent landslides. An asymmetrical cuesta terrain is featured by a steep escarpment on one side and a gentle slope on the other (Davis 1915; Peterek and Schröder 2010). Multiple landslides occurred in a cuesta landscape with folded laminar structures during the 2004 Mid-Niigata Prefecture Earthquake, Japan (Chigira and Yagi 2006). Previous research on landslides in cuesta landscapes has primarily focused on rock falls on cuesta escarpments or small-scale slump-style slides (Cruden and Hu 1999; Grozavu. et al. 2010; Schmid and Meitz 2000). On the other hand, only a few studies, such as Kuroda (1964), addressed landslides on the cuesta's back slopes. This is perhaps because landslides occurring on the escarpments of cuestas have been much more than those on the back slopes. However, translational slides on the cuesta's back slopes are basically bedrock slides; they are fast, regardless of the cause, and can be as large as 1 km in width and length. Therefore, these landslides can pose significant risks of severe damage to their slopes and areas at their feet.

We focused on the intrinsic features of the cuesta's back slopes, such as layers coming off and sliding down one after another along the rock's bedding planes and cracks. In this study, we analyzed the relationship among geology, geological structure, cracks, and bedding planes associated with these landslides; the development of rivers and landslides; the triggers of landslides, such as earthquakes rainfalls, and snowmelt; and the recurrence of landslides. The primary aim of this study was to create valuable guidelines for engineering plans, prediction of landslides, and understanding the landslide mechanisms by focusing on the relationship between the landslide occurrence processes and the evolution of cuesta landscapes. This research shows that translational bedrock slides, which recur on the cuesta's back slopes as part of the denudation processes, play an essential role in the evolution of cuesta landscapes.

2 Methodology

Cuesta's back slope landslides of concern were surveyed between 1998 and today. They are landslides in the Hijiori region and Higashi-Naruse area, the Hijirigahana, Yokowatashi, and Nunomata landslides of Japan, the Goldau landslide of Switzerland, landslides along the Tamakoshi River in Nepal, and the Chiu-Fen-Erh-Shan and Tsaoling landslides in Taiwan. This study defines the cuesta's back slope as the gentler slope of the asymmetric cuesta with an inclination of 5 to 30° (Cruden and Hu 1999, and other references).

During the survey, we primarily recorded the geologies, geological structures, strikes and dips of bedrock, slope inclinations, landslide movement types (Varnes 1978; Cruden and Varnes 1996), and the directions of movement. We measured the cracks in bedrocks in the landslides and their surrounding areas. We targeted cracks in bedrocks that extend more than 1 m and measured their strikes and dips. These values are presented on a rose diagram or a stereo net. The analysis of cracks in the Chiu-Fen-Erh-Shan landslide of Taiwan is based on Wang et al. (2003).

The widths and directions of visible cracks on an outcrop can vary remarkably. Therefore, when the outcrop area was limited, the entire extent of the outcrop was explored, whereas, in large outcrops, we targeted valleys and rivers where base rocks are exposed. Here, we assume that a crack direction at a particular site is a dominant direction on a Rose diagram of the crack azimuths observed there.

We analyzed the movement of the Yokowatashi landslides in the time domain using MIDAS GTS for BESSRA software to discuss the detachment sequence of elastoplastic landslide masses.

3 Results

3.1 Descriptions of Featured Landslides

This chapter shows case histories by their causes, i.e., rainfalls/ snowmelt and earthquakes.

3.1.1 Cuesta Landslides Triggered by Rainfalls and Snowmelt Landslides in the Hijiori Region, Japan

The Hijiori region encompassing Okura village in Yamagata prefecture is approximately 15 km long and 10 km wide, extending from the Quaternary Hijiori caldera (about 4 km in diameter) northward to the Mogami River. It is a zone of frequent landslides (Fig. 1).

This region can be roughly divided into two sections: an area of Neogene sedimentary rocks that make up most of the

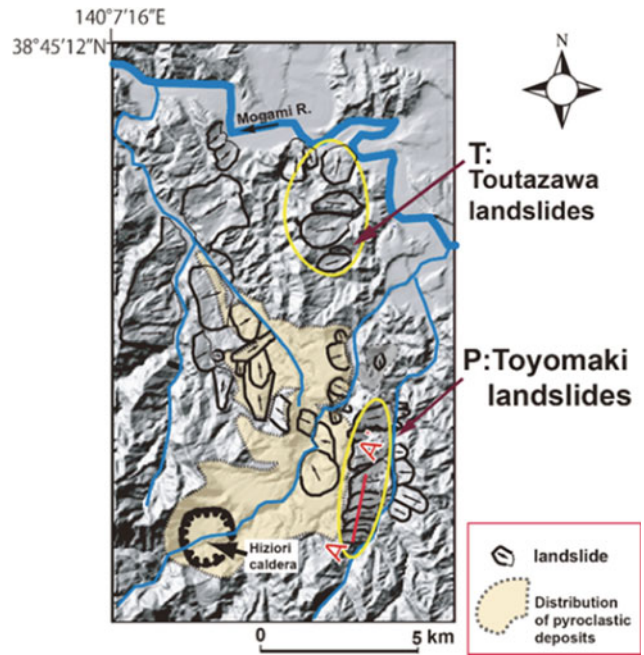


Fig. 1 The topography and landslide distribution in the Hijiori region (data added to a shaded relief map)

region's northern half and a southern area consisting of pyroclastic-flow deposits formed by the ejecta of the Hijiori caldera. The area of the Neogene sedimentary rocks in the north is hilly, with ridges between 50 and 300 m in relative height. Their ridgelines and rivers align in north–south direction, following azimuths of fold axes. Cuesta topography is well developed here. The steep slopes on the western sides of the ridges incline 30° or more prominent, and the eastern sides have gentle slopes of 5 to 20°. The Toutazawa landslides are in this region (T in Fig. 1).

The activities of the Toutazawa landslides are dominant on the cuesta's back slopes, where a homoclinal folding structure dipping to the east features the terrain.

The cuesta's gentle back slope steps down. These steps control the movements of the landslide masses perching above ((a) in Fig. 2). The upper landslide masses on the stepped back slope move along these steps about 50 to 60° off the direction of the maximum dip. Due to erosive/depositional actions, these landslide masses can gradually be leveled ((b) in Fig. 2). Eventually, each transverse cross-section of these landslide masses has an asymmetric inverted triangle shape.

The maximum snow depth here exceeds 200 cm. Many of these landslides occur during the snowmelt season, perhaps due to increased pore water pressure associated with melt-water infiltration into the landslide masses with the asymmetric inverted triangle cross-sections.

The Toyomaki landslides are in the area containing Quaternary pyroclastic flow deposits (P in Fig. 1). The

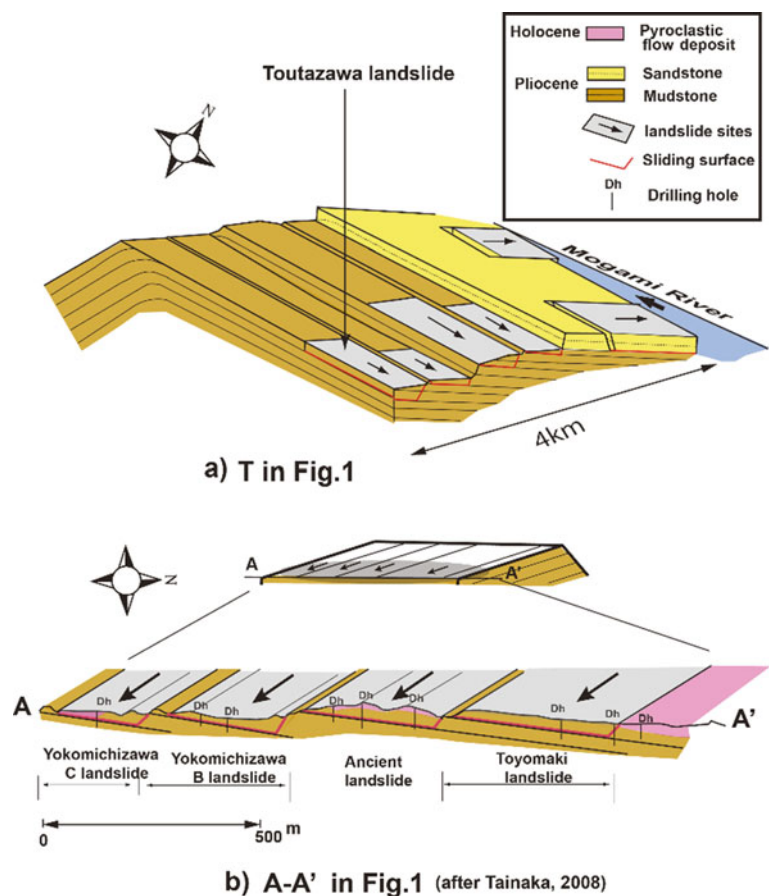
landslides with Pyroclastic flow deposit covers are more extensive than those with no pyroclastic soil cover (such as the Toutazawa landslides). The landslide masses with the pyroclastic soil covers are as thick as 150 m. The Toyomaki landslides consist of five landslides that occurred close to each other within a 5 km wide and 1 km long area. The entire terrain features and the estimated age of the pyroclastic flow deposits suggest significant displacements occurred first as a primary rockslide. Then, the pyroclastic flow covered the whole landslides (Abe et al. 2002), followed by repetitive sliding events. As revealed by borehole drillings on the sliding surface, the transverse cross-section of the landslide is an asymmetrical inverted triangle resting on the sliding surface dipping to the north. The landslide mass moves about 10° off the maximum dip of the strata (b in Fig. 2). All landslides in the Toyomaki landslides occurred during snowmelt, suggesting that a large amount of groundwater has played a role in the occurrence mechanism of landslides with asymmetrical cross-sections on their sliding surfaces.

3.1.2 Landslides in the Higashi-Naruse Region, Japan

Higashi-naruse, an area of frequent landslide occurrences, is located in the Ou Mountain range in the Tohoku region of Japan. Many landslides here occur as translational rockslides in Miocene siliceous mudstones formations. They are roughly divided into two groups: the Yachi landslides on the left bank of the Naruse River and the Yanagisawa landslides, the toe section of which is on the right bank of the Naruse River (Fig. 3). In the Yachi landslides, a cluster of multiple landslides is seen on the cuesta's back slopes region, covering a 7 km by 3 km area. The adjacent Okamizawa and Yanagisawa landslides cover a 4 km by 2.5 km area on the cuesta's back slopes (Fig. 3).

Large-scale landslide topography covering a 6 km by 3 km area is present in the Yachi landslides. The west side of the crown of this vast landslide topography is a cuesta scarp. The landslides are on the cuesta's back slopes, dipping between 5 and 23° . Excavation of the head section of the landslide and drilling of test pits have identified the

Fig. 2 Model of the Toutazawa landslides (a) and the cross-section of the Toyomaki landslides (b)



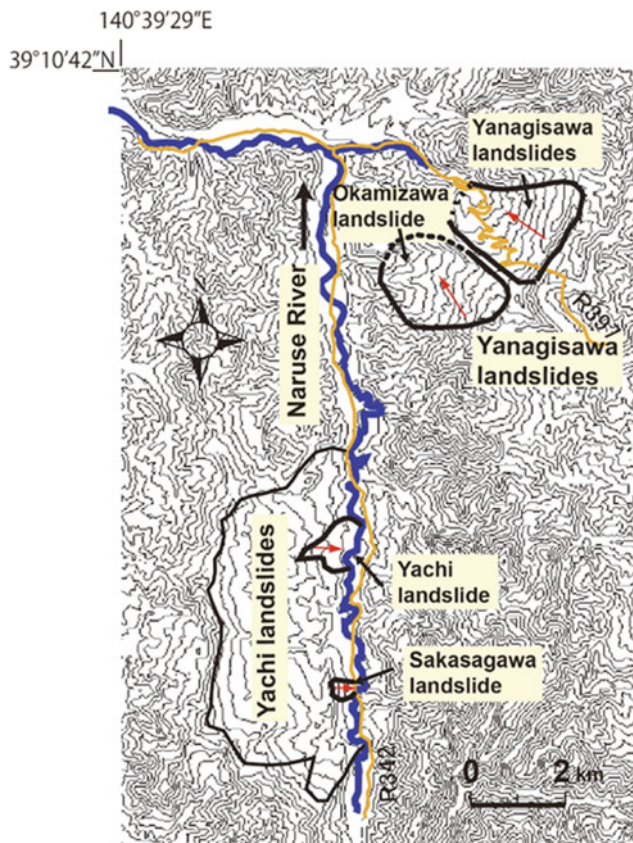


Fig.3 Landslides of the Higashinaruse region (after Moriya et al. 2008)

sliding surface of the Yachi landslide as a tuff layer within a siliceous mudstone layer. The Okamizawa and Yanagisawa landslides are translational rockslides that slide on a seam of tuff or black mudstone within a highly developed level containing siliceous mudstones.

These two landslides can be further subdivided into smaller slides. Data obtained from field mapping, borehole drilling, and geological investigations for the construction of catchment wells have revealed that cuesta's steps separate these landslide masses, and each landslide mass moves individually on its sliding surface.

3.1.3 The Goldau Landslide, Swiss Alps

The Goldau landslide (Fig. 4) in the Swiss Alps occurred in 1806 on a cuesta's back slope located 1500 m above sea level following heavy rainfall (Thuro and Hatem 2010). A massive volume of rock ($10\text{--}50 \times 10^6 \text{ m}^3$) plunged into Lake Lauerz (Lauerzersee), generating a landslide tsunami that claimed 457 lives and left 206 missing persons (Zehnder 1988). Three such events are known to have happened from geomorphic and historical evidence (Fig. 4). Currently, a discernible displacement can be identified on the east side of the region, causing yet growing fear of another large-scale

rockslide. The past slides dipping 20 to 30° are 200 to 700 m wide and 1000 to 2000 m long. The flank of each displaced mass shows a steep escarpment.

The area's geology alternates between conglomerate with sandstone and intercalated marl in a Miocene molasse. The sliding surface is presumed to have developed within the marl section, where fragmented marl has become clay.

The dips of the sliding surfaces are $20\text{--}30^\circ$. In the newest landslide that moved in 1806 ((3) in Fig. 4), the joints are mainly parallel or orthogonal to the direction of the landslide movement. The inclination of the sliding surface becomes steeper from 20 to 30° as we move up stepwise slopes from (1) to (3) in Fig. 4. The step between slopes (1) and (2) is approximately 1 m high, while the 0–20 cm high step between (2) and (3) inclines gently. These steps resemble the stepwise slide surfaces observed in the Higashinaruse area described above and the Hijirigahana landslides in the Niigata-ken Chuetsu-Oki Earthquake of 2007 in Japan. The prominent 3 to 5 m scarp is at the uppermost part of the landslide ((3) in Fig. 4). The stationary remains of the slide lie above this scarp. Many cracks observed on the soil remains can be an early sign of a coming landslide. In some places, the orientation of displacements obliquely crosses the maximum dip of the strata. Therefore, the surface water on this landslide mass flows towards the eastern flank of the landslide, where a stream emerges. Part of this water flows into the base of displaced material ((4) in Fig. 4) adjacent to the eastern side and may act as one of the triggering factors of the next sliding event.

3.1.4 Landslides along the Tamakoshi River, Nepal

Many landslides in Nepal are attributed to the steep Himalayan terrain as well as geological features such as the Main Central Thrust (MCT) and Main Boundary Thrust (MBT), which are large-scale thrust faults with nappe structures (Abe et al. 1999). Charikot, on the Tamakoshi River, is situated in the Lower Himalayas of central Nepal. The area has an average altitude of approximately 1000–2000 m, and the bedrock is Precambrian to Paleozoic low-grade Augen gneiss (Fig. 5).

Unlike the landslides in the fractured sections of the large-scale tectonic lines in Nepal, many landslides in this region are influenced by rock characteristics such as schistosity, joints, and cracks. There is an area of synclines with an east–west axis around Charikot, and cuestas with dip slopes of $10\text{--}20^\circ$ form on the limbs of these folds, dipping north and south. The steps have developed in an east–west direction on the slopes.

The Tamakoshi River flows from north to south at the toe of these landslides. Streams flowing into the Tamakoshi River have cut both sides of each landslide down to

Fig. 4 The Goldau landslide: (1) Prehistoric landslide, (2) the 1222 Rothen slide, (3) the 1806 rockslide, (4) future event? (Photo by Google Earth. History of landslide activity is after Thuro and Hatem 2010)

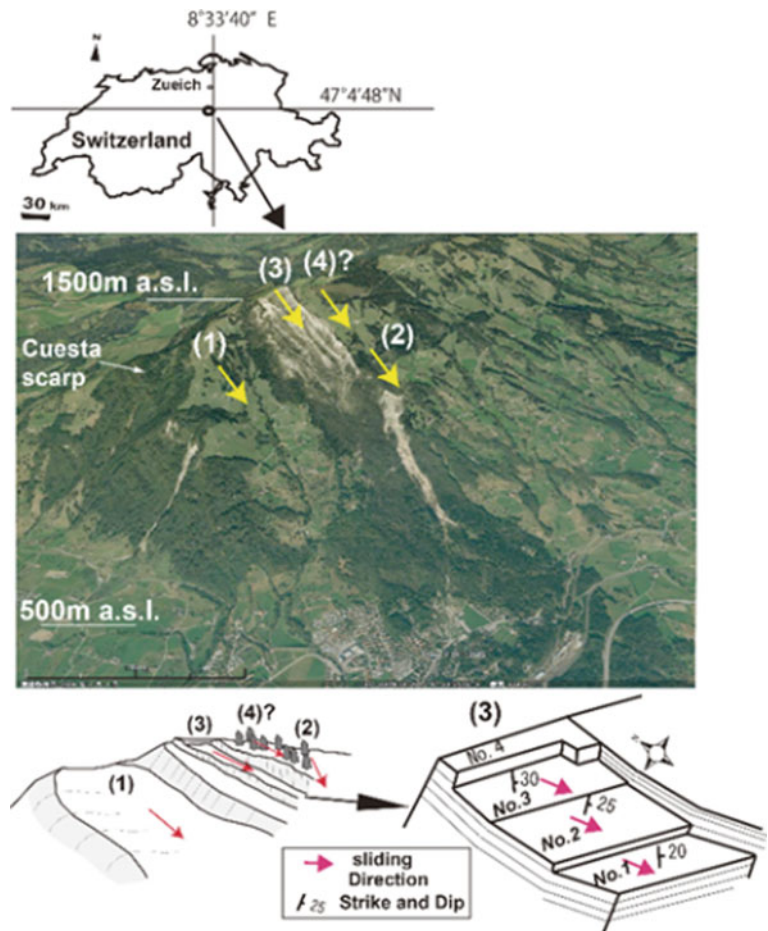
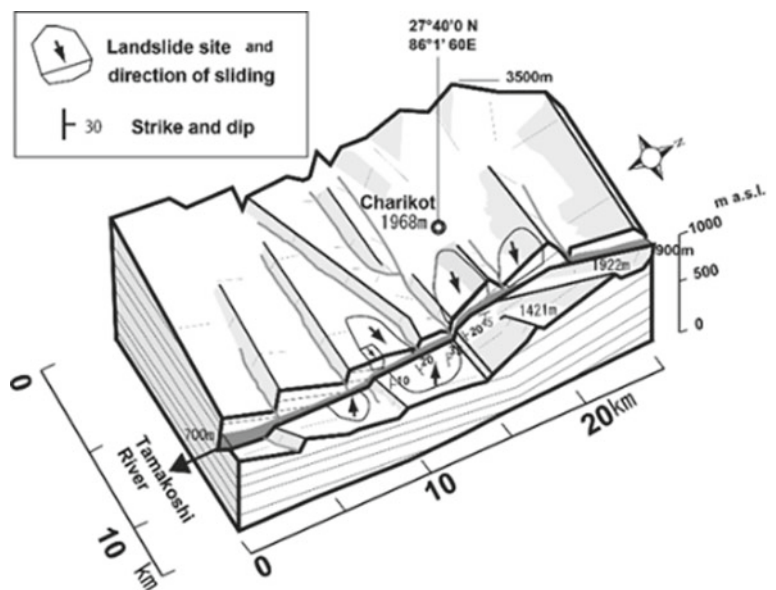


Fig.5 Schematic diagram of the cuesta landscape on the banks of the Tamakoshi River and landslides



lower elevations. Translational landslides along the schistosity and circular landslides are in the weathered layers on the cuesta's back slopes. Similar landslides on the cuesta's back slopes are also found in the Precambrian phyllite

along the Sunkoshi River and the Roshi River, one of the tributaries of the Sunkoshi. Both are located around 50 km northwest and southwest of the said translational slides near Charikot.

3.2 Earthquake-Induced Landslides

3.2.1 The Yokowatashi Landslide, Japan

Japan's 2004 M6.8 Mid-Niigata Prefecture Earthquake was a significant inland earthquake claiming 68 lives. Many landslides occurred in the vicinity of the epicenter of this earthquake (e.g., Chigira and Yagi 2006; Kieffer et al. 2006), which is located in a mountainous region 25 to 400 m above sea level. Geological features in this area include alternating beds of Pliocene sandstone, mudstone, and siltstone with a highly developed north-south trending composite fold structure.

The Yokowatashi landslide (Fig. 6), one of many that occurred during the 2004 Mid-Niigata Earthquake, is located on a cuesta 50 to 100 m above sea level, where an alluvial plain of Shinano River opens up at the western end of the hilly terrain.

Within a lateral distance of 250 m, three landslides of Pliocene muddy siltstone moved together towards the Shinano River. The sliding surface is a seam of sandy tuff intercalated within siltstone. The surface stretching from A to F in Fig. 6 is terraced with 1 to 2 m high southeast trending steps. In addition to the displaced locations in the 2004 Mid-Niigata Prefecture Earthquake (B, D, and F in Fig. 6), other locations (A, C, and E in Fig. 6) also show planar dip-slopes that presumably resulted from past rockslides. Incidentally, no landslides have been identified on the cuesta scarp here. The conglomeratic strata that make up the topmost layer of the Yokowatashi landslide (see the

conglomerate layer in Fig. 6) are key to understanding the history of past slide events here. The translational rockslides are assumed to have taken place in succession from north to south.

The northernmost stream initially developed along cracks and cut the slope down to the lower elevation to expose a loose plane along the creek. This process reduced the resisting force against the landslide mass south of the stream, which eventually caused the translational landslides.

A large planar piece of rock remains partially atop Slope B and over a large portion of Slope C. Large rock blocks on Slopes E and F are perhaps the remnants of the ridge section left by an earlier slide. As described later, the above is one of the most often identified features of the earthquake-triggered cuesta landslides, and Fig. 7 shows a chronological summary of the Yokowatashi landslides.

3.2.2 The Hijirigahana Landslide, Japan

Three years after the 2004 Mid-Niigata Prefecture Earthquake, the 2007 M6.8 Niigata-ken Chuetsu-Oki Earthquake occurred off the coast of Kashiwazaki near the epicenter of the earlier earthquake. This earthquake triggered a landslide on a cuesta's back slope in hilly coastal terrain.

The Hijirigahana landslide move along the slope at high speed and are 100 m wide, 200 m long, and 10 m thick. Some of the sliding masses have remained at the crown of the slope, but most of them slid down as translational rockslides, reaching the foot of the slope in one movement. Their slip surface was a bedding plane between Pliocene siltstone and coarse sandstone layers.

3.2.3 The Nunomata Landslide, Japan

In the 1914 M7.1 Senboku Earthquake, another inland earthquake, eight rockslides were reported in Akita Prefecture, northeast Japan (Ohashi 1915). They included the translational Nunomata landslide on the cuesta's back slope. It traveled 70 to 80 m down a slope of approximately 8°, creating a landslide dam. The landslide mass was 100 m wide, 300 m long, and 20 m thick. Our observations and analysis of this slide in a test pit at the head of the landslide confirm that the sliding surface lies within an intercalated sandstone between Pliocene siltstone layers. This sliding surface consists of a sandstone layer with the same softness as the sandy tuff in the Yokowatashi landslide.

3.2.4 The Chiu-Fen-Erh-Shan Landslide and the Tsaoling Landslide, Taiwan

The 1999 M7.3 Chi-chi Earthquake in central Taiwan triggered many landslides. Among those quake-induced landslides, the Chiu-Fen-Erh-Shan and the Tsaoling landslides are massive and occurred on the cuesta's back slopes of Neogene sedimentary rock units.

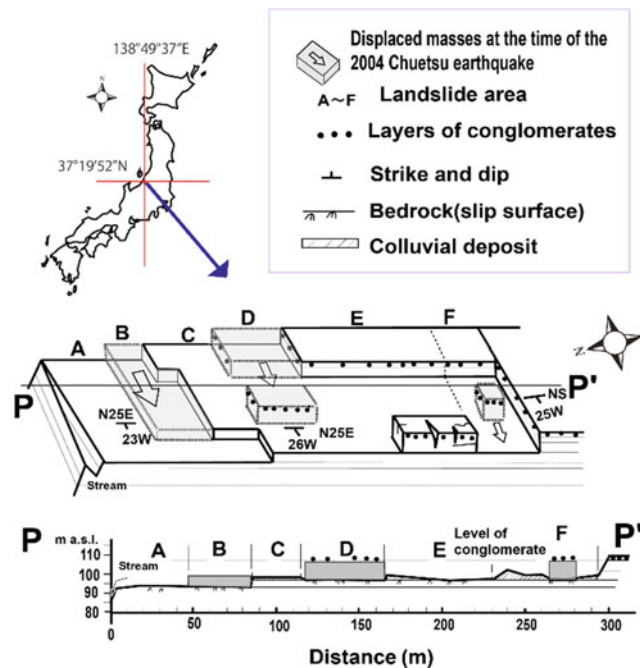
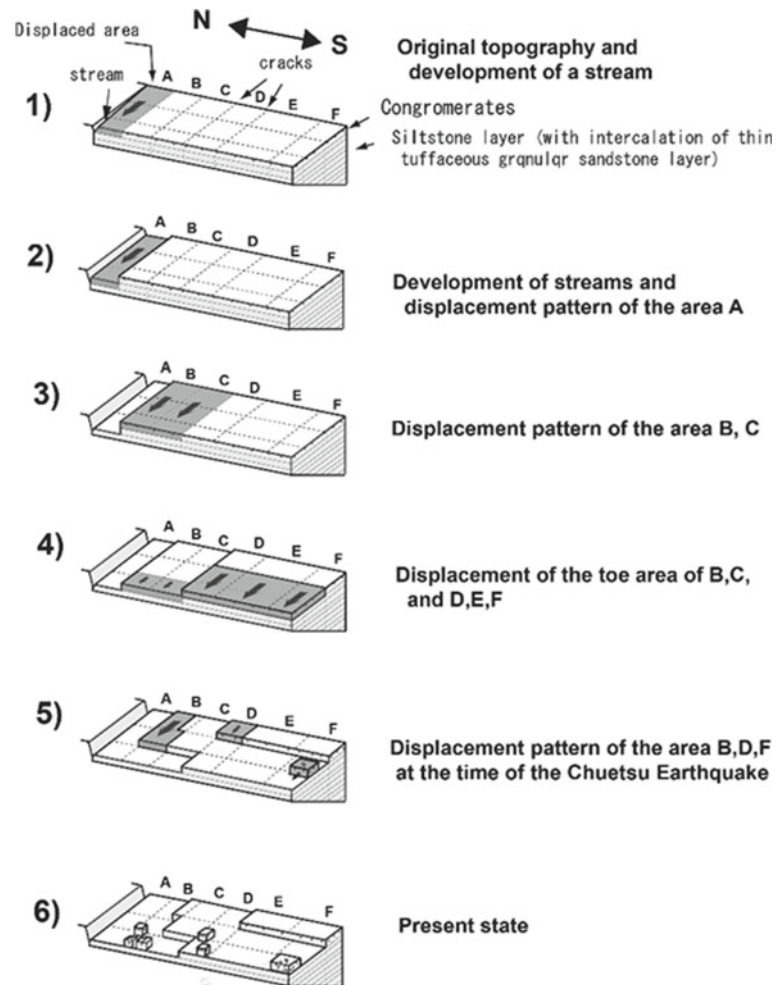


Fig. 6 Displacement model of the Yokowatashi landslide

Fig. 7 Schematic model of crack directions and the history of activity of the Yokowatashi landslide



The Chiu-Fen-Erh-Shan landslide is a 1100 m-wide, 1300 m-long translational rockslide that slid rapidly down the cuesta's back slope at a dip angle of 20 to 35°. The slide occurred in Miocene sandstone and shale formations, and its sliding surface corresponds to a transition in layering from silty mudstone to clay (Wang et al. 2003).

The Tsaoling landslide is a high-velocity translational rockslide approximately 1000 m wide and 1000 m long on the cuesta's back slope, dipping at 10 to 20°. This landslide mass is primarily Pliocene sandstone and shale, with its sliding surface on a seam of silty mudstone. The Tsaoling landslide is known to have moved four or five times after being triggered by earthquakes and precipitation (Chigira et al. 2003). At the time of our observations conducted seven years after the 1999 earthquake, about 2 m-deep longitudinal gullies had developed within the displaced material.

This cuesta landslide is rare in its cause, i.e., rainfall and earthquakes.

4 Discussion

4.1 Geological Properties and Geomorphic Features of Cuesta Landslides

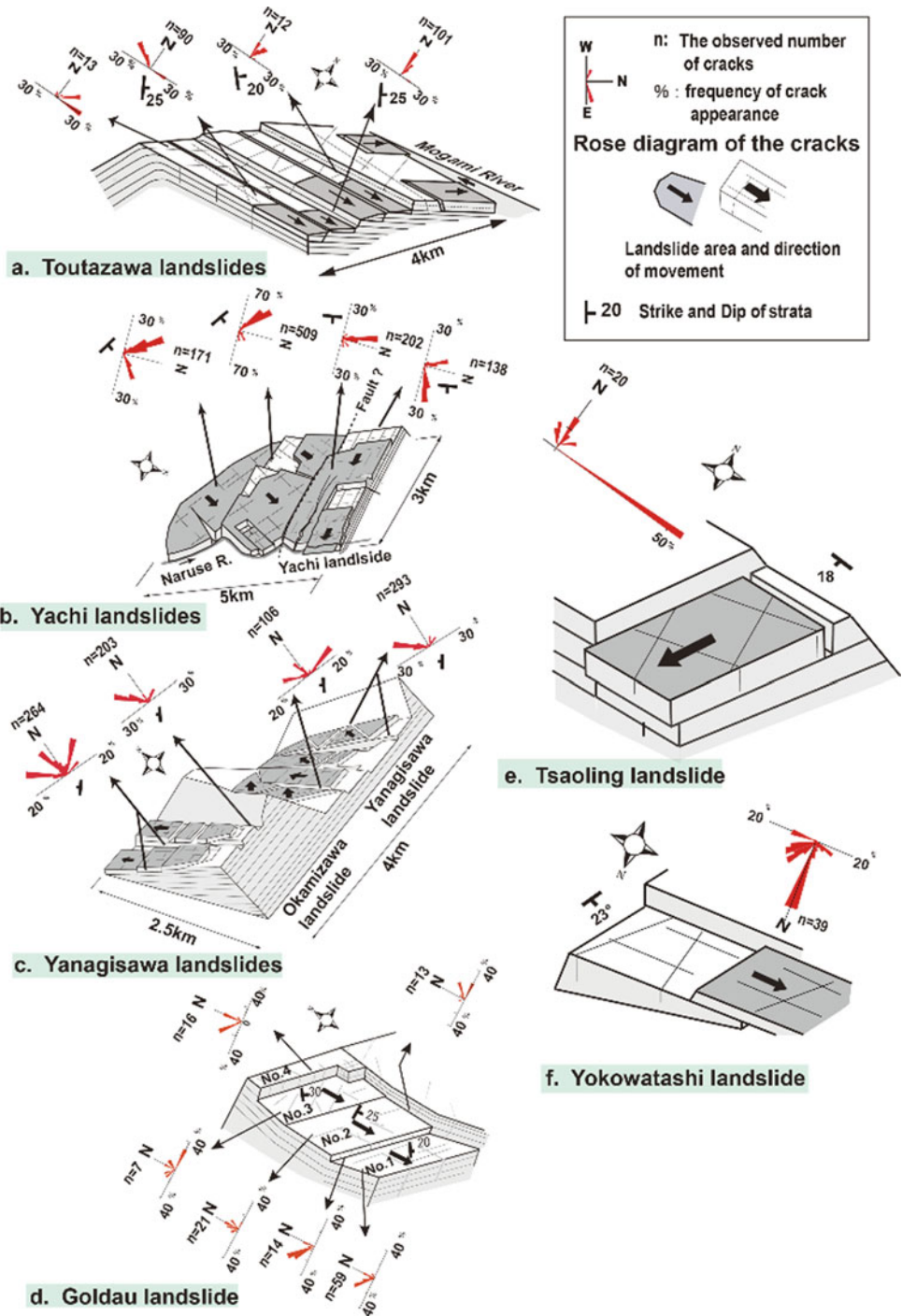
Many examples of cuesta landscapes shown in this paper are in relatively hard Neogene mudstones with intercalated layers (a few centimeters to a meter thick) of soft sandstone, mudstone, marl, or tuff. Some are in gneisses with well-developed schistosity. This feature indicates that landslides on these cuesta's back slopes occur as translational rockslides on sliding surfaces developed through the weak and thin layers of soft mudstone, marl, tuff, or sandstone. Moreover, as discussed below, the relationship between relatively systematic cracks closely related to the extent and direction of movement and occurrence history of landslides are often observed in such strata. These cracks are attributed to bedrock joints and folds as well as weathering.

4.2 Behaviors of Landslides, Dips of Strata, and Orientations of Rock Cracks

This section highlights the ranges and directions of rock-slides' movements and the relationship between the directions of valleys and the cracks in base rocks. We analyzed the directionality of the cracks in the bedrock in each landslide area (Fig. 8).

In the Toutazawa landslides, where landslide masses move toward Mogami River, the orientation of the crown scarp is constrained by an E-W trending crack, while an N-S crack constrains the flank of the landslides. The direction of movement tends to be almost identical to the direction of the maximum dip of the strata. Conversely, for landslides moving eastward, the orientation of the escarpment is constrained by a crack trending NW-SE, while NE-SW cracks

Fig. 8 Rock cracks and landslide behavior a-d: landslides triggered by rainfalls and snowmelt, e, f: earthquake induced landslides



constrain the orientation of the flank. The direction of movement of the landslide is 50–60° oblique to the direction of the maximum dip of the strata. Therefore, the cross-section of each sliding landslide mass is asymmetric, deepening toward the north (a in Fig. 8).

The Yachi landslides are divided into three areas, with the E-W trending valley as the boundary. Each area has a direction of movement that agrees with the direction of the maximum dip of the strata. The orientation of the crown scarp is constrained by NW–SE cracks (b in Fig. 8).

In the Yanagisawa landslides, the orientation of the crown scarp is constrained by an NW–SE trending crack. An N-S trending fault partially constrains the flank orientation of the landslide. The direction of movement in the Okamizawa landslide agrees with the maximum dip of the strata but is partially oblique in the Yanagisawa landslide (c in Fig. 8).

The areas of the Goldau landslide of 1806 have the orientation of the crown scarp constrained by NW–SE trending cracks. An N-S trending crack partially constrains the flank orientation of the landslide. The landslide moved toward the most significant inclination at the center. However, the greater part of the landslide mass moved south 30–40° off the maximum dip of the strata (d in Fig. 8).

The direction of movement of the Tsaoling landslide in Taiwan agrees with the maximum dip of the strata. The orientation of the crown scarp somewhat matches the direction of an E-W trending crack (e in Fig. 8). Wang et al. (2003) reported that though cracks constrained the mass movement of the Chiu-Fen-Erh-Shan landslide in the 1999 Chi-chi earthquake, the landslide mass moved toward the maximum dip of the strata.

In the Yokowatashi landslide, the orientation of the crown scarp is constrained by NE-SW trending cracks, while E-W trending cracks constrain the flank orientation of the landslide. The direction of movement of the landslide matches the direction of the maximum dip of the strata (f in Fig. 8).

These results indicate that cracks in the bedrock on the cuesta's back slopes control the orientations of the crowns/heads and flanks of the landslides. The direction of landslide movement is generally in the direction of the maximum dip of the strata when caused by earthquakes. On the other hand, when the cause is rainfall/snowmelt, the direction of movement tends to be oblique to the direction of maximum dip (Table 1).

The reasons why a landslide mass in a cuesta terrain can move oblique to the azimuth of the stratum's maximum dip are the followings:

- Difference in the azimuths of the maximum dip of the bedding plane, i.e., the slip surface and the stepwise offsets exposed on the strata.

- Difference between the river's flow direction scouring the slope toe to form a free surface at the slope's toe and that of the maximum dip of the bedding plane, i.e., the sliding surface.

In short, regardless of the direction of the maximum dip of the strata, a landslide mass tends to move towards rivers, i.e., where there are free surfaces with less resistance. Also, steps on the cuesta's backslope guide the landslide masses in their direction. Among landslides that moved off the direction of the strata's maximum dip, the landslide masses at Toutazawa and Toyomaki had asymmetric reverse triangular cross-sections.

4.3 The Behavior of Pore Water Pressure in a Landslide with a Laterally Asymmetrical Slide Surface

To understand the effect of groundwater on rain/snowmelt-induced landslides at Totazawa and Toyomaki with asymmetrical cross-sections, we focused on the Yokomichizawa B landslide at the southern end of the Toyomaki landslide (Figs. 1 and 2). We drilled six boreholes to measure the pore water pressures. The results showed that the pore water pressure was highest where the sliding surface was the deepest (Fig. 9). Unlike ordinary landslides where the increasing pore water pressure causes the effective stress over the whole sliding surface to decrease, the pore water pressure reaches its most significant value at the deepest point of the sliding surface. Since no landslide occurred during our measurement, we could not capture the movement of the landslide in relation to the pore water pressure buildup. Perhaps, groundwater drainage from the base of the reverse triangular cross-section through the drainage tunnels in the adjacent Yokomichizawa C and Toyomaki landslides certainly lowered the amount of landslide movement.

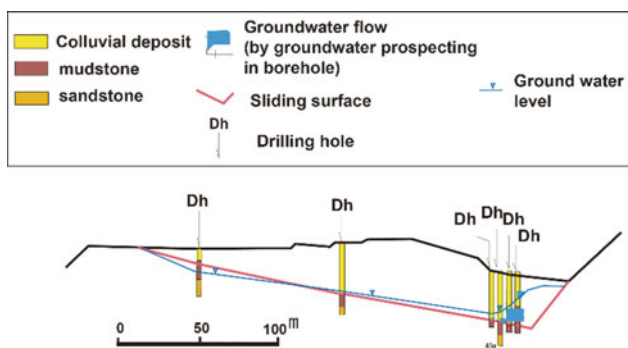
4.4 Mechanical Behavior of a Landslide on the Cuesta's Back Slope at the Time of an Earthquake

Tanaka et al. (2008) and Wakai et al. (2008) conducted 3D dynamic elastoplastic F.E.M. analyses on the Hitotsu-Minesawa landslide and Yokowatashi Landslides during the 2004 Mid-Niigata Prefecture Earthquake, where landslides are known to occur frequently. They reported that seismic acceleration was relatively high in ridges, and thus the shear stress was relatively high at the toes of these landslides.

An elastoplastic time-domain analysis was performed for the Yokowatashi landslides using MIDAS GTS for BESSRA software (Fig. 10). The underground input seismic motion for

Table 1 The characteristics of the featured landslides

Triggering factor	Country	Region	Landslide area	Slide units	Main geological property	Sliding surface	Slope angle	Relation between the slide direction and the maximum dip of the strata	Lateral topography
Rainfalls or snow melt	Japan	Hijiori	Totazawa	Totazawa others	Pliocene mudstone sandstone	Clay seam	5–20°	Cross oblique	Laterally asymmetry
			Toyomaki	Toyomaki Takamori Yokomitizawa and others	Pliocene mudstone sandstone	Clay seam	5–10°	Cross oblique	Laterally asymmetry
		Higashi naruse	Yanagisawa	Yanagisawa	Miocene hardshale	Clay seam	10–15°	Cross oblique parallel	Laterally asymmetry symmetry
				Okamizawa				Parallel	Laterally asymmetry
	Yachi	Yachi others	Clay seam	5–20°	Parallel	Laterally asymmetry			
		Swiss			Rigi	Goldau	Miocene conglomerate sandstone and marl	Clay seam	20–30°
	Nepal	Charikot	Along Tamakoshi river	Precambrian to Paleocene gneiss	Clay seam	18–25°	Cross oblique	Laterally asymmetry	
Earthquake	Japan	Tyuetsu	Yokowatahi	Pliocene mudstone sandstone	Seam of sandstone	20–25°	Parallel	Laterally symmetry	
		Tyuetsu oki	Hijirigahana	Pliocene mudstone sandstone	Clay seam	25–30°			
		Senboku	Nunomata	Pliocene mudstone sandstone	Seam of sandstone	8–10°			
	Taiwan	Nantou ken	Chiu-fen-erh-shan	Miocene mudstone sandstone	Clay seam	20–35°	Parallel Wang W.N. et al.(2003)		
		Yunlin ken	Tsaoling	Pliocene mudstone sandstone	Clay seam	10–20°	Parallel		

**Fig. 9** Cross-sectional profile and the water head level of the Yokomichizawa B landslide ((b) in Fig. 2)

the 3D model (91 m below sea level) was obtained to adjust the observed strong ground motion at the Takezawa observatory (J.M.A.) (Wakai et al. 2008). The rock sliding sequence realized in the numerical simulations was:

1. The amplified acceleration forcibly shook the cuesta ridge.
2. Shear stress was first concentrated around the toe part of the landslide mass.
3. Then the intense shear stress developed along the base of each exposed step (escarpment) of the cuesta.
4. Then rapid rockslides followed.

Applied physical value

Classification of strata	Thickness of strata		young's modulus E(kN/m ²)	Poisson's ratio γ	Internal frictional angle (ø)	Cohesion C(kN/m ²)	Unit weight r (kN/m ³)
	(m)	(GL-m)					
Flood plane sediments	5	0-5	58860	0.45	25	9.81	15.696
	25	5-30	235440	0.40	35	9.81	17.658
	50	30-80	5209110	0.30	40	981.00	19.620
	Engineering base	80-Engineering base	5209110	0.30	40	981.00	19.620
pliocene siltstone	5	0-5	117720	0.40	30	9.81	17.658
	25	5-30	1353780	0.35	35	98.10	19.620
	50	30-80	5209110	0.30	40	981.00	19.620
	Engineering base	80-Engineering base	5209110	0.30	40	981.00	19.620

Engineering base is EL-91m

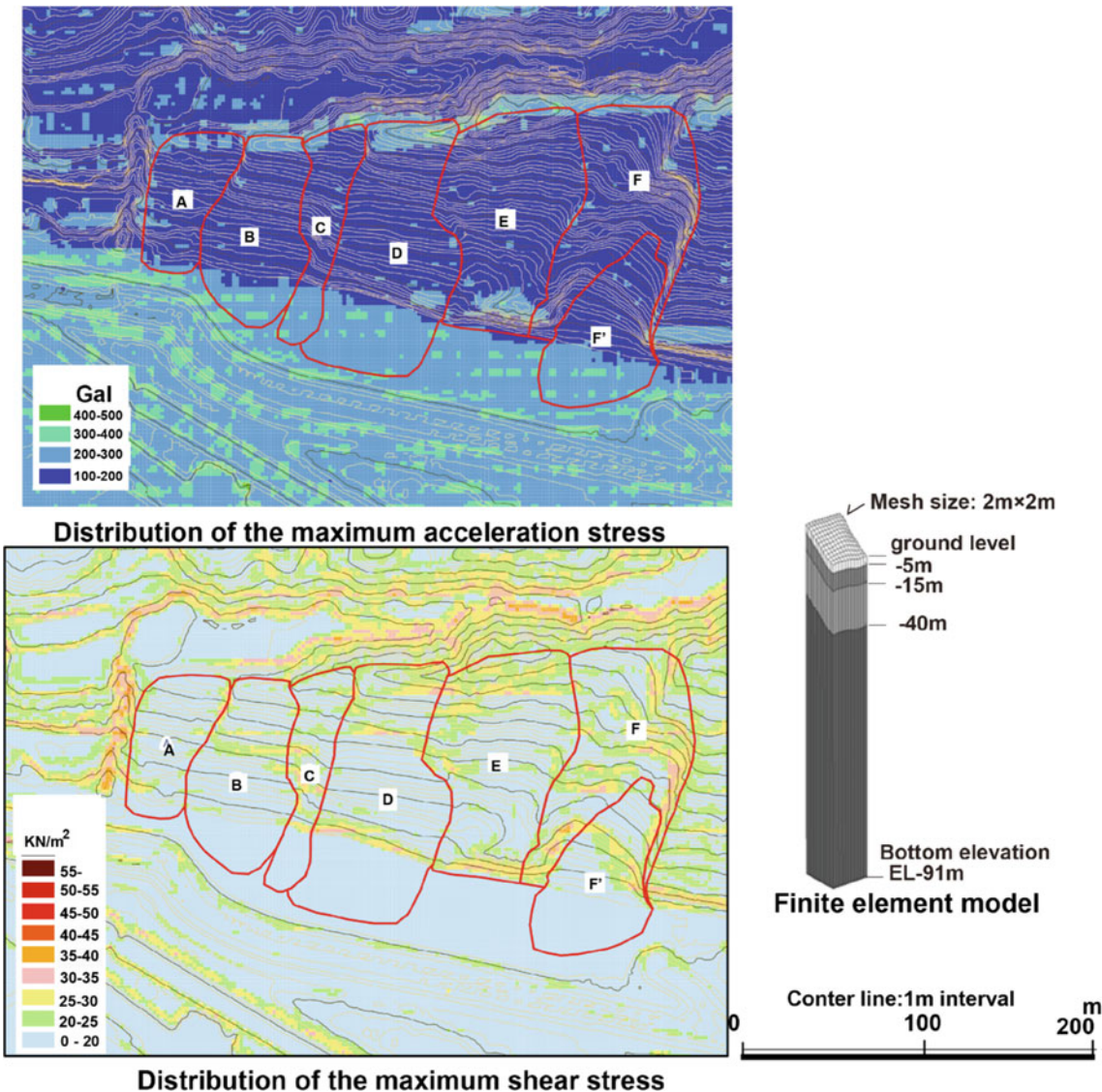


Fig. 10 The 3D dynamic elasto-plastic response FEM analysis of the Yokowatashi landslide area

As seen in the cases of Yokowatashi, Hijirigahana, and Chiu-Fen-Erh-Shan, earthquake-triggered translational landslides can leave parts of their moving masses atop the cuesta's back slopes. This finding suggests that shear stress acting at the toe and flanks of the landslide, rather than horizontal

acceleration, is most strongly associated with sliding. The step-like offset along the neighboring landslide masses' edges is essential for understanding the retrogressive sequence of sliding events (Fig. 7). The stream cutting down the northern end of the Yokowatashi landslide area likely initiated the primary landslide.

4.5 Movement of Landslides and the Cuesta Landscape

Many landslides on the cuesta's back slopes of well-developed sedimentary rock units -especially mudstone- that dominate cuesta landscapes occur as translational rockslides. These landslides touching each other can form a step-like landscape. Bedding, cracks, and stepwise boundaries of these masses can control the movements of the landslide masses, causing directions of these mass movements to differ from each other and thus affect the detaching sequence. River erosion at the slopes' toes also contributes to the landslide mass movement (Fig. 11).

As the fluvial erosion develops, retrogressive detaching of landslide masses occurs repeatedly, and intact sliding surfaces appear one after another.

When a landslide mass has an asymmetric inverse triangular transverse cross-section, underground water gathers around the deepest vertex of the triangle. Thus, the landslide initiation can differ from a generally observed landslide. Earthquake-induced large landslides on cuesta's back slopes may have repeated over a long geological time. Therefore, knowing landslide histories is an essential subject of study to be prepared for the next.

According to the current view, cuesta landscapes are the product of differential erosion. However, the cyclic processes of geomorphological evolution, i.e., the development of cracks and the consequent formation of a river, followed

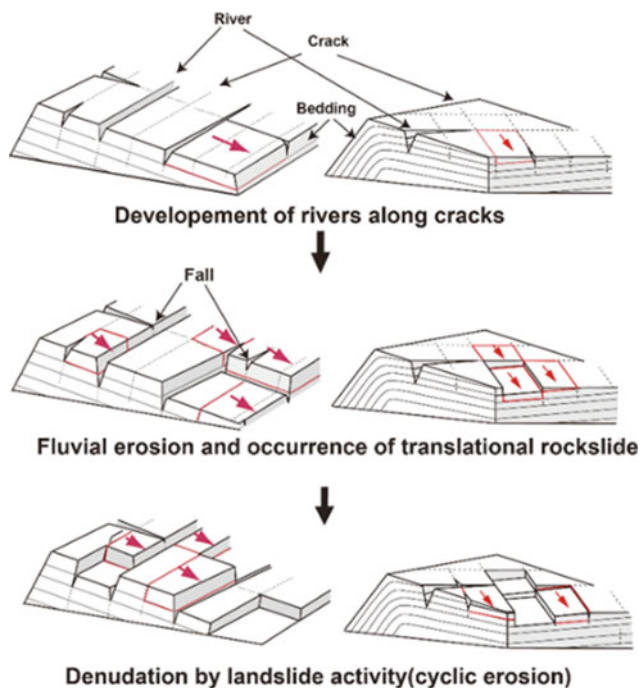


Fig. 11 Schematic models of the landslide history induced by the development of cracks and streams

by denudation and landslides, also have an essential role in the processes that lead to the formation of cuesta landscapes.

5 Conclusions

In this study, we focused on the mechanisms of landslides on the cuesta's back slopes, which are the most commonly occurring as large-scale landslides in cuesta landscapes. We also examined the role of these landslides on the geomorphological evolution of cuesta terrains. We came to the following conclusions:

1. The extents, forms, and movement directions of many landslides in the cuesta's back slopes depend on the bedding of strata, bedrock cracks, and rivers formed along the cracks. The landslides occur as slab-shaped translational slides moving on a bedding plane.
2. In general, landslides occur on slopes where the same mass moves over a long time and undergoes weathering and fracturing. Whereas most landslides on the cuesta's back slopes recur, causing an intact bedding plane to appear as a new sliding surface, thus maintaining the overall form of the cuesta's back slopes.
3. Direction of a rain/snowmelt-induced landslide mass movement often differs from the direction of the maximum dip of the strata. Conversely, an earthquake-induced landslide mass tends to move in the same direction as the strata's maximum dip.
4. When a landslide mass has an asymmetric reverse-triangular cross-section, underground water gathers the deepest vertex of the triangle, affecting the detaching process. Earthquake-induced landslides are often a sequence of detaching events of landslide masses touching each other. The sequence is affected by the river erosion of the landslide toe and intense shear forces localized at the toes and lower flanks of landslide masses.

The results suggest that these translational bedrock landslides occurring on the cuesta's back slopes have repeatedly denuded intact sliding surfaces over the long term while maintaining the cuesta landscape.

Acknowledgements We thank the Shinjo River Office of the Ministry of Land, Infrastructure and Transport for help in compiling data.

References

- Abe S, Higaki D, Dangol V (1999) Types of slope movement and their relation to geology, geological structures and topography in Central Nepal. *J Jpn Landslide Soc* 33(3):108–116 (in Japanese with English abstract)

- Abe S, Takahashi A, Satou K, Higaki D (2002) Slope evolution processes of landslides around the quaternary volcanoes in the Tohoku district, Japan. A case study in the surrounding area of the Hijiori caldera, Yamagata Prefecture. *J Jpn Landslide Soc* 38(4):10–17 (in Japanese with English abstract)
- Chigira M, Wang WN, Furuya T, Kamai T (2003) Geological causes and geomorphological precursors of the Tsaoling landslide triggered by the 1999 Chi-Chi earthquake, Taiwan. *Eng Geol* 68:259–273
- Chigira M, Yagi H (2006) Geological and geomorphological characteristics of landslides triggered by the 2004 Mid Niigata prefecture earthquake in Japan. *Eng Geol* 82:202–221
- Cruden DM, Varnes DJ (1996) Landslides types and processes, landslides investigation and mitigation. In: Turner AK, Schuster RL (eds) TRB special report 247. National Academy Press, Washington D.C., pp 36–72
- Cruden DM, Hu XQ (1999) The shapes of some mountain peaks in the Canadian Rockies. *Earth Surf Proc Land* 24:1229–1241
- Davis WM (1915) The principles of geographical description. *Ann Assoc Amer Geogr* 5:61–105
- Grozavu A, Mărgărint MC, Patriche CV (2010) GIS applications for landslide susceptibility assessment: a case study in Iasi County (Moldavian Plateau, Romania), Risk Analysis VII & Brownfields V. Wit Press, pp 393–404
- Kieffer DS, Jibson R, Rathje EM, Kelson K (2006) Landslides triggered by the 2004 Niigata Ken Chuetsu, Japan, earthquake. *Earth Spectra* 22(S1):47–73
- Kuroda K (1964) Geomorphological developments of landslide areas in Noto peninsular and other places. *Landslides Jpn Landslide Soc* 1(2):9–18 (in Japanese)
- Moriya H, Abe S, Higaki D (2008) Deformation and crushing structure of moving blocks in Tertiary hard mud stone landslides. In: Proceedings of the international conference on management of landslide hazard in the Asia-Pacific region, the japan landslide society, pp 311–322. (in Japanese with English abstract)
- Ohashi R (1915) On the earthquake of 1914 in Akita. Reports of the Imperial Earthquake Investigation Committee 82:37–42 (in Japanese)
- Petek A, Schroöder B (2010) Geomorphologic evolution of the cuesta landscapes around the Northern Franconian Alb—review and synthesis. *Zeitschrift Für Geomorphologie* 54(3):305–345
- Schmidt KH, Meitz P (2000) Effects of increasing humidity on slope geomorphology: cuesta scarps on the Colorado Plateau, USA. In: The hydrology geomorphology interface: rainfall, floods, sedimentation, land use (proceedings of the Jerusalem conference, May 1999), IAMS Publication 261:165–181
- Tainaka O (2008) Mechanism and countermeasure of the Toyomaki and the Hirane landslides, Tohoku district, Japan. In: Proceedings of the international conference on management of landslide hazard in the Asia-Pacific region, the japan landslide society, pp 266–272
- Tanaka N, Abe S, Wakai A, Kawabata H, Yoshimatsu H (2008) Occurrence mechanism of rockslide at the time of the Chuetsu earthquake in 2004—a dynamic response analysis by using a simple cyclic loading model. In: Chen et al (eds) Landslides and engineered slopes, Taylor & Francis Group, London, pp 939–944
- Thuro K, Hatem M goldau landslide event-analysis of large rockslide (2010) The 1806. In: Williams et al (eds) Geologically active proceedings of the 11th IAEG congress, pp 3693–3700. CRC Press. ISBN 978-0-415-60034-7
- Varnes DJ (1978) Slope movement types and processes. In: Schuster RL, Krizek RJ (eds) Landslides: analysis and control, transportation and road research board, special report no. 176. National Academy of Science, Washington D. C., pp 11–33
- Wakai A, Tanaka N, Abe S, Yoshimatsu H, Yamabe K, Watanabe T (2008) Large-area damage prediction system based on finite element method for risk assessment of seismic slope failure in mountains area. *J Jpn Landslide Soc* 45(3):21–32 (in Japanese with English abstract)
- Wakai A, Ugai K, Onoue A, Kuroda S, Higuchi K (2010) Numerical modeling of an earthquake-induced landslide considering the strain-softening characteristics at the bedding plane. *Soils Found Jpn Geotech Soc* 50(4):533–545 (in Japanese with English abstract)
- Wang WN, Chigira M, Furuya T (2003) Geological and geomorphological precursors of the Chiu-fen-erh-shan landslide triggered by the Chi-chi earthquake in central Taiwan. *Eng Geol* 69:1–13
- Zehnder JN (1988) Der Goldaur Bergsturz, Bergsturz museum Goldaw, p 272

Open Access This chapter is licensed under the terms of the Creative Commons Attribution 4.0 International License (<http://creativecommons.org/licenses/by/4.0/>), which permits use, sharing, adaptation, distribution and reproduction in any medium or format, as long as you give appropriate credit to the original author(s) and the source, provide a link to the Creative Commons license and indicate if changes were made.



The images or other third party material in this chapter are included in the chapter's Creative Commons license, unless indicated otherwise in a credit line to the material. If material is not included in the chapter's Creative Commons license and your intended use is not permitted by statutory regulation or exceeds the permitted use, you will need to obtain permission directly from the copyright holder.



Application of Spectral Element Method (SEM) in Slope Instability Analysis

Ram Chandra Tiwari and Netra Prakash Bhandary

Abstract

Spectral element framework for slope instability analysis includes Spectral Element Method (SEM) formulation, system requirements for serial and parallel computations, model preparation with hexahedral meshing in Cubit or Trelis, meshing and mapping technique (h- and p-refinement techniques) according to SEM, applying boundary conditions for 2D and 3D, defining inputs for material model, ground water table, seismic loading as well as processing and visualizing the results in Tecplot and ParaView. Within this framework, the safety factor in slope stability is computed and visualized with greater spectral accuracy and stability.

Keywords

Spectral element method • Slope • Stability

1 Introduction

Spectral element method (SEM) along with meshing and mapping technique is discussed by Patera (1984), Canuto et al. (1988), Serini (1994), Faccioli et al. (1997), Komatitschi and Vilotte (1998), Komatitsch and Tromp (1999), Peter et al. (2011), Gharti et. al. (2012) and Tiwari et al. (2013), and so on. In this article, we introduce and discuss SEM techniques and tools required for the use of a SEM program called ‘Specfem_Geotech’ developed by Gharti

R. C. Tiwari
Department of Civil Engineering, Institute of Engineering,
Tribhuvan University, Pulchowk Campus, Lalitpur, Nepal
e-mail: rct2075ce_rctiwari@pcampus.edu.np

N. P. Bhandary (✉)
Department of Environmental Design, Faculty of Collaborative
Regional Innovation, Ehime University, Matsuyama, 791-8577,
Japan
e-mail: netra@ehime-u.ac.jp

et al. (2011, 2012). This program is parallelized using message passing interface (MPI) according to Gropp et al. (1994) and Pacheco (1997), based on the domain decomposition method and implements open-source graph partitioning library ‘SCOTCH’ to separate the domain according to Pellegrini and Roman (1996). The program employs some of the codes from the ‘Programming the finite element method book’ written by Smith and Griffiths (2004) and the element-by-element preconditioned conjugate gradient method according to King and Sonnad (1987) and Barragy and Carey (1988) to solve linear equations. The Mohr–Coulomb failure criterion in the visco-plastic strain method has been implemented as per Zienkiewicz and Corneau (1974). Along with these techniques and tools, the meshing tool ‘Cubit’ or ‘Trelis’ (www.cubit.sandia.gov) is used for hexahedral meshing, and visualization tools like ‘Tecplot Focus2016R1’ (www.tecplot.com) and ‘ParaView’ (www.paraview.org) are used to visualize the results in 2D and 3D. The following numerical tools are used to compute safety factor in slope instability analysis (Table 1).

2 SEM Approach

The FEM (i.e., Finite Element Method) is not efficient to integrate high-order polynomial equations and demands a more sophisticated computing facility since it requires solving a whole mass matrix. Fine meshes are required for the numerical convergence and consideration of progressive failure also demands an increased number of iterations. In this context, a high-order FEM, known as SEM, is employed to evaluate the stability of slopes.

SEM employs nodal quadrature, namely, Gauss-Legendre-Lobatto quadrature. In nodal quadrature, interpolation nodes coincide with integration points. The coincidence of integration and interpolation points has two main advantages: (1) interpolation is not necessary to determine nodal quantities from quantities at quadrature points and vice-versa, thus

Table 1 Numerical tools employed for SEM program

Stage	Tool	Function
Input	Cubit or Trelis	Create 3D model Create and refine mesh Assign boundary conditions Export to Exodus file format
Processing	Cygwin, Scotch, MPI/openMPI Specfem3D_Geotceh	Cygwin: to simulate Unix environment within Windows Scotch: graph partitioning MPI: message passing interface for parallel simulations Specfem3d_Geotech Converts Exodus to ASCII Input format Performs all computations
Output	Tecplot Focus2016R1 ParaView	Tecplot: preparation of various charts in 2D and 3D ParaView: visualization of stress and displacement contours in 3D

simplifying the computation of the stiffness matrix, strain, stress, etc. and (2) interpolating functions become orthogonal on quadrature points, resulting in a diagonal mass matrix, thereby simplifying the time-consuming algorithm (Fig. 1). SEM method adopts the geometric flexibility of finite elements and implements high order polynomial equations, which lead to high numerical stability as well as reliable spectral accuracy in less computing time.

3 Model Tests

3.1 H-Refinement

H-refinement refers to the change in the mesh size of a numerical model. In FEM, the H-refinement technique is

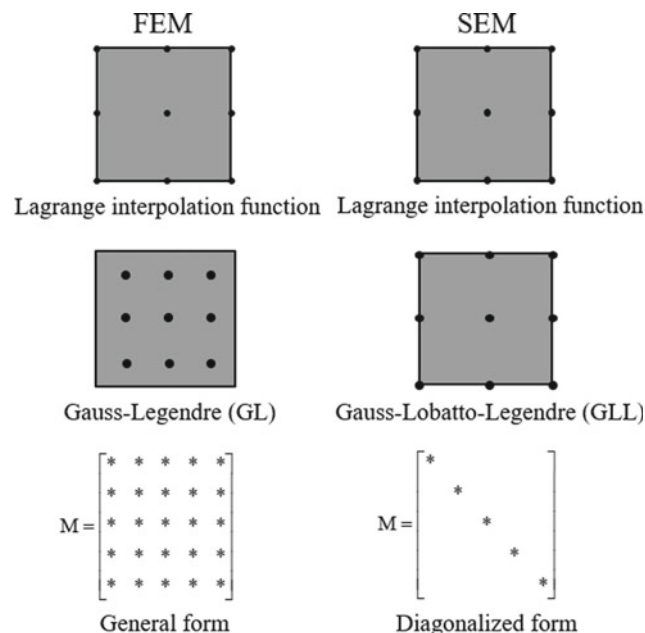


Fig. 1 Comparison between FEM and SEM

often employed in the region having irregular geometry. However, Cubit/Trelis does not have the ability to refine mesh in a particular region. Hence, the mesh size of the entire model is varied and tested for variation of factor of safety (FOS) and computation time. The H-refinement technique is shown in Fig. 2, and the models with varied mesh sizes (i.e., Element size: 2–4 m and Elemental budget: 1968–268 Nos.) are illustrated in Fig. 3a–d. The overall SEM approach is shown in Fig. 4, which also includes numerical tests. Spectral and elastoplastic tests are also indicated. The spectral test includes (1) modelling domain, (2) boundary condition, (3) h- and p-refinement, and (4) spectral accuracy while the elastoplastic test includes phi-nu inequality, elastic modulus, poisson’s ratio, and material dilation.

To evaluate the stability of landslide slopes the numerical scheme shown in Fig. 4 needs to be followed. The numerical and computational scheme accommodates hexahedral meshing and mapping techniques along with material and model preparation.

The results from the H-refinement test are shown in Table 2 and Fig. 5.

The test showed that a mesh size of 2.5 m yields factor of safety (FOS) accurately with the least computation time. Hence, a mesh size of 2.5 m has been adopted in batch processing.

3.2 P-Refinement

Accurate numerical computation can be varied by varying the degree of the polynomial of the shape function. A P-refinement test is performed to determine the GLL value that yields FOS with reasonable accuracy with the least computation time. The mapping technique in SEM is shown in Fig. 6.

The results obtained from the test are as illustrated in Table 3 and Fig. 7.

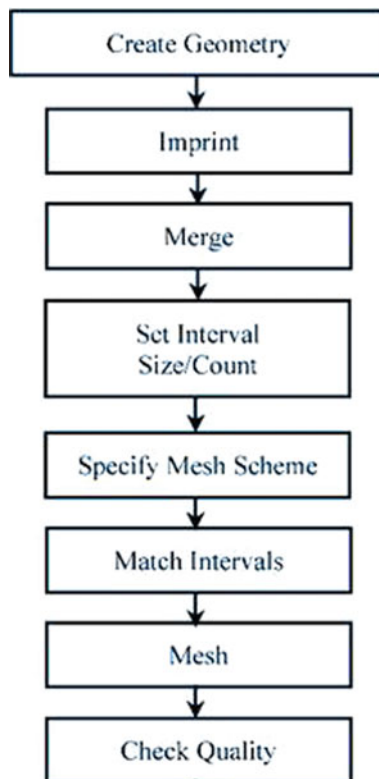


Fig. 2 Spectral meshing technique (as per Tiwari et al. 2013)

3.3 Partitioning

To understand the effect of parallel processing on computation time, a domain having 2568 elements is decomposed

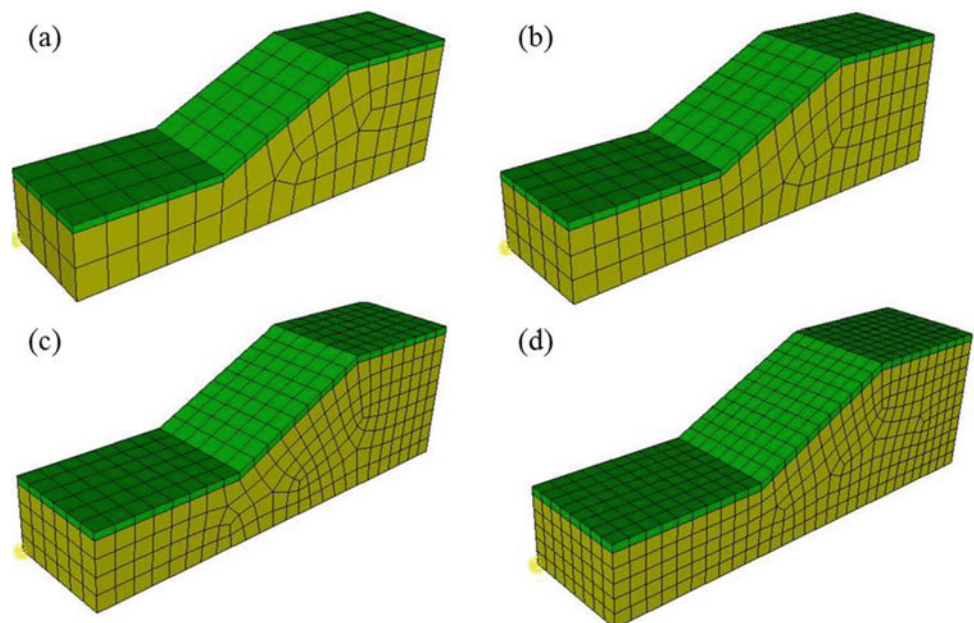
into various partitions, as visualized in Fig. 8. Domain is decomposed such that the number of partitions is equal to the number of cores intended to be used for simulation. The results obtained from the simulation are shown in Table 4 and Fig. 9.

From the P-refinement test, GLL 3 was found to yield FOS with reasonable accuracy in the least time. Hence, GLL 3 was adopted batch processing.

Figure 9 shows that parallel processing is significantly faster than serial processing. There is almost a one-fourth reduction in computation time while using four cores as compared to a single core. However, the rate at which the computation time decreases onwards is very gradual. Hence, an increase in the number of processors does not necessarily mean a reduction in computation time. It depends on system configuration and must be tested independently for each system for optimum results.

Procedure for the computation of factor of safety for all the model combinations is carried out as shown in the flow charts below (Figs. 10 and 11). The procedure is divided into two stages. In the first stage, the basic slope models are prepared and various tests such as H, P refinements, and quality checks are performed in the local PC. Once the models are found suitable for the purpose of computation of FOS, they are uploaded to the server. The codes are executed in the order as shown in the flowcharts to generate the simulation files for Specfem3D_Geotech, to generate a batch file for the execution of the simulation, and to extract FOS after all the simulations are completed. Figures 10 and 11 show respectively the detailed procedure followed on a local PC and a server.

Fig. 3 Model showing various elemental size and budget:
a element size 4 m numbers 268,
b element size 3 m numbers 550,
c element size 2.5 m numbers 1074, and
d element size 2 m number 1968



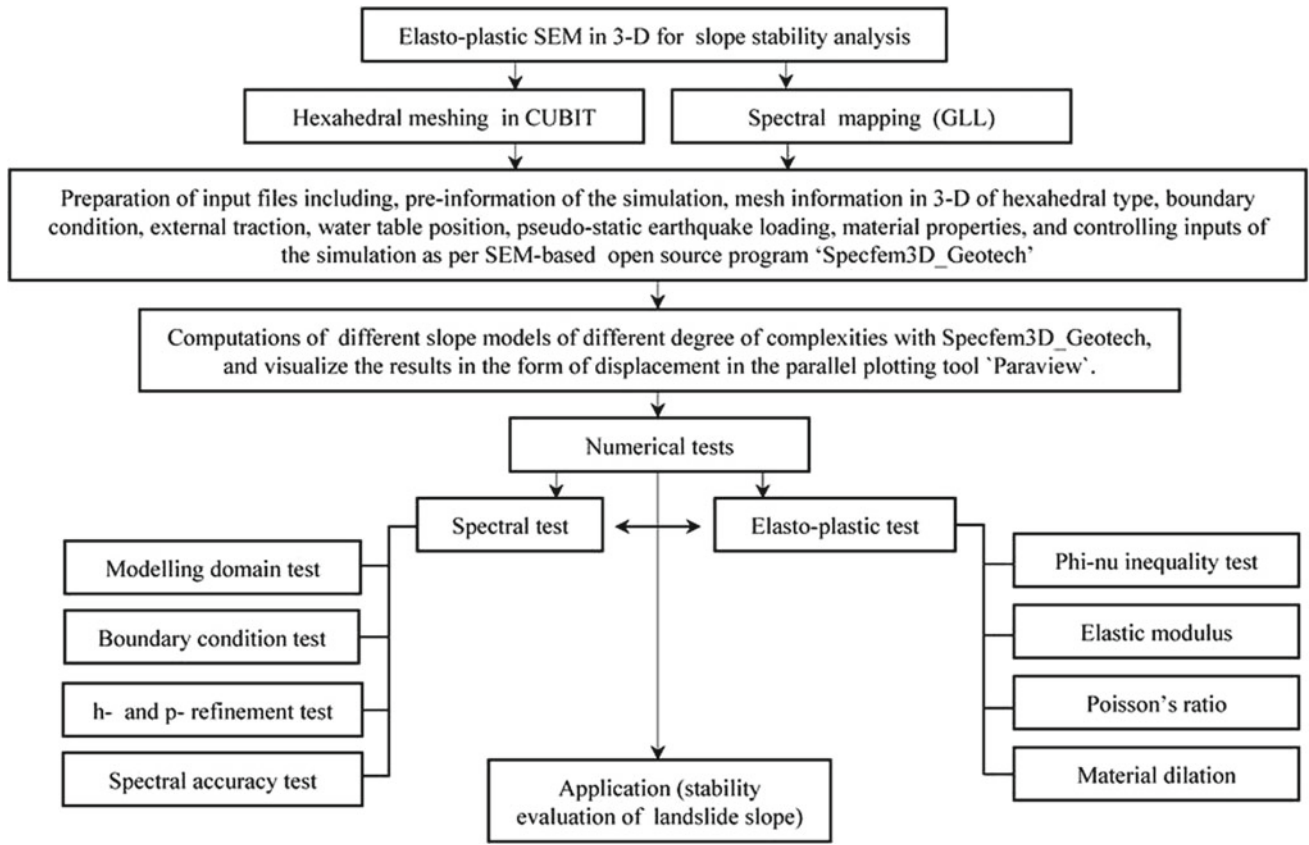


Fig. 4 SEM approach with Specfem3D_Geotech

Table 2 Computation time for various element budget

Element size/number	2 m (1968)	2.5 (1074)	3 m (550)	4 m (268)	5 m (135)
Time (seconds)	4995	2439	915	334	250

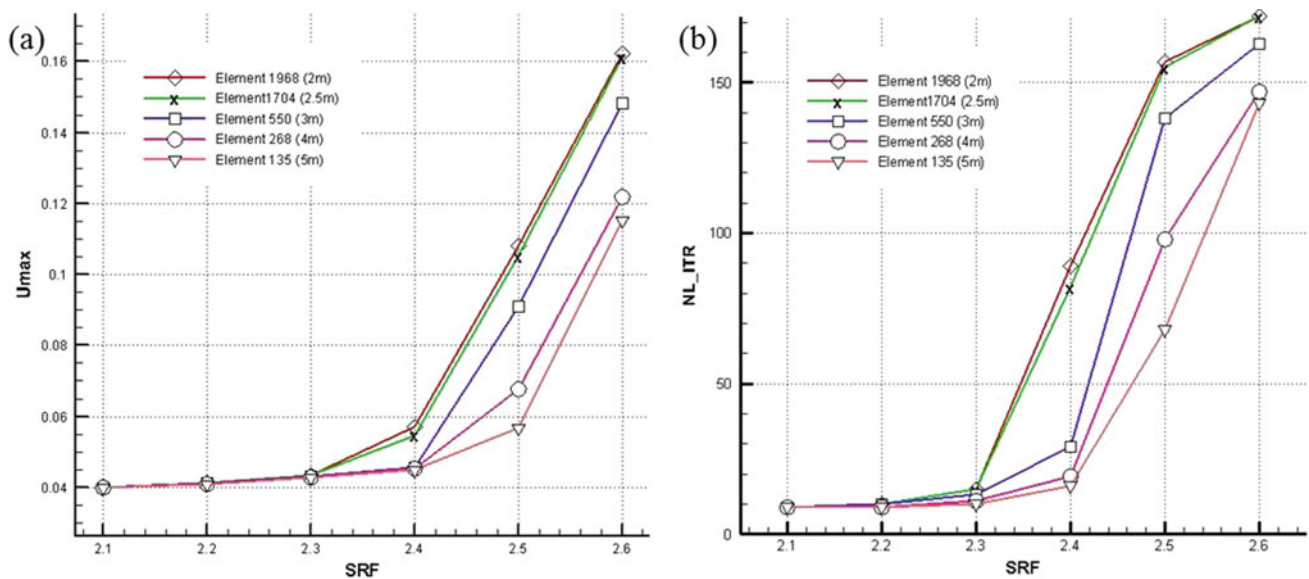


Fig. 5 H-refinement tests: a Umax versus SRF and b NL_ITR versus SRF

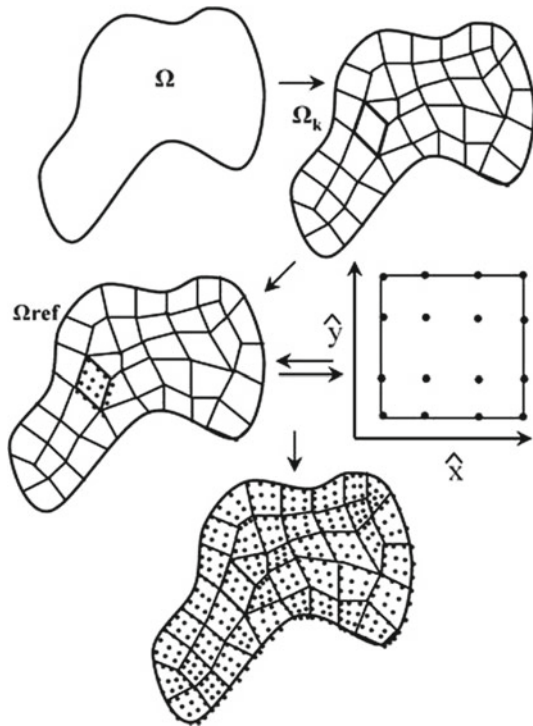


Fig. 6 Spectral mapping techniques (Tiwari et al. 2013)

Table 3 Variation of computation time with GLL points

GLL	2	3	4	5
Seconds	3.8405	132.4453	2419	24,180

The function of each code is listed below:

- Code-1: Generates simulation files Specfem3D_Geotech, generates batch file to execute all simulations without human intervention.
- Code-2: Checks the results of the completed simulation and determines if models have undergone plastic deformation. Generates Batch file for the models that are yet to undergo plastic deformation.
- Code-3: Extracts FOS from the results and generates Charts for Tecplot focus2016R1 or Tecplot 360 for all models.

In this method, we have employed strength reduction technique to get critical value of factor of safety (Griffiths and Lane 1999; Chen et al. 2007). Stability by strength reduction is a procedure where the factor of safety is obtained by weakening the soil in steps until the slope “fails.” The factor of safety is deemed to be the factor by which the soil strength needs to be reduced to reach failure. This method allows systematic reduction in soil strength by

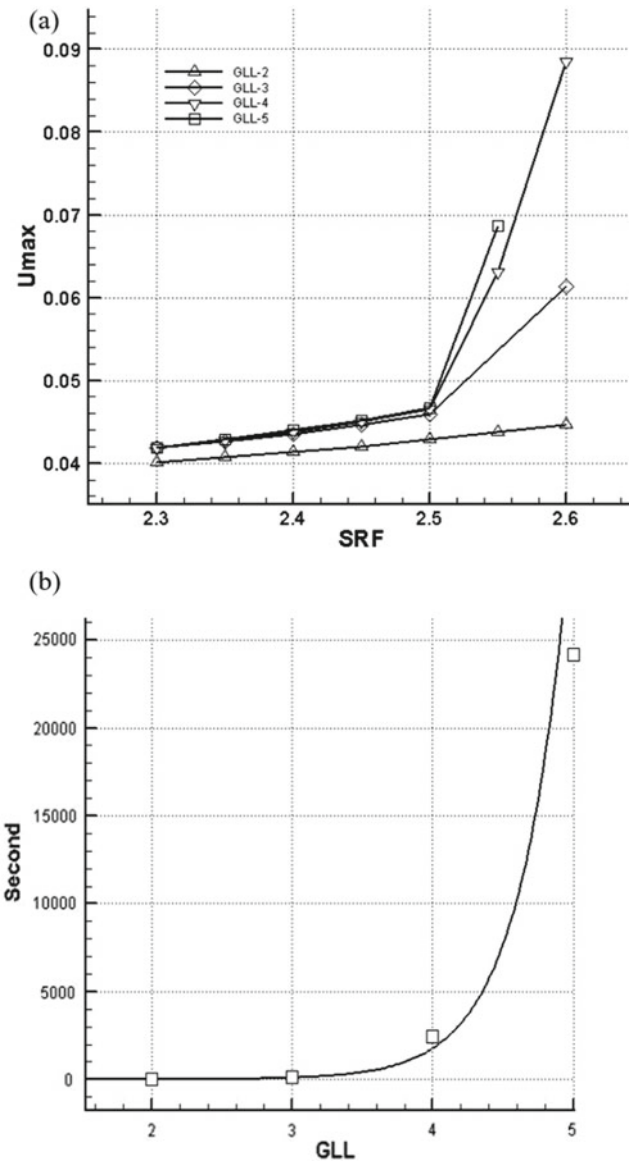


Fig. 7 P-refinement tests: **a** SRF versus displacement at various GLL points and **b** variation of computation time with increase in GLL points

introducing SRF to reduce the frictional and cohesion component of shear strength of the basic equation of $\tau = \sigma \tan \phi' + c'$.

$$\phi'_f = \tan^{-1} \left(\frac{\tan \phi'}{\text{SRF}} \right) \quad (1)$$

$$c'_f = \frac{c'}{\text{SRF}} \quad (2)$$

where, ϕ'_f and c'_f are known as reduced angle of internal friction and cohesion. In this method, a nodal displacement is significantly observed at a failure point and the points after failure initiation need several iterations to converge to a

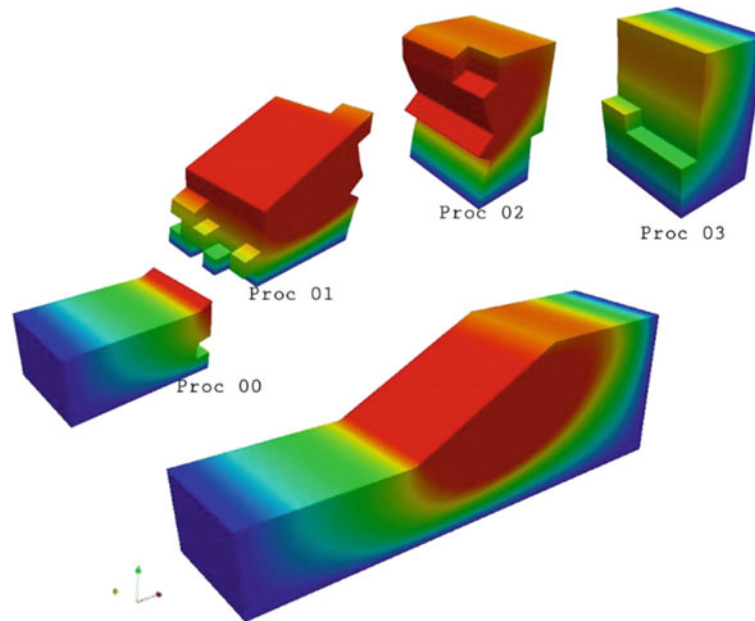


Fig. 8 Domain decomposition for 4 cores visualized using ParaView

Table 4 Variation of computation time with the number of processors (Pro(s)) employed

Pro (s)	1	4	8	16	20	24
Seconds	724.8906	200.0078	138.9648	106.3828	98.9352	106.6576

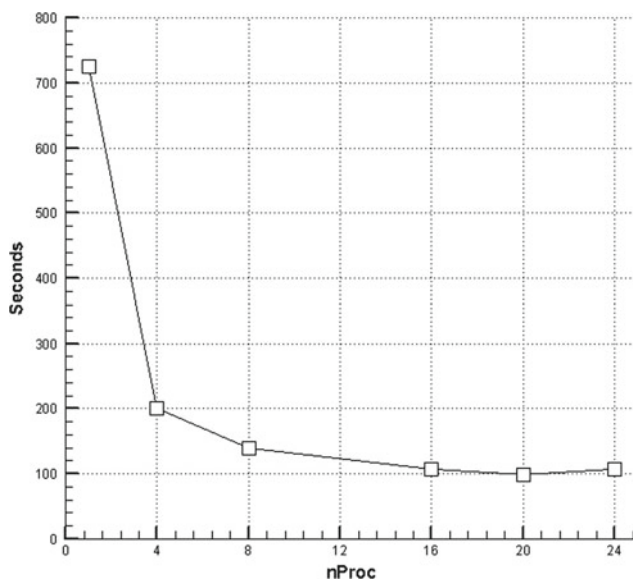


Fig. 9 Computation time with no. of processors

solution. Boundary conditions have significant effects on stability of slopes. FOS varies as per boundary conditions. In general, there are four kinds of boundary conditions (Fig. 12).

- (1) Vertical rollers at left, right as well as front and rear faces, and fixed boundary at the bottom face,
- (2) Vertical rollers at left, right, and rear faces and fixed at front and bottom faces,
- (3) Vertical rollers at left, right, and front faces and fixed at rear and bottom faces, and
- (4) Vertical roller boundary at left and right faces and fixed boundaries at front, rear, and bottom faces.

4 Modeling with Specfem3D_Geotech

It is a free and open-source command-driven program for 3D landslide slope stability analysis based on the SEM. The program can run in a serial and parallel or in multi-core machines or in large clusters. The program is written in FORTRAN 90 and parallelized using message passing interface (MPI or openMPI) based on the domain decomposition method. The open-source graph partitioning library SCOTCH is used for the domain decomposition. This program does not have inbuilt meshing. It does not automatically determine the FOS of slope stability. After plotting the series of safety factors versus maximum displacement, FOS can be determined for the given slope.

4.1 System Requirement

To run the serial and parallel version of Specfem3D_Geotech program, Linux working environment is required by

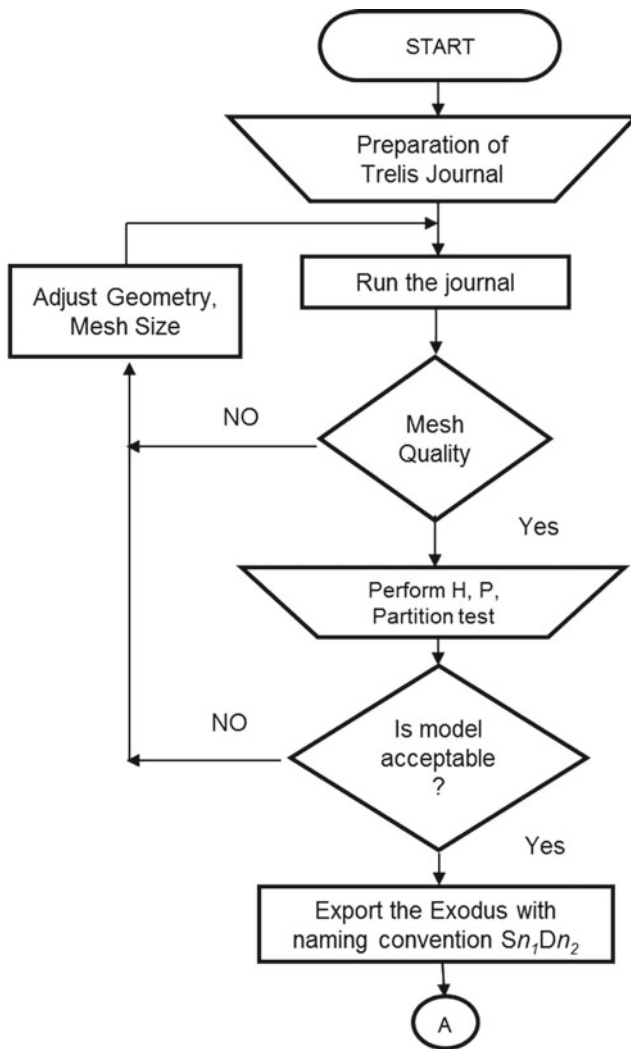


Fig. 10 Procedure carried out on a local PC

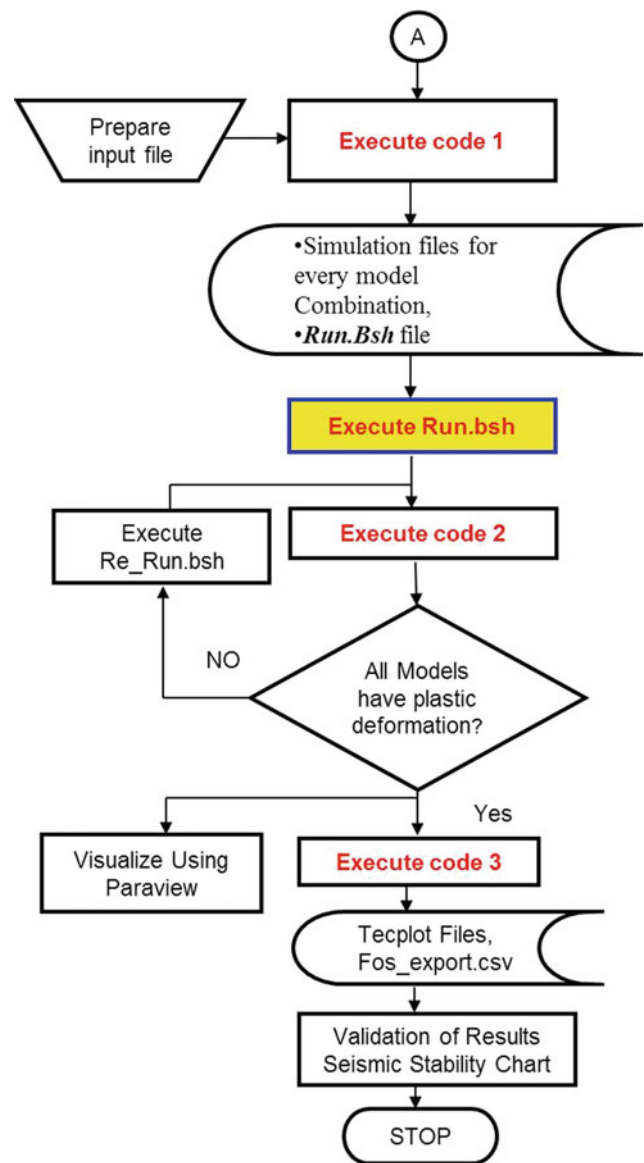


Fig. 11 Procedure carried in server

either installing Cygwin program on computer of window operating system or making Linux operating system. While installing the Cygwin, the following platforms are selected accordingly (www.cygwin.com).

- Base (automatically selected)
- Gcc-core-GNU Compiler collection (C, openMP)
- Gccfortran
- Make-The GNU version of make utility
- Automake 1.10
- Openssl-openssl
- Openssl-devel
- Openssl100
- Ssh-(autossh, libssh2-devel, libssh2_1, openssh)
- Vim-(gvim, vim and vimcommon)
- Scp
- Ftp-(lftp, tftp, tftp Server)
- Shell-xterm-emulator and
- Utilities-cygutilities

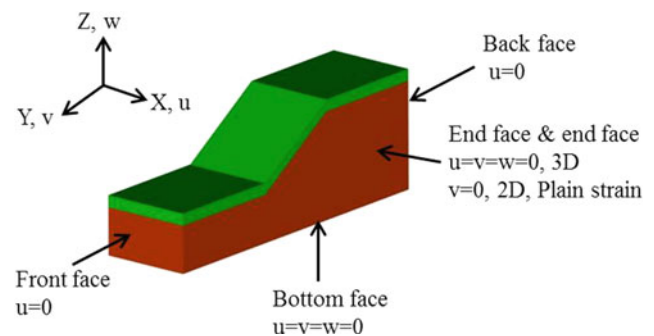


Fig. 12 Boundary conditions for 2D and 3D problems in slope stability analysis

To assure the correct installation, type 'gfortran' in a command prompt and make sure that there is a display of text 'no input found.' If Command prompt does not display such text, the program is not installed correctly.

4.2 Model Preparation

Exact topography is needed to make a realistic model. The surface complexity of the model depends on the contours available. Therefore, contours of the suitable interval must be chosen to simplify the model. A total station survey would be good enough to capture the detail topographic features by producing contours of suitable intervals of the area. Based on those contours, both 2D and 3D models are prepared. If there is no such case of doing a topographic survey and producing exact contour maps, topographic data can be explored from Google Earth or any other similar tools and techniques.

4.3 2D Models

Following three steps must be followed to prepare 2D models.

- (1) Extracting the topographic data from Google earth. To extract topographic data from Google earth, following steps must be followed.
 - (i) Create path in Google Earth within the study area (set distance in meter),
 - (ii) Name the drawn path in step (1) and click on 'ok'
 - (iii) Right click on the path of temporary location and save as my places in '.kml' format in required location (for example: Jure.kml, Jure landslide, Sindhupalchowk, Nepal (27° 46'1.55" N latitude and 85° 52'17.10" E longitude))
- (2) Save extracted '.kml' file to '.csv'

To save the extracted '.kml' file to '.csv,' following steps must be followed.

 - (i) Open TCX converter,
 - (ii) Open the file in TCX converter (open Jure.kml),
 - (iii) Click on track modify and then update altitude (the altitude initially shows zero value after updating the RL above mean sea level appears), and
 - (iv) Export the file in '.csv' format (for example: Jure.csv).
- (3) Preparing model in AutoCAD CIVIL3D

The 2D models must be prepared in AutoCAD CIVIL3D program in the following manner.

 - (i) Open AutoCAD CIVIL 3D,

- (ii) Import the file in keep point format NEZ (The latitude and longitude degree should be multiplying by 111000 m) (Zoom extents if imported points not visible),
- (iii) Create TIN surface,
- (iv) Add points to surface and manage surface properties to display the contour interval,
- (v) Create alignment with alignment creation tools. We created left section (1-1), Middle (2-2), Right (3-3) in case of Jure landslide,
- (vi) Create profile,
- (vii) Draw polyline above profile line. Draw the closed polyline as per the required strata of the model,
- (viii) Move the polyline drawn in step (vii) to the origin, and align with 'xz' face by rotation, so that it is easier to give dimensions,
- (ix) Extrude the 2-D surface to required depth and
- (x) Save the solid extruded volume to ASCII '.sat' format (for example: Jure.sat).

4.4 3D Models

To create 3D model, three major steps of 2D model i.e., (1) Extracting the topographic data, (2) how to save extracted data and (3) model preparation in AutoCAD CIVIL3D up to 1–4 steps each would be same and then follow the following steps:

- (1) The prepared surface is in 3D surface, view it in different styles like isometric or any custom view by 3D orbit rotator,
- (2) Choose the contour interval accordingly as the size of the study area (for example 20 m intervals in Jure landslide),
- (3) Draw splines over contour with best fit,
- (4) Copy the drawn contour to the new location, visualize them and found match with original contour, Creates the surface of the contours with loft command. Select cross-section only for lofting option,
- (5) Use thicken command to convert surface to volume (Because the import of cubit should be volume object and .sat format),
- (6) Then draw a box using 'BOX' command of exact model size (The model size should be less than counter surface to operate subtract command),
- (7) Move the box to volume created so that volumes clearly intersect the box,
- (8) Use 'SUBTRACT' command to subtract volume created in '7' from the box (1st select the box and then the volume),

- (9) Then use 'SEPARATE' command to separate the subtracted volume,
- (10) Delete the upper surface,
- (11) Extend the box in z-direction to get the model according to the required depth of the model,
- (12) Move the object or align the object with co-ordinate (0, 0, 0) with front face left side bottom vertex as origin and
- (13) The model prepared in AutoCAD 3D is exported to '.SAT' file format.

4.5 Models in Cubit/Trelis

The process of preparing 2D and 3D models in Cubit is more or less similar except in selecting their boundary conditions. The 2D model can also directly be prepared in Cubit if (x, z) coordinate of each profile points are known. The easiest way to prepare model here would be by creating solid model in AutoCAD in the following manner (Figs. 13 and 14).

- (1) The SAT file prepared in AutoCAD 3D is imported in cubit (Jure.sat) and
- (2) To prepare meshable body and to check mesh quality, following works must be done.
 - (i) Run heal analyzer to remove invalid topology,
 - (ii) Remove small surfaces,
 - (iii) Modify blend surfaces,
 - (iv) Decompose volume,
 - (v) Set sources and targets and
 - (vi) Force sweep topology.

Above work can be done from power tool, command panel and command line. Next steps of this process are as follows.

- (3) 'Imprint all' command merges all for sharing of same surface if adjacent volume,
- (4) Meshing operation can be done with the following steps: command panel—meshing—volume—intervals—selecting volume—constant size and giving the size of mesh,
- (5) To check mesh quality, following steps would be followed: command panel—meshing—volume—mesh quality—quality metrics—selecting volume—quality metric (shape)—picking the choice display graphical summary,
- (6) By seeing the graphical summary of the mesh quality, number of mesh of that quality, we decided the way to decompose the model i.e., orientation of cutting,
- (7) To decompose the volume, there is a different method of cutting in Cubit: command panel—volume—web

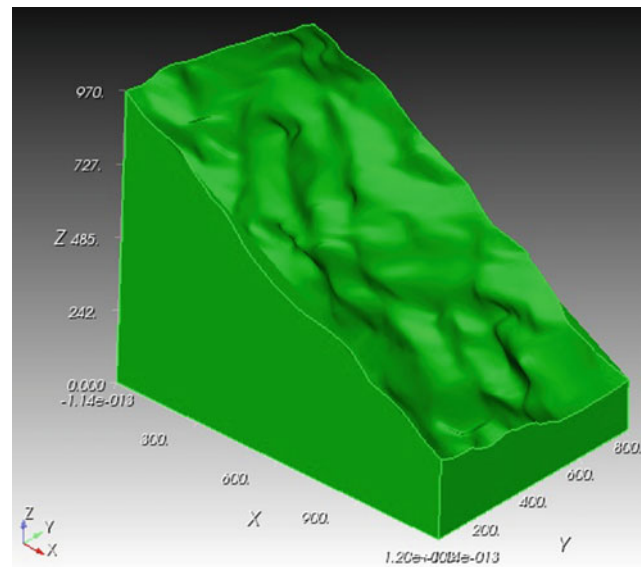


Fig. 13 3D Model of Jure, Sindhupalchowk landslide without Meshing (27° 46'1.55" N latitude and 85° 52'17.10" E longitude)

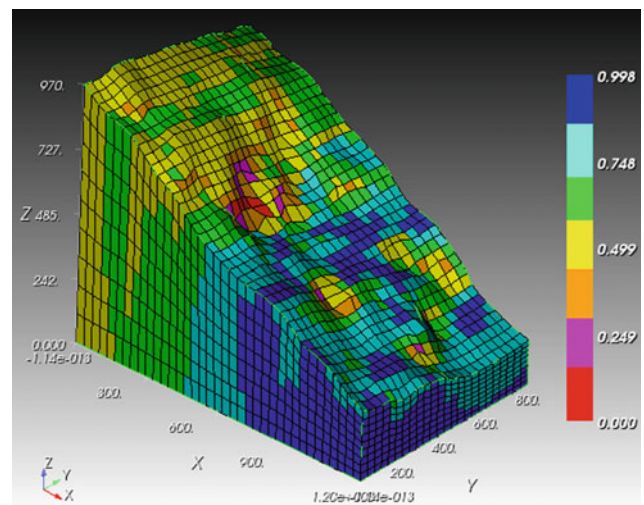


Fig. 14 3D Model of Jure Sindhupalchowk landslide with Meshing (27°46'1.55°N latitude and 85°52'17.10°E longitude)

cut: we use the various web cut method according to suitability of orientation and location of cutting plane,

- (8) If the mesh quality is not found good enough then steps 5–7 would be repeated with different meshing and mapping scheme,
- (9) Then do 'Compress all,'
- (10) Then, define all volumes of blocks,
- (11) Define surfaces as sideset for the implementation of boundary condition,
- (12) Define boundary condition according to the real field scenario.

- (13) Then the model is exported as exodus file (.exe) to Directory/text/utilities and saved as .e file.

The SEM program reads text files only. The exodus files from Cubit/Trelis need to be changed to a text file. Then, the .SEM file is edited as per requirement according to process mentioned in editing .SEM file.

Figure 14 shows the hexahedral meshing in the 3D domain along with quality meshing and mapping. Inaccuracy of the result and termination of the program is mainly due to the lack of quality meshing and mapping. Thus, h- and p- refinement techniques are employed to limit the numerical and computational errors. The numerical and computational stability can only be achieved if proper h- and p- refinement efforts have been employed in the model.

5 Inputs for Specfem3D_Geotech

5.1 Material Properties

The material model is prepared with six soil parameters. They are gamma, γ_m , ν , ϕ , c , and ψ . Here, 'gamma' is the unit weight of the soil, ' γ_m ' is the Young's Modulus of soil, ' ν ' is the Poisson's ratio, ' ϕ ' is the angle of internal friction of soil, ' c ' is the cohesion coefficient, ' ψ ' is the dilation angle.

5.2 Ground Water Table (GWT)

To prepare the input file of ground water table, position of GWT at borehole locations should be identified.

5.3 Seismic Input

The horizontal seismic acceleration in Nepal varies from 0.1 to 0.5 g. Direction of acceleration may vary with respect to the orientation of slope. After the completion of computations, '.case' and 'summary' files can be viewed in Tecplot and Paraview. Tacplot and Paraviews are the powerful visualization tools for 2D and 3D.

5.4 Output Visualization

The output of the SEM program can be visualized in different forms .DAT file is prepared based on summary file in the form of 'SRF,' non-linear iterations (NL_ITERs) (numbers) and maximum displacement (UMAX) (m). DAT

file is then opened to Tecplot focus2016 R1 program to plot the graph of SRF versus maximum displacement and SRF versus NL_ITERs. Scaling and sizing different features of graph are edited with various tools as per requirements.

The factor of safety is then determined as per the judgment on critical factor of safety. The critical value of SRF is a point where displacement is abruptly changed to maximum. It can be further correlated with non-linear iteration. At certain SRF, the non-linear iteration is also suddenly changed to maximum value. The factor of safety is then interpreted with different variables like dry condition, fully saturated conditions, and seismic motion condition. The progressive failure can be visualized in 3D visualization tool Paraview by opening '.case' files. The results can be captured or exported to '.jpg' file format.

Tacplot is used to visualize results in 2D. Data management and further editing, if any, would be possible in Tacplot focus program. As an example, notepad or text file '.txt' can be prepared in for two variables: (1) strength reduction factor (SRF) and (2) maximum Displacement (m). SRF varies from 0.1 to 1.2, altogether inserted 12 values in case first. Similarly, displacement values in each SRF are needed in each case of modeling.

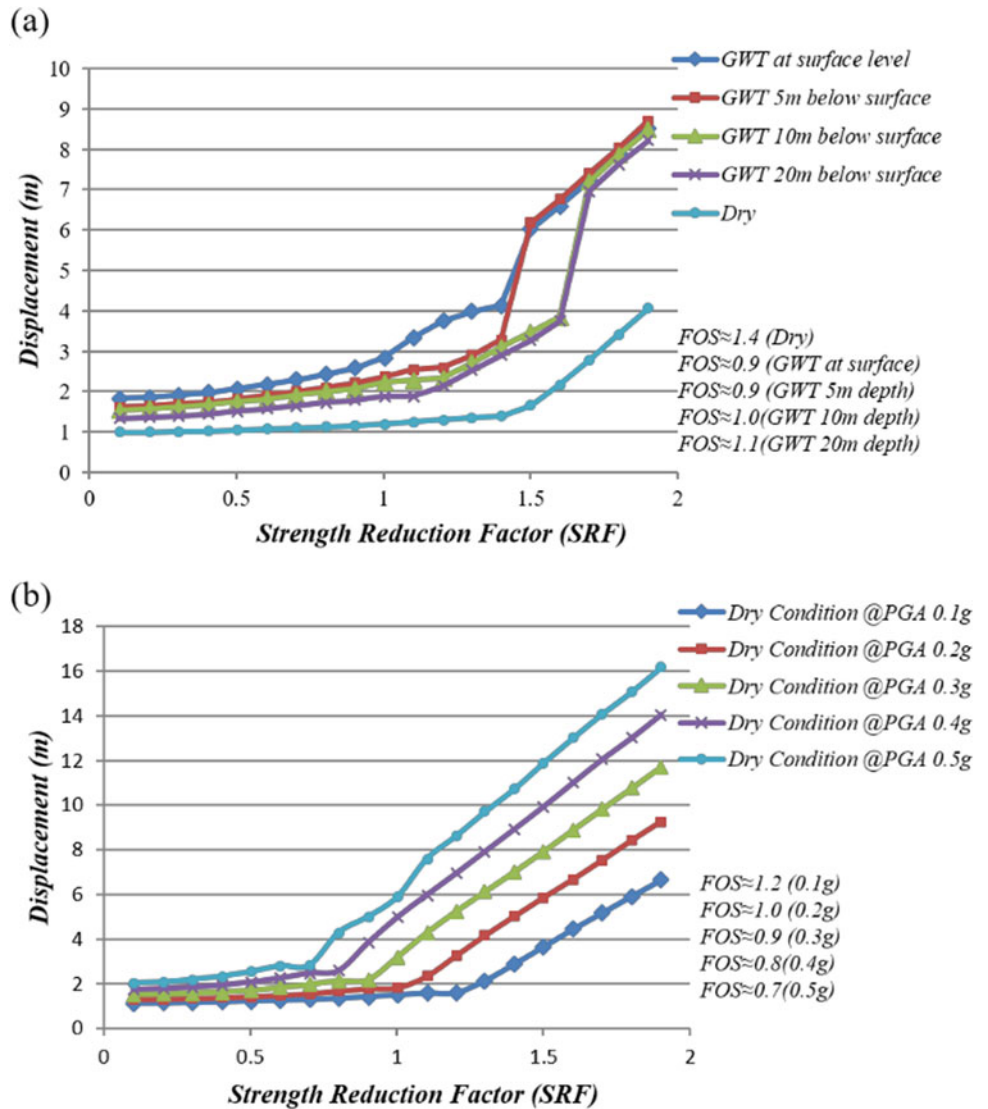
The material model presented in Table 5 below for debris is taken from USCS soil classification system as adopted by Krahenbuhl and Wagner (1983). The material model for rock is taken as: (1) Material: Schist inter bedded with Phyllite, (2) Failure Criteria: Mohr-Coulomb, (3) Unit weight = 27 kN/m³, (4) Modulus of elasticity of rock mass = 29,903,000 kPa \approx 30 MPa, (5) Poisson ratio = 0.3 and (6) Angle of internal friction = 32.50° (as per Hoek and Diederichs 2006; Hoek 2007). The pseudostatic seismic stability of the slope is proposed. In Jure area, the maximum PGA is 250 gal according to the seismic hazard map developed by Department of Mines and Geology (Pandey et al. 2002). So, the seismic loading PGA of 0.1 to 0.5 g are varied in the models accordingly.

Figure 15 shows the computational results in varying groundwater and seismic slope condition: (a) Displacement (m) versus SRF at dry and GWT at the surface and (b) Displacement (m) versus SRF seismic loading condition in case of Jure landslide model, Nepal. The abrupt change in slope as noticed would be the critical SRF. Similar results can be obtained in 2D domains. However, the complexity of the domain can be well captured in 3D domains as compared to 2D. The safety factor thus obtained in 3D models seems to be more accurate than the 2D if the complexity issue of the modelling domain is well addressed. In this way, the SEM scheme replaces the huge computational burden in FEM. SEM approach can be employed for soil and rock slopes.

Table 5 Debris parameter according to USCS as adopted by Krahenbuhl and Wagner (1983)

Group	Soil condition	γ (kN/m ³)	C (kN/m ²)	ϕ (Degree)
GM-CL	Dry	19.0	6.0	30.0
	Saturated	21.0	3.0	29.0

Fig. 15 Computational results in varying ground water and seismic slope condition: **a** displacement (m) versus SRF at dry and GWT at surface and **b** displacement (m) versus SRF seismic loading condition



6 Conclusions

Spectral element method is an elegant formulation of the FEM with a high degree piecewise polynomial basis. In this method, the interpolation nodes of an element and the numerical integration points are cited in the same points. Here, with the coincidence of integration and interpolation points, the interpolating functions become orthogonal, resulting in a diagonal mass matrix, which significantly simplifies the computational procedures and drastically

reduces the computational costs. The SEM procedure has three major benefits over the existing FEM procedures: (1) geometrical flexibility, (2) high computational efficiency, and (3) reliable spectral accuracy (i.e., exponential reduction of errors with increasing degree of polynomials). The higher spectral degree in SEM replaces the huge computational burden of FEM. Then, the safety factors thus obtained seems to be accurate values as per the material properties and slope model supplied which can encouragingly be used in effective design and implementation of various landslide slope stability works.

Acknowledgements We would like to acknowledge the Japanese Society for the Promotion of Science (JSPS) for providing this research opportunity. We would also like to acknowledge Mr. Pujan Giri, M.Sc. Student in Geotechnical Engineering, Institute of Engineering, Pulchowk Campus, Tribhuvan University for his effort in numerical and computational works.

References

- Ahrens J, Geveci, B, Law, C (2005) ParaView: an end-user tool for large data visualization, visualization handbook, Elsevier. ISBN-13: 978-0123875822. <http://www.paraview.org>. Last Accessed 18 Jul 2021
- Anderson DA, Tannehill JC, Pletcher RH (1984) CUBIT 15.3 user documentation, SAND2017-6895 W. Sandia National Laboratories. <http://www.cubit.sandia.gov>. Last Accessed 17 Jul 2021
- Barragy E, Carey GF (1988) A parallel element-by-element solution scheme. *Int J Numer Meth Eng* 26(11):2367–2382
- Canuto C, Hussaini MY, Quarteroni A, Zang TA (1988) Spectral methods in fluid mechanics. Springer, Berlin. <https://doi.org/10.1007/978-3-642-84108-8>
- Chen JX, Ke PZ, Zhang G (2007) Slope stability analysis by strength reduction elasto-plastic FEM. *Key Eng Mater* 345–346:625–628. <https://doi.org/10.4028/www.scientific.net/kem>
- Cygwin (2021) This is the home of the Cygwin project. <http://www.cygwin.com>. Last Accessed 15 June 2021
- Faccioli E, Maggio F, Paolucci R, Quarteroni A (1997) 2D and 3D elastic wave propagation by a pseudo-spectral domain decomposition method. *J Seismolog* 1(3):237–251
- Gharti HN, Komatitsch D, Oye V, Martin R, Tromp J (2011) SPEC3D_GEOTECH 1.0 Beta User Manual
- Gharti HN, Komatitsch D, Oye V, Martin R, Tromp J (2012) Application of an elastoplastic spectral-element method to 3D slope stability analysis. *Int J Num Methods Eng* 91(1):1–26
- Griffiths DV, Lane PA (1999) Slope stability analysis by finite elements. *Geotechnique* 49(3):387–403
- Gropp W, Lusk E, Skjellum A (1994) Using MPI, portable parallel programming with the message passing interface. Computing and processing. MIT press, Cambridge, USA, p 336. ISBN: 9780262527392
- King RB, Sonnad V (1987) Implementation of an element-by-element solution algorithm for the finite element method on a coarse-grained parallel computer. *Comput Methods Appl Mech Eng* 65(1):47–59
- Krahenbuhl, J, Wagner A (1983) “Survey, design, and construction of trail suspension bridges for remote areas”, SKAT. Swiss Center for Appropriate Technology in St. Gallen, Switzerland. Survey, design, and construction of trail suspension bridges for remote areas. (OCOLC) 692980053
- Komatitsch D, Tromp J (1999) Introduction to the spectral element method for the three-dimensional seismic wave propagation. *Geophys J Int* 139(3):806–822
- Komatitsch D, Vilotte JP (1998) The spectral element method, an efficient tool to simulate the seismic response of 2D and 3D geological structures. *Bullet Seismol Soc Am* 88(2):368–392
- Law KH (1986) A parallel finite element solution method. *Comput Struct* 23(6):845–858
- Pacheco P (1997) Parallel programming with MPI. Morgan Kaufmann Publishers Inc. 340 Pine Street, Sixth Floor San Francisco, CA, United States, p 418. ISBN:978-1-55860-339-4
- Patera AT (1984) A spectral element method for fluid mechanics: laminar flow in a channel expansion. *J Comput Phys* 54(3):468–488
- Pellegrini F, Roman J (1996) Scotch: A software package for static mapping by dual recursive bipartitioning of process and architecture graphs. In: Liddell H, Colbrook A, Hertzberger B, Sloot P (eds) High-performance computing and networking. HPCN-Europe 1996. Lecture Notes in Computer Science Vol 1067. Springer, Berlin, Heidelberg, pp 493–498
- Peter D, Komatitsch D, Luo Y, Martin R, Le GN, Casarotti E, Le LP, Magnoni F, Liu Q, Blitz C, Nissen-Meyer T, Basini P, Tromp J (2011) Forward and adjoint simulations of seismic wave propagation on fully unsaturated hexahedral meshes. *Geophys J Int* 186(2):721–739
- Seriani G (1994) 3D large-scale wave propagation modeling by spectral element method on Cray T3E multiprocessor. *Comput Methods Appl Mech Eng* 164(1):235–247
- Smith IM, Griffiths DV (2004) Programming the finite element method. John Wiley and Sons and location. (ISBN_number_)
- Tecplot (2021) Tacplot. <http://www.tecplot.com>. Last Accessed 20 Jul 2021
- Tiwari RC, Bhandary NP, Yatabe R (2013) High-order FEM formulation for 3-D slope instability. *Appl Math* 4(5A). <https://doi.org/10.4236/am.2013.45A002>
- Zienkiewicz O, Corneau I (1974) Visco-plasticity—plasticity and creep in elastic solids—a unified numerical solution approach. *Int J Numer Meth Eng* 8(4):821–845

Open Access This chapter is licensed under the terms of the Creative Commons Attribution 4.0 International License (<http://creativecommons.org/licenses/by/4.0/>), which permits use, sharing, adaptation, distribution and reproduction in any medium or format, as long as you give appropriate credit to the original author(s) and the source, provide a link to the Creative Commons license and indicate if changes were made.

The images or other third party material in this chapter are included in the chapter’s Creative Commons license, unless indicated otherwise in a credit line to the material. If material is not included in the chapter’s Creative Commons license and your intended use is not permitted by statutory regulation or exceeds the permitted use, you will need to obtain permission directly from the copyright holder.





Climate Change-Induced Regional Landslide Hazard and Exposure Assessment for Aiding Climate Resilient Road Infrastructure Planning: A Case Study in Bagmati and Madhesh Provinces, Nepal

I Putu Krishna Wijaya, Peeranan Towashiraporn, Anish Joshi, Susantha Jayasinghe, Anggraini Dewi, and Md. Nurul Alam

Abstract

Nepal's hilly and mountainous regions are highly susceptible to landslides triggered by extreme precipitations. The prevalence of such landslides has increased due to climate change-induced extreme hydro-meteorological conditions. These recurring landslides have significantly impacted the road transport infrastructure, which is the economic lifeline for cities and socio-economic mobility of rural communities in the hilly and mountainous regions of the country. This study modelled extreme rainfall scenarios for the current 1976–2005 baseline and future horizons of 2030, 2050, and 2080 to develop high-resolution 1 km × 1 km mean precipitation datasets under RCP4.5 and RCP8.5. Based on these extreme precipitation scenarios, we developed high-resolution landslide hazard models adopting integrated weighted index by combining the Frequency Ratio (FR) and Analytical Hierarchical Process (AHP) methods using multi-variate factors. The multi-variate factors included three terrain parameters—slope, aspect, and elevation; two soil parameters—lithology and soil type; two Euclidean distance parameters from the likely sources—distance from the lineaments and distance from the stream/river; an anthropogenic parameter—land use; and the climate parameter—the mean annual rainfall for four-time horizons and two RCPs. These parameters were spatially modelled and combined using the weighted overlay method to generate a landslide hazard model. As demonstration case studies, the landslide hazard models were developed for Bagmati and Madhesh provinces. The models were validated using the Receiver Operating Characteristic curve (ROC) approach, which showed a satisfactory 81–86% accuracy in the study area. Spatial exposure analysis of the road network assets under the

Strategic Road Network (SRN) was completed for seven landslide hazard scenarios. In both Bagmati and Madhesh provinces, the exposure analysis showed that the proportion of road sections exposed to landslide hazard significantly increases for the future climate change scenarios compared to the current baseline scenario.

Keywords

Climate change-induced landslide • Landslide hazard • Exposure assessment

1 Introduction

According to Thapa (2015), from 1971 to 2015, landslides killed approximately 200 people in Nepal each year, with one of the most severe landslide events in July 1993, killing 1336 people in central Nepal. The risk of slope failure has been further exacerbated due to the extreme rainfall events caused by climate change. We studied landslide hazards owing to extreme rainfall events in Bagmati and Madhesh provinces under several climate change scenarios. We developed high-resolution 1 km × 1 km downscaled extreme rainfall projections under selected extreme Global Climate Models (GCMs) from the Coupled Model Inter-comparison Project Phase 5 (CMIP5), GCMs, with representative concentration pathways (RCP4.5 and RCP8.5) scenarios for 1976–2005 (baseline) as well as the 2030s, 2050s, and 2080s. Based on these extreme rainfall scenarios, we modelled and mapped rainfall-triggered regional landslide hazards by merging the Frequency Ratio (FR) and the Analytical Hierarchy Process (AHP) techniques. The developed approach applies Geographic Information System (GIS) as a tool along with open data to develop the regional landslide hazard models. The study aims to understand better the spatial distribution of landslide hazard levels for current climate conditions and future time

I. P. K. Wijaya · P. Towashiraporn (✉) · A. Joshi · S. Jayasinghe · A. Dewi · Md.N. Alam
Asian Disaster Preparedness Center, Phaholyothin Road,
Phyathai, Bangkok, 10400, Thailand
e-mail: peeranan@adpc.net

© The Author(s) 2023

K. Sassa et al. (eds.), *Progress in Landslide Research and Technology, Volume 1 Issue 1, 2022*,
Progress in Landslide Research and Technology, https://doi.org/10.1007/978-3-031-16898-7_12

horizons and the potential exposure levels of the road transport infrastructure to the landslide hazard scenarios.

Exposure to climate-related extremes and hazards is the first step in assessing the vulnerability and risk of the system. In the context of a transport system, if an asset or system is located in a region directly affected by climate change and climate-induced hazards, it is referred to as “exposure” (Filosa et al. 2017).

2 Description of the Study Area

Bagmati and Madhesh Provinces are situated in the central region of Nepal, bordering Provinces 1 to the east, India to the south, Gandaki Province to the west, and China to the north. Bagmati and Madhesh Provinces are located in between latitudes of 27° 4' and 28° 19' N, and longitudes of 83° 56' and 86° 59' E (Fig. 1). Bagmati Province has thirteen districts and encompasses a total area of 20,300 km². Madhesh Province has eight districts and covers an area of 9661 km².

The road network in Nepal comprises the Strategic Road Network (SRN), which is maintained by the Department of Roads (DoR), and the Local Road Network (LRN), which is maintained by local governments (GoN/World Bank 2013). The spatial distribution of SRN is shown in Fig. 1. The total lengths of SRN roads in Bagmati and Madhesh Provinces are 2544 km and 1466 km, respectively (GoN/DoR 2018). The road density (km/100 km²) of SRN roads in Bagmati and Madhesh Provinces are 12.5 and 15.21, respectively (GoN/DoR 2018).

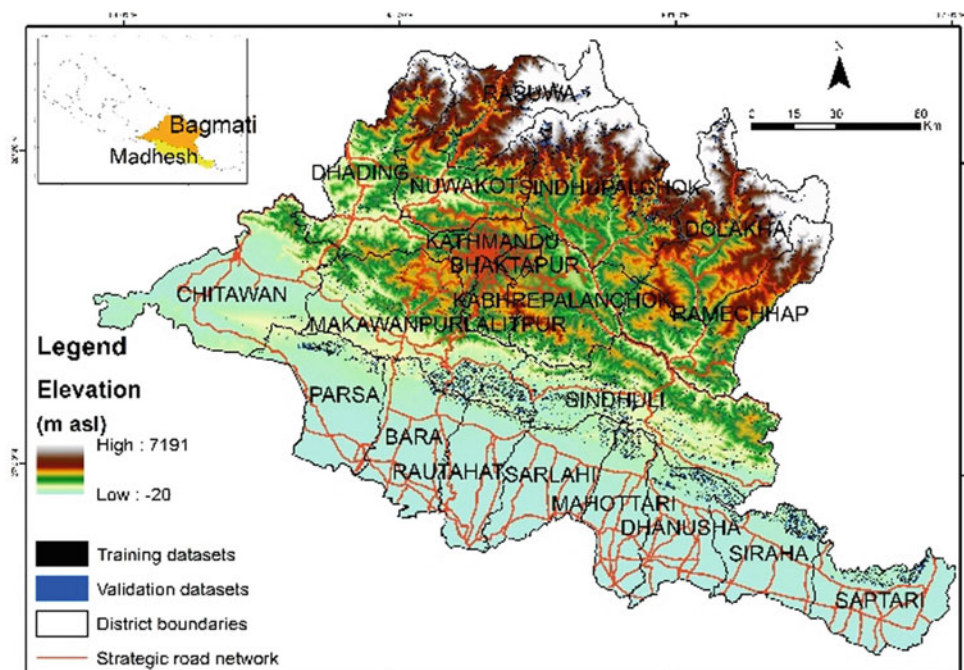
The study area is divided into five physiographic regions: the High Himalaya, High Mountain, Middle Mountain, Siwalik (Chure), and the Terai zones (Upreti and Dhital 1996). Land area in Bagmati Province spans from Siwalik region characterized by highly dissected sloping terrain, Middle Mountain with steep terrain, and High Mountain and High Himalayas with very steep mountainous terrain and very high prevalence of landslides. The majority of land in Madhesh Province is located in the flat Terai Region with northern areas in the Siwalik Hills, where the majority of landslides occur. Tectonically, those physiographical zones are separated by three thrust faults, viz. the Main Boundary, Main Central, and Main Frontal Thrust. The regional geology of the study area is divided into four tectonic zones, viz. Terai, Sub-Himalayan, Lesser Himalayan, and Higher Himalayan zones (Dhital 2015).

According to Dahal (2015), small and large-scale landslides occur in Nepal. The majority of small-scale landslides are discovered to develop on large-scale landslides. In many cases, the shallow rotational and translational landslides merge into the mainstream valley, resulting in devastating debris flows at nearby highways or communities.

3 Analysis Input Data

Three important datasets were compiled to map and analyze the landslide hazard viz the landslide inventory data, landslide controlling factors dataset, and landslide triggering factor (rainfall) dataset.

Fig. 1 Digital map shows the location, topography, and distribution of strategic road network (SRN) of the study area



3.1 Landslide Inventory Map

The landslide inventory data was generated by Durham University and the National Society for Earthquake Technology of Nepal (NSET) under a project funded by the Department for International Development of the United Kingdom (DFID) - DFID/NERC SHEAR project number: 201844, in collaboration with the Durable Solutions 2 project. In this study, the data is on polygon shapefile, and we used the post-monsoon data of 2020 as landslide datasets. The landslides in the landslide inventory were randomly divided into two subsets, i.e., the training set area (80%) and the test/validation set area (20%), as suggested by Getachew and Meten (2021). The landslide size in the study area varied from 0.01 to 1.3 km².

3.2 Landslide Controlling Factors Map

Pawluszek and Borkowski (2017) mentioned that there are no specific rules for defining the number of controlling factors sufficient for the landslide hazard analysis. With the combination of the works of literature mentioned above and the nature of the study area, nine different thematic layers together with terrain slope (°), distance from lineaments (m), distance from streams (m), elevation (m), lithology, soil, rainfall, land use, and terrain aspect were taken into consideration. The landslide controlling factor maps were rasterized with 12.5 m × 12.5 m pixels, and each raster was reclassified into appropriate thematic classes.

3.3 Rainfall Datasets and Projected Scenarios

Climate projections are widely used to understand climate extremes and their probability of occurrence in the future. Development of climate change projections, including regional and national level projections for climate extremes, could be accessed from four sources such as the Global Climate Models (GCMs), the Regional Climate Models (RCMs), from an understanding of the regional and national climate influences, and from the historical climate change

recently observed (Seneviratne et al. 2012; Knutti et al. 2010; Christensen et al. 2007). As illustrated in Fig. 2, the suggested climate impact modelling methodology for identifying extreme events in the study area comprises six methodological steps.

As the current study focuses on identifying future extreme occurrences to determine the maximum hazardous levels for the study area, it is essential to choose those GCMs that give extreme conditions in the targeted areas in the future. The future climate scenarios for 2030 (averaging 2016–2045), 2050 (averaging 2036–2065), and 2080 (averaging 2066–2095) are developed in the study area based on current climate (rainfall and mean temperature from 1976 to 2005) across the same study region during the wet season. Because landslides are more common during the rainy (monsoon) season, it is thought to be the best time period to choose suitable GCMs. Then a skills test is suggested for the identification of the models. The Skill Test entails calculating the change in annual mean temperature (ΔT) and percent change in yearly precipitation ($\Delta P\%$) from each of the models (CMIP5 models).

4 Analysis Methods

The integrated weighted index method was used in this study. The integrated weighted index method was applied by merging the analytical hierarchy process (AHP) and the Frequency Ratio (FR) method. The integration between these two methods has been peer-reviewed by Yi et al. (2019), Mondal and Maiti (2013), and El Jazouli et al. (2019). There are four important processes in the integrated weighted index method. The first step is to determine the relative importance of landslide controlling and triggering parameters using the AHP technique (Fig. 3). The second step is to describe a mutual relationship between the location of landslides and the controlling & triggering parameters by using the FR method. In the third step, landslide hazard maps were created using the weighted overlay tool in a GIS environment. In the fourth and last step, the operating characteristics curve (ROC) technique was used to validate the results of landslide hazard model predictions (Fig. 3).

Fig. 2 Climate impact modeling for evaluating risks from severe landslides utilizing downscaled GCMs

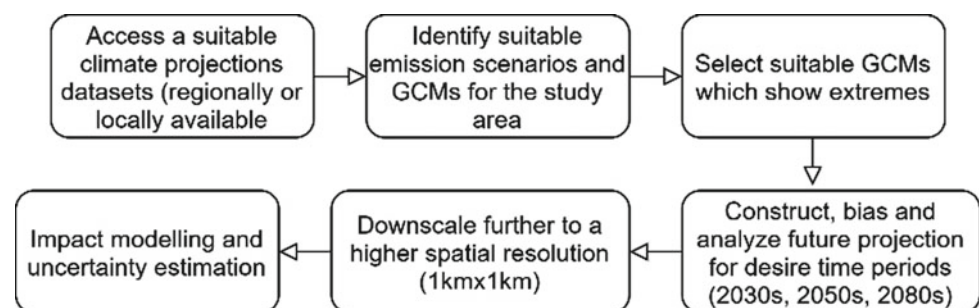
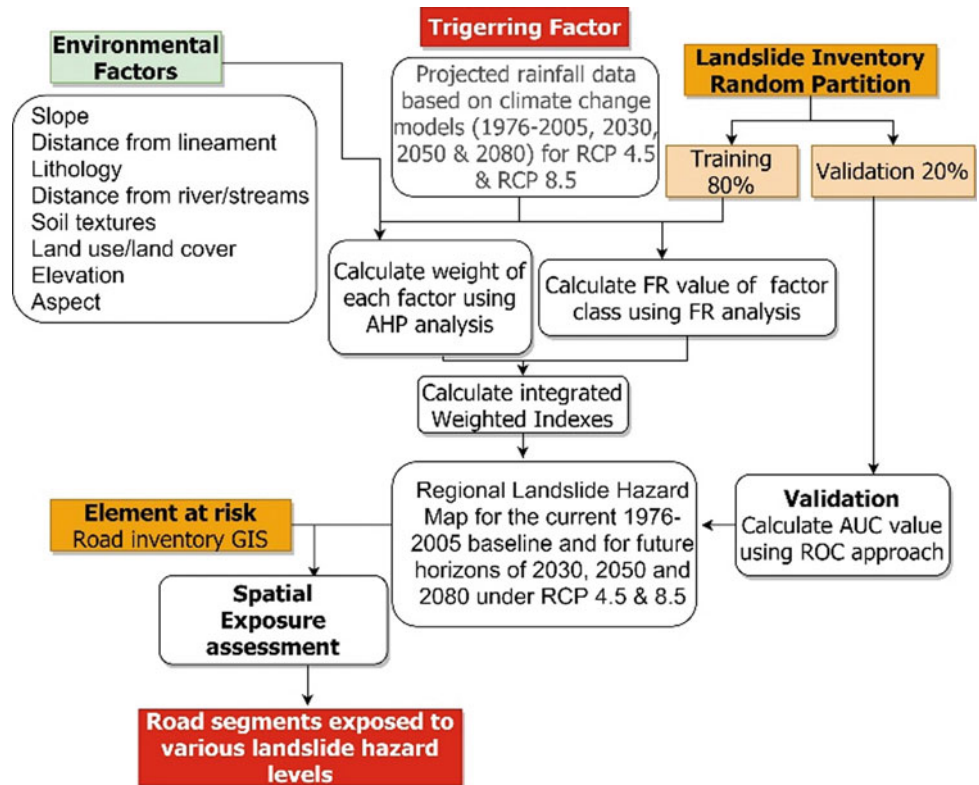


Fig. 3 Flow chart with study approaches



4.1 Frequency Ratio Method

Frequency ratio (FR) values represent the connection between the landslide occurrence and the classes of every single controlling and triggering parameter. In terms of landslide evaluation and prediction, the frequency ratio approach is one of the most widely used statistical methods (Mandal and Mondal 2019). The FR relates the likelihood of the presence to the absence of landslide occurrence (Lee and Pradhan 2007). The landslide hazard can be evaluated from the spatial relationship between the controlling factor and landslides occurrences. The greater the FR ratio is the stronger is the link among the landslide controlling and triggering parameters and the incidence of landslides (Lee and Pradhan 2007).

The frequency ratio value is computed as described in the following formula:

$$FR_i = \frac{N_{cell}(S_i)/N_{cell}(N_i)}{\sum N_{cell}(S_i)/\sum N_{cell}(N_i)} \quad (1)$$

where, $N_{cell}(S_i)$ is the number of grid cells in class I that have been identified as landslides, and $N_{cell}(N_i)$ is the total number of grid cells in class I in the entire area. The total number of grid cells that have been identified as landslides in the entire area is $\sum N_{cell}(S_i)$, while the total number of grid cells in the entire area is $\sum N_{cell}(N_i)$.

4.2 Analytical Hierarchy Process (AHP) Method

The analytical hierarchy process (AHP) method was first proposed by Saaty (1982, 1991, 2000) and is widely applied in the decision-making paradigm. AHP avoids the difficulties associated with random weights and rating systems by allowing judgment to influence relative importance features or weights rather than randomly assigning those features (Yalcin 2008).

CR stands for the likelihood that the matrix judgments were created at random, as follows:

$$CR = \frac{CI}{RI} \quad (2)$$

Based on the arrangement of Malczewski's matrix (1999), RI is the average of the resultant consistency index, and CI is the consistency index and may be represented as:

$$CI = \frac{(\lambda_{\max} - n)}{(n - 1)} \quad (3)$$

where λ_{\max} is the matrix's largest value, which may be easily computed from the matrix, and n is the matrix's order. R is a value that ranges from 0 to 1. A consistency ratio near one implies that the matrix's rating was most likely generated randomly. A decent level of consistency is one with a consistency ratio of 0.10 or less (Malczewski 1999).

4.3 Integrated Weighted Index Method

FR is a statistical model based on data that can determine the spatial correlation between landslide locations and the controlling and triggering parameters (Yi et al. 2019). The FR technique, on the other hand, does not take into account the interdependence of controlling and triggering parameters. The AHP technique is a critical multiple-criteria decision-making method to address this problem. To a certain degree, the integrated approach retains the benefits of the FR and AHP methods while reducing their limitations.

By combining the FR and AHP techniques, the integrated weighted model examined the connection among the controlling and triggering parameters as well as the effect of each landslide controlling and triggering parameters on landslide frequency. The following formula can be used to obtain the integrated weighted index:

$$I = \sum_i^m (W_i \times FR_i) \quad (4)$$

where m is the number of controlling and triggering factors, W_i denotes the weight assigned to each controlling and triggering factor using the AHP method, and FR_i denotes the FR value assigned to the i th controlling and triggering factor using the FR method.

4.4 Validation Method

Validation of the model predictions is critical for landslide hazard mapping. The receiver operating characteristics curve (ROC) technique (Brenning 2005) was used to assess the effectiveness of the integrated weighted index model. The ROC curve is a plot of the model prediction's sensitivity (percent of true positives) against the complement of its specificity (proportion of false positives, Jaiswal 2011). The true positive rate (TPR) was plotted in contradiction of the false positive rate (FPR) on the ROC curve, with TPR on the y-axis and FPR on the x-axis.

Specificity is the probability that a mapping unit with no landslide is correctly classified 1-specificity is the false positive rate measured along the curve's x-axis (Jaiswal 2011). The area under the curve (AUC) ranged between 0.5 and 1.0, where a value of 1.0 suggested that the model performed perfectly, but a value near 0.5 indicated that the model performed poorly.

4.5 Exposure Assessment Method

The exposure of roads under the SRN is assessed as the physical exposure which is spatially exposed to the landslide

hazard areas. The physical exposure of the road network is assessed as "the ratio or the proportion of road section length potentially affected by landslides in the current climate scenario and future climate change scenarios to the total length of the road," the landslide being represented by the landslide hazard and the severity represented by the hazard classes. The exposure index for a road segment is calculated as

$$E_i = \frac{L_r}{L_i} \times 100 \quad (5)$$

and the road exposure index for entire region (province) is calculated as

$$E = \frac{\sum_{i=1}^n L_{ri}}{\sum_{i=1}^n L_i} \times 100 \quad (6)$$

where, E_i is the exposure index of road segment i with the total length of L_i and landslide exposed length of L_r . E is the exposure index of the road in the entire geographic region calculated as the proportion of the total length.

The landslide exposed length L_r for each road section is calculated using spatial overlay analysis of the existing SRN road network data (GoN/DoR 2018) with landslide hazard scenario maps of the current baseline period (1976–2005) and future climate change scenarios (2030, 2050 and 2080) in a GIS environment.

5 Results

5.1 Regional Landslide Hazard Maps

The weight for each controlling & triggering parameter was assigned using the analytic hierarchy process approach. The larger the weight is, the more significant the impact on landslide occurrences may be. The comparison quality is described by the consistency ratio (CR). Some works of literature related to landslides hazard mapping were investigated to find the appropriate correlation between the controlling and triggering factors (Mandal and Mondal 2019; Sonker et al. 2021; Yi et al. 2019).

Four factors considered to be the most important landslide controlling and triggering factors were slope, lithology, rainfall, and distance from lineaments. Thus, in this study, those four factors were given a higher weight than the other controlling factors. Some studies found no significant influence of aspect on slope stability (Ayalew and Yamagishi 2005), while some others found its effect on landslide initiation (Dai and Lee 2002). Thus, low weight was given to the aspect factor.

As mentioned above, in the AHP analysis, the consistency ratio characterizes the comparison's reliability. In this study, the consistency ratio (CR) of the matrix of paired

comparisons between the nine controlling and triggering factors in the hazard map is 0.012. A consistency ratio of 0.10 or less is considered a satisfactory degree of consistency (Malczewski 1999). Even though the consistency ratio of this study is consistent (0.012), the pair-wise comparison is subjective, and the precision is heavily reliant on the expert's perspective. In order to reduce the subjectivity, the integrated weighted index model by combining FR and AHP was applied.

Based on the pairwise comparison matrix of AHP, the weight of slope was the highest (0.205 suggesting that slope has the greatest effect on the frequency of landslides). The weight of distance from lineaments and rainfall were the second and third highest (0.198 and 0.174, respectively), followed by lithology (0.134), soil (0.067), and distance from streams (0.061). Finally, the weights of aspect, elevation, and land use were the lowest (0.054). This suggested that these three parameters had the lowest impact on the prevalence of the landslide. The application of the integrated weighted index model demonstrated that landslide hazard levels were essentially compatible with landslide occurrence.

A total of seven maps of landslide hazard were developed from two RCP4.5 and RCP8.5 for time horizons 2030s, 2050s, and 2080s and baseline (1976–2005). The landslide hazard maps were divided into five categories: very low, low, moderate, high, and very high (Fig. 7). The total area of landslide hazard was quantified by calculating the area geometry in the GIS environment.

Based on the acquired landslide hazard maps, the area for each hazard level in scenarios shows different values. In the RCP8.5 scenario, for time horizon 2030, 2050, and 2080s,

the hazardous zones, including zones with extremely high and high hazard levels, cover about 24%, 25%, and 30% of the study area, respectively.

In the case of the RCP4.5 scenario for time horizon 2030, 2050, and 2080, the very high and high hazard level zones covered approximately 22%, 23%, and 24% of the study area, respectively. The highest area value (8994 km²) of the high to very high hazard level was reached by the hazard map of RCP8.5 for time horizon 2080, where most of the high-very high hazard area is located in Bagmati province (8862 km²) and a small part of Madhesh province (132 km², Tables 1 and 2). Concerning the hazard maps of RCP4.5 and RCP8.5 for time horizon 2030, 2050, and 2080, most parts of high to very high-level hazard zones are mainly distributed in Bagmati Province, especially in Rasuwa, Niwakot, Sindhupalohok, Dolahak, Dhading, Nuwakot, Ramechhap, the southern part of Lalitpur, north and north-western part of Chitawan, Makawanpur, and Sindhuli district (Fig. 7).

5.2 Validation of Landslide Hazard Maps

Validation of modelled outputs is critical to evaluate the landslide hazard map results. A sample dataset of 8813 landslides was used as a validation dataset from the total (43,519 landslides sample dataset) to validate the reliability of the landslide hazard model.

The AUC values for the landslide hazard map (current climate and future projected scenarios) varied from 81 to 86%, which showed that the integrated weighted index

Table 1 Total area of landslide hazards in Bagmati Provinces for current climate (baseline), future scenarios and periods

Hazard area	Baseline (km ²)	RCP4.5 (km ²)			RCP8.5 (km ²)		
	1976–2005	2030	2050	2080	2030	2050	2080
Very low	814	745	645	601	620	591	261
Low	5345	5237	5063	4842	4791	4758	3457
Moderate	7613	7662	7671	7712	7652	7670	7682
High	4940	5029	5197	5246	5321	5340	6353
Very high	1550	1589	1686	1861	1878	1903	2509

Table 2 Total area of landslide hazards in Madhesh Provinces for current climate (baseline), future scenarios and periods

Hazard area	Baseline (km ²)	RCP4.5 (km ²)			RCP8.5 (km ²)		
	1976–2005	2030	2050	2080	2030	2050	2080
Very low	5100	4614	4416	4269	4306	4272	3382
Low	3782	4008	4132	4259	4222	4247	4598
Moderate	612	855	925	944	947	951	1428
High	46	62	66	67	64	69	130
Very high	0	1	1	1	1	1	2

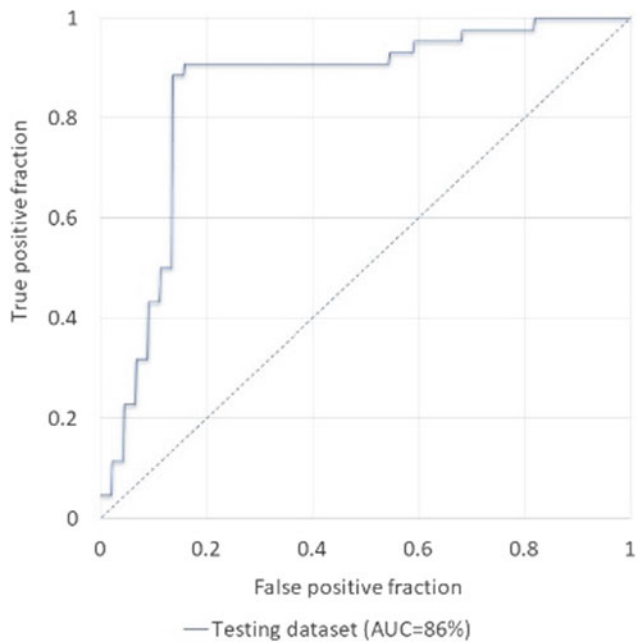


Fig. 4 The integrated weighted index model's forecast effectiveness. An example of ROC of landslide hazard map for time horizon 2080s with RCP8.5

model used in this analysis has a high degree of predictability. Figure 4 showed the ROC of the landslide hazard map for time horizon 2080s with RCP8.5.

5.3 Exposure Assessment Results

Exposure assessments of SRN roads in the study provinces were done for seven landslide hazard scenarios. In Bagmati Province, the majority of roads have low (35.5%) and

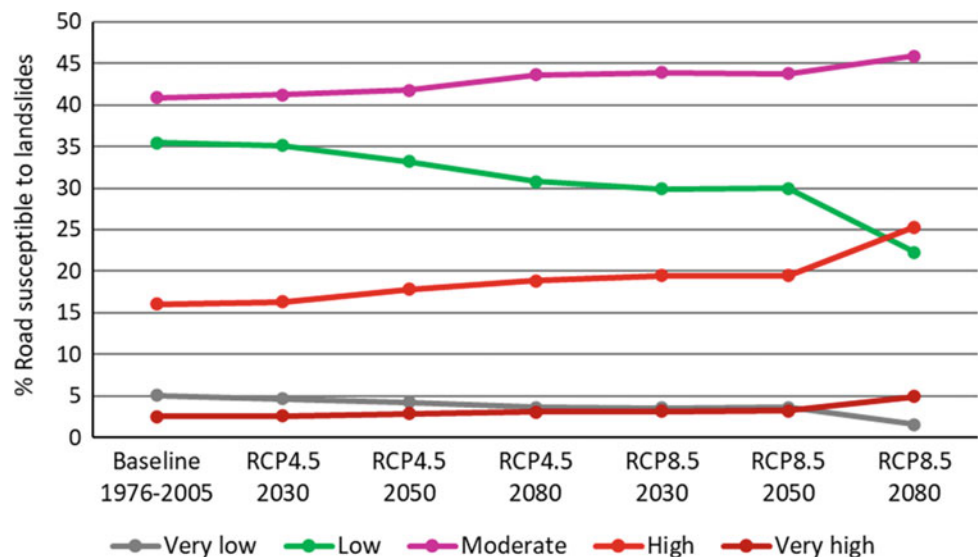
medium (40.9%) risk to landslides in the baseline period, with 16 and 2.5% lengths of the roads exposed to high and very high landslide hazards. The proportion of road length exposed to very low and low landslide hazards decreases in all the time horizons for RCP4.5 and RCP8.5. It consequently increases in moderate, high, and very high hazardous categories compared to the baseline years (Fig. 5). Exposure to moderate, high, and very high hazard increases significantly for the RCP8.5 scenario in 2080.

For Madhesh Province, the majority proportion (68%) of the road is exposed to very low landslide hazard, with 31% low and negligible 0.9% to moderate hazard in the baseline period. The very low hazard proportion of the roads decreases significantly in the future horizons, consequently with a significant increase in the proportion of road length exposed to low and moderate hazardous landslides (Figs. 6 and 7).

6 Discussion

Compared to the landslide-hazardous areas modelled for the current baseline climate conditions (1976–2005), the landslide-hazardous areas increase significantly in extreme rainfall conditions for the future climate change scenarios for both RCPs. Results revealed that the regions with very high landslide hazard increased to 312 km² (for RCP4.5) and 961 km² (for RCP8.5) in the 2080s. Thus, it is predicted that landslide hazards will increase in future time horizons (in the 2030s, 2050s, and 2080s). RCP8.5 scenario showed larger hazardous areas than RCP4.5 in future time horizons, as RCP8.5 models predicted heavier rainfall than RCP4.5. In future periods, the Bagmati Province and northern part of Madhesh Province are likely to have higher landslide hazard areas than the current condition. In particular, it is predicted

Fig. 5 Proportion SRN Road hazardous to current and future landslide scenarios in Bagmati Province



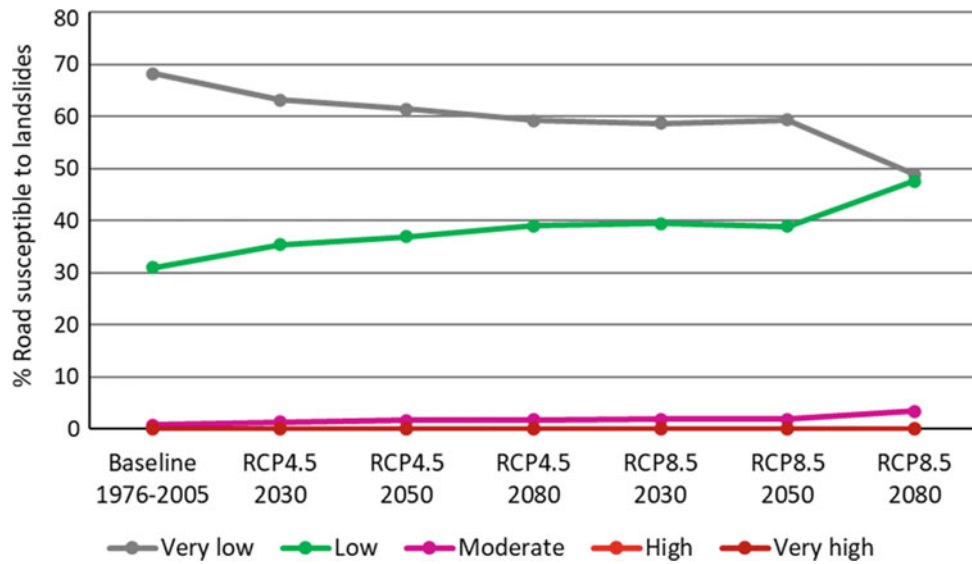


Fig. 6 Proportion SRN Road hazardous to current and future landslide scenarios in Madhesh Province

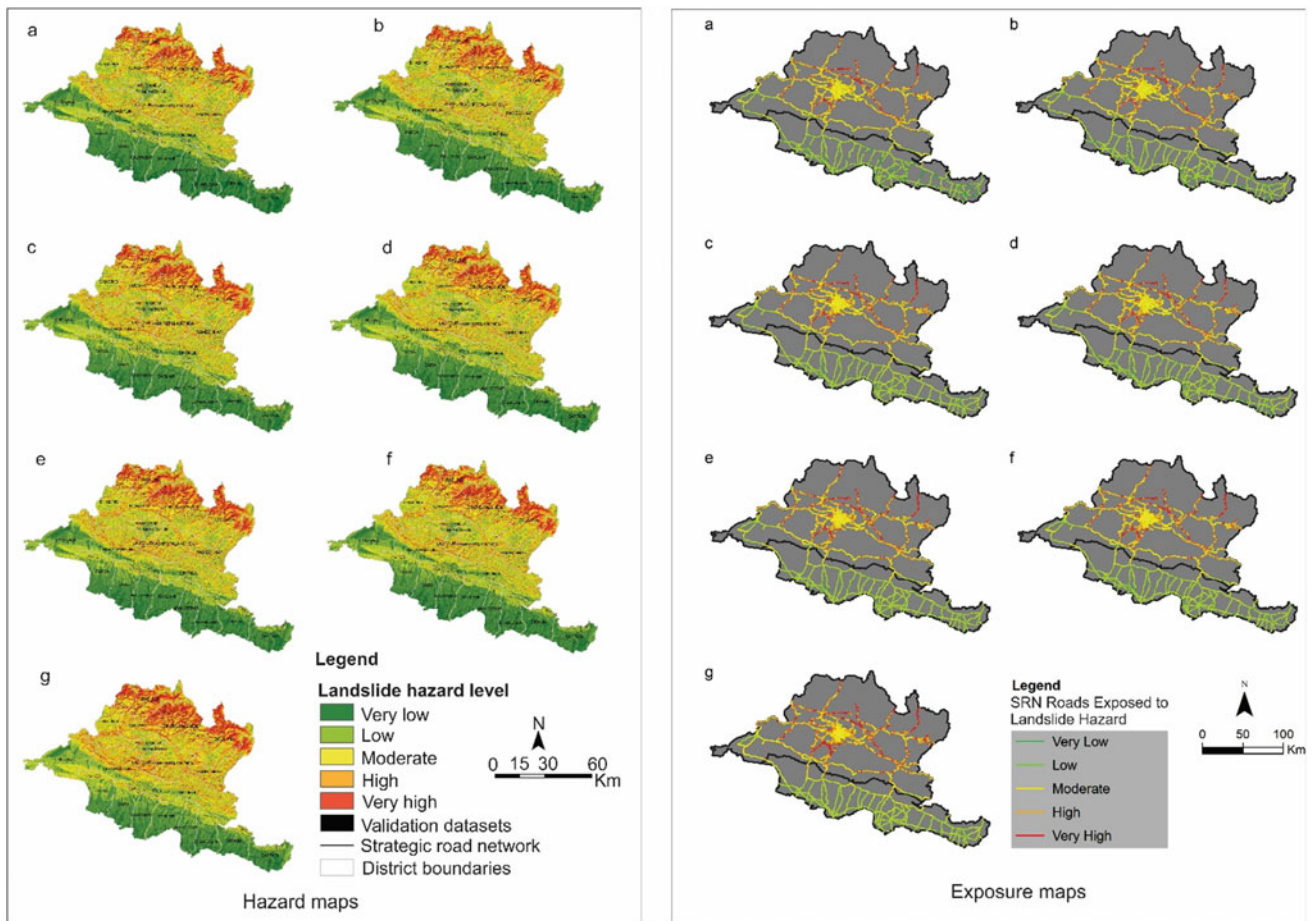


Fig. 7 Landslide hazard and exposure maps for **a** baseline period (1976–2005), **b** time horizon 2030s for RCP4.5, **c** time horizon 2030s with RCP8.5, **d** time horizon 2050s for RCP4.5, **e** time horizon 2050s

for RCP8.5, **f** time horizon 2080s for RCP4.5 and **g** time horizon 2080s for RCP8.5

that landslide hazards in Bagmati and the northern area of Madhesh Provinces would increase in the 2030s (2016–2045), 2050s (2036–2065), and 2080s (2066–2095) in both RCP scenarios. In both scenarios, the landslide-hazardous areas for the 2080s were predicted to expand significantly to the area adjacent to Rasuwa, Sindhupalchok, and Dolakha districts.

The hazard map for time horizon 2080 with RCP8.5 represents the worst-case scenario for landslides. Although the majority of the study area (31%) was predicted to be on moderately hazardous to future landslides, 30% was indeed in the high and very high hazardous categories. The unsafe areas mentioned in the previous section require immediate mitigation actions. Reactivation of existing landslide sites and new landslides may occur, particularly along lineaments. The findings revealed the dependability (indicated by the AUC value that showed a satisfactory result of 81–86% accuracy) and practicality of the integrated weighted index model in regional landslide hazard mapping.

In Bagmati Province, the proportion of road length hazardous to very low and low landslides decreases for RCP4.5 scenarios. Consequently, the proportion increases for moderate, high, and very high landslide hazards for 2030, 2050 and 2080 horizons. Similarly, in Madhesh Province, the proportion of road length in low hazardous areas decreases in the future horizons, consequently with a significant increase in low and moderate hazards.

7 Conclusions

The landslide hazard modelling and mapping spatially locate the regions hazardous to landslides due to multi-variate factors under the extreme rainfall conditions for the current and projected future time horizons. Seven maps of landslide hazard were created, representing scenarios for RCP4.5 and RCP8.5 for future time horizons 2030s, 2050s, and 2080s and the current (1976–2005) baseline period. The significant increase in very high landslide hazardous areas between the baseline period and the long-term horizon in 2080 (for RCP8.5 scenario) indicates that the extreme rainfall due to climate change will substantially increase landslides at Bagmati and Madhesh provinces. These landslide hazard models and maps enable decision-making in the planning of road infrastructure through relatively safer areas indicated by very low, low, and/or moderate hazardous areas. Planning, designing, and construction of road infrastructure in the moderate hazardous areas may require road design parameters to adapt and/or mitigate the impacts of landslide hazards. Moderate hazardous areas may also be managed through climate adaptive measures, including green-grey infrastructures such as the incorporation of Nature-based Solutions (NbS) along with engineering solutions. These landslide

hazard maps will further support vulnerability assessment of strategic roads in the provinces and identify critical road segments for planning and implementing climate adaptation measures and activities to enhance the climate resilience of the road infrastructure in the provinces.

The exposure analysis showed that the exposure levels of the roads to landslides would significantly increase in the future due to climate change impacts. The identification and mapping of road sections exposed to higher levels of landslide hazard enable road sector authorities to prioritize adaptation actions in these stretches of the road. Further, the exposure assessment provides an opportunity to target a more detailed study to model and quantify the hazard risk to the road transport network due to specific landslides that could occur in hazardous areas.

Acknowledgements This study was made possible by the Climate Adaptation and Resilience (CARE) for South Asia Project, implemented by Asian Disaster Preparedness Center (ADPC) with the support of World Bank. The landslide inventory data was developed under UKRI-DFID SHEAR program (201844-112) and obtained from National Disaster Risk Reduction and Management Authority (NDRRMA) of Nepal for the study. We advise that the political/administrative boundary representation on the maps is not necessarily authoritative.

References

- Ayalew L, Yamagishi, H (2005) The application of GIS-based logistic regression for landslide susceptibility mapping in the Kakuda-Yahiko Mountains, Central Japan. *Geomorphology* 65:15–31. <https://doi.org/10.1016/j.geomorph.2004.06.010>
- Brenning A (2005) Spatial prediction models for landslide hazards: review, comparison and evaluation. *Nat Hazards Earth Syst Sci* 5:853–862
- Christensen JH, Hewitson B, Busuioac A, Chen A, Gau X, Held I, Jones R, Kolli R, Kwon W, Laprise R, Magaña Rueda V, Mearns L, Menéndez C, Räisänen J, Rinke A, Sarr A, Whetton P (2007) Regional climate projections. In: Solomon S, Qin D, Manning M, Chen Z, Marquis M, Averyt KB, Tignor M, Miller HL (eds) *Climate change 2007: the physical science basis. Contribution of working group I to the fourth assessment report of the intergovernmental panel on climate change*. Cambridge University Press, Cambridge, UK, pp 847–940
- Dahal RK (2015) Earthquake-induced slope failure susceptibility in east Nepal. *J Nepal Geol Soc* 49:49–56
- Dai FC, Lee CF (2002) Landslide characteristics and slope instability modelling using GIS, Lantau Island, Hong Kong. *Geomorphology* 42:213–228
- Dhital M (2015) Geology of the Nepal Himalaya: regional perspective of the classic collided orogen. <https://doi.org/10.1007/978-3-319-02496-7>
- El Jazouli A, Barakat A, Khellouk R (2019) GIS-multicriteria evaluation using AHP for landslide susceptibility mapping in Oum Er Rbia high basin (Morocco). *Geoenviron Disast* 6:3
- Filosa G, Plovnick A, Stahl L, Miller R, Pickrell D (2017) *Vulnerability assessment and adaptation framework*, 3rd edn. U.S. Department of Transportation Federal Highway Administration, Federal Highway Administration, Cambridge, MA. https://www.fhwa.dot.gov/environment/sustainability/resilience/adaptation_framework/

- Getachew N, Meten M (2021) Weights of evidence modeling for landslide susceptibility mapping of Kabi-Gebro locality, Gundomeskel area, Central Ethiopia. *Geoenviron Disast* 8:6
- GoN/DoR (2018) Statistics of strategic road network SSRN 2017/2018. HMIS-ICT Unit, Department of Roads
- GoN/World Bank (2013) Nepal Road Sector Assessment Study. World Bank
- Jaiswal P (2011) Landslide risk quantification along transportation corridors based on historical information. University of Twente, Faculty of Geo-Information Science and Earth Observation (ITC)
- Knutti R, Abramowitz G, Collins M, Eyring V, Glecker PJ, Hewitson B, Mearns L (2010) Good practice guidance paper on assessing and combining multi model climate projections. In: Stocker TF, Dahe Q, Plattner GK, Tignor M, Midgley PM (eds) Meeting report of the intergovernmental panel on climate change expert meeting on assessing and combining multimodel climate projections. IPCC Working Group I Technical Support Unit, University of Bern, Bern, Switzerland, pp 1–13
- Lee S, Pradhan B (2007) Landslide hazard mapping at Selangor, Malaysia using frequency neural network model at Cameron Highland, Malaysia. *Landslides* 7:13–30
- Malczewski J (1999) GIS and multicriteria decision analysis. Wiley, New York
- Mandal S, Mondal S (2019) Probabilistic approaches and landslide susceptibility. *Geoinformatics and modelling of landslide susceptibility and risk. environmental science and engineering. Springer book series (ESE)*, pp 145–163
- Mondal S, Maiti R (2013) Integrating the analytical hierarchy process (AHP) and the frequency ratio (FR) model in landslide susceptibility mapping of Shiv-khola watershed, Darjeeling Himalaya. *Int J Disaster Risk Sci* 4:200–212
- Pawluszek K, Borkowski A (2017) Impact of DEM-derived factors and analytical hierarchy process on landslide susceptibility mapping in the region of Rożnów Lake, Poland. *Nat Hazards* 86:919–952
- Saaty TL, Vargas LG (1982) The logic of priorities; applications in business, energy, health, and transportation. Kluwer-Nijhoff. Reprinted in Paperback, Boston (1991), RWS Publications, Pittsburgh
- Saaty TL, Vargas LG (1991) Prediction. Kluwer Academic, Projection and Forecasting, Boston
- Saaty TL, Vargas LG (2000) Models. Kluwer Academic Publishers, Methods, Concepts and Applications of the Analytic Hierarchy Process, Boston
- Seneviratne SI, Nicholls N, Easterling D, Goodess CM, Kanae S, Kossin J, Luo Y, Marengo J, McInnes K, Rahimi M, Reichstein M, Sorteberg A, Vera C, Zhang X (2012) Changes in climate extremes and their impacts on the natural physical environment. In: Field CB, Barros V, Stocker TF, Qin D, Dokken DJ, Ebi KL, Mastrandrea MD, Mach KJ, Plattner GK, Allen SK, Tignor M, Midgley PM (eds) Managing the risks of extreme events and disasters to advance climate change adaptation. A Special Report of Working Groups I and II of the Intergovernmental Panel on Climate Change (IPCC). Cambridge University Press, Cambridge, UK, and New York, NY, USA, pp 109–230
- Sonker I, Tripathi J, Singh, AK (2021) Landslide susceptibility zonation using geospatial technique and analytical hierarchy process in Sikkim Himalaya. *Quat Sci Adv* 4:100039. <https://doi.org/10.1016/j.qsa.2021.100039>
- Thapa PB (2015) Occurrence of landslides in Nepal and their mitigation options. *J Nepal Geol Soc* 49(1):17–28
- Upreti BN, Dhital MR (1996) Landslide studies and management in Nepal. ICIMOD, Nepal, p 87
- Yalcin A (2008) GIS-based landslide susceptibility mapping using analytical hierarchy process and bivariate statistics in Ardesen (Turkey): comparisons of results and confirmations, *Catena*, p 72
- Yi Y, Zhang Z, Zhang W, Xu Q, Deng C, Li Q () GIS-based earthquake-triggered-landslide susceptibility mapping with an integrated weighted index model in Jiuzhaigou region of Sichuan Province, China. *Nat Hazards Earth Syst Sci* 19. <https://www.nepal2015eq.webspace.durham.ac.uk/>

Open Access This chapter is licensed under the terms of the Creative Commons Attribution 4.0 International License (<http://creativecommons.org/licenses/by/4.0/>), which permits use, sharing, adaptation, distribution and reproduction in any medium or format, as long as you give appropriate credit to the original author(s) and the source, provide a link to the Creative Commons license and indicate if changes were made.

The images or other third party material in this chapter are included in the chapter's Creative Commons license, unless indicated otherwise in a credit line to the material. If material is not included in the chapter's Creative Commons license and your intended use is not permitted by statutory regulation or exceeds the permitted use, you will need to obtain permission directly from the copyright holder.





Using Experimental Models to Calibrate Numerical Models for Slope Stability and Deformation Analysis

Binod Tiwari and Duc Tran

Abstract

Landslides cause significant loss of lives and properties globally. Rainfall and earthquake are considered to be two frequent causes of landslides although there are dozens of natural or anthropogenic triggers of landslides. Experimental or numerical analyses by varying a single parameter—while keeping other triggers constant—help researchers/practitioners to understand the influence of each triggering factor on slope stability/landslides. However, experimental modeling of landslides in laboratory is exhaustive, time consuming, and expensive process. There are various experimental methods available for such modeling—ranging from centrifuge modeling to small scale 1 g models—depending on the need, available resources, and funds. With the wide availability of materials and development of better sensors/instruments, our capability to perform laboratory experiments, specifically for landslide modeling, has been much easier and accessible in recent decades. Such experiments are valuable to calibrate numerical models so that various analyses can be performed on the real-world problems. In this study, we prepared laboratory scale slopes in Plexiglas containers at varying densities and slope inclinations, and instrumented the slopes properly to measure real time suction, displacement, advancement of wetting front, and accelerations at various locations and depths within the model. The slopes were subjected to rainfall and/or earthquake shaking to evaluate the effect of rainfall and earthquakes—separately and combined—on slope stability. The experimental results were used to calibrate the numerical modeling effort so that a full spectrum of sensitivity analyses could be performed for a slope located in an expensive neighborhood of Southern California.

Keywords

Landslides • Experimental modeling • Numerical modeling • Suction • Rainfall • Tensiometer • Slope stability

1 Background

Landslides cause billions of dollars of loss in properties and kill thousands of people annually worldwide. Causes of landslides span from many factors including heavy rainfall, snow melt, volcanic eruption, earthquake, changes in surface or ground water level, stream bank erosion, loss of vegetation cover, deforestation, wildfires, poor construction practice, improper design of infrastructure, and poor water management practice. These factors cause disturbance to naturally stable slopes and add into factors causing slope instability, which eventually yield mass movement in the form of landslides, slope failures, mudslides, and debris flows. While each of these factors either solely or in combination with two or more other factors are responsible for triggering hundreds of thousands of landslides every year, heavy rainfall, earthquake or combination of both account for majority of the mass movements. With a geometric increase in the number of significant earthquakes and a significant increase in global precipitation anomaly due to global warming associated climate change, there has been a geometric increase in the number of significant mass movements every year (Ajmera and Tiwari 2021).

Due the increase in the number of mass movements annually, there has been significant progress in research and development related to understanding behavior of mass movement caused by the triggers mentioned earlier through various methods including theoretical analyses, statistical analyses including artificial intelligence, remote sensing techniques, instrumentation with better equipment/tools

B. Tiwari (✉) · D. Tran
Department of Civil and Environmental Engineering, California
State University, Fullerton, Fullerton, CA 92831, USA
e-mail: btiwari@fullerton.edu

© The Author(s) 2023

K. Sassa et al. (eds.), *Progress in Landslide Research and Technology, Volume 1 Issue 1, 2022*,
Progress in Landslide Research and Technology, https://doi.org/10.1007/978-3-031-16898-7_13

including internet of the things, and experimental as well as numerical modeling techniques. Although some methods are better than others for specific projects depending on the scope of the project, availability of information, or implementation cost, each method has its own merit in analyzing landslide projects. However, if affordable, a combination of these methods will always provide the most accurate results.

Experimental modeling techniques, although very expensive, have been very effective in understanding the mechanism of slope stability or mass movement subjected to one or a combination of triggering factors. These experimental methods include element level flume tests, laboratory scale experimental slope models (Tiwari et al. 2018, 2013; Tiwari and Caballero 2015), field tests, and centrifuge modeling. Each of these techniques have their own benefits as well as limitations. However, the best method is generally chosen based on the scope of the project, availability of the equipment/tools, and project funds. While flume tests are generally performed to study the source and run-out of failed mass during rainfall events, laboratory scale experimental modeling are more appropriate to evaluate, numerically, the influence of triggers such as rainfall and earthquakes on seepage velocity and slope deformation. In the field tests, although very expensive, influence of rainfall on mass movement is studied on actual slopes. All these techniques offer 1 g level stresses only; as such, they may not represent actual field level stresses on slopes. Centrifuge models, although having their own merits and challenges, are helpful in studying slope behavior at high stress levels. Nonetheless these experimental models will help in calibrating numerical models, specifically for slopes subjected to different external triggers, so that multiple scenarios can be studied at the field scale. There are a large number of software available for such numerical modeling—ranging from simple to complicated or relatively low cost to expensive—in addition to the availability of several open source coding.

Although experimental modeling of various sizes and scopes are available in practice, this study focuses on a small scale, laboratory based, models to evaluate the seepage velocity, suction, and deformation of slopes subjected to rainfall and/or earthquake induced shaking. Ten different slopes were prepared with varying compaction densities and slope gradients, and subjected to different rainfall intensities and seismic accelerations. The results obtained from the experimental study have been used to calibrate the numerical models so that effect of different intensity of rainfall and earthquake shakings on slope stability could be observed for different gradients and densities using the numerical modeling exercise. The following sections will describe the experimental procedures, data analyses, results, discussion, and a brief summary based on the outcomes of this study.

2 Methodology

2.1 Experimental Modeling

A truck-full of soil was collected from a landslide site at Mission Viejo, Southern California. Various laboratory tests, such as sieve and hydrometer analyses, specific gravity tests, standard Proctor compaction tests, Atterberg limit tests, falling head permeability tests, and direct shear tests were performed on the collected soil samples following the guidelines outlined in the pertinent ASTM standards. Direct shear tests were conducted for soils at different degrees of saturation. The slope materials were sieved through 4.75 mm size sieve so that only smaller sized materials could be used in the laboratory scale models.

The air-dried soil was mixed with water uniformly to prepare a moist sample having ~12% moisture content. While preparing the model slopes, bottom of the 1.2 m \times 1.2 m sized Plexiglas container was installed with Polyethylene pipes having numerous holes—drilled in a staggered way and wrapped with geo-textile—that was buried under 5 cm thick gravel layer. A geotextile layer was installed between the compacted slope and the drainage layer to act as a filter layer. The moist soil was compacted on the geotextile layer—in 5 cm thick layers—at the pre-defined densities. Each layer of compacted soil slope was prepared until the desired height of the slope achieved. The desired geometries of the slopes were marked on the Plexiglas container to guide the compaction effort. Figure 1 illustrates the process involved in making the experimental model slopes. Separate slopes were prepared for two different slope gradients—40° and 45°—at three different void ratios (or densities)—0.89, 1.0, and 1.2—as illustrated in Table 1.

The compacted slopes were installed with miniature tensiometers that were calibrated prior to installation. Calibration of tensiometers prior to placement is extremely important to avoid erroneous suction measurements during the rainfall event. Small holes were drilled into the slope up to the desired depths at the spatial location (Fig. 2) to install the tensiometers (Fig. 3). Those holes were backfilled with the soil after the installation of tensiometers and then the top of the drill holes were sealed with bentonite slurry to avoid rainwater percolating down through the backfilled hole (Fig. 4). Moreover, several copper wire extensometers were installed at pre-defined locations (Fig. 5) as illustrated in Fig. 6 to measure the slope deformation at various locations during and at the end of the experiments.

The experimental models prepared as explained above were than subjected to two different rainfall intensities (1.68 and 3.6 cm/h) and three levels of seismic shaking events (0.1–0.3 g accelerations; 1–3 Hz frequencies), as illustrated in Table 2. The rainfall events were applied through a



Fig. 1 Process for the preparation of experimental model slopes

Table 1 Geometries and densities of the model slopes used for this study

Model number	Slope gradient (Deg)	Void ratio
1	40	0.89
2	40	1.00
3	40	1.20
4	40	1.20
5	40	0.89
6	45	0.89
7	45	1.00
8	45	1.20
9	45	1.00
10	40	1.20

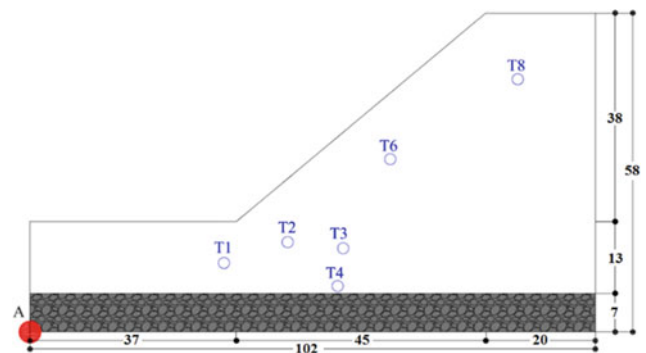


Fig. 2 Locations of the tensiometers at different depths (Decagon T5 tensiometers)



Fig. 3 Drilling in the slope to install the miniature tensiometer

laboratory scaled custom designed sprinkler system (Fig. 7), and the seismic events were applied after preparing the model on the shaking table, shaking with actuators, and saturating them with rainfall (Fig. 8).

During the rainfall events, advancements of the wetting fronts were traced—every 15 min—while suction values



Fig. 4 Backfilling of the top surface of tensiometer location with bentonite slurry

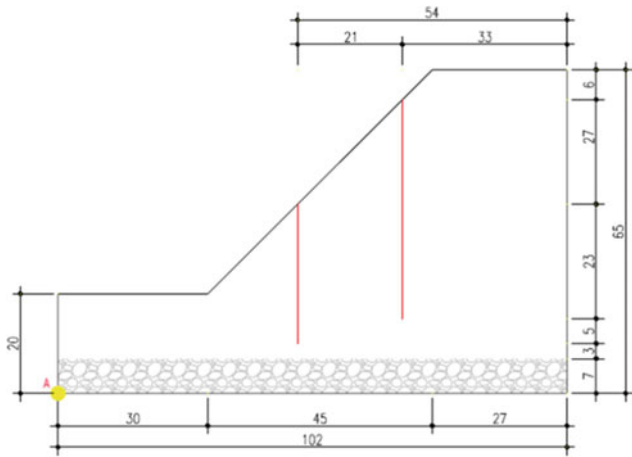


Fig. 5 Location of copper wire inclinometers (units = cm)

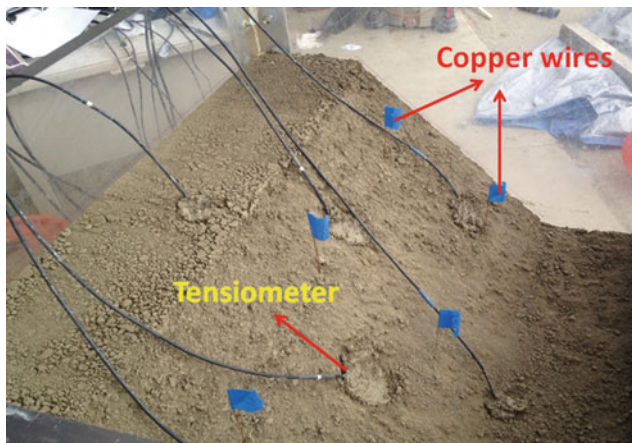


Fig. 6 Installed copper wire inclinometers

were recorded with the tensiometers every second. Suction values were also recorded during the seismic events to measure the change in suction during seismic events. Moreover, deformations of the slopes were measured using high resolution cameras (surface, real time) and the copper

Table 2 Rainfall intensities (prior to seismic motion) and seismic motions applied to the models

Model number	Rainfall intensity (cm/h)	Seismic motions
1	1.68	0
2	1.68	0
3	1.68	0
4	3.60	0
5	3.60	0
6	3.60	0
7	3.60	0
8	3.60	0
9	1.68	0
10	3.60	0.1–0.3 g 1–3 Hz



Fig. 7 Custom designed sprinkler system used for this study

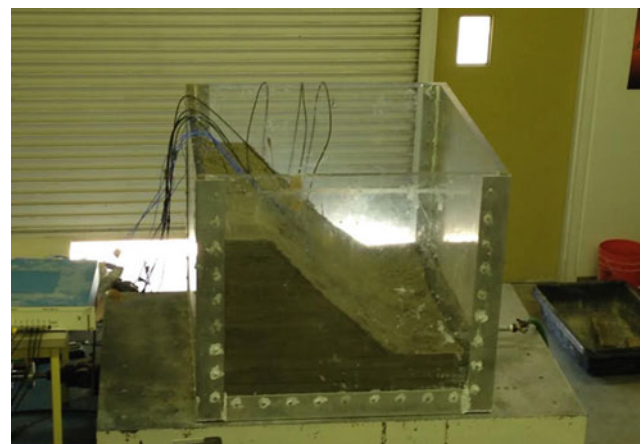


Fig. 8 Slope models prior to shaking on the shaking table

wire extensometers (depth-wise, at the end of the test). Degrees of saturations for soil at the tensiometer locations were measured at the end of the rainfall event.

2.2 Numerical Modeling

Numerical models were developed for the slope models at the same geometry and densities as used in the experimental modeling. Slope/W, Seep/W, and Sigma/W platforms of the GeoStudio software were used for static analysis and Quake/W was used for the seismic analysis. Prior to the initiation of numerical modeling to acquire various parameters, numerical modeling parameters for Seep/W were calibrated with the experimental results, specifically with the wetting front locations and suctions at different locations and time spans. To perform finite element analysis for experimental models in this study, Sigma/W was used. Before performing the stability analysis, steady-state seepage analysis was performed first to obtain initial pore-water pressure condition to be matched with the experimental information, and then the model was imported into the Sigma/W for transient analysis state. Sigma/W allows simulating rainfall on the slope in desired amount of time. Change in pore-water pressure with rainfall duration was also calculated by using this module. The required parameters for the numerical analysis were taken from laboratory experiment (Table 3). There were a few assumptions made in this analysis: (a) infiltration was considered as the only effect on seepage condition within the slope, and the evaporation on the surface of the slope was ignored during the numerical analysis; (b) if rainfall intensity is smaller than the saturated hydraulic conductivity, all rainfall infiltrates into the surface, and the excess amount will runoff and flow down the slope. In Seep/W, a “q” unit flux boundary condition is assigned as the rainfall intensity, which was 1.68 or 3.6 cm/h. This flux value is applied along the surfaces of the slope, as shown in Fig. 9. In Sigma/W, there were a few assumptions for input parameters, such as Young’s modulus and Poisson’s ratio. Typical values of Young’s modulus for cohesive material obtained from literature for high plasticity clay (CH)—7000 kPa for void ratio of 0.89, 5500 kPa for void ratio of 1, and 4000 kPa for void ratio of 1.2—were used. The value of Poisson’s ratio used was 0.45. Details of the numerical analysis using these platforms are available in Tran (2017).

Table 3 Parameters used in numerical modeling of model 1

Parameter	Values
Void ratio	0.89
Hydraulic conductivity (m/s)	4×10^{-9}
Rainfall intensity (cm/h)	1.69
Young modulus (kPa)	5000
Poisson’s ratio	0.45

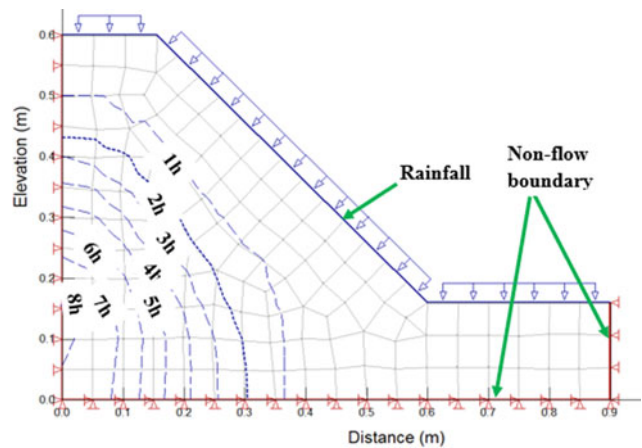


Fig. 9 Boundary conditions and grid set-up for numerical modeling

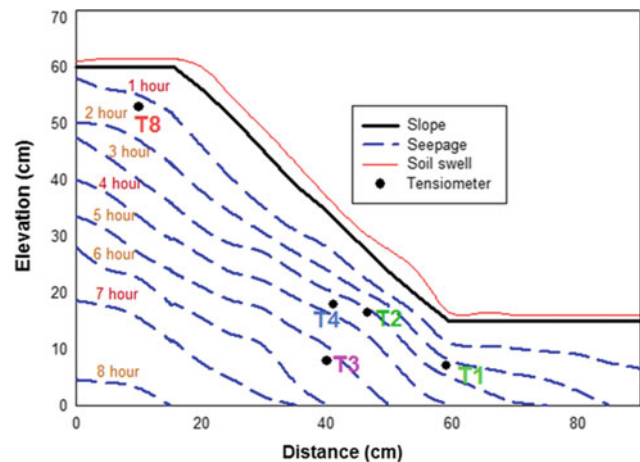


Fig. 10 Advancement of wetting front with time—recorded by eye-observation through the Plexiglas container

3 Results and Discussion

3.1 Laboratory Experiments

Presented in Fig. 10 is a sample wetting front locations—separated every hour—for Model 2. Time vs suction recording at 5 tensiometer locations on this model are presented in Fig. 11. Results presented on Fig. 10 can be used to estimate the time required for the water to reach tensiometers and reduce the suction to ~ 0 kPa. Please note that tensiometers were installed half way from the edge of the slope while wetting fronts were measured at the edge of the slope. As can be observed in Table 4, time required for the tensiometer to cease suction is very close to the time the wetting front advanced to those tensiometers, except in Tensiometer 3 (T3). From the pattern of the suction variation with time, observed in Fig. 11, it is clear that this

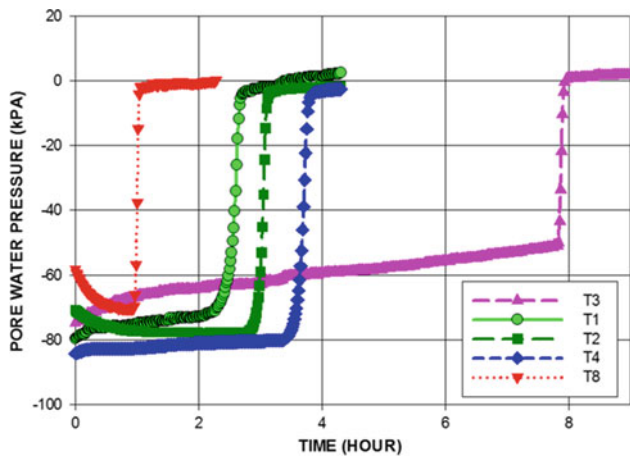


Fig. 11 Variation of suction with time—recorded by the tensiometers

tensiometer had some recording issues during the initial period. Similar results were obtained for other models as well. Please also note that as the soil was compacted at higher density for this model, soil swelled after the slope became saturated as can be observed in Fig. 10 for the post-experiment slope.

Deflection of the copper wire extensometers with depth shows the location that had the maximum deformation. Presented in Fig. 12 are the deflections of copper wires for Model 3. Deflection of the copper wire extensometers helped to predict the plane that has maximum deformation for Model 3, as presented in Fig. 13.

The wetting front information presented in Fig. 10 has been used to calculate seepage velocity for all 10 models so that variation in seepage velocity on slopes with soil density and intensity of rainfall could be developed. Presented in Fig. 14 is the relationship between seepage velocity and void ratio for two different rainfall intensities. Likewise, Fig. 15 shows the variation in seepage velocity with infiltration rate. Similar results were obtained for the 45° slope as well.

The results obtained from the experimental modeling were compared with the results obtained from the numerical analysis using Seep/W. As can be observed in Figs. 16 and 17, the results obtained from the numerical modeling in models with 40° slopes were close to that from the

experimental modeling. This is the way how calibrations of the numerical models were performed. Similar results were observed for the 45° slopes as well.

Critical failure planes were also obtained through numerical analysis using Sigma/W, as presented in Fig. 18 (for Model 1). Presented in Figs. 19 and 20 are the comparison of weakest planes obtained with experimental and numerical analyses for Models 6 and 2, respectively.

The comparison between seepage velocities and deformation obtained from both numerical and experimental modeling was useful to calibrate the numerical models, as explained earlier. With the Slope/W function of the Geo-Studio, reduction in safety factors with an increase in rainfall duration for the experimental models were calculated at the critical/weakest planes using Spencer’s Method. Although the factors of safety were higher than 1 and the models did not fail, there was a drastic reduction in safety factors with an increase in rainfall duration for all slopes, with denser slopes having a lower reduction rate. Results of the numerical analysis related to safety factor reduction with rainfall duration for 40° slopes having different soil densities, subjected rainfall intensities of 1.68 cm/h and 3.6 cm/h are presented in Figs. 21 and 22, respectively. Similar results for the 45° slopes at the rainfall intensity of 3.6 cm/h are presented in Fig. 23, for comparison.

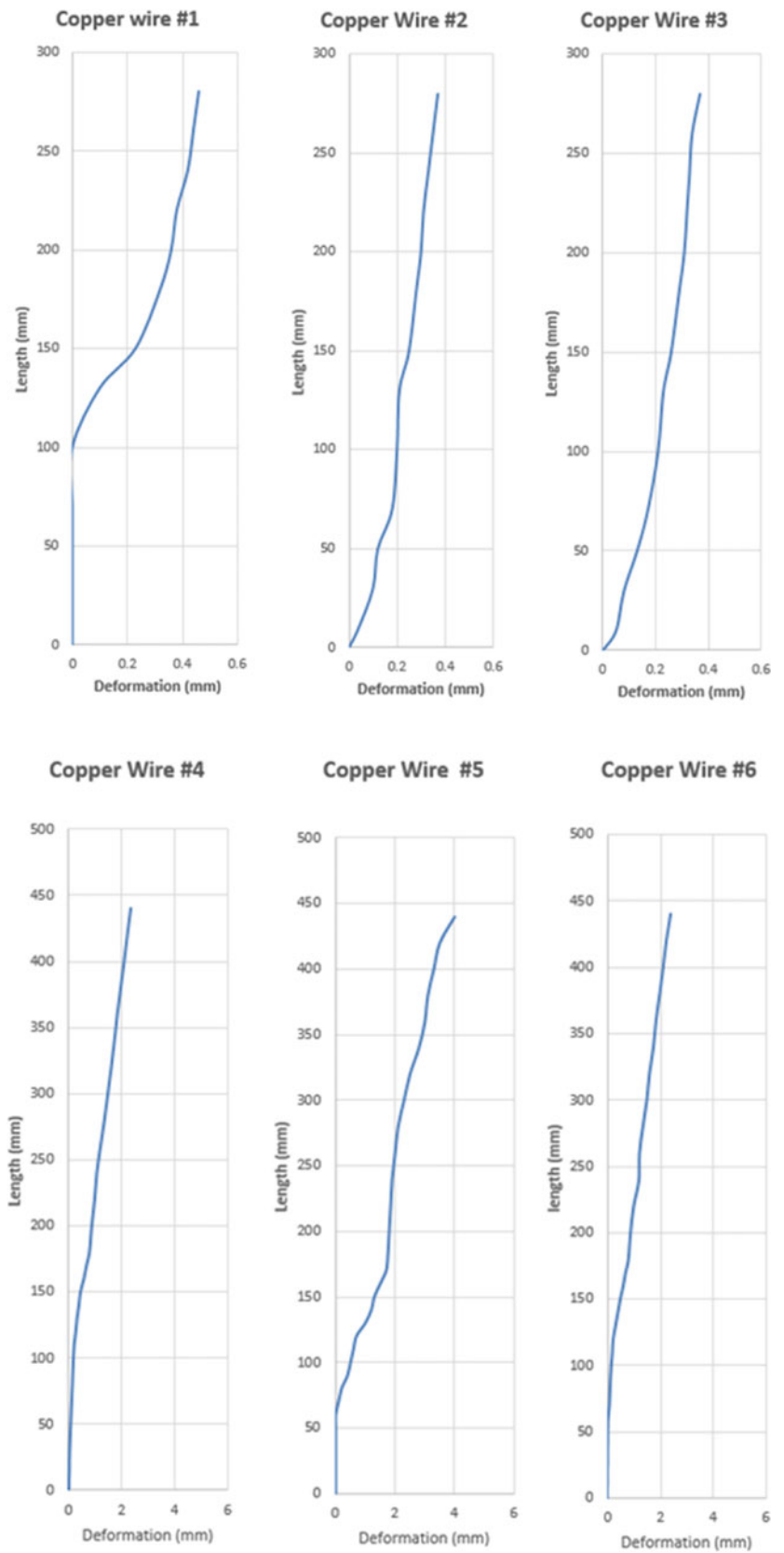
As explained in the previous section, slope models were prepared in the Plexiglas container to make a 40° slope at the void ratio of 1.2 (Model 10). Tensiometer devices and accelerometers were installed at different depths within the slope. First, the slopes were subjected to a series of sinusoidal waves for 20 cycles, separately at the frequencies of 1, 2, 3 Hz and accelerations of 0.1, 0.2, 0.24, and 0.3 g. In addition, ground motion recorded at station 90,095 during the 1994 Northridge Earthquake was also applied. Figure 24 shows the ground motion applied to the model.

Right after the shaking event, the sprinkler system was set on the top of the Plexiglas container. Rainfall intensity of 3.6 cm/h was introduced to the slope. Figure 25 shows the variation in pore water pressure during the shaking stage. As can be observed in Fig. 25, there is no change in suction in the compacted soil during shaking. Presented in Fig. 26 is the variation in suction during the rainfall event, observed

Table 4 Time required for the wetting fronts to reach tensiometers and the tensiometers to drop suction to ~0 kPa

Tensiometer location	Time required for wetting fronts to reach tensiometers (h)	Time required for tensiometers to drop suction values to ~0 kPa (h)
T1	2.5	2.5
T2	3.0	3.0
T3	5.2	7.9
T4	3.5	3.9
T8	1.2	1.2

Fig. 12 Copper wire deflections observed after the experiment in model 3 (x-axis exaggerated)



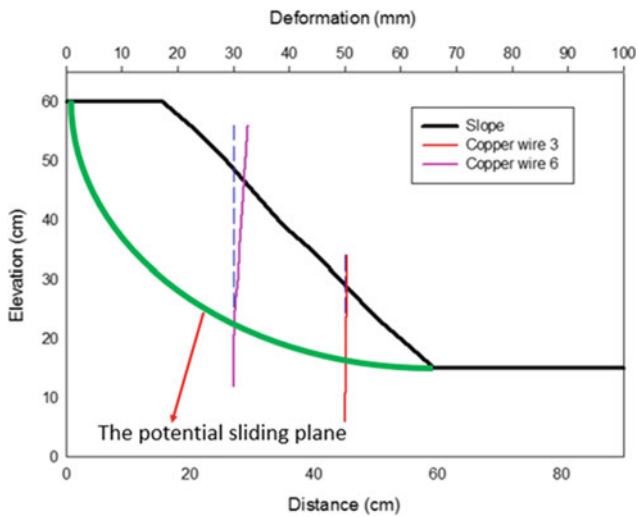


Fig. 13 Predicted weakest plane in model 3

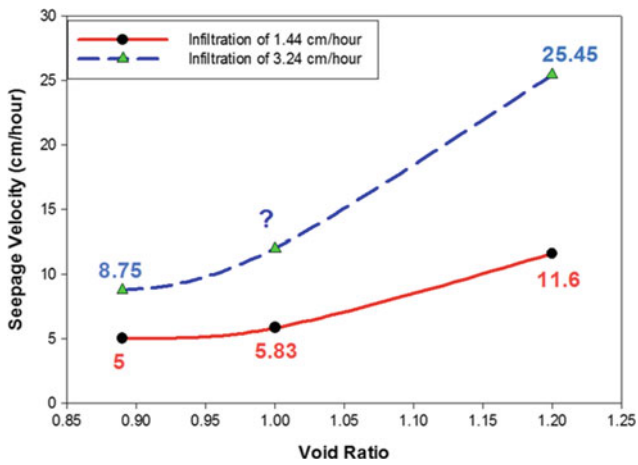


Fig. 14 Variation of seepage velocity with void ratio for two different intensities of rainfall for 40° slope. Data for point ‘?’ was obtained from the numerical analysis

with the tensiometers. Deformation observed with the copper wire and the potential sliding plane obtained with Sigma/W for the slope subjected to rainfall after the seismic event is presented in Fig. 27. As can be observed in Fig. 27, deformation of the slope decreased after the model was shaken with a series of seismic events; and the potential sliding planes obtained from the numerical and experimental results were similar. Figure 28 shows the comparison of factors of safety obtained for static slope and same slope subjected to post-seismic event rainfall event. As observed in Fig. 28, safety factors have increased for the same slope after the shaking event due to the increase in soil density after the shaking event; please note that Model 10 had the highest void ratio, i.e. lowest compaction density.

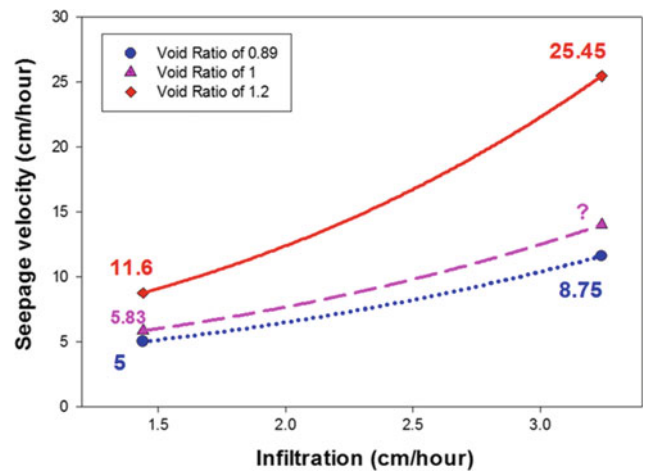


Fig. 15 Variation of seepage velocity with intensity of rainfall for three different void ratios for 40° slope

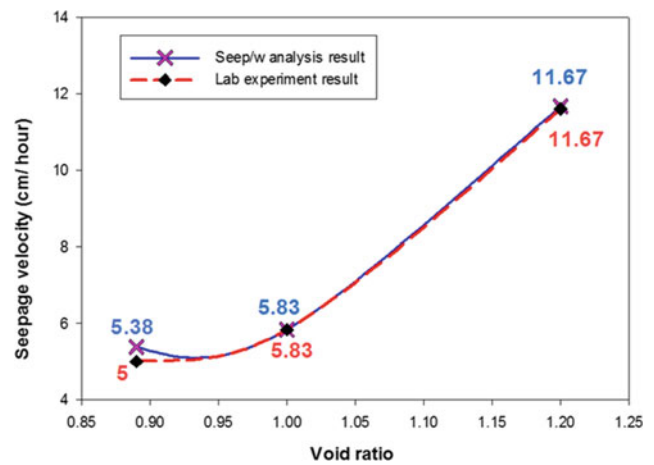


Fig. 16 Seepage velocities from numerical and experimental models for 40° slope; rainfall intensity 1.68 cm/h

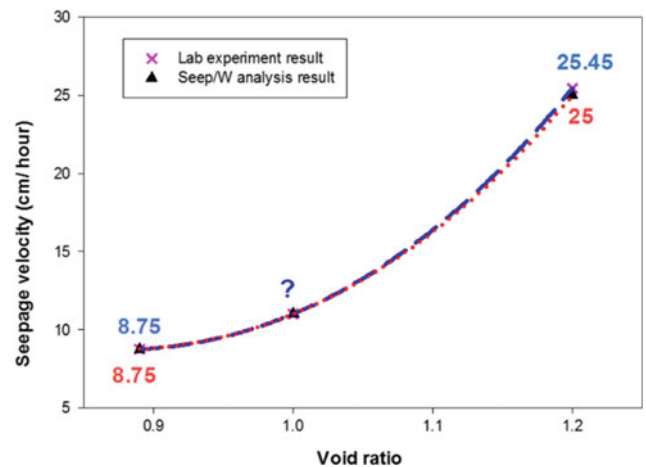


Fig. 17 Seepage velocities from numerical and experimental models for 40° slope; rainfall intensity 3.6 cm/h

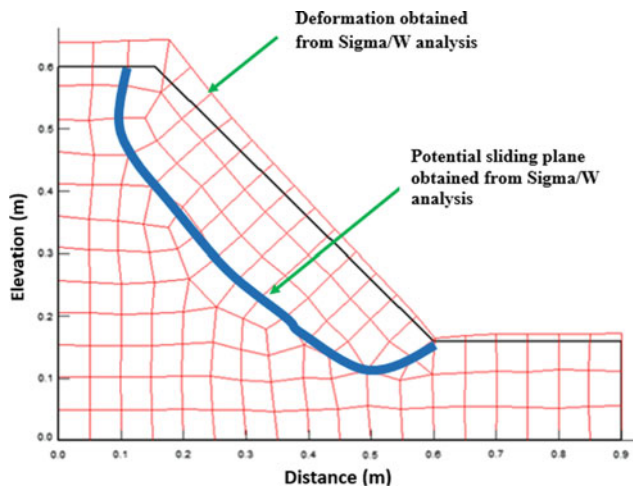


Fig. 18 Weakest plane obtained from numerical analysis—Sigma/W for model 1

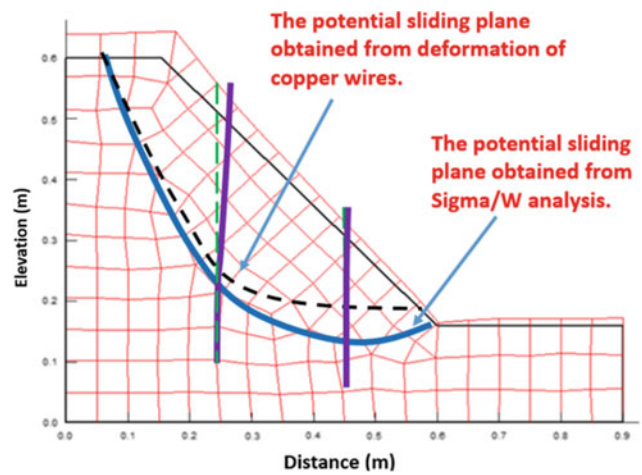


Fig. 20 Weakest plane obtained from numerical and experimental analyses—Sigma/W for model 2

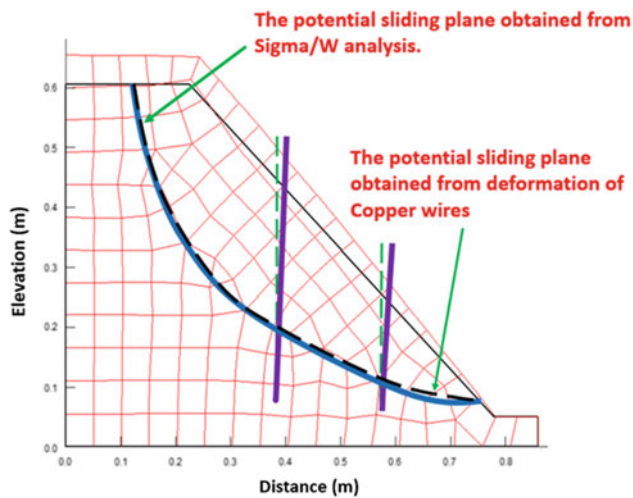


Fig. 19 Weakest plane obtained from numerical and experimental analyses—Sigma/W for model 6

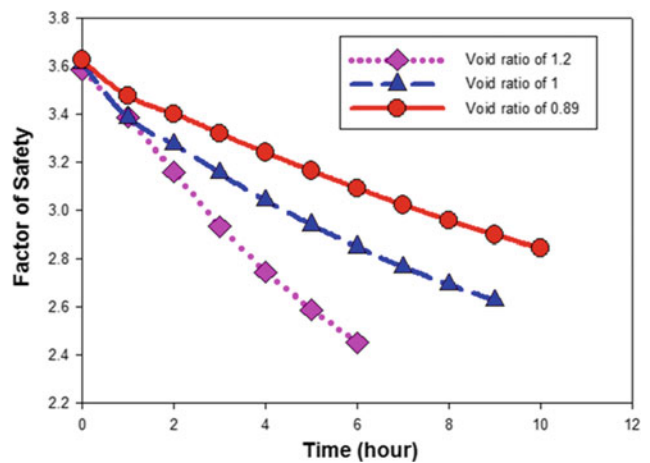


Fig. 21 Variation in safety factor with rainfall duration in 40° slope model subjected to 1.68 cm/h rainfall

4 Summary and Conclusion

Extensive experimental modeling efforts were made on slopes prepared at two different slope gradients and three different densities. Those experiments included preparing the slopes, instrumenting them with tensiometers and extensometers, and subjecting the slopes to two different intensities of rainfall until the slopes got saturated. The suction values and extensometer deformations were recorded and the results were compared with the results obtained from the wetting front advancement with time. Moreover, numerical analyses were performed on all the slopes to calibrate the numerical analyses parameters. Results obtained from Seep/W on seepage velocities and Sigma/W on deformation matched well with the results obtained from the wetting

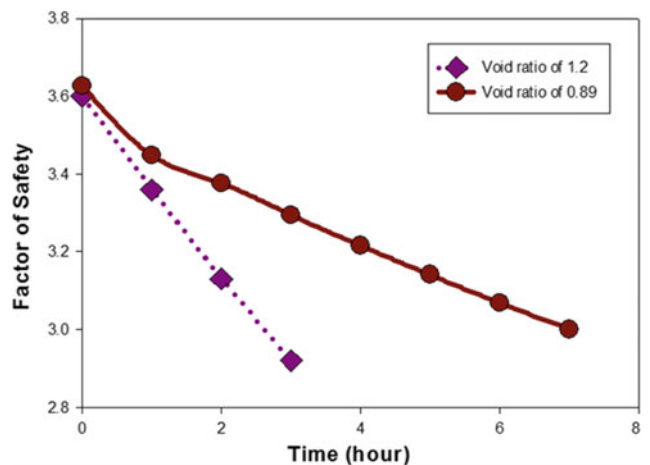


Fig. 22 Variation in safety factor with rainfall duration in 40° slope model subjected to 3.6 cm/h rainfall

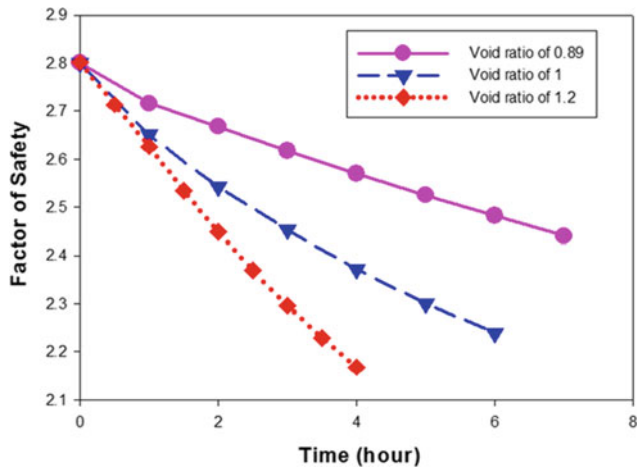


Fig. 23 Variation in safety factor with rainfall duration in 45° slope model subjected to 1.68 cm/h rainfall

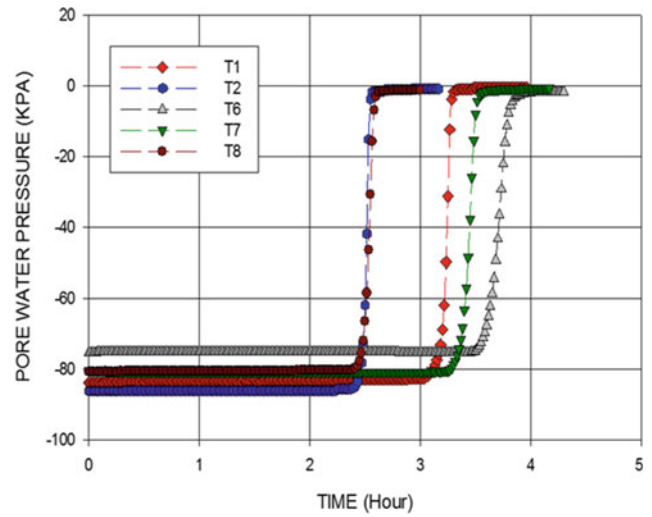


Fig. 26 Variation in suction with time during the post-earthquake rainfall event

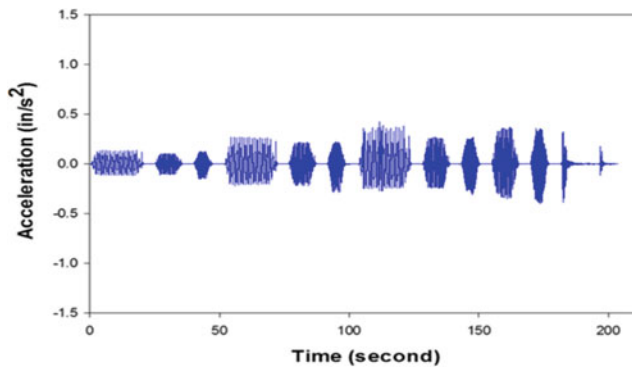


Fig. 24 Ground motion applied to model 10 prior to the application of rainfall event

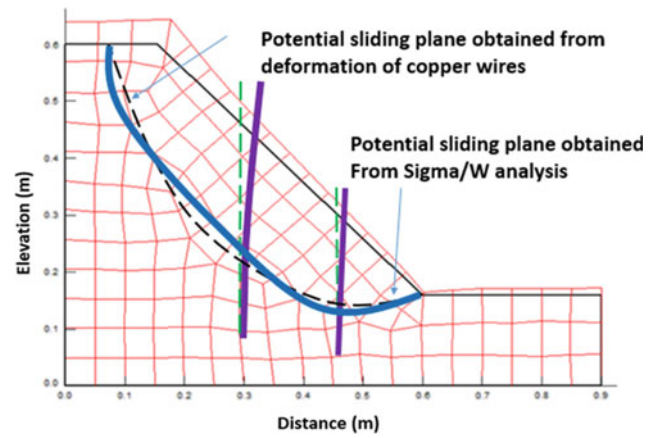


Fig. 27 Potential sliding planes observed on model 10 with experimental and numerical results

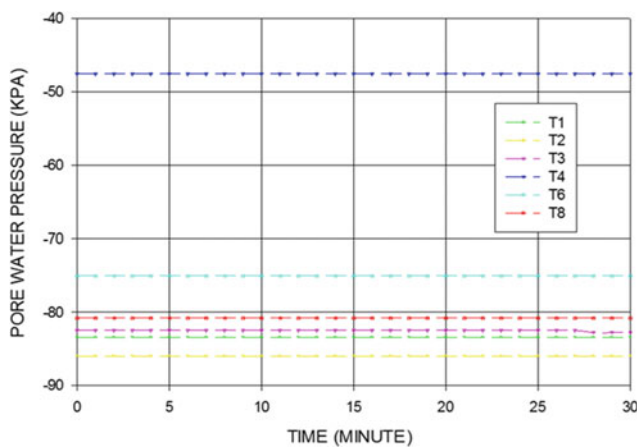


Fig. 25 Variation in suction with time during the shaking event

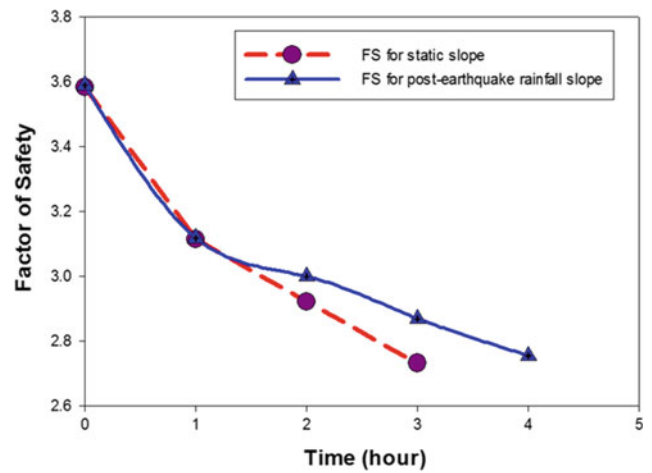


Fig. 28 Variation of the factors of Safety on Model 10 with time for static and seismic loading

fronts/tensiometer recordings and copper wire deformation, respectively. The calibrated numerical models were used to calculate the factors of safety of slopes with the duration of rainfall using Slope/W module of GeoStudio. In addition to the static experiments, slope model that had the lowest density was shaken on the shaking table with a series of seismic motions and change in suction during the shaking was observed. It was observed that there was no change in suction with seismic shaking. When the shaken slope was subjected to a rainfall event, there was a reduction in seepage velocity and deformation compared to the same slope that was not subjected to seismic events. Such reduction in seepage velocity has been attributed to the increase in density of the soil during and after shaking. This study provides a complete information about how various soil and ground parameters influence stability of slopes and how numerical models can be calibrated with the experimental modeling results to apply the calibrated numerical models for field slopes/landslides.

Acknowledgements The project was funded by Intramural Grant at California State University, Fullerton. The authors would like to thank

Dr. Beena Ajmera, Hector Zazueta, Sharif Mohiuddin, Mohamad Sadik Khan, Juan Reyna, Jennifer Lowes, Hari Woli, and dozens of community college and high school interns who were involved in this study.

References

- Ajmera B, Tiwari B (2021) Recent advances in the methods of slope stability and deformation analyses. Understanding and reducing landslide disaster risk. WLF2020. ICL Contribution to Landslide Disaster Risk Reduction, Kyoto, pp 4, 81–108
- Tiwari B, Ajmera B, Khalid M, Donyanavard S, Chavez R (2018) Influence of slope density on the stability and deformation of clayey slopes. *Geotech Special Publ* 297:293–301
- Tiwari B, Caballero S (2015) Experimental model of rainfall induced slope failure in compacted clays. *Geotech Special Publ ASCE* 256:1217–1226
- Tiwari B, Lewis A, Ferrar E (2013) Experimental simulation of rainfall and seismic effects to trigger slope failures. *Geotech Special Publ ASCE* 231(1):448–451
- Tran D (2017) Effect of rainfall and seismic activities on compacted clay slopes having different void ratios and inclinations. MS thesis, California State Univ., Fullerton, California

Open Access This chapter is licensed under the terms of the Creative Commons Attribution 4.0 International License (<http://creativecommons.org/licenses/by/4.0/>), which permits use, sharing, adaptation, distribution and reproduction in any medium or format, as long as you give appropriate credit to the original author(s) and the source, provide a link to the Creative Commons license and indicate if changes were made.

The images or other third party material in this chapter are included in the chapter's Creative Commons license, unless indicated otherwise in a credit line to the material. If material is not included in the chapter's Creative Commons license and your intended use is not permitted by statutory regulation or exceeds the permitted use, you will need to obtain permission directly from the copyright holder.





Sustainability of Geosynthetics-Based Landslide Stabilization Solutions

Ivan P. Damians, Yoshihisa Miyata, Pietro Rimoldi, Nathalie Touze, and John Kraus

Abstract

This paper considers the sustainability of geosynthetics-based solutions to mitigate landslide risks. The different types of geosynthetics are briefly described, along with their functions and applications relevant to landslides, emphasizing reinforcement. The paper identifies the sustainability factors to consider when applying geosynthetics for these purposes. The paper then presents an overview based on existing literature to illustrate how geosynthetics typically outperform traditional methods across a range of sustainability criteria across the entire life cycle. The paper shows lastly how the value integrated model for sustainable evaluations (MIVES) tool can be applied to evaluate and compare alternative methods for remediation of landslides and recommends further studies using this tool.

Keywords

Geosynthetics • Landslides • Sustainability assessment • MIVES

1 Introduction

Landslides have occurred since time immemorial, even without any land transformation generated by human actions. They can occur worldwide, with little distinction across geographical locations, and represent one of the most common geological events.

Historically, different construction solutions have been considered with the aim of avoiding ground displacements, especially where there is risk to life or where infrastructure, buildings, or service installations are vulnerable to damage. It is essential to choose the appropriate solution based on a solid understanding of the causes of landslides. Among the natural causes, the most frequent are rainwater infiltration, rising groundwater levels, loss of vegetated surface, erosion, and weathering.

Human land use and related ground transformation often increase the potential for landslides, for example, as a consequence of construction, earthworks, and urbanization—i.e., modification of previously stable geometries and/or loading conditions. Other significant factors include deforestation (change of the previous surface scenario that may include deep-rooted vegetation removal), blasting and mining, and agricultural and forestry activities.

Appropriate preventative measures can be active or passive, depending on the specific factors. Active interventions may include direct ground modifications or measures to rectify previous potentially unstable scenarios by modifying the geometry of the land or strengthening the ground. Examples of passive approaches include mechanical protective measures, drainage, filtration, and separation.

I. P. Damians (✉)

Department of Civil and Environmental Engineering, University Politècnica de Catalunya-Barcelona Tech (UPC), & International Centre for Numerical Methods in Engineering (CIMNE), 08034 Barcelona, Spain
e-mail: ivan.puig@upc.edu

Y. Miyata

Department of Civil Engineering, National Defense Academy of Japan, Yokosuka, 239-8686, Japan
e-mail: miyata@geotech-research.jp

P. Rimoldi

Eng. Pietro Rimoldi, Civil Engineering Consultant, Corso Garibaldi 125, 20121 Milano, Italy

N. Touze

University Paris-Saclay, INRAE, SDAR, 78352 Jouy-en-Josas, France
e-mail: nathalie.touze@inrae.fr

J. Kraus

International Geosynthetics Society (IGS), 9225 Bee Cave Rd Building B, Suite 206, Austin, 78733, TX, USA

© The Author(s) 2023

K. Sassa et al. (eds.), *Progress in Landslide Research and Technology, Volume 1 Issue 1, 2022*, Progress in Landslide Research and Technology, https://doi.org/10.1007/978-3-031-16898-7_14

Geosynthetics are durable polymers that provide high performance, and they often contribute to making infrastructures more sustainable in many aspects. Nowadays, polymeric materials are used routinely for soil reinforcement and stabilization, barrier systems and hydraulic drainage within the civil engineering framework. Fibrous filter fabric products were already used in ancient times to improve the mechanical performance of soil, using natural fabrics or vegetation. But, in the final third of the twentieth century, more stable and durable products were available, following the advent of polymeric materials. As the technology advanced, its effectiveness increased significantly, and previously unknown or unconsidered applications became viable.

The list of the most commonly used geosynthetic products currently available is extensive. It includes geotextiles, geogrids, geonets, geomembranes, geocells, and geocomposites. These products consist of diverse materials, typically polyamide, polyester, polyethylene, polypropylene, polyvinylchloride, ethylene and copolymer. They take various forms, usually sheets, grids, cells, or strips. This diversity of material and form leads to performance that is well adapted to the specific needs of the required function.

2 Geosynthetics for Landslide Prevention

Within the many civil engineering applications where geosynthetics play a fundamental role, their use in landslide stabilization projects is not new. The main related functions for landslide stability purposes are filtration, drainage, protection and reinforcement. Geosynthetics demonstrate several significant mechanical/functional/technical advantages.

Engineers can prevent landslides in various ways using geosynthetics:

- using geotextiles and geomembranes to perform barrier function and/or filter function, which prevents the effects of water seepage;
- using high strength geosynthetics to reinforce the soil, thus making stable even for very steep slopes;
- using geomats and geocells for hold topsoil in place, thus preventing slippage;
- using geocomposite drains to allow excess rainwater to disperse safely, without washing the soil away; and/or
- applying geosynthetics for erosion control to the surfaces of slopes to encourage the growth of new vegetation and provide anchorage to the root structures, thereby increasing their erosion resistance under significant hydraulic stresses, further stabilizing slopes through natural means.

For landslide mitigation, geosynthetics are often utilized to provide tensile strength and added stiffness to the soil,

which is basically strong in compression, to achieve a safe level. Geosynthetic reinforcements combine high tensile strength (up to 1000 kN/m in some products) with limited tensile creep, improved interaction with the surrounding soil material, and resistance to chemical/biological degradation and environmental ageing.

Since 1980 geosynthetics, and particularly geogrids, have been extensively used for the construction of Reinforced Soil Structures (RSSs), and in many landslide stabilization projects, for slopes as high as 60 m (Cambiaghi and Rimoldi 1991; Cazzuffi et al. 1995; Coluzzi et al. 1996; Coluzzi et al. 1996; Coluzzi et al. 1997; Dikran and Rimoldi 1994; Manni and Rimoldi, 2006; Rimoldi 1996; Rimoldi and Ricciuti 1992; Rimoldi and Scotto 2012).

RSSs have been designed and built even in highly seismic areas (Rimoldi 2018) using cohesive/ marginal fills (Giroud et al. 2014).

Layers of geosynthetic reinforcement are used to stabilize slopes against potential deep-seated failure using horizontal layers of primary reinforcement. The reinforced slope may be part of slope reinstatement and/or used to strengthen the sides of earth fill embankments.

The reinforcement layers allow slope faces to be constructed at steeper angles than the unreinforced slope. It may be necessary to stabilize the face of the slope (particularly during fill placement and compaction) by using relatively short and more tightly spaced secondary reinforcement and/or wrapping the reinforcement layers at the face. In most cases, the face of the slope must be protected against erosion. An interceptor drain may be required to eliminate seepage forces in the reinforced soil zone. Figure 1 shows the scheme of a reinforced soil slope, and Fig. 2 shows an example of a remediated slope with a reinforced slope structure.

Recently, Rimoldi et al. (2021) reported on geosynthetic reinforced soil structures for slope stabilization and landslide rehabilitation in Asia, including slope reinforcement and

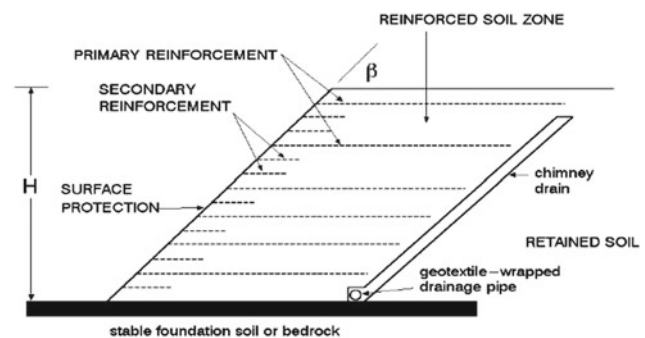


Fig. 1 Scheme of a geosynthetic reinforced soil slope (from IGS leaflet “Geosynthetics in Slopes over Stable Foundations”)

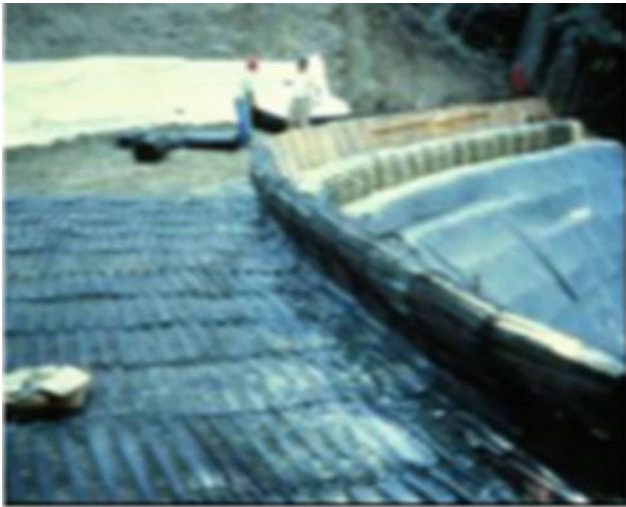


Fig. 2 Example of remediated slope with reinforced slope structure (from IGS leaflet “Geosynthetics in Slopes over Stable Foundations”)

drainage (Fig. 3). In most applications, geosynthetics usually offer lower production costs than traditional solutions. Geosynthetics can be shown to be the best products used in landslide rehabilitation and natural disaster reconstruction through life cycle cost analysis. In fact, there are several advantages when using geosynthetics: space savings; avoidance of costly ‘remove and replace’ methods; possible use of locally available lower quality backfill materials; low maintenance due to long life cycle; lower time and labour costs, because geosynthetics are easy to install, use less backfill material and require no special equipment; increased reliability of designed solutions thanks to geosynthetics’ guaranteed mechanical and hydraulic properties.

3 Sustainability

As an integral part of civil engineering design decision-making, sustainability criteria are becoming more common (e.g., Aguado et al. 2012; MacAskill and Guthrie 2013), including in geotechnical engineering projects (Basu et al. 2014; Holt et al. 2010). Sustainability and sustainable development include the capacity to carry out an activity (such as manufacturing or constructing a product or structure) with minimal or no impact (BSI 2012; Josa and Alavedra 2006; WCED 1987). However, sustainability is more broadly defined as satisfying three sets of requirements or pillars based on environmental, economic and societal/technical/ functional criteria (Afnor Group 2012; ISO 2019). Sustainability objectives can vary between project types and



a)



b)



c)



d)

Fig. 3 Geosynthetic reinforced soil structures for slope stabilization and landslide rehabilitation in Asia (from Rimoldi et al. 2021): **a** reinforced soil structure along the river Myittha in Myanmar, as a remedial work of an existing collapsed concrete masonry wall, **b** installation of gravel layer wrapped with nonwoven geotextile as drainage material, **c** rainwater runoff triggered a slope collapse, and **d** installation of geosynthetic reinforcements and view of the completed slope remediation

within different categories due to differences in costs of materials, construction, maintenance, environmental and societal impacts, etc.

Sustainable design involves finding a satisfactory balance between these competing objectives (Basu and Puppala 2015; Josa and Alavedra 2006; Josa et al. 2008). A key feature of sustainable design is a structure or project lifetime ‘cradle-to-grave’ perspective, although ‘cradle-to-operation’ or ‘cradle-to-gate’ are also common (ISO 2006a, b). In slope stability, lifetime use is considered in six stages comprising (1) **extraction and processing** of raw materials, (2) **production of materials** required for each alternative approach (including the extraction and treatment of aggregates, specific geosynthetic products production, and all/other products/processes involved, etc.), (3) **construction/execution/installation** of the alternative and all related/involved works including necessary controls/checking tasks during construction, (4) **maintenance** involved in the whole service life, including eventual final stage, (5) **demolition** up to achieving (6) **end-of-life** stage of the solution. All these tasks are directly related to energy consumption both for direct execution and indirectly, e.g., transport. Obviously, this lifetime has to be the same for all alternatives under comparison, which is included in the definition of the functional unit, fixed between them.

Therefore, sustainability is understood and standardized in the context of our global systems to encompass environmental, economic and social impacts, where the needs of the present generation are met without compromising those of future generations. From this sustainability point of view, geosynthetics have proven themselves as suitable solutions in many civil engineering applications. Often, they represent the best option across multiple sustainability factors, particularly for landslide stability purposes. Whether in landslide or other applications, when compared with conventional approaches, geosynthetics-based solutions have demonstrated reduced material use and lower costs for materials, construction and maintenance works.

In general terms, **economically**, at the construction level of slope stabilization, different studies have proven that a construction solution that opts for geocomposites is much more economical and efficient. The use of geosynthetics may reduce or even eliminate waste deposits. Furthermore, geosynthetics can also serve as reinforcing and/or drainage materials to accelerate the consolidation of soft subgrades, thereby reducing execution times, transportation, and general construction-related costs.

Geosynthetics also deliver superior **environmental** performance in terms of a smaller carbon footprint and effective climate mitigation and adaptation. Material displacements are considerably reduced, and the tools and equipment used for installation are much simpler than traditional methods. Transportation is also much easier, and there is no need for highly qualified personnel to perform installation and

construction. Compared with conventional options, significant savings are typically obtained (Christopher 2014).

Geosynthetics also bring significant **social, technical and functional** benefits in comparison with other foundation-stabilization methods such as dewatering, excavation, and replacement with certain granular materials or chemical stabilization. Compared with traditional drainage methods (i.e., sand and gravel), a key advantage is that geosynthetics-based solutions significantly reduce the required thickness of aggregate layers compared with conventional solutions. Also, geosynthetic products typically work better than the geotechnical materials they replace and the performance improvement is gained by using manufactured materials with fully known properties.

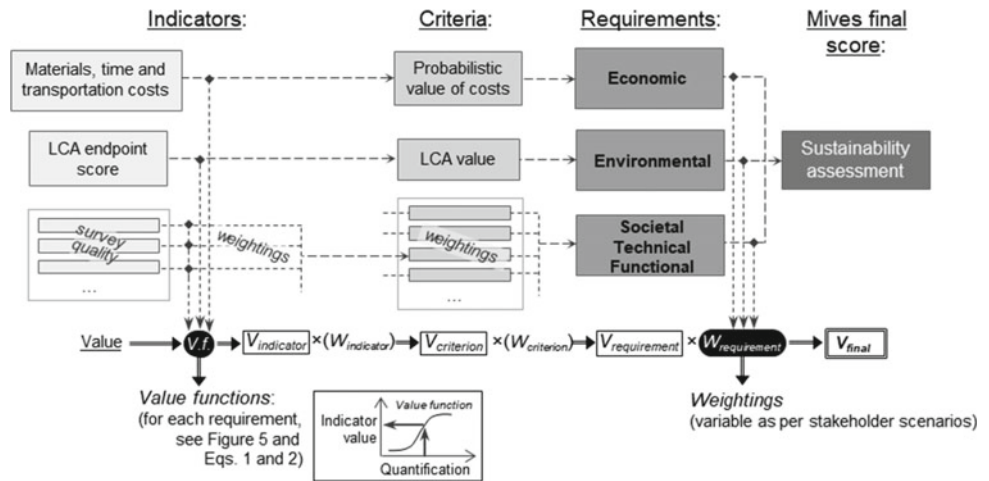
3.1 Sustainability Assessment: MIVES Methodology for the Case of Slope Stability Remediation Alternatives. General Approach

A sustainability assessment model should be based on value theory and multi-attribute assumptions. For slope stabilization performances, a value integrated model for sustainability evaluations (MIVES) methodology may be used (Josa et al. 2008), as has already been done for other civil engineering applications. Damians et al. (2018) present a clear and direct application for retaining wall structures, which can be used here as a reference for slope stability applications.

The MIVES method (hosted in free software available at: <https://deca.upc.edu/es/proyectos/mives/descargas>) can be used for quantitative sustainability assessment of any defined functional unit for which inputs and outputs can be related for each requirement level or pillar category by using multicriteria analyses.

As already stated, a proper definition of the functional unit is crucial for a correct comparison between alternative solutions (in this case, for example, according to different measures/actions to remediate unstable slopes, affecting the same extension area, etc.). According to the functional unit, the full inventory of materials and actions related to each case study analysis is required (indicator items list). The sustainability assessment methodology and related outcomes using the MIVES approach can be understood from the flow chart in Fig. 4, where the requirements tree is defined by a hierarchical process. Sustainability requirements refer to environmental, economic and societal/ technical/ functional pillars (the basic/standardized pillar categories defining sustainability; ISO 2019). Each category is defined by criteria with three or more quantifiable indicators. Each multicriteria analysis ends with a single numerical score (V_{final}) suitable for objective decision-making between the different

Fig. 4 Sustainability assessment flow chart or requirements tree proposal for landslide applications (modified from Damians et al. 2018)



project alternatives under consideration. The global process of assigning values and weighting to each indicator—criteria—requirement level to arrive at a final MIVES score (V_{final}) is shown below the flow chart in Fig. 4 and explained.

3.2 Sustainability Requirements Definition

For slope stability purposes, as typically done in many other areas, the **economic pillar** can focus on project costs. These costs accrue from the manufacturing and transportation of construction materials, anticipated material losses, on-site fabrication of structural remediation components, including labour and the like. For cradle-to-grave sustainability assessment, these costs include operation but also maintenance and, if included in the functional unit lifetime definition, final dismantling and disposal of materials.

Cost variability is common in civil and construction engineering projects (depending on the project's specifics, site of the works, types of suppliers, materials/specifications, etc.). Probabilistic cost analysis is recommended. While cost can be finally grouped as a single indicator, it may also be split with regard to costing types (in such cases, probabilistic analysis may be applied to some indicators only).

The **environmental pillar** focuses on environmental impacts and is most often addressed through a life cycle assessment (LCA) approach. Fraser et al. (2012), Heerten (2012), Stucki et al. (2011), and Damians et al. (2017) present examples where LCA approaches were applied in studies of different geosynthetic applications to civil engineering. An LCA should ideally consider all possible environmental impacts of any construction process and materials used in the project works (ISO 2006b). Midpoint (pM) indicators (e.g., tonnes carbon dioxide equivalent (tCO_2e)) are used to identify intermediate effects of pollutants, and damage models are used to compute endpoint

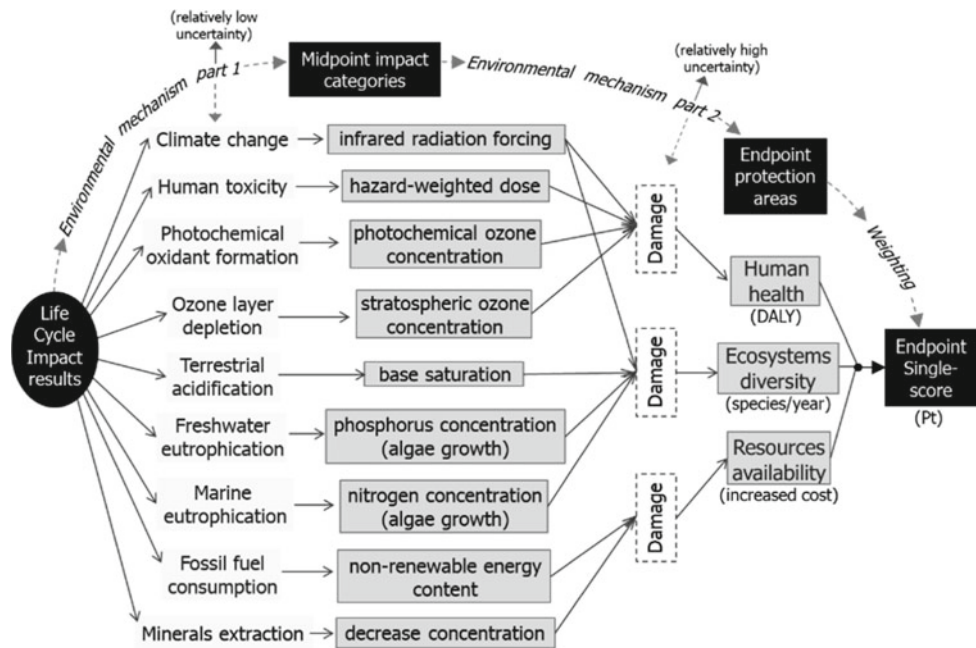
(Ep) indicators, which are combined to give a 'final-effects' LCA endpoint score. Quantification of environmental impacts is well established in the scientific literature, and databases are available. Damage categories can be weighted based on socio-political factors and uncertainty in calculations when computing the final (dimensionless) endpoint score for project alternatives in LCA. This score can then be used for decision-making based on environmental impacts alone (Bare et al. 2000). Figure 5 presents the relationship between the life cycle impacts, midpoint indicators and endpoint indicators for nine categories. Different environmental midpoint impact categories can be included according to the specific alternatives analysed, and site-application effects representation for specific slope stability purposes.

The **societal/technical/functional pillar** captures requirements related to issues such as aesthetics, safety, ease of design and constructability, among many other considerations including, for example, technical issues/considerations regarding the specific products available and/or to apply for slope stability purposes. These issues vary according to subjective importance and assessment. A practical strategy to quantify these issues is to develop a survey tool that representative agents, stakeholders and suitably qualified professionals can fill out. The results can be weighted using analytic hierarchy process techniques (Saaty 2008).

4 MIVES in Brief

Multi-attribute utility theory and value analysis provide a rigorous framework through a process of hierarchy, evaluation, valuation, weighting and aggregation. Once the requirements/ criteria/ indicators are defined by **hierarchy (1st stage;** see requirements tree in Fig. 4), all indicators (including the whole inventory of materials and processes

Fig. 5 Relationship between life cycle impacts, midpoint and endpoint indicators, ReCiPe method (modified from Goedkoop et al. 2008)



involved as indicator items) must be properly defined and categorized by **evaluation (2nd stage)**. The inventory of materials and processes have to be determined for the specific functional unit definition, which shall logically be the same for all alternatives selected for the sustainability assessment. After that, it is necessary to compare the resulting quantifications between all indicators from the three pillars through due **valuation (3rd stage)**.

The definition of the decision-making options (or stakeholder scenarios) and related sensitivities is done by **weighting (4th stage)** to the requirements or pillars ($W_{\text{requirement}}$). It should be noted that the weighting process is applied to all indicators ($W_{\text{indicator}}$) and criteria ($W_{\text{criterion}}$) and/or in all possible layers/sub-criteria—if there are—within the same requirement level. However, in some cases, a particular indicator/criterion's weighting may not be influenced by the stakeholder scenario and must be assumed separately/independently as per technical criteria.

Finally, summation of values and linked weights for each step within the flow chart (requirements tree) shall be done by **aggregation (5th stage)**, achieving the final MIVES result/score (V_{final}) and obtaining the best alternative in terms of sustainability. Thus, each option is assessed independently, with the best solution identified as the option with the best aggregate score.

An important feature of the MIVES sustainability assessment model is that the strength of each option is influenced by the strength of the competing options during the scoring calculations for each of the three pillar categories or requirements.

5 Evaluation Process: The Value Functions

Evaluation is usually difficult because indicators are often not directly comparable. This is what happens, for example, when safety factors (non-dimensional) are compared with related financial costs, or if the execution/installation time of specific construction actions for a particular alternative is balanced against tons of CO_2 generated. Even when using the same quantification unit, in many cases, it is difficult to compare indicators (for example, when comparing costs derived from different stages/concepts/processes involved in the same product or alternative). Accordingly, it is necessary to translate all the indicators into a common/single one to allow comparison. This transformation is done by the value functions, which can be defined by different trends, adopting different forms (i.e., linear, concave, convex, sigmoidal, etc.), as appropriate. Examples of value functions are shown in Fig. 6. Value functions can also be discrete or non-continuous. Value functions are used as converters from original indicator quantifications (X-axis) to dimensionless indicator values ($V_{\text{indicator}}$) between 0 and 1 (y-axis; see Fig. 6). While a value function trend should be established (e.g., higher value for: lower cost, lower environmental impacts, better protection, better functionality/ robustness/ resilience, lower labour, and technical-specific requirements, lower land used, etc.), the shape of this function may be difficult to define.

A good way to properly define function shape is to begin by identifying the real maximum/minimum indicator scores

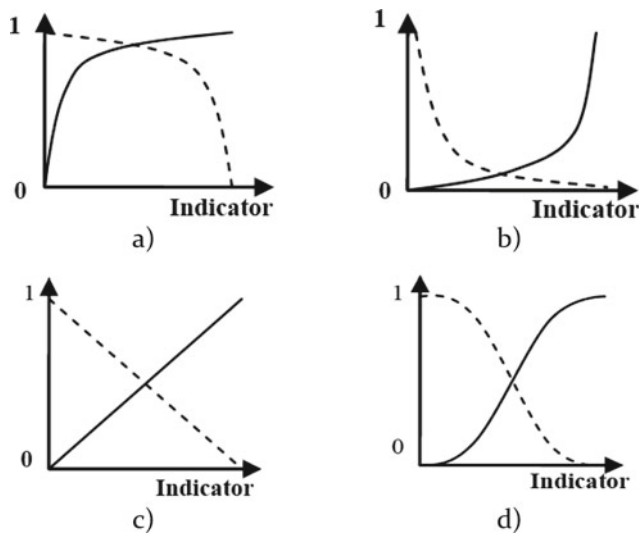


Fig. 6 Different types and tendencies of value functions: **a** concave, **b** convex, **c** linear, and **d** S-shape (modified from Alarcón et al. 2011)

(quantification) for inclusion. It is not necessary to define maxima and minima according to the values suggested by each alternative solution, as objective limits may have been set independently, e.g., security factors must be met regardless of cost or idealized values—such as net-zero carbon—may have been set to force alternatives to achieve them.

Once minima and maxima are defined, it is necessary to identify the desired approach for alternatives that are close to these limits. How much do we want to penalize for being close to the unwanted limit? How convenient is it to segregate alternative solutions close to the set boundaries? For economic impacts, lower costs to low probable limits (very efficient use of materials and no losses of any kind) can be established for the highest possible value (i.e., $V_{\text{economic-indicator}} = 1$). For environmental impacts, idealized limits can be established, although none of the analysed solutions is required to achieve the higher value limit with $V_{\text{environmental-indicator}} = 1$. Although there are different ways to define the value functions, Eq. (1) is proposed below (after Alarcón et al. 2011) and has been already used in many civil engineering applications (Aguado et al. 2012; Viñolas 2011; Damians et al. 2017; Pujadas et al. 2017; Josa et al. 2020; among others).

$$V_{\text{indicator}} = B \left(1 - e^{-K \left(\frac{|x - S_{\text{min}}|}{c} \right)^P} \right) \quad (1)$$

where:

V_i is the value of the indicator being evaluated.

S_{min} is the point of minimum satisfaction, with a value of 0.

X is the abscissa that generates a value equal to $V_{\text{indicator}}$

P defines approximately the shape of the curve: concave, convex, linear or S-shaped (see Fig. 6). If $P < 1$ the curve is concave; if $P > 1$ the curve is convex or S-shaped, if $P = 1$ it is linear.

C is a parameter that approximately defines the x -value of the point of inflexion for curves with $P > 1$.

K is a parameter that approximately defines the y -value at the point C .

B is a factor that allows the function to remain within the range from 0 to 1. It is assumed that the highest level of satisfaction has a value of 1. This factor is determined by Eq. (2).

$$B = \left(1 - e^{-K \left(\frac{S_{\text{max}} - S_{\text{min}}}{c} \right)^P} \right)^{-1} \quad (2)$$

where:

S_{max} is the point of maximum satisfaction, with a value of 1.

6 Conclusion

Multiple technological advances have allowed progress in many fields of civil engineering, enabling significant reductions in atmospheric CO₂ emissions, cost savings for personnel and construction material, and enhanced effectiveness compared with traditional solutions.

Many studies demonstrate that geosynthetic materials significantly contribute to preventing, avoiding, or reducing the potentially catastrophic effects caused by land changes and soil erosion. Their use not only saves time and money in installation but can also save lives. Sustainability assessment methods that account for environmental impact, cost and societal/functional considerations are becoming an important civil engineering tool for selecting the best option among multiple solutions performing the same function.

A suitable methodology to assess different alternatives for remediation of slope instability is available through the MIVES tool and presented in this study. Other landslide mitigation application cases should be analysed, applying specific protocols or particular model features based on the proposed methodology. Further developments and examples of practical use of the MIVES are expected in the future.

References

- AFNOR Group (2012) CEN/TC 350: sustainability of construction works. AFNOR Group
- Aguado A, del Caño A, de la Cruz MP, Gómez D, Josa A (2012) Sustainability assessment of concrete structures within the Spanish structural concrete code. *ASCE J Constr Eng Manage* 138(2):268–276
- Alarcon B, Aguado A, Manga R, Josa A (2011) A value function for assessing sustainability: application to industrial buildings. *Sustainability* 3(1):35–50
- Bare JC, Hofstetter P, Pennington D, Udo de Hades HA (2000) Midpoints versus endpoints: the sacrifices and benefits. *Int J Life Cycle Ass* 5(6):319–326
- Basu D, Misra A, Puppala AJ (2014) Sustainability and geotechnical engineering: perspectives and review. *Can Geotech J* 52(1):96–113
- BSI (2012) BS EN 15804: sustainability of construction works—environmental product declarations—core rules for the product category of construction products. BSI
- Cambiaghi A, Rimoldi P (1991) The use of geogrids in landslide control works: a case history from Valtellina (Northern Italy). In: *Proceedings of international conference on slope stability engineering—developments and applications*. Isle of Wight
- Cazzuffi D, Giusti G, Rimoldi P (1995) Lessons learned from the loss of performance of a 47m high geotextile reinforced slope subsequently replaced with a geogrid reinforced slope. In: Giroud JP, Soderman K L (eds) *Geosynthetics: lessons learned from Failures*. IFAI, Roseville
- Christopher BR (2014) Costs savings by using construction methods with geosynthetics. In: *Proceedings 10ICG—10th international conference on geosynthetics*, 21–25 Sept., Berlin
- Coluzzi E, Montanelli F, Recalcati P, Rimoldi P, Zinesi M (1997) Preliminary results from an instrumented geogrid reinforced slope for the stabilisation of the Montone hill in central Italy. In: *Proceedings of international conference on mechanical stabilized backfill*. Denver, Colorado
- Coluzzi E, Recalcati P, Rimoldi P (1996) Landslide repairs with green faced reinforced walls. In: *Proceedings International seminar on environmental geotechnology with geosynthetics—INTSEMEGG '96*. New Delhi
- Damians IP, Bathurst RJ, Adroguer E, Josa A, Lloret A (2018) Sustainability assessment of earth retaining wall structures. *ICE Env Geotech* 5(4):187–203
- Damians IP, Bathurst RJ, Adroguer E, Josa A, Lloret A (2017) Environmental assessment of earth retaining wall structures. *ICE Environ Geotech* 4(6)
- Dikran S, Rimoldi P (1994) The use of geogrids to increase the stability of slopes. In: *Proceedings of international conference on landslides, slope stability & the safety of infra-structures*. Kuala Lumpur
- Fraser I, Elsing A, Stucki M et al (2012) Comparative life cycle assessment of geosynthetics versus conventional construction materials, a study on behalf of the E.A.G.M., case 4, soil retaining wall. In: *Proceedings of the 5th European geosynthetics congress*, Valencia, vol 4, pp 218–222
- Giroud J P, Naughton P J, Rimoldi P, Scotto M (2014) Design of reinforced slopes and walls with low-permeability fills using draining geogrids. In: *Proceedings 10ICG—10th international conference on geosynthetics*. Berlin
- Goedkoop M, Heijungs R, Huijbregts M et al (2008) ReCiPe 2008. A life cycle impact assessment method which comprises harmonised category indicators at the midpoint and the endpoint level, report I: characterisation. Den Haag. See <http://www.lcia-recipe.net/>
- Heerten G (2012) Reduction of climate-damaging gases in geotechnical engineering practice using geosynthetics. *Geotext Geomem* 30:43–49
- Holt DG, Jefferson I, Braithwaite PA, Chapman DN (2010) Embedding sustainability into geotechnics—part A: methodology. *Proc Inst Civil Eng Eng Sustain* 163(3):127–135
- ISO (International Organization for Standardization) (2006a) ISO 14040: Environmental management—life cycle assessment—principles and framework. ISO, Geneva
- ISO (2006b) ISO 14044: environmental management—life cycle assessment—requirements and guidelines. ISO, Geneva
- ISO (2019) ISO 21931: sustainability in buildings and civil engineering works—framework for methods of assessment of the environmental, social and economic performance of construction works as a basis for sustainability assessment—part 2: civil engineering works. ISO, Geneva
- Josa A, Alavedra P (2006) El concepto de sostenibilidad. In: Losada R, Rojí E, Cuadrado J (eds) *La Medida de la Sostenibilidad en Edificación Industrial: MIVES*. Universidad Politécnica de Valencia, Universitat Politècnica de Catalunya and Labein-Tecnalia, Bilbao, Spain, pp 59–70
- Josa A, San José T and Cuadrado J (2008) El caso de la EHE. In *Jornada sobre Sostenibilidad en la Tecnología del Hormigón: MIVES, una Herramienta de Apoyo a la Toma de Decisiones*, Barcelona, pp 84–95
- Josa I, Pons O, de la Fuente A, Aguado A (2020) Multi-criteria decision-making model to assess the sustainability of girders and trusses: case study for roofs of sports halls. *J Clean Prod* 249
- MacAskill K, Guthrie P (2013) Risk-based approaches to sustainability in civil engineering. *Proc Inst Civil Eng Eng Sustain* 166(4):181–190
- Manni E, Rimoldi P (2006) A complex segmental concrete block retaining wall structure for the reconstruction of a historical bridge. In: *Proceedings ICG 8—8th international conference on geosynthetics*. Yokohama
- Pujadas P, Pardo-Bosch F, Aguado-Renter A, Aguado A (2017) MIVES multi-criteria approach for the evaluation, prioritization, and selection of public investment projects. A case study in the city of Barcelona. *Land Use Policy* 64:29–37
- Rimoldi P (1996) Geogrid reinforced walls, slopes and landslides: technical solutions and construction methods. In: *Proceedings international seminar on environmental geotechnology with geosynthetics—INTSEMEGG '96*. New Delhi
- Rimoldi P (2018) Design and construction of reinforced walls in Italy in complex static and seismic conditions. In: *Proceedings 11ICG, 11th international conference on geosynthetics*. Seoul
- Rimoldi P, Ricciuti A (1992) The role of geogrid reinforced embankments in landslide stabilization: theory and practice in Italy. In: *Proceedings 6th international symposium on landslides*. Christchurch
- Rimoldi P, Scotto M (2012) Hybrid reinforced soil structures for high walls and slopes. In: *Proceedings GeoAmericas 2012 conference* Lima
- Rimoldi P, Lelli M, Pezzano P, Trovato F (2021) Geosynthetic reinforced soil structures for slope stabilization and landslide

- rehabilitation in Asia. In: Vilímek V et al (eds) Understanding and reducing landslide disaster risk. ICL contribution to landslide disaster risk reduction. Springer Nature, Switzerland, pp 397–404
- Saaty T (2008) Decision making with the analytic hierarchy process. *Int J Serv Sci* 1(1):83–98
- Stucki M, Büsser S, Itten R, Frischknecht R and Wallbaum H (2011) Comparative life cycle assessment of geosynthetics versus conventional construction materials. Eur. Ass. of Geosynthetics Manufacturers, ESU-services, Uster, ETH Zürich
- Viñolas B (2011) Applications and methodology advances in MIVES multicriteria valorations. Doctoral thesis. Universitat Politècnica de Catalunya-BarcelonaTech
- WCED (World Commission on Environment and Development) (1987) Our common future: report of the world commission on environment and development. Oxford University Press, Oxford, UK

Open Access This chapter is licensed under the terms of the Creative Commons Attribution 4.0 International License (<http://creativecommons.org/licenses/by/4.0/>), which permits use, sharing, adaptation, distribution and reproduction in any medium or format, as long as you give appropriate credit to the original author(s) and the source, provide a link to the Creative Commons license and indicate if changes were made.

The images or other third party material in this chapter are included in the chapter's Creative Commons license, unless indicated otherwise in a credit line to the material. If material is not included in the chapter's Creative Commons license and your intended use is not permitted by statutory regulation or exceeds the permitted use, you will need to obtain permission directly from the copyright holder.



Review Articles



Establishment of the Disaster Risk Reduction Unit in UNESCO and UNESCO's Contribution to Global Resilience

Lesly Mercedes Barriga Delgado, Irina Pavlova, Soichiro Yasukawa, and Sergio Esperancinha

Abstract

The occurrence of catastrophes has increased considerably in recent decades. Climate change, urban pressure and lack of disaster preparedness are increasingly transforming natural hazards into disasters, causing multiple losses. In the last decades, Disaster Risk Reduction (DRR) has captured significant attention as the main approach to reduce vulnerabilities and exposure and improve preparedness to protect regional, national and local development. One of the main international agreements adopted to strengthen and enhance society's resilience is the Sendai Framework for Disaster Risk Reduction (2015–2030), which emphasises the need for more inclusive, multi-hazard DRR processes and its synergies with climate change, health, and sustainable development. Within this framework, UNESCO enhances preparedness and builds resilience at all levels through multi-hazard, multi-discipline, and multi-stakeholder DRR mechanisms, supporting the Member States particularly on eight thematic. Likewise, UNESCO has been a catalyst for international, interdisciplinary cooperation in many aspects of disaster risk reduction and mitigation. The organisation has supported activities of international DRR programmes, such as International Consortium on Landslides (ICL), as part of its global contributions to this and other international agreements.

Keywords

DRR • Disasters • Resilience • Multi-hazard • Multi-stakeholder • Multi-discipline approach

1 The Impact of Natural Hazards

Floods, hurricanes, earthquakes, volcanoes, cyclones, landslides and wildfires have shaped the Earth's landscape for millennia, interacting with human settlements since the dawn of civilization (Chaudhary and Piracha 2021). Such encounters have had considerable impact on human life and property, disturbing and altering the livelihoods of populations worldwide (UNESCO and UNICEF 2012).

The occurrence of disasters has increased significantly over the last six decades (Chaudhary and Piracha 2021). Climate Change (CC), urban pressure and the lack of disaster preparedness are increasingly transforming natural hazards into catastrophes, causing multiple losses. It is estimated that around 85% of the world's population has been distressed by at least one natural hazard in the past 30 years (Chaudhary and Piracha 2021). Since the 1990s, there has been a fluctuating trend of increasing direct socio-economic impacts due to disaster events, exacerbated in developing countries where 90% of the casualties occur (Chaudhary and Piracha 2021; Academy of Disaster Reduction and Emergency Management et al. 2020). Worldwide, from 2000 to 2019, disasters have caused US\$1.23 trillion in damages, claimed 1.23 million lives and affected over 4 billion people (UNDRR 2020).

With an increasing frequency and magnitude of extreme meteorological events as a result of climate change, losses associated with disasters are on the rise (UNDRR 2019). In the last few years, risks associated with climate extremes have been amplified by the COVID-19 pandemic, creating compound impacts and diminishing resilience to future disturbances (Walton et al. 2021). From the start of the pandemic through August 2021, extreme weather events

L. M. Barriga Delgado · I. Pavlova · S. Yasukawa (✉) · S. Esperancinha
Science Sector, Disaster Risk Reduction Unit, UNESCO,
75007 Paris, France
e-mail: s.yasukawa@unesco.org

L. M. Barriga Delgado
e-mail: lm.barriga-delgado@unesco.org

I. Pavlova
e-mail: i.pavlova@unesco.org

S. Esperancinha
e-mail: s.esperancinha@unesco.org

have affected 139.2 million people and claimed 17,242 lives in 433 disaster events (Walton et al. 2021). The vulnerability of poorer populations to extreme hydro-meteorological events has been aggravated, with their recovery after a disaster becoming more difficult given the pandemic economic impact (Walton et al. 2021).

2 Disaster Risk Reduction and the Sendai Framework

Over the past decades, Disaster Risk Reduction (DRR) has captured significant attention as the main approach to improve resilience and protect socio-economic development at different levels (Van Niekerk and Terblanché-Greeff 2017). Advances in DRR research have demonstrated the critical need to move from disaster response to the identification, evaluation and ranking of vulnerabilities and risks and their unequal distribution among populations (Aitsi-Selmi et al. 2015).

In 2015, a voluntary pathway was established to ensure that DRR policy reflects the complexity and evolving understanding of disaster risks in the twenty-first century (Aitsi-Selmi et al. 2015), the Sendai Framework for Disaster Risk Reduction (SFDRR) 2015–2030. This agreement constitutes a long-term international compromise that aims to protect lives, livelihoods and infrastructure along with cultural and natural heritage from man-made and natural hazards over 15 years (Kelman 2015; Wahlström 2015). This major ambition was adopted at the UN Third World Conference on Disaster Reduction (WCDR) held in Sendai, Japan and endorsed by the UN General Assembly in June 2015, following the Hyogo Framework for Action 2005–2015 (UNDRR 2019). Nevertheless, and unlike the Hyogo Framework, SFDRR places greater emphasis on the need for a more inclusive and all-hazards DRR process that incorporates both bottom-up and top-down actions, local knowledge and expertise, with attention to the synergies between DRR, climate change, health, and sustainable development (Aitsi-Selmi et al. 2015). Likewise, SFDRR recognizes the importance of a people-centred approach in the designing and implementation of DRR policies and plans at all levels, in accordance with its seven global targets and four priorities of action (Stough and Kang 2015).

- Priority 1: Understanding disaster risk
- Priority 2: Strengthening disaster risk governance to manage disaster risk
- Priority 3: Investing in disaster risk reduction for resilience
- Priority 4: Enhancing disaster preparedness for effective response and to Build Back Better in recovery, rehabilitation, and reconstruction.

3 UNESCO and the Establishment of the Disaster Risk Reduction Unit

UNESCO operates at the interface between natural and social sciences, education, culture and communication, playing a vital role in building a global culture of resilience.

The organisation has been strongly involved in DRR since the 1960s with studies on earthquakes and oceanography, expanding since then its fields of action to other hazard categories, adaptation and mitigation activities. The scientific and technical work in DRR is essentially promoted by UNESCO's International and Intergovernmental Science Programmes, namely the International Geoscience and Geoparks Programme (IGGP) (UNESCO n.d.), the Man and Biosphere Programme (MAB) (UNESCO n.d.), the Intergovernmental Oceanographic Commission (IOC) (IOC-UNESCO n.d.) and the International Hydrological Programme (IHP) (UNESCO n.d.).

At the end of 2021, and following an increase in requests for support from national governments, UNESCO Member States approved the creation of an independent DRR unit under the Assistant Director-General for Natural Sciences in the context of the recent approval of the Program and Budget for 2022–2025. This cross-sectoral unit aims to coordinate UNESCO's work on DRR and with the above-mentioned programs and mainstream the topic in the organization and UN entities.

4 UNESCO's Approach on Disaster Risk Reduction

Following the SFDRR premises, UNESCO enhances preparedness and builds resilience at all levels through multi-hazard, multi-discipline, and multi-stakeholder DRR mechanisms, supporting the Member States particularly on (1) Science, Technology and Innovation (STI) for Resilience; (2) Early Warning Systems (EWS); (3) Built Environment; (4) School Safety (5) Disaster Risk Reduction for Culture and Sites; (6) Ecosystem-based Disaster Risk Reduction (Eco-DRR); (7) Post-disaster Response; and (8) Risk Governance and Social Resilience (UNESCO n.d.).

Through a multi-disciplinary approach, UNESCO builds capacities and fosters partnerships to support a holistic understanding of climate crises and natural hazards and thus scientific and technical disaster prevention, preparation, response and recovery. UNESCO makes the most of its comparative advantage by combining its expertise in earth, ocean, water and ecological sciences with its mandate in education, social sciences, communication, information and heritage preservation towards achieving resilient societies. Under its responsibilities, UNESCO supports countries in DRR capacity-building, working in close collaboration with

governments, the private sector and the overall UN system to support Member States with their commitments and aspirations contained in the Nationally Determined Contributions (NDCs) and the UNFCCC Paris Agreement.

In addition, UNESCO adopts a multi-hazard and multi-stakeholder engagement approach to the challenges of disaster risks and climate change adaptation and mitigation. Multi-hazard approach is necessary as one hazard may have cascading effects such as earthquake to tsunami, storm to flood, warming climate to glacier melting. UNESCO is in a good position as it covers both weather and geo-related hazards, giving DRR policy/technical directions based on scientific evidence. Multi-stakeholder approach allows academics, civil society, the private and public sectors to collaborate in establishing risk prevention plans and strategies. The engagement of different stakeholders and organisations working at different scales of governance leads to more coordinated and integrated DRR actions and projects. In this regard, UNESCO supports the creation of spaces for the empowerment and active participation of all-level stakeholders in DRR processes.

5 UNESCO's Contribution to Major Global Challenges

As mentioned, UNESCO's contribution to DRR focuses on eight thematics.

Science Technology and Information (STI)—UNESCO's take on STI involves the enhancement and application of citizen science, participatory research, local and indigenous knowledge and development, and advanced Information and Communication Technologies (ICTs) to enhance local disaster preparedness and readiness. In Eastern Africa for example, UNESCO developed a mobile AI Chatbot to facilitate risk communication between citizens and public sectors before, during and after the occurrence of hazardous events. More than 700 public servants were trained for this AI tool between 2020 and 2021.

Early Warning Systems (EWS)—Significant efforts have been undertaken by UNESCO to strengthen EWS development, particularly in countries with significant challenges and vulnerabilities. In Ghana (2019), Morocco and Croatia (2021) for instance, UNESCO supported the donation and instalment of equipment for seismic monitoring provided by the Japanese company Challenge. Likewise, in 2020, 19 countries received expert support from the organisation to strengthen their early warning systems for tsunamis, floods and earthquakes.

Built Environment—UNESCO supports its Member States in strengthening capacities and construction-policy sectors to increase the safety of their built environment and thus reduce the socio-economic impact of disastrous events. The project “Capacity Building for Disaster Risk Reduction in the Built Environment in Latin America and the Caribbean” is the latest UNESCO project concerning this issue. The three-year initiative also known as BERLAC, started in 2020 and has six target countries (Cuba, Dominican Republic, Guatemala, Mexico, Peru and Haiti) and four components: (1) secure safer new buildings, (2) school facilities safety, (3) strengthen existing buildings, and (4) develop risk-informed policymaking.

School Safety—UNESCO is actively engaged in empowering schools and their communities to enhance school safety. To do so, UNESCO deploys a multi-hazard school safety assessment methodology known as VISUS (Visual Inspection for defining Safety Upgrading Strategies), developed in close collaboration with the University of Udine (Italy). The methodology has been successfully tested in seven countries, assessing the safety of more than 500,000 students and educational staff. In 2022, UNESCO is planning to evaluate the safety of 100 school buildings in the Dominican Republic, using the same methodology.

DRR for Culture and Sites—Acknowledging the value and importance of safeguarding cultural heritage, UNESCO and the Caribbean Disaster Emergency Management Agency (CDEMA) conducted in 2020 a regional workshop to raise awareness and foster synergies on disaster resilience in the Caribbean culture sector. UNESCO is currently supporting the incorporation of the workshop results into national/local DRR policies and plans for the culture sector and selected World Heritage sites in the region.

Eco-DRR—UNESCO promotes the conservation and sustainable management of natural ecosystems to prevent and mitigate natural hazards and climate change impacts. Currently, UNESCO is involved in the EU-funded OPER-ANDUM project, which aims to reduce hydro-meteorological risks in European rural territories through nature-based solutions (NbS).

Post-disaster Response—UNESCO assists Member States in post-disaster response to assess damage and losses, and to identify recovery and reconstruction needs. In the last years and after earthquake events, UNESCO dispatched engineers and seismologists to Turkey, Philippines and Iran for carrying out post-earthquake field investigations and drawing lessons towards better preparedness, response, and recovery.

Risk Governance and Social Resilience—UNESCO promotes civil society engagement in the management of disaster risk, encouraging the formation of youth networks that will contribute for the mainstreaming of DRR in their communities and governments. In recent years, and with the support of UN agencies and regional organisations, UNESCO has established youth platforms in Asia (U-INSPIRE in 2019), Africa (AYAB-DRR in 2020) and the Caribbean (CARIDIMA in 2021). Furthermore, during 2020, 31 countries were supported technically by UNESCO in updating national policy preparedness frameworks, prioritising small island developing states (SIDS) and African countries.

6 UNESCO's Partnership with ICL

ICL was founded in 2002 during the UNESCO-Kyoto University Joint Symposium on “Landslide Risk Mitigation and Protection of Cultural and Natural Heritage” as an activity of International Geoscience Programme project 425 “IGCP-425 Landslide hazard assessment and mitigation for cultural heritage sites and other locations of high societal value.” The first session of the Board of Representatives (BOR) of ICL was organised at UNESCO Headquarters on 19–21 November 2002. Initial members of ICL agreed to launch the International Programme on Landslides (IPL) and adopted eight coordinating projects and 14 member projects of IPL. Since its establishment, UNESCO has continuously supported ICL/IPL activities (Sassa 2005; Sassa et al. 2022), such as the UNITWIN (University Twinning and Networking) Cooperation Programme on Landslide risk mitigation for society and the environment (ICL 2015), the World Landslide Forum, the IPL Awards for Success and the Journal of the International Consortium on Landslides (ICL 2012).

During the Third UN World Conference on Disaster Risk Reduction (WCDRR) in March 2015, ICL took the initiative of organising together with IPL, the Japanese Ministry of Land, Infrastructure, Transport and Tourism (MLIT), UNESCO and others the Working Session “Underlying Risk Factors”. As an outcome of the session, the “ISDR-ICL Sendai Partnerships 2015–2025 for global promotion of understanding and reducing landslide disaster risk” was signed by a number of key international organisations, including UNESCO (Fig. 1) (Sassa 2015). These partnerships have been mobilized to pursue prevention, provide practical solutions, education, communication and public outreach to understand and reduce landslide disaster risk.

UNESCO appreciates the continuous commitment of ICL global partners on long-term reduction of landslides disaster risk, which has been translated into the establishment of the Kyoto Landslide Commitment (KLC) 2020, which was launched on 5 November with 90 signatory organisations including UNESCO. The continuity of the Sendai



Fig. 1 The signers from the first 16 signatory organisations with ICL officers after the signing of the ISDR-ICL Sendai Partnerships 2015–2025 document (Sassa 2015)

Partnership 2015–2025 through the KLC2020 will allow greater significant outcomes in the development of resilient sustainable societies in many landslides’ prone areas. This framework could not have come at a better time, considering the intensification of landslide risks due to climate change and global warming.

UNESCO is committed to the promotion and implementation of the ISDR-ICL Sendai Partnerships 2015–2025 and KLC2020. In this context and in line with its mandate, UNESCO’s DRR unit will continue to support the development of global, regional and national multi-hazard EWS, the improvement of the scientific basis for developing technologies and tools for landslide multi-risk identification and management, the enhancement of schools and communities preparedness and response, the provision of policy and technical assistance to strength capacity for floods and landslide monitoring and forecasting, the increase in research, partnerships and international scientific cooperation, and the collaboration with international partners, sectors, UNESCO field offices, UNESCO chairs and Category II Centres in the topic.

References

- Academy of Disaster Reduction, Emergency Management, Ministry of Emergency Management - Ministry of Education, National Disaster Reduction Center of China, Ministry of Emergency Management, Information institute of the Ministry of Emergency Management, (2020) 2019 Global Natural Disaster Assessment Report. Academy of Disaster Reduction, Emergency Management, Beijing, 88 p
- Aitsi-Selmi A, Egawa S, Sasaki H, Wannous C, Murray V (2015) The Sendai framework for disaster risk reduction: renewing the global commitment to people’s resilience, health, and well-being. *Int J Disaster Risk Sci* 6:164–176. <https://doi.org/10.1007/s13753-015-0050-9>
- Chaudhary MT, Piracha A (2021) Natural disasters—origins, impacts management. *Encyclopedia* 1:1101–1131. <https://doi.org/10.3390/encyclopedia10400842021>
- ICL (2015) UNITWIN programme. <http://icl.iplhq.org/category/icl/unitwin-programme-icl>
- IOC-UNESCO (n.d.) Intergovernmental Oceanographic Commission of UNESCO. <https://ioc.unesco.org/>. Accessed on 18 Mar 2022

- ICL (2012) ICL leaflet 2012. <http://icl.ipihq.org/category/icl/leaflet-and-publications/>
- Kelman I (2015) Climate change and the Sendai framework for disaster risk reduction. *Int J Disaster Risk Sci* 6:117–127. <https://doi.org/10.1007/s13753-015-0046-5>
- Van Niekerk D, Terblanché-Greeff A (2017) Handbook of anticipation, Poli R (ed). Cham: Springer (ISBN_978-3-319-91553-1), 1733 p. https://doi.org/10.1007/978-3-319-31737-3_90-1
- Sassa K (2005) ICL history and activities. In: Sassa K, Fukuoka H, Wang F, Wang G (eds) Landslides—risk analysis and sustainable disaster management. Springer, pp 3–21
- Sassa K (2015) ISDR-ICL Sendai partnership 2015–2025 for global promotion of understanding and reducing landslide disaster risk. *Landslides* 12(4):631–640
- Sassa K, Canuti P, Bobrowsky P, Casagli N (2022). International consortium on landslides: from IDNDR, IGCP, UNITWIN, WCDRR 2 & 3 to Kyoto landslide commitment 2020. *Progress in Landslide Research and Technology*, vol 1, No 1 (in press)
- Stough LM, Kang D (2015) The Sendai framework for disaster risk reduction and persons with disabilities. *Int J Disaster Risk Sci* 6:140–149. <https://doi.org/10.1007/s13753-015-0051-8>
- UNDRR (2020) The human cost of disasters: an overview of the last 20 years (2000–2019). UNDRR, Geneva, p 17p
- UNDRR (2019) Global assessment report on disaster risk reduction 2019. UNDRR, Geneva (ISBN_978-92-f1-004180-5), 425 p
- UNESCO (n.d.) Hydrology (IHP). <https://en.unesco.org/themes/water-security/hydrology>. Accessed on 18 Mar 2022
- UNESCO (n.d.) Disaster risk reduction. <https://en.unesco.org/disaster-risk-reduction>. Accessed on 18 Mar 2022
- UNESCO, UNICEF (2012) Disaster risk reduction in school curricula: case studies from thirty countries. <https://www.google.com.pe/url?sa=t&rct=j&q=&esrc=s&source=web&cd=&cad=rja&uact=8&ved=2ahUKEwimkrSr3ODxAhUI>. Accessed on 20 Mar 2022
- UNESCO (n.d.) International geoscience and geoparks programme (IGGP). <https://en.unesco.org/international-geoscience-and-geoparks-programme>. Accessed on 18 Mar 2022
- UNESCO (n.d.) Man and the biosphere (MAB). Programme. <https://en.unesco.org/mab>. Accessed on 18 Mar 2022
- Wahlström M (2015) New Sendai framework strengthens focus on reducing disaster risk. *Int J Disaster Risk Sci* 6:200–201. <https://doi.org/10.1007/s13753-015-0057-2>
- Walton D, Arrighi J, van Aalst M, Claudet M (2021) The compound impact of extreme weather events and COVID-19. IFRC, Geneva, p 34p

Open Access This chapter is licensed under the terms of the Creative Commons Attribution 4.0 International License (<http://creativecommons.org/licenses/by/4.0/>), which permits use, sharing, adaptation, distribution and reproduction in any medium or format, as long as you give appropriate credit to the original author(s) and the source, provide a link to the Creative Commons license and indicate if changes were made.



The images or other third party material in this chapter are included in the chapter's Creative Commons license, unless indicated otherwise in a credit line to the material. If material is not included in the chapter's Creative Commons license and your intended use is not permitted by statutory regulation or exceeds the permitted use, you will need to obtain permission directly from the copyright holder.

**IPL Projects, World Centres of Excellence
on Landslide Risk Reduction, and Kyoto Landslide
Commitment 2020**



Early Warning System Against Rainfall-Induced Landslide in Sri Lanka

Kazuo Konagai, Asiri Karunawardena, Kithsiri N. Bandara, Kyoji Sassa, Ryo Onishi, Ryosuke Uzuoka, Shiho Asano, Katsuo Sasahara, Sanchitha Jayakody, and Imaaya Ariyaratna

Abstract

Based on solid evidence, scientists attribute the global warming trend observed since the mid-twentieth century to the human expansion of the “greenhouse effect.” Extreme rainfall events have become more frequent worldwide, resulting in hydro-meteorological hazards creating more deaths and devastation. One of the most remarkable disasters of rain-induced rapid long-traveling landslides (RRLL) in Sri Lanka took place at Aranayake, 70 km east of Colombo, in 2016 (JICA Survey Team (2016), Survey results of Aranayake Disaster, JICA. URL: <https://www.jica.go.jp/srilanka/english/office/topics/c8h0vm00006ufwhl-att/160720.pdf> [Last accessed: April 14, 2020]). The fluidized landslide mass ran over an about 2 km distance claiming the lives of 125 people. This tragic event highlighted the importance of reliable early warning and disaster management mechanisms even more than ever because the presence of these hidden unstable soil

masses, as well as their run-out distances, are hardly predicted. Once they start sliding, it is almost impossible to stop them. Since 2020 (after the preceding period of 2019), both the National Building Research Organization, Sri Lanka (NBRO) and the International Consortium on Landslides (ICL) have jointly started a new 5-year research project, “Development of early warning technology of Rain-induced Rapid and Long-travelling Landslides (Project RRLL),” within the framework of SATREPS. SATREPS, standing for “Science and Technology Research Partnership for Sustainable Development,” is a Japanese government program promoting international joint research. This article reports on the outline of the project, including its background, goals, plans of plots for developing critical technologies for the early warning system, etc.

Keywords

RRLLs • SATREPS • Sri Lanka

K. Konagai (✉) · K. Sassa
International Consortium On Landslides, Secretariat, Kyoto,
606-8226, Japan
e-mail: konagai@iclhq.org

A. Karunawardena · K. N. Bandara
National Building Research Organization, Colombo, 00500, Sri
Lanka
e-mail: asiri13@hotmail.com

R. Onishi
Tokyo Institute of Technology, Tokyo, 152-8550, Japan
e-mail: onishi.ryo@gsic.titech.ac.jp

R. Uzuoka · S. Jayakody
Disaster Prevention Research Institute, Kyoto University, Kyoto,
611-0011, Japan
e-mail: uzuoka.ryosuke.6z@kyoto-u.ac.jp

S. Asano
Forestry and Forest Products Research Institute, Ibaraki,
305-8687, Japan
e-mail: shiho03@ffpri.affrc.go.jp

K. Sasahara · I. Ariyaratna
Kochi University, Kochi, 780-8520, Japan
e-mail: sasahara@kochi-u.ac.jp

1 Introduction

As an isolated island within the Northern Indian Ocean, Sri Lanka experiences extreme rainfalls in two monsoon seasons in response to the bi-annual reversing monsoonal winds (Department of Meteorology, Sri Lanka 2020). Particularly the south-western monsoon from May to September brings rain to the southwest mountainous area of Sri Lanka. Out of 25 administrative districts in Sri Lanka, ten districts, approximately 30% of the total land area of the Island, are the most prone to landslides. Landslides in Sri Lanka, mainly due to natural causative factors, have long been remote and isolated events. However, these landslide-prone areas have become the primary area of tea and cinnamon plantations; thus, about 35% of the population of Sri Lanka live in these areas nowadays.

Moreover, post-civil-war Sri Lanka has been attracting tourists with 5 of 7 UNESCO cultural and natural world heritages of Sri Lanka located in landslide-prone areas. Studies have revealed that human-induced interventions such as rapid urbanization, population growth toward the foot of mountains, inappropriate land management, deforestation in steep slopes, etc., have influenced nearly 70% of the landslides in Sri Lanka. One of the most remarkable disasters to mention took place at Aranayake in Kegalle District, 70 km east of Colombo (JICA Survey Team 2016). The fluidized landslide mass ran over a 2 km distance killing 125 people. These hidden unstable soil masses are difficult to find in advance, and their long run-out distances are hard to predict. Once they start sliding, it is almost impossible to stop them. Thus, this tragic event at Aranayake highlights the importance of sophisticated early warning and efficient disaster management protocols.

Since 2020 (after the preceding period of 2019), both the National Building Research Organization, Sri Lanka (NBRO hereafter) and the International Consortium on Landslides (ICL hereafter) have jointly started a new 5-years project for Sri Lanka titled “Development of early warning technology of Rain-induced Rapid and Long-travelling Landslides (Project RRL hereafter).” The project is within the framework of SATREPS. SATREPS, “Science and Technology Research Partnership for Sustainable Development,” is a Japanese government program with two funding organizations, Japan International Cooperation Agency (JICA hereafter) and the Japan Science and Technology Agency (JST hereafter), that promote international joint research. JICA has proactively contributed to building a rational landslide disaster mitigation framework for Sri Lanka. This project aiming to develop cutting-edge technologies for one-day-in-advance forecasts of the occurrence of RRLs is indeed complementary to all efforts that JICA has been deploying in this country. This article outlines the background story that led up to the project, the project’s framework, and some noteworthy developments in the technology for implementing the early warning protocols.

2 Background Story

2.1 Recent Landslides in Sri Lanka

The technologies to stabilize reactivated and creeping landslide masses have progressed much because we can identify their locations. However, the number of recent tragic events in Sri Lanka shows a soaring trend in general, with some remarkable spikes in 2003, 2007, 2011, 2014, 2016, and 2017, as shown in Figs. 1 and 2. These events highlight the difficulty in coping with the devastations caused by RRLs. We can identify neither their locations nor early signs of movement in

advance. Therefore, implementing advanced and feasible technologies for early warnings of RRLs is crucial.

2.2 EWS in Sri Lanka

Landslide Early Warning System (EWS) plays a significant role as a non-structural risk reduction method on rainfall-induced landslides. The National Building Research Organization (NBRO) is the authorized body for landslide Early Warning (EW) in Sri Lanka. It has provided two kinds of EWS since 2007: the first one is the Regional Landslide Early Warning (RLEW) based on the rainfall thresholds (NBRO 2022a). The other is the Site-Specific Landslide Early Warning based on sophisticated measurement instruments or community-based landslide warning (NBRO 2022a).

The first EWS (RLEW) started in 2007. The warning on a regional scale goes off based on predefined rainfall threshold limits under three levels, i.e., watch, alert, and evacuation respectively at 75 mm/day, 100 mm/day, and 150 mm/day or 75 mm/h. The NBRO uses an automated network of 325 rain gauges (Fig. 3) established in the landslide-prone areas of the country to obtain real-time rainfall data, based on which the early warnings are issued. The messages were notified directly to local people through not only the Web of NBRO, but also radio communication, television, telephone, and bells on sites from local agencies, which have the responsibilities for the safety of local people. But some problems have been emerging through the implementation process of the system. Warning messages do not always efficiently reach local people, and local people often ignore the message even when they have adequately spread to the people. Moreover, there have been many false-negative and false-positive predictions of landslide occurrences, making people think that the EW messages are just like the tale of “The Boy Who Cried, Wolf.”

NBRO, given official development assistance from JICA, started implementing the second method, site-specific EWS and the Community-Based Landslide Early Warning (CBLEW) approach for the landslide vulnerable communities identified in the country from 2016 to solve the problems mentioned above. Site-specific information is necessary for a more reliable warning for a specific slope. It was thus a practical solution to save more lives in line with the four priorities of the Sendai Framework for Disaster Risk Reduction 2015–2030.

The CBLEW approach aims to empower the communities and establish systematic preparedness plans for timely self-evacuation of communities in case of a landslide event. In this course, the communities get education on preparedness and self-decision based on the rainfall data obtained by manual rain gauges distributed in the village. The CBLEW approach consists of the following:

Fig. 1 Number of landslides and deaths from 2003 to 2021 (Credit NBRO)

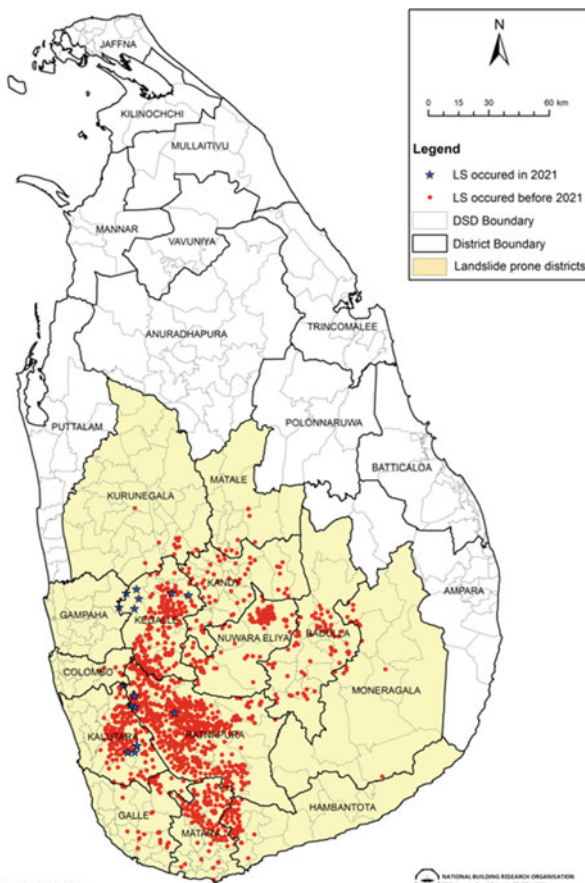
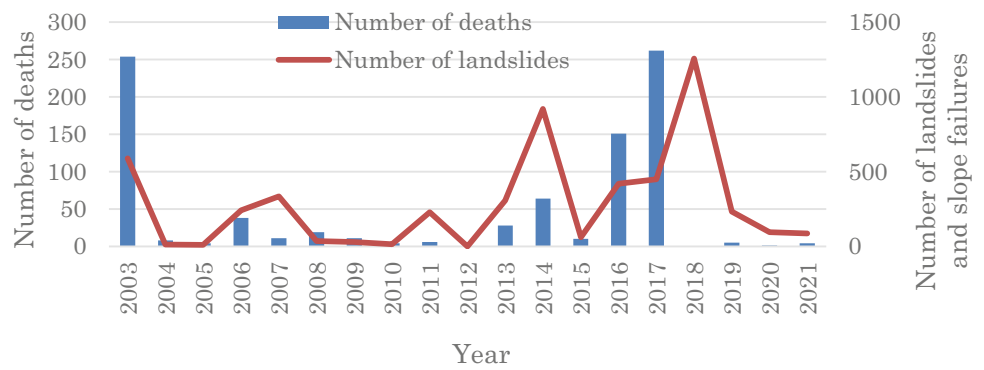


Fig. 2 Locations of landslides from 2003 to 2017 (Credit NBRO)

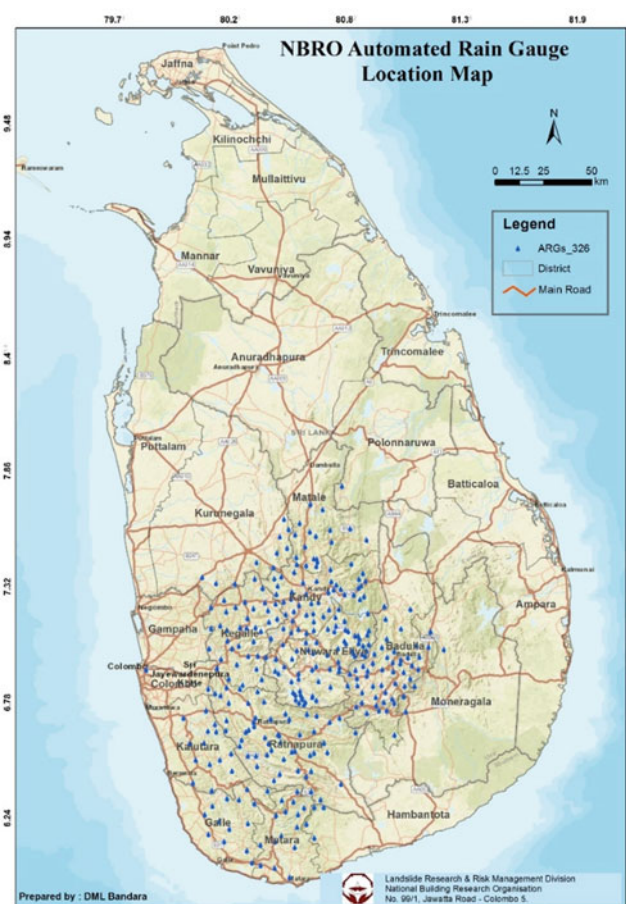


Fig. 3 Distribution of automatic rain gauges in Sri Lanka (Credit NBRO)

- (1) Site selection by NBRO based on its preliminary landslide investigation reports and landslide hazard zonation maps (NBRO 2022b),
- (2) Awareness programs for local government officers to familiarize them with the project, and
- (3) Awareness programs for local communities to give knowledge about the following:
 - What a landslide is,
 - What pre-symptoms people can observe,
 - Risk reduction techniques, and

- How the community people can create a community risk map (Fig. 4, next page), install manual rain gauges (Fig. 5, next page) and extensometers (Fig. 6, next page), and sirens in the community.

However, fatal landslides/slope failures that continue happening in the country remind us of the current need for a more sophisticated early warning system. At first, developing novel approaches such as precipitation nowcast and



Fig. 4 Example of community hazard map (Credit NBRO)

forecast techniques is mandatory for improving landslide early warnings. Behind this, we have the drastic change in monsoon and cyclone patterns in the Indian Ocean, responsible for unpredictable extreme events such as intense and localized rain impacts. Secondly, we need to examine the zoning for the EWS, which currently follows the administrative zoning. It is perhaps more rational to issue a warning considering the catchment boundaries. Thirdly, site-specific EWS will be more accurate given more reliable geotechnical parameters.

As mentioned above, RRLs are the most troublesome among all types of landslides because the movements of soil masses are associated with liquefactions of whole masses and along sliding surfaces. Their motions are swift and extremely dangerous. Therefore, a pressing need is to develop an effective early-warning system that predicts RRL occurrences one day in advance. Advancements in technology for landslide disaster mitigation are remarkable in the international world of the academy, with the ICL as the core organization. They include forecasting localized precipitation events, early detection of ground movements, and relaying timely early warning to the last mile, namely,

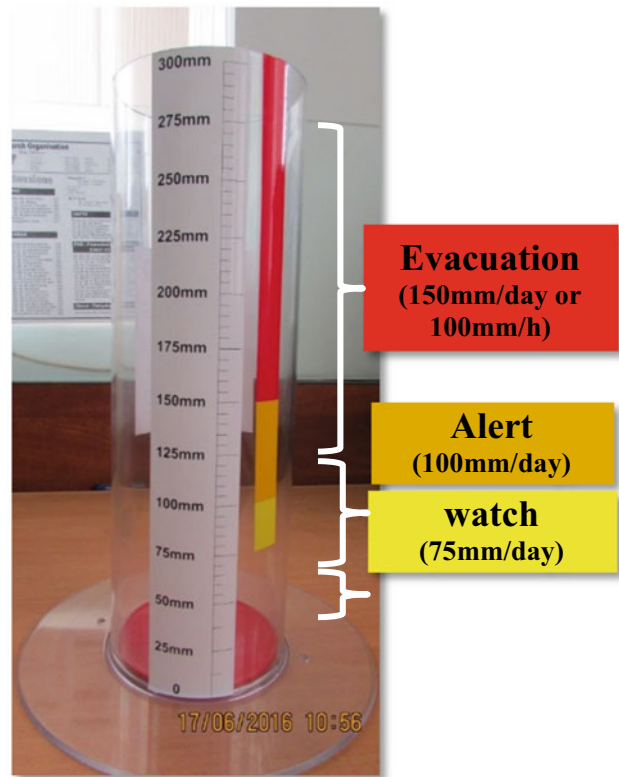


Fig. 5 Hand-made rain gauge (Credit NBRO)

residents at landslide risk. Among them, the critical technologies for the development of RRL EWS are:

- (1) Time prediction of heavy rainfalls and pore water pressure build-ups,
- (2) Site prediction of landslide initiations and motions, and
- (3) Effective risk communication and public education.

In light of this situation, we have started a new 5-year project between ICL on the Japanese side and NBRO on the Sri Lankan side in 2020 (Japan Science and Technology Agency 2020). The project is entitled “Development of Early Warning Technology of Rain-Induced Rapid and Long-Travelling Landslides,” in short, “Project RRL.” As said, this 5-year project, which officially started in 2020, is one of the SATREPS projects.

3 Project RRL

3.1 Planning and Kickoff

The “Sendai Framework for Disaster Risk Reduction 2015–2030” is an international document adopted by the United Nations member states between 14 and 18 March 2015 at the World Conference on Disaster Risk Reduction held in

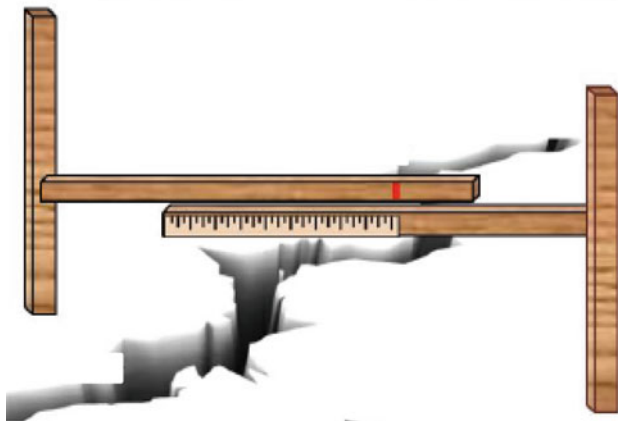


Fig. 6 Handmade extensometer (Credit NBRO)

Sendai, Japan. This document outlines seven clear targets and four priorities for action to prevent new and reduce existing disaster risks (UNISDR Prevention Web 2015):

- (1) Understanding disaster risk,
- (2) Strengthening disaster risk governance to manage disaster risk,
- (3) Investing in disaster reduction for resilience, and
- (4) Enhancing disaster preparedness for effective response and “Build Back Better” in recovery, rehabilitation, and reconstruction.

Sri Lanka has made a solid commitment to implementing the Sendai Framework for Disaster Risk Reduction 2015–2030. The commitment includes:

- (1) Establishing the Roadmap for disaster risk reduction “Safe and Resilient Sri Lanka” developed by JICA (UDR Prevention Web 2005) for the Ministry of Disaster Management of Sri Lanka, and
- (2) Joining the “ISDR-ICL Sendai Partnerships 2015–2025 for global promotion of understanding and reducing landslide disaster risk” (Sassa 2015).

The Partnership was officially adopted at the ICL-IPL Sendai Partnership Conference on 11–15 March 2015 (Fig. 7). Both NBRO and Central Engineering Consultancy Bureau (CECB), who joined the conference and signed the Sendai Partnership, envisaged together with relevant signatories the first plan for this SATREPS project. After thorough discussions, it passed the final selection round on May 16, 2019, that the new 5-year SATREPS project for Sri Lanka concerning “Development of early warning technology of Rain-induced Rapid and Long-travelling Landslides (Project RRL)” would start in 2020.

A signing ceremony for the Minutes of Meeting (MM) between NBRO, Sri Lanka, and JICA, Japan, was held on October 15, 2019, at the auditorium of NBRO (Fig. 8). Mr. Satoshi Nakamura, Leader, Detailed Planning Survey Team, JICA, Japan, and Eng. (Dr.) Asiri Karunawardena, Director General, NBRO, Sri Lanka, signed the MM toward implementing Project RRL. In the same signing ceremony, Collaborative Research Agreement (CRA) between NBRO, Sri Lanka, and ICL was also signed by Eng. (Dr.) Asiri Karunawardena, Director General, NBRO, Prof. Kazuo Konagai, Leader on the Japanese side of Project RRL, Principal Researcher, Prof. Kyoji Sassa, Secretary-General, and Prof. Kaoru Takara, Executive Director of ICL.

The following officers signed Record of Discussions of the Project RRL: Mr. Fusato Tanaka, Chief Representative, JICA Sri Lanka Office, Eng. (Dr.) Asiri Karunawardena, Director General, NBRO, Major General (Retired), Kamal Gunaratne, Secretary, Ministry of Defence and Mr. Ajith Abeysekera, Director General, Department of External Resources, Ministry of Finance. This Record of Discussion is an official agreement between both governments to confirm the implementation of the 5 year Project RRL starting on February 5, 2020.

Technical Cooperation Agreement for pursuing the Project RRL over the five years from March 1, 2020, to February 28, 2020, was implemented between JICA and ICL.

JICA and ICL signed the contract for the first year of Project RRL with the consent of both parties. The first year started on March 1, 2020, and ended on May 31, 2021.

3.2 Implementation Structure

Figure 9 shows the implementation structure of Project RRL. The project is carried out exclusively by members of the Joint Coordination Committee (JCC). Simultaneously, it is also open through the “Landslide Technical Forum” to anyone interested in it. The JCC members are signatory entities of the Record of Discussion



Fig. 7 Signing ceremony of ISDR-ICL Sendai Partnerships 2015–2025 (Sassa 2015)



Fig. 8 Signing ceremony on Oct. 15, 2019 for the minutes of meeting (MM) between NBRO, Sri Lanka and JICA, Japan

that JICA and the implementing agencies on the Sri Lankan side signed.

On the Sri Lankan side, we have:

- (1) NBRO as the primary implementing agency and thus the Secretariat of JCC,
- (2) Disaster Management Center (DMC),
- (3) Department of Meteorology (DOM), and
- (4) Department of Irrigation (DOI).

(1) NBRO, (2) DMC, and (3) DOM are currently under the purview of the Ministry of Internal Security, Home Affairs, and Disaster Management, while (4) DOI is a department of the Ministry of Irrigation. Just when the project officially started, the COVID-19 pandemic started spreading worldwide. To further promote our activities

under this harsh condition, we got new JCC members since the 1st JCC meeting held in April 2021. They are:

- (5) Central Engineering Consultancy Bureau (CECB) and
- (6) Two individual professors from three major universities in Sri Lanka.

On the Japanese side, which the Japan Science and Technology Agency (JST) financially supports, we have:

- (7) The headquarters of ICL as the entity leading the project,
- (8) Tokyo Institute of Technology (TIT),
- (9) Disaster Prevention Research Institute (DPRI) of Kyoto University,
- (10) Forestry and Forest Product Research Institute (FFPRI), and

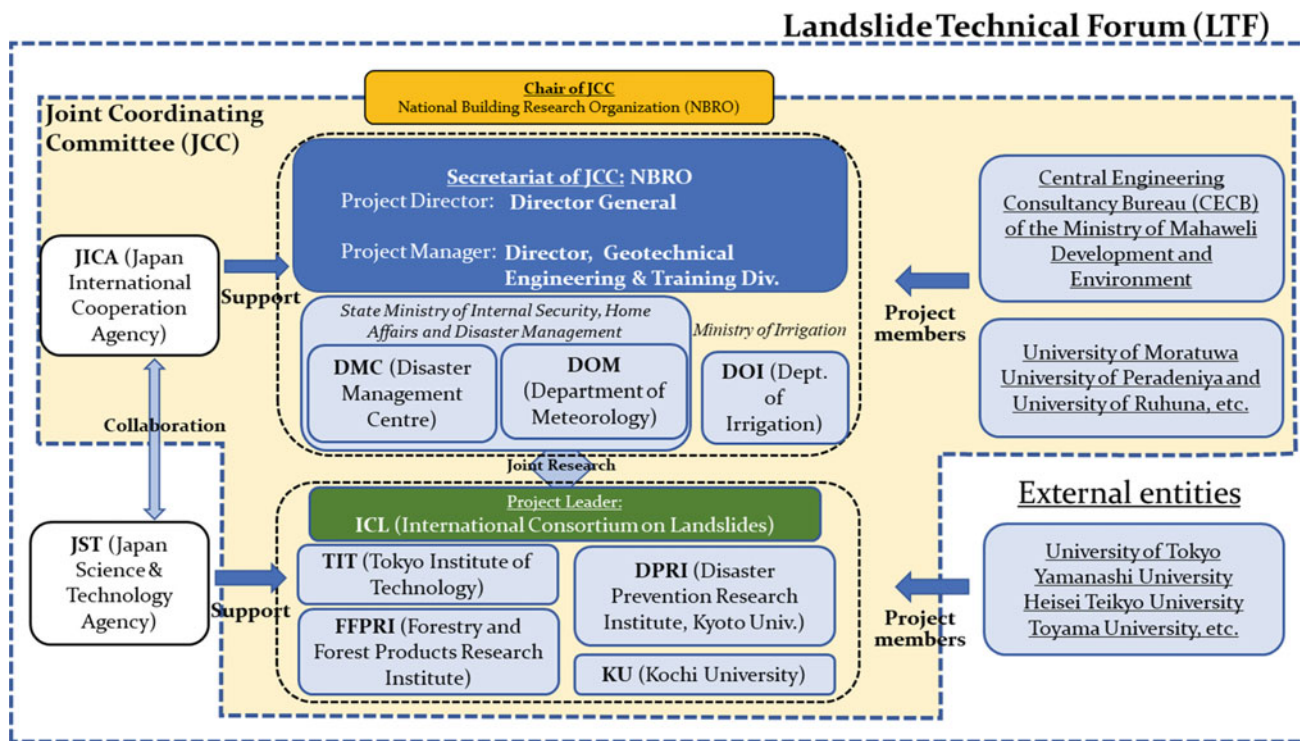


Fig. 9 Implementation structure for project RRL (as of November 2021)

(11) Kochi University.

In addition to these entities and organizations, we have individual researchers joining the Project as official members from external entities.

4 Pilot Study Sites

Geologically, the island of Sri Lanka is an extension of Peninsular India and forms part of the Indian Shield, one of the oldest and most stable parts of the earth’s crust. Previous studies have suggested that the larger part of the landslide-prone areas is covered with thick weathered gneiss metamorphosed during Precambrian Era. The tropical climate has favored deep weathering of these metamorphic rocks reaching tens of meters in these mountains with dense tropical vegetation drapes. Two pilot study sites, Aranayake and Athwelthota, are selected as representatives of two major types of RRL (Fig. 10).

4.1 Aranayake Landslide Area

Aranayake landslide was triggered on May 17, 2016, by exceptional rainfall associated with a slow-moving tropical cyclone. The fluidized landslide mass from the relative

elevation of about 600 m ran over an approximately 2 km distance claiming the lives of 125 people. This landslide is unique because it is much more prominent in size and runout distance than the others. Though this type of landslide rarely occurs, a large RRL can cause a big disaster. This landslide mass ran across two local communities, Elagipitiya and Debatthama Pallegage, with about 1500 and 1100 inhabitants, respectively. Summing up populations of the neighboring communities with similar risks of this type of RRL expected, the number of beneficiaries of this project will be at least several thousand.

4.2 Athwelthota Landslide Area

This landslide, which occurred in the Athwelthota area, Baduraliya District, on May 26, 2017, destroyed nine houses, killed nine people, and stopped traffic on a national highway. Each landslide of the Athwelthota type will not cause a surprisingly large disaster, but the number of landslides of this type can be huge, causing extensive losses of human lives and properties.

During the heavy rain of 2017, 37 RRLs reportedly took place all at once, claiming the lives of 262 people. There remains unstable soil masses above the two pilot study sites perching in and around the tops of the exposed bare-earth slopes. We will install necessary equipment on/in these soil

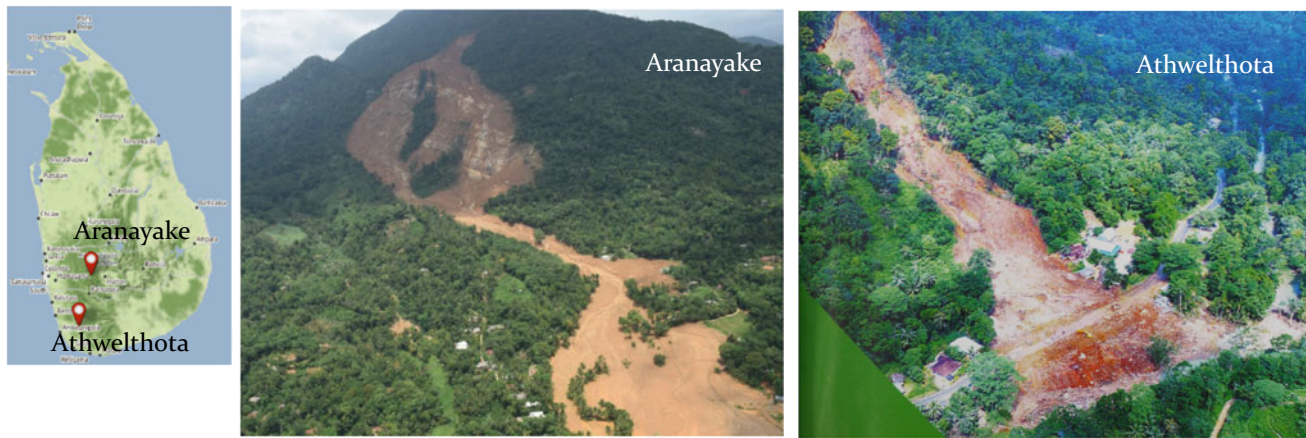


Fig. 10 Pilot study sites: (Left) Alanayake landslide in 2016, and (Right) Athwelthota landslide in 2017 (credit NBRO)

masses to measure the causal factors of landslides and creeping deformations. These pieces of equipment include pore pressure sensors, inclinometers, borehole extensometers, etc. We also monitor the movements of these soil masses with Persistent Scatterer Interferometric Synthetic Aperture Radar (PSInSAR). PSInSAR is a remote sensing technique that uses radar signals from a satellite to measure the ground displacement accurately. The method thus allows us to track the motion of each scatterer structure placed on the ground. These measurements will help develop infiltration models for the weathered gneiss in these areas.

5 Preliminary Study of Aranayake RRL

Natural disasters such as landslides can repeatedly occur in and around the same area, and we often find traces of past tragic events remaining on the terrain. We can also see early signs of future events in the topographical features. Figure 11 shows polygons with possible landslide blocks and rock creep areas image-interpreted from the digital elevation model of Aranayake, the 2016 RRL (Polygon A) disaster-hit area. In this figure, a clear depression B does not take the appearance of a river valley (such as E) formed by vertical erosional downcutting. This depression might be the source area of a large past RRL, and the debris mass from this area B might have deposited on area C. Meanwhile, an unstable soil mass (D) remains immediately behind the scar of the bare earth exposed in the 2016 RRL. Although an RRL has not occurred yet, the creeping movement may help debris gradually accumulate to reach its stability limit. Given the image interpretation mentioned above and assuming that the inherent soil parameters differ little from those at the 2016 Aranayake landslide zone, LS-RAPID simulations were conducted to examine the following:

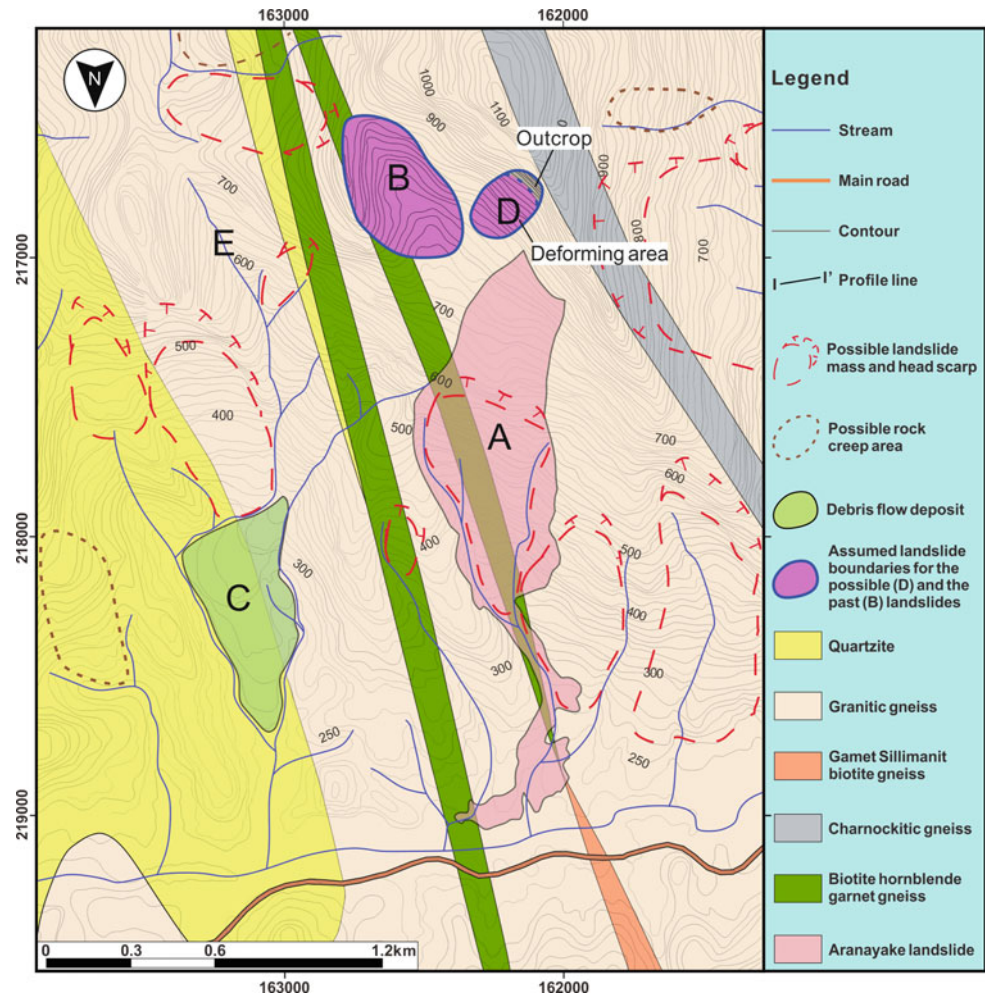
- (1) If the LS-RAPID simulation would reproduce the 2016 RRL event (A),
- (2) If the past RRL (B) likely happened, and
- (3) How far out the future potential RRL (D) can run out.

LS-RAPID is an integrated model that simulates landslide masses' initiation and downward movements (Sassa et al. 2010).

We took two soil samples (S-1, S-2) for testing from the Aranayake RRL source area as marked in Fig. 12b. These soil samples were weathered matters of granitic gneiss with grain size distribution curves shown in Fig. 12c. We then conducted a series of ring shear tests using the ICL-2 ring shear apparatus (Khang et al. 2018). These tests allow us to obtain mechanical parameters and the critical displacements, namely DU at which strength reduction starts and DL at which strength converges on its residual value. These parameters are all necessary for the simulations. Undrained tests were then performed under the monotonic stress control, with the initial normal stress σ and its increment $\Delta\sigma$ set at 500 kPa and 1 kPa/s, respectively; the initial shear stress τ and its increment $\Delta\tau$ set at 200 kPa and 1 kPa/s. The normal stress was firstly increased to the predetermined value (500 kPa) in a drained condition to avoid the generation of excess pore water pressure. The drain valve was then shut to realize the undrained condition before shearing. The applied initial normal stress was determined, taking into account the landslide mass's average thickness (25 m). The initial shear stress was finally calculated from this normal stress and the slope angle.

When the effective stress path reaches the failure line, it decreases due to pore pressure buildup along the failure line until the mobilized shear stress reaches the steady-state value. This behavior reflects the sliding-surface liquefaction associated with grain crushing and the collapse of grain

Fig. 11 Possible landslide blocks and rock creep areas image-interpreted from the digital elevation model of Aranayake (Tan et al. 2020)



fabrics (Sassa et al. 2004, 2010, 2015). As plotted in Fig. 13c, when undrained shearing begins, the stress path in the drained equilibrium with the initial normal stress of 500 kPa (indicated in Fig. 13c) goes obliquely upward, reflecting the porewater pressure buildup. After it reaches the failure line (39°), it decreases along the failure line until it reaches the steady-state shear resistance of 30 kPa. The friction angle holds its peak value (ϕ_p) in the pre-failure state until the shear displacement DL is reached (point of failure), then shear strength reduces as the shear displacement develops from DL to DU. DL and DU values observed in this test are marked in Fig. 13b.

The 2016 Aranayake RRL was reproduced in an LS-RAPID numerical simulation to examine its initiation and motion processes. Figure 14 shows the downslope movement of the Aranayake landslide mass frame-by-frame. The landslide mass shows an early sign of being detached at the center of the source area (stage 1), at the elapsed time (from the beginning of simulation) of 40 h 33 m, and the pore pressure ratio (r_u) increases to 0.20. The whole landslide mass then starts sliding at 66 h 06 m ($r_u = 0.28$) (stage 2). The simulated landslide initiation time coincides roughly

with the actual time, proving the reliability of the simulation. The landslide flow then splits into two runoff paths until they join each other again, where a remarkable volume of debris stagnates (stage 3). Finally, the landslide flow stops at 66 h 08 m (stage 4). Given the satisfactory agreement between the simulated and the observed processes of the Aranayake mass movement, the same geotechnical parameters were used for LS-RAPID simulations to discuss the possible neighboring soil wasting processes. Figures 15 and 16, respectively, show how the soil mass, which could have been detached in the past, moved downslope, and how the unstable soil mass, which still perches atop of the Alanayake mountain slope just behind the scar of the 2016 RRL, can move downslope (Tan et al. 2020). For the future RRL case, shallow and deep potential sliding surfaces were assumed to develop through the unstable soil mass. With no information about precipitations for the past and future RRLs, the pore pressure ratio r_u was assumed to increase at a steady rate of 0.01/s. These simulations show the potential distal ends when a jumble of wood and soil comes down as the leading wave of a possible debris flow, thus, bringing to light areas of special warning.

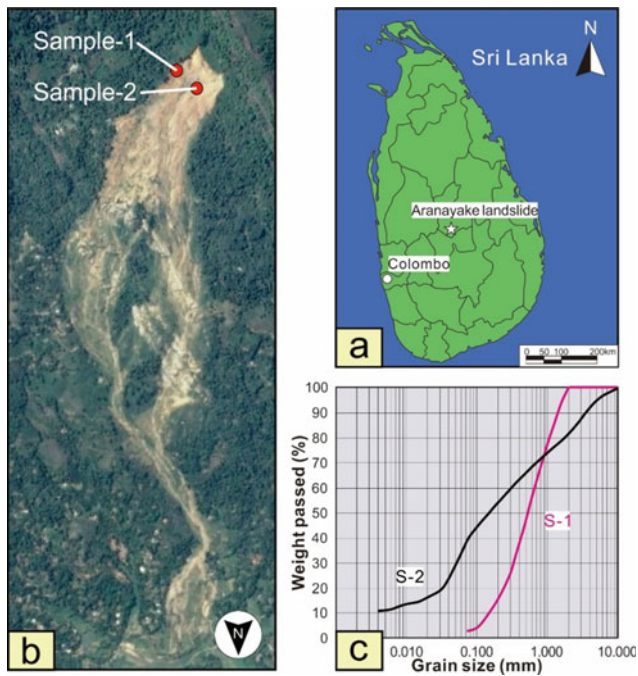


Fig. 12 a Location of the landslide region b Satellite picture of the Aranayake landslide and the sampling site. c Grain size distribution of the sample (Dang et al. 2019)

6 Technologies to Develop

This project has the following three groups, G1, G2, and G3:

G1 works as a hub for this joint research and integrates unique technologies developed at the two pilot sites by Groups 2 and 3. Through this activity, Sri Lankan scientists and researchers enhance their ability to cope with the RRLD disaster mitigation.

G2 develops technologies for (1) 24 h in-advance prediction of heavy rainfalls and (2) assessing groundwater pressure build-up, initiation of an RRLD, and its flowing dynamics.

G3 strengthens RRLD risk communication protocol, developing an augmented reality system for sharing predicted risk information and providing public education to develop the capacities of the communities.

As said before, essential technologies that the three groups mentioned above will develop are for:

- (1) Precise weather forecasts in mountainous regions,
- (2) Prediction of groundwater pressure build-up, identification of RRLDs locations and their moving areas, and
- (3) Effective risk communication and public education.

Details for each technology follow.

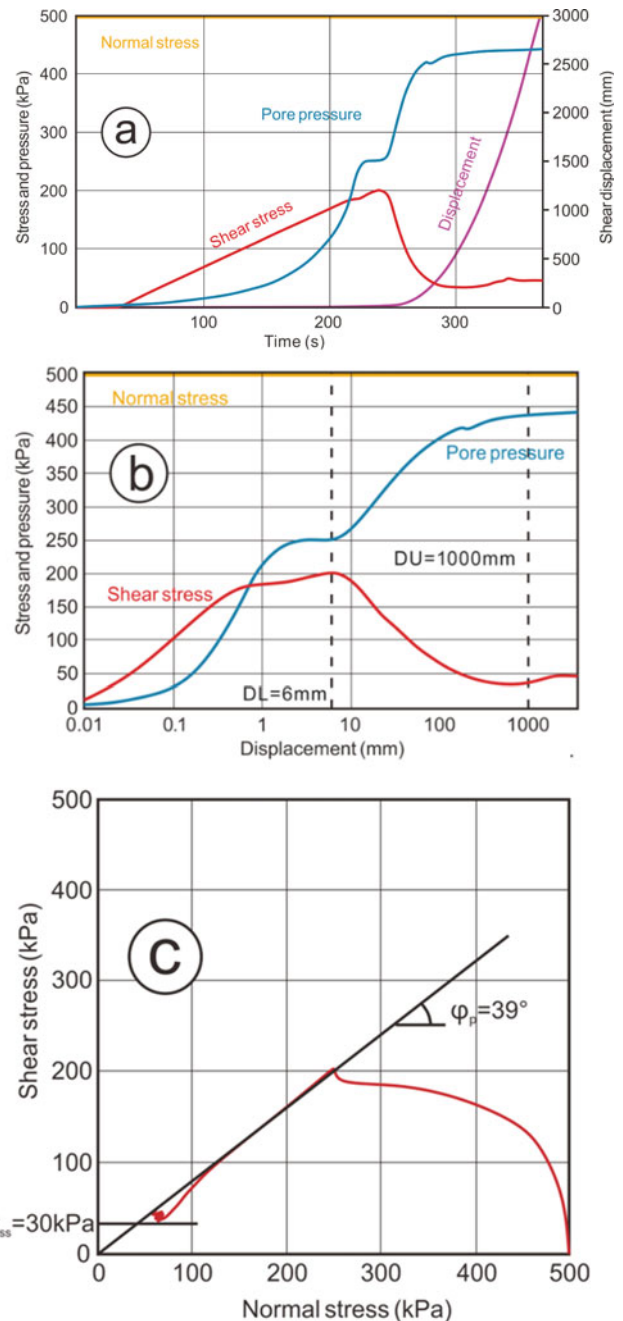


Fig. 13 Result of the undrained stress control test on S-2 using ICL-2 apparatus. a Time-series curves. b Stress-displacement curves. c Stress path. Result of S-1 is not employed as increasing the pore pressure failed to trigger the landslide. The reasons are available in Dang et al. (2019)

6.1 Precise Weather Forecast in Mountain Regions

The southwest region of Sri Lanka, where the south-western monsoon brings heavy rain between May to September, is our target region for the precise weather forecast. However, the technology should apply to wherever we need it.

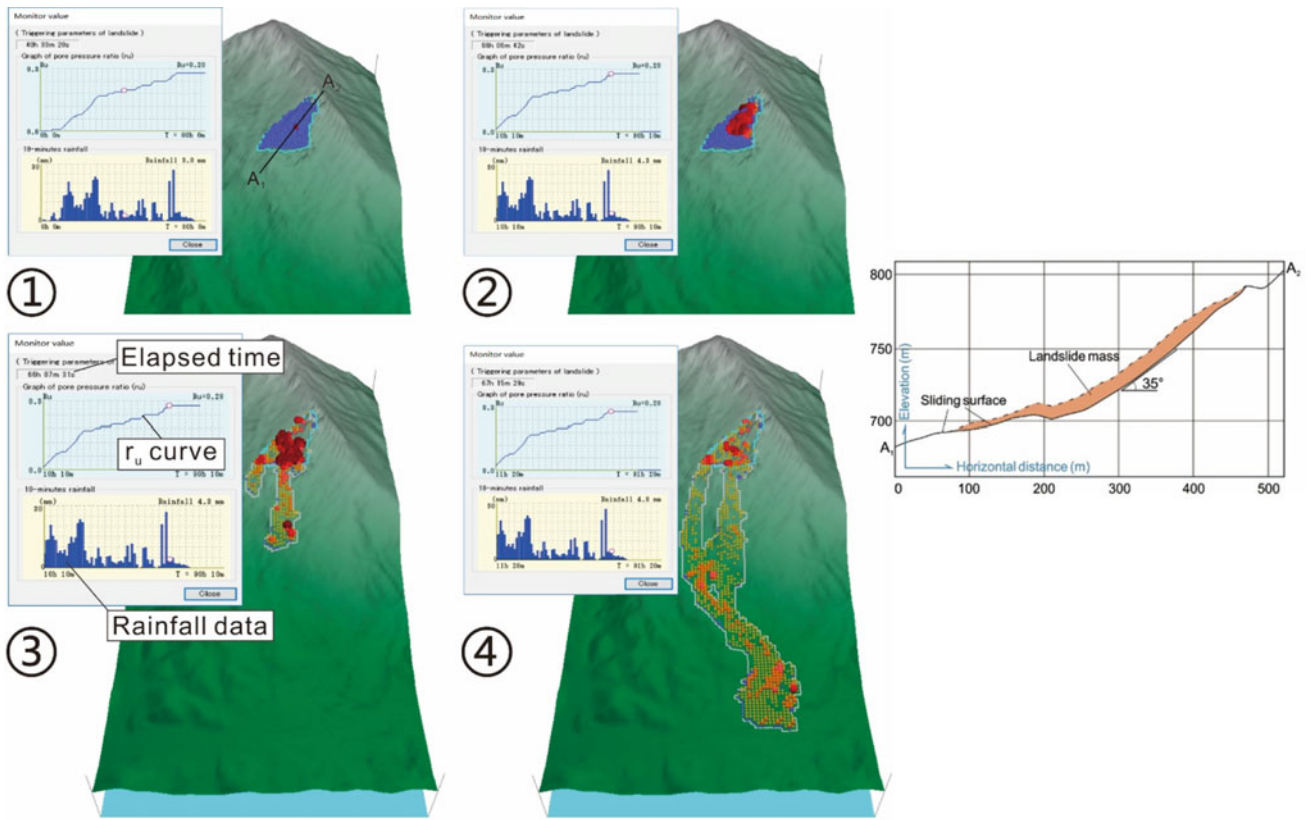


Fig. 14 Reproduction of the 2016 Aranayake RRL on LS-RAPID. The A_1 – A_2 profile is shown on the right. (Dang et al. 2019)

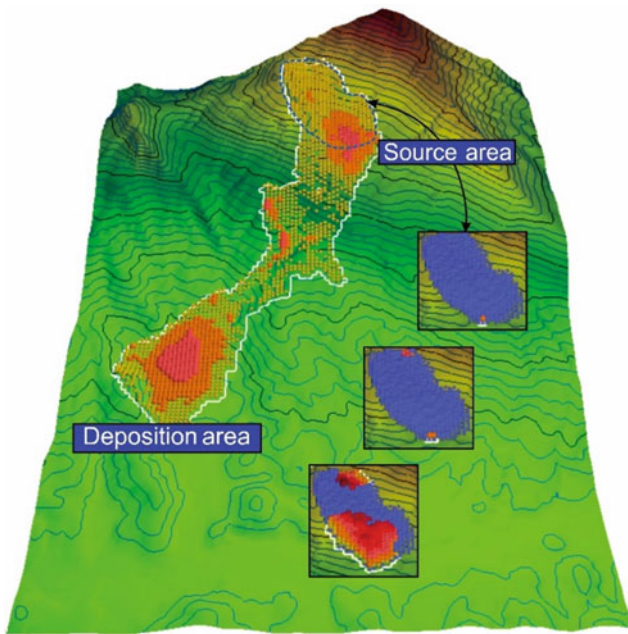


Fig. 15 Runout of the past possible RRL (Tan et al. 2020)

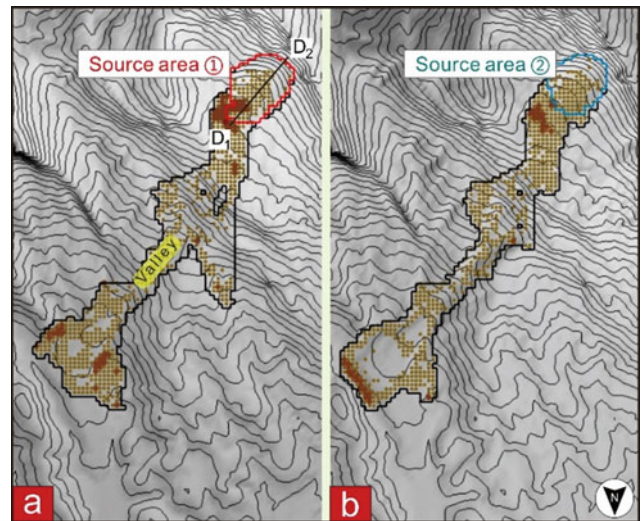


Fig. 16 Runout of the future potential RRL reproduced on LS-RAPID. **a** For a deep-seated RRL and **b** for shallow-seated RRL (Tan et al. 2020)

Looking ahead to worldwide applications in the future, we use MSSG as our generic platform for the precise weather forecast from this perspective. The developers of this MSSG join the research activity of G2 to help develop the rainfall prediction system suitable for Sri Lanka.

MSSG, standing for Multi-Scale Simulator for the Geo-Environment, is an atmosphere–ocean coupled non-hydrostatic model aimed at seamless simulations from global to local scales. MSSG consists of atmospheric (MSSG-A) and ocean (MSSG-O) components (e.g., Takahashi et al. 2007, 2013; Onishi and Takahashi 2012). MSSG adopts a conventional latitude–longitude grid system for regional simulations and the Yin-Yang grid system (Kageyama and Sato 2004; Baba et al. 2010, Fig. 17a), consisting of two overlapping latitude–longitude grids, thus avoiding the polar singularity problem, for global simulations.

MSSG can consider the precise topographic effect and the boundary-layer turbulence that affects the cumulonimbus clouds development, (Seifert and Onishi 2016) particularly over slopes against the wind. Thus, it is suitable for better one-day-ahead predictions of heavy rainfalls in the mountains.

Given the initial condition of weather variables such as winds, temperatures, atmospheric pressures, etc., three days before the Aranayake Landslide of May 2016 in Sri Lanka, MSSG simulated cumulative rain falls at Aranayake. Figure 18 shows the rainfall accumulation at Aranayake (80.4546E and 7.1476N) from 00:00 UTC May 14, 2016. The figure shows three curves:

- (1) For the simulation considering the turbulence enhancement (Case-T),
- (2) For the simulation not considering the turbulence enhancement (Case- NoT), and
- (3) The rain gauge record near Aranayake.

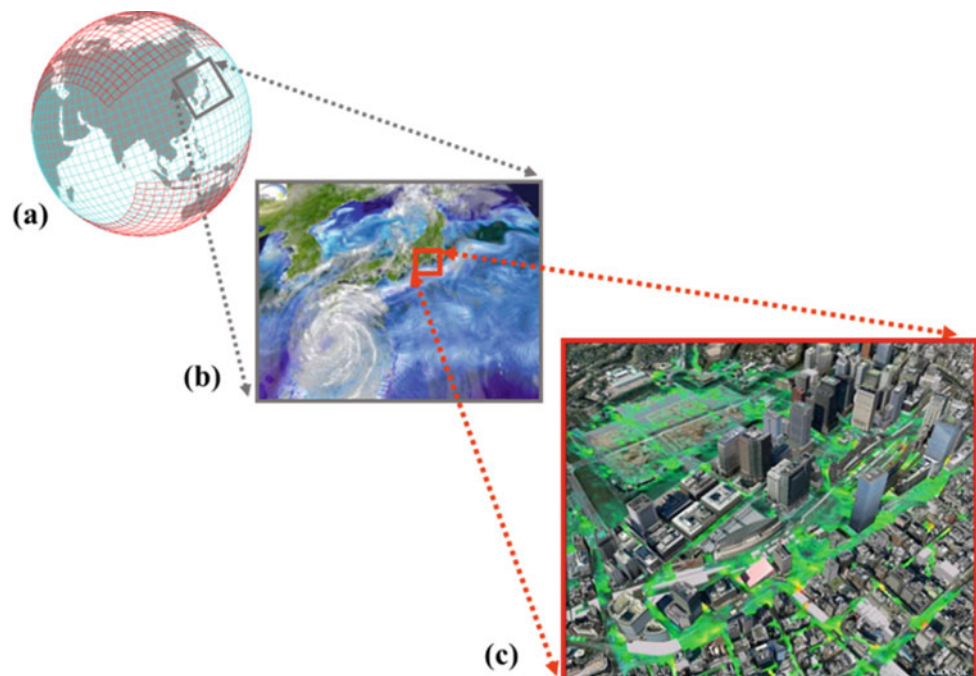
Though the reproduced timings of heavy rainfall events are off from the recorded ones, they successfully produced the total rainfall at the end. The Case-T shows a more significant amount of rain than the Case-NoT, which indicates the turbulence enhancement impacted the orographic rain.

One more successful example is in Western Japan, which suffered vast devastation by the successive heavy downpours in late June through mid-July 2018. Figure 19 shows the 6-h rainfall accumulation over Hiroshima. MSSG successfully reproduced the line-shaped torrential rainfall area, with a length of approximately 70 km in the southwest to the northeast direction and a width of roughly 20 km.

These simulations on MSSG usually require substantial computer resources. For example, the simulation shown in Fig. 19 was conducted on a supercomputer at JAMSTEC with the upper-level computation nest covering a 200 km by 200 km area of the island and the lower-level nest at the resolution of 500 m by 500 m.

The challenge in the one-day-ahead weather prediction in Sri Lanka is that we need to run the MSSG on an affordable workstation. To make it possible, a technique to construct rationally new data points from a low-resolution simulation

Fig. 17 MSSG is designed to be applicable to **a** global scale, **b** meso scales and **c** up to urban scales. The Yin-Yang grid system, which consists of two overlapping latitude–longitude grids indicated in blue and red, was adopted for global simulations



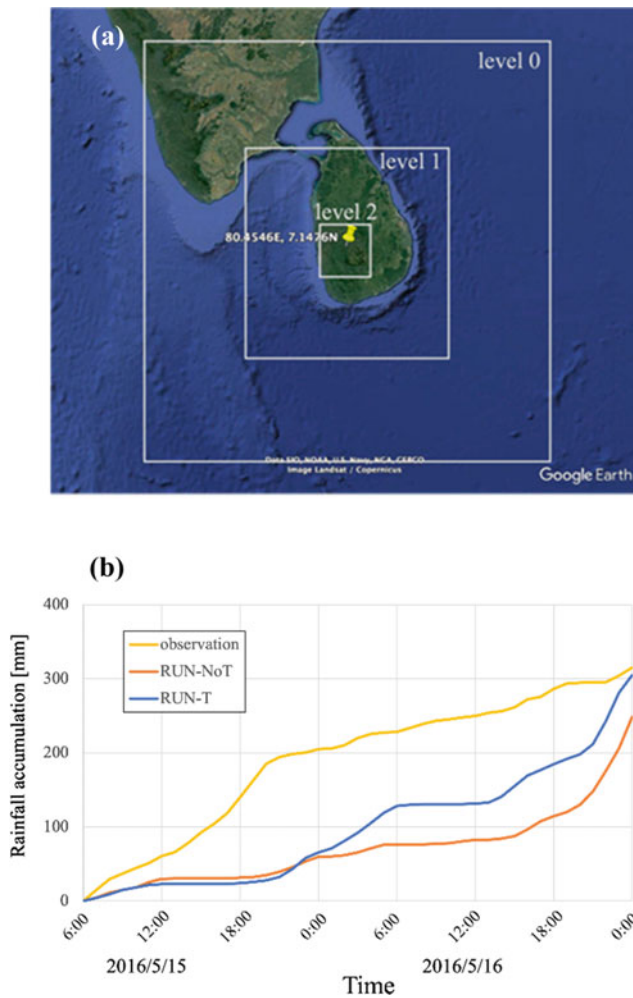


Fig. 18 **a** Computational nesting domains for the Aranayake rainfall simulation. **b** Rainfall accumulation from 06:00 UTC on 15 May, 2016

on the workstation is being developed by applying machine learning technology with good references obtained from simulations on the supercomputer (Onishi et al. 2019).

6.2 Predicting Groundwater Pressure Build-Up

The process of groundwater pressure buildup can trigger an RRL, and thus it is vital to study the process rationally. For this purpose, researchers at the Disaster Prevention Research Institute (DPRI), Kyoto University, conduct geotechnical centrifuge tests, which are helpful for scale modeling of any large-scale nonlinear problem for which gravity is a primary driving force. With a radius of 2.5 m and a maximum payload of 24 g ton, the centrifuge at DPRI can produce 200 g's of centrifugal acceleration at its effective radius (Fig. 20).

Studying rainfall-induced slope failures via centrifuge modeling has a long history, and nozzle system is one of the commonly used rainfalls simulating options (Take et al.

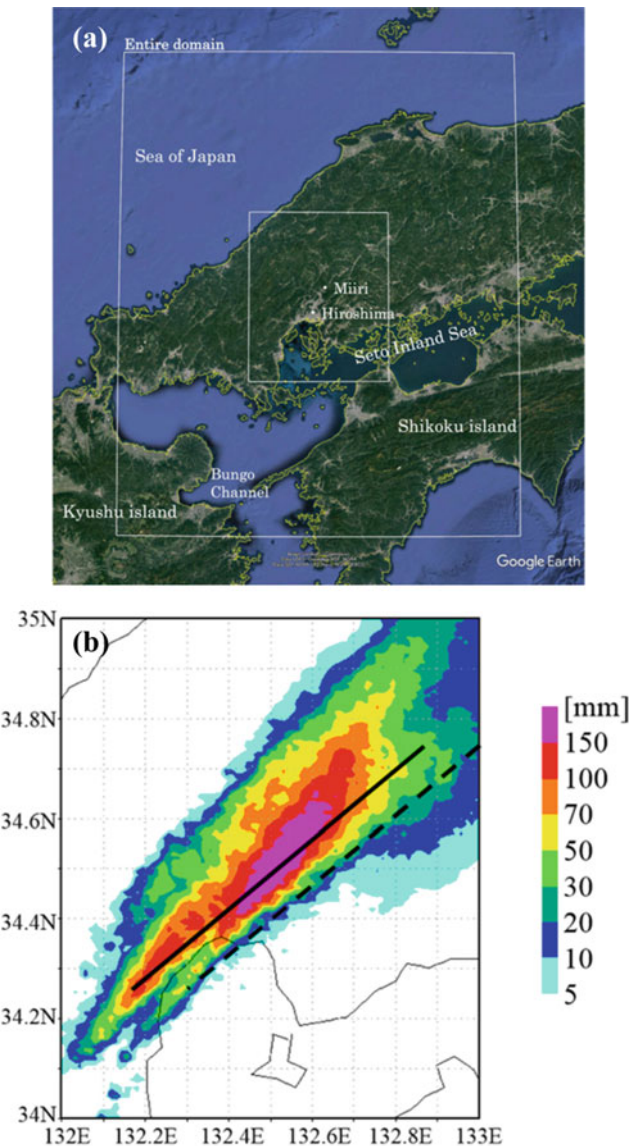


Fig. 19 **a** The computational domain. **b** The horizontal distribution of the 6-h (11 pm–5 am) rainfall accumulation over Hiroshima. **c** A three-dimensional visualization of the cloud distribution over Hiroshima at 00:10 am viewed from the southeast direction. The dashed line corresponds to the solid line in (b)

2004; Ling et al. 2009; Bhattacharjee and Viswanadham 2018). In this experiment, steady and constant downpours are realized in a rigid soil container ($600 \times 300 \times 140$ mm inside) as water flows from 18 misting spray nozzles attached at the top (Xu et al. 2021).

Of particular note is that the soils from mountain slopes in Sri Lanka are weathered fragments of Pre-Cambrian gneiss rock with fine contents ranging from 30 to 40%. In the light of the current circumstances of the COVID-19 pandemic, not the soils from Sri Lanka but weathered granite soil, which is particularly dominant in western Japan and often known as Masado, is used in the experiments. The particle size distribution of this soil says this is well-graded sand with silt. The required amount of the dry soil was moistened with the predetermined amount of water for the specific water content and kept in sealed bags for 24 h to homogenize the soil in terms of water content. The soil was then compacted using the wet-tamping method in layers of 20 mm thickness. During this compaction, Pore Pressure Transducers (PPTs) were placed at predetermined locations shown in Fig. 21. Finally, the soil was cut and shaped to provide the required geometry.

With time, the downpour from the misting spray nozzles led to pore water pressure (PWP) buildup. As shown in Fig. 22, the buildups of the pore pressure at different locations in the soil mass were reproduced in the analyses adopting a simple elastic constitutive model with the soil–water characteristic curve (SWCC) based on the van Genuchten (VG) model (Van Genuchten 1980). The governing equations for the numerical analysis are available in Uzuoka and Borja (2012). The first step of the numerical simulation was to put the soil mass in the steadily increasing gravitational field up to 50 G. Then, the water started seeping into the ground from the flux boundary. The aerial elements were placed immediately above the slope surface to reproduce the smooth infiltration across the air–soil boundary (Uzuoka et al. 2011). The reproduced pore pressure buildups are in good agreement with those observed, as shown in Fig. 23.

6.3 Effective Risk Communication and Public Education

It will take several hours to make a one-day-in-advance forecast of the occurrence of RRLs using the computer programs mentioned above (MSSG, LS-RAPID, etc.) on high-performance workstations. The obtained results will then be timely relayed to the last mile as augmented reality dioramas of the predicted rains and RRLs with a bird's-eye view of the terrain as its background on tablets' and PC screens (Fig. 24). The system physically allows for bi-directional communication between transmitter and receiver sides.

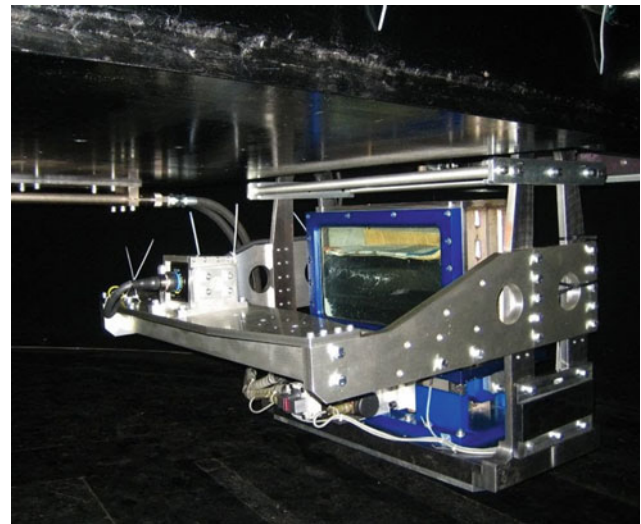


Fig. 20 Geotechnical centrifuge at DPRI, Kyoto University (DPRI Geotechnical Centrifuge Center 2010)

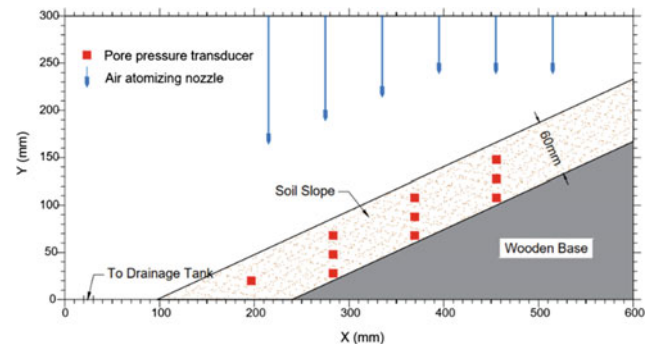


Fig. 21 Schematic diagram of the centrifuge model

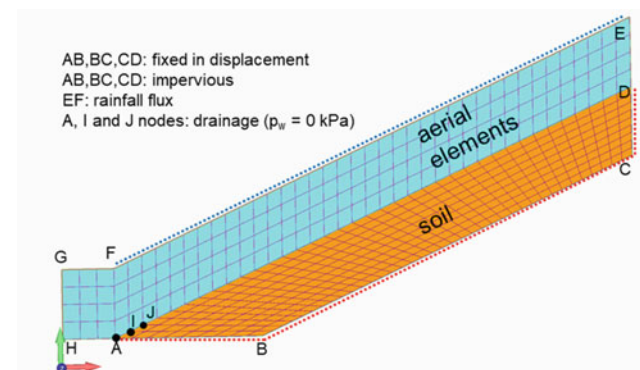


Fig. 22 Numerical model

However, we need to take the following into account for better implementation strategies:

- (1) In Sri Lanka, districts are the second level administrative divisions under provinces (Statoids 2015). Each district, administered under a District Secretary, is

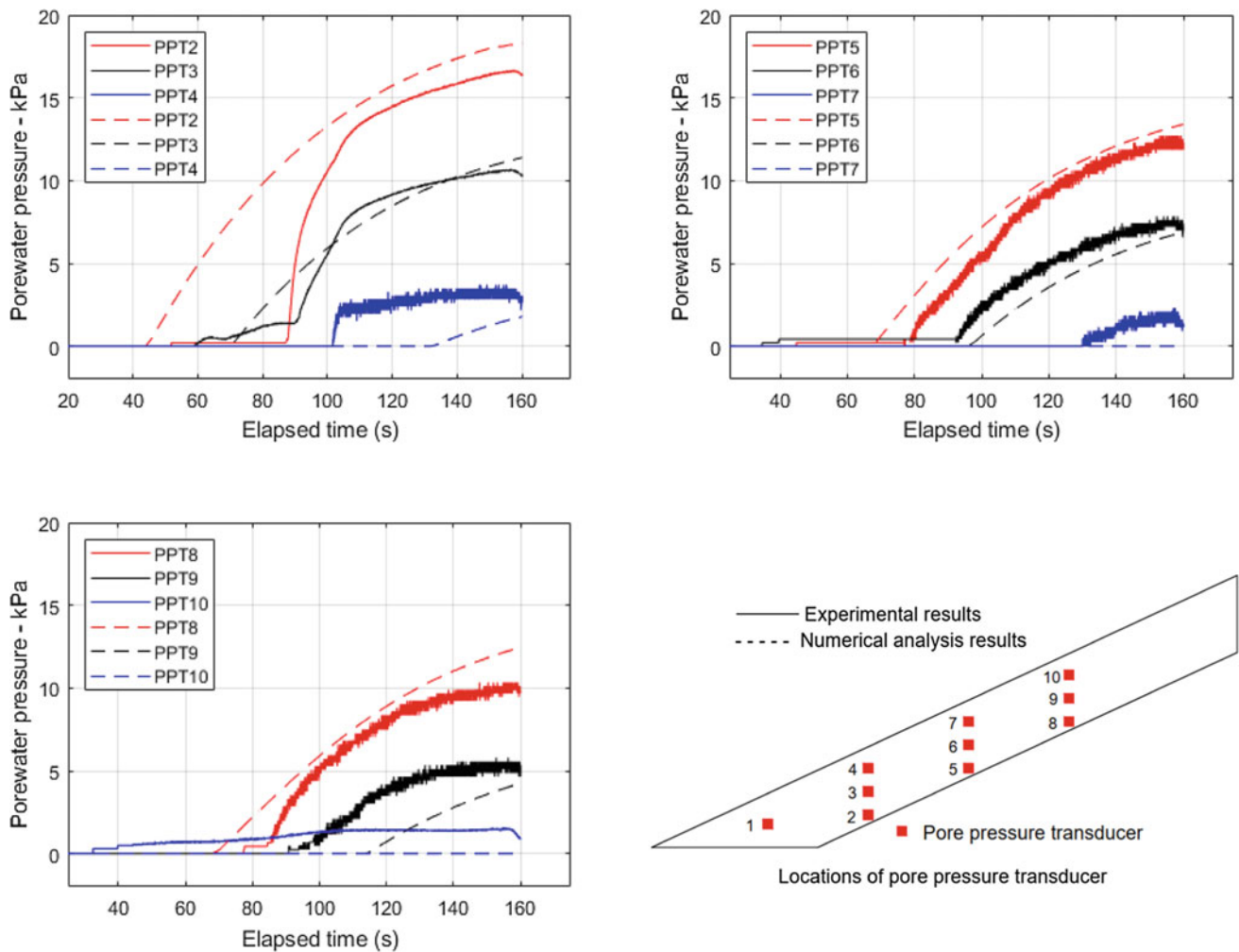


Fig. 23 Comparison of pwp development of experimental results (Test A) and numerical results

divided into several Divisional Secretary’s (DS) divisions, which are further subdivided into extremely many local communities called “Grama Niladhari (GN)” divisions.

- (2) The number of local GN divisions in RRLl-prone areas is increasing year by year reflecting human interventions.
- (3) Though the Disaster Management Centre (DMC) of the Ministry of Défense has sole authority in terms of the issuance of evacuation alerts and evacuation orders, each Divisional Secretary (DS) can use his/her discretion in taking necessary actions in case of urgency.
- (4) NBRO has been helping their decisions providing information alerting them of landslides.
- (5) In this regard, both NBRO and JICA has started a joint project “Project SABO” (NBRO and JICA 2020), for capacity strengthening on development of non-structural measures for landslide risk reduction. The goals include: (a) strengthening of hazard mapping and risk assessment capacity, and (b) revision of regional-level early

warning issuance criteria, etc. Thus, Project RRLl is expected to play a complementary role with Project SABO, providing proactive information that allows people to take precautions against RRLls (Fig. 25, NBRO and JICA 2020).

As said in the “Background story,” NBRO has had local community people actively involved in the Community-Based Landslide Early Warning (CBLEW). The AR image of potential heavy rains and RRLls displayed one day in advance on tablets and PC screens will undoubtedly help them keep further watchful eyes on the movements of potentially dangerous slopes. In this light, people should know the intrinsic nature of the creeping ground movement, which can be a precursor of the RRLl. The researchers at Kochi University study this nature using model slopes with different slope angles, water contents, etc., built in a steel flume (Fig. 26). Behind their experiments is the empirical finding by Fukuzono (1985). Fukuzono reported a linear relationship between the logarithm of

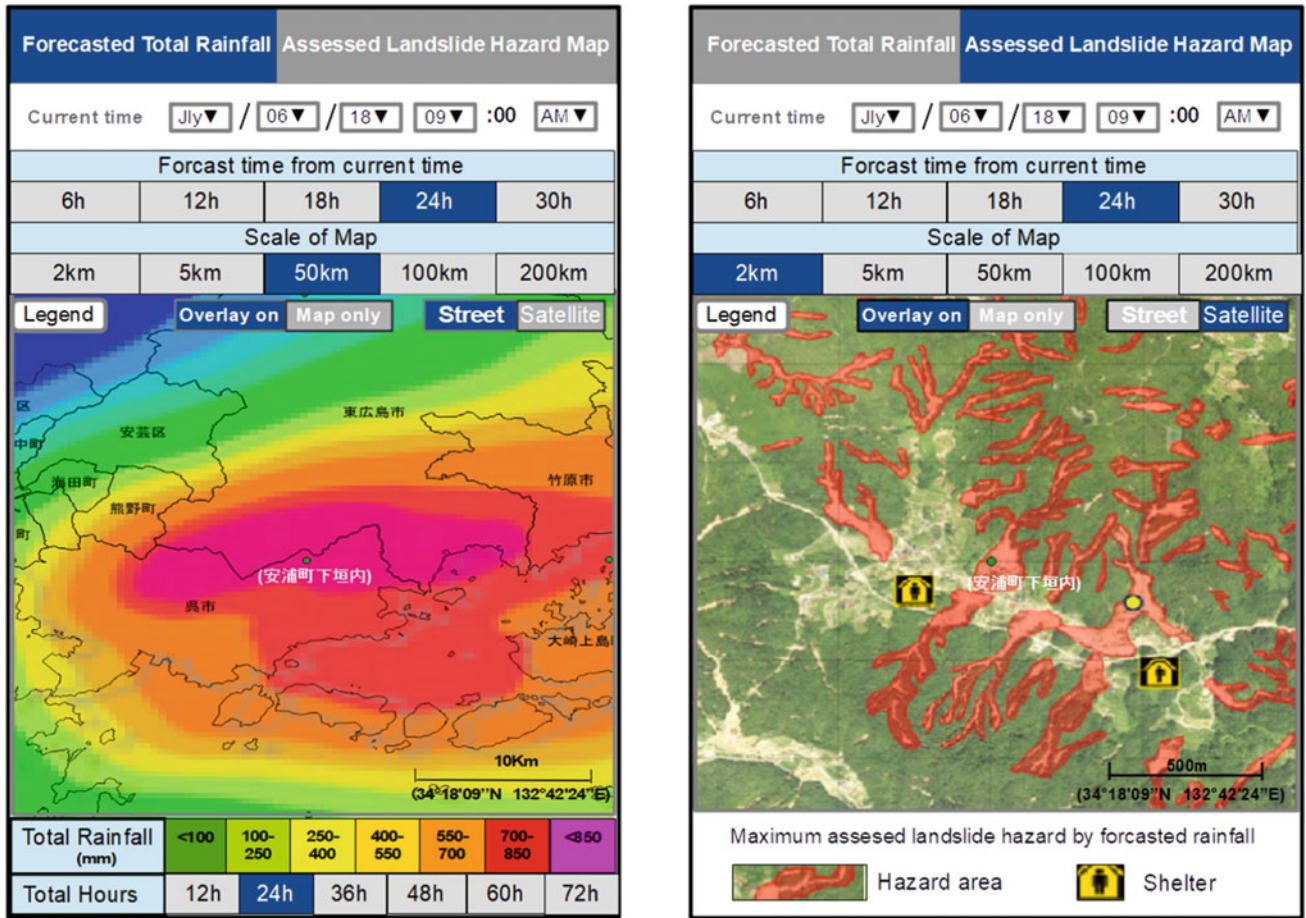
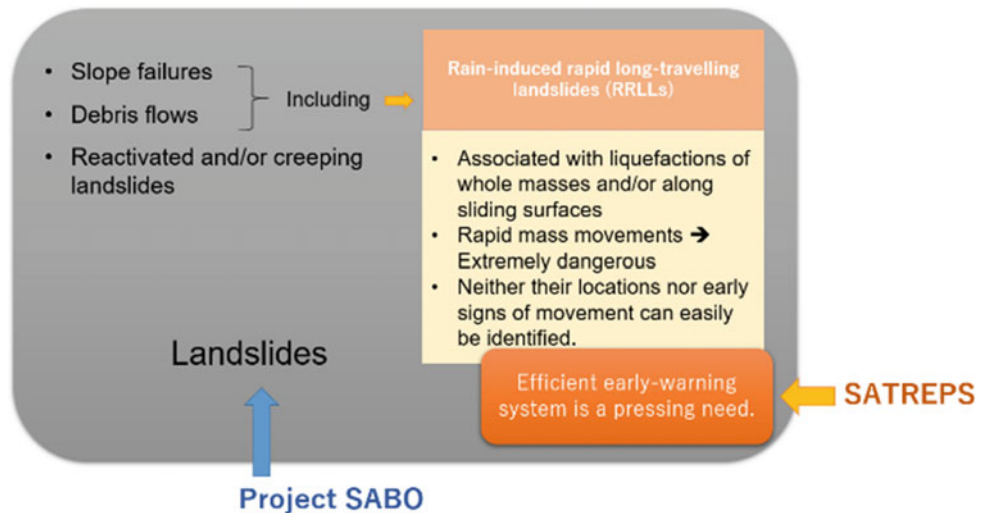


Fig. 24 Rendering image of augmented reality dioramas of the predicted rains and locations of RRLs with a bird’s-eye view of the area as their background on tablet’s screen

Fig. 25 Rain-induced landslides to be covered by both project SABO and project RRL (SATREPS)



acceleration and the logarithm of velocity for the tertiary (or accelerating) creeping movement of a landslide mass with an increasing creep rate, which leads to a landslide.

They have examined three different cases with different slope angles and water contents (Table 1). The three model slopes were prepared with highly weathered granite sand

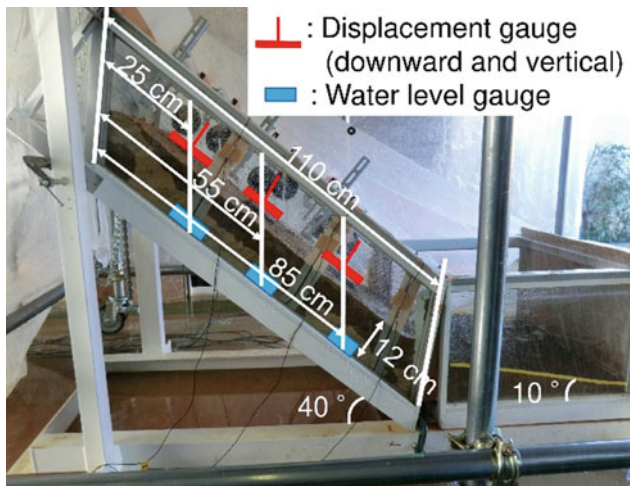


Fig. 26 Slope model prepared in a steel flume (Sasahara 2021)

Table 1 Three cases examined (Sasahara 2021)

	Case 1	Case 2	Case 3
Rainfall intensity (mm/h)	46	46	46
Dry unit weight (g/cm ³)	1.32	1.21	1.32
Water content (%)	0	15.1	0
Upper slope angle (deg.)	40	40	35

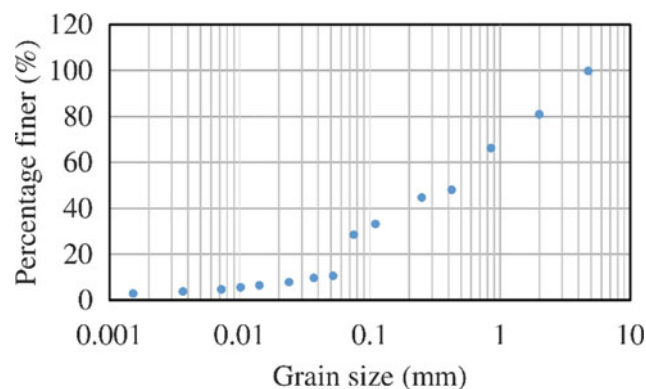


Fig. 27 Grain size distribution of the soil for the model (Sasahara 2021)

(Fig. 27, Masado in Japanese), and steady artificial rainfalls of 46 mm/h were given to these slopes. These slopes showed different buildups of displacements, as shown in Fig. 28. Displacements also differed from location to location on each slope surface. However, it is surprising that the logarithm of acceleration takes almost the same ascending line as the logarithm of velocity increases, no matter the slope geometry and water content, as shown in Fig. 29. The scatter in the plots, particularly for Case 2, are due to the

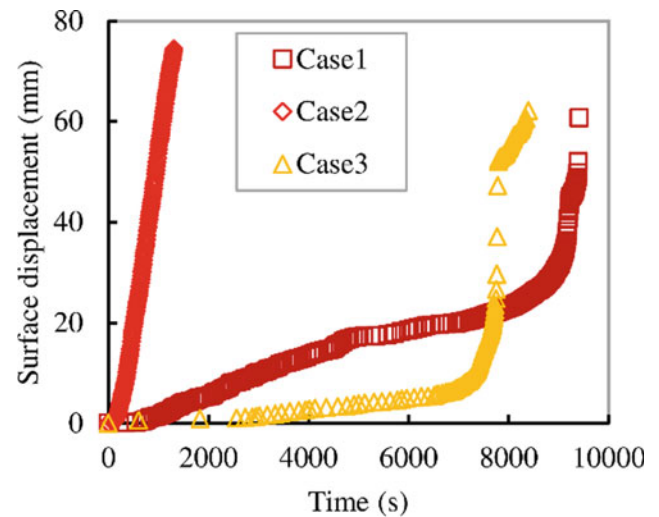


Fig. 28 Displacement buildups for three slope cases: the target plate for displacement measurement was placed 85 cm downslope from the upper end of the flume (Sasahara 2021)

spontaneous formation of a bulge at the toe part of the slope. Once people find they are somewhere on this unique line, they should take proactive actions to prepare for the potential RLL disaster. Further studies will be necessary to work out detailed action plans.

7 Summary

Influenced by the effects of global climate change and, more seriously, by human-induced interventions in landslide-prone areas, the number of tragic RLL events in Sri Lanka has been on a general soaring trend with some remarkable spikes in 2003, 2007, 2011, 2014, 2016, and 2017. In this situation, ICL and NBRO have started this project, “Development of early warning technology of rain-induced rapid and long-traveling landslides in Sri Lanka” (Project RLL) in 2020 after the preceding period of 2019. The project is in line with the activities of the Sri Lanka Comprehensive Disaster Management Programme, output 1.3 “National and community level landslide early warning system is in place.” NBRO has been running one more JICA technical cooperation project, Project SABO, to strengthen the development of non-structural measures for landslide risk reduction. Project RLL is thus complementary with Project SABO providing extra lead time for emergency responses evacuations, namely, one of the most critical missing pieces of the jigsaw puzzle for landslide-hazard mitigation.

The critical technologies to be developed in Project RLL include:

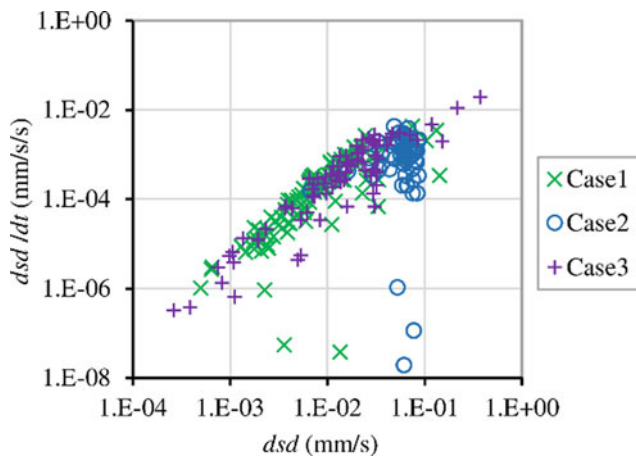


Fig. 29 Logarithms of acceleration and logarithms of velocity for three different cases: the target plate for displacement measurement was placed 85 cm downslope from the upper end of the flume (Sasahara 2021)

- 24 h in-advance prediction of heavy rainfalls in mountains,
- Assessing groundwater pressure build-up, initiation of an RRL, its flowing dynamics, and
- Effective risk communication and public education.

For the (1) 24 h in-advance prediction of heavy rainfalls in the mountains, we use MSSG (Multi-Scale Simulator for the Geo-Environment) as our generic platform for the precise weather forecast. MSSG can consider the topographic effect and thus the boundary-layer turbulence that affects the cumulonimbus clouds development (Seifert and Onishi 2016), particularly over slopes against the wind. It is, therefore, suitable for better one-day-ahead rainfall predictions, particularly in the mountains. The current challenge at the Tokyo Institute of Technology is to run the MSSG on an affordable workstation. To make this possible, a technique to construct rationally new data points from a low-resolution simulation on the workstation is being developed by applying machine learning technology.

For (2) assessing groundwater pressure buildup, researchers at the Disaster Prevention Research Institute (DPRI), Kyoto University, conduct geotechnical centrifuge tests, which are helpful for scale modeling of any large-scale nonlinear problem for which gravity is a primary driving force. Of particular note is that the soils from mountain slopes in Sri Lanka are weathered fragments of Pre-Cambrian gneiss rock with fine contents ranging from 30 to 40%. Thus, well-graded sand with the inclusion of silt was used in the experiments. The pore pressure buildups at different soil mass locations were successfully reproduced in numerical simulations, thus validating the numerical model.

For (3) effective risk communication, the communication tool to be developed will timely relay the prediction to the

last mile as augmented reality dioramas of the potential rains and RRLs with a terrain image displayed on tablets and PC screens. The AR image of possible heavy rains and RRLs displayed on screens will undoubtedly help the local people and officers keep further watchful eyes on the movements of potentially dangerous slopes. Researchers at Kochi University have found that the logarithm of acceleration of the creeping landslide mass takes almost the same ascending line as the logarithm of velocity increases, regardless of the slope geometry and water content. Once people find they are somewhere on this unique line, they will take proactive actions to prepare for the potential RRL disaster. This finding is what people should learn through the educational program to be developed.

Acknowledgements Amid the currently ongoing coronavirus pandemic, we are now figuring out how we will firmly pursue “Project RRL” in line with our developed strategy. The good thing is that scientists and all supporters from both governments are united in our shared belief that the project will undoubtedly contribute to the Sustainable Development Goals (SDGs) of the United Nations. Among all goals, the project serves Goal 11, “Make cities and human settlements inclusive, safe, resilient and sustainable,” through the landslide risk reduction for human settlements in mountainous areas and urban areas close to mountains. We would like to give special thanks to Mr. Satoshi Nakamura, Director, Mr. Naoya Orita, Mr. Haruki Ogasa, Assistant Directors at the Disaster Risk Reduction Team, JICA, Prof. Takashi Asaeda, Research Supervisor, Mr. Kazuo Anazawa, Senior Associate Research Supervisor at JST, Mr. Takayuki Nagai, JICA expert, Mr. Kiyofumi Takashima, and Ms. Yurie Hirabayashi, JICA Sri Lanka Office. Without their support, it would not have been possible for the authors to reach the project’s current stage. We must also thank officers and scientists from NBRO, DOM, DMC, DMI, Central Engineering Consultancy Bureau (CECB), and three major universities in Sri Lanka. They attended the RRL Workshop at the Ministry of Irrigation, Water Resources, and Disaster Management (supervisory authority of NBRO of that time) on June 20, 2018, two Joint Coordination Committee Meetings held on April 22 and November 4, 2021. Their comments have inspired the authors, particularly in the harsh situation of the COVID-19 pandemic. Significantly, Mr. N.A.S. Kumara, Secretary of the Ministry, has given valuable comments in the first RRL workshop from a broad perspective. Also, Major General (Rtd) Sudantha Ranasinghe, Director General of the DMC, provided us with an overview of DMC missions and the roles expected for DMC to pursue in the Project RRL. Last but not least, the authors are greatly indebted to Dr. Kiyoharu Hirota, Dr. Khang Dang, Dr. Ms. Kumiko Fujita, and Ms. Mie Ueda at ICL, for their ceaseless efforts to support the project.

References

- Bhattacharjee D, Viswanadham BVS (2018) Design and performance of an in-flight rainfall simulator in a geotechnical centrifuge. *Geotech Test J* 41(1):72–91
- Dang K, Sassa K, Konagai K, Karunawardena A, Bandara RMS, Hirota K, Tan Q, Ha ND (2019) Recent rainfall-induced rapid and long-traveling landslide on 17 May 2016 in Aranayaka, Kagelle District, Sri Lanka. *Landslides* 16:155–164. <https://doi.org/10.1007/s10346-018-1089-7>

- Department of Meteorology (2020) Sri Lanka, Climate of Sri Lanka. http://www.meteo.gov.lk/index.php?option=com_content&view=article&id=94&Itemid=310&lang=en. Accessed on 14 Apr 2020
- DPRI Geotechnical Centrifuge Center (2010) <https://sites.google.com/dpri.kyoto-u.ac.jp/centrifuge>
- Fukuzono T (1985) A new method for predicting the failure time of a slope. In: Proceedings of the IVth international conference and field workshop on landslides, Tokyo, pp 145–150
- Japan Science and Technology Agency (2020) SATREPS for the earth, for the next generation. <https://www.jst.go.jp/global/english/>. Accessed on 12 Feb 2021
- JICA Survey Team (2016) Survey results of Aranayake Disaster, JICA. <https://www.jica.go.jp/srilanka/english/office/topics/c8h0vm00006ufwhl-att/160720.pdf>. Accessed on 14 Apr 2020
- Ling HI, Wu M-H, Leshchinsky D, Leshchinsky B (2009) Centrifuge modeling of slope instability. *J Geotech Geoenviron Eng* 135 (6):758–767
- National Building Research Organization, NBRO (2022a) Landslide early warning. http://www.nbro.gov.lk/index.php?option=com_content&view=article&id=116&lang=en
- National Building Research Organization, NBRO (2022b) Landslide hazard zonation mapping. https://www.nbro.gov.lk/index.php?option=com_content&view=article&id=48&Itemid=264&lang=en
- National Building Research Organization (NBRO) & Japan International Cooperation Agency (JICA) (2020c) Project for capacity strengthening on development of non-structural measures for landslide risk reduction (Project SABO). http://www.nbro.gov.lk/index.php?option=com_content&view=article&id=197&catid=2&Itemid=101&lang=en. Accessed on 14 Apr 2020c
- Onishi R, Takahashi K (2012) A warm-bin-cold-bulk hybrid cloud microphysical model. *J Atmos Sci* 69:1474–1497
- Onishi R, Sugiyama D, Matsuda K (2019) Super-resolution simulation for real-time prediction of urban micrometeorology. *SOLA* 15:178–182
- Sasahara K (2021) Velocity and acceleration of surface displacement in sandy model slope with various slope conditions. In: Chapter 37, understanding and reducing landslide disaster risk, world landslide forum, vol 5, Springer. https://doi.org/10.1007/978-3-030-60311-3_37
- Sassa K, Nagai O, Solidum R, Yamazaki Y, Ohta H (2010) An integrated model simulating the initiation and motion of earthquake and rain induced rapid landslides and its application to the 2006 Leyte landslide. *Landslides* 7(3):219–236
- Sassa K (2015) ISDR-ICL Sendai partnerships 2015–2025 for global promotion of understanding and reducing landslide disaster risk. *Landslides* 12:631–640. <https://doi.org/10.1007/s10346-015-0586-1>
- Seifert A, Onishi R (2016) Turbulence effects on warm-rain formation in precipitating shallow convection revisited. *Atmos Chem Phys* 16:12127–12141
- Statoids (2015) Divisions of Sri Lanka. <http://www.statoids.com/y/lk.html>. Accessed on 14 Apr 2020
- Takahashi K, Peng X, Onishi R, Ohdaira M, Goto K (2007) Multi-scale simulator for the geo-environment: MSSG and simulations, use of high-performance computing in meteorology, pp 36–54
- Takahashi K, Onishi R, Baba Y, Kida S, Matsuda K, Goto K, Fuchigami H (2013) Challenge toward the prediction of typhoon behavior and down pour. *J Phys Conf Ser* 454:012072
- Take WA, Bolton MD, Wong PCP, Yeung FJ (2004) Evaluation of landslide triggering mechanisms in model fill slopes. *Landslides* 1 (3):173–184
- Tan Q, Sassa K, Dang K, Konagai K, Karunawardena A, Bandara RMS, Tang H, Sato G (2020) Estimation of the past and future landslide hazards in the neighboring slopes of the 2016 Aranayake landslide, Sri Lanka. *Landslides* 17. <https://doi.org/10.1007/s10346-020-01419-1>
- UDR Prevention Web (2005) Towards a safer Sri Lanka: Road map for disaster risk management. <https://www.preventionweb.net/publication/towards-safer-sri-lanka-road-map-disaster-risk-management>. Accessed on 15 Feb 2022
- UNISDR Prevention Web (2015) Sendai framework for disaster risk reduction 2015–2030. In: UN world conference on disaster risk reduction, 14–18 March 2015, Sendai. <https://www.wcdrr.org/preparatory/post2015.html>. Accessed on 15 Feb 2022
- Uzuoka R, Kazama M, Sento N (2011) Soil-water-air coupled analysis on seepage and overtopping behavior of river levee. In: Proceedings 14th Asian regional conference on soil mechanics and geotechnical engineering, ARC 2011, Hong Kong
- Uzuoka R, Borja RI (2012) Dynamics of unsaturated poroelastic solids at finite strain. *Int J Numer Anal Meth Geomech* 36(13):1535–1573
- Van Genuchten MTh (1980) A closed-form equation for predicting the hydraulic conductivity of unsaturated soils. *Soil Sci Soc Am J* 44 (5):892–898
- Xu J, Ueda K, Uzuoka R (2021) Evaluation of failure of slopes with shaking-induced cracks in response to rainfall. *Landslides*

Open Access This chapter is licensed under the terms of the Creative Commons Attribution 4.0 International License (<http://creativecommons.org/licenses/by/4.0/>), which permits use, sharing, adaptation, distribution and reproduction in any medium or format, as long as you give appropriate credit to the original author(s) and the source, provide a link to the Creative Commons license and indicate if changes were made.

The images or other third party material in this chapter are included in the chapter's Creative Commons license, unless indicated otherwise in a credit line to the material. If material is not included in the chapter's Creative Commons license and your intended use is not permitted by statutory regulation or exceeds the permitted use, you will need to obtain permission directly from the copyright holder.





Real-Time High-Resolution Prediction of Orographic Rainfall for Early Warning of Landslides

Ryo Onishi, Joe Hirai, Dmitry Kolomenskiy, and Yuki Yasuda

Abstract

Heavy rainfall often causes devastating landslides. Early warning based on reliable rainfall prediction can help reduce human and economic damages. This paper describes a recent development of reliable high-resolution prediction of orographic (topographic) rainfall using our next-generation numerical weather prediction model, the Multi-Scale Simulator for the Geoenvironment (MSSG). High-resolution computing is required for reliable rainfall prediction, and the MSSG can run with very high resolutions. Robust cloud microphysics is another key to realizing reliable predictions of orographic clouds, where the atmospheric boundary turbulence can affect. This paper clarifies that in-cloud turbulence can enhance cloud development. The recent cloud microphysics model that can consider turbulence enhancement is newly implemented in the MSSG. The emerging machine-learning technology is also coupled with the MSSG for reliable operational predictions. We show the recent development towards reliable predictions of orographic rainfall for realizing early warning of landslides.

Keywords

Multi-scale weather simulation • Orographic rainfall • Turbulence enhancement of cloud development • Super-resolution simulation • Deep neural network

1 Introduction

Most tragic landslides are caused by heavy rainfall. For example, the most tragic landslide disaster for recent Japan happened in Hiroshima in August 2014. A series of landslides following local heavy rain reportedly killed seventy-four people. An automated observatory recorded over 200 mm rainfall accumulation within 3 h. This intense rainfall within such a short period made it difficult to issue an early warning, and unfortunately, the evacuation advisory by Hiroshima prefecture was too late.

Reliable rainfall prediction is undoubtedly needed for early warning. There are several numerical weather prediction models available in the world. Examples are WRF (www.wrf-model.org) in the United States, ASUCA in Japan, and COSMO (www.cosmo-model.org) in Germany. These are called regional models as they target regional- (or meso-) scale weather with O(1 km) horizontal resolution. Such regional models are usually for short-term forecasts. However, it is often valuable for early warning if the chance of heavy rain is predicted more than two days before. The regional models need, for forecast, boundary conditions provided by global models. Global models are generally run with O(10 km) horizontal resolutions and guide long-term forecasts (usually more than 2 days). Due to the coarse horizontal grid of O(10 km), the global models need the aid of cumulus parameterization and are usually not good at local heavy rain predictions.

The recent development of supercomputer systems allows us to run global simulations with O(1 km) horizontal resolutions or even finer resolutions with O(100 m) without the

R. Onishi (✉) · Y. Yasuda
Tokyo Institute of Technology, Global Scientific Information and
Computing Center, Tokyo, 1528550, Japan
e-mail: onishi.ryo@gsic.titech.ac.jp

Y. Yasuda
e-mail: yasuda.y.aa@m.titech.ac.jp

J. Hirai
Tokyo Institute of Technology, Department of
MechanicalEngineering, Tokyo, Japan
e-mail: hirai.j.ab@m.titech.ac.jp

D. Kolomenskiy
Skolkovo Institute of Science and Technology, Skoltech Center
for Design, Manufacturing, and Materials, Moscow, Russia

aid of cumulus parameterizations. The Multi-Scale Simulator for the Geoenvironment (MSSG; Takahashi et al. 2013 and references therein) can serve for such simulations.

The following subsection briefly reviews the numerical weather prediction models. We then explain the multi-scale weather prediction model MSSG. Some examples of MSSG simulations for heavy rain events are shown. We finally describe the recent integrated technology of machine-learning and computer simulation technologies for operational real-time prediction systems.

2 Multi-scale Weather Prediction Model—Multi-scale Simulator for the Geoenvironment (MSSG)

2.1 Overview

Two types of models are in use for numerical weather prediction (NWP): global and regional models. Global models generally run with $O(10\text{ km})$ horizontal resolutions and guide long-term forecasts (usually more than two days). Regional models are used for shorter-term forecasts and run with $O(1\text{ km})$ horizontal resolutions. Some meteorological processes are too small to be explicitly included for the global models. Then the so-called parameterization is a way for representing these processes by relating them to grid-scale variables. For example, a typical cumulus cloud has a scale of $O(1\text{--}10\text{ km})$, much smaller than the horizontal resolutions of global models. The convection process by cumulus clouds should be parameterized, and the parameterization is called cumulus parameterization, on which most of the global models rely.

The recent development of supercomputer systems allows us to run global simulations with $O(1\text{ km})$ horizontal resolutions without the aid of cumulus parameterizations. The Multi-Scale Simulator for the Geoenvironment (MSSG; Takahashi et al. 2006, 2013 and references therein) can serve for such simulations.

The MSSG is an atmosphere-ocean coupled non-hydrostatic model aimed at seamless simulations from global to local scales (Fig. 1). MSSG consists of atmospheric (MSSG-A) and ocean (MSSG-O) components. MSSG adopts a conventional latitude-longitude grid system for regional simulations and the Yin-Yang grid system (Kageyama and Sato 2004; Baba et al. 2010), consisting of two overlapping latitude-longitude grids, thus avoiding the polar singularity problem, for global simulations. MSSG has been serving a wide range of applications. A global atmosphere-ocean coupled simulation was performed at an 11 km horizontal resolution with a nested region at a 2.7 km horizontal resolution. It successfully showed sea surface cooling induced by a typhoon along the track (Takahashi

et al. 2013). High-resolution global typhoon simulations were conducted with 7 km horizontal resolutions to clarify the potential of high resolutions for typhoon track predictions (Nakano et al. 2017). High-resolution regional atmospheric simulations were conducted to investigate the influences of the choice of cloud microphysics scheme and that of in-cloud turbulence on the development of clouds (Onishi et al. 2012, 2015). MSSG-O has been used to investigate the dispersion of radionuclides released from the Fukushima Dai-ichi nuclear power plant with 2 km horizontal resolution (Choi et al. 2013) and the effect of wind on long-term summer water temperature trends in Tokyo Bay, Japan, with 200 m horizontal resolution (Lu et al. 2015). MSSG-A has been applied to building-resolving urban atmosphere simulations with 5 m spatial resolutions to clarify heat environments on streets (Takahashi et al. 2013; Matsuda et al. 2018; Kamiya et al. 2019) (Fig. 1).

2.2 Dynamical Core of the Atmosphere Component

The dynamical core of MSSG-A is based on the non-hydrostatic equations and predicts the three wind components—air density, water vapor mixing ratio, and pressure.

The third-order Runge–Kutta scheme is used for time integrations. The fast terms relating to acoustic and gravity waves are calculated separately with a shorter time step (Wicker and Skamarock 2002). A fifth-order upwind scheme (Wicker and Skamarock 2002) was chosen for momentum advection and the second-order weighted average flux (WAF) scheme with the Superbee flux limiter (Toro 1989) for scalar advection. For turbulent diffusion, the Mellor–Yamada–Nakanishi–Niino level 2.5 scheme (Nakanishi and Niino 2009) is used. The MSSG-Bulk model (Onishi and Takahashi 2012), which is a six-category bulk cloud microphysics model (see the following subsection for detail), is used for explicit cloud physics, and “Model-Simulation-radiation TRaNsfer code” (MSTRNX; Sekiguchi and Nakajima 2008) is used for calculating longwave and shortwave radiation transfers.

2.3 Cloud Microphysics

The bulk cloud microphysics model in MSSG (MSSG-Bulk model; Onishi and Takahashi 2012) computes the temporal evolutions of mixing ratios of water vapor, cloud water, rain, cloud ice, snow and graupel, and in addition, the number density of cloud ice particles. Thus, the bulk model is a one-moment model for warm rain processes and a partial two-moment model for cold rain processes.

Figure 2 shows the cloud microphysical processes considered in MSSG-Bulk. The prognostic variables are the

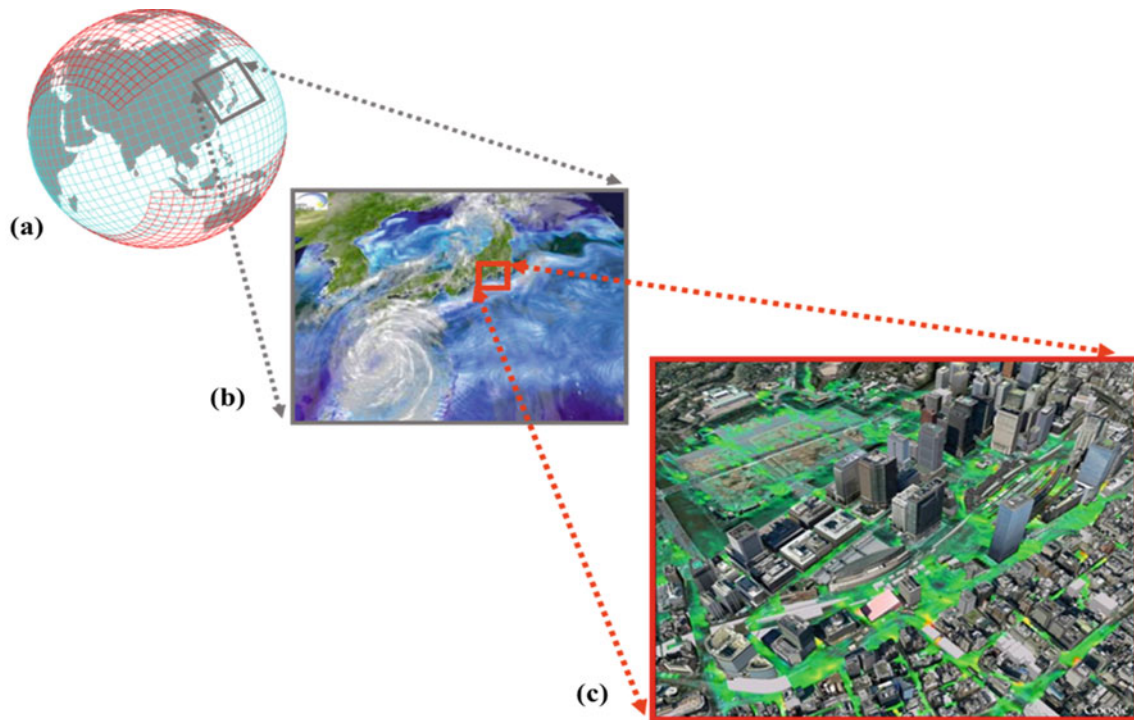
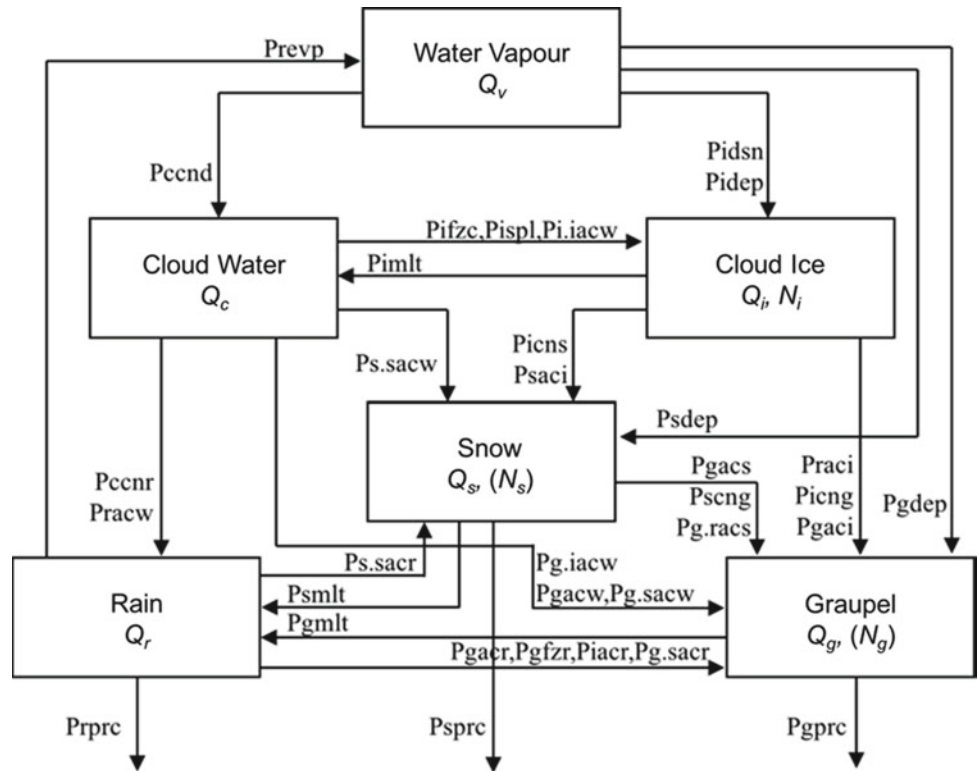


Fig. 1 MSSG is designed to be applicable to **a** global scale, **b** meso scales and up to **c** urban scales. The Yin-Yang grid system, which consists of two overlapping latitude–longitude grids indicated in blue and red, is adopted for global simulations

Fig. 2 Cloud microphysical processes in MSSG-bulk



mixing ratios of water vapor, cloud, rain, cloud ice, snow, graupel, and the number concentration of cloud ice; Q_v , Q_c , Q_r , Q_i , Q_s , Q_g and N_i , respectively.

MSSG also has the warm-bin/cold-bulk hybrid cloud microphysical model named MSSG-Bin (Onishi and Takahashi 2012). In that hybrid model, a spectral bin scheme is used for liquid droplets, while a bulk scheme is used for solid (ice) particles. That is, the expensive but more reliable spectral bin scheme treats the relatively well-understood physics of the liquid phase, and the computationally efficient but less robust bulk scheme is used to treat the poorly understood physics of the ice phase.

3 Rainfall Predictions

3.1 Regional Numerical Weather Prediction

MSSG weather simulations have been applied to several heavy rain events. Examples are the locally heavy rain event in Zoshigaya, Japan, on 4th September 2005 and in Hiroshima, Japan, on 19th and 20th August 2014.

The Zoshigaya heavy rain happened on 4th September 2005, associated with mesoscale convective systems caused severe urban flooding in Suginami ward, in the heart of the Tokyo metropolitan city. An MSSG simulation was performed on 1 km horizontal resolution and 32 vertical layers for the computational domain shown in Fig. 3. The initial data were obtained by interpolating the Grid Point Value (GPV) data at 06:00 UTC on 4th September 2005 provided

by Japan Meteorological Business Support Center. Figure 4 shows the surface precipitation at 00:00 on 5th September 2005, when a strong rain band lay east of Tokyo and Kanagawa. The local maximum precipitation was underestimated, but MSSG successfully reproduced the south-north rain band.

The Hiroshima heavy rain happened on 19th and 20th August 2014, which led to devastating landslides. The regional MSSG simulation was applied to reproduce this event (Hiruma et al. 2022).

Figure 5a shows the horizontal computational domain, which covers a part of the Chugoku, Shikoku, and Kyushu regions, Japan. The number of grid points was $N_\lambda \times N_\phi \times N_z = 648 \times 648 \times 207$, where subscripts λ , ϕ , and z denote longitudinal, latitudinal, and altitudinal directions, respectively. The horizontal grid spacing $\Delta x_\lambda = \Delta x_\phi$ was set to 500 m both for latitudinal and longitudinal directions. The domain height was 30 km, and a damping layer was laid in the top 1/3 of the domain. The vertical grid spacing Δz was varied from 14 m for the lowest layer to 123 m for the highest layer. The simulation start time was set to 9 pm in Japan Standard Time (JST; 9 h ahead to the coordinated universal time, UCM) on 19th August 2014 and the duration to 8 h.

Figure 5b shows the 6-h rainfall accumulation over Hiroshima. This figure shows that the MSSG simulation successfully reproduced the line-shaped heavy rainfall area, with a length of approximately 70 km in the southwest to the northeast direction and a width of approximately 20 km. The most intense simulated rainfall area was located on the east side of Hiroshima city and was shifted eastward by only

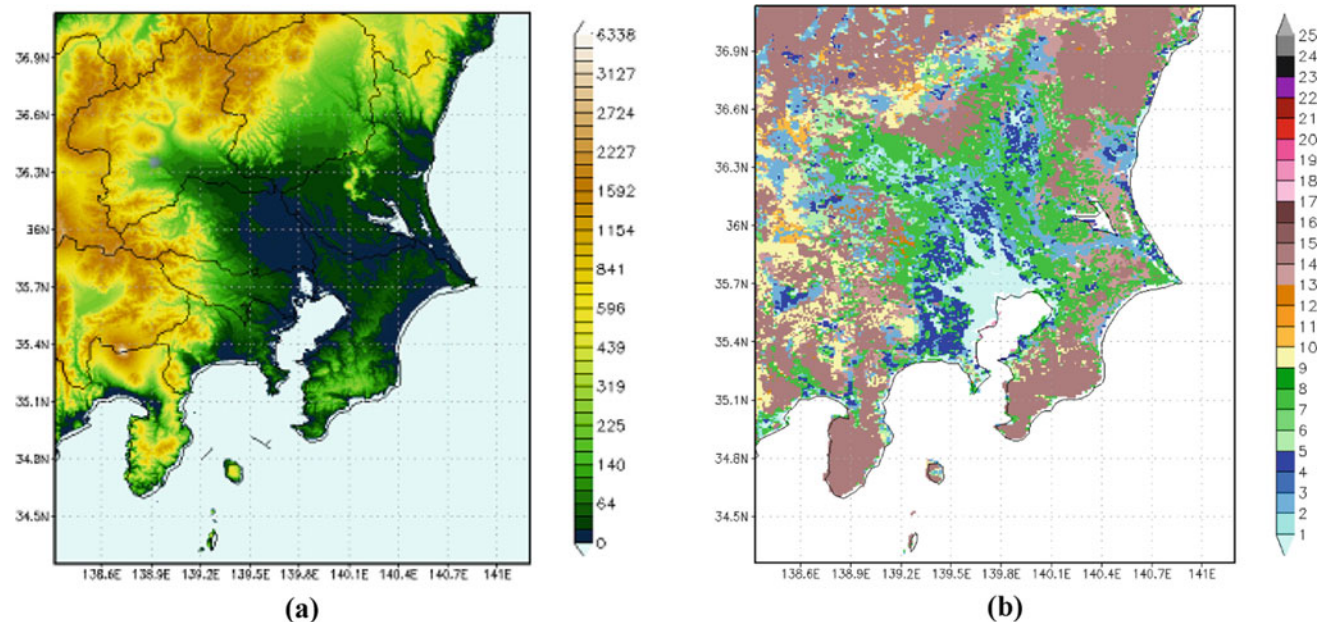


Fig. 3 Computed area showing **a** the orographic elevation and **b** the land use index

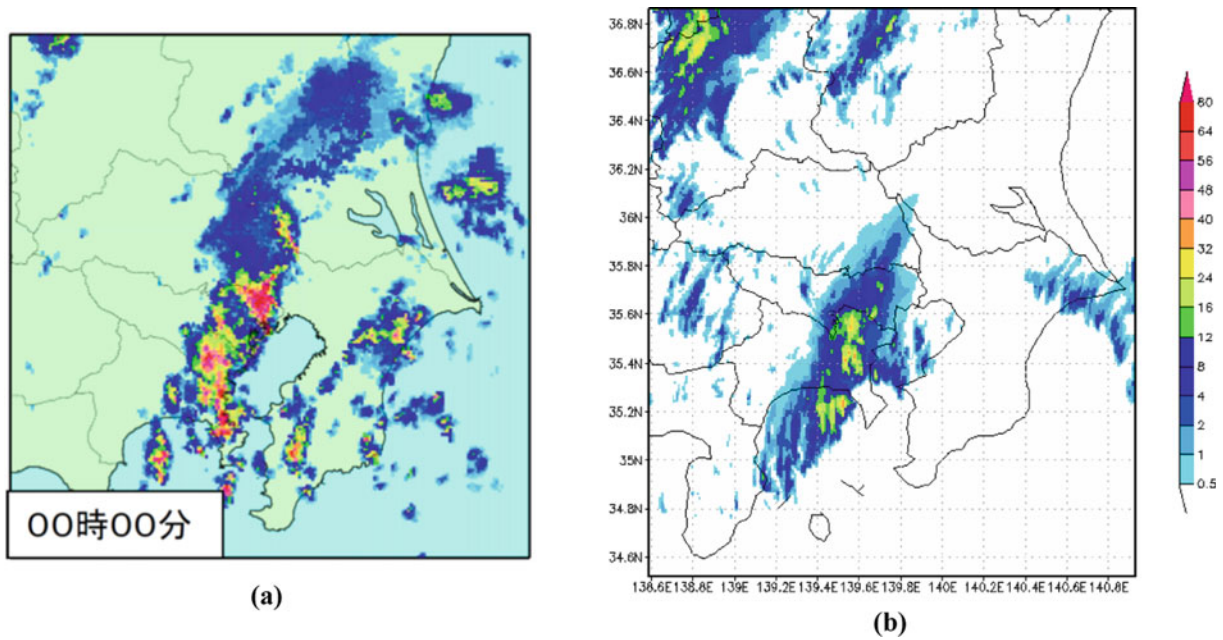


Fig. 4 Surface precipitation at 00:00 JST on 4 September 2005 from **a** the radar observation (Tokyo District Meteorological Observatory) and **b** the MSSG simulation result

around 20 km compared with JMA radar observations. Figure 5c shows a three-dimensional visualization of the cloud distribution over Hiroshima at 00:10 am viewed from the southeast direction. It was visualized using the open software named VDVGE (Kawahara et al. 2015). For this visualization, we ran a 100 m grid-spacing simulation for 10 min starting at 12 am from a linearly-interpolated 500 m grid-spacing model state. The total mixing ratios of non-sedimenting hydrometeors—i.e., cloud water and cloud ice—are shaded in white, whereas those of sedimenting hydrometeors—i.e., rain, graupel and snow—are colored in red. The images are stretched by a factor of three in the vertical direction to aid recognition of the convective system. This visualization shows a typical three-dimensional shape of a storm training, consisting of a chain of cumulonimbus lines.

3.2 Effect of Turbulence Enhancement on Orographic Precipitation

The turbulence-enhanced collision rate of cloud droplets may explain the rapid growth of cloud droplets, which often result in fast rain initiation in the early stages of cloud development (Falkovich and Pumir 2007; Grabowski and Wang 2013).

The change rate of particle number density, $n_f(r, x_i, t)$, by the stochastic collision-coalescence process is represented by

$$\frac{dn_f(r)}{dt} = \frac{1}{2} \int_0^{\infty} K_c(r', r') n_f(r') n_f(r') dr' - \int_0^{\infty} K_c(r, r') n_f(r) n_f(r') dr' \quad (1)$$

where $r' = (r^3 - r'^3)^{1/3}$ and $K_c(r_1, r_2)$ is the collision kernel describing the rate at which a particle of radius r_1 is collected by a particle of radius r_2 . The conventional collision kernel model is the hydrodynamic kernel model, which describes the collision due to the settling velocity difference between two particles of different sizes

$$\langle K_{c,hydr}(r_1, r_2) \rangle = \pi R_{12}^2 |V_{p,1} - V_{p,2}|, \quad (2)$$

where $\langle \rangle$ denotes an ensemble average, $R_{12} (= r_1 + r_2)$ is the collision radius and $V_{p,i}$ is the settling velocity of particles with radius r_i . This hydrodynamic kernel cannot describe the collisions due to turbulence since it contains no flow parameters.

The turbulent collision kernel that involves the turbulence effects can be written in the following form (Wang et al. 1998).

$$\langle K_{c,turb}(r_1, r_2) \rangle = 2\pi R_{12}^2 \langle w_r(x = R_{12}) \rangle g_{12}(x = R_{12}) \quad (3)$$

Here $w_r(x = R_{12})$ is the radial relative velocity at contact separation and describes the turbulence-enhanced relative velocities of two colliding particles. The term, $g_{12}(x = R_{12})$,

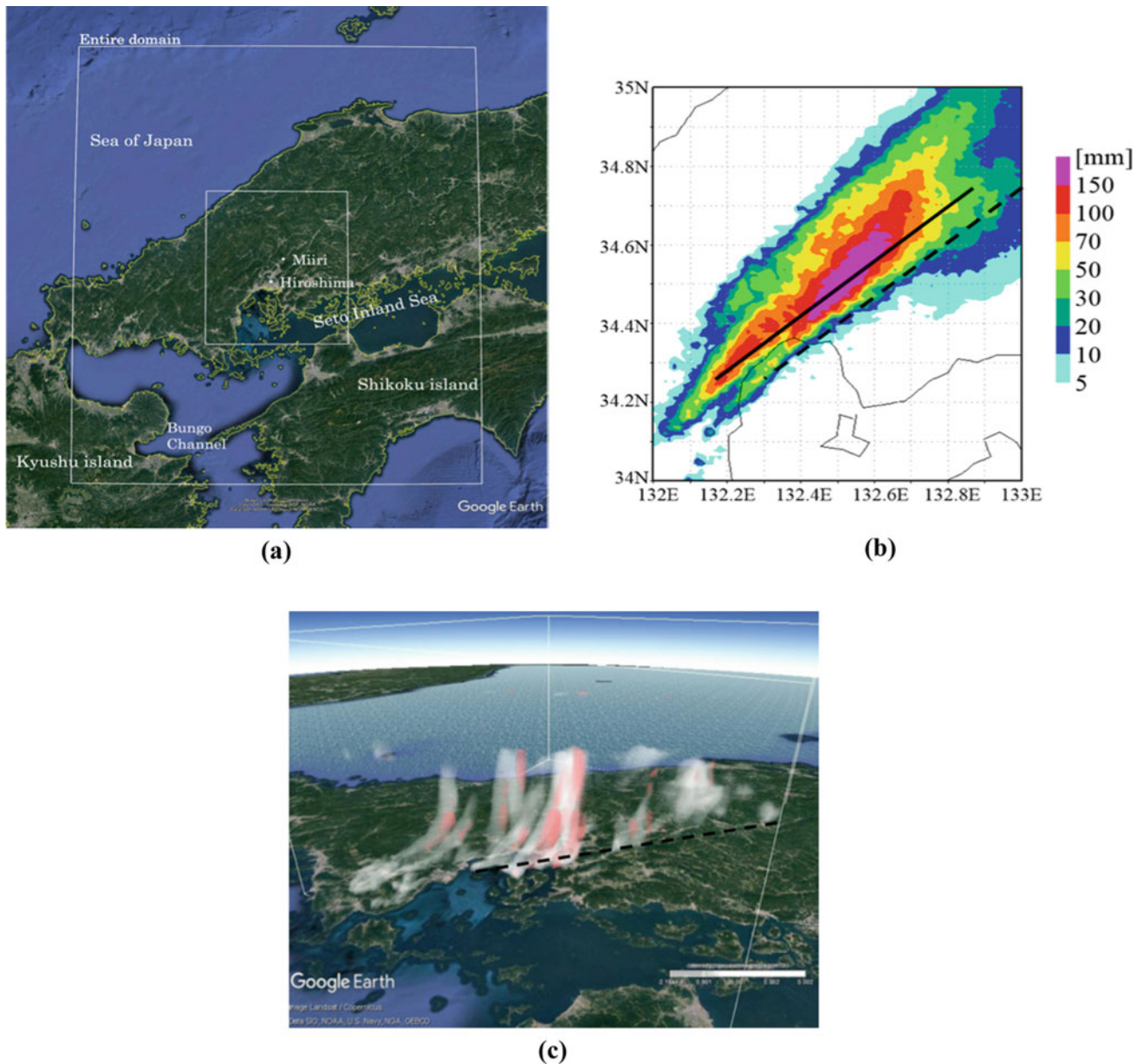


Fig. 5 **a** Computational domain. **b** Horizontal distribution of the 6-h (11 pm–5 am) rainfall accumulation over Hiroshima. **c** A three-dimensional visualization of the cloud distribution over

Hiroshima at 00:10 am viewed from the southeast direction. The dashed line corresponds to the solid line in (b)

is the radial distribution function (RDF) at contact separation, the so-called the “accumulation effect,” which measures the effect of particle preferential distributions. Currently, there are a couple of models available for the turbulent kernel based on Eq. (3). Examples are the Ayala-Wang model (Ayala et al. 2008; Wang et al. 2008) and our developed model (Onishi model; Onishi et al. 2015). This study adopted the latter model to investigate the turbulent collisions on cloud development.

Figure 6 shows the computational domain for mesoscale orographic flow over Mt. Hiei, located between Kyoto and

Shiga prefectures. The MSSG simulation with the MSSG-Bin cloud microphysics model was performed for the domain whose domain was $40 \text{ km} \times 20 \text{ km} \times 15 \text{ km}$ in the x - (streamwise), y - (spanwise), and z - (vertical) directions. The number of numerical grid points used were $400 \times 200 \times 48$. Horizontal computational grids were regular, and the height-based, terrain-following-coordinate system has been chosen for the vertical direction. The minimum vertical spacing was 10 m in the vicinity of the surface, and the maximum one was 500 m at the top of the domain. The moist air, whose relative humidity was 95%, flew into the domain with the

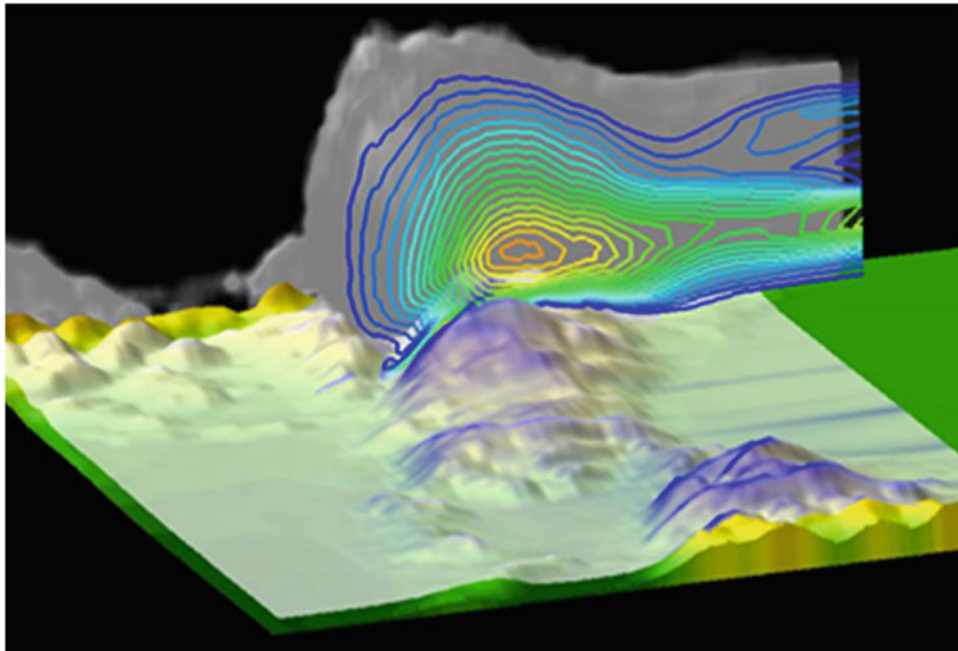


Fig. 6 Bird-eye's view of the computational domain. A snapshot of three-dimensional cloud distribution (in white) and the surface precipitation (in blue) are also drawn

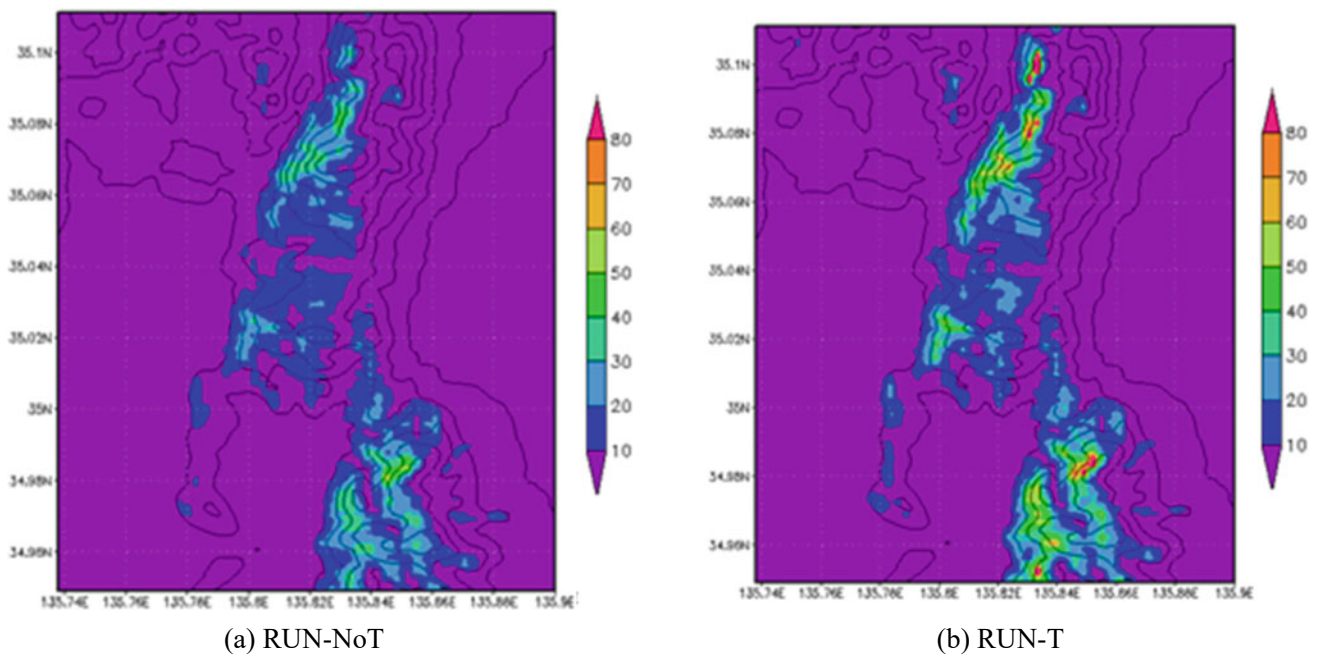


Fig. 7 Surface precipitation for **a** RUN-NoT and **b** RUN-T. Large part of surface precipitation was seen in windward slope. It was clearly shown that the precipitation is enhanced by turbulent collisions of cloud droplets

streamwise velocity $U_0 = 15$ m/s toward the east. In the MSSG-Bin model, 33 bins (classes) were used for so-called mass-doubling size resolution. The droplet collision growth was calculated using Eq. (1). Using the collision kernel model of Eq. (2) (RUN-NoT) or that of Eq. (3) (RUN-T).

Figure 7 shows the surface precipitation obtained from RUN-NoT and RUN-T. It shows a large part of surface precipitation in windward slopes. This means that the local orography governs the present precipitation process. Intense precipitation, over 80 mm/h, is observed in

RUN-T, indicating that the precipitation is significantly enhanced by turbulent collisions of cloud droplets.

3.3 Bulk Parameterizations of Turbulence-Aware Cloud Growth

In the previous subsection, the spectral-bin cloud microphysics scheme was used to investigate the role of turbulent collisions of cloud droplets. The spectral bin simulation is computationally expensive and cannot be used for operational weather prediction simulations.

The influence of turbulence on droplet growth has been parameterized for bulk cloud microphysics schemes in Seifert and Onishi (2016) and Onishi and Seifert (2016). Their bulk parameterization has been implemented in MSSG.

The auto-conversion term, denoted by P_{cnnr} in Fig. 2, is parameterized as

$$P_{cnnr} = \frac{k_{cc,0} (\mu + 2)(\mu + 4)}{20x^* (\mu + 1)^2} Q_c^2 \bar{x}_c^{-2} \left[1 + \frac{\Phi_{au}(\tau)}{(1 - \tau)^2} \right] \eta_{au}, \quad (4)$$

where $\bar{x}_c (= Q_c / N_c)$, where N_c is the number density of cloud droplets) shows the mean cloud droplet mass, x^* is the separating mass between cloud and rain drops, and η_{au} shows the enhancement factor by turbulence. The dimensionless ratio $\tau = Q_r / (Q_c + Q_r)$ acts as an internal timescale and modulates the auto-conversion rate through the universal function $\Phi_{au}(\tau)$. The enhancement η_{au} is given by

$$\eta_{au} = 1 + \epsilon Re_\lambda^p \left[\alpha_{cc}(v) \exp \left\{ - \left[\frac{\bar{r}_c - r_{cc}(v)}{\sigma_{cc}(v)} \right] \right\} + \beta_{cc} \right], \quad (4)$$

where $\bar{r}_c (= (x_c / \rho_w)^{1/3}$, where ρ_w is the water density) is the mean radius of cloud droplets, ϵ is the energy dissipation rate and $Re_\lambda = u' l_\lambda / \nu$, where u' is the RMS of velocity fluctuations and l_λ the Taylor microscale and ν the kinematic viscosity) is the Taylor-microscale-based Reynolds number. In the case of $\eta_{au} = 1$, the turbulence enhancement is neglected. The turbulence characteristic variables ϵ and Re_λ can be estimated from grid-scale quantities, assuming local isotropic homogeneous turbulence.

The accretion term, denoted by P_{accc} in Fig. 2, is parameterized as

$$P_{accc} = k_{cr,0} Q_c Q_r \Phi_{ac}(\tau) \eta_{ac} \quad (5)$$

where η_{ac} shows the enhancement factor by turbulence and modeled as

$$\eta_{ac} = 1 + c_r \epsilon \left(\frac{x^*}{\bar{x}_r} \right)^{\frac{2}{3}}, \quad (6)$$

where \bar{x}_r is the mean mass of rain drops. In case $\eta_{ac} = 1$, the turbulence effect is neglected.

Seifert and Onishi (2016) proposed the parameterizations for two-moment methods, where the number densities in addition to the mass mixing ratios are calculated. The mean masses of cloud and rain categories, \bar{x}_c and \bar{x}_r , respectively, are calculated from the mass mixing ratios $Q_{\{c/r\}}$ and number densities $N_{\{c/r\}}$ as

$$\bar{x}_{\{c/r\}} = \frac{Q_{\{c/r\}}}{N_{\{c/r\}}} \quad (7)$$

The MSSG-Bulk method in the MSSG is based on a one-moment method, where only mass mixing ratios are calculated. The mean masses of cloud and rain categories are estimated by

$$\bar{x}_{\{c/r\}} = \frac{Q_{\{c/r\}}}{N_{\{c0/r0\}}}, \quad (9)$$

where the cloud number density, $N_{c,0}$, is set to $7.0 \times 10^7 \text{ m}^{-3}$ (constant) and the rain number density $N_{r,0}$ is calculated from Q_r using the formulation proposed in Thompson et al. (2004).

3.4 Sri Lanka Rainfall Simulation with the Turbulence-Aware Bulk Cloud Parameterizations

The MSSG model was applied to Aranayake heavy rainfall event in Sri Lanka in May 2016, which caused devastating landslides resulting in over 150 casualties.

Figure 8a shows the computational nesting domains. Three-layer nesting domains were used. The horizontal resolutions were 8 km, 2 km, and 500 m. The number of horizontal grids was $N_\lambda \times N_\phi = 128 \times 128$ for the 8 km-resolution domain, and $N_\lambda \times N_\phi = 256 \times 256$ for the 2 km- and 500 m-resolution domains. Irregular grid spacings were used for the vertical direction with the same number of vertical grids, $N_z = 55$, for all the three nesting domains for the height of 40 km. The simulation was conducted for three days starting from 00:00UTC 14 May 2016.

Figure 8b shows the rainfall accumulation at Aranayake (80.4546E and 7.1476 N) from 06:00UTC 15 May, 2016. The simulation results for both Case-NoT (turbulence enhancement not considered) and Case-T (turbulence enhancement considered) cases are drawn together with the observation. Though the simulation results did not reproduce timings of heavy rainfalls, they successfully reproduced the total rainfall at the end. Case-T shows a larger amount of rainfall than Case-NoT, which indicates the turbulence enhancement made an impact on the orographic rainfall. Interestingly, turbulence impact fluctuated from time to time.

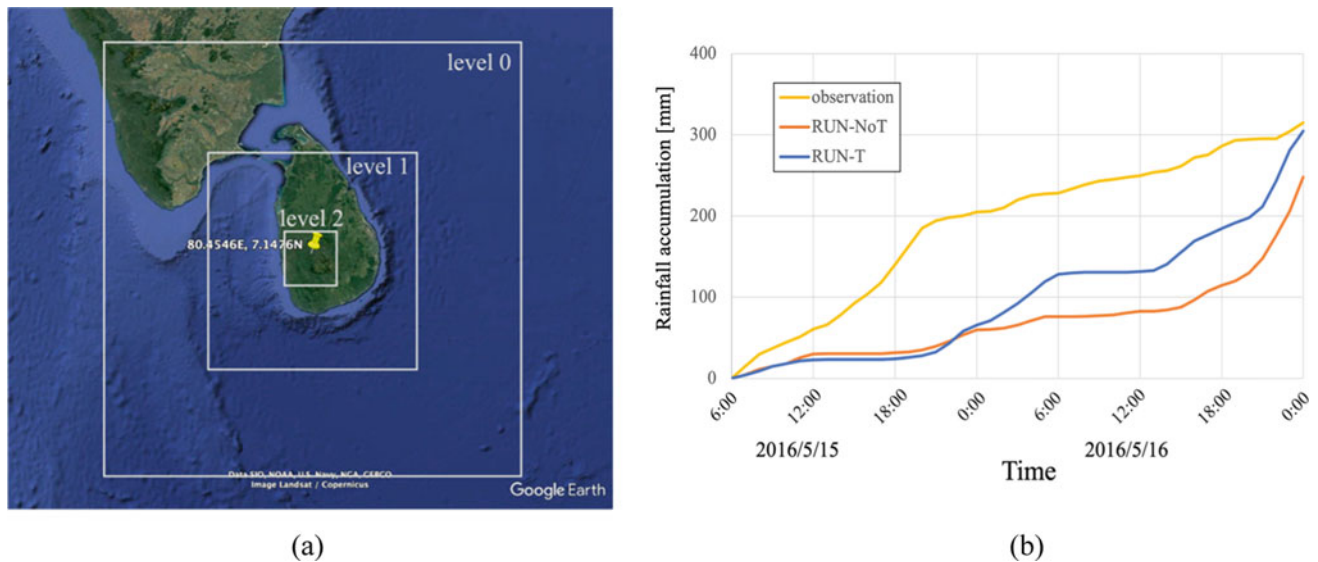


Fig. 8 **a** Computational nesting domains for the Aranayake rainfall simulation. **b** Rainfall accumulation from 06:00UTC on 15 May 2016

For example, there is little difference between Case-NoT and Case-T for the rainfall around 09:00UTC on 15 May, while the large difference between the two for the rainfall around 03:00UTC on 16 May. This means that the turbulence enhancement of droplet growth can have a large impact on certain weather conditions, and the present bulk parameterization can represent that impact. Future research is expected to clarify the weather condition under which the turbulence enhancement becomes relevant.

4 Realtime Operational Prediction System

4.1 Operational Prediction System

The operational prediction system consists of pre-processing, weather simulation and post-processing (Fig. 9). Pre-processing includes preparing the initial and boundary data for MSSG forecast simulations, including the

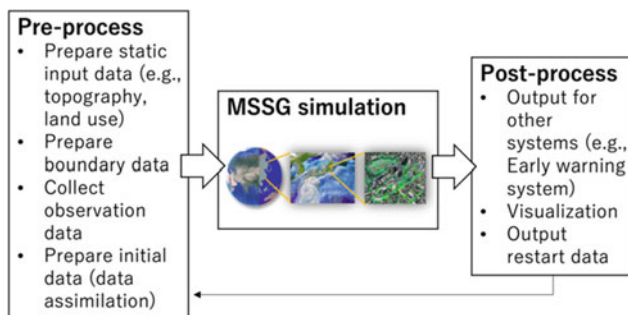


Fig. 9 Flow chart of an operational real-time weather forecasting system

data assimilation module that produces the analysis data considering the observations. Downloading the observation data is a part of the data assimilation module.

The MSSG weather simulation runs on various computer systems, either notebook PCs or supercomputers. The computer performance limits the domain size, spatial resolution, and forecast leading time. In the current situation (in the year 2022), the ordinary desktop workstation can run 24 h simulations for a $200 \text{ km} \times 200 \text{ km}$ domain with 2 km horizontal resolutions within 1 h. Supercomputers can run 1000 times larger or faster simulations.

In post-processing, the results are analyzed, visualized, and transferred to other systems, such as the early warning system. The visualization cost as well as the storage cost (Kolomenskiy et al. 2021) largely depends on the data size. Two-dimensional visualizations do not require much time, but three-dimensional ones usually do. The post-analysis includes machine learning such as super-resolution, which remap low-resolution prediction maps into high-resolution ones. This super-resolution technology will appear in the following subsection.

4.2 Super-Resolution Simulation System for High-Resolution Prediction Maps

Downscaling techniques are used to upconvert the low-spatial resolution models through dynamical and statistical modeling. Various machine-learning models, including artificial neural networks (Cannon 2011) and support vector machines (Ghosh 2010), have been applied for downscaling. Dong et al. (2014) applied the convolutional neural network (CNN) to the super-resolution

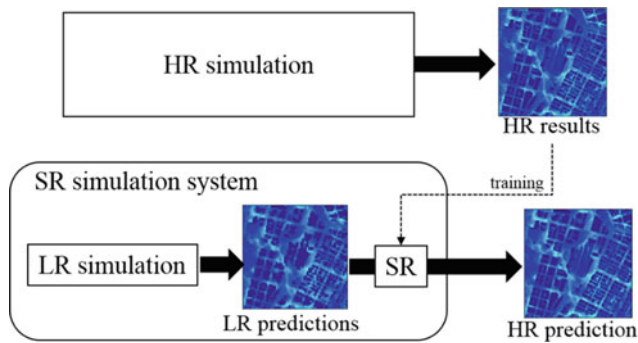


Fig. 10 Super-resolution (SR) simulation system for operational real-time high-resolution prediction. Instead of performing high-resolution (HR) simulations to obtain HR results, low-resolution (LR) simulations are performed. The obtained LR results are converted into HR ones via SR mapping with a deep convolutional neural network (CNN) trained using the dataset obtained from HR simulations

(SR) and reported that the CNN-based SR outperforms conventional mapping methods. Vandal et al. (2018) applied a CNN-based SR for climate change projections downscaling and reported the advantage of the CNN-based SR compared to the statistical downscaling and traditional SR. Onishi et al. (2019) applied a CNN-based SR to urban micrometeorology and confirmed its robustness. Onishi et al. (2019) further proposed the SR simulation system that utilizes the CNN-based SR technology. The SR simulation system can realize real-time high-fidelity prediction maps on a desktop computer in local offices.

Figure 10 shows the SR simulation system. HR numerical simulations provide better predictions than those obtained using LR simulations, but they are more computationally expensive than LR ones. The SR simulation

system consists of an LR simulation and an SR method that maps the resultant LR prediction images to HR ones. This combination provides predictions as good as those obtained using the corresponding HR simulation with a much lower computational cost.

For example, we assume that the HR is 500 m resolution and LR is 2 km resolution for local orographic rainfall prediction. A 500 m horizontal resolution would be required for resolving local slopes, while such an HR weather simulation would require computational time, hindering real-time operations on consumer computers.

Figure 11 shows the recently proposed SR neural network (Yasuda et al. 2022) that can be used for the rainfall prediction map. Several input channels can be used to obtain the output, i.e., the HR rainfall map. For example, the HR topography map would definitely help to improve the accuracy of the SR. The SR neural network is to be trained by a set of HR and LR simulation results. The HR simulations would be performed on supercomputers at a high cost. In the operational stage, however, the LR simulation requires much less computational cost. This SR system is thus promising for real-time prediction services for local communities, which would not have large computational resources.

For example, let us assume a two nesting layer simulation with a horizontal resolution of 8 and 2 km with 64×64 grid points. It takes 1 h for 25 h prediction on Intel Core i7 quadcore on 2.3 GHz, a common consumer CPU. This simulation provides the rainfall prediction map with a 2 km resolution for a $128 \text{ km} \times 128 \text{ km}$ area with 24 h leading time. This 2 km resolution map can be super-resolved (up-converted) into a 500 m resolution map that can resolve

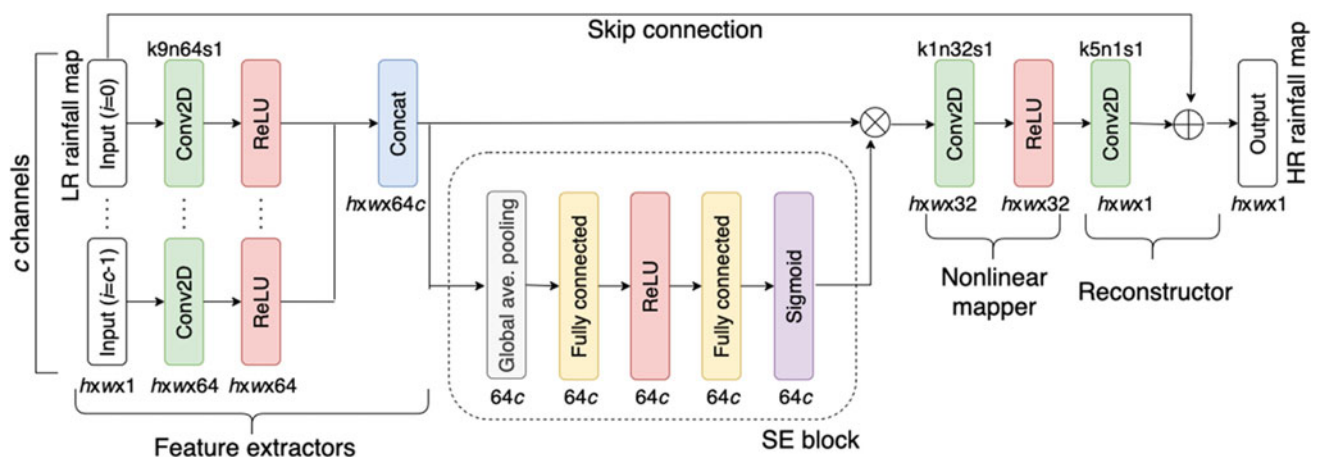


Fig. 11 Squeeze-and-excitation super-resolution convolutional neural network (SE-SRCNN) for remapping low-resolution rainfall prediction maps into high-resolution ones. The labels above the rectangles of “Conv2D” display kernel size, number of filters, and stride size; for

instance, “k9n64s1” means that the kernel size is 9×9 , the number of filters 64, and the stride size 1×1 . The image height h and width w are 64 in the present figure. The SE block is kept even when the number of inputs c is 1

individual mountain slopes. It takes only milliseconds for the conversion (i.e., inference), and it would not affect the leading time. In the end, the high-fidelity rainfall prediction map with 500 m resolution for 24 h ahead, which can be useful for local early warning systems, can be provided on a consumer PC.

5 Conclusions

We have described a recent development of our next-generation numerical weather prediction model—the Multi-Scale Simulator for the Geoenvironment (MSSG). MSSG is categorized as a global cloud-resolving model that can be used for both global and regional simulations with high resolution without the aid of cumulus parameterization. The examples have shown that MSSG has good prediction skills for the investigation of detailed orographic local rainfall. MSSG can thus be a promising numerical weather prediction model for early warning of landslides.

MSSG has successfully reproduced heavy rains associated with typhoons and a band-shaped precipitation system (Senjo-Koutai in Japanese). The turbulence-aware cloud microphysics model has been implemented in the MSSG. This can bring the extra ability of reliable predictions of orographic rainfall to MSSG.

In order to reproduce local orographic rainfall, the simulation needs enough fine resolutions with $O(100\text{ m})$ to resolve individual local slopes. In the case of an early warning system for a local community, the system should preferably be compact like a desktop PC. The feasible rainfall forecast simulation will have $O(1\text{ km})$ horizontal resolutions, much coarser than $O(100\text{ m})$ resolutions, due to the limited computational speed. The super-resolution simulation system, which relies on recent machine-learning technologies, can help obtain high-resolution rainfall prediction maps that can resolve individual slopes in short operational cycles.

We now have the MSSG and the super-resolution simulation system. The high-resolution rainfall prediction maps can be obtained in real-time, e.g., 24-h rainfall forecast maps can be updated in an hour. The rainfall prediction maps are then transferred to the landslide simulation model and to the early warning system. We hope this integrated system will help construct a safe society free from victims due to landslides.

Acknowledgements This research was partially supported by Science and Technology Research Partnership for Sustainable Development (SATREPS), Japan Science and Technology Agency (JST)/Japan International Cooperation Agency (JICA). The numerical simulations were performed on the Earth Simulator of the Japan Agency for Marine-Earth Science and Technology (JAMSTEC) and on TSU-BAME 3.0 of the Tokyo Institute of Technology.

References

- Ayala O, Rosa B, Wang L-P (2008) Effects of turbulence on the geometric collision rate of sedimenting droplets. Part 2. Theory and parameterization. *New J Phys* 10:075 016
- Baba Y, Takahashi K, Sugimura T, Goto K (2010) Dynamical core of an atmospheric general circulation model on a yin–yang grid. *Mon Weather Rev* 138:3988–4005
- Cannon AJ (2011) Quantile regression neural networks: implementation in R and application to precipitation downscaling. *Comput Geosci* 37:1277–1284
- Choi Y, Kida S, Takahashi K (2013) The impact of oceanic circulation and phase transfer on the dispersion of radionuclides released from the Fukushima Dai-ichi Nuclear Power Plant. *Biogeosciences* 10:4911–4925
- Dong C, Loy CC, He K, Tang X (2014) Learning a deep convolutional network for image super-resolution. In: *European conference on computer vision (ECCV)*, pp 184–199
- Falkovich G, Pumir A (2007) Sling effect in collisions of water droplets in turbulent clouds. *J Atmos Sci* 64:4497–4505
- Ghosh S (2010) SVM-PGSL coupled approach for statistical downscaling to predict rainfall from GCM output. *J Geophys Res Atmos* 115:D22102
- Grabowski WW, Wang L-P (2013) Growth of cloud droplets in a turbulent environment. *Annu Rev Fluid Mech* 45:293–324
- Hiruma D, Onishi R, Takahashi K, Fukagata K (2022) Sensitivity study on storm modulation is feasible through a strategic use of consumer air conditioners. *Atmos Sci Lett* e1091. <https://doi.org/10.1002/asl.1091>
- Kageyama A, Sato T (2004) The Yin-Yang grid: an overset grid in spherical geometry. *Geochem Geophys Geosyst* 5:Q09005
- Kamiya T, Onishi R, Koderia S, Hirata A (2019) Estimation of time-course core temperature and water loss in realistic adult and child models with urban micrometeorology prediction. *Int J Environ Res Public Health* 16:5097
- Kawahara S, Onishi R, Goto K, Takahashi K (2015) Realistic representation of clouds in Google Earth. In: *Proceedings SIGGRAPH Asia 2015 VHPC*. <https://doi.org/10.1145/2818517.2818541>
- Kolomenskiy D, Onishi R, Uehara H (2021) Data compression for environmental flow simulations. *J Visual*. <https://doi.org/10.1007/s12650-021-00813-8>
- Lu L-F, Onishi R, Takahashi K (2015) The effect of wind on long-term summer water temperature trends in Tokyo Bay, Japan. *Ocean Dyn* 65:919–930
- Nakanishi M, Niino H (2009) Development of an improved turbulence closure model for the atmospheric boundary layer. *J Meteor Soc Japan* 87:895–912
- Nakano M, Wada A, Sawada M, Yoshimura H, Onishi R, Kawahara S, Sasaki W, Nasuno T, Yamaguchi M, Iriguchi T, Sugi M, Takeuchi Y (2017) Global 7-km mesh nonhydrostatic model intercomparison project for improving TYphoon forecast (TYMIP-G7): experimental design and preliminary results. *Geosci Model Devel* 10:1363–1381
- Matsuda K, Onishi R, Takahashi K (2018) Tree-crown-resolving large-eddy simulation coupled with three-dimensional radiative transfer model. *J Wind Eng Ind Aerodyn* 173:53–66
- Onishi R, Takahashi K (2012) A warm-bin–cold-bulk hybrid cloud microphysical model. *J Atmos Sci* 69:1474–1497
- Onishi R, Matsuda K, Takahashi K (2015) Lagrangian tracking simulation of droplet growth in turbulence—turbulence enhancement of autoconversion rate. *J Atmos Sci* 72:2591–2607
- Onishi R, Sugiyama D, Matsuda K (2019) Super-resolution simulation for real-time prediction of urban micrometeorology. *SOLA* 15:178–182

- Onishi R, Seifert A (2016) Reynolds-number dependence of turbulence enhancement on collision growth. *Atmos Chem Phys* 16:12441–12455
- Seifert A, Onishi R (2016) Turbulence effects on warm-rain formation in precipitating shallow convection revisited. *Atmos Chem Phys* 16:12127–12141
- Sekiguchi M, Nakajima T (2008) A k-distribution-based radiation code and its computational optimization for an atmospheric general circulation model. *J Quant Spectrosc Radiat Transfer* 109:2779–2793
- Takahashi K, Onishi R, Baba Y, Kida S, Matsuda K, Goto K, Fuchigami H (2013) Challenge toward the prediction of typhoon behaviour and down pour. *J Phys: Conf Ser* 454(012):072
- Takahashi K, Peng X, Onishi R, Ohdaira M, Goto K, Fuchigami H, Sugimura T (2006) Multi-scale weather/climate simulations with multi-scale simulator for the geoenvironment (MSSG) on the earth simulator. In: Annual report of the earth simulator center, April 2005–March 2006, pp 31–39
- Toro EF (1989) A weighted average flux method for hyperbolic conservation laws. *Proc Roy Soc London* A423:401–418
- Vandal T, Kodra E, Ganguly S, Michaelis A, Nemani R, Ganguly AR (2018) Generating high resolution climate change projections through single image super-resolution: an abridged version. In: Proceedings 27th international joint conference on artificial intelligence (IJCAI-18), pp 5389–5393
- Wang L-P, Ayala O, Rosa B, Grabowski WW (2008) Turbulent collision efficiency of heavy particles relevant to cloud droplets. *New J Phys* 10(075):013
- Wang L-P, Wexler AS, Zhou Y (1998) Statistical mechanical descriptions of turbulent coagulation. *Phys Fluids* 10:2647–2651
- Wicker LJ, Skamarock WC (2002) Time-splitting methods for elastic models using forward time schemes. *Mon Weather Rev* 130:2088–2097
- Yasuda Y, Onishi R, Hirokawa Y, Kolomenskiy D, Sugiyama D (2022) Super-resolution of near-surface temperature utilizing physical quantities for real-time prediction of urban micrometeorology. *Build Environ* 209:108597

Open Access This chapter is licensed under the terms of the Creative Commons Attribution 4.0 International License (<http://creativecommons.org/licenses/by/4.0/>), which permits use, sharing, adaptation, distribution and reproduction in any medium or format, as long as you give appropriate credit to the original author(s) and the source, provide a link to the Creative Commons license and indicate if changes were made.



The images or other third party material in this chapter are included in the chapter's Creative Commons license, unless indicated otherwise in a credit line to the material. If material is not included in the chapter's Creative Commons license and your intended use is not permitted by statutory regulation or exceeds the permitted use, you will need to obtain permission directly from the copyright holder.



IPL Project 202: Landslide Monitoring Best Practices for Climate-Resilient Railway Transportation Corridors in Southwestern British Columbia, Canada

David Huntley, Peter Bobrowsky, Roger MacLeod, Drew Rotheram-Clarke, Robert Cocking, Jamel Joseph, Jessica Holmes, Kevin Sattler, Jonathan Chambers, Philip Meldrum, Paul Wilkinson, Shane Donohue, and David Elwood

Abstract

The paper outlines landslide mapping and change-detection monitoring protocols based on the successes of ICL-IPL Project 202 in southwestern British Columbia, Canada. In this region, ice sheets, glaciers, permafrost, rivers and oceans, high relief, and biogeoclimatic characteristics contribute to produce distinctive landslide assemblages. Bedrock and drift-covered slopes along the transportation corridors are prone to mass-wasting when favourable conditions exist. In high-relief mountainous areas, rapidly moving landslides include rock and debris avalanches, rock and debris falls, debris flows and torrents, and lahars. In areas with moderate to low relief, rapid to slow mass movements include rockslides and slumps, debris or earth slides and slumps, and earth flows. Slow-moving landslides include rock glaciers, rock and

soil creep, solifluction, and lateral spreads in bedrock and surficial deposits. Research in the Thompson River Valley aims to gain a better understanding of how geological conditions, extreme weather events and climate change influence landslide activity along the national railway corridor. Remote sensing datasets, consolidated in a geographic information system, capture the spatial relationships between landslide distribution and specific terrain features, at-risk infrastructure, and the environmental conditions expected to correlate with landslide incidence and magnitude. Reliable real-time monitoring solutions for critical railway infrastructure (e.g., ballast, tracks, retaining walls, tunnels and bridges) able to withstand the harsh environmental conditions of Canada are highlighted. The provision of fundamental geoscience and baseline geospatial monitoring allows stakeholders to develop robust risk tolerance, remedia-

D. Huntley (✉) · D. Rotheram-Clarke · R. Cocking · J. Joseph
Geological Survey of Canada, 1500-605 Robson Street,
Vancouver, BC V6B 5J3, Canada
e-mail: david.huntley@nrcan-mcan.gc.ca

D. Rotheram-Clarke
e-mail: drew.rotheram-clarke@nrcan-mcan.gc.ca

R. Cocking
e-mail: robert.cocking@nrcan-mcan.gc.ca

J. Joseph
e-mail: jamel.joseph@nrcan-mcan.gc.ca

P. Bobrowsky · R. MacLeod
Geological Survey of Canada, 9860 West Saanich Road, Sidney,
BC V8L 4B2, Canada
e-mail: peter.bobrowsky@nrcan-mcan.gc.ca

R. MacLeod
e-mail: roger.macleod@nrcan-mcan.gc.ca

J. Holmes
School of Engineering, Newcastle University, Newcastle upon
Tyne, NE1 7RU, UK
e-mail: jessica.holmes@ncl.ac.uk

K. Sattler
College of Engineering, University of Saskatchewan, 57 Campus
Drive, Saskatoon, SK S7N 5A9, Canada
e-mail: kevin.sattler@usask.ca

J. Chambers · P. Meldrum · P. Wilkinson
British Geological Survey, Keyworth, Nottingham, NG12 5GG,
UK
e-mail: jecha@bgs.ac.uk

P. Meldrum
e-mail: pime@bgs.ac.uk

P. Wilkinson
e-mail: pbw@bgs.ac.uk

S. Donohue
School of Civil Engineering, University College Dublin, Dublin,
NE1 7RU, Ireland
e-mail: shane.donohue@ucd.ie

D. Elwood
57 Campus Drive, Saskatoon, SK S7N 5A9, Canada
e-mail: david.elwood@usask.ca

tion, and mitigation strategies to maintain the resilience and accessibility of critical transportation infrastructure, while also protecting the natural environment, community stakeholders, and the Canadian economy. We conclude by proposing a best-practice solution involving three levels of investigation to describe the form and function of the wide range of rapid and slow-moving landslides occurring across Canada, which is also applicable elsewhere.

Keywords

National railway infrastructure • Landslide change-detection monitoring • Satellite InSAR analysis • UAV photogrammetry • RTK-GNSS surveys • Continuous ERT

1 Introduction

Canada's national railway network is the dominant mode for exporting natural resources (e.g., coal, oil, grain, potash, forest products) to deep-water marine terminals; and for intermodal goods entering continental North America from global markets. Unfortunately, across much of the continent (Fig. 1), railway infrastructure and operations are confined to transportation corridors with slopes susceptible to a broad range of landslide processes (Geertsema et al. 2009a, b; Bobrowsky and Dominguez 2012). Landslide form and function are dependent upon regional physiographic setting (montane belts, high plateaus, prairies, lowlands), environmental conditions (past and present), and local geology (solid and drift). Regionally, the diverse bedrock geology, wide range of surficial deposits, along with high relief in mountains, plateaus and deeply incised valleys (Fig. 1) favours a broad range of rapid- to slow-moving landslides (Table 1).

Where transportation corridors traverse unstable slopes, varying degrees of damage to vulnerable infrastructure, or service delays caused by landslides have potential local and national economic, social, and environmental consequences. A landslide-resilient national transportation railway network requires sustainable, cost-effective management of service operations to meet future socioeconomic needs while protecting the natural environment and public. In a scenario of future extreme weather events and climate change, railway infrastructure and operations are expected to face unique challenges in design, monitoring, adaptation, mitigation, reclamation and restoration. An understanding of the geographic distribution and temporal range of earth materials and geological hazards is fundamental to effective hazard management and risk reduction safety (cf. Jespersen-Groth et al. 2009; Laimer 2017).

Here, we present a monitoring framework for railway disaster risk-reduction that incorporates: (1) fundamental spatial and temporal information on geological, geophysical, and geotechnical properties of landslides at national, regional and local scales; with (2) site-specific benchmark monitoring acquired using an array of remote sensing platforms; and (3) in-situ change-detection monitoring technologies and methodologies.

2 Study Area

Because of its socioeconomic primacy, the focus of attention is on landslide processes adversely affecting the national railway corridors connecting the deep-water ports of Vancouver and Squamish in southwestern British Columbia (BC) to the rest of Canada (Fig. 1). From these coastal ports, the Canadian National (CN) and Canadian Pacific (CP) railway corridors traverse mountainous and rolling plateau terrain, running through deeply incised valleys and along the steep shorelines of fjords and lakes (Fig. 2a–c). Gentle to steep bedrock slopes along these transportation corridors are mantled by surficial deposits susceptible to a range of rapid- to slow-moving landslides (Table 1).

CN and CP railway transportation corridors are usually <1 km from river channels, fjord coastlines, and lakeshores to maintain an optimal grade (Fig. 2d–f). Located so, railway tracks and infrastructure are prone to damage by landslides, floods, wildfires, and other geological hazards. Local physiography, weather conditions, geological hazards, and land-use activities present local and national economic, social, and environmental challenges (cf. Schuster and Fleming 1986; Haque et al. 2016; Blais-Stevens 2020).

The strategic importance of these vital corridors, along with the need to understand and manage the safety risks related to landslides, make on-site investigations a strategic priority for governments, academia, and the rail industry (Bunce and Chadwick 2012; Hendry et al. 2015). Combining field-based landslide investigation with multi-year geospatial and in-situ time-series monitoring leads to a more resilient railway national transportation network able to meet Canada's future socioeconomic needs, while ensuring protection of the environment and resource-based communities from landslides related to extreme weather events and climate change.

2.1 ICL Project 202 Landslide Laboratory

Thompson River with its several slides and history afford a study of known slides that, with certainty, experience dynamic behaviour during monitoring efforts. Landslides

along a ten-kilometre stretch of the Thompson River valley between the communities of Ashcroft and Spences Bridge (Fig. 3) have negatively impacted critical railway infrastructure, arable land, fisheries, and other natural resources since the 1880s (Stanton 1898; Evans 1984).

In the late nineteenth century, terraces were intensively irrigated for agricultural land use and toe slopes were incised and over-steepened during railway construction (Stanton 1898; Evans 1984; Clague and Evans 2003). Prehistoric mass movements were consequently reactivated as sudden

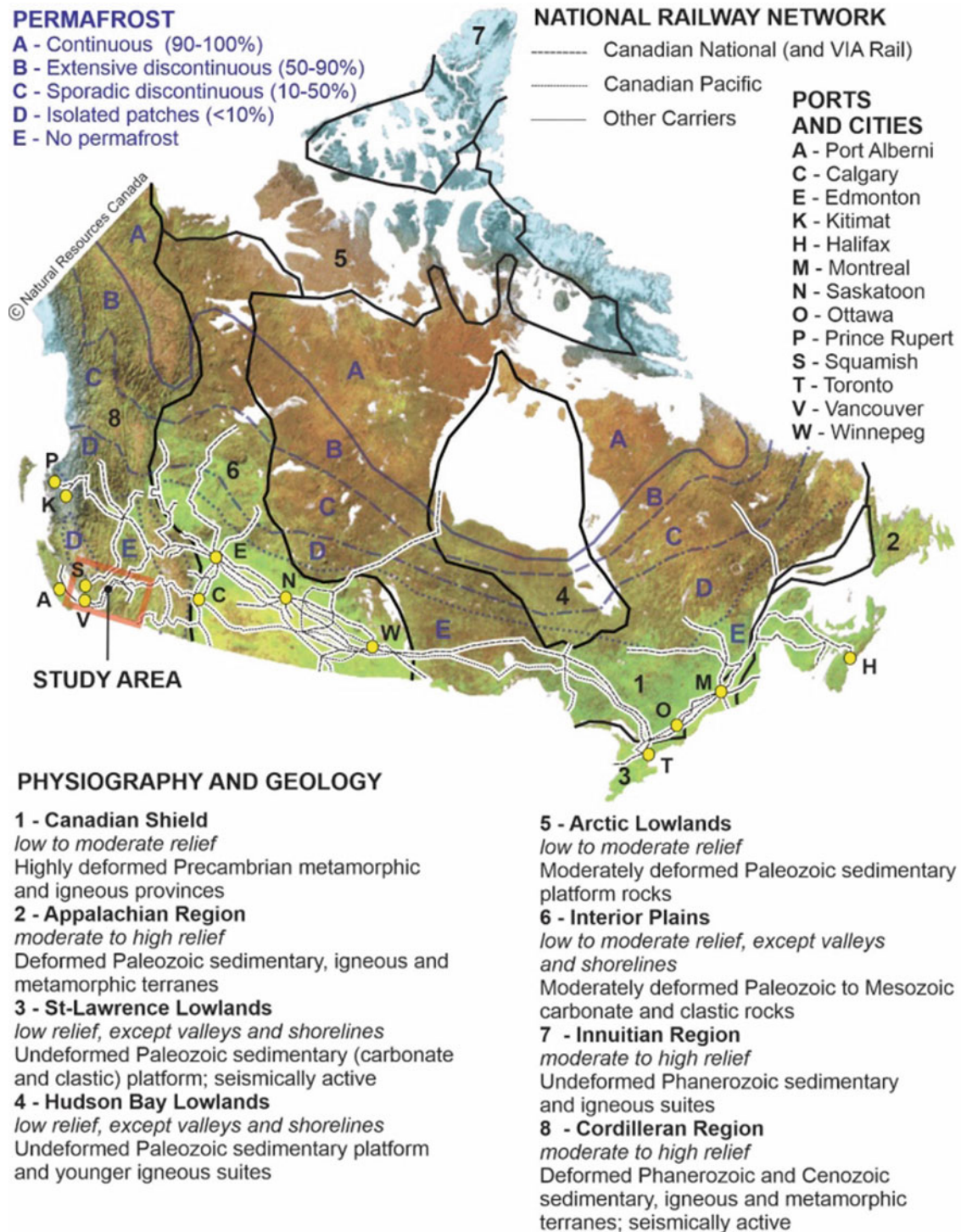


Fig. 1 Physiography, geology, and permafrost zones of Canada, showing extent of national railway network, major ports, population centres, and location of study area (after Bostock 2014)

Table 1 Surficial materials and landslides of southwestern BC (terrain classification after Howes and Kenk 1997; Hervás and Bobrowsky 2009; Highland and Bobrowsky 2008). See Fig. 2 for terrain code legend (after Deblonde et al. 2018)

Landslide classification	Surficial geology susceptible to failure
<i>Rapid mass movement (R)</i> (annual displacement = $m \text{ year}^{-1}$ to $km \text{ year}^{-1}$)	
Rock avalanche	R
Debris avalanche	C, GF, GL, T
Rock fall + Topple	R
Debris fall	C, GF, T
Debris flow	C, GL, GW, T
Debris torrent	A, C, GL, GF
Lahar	R, C, T, GF
<i>Rapid to slow mass movement (R, F)</i> (annual displacement = $cm \text{ year}^{-1}$ to $m \text{ year}^{-1}$)	
Rock slide + slump	R
Debris / Earth slide + slump	C, GF, GL, T
Earth flow	C, GF, GL, T
<i>Slow mass movement (F)</i> (annual displacement = $mm \text{ year}^{-1}$ to $m \text{ year}^{-1}$)	
Rock creep + Rock glaciers	R, C
Soil creep + Solifluction	A, C, GF, GL, GW, T
Lateral spreading (bedrock and earth)	R, C, GL, GW, T

onset, rapid retrogressive flow-slides during the fall and winter months. The economic importance of this transportation corridor, along with the need to understand and manage the safety risk related to the landslides that threaten the route, mandate the Thompson River valley a monitoring priority for Natural Resources Canada (NRCAN) and the Geological Survey of Canada (GSC).

3 Methods and Results

Monitoring unstable slopes and infrastructure at risk is a cost-effective hazard management practice in southwestern BC that also provides important geoscience information to help develop appropriate stakeholder mitigation and adaptation measures (Bunce and Chadwick 2012; Huntley et al. 2021a). Here, we outline landslide mapping and change-detection monitoring protocols based on the successes of ICL-IPL Project 202 in the Thompson River valley railway transportation corridor that incorporate diverse historical time-series and near real-time geoscience datasets.

3.1 Monitoring to Understand Landslide Form

Descriptions of local topographic, bathymetric, surficial and bedrock geological conditions, including earth materials and landforms, and their hydrological properties are essential for understanding landslide compositions, structures, and

behaviours. Geospatial relationships between landslide distribution and specific terrain features, and the environmental conditions triggering instability are determined from field-based, on-site geological and geophysical studies, combined with geotechnical, petrophysical, and geochemical laboratory analysis, which are then codified and quantified in geographic information systems (GIS).

3.2 Remote Sensing and Field Surveys

Understanding form and function begins with terrain analysis and landslide inventory. Terrain polygons and features characteristic of landslide activity are delimited on optical satellite imagery (e.g., Landsat, WorldView), conventional air photographs, and unoccupied aerial vehicle (UAV) photogrammetry. Terrain and landslide classifications are benchmarked by ground observations of slope gradient, surficial materials, material texture, material thickness, slope morphology, moisture conditions, ongoing geomorphic processes, and land cover (Figs. 4b, 5; Huntley and Bobrowsky 2014; Huntley et al. 2017a, 2019a, 2020a; b, c; Holmes et al. 2018, 2020). Terrain and landslides are codified following British Columbia (Howes and Kenk 1997) and GSC mapping standards (Deblonde et al. 2018).

For the Thompson River valley, landslide distribution is influenced by the distribution of forests, shrub lands, grasslands, wetlands, water, croplands, and railway infrastructure. Vegetation cover generally contributes to increased slope

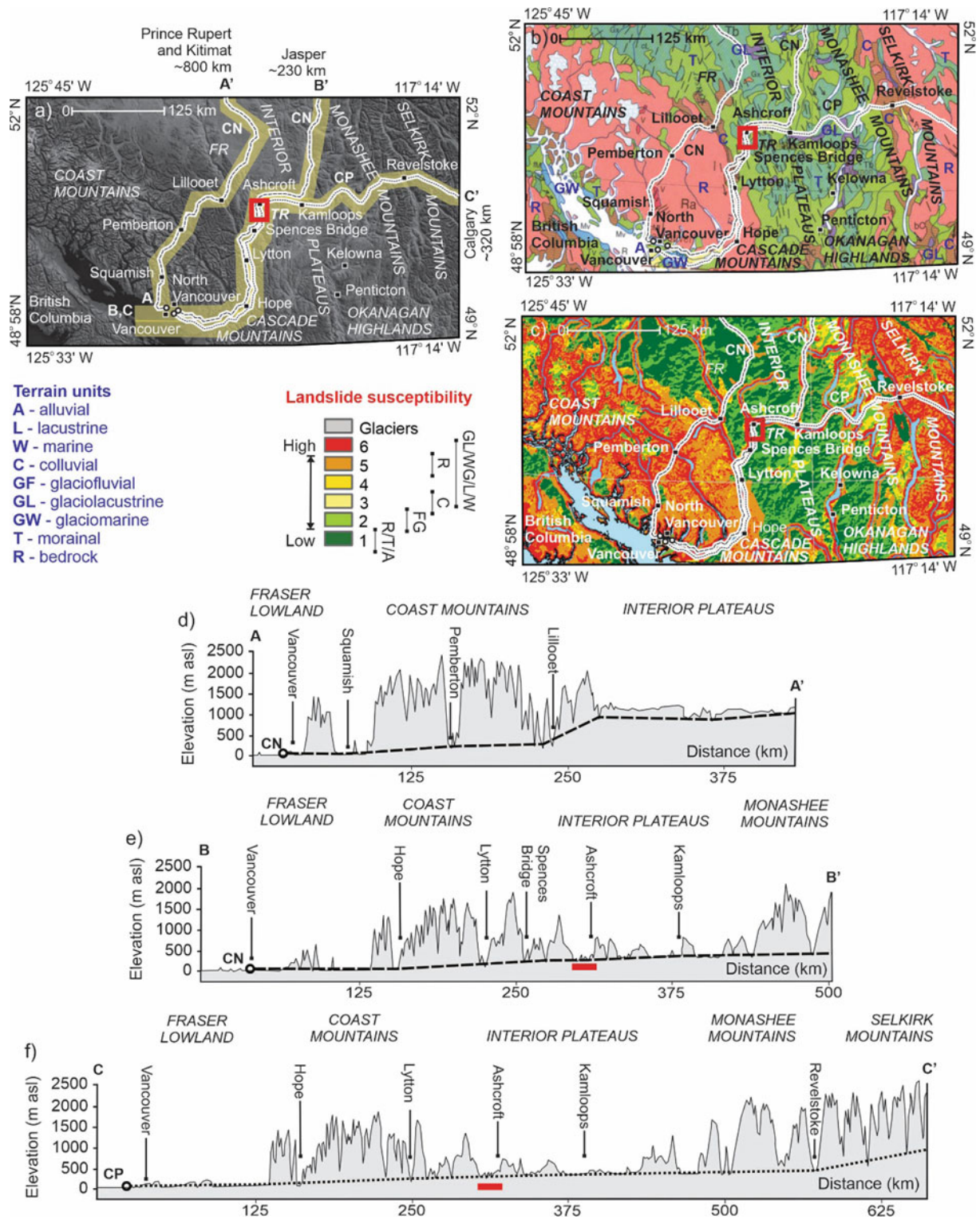


Fig. 2 CN and CP railway corridors traversing southwestern BC: **a** Topography and physiography, showing location of cross-sections along CN and CP transportation corridors, key urban settlements, and major physiographic elements. **b** Surficial geology (modified from Fulton 1995; Deblonde et al. 2018). **c** Landslide susceptibility (modified from Bobrowsky and Dominguez 2012). **d** A-A'—CN

secondary railway corridor to north-central British Columbia. **e** B-B'—CN primary railway corridor to eastern Canada. **f** C-C'—CP primary railway corridor to eastern Canada. Approximate rail grades shown as black dashed (CN) and dotted (CP) lines. FR—Fraser River; TR—Thompson River

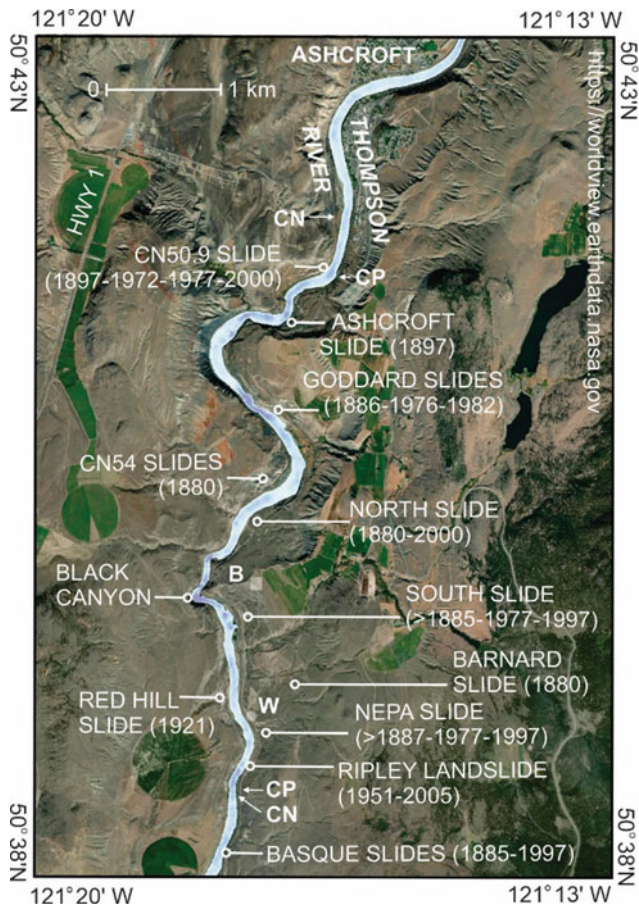


Fig. 3 Landslides of the Thompson River valley and railway transportation corridor; prime ground control point, survey base station (B); weather station (W). Topographic layer merges World Imagery with a DEM of Canada generated from Aster GDEM v2 worldwide elevation data (1 arc-second resolution)

stability through the action of binding roots and water absorption in soils. However, extensive, deep-penetrating roots on steep slopes also contributes to the mechanical and chemical weathering of soils and parent materials by

Fig. 4 Landslide monitoring best practices along the national railway transportation corridor in the Thompson River valley, southwestern BC. **a** RS2 InSAR change detection, showing average linear displacement rate rastered at 3 cm yr⁻¹, with purple polygons delimiting 4-sigma confidence levels (Huntley et al. 2021e). **b** Surficial geological mapping describing sediments and landslide characteristics (Huntley et al. 2020a). **c, d** Shallow geophysical surveys provide data for interpretation of sub-surface geology and landslide structure (Huntley et al. 2019a). **e** Boreholes, instrumented to monitor groundwater pressure and slope displacement, provide additional *in-situ* geological, geophysical, geochemical, and geotechnical data on subsurface conditions (Hendry et al. 2015; Sattler et al. 2018). **f** UAV photogrammetric data used to generate DSMs and DEMs of landslides, and for change-detection monitoring (see Huntley et al. 2021a). **g** GPR, single-beam acoustic and multi-beam bathymetric datasets provide information on portions of active landslides submerged beneath Thompson River (Huntley et al. 2019a, 2021a). **h** Trihedral aluminum

providing additional materials for remobilization if triggered by other factors (e.g., seismic shaking and precipitation events). Lying leeward of the Coast Mountains, the valley experiences semi-arid conditions with annual precipitation as rainfall and snow <2700 mm (Dominguez-Cuesta and Bobrowsky 2011). Greater cyclic and seasonal ground moisture changes due to evapotranspiration varying strongly between winter and summer will also drive deterioration.

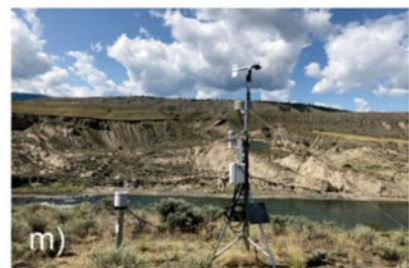
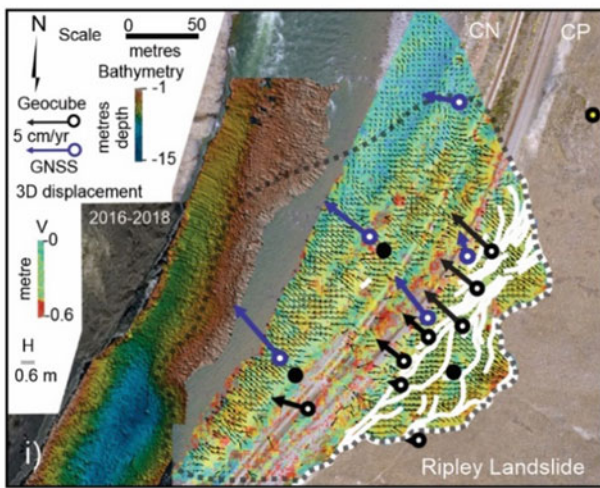
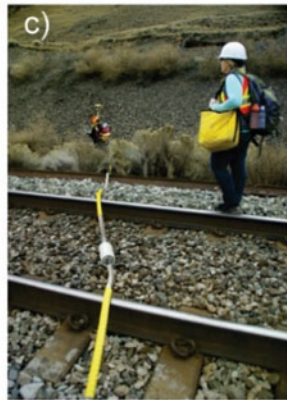
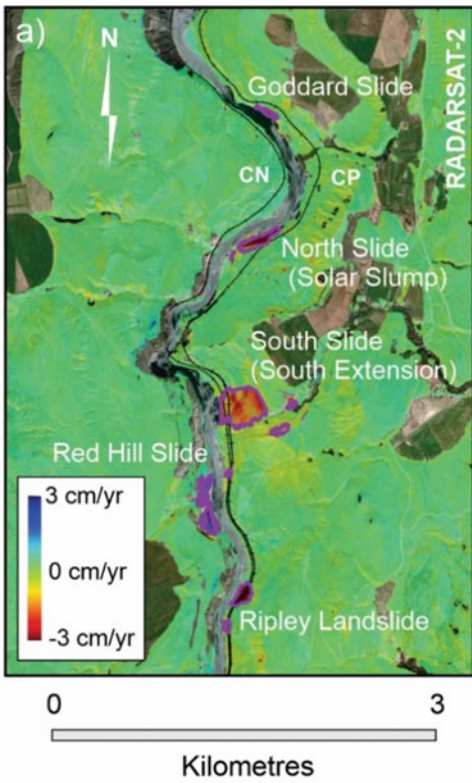
Nine surficial material classes are recognized; distinguished by genetic origin, material texture and thickness, slope gradient and morphology, moisture conditions, and active geomorphic processes (Fig. 2b and Table 1). Bedrock influences slope hazards where surficial cover is thin, for example on terrain with slopes >35°. Elsewhere, drift cover is thicker and surficial materials have a greater influence on slope instability. Large retrogressive rotational-translational earth-debris slides were initially triggered by deep incision of Pleistocene fill in the Thompson River valley during the early Holocene (Clague and Evans 2003).

Subsequently, the river has influenced slope stability and landslide susceptibility by changing (a) the pore water pressure in the slope mass, and along rupture surfaces; (b) the supporting force on landslide toes; and (c) through cut-bank erosion, thereby affecting the geometry of the landslide. Back-tilted blocks and rapid debris slumps move over weak, curvilinear rupture zones in glaciolacustrine clay-silt units confined between overlying till and underlying bedrock (Porter et al. 2002; Eshraghian et al. 2007, 2008; Huntley et al. 2020a).

3.3 Geophysical Surveys and In-Situ Monitoring

Geophysical surveys, borehole logging, and laboratory analysis of geotechnical and geochemical properties of earth materials, including stratigraphic layers and structures (e.g., joints, faults, shear planes and tension cracks) provide additional information on internal geological structures and

corner reflectors installed on active landslides enhance the resolution of persistent scatterer InSAR change-detection (Journault et al. 2018). **i** Surface displacement data derived from UAV overflights and multi-beam bathymetry data; plotted with RTK-GNSS and d-GNSS displacement data (stable d-GNSS unit—yellow dot; active d-GNSS unit—black and white dot; inactive Geocube™—black dot; active GCP—blue dot) (Huntley et al. 2021a). **j** Repeat RTK-GNSS surveys of GCPs on active landslides benchmark displacement estimates from InSAR and UAV datasets (Huntley et al. 2021a). **k** Geocube™ d-GNSS network installed at Ripley Landslide and South Slide provide near real-time displacement measurements (Huntley et al. 2020b). **l** Fibre Bragg Grating and Brillouin Optical Time Domain Reflectometry strain monitoring of lock-block retaining wall at Ripley Landslide (Huntley et al. 2017c). **m** Weather station continuously records precipitation, snowfall, air temperature, wind speed and direction (Huntley et al. 2020a)



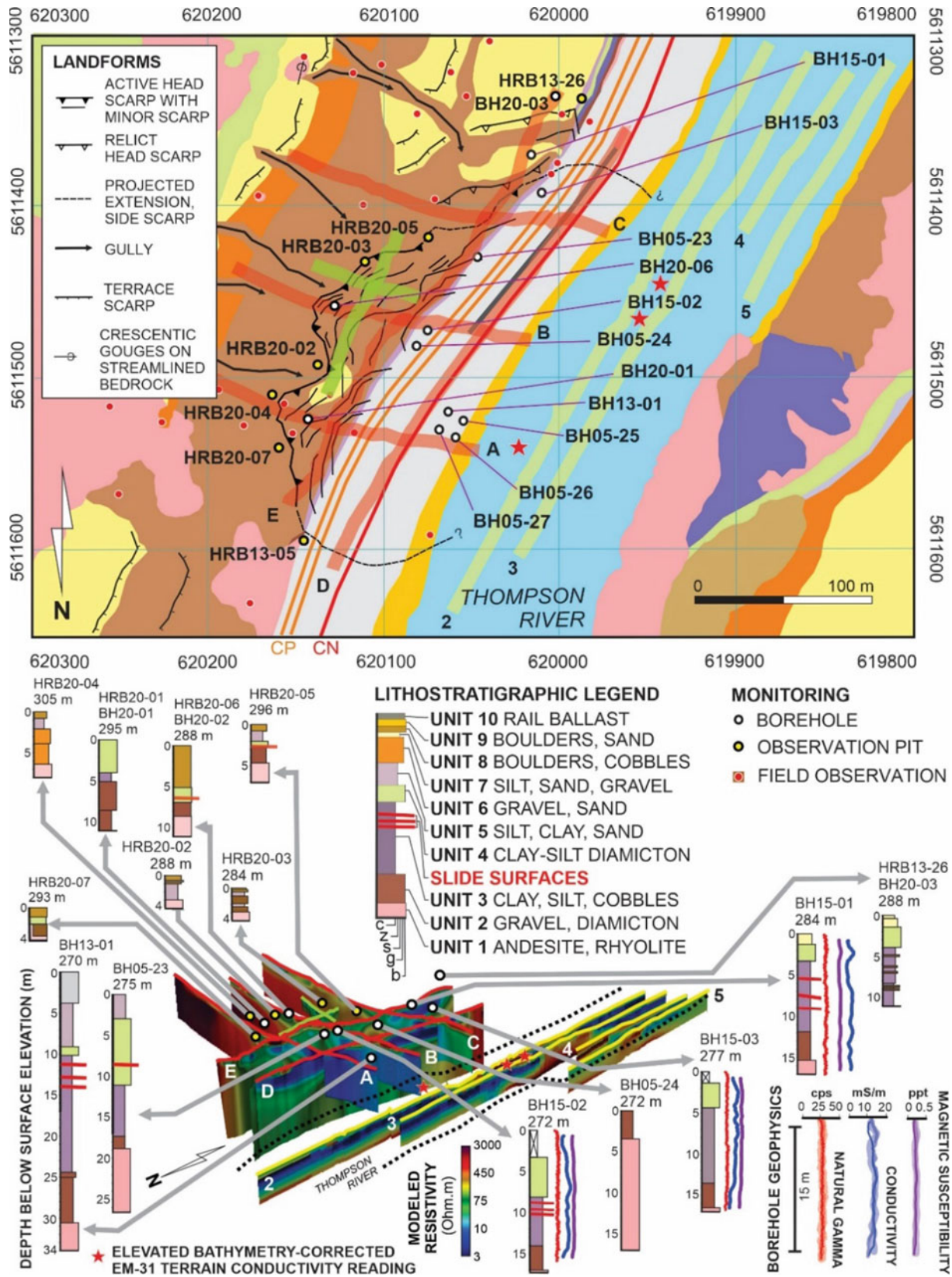


Fig. 5 GIS output generated from field studies and laboratory results. Surficial hydrogeological units and landforms of Ripley Landslide, in the Thompson River valley, southwestern BC, as revealed by field-based mapping and geophysical surveys (after Huntley and Bobrowsky 2014; Huntley et al 2019c, 2020a). Locations of logged and monitored boreholes, observation pits, field observations, and ERT

survey lines indicated on surficial geology map. ERT pseudosections produced by the British Geological Survey (© UK Research and Innovation 2020). Terrestrial ERT survey—red lines (A-E); waterborne ERT and EM-31 survey—yellow lines (2-5); PRIME installation—green lines (oriented N-S and E-W, see Fig. 6)

failure mechanisms, as well as how and where groundwater flows through landslide bodies and surrounding bedrock (cf. Whiteley et al. 2019).

Electrical resistivity tomography (ERT), frequency modulated electromagnetic conductivity (FEM), ground-penetrating radar (GPR), seismic primary wave refraction (PWR), and multichannel analysis of shear waves (MASW) surveys provide the most useful information on the distribution earth materials, in addition to the distribution and quantity of groundwater (Figs. 4c, d, 5 and 6; Huntley et al. 2017a, 2019a). Geophysical methods adopted for hydrogeological logging of observation wells include down-hole measurement of natural gamma radiation (GR), induction conductivity (IC) and magnetic susceptibility (MS) (Fig. 5). Subsurface borehole monitoring (Fig. 4e), combining ShapeAccelArray inclinometry with piezometer head levels, indicate that the landslides studied in the Thompson River valley are failing along sub-horizontal, weak, basal shear surfaces in highly plastic clay beds that extend under the river (Porter et al. 2002; Eshraghian et al. 2007, 2008).

At Ripley Landslide, detailed borehole logging shows that the central and northern parts are translating sub-horizontally (2.1° – 2.5°), whereas the southern portion near a lock-block retaining wall has a steeper (28°) slide surface (Fig. 5; Macciotta et al. 2014; Hendry et al. 2015; Schafer et al. 2015).

3.4 Aerial and Bathymetric Surveys

UAVs allow flexible, inexpensive acquisition of low-altitude aerial images, while various off-the-shelf photogrammetric Structure from Motion (SfM) software packages enable production of high-resolution digital surface models (DSM), digital elevation models (DEM) and orthophoto mosaics from such images. These UAV surveys help characterize landslide surface morphology and the spatial extent of displacement (Fig. 4f).

DSMs and corresponding orthophoto mosaics provide very high spatial resolution datasets (2 cm) enabling detailed topographical and textural information (cf. Huntley et al. 2020a, 2021a). UAVs, when equipped with a LiDAR sensor, penetrate the vegetation cover and provide elevation data in areas where the photogrammetry based on SfM method is not likely to produce a representative ground surface. Merged mosaics and DSMs capture the surface condition of landslides, and the extent of bare earth and vegetation growth (e.g., grasses, shrubs, and trees). Metre-scale anthropogenic features (e.g., train tracks, lock-block retaining walls, culverts) are resolvable in high-resolution raster imagery.

Bathymetric surveys better characterize the geometry of submerged landslide toe slopes and identify reaches with

channel incision and erosion. GPR, ERT, and acoustic single-beam and multi-beam river surveys (Fig. 4g) reveal variations in channel bed composition ranging from sand and silt draping bedrock to coarse gravel and boulders overlying clay-rich valley fill (Huntley et al. 2019a, b, c, 2021a). Shallow waters (riffles) with rapids lie adjacent to stable terrain, separated by deep scour pools (up to 5 m below river level) adjacent active slide toes.

3.5 Monitoring to Determine Landslide Function

Although some landslides in the Thompson River valley failed and moved rapidly in the past, today all are slow-moving compound features within Pleistocene valley fill (Porter et al. 2002; Eshraghian et al. 2007, 2008; Bunce and Chadwick 2012; Huntley et al. 2020a, b; Fig. 4a). Temporal relationships between landslides and the environmental conditions triggering instability are determined from time-series monitoring and GIS analyses of satellite Interferometric Synthetic Aperture Radar (InSAR), UAV photographs, and ground-based real-time kinematic ground-based global navigation satellite system (RTK-GNSS) surveys (Eshraghian et al. 2008; Bunce and Chadwick 2012; Huntley et al. 2020a, b; Fig. 4a).

3.6 InSAR Change-Detection Monitoring

Satellite remote sensing is an effective first approach for determining the risks posed from ground hazards than other site investigation (Fig. 4a). InSAR provides the best opportunity to determine the extent of landslide activity in the Thompson River valley (Journault et al. 2016, 2018; Huntley et al. 2017b). Slope deformation is monitored using persistent scatterer InSAR techniques, with landslide mapping, modelling, back-analysis of deformation velocities, and long-term deformation trends derived from datasets (e.g., Macciotta et al. 2014; Journault et al. 2016, 2018; Huntley et al. 2017c). Trihedral aluminium corner reflectors, permanent coherent artificial InSAR targets, improves the precision and accuracy of subsequent image processing of images (Fig. 4h). Different line-of-sight (LoS) viewing geometries allow for the projection of vertical and horizontal displacement. Ground movement measured by space-borne InSAR produces results with precision comparable to RTK-GNSS measurements, but with the advantage of monitoring displacement over large areas (Huntley et al. 2017c; Journault et al. 2018).

InSAR monitoring indicates at least five large volume rotational-translational landslides remain active and have potential to adversely impact CN and CP railway

infrastructure and services (Fig. 4a; Journault et al. 2016, 2018; Huntley et al. 2017b, 2021a, b, c). Satellite InSAR platforms with repeat visit times of weeks (e.g., RADARSAT-2 [RS2] and SENTINEL-1 [S1]) to days (e.g., RADARSAT Constellation Mission [RCM]) provide rapid monitoring capability with cm-scale precision and accuracy when periodically benchmarked with ground-based RTK-GNSS measurements and UAV photogrammetry. The combination of relatively high spatial and temporal resolution offered by RCM resolves rapid movement over small areas that would otherwise be aliased by the coarser spatial and temporal resolution of RS2 and S1 (Huntley et al. 2021b, c, d). Ground movement is shown to be generally concentrated within the main body of most sliding masses (Fig. 4a). Rates of displacement detected by InSAR vary seasonally, with slower displacement rates occurring during the May to August interval, and higher values from September to April.

3.7 UAV Change-Detection Monitoring

Rigorous change detection requires an accurate and precise elevation model to serve as a reference base topographic map. Repeat UAV surveys have aimed to better characterize the spatial extent, magnitude and direction of landslide movement in the Thompson River valley (Huntley et al. 2021a, d). Planimetric displacement of landslides are first mapped using image co-correlation analysis processing of time-sequenced hill-shaded UAV DSMs. Parameters during hill-shading that align the orientation of the landslide with the simulated sun are used to draw out features for displacement detection. Areas of vegetation and recent track ballast work on hill-shaded images are masked prior to processing to reduce the areas with substantial change not related to slide movement. Two images are created for E/W (X) and N/S (Y) displacement, while elevation changes (Z) are derived from the DSM. These values are added, and then squared to produce a single raster containing 3D displacement values that are all positive, with larger values representing more displacement (Fig. 4i; Huntley et al. 2021a, d).

3.8 RTK-GNSS Change-Detection Monitoring

Repeat RTK-GNSS ground surveys aim to better characterize the magnitude and direction of landslide movement over time (Fig. 4j). GNSS techniques have been successfully employed to determine the three-dimensional coordinates of moving points on landslides (Macciotta et al. 2014; Rodriguez et al. 2018). Ground control points (GCP) are

established across the slope using stable boulders and anthropogenic features on, and adjacent to the landslide. A reference base station was established on a stable post-glacial terrace near Black Canyon, 3 km north of the Ripley Landslide (B, Fig. 3). GNSS monuments (Bunce and Chadwick 2012; Macciotta et al. 2014) provide continuous, near real-time monitoring of surface displacement, but only at three trackside locations.

Repeat RTK-GNSS surveys provide point position data across much of the slide body. However, this method generates limited information on the seasonal variation in displacement rates and amounts. Moreover, periodic and continuous monitoring of GCPs and railway infrastructure with small and slow annual displacements ($<10 \text{ cm year}^{-1}$) is particularly challenging in an environment with a semi-arid intermontane climate, and an extreme temperature range of -30 to $+40$ °C. A Geocube (GeoKylia)TM continuous differential (D)GNSS network installed at the Ripley Landslide addresses both issues of spatial and temporal coverage (Fig. 4k). Two areas of maximum displacement recorded by the DGNSS network coincide with maximum displacement indicated by InSAR and UAV analysis. The larger northern zone spans the CN and CP tracks, while a smaller zone at the south end of the landslide near the lock-block retaining wall (Macciotta et al. 2014; Rodriguez et al. 2018; Huntley et al. 2020b, 2021a).

3.9 In-Situ Instrumental Change-Detection Monitoring

Elevated soil moisture was recognized as a driver of slope failure in the Thompson River valley since the first slope stability study in the area (Stanton 1898). Regional and local groundwater conditions contribute to high pore pressures and slope instability along the transportation corridor. Since clay impedes groundwater flow, pore pressure increases along the surface of clay layers, resulting in reduced material strength and decreased slope stability (Porter et al. 2002; Clague and Evans 2003). Piezometers on active landslides record upward hydraulic gradients and elevated pore pressures, confirming toe slopes are in a discharge zone of a regional groundwater flow system (Eshraghian et al. 2008; Hendry et al. 2015).

A strong correlation between river stage and pore pressures suggests Thompson River controls the distribution of groundwater in the slide mass by acting as a lower hydraulic boundary for the regional groundwater regime within the fractured bedrock; and by allowing horizontal connectivity through higher conductivity layers of fluvial cobbles, gravels and sands (Hendry et al. 2015; Schafer et al. 2015).

Proactive infrastructure monitoring and evaluation (PRIME) with continuous ERT and soil moisture

acquisitions capture subsurface responses in interannual and seasonal variations in precipitation, in addition to temperature, surface runoff, and snowmelt (Fig. 6a–g; Sattler et al. 2018, 2020; Holmes et al. 2018, 2020; Huntley et al. 2019b, c). Noticeable increases in rate of movement occur when high, prolonged flows of Thompson River sustained by snowmelt are followed by low flows through the autumn and winter months (Macciotta et al. 2014; Schafer et al. 2015; Tappenden 2016). The greatest displacement rates occur from November to March when transitional ground conditions allow snowmelt and rainfall to penetrate deep into the still frozen (or thawing) slide body by way of tension cracks, planar fractures, and bedding surfaces (Fig. 6c, e, g). Resistivity and soil suction show similar seasonal trends, responding cyclically to changing weather conditions from December to March (Fig. 6d, f, h).

Fibre Bragg grating (FBG) and Brillouin optical time domain reflectometry (BOTDR) indicate peak strain rates in the lock-block retaining wall at the south end of the Ripley Landslide also occur in the fall and winter months (Fig. 4l; Huntley et al. 2017c).

In the Thompson River valley, InSAR interferometry, UAV photogrammetry, RTK-GNSS, piezometers, ERT monitoring, and fibre optic reflectometry all show peak movement occurs through winter to spring, indicating factors other than changes in river and groundwater levels influence landslide activity. To understand climatic controls, local weather conditions, including wind speed and direction, rainfall and snow depth, air temperature, ground temperature, and soil matric suction are monitored (W, Figs. 3 and 4m). Weather station data confirm that major precipitation events occur mostly between fall and spring when landslide activity increases (Fig. 6b). Fluctuations in temperature over the winter months also contribute to intervals of landslide activity with thawing soil moisture recharging groundwater (Holmes et al. 2018, 2020; Huntley et al. 2019a, b, c; Sattler et al. 2020, 2021).

4 Discussion and Synthesis

4.1 Landslides and Consequences

Across Canada, relief, slope, aspect, distance from hydrological features, environmental conditions, surficial geology, and land cover conspire to produce a wide range of rapid and slow-moving landslides (Table 1) with the potential to impact railway infrastructure and operations. Landslides have been responsible for numerous casualties, injuries and deaths, costly damage to transportation infrastructure and property, socioeconomic losses, and environmental degradation since the late eighteenth century (Blais-Stevens 2020). Since the late 1800s, the operational and economic

consequences of slope failure along the national railway transportation corridors have depended on the scale and rate of movement, and temporal relationship between landslide activity and train timetables.

In the Thompson River valley transportation corridor (Fig. 3), small ($<10 \text{ cm year}^{-1}$), incremental surface displacements detected by InSAR, UAVs and periodic RTK-GNSS surveys contribute to minor track misalignment, requiring short-term (seasonal) reorganization of train schedules to allow the safe addition of ballast and realignment of tracks, and to avoid significant time-tabling impacts (i.e., intrinsic consequences). In contrast, frequent, rapid, large and widespread ground movements are a concern for railway companies, government agencies and local communities. Greater surface displacement will damage bridges, culverts, retaining walls and access roads, and cause major track misalignment with the potential for train derailments and service disruption. Potential accompanying negative environmental impacts (i.e., extrinsic consequences) include the loss of natural resources, including fish, wildfowl, game animals, cattle and crops, and potable water for communities.

Global climate change is anticipated to lead to more extreme regional weather events across Canada, along with an increase in the frequency and magnitude of landslides, floods, wildfires and other geological hazards in all provinces and territories (Sauchyn and Nelson 1999; Couture and Evans 2006; St. George 2007). For example, increasing precipitation and higher sustained river flows will change groundwater pressures on slide rupture surfaces extending below rivers and lakes, contributing to increased instability of slopes along the national railway transportation corridors. Climate-driven geological hazards can potentially compromise the safe and secure transport of rural resources and intermodal goods across the continent. A cascade of resulting negative intrinsic and extrinsic consequences for transportation and energy infrastructure, supply chains for goods and services, as well as the environment, will challenge the integrity and resilience of national transportation infrastructure and local communities (Evans and Clague 1997; Geertsema et al. 2006a, b; Blais-Stevens 2020).

The extreme storm system of November 14, 2021, in southwestern BC and its aftermath illustrates such a cascade of events. Following a dryer-than-normal summer and wetter-than-normal fall along all major transportation corridors through the Cascades and Coast Mountains (Fig. 2), wildfire-disturbed slopes received $>100 \text{ mm}$ of rain in 24 h (and up to 300 mm over 48 h) during an extreme “atmospheric river event” (<https://weather.gc.ca/> [URL 2021]). Along with the loss of life (human and livestock), railways, highways, pipelines, power transmission networks, light industrial, and rural–urban infrastructure (e.g., potable water conduits and sewage treatment plants) sustained significant damage because of widespread storm-driven landslides and

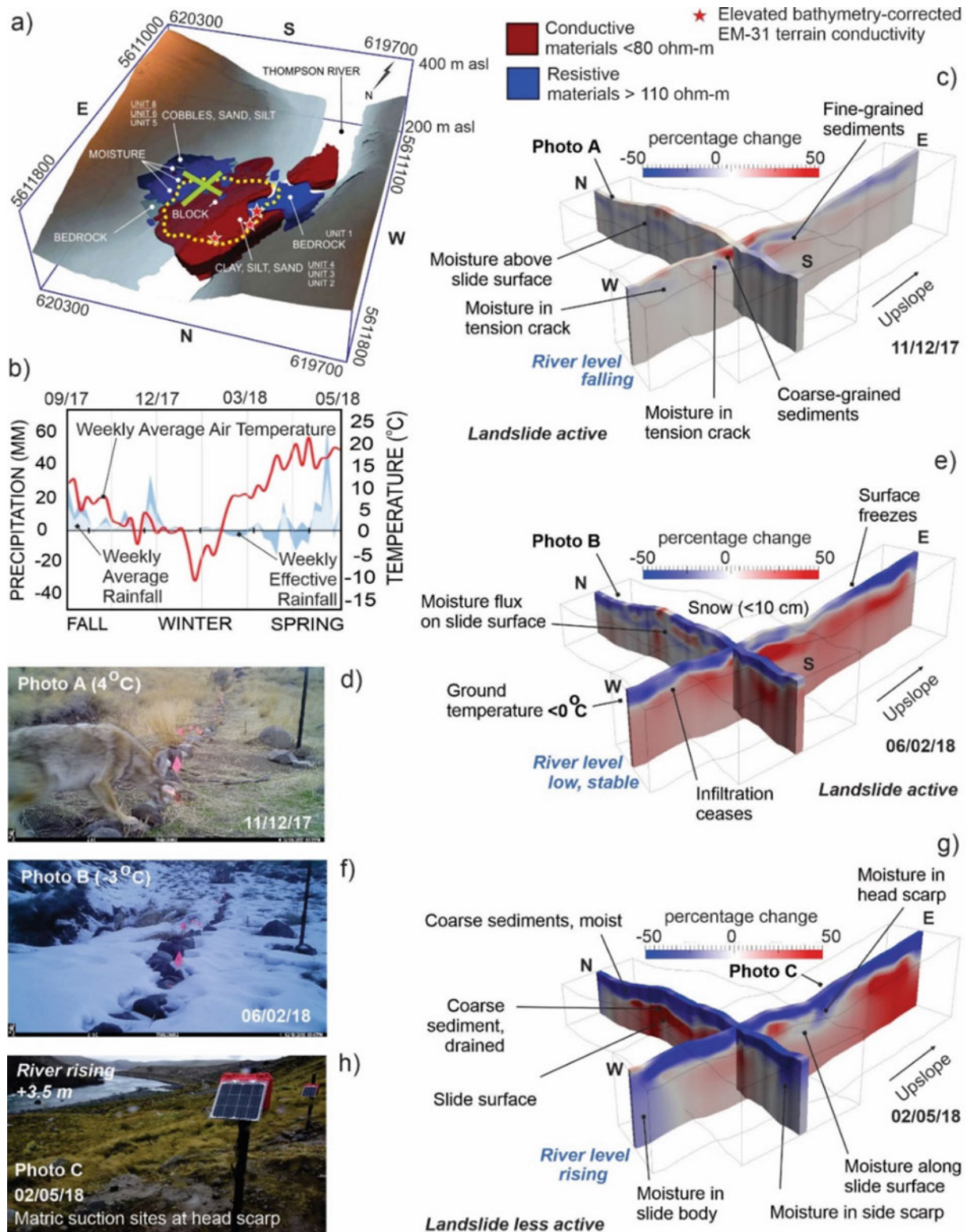


Fig. 6 In-situ ERT time-series monitoring observations, results and interpretation for the Ripley Landslide, in the Thompson River valley, southwestern BC. **a** 3D block diagram of merged ERT data captures a static proxy image of subsurface resistive and conductive earth materials (see Fig. 5). **b** Precipitation, expressed as a weekly average rainfall and effective rainfall; and temperature expressed as a weekly average from September 2017 to May 2018 (Holmes et al. 2020; Sattler

et al. 2020). **c, d** Resistivity profile of PRIME cross-sections (north-south, east-west) with observations of ground conditions and changes in resistivity (Ωm) from December 5, 2017. **e, f** Ground and resistivity conditions February 6, 2018. **g, h** Ground and resistivity conditions for May 2, 2018 (after Holmes et al. 2018; Sattler et al. 2018; Huntley et al. 2019c; British Geological Survey ©UK Research and Innovation 2020)

flooding. The costly relocation of whole communities and reorganization of transportation and shipping schedules led to national socioeconomic losses through service disruption and broken supply chains extending well beyond the winter of 2021–2022. Long-term negative environmental consequences include widespread contamination of agricultural lands and damage to natural fish and wildlife habitats.

4.2 Landslide Mitigation and Monitoring Best Practices

Geotechnical mitigation solutions for landslides can carry significant economic costs and environmental consequences, especially when measures fail to stabilize the slopes of concern (Bunce and Chadwick 2012). In closing, we propose a best-practice solution incorporating three levels of investigation to describe the form and function of the wide range of rapid and slow-moving landslides occurring across Canada in a range of physiographic settings (Fig. 7). Geospatial and temporal change-detection monitoring of active landslides and at-risk infrastructure is a cost-effective hazard management practice that provides important geoscience information to help develop appropriate early warning, mitigation, and adaptation measures in response to extreme weather events driven by climate change.

4.3 Level I Investigation (Fundamental Geoscience)

All landslide studies begin with the acquisition of fundamental geoscience information on earth materials, landforms, and their behaviours. GIS landslide inventories are based on the interpretation of high-resolution optical and hyperspectral satellite imagery, air photos, and UAV photogrammetry (Fig. 7). On-site investigations of slope and drainage, bedrock and structures, surficial geology and geomorphology, and vegetation and land cover, when combined with borehole logging, geophysical surveys, petrological and geochemical analyses, and geotechnical studies provide fundamental geoscience information on terrain units and landforms susceptible to mass-movement landslides (Fig. 7).

Landslide inventories and susceptibility maps (e.g., Fig. 2c) allow stakeholders to recognize slopes of concern for further investigation and identify the most suitable geological indicators for level II and III monitoring (Fig. 7). GIS and derivative maps that delimit unstable and potentially unstable terrain are invaluable tools for landslide monitoring and risk management since they can be applied to calculate spatial relationships between landslide distribution, specific

terrain features, and environmental conditions expected to correlate with landslide incidence.

Although non-systematic datasets have unequal reliability, accuracy and precision, they nevertheless provide useful insight into landslide distribution at various scales and help focus attention on areas of interest where rigorous qualitative analyses are warranted (Fig. 7).

4.4 Level II Investigation (Geospatial Benchmarks)

For landslides of concern and terrain susceptible to mass-wasting identified in a Level I investigation, ground-based RTK-GNSS measurements with cm-scale precision and accuracy periodically benchmark displacement values determined from satellite InSAR and UAV change-detection datasets (Fig. 7).

As highlighted by the case study in the Thompson River valley, slow-moving mass movements (e.g., rock slumps, debris slides and earth flows) are most effectively monitored by combining InSAR, UAV and RTK-GNSS monitoring. Shallow geophysical and bathymetric surveys also contribute an understanding of the composition and behaviour of a range of slow-moving landslides. Like other parts of Canada, the landscape and harsh environment of southwestern BC presents logistical challenges for installation, and instrumentation of geophysical and continuous GNSS measurements. Permanent GNSS stations and GCPs are less appropriate for monitoring rapid mass movements in steep, mountainous areas with rock avalanches, debris flows and lahars, or in low relief permafrost terrain with active layer detachments and thaw flows where they are prone to damage and loss of data.

4.5 Level III Investigation (Time-Series Monitoring)

Steep, mountainous terrain also presents logistical challenges for installation and *in-situ* time-series monitoring of rapid-moving rock avalanches, debris flows and lahars in steep, are prone to damage and loss of data. In a Level III investigation, lithological, geophysical, geochemical and geotechnical properties, and other environmental conditions (e.g., river and groundwater levels, soil moisture, weather variables), recognized as drivers of landslide activity and benchmarked during levels I-II, are selected for *in-situ* time-series monitoring.

Level III investigations are most suitable for slower moving landslides where boreholes can be drilled for monitoring and unstable slopes instrumented safely. In the

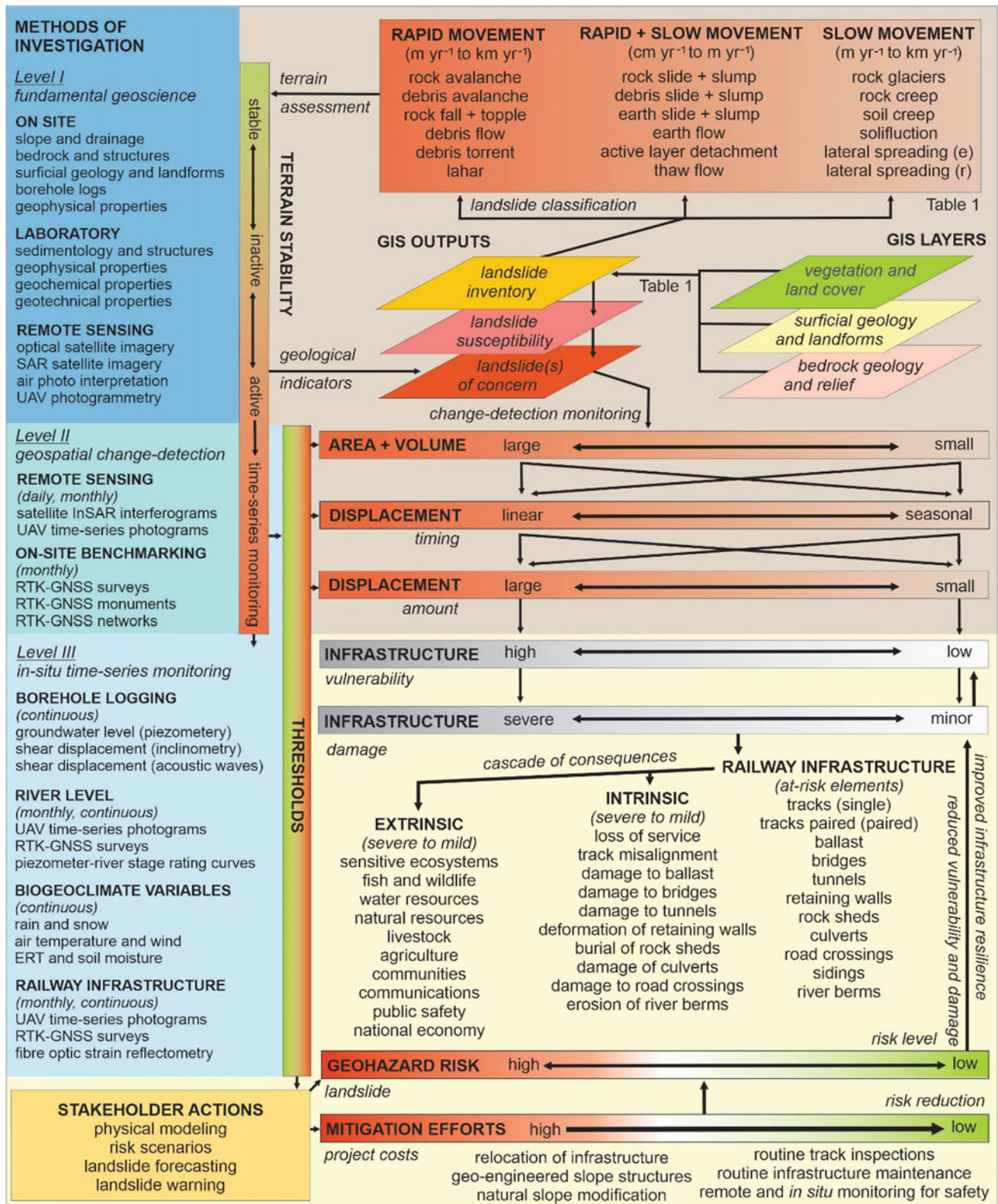


Fig. 7 Conceptual model outlining three levels of investigation to classify, determine susceptibility, and identify landslides of concern for monitoring. Inventory maps, geospatial change-detection, and in-situ time-series monitoring define the interactions between landslides of varying sizes, displacement amounts, and timing of activity; and

contribute to estimates of infrastructure vulnerability, anticipated damage, and cascade of consequences contributing to landslide risk. Mitigation solutions reduce the risks to railway transportation corridors running through terrain susceptible to landslides

Thompson valley transportation corridor, Level III InSAR, UAV and RTK-GNSS change-detection datasets conclusively show that geotechnical solutions to stabilize slopes based on current physical models are only partly successful (Journault et al. 2016, 2018; Huntley et al. 2017b, 2021c, e). To better understand the impacts of climate, landslide behaviour is further investigated through time-series monitoring of slopes and infrastructure (e.g., fibre optic reflectometry), boreholes (e.g., piezometers, inclinometers, and acoustic emissions), and weather variables (e.g., rain gauges, snow sensors, thermistors, anemometers, soil moisture meters).

The key goal of geological indicator time-series monitoring is the derivation of thresholds for driving factors that influence landslide dimensions and displacement values (Fig. 7).

4.6 Stakeholder Actions (Climate-Resilient Infrastructure)

The severity of damage to vulnerable railway infrastructure (e.g., tracks, ballast, tunnels, bridges and retaining walls) is a consequence of the areal extent and volume of the landslide (s), temporal changes in landslide activity, and the magnitude of displacement detected during level I–III investigations (Fig. 7). In addition, climate-driven mass-wasting will affect, to varying degrees, sensitive ecosystems, fish, wildlife and water resources, agricultural lands and livestock, communities and people living in proximity to railway infrastructure, and ultimately, supply chains and the national economy (Fig. 7).

Environmental thresholds derived from multi-year datasets capturing spatial and temporal changes in landslide activity in proximity to critical transportation infrastructure enable stakeholders to build robust monitoring and early warning systems, cost-effective mitigation measures, and reliable risk management strategies (Fig. 7). Geospatial and in-situ time-series datasets improve the safety, security and resilience of transportation infrastructure to climate-driven geological hazards, reducing risks to the economy, environment, natural resources and public safety.

Acknowledgements The Government of Canada, through the Ministry of Transport and Ministry of Natural Resources, is funding field-based landslide research in the Thompson River valley, BC, and elsewhere across Canada. The authors wish to acknowledge the support of Danny Wong (Canadian Pacific Railways, Calgary, Alberta) and Trevor Evans (Canadian National Railways, Kamloops, British Columbia). University partners include Michael Hendry, Renato Macciotta, and Sohrab Sharifi (University of Alberta, Edmonton, Alberta). Bathymetric surveys were completed with the assistance of Tim Funk (Funktionale, Kamloops, British Columbia), Paul Bauman, Graham Young and team (Advisian-Worley Parsons Group, Calgary, Alberta), and Jacques Gagne (Department of Fisheries and Oceans,

Sidney, British Columbia). Andy Pon and colleagues (3vGeomatics, Vancouver, British Columbia), Pano Skrivanos (Pacific UAV, Sidney, British Columbia), Bill Lakeland and Alec Wilson (Spexi Geospatial Inc.) provided technical assistance with InSAR and UAV analyses. Remi Usquin and Frédéric Verluise, Ophelia Sensors (Paris, France), provided tireless Geocube™ support. Philip LeSueur provided an internal Geological Survey of Canada critical peer review of the draft manuscript.

References

- Blais-Stevens A (2020) Historical landslides that have resulted in fatalities in Canada (1771–2019). Geological Survey of Canada, Open File 8392, 1 sheet. <https://doi.org/10.4095/326167>
- Blais-Stevens A, Couture R, Page A, Koch J, Clague J, Lipovsky P (2010) Landslide susceptibility, hazard and risk assessments along pipeline corridors in Canada. In: Proceedings of the 63rd Canadian geotechnical conference and 6th Canadian permafrost conference, pp 878–885
- Bobrowsky PT, Dominguez MJ (2012) Landslide susceptibility map of Canada. Geological Survey of Canada, Open File 7228, 1:6 million-scale map: 1 sheet. <https://doi.org/10.4095/291902>
- Bostock HS (2014) Geology, physiographic regions of Canada. Geological Survey of Canada, Map 1254A, 2nd ed, scale 1:5 million-scale map, 3 sheets. <https://doi.org/10.4095/293408>
- Bunce C, Chadwick I (2012) GPS monitoring of a landslide for railways. In: Landslides and engineered slopes—protecting society through improved understanding, pp 1373–1379
- Clague J, Evans S (2003) Geologic framework for large historic landslides in Thompson River valley, British Columbia. *Environ Eng Geosci* 9:201–212
- Couture R, Evans S (2006) Slow-moving disintegrating rockslides on mountain slopes. In: Evans S et al (eds) Landslides from massive rock slope failure: proceedings of the NATO advanced research workshop on massive rock slope failure: new models for hazard assessment, NATO science series, sub-series IV: earth and environmental sciences, vol 49, pp 377–393
- Deblonde C, Cocking R, Kerr D, Campbell J, Eagles S, Everett D, Huntley D, Inglis E, Parent M, Plouffe A, Robertson L, Smith I, Weatherston A (2018) Science language for an integrated Geological Survey of Canada data model for surficial geology maps (Version 2.3.14). Geological Survey of Canada, Open File 8236: 50 p, 2 sheets
- Dominguez-Cuesta M, Bobrowsky P (2011) Proposed landslide susceptibility map of Canada based on GIS. In: Proceedings of the second world landslide forum, 8 p
- Eshraghian A, Martin C, Cruden D (2007) Complex earth slides in the Thompson River Valley, Ashcroft, British Columbia. *Environ Eng Geosci* XIII:161–181
- Eshraghian A, Martin C, Morgenstern N (2008) Movement triggers and mechanisms of two earth slides in the Thompson River Valley, British Columbia, Canada. *Can Geotech J* 45:1189–1209
- Evans S (1984) The 1880 landslide dam on Thompson River, near Ashcroft, British Columbia. Geological Survey of Canada. *Current Res Part A Paper* 84-1A:655–658
- Evans S, Clague J (1997) The impact of climate change on catastrophic geomorphic processes in the mountains of British Columbia, Yukon, and Alberta. In: Taylor E, Taylor B (eds) Responding to global climate change in British Columbia and Yukon, Vol I of the Canada Country Study: climate impacts and adaptation, Chap 7, 16 p
- Fulton R (Compiler) (1995) Surficial materials of Canada. Geological Survey of Canada, Map 1880A, scale 1:5,000,000

- Geertsema M, Clague J, Schwab J, Evans S (2006a) An overview of recent large catastrophic landslides in northern British Columbia, Canada. *Eng Geol* 83:120–143
- Geertsema M, Schwab J, Blais-Stevens A (2006b) Landslides impacting linear infrastructure in west-central British Columbia. In: *Proceedings of the 1st specialty conference on disaster mitigation*, pp DM 1–10
- Geertsema M, Highland L, Vaugeouis L (2009a) Environmental impact of landslides. In: *Landslides—disaster risk reduction*, pp 589–607
- Geertsema M, Schwab J, Blais-Stevens A, Sakals M (2009b) Landslides impacting linear infrastructure in west central British Columbia. *Nat Hazards* 48:59–72
- Haque U, Blum P, da Silva P, Andersen P, Pilz J, Chalov S, Malet J-P, Auflič M, Andres N, Poyiadji P, Lamas P, Zhang W, Peshevski I, Pétursson H, Kurt T, Dobrev N, Garcí-Davalillo J, Halkia M, Ferri S, Gaprindashvili G, Engström J, Keellings D (2016) Fatal landslides in Europe. *Landslides* 13:1545–1554
- Hendry M, Macciotta R, Martin D (2015) Effect of Thompson River elevation on velocity and instability of Ripley Slide. *Can Geotech J* 52(3):257–267
- Hervás J, Bobrowsky P (2009) Mapping: inventories, susceptibility. Hazard and risk. In: *Landslides—disaster risk reduction*, pp 321–349
- Highland L, Bobrowsky P (2008) *The landslide handbook—a guide to understanding landslides*. U.S. Geological Survey Circular 1325, 129 p
- Holmes J, Chambers J, Donohue S., Huntley D, Bobrowsky P, Meldrum P, Uhlemann S, Wilkinson P, Swift R (2018) The use of near surface geophysical methods for assessing the condition of transport infrastructure. *Civil Engineering Research Association, Special Issue on Structural Integrity of Civil Engineering Infrastructure*. *J Struct Integrity Maintenance*, 6
- Holmes J, Chambers J, Meldrum P, Wilkinson B, Williamson P, Huntley D, Sattler K, Elwood D, Sivakumar V, Reeves H, Donohue S (2020) 4-Dimensional electrical resistivity tomography for continuous, near-real time monitoring of a landslide affecting transport infrastructure in British Columbia, Canada. *Near Surface Geophys* 15. <https://doi.org/10.1002/nsg.12102>
- Howes D, Kenk E (1997) *Terrain classification system for British Columbia*. Province of British Columbia, Ministry of Crown Lands, 102 p
- Huntley D, Bobrowsky P (2014) *Surficial geology and monitoring of the Ripley Slide, near Ashcroft, British Columbia, Canada*; Geological Survey of Canada, Open File 7531, 21 p
- Huntley D, Bobrowsky P, Parry N, Bauman P, Candy C, Best M (2017a) Ripley landslide: the geophysical structure of a slow-moving landslide near Ashcroft, British Columbia, Canada. Geological Survey of Canada, Open File 8062, 59 p
- Huntley D, Bobrowsky P, Charbonneau F, Journault J, Hendry M (2017b) Innovative landslide change detection monitoring: application of spaceborne InSAR techniques in the Thompson River valley, British Columbia, Canada. In: *Landslide research and risk reduction for advancing culture and living with natural hazards*, vol 3, 4th world landslide forum (ICL-IPL), Ljubljana, Slovenia 29-May–2 June 2017b. Springer Nature, 13 p
- Huntley D, Bobrowsky P, Zhang Q, Zhang X, Lv Z. (2017c) Fibre Bragg grating and Brillouin optical time domain reflectometry monitoring manual for the Ripley landslide, near Ashcroft, British Columbia. GSC Open File 8258, 66 p
- Huntley D, Bobrowsky P, Hendry M, Macciotta R, Best M (2019a) Multi-technique geophysical investigation of a very slow-moving landslide near Ashcroft, British Columbia, Canada. *J Environ Eng Geophys* 24(1):85–108. <https://doi.org/10.2113/JEEG24.1.87>
- Huntley D, Bobrowsky P, Sattler K, Elwood D, Holmes J, Chambers J, Meldrum P, Holmes J, Wilkinson P, Hendry, M., Macciotta R (2019b) PRIME installation in Canada: protecting national railway infrastructure by monitoring moisture in an active landslide near Ashcroft, British Columbia. Geological Survey of Canada, Open File 8548, 1 sheet. <https://doi.org/10.4095/314548>
- Huntley D, Bobrowsky P, Hendry M, Macciotta R, Elwood D, Sattler K, Chambers J, Meldrum P (2019c) Application of multi-dimensional electrical resistivity tomography datasets to investigate a very slow-moving landslide near Ashcroft, British Columbia, Canada. *Landslides* 16:1033–1042. <https://doi.org/10.1007/s10346-019-01147-1>
- Huntley D, Holmes J, Bobrowsky P, Chambers J, Meldrum P, Wilkinson P, Elwood D, Sattler K, Hendry M, Macciotta R (2020a) Hydrogeological and geophysical properties of the very slow-moving Ripley Landslide, Thompson River valley, British Columbia. *Can J Earth Sci* 57:1371–1391. <https://doi.org/10.1139/cjes-2019-0187>
- Huntley D, Bobrowsky P, Cocking R, Joseph J, Neelands N, MacLeod R, Rotheram-Clarke D, Usquin R, Verluise F (2020b) Installation, operation and evaluation of an innovative global navigation satellite system monitoring technology at Ripley Landslide and South Slide, near Ashcroft, British Columbia. Geological Survey of Canada, Open File 8742, 36 p
- Huntley D, Bobrowsky P, MacLeod R, Cocking R, Joseph J, Rotheram-Clarke D (2021a) Ensuring resilient socio-economic infrastructure: field testing innovative differential GNSS-InSAR-UAV monitoring technologies in mountainous terrain near Ashcroft, British Columbia, Canada. *J Mountain Sci* 18(1):1–20. <https://doi.org/10.1007/s11629-020-6552-y>
- Huntley D, Rotheram-Clarke D, Cocking R, Joseph J (2021b) Landslide change detection monitoring with a benchmarked RADARSAT CONSTELLATION MISSION high temporal resolution dataset. Institute of Electrical and Electronic Engineers. In: *International geoscience and remote sensing symposium, Special Volume*, 4 p
- Huntley D, Rotheram-Clarke D, Pon A, Tomaszewicz A, Leighton J, Cocking R, Joseph J (2021c) Benchmarking RADARSAT-2, SENTINEL-1 and RADARSAT CONSTELLATION MISSION change detection monitoring at North Slide, Thompson River valley, British Columbia: implications for a landslide-resilient national railway network. *Canadian J Remote Sens* 23. <https://doi.org/10.1080/07038992.2021.1937968>
- Huntley D, Bobrowsky P, Rotheram-Clarke D, MacLeod R, Cocking R, Joseph J, Holmes J, Donohue S, Chambers, J., Meldrum P, Wilkinson P, Hendry M, Macciotta R (2021d) Protecting Canada's railway network using remote sensing technologies. In: *Advances in remote sensing for infrastructure*, Springer International Publishing, 26 p. https://doi.org/10.36487/AGC_repo/2025_09
- Huntley D, Rotheram-Clarke D, Cocking R, Joseph J, Bobrowsky P (2021e) *Understanding Plateau and Prairie Landslides: annual report on landslide research in the Thompson River valley, British Columbia, and the Assiniboine River valley, Manitoba-Saskatchewan (2020–2021e to 2021e–2022)*. Geological Survey of Canada, Open File 8838, 73 p
- Jespersen-Groth P, Potthoff D, Clausen J, Huisman D, Kroon L, Marotí G, Nielsen M (2009) Disruption management in passenger railway transportation. In: *Robust and online large-scale optimization*. Springer, pp 399–421
- Journault J, Macciotta R, Hendry M, Charbonneau F, Bobrowsky P, Huntley D, Bunce C, Edwards T (2016) Identification and quantification of concentrated movement zones within the Thompson River valley using satellite borne InSAR. *Canadian Geotechnical Society*. In: *Proceedings volume of geoVancouver 2016 annual meeting*, 13 p
- Journault J, Macciotta R, Hendry M, Charbonneau F, Huntley D, Bobrowsky P (2018) Measuring displacements of the Thompson

- River valley landslides, south of Ashcroft, B.C., Canada, using satellite InSAR. *Landslides* 15(4):621–636. <https://doi.org/10.1007/s10346-017-0900-1>
- Laimer H (2017) Anthropogenically-induced landslides—a challenge for railway infrastructure in mountainous regions. *Eng Geol* 222:92–101
- Macciotta R, Hendry M, Martin D, Elwood D, Lan H, Huntley D, Bobrowsky P, Sladen W, Bunce C, Choi E, Edwards T (2014) Monitoring of the Ripley Slide in the Thompson River Valley, B.C. *Geohazards* 6. In: Symposium, proceedings volume, Kingston, Ontario, 1 p
- Porter M, Savigny K, Keegan T, Bunce C, MacKay C (2002) Controls on stability of the Thompson River landslides. In: Canadian geotechnical society, ground and water—theory to practice, proceedings of the 55th Canadian geotechnical conference, pp 1393–1400
- Rodriguez J, Hendry M, Macciotta R, Evans T (2018) Cost-effective landslide monitoring GPS: characteristics, implementation and results. *Geohazards* 7, Proceedings Paper, 8 p
- Sassa K (2004) The international consortium on landslides. *Landslides* 1:91–94. <https://doi.org/10.1007/s10346-004-0012-6>
- Sattler K, Elwood D, Hendry M, Macciotta R, Huntley D, Bobrowsky P, Meldrum P (2018) Real-time monitoring of soil water content and suction in slow-moving landslide. In: *GeoEdmonton 2018*, proceedings paper, 8 p
- Sattler K, Elwood D, Hendry M, Huntley D, Holmes J, Wilkinson P (2020) Effect of pore-pressure dynamics on progressive failure in clay shale landslides. *Landslides* 17. https://doi.org/10.1007/978-3-030-60706-7_45
- Sattler K, Elwood D, Hendry M, Berscheid B, Marcotte B, Abdulrazagh P, Huntley D (2021) Field collection of geotechnical measurements for remote or low-cost data-logging requirements. *Geotech Test J* 45(1):35. <https://doi.org/10.1520/GTJ20200323>
- Sauchyn D, Nelson H (1999) Origin and erosion of the police point landslide, Cypress Hills, Alberta. In *Holocene climate and environmental change in the Palliser Triangle: a geoscientific context for evaluation the impacts of climate change on the southern Canadian prairies*. *Geol Survey Canada Bulletin* 534:257–265
- Schafer M, Macciotta R, Hendry M, Martin D, Bobrowsky P, Huntley D, Bunce C, Edwards T (2015) Instrumenting and monitoring a slow moving landslide. *GeoQuebec 2015 Paper*, 7 p
- Schuster R, Fleming R (1986) Economic losses and fatalities due to landslides. *Bulletin Assoc Eng Geol* XXIII 1:11–28
- Stanton R (1898) The great land-slides on the Canadian Pacific Railway in British Columbia. *Proc Civil Eng* 132:1–48
- St. George S (2007) Stream flow in the Winnipeg River basin, Canada: trends, extremes and climate linkages. *J Hydrol* 332:396–411
- Tappenden K (2016) Impact of climate variability on landslide activity in the Thompson River Valley Near Ashcroft, B.C. In: *Proceedings of the 69th Canadian geotechnical conference*, October 2–5, 2016. Vancouver, 10 p
- Whiteley J, Chambers J, Uhlemann S, Wilkinson P, Kendall J (2019) Geophysical monitoring of moisture-induced landslides: A review. *Rev Geophys* 57:106–145. <https://doi.org/10.1029/2018RG000603>

Open Access This chapter is licensed under the terms of the Creative Commons Attribution 4.0 International License (<http://creativecommons.org/licenses/by/4.0/>), which permits use, sharing, adaptation, distribution and reproduction in any medium or format, as long as you give appropriate credit to the original author(s) and the source, provide a link to the Creative Commons license and indicate if changes were made.



The images or other third party material in this chapter are included in the chapter's Creative Commons license, unless indicated otherwise in a credit line to the material. If material is not included in the chapter's Creative Commons license and your intended use is not permitted by statutory regulation or exceeds the permitted use, you will need to obtain permission directly from the copyright holder.



Advanced Technologies for Landslides— ATLaS (WCoE 2020–2023)

Nicola Casagli, Veronica Tofani, Sandro Moretti, Riccardo Fanti,
Giovanni Gigli, Silvia Bianchini, Samuele Segoni, William Frodella,
and Tommaso Carlà

Abstract

The UNESCO Chair on Prevention and Sustainable Management of Geo-Hydrological Hazards, University of Florence has been a member of the International Consortium on Landslides (ICL) since 2002. It was designated as one of World Centres of Excellence (WCoE) for Landslide Risk Reduction five times for 2008–2011, 2011–2014, 2014–2017, 2017–2020 and 2020–2023, with a project entitled “Advanced Technologies for Landslides”. In this paper, we describe the activities carried out by the UNESCO Chair as a member of ICL and as WCoE, and its contribution to the risk reduction policies promoted by the 2020 Kyoto Commitment.

Keywords

Landslides • Monitoring • Remote sensing • Risk reduction • Kyoto commitment

1 Introduction

The UNESCO Chair on Prevention and Sustainable Management of Geo-hydrological Hazards (UNESCO Chair) was funded in 2016 at University of Florence (UNIFI), a major academic organization for research and higher education in Italy. The UNESCO chair carries out research and development (R&D) for the prevention and management of landslides, in order to support policies and actions of risk reduction.

The University of Florence (UNIFI) is a founding member of ICL since 2002 and in 2008 was named as a World Centre of Excellence (WCoE) on Landslide Risk Reduction for the triennium 2008–2011 by the Global Promotion Committee of International Programme on Landslides of UN-ISDR. This recognition was reaffirmed four times over for 2011–2014, 2014–2017, 2017–2020 and 2020–2023.

In particular, in the framework of the project ATLaS (Advanced Technologies for LandSlides), the WCoE focuses on research activities concerning the landslide monitoring and early warning through innovative technologies, exploitation of EO (Earth Observation) data and technology to detect, map, monitor and forecast ground deformations, regional forecasting models and on activities related to education and training on landslides risk reduction.

The expertise of the WCoE research team includes remote-sensing techniques and application of space-borne and ground-based SAR interferometry, monitoring ground instabilities and development of early warning systems and GIS-based quantitative models for hazard and risk prediction.

N. Casagli · V. Tofani (✉) · S. Moretti · R. Fanti · G. Gigli ·
S. Bianchini · S. Segoni · W. Frodella · T. Carlà
Department of Earth Sciences, University of Florence,
Via G. La Pira 4, 50121 Florence, Italy
e-mail: veronica.tofani@unifi.it

N. Casagli
e-mail: nicola.casagli@unifi.it

S. Moretti
e-mail: sandro.moretti@unifi.it

R. Fanti
e-mail: riccardo.fanti@unifi.it

G. Gigli
e-mail: giovanni.gigli@unifi.it

S. Bianchini
e-mail: silvia.bianchini@unifi.it

S. Segoni
e-mail: samuele.segoni@unifi.it

W. Frodella
e-mail: william.frodella@unifi.it

T. Carlà
e-mail: tommaso.carla@unifi.it

The group participates in research and technological development projects in several areas of the world, often in active collaboration with international, national, and regional organizations and agencies. Since 2002, the UNESCO Chair has coordinated or has been involved in several ICL/IPL projects and is the proposer of the ICL Italian network that was officially established in December 2018.

Based on the expertise gathered during the last years in the abovementioned activities, the UNESCO Chair can provide its contribution to Kyoto 2020 Commitment for Global Promotion of Understanding and Reducing Landslide Disaster Risk that signed the Kyoto Commitment during the 2019 ICL-IPL Conference which at UNESCO Headquarters, Paris, on 16–19 September 2019 (Sassa 2018a, b, c; 2019).

2 Research Activity of WCoE

The WCoE ATLaS project focuses on the three main activities structured in three packages:

WP1—Monitoring unstable slopes and integration of different techniques for the set-up of early warning systems.

WP2—EO data for mapping, characterization and monitoring of landslides.

WP3—Landslide risk assessment and regional landslide forecasting models.

2.1 WP1

This activity focuses on the application of innovative monitoring techniques to estimate the deformational evolution of the landslide events (in space and time) and to implement the most suitable operational early warning systems (EWS), according to different critical situations (Carlà et al. 2017, 2019a, b; Frodella et al. 2018; Bardi et al. 2017). Several sites are monitored in Italy and all of them were monitored by using advanced sensors and portable instrumentations as ground-based synthetic aperture radar interferometers (GB-InSAR), terrestrial laser scanning (LIDAR), satellite interferometry (PS-InSAR), UAVs equipped with different sensors, GPS antennas, infrared thermography and traditional instrumentation (e.g. strain gauges, inclinometers, piezometers) (Del Soldato et al. 2018a; Di Traglia et al. 2018; Rossi et al. 2018; Casagli et al. 2017; Frodella et al. 2017; Lombardi et al. 2017; Carlà et al. 2019a, b).

As the use of these techniques has proliferated over the years, the advantages provided by the implementation of long-term monitoring campaigns for understanding the mechanism of complex slope instabilities have become increasingly apparent. One such example is represented by the Ruinon rockslide (Central Italian Alps), a ~ 30 million m^3 highly disaggregated translational slide in phyllites and

blocky/chaotic debris (Crosta and Agliardi 2003), which has been continuously monitored for more than a decade by means of a ground-based radar interferometer (Crosta et al. 2017). Phases of intense reactivation in the mid-lower part of the slide area have repeatedly caused the closure of a road travelling along the adjacent valley floor and the consequent isolation of a nearby village. For instance, in the summer of 2019, surface velocities locally increased to unprecedented values and often exceeded 1 m/day.

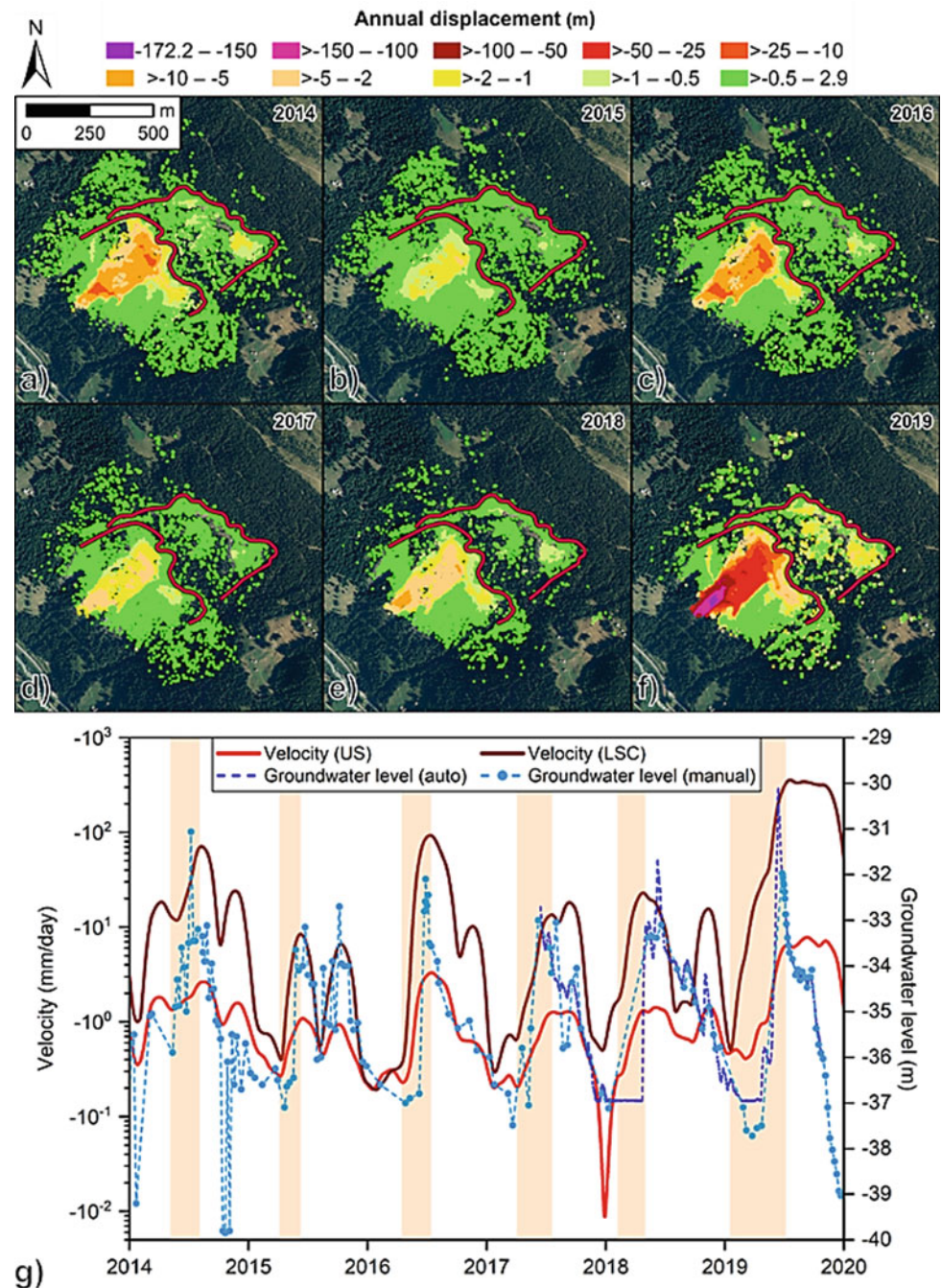
Most of the instrumentation installed on the slide area (mainly wire extensometers and borehole inclinometers) was therefore progressively damaged, leaving the GB-InSAR system as the sole operational tool for quantifying the slope displacements in space and time. This large set of data was exploited to directly or indirectly derive an updated assessment of the thickness of upper debris affected by greater deformation; the differences in deformation behaviour at different slide locations and depths; and the nature of hydrological forcing behind the recent reactivation phases (Carlà et al. 2021). In particular, slope displacements were combined with groundwater level measurements from two standpipe piezometers located behind the upper limit of the slide area. Readings at one of the two standpipe piezometers were carried out at irregular intervals since April 2012, while the second instrument was put into operation in June 2017 and equipped with a data logger for automatic piezometric monitoring at a fixed interval of 30 min.

It was observed that velocities cyclically increased up to their maximum yearly value in late spring or early summer, closely following sharp rises of groundwater level—as most likely determined by the superimposition of rainfalls and seasonal snowmelt at higher elevations (Fig. 1).

In addition, reactivations of secondary importance were revealed to occasionally occur during the fall, when heavy rainfalls were associated with small temporary reversals of the otherwise decreasing trend of groundwater level. Eventually, a clear exponential-like correlation between the yearly peak of surface velocity and the yearly peak of groundwater level was identified (Carlà et al. 2021), highlighting how even small variations of the latter variable may profoundly alter the evolutionary trends of complex slope instabilities. The experience gained at Ruinon also supports the proposition that long-term GBInSAR monitoring may be an essential tool in the case of highly disaggregated and rapidly evolving alpine rockslides that being subject to recurrent reactivations and associated large displacements would otherwise be difficult to investigate owing to the difficult accessibility of the site. The instrument was in fact essential for setting up a management strategy for the adjacent road at risk based on a scale of differentiated early-warning thresholds.

More specifically, by exploiting the spatial properties of interferometric data, the slide area was divided into several

Fig. 1 Annual cumulative displacements of the Ruinon slide area measured by the GBInSAR system from 2014 to 2019 (a–f), and dependency between slide velocity and groundwater level (h). US and LSC are abbreviations for Upper Scarp and Lower Scarp, respectively, which are the two main geomorphological features within the Ruinon slide area (see red lines in panels a–f). Accordingly, values of US velocity derive from averaging all pixels located between the upper and lower scarp, whereas values of LSC velocity derive from averaging all pixels located downslope of the lower scarp. In g), yellow areas delimit the periods of sustained increase of velocities in late spring and/or early summer



sub-sectors, each one having a characteristic deformation behaviour. The presence of multiple mutually interacting blocks is in fact common in these types of landslides because of local variations in material composition, rupture surface (s) geometry, and/or degree of slope damage.

2.2 WP2

This activity is devoted to the application of high resolution EO data for the ground deformation mapping and

monitoring with millimetric precision, from local to regional scales. The final aim is a satellite surveillance system based on all the Earth Observation data (radar hyperspectral) available from several constellations of satellites.

WP2 activities deal with the development of satellite surveillance system exploiting Earth Observation (EO) data (radar, multi- and hyperspectral data) for the identification, mapping and monitoring of ground deformations associated with landslides from local to regional scales (Solari et al. 2020). In particular, advanced multi-temporal InSAR techniques are successfully exploited for detecting and

characterizing slow-moving ground surface displacements thanks to their millimetre precision and wide area coverage. Applications rely on historical SAR archives at medium resolution (e.g., ERS and ENVISAT, RADARSAT images) and on data from currently operative satellites at high resolution (e.g., COSMO-SkyMed constellation). Moreover, nowadays the availability of regular and systematic Sentinel-1 SAR data acquisitions with short revisiting time (e.g., 12 days) combined with advances in InSAR processing algorithm across time allows not only the mapping of geo-hydrological phenomena (for instance, for updating pre-existing landslide inventories), but also to perform recurring monitoring of the deformative scenario at a regional scale (Raspini et al. 2018; Bianchini et al. 2018).

An innovative monitoring system based on the systematic processing of current Sentinel-1 data has been set up and tested in Italy on Tuscany Region (since 2016), Valle d'Aosta (since 2018) and Veneto Region (since 2019) (Fig. 2a). Such satellite-based services rely on PSI data elaborated through SqueeSAR algorithm (Ferretti et al. 2011) and consist in two activities named “PS mapping” and “PS monitoring”.

The “PS mapping” activity exploited PSI-based ground deformation maps and semi-automatic hotspot-like analysis to map the most relevant long-term active deformational processes on the whole regional territory, as they represent the fastest moving areas, e.g., mainly related to already known or not known landslides (Fig. 2b) (Bianchini et al. 2021).

The “PS monitoring” activity is based on regularly updated terrain deformation maps from systematic processing of Sentinel-1 data stack (e.g., after every new satellite acquisition: 12 days). In more detail, once a new Sentinel-1 image is available, it is automatically downloaded and added to the existing SAR archive and the new data stack is entirely reprocessed to generate new ground deformation maps, providing an updated view of the regional deformational scenario (Fig. 2c) (Confuorto et al. 2021). The time series of displacement of each radar benchmark is systematically analyzed to promptly detect any velocity-change in the deformation pattern, in order to identify the so-called Anomalous Point (AP), e.g., measurement PSI points that show trend variations or abrupt velocity changes (e.g. related to landslide accelerations) in the time series (Raspini et al. 2019).

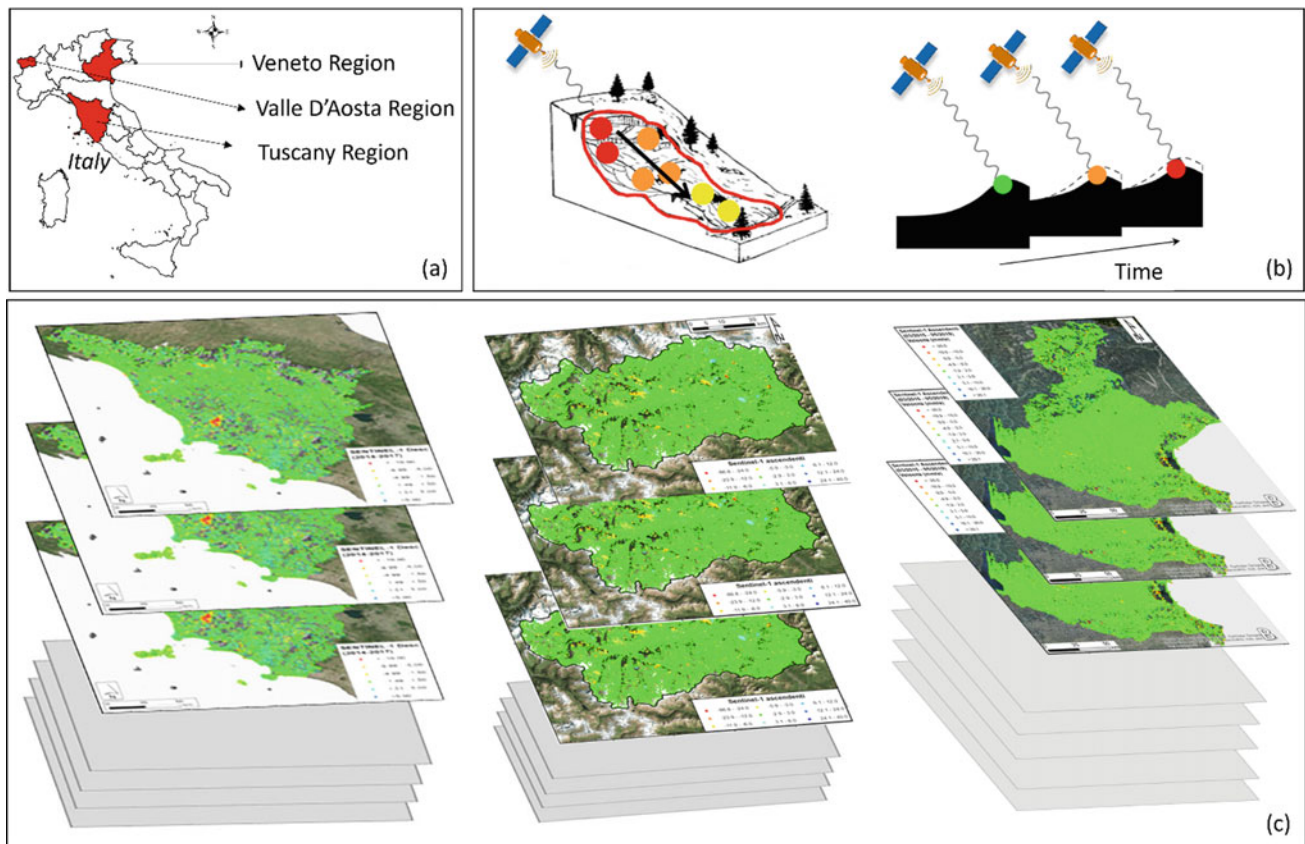


Fig. 2 Satellite-based services at regional scale in Italy: **a** Location of Tuscany, Valle d'Aosta, Veneto Region in Italy; **b** Example of “PS mapping” activity to highlight highest ground motion rates and of “PS

monitoring” activity to periodically scan the territory across time; **c** Sketch of systematically updated ground deformation maps based on Sentinel-1 PSI data of Tuscany, Valle d'Aosta, Veneto Region

This near-real-time monitoring of ground instability at regional scale has demonstrated to be very useful tool as it scans periodically the territory and rapidly points out the fastest deformations and most hazardous sites over the entire regional area. The sites where significant AP are retrieved need to be reported and can be notified to the regional authority for in-situ validation or for further analysis within risk mitigation strategies.

2.3 WP3

WP3 activities focus on developing operational and pre-operational regional scale landslide early warning systems (RLEWS). This objective is achieved by a multiscale approach integrating different methodologies, including statistical rainfall thresholds, landslide susceptibility assessment, and distributed physically based modelling.

To date, statistical rainfall thresholds are the state-of-the-art technique used for RLEWS (Segoni et al. 2018a). ATLaS is active on this topic with several research projects aimed at: (i) developing innovative approaches, as the use of 3D rainfall thresholds that are operated daily by the Emilia Romagna Region Civil Protection (Rosi et al. 2021) (Fig. 3); (ii) transferring consolidated approaches (namely, the models MaCumBA and SIGMA) to new test sites (including developing countries), customizing the model design and RLEWS settings according to the technical constraints and the physical features encountered in the new sites (Abraham et al. 2020a); (iii) hybridizing the rainfall threshold approach with other methodologies such as landslide susceptibility maps, to get a finer spatial resolution (Segoni et al. 2018b) or by integrating slope-scale instrumental monitoring in the rainfall threshold-based RLEWS algorithms to reduce false alarms (Abraham et al. 2020b).

With respect to physically based modelling, to date this approach is used for early warning only at the slope scale or in small areas. In contrast, the efforts of ATLaS are mainly aimed at applying this approach over very wide areas (e.g., hundreds or thousands of square kilometres) to establish prototypal RLEWS for rainfall-induced shallow landslides.

To pursue this objective, a High-Resolution Slope Stability Simulator (HIRESS—Rossi et al. 2013) has been developed and for its implementation, several issues have been addressed. One of the main constraints is the difficulty in coping with the high spatial variability of the values assumed by geotechnical and hydrological parameters like cohesion, internal friction angle, hydraulic conductivity and so on, which are inputs to the slope stability model.

To this end, efforts are continuously accomplished to measure such parameters in as many sample points as possible, assessing the statistical distribution of their values over lithological or geomorphological units and reproducing the

same variability with a Monte Carlo approach when feeding the slope stability model (Tofani et al. 2017; Salvatici et al. 2018).

The research about the input parameters also includes the stabilizing effect exerted by roots systems. To this aim HIR-ESSS formulation has been modified to include the additional root cohesion and studies have been undertaken to characterize how to correctly parameterize this additional factor (Cuomo et al. 2021; Masi et al. 2021). In addition, the application to operational RLEWS demands a robust criterium to interpret the model outputs and to convert them in warnings. The raw outputs of the model, which consists of slope failure probability at the pixel level, are aggregated over larger spatial units (e.g., slope units or small basins) according to a criterium that is necessarily very site specific and dependent on the needs of the end-users. Therefore, a semi-automated tool has been developed to objectively identify the criterium that maximizes the correct predictions while minimizing the errors (Bulzinetti et al. 2021). With these features, it has been possible to apply HIRESS to several Italian test sites ranging from 18 km² to 3500 km² in areal extension, demonstrating a promising potential for a pre-operational use.

The activities pursued in WP3 allow the setting up of RLEWSs with a multi-tier framework: the rainfall thresholds technique allows for warnings differentiated over large alert, while with a combined approach using rainfall thresholds and susceptibility maps the spatial resolution can be refined up to the municipality level (whose width is typically in the order of tens of square kilometres); and finally finer-spatial resolution warnings can be obtained with the physically based modeling, which starts from landslide triggering probabilities at the pixel level (typically, 10 m cell size) which are aggregated to issue warnings over spatial units whose extension is typically on the order of 1 km².

3 IPL Projects

Since its involvement in ICL, the UNESCO Chair has proposed several IPL projects. Currently, the active projects are:

- IPL196: Development and applications of a multi-sensors drone for geohazards monitoring and mapping, Proposer: Veronica Tofani
- IPL198: Multi-scale rainfall triggering models for Early Warning of Landslides (MUSE), Proposer: Filippo Catani
- IPL 221: PS continuous streaming for landslide monitoring and mapping, Proposer: Federico Raspini and Silvia Bianchini

IPL 196 has the objective to test the applicability of a multi-sensors drone for the mapping and monitoring of geohazards. In particular, the project has two specific

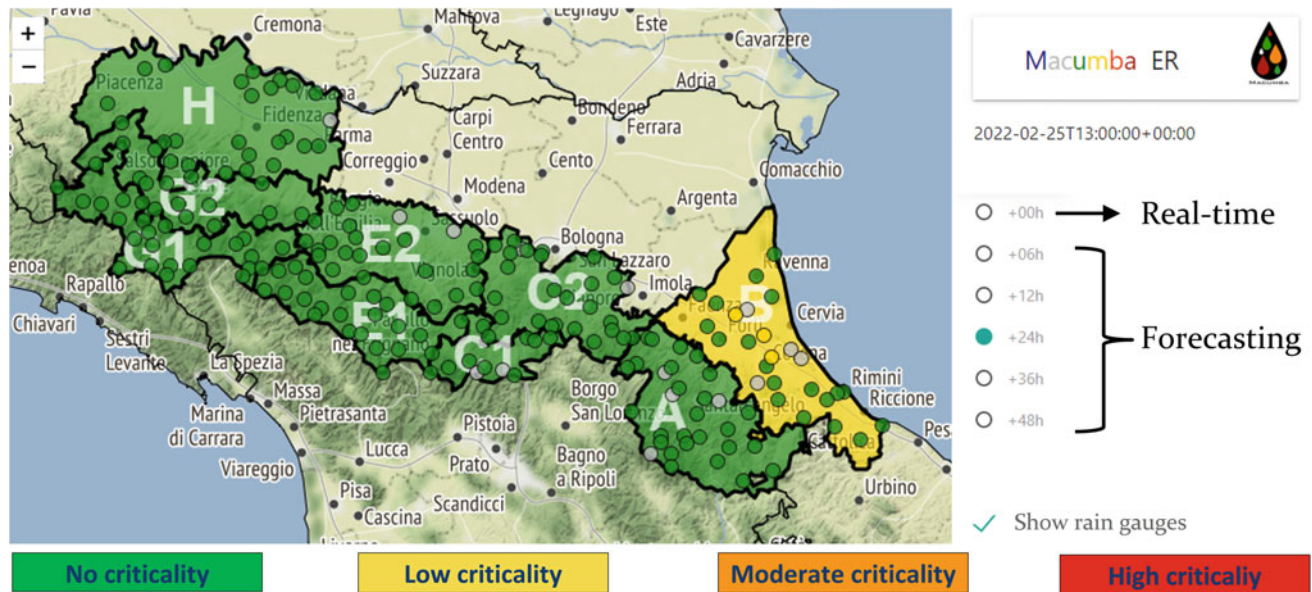


Fig. 3 Overview of the web interface of the RLEWS based on 3D rainfall thresholds, which is currently operated in the hilly and mountainous sectors of Emilia Romagna region

objectives: (i) development of the drone, sensors, safety and automation and (ii) application of the drone as a platform of integrated sensors (multispectral sensor, visible light camera, infrared camera and LIDAR) for the mapping and monitoring of geohazards.

IPL 198 aims at the enhancement of knowledge and methodologies related to the integration of landslide prediction models at different scales to build an effective operational multi-scale system for real-time early warning of rainfall triggered mass movements.

The objective of IPL 221 is to perform the transition from historical analysis of radar satellite image archives to real-time monitoring of ground deformation at regional scale using radar satellite scenes. To accomplish this objective, the short revisiting time and regularity of acquisitions of Sentinel-1 constellation of SAR (Synthetic Aperture Radar) satellite sensors were exploited.

The activity reports are regularly published in the ICL IPL website, while their outcomes have been published in the *Landslides* journal (IPL-196, Rossi et al. 2018; IPL-198, Tofani et al. 2017; IPL-221, Raspini et al. 2019).

4 Contribution to Kyoto 2020 Commitment

As a member of the International Consortium on Landslides (ICL) the UNESCO Chair is signatory of the ISDR-ICL Sendai Partnership 2015–2025 (Sassa 2015). The Sendai Partnership was accepted and signed during the 3rd United Nations World Conference on Disaster Risk Reduction (WCDRR) in Sendai (March 11-15th 2015). During the

4th World Landslide Forum (WLF4), held in Ljubljana from May 29-June 2 2017, the Chair has contributed to the “Ljubljana Declaration” on Landslide Risk Reduction, together with all of the participants to the forum, as a further commitment on the part of the global landslide community to the Sendai Framework for Disaster Risk Reduction 2015–2030 (Sassa 2017).

The Chair has been signatory and promoter of the Kyoto 2020 Commitment (KLC2020) for global promotion of understanding and reducing landslide disaster risk, during the 2019 ICL-IPL Conference at UNESCO Headquarters, Paris, on 16–19 September 2019. The Kyoto 2020 Commitment is a duty to the Sendai Landslide Partnerships 2015–2025, the Sendai Framework for Disaster Risk Reduction 2015–2030, the 2030 Agenda Sustainable Development Goals, the New Urban Agenda, and the Paris Climate Agreement (Sassa 2019).

The UNESCO Chair, in line with the activity carried out in the framework of the WCoE and IPL projects, will particularly contribute to some priority actions of Kyoto 2020 Commitment (Sassa 2018c):

Action 1: Promote the development of people-centered early warning technology for landslides with increased precision and reliable prediction both in time and location, especially in a changing climate context.

Action 2: Advance hazard and vulnerability mapping, including vulnerability and risk assessment with increased precision, as well as reliability as part of multi-hazard risk identification and management.

Action 3: Improve the technologies for monitoring, testing, analyzing, simulating, and effective early warning for

landslides suitable for specific regions considering natural, cultural, and financial aspects.

Action 6: Investigate the effect of climate change on rainfall-induced landslides and promote the development of effective rainfall forecasting models to provide earlier warning and evacuation especially in developing countries.

Action 9: Foster new initiatives to study research frontiers in understanding and reducing landslide disaster risk by promoting joint efforts by researchers, policy makers and funding agencies.

In the framework of the contribution to policies for risk reduction, the UNESCO Chair contributed to the organization of the 5th World Forum on landslides (WLF5), which due to the COVID-19 pandemic was held in mixed virtual and in-person mode from November 2–6, 2021 in Kyoto (Japan) (Fig. 5).

The UNESCO Chair is currently organizing the 6th World Landslide Forum, which will be held in Florence from the 14th to the 17th of November 2023 (Fig. 4). The Forum will have the theme “Landslide Science for Sustainable Development.” The event is jointly organized by the International Consortium on Landslides (Kyoto, Japan), the International Programme on Landslides (IPL) and the UNESCO Chair on Prevention and Sustainable Management of Geohydrological Hazards at the University of Florence.

The Forum is focused on Landslide Science for Sustainable Development, as a contribution to the Kyoto 2020 Commitment for global promotion of understanding and reducing landslide disaster risk (KLC2020).

The aim of the Forum is to provide a platform to achieve a fruitful cooperation among landslide researchers to define

shared priority actions for landslide risk reduction on a global scale. The Forum will deal with the main aspects related to landslide analysis: landslide monitoring and early warning, landslide modelling, landslide hazard and risk assessment, mitigation techniques, landslide triggering mechanism and climate change. In line with the 2030 Agenda and the Sustainable Development Goals, the Forum will be a sustainable event. The Forum is hosted in Florence city center, with everything at walking distance and no printed material. The Forum programme and proceedings will be distributed to the participants in electronic format.

The Forum will focus on 6 main themes:

- Theme 1: Kyoto Landslide Commitment for sustainable development
- Theme 2: Remote sensing, monitoring and early warning
- Theme 3: Testing, modeling, and mitigation techniques
- Theme 4: Mapping, hazard, risk assessment and management
- Theme 5: Climate change, extreme weather, earthquakes, and landslides
- Theme 6: Progress in landslide science and applications

5 ICL Italian Network

The ICL Italian network was officially established in December 2018 during the ICL-IPL Conference, held in Kyoto on 1–4 December 2018. ICL Italian network, proposed and coordinated by the UNESCO Chair on Prevention

Fig. 4 Home page of the 6th World Landslide Forum Website (<https://wlf6.org>)



and Sustainable Management of Geo-hydrological hazards, currently counts 13 ICL members (7 Full members, 5 Associates and 1 Supporter) (Casagli and Tofani 2018).

The general objective of the Italian ICL Network is to contribute at a national level to the Sendai Partnership for Disaster Risk Reduction 2015–2025 for the national promotion of understanding, prevention and sustainable management of landslide risk disaster, for the safety of human life, society and the environment and to the Kyoto Commitment 2020 for Global Promotion of Understanding and Reducing Landslide Disaster Risk.

The Italian ICL network on landslides is formed by well-established scientific institutions, recognized both at national and international levels, with a long-dated expertise on landslide research for hydrogeological hazard assessment and landslide disaster risk reduction. The network partners have also developed strong and widespread synergies with national, regional and local administrations, technical stakeholders, and end-users for developing policies and procedures for landslide disaster prevention, management and mitigation.

On March 26, 2021, a virtual meeting of the Italian Network of ICL took place. During the meeting, the activities carried out by ICL were discussed with reference to the organization of WLF5 and WLF6. It was also discussed how to improve networking activities between the Italian partners of ICL through the strengthening of joint research and training activities. During the meeting, Dr. Claudio Margottini was appointed as coordinator of the Italian Network for the next three years.

References

- Abraham MT, Satyam N, Kushal S, Rosi A, Pradhan B, Segoni S (2020a) Rainfall threshold estimation and landslide forecasting for Kalimpong India Using SIGMA model. *Water* 12(4):1195
- Abraham MT, Satyam N, Bulzinetti MA, Pradhan B, Pham BT, Segoni S (2020b) Using field-based monitoring to enhance the performance of rainfall thresholds for landslide warning. *Water* 12(12):3453
- Bardi F, Raspini F, Frodella W, Lombardi L, Nocentini M, Gigli G, Morelli S, Corsini A, Casagli N (2017) Monitoring the rapid-moving reactivation of earth flows by means of GB-InSAR: the April 2013 Capriglio landslide (Northern Apennines, Italy). *Remote Sens* 9(2):165
- Bianchini S, Raspini F, Solari L, Del Soldato M, Ciampalini A, Rosi A, Casagli N (2018) From picture to movie: twenty years of ground deformation recording over Tuscany region (Italy) with satellite InSAR. *Frontiers Earth Sci*, 177
- Bianchini S, Solari L, Bertolo D, Thuegaz P, Catani F (2021) Integration of satellite interferometric data in civil protection strategies for landslide studies at a regional scale. *Remote Sens* 13(10):1881
- Bulzinetti MA, Segoni S, Pappafico G, Masi EB, Rossi G, Tofani V (2021) A tool for the automatic aggregation and validation of the results of physically based distributed slope stability models. *Water* 13(17):2313
- Carlà T, Intrieri E, Di Traglia F, Nolesini T, Gigli G, Casagli N (2017) Guidelines on the use of inverse velocity method as a tool for setting alarm thresholds and forecasting landslides and structure collapses. *Landslides* 14(2):517–534
- Carlà T, Tofani V, Lombardi L, Raspini F, Bianchini S, Bertolo D, Thuegaz P, Casagli N (2019a) Combination of GNSS, satellite InSAR, and GBInSAR remote sensing monitoring to improve the understanding of a large landslide in high alpine environment. *Geomorphology* 335:62–75
- Carlà T, Nolesini T, Solari L, Rivolta C, Dei Cas L, Casagli N (2019b) Rockfall forecasting and risk management along a major transportation corridor in the Alps through ground-based radar interferometry. *Landslides* 16:1425–1435
- Carlà T, Gigli G, Lombardi L, Nocentini M, Carlà T (2021) Monitoring and analysis of the exceptional displacements affecting debris at the top of a highly disaggregated rockslide. *Eng Geol* 294:106345
- Casagli N, Frodella W, Morelli S, Tofani V, Ciampalini A, Intrieri E, Raspini F, Rossi G, Tanteri L, Lu P (2017) Spaceborne, UAV and ground-based remote sensing techniques for landslide mapping, monitoring and early warning. *Geoenviron Disasters* 4(9):27p
- Confuorto P, Del Soldato M, Solari L, Festa D, Bianchini S, Raspini F, Casagli N (2021) Sentinel-1-based monitoring services at regional scale in Italy: state of the art and main findings. *Int J Appl Earth Obs Geoinf* 102:102448
- Crosta GB, Agliardi F (2003) Failure forecast for large rockslides by surface displacement measurements. *Can Geotech J* 40:176–191
- Crosta GB, Agliardi F, Rivolta C, Alberti S, Dei Cas L (2017) Long-term evolution and early warning strategies for complex rockslides by real-time monitoring. *Landslides* 14:1615–1632
- Cuomo S, Masi EB, Tofani V, Moscariello M, Rossi G, Matano F (2021) Multiseasonal probabilistic slope stability analysis of a large area of unsaturated pyroclastic soils. *Landslides* 18(4):1259–1274
- Del Soldato M, Riquelme A, Bianchini S, Tomàs R, Di Martire D, De Vita P, Moretti S, Calcaterra D (2018) Multisource data integration to investigate one century of evolution for the Agnone landslide (Molise, southern Italy). *Landslides* 78:2387–2408
- Di Traglia F, Nolesini T, Ciampalini A, Solari L, Frodella W, Bellotti F, Fumagalli A, De Rosa G, Casagli N (2018) Tracking morphological changes and slope instability using spaceborne and ground-based SAR data. *Geomorphology* 300:95–112
- Ferretti A, Fumagalli A, Novali F, Prati C, Rocca F, Rucci A (2011) A new algorithm for processing interferometric data-stacks: SqueeSAR. *IEEE Trans Geosci Remote Sens* 49:3460–3470
- Frodella W, Ciampalini A, Bardi F, Salvatici T, Di Traglia F, Basile G, Casagli N (2018) A method for assessing and managing landslide residual hazard in urban areas. *Landslides* 15:183–197
- Frodella W, Gigli G, Morelli S, Lombardi L, Casagli N (2017) Landslide mapping and characterization through infrared thermography (IRT): suggestions for a methodological approach from some case studies. *Remote Sens* 9(12):1281
- Masi EB, Segoni S, Tofani V (2021) Root reinforcement in slope stability models: a review. *Geosci* 11(5):212
- Raspini F, Bianchini S, Ciampalini A, Del Soldato M, Solari L, Novali F, Del Conte S, Rucci A, Ferretti A, Casagli N (2018) Continuous, semi-automatic monitoring of ground deformation using sentinel-1 satellites. *Sci Rep* 8(1):1–11
- Raspini F, Bianchini S, Ciampalini A, Del Soldato M, Montalti R, Solari L, Casagli N (2019) Persistent scatterers continuous streaming for landslide monitoring and mapping: the case of the Tuscany region (Italy). *Landslides* 16(10):2033–2044
- Rosi A, Segoni S, Canavesi V, Monni A, Gallucci A, Casagli N (2021) Definition of 3D rainfall thresholds to increase operative landslide early warning system performances. *Landslides* 18(3):1045–1057

- Rossi G, Catani F, Leoni L, Segoni S, Tofani V (2013) HIRESSS: a physically based slope stability simulator for HPC applications. *Nat Hazards Earth Syst Sci* 13:151–166
- Rossi G, Tanteri L, Tofani V, Vannocci P, Moretti S, Casagli N (2018) Multitemporal UAV surveys for landslide mapping and characterization. *Landslides* 15(5):1045–1052
- Salvatici T, Tofani V, Rossi G, D'Ambrosio M, Tacconi Stefanelli C, Masi EB, Rosi A, Pazzi V, Vannocci P, Petrolo M, Catani F, Ratto S, Stevenin H, Casagli N (2018) Application of a physically based model to forecast shallow landslides at a regional scale. *Nat Hazard* 18(7):1919–1935
- Sassa K (2015) ISDR-ICL Sendai Partnerships 2015–2025 for global promotion of understanding and reducing landslide disaster risk. *Landslides* 12(4):631–640
- Sassa K (2017) The 2017 Ljubljana declaration on landslide risk reduction and the Kyoto 2020 commitment for global promotion of understanding and reducing landslide disaster risk. *Landslides* 14(4):1289–1296
- Sassa K (2018a) Zero draft of the Kyoto 2020 commitment for global promotion of understanding and reducing landslide disaster risk. *Landslides* 15(3):389–392
- Sassa K (2018b) The Fifth world landslide forum—implementing and monitoring the ISDR-ICL Sendai partnerships 2015–2025 - organization plans, themes and sessions. *Landslides* 15(3):617–620
- Sassa K (2018c) ICL journal “Landslides” and the Kyoto 2020 commitment. *Landslides* 15(9):1705–1712
- Sassa K (2019) The fifth world landslide forum and the final draft of the Kyoto 2020 commitment. *Landslides* 16(2):201–221
- Segoni S, Piciullo L, Gariano SL (2018a) A review of the recent literature on rainfall thresholds for landslide occurrence. *Landslides* 15(8):1483–1501
- Segoni S, Tofani V, Rosi A, Catani F, Casagli N (2018b) Combination of rainfall thresholds and susceptibility maps for dynamic landslide hazard assessment at regional scale. *Front Earth Sci* 6:1–11
- Solari L, Del Soldato M, Raspini F, Barra A, Bianchini S, Confuorto P, Casagli N, Crosetto M (2020) Review of satellite interferometry for landslide detection in Italy. *Remote Sensing* 12(8):1351
- Tofani V, Bicocchi G, Rossi G, Segoni S, D'Ambrosio M, Casagli N, Catani F (2017) Soil characterization for shallow landslides modeling: a case study in the Northern Apennines (Central Italy). *Landslides* 14(2):755–770

Open Access This chapter is licensed under the terms of the Creative Commons Attribution 4.0 International License (<http://creativecommons.org/licenses/by/4.0/>), which permits use, sharing, adaptation, distribution and reproduction in any medium or format, as long as you give appropriate credit to the original author(s) and the source, provide a link to the Creative Commons license and indicate if changes were made.

The images or other third party material in this chapter are included in the chapter's Creative Commons license, unless indicated otherwise in a credit line to the material. If material is not included in the chapter's Creative Commons license and your intended use is not permitted by statutory regulation or exceeds the permitted use, you will need to obtain permission directly from the copyright holder.





Strengthening the Resilience by Implementing a Standard for Landslide Early Warning System

Teuku Faisal Fathani, Dwikorita Karnawati, Wahyu Wilopo,
and Hendy Setiawan

Abstract

The implementation of early warning systems is in line with the Sendai Framework for Disaster Risk Reduction (SFDRR) 2015–2030. The Sendai Framework Priority 4 emphasizes improvement of preparedness and anticipation of disasters by establishing communities' resilience to disaster. The development of a simple, low-cost early warning system that is universally accessible is needed to achieve the goals of the Sendai Framework. Universitas Gadjah Mada, incorporated with the Indonesian Standardization Agency (BSN) and the Indonesian Disaster Management Authority (BNPB), has promoted a new standard for community-based landslide early warning systems to the International Organization for Standardization (ISO). This standard, published as ISO 22327:2018, empowers individuals and communities vulnerable to landslides to act in sufficient time, and in appropriate ways to reduce the possibility of injuries, loss of life, and damage to property and the environment. It is designed to encourage communities to play a more active role in their own protection. ISO 22327:2018 adopts the concept of a people-centered early warning system by UNISDR (2006) to be used by communities vulnerable to landslides, and by government and non-governmental organizations at central, provincial, districts, sub-district, and village levels.

Keywords

Risk assessment • Monitoring and warning technology • Risk communication • Disaster response

1 Introduction

Indonesia is geologically complex, being at the junction of three major active plates: Eurasia, Indo-Australian, and Pacific. Although this setting richly endows Indonesia with natural resources, it also makes the country prone to disasters such as volcano eruptions, earthquakes, tsunamis, landslides, floods, liquefaction, and flows. Plate movement, active faults, volcanic activities, weathering rates, and heavy rainfall all influence hazard occurrences in Indonesia.

The Indonesian Disaster Management Authority (BNPB) data shows that the number of disaster events in Indonesia increased significantly from 2010 to 2019, as shown in Fig. 1 (BNPB 2020). In 2019, 9391 disasters occurred and leading to 911 people dead or missing, 2163 injured, and 5372 million people directly affected and displaced. Landslides were ranked fourth after wildfire, tornadoes, drought as the most frequent disasters in 2019.

Landslides are widespread and frequently occur around the world. The natural phenomenon is controlled by slope condition, geology, geological structures, land use of slopes, and they are triggered by heavy rainfall or earthquakes. Landslides can cause significant losses and damages when occurring in highly populated areas. Intensive development in susceptible areas increases disaster risks. On the other hand, knowledge and ability of the community to implement disaster mitigation in general are low.

The intensity of landslide occurrence in Indonesia during the past decade has increased and disaster areas are more widespread, as illustrated in Fig. 2. This is a consequence of the increase in non-eco-friendly land use, high rainfall intensity with a long duration, and an increase in frequency

T. F. Fathani (✉)

Department of Civil and Environmental Engineering, Universitas Gadjah Mada, Jl. Grafika 2, Yogyakarta, 55281, Indonesia
e-mail: tfathani@ugm.ac.id

D. Karnawati

Meteorological, Climatological, and Geophysical Agency,
Jl. Angkasa 1 No.2 Kemayoran, DKI Jakarta, 10610, Indonesia

W. Wilopo · H. Setiawan

Department of Geological Engineering, Universitas Gadjah Mada,
Jl. Grafika 2, Yogyakarta, 55281, Indonesia

© The Author(s) 2023

K. Sassa et al. (eds.), *Progress in Landslide Research and Technology, Volume 1 Issue 1, 2022*,
Progress in Landslide Research and Technology, https://doi.org/10.1007/978-3-031-16898-7_20

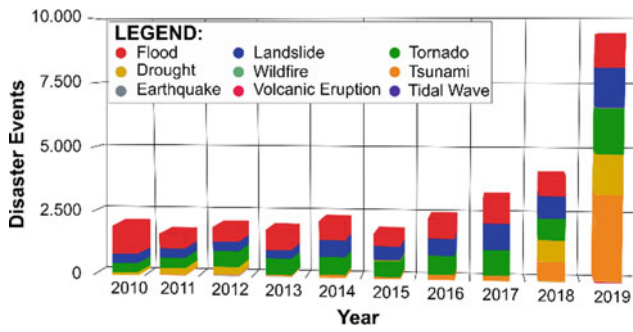


Fig. 1 Disaster events in Indonesia in 2010–2019 (BNPB 2020)

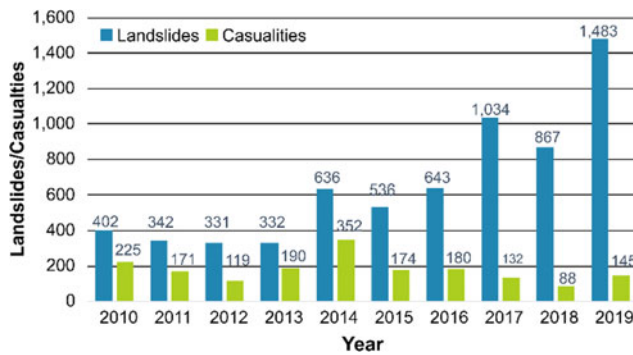


Fig. 2 Data on landslides and casualties from 2010–2019 (BNPB 2020)

of earthquake occurrence. Most areas susceptible to landslides are fertile lands with abundant groundwater, on which settlement areas, farmlands, and paddy fields have been developed, with construction of essential supporting infrastructure. Substantial regions of high landslide susceptibility are found in the mountain belt of Indonesia, for example in

Bukit Barisan. Susceptible terrain is extensively developed in these remote rural areas. Consequently, relocating settlements and infrastructure is not easy, and may be very costly. Susceptible conditions and other factors such as density and population, infrastructures and building conditions, economic level, and regional capacity, contribute to an area's risk level (Hufschmidt et al. 2005; Crozier and Glade 2005).

About 108.8 million people live in moderately to highly landslide susceptible zones, out of which 15.2 million live in highly susceptible zones in 228 districts in Indonesia (BNPB 2020). In 2019, there were 1483 landslides in Indonesia that involved 145 casualties, 9473 affected people, and major economic, physical, and environmental losses. As almost every region in Indonesia has a high potential of landslides, a collective effort to strengthen mitigation capability, risk reduction, and disaster management is greatly needed.

According to landslide hazard map (Fig. 3), the areas with high risk to landslides are those in the western parts of Sumatera Island, along the Bukit Barisan mountain belt; the southern and central parts of Java Island, Bali, Nusa Tenggara, almost every part of Sulawesi Island, Maluku, the southern and central parts of Papua. The total number of people affected by landslide risk in Indonesia is 194 million, with the potential loss of USD 13 billion (BNPB 2019).

2 Disaster Management Policy and Strategy

Due to the high propensity of the country to disasters, the Indonesian government is committed to reducing disaster risk by placing disaster risk reduction as one of the national development priorities. National policies in disaster management started to receive attention following the tsunami and earthquake in Aceh and Nias at the end of 2004.

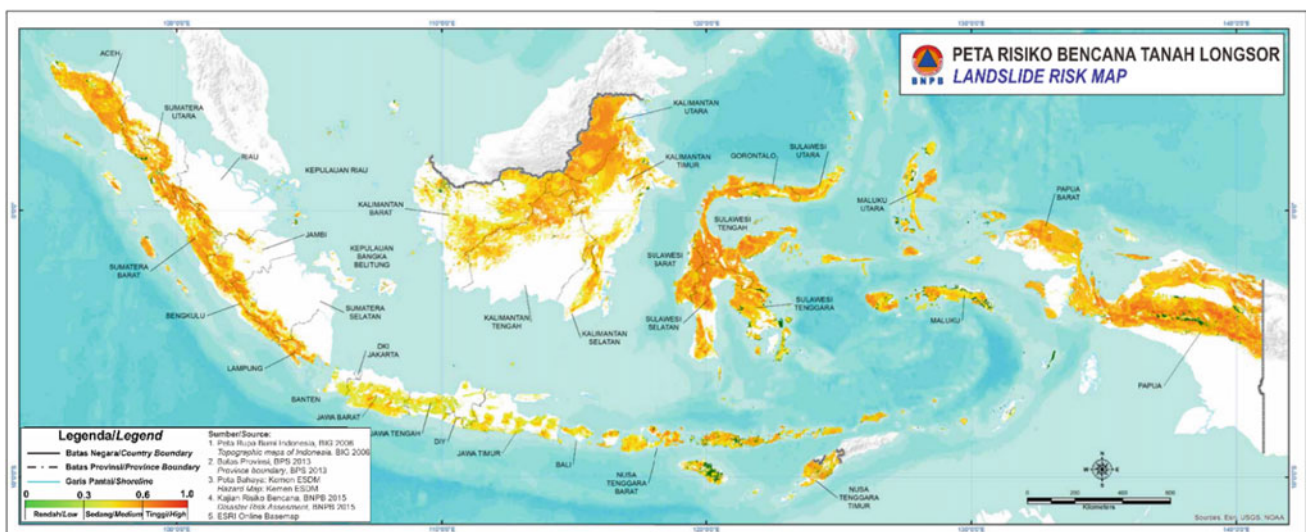


Fig. 3 Landslide hazard map of Indonesia (BNPB 2019)

The enactment of Law No 24 of 2007 on Disaster Management and its Government Regulation, established the National Disaster Management Agency (BNPB) at the national level and the Regional Disaster Management Agency (BPBD) at provincial and district levels.

Paradigm shifts in disaster management have been implemented, namely: (1) from response-oriented approach *to* mitigation-oriented strategy, (2) from sectoral approach *to* multi-sectoral approach, (3) from government responsibility *to* collective responsibility, (4) from centralization *to* decentralization, and (5) from being emergency response-oriented *to* becoming disaster risk reduction oriented (Bappenas 2014).

As one of the strategic environmental priorities, the National Mid-Term Development Plan (RPJMN) 2015–2019 specified that disaster management integrates policies and Disaster Risk Reduction (DRR) strategies with global climate change adaptation. To this end, the Disaster Management Strategies are focused on: (1) the internalization of DRR in the framework of sustainable development at the national and regional level; (2) the reduction of disaster vulnerability level; and (3) capacity building of disaster management implementation (Bappenas 2014).

The consistency of the government and other stakeholders, including universities, is necessary to formulate and realize disaster management strategies. The Disaster Management National Plan (Renas-PB, 2010–2014) evaluation shows that the general activities for all hazards ran well. However, specific activities for each hazard did not perform as well as the general activities. Accordingly, in 2014, Universitas Gadjah Mada contributed to developing the landslides risk reduction masterplan in Renas-PB 2015–2019 and directly instituted the disaster management action plan in Indonesia (BNPB 2014).

Disaster management measures are a tremendous challenge and responsibility that should be carried out with a sustainable, measured, and structured strategy. Over the last decade, Indonesia has learned many important lessons in disaster management. It has implemented numerous changes, particularly by establishing a disaster management system emphasizing disaster risk reduction.

One of the most effective mitigation measures is the implementation of an early warning system with appropriate technologies. The disaster management strategy begins with risk assessment and mapping to determine high risk areas and countermeasure priority, followed by the utilization of various numerical modellings to predict disaster impacts and mechanisms. The next step is to determine the most appropriate structural or non-structural disaster management method. This strategy has been accepted as a national standard in Indonesia and an international guideline for disaster risk reduction around the world (Fathani 2019). It has been implemented in Myanmar and in 33 provinces, 124 cities/

districts in Indonesia, involving the national government, the local government, the local universities and private sectors, and local communities.

3 Development of Landslide Early Warning System

Landslide countermeasures can be conducted structurally or non-structurally. Structural countermeasures include modification of slope geometry, slope reinforcement and retention, drainage management, and relocation to safer areas for people living in high-risk areas (red zones). Non-structural mitigation focuses on community knowledge and preparedness, improving institutional capacity building, all supported by policies and regulations. Every disaster event is unique as it occurs under different geomorphology-geology-geotechnical conditions. Thus, it is not appropriate to apply the same countermeasure method to every case. Risk assessment is the key to planning the appropriate countermeasure technologies and methods (Karnawati et al. 2013).

Structural and environmental conservation are crucial as the only measures that prevent or reduce potential disaster risk. However, implementing these types of measure is very costly. One such mitigation measure is to relocate people living in landslide susceptible areas to safer terrain. This is a challenge because of the large population numbers often involved, resistance from settled people (i.e., the cultural-economic-socio aspect), and budget limitations. Therefore, an effective disaster risk reduction measure implemented under this condition is a nonstructural mitigation: improving community preparedness by installing a landslide monitoring system.

Universitas Gadjah Mada (UGM) has developed a simple early warning system in collaboration with BNPB and Ministry of Village, Development of Disadvantaged Regions, and Transmigration (KPDRT) that has been operating since 2006. The development of the landslide monitoring technology began when imported landslide monitoring devices were installed in Kulon Progo District in 2000–2002. Unfortunately, these monitoring systems were easily damaged, and with repair needing to be performed abroad, functionality was difficult to maintain.

Unfortunately, people living in high-risk areas typically have poor education, are in middle to lower economic classes, and have limited knowledge and resources for maintenance of monitoring systems and accessible community infrastructure (Fathani et al. 2014). For this reason, UGM has developed more exciting, engaging, and understandable low-cost and simple disaster risk reduction tools. The monitoring systems use local materials and incorporate observations of landslides and other natural disasters, and are directly managed by impacted communities.

The first-generation monitoring systems were an extensometer and a manually recorded rain gauge. Both were designed with the goal that communities could independently produce and repair these monitoring tools. Extensometers and rain gauges were installed in Banjarnegara District and Situbondo District in 2007, then in Karanganyar District in 2008. The manufacturing of these tools involved small and medium size enterprises in Central Java Province and the Special Region of Yogyakarta. Early warning included not only the installation of monitoring tools, but also a technical and cultural-economic-socio assessment that enabled communities to understand the function of the installed systems, and how to independently operate and maintain them (Karnawati et al. 2011; Fathani et al. 2014).

4 Implementation of Disaster Early Warning System

4.1 Establishment of a Landslide Early Warning System

Research in landslide early warning systems keeps evolving, with various generations of early detection tools under development. Landslide early warning systems are installed in the Sumatera, Java, Kalimantan, Sulawesi, and Papua districts. Funding comes not only from the government, but also from several mining and energy companies. Nevertheless, many issues remain. For example, non-optimal

supporting infrastructure and sensors, stolen and poorly maintained tools limit reliability and utility. Accordingly, the UGM team developed a strategy for the early warning system implementation that incorporates nontechnical and technical aspects to the installation. This multidisciplinary approach involved engineering, sociology, anthropology, psychology, economics, and agriculture (Karnawati et al. 2013; Fathani and Karnawati 2018).

Incorporating multidisciplinary technical and social approaches enriches the early warning system concept. A seven sub-system approach begins with: (1) risk assessments, (2) information dissemination, and (3) establishment of disaster preparedness teams. These initial stages are followed by: (4) development of evacuation route maps and (5) development of Standard Operating Procedures (SOP). Next comes (6) the installation of the early warning systems and evacuation drills, and lastly, (7) the establishment of commitments between communities, village councils, and district governments on the operation and maintenance of early warning systems that guarantee the sustainability of installed systems (Fathani et al. 2016, 2017). It is not necessary for evacuation route maps to conform with cartographic rules, so long as they are understandable to the communities affected (Fathani and Legono 2011; Karnawati et al. 2018; Setiawan et al. 2021).

Student Community Services are also involved in the implementation of landslide early warning systems at numerous sites in Indonesia such as Karanganyar District, Banjarnegara District, Banyumas District, Boyolali District, Sumatera Barat Province, and others (Fig. 4).

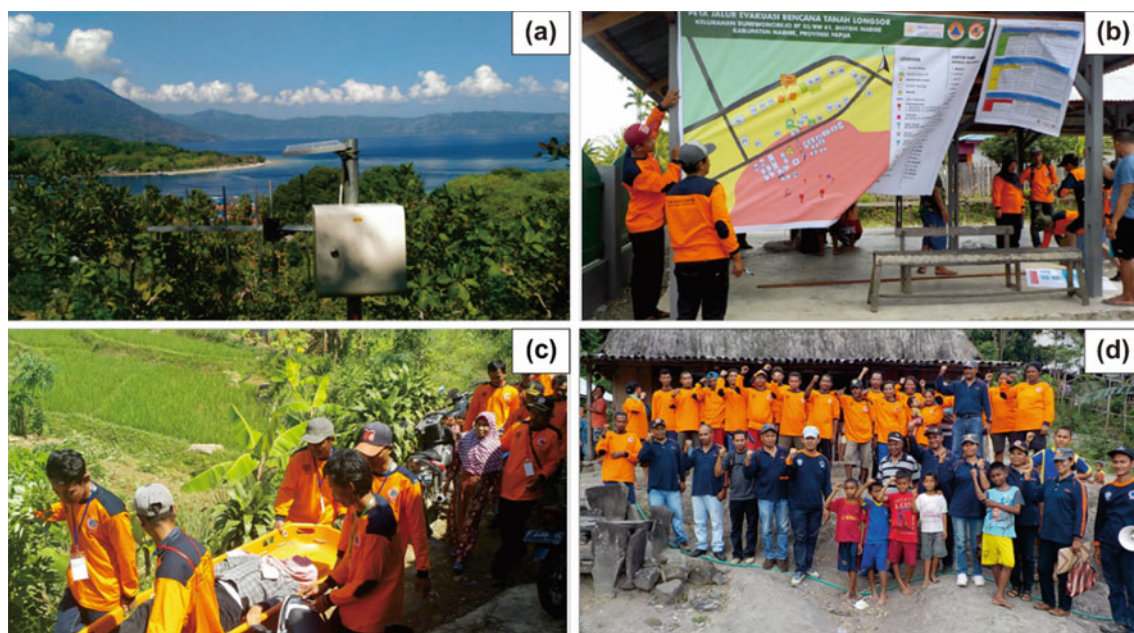


Fig. 4 a Installation of extensometer; b A community landslide evacuation map; c Evacuation drill; d The local disaster preparedness team and UGM facilitator team

5 Gajah Mada Early Warning System (GAMA-EWS)

GAMA-EWS is designed to monitor, detect, and give early warning for sedimentary disasters such as landslides, floods, flash floods, and debris flows. The system comprises of an extensometer (a lateral, vertical, or rotational ground movement detection tool), tiltmeter (instruments used to measure ground tilt in slopes), inclinometer (instruments used to measure displacement in slip surface), and ultrasonic sensor (instruments used to measure the change in water level) integrated and connected into one field server.

The current system is the 7th generation of GAMA-EWS since the innovation was developed in 2006. By 2020, about 40 variants of detection tools, namely the extensometer (upper/underground), crackmeter, tiltmeter, inclinometer, rain gauge, ultrasonic water level sensor, and groundwater sensor were developed. These early warning tools, manufactured with appropriate technologies, use 90% local components and manufactured by PT. GAMA-InaTEK as a subsidiary of UGM.

This process involves small and medium enterprises in the Special Region of Yogyakarta and Central Java Province. Manufacturing and design are monitored by the Center of Excellence of Technological Innovation for

Disaster Mitigation UGM (PUI GAMA-InaTEK). The information on disaster early warning systems received by local authorities and the community is delivered in real-time via sirens, speakers, SMS blasting, email, website hosted on the GSM network, Wi-Fi, radio frequency, and via satellite.

The main components of GAMA-EWS are: (1) multiple sensors to monitor and collect field data; (2) a server and online system to receive and process the data; and (3) a warning system to improve the community preparedness in disaster emergencies, as illustrated in Fig. 5. All components work automatically through a telemetry system that has an independent energy source (solar panel) and operates wirelessly. Therefore, the early warning system can work effectively, particularly in remotely located hazard areas. GAMA-EWS has several advantages: it is easy to install, has flexible trusses, does not need electricity supply from PLN (using solar energy), and is easy to operate and maintain.

By 2021, GAMA-EWS has been installed in 33 provinces, 124 districts, and more than 500 villages in Indonesia. The implementation of the system is a collaboration between UGM and several institutions such as BNPB, BPBD, KPDTT, and in cooperation with numerous mining and energy companies, as shown in Fig. 6. In addition, the GAMA-EWS detection tools and early warning system have been implemented outside Indonesia, for example, in Myanmar.

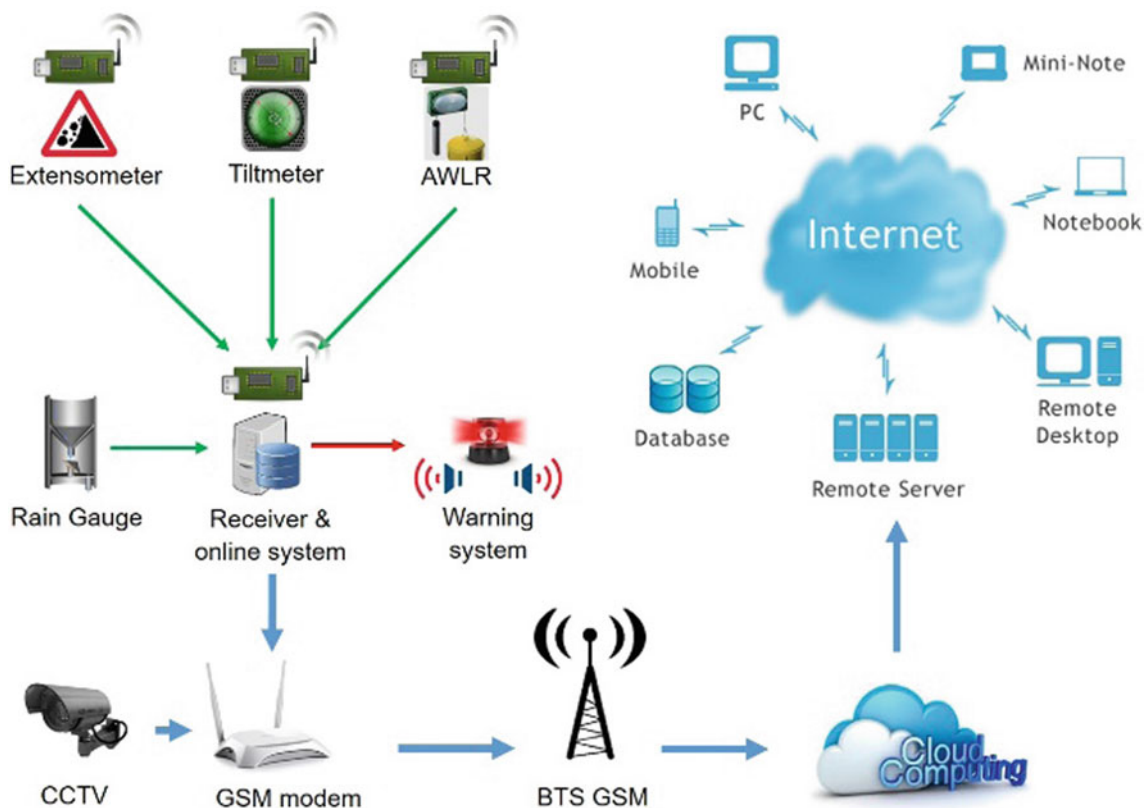


Fig. 5 Detection of hazard zone and early warning information flow

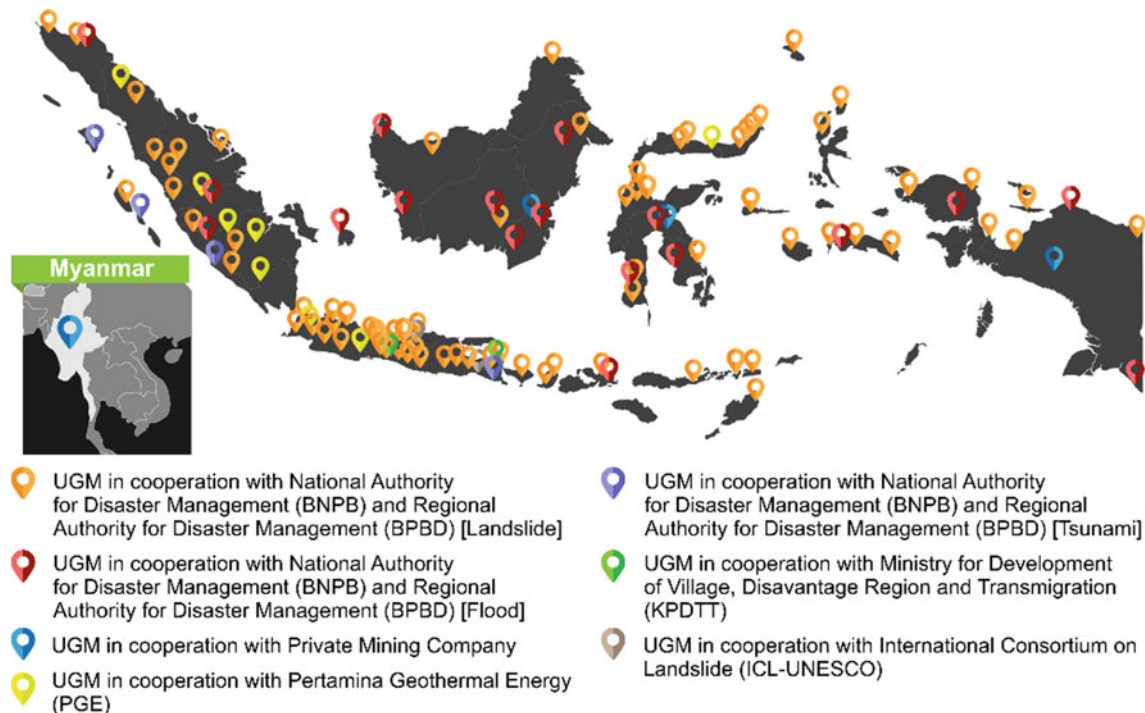


Fig. 6 Locations of landslides and floods early warning system implementation (2007–2021)

In addition to the landslide early warning system, GAMA-EWS has also developed early warning systems for floods, flash floods, and debris flows implemented in numerous regions of Indonesia (Fathani and Legono 2013). The implementation of the early warning system is conducted through the UGM thematic Student Community Service and involves local universities and communities as the subject and the object of the activity. For the implementation of the system, the national, regional, and village governments, as well as local communities play significant roles in the operation and maintenance of their early warning systems.

6 Formulation of International and National Standard

6.1 Indonesian Standard of SNI 8235:2017 on Landslide Early Warning System

According to UN-ISDR (2006), an effective and comprehensive early warning system comprises four interconnected key elements: (1) risk knowledge; (2) warning service and monitoring technology; (3) communication and dissemination; and (4) response-ability. The challenge is not in technology development; rather it is in their implementation, which involves communities living in the vulnerable areas,

and coordination between all levels of government, the private sector, and other stakeholders.

Consequently, UGM has developed a sediment disaster early warning system that integrates the social and technical systems that have effectively worked through the installation, operational, and maintenance phases. Referring to the four key elements above, UGM, supported by BNPB and BSN, developed a pragmatic landslide early warning system. This system comprises seven main activities: (1) Risk assessment, (2) Dissemination and communication on disaster knowledge, (3) Establishment of a disaster preparedness team, (4) Development of an operational evacuation manual, (5) Building a practical SOP, (6) Developing an evacuation drill, monitoring and early warning technology, and (7) Building the commitment of local authorities and communities to operate and maintain all components of the landslide early warning system (Fathani et al. 2016; 2017).

7 ISO 22327:2018 on Community Based Landslide Early Warning System

Indonesia, through BNPB, is a Center of World Excellence in Disaster Risk Reduction. Consequently, BNPB and UGM have encouraged the landslide early warning SNI to be adopted as an international standard (ISO) global guideline. In the 2nd Plenary Meeting ISO/Technical Committee

(ISO/TC) 292 in Bali in December 2015, Indonesia officially proposed the landslide early warning SNI draft to be ISO 22327 entitled *Guidelines for Implementing Community-based Landslide Early Warning System*.

After a long technical discussion, at the 5th 292 ISO/TC meeting in Sydney, Australia, in March 2018, the proposed landslide early warning international standard was approved and adopted as ISO 22327:2018 *Security and Resilience-Emergency Management: Guidelines for implementation of a community landslide early warning system*. This is a follow up to SNI 8235:2017, established the previous year. It is a significant achievement since ISO 22327:2018 is the first international standard proposed by Indonesia, and the first from a developing country.

This means that every country could adopt this standard and state it in the early warning system implementation contract. The concept of early warning system comprising 7 sub-systems are fully implemented in Indonesia and Myanmar. Other countries such as Bangladesh and Argentina have started to adopt the standard.

As a result of the ISO 22327:2018, the International Organization for Standardization (ISO) assigned Indonesia to develop the General Standard for Multi-Hazards Early Warning System (ISO 22328-1:2020), complete with Technical Specification for multiple hazards such as tsunamis, volcanic eruptions, and floods. The document was in the process of finalization at the time of going to press (June 2022).

8 Conclusions

Creating innovative hazard monitoring systems takes a long time, requiring the study of basic processes by institutes of higher education, and dissemination of useful hazard information to maintain people's interest. The disaster early warning system developed by Universitas Gadjah Mada, as an ICL member and a World Center of Excellence on Landslide Disaster Risk Reduction (WCoE-07), has been published as a national and international standard. However, intensive innovation, evaluation, and improvement is constantly undertaken. The challenges in conducting these are many, such as maintaining the sustainability, in this case, the endurance of the stakeholders. An appropriate strategy to maintain the awareness and preparedness of the community is needed. After a disaster, the community awareness and preparedness increase but they diminish after a period of time. Another challenge is media exposure. The media should actively deliver information on the importance of disaster risk reduction, mitigation, and early warning system prior to disasters instead of post-disaster. Innovation must be carried out continuously to develop equipment that is low maintenance and functions well in minimum conditions (weather,

humidity, etc.). In addition to landslide monitoring, UGM has implemented the early warning system concept and strategy for other hazards leading to disasters, including volcanic eruptions, debris flows, seasonal floods, and flash floods.

The challenges in disaster management are still numerous and various. Through the innovation efforts and strategies initiated by UGM, national resilience and sustainability in disaster risk management is maintained. The success of the implementation of the early warning system is achieved through multidisciplinary collaboration, with full support from national and regional governments, and private sector stakeholders. In the future, UGM will continue to innovate with multiple parties to establish national technology sovereignty and disaster risk reduction globally.

Acknowledgements We would like to express our great appreciation to the Indonesian Disaster Management Authority (BNPB) for supporting this research activity. We would also like to thank Prof. Irasema Alcántara-Ayala (National Autonomous University of Mexico) and Dr. David Huntley (Geological Survey of Canada) for their valuable and constructive suggestions.

References

- Bappenas (2014) Rencana Pembangunan Jangka Menengah Nasional (RPJMN) 2015–2019. *Buku III Agenda Pembangunan Wilayah*, KPPN/Bappenas: 1–1–1–48
- BNPB (2020) *Risiko Bencana Indonesia (RBI)*. Direktorat Pengurangan Risiko Bencana, BNPB, Jakarta. <https://bnpb.cloud/dibi> last access 28 Mei 2020
- BNPB (2019) *Risiko Bencana Indonesia (RBI)*. Direktorat Pengurangan Risiko Bencana, BNPB, Jakarta. <https://bnpb.cloud/dibi> last access 21 October 2019.
- BNPB (2014) *Rencana Nasional Penanggulangan Bencana (2015–2019)*. Badan Nasional Penanggulangan Bencana, Jakarta.
- Crozier MJ, Glade T (2005) Landslide hazard and risk: issues, concepts and approach. In: Glade T, Anderson MG, Crozier MJ (eds) *Landslide hazard and risk*. Wiley, Chichester, pp 1–40
- Fathani T F (2019) Strategic program and technological innovation for landslide disaster risk reduction. In: Proceedings 23rd annual national conference on geotechnical engineering (PIT XXIII HATTI), pp 12–13 November 2019. Jakarta
- Fathani TF, Karnawati D (2018) TXT-tool 2.062–1.1: a landslide monitoring and early warning system. In: Sassa K et al (eds) *Landslide dynamics: ISDR-ICL landslide interactive teaching tools*, vol 1. Fundamentals, mapping and monitoring. Springer, Cham, pp 297–308. https://doi.org/10.1007/978-3-319-57774-6_21
- Fathani TF, Karnawati D, Wilopo W (2017) Promoting a global standard for community-based landslide early warning system. In: Sassa K, Mikoš M, Yin Y. (eds) *Advancing culture of living with landslides*, vol 1. ISDR-ICL Sendai Partnerships 2015–2025. Springer, Cham, pp 355–361. https://doi.org/10.1007/978-3-319-59469-9_30
- Fathani TF, Karnawati D, Wilopo W (2016) An integrated methodology to develop a standard for landslide early warning systems. *J Nat Hazards Earth Syst Sci* 16(9):2123–2135. <https://doi.org/10.5194/nhess-16-2123-2016>
- Fathani TF, Karnawati D, Wilopo W (2014) An adaptive and sustained landslide monitoring and early warning system. In: Sassa K,

- Canuti P, and Yin Y (eds) *Landslide science for a safer geoenvironment vol 2. Methods of landslide studies*. Springer, Cham, pp 563–567. https://doi.org/10.1007/978-3-319-05050-8_87
- Fathani TF, Legono D (2013) The application of monitoring and early warning system of rainfall-triggered debris flow at Merapi Volcano, Central Java, Indonesia. In: Wang F et al (eds) *Progress of geo-disaster mitigation technology in Asia*. Environmental science and engineering. Springer, Berlin, Heidelberg, pp 263–275. https://doi.org/10.1007/978-3-642-29107-4_13
- Fathani TF, Legono D (2011) A self-evacuation drill development program for community resilience against mount merapi disaster. In: *Proceeding of international workshop on multimodal sediment disasters triggered by heavy rainfall and earthquake and the countermeasures*, 8–9 March 2011. Yogyakarta, Indonesia pp 125–136
- Hufschmidt G, Crozier M, Glade T (2005) Evolution of natural risk: research framework and perspectives. *Nat Hazard* 5(3):375–387. <https://doi.org/10.5194/nhess-5-375-2005>
- Karnawati D, Fathani TF, Wilopo W, Andayani B (2018) TXT-tool 4.062–1.1: community hazard maps for landslide risk reduction. In: Sassa K et al (eds) *Landslide dynamics: ISDR-ICL landslide interactive teaching tools vol 2. Testing, risk management and country practices*. Springer, Cham, pp 599–606. https://doi.org/10.1007/978-3-319-57777-7_36
- Karnawati D, Fathani TF, Wilopo W, Andayani B (2013) Hybrid socio-technical approach for landslide risk reduction in Indonesia. In: Wang F, Miyajima M, Li T, Shan W, Fathani T F (eds) *Progress of geo-disaster mitigation technology in Asia*. Springer, Berlin, Heidelberg, pp 157–169. https://doi.org/10.1007/978-3-642-29107-4_7
- Karnawati D, Fathani TF, Ignatius S, Andayani B, Legono D, Burton PW (2011) Landslide hazard and community-based risk reduction effort in Karanganyar and the surrounding area, central Java, Indonesia. *J Mt Sci* 8:149–153. <https://doi.org/10.1007/s11629-011-2107-6>
- Setiawan H, Retnaningrum E, Arrisaldi T, Wilopo W (2021) Capacity building and community preparedness towards landslide disaster in Pagerharjo Village, Kulon Progo Regency of Yogyakarta, Indonesia. In: Sassa K et al (eds) *Understanding and reducing landslide disaster risk*. WLF 2020. ICL contribution to landslide disaster risk reduction. Springer, Cham, pp 603–610. https://doi.org/10.1007/978-3-030-60196-6_54
- UN-ISDR (2006) *Developing an early warning system: a checklist*, The Third International Conference on Early Warning (EWC III), available at <http://www.unisdr.org/2006/ppew/info-resources/ewc3/checklist/English.pdf>. Last accessed Feb 2022

Open Access This chapter is licensed under the terms of the Creative Commons Attribution 4.0 International License (<http://creativecommons.org/licenses/by/4.0/>), which permits use, sharing, adaptation, distribution and reproduction in any medium or format, as long as you give appropriate credit to the original author(s) and the source, provide a link to the Creative Commons license and indicate if changes were made.

The images or other third party material in this chapter are included in the chapter's Creative Commons license, unless indicated otherwise in a credit line to the material. If material is not included in the chapter's Creative Commons license and your intended use is not permitted by statutory regulation or exceeds the permitted use, you will need to obtain permission directly from the copyright holder.





Central Asia Rockslides Inventory: Compilation, Analysis and Training—Progress of the IPL WCoE

Alexander Strom

Abstract

JSC “Hydroproject Institute” together with Institute of Seismology of National Academy of Sciences of Kyrgyz Republic were awarded a World Centre of Excellence on Landslide Risk Reduction (WCoE) since the 1st World Landslide Forum in 2008. This award was confirmed during the 2nd, 3rd, 4th and 5th World Landslide Forums. The core activity of this WCoE is the Kokomeren Summer School on Rockslides and Related Phenomena—a two-week long annual field training course aimed to acquaint students and young landslide researchers with unique and very didactic examples of large-scale rockslides, rock avalanches and manifestations of active tectonics abundant in the Kokomeren River basin in Central Tien Shan. Further development of these activities evolved in compilation of the complete rockslide database of the entire Central Asia Region embracing Pamir, Tien Shan and Dzungaria that belong to six states—Afghanistan, China, Kazakhstan, Kyrgyzstan, Tajikistan, and Uzbekistan.

Keywords

Rockslide • Rock avalanche • Field training • Database • Inventory

1 Introduction

Central Asia region embracing Pamir, Tien Shan and Dzungarian mountain systems located in six states—Afghanistan, China, Kazakhstan, Kyrgyzstan, Tajikistan,

and Uzbekistan, is one of the global landslide hotspots (Nadim et al. 2006). Unique combination of rugged terrain, arid climate and lack of vegetation, active tectonics and high seismicity provides conditions quite favorable both for landslides formation and for their identification, mapping and detailed study at both regional and site-specific scales. It is fully applied to the study of large-scale rockslides and rock avalanches—the most destructive and most hazardous types of landslides in mountainous regions.

Complex study of these hazardous phenomena, compilation of the regional inventory of rockslides exceeding 1 million cubic meters in volume, and organization of an annual two-week field training course for students and young researchers interested in studying these natural phenomena are the main aims of the multi-year joint project of the JSC “Hydroproject Institute” (Moscow) and Institute of Seismology of National Academy of Sciences of Kyrgyz Republic. These organizations were awarded as World Centre of Excellence on Landslide Risk Reduction (WCoE) since the 1st World Landslide Forum in 2008.

Seventeen years of development and progress of these activities as well as our future plans are described in brief hereafter.

2 Field Training Course—The Kokomeren Summer School

The Kokomeren Summer School on Rockslides and Related Phenomena started in 2006. It was skipped in 2010 due to political crisis in Kyrgyzstan and in 2020–2021 due to the COVID-19 pandemic but was resumed in 2022. The Kokomeren Summer School (KSS) is a two-week long field training course during which the entire group led by the author visit rockslides, rock avalanches and rockslide dams where various peculiarities of these natural phenomena are demonstrated and explained in detail.

A. Strom (✉)
Geodynamics Research Centre, JSC “Hydroproject Institute”,
125993, 2, Volokolamsk Highway, Moscow, Russia
e-mail: strom.alexandr@yandex.ru

The first KSS was preceded by the 2005 special field reconnaissance during which most interesting and didactic sites were selected and studied. Data collected during this field trip as well as those collected by organizers during their previous work in the study area were summarized in the full-color detailed guidebook. These activities were performed within the frames of the IPL M-111 project supported by the International Consortium on Landslides (ICL) and followed later by the C-106-2/IPL-106-2 projects. In 2017–2019, and in 2022, the KSS was supported partially by the Central Asian UNESCO office that covered the expenses of four participants, one each from Kyrgyzstan, Kazakhstan, Uzbekistan and Tajikistan. Almost each year some new study sites or new field routes have been found and included in the new versions of the Guidebook. The latest one is available at the ICL and IPL websites.

During fourteen years of the KSS, 159 students, young researchers, and several experienced experts from Argentina, Austria, Belgium, China (including Hong Kong), Chinese Taipei, Czech Republic, France, Germany, Great Britain, Italy, Japan, Kazakhstan, Korea, Kyrgyzstan, New Zealand, Poland, Russia, Slovakia, Slovenia, Switzerland, Spain, Tajikistan, USA and Uzbekistan have attended this field training course (Table 1). Some of them attended two courses.

This area (Fig. 1) was selected for field training course due to quite favorable combination of several factors: (1) unique variability of rockslide morphological types and subtypes (Strom 2021); (2) excellent exposure of both morphology of the studied features and of their internal structure; (3) impressive manifestation of neotectonics and active faulting in the study area that form the prerequisites of large-scale rockslides formation; (4) attainability of almost all study sites that require up to two hours driving and several kilometers long hiking to reach them; and (5) closeness of the area to Bishkek—route from Bishkek airport to base camp takes 5–6 h, depending on weather conditions.

During daily field trips the attendees visited numerous rockslides and rock avalanches, the largest of which—the Kokomeren rockslide was about 1.5 km³ in volume and formed the dam up to 400 m high, nowadays completely

dissected by erosion (Fig. 2). There are also impressive evidence of river damming (Fig. 3) and of the subsequent outburst floods (Fig. 4)—the secondary and the tertiary effects of large-scale rock slope failures that can be even more destructive than rockslides themselves.

The KSS attendees also have a chance to be acquainted with the traditional lifestyle of very friendly and hospitable local people and to taste local food and traditional drink of nomads—kumis—fermented horse milk (Figs. 5 and 6).

Such field training proved its efficiency—many unclear or controversial peculiarities of the studied phenomena can be explored and explained directly on site. Several participants of the KSS from the European and Asian countries came to Kyrgyzstan again with their own research projects to continue studying excellent manifestations of rock slope instability, both in the same parts of the Tien Shan and in other parts of this mountain system.

3 Central Asian Rockslide Database—Compilation and Analysis

Preparation of the Summer School Guidebook along with the study of numerous rockslides, rock avalanches and deep-seated gravitational slope deformations (DSGSD) performed in different parts of the Central Asian mountains, was a starting point for compilation of the complete large-scale rockslide inventory and database of the entire Central Asian region (Strom and Abdrakhmatov 2017) (Fig. 7). This database includes ca. 1000 case studies in the Djungaria, Tien Shan and Pamir Mountain systems, for about 600 of which quantitative and qualitative parameters characterizing their headscarps, deposits and the dammed lakes are provided. Results of these studies have been summarized in the monograph “Rockslides and rock avalanches of Central Asia: distribution, morphology, and internal structure” (Strom and Abdrakhmatov 2018) published by Elsevier (ISBN: 978-0-12-803204-6). The database is available as an Excel spreadsheet at the Elsevier website (<https://www.elsevier.com/books/rockslides-and-rock-avalanches-of-central-asia/strom/978-0-12-803204-6>) as part of the supplementary

Table 1 Number of participants attending the KSS

Year	Attendees	Year	Attendees
2006	2	2014	12
2007	5	2015	5
2008	7	2016	19
2009	8	2017	16
2011	10	2018	23
2012	13	2019	21
2013	8	2022	10

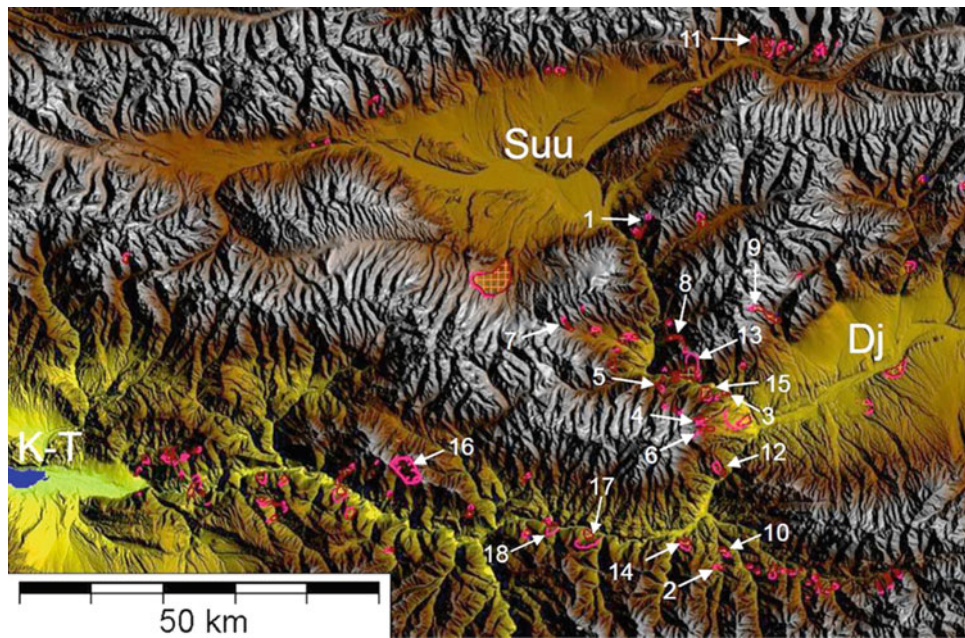


Fig. 1 Large landslides, rock avalanches and caldera-like collapses in the Kokomeran River basin and adjacent part of the Naryn River basin. Suu, Dj and K-T—the Suusamy, the Djungal and the Ketmen-Tiube intermountain depressions. Selected features most of which are demonstrated during the training course: 1—Seit; 2—Ak-Kiol; 3—

Mini-Köfels; 4—Kashkasu; 5—Northern Karakungey; 6—Southern Karakungey; 7—Chongsu; 8—Sarysu; 9—Ming-Teke; 10—Lower Ak-Kiol; 11—Snake-Head; 12—Lower-Aral; 13—Kokomeran; 14—Ornok; 15—Displaced Peneplain; 16—Kyzylkiol caldera-like collapse; 17—Karachauli; and 18—Lower Kokomeran

Fig. 2 Overview of the Kokomeran Rockslide whose ca. 400 m high body had been completely dissected by erosion



material and can be provided by the author upon the request as well.

Unique and didactic examples of rockslides, most of which converted into flow-like rock avalanches (Fig. 8), of the existing, silted and breached rockslide dams (Figs. 9, 10 and 11) and of the DSGSDs (Fig. 12) have been identified throughout the entire Central Asia Region—from the Djungarian Range in the North to Pamir and Afghan Badakhshan in the South and from Eastern Tien Shan in

Xinjiang, China, to its westernmost part in Uzbekistan and Tajikistan. Some of case studies are really unique due to their size and expressiveness (Fig. 13).

Large number of the quantified rockslides and rock avalanches allowed establishing statistical relationships between parameters, characterizing the collapsed rock massif—its volume and height drop and parameters that are used to describe their mobility (runout, angle of reach, affected area) (Strom 2018; Strom and Abdrakhmatov 2018; Strom et al.

Fig. 3 Succession of lacustrine sediments accumulated in the lake dammed by the Kokomeren rockslide (above) and composition of its basal unit—mixture of dark-grey Paleozoic metasediments rubble and red Neogene claystone



2019). These relationships, some of which are characterized by very high correlation coefficients ($R^2 > 0.9$), can be used for fast assessment of the landslide hazards and associated risks if the potentially unstable slope is identified and its height and volume are estimated.

Parts of the entire database were used for testing new software developed for automatic generation of landslide profiles (Li et al. 2020) and for elaboration of the more strict determination of landslide longitudinal shape (Li et al. 2022).

Fig. 4 Terrace-like body downstream from the breached 70 m high Lower Aral rock avalanche dam. These deposits left by the final phases of the outburst flood are composed of layers of angular unrounded clasts



Fig. 5 Participants of the 2018 KSS with local family



The Central Asian rockslide database serves as a reference point for various regional and site-specific studies of natural hazards and risks associated with rockslides, rock avalanches and rockslide dams (e.g. Fomenko et al. 2020; Jones et al. 2021). It has been also used for the landslide susceptibility assessment of the Central Asian states performed within the frames of the ongoing World Bank funded project. In future, the database will be enlarged by quantifying those case studies whose parameters have not been measured yet.

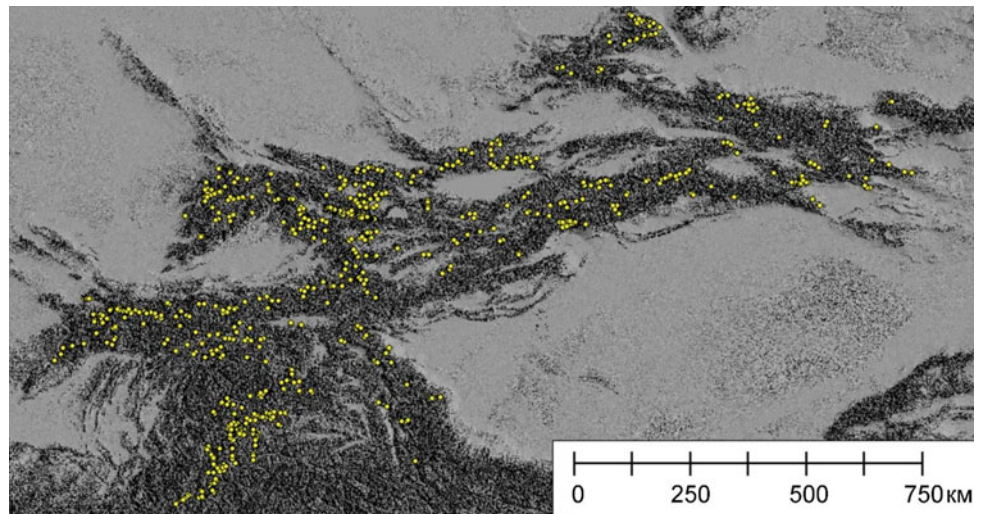
4 Conclusions

Activities of the World Centre of Excellence (WCoE) of JSC “Hydroproject Institute” and of Institute of Seismology of National Academy of Sciences of Kyrgyz Republic are focused on the study of the most disastrous types of landslides in mountainous regions—large-scale rockslides and rock avalanches.

Fig. 6 Drinking kumis in the shepherd's yurt



Fig. 7 Spatial distribution of large rockslides, rock avalanches and DSGSDs' in the Central Asian region



WCoE performs both scientific (compilation of the Central Asian rockslide database and study of the most informative features) and educational (Kokomeren Summer School) tasks. Besides, results of our studies have been used and will be used in future for practical purposes—to assess landslide and seismic hazards of the particular sites and associated risks.

Acknowledgements I am grateful to Prof. Kanatbek Abdrakhmatov, who along with valuable scientific contributions, charged himself with organization of the camping, local transportation, and other arrangements of the Kokomeren Summer School. I also want to express my gratitude to Prof. Kyoji Sassa for his permanent support to our activities.

Fig. 8 The 7.5 km long Chukurchak rock avalanche, Tien Shan, Kyrgyzstan. Headscarp is marked by elevation marks 2970 and 2250 m a.s.l., while other elevation marks are placed at the front of rock avalanche branches

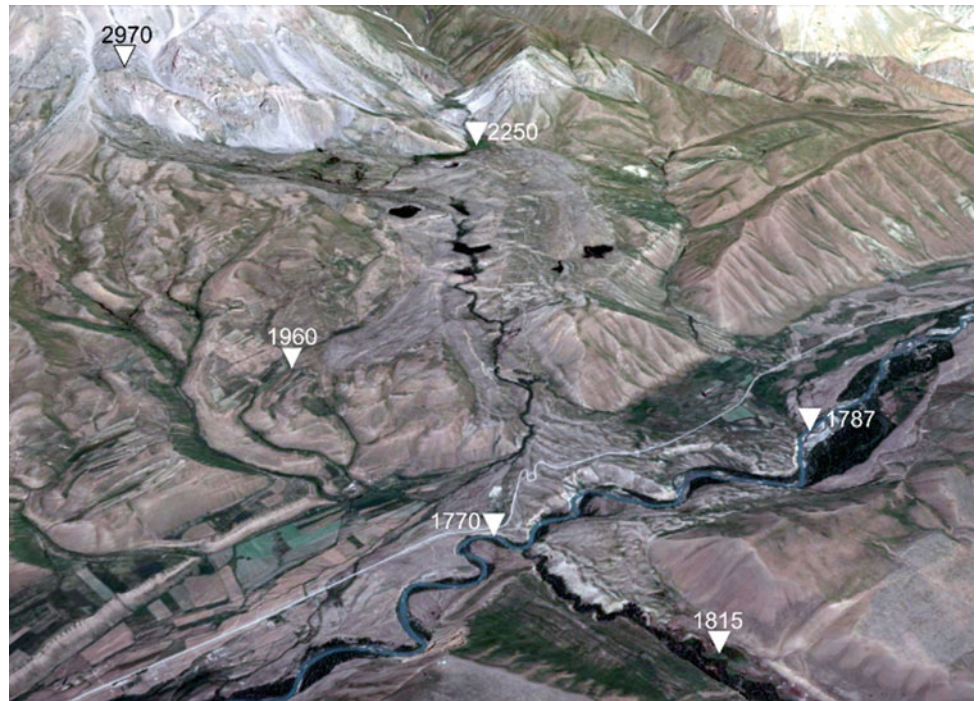


Fig. 9 Rockslide (rock avalanche) dam of the Big Almaty Lake, Kazakhstan. Red arrows mark the headscarp at 3000–3300 m a.s.l.; yellow arrows—rock avalanche front. Lake level was raised by small earthfill dam

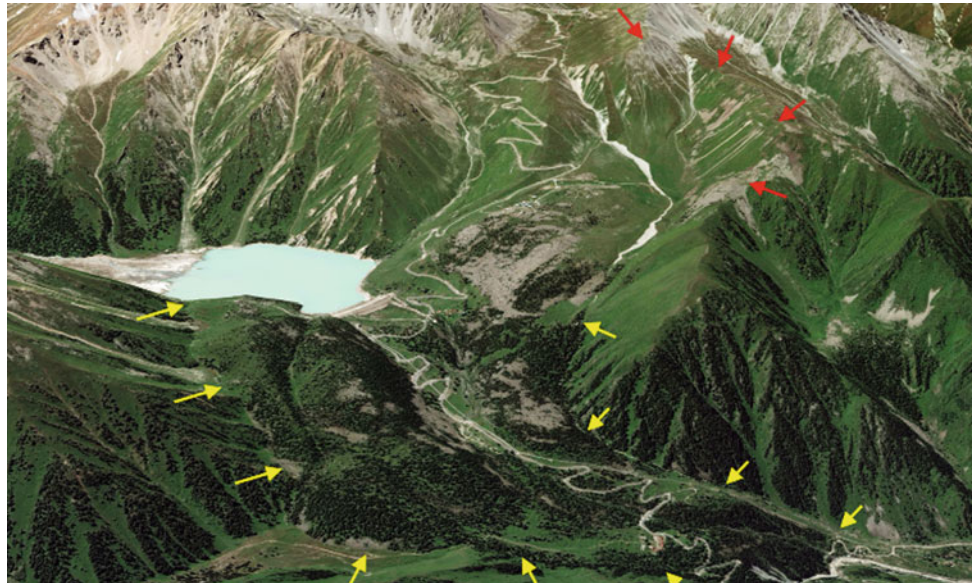


Fig. 10 Rockslide dam in Chinese Pamir and completely silted and forested dammed lake

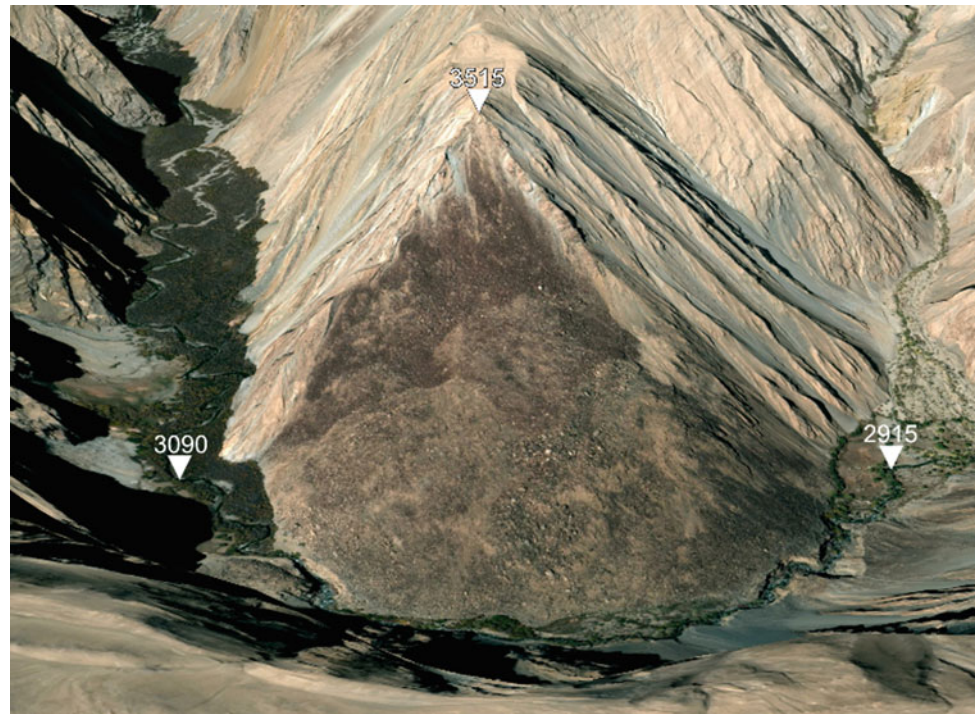


Fig. 11 Gigantic breached natural dam ca. 500 m high at the junction of the Dura and Munjiang River in the Kokcha River basin in Afghanistan. It was formed by the Pazhuk rockslide about 3 km³ in volume



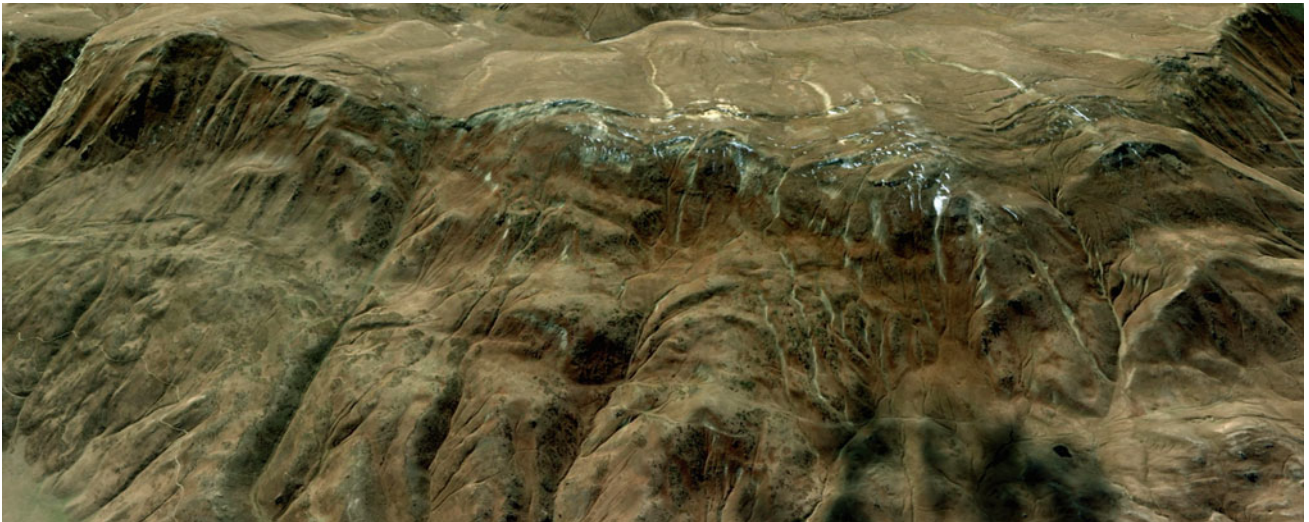


Fig. 12 Ca. 5 km long DSGSD at the northern slope of the Peter the First Range, Tajikistan

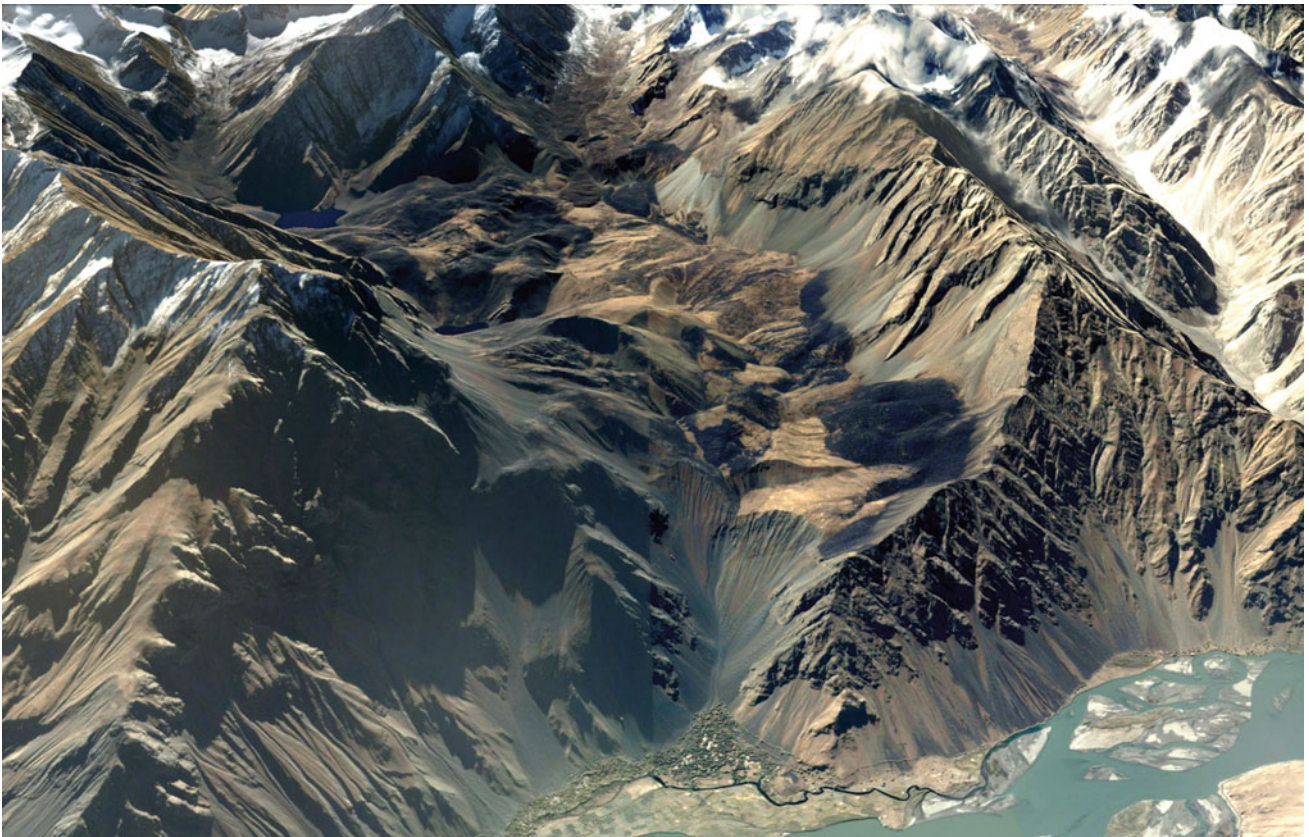


Fig. 13 Oblique view of the tremendous Padjvar rockslide in Afghan Badakhshan ca. 6 km^3 in volume. The entire ridge about 6 km long collapsed in the adjacent valley of the left tributary of the Pianj River and filled it almost completely with the deposits up to 650–700 m thick that cover 19.72 km^2 , while the total affected area is about 27 km^2

References

- Fomenko I, Strom A, Zerkal O (2020) Possibility of landslide damming in the Vakhsh River catchment and its effect on the hydraulic schemes and population. In: Proceedings of SCG-XIII international symposium on landslides. Cartagena, Colombia. June 15th–19th-2020, Article 164
- International Consortium on Landslides (ICL) Landslide field school guidebook. <https://icl.iplhq.org/category/icl/leaflet-and-publications/>
- International Program on Landslides (IPL) Announcements and news. In: 2017 International summer school on rockslides and related phenomena in the Kokomeren River Valley (Kyrgyzstan). Download Guidebook. <https://iplhq.org/category/iplhq/announcements-and-news/>
- Jones N, Manconi A, Strom A (2021) Active landslides in the Rogun Catchment, Tajikistan, and their river damming hazard potential. *Landslides* 18:3599–3613. <https://doi.org/10.1007/s10346-021-01706-5>
- Li L, Lan H, Strom A (2020) Automatic generation of landslide profile for complementing landslide inventory. *Geomat Nat Hazards Risk* 11:1000–1030. <https://doi.org/10.1080/19475705.2020.1766578>
- Li L, Lan H, Strom A, Macciotta R (2022) Landslide longitudinal shape: a new concept for complementing landslide aspect ratio. *Landslides*. <https://doi.org/10.1007/s10346-021-01828-w>
- Nadim F, Kjekstad O, Peduzzi P, Herold C, Jaedicke C (2006) Global landslide and avalanche hotspots. *Landslides* 3:159–173
- Strom A (2018) Large-scale rockslide inventory of the Central Asia region: data and analysis. In: Shakoor A, Cato K (eds) IAEG/AEG annual meeting proceedings, San Francisco, California, 2018, 1 pp 145–153. https://doi.org/10.1007/978-3-319-93124-1_18
- Strom A (2021) Rock avalanches: basic characteristics and classification criteria. In: Vilimek V, Wang F, Strom A et al (eds) Understanding and reducing landslide disaster risk, vol 5, pp 3–23
- Strom A, Abdrakhmatov K (2017) Large-scale rockslide inventories: from the Kokomeren River Basin to the Entire Central Asia Region (WCoE 2014–2017, IPL-106-2). In: Sassa K et al (eds) Advancing culture of living with landslides, vol 1, pp 339–346. https://doi.org/10.1007/978-3-319-59469-9_28
- Strom A, Abdrakhmatov K (2018) Rockslides and rock avalanches of Central Asia: distribution, morphology, and internal structure. Elsevier, 459 p. ISBN: 978-0-12-803204-6
- Strom A, Li L, Lan H (2019) Rock avalanche mobility: optimal characterization and the effects of confinement. *Landslides* 16:1437–1452. <https://doi.org/10.1007/s10346-019-01181-z>

Open Access This chapter is licensed under the terms of the Creative Commons Attribution 4.0 International License (<http://creativecommons.org/licenses/by/4.0/>), which permits use, sharing, adaptation, distribution and reproduction in any medium or format, as long as you give appropriate credit to the original author(s) and the source, provide a link to the Creative Commons license and indicate if changes were made.



The images or other third party material in this chapter are included in the chapter's Creative Commons license, unless indicated otherwise in a credit line to the material. If material is not included in the chapter's Creative Commons license and your intended use is not permitted by statutory regulation or exceeds the permitted use, you will need to obtain permission directly from the copyright holder.



A Global Database of Giant Landslides on Volcanic Islands

Matt Rowberry, Jan Klimeš, Jan Blahůt, Jan Balek, and Michal Kusák

Abstract

This paper describes a comprehensive online database of giant landslides on volcanic islands compiled by researchers from the Institute of Rock Structure and Mechanics, Czech Academy of Sciences, in the framework of IPL Project 212. The database was constructed from 2016 to 2018. It comprises a total of seventy-five events from the Atlantic Ocean and Mediterranean Sea, sixty-seven events from the Pacific Ocean, and forty events from the Indian Ocean. In this paper some of the main benefits of landslide inventories and thematic databases are outlined and the global distribution of giant landslides on volcanic islands is described in depth. The database is hosted on the website of the Institute of Rock Structure & Mechanics and records can be downloaded as a spreadsheet or kml file for integration in a number of geospatial programs including ArcGIS and Google Earth. However, since completion of the database in 2018, a number of potentially significant studies of giant landslides on volcanic islands have been published from archipelagos in the Atlantic and Pacific Oceans while outstanding modern analogues for past events are represented by the collapse of Anak Krakatau on 22 December 2018 and the collapse of Hunga Tonga-Hunga Ha'apai on 15 January 2022. Consequently, the recent literature will be scrutinized with the aim of updating information already contained in the database while two new layers are planned: the first of these will provide information about recent volcanic collapses and the second will provide information about the long-term instrumental monitoring of giant landslides. It is intended that the second release of the database will be available online in early 2023.

Keywords

Giant landslides • Landslide inventories • Thematic databases • Debris avalanches • Slumps • Volcanic islands

1 Introduction

In the 1960s it was shown that the Hawaiian Ridge hosted a pair of giant landslides (Moore 1964) but the geomorphological evidence used to document these events was not greeted with universal enthusiasm (Langford and Brill 1972). Not only were the original observations corroborated by later research but it has become clear that the vast majority of volcanoes are prone to episodes of slope instability and subsequent structural failure (McGuire 1996). Indeed it is now known that the structural failure of a volcano can create some of the largest landforms generated in a single geological moment (Whelan and Kelletat 2003). Instability may be caused by magma emplacement, peripheral erosion, the overloading of slopes, or the oversteepening of slopes while subsequent failure may be triggered by a suite of climatic, magmatic, or seismogenic processes (McGuire 1996). The potential for instability may be increased on oceanic island volcanoes due to edifice spreading along weak sedimentary horizons or in response to seaward creeping masses of olivine cumulate (Fig. 1). In many instances, it is probable that more than one preparatory factor is operating prior to the initiation of a specific trigger.

The seafloors and subsurfaces of numerous volcanic archipelagos have now been imaged in unprecedented detail thanks to advances in a range of geophysical techniques such as single and multibeam echo sounders, sidescan sonar, and reflection and refraction seismic surveys (e.g. Crutchley and Kopp 2018; Hughes Clark 2018; Klaucke 2018). Giant landslides on volcanic islands transport hundreds of thousands of cubic metres to hundreds of cubic kilometres of

M. Rowberry (✉) · J. Klimeš · J. Blahůt · J. Balek · M. Kusák
Institute of Rock Structure & Mechanics, Czech Academy of Sciences, Prague, Czech Republic
e-mail: rowberry@irms.cas.cz

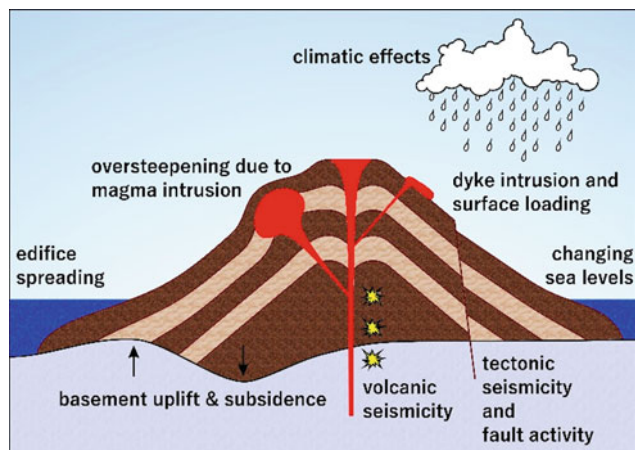


Fig. 1 Factors contributing towards the development of structural instability at active volcanoes (modified from McGuire 1996)

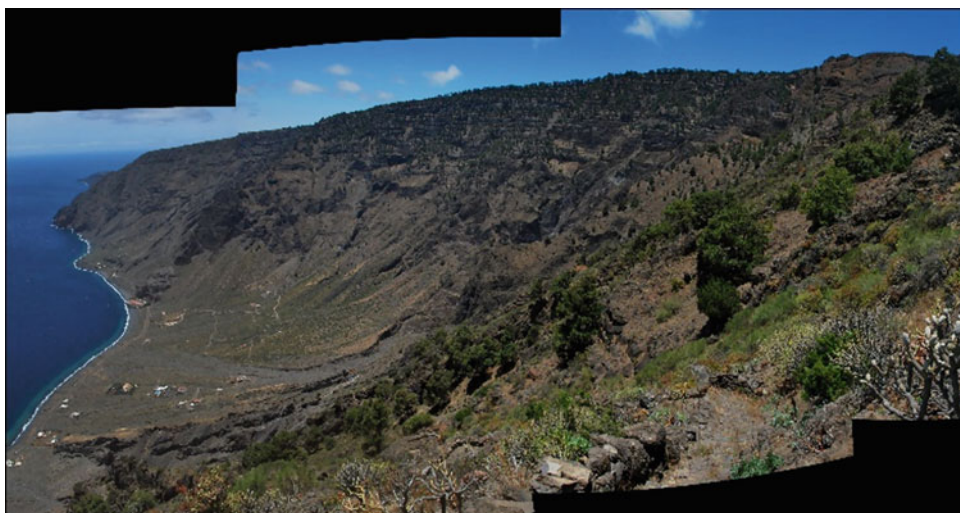
material and create arcuate embayments and steep cliffs (Fig. 2). Through time these features are degraded by erosion and partially or completely hidden by further volcanism. Their deposits can be transported for hundreds of kilometres and can extend over areas of many hundreds of square kilometres (Masson et al. 2002). In the sea, these accumulations are often well preserved but they tend to lie at considerable depths so investigating their internal structure requires access to—usually proprietary—borehole data. Consequently, giant landslides on volcanic islands remain among the most poorly studied types of terrestrial landslide despite their global distribution and potential to generate catastrophic failures and tsunamis (Day et al. 2015; Ramalho et al. 2015).

Insufficient information pertaining to the internal structure of giant landslides on volcanic islands means that such events are poorly defined. They are usually interpreted as either debris avalanches or slumps; debris avalanches are

thought to reflect a sudden single catastrophic event while slumps are thought to reflect protracted slope deformation. Evidence for both of these end members are sometimes found in a single archipelago, occasionally even on a single volcanic edifice, such as on the main island of Hawai‘i and on El Hierro in the Canary Islands. Furthermore, some debris avalanches have been reinterpreted as multistage collapses (Hunt et al. 2013) while some slumps present evidence for recurring periods of rapid slip (Blahůt et al. 2020). It is also possible that structural failure then triggers an eruption in much the same way as was seen on Mount Saint Helens in May 1980. In such a scenario, evidence for the initial structural failure could disappear almost instantaneously. There is also the possibility that slumps transition into catastrophic debris avalanches but no unequivocal evidence for this has yet been recognised.

Until recently, information about giant landslides on volcanic islands had not been rationalised into a single online resource. Here an outline of the first comprehensive global database of giant landslides on volcanic islands is presented. The database was compiled over a three year period from 2016 to 2018: the first year concentrated on investigating events in the Atlantic Ocean; the second year concentrated on investigating events in the Pacific Ocean; and the third year concentrated on investigating events in the Indian Ocean. In this paper, attention focuses, first, on the benefits of landslide inventories and thematic databases, second, on the global distribution of giant landslides on volcanic islands and, third, on plans to update the database and implement some changes. It is hoped that the database will be used by the research community to investigate the spatial and temporal distribution of such landslides, to investigate their morphometric characteristics in more detail, and to assess the hazard and potential risks posed by future events. The complete database is available at: <https://www.irms.cas.cz/ext/giantlandslides>.

Fig. 2 An example of an arcuate embayment and steep cliffs formed by a giant landslide on a volcanic island: the Las Playas debris avalanche on El Hierro in the Canary Islands (photograph by Jan Klimeš)



2 Landslide Inventories and Thematic Databases

Landslide inventories and thematic databases provide essential information needed to assess the spatial and temporal distribution of landslides, their preparatory factors and triggers, and their negative societal impacts (Guzzetti et al. 2012). The scope of such inventories and databases can be regional (Blahůt et al. 2012; Strozzi et al. 2018) or global (Kirschbaum et al. 2010; Froude and Petley 2018) or it can extend beyond the Earth to cover extraterrestrial bodies such as Mars (Brunetti et al. 2014; Crosta et al. 2018). Despite their importance, it is sometimes difficult to access information about landslide databases in terms of, for example, their completeness, format, and structure and such information is necessary in order to be able to generate reliable susceptibility, hazard, and risk assessments (Van Den Eeckhaut and Hervás 2012). Nonetheless, in many instances the rapid preparation of more reliable and relevant landslide inventories is being facilitated by advancing technologies coupled with data mining from media reports (e.g. Kreuzer and Damm 2020; Franceschini et al. 2022) or social networks (e.g. Pennington et al. 2015; Juang et al. 2019).

There is still the fundamental issue that landslide inventories have only been prepared for a small proportion of the globe. In terrestrial settings, it has been estimated that inventory mapping covers only around one percent of the total land surface (Guzzetti et al. 2012). In submarine settings, this figure is thought to be lower, in light of the fact that more than three quarters of the seafloor is still not mapped at a resolution of 1 km (Jakobsson 2020). However, there are an increasing number of inventories and databases that have focused on compiling information about submarine landslides (Camerlenghi et al. 2010; Urlaub et al. 2013; Gamboa et al. 2021). These are particularly useful because such landslides have the potential to cause devastating tsunamis in coastal regions far from the triggering event. However, due to the financial and time constraints associated with seafloor mapping, there is a tendency for submarine landslide inventories to come from regions of high economic importance (Chaytor et al. 2009; Katz et al. 2015). It is anticipated that in the future an increasing number of giant landslides will be recognised in more remote, less prosperous volcanic islands such as those in the Subantarctic.

3 Database Structure

The term giant landslide is used here to refer to any mass movement whose main body can be defined with some degree of confidence and whose volume is in the order of cubic kilometres while the term volcanic island is restricted

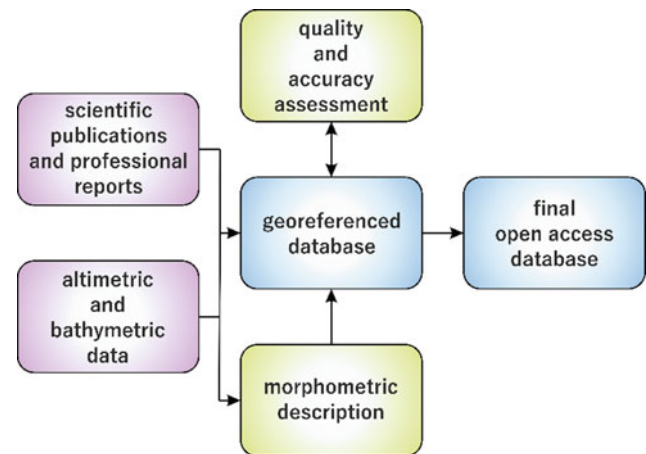


Fig. 3 Flow diagram outlining our approach to construction of the giant landslides on volcanic islands database (modified from Blahůt et al. 2018a)

to only those islands whose origins are entirely volcanic (Blahůt et al. 2018a, 2019). The majority of the information found in the database has been sourced from peer reviewed scientific publications—both manuscripts and book chapters—while a small proportion comes from other sources such as professionals reports and technical documents. This information has been supplemented by insights gleaned from altimetric and bathymetric models. For the European islands—including those that comprise the autonomous community of Spain, the Canary Islands, and those that comprise the two autonomous regions of Portugal, Azores and Madeira—altimetric data were obtained from the Shuttle Radar Topography Mission (SRTM 2019) and bathymetric data were obtained from the European Marine Observation & Data Network (EMODNET 2019). In all other cases—including the French overseas department of La Réunion—the altimetric data and the bathymetric data were obtained from the Global Multi Resolution Topography (GMRT 2019). To define the spatial characteristics of each giant landslide it has been necessary to georeference published maps using ArcGIS. The georeferenced maps have been subjected to rigorous accuracy assessments prior to inclusion of the data in the database (Fig. 3). A complete list of all the parameters included in the database is presented on Table 1.

4 Global Distribution

4.1 North Atlantic Ocean

In the North Atlantic Ocean, giant landslides have been recognised in the archipelagos of Madeira, the Azores, the Canary Islands, the Cape Verde Islands, and the Lesser Antilles (Fig. 4). The database includes eight events from the

Table 1 Data compiled in the giant landslide on volcanic island database. Uncertainties in these data are described in more detail elsewhere (Blahút et al. 2019)

Name	The name of the giant landslide
Island	The name of the volcanic island hosting the landslide
Archipelago	The name of the archipelago to which the island belongs
Type	The type of mass movement according to the source document
Island age	The age—often given as a range—asccribed to the volcanic edifice
Island age: mean	The mean of the age range asccribed to the volcanic edifice
Source	Source document or documents used for georeferencing the landslide
Bathymetric method	Method used to create the maps in the source document(s)
Landslide age	The age—often given as a range—asccribed to the landslide
Landslide age: mean	The mean of the age range asccribed to the landslide
Total volume	The volume—often given as a range—asccribed to the landslide
Volume: mean	The mean of the volume range asccribed to the landslide
Area	The area of the landslide derived from the georeferenced map
Width	The width of the landslide derived from the georeferenced map
Length	The length of the landslide derived from the georeferenced map
Perimeter length	The perimeter length of the landslide derived from the georeferenced map
W—gHM (J)	The potential energy of the landslide (see Blahút et al. 2019)
Hmax	Maximum elevation of the landslide derived from the georeferenced map
Hmin	Minimum elevation of the landslide derived from the georeferenced map
ΔH	The fall height of the landslide derived from the georeferenced map
Complete	Is a complete outline of the areal extent of the landslide defined
H/L	The apparent friction coefficient of the landslide
Mean slope	The mean gradient of the landslide
L/H	The relative runout of the landslide

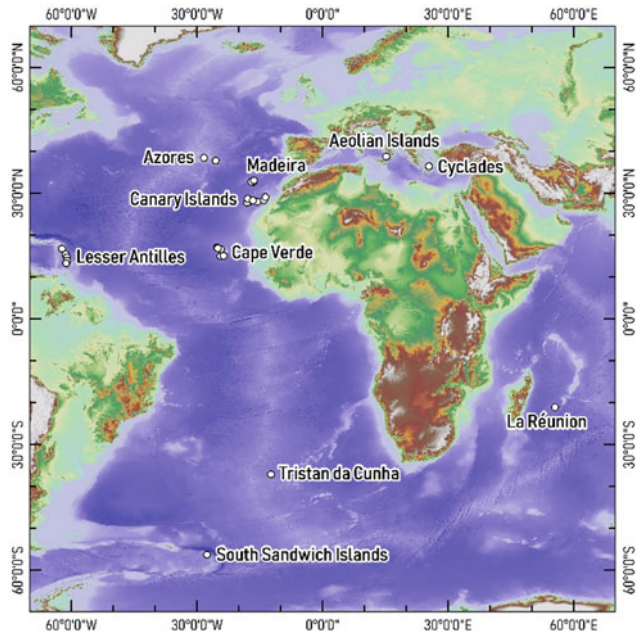


Fig. 4 Distribution of giant landslides on volcanic islands from the Atlantic and Indian Oceans. Global relief model derived from Global Bathymetry and Topography at 15 Arc Sec: SRTM15 + V2.1 (Tozer et al. 2019)

volcanoes of Madeira. Seafloor mapping of this region has been performed using multibeam echosounder. Four giant landslides are known from the main island of Madeira while two are known from each of the islands of Desertas and Porto Santo (Quartau et al. 2018). The database includes five events from the volcanoes of the Azores. Seafloor mapping of this region has also been performed using multibeam echosounder. Four giant landslides are known from the island of Pico (Costa et al. 2014; Omira et al. 2016) and one is known from the island of São Miguel (Sibrant et al. 2015).

The database includes thirty two events from the volcanoes of the Canary Islands. Seafloor mapping of this region has been performed using side scan sonar and multibeam echosounder. Nine giant landslides are known from the island of La Gomera, seven are known from El Hierro, seven are known from Tenerife, four are known from Gran Canaria, three are known from La Palma, and one is known from each of the islands of Fuerteventura and Lanzarote (Carracedo et al. 1999; Urgeles et al. 1999; Gee et al. 2001; Krastel et al. 2001; Masson et al. 2002; Acosta et al. 2003; Ancochea et al. 2006; Casillas et al. 2010; Dávila Harris et al. 2011; Hunt et al. 2011; Boulesteix et al. 2013; Hunt et al. 2014; Becerril et al. 2016; León et al. 2017).

The database incorporates twelve events from the volcanoes of Cape Verde. Seafloor mapping of this region has been performed using multibeam echosounder. Four giant landslides are known from each of the Barlavento Islands of Santo Antão and São Nicolau, two are known from the Sotavento Island of Fogo, one is known from the Barlavento Island of São Vicente, and one is known from the Sotavento Island of Santiago (Le Bas et al. 2007; Masson et al. 2008). In addition, the database incorporates thirteen events from the volcanoes of the Lesser Antilles. Seafloor mapping of this region has also been performed using multibeam echosounder. Seven giant landslides are known from the Leeward Island of Montserrat, three are known from the Windward Island of Martinique, and one is known from each of the Windward Islands of Dominica, Santa Lucia, and St Vincent (Deplus et al. 2001; Brunet et al. 2016; Coussens et al. 2016).

4.2 Mediterranean Sea

In the Mediterranean Sea giant landslides have been recognised in the Aeolian Islands and the Cyclades (Fig. 4). Seafloor mapping around the Aeolian Islands has been performed using side scan sonar and multibeam echosounder while it has been performed using multibeam echosounder around the Cyclades. From the Aeolian Islands, one giant landslide is known from the island of Stromboli (Romagnoli et al. 2009). From the Cyclades, two giant landslides are known from the island of Santorini (Hooft et al. 2017).

4.3 South Atlantic Ocean

In the South Atlantic Ocean, giant landslides have been recognised in the archipelagos of Tristan da Cunha and the South Sandwich Islands (Fig. 4). Seafloor mapping around Tristan da Cunha has been performed using side scan sonar while multibeam echosounder has been used around the South Sandwich Islands. From Tristan da Cunha, one giant landslide is known from the main island of Tristan da Cunha (Holcomb and Searle 1991). From the South Sandwich Islands, one giant landslide is known from the Traversay Island of Zavodovski (Leat et al. 2010).

4.4 Indian Ocean

In the Indian Ocean giant landslides have been recognised in the Mascarenhas Archipelago (Fig. 4). The database includes forty events from the island of La Réunion (Oehler et al. 2008). Seafloor mapping of this region has been performed using deep tow side scan sonar and multibeam

echosounder. No other volcanic edifice is thought to have hosted so many giant landslides and yet these are the only events hitherto identified in the Indian Ocean.

4.5 Northern Pacific Ocean

In the northern Pacific Ocean giant landslides have been recognised in the Aleutian Arc—including Alaska—and in the Hawaiian Islands (Fig. 5). The database includes four events from Alaska and nine events from the volcanoes of the Aleutian Arc. Seafloor mapping around Alaska has been performed using multibeam echosounder while side scan sonar and multibeam echosounder has been used around other parts of the Aleutian Arc. From Alaska, four giant landslides are known from Augustine Island (Begét and Kienle 1992; Waythomas et al. 2006). From the Aleutian Arc, three giant landslides are known from the Delarof Island of Gareloi, one is known from each of the Rat Islands of Kiska and Segula, and one is known from each of the Andreanof Islands of Great Sitkin, Bobrof, Kanaga, and Tanaga (Coombs et al. 2007).

The database includes nineteen events from the volcanoes of the Hawaiian Islands. Seafloor mapping in this region has been performed using side scan sonar. Eleven giant landslides are known from the main island of Hawai'i, three are known from the island of O'ahu, two are known from the island of Kaua'i, and one is known from each of the islands

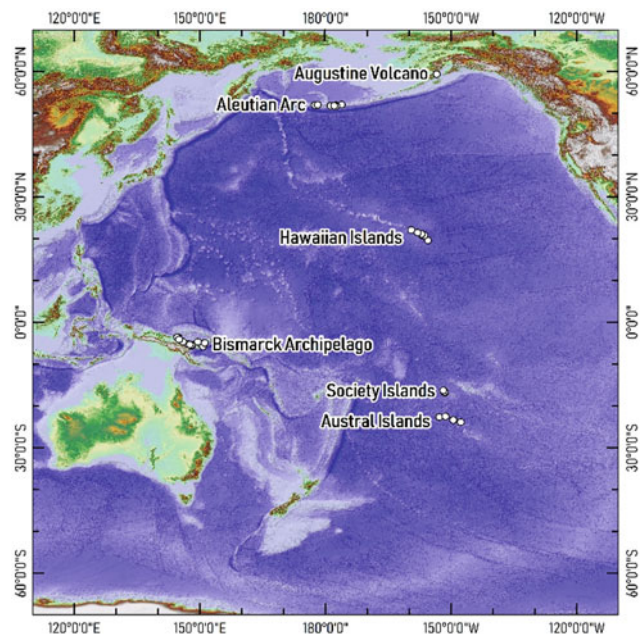


Fig. 5 Distribution of giant landslides on volcanic islands from the Pacific Ocean. Global relief model derived from Global Bathymetry and Topography at 15 Arc Sec: SRTM15 + V2.1 (Tozer et al. 2019)

of Lana'i, Maui, and Moloka'i (Lipman et al. 1988; Moore et al. 1989, 1994; McMurtry et al. 2004). The inventory of giant landslides on the Hawaiian Islands is exceptional in the sense that it includes the only instance of a sandrubble flow—from the island of Hawai'i—as well as seven slumps from three different islands—five from the island of Hawai'i, one from Maui, and one from O'ahu.

4.6 Southern Pacific Ocean

In the southern Pacific Ocean giant landslides have been recognised in the Bismarck Archipelago and in French Polynesia (Fig. 5). The database incorporates thirteen events from the volcanoes of the Bismarck Archipelago. Seafloor mapping in this region has been performed using side scan sonar and multibeam echosounder. Two giant landslides are known from each of the Madang Province islands of Crown and Karkar, one is known from the Madang Province island of Manam, one is known from each of the East Sepik Province islands of Bam and Kadovar, one is known from each of the Morobe Province islands of Ritter, Sakar, Tolokiwa, one is known from each of the West New Britain Province islands of Garove, Lolobau, and New Britain (Silver et al. 2009; Day et al. 2015).

The database includes twenty-two events from the volcanoes of French Polynesia. Seafloor mapping in this region has been performed using single beam and multibeam echosounder. From the Austral Islands, four giant landslides are known from Rūrutu Island, three from Tupua'i Island, three from Ra'ivāvae Island, and two from Rimatarā Island (Clouard and Bonneville 2004). From the Society Islands, three giant landslides are known from the Leeward Island of Bora Bora, two from the Leeward Island of Raiatea, two from the Leeward Island of Taha'a, one from the Leeward Island of Tupai (Clouard and Bonneville 2004) along with two from the Windward Island of Tahiti (Clouard et al. 2001; Hildenbrand et al. 2006).

5 Future Plans for the Database

More than three years have passed since the full database of giant landslides on volcanic islands first appeared as an online resource. On the basis of information contained in the database, it has been possible to investigate the basic morphometric characteristics of the giant landslides and the relationships that exist between these characteristics (Blahūt et al. 2019). Until now, the database has not helped to shed any light on the association between giant landslides and megatsunamis, while the information contained in the database has not yet been used as part of a susceptibility, hazard, and risk assessment.

In the intervening period, important new research on giant landslides has been published from many parts of the Atlantic Ocean including Cape Verde (Martínez-Moreno et al. 2018; Barrett et al. 2020; Cornu et al. 2021), the Azores (Hildenbrand et al. 2018; Marques et al. 2020, 2021), the Canary Islands (Coello-Bravo et al. 2020), and the Lesser Antilles (Solaro et al. 2020) as well as the Bismarck Archipelago in the Pacific Ocean (Watt et al. 2019). Moreover, the collapse of Anak Krakatau on 22 December 2018 stimulated much research (Williams et al. 2019; Grilli et al. 2019, 2021; Hunt et al. 2021; Cutler et al. 2022) and it is anticipated that the collapse of Hunga Tonga-Hunga Ha'apai on 15 January 2022 will provide the impetus for many new studies. Consequently, this feels like an auspicious time to update the global giant landslides on volcanic islands database.

First, the recent literature will be scrutinised with the aim of updating the information already contained in the database. Second, two new layers will be added. The first of these layers will provide information about recent volcanic collapses such as those of Anak Krakatau and Hunga Tonga-Hunga Ha'apai. Synthesising information about these events is important because they represent outstanding analogues for past collapses. The second of these layers will provide information about the long term monitoring of giant landslides on volcanic islands through direct instrumental methods such as dilatometric gauges (Blahūt et al. 2017, 2018b) and GNSS (Owen et al. 2000; Hildebrand et al. 2012). Such monitoring is important because it serves to verify remote sensing observations, which could be especially helpful in relation to hazard assessment. It is intended that the second release of the giant landslides on volcanic islands database will be available online in early 2023.

6 Conclusions

Landslide inventories and thematic databases provide essential information needed to assess the spatial and temporal distribution of landslides, their preparatory factors and triggers, and their negative societal impacts. In this paper, an online database of giant landslides on volcanic islands has been described. The database was constructed from 2016 to 2018 and comprises a total of seventy-five events from the Atlantic Ocean and Mediterranean Sea, sixty-seven events from the Pacific Ocean, and forty events from the Indian Ocean. However, there is now a clear need to update the existing database in light of potentially significant recent research from archipelagos in the Atlantic and Pacific Oceans coupled with major collapses on Anak Krakatau and Hunga Tonga-Hunga Ha'apai. Two new layers will provide information about recent volcanic collapses and the long-term instrumental monitoring of giant landslides. The second release of the database should be available online in early 2023.

Acknowledgements The global database of giant landslides on volcanic islands represents the main output from IPL Project 212. Construction of the database has been supported by the conceptual development research organisation of the Institute of Rock Structure & Mechanics CAS (RVO:67985891). Our field studies in the Canary Islands have been conducted thanks to the National Geographic Society through the Waitt Grants Program (Project No. W244-12), the Czech Science Foundation (Project No. GJ16-12227Y), and a bilateral Mobility Plus Project (Project No. FNRS-20-01).

References

- Acosta J, Uchupi E, Muñoz A, Herranz P, Palomo C, Ballesteros M, ZEE Working Group (2003) Geologic evolution of the Canarian Islands of Lanzarote, Fuerteventura, Gran Canaria, and La Gomera and comparison of landslides at these islands with those at Tenerife, La Palma, and El Hierro. *Mar Geophys Res* 24:1–40. <https://doi.org/10.1007/s11001-004-1513-3>
- Ancochea E, Hernán F, Huertas M, Brändle J, Herrera R (2006) A new chronostratigraphical and evolutionary model for La Gomera: implications for the overall evolution of the Canarian Archipelago. *J Volcanol Geotherm Res* 157:271–293. <https://doi.org/10.1016/j.jvolgeores.2006.04.001>
- Barrett R, Lebas E, Ramalho R, Klaucke I, Kutterolf S, Klügel A, Lindhorst K, Gross F, Krastel S (2020) Revisiting the tsunamigenic volcanic flank collapse of Fogo island in the Cape Verdes, offshore West Africa. In: Georgiopoulou A, Amy L, Benetti S, Chaytor J, Clare M, Gamboa D, Haughton P, Moernaut J, Mountjoy J (eds) *Subaqueous mass movements and their consequences: advances in process understanding, monitoring and hazard assessments*. *Geol Soc Lond, Spec Pub* 500, pp 13–26. <https://doi.org/10.1144/SP500-2019-187>
- Becerril L, Galve J, Morales J, Romero C, Sánchez N, Martí J, Galindo I (2016) Volcanostructure of El Hierro (Canary Islands). *J Maps* 12 (S1):43–52. <https://doi.org/10.1080/17445647.2016.1157767>
- Begét J, Kienle J (1992) Cyclic formation of debris avalanches at Mount St Augustine Volcano. *Nature* 356:701–704. <https://doi.org/10.1038/356701a0>
- Blahůt J, Balek J, Klimeš J, Rowberry M, Kusák M, Kalina J (2019) A comprehensive global database of giant landslides on volcanic islands. *Landslides* 16:2045–2052. <https://doi.org/10.1007/s10346-019-01275-8>
- Blahůt J, Baroň I, Sokol L, Meletlidis S, Klimeš J, Rowberry M, Melichar R, García-Cañada L, Martí X (2018a) Large landslide stress states calculated following extreme climatic and tectonic events on El Hierro, Canary Islands. *Landslides* 15:1801–1814. <https://doi.org/10.1007/s10346-018-0993-1>
- Blahůt J, Klimeš J, Rowberry M, Kusák M (2018b) Database of giant landslides on volcanic islands—first results from the Atlantic Ocean. *Landslides* 15:823–827. <https://doi.org/10.1007/s10346-018-0967-3>
- Blahůt J, Mitrovic-Woodell I, Baroň I, René M, Rowberry M, Blard P, Hartvich F, Meletlidis S (2020) Volcanic edifice slip events recorded on the fault plane of the San Andrés Landslide, El Hierro Canary Islands. *Tectonophysics* 776:228317. <https://doi.org/10.1016/j.tecto.2019.228317>
- Blahůt J, Poretti I, De Amicis M, Sterlacchini S (2012) Database of geohydrological disasters for civil protection purposes. *Nat Hazards* 60:1065–1083. <https://doi.org/10.1007/s11069-011-9893-6>
- Blahůt J, Rowberry M, Balek J, Klimeš J, Baroň I, Meletlidis S, Martí X (2017) Monitoring giant landslide detachment planes in the era of big data analytics. In: Mikoš M, Arbanas Ž, Yin Y, Sassa K (eds) *Advancing culture of living with landslides*. Springer, Cham, pp 333–340. https://doi.org/10.1007/978-3-319-53487-9_38
- Boulesteix T, Hildenbrand A, Soler V, Quidelleur X, Gillot P (2013) Coeval giant landslides in the Canary Islands: implications for global, regional, and local triggers of giant flank collapses on oceanic volcanoes. *J Volcanol Geotherm Res* 257:90–98. <https://doi.org/10.1016/j.jvolgeores.2013.03.008>
- Brunet M, Le Friant A, Boudon G, Lafuerza S, Talling P, Hornbach M, Ishizuka O, Lebas E, Guyard H, IODP Expedition 340 Science Party (2016) Composition, geometry, and emplacement dynamics of a large volcanic island landslide offshore Martinique: from volcano flank collapse to seafloor sediment failure? *Geochem Geophys Geosyst* 17:699–724. <https://doi.org/10.1002/2015GC006034>
- Brunetti M, Guzzetti F, Cardinali M, Fiorucci F, Santangelo M, Mancinelli P, Komatsu G, Borselli L (2014) Analysis of a new geomorphological inventory of landslides in Valles Marineris, Mars. *Earth Planet Sci Lett* 405:156–168. <https://doi.org/10.1016/j.epsl.2014.08.025>
- Camerlenghi A, Urgeles R, Fantoni L (2010) A database on submarine landslides of the Mediterranean Sea. In: Mosher D, Shipp R, Moscardelli L, Chaytor J, Baxter C, Lee H, Urgeles R (eds) *Submarine mass movements and their consequences*. Springer, Dordrecht, pp 503–513. https://doi.org/10.1007/978-90-481-3071-9_41
- Carracedo J, Day S, Guillou H, Pérez Torrado F (1999) Giant Quaternary landslides in the evolution of La Palma and El Hierro, Canary Islands. *J Volcanol Geotherm Res* 94:169–190. [https://doi.org/10.1016/S0377-0273\(99\)00102-X](https://doi.org/10.1016/S0377-0273(99)00102-X)
- Casillas R, Fernández C, Colmenero J, De La Nuez J, García-Navarro E, Martín M (2010) Deformation structures associated with the Tazo landslide (La Gomera, Canary Islands). *Bull Volcanol* 72:945–960. <https://doi.org/10.1007/s00445-010-0373-8>
- Chaytor J, Ten Brink U, Solow A, Andrews B (2009) Size distribution of submarine landslides along the U.S Atlantic Margin. *Mar Geol* 264:16–27. <https://doi.org/10.1016/j.margeo.2008.08.007>
- Clouard V, Bonneville A (2004) Submarine landslides in French Polynesia. In: Hekinian R, Stoffers P, Cheminée J (eds) *Oceanic hotspots: intraplate submarine magmatism and tectonism*. Springer, Heidelberg, pp 209–238. https://doi.org/10.1007/978-3-642-18782-7_7
- Clouard V, Bonneville A, Gillot P (2001) A giant landslide on the southern flank of Tahiti Island, French Polynesia. *Geophys Res Lett* 28:2253–2256. <https://doi.org/10.1029/2000GL012604>
- Coello-Bravo J, Márquez Á, Herrera R, Huertas M, Ancochea E (2020) Multiple related flank collapses on volcanic oceanic islands: evidence from the debris avalanche deposits in the Orotava Valley water galleries (Tenerife, Canary Islands). *J Volcanol Geotherm Res* 401:106980. <https://doi.org/10.1016/j.jvolgeores.2020.106980>
- Coombs M, White S, Scholl D (2007) Massive edifice failure at Aleutian Arc Volcanoes. *Earth Planet Sci Lett* 256:403–418. <https://doi.org/10.1016/j.epsl.2007.01.030>
- Cornu M, Paris R, Doucelance R, Bachélery P, Bosq C, Auclair D, Benbakkar M, Gannoun A, Guillou H (2021) Exploring the links between volcano flank collapse and the magmatic evolution of an ocean island volcano: Fogo Cape, Verde. *Sci Rep* 11:17478. <https://doi.org/10.1038/s41598-021-96897-1>
- Costa A, Marques F, Hildenbrand A, Sibrant A, Catita C (2014) Large scale catastrophic flank collapses in a steep volcanic ridge: the Pico-Faial Ridge, Azores Triple Junction. *J Volcanol Geotherm Res* 272:111–125. <https://doi.org/10.1016/j.jvolgeores.2014.01.002>
- Coussens M, Wall-Palmer D, Talling P, Watt S, Cassidy M, Jutzeler M, Clare M, Hunt J, Manga M, Gernon T, Palmer M, Hatter S, Boudon G, Endo D, Fujinawa A, Hatfield R, Hornbach M, Ishizuka O, Kataoka K, Le Friant A, Maeno F, McCanta M, Stinton A (2016) The relationship between eruptive activity, flank collapse, and sea level at volcanic islands: a long term (>1 Ma) record offshore Montserrat, Lesser Antilles. *Geochem Geophys Geosyst* 17:2591–2611. <https://doi.org/10.1002/2015GC006053>

- Crosta G, Frattini P, Valbuzzi E, De Blasio F (2018) Introducing a new inventory of large Martian landslides. *Earth Space Sci* 5:89–119. <https://doi.org/10.1002/2017EA000324>
- Crutchley G, Kopp H (2018) Reflection and refraction seismic methods. In: Micallef A, Krastel S, Savini A (eds) *Submarine geomorphology*. Springer, Cham, pp 43–62. https://doi.org/10.1007/978-3-319-57852-1_4
- Cutler K, Watt S, Cassidy M, Madden-Nadeau A, Engwell S, Abdurrahman M, Nurshal M, Tappin D, Carey S, Novellino A, Hayer C, Hunt J, Day S, Grilli S, Kurniawan I, Kartadinata N (2022) Downward propagating eruption following vent unloading implies no direct magmatic trigger for the 2018 lateral collapse of Anak Krakatau. *Earth Planet Sci Lett* 578:117332. <https://doi.org/10.1016/j.epsl.2021.117332>
- Dávila Harris P, Branney M, Storey M (2011) Large eruption triggered ocean island landslide at Tenerife: onshore record and long term effects on hazardous pyroclastic dispersal. *Geology* 39:951–954. <https://doi.org/10.1130/G31994.1>
- Day S, Llanes P, Silver E, Hoffmann G, Ward S, Driscoll N (2015) Submarine landslide deposits of the historical lateral collapse of Ritter Island, Papua New Guinea. *Mar Pet Geol* 67:419–438. <https://doi.org/10.1016/j.marpetgeo.2015.05.017>
- Deplus C, Le Friant A, Boudon G, Komorowski J, Villemant B, Harford C, Ségoufin J, Cheminée J (2001) Submarine evidence for large scale debris avalanches in the Lesser Antilles Arc. *Earth Planet Sci Lett* 192:145–157. [https://doi.org/10.1016/S0012-821X\(01\)00444-7](https://doi.org/10.1016/S0012-821X(01)00444-7)
- EMODNET (2019) European marine observation and data network. <http://www.emodnet.eu/geoviewer>. Last accessed 20 June 2019
- Franceschini R, Rosi A, Catani F, Casagli N (2022) Exploring a landslide inventory created by automated web data mining: the case of Italy. *Landslides* 19:841–853. <https://doi.org/10.1007/s10346-021-01799-y>
- Froude M, Petley D (2018) Global fatal landslide occurrence from 2004 to 2016. *Nat Hazards Earth Syst Sci* 18:2161–2181. <https://doi.org/10.5194/nhess-18-2161-2018>
- Gamboa D, Omira R, Terrinha P (2021) A database of submarine landslides offshore west and southwest Iberia. *Sci Data* 8:185. <https://doi.org/10.1038/s41597-021-00969-w>
- Gee M, Watts A, Masson D, Mitchell N (2001) Landslides and the evolution of El Hierro in the Canary Islands. *Mar Geol* 177:271–293. [https://doi.org/10.1016/S0025-3227\(01\)00153-0](https://doi.org/10.1016/S0025-3227(01)00153-0)
- GMRT (2019) Global multi resolution topography v 3.4. <http://www.marine-geo.org/tools/GMRTMapTool>. Last accessed 20 June 2019
- Grilli S, Tappin D, Carey S, Watt S, Ward S, Grilli A, Engwell S, Zhang C, Kirby J, Schambach L, Muin M (2019) Modelling of the tsunami from the December 22, 2018 lateral collapse of Anak Krakatau volcano in the Sunda Straits, Indonesia. *Sci Rep* 9:11946. <https://doi.org/10.1038/s41598-019-48327-6>
- Grilli S, Zhang C, Kirby J, Grilli A, Tappin D, Watt S, Hunt J, Novellino A, Engwell S, Nurshal M, Abdurrahman M, Cassidy M, Madden-Nadeau A, Day S (2021) Modeling of the Dec. 22nd 2018 Anak Krakatau volcano lateral collapse and tsunami based on recent field surveys: comparison with observed tsunami impact. *Mar Geol* 440:106566. <https://doi.org/10.1016/j.margeo.2021.106566>
- Guzzetti F, Mondini A, Cardinali M, Fiorucci F, Santangelo M, Chang K (2012) Landslide inventory maps: new tools for an old problem. *Earth-Sci Rev* 112:42–66. <https://doi.org/10.1016/j.earscirev.2012.02.001>
- Hildenbrand A, Gillot P, Bonneville A (2006) Offshore evidence for a huge landslide of the northern flank of Tahiti-Nui (French Polynesia). *Geochem Geophys Geosyst* 7:Q03006. <https://doi.org/10.1029/2005GC001003>
- Hildenbrand A, Marques F, Catalão J (2018) Large scale mass wasting on small volcanic islands revealed by the study of Flores Island (Azores). *Sci Rep* 8:13898. <https://doi.org/10.1038/s41598-018-32253-0>
- Hildebrand A, Marques F, Catalão J, Catita C, Costa A (2012) Large scale active slump of the southeastern flank of Pico Island, Azores. *Geology* 40:939–942. <https://doi.org/10.1130/G33303.1>
- Holcomb R, Searle R (1991) Large landslides from oceanic volcanoes. *Mar Geotechnol* 10:19–32. <https://doi.org/10.1080/10641199109379880>
- Hoofft E, Nomikou P, Toomey D, Lampridou D, Getz C, Christopoulou M, O'Hara D, Arnoux G, Bodmer M, Gray M, Heath B, Vanderbeek B (2017) Backarc tectonism, volcanism, and mass wasting shape seafloor morphology in the Santorini-Christiana-Amorgos region of the Hellenic Volcanic Arc. *Tectonophysics* 712–713:396–414. <https://doi.org/10.1016/j.tecto.2017.06.005>
- Hughes Clark J (2018) Multibeam echosounders. In: Micallef A, Krastel S, Savini A (eds) *Submarine geomorphology*. Springer, Cham, pp 25–41. https://doi.org/10.1007/978-3-319-57852-1_3
- Hunt J, Talling P, Clare M, Jarvis I, Wynn R (2014) Long term (17 Ma) turbidite record of the timing and frequency of large flank collapses of the Canary Islands. *Geochem Geophys Geosyst* 15:3322–3345. <https://doi.org/10.1002/2014GC005232>
- Hunt J, Tappin D, Watt S, Susilohadi S, Novellino A, Ebmeier S, Cassidy M, Engwell S, Grilli S, Hanif M, Priyanto W, Clare M, Abdurrahman M, Udrekh U (2021) Submarine landslide megablocks show half of Anak Krakatau island failed on December 22nd 2018. *Nat Commun* 12:2827. <https://doi.org/10.1038/s41467-021-22610-5>
- Hunt J, Wynn R, Masson D, Talling P, Teagle D (2011) Sedimentological and geochemical evidence for multistage failure of volcanic island landslides: a case study from Icod landslide on north Tenerife, Canary Islands. *Geochem Geophys Geosyst* 12:Q12007. <https://doi.org/10.1029/2011GC003740>
- Hunt J, Wynn R, Talling P, Masson D (2013) Multistage collapse of eight western Canary Island landslides in the last 1.5 Ma: sedimentological and geochemical evidence from subunits in submarine flow deposits. *Geochem Geophys Geosyst* 14:2159–2181. <https://doi.org/10.1002/ggge.20138>
- Jakobsson M (2020) Roadmap for future ocean floor mapping. The Nippon Foundation - General Bathymetric Chart of the Oceans - Seabed 2030. Downloaded from <https://seabed2030.org>
- Juang C, Stanley T, Kirschbaum D (2019) Using citizen science to expand the global map of landslides: introducing the Cooperative Open Online Landslide Repository (COOLR). *PLoS ONE* 14: e0218657. <https://doi.org/10.1371/journal.pone.0218657>
- Katz O, Reuven E, Aharonov E (2015) Submarine landslides and fault scarps along the eastern Mediterranean Israeli continental slope. *Mar Geol* 369:100–115. <https://doi.org/10.1016/j.margeo.2015.08.006>
- Kirschbaum D, Adler R, Hong Y, Hill S, Lerner-Lam A (2010) A global landslide catalog for hazard applications: method, results, and limitations. *Nat Hazards* 52:561–575. <https://doi.org/10.1007/s11069-009-9401-4>
- Klaucke I (2018) Sidescan sonar. In: Micallef A, Krastel S, Savini A (eds) *Submarine geomorphology*. Springer, Cham, pp 13–24. https://doi.org/10.1007/978-3-319-57852-1_2
- Krastel S, Schmincke H, Jacobs C, Rihm R, Le Bas T, Alibés B (2001) Submarine landslides around the Canary Islands. *J Geophys Res-Solid Earth* 106:977–997. <https://doi.org/10.1029/2000JB900413>
- Kreuzer T, Damm B (2020) Automated digital data acquisition for landslide inventories. *Landslides* 17:2205–2215. <https://doi.org/10.1007/s10346-020-01431-5>
- Langford S, Brill R (1972) Giant submarine landslides on the Hawaiian Ridge: a rebuttal. *Pac Sci* 26:254–258

- Leat P, Tate A, Tappin D, Day S, Owen M (2010) Growth and mass wasting of volcanic centers in the northern South Sandwich Arc, South Atlantic, revealed by new multibeam mapping. *Mar Geol* 275:110–126. <https://doi.org/10.1016/j.margeo.2010.05.001>
- Le Bas T, Masson D, Holtom R, Grevemeyer I (2007) Slope failures of the flanks of the southern Cape Verde Islands. In: Lykousis V, Sakellariou D, Locat J (eds) *Submarine mass movements and their consequences*. Springer, Dordrecht, pp 337–345. https://doi.org/10.1007/978-1-4020-6512-5_35
- León R, Somoza L, Urgeles R, Medialdea T, Ferrer M, Biain A, García-Crespo J, Mediato J, Galindo I, Yepes J, González F, Gimenez-Moreno J (2017) Multi-event oceanic island landslides: new onshore-offshore insights from El Hierro Island, Canary Archipelago. *Mar Geol* 393:156–175. <https://doi.org/10.1016/j.margeo.2016.07.001>
- Lipman P, Normark W, Moore J, Wilson J, Gutmacher C (1988) The giant submarine Alike debris slide, Mauna Loa, Hawaii. *J Geophys Res-Solid Earth* 93:4279–4299. <https://doi.org/10.1029/JB093iB05p04279>
- Marques F, Hildenbrand A, Costa A, Sibrant A (2020) The evolution of Santa Maria Island in the context of the Azores Triple Junction. *Bull Volcanol* 82:39. <https://doi.org/10.1007/s00445-020-01378-4>
- Marques F, Catalão J, Hübscher C, Costa A, Hildenbrand A, Zeyen H, Nomikou P, Lebas E, Zanon V (2021) The shaping of a volcanic ridge in a tectonically active setting: the Pico-Faial Ridge in the Azores Triple Junction. *Geomorphology* 378:107612. <https://doi.org/10.1016/j.geomorph.2021.107612>
- Martínez-Moreno F, Monteiro Santos F, Madeira J, Pous J, Bernardo I, Soares A, Esteves M, Adão F, Ribeiro J, Mata J, Brum da Silveira A (2018) Investigating collapse structures in oceanic islands using magnetotelluric surveys: the case of Fogo Island in Cape Verde. *J Volcanol Geotherm Res* 357:152–162. <https://doi.org/10.1016/j.jvolgeores.2018.04.028>
- Masson D, Le Bas T, Grevemeyer I, Weinrebe W (2008) Flank collapse and large scale landsliding in the Cape Verde Islands, off West Africa. *Geochem Geophys Geosyst* 9:Q07015. <https://doi.org/10.1029/2008GC001983>
- Masson D, Watts A, Gee M, Urgeles R, Mitchell N, Le Bas T, Canals M (2002) Slope failures on the flanks of the western Canary Islands. *Earth-Sci Rev* 57:1–35. [https://doi.org/10.1016/S0012-8252\(01\)00069-1](https://doi.org/10.1016/S0012-8252(01)00069-1)
- McGuire W (1996) Volcano instability: a review of contemporary themes. In: McGuire W, Jones A, Neuberger J (eds) *Volcano instability on earth and other planets*. *Geol Soc Lond, Spec Pub* 110, pp 1–23. <https://doi.org/10.1017/S0016756897216468>
- McMurtry G, Watts P, Fryer G, Smith J, Imamura F (2004) Giant landslides, megatsunamis, and paleo-sea level in the Hawaiian Islands. *Mar Geol* 203:219–233. [https://doi.org/10.1016/S0025-3227\(03\)00306-2](https://doi.org/10.1016/S0025-3227(03)00306-2)
- Moore J (1964) Giant submarine landslides on the Hawaiian Ridge. US Geological Survey Professional Paper 501-D:95-98
- Moore J, Clague D, Holcomb R, Lipman P, Normark W, Torresan M (1989) Prodigious submarine landslides on the Hawaiian Ridge. *J Geophys Res-Solid Earth* 94:17465–17484. <https://doi.org/10.1029/JB094iB12p17465>
- Moore J, Normark W, Holcomb R (1994) Giant Hawaiian underwater landslides. *Science* 264:46–47. <https://doi.org/10.1126/science.264.5155.46>
- Oehler J, Lénat J, Labazuy P (2008) Growth and collapse of the Reunion Island Volcanoes. *Bull Volcanol* 70:717–742. <https://doi.org/10.1007/s00445-007-0163-0>
- Omira R, Quartau R, Ramalho I, Baptista M, Mitchell N (2016) The tsunami effects of a collapse of a volcanic island on a semienclosed basin. In: Duarte J, Schellart W (eds) *Plate boundaries and natural hazards*. Wiley, Hoboken, pp 271–287. <https://doi.org/10.1002/9781119054146.ch13>
- Owen S, Segall P, Lisowski M, Miklius A, Denlinger R, Sako M (2000) Rapid deformation of Kilauea Volcano: global positioning system measurements between 1990 and 1996. *J Geophys Res-Solid Earth* 105(B8):18983–18998. <https://doi.org/10.1029/2000JB900109>
- Pennington C, Freeborough K, Dashwood C, Dijkstra T, Lawrie K (2015) The national landslide database of Great Britain: acquisition, communication, and the role of social media. *Geomorphology* 249:44–51. <https://doi.org/10.1016/j.geomorph.2015.03.013>
- Quartau R, Ramalho R, Madeira J, Santos R, Rodrigues A, Roque C, Carrara G, Brum da Silveira A (2018) Gravitational, erosional, and depositional processes on volcanic ocean islands: insights from the submarine morphology of Madeira archipelago. *Earth Planet Sci Lett* 482:288–299. <https://doi.org/10.1016/j.epsl.2017.11.003>
- Ramalho R, Winckler G, Madeira J, Helffrich G, Hipólito A, Quartau R, Adena K, Schaefer J (2015) Hazard potential of volcanic flank collapses raised by new megatsunami evidence. *Sci Adv* 1: e1500456. <https://doi.org/10.1126/sciadv.1500456>
- Romagnoli C, Kokelaar P, Casalbore D, Chiocci F (2009) Lateral collapses and active sedimentary processes on the northwestern flank of Stromboli Volcano, Italy. *Mar Geol* 265:101–119. <https://doi.org/10.1016/j.margeo.2009.06.013>
- Sibrant A, Hildenbrand A, Marques F, Weiss B, Boulesteix T, Hübscher C, Lüdmann T, Costa A, Catalão J (2015) Morphostructural evolution of a volcanic island developed inside an active oceanic rift: S. Miguel Island (Terceira Rift, Azores). *J Volcanol Geotherm Res* 301:90–106. <https://doi.org/10.1016/j.jvolgeores.2015.04.011>
- Silver E, Day S, Ward S, Hoffmann G, Llanes P, Driscoll N, Appelgate B, Saunders S (2009) Volcano collapse and tsunami generation in the Bismarck Volcanic Arc, Papua New Guinea. *J Volcanol Geotherm Res* 186:210–222. <https://doi.org/10.1016/j.jvolgeores.2009.06.013>
- Solaro C, Boudon G, Le Friant A, Balcone-Boissard H, Emmanuel L, Paterne M, Expedition Science Party IODP (2020) New insights into the recent eruptive and collapse history of Montagne Pelée (Lesser Antilles Arc) from offshore marine drilling site U1401A (IODP Expedition 340). *J Volcanol Geotherm Res* 403:107001. <https://doi.org/10.1016/j.jvolgeores.2020.107001>
- SRTM (2019) Shuttle radar topography mission, v 3.0. <https://www2.jpl.nasa.gov/srtm>. Last accessed 20 June 2019
- Strozi T, Klimeš J, Frey H, Caduff R, Huggel C, Wegmüller U, Rapre A (2018) Satellite SAR interferometry for the improved assessment of the state of activity of landslides: a case study from the Cordilleras of Peru. *Remote Sens Environ* 217:111–125. <https://doi.org/10.1016/j.rse.2018.08.014>
- Tozer B, Sandwell D, Smith W, Olson C, Beale J, Wessel P (2019) Global bathymetry and topography at 15 arc sec: SRTM15+. *Earth Space Sci* 6:1847–1864. <https://doi.org/10.1029/2019EA000658>
- Urgeles R, Masson D, Canals M, Watts A, Le Bas T (1999) Recurrent large scale landsliding on the west flank of La Palma, Canary Islands. *J Geophys Res-Solid Earth* 104:25331–25348. <https://doi.org/10.1029/1999JB900243>
- Uruba M, Talling P, Masson D (2013) Timing and frequency of large submarine landslides: implications for understanding triggers and future geohazard. *Quat Sci Rev* 72:63–82. <https://doi.org/10.1016/j.quascirev.2013.04.020>
- Van Den Eeckhaut M, Hervás J (2012) State of the art of national landslide databases in Europe and their potential for assessing landslide susceptibility, hazard, and risk. *Geomorphology* 139–140:545–558. <https://doi.org/10.1016/j.geomorph.2011.12.006>

- Watt S, Karstens J, Micallef A, Berndt C, Urlaub M, Ray M, Desai A, Sammartini M, Klauke I, Böttner C, Day S, Downes H, Kühn M, Elger J (2019) From catastrophic collapse to multiphase deposition: flow transformation, seafloor interaction and triggered eruption following a volcanic island landslide. *Earth Planet Sci Lett* 517:135–147. <https://doi.org/10.1016/j.epsl.2019.04.024>
- Waythomas C, Watts P, Walder J (2006) Numerical simulation of tsunami generation by cold volcanic mass flows at Augustine Volcano, Alaska. *Nat Hazards Earth Syst Sci* 6:671–685. <https://doi.org/10.5194/nhess-6-671-2006>
- Whelan F, Kelletat D (2003) Submarine slides on volcanic islands—a source for megatsunamis in the Quaternary. *Prog Phys Geogr* 27:198–216. <https://doi.org/10.1191/0309133303pp367ra>
- Williams R, Rowley P, Garthwaite M (2019) Reconstructing the Anak Krakatau flank collapse that caused the December 2018 Indonesian tsunami. *Geology* 47:973–976. <https://doi.org/10.1130/G46517.1>

Open Access This chapter is licensed under the terms of the Creative Commons Attribution 4.0 International License (<http://creativecommons.org/licenses/by/4.0/>), which permits use, sharing, adaptation, distribution and reproduction in any medium or format, as long as you give appropriate credit to the original author(s) and the source, provide a link to the Creative Commons license and indicate if changes were made.

The images or other third party material in this chapter are included in the chapter's Creative Commons license, unless indicated otherwise in a credit line to the material. If material is not included in the chapter's Creative Commons license and your intended use is not permitted by statutory regulation or exceeds the permitted use, you will need to obtain permission directly from the copyright holder.





Landslide Disasters Caused by the 2018 Eastern Iburi Earthquake in Hokkaido Japan and the Countermeasures to Completely Prevent the Similar Disasters in the Future

Fawu Wang and Kounghoon Nam

Abstract

The catastrophic 2018 Hokkaido Eastern Iburi Earthquake triggered thousands of shallow liquefied landslides in pyroclastic fall deposits one day after the passage of Typhoon Jebi. The landslides were highly mobile and had long runouts. This study reports novel findings pertaining to distinctive properties of the widely distributed, weathered Plinian Ta-d tephra deposit from Tarumae volcano and their impact on the spatial clustering of the Iburi landslides. Distribution of the landslides is positively correlated with the spatial distribution of the Ta-d tephra. Liquefaction occurred in the weathered Ta-d pumice that has lower soil strength than other local pumice units, despite the absence of unconfined groundwater. The volumetric soil moisture content of weathered Ta-d pumice is very high (> 90%) and exceeds other soil layers, regardless of precipitation variation. The presence of hydrated halloysite was confirmed by X-ray diffraction. The halloysite enhances the shaking-triggered liquefaction because it maintains weathered Ta-d pumice in a highly saturated and exceedingly loose state, even in the absence of unconfined groundwater.

Keywords

Iburi earthquake • Landslides • Liquefaction • Ta-d pumice • Hydrated halloysite

1 Introduction

A magnitude (M_j) 6.7 earthquake occurred on 6 September 2018 at a depth of approximately 35 km in the central and eastern Iburi regions of Hokkaido in Northern Japan. The reported damage included 41 fatalities, 691 injured persons, and 1,016 completely collapsed houses. The Japan Meteorological Agency (JMA) designated this earthquake the 2018 Hokkaido Eastern Iburi Earthquake (Fujiwara et al. 2019). Most of the landslides (5627 failures) occurred intensively between the epicenter and the station that recorded the highest peak ground acceleration (No. HKD 127, Japan). Hundreds of aftershocks followed the main shock. Moreover, in Iburi region, there is a high possibility of earthquakes occurring in the future. Effective countermeasure works are required for sustainable management and disaster mitigation in the study area.

2 Study Area and Geological Settings

Hokkaido is located in one of the most tectonically active regions in the world. It is subjected to westward subduction of the Pacific Plate and convergence between the North American and Eurasian Plates (Kimura 1994; Tamaki et al. 2010). More specifically, due to the collision of the Northeast Honshu Arc-Japan Trench and the Kuril Arc-Trench, Hokkaido presents complex tectonic associations and geological features (Arita et al. 1998). Numerous earthquakes have occurred along the southwestern region of the Kuril Trench, such as the 1993 Mw 7.6 Kushiro-Oki earthquake, the 1994 MJMA 8.1 Hokkaido-Toho-Oki earthquake, and the 2003 Mw 8.3 Tokachi-Oki earthquake (Arita et al. 1998; Okamura et al. 2008). The Hidaka Collision Zone, which is an area of deformation characterized by right-lateral strike-slip movement in central Hokkaido, consists of five belts, i.e., the Sorachi-Yezo Belt (SY), the Idonnappu Belt (ID), the Hidaka Belt (HD), the Yubetsu Belt (YB), and the

F. Wang (✉) · K. Nam
College of Civil Engineering, Tongji University, Shanghai,
20092, China
e-mail: wangfw@tongji.edu.cn

K. Nam
e-mail: soilnam@tongji.edu.cn

Tokoro Belt (TB) (Fig. 1) (Kimura 1983). Their ages range from the Late Jurassic to Paleogene (Kimura 1983). The study area is situated at the frontal fold and thrust belt created by the westward vergence of the Hidaka Mountains (Ozaki and Taku 2014) and extending to an adjoining lowland terrace (Ishikari Depression). Faults and active faults in this region are extremely developed with near north-south strikes, especially at the Eastern Boundary Fault Zone of the Ishikari Lowland (Fig. 2).

The main part of the Eastern Boundary Fault Zone of the Ishikari Lowland originates from Bibai and ends at Abira, Yufutsu, with a convex curve distribution striking from NNE/SSW to NNW/SSE. Two reverse active fault zones (behavioral segments) of the Eastern Boundary Fault Zone of the Ishikari Lowland (i.e., the Yufutsu faults and the Maoi faults) run across the study area. Another active fault, the Karumai behavioral segment, is located southwest to the epicenter of the Iburi earthquake (Fig. 2).

Two major faults, the Atsuma and Biratori faults, with a general NNW/SSE trend, are in the central study area. Eighteen geological units (including water) were classified based on a 1:200,000 seamless geological map and the Seamless Geoinformation of Coastal Zone “Southern Coastal Zone of the Ishikari Depression” (Ozaki and Taku 2014) published by the Geological Survey of Japan, AIST. The outcropped strata in the area are dominated by Neogene and

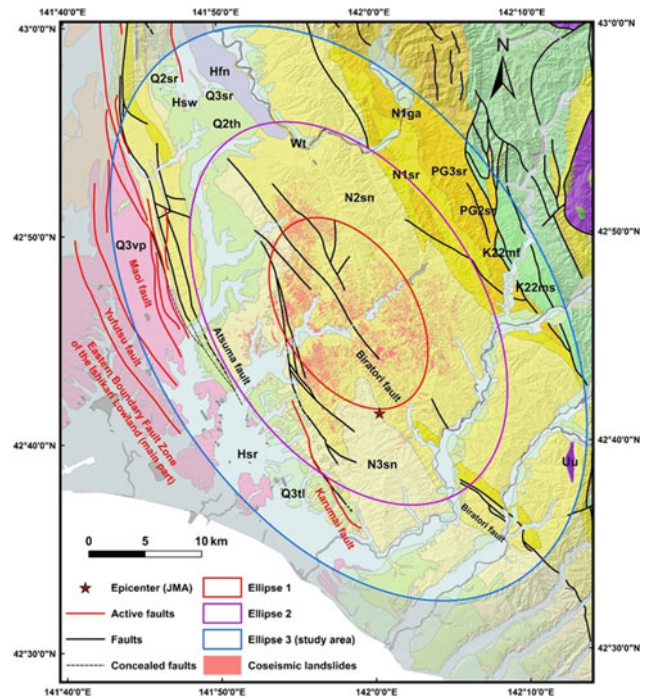
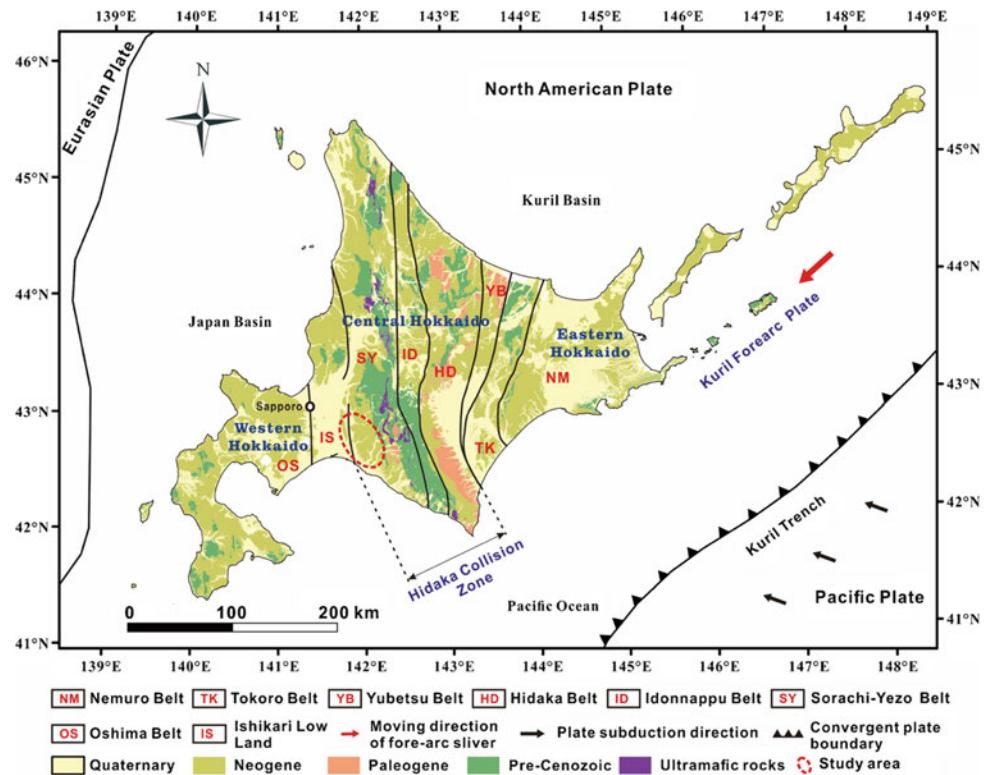


Fig. 2 Geological setting of the study area. Geological units and (active) faults are categorized based on the 1:200,000 seamless geological map published by the Geological Survey of Japan, AIST. The descriptions of geological units (such as N2sn, Hsr, Q3tl, and Q3vp) are listed in Table 1

Fig. 1 Simplified tectonic setting and geochronology around Hokkaido. Tectonic divisions are modified after Kimura (1994), Arita et al. (1998), Takashima et al. (2002), Zhang et al. (2019). Plates boundaries are derived from U.S. Geological Survey. Geochronologic map is classified based on 1:200,000 geological map of Japan from Geological Survey of Japan, AIST



Quaternary marine and non-marine sedimentary rocks and Late Pleistocene non-alkaline pyroclastic flow rocks (Ozaki and Taku 2014). The eastern part is characterized by rugged terrain along with high elevations and presents complex lithologic characteristics. The main strata of the eastern area are represented by Eocene to Oligocene coal-bearing fluvial and marine sedimentary rocks, Early Miocene to Middle Miocene mudstone, sandstone, and alternating beds of sandstone and mudstone with conglomerate and tuff, and Late Cretaceous marine muddy turbidite and mudstone. In addition, ultramafic rocks and Early to Middle Miocene mafic plutonic rocks (which may indicate complex tectonic movement) are also scattered in the vicinity. The hilly terrain is mainly derived from Tarumae Caldera. At least three cyclothem interbedded layers, i.e., Tarumae-d pyroclastic fall deposits, Tarumae-c pyroclastic fall deposits and Tarumae-a, b pyroclastic flow deposits were determined (Tajika et al. 2016). The nethermost layer comprised paleosol (Ta-d loam) and Tarumae-d pyroclastic fall deposits (8–9 ka), including lithic fragments (Ta-d1) and pumice fall (Ta-d2). Middle humus and Tarumae-c pyroclastic fall deposits (2.5–3 ka) constituted the second layer. Humic surface soil, Tarumae-a pyroclastic fall deposits, and Tarumae-b

pyroclastic fall deposits at the top make up the surface layer (Tajika et al. 2016). The total depth of the pyroclastic tephra deposits distributed in the study area above is approximately 4–5 m (Yamagishi and Yamazaki 2018). The central study area is underlain by Middle Miocene to Pliocene mudstone, siltstone, sandstone, and conglomerate. The western part is located in the Ishikari Lowland and consists of Late Pleistocene to Holocene fluvial deposits and Late Pleistocene non-alkaline pyroclastic flow rocks.

To better understand the general features of the study area and to evaluate the effect of primary and triggering factors on landsliding, three terms in addition to the aforementioned CA (class area), LSN (landslide number), and LSA (landslide area) are introduced in this study. These are TLSN (total landslide number), TLSA (total landslide area), and TCA (total class area). Another two indexes, i.e., LSAP (percentage of landslide area) and CAP (class area percentage), in addition to the above-mentioned LSNP (landslide number percentage) and LC (landslide concentration), are also described herein. LSNP (LSAP) represents the percentage of number (area) of landslides in one class. LC shows the landslide density of certain class. CAP is the area percentage of one class to the total classes (Table 1).

Table 1 Classification of geological units and coseismic landslides that occurred in each unit

Code	Age	Lithology	CA (km ²)	LSN	LSA (km ²)
N2sn	Middle to late miocene	Sandstone, mudstone, conglomerate, and sandstone (with tuff)	606.3	4924	41.7
N3sn	Late miocene to pliocene	Diatomaceous siltstone with sandstone and conglomerate	199.1	517	3.1
Hsr	Late pleistocene to holocene	Clay, silt, sand, gravel, and peat	230.4	88	1.1
Q2th	Middle pleistocene	Mud, sand, gravel, and peat	129.2	40	0.1
N1sr	Early miocene to middle miocene	Mudstone, sandstone, and conglomerate (with tuff)	82.7	20	0.1
Q2sr	Middle pleistocene	Mud, sand, gravel, and peat	17.1	23	0.2
Q3tl	Late pleistocene	Mud, sand, gravel, peat, and volcanic materials	53.5	8	0.1
PG3sr	Late eocene to early oligocene	Tuffaceous siltstone with sandstone and conglomerate	79.3	2	0.002
Q3sr	Late pleistocene	Sand and volcanic ash sand	0.1	0	0
Hsw	Late pleistocene to holocene	Swamp deposits	0.9	0	0
PG2sr	Middle eocene	Sandstone, mudstone, and conglomerate (with coal and tuff)	1	0	0
N1ga	Early to middle miocene	Basaltic andesite	0.3	0	0
K22mf	Late cretaceous	Marine muddy turbidite	4.8	0	0
Q3vp	Late pleistocene	Rhyolite pumice block, lapilli, and ash	84	0	0
Hfn	Late pleistocene to holocene	Fan deposits gravel, sand, and mud (with peat and volcanic ash)	21.8	0	0
Uu	Unknown	Ultramafic rocks	1.8	0	0
K22ms	Late cretaceous	Marine sandstone	32.3	0	0
Wt		Water	12.5	3	0.04
Total			1557.2	5625	46.3

Modified from Zhang et al. (2019)

3 Coseismic Landslides Generated by Iburi Earthquake

Based on the field investigation, the Iburi landslides are mainly shallow translational landslides with planar slip surfaces. Most landslides are characterized by high mobility and long run-out distances, and almost all the upper slip surfaces are exposed. The shallow landslides began from the collapse of the gully head, incorporated a vast sliding mass along the valley, heaped irregularly at the gully mouth, and ruined several houses and drainage system (Fig. 3a–d). These figures illustrate the soil composition of the landslide in the right flank and in the scarp integrated sliding body. The left-hand side of the scarp, which is located near the ridge of the hill slope and did not collapse due to its shallower dip angle, exhibits a stratigraphic sequence of pyroclastic deposits originating from the Tarumai Volcano. Isopach contour map and field investigation show that Ta-b (AD 1667), Ta-c (ca. 2.5 ka), and Ta-d (ca. 9 ka), with two layers of interbedded Andosols, indicating that this material

corresponds to the pale-brown, clay-rich deposit found on the scarp. The thicknesses of Ta-d, En-a and Spfa-1 pyroclastic fall deposits are 0.3–1.0 m, 0.1–1.0 m and 3–4 m respectively. The top layer has a gray-colored fine humic surface with a depth of about 300 mm. The middle layer is composed of middle humus and Tarumae-c pyroclastic fall deposits formed about 2000 years ago, while the bottom layer is composed of brownish and grayish pumice. The grain size of the bottom layer decreases from the lower to upper part. The potential sliding surface is located in the grayish-green dense pumice deposited about 9000 years ago. The soil composition is closely related to the historic eruption and repose of the Tarumae Volcano (Tajika et al. 2016), and most coseismic landslides occurred in the interface between Ta-d pumice layers. It is discovered through the field reconnaissance that the sliding mass moved along the planar interface of the Ta-d pumice and the underlying paleosol. Sliding zone liquefaction and grain crushing occurred within the saturated pumice layers during the down-slope motion. The crushed and liquified pumice layers

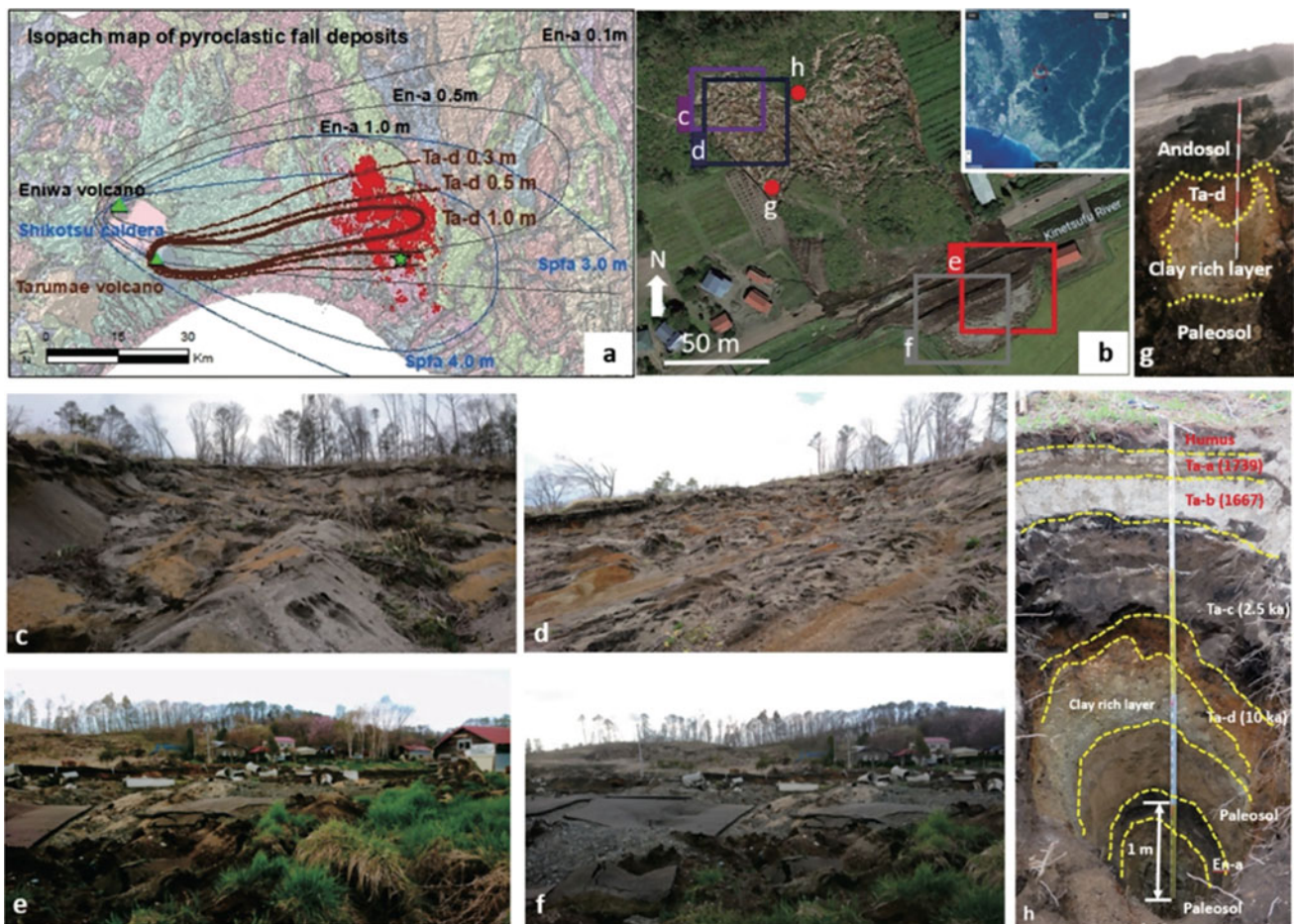


Fig. 3 Isopach map of pyroclastic fall deposits (Ta-a, Ta-b, Ta-c, Ta-d, En-a and Spfa-1) and field investigation on sliding surface (general view: a–d, and soil profiling: e and f)

spread in the deposition area and resulted in the extension of the upper sliding mass in horizontal directions. The slope angle after failure remains unchanged as the pyroclastic fall deposits were evenly deposited on the original slope surface. A sharp-free face appears at the scarp and creates a high possibility of retrogressive slope failure due to future seismic oscillation. According to Kameda et al. (2019), the clay-rich Ta-d layer including halloysite-bearing soils acted as the sole weak and failure plane within the volcanic deposits covering the slopes (Fig. 4). The liquefaction and fluidization of this specific horizon provided the prerequisite conditions for the seismic triggering of the recent landslides.

4 Soil Properties of Ta-d Unit

Although most recent studies have noted the widespread association of Iburi landslides with the Ta-d unit, there has been limited examination of the mechanical and hydrological properties of this deposit. To this end, we carried out a series of in-situ investigations (trench observation, in-situ volumetric soil moisture content (W_v) measurement, and hardness testing) and laboratory tests (grain size analysis, water content measurement, and void ratio testing) on the pyroclastic fall deposits comprising the sliding mass and sliding zone. Based on soil physical properties, the Ta-d unit can be subdivided into four subunits, i.e., pumice with ash (Ta-d P&A), high liquid limit volcanic cohesive soil (Ta-d VH2), medium gravely soil (Ta-d MG), and coarse sandy soil (Ta-d CS). A representative stratigraphic section and stratigraphic column depicting soil composition of the Iburi landslides is illustrated in Fig. 5. Grain size analysis shows that Ta-d pumice has a significant clay content, with a peak of > 20% in Ta-d VH2 (Fig. 5), whereas clay-sized particles are virtually absent in other layers (even in humus or paleosols). Moreover, Ta-d VH2 must have maintained a nearly fully saturated state during the Iburi earthquake, as W_v reaches a peak of approximately 100% in Ta-d VH2 (Fig. 5).

To verify the nearly fully saturated state of Ta-d VH2, the W_v measurement of watermelon and pear were conducted in laboratory as well. For easy comparison, the W_vs of watermelon and pear measurement were tested with the volumetric soil moisture sensors (SE-STEWD-3-WET) those were applied in the W_v measurement of the Ta-d VH2 and all tests were repeated five times. Similarly, the maximum and minimum values were excluded. The W_v of watermelon ranges from 84.6 to 94.4%, and the W_v of pear fluctuates between 85.3 and 94.4%. This means the water content of Ta-d VH2 is even higher than that of watermelon. The high W_v thus not only indicates a high saturation degree of Ta-d VH2, but also signifies a loose state. Similarly, the highest water content value was also observed in undisturbed soil in Ta-d VH2. The high degree of saturation of Ta-d VH2 fully explains the high mobility of the Iburi landslides, one of their striking features. In addition to high saturation, low soil strength is a property favorable to slope failure. Uniaxial compression strength values obtained in hardness tests reach their minimum (almost zero) in Ta-d VH2, indicating extremely low soil strength (Fig. 6). Void ratios of undisturbed soils were also tested, and the highest void ratio of eight was identified in Ta-d pumice (Fig. 6). The Ta-d MG subunit is mainly composed of relatively sound pumice grains with highest void ratio. In summary, Fig. 6 shows how very low uniaxial compression strength coincides with very high W_v in Ta-d VH2, along with high vesicularity. This combination indicates that Ta-d VH2 existed in a highly saturated and loose state with low soil strength, facilitating the widespread occurrence of the Iburi landslides.

5 Countermeasure Works

Since earthquake occurrence in Hokkaido is frequent, it is estimated that the similar phenomenon of rapid and long runout landslides will be triggered by earthquake in the

Fig. 4 Schematic cross-section of pyroclastic fall deposits in study area based on XRD patterns for air-dried (blue lines) and heated (red lines) samples. Hy = halloysite, Qz = quartz, Pl = plagioclase, Po = portlandite (cross section modified from Zhang et al. 2019; Wang et al. 2021)

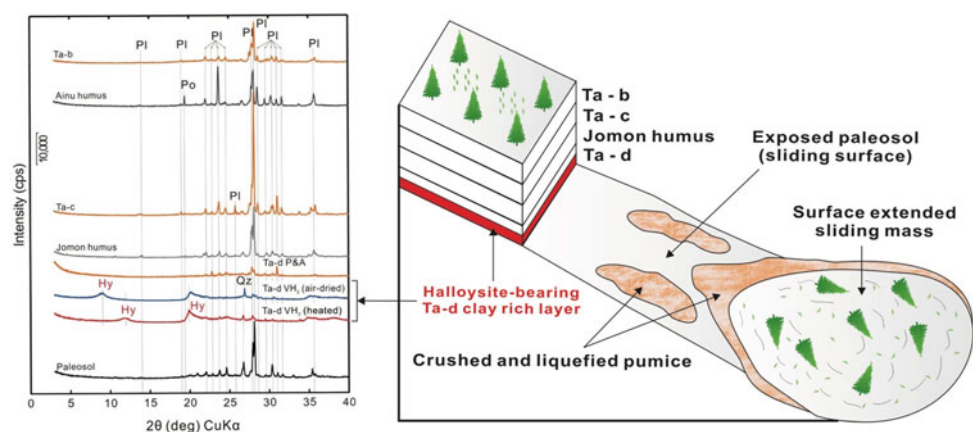
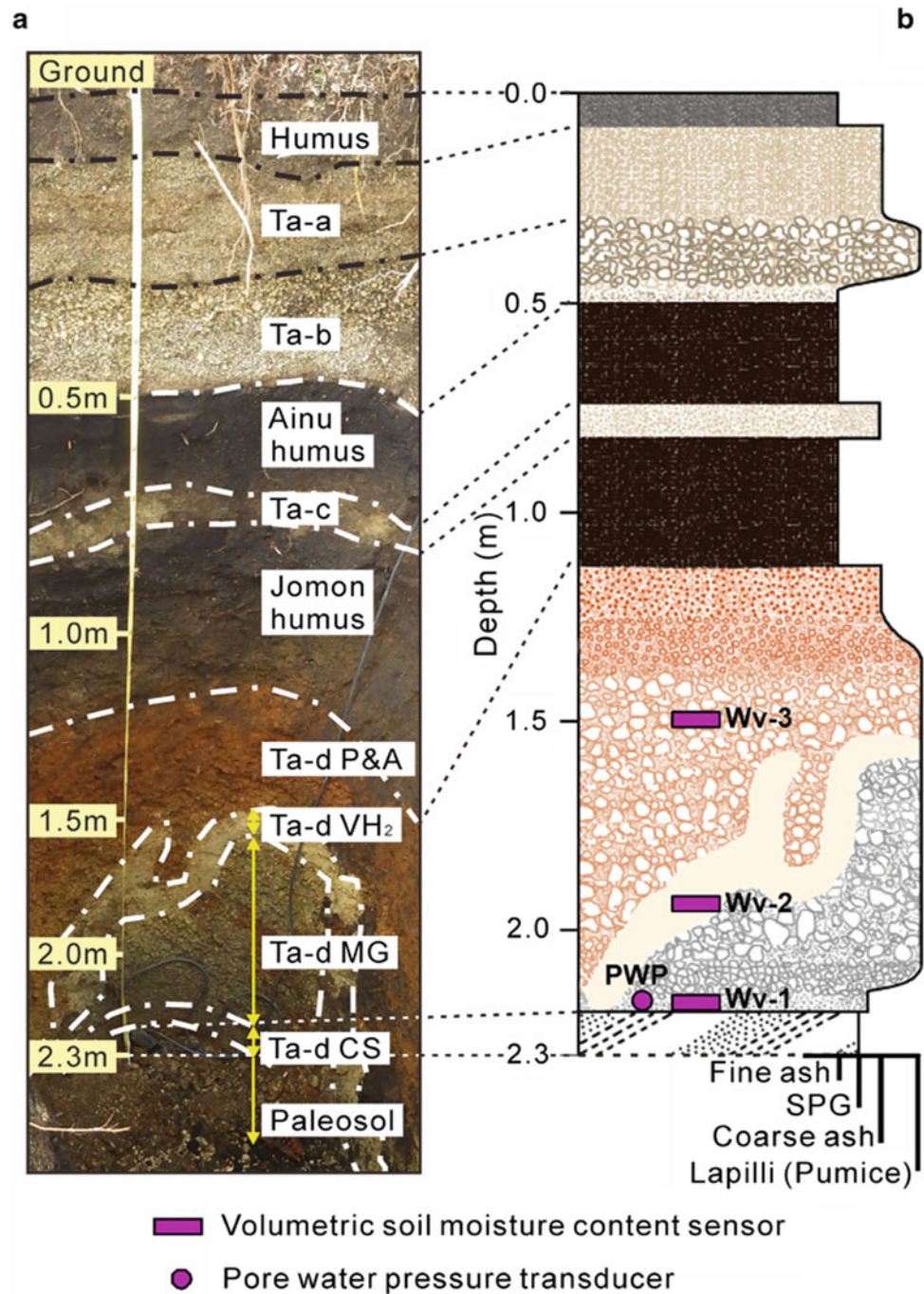


Fig. 5 **a** Representative stratigraphic section at the crown of LS1 and **b** stratigraphic column showing locations of in-situ monitoring sensors (modified from Wang et al. 2021)



same area again (Hua et al. 2019; Kameda et al. 2019). How to protect the local people from the landslide disaster, and how to keep the facilities safe during the earthquake are big questions to be answered by the local administration agency. Considering the earthquake of the same intensity or higher will occur again, and the weathering of the volcanic ashes will go deeper, if no action is taken to change the current geological and

geomorphological condition, the same disaster will certainly happen in the future. Photos in Fig. 7 show the slopes after removing the surficial volcanic ashes. This kind of work has been conducted in the area covered by volcanic ashes including Ta-d, which has potential to become to slide and threaten the safety of people and infrastructures. It is a rare case over the world, and it is of high value to learn from it.

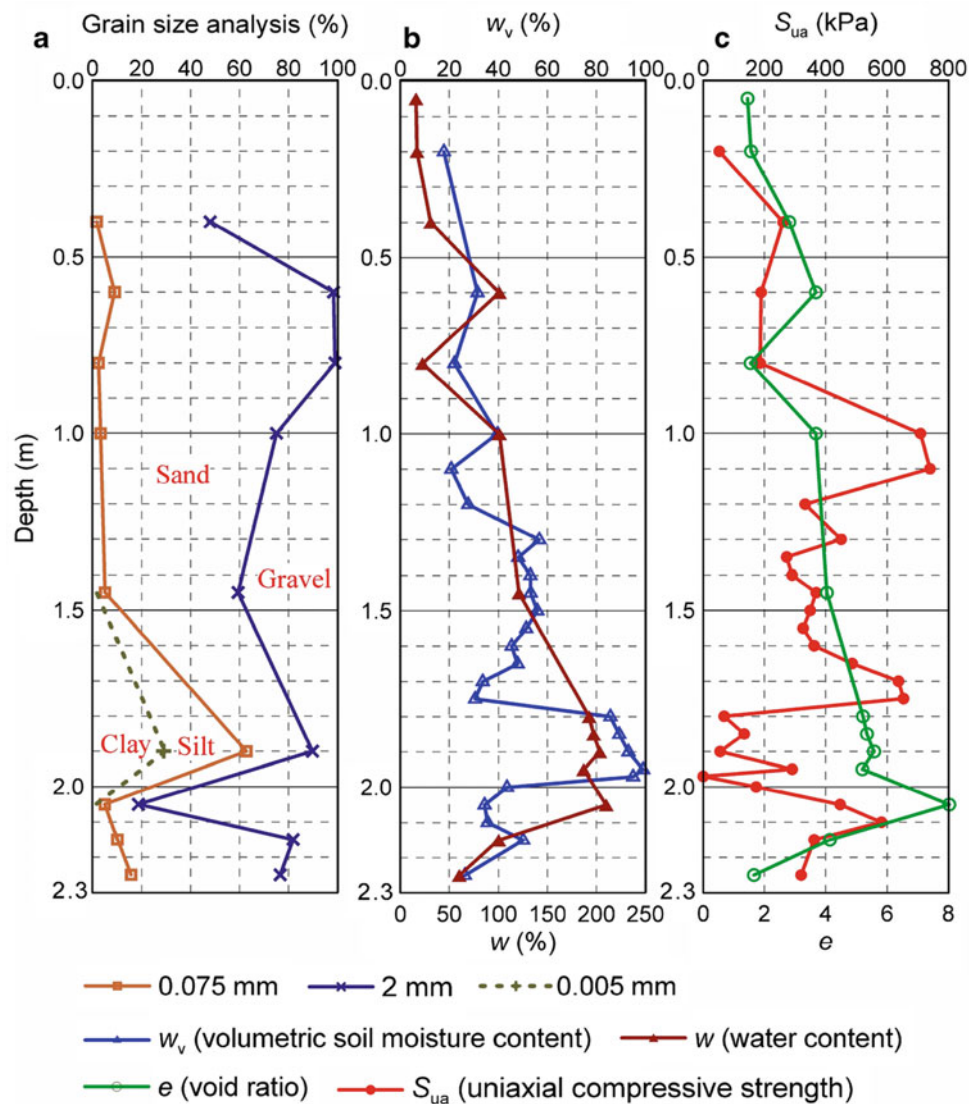


Fig. 6 Soil geotechnical properties along the stratigraphic section at the crown of LS1: **a** Grain size analysis, **b** Volumetric soil moisture content, and **c** Uniaxial compressive strength (modified from Wang et al. 2021)

6 Conclusions

This study is based on the field investigations on concurrent failure of Iburi landslides in Ta-d, and a series of causative tracing studies were then carried out systematically. The positive correlation between spatial clustering of Iburi landslides and the spatial distribution of the Ta-d pumice verifies the crucial role of the Ta-d unit on Iburi landslide distribution from a macroscopic point of view. The causative-tracing study concerning the prevalent occurrence of Iburi landslides in Ta-d led to the recognition of Ta-d and the discovery of its distinguishing properties. Further

exploration of the reason for the generation of distinguishing properties of Ta-d, especially the high saturation, led to our most important finding in this work: the high saturation results from the water-conservation or water-absorption of Ta-d, rather than the preceding rainfall recorded during our long-term monitoring. The water-conservation or water-absorption of Ta-d is rationalized by the occurrence of halloysite. This work argues against the previously stated influence of preceding precipitation on the Iburi landslides and emphasizes the role of distinguishable properties of certain pyroclastic fall deposits on coseismic landslides, even though coseismic landslides are unquestionably affected by factors such as seismic shaking, topography,

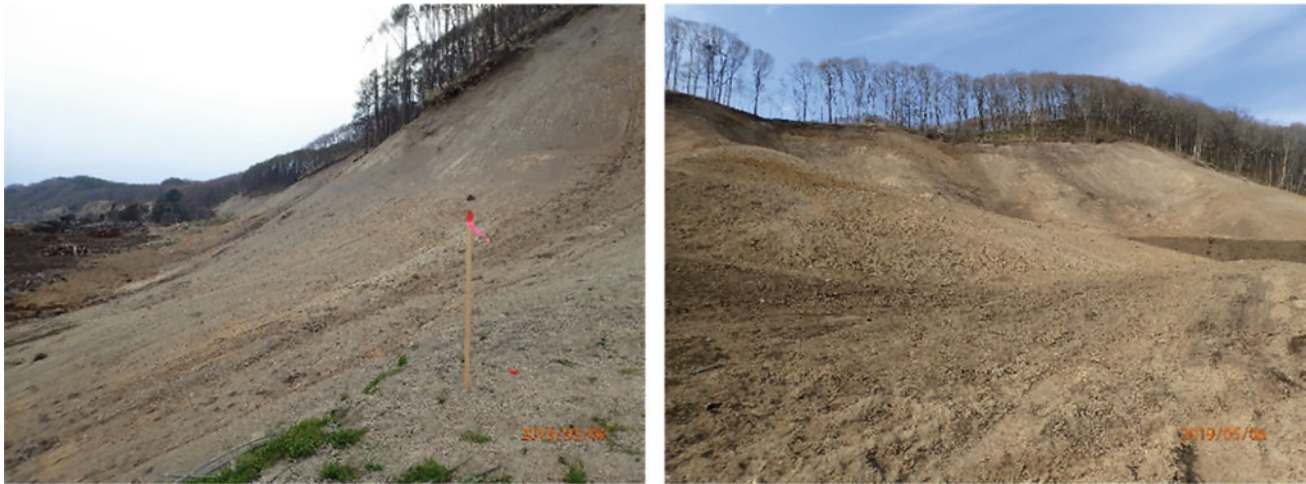


Fig. 7 The photos showing the slopes after removing the surficial volcanic ashes

geological context, and tectonic assembly, among others. Moreover, the correlation analysis between tephra dispersal and coseismic landslide distribution, combined with discovery of halloysite and its potential role in slope destabilization, provides new thoughts for land use management, and geo-hazard risk assessment and reduction, especially in volcanic terranes at active margins world-wide.

Acknowledgements We express our sincere gratitude to J. Bo, P. Li, X. Li (Institute of Disaster Prevention, China), F. Ji (Chengdu University of Technology, China), A. Iio, J. Furuyama, E. Yokota, P. Dhungana (Shimane University, Japan) for their support during field work. We acknowledge support from the local government and geological museum in Atsuma, Hokkaido, Japan.

References

- Arita K, Ikawa T, Ito T, Yamamoto A, Saito M, Nishida Y, Satoh H, Kimura G, Watanabe T, Ikawa T, Kuroda T (1998) Crustal structure and tectonics of the Hidaka Collision Zone, Hokkaido (Japan), revealed by vibroseis seismic reflection and gravity surveys. *Tectonophysics* 290(3–4):197–210
- Fujiwara S, Nakano T, Morishita Y, Kobayashi T, Yarai H, Une H, Hayashi K (2019) Detection and interpretation of local surface deformation from the 2018 Hokkaido Eastern Iburu Earthquake using ALOS-2 SAR data. *Earth Planets Space* 71:64
- Hua Y, Zhao D, Xu Y, Wang Z (2019) Arc-arc collision caused the 2018 Eastern Iburu earthquake (M 6.7) in Hokkaido, Japan. *Sci Rep* 9(13914)
- Kameda J, Kamiya H, Masumoto H, Morisaki T, Hiratsuka T, Inaoi C (2019) Fluidized landslides triggered by the liquefaction of subsurface volcanic deposits during the 2018 Iburu–Tobu earthquake, Hokkaido. *Sci Rep* 9(13119)
- Kimura G (1983) Collision tectonics in Hokkaido and Sakhalin. *Accretion tectonics in the Circum-Pacific regions* 123–134
- Kimura G (1994) The latest cretaceous-early paleogene rapid growth of accretionary complex and exhumation of high pressure series metamorphic rocks in Northwestern Pacific margin. *J Geophys Res Solid Earth* 99(B11):22147–22164
- Ozaki M, Taku K (2014) 1:200,000 land geological map in the Ishikari depression and its surrounding area with explanatory note. Seamless Geoinformation of coastal zone B southern coastal zone of the Ishikari depression, seamless geological map of coastal zone S-4, Geological Survey of Japan ALST
- Okamura Y, Tsujino T, Arai K, Sasaki T, Satake K, Joshima M (2008) Fore arc structure and plate boundary earthquake sources along the southwestern Kuril subduction zone. *J Geophys Res Solid Earth* 113(B6)
- Tajika J, Ohtsu S, Inui T (2016) Interior structure and sliding process of landslide body composed of stratified pyroclastic fall deposits at the Apporo 1 archaeological site, southeastern margin of the Ishikari Lowland, Hokkaido, Northern Japan. *J Geol Soc Japan* 122(1):23–35
- Tamaki M, Kusumoto S, Itoh Y (2010) Formation and deformation processes of late paleogene sedimentary basins in southern central Hokkaido, Japan: paleomagnetic and numerical modeling approach. *Island Arc* 19(2):243–258
- Takashima R, Nishi H, Yoshida T (2002) Geology, petrology and tectonic setting of the Late Jurassic ophiolite in Hokkaido, Japan. *J Asian Earth Sci* 21(2):197–215
- Wang F, Zhang S, Li R, Zhou R, Auer A, Ohira H, Dai Z, Inui T (2021) Hydrated halloysite: the pesky stuff responsible for a cascade of landslides triggered by the 2018 Iburu earthquake, Japan. *Landslides* 18(8):2869–2880
- Yamagishi H, Yamazaki F (2018) Landslides by the 2018 Hokkaido Iburu–Tobu Earthquake on September 6. *Landslides* 15(12):2521–2524
- Zhang S, Li R, Wang F, Iio A (2019) Characteristics of landslides triggered by the 2018 Hokkaido Eastern Iburu earthquake, Northern Japan. *Landslides* 16(9):1691–1708

Open Access This chapter is licensed under the terms of the Creative Commons Attribution 4.0 International License (<http://creativecommons.org/licenses/by/4.0/>), which permits use, sharing, adaptation, distribution and reproduction in any medium or format, as long as you give appropriate credit to the original author(s) and the source, provide a link to the Creative Commons license and indicate if changes were made.

The images or other third party material in this chapter are included in the chapter's Creative Commons license, unless indicated otherwise in a credit line to the material. If material is not included in the chapter's Creative Commons license and your intended use is not permitted by statutory regulation or exceeds the permitted use, you will need to obtain permission directly from the copyright holder.





Landslide Travel Distances in Colombia from National Landslide Database Analysis

Steven Moncayo and Guillermo Ávila

Abstract

The analysis of landslide processes and consequent damages constitutes an important aspect in risk assessment. The potential reach zones of a landslide can be estimated by analyzing the behavior of past events under particular geological, geomorphological, and climatic conditions. Although landslide risk models have been developed for temperate zones, little information is available for tropical countries, so empirical equations are used without validation. In this study, a dataset comprising characteristic parameters for 123 landslides from the Andean region of Colombia was compiled from the digital inventory of the Colombian Geological Survey Mass Movement Information System (SIMMA). Empirical landslide travel-distance models were developed using simple and multiple regression techniques. The results revealed that the volume of the displaced mass, the slope angle, the maximum landslide height, and geomorphological environment were the predominant factors controlling the landslides travel distances in the study area. Similarly, a strong correlation was found between the planimetric area and landslide volume, validating the model of Iverson et al. (1998) (Iverson et al., in *Geol Soc Am Bull* 110:972–984, 1998). The proposed models show a reasonable fit between the observed and predicted values, and exhibited higher prediction capacity than other models in the literature. An example of application of the prediction equations developed here illustrates the procedure to delineate landslide hazard zones for different exceedance probabilities.

Keywords

Empirical relationships • Hazard • Landslide • Travel distance • Statistical analysis

1 Introduction

One of the most important concepts in a landslide hazard assessment is travel distance, and its evaluation constitutes a key element for determining areas exposed to these events. There are several methodologies for estimating the travel length of landslides; for example, numerical models or physical scale models. Most commonly, distances are estimated based on empirical correlations obtained from the analysis of previous events. Landslide travel distances are measured and correlated with variables such as the angle of slope, the volume, types of materials, geological and geomorphological characteristics, and the maximum landslide height, among others (e.g., Corominas 1996; Finlay et al. 1999; Guo et al. 2014; Rickenmann 1999). Unfortunately, correlations are only applicable to the regions where they are developed, so it is necessary to produce local equations where landslide reach studies are scarce, especially in heavily populated tropical environments.

This study uses information from 123 events in the Andean zone of Colombia. Simple and multiple regression statistical techniques are applied to obtain linear equations with the best goodness of fit for determining the extent of landslides from certain influencing factors. Subsequently, the equations obtained are validated and the prediction capacity is compared with other models available in the literature. Finally, an application of the empirical-statistical models in the hazard zonation processes is presented.

S. Moncayo (✉) · G. Ávila
Department of Civil and Agricultural Engineering, Universidad
Nacional de Colombia, Bogotá, D.C., Colombia
e-mail: csmoncayo@unal.edu.co

G. Ávila
e-mail: geavilaa@unal.edu.co

2 Materials and Methods

2.1 Study Area

The information that serves as the basis for this study corresponds to the Andean zone of Colombia. This landslide-prone zone extends from the border with Ecuador in the south, to the border with Venezuela in the northeast, as shown in Fig. 1. The region has an area of 305000 km², and an average elevation of 2000 m above sea level, ranging from areas close to sea level to peaks over 5000 m above sea level. This is the most populated area in the country, encompassing several cities connected by numerous roads. Many of the reported landslides are associated with the intensive road network, urban expansion, and industrial development.

From a physical point of view, this area offers a high degree of complexity due to the tropical climate conditions with high levels of rainfall. Rainfall amounts vary from 1500 mm to more than 3000 mm per year, while mean temperatures range between 8 °C in high mountain areas, up to 28 °C in the valley floors. The complex geology, with the presence of active geological faults in a predominant SW-NE direction, and highly variable soil thicknesses between a few centimeters and several meters, results in the

occurrence of frequent landslides of multiple dimensions, and broad range of travel distances. These conditions contribute to dense vegetation cover and limit land use in the region, and negatively affect the terrain, in such a way that 91% of the total area of the Andean region in Colombia is located in a medium to high landslide hazard category (De Leon 2018).

2.2 Landslide Data

The Colombian Geological Survey oversees the management of a national digital inventory of landslides called the Mass Movement Information System (SIMMA). This system records, stores, and displays information on the most important landslides in Colombia. Records extend from the beginning of the twentieth century to the present, although most data correspond to events occurring over the last 30 years. The inventory is the result of extensive fieldwork undertaken by specialized professionals following the guidelines of the “Andean Multinational Project: Geosciences for the Andean Communities”. The database adopts the Cruden and Varnes (1996) classification system and distinguishes five types of failure mechanisms: fall, flow, lateral spread, slide, and topple.

Fig. 1 Distribution map of the 123 landslides in the Andean region of Colombia



For the purposes of this study, 5994 events corresponding to the period 1900–2019 were initially collected from the SIMMA inventory. An exhaustive depuration of the data was then undertaken. Lateral spreads and topples were excluded because landslide mobility models generally do not include these types of slope failures. In many cases, the information available, even though very useful in identifying the occurrence and characteristics of the landslides, was incomplete with respect to travel distance, or presented some inconsistency for analyses. It was, therefore, necessary to discard many records and use only those with complete information. The number of useful data points was then reduced from 5994 to only 123. This ensured only the most reliable information was used in the regression analyses, and that data volumes were similar to those reported in other studies (e.g., Guo et al. 2014; Qiu et al. 2018).

To validate the statistical models under development, data were divided into two subsets. The first subset was the training dataset from which empirical equations were obtained. The second corresponded to the test dataset, used to evaluate the accuracy of resulting models. Approximately 81% of the data were used to build the training dataset, and 19% to build the test dataset. Through simple random sampling, 100 landslides were selected to build the statistical models, and the remaining 23 for validation.

The spatial distribution of the landslides used for the analyses is shown in Fig. 1. Yellow triangles correspond to training landslide data and red triangles to test landslides data.

2.3 Definition of Terms

Certain attributes described the anatomy of the movement of each registered landslide. These attributes were subsequently used in an analysis of mobility events. The descriptions were based on those published by the IAEG (1990). The travel distance (L) was the horizontal distance from the crown of the sliding source to the toe of the displaced mass. The maximum landslide height (H) was the difference in elevation between the crown and the toe of the landslide. The slope angle (θ) referred to the mean value of the slope gradient before failure. The landslide area (A) was the horizontal projection of the landslide polygon that comprises the total area of the movement. The scheme of a landslide showing each of these attributes is shown in Fig. 2. Another of the attributes analyzed, but not shown in Fig. 2, was the volume (V), which referred to the total volume of the displaced mass. Volume was obtained by multiplying the total area affected by the average thickness of the landslide.

Additionally, six qualitative attributes were collected to describe each landslide in the database. The same attributes were used to develop the statistical models.

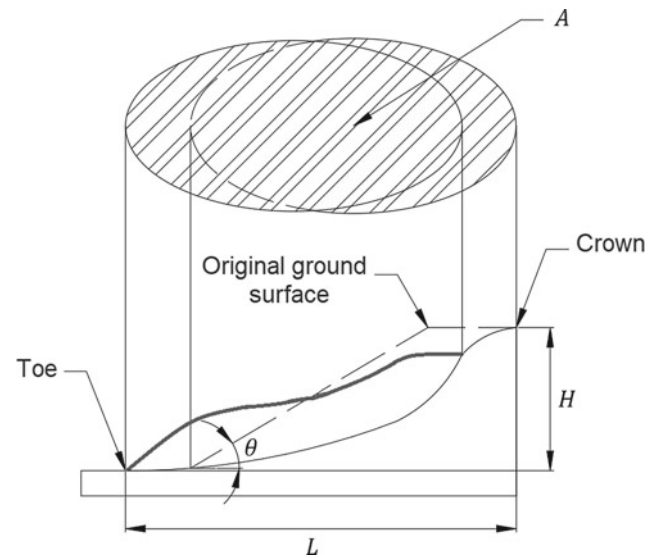


Fig. 2 Conceptual diagram of the anatomy of a landslide. Modified from IAEG (1990)

- (1) The *Geomorphological Environment* attribute was divided into five types: denudational, structural, fluvial, glacial, and volcanic.
- (2) The *Triggering Factor* attribute was divided into six categories: rainfall, erosion, poor drainage management, undermining, mixed, and other (includes ice melt and artificial vibration).
- (3) The *Water Content* attribute was divided into four categories: dry, slightly moist, moist, and very moist.
- (4) The *Lithology* attribute was divided into five types: igneous rock, sedimentary rock, metamorphic rock, deposit, and mixed lithology.
- (5) The *Landslide Type* attribute was divided into four categories: rotational landslide, translational landslide, flow, and fall.
- (6) The *Obstruction* attribute was divided into three types: obstructed travel path, partial obstruction, and no obstruction.

2.4 Methods

Travel distance is evaluated using diverse analysis methods, including empirical, analytical, and numerical methods. Empirical methods, unlike analytical and numerical approaches, consider simpler parameters. For this reason, empirical methods are frequently used as a preliminary evaluation of travel distance when rheological parameters or mechanical details of the movement are not available or required. In addition, simple empirical tools offer a practical method of prediction, especially in regions where information is limited

(Guo et al. 2014; Whittall et al. 2017). A common practice is to relate the mobility of landslides to the most important geometric parameters, mobility being generally represented by the travel distance, or the reach angle. As defined by Heim (1932), this is the angle of the line connecting the highest point from the source of the landslide with the distal margin of the displaced mass (Chen et al. 2015). It is calculated as the arctangent of the ratio H/L, which is equivalent to the coefficient of friction (Shreve 1968). Early authors noted a clear relationship between mobility and volume of the displaced mass (Hsü 1975; Scheidegger 1973). The incidence of other factors on the reach of mass movements was later confirmed.

Other authors consider a two-dimensional approach, such as the one described by Iverson et al. (1998). These researchers obtained a power-law relationship between the planimetric area and volume of the displaced mass through a mass balance approach, with an exponent equal to 2/3. This value was subsequently validated in later studies (e.g., Berti and Simoni 2007; Crosta et al. 2003; Scheidl and Rickenmann 2010). Empirical methods lead to prediction equations through the application of a variety of statistical tools but require validation and adjustment for local conditions, such as those presented here.

In this work, simple and multiple regression techniques were used to obtain the best prediction models to apply to the travel distances from the training dataset of the study region. Initially, the one-to-one relationships between the travel distance and main morphometric parameters were evaluated: maximum landslide height, slope angle, and displaced volume. Later, an area-volume model was obtained to validate the model of Iverson et al. (1998).

To improve the relationships obtained with the simple regression technique, multiple linear regression models were designed. The independent variables used in this analysis were three geometric variables (V, H, θ) and six qualitative variables (Geomorphological Environment, Water Content, Triggering Factor, Lithology, Landslide Type, and Obstruction). Two multiple regression methods were used: the backward elimination method, and the forward selection method. The elimination or selection criteria used were the p-value, and the adjusted coefficient of determination (adjusted R²) criteria. After obtaining the best prediction models, it was necessary to verify that the assumptions of the linear model were met, namely: linearity, normality, homoscedasticity, independence, and non-collinearity. This was achieved using the *gvlma* (), *shapiro.test* (), *ncvTest* (), *durbinWatsonTest* () and *vif* () functions of the R software, respectively; corresponding to different statistical tests that evaluated each of the assumptions.

The travel distance regression models were first validated by self-verification using the training landslides. The models were then applied to the test set, and the average errors of the two datasets were calculated. For local landslides to have a

point of comparison, average errors were calculated after applying other correlation equations developed by other authors outside the study area. Mean absolute percentage error (MAPE) and root mean square error (RMSE) were used for this task. There were defined by Eqs. (1) and (2).

$$\text{MAPE} = \frac{1}{n} \left(\sum_{i=1}^n \left| \frac{\hat{y}_i - y_i}{y_i} \right| \times 100\% \right) \quad (1)$$

$$\text{RMSE} = \sqrt{\frac{\sum_{i=1}^n (\hat{y}_i - y_i)^2}{n}} \quad (2)$$

Where \hat{y}_i and y_i were the predicted and observed values, respectively, and n the number of observations. Using these two error measures together provided extra context on the quality of the fit.

An advantage of empirical models was that the inherent dispersion of the data made it possible to express outputs in quantitative statistical terms (McDougall 2017). Following this logic, and making use of statistical inference tools, it was possible to transform the prediction intervals for a given model in terms of exceedance probabilities. This made it possible to construct a preliminary landslide mobility hazard map. In this study, the models developed for both travel distance and landslide area were used to generate a preliminary hazard map from a landslide record that was not included in the training and test datasets.

3 Results and Discussion

3.1 Distribution of Landslides in the Andean Region

Table 1 shows the descriptive statistics for the numerical variables of the training dataset, including: number of observations (N), mean, standard deviation (StDev), median, range, skewness, and kurtosis. The variables of Table 1 present a positive skewness, so it was necessary to transform each by means of a logarithmic transformation, thus allowing them to comply with statistical normality.

On the other hand, the database records six categorical variables, whose distribution conditions the statistical models since each category influences the mobility of landslides in a certain way. The Geomorphological Environment variable is distributed as follows: 39 events come from denudational environments, 34 from structural environments, 19 correspond to volcanic environments, and finally, glacial and fluvial environments have 4 events. The Triggering Factor variable has 60 landslides in the erosion category, 27 in the rainfall category, 4 in the mixed category, and 3 events in the remaining categories. Regarding the Water Content variable, 40 landslides were identified within

Table 1 Descriptive statistics of the numerical variables of the database

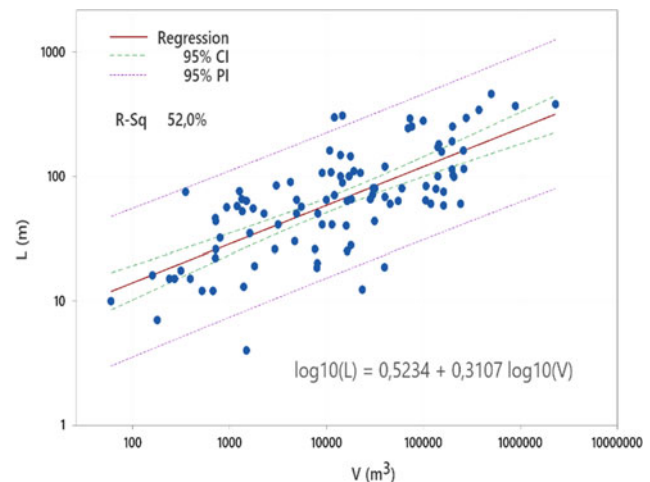
Variable	N	Mean	StDev	Median	Range	Skewness	Kurtosis
L (m)	100	94.95	93.46	64.45	456.00	1.86	3.18
H (m)	100	50.28	55.04	30.00	308.00	2.73	8.45
θ (°)	100	44.25	17.61	40.00	72.00	0.42	-0.57
V (m ³)	100	85,862.54	252,844.68	14,205.00	2,279,940.00	7.11	58.92
A (m ²)	100	11,490.73	26,370.80	3,584.00	186,950.38	4.94	27.49

the moist category, 31 within the slightly moist category, 17 within the very moist category, and 12 within the dry category. Regarding the Lithology, 32 landslides come from a lithology derived from igneous rocks, 27 landslides from a lithology of sedimentary rocks, 15 landslides from a lithology of metamorphic rocks, 13 landslides come from deposits, and 13 from a mixed lithology. The Landslide Type variable presents the following distribution: 59 landslides correspond to translational landslides, 34 to rotational landslides, 4 to falls, and 3 to flows. Regarding the Obstruction variable, 67 landslides had an obstruction in their travel path, 25 did not, and 8 landslides were partly obstructed.

3.2 Relationship Between Mobility and Landslide Volume

It is observed that the H/L ratio tends to decrease with an increase in landslide volume, i.e., the greater the volume, the greater the travel distance of the landslide. The first to notice this behavior was Heim (1932). Later, Scheidegger (1973) used this concept to make predictions through a regression line, establishing that the equivalent friction coefficient decreases with volume for values greater than 10^5 m³ and that below this threshold, movements exhibit a constant reach angle. Hsü (1975) arrived at a similar conclusion, and Corominas (1996) recognized that the volume of small events also influences landslide mobility.

Controversial conclusions have been reached when studying the effect of volume on the reach of mass movements. Kilburn and Sørensen (1998) developed an analytical model in which they observed a clear dependence of H/L on volume. Legros (2002) found a positive relationship between travel distance and volume for both volcanic submarine landslides and non-volcanic submarine landslides, despite the marked differences between the environments in which they are triggered. Budetta and de Riso (2004) also found a good correlation between the two variables for debris flows in Italy. In contrast, Okura et al. (2003) and Hunter and Fell (2003) did not find a clear relationship between volume and the H/L parameter. Some authors, such as Skermer (1985), have established that there is no clear relationship between H/L and volume, and that mobility is determined by the

**Fig. 3** Relationship between travel distance and landslide volume

height of fall. The higher the landslide initiation is the greater will be the travel distance (Corominas, 1996). Staron and Lajeunesse (2009) stated that the correlation between the volume and mobility of a landslide is purely geometric, and does not contain information about the dynamics of the movement.

Figure 3 illustrates the relationship between travel distance and volume in a log–log plot for the study region. The line of best fit is shown along with its equation, the 95% confidence and prediction intervals, and the value of the coefficient of determination (R^2). Observe that there is an increase in mobility with the increase in the displaced volume. Although this is in agreement with most of the studies presented in the literature, the coefficient R^2 (0.52) indicates the model has a poor goodness of fit, since volume is not the only factor controlling landslide mobility.

3.3 Relationship Between Travel Distance and Maximum Landslide Height

The relationship between these two variables is often used to model average equivalent coefficients of friction. Some studies examine the effects of topography on landslide mobility (e.g., Finlay et al. 1999; Hunter and Fell 2003). Basharat and Rohn (2015) confirm the relationship between

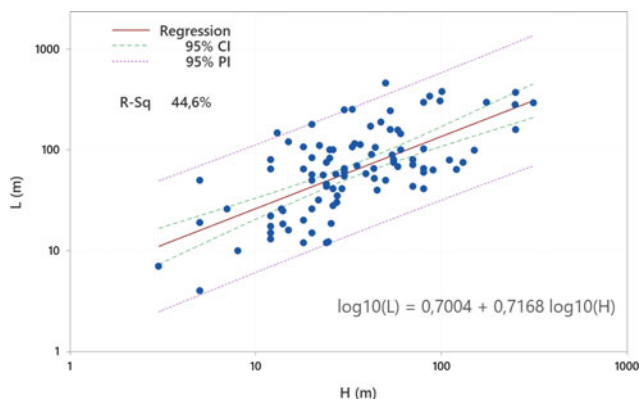


Fig. 4 Relationship between travel distance and maximum landslide height

travel distance and fall height in a logarithmic plot applied to earthquake-induced rockfall events in northeastern Himalayas, Pakistan. This relationship is explained by taking into account that the height of fall governs the potential energy, which makes it responsible for the speed of the landslide, and its travel distance when it is transformed into kinetic energy. Therefore, a greater height of fall leads to a higher speed, and thus a longer travel distance (Corominas 1996; Guo et al. 2014). Other authors indicate that maximum landslide height does not influence the extent of the displaced mass, and is of secondary importance, simply adding dispersion to the analysis (Davies 1982; Hsü 1975; Legros 2002). However, making height an independent variable improves multiple regression models (Finlay et al. 1999; Qiu et al. 2017). Figure 4 shows a trend of increasing travel distance with increasing maximum height. Nevertheless, the model does not present a strong goodness of fit ($R^2 = 0.45$).

3.4 Relationship Between Travel Distance and Slope Angle

In the literature, slope angle has an established negative relationship with travel distance. For example, numerical simulations by Okura et al. (2000) find a positive relationship between H/L and the slope angle: that is, the greater the angle, the shorter the travel distance. Hattanji and Moriwaki (2009), after analyzing a set of relict landslides in Japan, confirm that the equivalent friction coefficient increases with increasing slope steepness (Qiu et al. 2017). Hühnerbach and Masson (2004) conclude that the positive relationship between volume and travel distance supports the relationship with the angle of inclination, since it is common to associate large events with low slopes.

Figure 5 confirms the negative relationship between the travel distance and slope angle; however, the fit is very weak

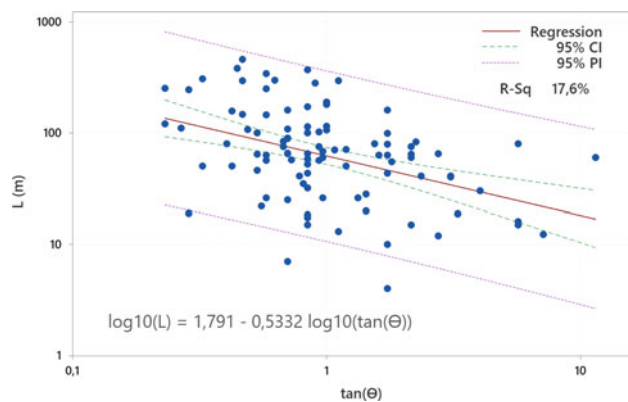


Fig. 5 Relationship between travel distance and slope angle

($R^2 = 0.18$). The data present a large dispersion around the line of best fit, which supports the hypothesis that a single factor, as the slope angle, is not capable of explaining the mobility of landslides.

3.5 Area-Volume Model

Sometimes mass movements not only propagate forward, but also laterally if orthogonal forces occurring during the movement exceed the basal friction of the soil (Strom et al. 2019). This condition creates the need to analyze the landslide area as a mobility index. The study by Iverson et al. (1998) is noteworthy in the literature. These authors establish that the planimetric area is proportional to the volume displaced with an exponent equal to $2/3$. This value is in accordance with the assumption of geometric proportionality (Crosta et al. 2003).

Figure 6 illustrates the relationship between the landslide planimetric area and displaced volume for the study area training dataset (logarithmic relationship, base 10), whose equation is given by (3).

$$\text{LogA} = 1.012 + 0.624\text{LogV} \quad (3)$$

Figure 6 shows a good fit between the variables, with a high coefficient of determination (0.84). The slope of the line is very close to that reported by Iverson et al. (1998). Through a hypothesis test, these authors derive a statistical significance of equaling the best-fit slope with a value equal to $2/3$. Using relevant statistical inference tools, and the help of the t-statistic and p-value, our test results produce a t-statistic equal to -1.550 , and a p-value of 0.124. Thus, it not possible to reject the null hypothesis that the data can be fitted to a linear model with a slope equal to $2/3$ on a log-log plot.

Figure 7 shows the line resulting from the previous procedure, whose equation is given by (4).

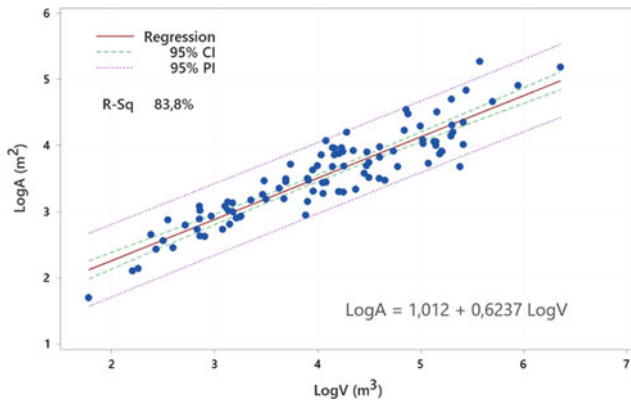


Fig. 6 Power-law relationship between planimetric area and landslide volume for different datasets in the form of Eq. (5)

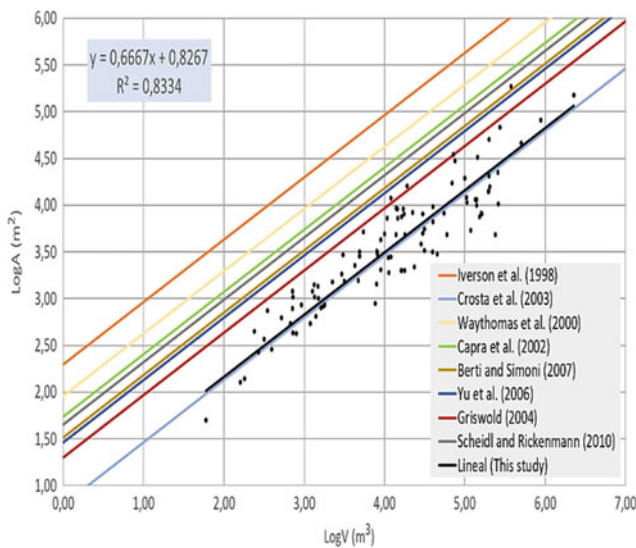


Fig. 7 Line of best fit for the area-volume model

$$\text{Log}A = 0.827 + 2/3\text{Log}V \quad (4)$$

Additionally, Fig. 7 overlaps the regression lines for different international studies that validate Iverson et al. (1998). Equation (4) can be written as a power-law following the properties of the logarithm, according to Eq. (5).

$$A = 6.71V^{2/3} \quad (5)$$

The form of Eq. (5) is useful as it allows conclusions to be drawn about differences in mobility when different types of landslides and materials are analyzed under particular geological conditions. For example, Fig. 7 shows that landslides in the Andean region of Colombia exhibit much lower propagation values than reported in studies from other parts of the world. Most Andean events correspond to rotational and translational landslides. This contrasts with

other studies focusing on phenomena with greater mobility, such as debris flows or lahars. The equation derived from the coarse debris flow research of Crosta et al. (2003) has a coefficient similar to that of this study. In Fig. 7, the line with the highest coefficient that accompanies the volume corresponds to the work of Iverson et al. (1998). That paper reports a value equal to 200 and is mostly applied to lahars. The implication of this value is that those phenomena can flood areas 30 times larger than other landslides in the database of this study. The analysis of this coefficient and the comparison for different regions is important since this contains information about the properties of the flow during the depositional phase (Scheidl and Rickenmann 2010).

3.6 Travel Distance Multiple Regression Model

Simple regression models show that the landslide travel distance cannot be explained with a single factor. For this reason, a multiple regression model is developed to improve the fit equations obtained with simple regression. Three geometric variables are used: V , H , and $\tan(\theta)$ in logarithmic form, and the six qualitative variables from the study database. The regression model incorporates the four statistical variable selection methods described.

These results reveal that the volume of the displaced mass, the maximum height of the landslide, the slope angle, and the geomorphological environment were the most influential variables regarding travel distance. These variables were found to be statistically significant (p -value less than 0.05). The resulting equation for predicting the travel distance of landslides in the study region is expressed by Eq. (6).

$$\text{Log}L = 0.263 + 0.156\text{Log}V + 0.617\text{Log}H - 0.521\text{Log}\tan(\theta) + \text{GE} \quad (6)$$

In Eq. (6) the value of the term “GE” (Geomorphological Environment) depends on the category that needs to be evaluated. The reference level is the denudation environment ($\text{GE} = 0$). For a structural environment, $\text{GE} = -0.155$; for a fluvial environment, $\text{GE} = -0.149$; for a volcanic environment, $\text{GE} = 0.052$; and for a glacial environment, $\text{GE} = 0.053$. Eq. (6) has a coefficient of multiple determination of 0.85, which represents a strong goodness of fit and means the model can explain 85% of the variability of the dependent variable. The statistical model satisfies the assumptions of linearity, normality, homoscedasticity, independence, and noncollinearity (all tests yield p -values greater than the 0.05 significance level used). The model was also tested for statistical significance with the help of the F statistic; obtaining a p -value below the significance level (0.05), i.e., this condition is met.

Equation (6) reflects the same trends observed in the one-to-one relationships. For example, coefficients that correspond to the volume and the maximum height are positive. That is; an increase in these variables leads to an increase in the response variable, which in this case is the travel distance. On the other hand, the coefficient value for slope angle is negative, reflecting an inverse relationship with the dependent variable, similar to what is shown in Fig. 5.

The statistical model reveals the importance of geomorphology as a factor influencing travel distance. The results show that landslides in volcanic and glacial settings are more mobile than in other environments. This is in agreement with international literature indicating volcanic events achieve greater travel distances due to their ability to involve larger volumes of water when compared with other landslide types (Hayashi and Self 1992; Korup et al. 2013; Siebert 1984; Ui 1983; Voight et al. 1983).

The model of Eq. (6) requires that practicing professionals have knowledge about the geomorphology of the study area: a requirement that can be limited in many situations. For this reason, an alternative statistical model with only numerical variables was developed using the backward elimination method, whose equation is given by:

$$\text{LogL} = 0.286 + 0.159\text{LogV} + 0.563\text{LogH} - 0.618\text{Log}\tan(\theta) \quad (7)$$

Although this statistical model complies with all the assumptions evaluated for the previous one, the goodness of fit is lower, with a multiple R^2 equal to 0.82.

3.7 Model Validation

To evaluate their predictive capacity, Eqs. (6) and (7) are applied to the two datasets (training and test). The models of Qiu et al. (2018) and Rickenmann (1999) are also applied to the same sets. Table 2 shows the results of calculating the errors in the predictions, applying the four models using Eqs. (1) and (2). Considering that the predicted values refer to the travel distance, an inverse transformation of Eqs. (6) and (7) is performed to obtain the response variable in correct units.

In general, the MAPE for the models developed in this study are lower than for the international models. The Rickenmann (1999) model reports very large MAPE values that exceeds 200% because of the focus on debris flow research. Although the model of Qiu et al. (2018) reports low error values, it does not outperform the predictive capacity of the models developed here.

Regarding the RMSE, Eq. (6) has the lowest value among the evaluated models (93.67 m). Although this value may seem high, in long-runout landslides it represents only a small percentage of the total travel length, making it a good approximation. The best fit model for the study region has a MAPE equal to 31.25%, outperforming the alternative model (MAPE = 35.13%). This value is similar to the average error reported by other authors (Guo et al. 2014; Tang et al. 2012).

The previous results show that the models developed (full and alternative model) have a good prediction capacity for the Colombian Andes. Nevertheless, the models are limited, since they are specific to the study region, or in areas with similar geological and geomorphological settings. The errors in the predictions can be reduced if other variables that were not analyzed are considered. For example, the 3D effect of the travel path, the drag of material, the effect of pore pressure, and mechanical properties of the soil.

3.8 Application of Empirical-Statistical Models

The model of Eq. (6) is defined as an intermediate level model according to the guidelines of Fell et al. (2008), which allows its use in the elaboration of preliminary hazard maps. According to McDougall (2017), the prediction intervals of a statistical model can be translated as estimates of the probability of exceedance of the response variable (travel length or landslide area). For example, the line of best fit can be associated with a 50% exceedance probability (i.e., a 50% probability that future landslides of the same type and size will travel farther). Similarly, for a 95% prediction interval, the lower bound value is associated with an exceedance probability of 97.5%, and the upper bound with an

Table 2 Comparison of the prediction capacity for the proposed and international models for the estimation of the landslides travel distance. The units of the variables in the international models are the same as those used in Table 1

Model	MAPE Training data (%)	MAPE Test data (%)	MAPE Average (%)	RMSE (m)
Equation (6)	29.77	37.69	31.25	93.67
Equation (7)	34.58	37.53	35.13	101.16
Qiu et al. (2018) $L = 0.635V^{0.247}H^{0.536}\tan(\theta)^{-0.215}$	44.66	48.41	45.36	158.20
Rickenmann (1999) $L = 1.900V^{0.160}H^{0.830}$	226.61	304.18	241.11	412.38

exceedance probability of 2.5% (distribution of two tails). With different prediction intervals, more exceedance probability limits are obtained.

It is possible to obtain a preliminary landslide-mobility hazard map with these tools. As an example, a landslide in the study region not considered in the test and training datasets is used. This event corresponds to a landslide on October 26, 2007 in the municipality of Ricaurte, located in the department of Nariño, southern Colombia. The movement is classified as a rotational landslide developed in colluvium comprising strongly weathered rock blocks with a clayey matrix rich in iron oxides. The event is identified as wet and was triggered by pluvial erosion in a denudational environment. From the morphometric point of view, the maximum height is 80 m and it moved a total of 8000 m³ of material at an angle of 25°; the direction of motion with respect to north is 130°.

From the crown of the landslide, different probabilities of exceedance are calculated to define the hazard zones according to the models of Eqs. (3) and (6). The 50 and 95% prediction intervals are used, resulting in five hazard categories (Table 3). In summary, a travel distance and planimetric area values are obtained for each hazard category.

A 12.5 m resolution DEM of the event area and the ESRI software ArcGIS is used to create the preliminary hazard map. From the crown of the landslide, and with the help of the ArcMap Buffer 3D function, concentric circles are drawn as a guide to delimit each hazard level, and whose radii are determined by the travel distance indicated in Table 3. Additionally, concentric sectors are drawn on the circles with an area equal to that indicated in Table 3. The areal extent of each sector depends on the considered hazard level and takes into account the direction of movement (130° with respect to true north). The results of this procedure are shown in Fig. 8. This geometric approximation does not exactly represent reality since landslide forms will vary according to the conditions of each site. However, for

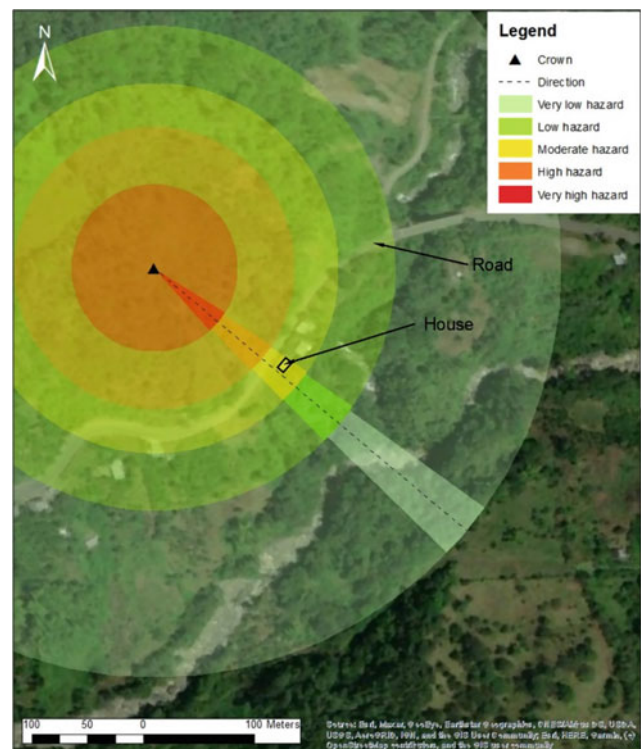


Fig. 8 Preliminary hazard map showing the reach zones of the landslide in the municipality of Ricaurte in 2007

practical purposes, and in preliminary phases of mapping, it is important to know the potential travel distance along with the planimetric area that may be reached by a landslide.

Figure 8 represents an example of a preliminary hazard map built from two empirical-statistical models. Although at first glance it seems “very simple”, the map is highly effective in identifying the exposed elements around the zone of influence of the landslide; in this case, a road and a house are located within a moderate hazard level sector. This map serves as a guide for decision makers and land planners involved in landslide risk management.

Table 3 Travel distance and landslide area limit values that define the hazard categories

Hazard level	Exceedance probability (%)	Travel distance (m)	Planimetric area (m ²)
Very high hazard	97.50	74.65	810.85
High hazard	75.00	125.93	1,832.69
Moderate hazard	50.00	165.05	2,795.50
Low Hazard	25.00	216.32	4,264.22
Very low hazard	2.50	364.92	9,637.85

4 Conclusions

In this study, a database of 123 well-documented landslides distributed across the Andean zone of Colombia. Most were rotational and translational landslides, and, to a much lesser extent, debris flows that exhibited a limited travel distance.

Various detailed statistical analyses were performed on a training subset of this dataset. The results of simple regressions reveal that travel distance is positively related to displaced volume and maximum slide height, and negatively related to slope angle. A strong correlation is observed between the planimetric landslide area and volume. Additionally, landslides from the study region follow the

area-volume relationship proposed by Iverson et al. (1998). Differences in the proposed regression line, when compared with those presented by other authors, are accounted for by considering variations in failure mechanism of the different landslides included in the datasets.

Simple landslide travel-distance models are improved by incorporating a multiple regression model using stepwise statistical methods. Results show that volume, maximum crown height, slope angle, and geomorphological environment are the variables with a predominant effect on landslide travel distance in the Colombian Andean zone. The multiple regression analyses found there to be no significant contribution from variables such as triggering factor, water content, lithology, landslide type, and obstruction. An alternative model with only numerical variables was also constructed. The equations developed are appropriate for use in tropical areas such as the Colombian Andes and other tropical cordilleran regions (e.g., SE Asia).

The accuracy of the two models is evaluated using training and test sets from database. Satisfactory error values are obtained when compared with the values derived from other models applied to the study area.

Empirical-statistical modeling and resulting preliminary hazard map incorporate travel distance and the planimetric areas. The most important function of this map is to identify possible zones affected by landslide processes.

References

- Basharat M, Rohn J (2015) Effects of volume on travel distance of mass movements triggered by the 2005 Kashmir earthquake, in the northeast Himalayas of Pakistan. *Nat Hazards* 77(1):273–292. <https://doi.org/10.1007/s11069-015-1590-4>
- Berti M, Simoni A (2007) Prediction of debris flow inundation areas using empirical mobility relationships. *Geomorphology* 90:144–161. <https://doi.org/10.1016/j.geomorph.2007.01.014>
- Budetta P, de Riso R (2004) The mobility of some debris flows in pyroclastic deposits of the northwestern Campanian region (southern Italy). *Bull Eng Geol Env* 63(4):293–302. <https://doi.org/10.1007/s10064-004-0244-7>
- Capra L, Macías JL, Scott KM, Abrams M, Garduño-Monroy VH (2002) Debris avalanches and debris flows transformed from collapses in the Trans-Mexican volcanic belt, Mexico—behavior, and implications for hazard assessment. *J Volcanol Geoth Res* 113:81–110
- Chen HX, Zhang L, Gao L, Zhu H, Zhang S (2015) Presenting regional shallow landslide movement on three-dimensional digital terrain. *Eng Geol* 195:122–134. <https://doi.org/10.1016/j.enggeo.2015.05.027>
- Corominas J (1996) The angle of reach as a mobility index for small and larger landslides. *Can Geotech J* 33:260–271. <https://doi.org/10.1139/t96-005>
- Crosta GB, Cucchiari S, Frattini P (2003) Validation of semi-empirical relationships for the definition of debris-flow behaviour in granular materials. In: Fourth international conference on debris-flow hazards mitigation: mechanics, prediction, and assessment. Mill Press, Rotterdam. pp 821–832
- Cruden DM, Varnes DJ (1996) Landslide types and processes. Landslides—investigation and mitigation: transportation research board, special report no. 247. National Academy Press, Washington, DC. pp 36–75
- Davies TRH (1982) Spreading of rock avalanche debris by mechanical fluidization. *Rock Mech* 15:9–24. <https://doi.org/10.1007/BF01239474>
- De Leon RD (2018) Impactos de los eventos recurrentes y sus causas en Colombia. Betancourt J (eds) UNGRD
- Fell R, Corominas J, Bonnard C, Cascini L, Leroi E, Savage WZ (2008) Guidelines for landslide susceptibility, hazard and risk zoning for land use planning. *Eng Geol* 102:85–98. <https://doi.org/10.1016/j.enggeo.2008.03.022>
- Finlay PJ, Mostyn GR, Fell R (1999) Landslide risk assessment: prediction of travel distance. *Can Geotech J* 36:556–562. <https://doi.org/10.1139/t99-012>
- Griswold J (2004) Mobility statistics and hazard mapping for non-volcanic debris flows and rock avalanches. MS thesis, Portland State University. Portland, EE.UU
- Guo D, Hamada M, He C, Wang Y, Zou Y (2014) An empirical model for landslide travel distance prediction in Wenchuan earthquake area. *Landslides* 11(2):281–291. <https://doi.org/10.1007/s10346-013-0444-y>
- Hattajji T, Moriwaki H (2009) Morphometric analysis of relic landslides using detailed landslide distribution maps: implications for forecasting travel distance of future landslides. *Geomorphology* 103(3):447–454. <https://doi.org/10.1016/j.geomorph.2008.07.009>
- Hayashi JN, Self S (1992) A comparison of pyroclastic flow and debris avalanche mobility. *J Geophys Res* 97(B6):9063–9071. <https://doi.org/10.1029/92JB00173>
- Heim A (1932) *Bergsturz und Menschenleben*. Fretz und Wasmuth, Zurich, 218 p
- Hsü KJ (1975) Catastrophic debris streams (sturzstroms) generated by rockfalls. *Geol Soc Am Bull* 86:129–140. [https://doi.org/10.1130/0016-7606\(1975\)86%3c129:CDSSGB%3e2.0.CO;2](https://doi.org/10.1130/0016-7606(1975)86%3c129:CDSSGB%3e2.0.CO;2)
- Hühnerbach V, Masson DG (2004) Landslides in the North Atlantic and its adjacent seas: an analysis of their morphology, setting and behaviour. *Mar Geol* 213:343–362. <https://doi.org/10.1016/j.margeo.2004.10.013>
- Hunter G, Fell R (2003) Travel distance angle for “rapid” landslides in constructed and natural soil slopes. *Can Geotech J* 40(6):1123–1141. <https://doi.org/10.1139/t03-061>
- IAEG (1990) Suggested nomenclature for landslides. *Bull Int Assoc Eng Geol* 41(1):13–16. <https://doi.org/10.1007/BF02590202>
- Iverson R, Schilling S, Vallance J (1998) Objective delineation of lahar-inundation hazard zones. *Geol Soc Am Bull* 110(8):972–984. [https://doi.org/10.1130/0016-7606\(1998\)110%3c0972:ODOLIH%3e2.3.CO;2](https://doi.org/10.1130/0016-7606(1998)110%3c0972:ODOLIH%3e2.3.CO;2)
- Kilburn CRJ, Sørensen SA (1998) Runout lengths of sturzstroms: the control of initial conditions and of fragment dynamics. *Journal of Geophysical Research: Solid Earth*. 103(B8):17877–17884. <https://doi.org/10.1029/98jb01074>
- Korup O, Schneider D, Huggel C, Dufresne A (2013) Long-Runout landslides. In: Marston RA, Stoffel M (eds) *Treatise on geomorphology*. Academic Press, San Diego, CA. (vol 7, ISBN 978-0-08-088522-3). <https://doi.org/10.1016/B978-0-12-374739-6.00164-0>
- Legros F (2002) The mobility of long-runout landslides. *Eng Geol* 63:301–331. [https://doi.org/10.1016/S0013-7952\(01\)00090-4](https://doi.org/10.1016/S0013-7952(01)00090-4)
- McDougall S (2017) 2014 Canadian geotechnical colloquium: landslide runout analysis—current practice and challenges. *Can Geotech J* 54(5):605–620. <https://doi.org/10.1139/cgj-2016-0104>
- Okura Y, Kitahara H, Kawanami A, Kurokawa U (2003) Topography and volume effects on travel distance of surface failure. *Eng Geol* 67:243–254. [https://doi.org/10.1016/S0013-7952\(02\)00183-7](https://doi.org/10.1016/S0013-7952(02)00183-7)

- Okura Y, Kitahara H, Sammori T (2000) Fluidization in dry landslides. *Eng Geol* 56:347–360. [https://doi.org/10.1016/S0013-7952\(99\)00118-0](https://doi.org/10.1016/S0013-7952(99)00118-0)
- Qiu H, Cui P, Hu S, Regmi AD, Wang X, Yang D (2018) Developing empirical relationships to predict loess slide travel distances: a case study on the Loess Plateau in China. *Bull Eng Geol Env* 77(4):1299–1309. <https://doi.org/10.1007/s10064-018-1328-0>
- Qiu H, Cui P, Regmi AD, Hu S, Wang X, Zhang Y, He Y (2017) Influence of topography and volume on mobility of loess slides within different slip surfaces. *CATENA* 157:180–188. <https://doi.org/10.1016/j.catena.2017.05.026>
- Rickenmann D (1999) Empirical relationships for debris flows. *Nat Hazards* 19:47–77. <https://doi.org/10.1023/A:1008064220727>
- Scheidegger AE (1973) On the prediction of the reach and velocity of catastrophic landslides. *Rock Mech* 5:231–236. <https://doi.org/10.1007/BF01301796>
- Scheidl C, Rickenmann D (2010) Empirical prediction of debris-flow mobility and deposition on fans. *Earth Surf Proc Land* 35(2):157–173. <https://doi.org/10.1002/esp.1897>
- Shreve RL (1968) The Blackhawk landslide. *Geol Soc America* 108:1–47
- Siebert L (1984) Large volcanic debris avalanches: characteristics of sources areas, deposits, and associated eruptions. *J Volcanol Geoth Res* 22:163–197. [https://doi.org/10.1016/0377-0273\(84\)90002-7](https://doi.org/10.1016/0377-0273(84)90002-7)
- Skemer NA (1985) Discussion of paper “nature and mechanics of the Mount St Helens rockslide-avalanche of 18 May 1980.” *Géotechnique* 35:357–362
- Staron L, Lajeunesse E (2009) Understanding how volume affects the mobility of dry debris flows. *Geophys Res Lett* 36(12). <https://doi.org/10.1029/2009GL038229>
- Strom A, Li L, Lan H (2019) Rock avalanche mobility: optimal characterization and the effects of confinement. *Landslides* 16(8):1437–1452. <https://doi.org/10.1007/s10346-019-01181-z>
- Tang C, Zhu J, Chang M, Ding J, Qi X (2012) An empirical-statistical model for predicting debris-flow runout zones in the Wenchuan earthquake area. *Quatern Int* 250:63–73. <https://doi.org/10.1016/j.quaint.2010.11.020>
- Ui T (1983) Volcanic dry avalanche deposits-identification and comparison with nonvolcanic debris stream deposits. *J Volcanol Geoth Res* 18:135–150. [https://doi.org/10.1016/0377-0273\(83\)90006-9](https://doi.org/10.1016/0377-0273(83)90006-9)
- Voight B, Janda RJ, Glicken H, Douglass PM (1983) Nature and mechanics of the Mount St Helens rockslide-avalanche of 18 May 1980. *Géotechnique* 33(3):243–273. <https://doi.org/10.1680/geot.1983.33.3.243>
- Waythomas C, Miller T, Begér J (2000) Record of Late Holocene debris avalanches and lahars at Iliamna Volcano, Alaska. *J Volcanol Geoth Res* 104:97–130. [https://doi.org/10.1016/S0377-0273\(00\)00202-X](https://doi.org/10.1016/S0377-0273(00)00202-X)
- Whittall J, Eberhardt E, McDougall S (2017) Runout analysis and mobility observations for large open pit slope failures. *Can Geotech J* 54(3):373–391. <https://doi.org/10.1139/cgj-2016-0255>
- Yu FC, Chen CY, Chen TC, Hung FY, Lin SC (2006) A GIS process for delimitating areas potentially endangered by debris flow. *Nat Hazards* 37:169–189. <https://doi.org/10.1007/s11069-005-4666-8>

Open Access This chapter is licensed under the terms of the Creative Commons Attribution 4.0 International License (<http://creativecommons.org/licenses/by/4.0/>), which permits use, sharing, adaptation, distribution and reproduction in any medium or format, as long as you give appropriate credit to the original author(s) and the source, provide a link to the Creative Commons license and indicate if changes were made.



The images or other third party material in this chapter are included in the chapter's Creative Commons license, unless indicated otherwise in a credit line to the material. If material is not included in the chapter's Creative Commons license and your intended use is not permitted by statutory regulation or exceeds the permitted use, you will need to obtain permission directly from the copyright holder.



Landform Geometry for Restoration of Mountain Roads and Landslide Hazard Resilience

A. A. Virajh Dias, H. M. J. M. K. Herath, and L. K. N. S. Kulathilake

Abstract

Traveling on a mountainous road is attractive but questionable under aggressive climatic conditions such as extreme rainstorms. Roads are often designed in different geological complexity overlaying upper and lower terrains. The complexity of slope geometries, potential deformities, ground discontinuities, soil-rock composite nature, factors incorporated in structural integrity, the complexity associated with infrastructure developments, and unstable landform have long been causes of the increasing cost of road constructions in hills. In many instances, landform geometries and the natures of slope observed in-situ allow us to understand many salient features that we need to know in the design to mitigate landslide threats. The extent to which we make the collective effort to gather many features of landforms and their static representations concludes its validity. Findings are more forced to be based on geometrical evidence of slopes and cross-checked with an appropriate design criterion. A provision should describe a design or construction method that is deemed to comply with the site-specific conditions. Such an approach will save the enormous cost of investigations, design, and simplification for numerical evaluations, and also contribute to an indirect approach to road restoration and improve an appropriate approach for resilience to landslide hazards.

Keywords

Landform • Geometry • Roads • Slopes • Landslide • Rockfall

1 Introduction

A mountain road is the most connecting way of community in a low country with far the most beautiful cities of the hill country (Fig. 1) by allowing transportation for vehicles and pedestrians. A landform is the silent feature of the ground and can be a crucial element in understanding the difficulty of infrastructure developments in the mountains. In many instances, widening mountain roads often pose a challenge in avoiding potential landslide hazards, mainly due to various landform features of the upper and lower slopes (Fig. 1).

2 Geomorphological Evidences of Failure

Landslide is often considered as a downward and outward movement of earth-formed material on hill slopes. It is usually triggered under extreme rainfall or ground shaking (seismicity). Fortunately, no records of landslides occurring during the dry season or due to seismicity are found in Sri Lanka. Geomorphological pieces of evidence such as topography, geology, hydrology, slope, groundwater, and land use are considered to be intrinsic and extrinsic variables. In contrast, extrinsic variables are accounted for improper land-use practices, roads, infrastructure developments, and man-made activities. The landslide initiation can be explained as the slip initiation of the upper sliding surface due to the loss of resistance of earth mass, where acceleration occurs towards the downward slope, and deceleration occurs in a lower section. In addition, the spatial distribution of landslide geometry clearly integrates potential energy relief of soil, rock, water, vegetative species, and other spatial element spreading over the landslide boundary. Many observations of such large-scale landslides were recorded in Sri Lanka during the last two to three decades, and some of those are depicted in Figs. 2, 3, 4, 5, 6, and 7.

The Mulhalkelle landslide (1989), Gampalakadawala (2003), and Aranayake landslide (2017) were identified as

A. A. Virajh Dias (✉) · H. M. J. M. K. Herath ·
L. K. N. S. Kulathilake
Natural Resources Management and Laboratory Services
(NRMLS), Central Engineering Consultancy Bureau (CECB),
No 415, Bouddhaloka Mawatha, Colombo 7, Sri Lanka
e-mail: virajhcecb@gmail.com



Fig. 1 From Kandy travel along the Teldeniya road and Kandy-Mahiyangana-Padiyatalawa to completely travel along the 18 Bend Road. (Photo by Attractions Sri Lanka 2019)



Fig. 2 Traffic disrupted (trees and rock has fallen in to the road) on to the road at 6th bend area of the Kandy-Mahiyangana “18 hairpin road”, 20th January, 2020 (Photo by Hirunews.lk 2020)

large-scale landslides in terms of physical dimensions, numbers of victims, transported earth mass volumes, damage to infrastructures, relief efforts, failure patterns, and geological complexities. All those landslides seriously impacted many road networks and economic development due to being located in agroecological zones of Sri Lanka (Panabokke 1996). Observations indicate the start of a landslide as a de-stabilization of a vast mass of earth on the hillslope, which is subjected to the high water saturation that might trigger regolith sliding on the bedrock interface. It can induce substantial failure on the adjoining steeper downslope, including large rock fragments embedded in wet soil. The moving earth masses of the Mulhalkelle landslide (Fig. 3), Gampalakadawala landslide (Fig. 4), and the Aranyake Landslide (Fig. 5) contained highly saturated regolith material (unconsolidated, loose, heterogeneous superficial deposits covering soil and solid rock). It was noted that the rock-soil interface was saturated due to the propagation of the perched water table closer to the interface. Finally, the displaced material appears to have turned into a



Fig. 3 This photo shows a stretch of a mountain slope destroyed by mudslide in Mulhalkelle, Nuwara Eliya district, 1986, NBRO Report (1988)



Fig. 4 Gampalakadawala Landslide (6 victims, Kalawana). Outburst floods resulted from mass movements temporarily blocking a “Delgoda Ganga” river at lower elevation, May, 2003

highly mobile flow, judging from damage to many elements at the lower elevation. The underlying geological structure of this area might be complex, jointed, highly foliated, and thus highly deformable structures. The rock surfaces visible



Fig. 5 Aranayake landslide in Sri Lanka is now thought to have killed about 122 people. The landslide was triggered by an exceptional rainfall associated with a slow-moving tropical cyclone, 2016. *Photo by Sri Lanka Red Cross*



Fig. 6 Sliding surface or the point of initiation of the Aranayake landslide in Sri Lanka, 2016 *Photo by Sri Lanka Red Cross (2016)*



Fig. 7 A landslide area at Kaluthara, 80 km from Colombo Sri Lanka on May 26, 2017, *Photo by The Straitstimes Asia (2017)*

on the remaining ridge have different inclinations from those exposed on the bedrock. Such geological complexities are usually difficult to explore before a landslide occurs. The mobile material appears to be weathered regolith interacting with a massive volume of groundwater during transportation of the earth material.

3 Study Background

This research aimed to develop a database of stable and unstable cut slopes (older than 20 years) through field verifications after heavy rainstorms recorded in the hilly/mountainous areas of Sri Lanka. The research started in late 2000 by implementing the “Pre-Feasibility Study for Designing Major Roads in Landslide Area” by the Central Engineering Consultancy Bureau (CECB 2000). The project was funded by the Japan International Cooperation Agency (JICA) through the Road Development Authority (RDA) of Sri Lanka. The activity was further studied under the IPL Certified Project ID-200, 2015, titled “An assessment of the rockfall susceptibility based on cut slopes adjacent to highways and railways,” implemented by the CECB. Subsequently, the study was carried out in 2003, 2006, 2008, 2012, 2016, and 2019. In addition, the CECB has been awarded the World Center of Excellence (WCoE) (Dias et al. 2017) for Landslide Risk Reduction under the theme of “Model Policy Framework, Standards and Guidelines” by the International Programme of Landslide (IPL) since 2014. The main objective of the study is investigating the design requirements of road cut slope stability along the (a) Ratnapura-Balangoda-Haputale highway, (b) Kandy-Gampola-Nuwara Eliya highway, and (c) Kandy- Hunnasgiriya-Madamaha Nuwara-Mahiyangana highway (See Fig. 8). Considering the ages of these highways, we realize that the non-engineered remedial designs adopted for the roads have stayed in balance with the road environments for 20 years or longer.

4 Landforms in Sri Lanka

Sri Lanka is characterized by a southern-central mountain range that rises to 2524 m above sea level at its peak (Erd., 1984). According to the various findings and documentation, the island consists of seven major landform units, viz. (i) coastal plain, (ii) continental shelf, (iii) circum-island peneplain, (iv) central massif, (v) Sabaragamuwa hills, (vi) Galoya hills and (vii) Elahera ridges (Erd.,1984).The entire area is covered by various landforms, from flat erosion



Fig. 8 Location map of the study and field verification survey locations. **a** Ratnapura-Balangoda-Haputale highway, **b** Kandy-Gampola-Nuwara Eliya highway and **c** Kandy-Hunnasgiriya-Madamaha Nuwara-Mahiyangana highway

or peneplain to a complex assemblage of mountains, ridges, plateaus, and valleys.

The mountainous landform is mainly due to geological and erosional history, which is considered one of the oldest and most stable parts of the earth's crust, namely Precambrian deposits in the Highland series (Cooray 1967). More than 90% of Sri Lanka is covered with highly crystalline, non-fossiliferous, Precambrian age, metamorphic rocks. These Precambrian rocks, which metamorphose under granulite facies and amphibolite facies, are subdivided into three groups based on lithology, structures, and ages of the rocks (Cooray 1984). Almost all hill country regions overlie highland series high grade, crystalline metamorphic rocks (Herath et al. 2014). The main rock types of this series are meta-sediments (quartzite, Marbles, garnet-sillimanite schists) and charnockite gneisses. Other rock types are biotite gneiss, hornblende-biotite gneiss and schists, and garnet-sillimanite gneiss (Cooray 1984).

5 Hydrological Records

In the late '80 s, when information was scarce, the landslide triggering rainfall threshold was placed at 200 mm in 72 h, provided rain in the area continued (Bhandari et al. 1992).

The above criterion did work partially; the probability of landslide occurrence as a rainfall intensity ratio spotlights the indicators that help assess the dynamic of rain-triggered

slope movements (Bhandari and Dias 1996). This study was conducted during the '90 s. The conditional probabilities were only examined partially in the case of reactivation of recent, seasonally active landslides. Rainfall records for the months of landslide events tell that 24 h rainfall associated with a landslide event was generally 2 to 23 times higher than the average daily rainfall (Bhandari and Dias 1996). The empirical rule is reasonably accurate if the average annual rainfall exceeds more than 3000 mm in the wet zone of the country.

The intense rainfall of 522 mm/day followed by a tropical storm on 15th May 2003 triggered 78 landslides in the Kalawana Division. Antecedent rainfalls during the ten days before the storm reached about 272 mm, increasing the soil moisture and causing soil surface erosion in various parts of Kalawana in the Ratnapura District. In November, the total three-day rainfall reached 656 mm and was the highest in 1947 (Dias and Gunathilaka 2014).

6 Landform Geometry and Mountainous Road Infrastructure

The mountainous slopes are predominantly convex-concave form and occasionally retain a planar slope segment within dipping slopes of in-situ rock. Dipping rock surfaces and many eroded rock slopes favor the development of various instabilities, and some lead to triggering significant landslides. Slope deformities and geometries initiate the natural degradation process of soil and rock, and history can be traced back millions of years (Fig. 9).

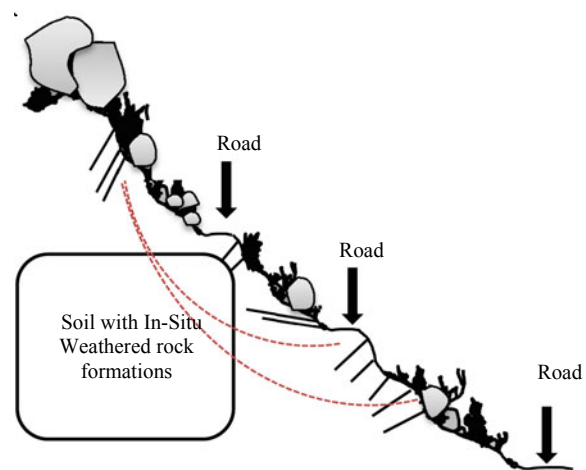


Fig. 9 Typical cross section of mountain hill slope

7 Data and Method of Approach

A total of 67 records were targeted for a detailed study out of 110 records of cuttings, bank failures, or landslides, as indicated in Table 1. The study is concerned with observations on the heights of failure, stable ground conditions, failure patterns, landforms, land uses, and geologies (Fig. 10).

7.1 Failure on Upper Slope Stability

The most common instabilities in roadside slopes mainly lie in immediate upper slope landform at which land-use practices were cultivation of economic crops (tea, vegetable), forestry, or home garden. The failure patterns are commonly associated with shallow rotational or translational failures

Table 1 Assessing potential stability according to the refined data

Point No.	Easting	Northing	Elevation MSL	Location	Type of failure	Slope angle	soil/rock type	Upper veg	h1/m	h2/m	Total H	toe wall	drain
POI 098	001-92-811	001-62-123	520	Kudawa, A4 Road	S	60.26	RS/HWR	HG	6.3	4.9	11.2	no	no
POI 103	001-95-434	002-64-209	569	Dambagahamada	S	63.43	SN	HG	4	–	4	no	yes
POI 104A	001-96-269	002-65-008	561	100 m away from Halgahawela (loc.10)	S	70.35	WR	HG	4	–	4	no	no
POI 113	001-98-399	001-67-353	563	Seelogama, A4 Road	S	74.05	RS/WR	HG	5	5	14	no	no
POI 115	001-98-999	001-67-802	557	Seelogama, A4 Road	S	63.43	MWR	HG	3	6	9	no	yes
POI 115A	001-98-999	001-67-802	557	Seelogama, A4 Road	S	74.05	MWR	HG	6	4	13	no	yes
POI 116	001-99-600	001-68-431	572	Belihuloya, A4 Road	S	66.8	MWR	HG	7	–	7	no	no
POI 119 A	001-99-600	001-68-431	572	Belihuloya, A4 Road	S	77.91	RS	FO	4.5	–	4.5	no	yes
POI 121	002-02-012	001-69-083	628	Pambahinna, A4Road	S	74.05	HWR	HG	5	–	5	no	no
POI 144	001-83-398	002-12-887	939	Pussellawa, A4Road	S	75.96	MWR/WR	TEA	4.5	5	9.5	no	no
POI 145A	001-84-234	002-12-875	976	Somagama, A4 Road	S	75.96	RS/WR	TEA	4	3	7	no	yes
POI 145C	001-84-234	002-12-875	976	Somagama, A4 Road	S	77.9	RS/WR	TEA	4	8	12	no	yes
POI 146	001-84-762	002-12-575	972	at Pssellawa Police Station	S	65.09	RS/HWR	HG	3.5	2.5	9	no	yes
POI 151	001-92-108	002-04-635	1271	Palagolla, A5 Road	S	77.9	HWR	HG	6	6	12	no	yes
POI 152	001-92-646	002-04-333	1379	Wedamulla	S	66.8	HWR	TEA	4.5	4.5	9	no	yes
POI092	00,191,834	00,161,429	541	Balangoda Bypass, AB7	S	75	RS	HG	4.0		4	no	yes
POI095	00,193,773	00,162,852	520	Imbulpe, A4 Road	S	59	HW/CWR	FO	8.7	7.1	15.8	no	yes
POI112	00,208,053	00,173,869	784	at 119 km post	S	58	CWR	FON	6.9	4.0	10.9	no	no
POI 099	001-93-222	002-62-014	519	Gammaduwa, Matale	F	57.26	RS/HWR	HG	6		6	no	no
POI 100	001-93-784	002-62-825	506	Gammaduwa, Matale	F	57.26	RS/HWR	HG	8	8	16	no	no
POI 101	001-93-729	001-63-376	513	Rathmalwinna	F	60.26	RS/HWR	HG	8	–	8	no	no
POI 102	001-95-253	002-64-205	550	Dambagahamada	F	66.8	HWR	HG	10	–	10	no	no
POI 104	001-96-269	002-65-008	561	Halgahawela	F	66.8	WR	HG	12	–	12	no	no
POI 105	001-97-107	001-66-090	481	Imbulpe, A4 Road	F	47.12	RS/WR	HG	7	–	7	no	no
POI 106	001-97-411	001-66-295	477	Imbulpe, A4 Road	F	70.35	WR	HG	8	–	8	no	yes
POI 107	001-97-605	001-66-409	512	Gilma-Imbulpe	F	60.26	RS/HWR	HG	7.2	2.5	9.7	no	yes
POI 107A	001-97-605	001-66-409	512	Gilma	F	63.43	HWR	HG	6.2	3	9.2	no	yes
POI 107B	001-97-605	001-66-409	512	Gilma	F	64.43	HWR	HG	6	3	9	no	yes
POI 108	001-97-638	001-66-510	513	Gilma	F	64.43	RS	HG	6.2	5	11.2	no	yes
POI 108A	001-97-638	001-66-510	513	about 50 m away	F	63.43	RS	HG	5.5	1.5	7	no	yes
POI 109	001-98-065	001-66-813	555	Imbulpe, A4 Road	F	77.91	RS/WR	HG	5	6	11	no	yes
POI 109A	001-98-065	001-66-813	555	Imbulpe, A4 Road	F	74.05	RS	HG	7	–	7	no	yes
POI 110	001-97-984	001-66-877	556	Imbulpe, A4 Road	F	60.26	RS/WR	HG	10	–	10	no	yes
POI 111	001-97-936	001-66-962	560	Imbulpe, A4 Road	F	63.43	HWR	HG	4.6	4.6	9.2	no	no

(continued)

Table 1 (continued)

Point No.	Easting	Northing	Elevation MSL	Location	Type of failure	Slope angle	soil/rock type	Upper veg	h1/m	h2/m	Total H	toe wall	drain
POI 112	001-98-093	002-67-115	565	Puwakgahawela old land slide	F	70.35	RS	FO	12	–	12	no	no
POI 114	001-98-452	001-67-478	558	Seelogama, A4 Road	F	60.26	RS/HWR	FO	12	–	12	no	yes
POI 115B	001-98-999	001-67-802	557	Seelogama, A4 Road	F	70.35	MWR	HG	6	5	15	no	yes
POI 118	002-00-221	001-68-818	613	Galagama, A4 Road	F	75.96	HWR/MWR	FO	4.5	–	4.5	no	yes
POI 118A	002-00-221	001-68-818	613	Galagama, A4 Road	F	79.88	HWR	FO	4.6	4.6	9.2	no	no
POI 118B	002-00-221	001-68-818	613	Galagama, A4 Road	F	75.96	HWR	FO	9	–	9	no	no
POI 119	002-00-466	001-68-615	634	Belihuloya, A4 Road	F	77.91	RS	FO	5	–	5	no	yes
POI 120	002-00-707	001-68-611	635	Belihuloya, A4 Road	F	77.91	WR	RF	6.5	–	6.5	no	no
POI 123	002-04-634	001-07-056	741	Dimbulgoda	F	60.25	WR	FO	6	6	12	no	yes
POI 124	002-04-954	001-70-226	758	Dimbulgoda	F	58.73	HWR	FO	8	6	16.5	no	no
POI 125 A	002-08-021	001-73-804	787	Kalupahana, A4 Road	F	63.43	RS	FO	5	4	14	no	no
POI 126	002-09-051	001-74-045	787	Sapugaha watta, Kalupahana—near the tunnel	F	63.43	RS/COL	HG	7	7	15	no	no
POI 128	002-13-981	001-73-672	973	Beragla, A4 Road	F	75.96	MWR	HG	7.5	4	11.5	no	no
POI 130	002-20-140	001-74-071	1400	Boralumankoda, A5 Road	F	80.67	WR	HG	3	11	14	no	no
POI 137	001-80-176	002-26-771	532	at 2 km post-Kandy Gampola road	F	75.96	RS/HWR	HG	5.5	2	7.5	no	yes
POI 138A	001-78-644	002-16-667	516	Boralumankada, Gampola—N'eliya road	F	79.87	RS	HG	4.5	6	10.5	no	no
POI 139	001-78-674	002-16-346	540	Ulapane, A5 Road	F	77.9	RS/HWR	HG	5	2	7	yes	no
POI 139A	001-78-674	002-16-346	540	Ulapane, A5 Road	F	77.9	RS/HWR	HG	3	3	6	yes	no
POI 140	001-79-956	002-14-552	595	Ulapane, A5 Road	F	70.35	RS/WR	HG	5	5	10	no	yes
POI 141	001-80-730	002-13-291	737	Ulapane, A5 Road	F	77.9	MWR	HG	2.6	2	4.6	no	no
POI 143	001-82-684	002-12-900	888	Udawalpala, A5 Road	F	77.9	RS/HWR	TEA	6	2	8	no	yes
POI 143A	001-82-684	002-12-900	888	Udawalpala, A5 Road	F	79.87	RS/HWR	TEA	3.5	–	3.5	no	no
POI 145	001-84-234	002-12-875	976	Pussellawa, A5 Road	F	75.96	RS/HWR	TEA	4	10	14	no	yes
POI 145B	001-84-234	002-12-875	976	Pussellawa, A5 Road, Near to KP 145	F	77.9	RS/WR	TEA	4	6	10	no	yes
POI 145D	001-84-234	002-12-875	976	Pussellawa, A5 Road, Near to KP 145	F	79.87	RS/WR	TEA	4	5	9	no	no
POI093	00,192,751	00,162,136	523	Balangoda, A4 Road	F	59	RS	HG	8.5		8.5	no	yes
POI094	00,192,946	00,162,157	511	Balangoda, A4 Road	F	75	RS/WR	HG	4.5		4.5	no	yes
POI096	00,195,268	00,164,219	553	at damaged house	F	45	HW/CWR	FO	10.0		10	no	no
POI100	00,198,069	00,166,812	550	Belihuloya, A4 Road	F	79	HWR	FO	6.2		6.2	no	yes
POI102	00,197,921	00,166,950	565	Belihuloya, A4 Road	F	79	CWR	FO	4.5	2.0	6.5	no	
POI105	00,200,267	00,168,785	635	near Belihuloya	F	73	RS	FO	4.9	2.3	7.1	no	yes
POI109	00,200,717	00,168,634	640	Wellawaya, A4 Road	F	72	RS/CWR	FO	6.1		6.1	no	yes
POI110	00,200,746	00,168,679	640	abt 50 m frm POI 109 and 159 km post	F	67	RS/CWR	FON	7.8		7.8	no	no

F Fail, S Stable, RS Residual Soil, HWR Highly Weathered Rock, MWR Moderately Weathered Rock, WR Weathered Rock, CWR Completely weathered rock, COL Colluvium, FO Forest, HG Home Garden, FON Natural Forest reservation, TEA Tea, KP Kilometer post.

The overall location specific data was more than 110 locations and refined below according to most viable for design supportive road sections in mountain slope.

followed by a flowage mass. Observations revealed the fact that heavy rainfall events trigger failures (Fig. 11).

Weathered rock with upper slope de-stability

Soil layer contact with impermeable bedrock leads to increased pore water pressure at the interface of soil and

rock and ultimately causes a significant reduction of shear strength. The maximum permissible strain of soil material cannot withstand in-situ and leads to move downward and outward movement (see Figs. 12, 13 and 14).



Fig. 10 Upper and lower slope de-stabilization after construction of a road in mountain environment



Fig. 12 Failure observation of a road side slope cut section which was constructed at 0.5 to 3.5 m high without any retaining structures



Fig. 11 Immediate upper slope (slope section above the road) de-stabilization, Kalawana, Ratnapura, 2003

8 Evaluation of Landform Restoration Potential

The landslide is ‘almost all varieties of mass movements on slope including rockfalls, topples and debris flow sliding mass’ defined by Varnes 1984. The landslide body entrains a large volume of residual surface soil and then moves downstream along a gully to produce a debris flow disaster (Gao et al. 2017). The evaluation focused mainly on site-specific data collected during investigations, planning, designs, construction works, and widening of mountain roads. The number of road guidelines and specifications that describe site-specific design optimization of mountain roads is limited (Wyllie 1987). Therefore, experiences in understanding the process of slope degradation, refinements for site-specific issues, reactions to natural events, and historical records are critical tools

for understanding mountain road restoration works. The findings obtained through the study will create an appropriate environment for the decision-making process for roadway designs and mountain travels.

Some of the observations of the first-hand records were bound with geological evidence, landform patterns, land use, and improving the decision-making process towards reducing landslide vulnerability of roadway. Therefore, the following observations (see Figs. 15, 16, 17, and 18) are concluded as a decision-making tool for understanding observation-based approaches for assessing the potential stability based on the refined database of the study.

8.1 In-Situ Formed Weathered Rock or Completely Weathered Soil Form Geometries

Soil slopes fail differently, depending on the site settings (upper and lower slope stability), geometry, resistance to erosion, and other topographical factors. However, the numerical simulations have shown the collapse patterns, Type-a and Type-b in Figs. 15 and 16 are less likely to occur. And resistance to collapse is mainly governed by the unsaturated soil parameters. However, any prolonged heavy rainstorms will saturate the soil surface. In such instances, shallow slope failures are significant (Russel et al. 2008). According to the site records, a relatively low-cost, eco-friendly remedial design will help enhance the slope stability.

8.2 De-Stabilized Soil, Colluvium or Rock-Soil Complex Form of Geological Sections

Type-c and Type-d geometries (Figs.17 and 18) usually contain complex forms of stability. Many uncertainties are



Fig. 13 Example of rock formed failures along the road side slope. Wedge failure, translational slides and falling rocks are very much significant along the road sides. High hazard potential zone can be observed due to foliated and jointed rock formations



Fig. 14 Some stable landforms were also noticed during investigations. Highly to completely weathered rock surfaces consist of unsaturated soils, each having different visual and physical characteristics. Surface erosional potential is high if the weathered surface

contains any soluble minerals of metamorphic rocks. Usually, those sections stay stable for 20–40 years or more with minor surface improvements

among site-specific observations. The movements of rocks and rock-soil composites are two different modes of failure under those circumstances. Falling, rolling, bouncing, and sliding of rock are major sequences of de-stabilizing mechanisms (Brawner et al. 1975 and 1994) of failure related to the above. Therefore, a detailed study on geometries, energy, and simulations in different scenarios will conclude the appropriate remedial designs.

9 Statistical Interpretation of Data

Landform geometrical features coupled with mountain road restoration works for enhancing landslide hazard resilience were further interpreted through a statistically determined

approach. Many site-specific construction works are relatively old, more than 20–30 years at the data collection, and the research has continued since 2000. The historical data usage approach mainly focused on observations of weather-associated consequences as a tool for understanding roadside slope stability potential. The statistical interpretation primarily focused on understanding the way to reduce the cost of landslide remediation work and, thus, the appropriate roadway design on a mountain slope. The landform is a feature on the terrain's surface, which is further subdivided based on land use. We interpreted the collapsed and intact slope landforms in terms of land use, slope angle, slope height, and slope azimuth, as shown in Figs. 19, 20, and 21.

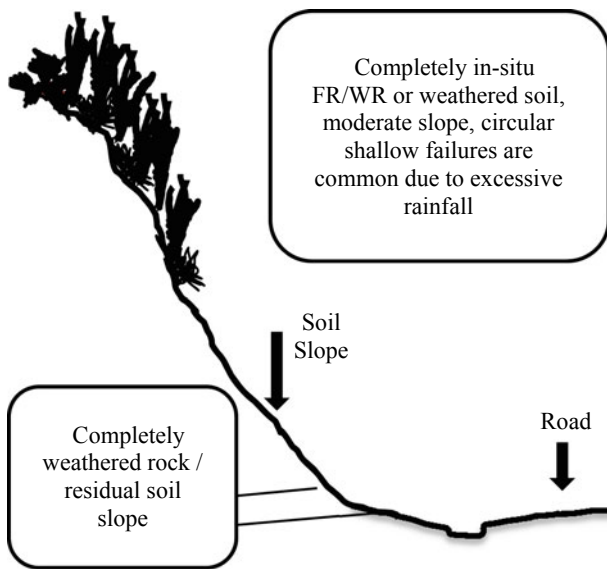


Fig. 15 Type-a: No rocks/rock outcrop at the upper slope, lower slope is stable or failed with in-situ residual soil formations. Limited or less potential threat of slope failures

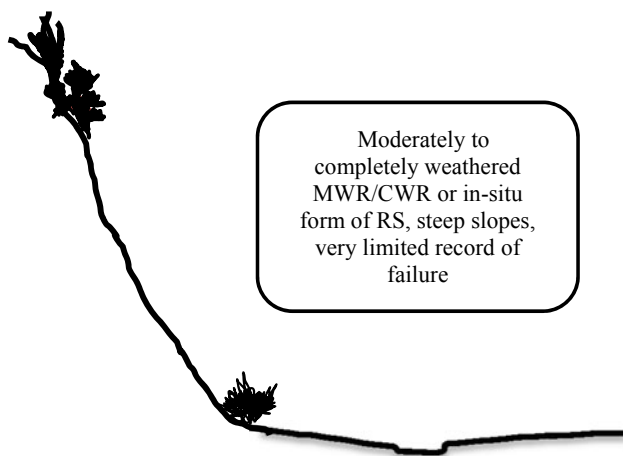


Fig. 16 Type-b: In-situ formed soil or completely weathered rock, less tendency or less potential slope failure according to field evidences

An illustrative example of the landform interpretation (Fig. 22) highlights the importance of studies on landform geometry of mountain road restoration. The studies significantly optimize the cost of total slope remedial measures against slope degradation in mountain road construction. Though observations were limited to 67 case histories, more data will support more corrective decisions during road designs.

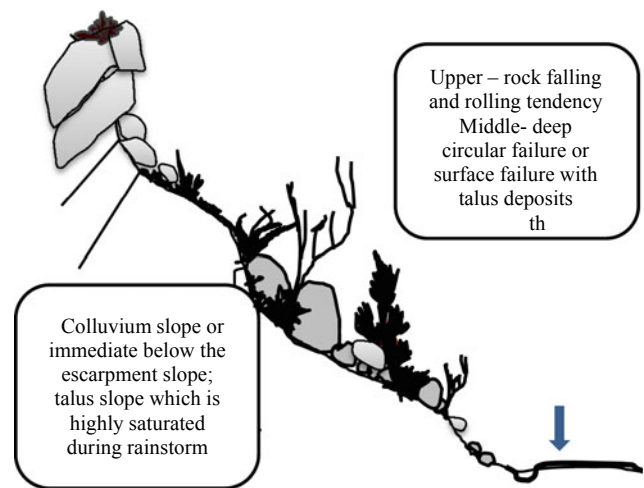


Fig. 17 Type-c: Rock falling, bouncing and rolling tendency of escarpment slope segments. Highly potential failure records at road side slope

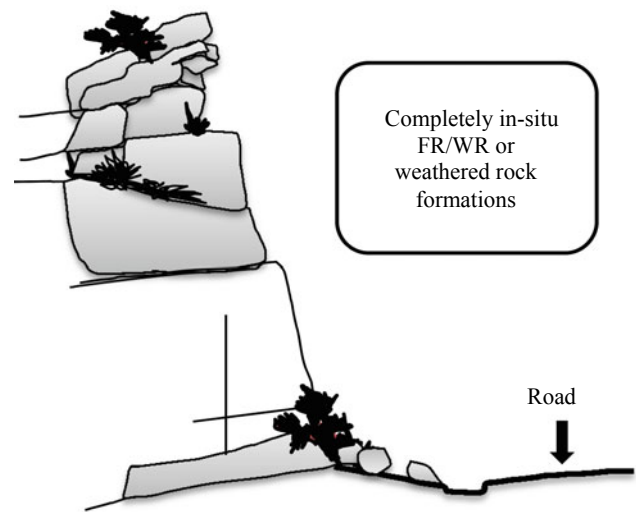


Fig. 18 Type-d: Completely rock slope, moderately to highly jointed/foliated rock face; Limited failure records, but highly potential rock falling, bouncing and rolling

10 Conclusion

Spatial interpretation and a case study

Hilly terrains in Sri Lanka, belonging to the humid weather pattern caused by global climate change, are wet and deserve attention in planning, designing, constructing, and maintaining mountain roads. Unsaturated residual soil

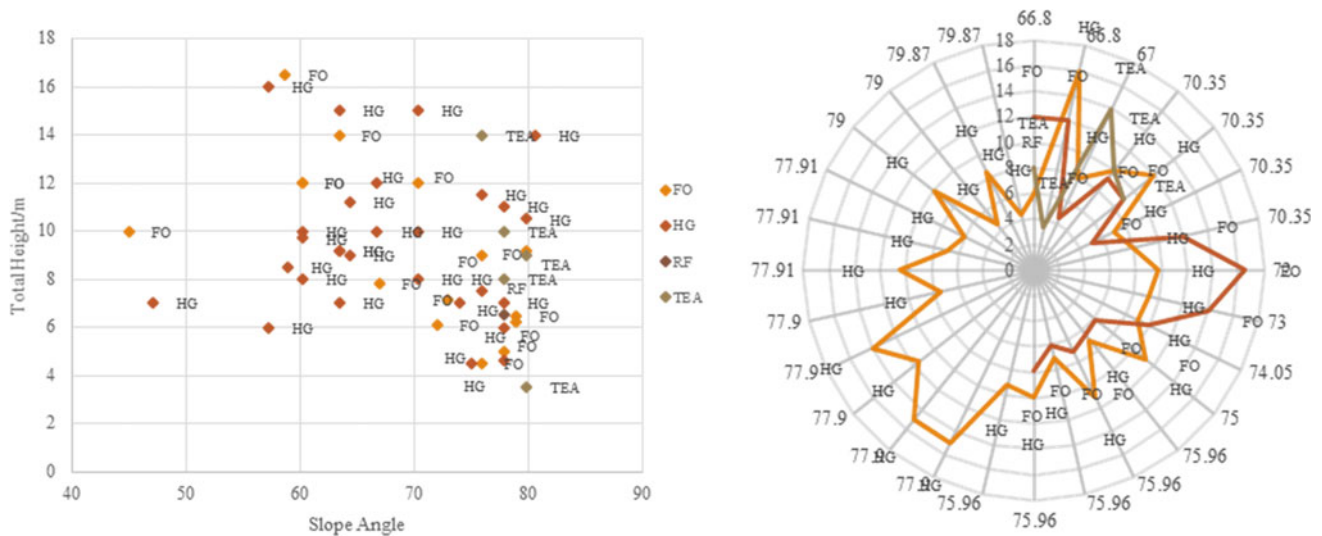


Fig. 19 Unstable slope records of stability plots for Slope Angle vs Total Height of earth cutting against to Land use above the road/upper slope segment (FO-Forest, HG-Home Garden, RF-Reforestation, and TEA-tea plantation). Height below 3.2 m is stable

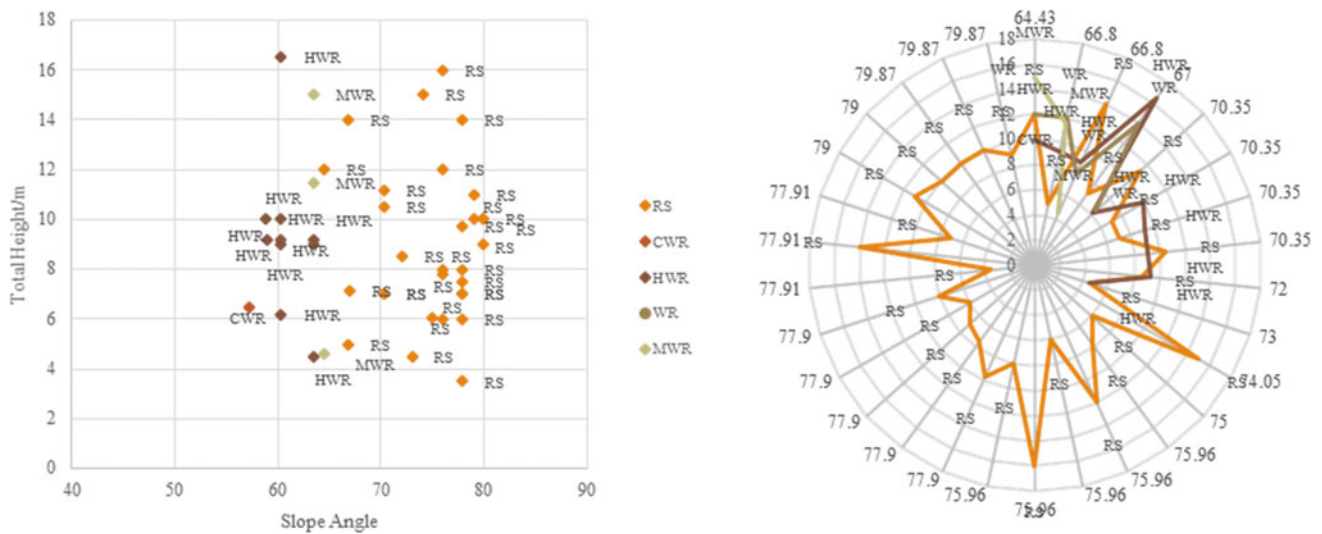


Fig. 20 Unstable slope records of stability plots for Slope Angle vs Total Height of earth cutting against Geology (ie. highly to completely weathered rock; HWR, MWR, CWR and residual soil condition; RS). Cutting Height below 4.6 m is stable

formations often cover these areas, indirectly contributing to high values of apparent cohesion during the non-saturated condition. Slopes of completely weathered soils (including highly weathered rocks) retain themselves in place due to the unsaturated behavior of soils, as shown in Fig. 21. Therefore, many cut-slopes of height not exceeding 3.2 m are potentially stable or can be restored with the least cost of remedial measures.

Land use in the upper slope significantly contributes to soil restoration potential. The geological complexity of cut

slope sections always needs to be toughly studied with an appropriate guideline of site-specific design.

The results of the study are summarized as follows.

- I. The complexity of slope geometries, potential deformities, ground discontinuities, and soil-rock composite nature are compulsory elements to understand and dominant parameters to describe the on-site stability of earth cut slope.
- II. Cut slopes of roads are often designed in different geological complexity overlaying upper and lower

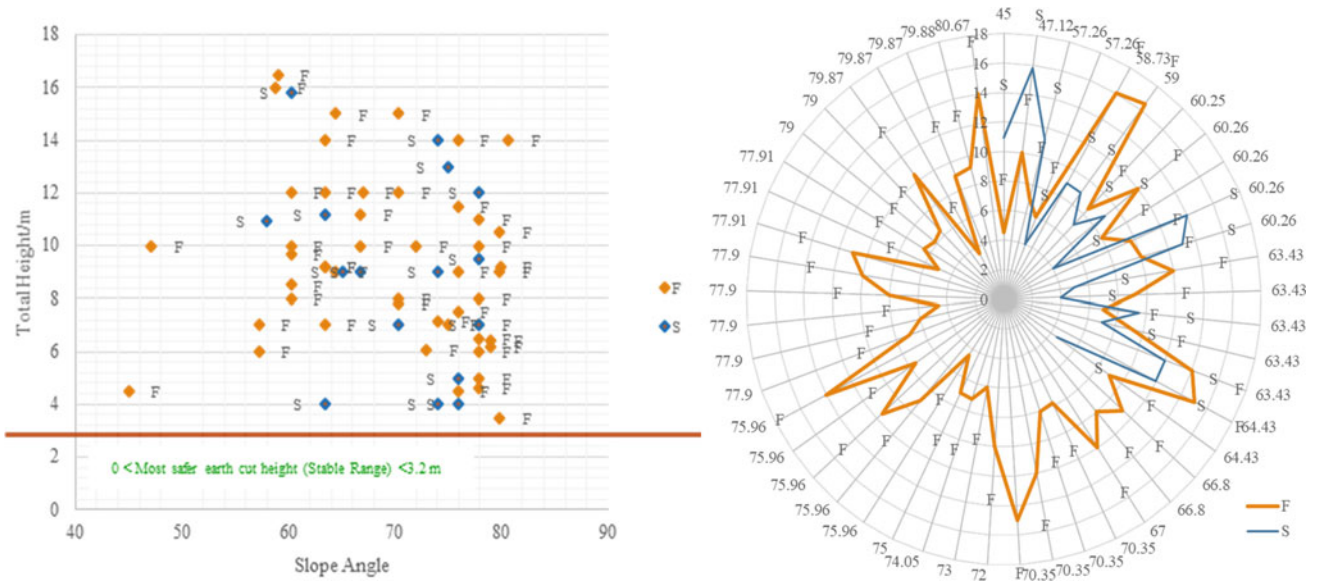


Fig. 21 Decision making stability plots for Slope Angle versus Total Height of Earth cut; Each point data contains different visual and physical characteristics including geology (highly to completely weathered rock, land surfaces), multiple landforms, stability criteria, failure-F and stable-S. Study concludes height below 3.2 m is stable even under different geological conditions or land use

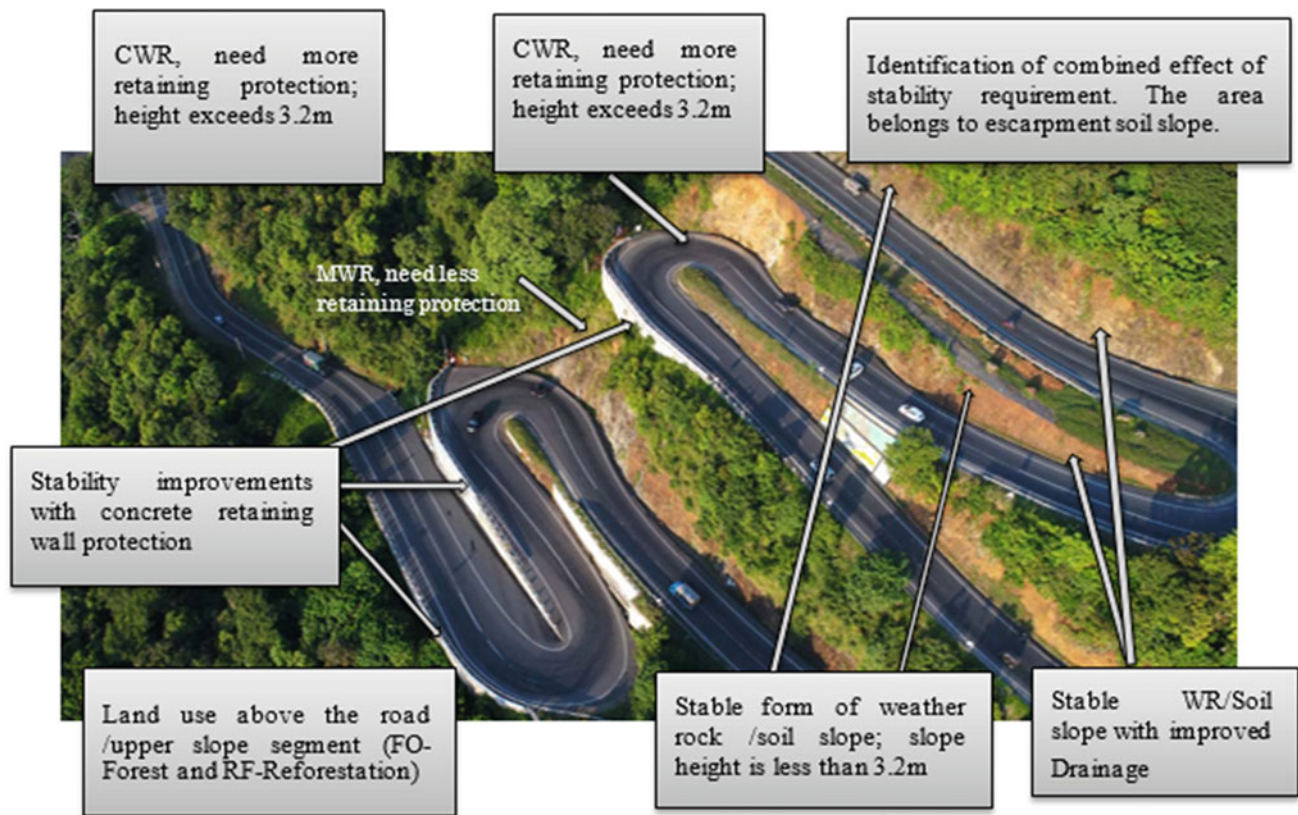


Fig. 22 Mountain slope stability measures adopted in “18 Hairpin Bend” Kandy-Mahiyangana highway (Photo by <https://www.mapakadavillage.lk/En/five-facets-about-mahiyanganaya/>), Sri Lanka

landforms. Therefore, accurate interpretation of those data is essential.

- III. Understanding factors incorporated in geo-structural integrity and potentially unstable landform are the key elements that decrease the cost of remedial measures on hill slopes.
- IV. In many instances, designing a wider section of mountain road is often challenging given landslide potential due to various landform features of upper and lower slopes.

Investigating and analyzing the soil properties and parameters that affect the stability of residual soil slope against all road cutting sections are usually expensive and time-consuming.

The above finding and approach allowed for site-specific generalization. Therefore, it is advisable to use additional criteria to predict the stability potential of cut slopes in road designs. More information about the cut slopes of mountain roads is required for more reliable prediction or design optimization.

More research on the road cut slope protections, data gathering of constructed slopes, data evaluation, and design of remedial measures will be recommended for very mountain regions/countries deep in mountains. They ultimately contribute to the development of landslide hazard resilience.

Acknowledgements This paper forms an integral part of the research under the World Centre of Excellence (WCoE) for Landslide Disaster Reduction implemented by the Natural Resources Management and Laboratory Services (NRMLS), Central Engineering Consultancy Bureau of the Ministry of Irrigation. It is published with their permission. However, the views expressed in the paper are those of the authors only. It is our pleasure to acknowledge Dr. (Ms.) W. A. D. Lakshani Weragoda for her valuable input for the interpretation of data and the staff of the Natural Resources Management and Laboratory Services for their continuous corporation and help extended to field works and preparation of this paper. Our thanks are due to the Eng. Iven de Silva, Chairman, Central Engineering Consultancy Bureau (CECB)/Secretary to the Ministry of Irrigation and Eng. G. R. A. S. Gunathilaka, General Manager, CECB, for the permission and encouragement.

References

- Attractions Sri Lanka (2019) 18 Bend Road, <https://www.attractionsinsrilanka.com/travel-directory/18-bend-road/>. (Last accessed on 30 Mar 2022)
- Bhandari RK, Senanayake KS, Thayalan N (1991) Pitfalls in the prediction on landslide through rainfall data. In: Bell DH (ed) *Landslides*, 2nd edn. A.A. Balkema, Rotterdam, pp 887–890
- Bhandari RK, Dias AAV (1996) Rain triggered slope movement as indicators of landslide dynamics. In: 7th international symposium on landslides, 17–21 June 1996, Trondheim, Norway
- Brawner CO, Wyllie DC (1975) Rock slope stability on railway Projects. In: Proceedings American railway engineering association regional meeting, Vancouver, B. C., American Railway Engineering Association, Washington, D.C., pp 8
- Brawner CO (1994) Rockfall hazard mitigation methods, participant workbook, NHI Course No. 13219. U.S. Department of Transportation, Federal Highway Administration, Publication No. FHWA SA-93-085
- Cooray PG (1967) An introduction to the geology of Ceylon. Ceylon National Museum Publication, Colombo, p 324
- Cooray PG (1984) Geology, with special reference to the pre-cambrian. In: Fernando CH (ed) *Ecology and biogeography in Sri Lanka*, The Hague, The Netherlands, W. Junk Publishers, pp 1–34
- Dias AAV, Gunathilaka AAJK (2014) Evaluation of sensitivity of the WAA and SINMAP models for landslide susceptibility risk mapping in Sri Lanka. In: Proceeding of the world landslide Forum3 (WLF3), Beijing, China, 2–6 June 2014. vol 2. *Landslide Science for a Safer Geoenvironment*, pp 167–173
- Dias AAV, Katuwala N, Herath HMJMk, Perera PVIP, Saha-bandu KLS, Rupasinghe N, (2017) Model policy frameworks, standards and guidelines on disaster reduction (WCoE 2014–2017). *Advancing culture of living with landslides; vol 1 ISRD-ICL Sendai Partnerships 2015–2025*, pp 365–374, Springer
- Erb DK (1984) Land forms and drainage. In: Fernando CH (ed) *Ecology and biogeography in Sri Lanka*. The Hague, The Netherlands, W. Junk Publishers, pp 35–63
- Gao Y, Yin YP, Li B, Feng Z, Wang WP, Zhang N, Xing AG (2017) Characteristics and numerical runout modeling of the heavy rainfall-induced catastrophic landslide-debris flow at Sanxicun, Dujiangyan, China, following the Wenchuan Ms 8.0 earthquake. *Landslides* 14:1–14
- Herath HM, Janaki MK, Kodagoda SSI, Dias AAV (2014) Shallow modes of slope failure in road earth cuttings in Sri Lanka. In: *Landslide science for a safer geoenvironment, world landslide forum3 (WLF3)*, Beijing, China, 2–6 June 2014; vol 2, pp 51–58; ISBN 978-3-319-05049-2. Springer
- Hiru News (2020) Traffic disrupted Daha Ata Wanguwa (18 Hairpin Bend) in Mahiyangana, <https://www.hirunews.lk/english/232733/traffic-disrupted-on-daha-ata-wanguwa-18-hairpin-bend-in-mahiyanganaya>. (Last accessed on 28 Mar 2022)
- Janaki HM, Herath MK, Jayasooriya JADNA, Dias AAV (2016) Geological stability of overhanging rock slopes. In: Proceedings of 2016 IPL Symposium, UNESCO, Paris November, pp 17–18
- NBRO Report (1988) Mulhalkele Landslide in 1986. Zero victims and damage to the general hospital premises at the Mulahalkele, Nuwara Eliya district in Sri Lanka, NBRO 1988
- Panabokke R (1996) Soils and agro-ecological environments of Sri Lanka. Natural resources, energy and science authority of Sri Lanka Pre-Feasibility Study for Designing Major Roads in Landslide Area (Published in vol 1 & vol 2), Central Engineering Consultancy Bureau, June, 2000, Sri Lanka. Project was funded by the Japan International Cooperation Agency (JICA) through the Road Development Authority (RDA) of Sri Lanka
- Russell CP, Santi P, Humphrey JD (2008) Modification and statistical analysis of the Colorado Rockfall hazard rating system: Report No. CDOT-2008-7, pp 139
- Sri Lanka Red Cross Society (2016) Red cross provides first aid and relief support to flood & landslide affected. <https://www.redcross.lk/main-news/180-persons-rescued-from-aranayaka-landslide-rescue-missions-well-underway/>. (Last accessed 29th Mar 2022)
- The StraitsTimes Asia. (2017) Sri Lanka appeals for help as floods cripple water supply. <https://www.straitstimes.com/asia/south-asia/sri-lanka-appeals-for-help-as-floods-cripple-water-supply>. (Last accessed on 31 Mar 2022)
- Varnes DJ (1984) Landslide hazard zonation: a review of principles and practice. *Natural Hazards*. UNESCO, Paris
- Wyllie DC (1987) Rock slope inventory system. In: Proceedings federal highway administration rockfall mitigation seminar, FHWA Region 10, Portland, Oreg., pp 25

Open Access This chapter is licensed under the terms of the Creative Commons Attribution 4.0 International License (<http://creativecommons.org/licenses/by/4.0/>), which permits use, sharing, adaptation, distribution and reproduction in any medium or format, as long as you give appropriate credit to the original author(s) and the source, provide a link to the Creative Commons license and indicate if changes were made.

The images or other third party material in this chapter are included in the chapter's Creative Commons license, unless indicated otherwise in a credit line to the material. If material is not included in the chapter's Creative Commons license and your intended use is not permitted by statutory regulation or exceeds the permitted use, you will need to obtain permission directly from the copyright holder.



ICL Landslide Teaching Tools



LS-RAPID Manual with Video Tutorials

Beena Ajmera, Hossein Emami Ahari, Doan Huy Loi, Hendy Setiawan, Khang Dang, and Kyoji Sassa

Abstract

LS-RAPID is an integrated simulation model capable of capturing the entire landslide process starting from a state of stability to landslide initiation and movement to the mass deposition. This paper provides an overview of the use of LS-RAPID to simulate landslide case histories around the world, provides a manual for readers to begin using the program for simulations, and describes the use of the program for several models. Specific steps to use the basic and advanced features in LS-RAPID are provided within the paper. Additionally, video tutorials are provided to supplement the descriptive steps provided in this paper. These tutorials are developed to focus on individual aspects of the program. The paper concludes with three tutorials that provide a complete walk-through of the use of the program from start to finish. These tutorials are for (1) an example of a rainfall-induced failure, (2) an example of an earthquake-induced failure, and (3) the case study of the Atami debris flow. The Atami debris flow illustrates the ability of LS-RAPID to reproduce reliable

results associated with the initiation and runout motions of the observed failure.

Keywords

Computer simulation • LS-RAPID • Video tutorials • User manual • Examples

Supplementary Information

The online version contains supplementary material available at https://doi.org/10.1007/978-3-031-16898-7_26.

B. Ajmera (✉) · H. E. Ahari
Department of Civil, Construction and Environmental
Engineering, Iowa State University, Ames, IA, USA
e-mail: bajmera@iastate.edu

H. E. Ahari
e-mail: hemami@iastate.edu

D. H. Loi · K. Sassa
International Consortium On Landslides, Kyoto, Japan

H. Setiawan
Department of Geological Engineering, Gadjah Mada University,
Yogyakarta, Indonesia
e-mail: hendy.setiawan@ugm.ac.id

K. Dang
Department of Geotechnics and Infrastructure Development, VNU
University of Science, Hanoi, Vietnam

1 Chapter 1: Introduction

LS-RAPID was developed by Sassa et al. (2010) as an integrated landslide simulation model that aims to model the whole process of a landslide including the stable state, failure stage, post-failure shear strength reduction, landslide motion, steady state condition and the mass deposition stage. This model is an upgrade to a numerical simulation model for landslides proposed by Sassa (1988).

In principle, the LS-RAPID model is intended to integrate the initiation mechanism and the behavior motion of a landslide from the initial failure of the slope (stability analysis) to the mobilization and expansion of landslide materials (dynamic analysis) to the deposition stage. The user can also perform partial analysis for a landslide model, for example, only simulate the motion simulation, or conduct full mode simulation that includes initiation, motion and expansion. Within the LS-RAPID model, changes in the behavior of the landslide can be captured when the triggering factors are initiated.

The LS-RAPID model can accommodate landslide simulations for failures induced by rainfall as well as earthquakes. For rainfall-induced landslides, simulations can be undertaken by inputting either the pore water pressure ratio or using hourly rainfall data time series. For earthquake-induced landslides, the simulation can be conducted using the static mode with a seismic coefficient, cyclic loading or seismic loading provided from an earthquake peak ground acceleration time series record. The program can also consider

combined triggering factors, that involve both rainfall and earthquake conditions applied simultaneously. The application is based on the data that is inputted into the simulation.

1.1 Example Case Studies

LS-RAPID has been applied in the study of numerous landslide cases around the world. The use of LS-RAPID in some case studies was integrated with laboratory tests through undrained dynamic loading ring shear apparatus to obtain the dynamic and residual shear strength of soils, i.e., post-failure state during large shear displacements and the pore-water pressure conditions as input parameters. Meanwhile, other studies have used approximate parameters estimated from back analysis, results of peak shear strength and static geotechnical tests.

Table 1 present a list of case studies in which LS-RAPID models were utilized. These case studies involve landslides triggered by rainfall or earthquake and have already been published in journals, chapter books and conference proceedings. The relevant references for additional information about the case study are also provided.

2 Theoretical Background

2.1 Basic Principle and Governing Equations

The concept of the LS-RAPID model was established by considering that the unstable slope consists of the landslide mass and stable ground in a form of a vertical imaginary column (Fig. 1). The forces acting within this moving landslide mass include the weight of the column (W), the vertical seismic force (F_v), horizontal seismic forces in the x - and y -directions (F_x and F_y , respectively), lateral pressure acting both on side walls (P), shear resistance acting on the bottom and interface with the stable ground (R), the normal stress acting on the bottom (N) from the stable ground as a reaction to the normal component of the self-weight, and the pore pressure acting on the bottom (U).

Following Newton's laws of motion, the acceleration (a) of the landslide mass (m) will be the result of the sum of driving forces (self-weight and seismic force), shear resistance (R) and the change in lateral pressure (P), denoted as:

$$a \cdot m = (W + F_v + F_x + F_y) + \left(\frac{\partial P_x}{\partial x} \Delta x + \frac{\partial P_y}{\partial y} \Delta y \right) + R \quad (1)$$

However, the effects of forces N and U that are projected in the upward direction of the maximum slope line

contribute before the motion and work during the motion against the direction of the landslide mass movement. All stresses and displacements are projected and calculated in to the horizontal plane (Sassa 1988).

The left side of Eq. (1) is then projected in to the x -, y - and z -directions by considering the flows in and out of the column element with constant average velocity as shown below:

$$a_x = \frac{\partial u_0}{\partial t} + u_0 \frac{\partial u_0}{\partial x} + v_0 \frac{\partial u_0}{\partial y} + w_0 \frac{\partial u_0}{\partial z} \quad (2)$$

$$a_y = \frac{\partial v_0}{\partial t} + u_0 \frac{\partial v_0}{\partial x} + v_0 \frac{\partial v_0}{\partial y} + w_0 \frac{\partial v_0}{\partial z} \quad (3)$$

The velocity along z -direction is neglected since the simulation is typically conducted to understand the mechanism and motion behavior of the moving landslide mass in area.

To represent the moving landslide mass, the LS-RAPID model uses the soil flow to x -direction per unit width as flux M and the soil flow to y -direction per unit width as flux N , that are both associated with the velocities and the height of soil column (h). They are expressed as:

$$M = u_0 \cdot h \text{ and } N = v_0 \cdot h \quad (4)$$

Therefore, the left side of Eq. (1) will become Eqs. (5) and (6) below:

$$\frac{1}{h} \left\{ \frac{\partial M}{\partial t} + \frac{\partial}{\partial x} (u_0 M) + \frac{\partial}{\partial y} (v_0 M) \right\} = (W + F_v + F_x + F_y) + \left(\frac{\partial P_x}{\partial x} \Delta x + \frac{\partial P_y}{\partial y} \Delta y \right) + R \quad (5)$$

$$\frac{1}{h} \left\{ \frac{\partial N}{\partial t} + \frac{\partial}{\partial x} (u_0 N) + \frac{\partial}{\partial y} (v_0 N) \right\} = (W + F_v + F_x + F_y) + \left(\frac{\partial P_x}{\partial x} \Delta x + \frac{\partial P_y}{\partial y} \Delta y \right) + R \quad (6)$$

As a result of the moving landslide mass, the right side of Eq. (1) consists of:

- the gravity term, $(W + F_v + F_x + F_y)$
- the pressure term, $\frac{\partial P_x}{\partial x} \Delta x + \frac{\partial P_y}{\partial y} \Delta y$, and
- the shear resistance per unit area on x - y plane, R .

The gravity term, by including the seismic acceleration, is projected to x - and y -directions and associated with the vertical seismic acceleration ($g \times K_v$) and horizontal seismic acceleration acting on x - ($g \times K_x$) and y -directions ($g \times K_y$), as stated below (Fig. 2):

Table 1 Application of LS-RAPID in landslide case studies around the world

No	Case study	Country	References
1	Earthquake- and rain-induced rapid Leyte landslide	The Philippines	<p>Sassa K, Nagai O, Solidum R, Yamazaki Y, Ohta H (2010) An integrated model simulating the initiation and motion of earthquake and rain induced rapid landslides and its application to the 2006 Leyte landslide. <i>Landslides</i> 7:219–236. https://link.springer.com/article/10.1007/s10346-010-0230-z</p> <p>Tien P V, Sassa K, Khang D (2018) TXT-tool 3.081-1.1: An integrated model simulating the initiation and motion of earthquake and rain induced rapid landslides and its application to the 2006 Leyte landslide. In: Sassa K, Tiwari B, Liu KF, McSaveney M, Strom A, Setiawan H (eds) <i>Landslide Dynamics: ISDR-ICL Landslide Interactive Teaching Tools</i> pp 83–99. Springer, Cham. https://link.springer.com/chapter/10.1007/978-3-319-57777-7_2</p>
2	Senoumi submarine megaslide in Suruga Bay	Japan	<p>Sassa K, He B, Miyagi T, Strasser M, Konagai K, Ostric M, Setiawan H, Takara K, Nagai O, Yamashiki Y, Tutumi S (2012) A hypothesis of the Senoumi submarine megaslide in Suruga Bay in Japan—based on the undrained dynamic-loading ring shear tests and computer simulation. <i>Landslides</i> 9:439–455 https://link.springer.com/article/10.1007/s10346-012-0356-2</p> <p>Setiawan H, Sassa K, He B (2018) TXT-tool 3.081–1.3: A hypothesis of the Senoumi submarine megaslide in Suruga Bay in Japan – Based on the undrained dynamic-loading ring shear tests and computer simulation. In: Sassa K, Tiwari B, Liu KF, McSaveney M, Strom A, Setiawan H (eds) <i>Landslide Dynamics: ISDR-ICL Landslide Interactive Teaching Tools</i> pp 131–147. Springer, Cham https://link.springer.com/chapter/10.1007/978-3-319-57777-7_5</p>
3	Rainfall triggered rapid and long run-out Hiroshima landslide	Japan	<p>Sassa K, Fukuoka H, Sato Y, Takara K, Huy L D, Setiawan H, Tien P V, Khang D Q (2014) Initiation mechanism of rapid and long runout landslide and simulation of Hiroshima landslide disasters using the integrated simulation model (LS-RAPID). <i>Proceeding of International Forum “Urbanization and Landslide Disaster”</i>, Kyoto, Japan, 8 October 2014, pp: 85–112</p> <p>Huy LD, Sassa K, Fukuoka H, Sato Y, Takara K, Setiawan H, Tien PV, Dang K (2018) TXT-tool 3.081-1.4: Initiation mechanism of rapid and long run-out landslide and simulation of Hiroshima landslide disasters using the integrated simulation model (LS-RAPID). In: Sassa K, Tiwari B, Liu KF, McSaveney M, Strom A, Setiawan H (eds) <i>Landslide Dynamics: ISDR-ICL Landslide Interactive Teaching Tools</i> pp 149–168. Springer, Cham https://link.springer.com/chapter/10.1007/978-3-319-57777-7_6</p>
4	Kostanjek landslide, Zagreb	Croatia	<p>Gradiški K, Sassa K, He B, Arbanas Ž, Arbanas S M, Krkač M, Kvasnička P, Oštrić M (2018) TXT-tool 3.385-1.1: Application of Integrated Landslide Simulation Model LS-Rapid to the Kostanjek Landslide, Zagreb, Croatia. In: Sassa K, Tiwari B, Liu KF, McSaveney M, Strom A, Setiawan H (eds) <i>Landslide Dynamics: ISDR-ICL Landslide Interactive Teaching Tools</i> pp 101–109. Springer, Cham https://link.springer.com/chapter/10.1007/978-3-319-57777-7_3</p>
5	Landslide susceptibility on flysch slopes in Istra	Croatia	<p>Jovančević S D, Nagai O, Sassa K, Arbanas Ž (2018) TXT-tool 3.385-1.2: Deterministic Landslide Susceptibility Analyses Using LS-Rapid Software. In: Sassa K, Tiwari B, Liu KF, McSaveney M, Strom A, Setiawan H (eds) <i>Landslide Dynamics: ISDR-ICL Landslide Interactive Teaching Tools</i> pp 169–179. Springer, Cham https://link.springer.com/chapter/10.1007/978-3-319-57777-7_7</p>
6	Grohovo landslide, Rječina River Valley, Rijeka	Croatia	<p>Prodan M V, Jovančević S D, Arbanas A (2018) TXT-tool 3.385-1.3: Landslide Occurrence Prediction in the Rječina River Valley as a Base for an Early Warning System. In: Sassa K, Tiwari B, Liu KF, McSaveney M, Strom A, Setiawan H (eds) <i>Landslide Dynamics: ISDR-ICL Landslide Interactive Teaching Tools</i> pp 263–275. Springer, Cham https://link.springer.com/chapter/10.1007/978-3-319-57777-7_13</p>

(continued)

Table 1 (continued)

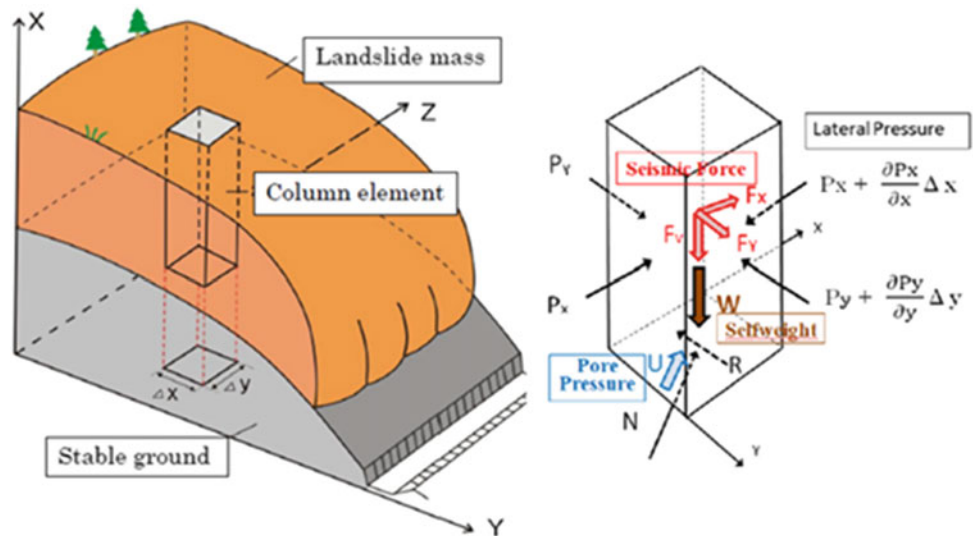
No	Case study	Country	References
7	The 1792 Unzen-Mayuyama megaslide	Japan	<p>Sassa, K., Dang, K., He, B. et al. (2014) A new high-stress undrained ring-shear apparatus and its application to the 1792 Unzen–Mayuyama megaslide in Japan. <i>Landslides</i> 11, 827–842 https://link.springer.com/article/10.1007/s10346-014-0501-1</p> <p>Sassa, K., Dang, K., Yanagisawa, H. et al. (2016) A new landslide-induced tsunami simulation model and its application to the 1792 Unzen-Mayuyama landslide-and-tsunami disaster. <i>Landslides</i> 13, 1405–1419 https://link.springer.com/article/10.1007/s10346-016-0691-9</p>
8	Earthquake- triggered Aratozawa landslide	Japan	<p>Setiawan H, Sassa K, Takara K, Ostric M, Miyagi T, Fukuoka H (2018) TXT-tool 4.081-1.2: Mechanism of the Aratozawa large-scale landslide induced by the 2008 Iwate-Miyagi earthquake. In: Sassa K, Tiwari B, Liu KF, McSaveney M, Strom A, Setiawan H (eds) <i>Landslide Dynamics: ISDR-ICL Landslide Interactive Teaching Tools</i> pp 819–831. Springer, Cham. https://link.springer.com/chapter/10.1007/978-3-319-57777-7_54</p> <p>Setiawan H, Sassa K, Takara K, Fukuoka H (2017) Detail study of the Aratozawa large-scale landslide in Miyagi Prefecture, Japan. In: Mikoš M., Vilímek V., Yin Y., Sassa K. (eds) <i>Advancing Culture of Living with Landslides</i> pp 473–480. WLF2017. Springer, Cham https://link.springer.com/chapter/10.1007/978-3-319-53483-1_56</p>
9	Kuridaira and Akatani landslides, the Kii Peninsula	Japan	<p>Van Tien P, Sassa K, Takara K, Fukuoka H, Dang K, Shibasaki T, Ha ND, Setiawan H, Loi DH (2018) Formation process of two massive dams following rainfall-induced deep-seated rapid landslide failures in the Kii Peninsula of Japan. <i>Landslides</i> 15: 1761–1778 https://link.springer.com/article/10.1007/s10346-018-0988-y</p>
10	Takanodai and Aso-ohashi landslides due to Kumamoto earthquake	Japan	<p>Dang, K., Sassa, K., Fukuoka, H. et al. (2016) Mechanism of two rapid and long-runout landslides in the 16 April 2016 Kumamoto earthquake using a ring-shear apparatus and computer simulation (LS-RAPID). <i>Landslides</i> 13, 1525–1534. https://link.springer.com/article/10.1007/s10346-016-0748-9</p>
11	Marappalam area of Nilgiris district, Tamil Nadu state	India	<p>Senthilkumar, V., Chandrasekaran, S. & Maji, V. (2017) Geotechnical characterization and analysis of rainfall-induced 2009 landslide at Marappalam area of Nilgiris district, Tamil Nadu state, India. <i>Landslides</i> 14, 1803–1814. https://link.springer.com/article/10.1007/s10346-017-0839-2</p>
12	Shenzhen landfill, Guangdong	China	<p>Yin, Y., Li, B., Wang, W., Zhan, L., Xue, Q., Gao, Y., Zhang, N., Chen, H., Liu, T., Li, A. (2016). Mechanism of the December 2015 catastrophic landslide at the Shenzhen landfill and controlling geotechnical risks of urbanization. <i>Engineering</i>, 2(2), 230–249 https://www.sciencedirect.com/science/article/pii/S209580991630950X</p>
13	Pasir Panjang landslide, Brebes Regency, Central Java	Indonesia	<p>Setiawan H, Wilopo W, Wiyoso T, Fathani TF, Karnawati D (2019) Investigation and numerical simulation of the 22 February 2018 landslide-triggered long-traveling debris flow at Pasir Panjang Village, Brebes Regency of Central Java, Indonesia. <i>Landslides</i>, Vol. 16(11): 2219–2232. First Online 5 August 2019 https://link.springer.com/article/10.1007/s10346-019-01245-0</p> <p>Setiawan H, Fathani TF, Wilopo W, Karnawati D (2019) Analysis of potential landslide and its motion behavior in Salem District, Brebes Regency, Central Java of Indonesia by using the LS-RAPID numerical simulation. <i>Proc. Int. Conf. on Landslide and Slope Stability SLOPE 2019</i> pp. E3(1–12), Bali, Indonesia</p>
14	Arayanake landslide	Sri Lanka	<p>Dang, K., Sassa, K., Konagai, K. et al. (2019) Recent rainfall-induced rapid and long-traveling landslide on 17 May 2016 in Aranayaka, Kagelle District, Sri Lanka. <i>Landslides</i> 16, 155–164. https://link.springer.com/article/10.1007/s10346-018-1089-7</p> <p>Tan, Q., Sassa, K., Dang, K. et al. (2020) Estimation of the past and future landslide hazards in the neighboring slopes of the 2016 Aranayake landslide, Sri Lanka. <i>Landslides</i> 17, 1727–1738 https://link.springer.com/article/10.1007/s10346-020-01419-1</p>

(continued)

Table 1 (continued)

No	Case study	Country	References
15	Shallow landslide, Halong City	Vietnam	Ha, N.D., Sayama, T., Sassa, K. et al. (2020) A coupled hydrological-geotechnical framework for forecasting shallow landslide hazard—a case study in Halong City, Vietnam. <i>Landslides</i> 17, 1619–1634 https://link.springer.com/article/10.1007/s10346-020-01385-8 Loi, D.H., Quang, L.H., Sassa, K. et al. (2017) The 28 July 2015 rapid landslide at Ha Long City, Quang Ninh, Vietnam. <i>Landslides</i> 14, 1207–1215. https://link.springer.com/article/10.1007/s10346-017-0814-y
16	Landslide induced tsunami, Truong River in Quang Nam province	Vietnam	Duc, D.M., Khang, D.Q., Duc, D.M. et al. (2020) Analysis and modeling of a landslide-induced tsunami-like wave across the Truong River in Quang Nam province, Vietnam. <i>Landslides</i> 17, 2329–2341 https://link.springer.com/article/10.1007/s10346-020-01434-2
17	Catastrophic landslide dam at Jure Village	Nepal	Van Tien, P., Luong, L. H., Sassa, K., Takara, K., Sumit, M., Thanh Nhan, T., Dang, K., Minh Duc, D. (2021). Mechanisms and Modeling of the Catastrophic Landslide Dam at Jure Village, Nepal. <i>Journal of Geotechnical and Geoenvironmental Engineering</i> , 147(11), 05,021,010 https://doi.org/10.1061/(ASCE)GT.1943-5606.0002637

Fig. 1 Column element within a moving landslide mass as basis of the LS-RAPID model (Sassa et al. 2010)



$$1 + K_v \text{ works in the } x \text{ - direction : } g \frac{\tan \alpha}{q+1} (1 + K_v) \quad (7)$$

$$(1 + K_v) \cdot k \cdot g \cdot \frac{\partial h}{\partial x} \text{ (x - direction)} \quad (11)$$

$$1 + K_v \text{ works in the } y \text{ - direction : } g \frac{\tan \beta}{q+1} (1 + K_v) \quad (8)$$

$$(1 + K_v) \cdot k \cdot g \cdot \frac{\partial h}{\partial y} \text{ (y - direction)} \quad (12)$$

$$\text{For horizontal acceleration along } x : g K_x \cos^2 \alpha \quad (9)$$

$$\text{For horizontal acceleration along } y : g K_y \cos^2 \alpha \quad (10)$$

The pressure term is the difference of the lateral pressure acting on both sides of columns in the x- and y-directions (Fig. 3), where the lateral pressure is expressed using the lateral earth pressure ratio (k), as shown in Eqs. (11) and (12).

According to Sassa (1988), shear resistance per unit area on the x–y plane is acting in the direction opposite to the direction of the movement of the landslide mass. The components of shear resistance in the x- and y- directions are given by Eqs. (13) and (14), respectively:

$$\frac{g}{(q+1)^{1/2}} \cdot \frac{u_o}{(u_o^2 + v_o^2 + w_o^2)^{1/2}} \{h_c(q+1) + (1-r_u) h \tan \phi_a\} \quad (13)$$

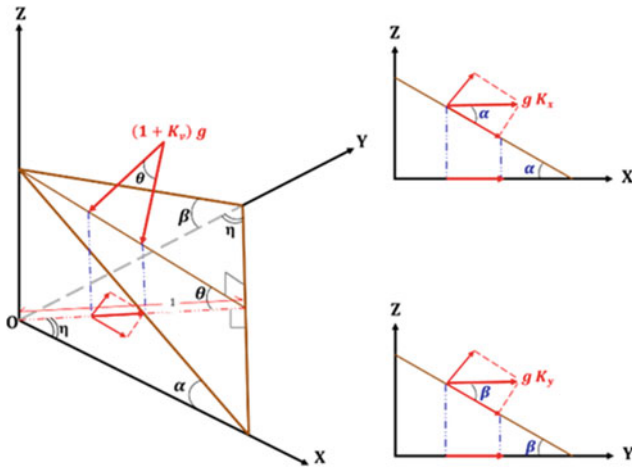


Fig. 2 Projection of (left) gravity and vertical seismic force and (right) gravity and horizontal seismic force

$$\frac{g}{(q+1)^{1/2}} \cdot \frac{v_o}{(u_o^2 + v_o^2 + w_o^2)^{1/2}} \{h_c(q+1) + (1-r_u)htan\phi_a\} \tag{14}$$

where $w_o = -(u_o \tan\alpha + v_o \tan\beta)$, while the effect of the apparent friction coefficient ($\tan\phi_a$), the pore pressure ratio (r_u) and cohesion in the unit of height (h_c) are dependent on the shear strength reduction stages.

Based on the deductions provided above, Eq. (1) can be completely expressed into the x- and y-directions as given by Eqs. (15) and (16), respectively below:

$$\begin{aligned} \frac{\partial M}{\partial t} + \frac{\partial}{\partial x}(u_o M) + \frac{\partial}{\partial y}(v_o M) = & gh \left\{ \frac{\tan\alpha}{q+1} (1+K_v) + K_x \cos^2\alpha \right\} \\ & - (1+K_v) k g h \frac{\partial h}{\partial x} \\ & - \frac{g}{(q+1)^{1/2}} \cdot \frac{u_o}{(u_o^2 + v_o^2 + w_o^2)^{1/2}} \\ & \cdot \{h_c(q+1) + (1-r_u)htan\phi_a\} \end{aligned} \tag{15}$$

$$\begin{aligned} \frac{\partial N}{\partial t} + \frac{\partial}{\partial x}(u_o N) + \frac{\partial}{\partial y}(v_o N) = & gh \left\{ \frac{\tan\beta}{q+1} (1+K_v) + K_x \cos^2\beta \right\} \\ & - (1+K_v) k g h \frac{\partial h}{\partial y} \\ & - \frac{g}{(q+1)^{1/2}} \cdot \frac{v_o}{(u_o^2 + v_o^2 + w_o^2)^{1/2}} \\ & \cdot \{h_c(q+1) + (1-r_u)htan\phi_a\} \end{aligned} \tag{16}$$

If it is assumed that the total density of the landslide mass does not change during motion, i.e., the sum of landslide mass flowing into a column (M, N) is balanced by the change in the height of the soil column, then:

$$\frac{\partial h}{\partial t} + \frac{\partial M}{\partial x} + \frac{\partial N}{\partial y} = 0 \tag{17}$$

Equations (15) to (17) were generated for both the processes of the landslide initiation and its motion. The variables in these equations are provided in Table 2.

The values of ϕ_a , h_c , and r_u vary across three conditions: (i) pre-failure state before shear displacement (start of shear reduction), (ii) transient state after failure up to a steady state, and (iii) steady state (residual state) after the end of strength reduction. The lateral earth pressure ratio in Eqs. (15) and (16) is expressed using Jaky's equation (Sassa 1988) as follows:

$$k = 1 - \sin\phi_{ia} \tag{18}$$

$$\tan\phi_{ia} = \frac{(c + (\sigma - u)\tan\phi_i)}{\sigma} \tag{19}$$

where $\tan\phi_{ia}$ is the apparent friction coefficient within the landslide mass and $\tan\phi_i$ is the effective friction coefficient within the landslide mass, which is not always the same as the effective friction coefficient during motion on the sliding surface (ϕ_m).

The value of k differs depending on whether the sample is in the liquefied state or in the rigid state. It can be expressed as follows:

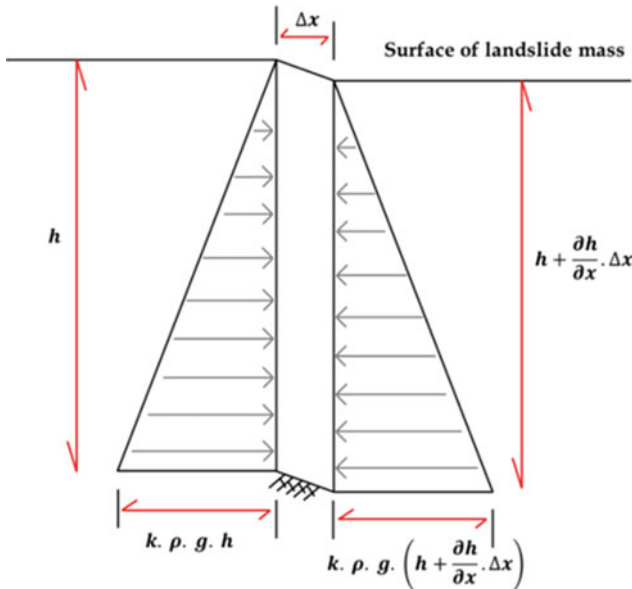


Fig. 3 Lateral pressure acting on a soil column

Table 2 Variables in the equations for LS-RAPID

Remarks	Description
h	Height of soil column within a mesh (depth of the moving mass)
g	Gravitational acceleration
α, β	Angles of the ground surface to the x-z plane and y-z plane, respectively
u_o, v_o, w_o	Velocity of a soil column in the x-, y-, and z- directions, respectively (velocity distribution in the z- direction is neglected by considering it to be a constant)
M, N	Discharge of soil per unit width in x- and y- directions ($M = u_o \cdot h$, $N = v_o \cdot h$), respectively
k	Ratio of lateral to vertical pressures
$\tan \phi_a$	Apparent friction coefficient mobilized at the sliding surface of the landslide
h_c	Cohesion (c) expressed in the unit of height ($c = \rho g h_c$, $\rho =$ density of soil)
q	$\tan^2 \alpha + \tan^2 \beta$
w_o	$-(u_o \tan \alpha + v_o \tan \beta)$
K_v, K_x, K_y	Seismic coefficients to the vertical, x- and y- directions, respectively
r_u	Pore pressure ratio (u/σ)

- Liquefied state, $\sigma = u$, $c = 0$, $\sin \phi_{ia} = 0$ and $k = 1.0$
- Rigid state, c is significant, $\sin \phi_{ia} = 1.0$ and $k = 0$

$$\tan \phi_{a(ss)} = \frac{\tau_{ss}}{\sigma} \quad (21)$$

An increase in the pore water pressure within a slope due to rainfall, rises of the groundwater table, and/or earthquakes may affect stresses, particularly along the susceptible sliding (slip) surface of a slope. A landslide occurs when the effective stress path in the stress-shear graph moves from the initial stress condition and reaches the peak failure line (ϕ_p). Volume reduction will take place as shear displacement progresses in saturated soils after failure as a result of grain crushing/soil particle breakage and the generation of excess pore water pressures.

The stress path will travel down along the failure line during motion of the landslide mass with certain friction (ϕ_m) angle until it reaches the steady (residual) state condition. The steady-state condition describes failure of the sample when there is no further grain crushing occurring at a constant value of pore water pressure with unchanged volume of the samples. Under this condition, only shear displacement occurs under a condition of constant shear resistance, which is known as the steady-state shear resistance. It is described by the following formula:

$$\tau_{ss} = \sigma_{ss} \tan \phi_m = \sigma_0 \tan \phi_{a(ss)} \quad (20)$$

where τ_{ss} and σ_{ss} are the shear and normal stresses, respectively, at the steady-state condition and $\tan \phi_{a(ss)}$ is the associated apparent friction coefficient. Thus, the apparent friction coefficient can be expressed as the ratio of steady-state shear resistance (τ_{ss}) and the initial normal stress acting on the sliding surface (σ_0), which corresponds to the total normal stress (σ) due to the in-situ soil weight in the simulation.

Ideally, from the ring shear tests, the apparent friction coefficient ($\tan \phi_{a(ss)}$) can be obtained by knowing the steady-state shear resistance (τ_{ss}) and the normal stress (σ). In addition, the concept of shear strength reduction during the progression of shear displacement from the pre-failure state to steady-state motion is shown in Fig. 4 (Sassa et al. 2010). The transient state from the peak state to the steady-state was observed when conducting ring shear tests (Sassa and Dang 2018). As an example of this shear-displacement relationship, Fig. 5 shows the shear strength reduction in terms of shear resistance (in kPa) with respect to the shear displacement (in mm, plotted in logarithmic scale) within a sample during a undrained cyclic loading test using a ring shear apparatus.

The shear strength reduction within the landslide mass consists of four stages, which are: (i) initial state, (ii) pre-failure state, (iii) transient state, and (iv) steady-state. In the initial state, soil stability is obtained under the peak friction coefficient ($\tan \phi_p$). The pre-failure state occurs when shear resistance reaches the peak friction coefficient due to rainfall, rises in the groundwater table, earthquakes or the combination of these factors. The critical shear displacement in the pre-failure state (stated as DL) indicates failure of soils and the occurrence of landslide. The transient state take place during the transition from failure point to the steady-state condition (Fig. 4). Pore pressure generation and shear strength reduction will occur during the transient state as a result of grain crushing, landslide mass mobilization and shear strength reduction. The critical shear displacement from the transition state to steady state condition is indicated by the end of shear reduction (stated as DU; Fig. 5). Th

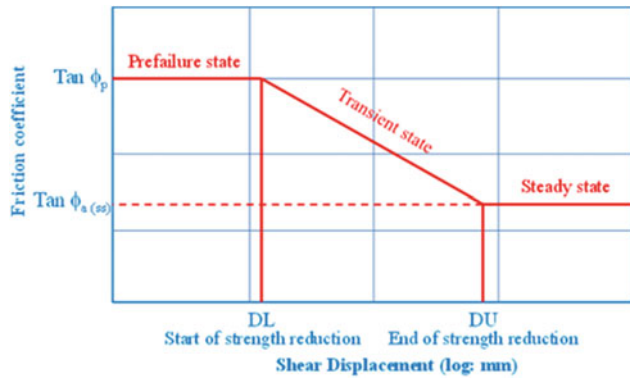


Fig. 4 Shear strength reduction during the progression of shear displacement (Sassa et al. 2010)

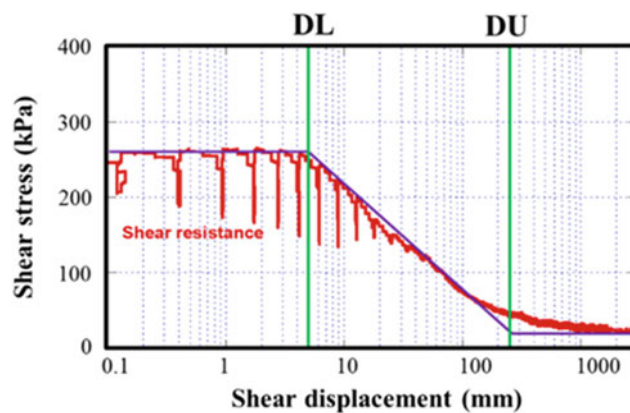


Fig. 5 Shear stress and shear displacement relationship in an undrained cyclic loading test on the Tertiary Sand (Sassa and Dang 2018)

friction coefficient represents the shear resistance during shear loading in the constant normal stress ($\Delta\sigma = 0$).

According to the description of the shear strength reduction stages above, the shear displacement (D), the friction coefficient ($\tan \phi$), and the effect of pore pressure ratio (r_u) can be expressed in each stage as follows:

- Initial deformation stage before failure ($D < DL$):

$$\tan \phi_a = \tan \phi_p$$

$$c = c_p$$

$$r_u = c_u$$

- Transient state after failure ($DL \leq D \leq DU$):

$$\tan \phi_a = \tan \phi_p - \frac{\log D - \log DL}{\log DU - \log DL} (\tan \phi_p - \tan \phi_{a(ss)})$$

$$c = c_p \left(1 - \frac{\log D - \log DL}{\log DU - \log DL} \right)$$

$$r_u = r_u \cdot \frac{\log DU - \log D}{\log DU - \log DL}$$

- Steady-state motion ($D > DU$):

$$\tan \phi_a = \tan \phi_{a(ss)}$$

$$c = 0$$

$$r_u = 0$$

3 User Manual

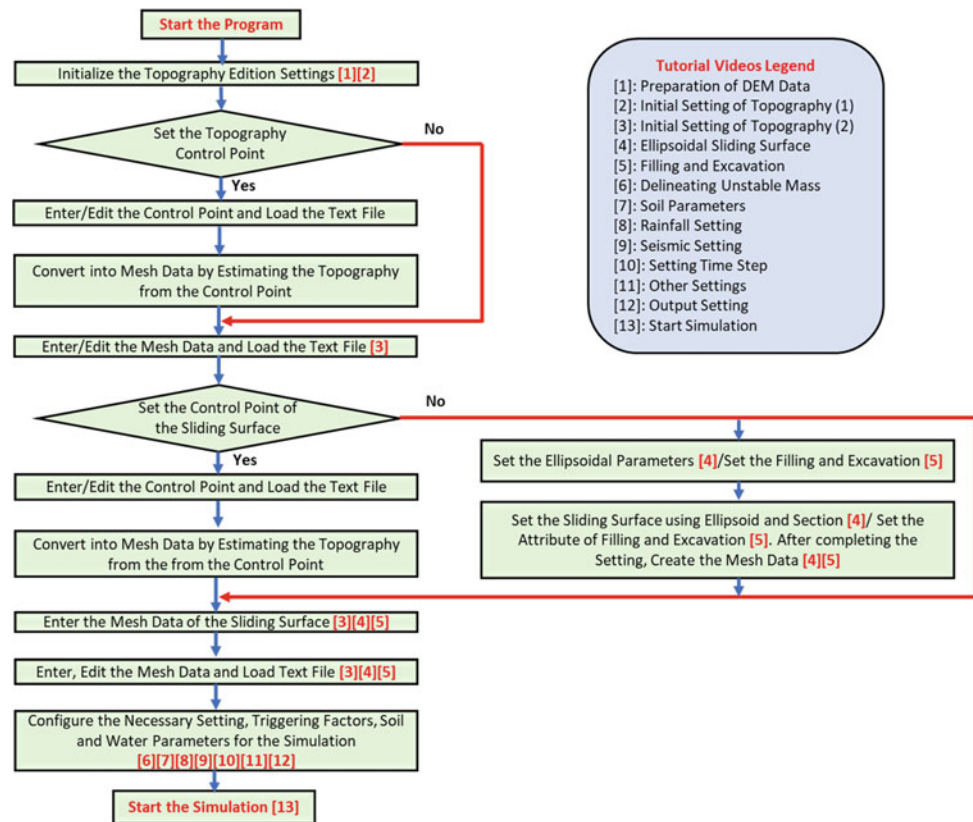
3.1 Simulation Overview

The steps involved in simulating a landslide using LS-RAPID are summarized in Fig. 6. The simulation begins with the establishment of settings that will allow viewing of the topography being modeled. Data related to the topography is then inputted into the program. There are two paths that can be taken to do so. In the first, a topography control point is established using which the topography is estimated. Alternatively, the mesh data for the topography is directly inputted and the control point is then established.

A process similar to the topography mesh and control point may be used to simulate the sliding surface and its associated control point. However, if a sliding surface mesh and/or control point are not available, the sliding surface for the landslide may be determined through several other means within LS-RAPID. Specifically, the sliding surface can be established using the ellipsoidal parameters or by modeling the filling and excavation processes. This information can then be converted into mesh data that establishes the sliding surface for the simulation.

The final steps before the start of the simulation will involve the configuration of various settings within LS-RAPID. In particular, it will be necessary to input the triggering factors (rainfall events, earthquake events or both), properties of the soils present in the landslide mass and sliding surface and properties of water. This chapter will contain detailed information about the specific steps necessary to simulate a landslide using LS-RAPID. Figure 6 also indicates video tutorials that are available for the simulation process. It is noted that depending on the available information and specific details of the landslide being simulated, several of the steps provided here may not be applicable. Interested users may also need to perform additional steps, not necessarily described in this section, to collect and format the data available for the purposes of their simulations.

Fig. 6 Flowchart containing steps for simulation using LS-RAPID



3.2 Preparation of the Digital Elevation Data Using DEMmake

Digital elevation models (DEMs) generally provide latitude, longitude and elevation information in an (x,y,z) format within a text file. Before this information can be used in simulations in LS-RAPID, it will be necessary to convert the text file into elevation mesh data. LS-RAPID is accompanied by a software, an Excel Spreadsheet titled, “DEMmake,” that allows the user to easily convert the DEM text file into the required elevation mesh data for the LS-RAPID input. A tutorial of the use of the DEMmake program, is titled, “1. Preparation of DEM Data.” A brief summary of the steps is provided below:

1. Open the DEMmake Excel program. The use of DEMmake will require that use of macros within Excel is enabled. If this is disabled, the setting can be changed by allowing content in the warning that appears at the top of the Excel file when DEMmake is opened. Macros can also be enabled by going to the “File” menu in Excel and selecting “Options.” From the dialog box titled, “Excel Options,” select “Trust Center” and then click the button for “Trust Center Settings” on the right. In the options on the left side, select “Macro settings” and then select the “Enable all macros (not recommended; potential dangerous code can run)” option. The opened DEMmake program will resemble the contents in Fig. 7.
2. Using the “Select Text-file” button at the top left of the DEMmake program, the text file containing the (x,y,z) coordinates should be selected. The data in the text file should be delineated (or separated) by commas or spaces for its use in the DEMmake program.
3. Automatically compute the range (minimum and maximum values) of the x-, y- and z-coordinates using the “Get Coordinate range information” button in the bottom right. The ranges for the x- and y-coordinates will be necessary in Step 4.
4. Transfer the ranges for the x- and y-coordinates (from Step 3) into the green “Grid” cells in the center of the DEMmake program. The interval of the x- and y- coordinates will then need to be specified in the “Pitch” column. Specifically, a pitch of 5.0 in the row containing x-coordinate information and a pitch of 10.0 in the row containing y-coordinate information would indicate that the difference between adjacent x-coordinates will be equal to 5.0, while the distance between adjacent y-coordinates is equal to 10.0. Based on the range of the coordinates and the pitch used, the number of grids will be automatically calculated. The user is cautioned against inputting any numbers in the grayed cells indicating the number of grids.
5. Now that all of the input information has been entered into the DEMmake program, it will be possible to

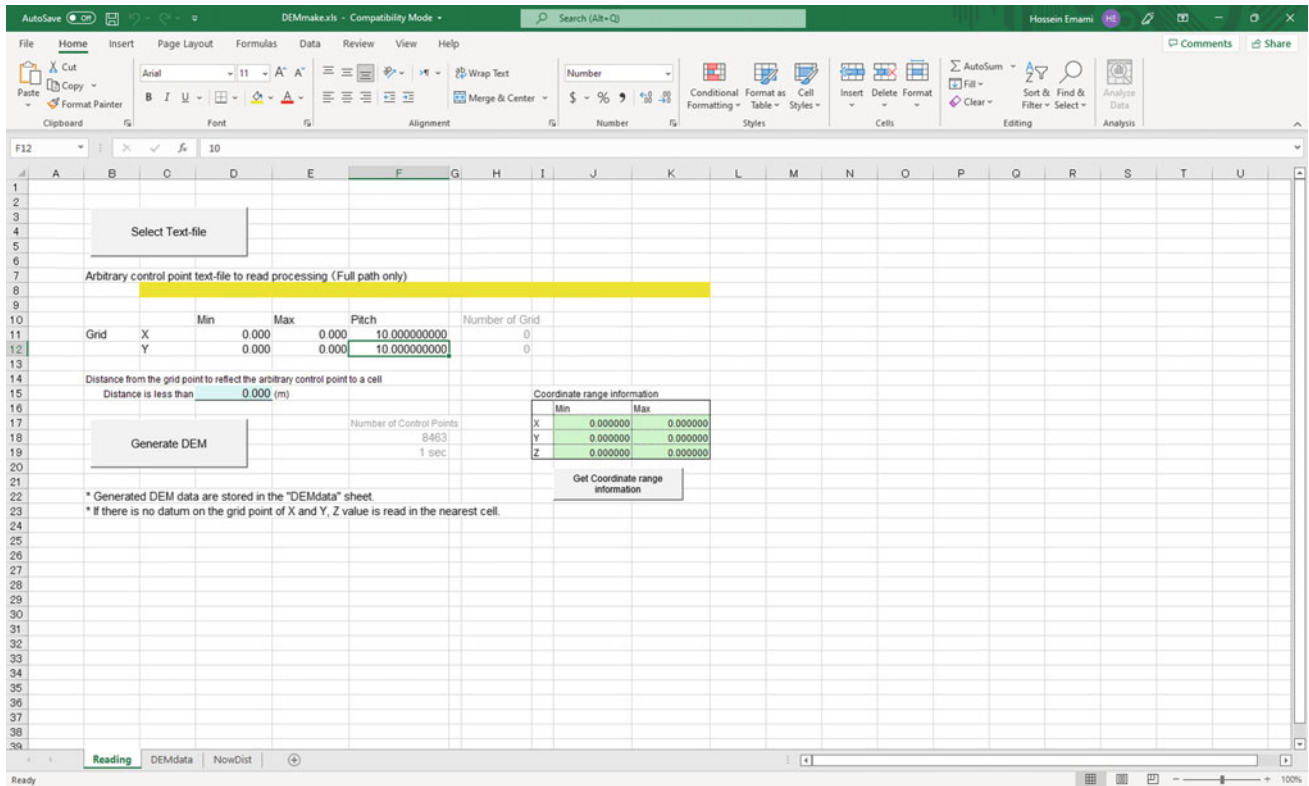


Fig. 7 Screenshot of DEMmake program when opened with macros enabled

generate the DEM data needed for the LS-RAPID simulation. To do so, click on the “Generate DEM” button. The DEM data that is generated will be stored in a separate Worksheet of the DEMmake Excel file. Specifically, the data will be found in the sheet titled, “DEMdata,” as shown in the screenshot in Fig. 8. In the cases when the control point was located at distance greater than the value specified in Step 5 from the grid point, the elevation (z-coordinate) information will not be provided in the DEM data generated. If an elevation value is necessary at a particular point, but not available in the DEMdata sheet, it may be necessary to make adjustments in Step 5 (by increasing the distance specified) and repeat this step.

The DEM data associated with the simulation area of interest for the LS-RAPID model should then be selected from the DEMdata sheet. When determining the Calculation Area for the LS-RAPID (as will be discussed later in this section), it will be necessary to know the number of mesh. This is equal to one less than the number of grids for the selected area. It is also possible to set-up the Simulation Area prior to generating the DEM data using DEMmake, as will be explained in the “Initial Topography” subsection later in this chapter. If this process is adapted, the number of grids will be automatically calculated by LS-RAPID.

3.3 Preparation of the Digital Elevation Data Using DEMmake

When LS-RAPID is first opened, there will be no information regarding the topography or details about the settings for the simulation. In this section, details regarding inputting this information to the program will be provided.

3.3.1 Simulation Area

The steps to establish the simulation area within LS-RAPID are provided below. A video tutorial titled, “2. Initial Setting of Topography 1” also describes this steps for interested users to follow.

1. Locate the “Flow” panel on the left side of the LS-RAPID program, as shown in Fig. 9. Within this panel, expand Section “1: Mesh” and click on the “Simulation area” button. A window titled, “Setting of simulation area and input-data type” will open and look similar to that shown in Fig. 10.
2. The minimum and maximum values of the x- and y-coordinates associated with the calculation area should be inputted in the top section titled, “Axial Setting of Calculation Area,” as shown in Fig. 10. LS-RAPID will allow inputs between $-999,999.999$ and $+999,999.999$ m.

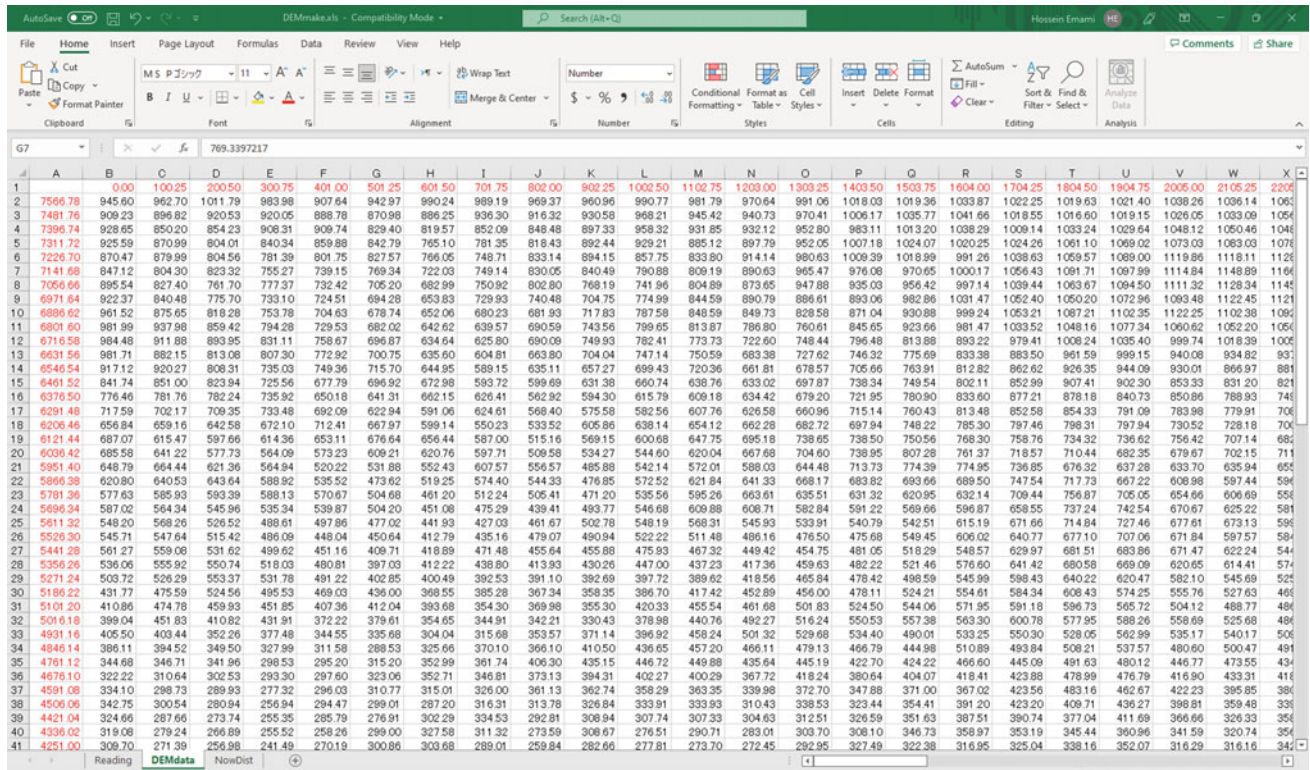


Fig. 8 Screenshot of the DEMdata worksheet of the DEMmake program

3. The second component of this window is the “Mesh Setting of Calculation Area” section. This section is used to input the pitch for the x- and y-directions. As with the DEMmake program, LS-RAPID will then automatically calculate the number of grids in both directions using the ranges from Step 2 and the input pitch values. LS-RAPID allows between 2 and 9999 numbers of mesh and pitch values between 0.001 and 999,999.99.
4. The simulation area along with the grid developed will be illustrated in the bottom part of the Setting of Simulation Area and Input-Data Type Window. In particular, the red box will delineate the extents of the calculation area, while the gray lines will indicate the location of the grid lines.
5. Upon clicking “Ok,” the calculation area will be displayed in the right panel of the LS-RAPID program, as shown in Fig. 11.

3.3.2 Editing Mesh

Slope Surface

As noted in the flow chart in Fig. 6, the topography can be established in LS-RAPID using one of two different approaches. In the first approach, the topography control points are added and a mesh is generated while in the second, the mesh is directly added into the program. The steps to generate a mesh from the topography control points are summarized below:

1. From the “Edit” menu in the toolbar at the top of the program, select the “Editing of Control Point” option, as illustrated in the screenshot in Fig. 12.
2. The control points can then be manually entered into the appropriate tab in the window that opens titled, “Editing of Control Point.” This window is presented in Fig. 13. For this section, the control points would be entered into the “Slope Surface Elevation” tab. Once the data has been entered into the tab, Click “Ok.”
3. In lieu of manual entry as described in Step 2, a text file containing the control point data may be imported into LS-RAPID. To do this, from the “File” menu in the Toolbar, select the “Read text data file” option. Next, click on the “Read (Ground Elevation) Control Point” to select the text file that contains the appropriate control point data. The options available in the “File” menu are shown in Figure 14. It is noted that the text file containing the control point data should be in a CSV format and separated by either a space, tab or comma to be properly read by LS-RAPID.
4. Once the control points have been inputted as described in Step 2 or have been imported following the instructions in Step 3, the results in the viewing panel will be similar to that shown in Fig. 15.
5. The control points will now need to be converted into a mesh. This is accomplished by selecting the “Transfer control point data to mesh data” option in the “Edit”

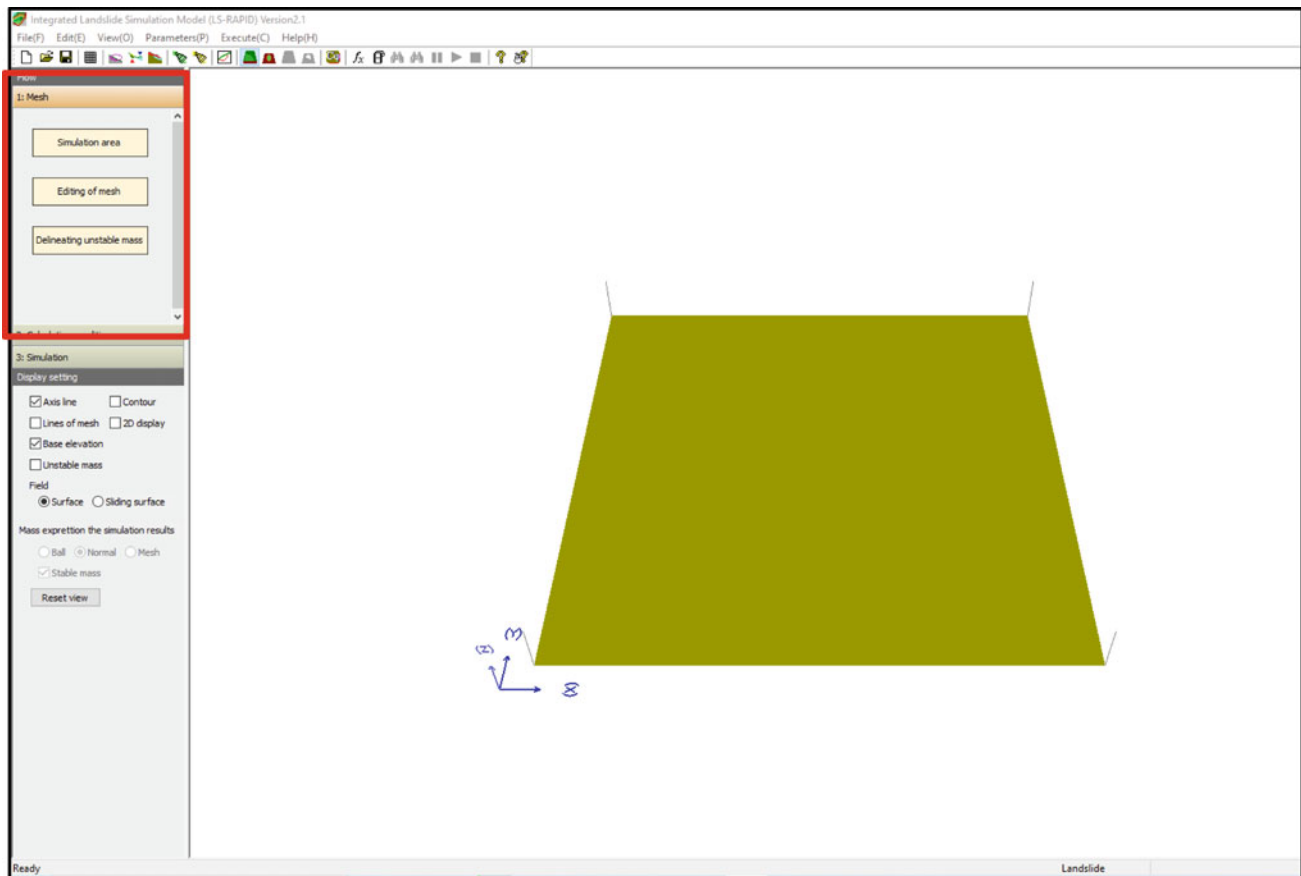


Fig. 9 Screenshot of the flow panel (in red box) in LS-RAPID

menu from the toolbar. This is shown in Fig. 12. The mesh topography based on the control point data will then be displayed in the viewing panel. An example is shown in Fig. 16. If necessary, control points can be edited using either Step 2 or Step 3 before.

Topography mesh data can also be directly added to LS-RAPID without the use of the control points using one of two different methods. The steps to both methods are summarized below:

Method 1: Importing Mesh Data into LS-RAPID.

1. The mesh data can be imported into LS-RAPID if a text file containing the data is available. To do so, select the “Read text data file” option from the “File” menu shown in Fig. 14. Next, click on the “Read (ground elevation) mesh data” option.
2. The text file containing the topography mesh data should be selected and the window closed. The result will be a topography mesh similar to that shown in Fig. 16.

Method 2: Inputting Mesh Data into LS-RAPID.

The steps for this process are summarized below, but can also be found in the video tutorial titled, “3. Initial Setting of Topography 2.”

1. Mesh data is added into the calculation area using the “Editing of Mesh” button in the “Flow” Panel under Section “1:Mesh,” as seen in Fig. 9.
2. A window titled, “Editing of mesh” will open containing several sections and tabs to input data. This window is shown in Fig. 17. The “Change header” section should be used to select the type of mesh representation provided in the rows and columns where data will be inputted. Specifically, when “Index” is selected, the mesh is represented with the numbers associated with the grid lines in the calculation area. Alternatively, the “Position” option will give the x- and y-coordinates of the calculation area where elevation data will be inputted. The one most appropriate for the simulation at hand should be selected.
3. The “Selection of input-data type” section will allow the users to select how the sliding mass will be defined. In particular, users may choose to provide the slope surface elevation and the sliding surface elevation using the

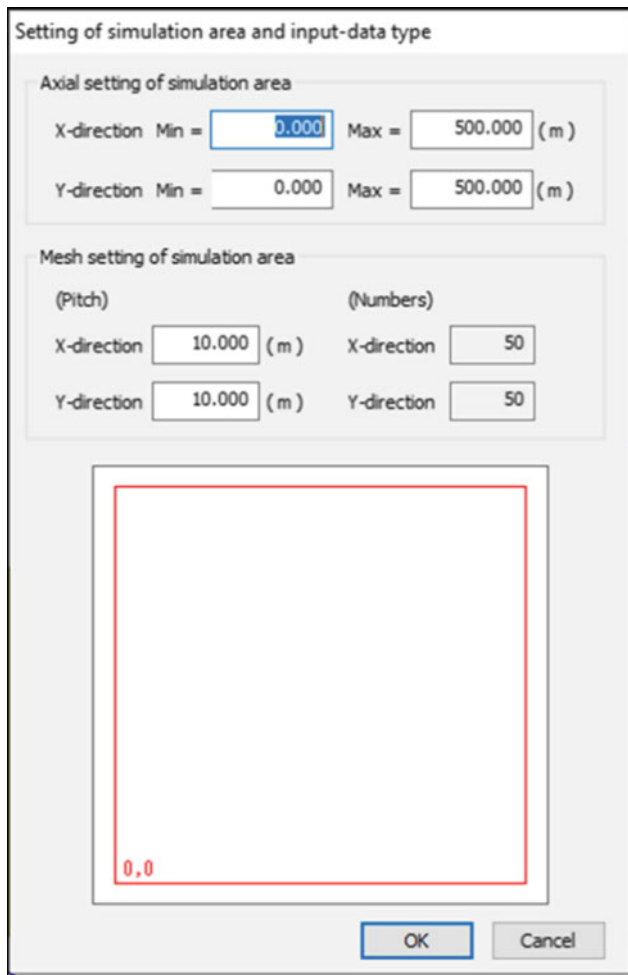


Fig. 10 Screenshot of the setting of simulation area and input-data type window

“Slope/Sliding Elev.” option. In this case, the thickness of the sliding mass will be automatically calculated. When the “Slope Elev./Mass Thickness” option is selected, the user must define the elevation of the slope surface and the thickness of the sliding mass. Using this information, LS-RAPID will automatically determine the elevations of the sliding surface. The final option available is “Sliding Elev./Mass Thickness” in which the slope surface elevation is automatically computed based on the inputted values of the sliding surface elevations and the thicknesses of the sliding mass.

4. The tabs that will allow data input will vary based on the option selected in Step 3. Data can be inputted into these tabs in one of three ways: (a) manually entering the data corresponding to the x- and y-coordinates shown in the table, (b) copy and pasting data from DEMmake, and (c) by adding a specific value to several selected cells using the “Set in selected rectangle” button.

5. The “Polygon Area” on/off toggle button in the top right corner of this window is another useful function. When this option is on, any shape can be creating in the topography with the left click of the mouse while simultaneously pressing the Ctrl and Shift keys on the keyboard. It is then possible to edit/add elevation information within the selected area.

Sliding Surface

The sliding surface for the landslide can be created in multiple ways. If information about the sliding surface is known, it can be inputted or imported into the LS-RAPID calculation area using steps that are analogous to those described above for the slope surface. In the cases when this information is not known, possible sliding surfaces can be created within LS-RAPID. These options are described in more detail in the next section.

3.4 Creating Possible Sliding Surfaces

When sliding surface elevation or sliding mass information is not available, there are several ways to establish potential sliding surfaces within LS-RAPID. This section will highlight two of those methods.

3.4.1 Ellipsoidal

In order to determine the possible sliding surface using the ellipsoidal parameters, it will be necessary to have the mesh data for the slope surface, for which the procedures were described previously. Thus, only the steps involved in the building of the sliding surface using this method are summarized below. Please note that users may also opt to follow the instructions in the video tutorial titled, “4. Ellipsoidal Sliding Surface.”

1. There are three different ways to reach the window in Fig. 18 to begin creating the ellipsoidal sliding surface.
 - a. Select the “Ellipsoid Sliding Surface setting” option from the “Edit” Menu (Fig. 12). Or,
 - b. From the Toolbar, select “Ellipsoid Sliding Surface setting” button. Or,
 - c. Open the “Editing of mesh” window in Fig. 17 by clicking the “Editing of mesh” button in Section “1: Mesh” from the “Flow” panel. Click the “Creation of sliding surface” button and select the “Create sliding surface section with section profile of ellipsoid (for new landslides)” before clicking “Ok.”
2. The process will begin with the selection of a longitudinal section. The section can be defined by either

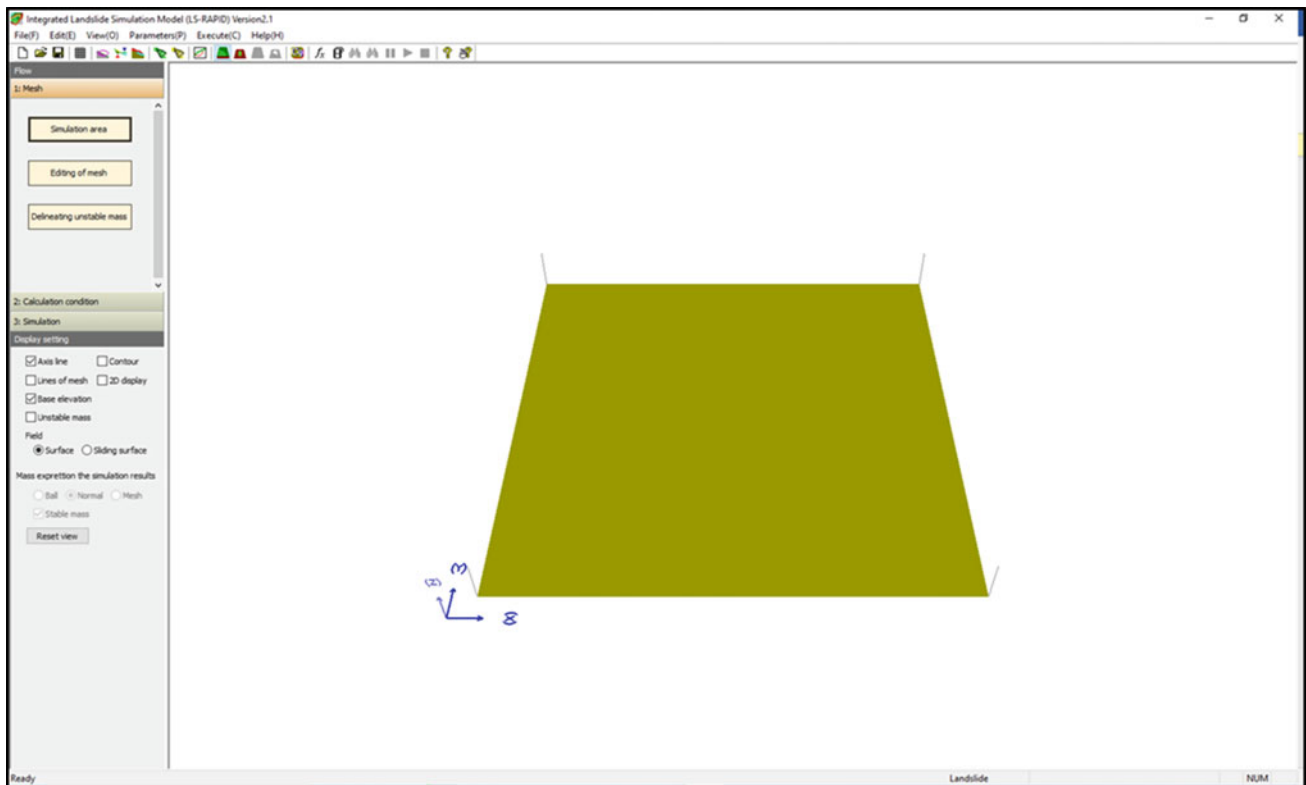


Fig. 11 Screenshot of calculation area

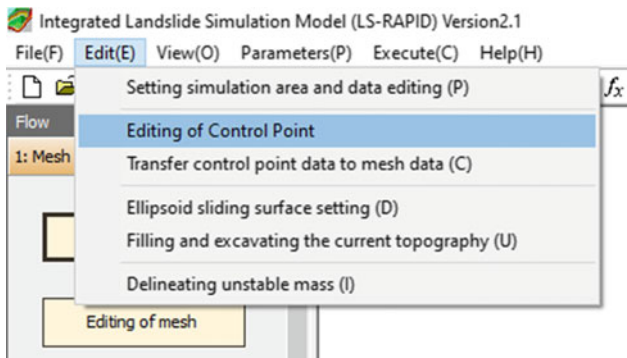


Fig. 12 Screenshot of edit menu in toolbar

inputting the x- and y-coordinates corresponding to the start and end points of the section in the table on the top left side of the window or by checking the “Input with a mouse” option and clicking the start and end points in the topographic map. The longitudinal section will be displayed in the figure on the right side of the window in Fig. 18.

- Locations through which the sliding surface will pass and the center of the ellipsoid will need to be inputted in the top part on the right side of the window. Specifically, the coordinates of two points through which the sliding surface passes should be entered into the table. As this



Fig. 13 Screenshot of the editing control point window

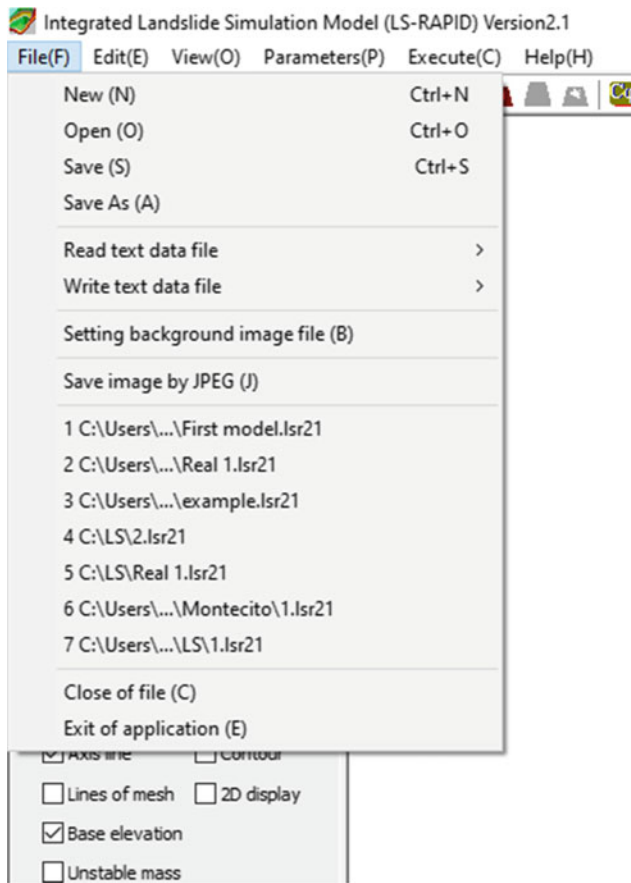


Fig. 14 File menu options for inputting control point data text file

information is entered, the points will be identified in the topographic map on the left side of the window.

4. The coordinates for the center of the ellipsoid should be entered into the third row in the table in the top part on the right side of the window. Once these coordinates are entered, the ellipsoid will be displayed in the figure just beneath the table.
5. In Steps 3 and 4, the coordinates were manually entered into the table on the top part of the right side of the window. In lieu of this, the locations for the points through which the ellipsoid passes along with the center of ellipsoid may also be inputted using the mouse. To do this, check the “Input with a mouse” box beneath the table and then click the locations of the two points through which ellipsoid passes and its center.
6. The points through which the ellipsoid passes along the cross-section will need to be specified in the bottom part of the right side of the window in Fig. 18. Analogous to the procedures described in Steps 3 to 5, the point through which the ellipsoid passes along the cross-section and the x-coordinate of the center of the ellipsoid can be entered manually in the bottom table or using a mouse after checking the “Input with a mouse”

Editing of Control Point

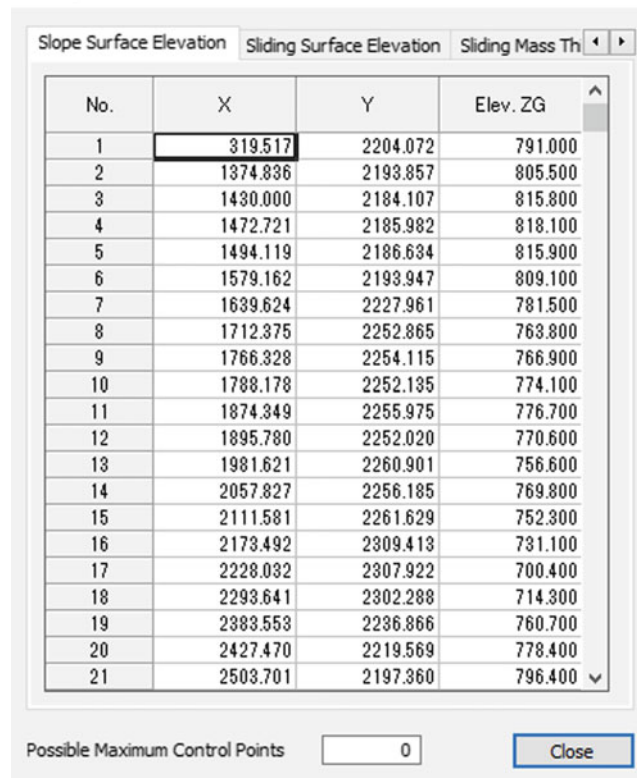


Fig. 15 Viewing panel with topography control point data

option. It is noted that prior information in this process will allow LS-RAPID to automatically determine the coordinates for Point D and z-coordinate for the center of the ellipsoid.

7. A sub-section can be created or edited using the radial buttons in “The current editing section” options at the top of the left side of the “Select profiles for drawing ellipsoidal sliding surface” window. The procedure is identical to that described above for the main section, except the locations will need to be adjusted to correspond to the sub-section.
8. Finally, the section at the top right of the window allows the user to re-size the images shown in the window. It also allows to user to determine if the section scales should be the same in the sections displayed in the window.

The ellipsoidal sliding surface generated using this procedure will then be displayed in the viewing panel in LS-RAPID. A dialog box will contain the characteristics of the ellipsoid.

3.4.2 Unstable/Bedrock Surface

The second method, described in this section, is used when the unstable/bedrock surface is known. When a landslide has occurred, the pre- and post-failure topography of the

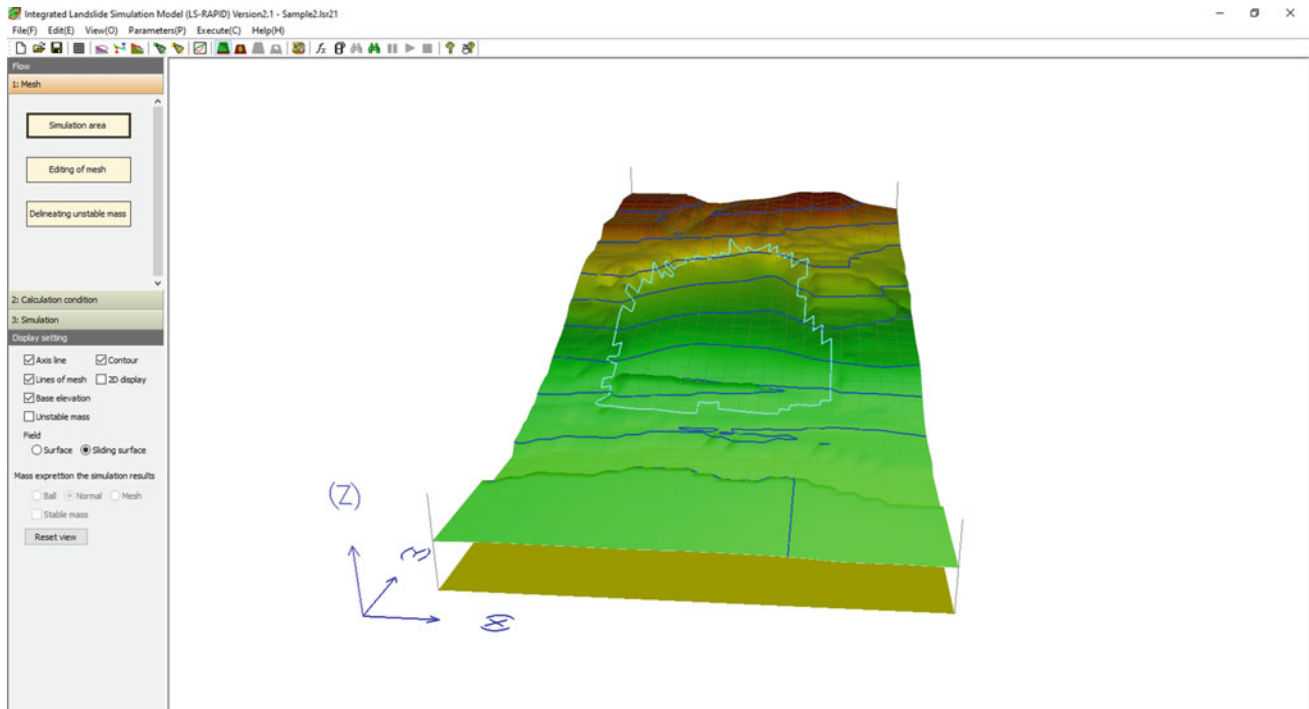


Fig. 16 Example of topography mesh in viewing panel

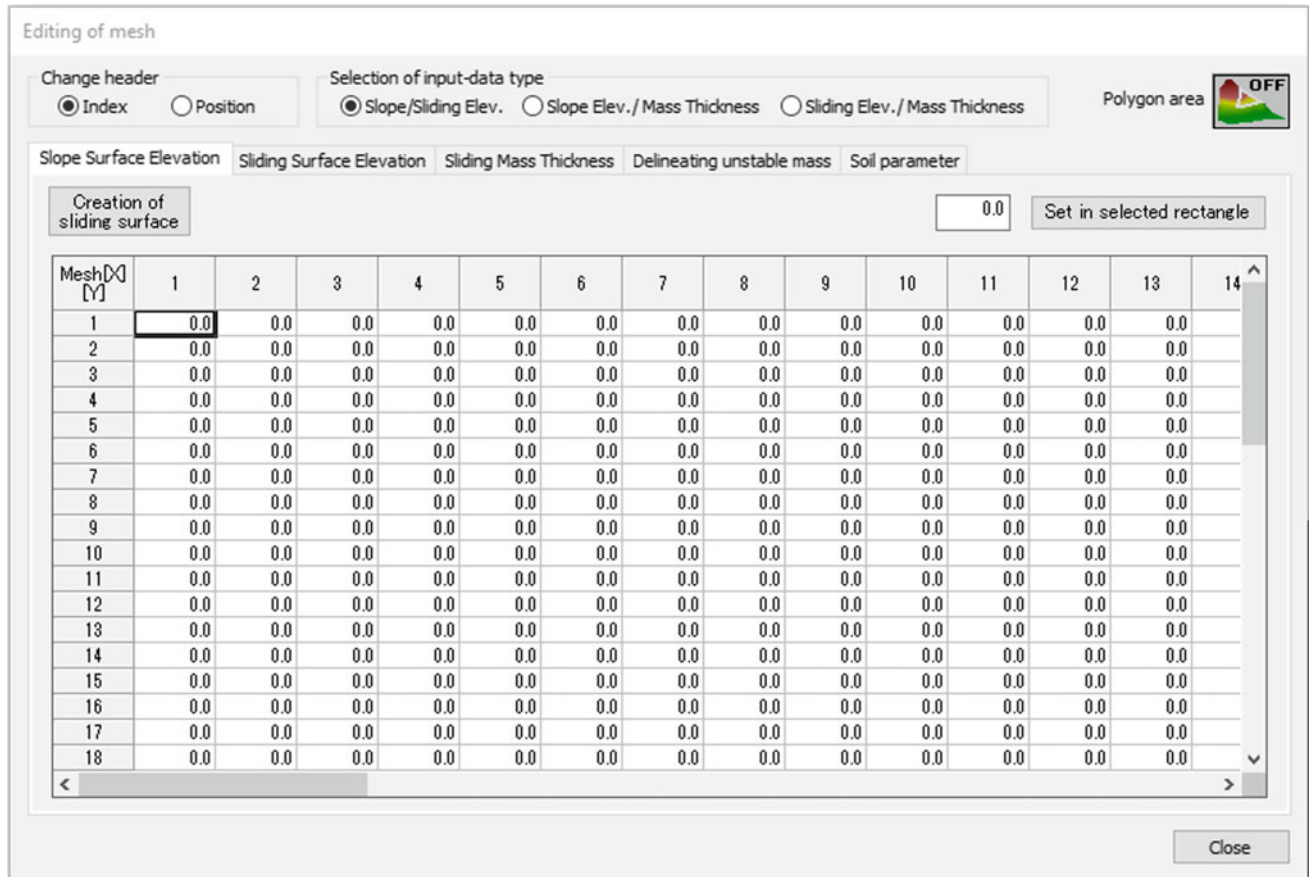


Fig. 17 Screenshot of the editing of mesh window

Fig. 18 Screenshot of the select profiles for drawing of ellipsoidal sliding surface window

Select profiles for drawing ellipsoidal sliding surface

The current editing section
 Main section Sub section

Select longitudinal section	X	Y
Starting point of a section		
Ending point of a section		

Input with a mouse

Coordinates are expressed as Xs along the crossing section, Ys along the longitudinal section, Zs along the vertical direction.

Decision of passing point of the sliding surface on the longitudinal section is automatically calculated from the elevation of the ground surface.

> When giving X coordinate of passing point and inputting Y coordinate as '*'

> When clicking the Left-side of mouse during pushing [Shift] key.

Resize option the Control
 Plane figure Longitudinal section Crossing section Section scale is same

Sliding surface on the longitudinal section	Y	Z
Passing point A		
Passing point B		
Center of ellipsoid on the longitudinal section		

Longitudinal section Input with a mouse

Sliding surface on the cross section	X	Z
Passing point C		
Passing Point D (Cross point of 2 sections)		
Center of ellipsoid on the crossing section		

Crossing section Input with a mouse

landslide area can be obtained and can be inputted as the slope and the sliding surface elevations. The steps are summarized below:

1. Input Slope Surface Elevation: The pre-failure topography is used to create the “Slope Surface Elevation” in the Section “1: Mesh.” The steps for inputting data were described in Sect. 3.3.2.
2. Input Sliding Surface Elevation: The post-failure topography is used to make the “Sliding Surface Elevation” in the Section “1: Mesh”. The method for entering this data is the same as that described in Step 1 above.
3. Determine the Source Area: The thickness of the sliding mass will be automatically computed based on the inputted value of the “Slope Surface Elevation” and “Sliding Surface Elevation.” This is shown in Fig. 19. To set the source area, in Section “1: Mesh” of the “Flow” Panel, choose the “Delineating unstable mass” button (shown in Fig. 9). From the “Editing of mesh” window, clicking “Set landslide source area (red)” button for the

cells that belong to the source area. An example of the result that will be obtained is shown in Fig. 19.

3.5 Fill and Excavate Topography

The sliding surface and original topography of the ground can be created using the fill and excavate options in LS-RAPID. The use of these options will require that the mesh data of the slope surface be inputted. The procedures are provided in the video tutorial titled, “5. Filling and Excavation,” while a brief summary of the steps is provided below:

1. To use the fill and excavate options in LS-RAPID, the “Filling and Excavating the Current Topography to Estimate Pre-failure Topography” window will be needed. This window, shown in Fig. 20, can be opened using one of the following three methods:
 - a. From the “Edit” menu in Fig. 12, select the “Recover (Source area/Deposition area)” option. Or,

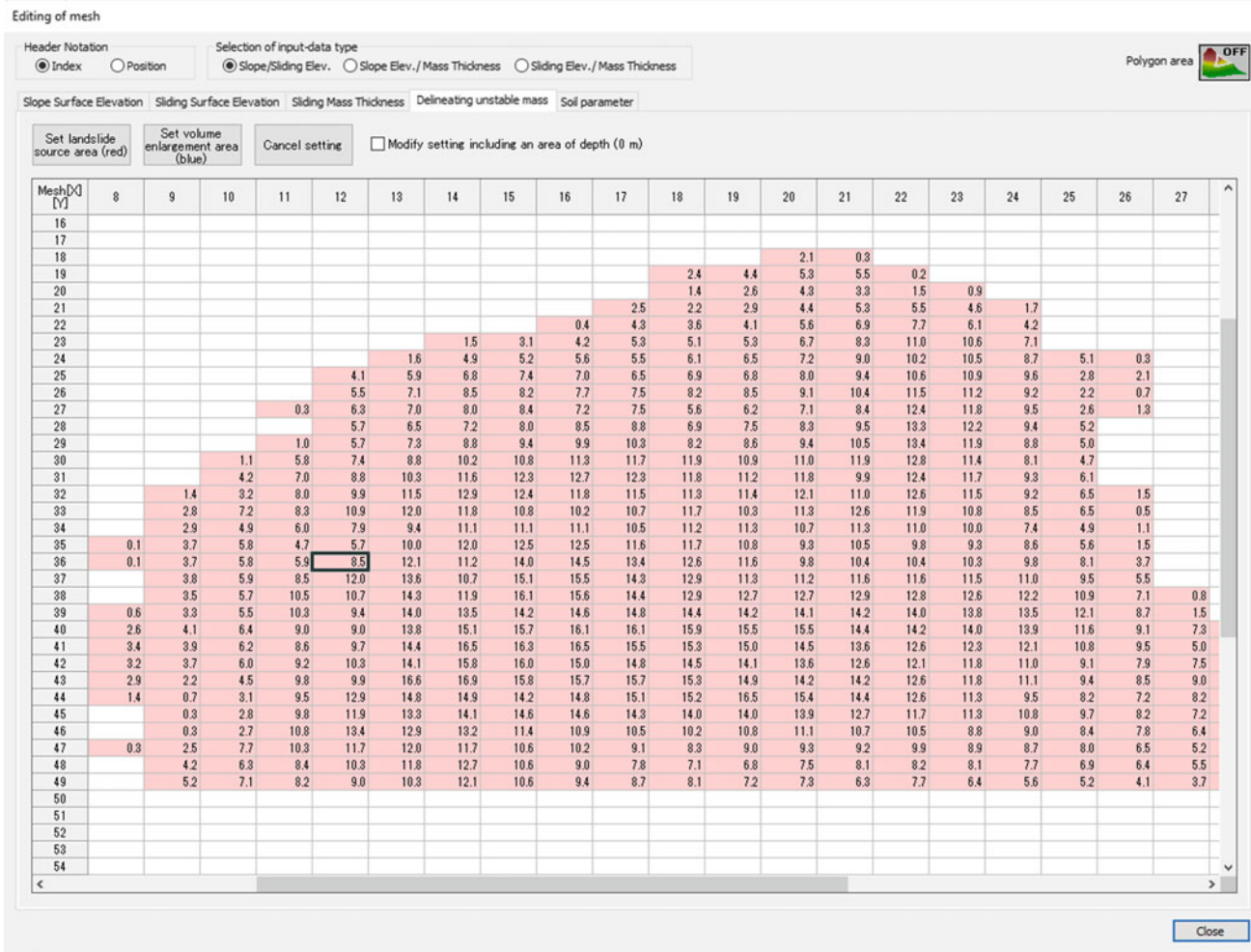


Fig. 19 Screenshot of the delineating unstable mass tab of the editing of mesh window

- b. Click the “Recover (Source area/Deposition area)” icon in the Toolbar. Or,
 - c. From the “Flow” panel, click on the “Editing of mesh” button in Section “1:Mesh” to get the “Editing of mesh” window in Fig. 17. After clicking on the “Creating of sliding surface” button, select, “Create sliding surface section with recovery setting (for previous landslides)” option and click “Ok.”
2. Landslides will cause differing changes to the topography that depend on the locations of the source and depositional areas. These zones should be delineated using the options in the “Delineate an area for modifying geographical features” section (Fig. 20). Specifically,
 - a. Source areas will be those that have experienced a reduction in the elevation as a result of the landslide. Therefore, the filling of these areas will be necessary to return to the original ground surface. These areas are defined by selecting the “Recovery of Source area by filling (Yellow)”. The source locations should then be selected in the “Input parameters on the mesh chart (Input depth of mass)” section in the window. Using the “Set for all” button, the selected cells or highlighted region will be set as the source area that needs to be filled to obtain the original ground surface.
 - b. On the other hand, deposition areas will have experienced an increase in the elevation from the landslide and will need to be excavated to reach to the original ground surface. The definition of the depositional area is very similar to the delineation of the source area. The radial button for “Recovery of Deposition area by excavation (Green)” should be selected. The cells for the depositional area should be selected in the “Input parameters on the mesh chart (Input depth of mass)” section. Finally, click on “Set for all” to assign the highlighted cells or section as the deposition area.

- c. If an error occurs, the “Undo of setting (White)” option can be used. Like the other options, the associated radial button should be selected, the cell/s that needs to be cleared should be selected from the “Input parameters on the mesh chart (Input depth of mass)” section and the “Set for all” button should be clicked.
 - d. The source and deposition areas or removal of these areas can also be selected using a mouse by checking the “Input with a mouse” box in the top left part of the window and then left clicking while pressing down the “Shift” key on the contour map. The “Set for all” button still needs to be clicked once the user is ready to assign the modification to the selected area/s.
3. Once the filling and excavation areas have been defined, it will be time to start the recovery of the original ground surface. This will be done through the “Start recovery (Source area/Deposition area)” section in the window. Once the direction of smoothing for the recovery is selected, click on the “Recalculation” button. The changes in the depth of the sliding mass will be tabulated in the “Input parameters on the mesh chart (Input depth of mass)” section once the recalculation is complete.
 4. Upon completion of the modifications to the topography to obtain the original ground surface, click “Ok (Reflection topographical recovery)” button. This will yield a confirmation message. To confirm that the recovered topography be added to the LS-RAPID model, click “Ok.” Otherwise, click “Cancel.”
 - a. When “Ok” is clicked, the slope surface inputted in LS-RAPID (that is, the slope surface prior to recovery) will be taken as the sliding surface. The new slope surface will be the source area that was created by filling. However, if only excavation was applied to the model, the sliding surface and slope surface will coincide and the original slope surface data will be deleted in these deposition area.
 - b. If “Cancel” is clicked, the confirmation window will disappear and the “Filling and Excavating the Current Topography to Estimate Pre-failure Topography” opened before (Fig. 20) will return.

In the fill regions, the recalculation process finds a standard line that best fits the current slope surface topography. If the elevation of the mesh is less than that of the standard line, the value is increased until the elevation of the mesh is equal to the elevation of the standard line. In the case, when the elevation of the mesh is greater than the elevation of the standard line, the recalculation process will not adjust the elevation. In contract, in excavate regions, the elevation of those regions where the mesh elevation is less than that of

the standard line will be increased to the elevation of the standard line. For all other mesh locations, the elevation remains unchanged.

Rather than using the automatic recalculation process described above, it is also possible to fill and excavate the source and deposition areas manually. To do so, the changes in the elevation (or the depth of the mass) should be entered into the “Input parameters on the mesh chart (Input depth of mass)” section in the “Filling and Excavating the Current Topography to Estimate Pre-failure Topography.” If manual inputs are entered, the input data will remain valid (or will be what is used in the computations) until the “Recalculation” button is clicked.

3.6 Determine Source and Enlargement Areas

After the slope and sliding surfaces have been modeled in LS-RAPID, it is possible to visualize the distribution of the unstable mass in the calculation area. Using this information, the landslide source area and the volume enlargement areas can be specified. The procedures to specify these areas are available in the video tutorial titled, “6. Delineating Unstable Mass.” The steps are also summarized below:

1. Open the “Editing of mesh” window from Fig. 17. As a reminder, this can be done in one of two different ways: (a) By selecting “Delineation of unstable mass” from the “Edit” menu, or (b) Clicking the “Delineating unstable mass” button in Section “1: Mesh” of the “Flow” Panel (Fig. 9).
2. In the “Editing of mesh” window, select the “Delineating unstable mass” tab to get to window in Fig. 21.
3. The cells corresponding to the source area or the volume enlargement area can now be assigned. To do this, the cells that belong to the source area should be selected and the “Set landslide source area (red)” button should be clicked. Similarly, by selecting the cells corresponding to the volume enlargement areas and clicking the “Set volume enlargement area (blue)” button, the selected cells will be said to belong to the volume enlargement area. The color of the cells will change to red if they have been assigned to the source area or blue if they have been assigned to the volume enlargement area. Unassigned cells will remain white.
4. If an error is made, the cell/s with errors can be selected and “Cancel setting” button can be clicked to remove the assignment of those cells to either the source area or the volume enlargement area.
5. Once the assignments have been made, click the “Set Completed” button.

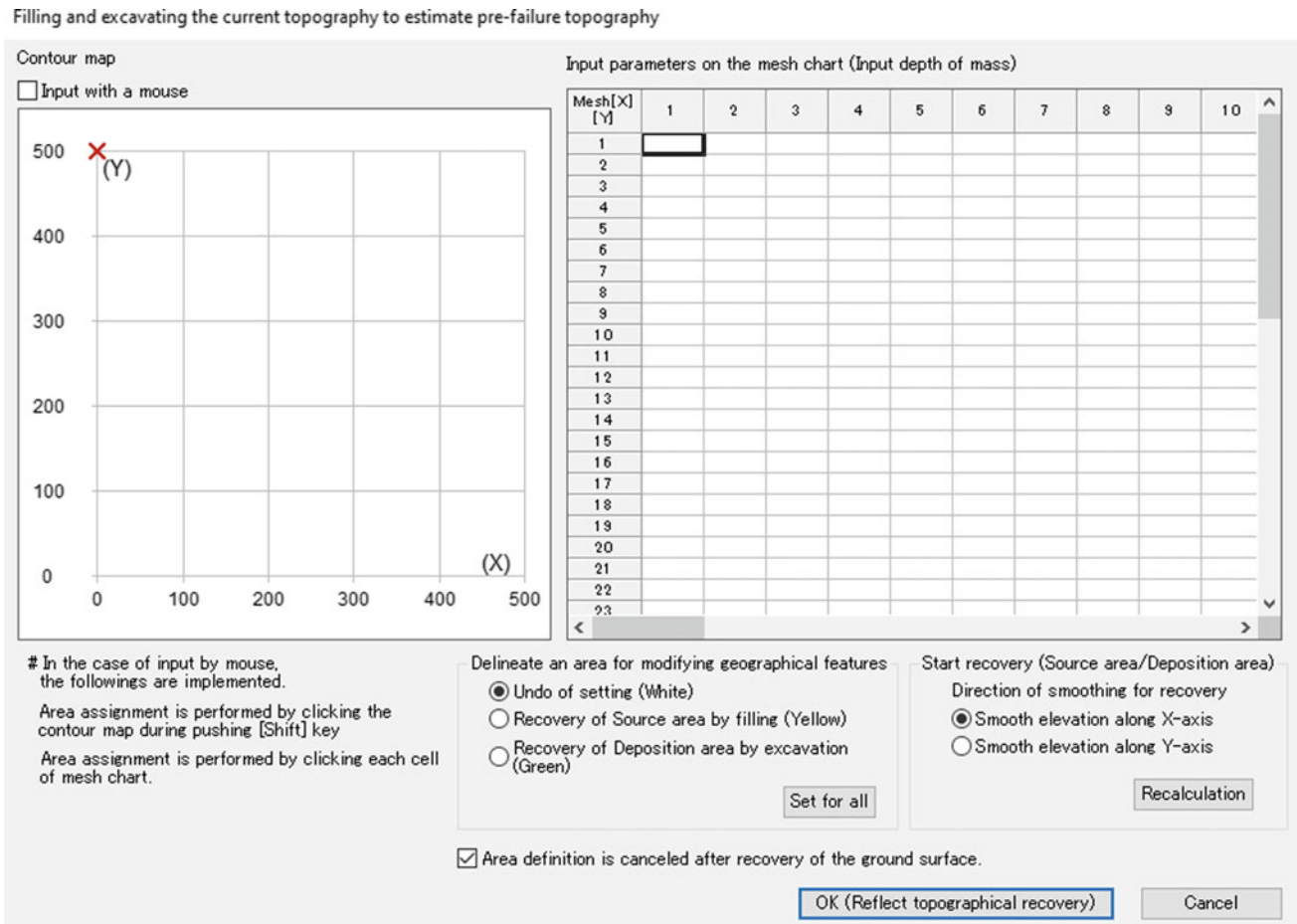
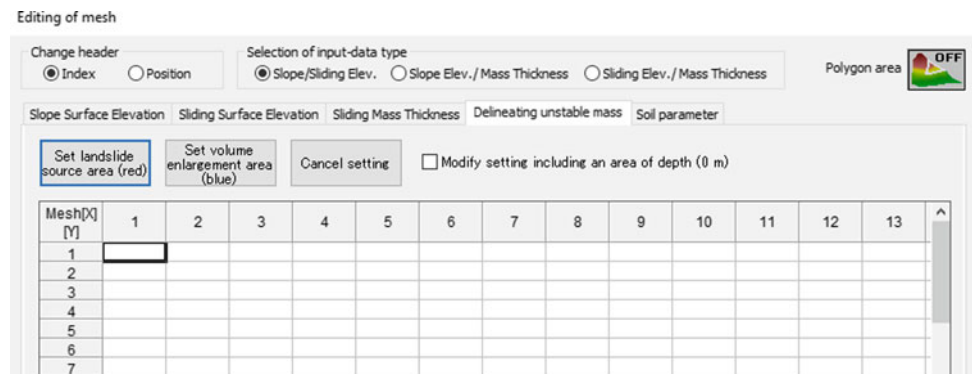


Fig. 20 Delineating unstable mass tab in the editing of mesh window

Fig. 21 Delineating unstable mass tab in the editing of mesh window



3.7 Input Soil Properties

Before the soil properties are inputted in to the LS-RAPID simulation, it is important to understand what soil properties will be needed and some of the ways that they can be obtained. Specifically, the following parameters will be needed for simulations in LS-RAPID:

- Lateral pressure ratio,
- Friction coefficient inside landslide mass,
- Friction coefficient during motion at sliding surface,
- Steady state shear resistance at sliding surface,
- Rate of excess pore-pressure generation, and
- Unit weight of mass.

In addition to the above parameters, the peak friction coefficient at sliding surface and the peak cohesion at sliding surface will be needed in simulations that consider strength reduction in full simulations.

The techniques to measure these parameters are provided in many geotechnical engineering textbooks with specific procedures in testing standards such as those by the American Society of Testing and Materials (ASTM). In addition, Tiwari and Ajmera (2018) describes all of the basic laboratory tests in a living document. Therefore, specific details regarding the measurement of these parameters is not provided here.

3.7.1 Typical Ranges

Typical ranges for the different soil properties are provided in this paper. Engineering judgement should be utilized if parameters are selected from the typical ranges provided here. Furthermore, it is noted that the information presented here is not a substitute for high quality sampling and testing, which, when appropriately applied, provides the best estimations of the field conditions.

Some typical values for the soil properties are summarized below:

- Lateral pressure ratio: 0.30–0.50
- Friction coefficient inside landslide mass: 0.36–0.58
- Friction coefficient during motion at sliding surface: 0.46–0.70
- Steady state shear resistance at sliding surface: 5–50 kPa
- Peak friction coefficient at sliding surface: 0.65–0.78
- Peak cohesion at sliding surface: 10–100 kPa.

The rate of excess pore pressure generation will have a value between 0 and 1.

3.7.2 Correlations

There are a number of correlations available in the literature to estimate the residual shear strengths of soils. Some of the available relationships at the time of publication are summarized in this section. More details are available in Tiwari and Ajmera (2020). Table 3 presents a summary of correlations for the residual shear strength available in the literature. Several relevant relationships are provided in Figs. 22, 23 and 24.

Table 3 Summary of available residual shear strength correlations

Liquid limit (LL)		Multiple parameters		
Relationship	References	Given	Relationship	References
$453.1LL^{-0.85}$	Cancelli (1977)	PI, σ_n'	Figs. 4 and 5	Hawkins and Privett (1985)
Fig. 1	Mesri and Cepeda-Diaz (1986)	LL, PI, CF, test type	Figs. 1 and 2	Collotta et al. (1989)
Plasticity index (PI)		CF, TT	Figs. 3 and 4	Figs. 3 and 4
Relationship	References	LL, CF, σ_n'	Fig. 4	Stark and Eid (1994)
Fig. 1	Voight (1973)	LL, CF, σ_n'	Fig. 4.3	Eid (1996)
$\frac{46.6}{PI^{0.446}}$	Kanji (1974) Kanji and Wolle (1977)	LL, M	Fig. 10	Tiwari and Marui (2003)
Fig. 6	Lupini et al. (1981)	PI, M	Fig. 11	Tiwari and Marui (2003)
Fig. 6	Gibo (1985)	LL, CF, σ_n'	For $CF < 20\%$ and $30 < LL < 80$	Stark and Hussain (2015)
Fig. 10	Borden and Putrich (1986)		$(\phi'_{r,s})_{50kPa} = 39.71 - 0.29LL + 6.63 \times 10^{-4}LL^2$	
Fig. 7	Müller-Vonmoss and Løken (1989)		$(\phi'_{r,s})_{100kPa} = 39.41 - 0.298LL + 6.81 \times 10^{-4}LL^2$	
Fig. 9	Tika and Hutchinson (1999)		$(\phi'_{r,s})_{400kPa} = 40.24 - 0.375LL + 1.36 \times 10^{-3}LL^2$	
			$(\phi'_{r,s})_{700kPa} = 40.34 - 0.412LL + 1.683 \times 10^{-3}LL^2$	
			For $25\% < CF < 45\%$ and $30 < LL < 130$,	
			$(\phi'_{r,s})_{50kPa} = 31.4 - 6.79 \times 10^{-3}LL - 3.616 \times 10^{-3}LL^2 + 1.864 \times 10^{-5}LL^3$	

(continued)

Table 3 (continued)

			$\left(\phi'_{r,s}\right)_{100kPa} = 29.8 - 3.627 \times 10^{-4}LL - 3.584 \times 10^{-3}LL^2 + 1.854 \times 10^{-5}LL^3$ $\left(\phi'_{r,s}\right)_{400kPa} = 28.4 - 5.622 \times 10^{-2}LL - 2.952 \times 10^{-3}LL^2 + 1.721 \times 10^{-5}LL^3$ $\left(\phi'_{r,s}\right)_{700kPa} = 28.05 - 0.208LL - 8.183 \times 10^{-4}LL^2 + 9.372 \times 10^{-6}LL^3$ For CF > 50% and 30 < LL, < 120, $\left(\phi'_{r,s}\right)_{50kPa} = 33.5 - 0.31LL + 3.9 \times 10^{-4}LL^2 + 4.4 \times 10^{-6}LL^3$ $\left(\phi'_{r,s}\right)_{100kPa} = 30.7 - 0.2504LL - 4.2053 \times 10^{-4}LL^2 + 8.0479 \times 10^{-6}LL^3$ $\left(\phi'_{r,s}\right)_{400kPa} = 29.42 - 0.2621LL - 4.011 \times 10^{-4}LL^2 + 8.718 \times 10^{-6}LL^3$ $\left(\phi'_{r,s}\right)_{700kPa} = 27.7 - 0.3233LL + 2.896 \times 10^{-4}LL^2 + 7.1131 \times 10^{-6}LL^3$ For CF > 50% and 120 < LL < 300, $\left(\phi'_{r,s}\right)_{50kPa} = 12.03 - 0.0215LL$ $\left(\phi'_{r,s}\right)_{100kPa} = 10.64 - 0.0183LL$ $\left(\phi'_{r,s}\right)_{400kPa} = 8.32 - 0.0114LL$ $\left(\phi'_{r,s}\right)_{700kPa} = 5.84 - 0.0049LL$	
Fig. 17	Toyota et al. (2009)	LL, CF, σ_n'	Fig. 7a	Eid et al. (2016)
Clay fraction (CF)		PI, CF, σ_n'	Fig. 7b	Eid et al. (2016)
Relationship	Reference	LL, M, ϕ_{fs}		
Fig. 7	Skempton (1964)	(Fully softened friction angle)	For kaolinite dominated soils, $\phi_{fs} - \phi_r = 6.128 \times 10^{-7}LL^3 - 0.00036LL^2 + 0.0751LL$ $\frac{\phi_{fs} - \phi_r}{\phi_{fs}} = -1.547 \times 10^{-7}LL^3 + 4.153 \times 10^{-5}LL^2 + 7.862 \times 10^{-4}LL$ $\frac{\phi_{fs} - \phi_r}{\phi_r} = 6.61 \times 10^{-5}LL^2 - 3.37 \times 10^{-4}LL$	Tiwari and Ajmera (2011)
Fig. 5	Lupini et al. (1981)			
Fig. 8	Tika and Hutchinson (1999)		For montmorillonite dominated soils with LL < 205, $\phi_{fs} - \phi_r = -0.00149LL^2 + 0.0704LL - 2.6868$ For montmorillonite dominated soils with LL < 180, $\frac{\phi_{fs} - \phi_r}{\phi_{fs}} = 1 \times 10^{-5}LL^2 + 0.001LL - 0.092$	
Mineralogy (M)			For montmorillonite dominated soils with LL < 145, $\frac{\phi_{fs} - \phi_r}{\phi_r} = 2 \times 10^{-8}LL^{3.596}$ For montmorillonite dominated soils with LL > 205, $\phi_{fs} - \phi_r = -1.893 \times 10^{-5}LL^2 + 0.00841LL + 4.5773$ For montmorillonite dominated soils with LL > 180, $\frac{\phi_{fs} - \phi_r}{\phi_{fs}} = -1.3 \times 10^{-6}LL^2 + 0.000692LL + 0.5018$ For montmorillonite dominated soils with LL < 145, $\frac{\phi_{fs} - \phi_r}{\phi_r} = 2.91 \times 10^{-8}LL^3 - 3.62 \times 10^{-5}LL^2 + 0.013LL$	
Relationship	Reference			
Fig. 6	Tiwari and Marui (2003)			
		PI, M, ϕ_{fs}	For kaolinite dominated soils, $\phi_{fs} - \phi_r = 1.123 \ln(PI) - 0.377$ $\frac{\phi_{fs} - \phi_r}{\phi_{fs}} = -2 \times 10^{-5}PI^2 + 0.0072PI$ $\frac{\phi_{fs} - \phi_r}{\phi_r} = 2.29 \times 10^{-5}PI^2 + 0.076PI$ For montmorillonite dominated soils with PI < 150, $\phi_{fs} - \phi_r = 0.012PI^{1.223}$ For montmorillonite dominated soils with PI < 120, $\frac{\phi_{fs} - \phi_r}{\phi_{fs}} = 3.8 \times 10^{-5}PI^2 + 0.000305PI + 0.003054$ $\frac{\phi_{fs} - \phi_r}{\phi_r} = 3 \times 10^{-5}PI^{2.219}$ For montmorillonite dominated soils with PI > 150, $\phi_{fs} - \phi_r = 9.7 \times 10^{-8}PI^3 - 1.1 \times 10^{-4}PI^2 + 0.033PI + 2.57$ For montmorillonite dominated soils with PI > 120, $\frac{\phi_{fs} - \phi_r}{\phi_{fs}} = 6.83 \times 10^{-9}PI^3 - 7.36 \times 10^{-6}PI^2 + 2.21 \times 10^{-3}PI + 0.396$ $\frac{\phi_{fs} - \phi_r}{\phi_r} = 4.27 \times 10^{-8}PI^3 - 4.41 \times 10^{-5}PI^2 + 0.012PI + 0.324$	Tiwari and Ajmera (2011)

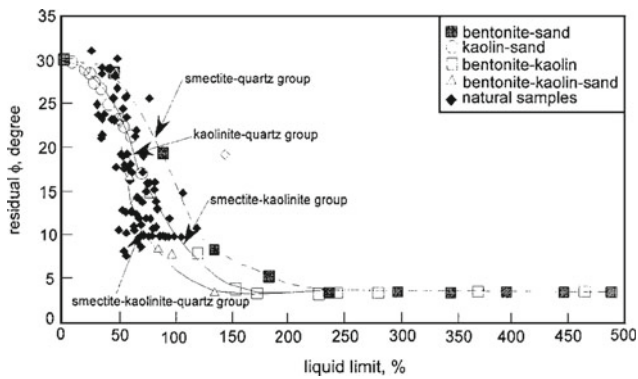


Fig. 22 Relationship from Tiwari and Marui (2003) for the residual friction angle in terms of the liquid limit and clay mineralogy

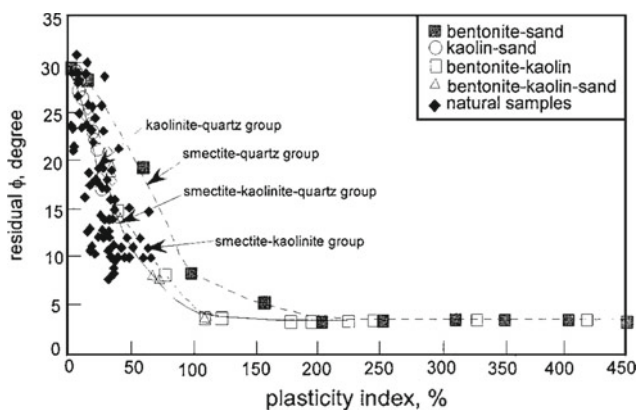


Fig. 23 Relationship from Tiwari and Marui (2003) for the residual friction angle in terms of the plasticity index and the clay mineralogy

3.7.3 Inputting Soil Properties in LS-RAPID

The procedures for inputting the soil properties in the LS-RAPID simulation are summarized below:

1. In the “Flow” panel, click on the “Soil parameters” button from Section “2: Calculation condition.” This section is shown in Fig. 25. The “Editing of Mesh” window from Fig. 17 will be displayed.
2. In the “Editing of Mesh” window, select the “Soil parameter” tab, as shown in Fig. 25.
3. The values of the parameter being edited should be entered. This can be done manually by entering the data corresponding to the x- and y-coordinates shown in the table if the “Position” radial button is selected under “Header” or to the x- and y- mesh indices if the “Index” radial button is selected. Alternatively, a specific value can be added to several selected cells using the “Set in selected rectangle” button.
4. These steps should be repeated until the values of eight different parameters are entered in the “SoilParameter” tab. These parameters are: (1) lateral pressure ratio, (2) friction coefficient inside landslide mass, (3) friction coefficient during motion at sliding surface, (4) steady state shear resistance at sliding surface, (5) rate of excess pore pressure generation, (6) peak friction coefficient at sliding surface, (7) peak cohesion at sliding surface, and (8) unit weight of mass. A description of the soil parameters can be obtained in LS-RAPID by clicking the “About parameters of soil characteristics” button. It is noted that except parameters 6 and 7 (peak friction angle and cohesion at

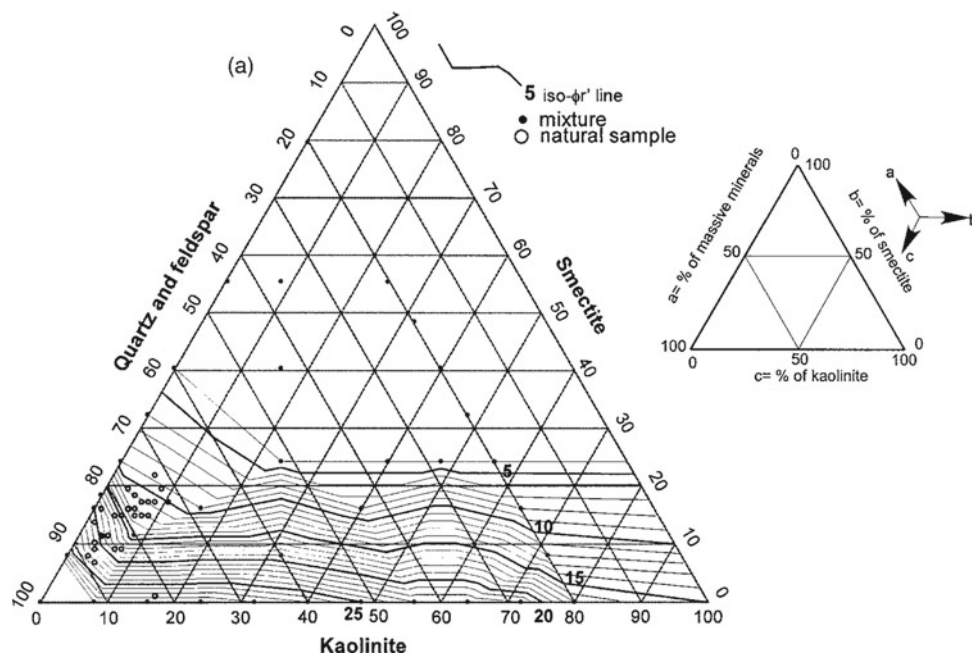


Fig. 24 Triangular correlation chart for clay mineralogy to estimate the residual friction angle developed by Tiwari and Marui (2003)

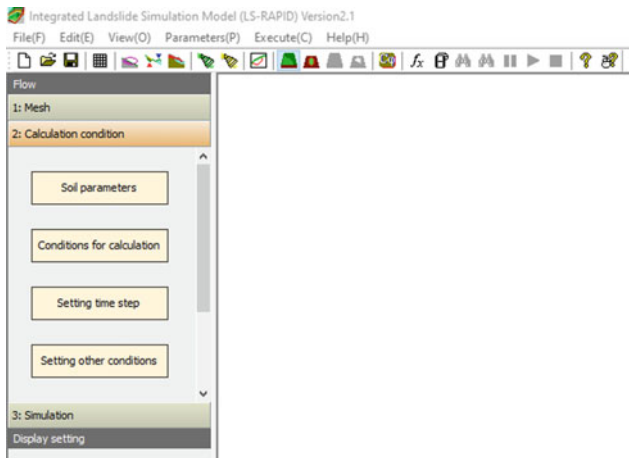


Fig. 25 Screenshot of section 2: calculation condition of the flow panel

sliding surface), all of the other parameters are required for the simulation. The parameter that is being edited will be indicated in the “Editing of Mesh” window with an asterisk (*) in the “Edit” column of the table. For example, in Fig. 26, the lateral pressure ratio is being edited.

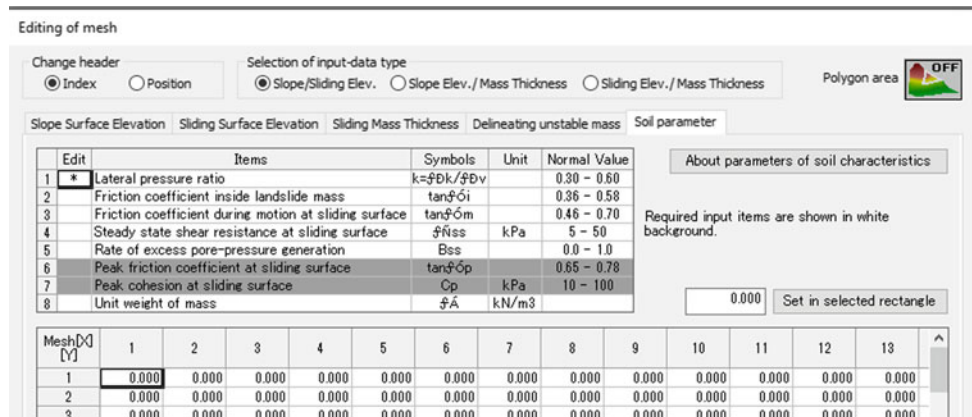
The procedures for inputting soil properties are also illustrated in the video tutorial titled, “7. Soil Parameters.”

3.8 Simulation Conditions

There are several different modes to simulate landslides in LS-RAPID. The procedures for performing these simulations are described below:

1. Open the “Set condition for calculation (Landslide)” window shown in Fig. 27 by clicking the “Conditions for calculation” button from Section “2:Calculation condition” in the “Flow” Panel on the left side of the program.

Fig. 26 Soil parameter tab in the editing of mesh window



2. The type of simulation that will be performed is selected from the “Condition of simulation” section in the “Set condition for calculation (Landslide)” window.
 - a. If only the motion needs to be determined, the “Motion simulation” radial button should be selected from the “Motion simulation” subsection.
 - b. Otherwise, a full mode simulation will need to be selected from the “Fullmode simulation (Initiation + Motion + Expansion)” subsection. Three radial buttons present the options available for the simulation type, namely, normal simulation, seismic simulation and rainfall simulation. Depending on the radial button selected, different options and parameter requirements will be made available on the “Set condition for calculation (Landslide)” window shown in Fig. 27.
 - i. Selection of the “Normal simulation” or “Seismic simulation” radial buttons will make available a check box for “With pore pressure.” This option allows pore water pressure to be considered as the trigger for the landslide. To use this option, rainfall data will be necessary.
 - ii. Details of normal and rainfall simulations procedures are provided in the video tutorial titled, “8. Setting for Rainfall Induced Landslide,” whereas, the seismic simulation procedures are in the video tutorial titled, “9. Settings for Earthquake Induced Landslide.”
3. To perform a normal simulation with pore pressure, the following steps will need to be followed:
 - a. In the “Method to give a graph of pore pressure ratio (ru)” section shown in Fig. 27, enter the time at which the rainfall begins in the “Time to start” box.
 - b. The pore water pressure condition will then need to be specified by selecting either the “Static” or “Survey” radial buttons.

Fig. 27 Set condition for calculation (landslide) window

- i. If the “Static” radial button is selected, the pore pressure ratio will remain constant at the “Ru” value specified for the “Duration” provided in the data entry boxes.
 - ii. Selection of the “Static” radial button will also provide an option to fluctuate the pore pressure value by checking the “Fluctuate a value” box. Checking this box will yield four locations requiring parameters. The user should enter the minimum pore pressure ratio in the “Min” box and the maximum value that the pore pressure ratio reaches in the “Max” box. The time required to reach this maximum pore pressure ratio should be entered in the “Max Time” box. In other words, at the start of the rainfall simulation, the pore pressure ratio will then begin at the value entered in the “Min” increasing to the value in the “Max” box over the duration noted in the “Max Time” box. This maximum value will then remain constant for the duration provided in the “Duration” data entry box.
 - iii. If the “Survey” radial button is selected, the rainfall will vary according to the pore pressure ratios provided at different time intervals. This pore pressure ratio as a function of time is specified by clicking the “Edition of ru” button, which will yield the “Pore pressure ratio” window shown in Fig. 28.
 - iv. The “Pore pressure ratio” will also contain a table in which the pore pressure ratios should be entered at different times of the rainfall event being simulated.
 - v. Once the rainfall data has been entered, Click “Ok” to return back to the “Set condition for simulation (Landslide)” window in Fig. 27.
 - vi. Visualization of the rainfall data can be obtained by clicking the “Graph preview” button in the bottom left corner of the Set condition for calculation (Landslide)” window in Fig. 27.
4. A rainfall simulation can be performed by selecting the “Rainfall simulation” radial button. The associated steps for this simulation are:
 - a. Click on the “Edition of rainfall” button to open the “Rainfall Data” window shown in Fig. 29.
 - b. The ten-minute rainfall intensities should be entered at different times of the rainfall event being simulated in the window in Fig. 29.
 - c. Once the data has been entered, click “Ok.”
 - d. As before, visualization of the rainfall data can be obtained by clicking the “Graph preview” button in the bottom left corner of the Set condition for calculation (Landslide)” window in Fig. 27.
 5. Procedures associated with the seismic simulations are described below. Note that the seismic waveforms can be visualized by clicking the “Graph preview” button in the bottom left corner of the Set condition for calculation (Landslide)” window in Fig. 27.
 - a. If pore pressure is also considered as part of the triggering mechanism, the “With pore pressure” box should be checked. This will require information to be entered into the “Method to give a graph of the pore pressure ratio (ru) section.” The procedures for this

entering the relevant information for this triggering mechanism have been explained in Step 3.

- b. The “Method to give a graph of seismic coefficient” section of the “Set condition for calculation (Landslide)” window will allow the user to input data related to the seismic excitation at the landslide location. The beginning of the seismic load will correspond to the time entered in the “Time to start” box.
- c. The user then has three options to apply the cyclic loads. These are given by the radial buttons labeled, “Static,” “Cyclic,” and “Seismic.” The options selected will determine whether the cyclic loads remain constant or fluctuate with time. Specifically, when “Static” is selected, the seismic coefficient will experience a linear variation with time. Data corresponding to the seismic coefficients should be entered into the “Static/Cyclic parameter setting” subsection. The selection of “Cyclic” will cause the seismic coefficient to fluctuate following a sine waveform. Furthermore, the

amplitude of the seismic coefficient will experience a linear change. Finally, seismic wave form data from an actual ground motion may be entered into the simulation when the “Seismic” option is selected. Thus, the seismic coefficient will vary based on the data inputted into the program.

- a. For the “Static” option,
 - i. Horizontal seismic coefficients will be entered by checking the “Horizontal seismic coefficient (Kh)” box. This coefficient can be entered in one of two ways: (1) Directional coefficients corresponding to the x- and y-directions can be entered in the boxes for the “X-direction coefficient Kx” and the “Y-direction coefficient Ky,” respectively, when the “Direction coefficient” radial button is selected, or (2) The horizontal coefficient can be entered directly by clicking the “Horizontal coefficient” radial button. In this option, the value of the horizontal coefficient and the corresponding seismic direction

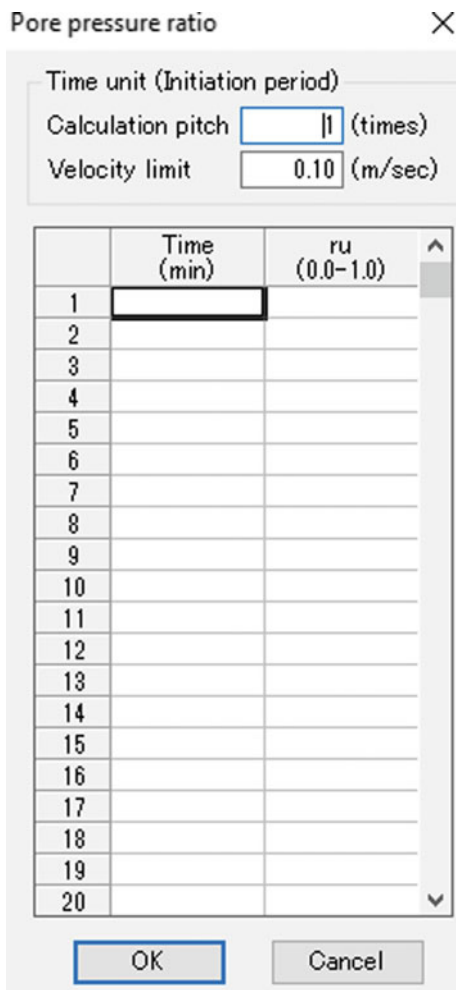


Fig. 28 Pore pressure ratio window obtained by clicking the edition of ru button in the set condition for calculation (landslide) window

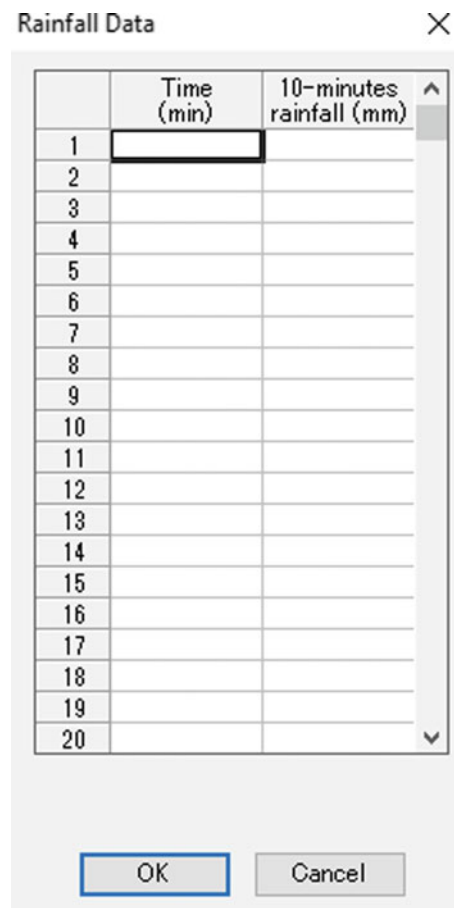


Fig. 29 Rainfall Data Window Opened when Edition of Rainfall Button in Clicked

- should be entered into the “Kh” and “Seismic direction θ_s ” boxes, respectively.
- ii. If a vertical seismic coefficient is needed, the “Vertical seismic coefficient (Kv)” box should be checked and the corresponding seismic coefficient should be entered into the data box.
 - iii. Clicking the “Substitute the direction of landslide profile” will cause the direction of the longitudinal landslide section to be set as the direction of the seismic coefficient if an ellipsoidal sliding surface was created.
 - iv. In the “Frequency/MaxTime/Duration” subsection, enter the “Duration” of the seismic load.
 - v. If the “Fluctuate a value” box is checked in the “Frequency/MaxTime/Duration” subsection of Fig. 27, the static seismic coefficient will begin at zero and linearly increase to the values of the seismic coefficients over the time specified in the “Max Time” box. The seismic coefficient will then remain constant before linearly decreasing from the maximum value to zero over the same “Max Time” duration. The total duration of the seismic load including the linear increase at the start and the linear decrease at the end will still correspond to the “Duration” value provided.
- b. For the “Cyclic” option,
- i. Follow the steps in given in Step 5.d.i to 5.d.iii.
 - ii. In the “Frequency/ MaxTime/ Duration” subsection, the frequency of the sinusoidal waveform should be entered in the “Hz” box and the number of cycles of loading in the “Total Cycle (N)” box.
 - iii. Checking the “Fluctuate a value” box will yield some additional options. Specifically, the number of cycles required to reach the maximum seismic coefficient should be entered in the “Kmax Cycle (N)” box. This will indicate the number of cycles over which the amplitude of the sine wave is increased to the maximum value specified. This increase will occur in a linear fashion. It also corresponds to the number of cycles at the end of the seismic waveform over which the maximum seismic coefficient is decreased to zero.
- c. For the “Seismic” option,
- i. Seismic coefficient data is entered by clicking on the “Edition of seismic waveform” button. This will open the “Data registration of seismic waveform” window. Figure 30 contains a screenshot of this window.
 - ii. A name for the waveform should be entered in the text box just beneath the text, “Case 1 Seismic Waveform.”
 - iii. In the table just beneath the name, the user should enter the time and corresponding values of the acceleration for the east-west, north-south and up-down directions. This information should inputted into the corresponding columns titled, “Time,” “EW-Acc,” “NS-Acc,” and “UD-Acc,” respectively. When entering the data, the time must be entered in chronological order with the corresponding acceleration values in the associated row.
 - iv. Up to three different seismic waveforms may be entered into the program. The steps for entering the data are the same, except the data will be entered to correspond to the seismic waveform case as shown in Fig. 30.
 - v. Once the seismic wave form data has been entered, click “Ok” to return to the “Set condition for calculation (Landslide)” window from Fig. 27.
 - vi. In the “Seismic parameter setting” subsection, the maximum seismic coefficients in the x-, y-, and vertical directions will be displayed in the “Kx max,” “Ky max,” and “Kv max” boxes, respectively. The amplitude of these waveforms can be scaled using the factors entered in the “EW Acc (gal)/980x,” “NS Acc (gal)/980x,” and “UD Acc (gal)/980x,” boxes, respectively.
6. Once the required data for the simulation have been entered using the procedures described above, the next section that will require user input will be the “Parameters for condition for strength reduction” in the “Set condition for calculation (Landslide)” window in Fig. 27. In the full mode simulations, the peak values of the friction coefficient and the cohesion are reduced to the normal motion values in the unstable mass. In other words, $\tan \phi_p$ and c_p will reduce to $\tan \phi_m$ and c_m , respectively.
- a. The reduction in the friction coefficient and the cohesion will commence when the travel length of the landslide reaches the distance specified in the “From (DL)” box and continue until the distance specified in the “To (DU)” box. Once the travel length exceeds the value in the “To (DU)” box, normal simulation will begin.
 - b. In the “Except source area (by depth of mass)” box, the user should specify the depth of the sliding mass (Δh_{cr}), which when reached will also trigger the start of the normal motion simulation signifying the completion of the reduction of the friction coefficient and cohesion.
 - i. Buoyancy can be incorporated into the simulation by checking the “Calculate submergence” in the “Setting of the submergence calculation” section. Doing so will allow the user to enter the depth of the ground water table (or the interface between

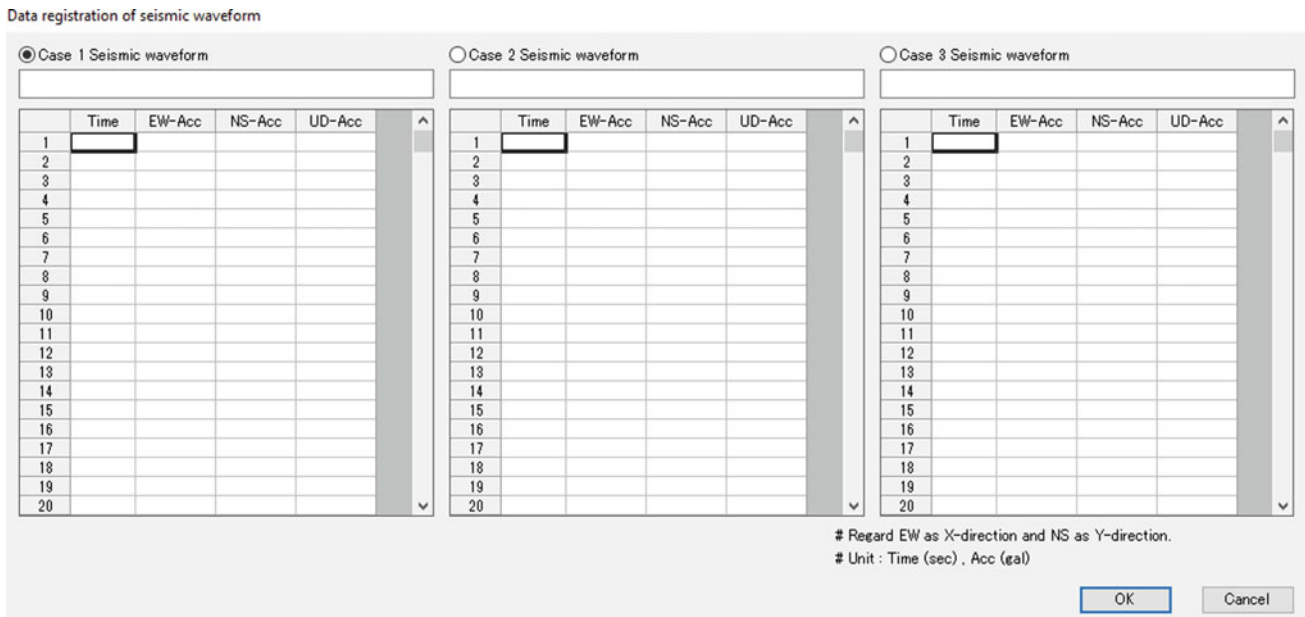


Fig. 30 Data registration of seismic waveform window screenshot

the submerged and unsubmerged soil) in the box for the “Level of the water surface.” The “unit weight of water (γ_w)” box should be used to specify the unit weight of water or the weight of water in a unit volume.

7. Once all of the simulation information has been entered, click the “Set Parameters” button in the bottom right corner of the “Set condition for calculation (Landslide)” window in Fig. 27.
8. The “Graph Preview” button in the bottom left corner of “Set condition for calculation (Landslide)” window will allow the user to view the ground motion that will be applied in the simulation based on the parameters entered in the steps described above.

3.9 Setting Time Steps

The degree by which the motion proceeds in the simulation can be adjusted by using a time step. The video tutorial titled, “10. Setting Time Step,” explains the procedure, which is also summarized below:

1. Open the “Setting time step” window presented in Fig. 31. This window can be obtained through the “Flow” panel on the left side of the LS-RAPID program. Under Section “2: Calculation condition,” click on the “Setting time step” button.

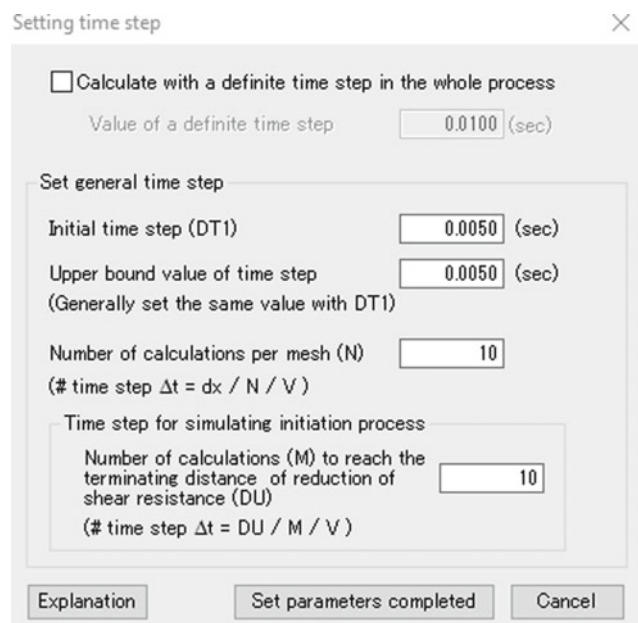


Fig. 31 Setting time step window

2. The time step can be set to remain constant throughout the simulation by checking the “Calculate with a definite time step in the whole process” box. Otherwise, the parameters in the “Set general time step” section should be edited.
3. The time step for the first step in the simulation should be specified in the “Initial time step (DT1)” box.
4. The next time step will be calculated from the average maximum velocity. In the event that this time step exceeds

- the value in the box labeled, “Upper bound value of time step,” the next time step will be value provided in this box.
- The number of calculations per mesh at which the next time step should be calculated should be provided in the next box.
 - In the subsection titled, “Time step for simulating initiation process,” the time step used in the initial simulation will be terminated as the reduction in the shear resistance will be complete. After reaching this distance, the simulation will use the time step corresponding to the motion simulation.

3.9.1 Setting of Other Conditions

There are several simulation settings that are not used very frequently. This section will quickly summarize those settings. To obtain these settings, click on the “Setting other conditions” button from Section “2: Calculation condition” in the “Flow” panel. The “Setting other conditions” window, displayed in Fig. 32, will open. The video tutorial describing these additional conditions is titled, “11. Setting Other Conditions.”

3.9.2 Non-frictional Energy Consumption

Checking the “Trigger non-frictional energy loss function” in the “Non-frictional energy consumption” section will cause this energy consumption to be considered in the simulation. It will be necessary to specify the coefficient, α , at which the non-frictional energy function is triggered. Two additional options also exist in this section, which allow the non-frictional energy loss function to be triggered when the specified velocity or specified depth of mass is reached, when the corresponding boxes are checked.

Fig. 32 Setting other conditions window screenshot

3.9.3 Other Settings

Under the “Set for” subsection, several other setting options are present. These are as summarized below:

- The “Threshold of flow rate (neglected below this value)” setting allows the user to specify the minimum amount of soil in the calculated mesh that is moving within a unit of time. When the flow is less than the value specified, the mesh rejects the flow. This value will depend on the size of the landslide, but a good initial estimate is 0.01 m³/sec.
- Landslide movements down a torrent will be concentrated along the torrent. However, some of the upper part of the landslide may cross over the ridge when it is higher than the ridge. Checking the “Calculate the case of crossing over a ridge” option will consider this effect.
- Increases in the lateral pressure are expected when the vertical stress increases. These increases depend on the lateral earth pressure coefficient. When the “Calculate increased lateral pressure at vertical earthquake loading” box is checked, this effect will be considered in the simulation.
- A cohesion value can be assigned to all of the geographical features of the landslide mass with the use of the “Cohesion inside mass” data box. Similarly, the cohesion along the entire sliding surface during landslide motion can be assigned using the “Cohesion at sliding surface during motion” box.
- During the simulation, the total volume of the soil mass should not change. However, in unsteady conditions, this volume may increase and the effect can be adjusted by increasing the velocity by a certain percentage before the simulation begins in the “Calibration parameter of calculated landslide mass” subsection.

3.9.4 Output Settings

The settings associated with the outputs from the simulation should be configured next. The following steps will describe how this configurations can be applied in LS-RAPID. Users may also refer to the video tutorial, titled “13. Output Setting for Landslide Simulation.” These settings can be accessed through the “Flow” Panel in Section “3: Simulation” by clicking the “Set calculation output” button. The “Output setting” window pictured in Fig. 33 will open. The options available in each section of this window will be discussed in this section.

3.9.5 Calculation Step Numbers (for Result Saving)

In the “Calculation step numbers (for result saving)” section of the “Output setting” window in Fig. 33, the value entered in the “Maximum step” data box will indicate the number of steps after which the results are drawn in the topographical

Fig. 33 Output setting window screenshot

display in LS-RAPID and when the results are saved. The “Drawing interval” represents the time (or step) interval at which the geographical features are updated during the simulation. Additionally, it also indicates the interval at which intermediate simulation results are saved.

The maximum x - and y - velocities will be obtained as an average of the corresponding results at a number of sample locations in each mesh. The number of samples that should be used for this average can be specified in the box labeled, “Necessary number of samplings to display U_{max} , V_{max} ” in the “Calculation step numbers (for result saving)” section.

The LS-RAPID simulation terminates when all solid features have stopped moving. A user may specify that the simulation continue beyond this point by specifying the “Minimum time for simulation.” This will cause the simulation to continue to run even after the all the solid features have stopped until the time entered is reached.

3.9.6 Output of Altitude Information

The “Output of altitude simulation” section primarily contains the settings to save output files. Specifically, when the “Output the altitude calculation result data” box is checked, elevation data after the simulation will be saved into the same folder as the project file. If a different location is desired, the user may specify the preferred location by using the open folder icon in the “Folder for output files” subsection. This location can be removed from the simulation by clicking the delete folder icon.

The three-dimensional view in the LS-RAPID display panel will not be updated when the “No refresh view during calculation” box is checked. It should be noted that the computations will be performed faster if the display does not

need to be periodically updated during the simulation process. Settings associated with the display during the simulation are set in the “Drawing” section of the “Output setting” window in Fig. 33. Details regarding these settings are provided next.

3.9.7 Drawing

During the simulation, the calculation time can be displayed in either seconds or hours by selecting the radial button next to “How to display calculation time” in the “Drawing” section. Any comments that should be displayed during the simulation should be provided in the text box under the “Comments field.”

When drawings are being periodically generated during the simulation, the “Waiting time for drawing result data” will indicate the time at which the output files for the altitude will be read and displayed. In the display, it may be of value to display the seismic and/or rainfall functions as the simulation progress. The length of the horizontal (or time) axis for these landslide triggers can be specified in the “Drawing period of landslide trigger” data box.

3.9.8 Output Options

The last section in the “Output settings” window shown in Fig. 33 is “Output settings.” Under the “Assign the head words for output files,” the word(s) that will proceed the names for all files and folders generated during the simulation can be specified. This is done by clicking the open folder icon and selecting the location at which the output files will be stored and typing the word(s) that should be used as a prefix in all of the output files and folders. It is noted that by default, the location shown in the window that opens when the open folder icon is clicked corresponds to

the location specified in the “Folder for output files” entry in the “Output of altitude information” section. These word(s) that serve as a prefix to the file and folder names can be deleted by clicking the delete folder icon.

By default, all of the data from the beginning of the simulation will be exported and saved. However, the user may also specify the range of steps across which the data should be saved if all of the data is not necessary. This can be done by entering the desired range values in the data boxes in “Step range to output calculation range.”

The text files that will be generated in the simulation can be formatted in the “<Text files>” subsection. Users have the choice between the use “Space” or “Comma” delimiters between data in the text files. The “Output Digit” will specify the number of decimal places that are provided for the depth of the soil mass in the text files, while “Output form” indicates how these data will be displayed. In particular, if “Matrix” is selected, the output data will be formatted in a matrix, whereas, the selection of “Control point form” will format the text files to have rows containing the mesh ID and the depth of soil mass.

The data that can be exported in the output files during the simulation can be selected from the check boxes at the bottom of the “<Text files>” subsection. When “VALUE” is selected, the depth of the unstable soil mass for each mesh will be saved, while “GRAPH” will display the depth of the unstable mass for each mesh graphically. The velocity of the soil mass can be outputted by checking the “U,” “V,” and/or “UV Bar” boxes. U and V represent the velocities in the x- and y-directions, respectively. The mean value of the velocity will be given by UV option.

The images generated during the simulation can be formatted using the options in the “<Picture files>” subsection. Images can be saved as “JPEG’ Files” and/or “AVI’ File” by checking the appropriate box(es). The number of images to be saved per second of the simulation should be specified in the box for “(frames/sec).” The area that will be included in the images is specified by the settings in the “Picture clipping area” subsection. Selection of “Application area” will focus on images associated with the regions with movement in a two-dimension plan view of the failure. By contrast, the selection of “3D-View area” will result in images containing three-dimension views of the simulation area based on the display in the viewing panel in the LS-RAPID program.

3.9.9 Background Images in Simulation

Users may find it valuable to have an image of the topography from Google Earth or other sources as the background for the simulation area. Steps to insert and display this image can be found in the “12. Setting Background Image for Topography” video tutorial. Additionally, the steps are briefly summarized in this section.

1. As shown in Fig. 34, select “Setting background image file (R)” from the “File(F)” menu. This will open in the “Setting background image file” window shown in Fig. 35.
2. Use the “Select File” button from the “Background image file” section to navigate to the location and select the file associated with the background image. Please note that only BMP and JPEG files can be used for this setting. Once the file has been selected, click the button labeled, “Open.”
3. The selected image will be displayed in the “(Image Preview)” section in the “Setting background image file” window shown in Fig. 35.
4. In the “Coordinate relation” section, specify the coordinates of the corners of the images. The labeling of these corners is identified in the “(Relation with simulation area)” section. Specifically, “Pos. A” refers to the bottom left corner of the images while “Pos. B” is the bottom right corner. Similarly, “Pos. C” and “Pos. D” correspond to the top right and top left corners, respectively. The x-coordinate should be entered in the cells under the “PX” column heading, whereas, the y-coordinates should to be entered in the “PY” column.
5. Click “Ok.” This will result in the background of the topography being replaced by the image selected based on the coordinates provided.

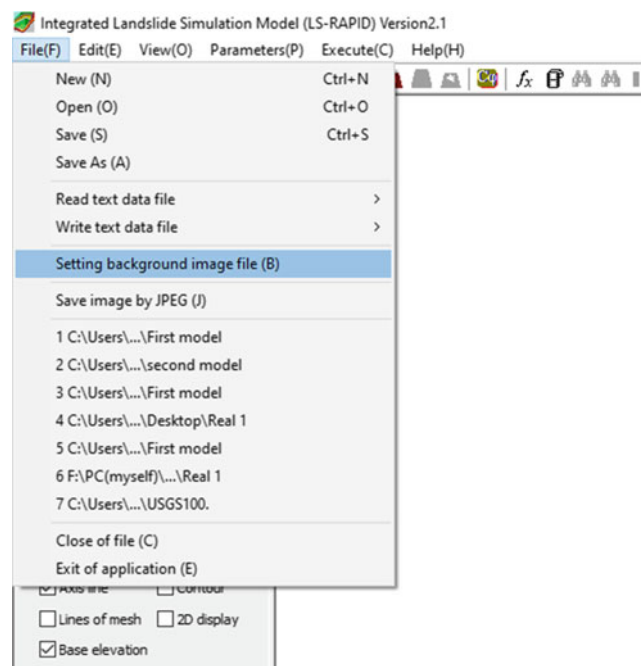


Fig. 34 Screenshot of file menu in LS-RAPID

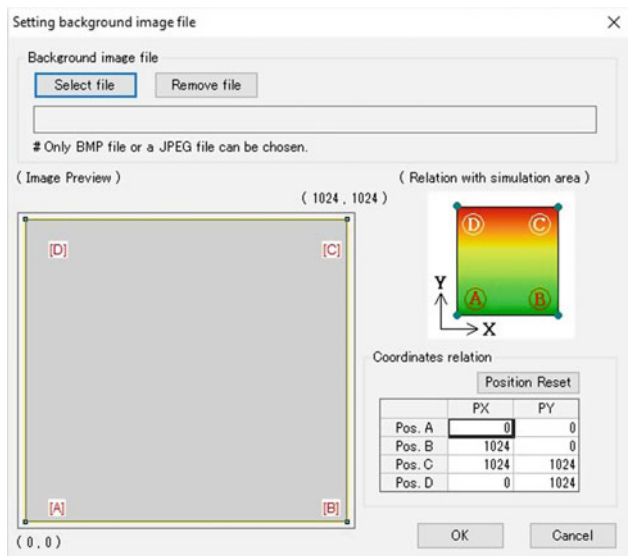


Fig. 35 Setting background image file window

3.9.10 Starting a Simulation and Displaying the Results

To begin the simulation, the user should click on the “Start simulation” button in Section “3: Simulation” of the “Flow” panel. Users may also refer to the video tutorial, titled “14. Start Simulation.” This will result in a notification, like that shown in Fig. 36, asking the user to confirm that the simulation should be started. When “Ok” is clicked, the simulation will begin. The pause, play and stop icons in the toolbar can be used to temporarily pause, restart and stop the simulation, respectively.

There are several options that can be used during the simulation. Clicking the black binoculars icon in the toolbar will open the “Mesh value monitor” window, similar to that pictured in Fig. 37. This window will display the mesh ID and associated values of various different parameters at the time step corresponding to when the black binoculars icon was clicked. The drop down menu at the top of this window will allow the user to select which of the various parameters used and/or generated at that specific time step should be displayed. Specifically, the following nine options are available: (1) friction coefficient at sliding surface, (2) cohesion at sliding surface, (3) present mass distribution, (4) velocity along x-axis, (5) velocity along y-axis, (6) flow rate along x-axis, (7) flow rate along y-axis, (8) accumulated mass displacement, and (9) maximum velocity record.

The green binoculars icon can be used to display the triggering factors in the simulation. Figure 38 contains the “Monitor value” window that is opened when the green binoculars icon is clicked. In this window, both the rainfall and earthquake loading information will be displayed.

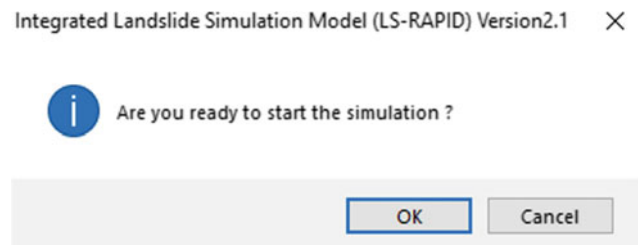


Fig. 36 Notification confirming the start of simulation when start simulation button is clicked

Upon the completion of the simulation, the simulation results can be displayed using the “Result of simulation” button. This button is located in Section “3: Simulation” in the Flow panel.

4 Examples and Tutorials

4.1 Generated Simple Slope with an Ellipsoidal Sliding Surface

Interested users may also follow a video tutorial with this example, titled, “15. Rainfall-Induced Simple Slope Landslide Tutorial.”

4.1.1 Initial Topography

Simulation Area

To create a simulation area within LS-RAPID for a simple slope, click on the “Simulation area” button in the Section “1: Mesh” within the “Flow” panel located on the left side of the program. This will result in the image in Fig. 9.

In the “Setting of simulation area and input-data type”, input values of the x- and y-coordinates, as indicated in Fig. 9. The simulation area will be 350 m in x-direction and 440 m in y-direction. The pitches for x- and y-directions are set as 10 m each in the second component of “Mesh setting of simulation area.” The numbers of grids are automatically calculated based on the inputted values of x- and y-coordinates and pitches. The simulation area is illustrated in the bottom part of the window. Click “OK” to complete setting of simulation area.

Editing Mesh

The second step is to establish the topography of the simple slope. In this example, the mesh data for the topography of the slope is estimated in an Excel file (as shown in Fig. 39) and then is inputted into LS-RAPID. Mesh data is added into the calculation area using “Editing of mesh” button of the Section “1: Mesh” in the “Flow” panel (Fig. 9).

Mesh value monitor

01) Friction coefficient at sliding surface (tan(Phi)) Step : 9428 Time : 46.9 sec DataCopy

Font - S Display 0 value Min = 0.2 (15,22) Max = 0.8 (1,1)

Mesh[X] [Y]	1	2	3	4	5	6	7	8	9	10	11	12	1	
1	0.800	0.800	0.800	0.800	0.800	0.800	0.800	0.800	0.800	0.800	0.800	0.800	C	
2	0.800	0.800	0.800	0.800	0.800	0.800	0.800	0.800	0.800	0.800	0.800	0.800	C	
3	0.800	0.800	0.800	0.800	0.800	0.800	0.800	0.800	0.800	0.800	0.800	0.800	C	
4	0.800	0.800	0.800	0.800	0.800	0.800	0.800	0.800	0.800	0.800	0.800	0.800	C	
5	0.800	0.800	0.800	0.800	0.800	0.800	0.800	0.800	0.800	0.800	0.800	0.800	C	
6	0.800	0.800	0.800	0.800	0.800	0.800	0.800	0.800	0.800	0.800	0.800	0.800	C	
7	0.800	0.800	0.800	0.800	0.800	0.800	0.800	0.800	0.800	0.800	0.800	0.800	C	
8	0.800	0.800	0.800	0.800	0.800	0.800	0.800	0.800	0.800	0.800	0.800	0.800	C	
9	0.800	0.800	0.800	0.800	0.800	0.800	0.800	0.800	0.800	0.800	0.800	0.800	C	
10	0.800	0.800	0.800	0.800	0.800	0.800	0.800	0.800	0.800	0.800	0.800	0.800	C	
11	0.800	0.800	0.800	0.800	0.800	0.800	0.800	0.800	0.800	0.800	0.800	0.800	C	
12	0.800	0.800	0.800	0.800	0.800	0.800	0.800	0.800	0.800	0.800	0.800	0.800	C	
13	0.800	0.800	0.800	0.800	0.800	0.800	0.800	0.800	0.800	0.800	0.800	0.800	C	
14	0.800	0.800	0.800	0.800	0.800	0.800	0.800	0.800	0.800	0.800	0.800	0.800	C	
15	0.800	0.800	0.800	0.800	0.800	0.800	0.800	0.800	0.800	0.800	0.800	0.800	C	
16	0.800	0.800	0.800	0.800	0.800	0.800	0.800	0.800	0.800	0.800	0.800	0.800	C	
17	0.800	0.800	0.800	0.800	0.800	0.800	0.800	0.800	0.800	0.800	0.800	0.800	C	
18	0.800	0.800	0.800	0.800	0.800	0.800	0.800	0.800	0.800	0.800	0.800	0.600	C	
19	0.800	0.800	0.800	0.800	0.800	0.800	0.800	0.800	0.800	0.800	0.800	0.600	C	
20	0.800	0.800	0.800	0.800	0.800	0.800	0.800	0.800	0.800	0.800	0.530	0.600	C	
21	0.800	0.800	0.800	0.800	0.800	0.800	0.800	0.800	0.800	0.800	0.800	0.360	C	
22	0.800	0.800	0.800	0.800	0.800	0.800	0.800	0.800	0.800	0.800	0.800	0.600	C	
23	0.800	0.800	0.800	0.800	0.800	0.800	0.800	0.800	0.800	0.800	0.800	0.600	C	
24	0.800	0.800	0.800	0.800	0.800	0.800	0.800	0.800	0.800	0.800	0.800	0.600	C	
25	0.800	0.800	0.800	0.800	0.800	0.800	0.800	0.800	0.800	0.800	0.600	0.315	C	
26	0.800	0.800	0.800	0.800	0.800	0.800	0.800	0.800	0.800	0.800	0.600	0.588	0.366	C
27	0.800	0.800	0.800	0.800	0.800	0.800	0.800	0.800	0.800	0.800	0.588	0.600	0.600	C

Fig. 37 Mesh value monitor window opened by black binocular icon

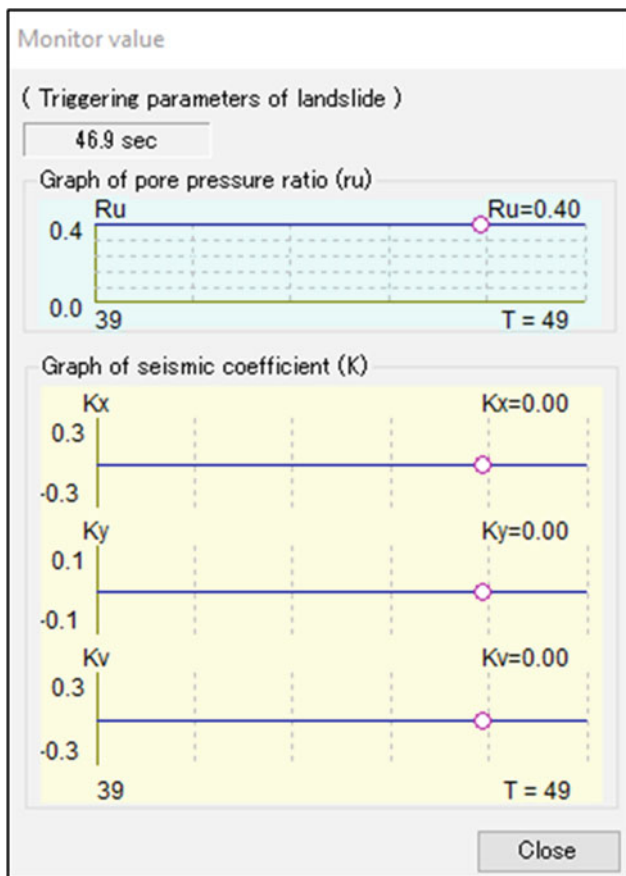


Fig. 38 Monitor value window opened by green binoculars icon

In the “Editing of mesh” window, select the “Index” option for the “Header Notation” section, select “Slope Elev./Mass Thickness” option in the “Selection of input-data type” section. In this case, the mesh is represented with the numbers associated with the grid lines in the calculation area and the slope surface elevation and the sliding mass thickness will be defined.

Topography data is inputted into the “Slope Surface Elevation” tab by copy-pasting from the Excel file. This step is illustrated in Fig. 40. The topography mesh of the simple slope will then be displayed in the viewing panel as shown in Fig. 41.

4.1.2 Creating Sliding Surface

The potential sliding surface is created using ellipsoidal parameters. As described previously in Sect. 3.4.1, the user can use one of the three different ways to begin creating the ellipsoidal sliding surface.

In this example, the longitudinal section is defined by inputting start (180, 450) and end (180, 150) points in the “Selection longitudinal section” table. The locations of passing points A, B, and the center of ellipsoid on the longitudinal section of the sliding surface are selected as (35, 110), (165, 50), and (200, 160), respectively. The locations of passing points C and the center of ellipsoid on the crossing section are (120, 95), (180, 160), respectively. The location of passing point D is automatically calculated. The parameters used in this example for this paper are shown in the screenshot in Fig. 42.

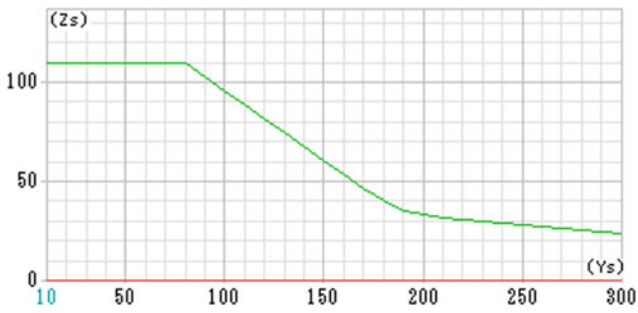


Fig. 39 Cross section of the simple slope

4.1.3 Delineating Unstable Mass

The delineating unstable mass step is used to specify the landslide source and enlargement areas. In Section “1: Mesh” of the “Flow” panel (Fig. 9), click the “Delineating unstable mass” button. Select all the cells corresponding to the source area and then click “Set landslide source area (red).” The color of the cells should change to red. The depth of unstable mass in the enlargement area is set to 5 m. Select

the cells corresponding to the volume enlargement areas and click the “Set volume enlargement area (blue)” button. The color of the cells of the volume enlargement area will become blue. This is illustrated in Fig. 43.

4.1.4 Input Soil Properties

In Section “2: Calculation condition” of the “Flow” panel, click on the “Soil parameter” button to input soil properties. Values of the parameters for this example are selected as approximately the average of the typical values suggested in the program and are specified in Table 4. Figure 44 shows the lateral earth pressures entered in the model.

4.1.5 Simulation of a Rainfall-Induced Landslide on Simple Slope

First, a rainfall-induced landslide simulation is performed on the geometry of the simple slope described previously in this chapter. The triggering factor of the landslide is considered to be a high-intensity or/and long-term rainfall, which causes a rise in level of the groundwater table. This will

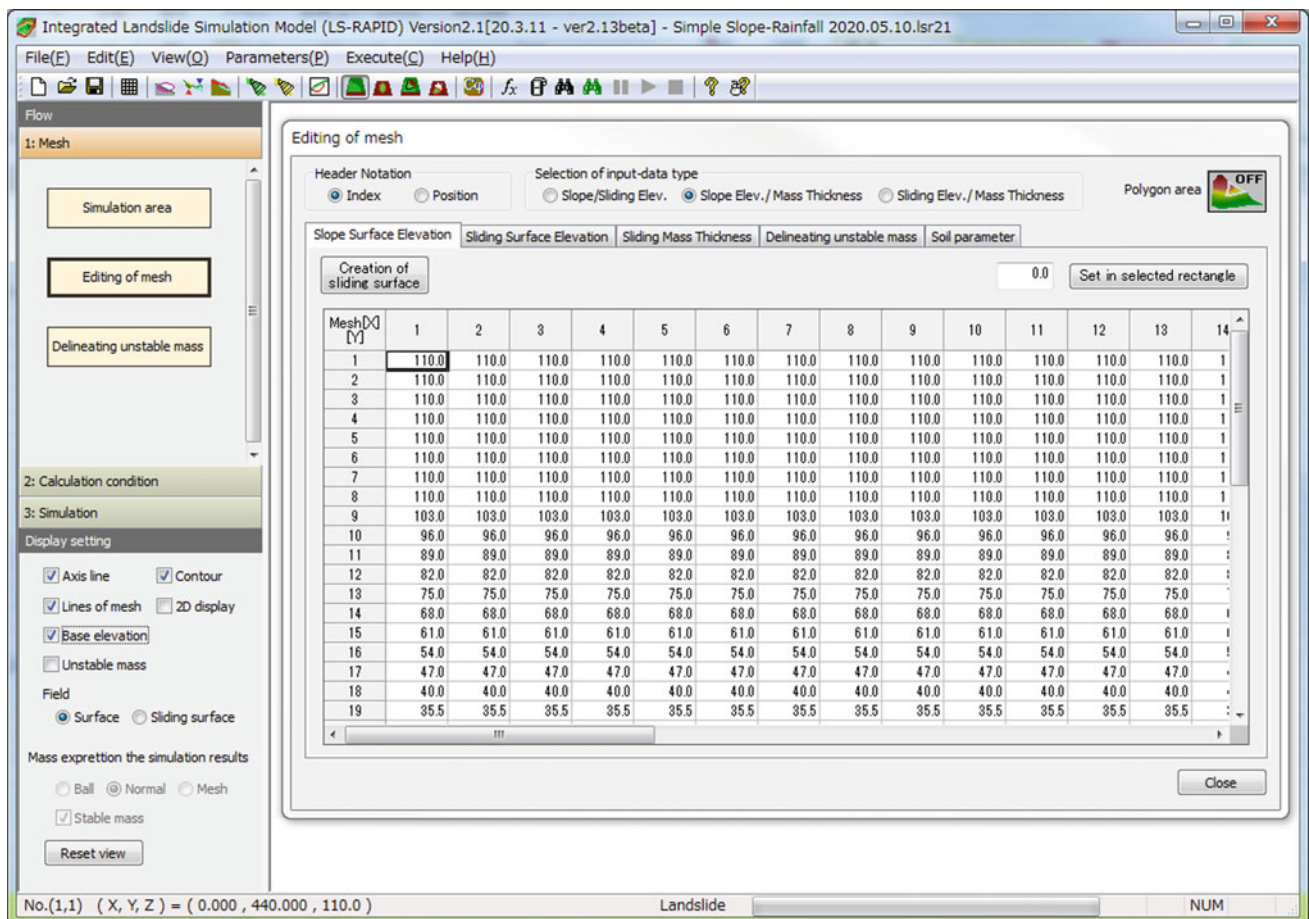


Fig. 40 Input topography mesh data into the calculation area using “editing of mesh”

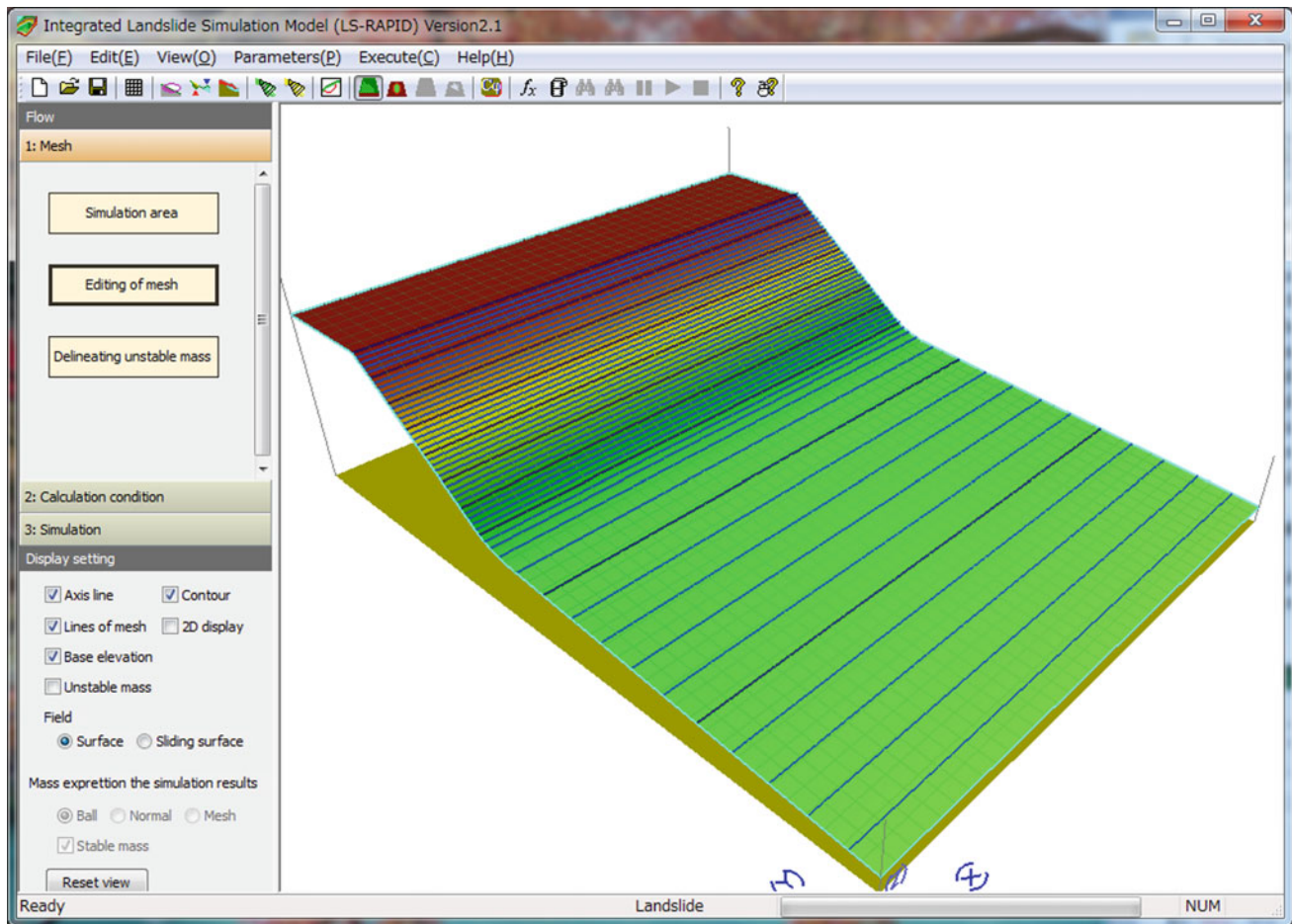


Fig. 41 Topography mesh of the simple slope example

subsequently cause an increase in the pore water pressure and an associated decrease in the shear strength on the sliding surface. The heavy rainfall used in the simulation occurred from 14 to 18 May 2016 which triggered the Aranayake catastrophic landslide in Sri Lanka (Dang et al. 2019). The observed rainfall data associated with this event is provided in Table 5. From the observed rainfall, the water pressure ratio (r_u) was calculated using a SLIDE model (Liao et al. 2010). The simulation is set to 80 h corresponding to the more than three days of the rainfall event.

Setting Simulation Conditions

In LS-RAPID, click on the “Conditions for calculation” button from Section “2: Calculation condition” in the “Flow” Panel to open the “Set condition for calculation (Landslide)” window. Figure 45 shows the window that will be open when these steps are followed.

Select the “Rainfall simulation” radial button to conduct a rainfall-induced landslide simulation. Click on the “Edition of rainfall” button to input the rainfall intensities (Fig. 46). For the “Method to give a graph of pore pressure

ratio (r_u),” select the “Survey” radial button and click on the “Edition of r_u ” button to input the pore pressure ratio data in the “Pore pressure ratio” window, as shown in Fig. 47. To reduce the computation time for the landslide simulation, the “Calculation pitch” and the “Velocity limit” are set as 36,000 times and 0.10 m/s, respectively. The pore pressure ratios estimated in Table 5 are entered into the “Pore pressure ratio” window. Once the rainfall and pore pressure ratio data have been entered, their graphs can be previewed, as shown in Fig. 48. Click the “Set Parameters” button in the bottom right corner of the “Set condition for calculation (Landslide)” window (Fig. 45) to complete this step.

Setting Time Steps and Other Conditions

For the example simple slope simulation, time steps and other conditions are set as illustrated in Figs. 49 and 50.

Output Settings

The simulation of the rainfall-induced simple slope landslide described in this section is long (80 h). The output settings

Select profiles for drawing ellipsoidal sliding surface

The current editing section
 Main section Sub section

Select longitudinal section	X	Y
Starting point of a section	180.000	450.000
Ending point of a section	180.000	150.000

Input with a mouse

[Layout of ellipsoid]
 Length of shorter axis of ellipsoid = 98.74
 Length of longer axis of ellipsoid = 184.38
 Length of depth axis of ellipsoid = 112.04
 The maximum vertical depth of sliding surface (m) = 35.06
 The volume of landslide mass along this section ($\times 10^3$ m³) = 196.5

Coordinates are expressed as Xs along the crossing section, Ys along the longitudinal section, Zs along the vertical direction.

Decision of passing point of the sliding surface on the longitudinal section is automatically calculated from the elevation of the ground surface.
 > When giving X coordinate of passing point and inputting Y coordinate as 'x'
 > When clicking the Left-side of mouse during pushing [Shift] key.

Resize option the Control
 Plane figure Longitudinal section Crossing section Section scale is same

Sliding surface on the longitudinal section	Y	Z
Passing point A	35.000	110.000
Passing point B	165.000	50.000
Center of ellipsoid on the longitudinal section	200.000	160.000

Longitudinal section Input with a mouse

Sliding surface on the cross section	X	Z
Passing point C	120.000	95.000
Passing Point D (Cross point of 2 sections)	180.000	65.872
Center of ellipsoid on the crossing section	180.000	160.000

Crossing section Input with a mouse

Fig. 42 Select profile to draw ellipsoidal sliding surface for the simple slope

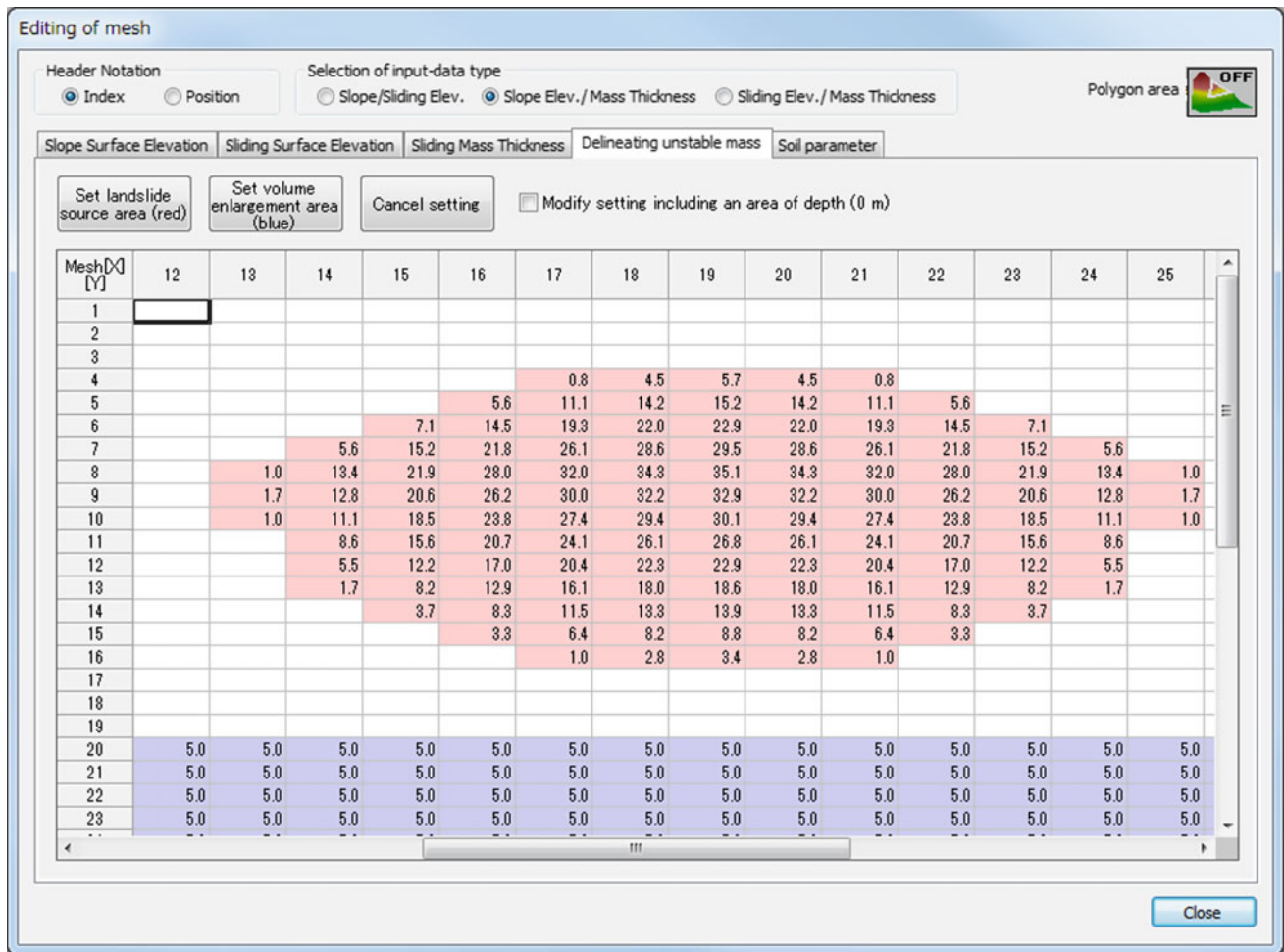


Fig. 43 Assignment of source and volume enlargement areas of the simple slope landslide example

Table 4 Soil parameter used in the simulation of the simple slope landslide

Soil Parameters	Normal value	Value used in simulation
Lateral pressure ratio ($k = \sigma_H/\sigma_v$)	0.30–0.60	0.45
Friction coefficient inside landslide mass ($\tan\phi_i$)	0.36–0.58	0.47
Friction coefficient during motion at sliding surface ($\tan\phi_m$)	0.46–0.70	0.58
Steady state shear resistance (τ_{ss} , kPa)	5–50	27.5
Rate of excess pore pressure generation (B_{ss})	0.0–1.0	0.8
Peak friction coefficient at sliding surface ($\tan\phi_p$)	0.65–0.78	0.72
Peak cohesion at sliding surface (c , kPa)	10–100	50
Unit weight of the mass (γ_r , kN/m ³)		20

selected for this example are shown in Fig. 51. The “Maximum step” is set to 20,000, the “Minimum time for simulation” and the “Drawing period of landslide trigger” are set to 57 h and 10 steps, respectively. The calculation time is set to display in hours. Other items were kept as default values.

Starting the Simulation and Displaying the Results

The results of the simulation of the rainfall-induced landslide on the simple slope are shown on Fig. 52. The cyan line represents the landslide mass in the source area, while the pink line shows the calculated sliding mass distribution area.

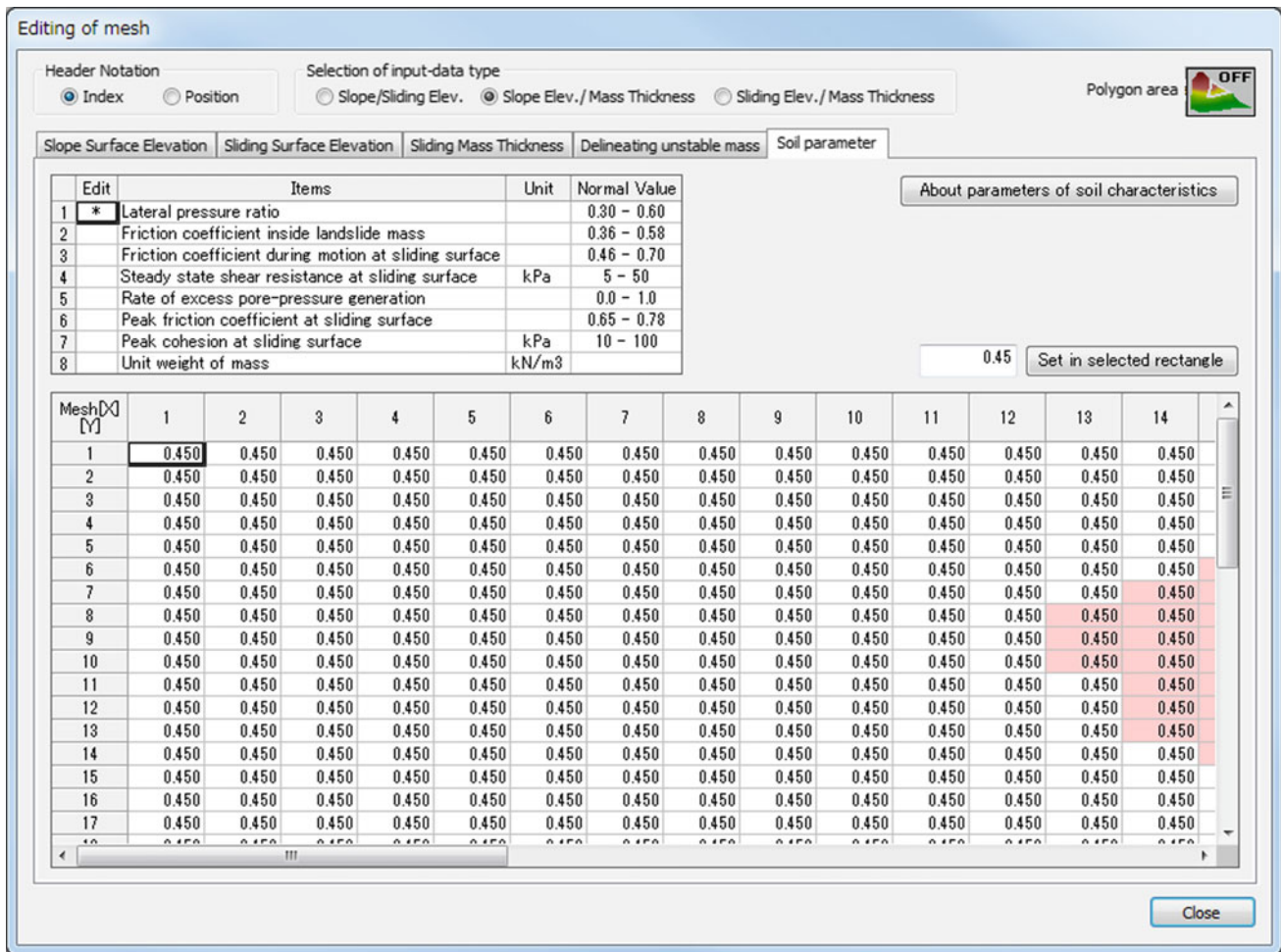


Fig. 44 Setting soil parameters (lateral pressure ratios) for the simple slope example

When the pore pressure ratio reaches 0.36 at 58 h 30 m 00 s, the failure initiates from the middle of the landslide source area. When the pore pressure ratio reaches 0.42 at 68 h 15 m 08 s, the entire landslide mass has formed and starts to move down at a speed of 20.6 m/s. At 68 h 15 m 42 s, the landslide mass has stopped moving and is completely deposited.

4.1.6 Simulation of an Earthquake-Induced Landslide on the Simple Slope

The second example is to simulate an earthquake-induced landslide on the designed simple slope. Since the slope geometry is the same as the rainfall-induced landslide simulation discussed previously, the steps associated with the creation of the geometry, entering soil properties, and other parameters are not described again. The reader is referred to previous sections in Sect. 4.

The 2008 Iwate-Miyagi earthquake record (MYG004), which triggered the Aratozawa landslides (Sassa 2014a; b) is used as the triggering factor for this example. The earthquake record is illustrated in Fig. 53.

A tutorial of the steps involved in performing this simulation is also included with this paper. This video tutorial is titled, “16. Earthquake-Induced Simple Slope Landslide Tutorial.” Interested users may opt to follow the steps in that video in lieu of the instructions provided below.

Setting Simulation Conditions

In LS-RAPID, click on the “Conditions for calculation” button from Section “2: Calculation condition” in the “Flow” Panel. This will open the “Set condition for calculation (Landslide)” window. A screenshot of this window was provided in Fig. 45.

Select the “Seismic simulation” radial button in the “Fullmode simulation (Initiation + Motion + Expansion)” section to conduct the earthquake-induced landslide simulation on the simple slope geometry, as shown in Fig. 54. In this example, pore pressure is not considered as part of the triggering mechanism. Click on the “Edition of seismic waveform” button in the “Method to give a graph of seismic coefficient” section to input the seismic data including name,

Table 5 Data of Aranyake rainfall and pore pressure ratios used in the simulation

Date (yyyy/m/d hh:mm)	Time (min)	Hourly rainfall (mm/hour)	Pore pressure ratio (ru)
2016/5/14 22:00	0	0	0.00
2016/5/14 23:00	60	0.75	0.00
2016/5/15 0:00	120	0.25	0.00
2016/5/15 1:00	180	0	0.00
2016/5/15 2:00	240	0.25	0.00
2016/5/15 3:00	300	2.5	0.00
2016/5/15 4:00	360	4.25	0.01
2016/5/15 5:00	420	1	0.01
2016/5/15 6:00	480	0.5	0.01
2016/5/15 7:00	540	1.5	0.01
2016/5/15 8:00	600	6.75	0.02
2016/5/15 9:00	660	13.25	0.03
2016/5/15 10:00	720	13.75	0.04
2016/5/15 11:00	780	20.75	0.06
2016/5/15 12:00	840	15.5	0.08
2016/5/15 13:00	900	13.5	0.09
2016/5/15 14:00	960	7.25	0.10
2016/5/15 15:00	1020	8.25	0.11
2016/5/15 16:00	1080	6.75	0.11
2016/5/15 17:00	1140	8.75	0.12
2016/5/15 18:00	1200	5.75	0.13
2016/5/15 19:00	1260	11.5	0.14
2016/5/15 20:00	1320	14.75	0.15
2016/5/15 21:00	1380	12.25	0.16
2016/5/15 22:00	1440	14.5	0.18
2016/5/15 23:00	1500	21.5	0.20
2016/5/16 0:00	1560	23.25	0.22
2016/5/16 1:00	1620	21.75	0.24
2016/5/16 2:00	1680	8.5	0.25
2016/5/16 3:00	1740	3.75	0.25
2016/5/16 4:00	1800	2.25	0.25
2016/5/16 5:00	1860	5	0.26
2016/5/16 6:00	1920	1	0.26
2016/5/16 7:00	1980	4.5	0.26
2016/5/16 8:00	2040	9.5	0.27
2016/5/16 9:00	2100	5.25	0.28
2016/5/16 10:00	2160	2.25	0.28
2016/5/16 11:00	2220	0.75	0.28
2016/5/16 12:00	2280	5.5	0.28
2016/5/16 13:00	2340	5.75	0.29
2016/5/16 14:00	2400	3	0.29

(continued)

Table 5 (continued)

Date (yyyy/m/d hh:mm)	Time (min)	Hourly rainfall (mm/hour)	Pore pressure ratio (ru)
2016/5/16 15:00	2460	2.5	0.29
2016/5/16 16:00	2520	2	0.29
2016/5/16 17:00	2580	3	0.30
2016/5/16 18:00	2640	3.5	0.30
2016/5/16 19:00	2700	2.5	0.30
2016/5/16 20:00	2760	5.25	0.31
2016/5/16 21:00	2820	10.75	0.32
2016/5/16 22:00	2880	2.75	0.32
2016/5/16 23:00	2940	11.5	0.33
2016/5/17 0:00	3000	7	0.34
2016/5/17 1:00	3060	1.5	0.34
2016/5/17 2:00	3120	0	0.34
2016/5/17 3:00	3180	0.5	0.34
2016/5/17 4:00	3240	9.5	0.34
2016/5/17 5:00	3300	9.75	0.35
2016/5/17 6:00	3360	4	0.36
2016/5/17 7:00	3420	1.75	0.36
2016/5/17 8:00	3480	4	0.36
2016/5/17 9:00	3540	0.25	0.36
2016/5/17 10:00	3600	0	0.36
2016/5/17 11:00	3660	0.75	0.36
2016/5/17 12:00	3720	21	0.38
2016/5/17 13:00	3780	2	0.38
2016/5/17 14:00	3840	26.75	0.41
2016/5/17 15:00	3900	4.25	0.41
2016/5/17 16:00	3960	4.25	0.41
2016/5/17 17:00	4020	4.75	0.42
2016/5/17 18:00	4080	2.25	0.42
2016/5/17 19:00	4140	2	0.42
2016/5/17 20:00	4200	2.25	0.42
2016/5/17 21:00	4260	1.25	0.42
2016/5/17 22:00	4320	1.5	0.42
2016/5/17 23:00	4380	1	0.42
2016/5/18 0:00	4440	0.25	0.42
2016/5/18 1:00	4500	0	0.42
2016/5/18 2:00	4560	0	0.42
2016/5/18 3:00	4620	0	0.42
2016/5/18 4:00	4680	0	0.42
2016/5/18 5:00	4740	0	0.42
2016/5/18 6:00	4800	0	0.42

Set condition for calculation (Landslide)

Condition of simulation

Motion simulation

Motion simulation

Fullmode simulation (Initiation + Motion + Expansion)

Normal simulation

Seismic simulation

Rainfall simulation Edition of rainfall

Method to give a graph of pore pressure ratio (ru)

Time to start (sec)

Static Fluctuate a value Min = Duration = (sec)

Max = Max Time = (sec)

Survey Edition of ru

Parameters of condition for strength reduction

Source area (by travel length) From (DL) To (DU) (mm)

Except source area (by depth of mass) $\Delta hcr =$ (m)

Setting of the submergence calculation

Calculate submergence

Level of the water surface (m)

Unit weight of water (γ_w) (kN/m³)

Graph preview

Method to give a graph of seismic coefficient

Time to start (sec)

Static Cyclic Seismic Edition of seismic waveform

Static / Cyclic parameter setting

Horizontal seismic coefficient (Kh)

Directional coefficient X-direction coefficient Kx =

Y-direction coefficient Ky =

Horizontal coefficient Kh =

Seismic direction $\theta_s =$ (deg)

Vertical seismic coefficient (Kv) Vertical coefficient Kv =

Substitute the direction of landslide profile

Frequency / MaxTime / Duration

Fluctuate a value

Duration = (sec) Hz =

Max Time = (sec) Total Cycle (N) =

Kmax Cycle (N) =

Seismic parameter setting

Kx max = EW Acc(gal)/980 x (times)

Ky max = NS Acc(gal)/980 x (times)

Kv max = UD Acc(gal)/980 x (times)

Set Parameters Cancel

Fig. 45 Set conditions for rainfall-induced landslide simulation

time and corresponding values of the acceleration for three directions, as illustrated in Fig. 55. In the “Seismic parameter setting” subsection (Fig. 54), the maximum seismic coefficients in the x-, y-, and vertical directions are kept the same as the values in the 2008 Iwate-Miyagi earthquake record (Fig. 53).

Once the seismic parameters for the simulation have been entered, their graphs can be previewed as shown in Fig. 56. Click the “Set Parameters” button in the bottom right corner of the “Set condition for calculation (Landslide)” window (Fig. 54) to complete this step.

Setting Time Steps and Other Conditions

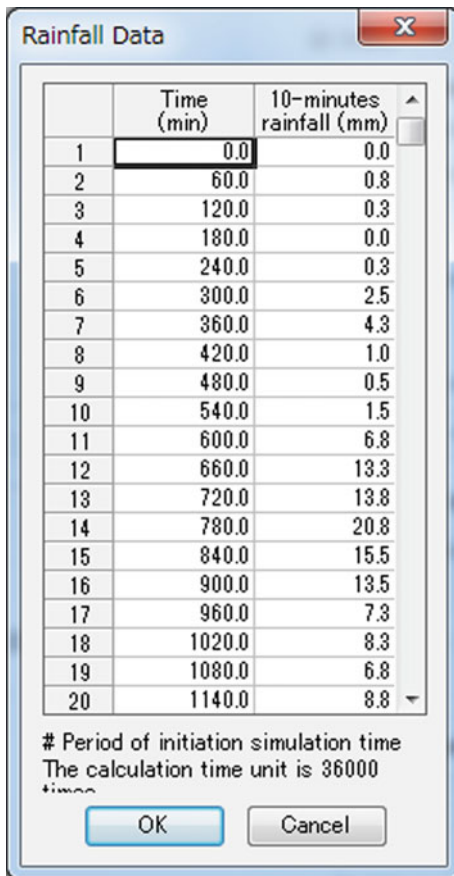
The time steps and other conditions of the earthquake-induced landslide simulation are set similar to the case of the rainfall-induced landslide simulation described earlier in this chapter. The values in this simulation can be found in Figs. 49 and 50.

Output Settings

Since the duration of the seismic waveform is about 300 s and the main shock occurs around 10 s, the output settings are selected to clearly show and cover the entire simulation process. As shown in Fig. 57, the “Maximum step” is set to 20,000, the “Drawing interval” is 0.1 s, and the “Minimum time for simulation” is 300 s. The “Drawing period of landslide trigger” is set to 10 s, which corresponds to the period of the main shock. The calculation time is select to display in seconds. All other items are kept at their default values.

Starting the Simulation and Displaying the Results

The results from the simulation of the earthquake-induced landslide on the simple slope are shown in Fig. 58. When the main shock of the earthquake strikes the slope at 4.3 s, failure initiates in the middle part of the source area. At 11.3 s, the entire landslide mass has formed and begins



	Time (min)	10-minutes rainfall (mm)
1	0.0	0.0
2	60.0	0.8
3	120.0	0.3
4	180.0	0.0
5	240.0	0.3
6	300.0	2.5
7	360.0	4.3
8	420.0	1.0
9	480.0	0.5
10	540.0	1.5
11	600.0	6.8
12	660.0	13.3
13	720.0	13.8
14	780.0	20.8
15	840.0	15.5
16	900.0	13.5
17	960.0	7.3
18	1020.0	8.3
19	1080.0	6.8
20	1140.0	8.8

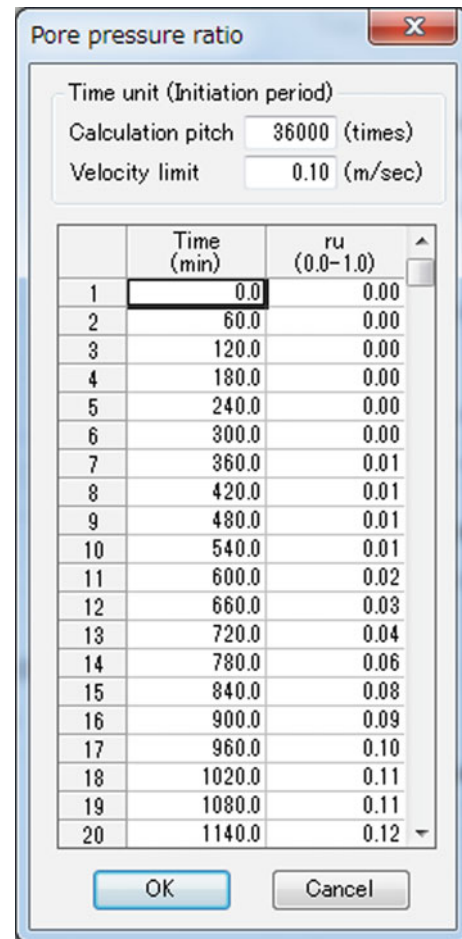
Period of initiation simulation time
The calculation time unit is 36000
times

Fig. 46 “Rainfall data” window with data from Aranayake rainfall provided in Table 5

moving downward at a velocity of 12.7 m/s during the earthquake shaking. At 56.4 s, the landslide mass has stopped moving. As before, in Fig. 58, the cyan line represents the landslide mass in the source area, while the red line shows the area of sliding mass distribution.

4.2 Application of LS-RAPID to Rain-Induced Landslides: A Case Study of Atami Debris Flow

From 1 to 3 July 2021, extreme rainfall occurred in the Atami District, Shizuoka Prefecture, Japan causing a catastrophic debris flow on 3 July 2021. A geological map with the debris flow is shown in Fig. 59. The Atami debris flow claimed 27 lives with one missing, three injuries and destroyed 54 houses, as of 10 February 2022 (Shizuoka Prefecture 2022). On 17 January 2022, International Consortium on Landslides (ICL) researchers investigated the landslide area. A sample was taken from immediately behind the exposed scar as shown in Fig. 59 and sent to the Kyoto ICL-SATREPS office for ring shear tests. As shown in



	Time (min)	ru (0.0-1.0)
1	0.0	0.00
2	60.0	0.00
3	120.0	0.00
4	180.0	0.00
5	240.0	0.00
6	300.0	0.00
7	360.0	0.01
8	420.0	0.01
9	480.0	0.01
10	540.0	0.01
11	600.0	0.02
12	660.0	0.03
13	720.0	0.04
14	780.0	0.06
15	840.0	0.08
16	900.0	0.09
17	960.0	0.10
18	1020.0	0.11
19	1080.0	0.11
20	1140.0	0.12

Fig. 47 “Pore pressure ratio” window with pore pressure ratio data from simple slope example

Fig. 59, the underlying geology of the source area is andesite to basaltic andesite lava and pyroclastic deposits, which are products of Hakone Volcano (Oikawa and Ishizuka 2011).

4.2.1 Ring-Shear Simulator

Speed control test is used as a basic soil test to obtain soil parameters. In undrained speed control tests, normal and shear stresses in the steady-state condition can be obtained as the mobilized and peak friction angles.

Slow shear speeds should be used in the tests on the fine-grained materials that have low coefficients of permeability and generate pore pressures slowly. The normal and shear stresses acting on the potential sliding surface were reproduced in the shear box. An undrained speed control test was conducted at a normal stress of 200 kPa, which corresponded to the landslide initiation in the field. Normal stress was increased to 200 kPa at a rate of $\Delta\sigma = 0.5$ kPa/s in the drained condition. After consolidation, the shear box was then changed into the undrained condition and shear displacement was increased at a rate of 0.01 mm/s.

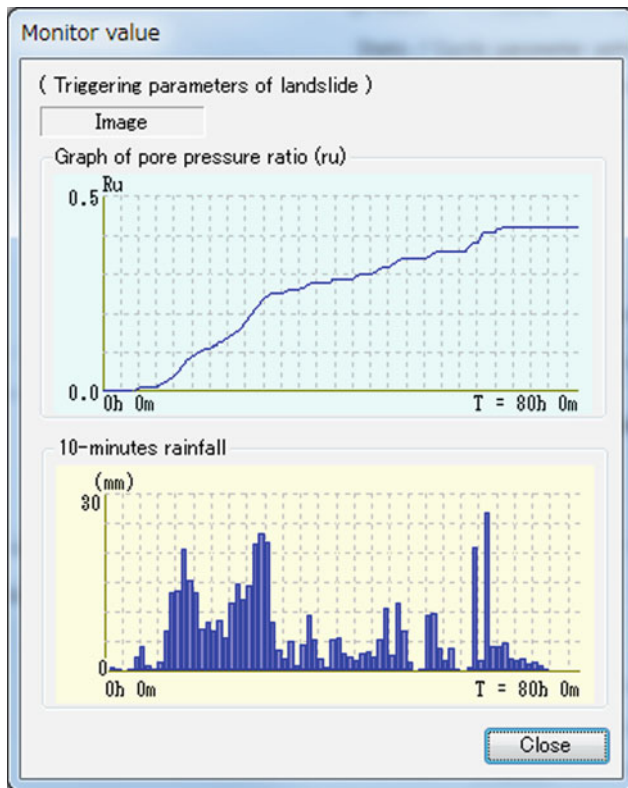


Fig. 48 (Bottom) Rainfall and (top) pore pressure ratio used as triggering factor for rainfall-induced landslide simulation

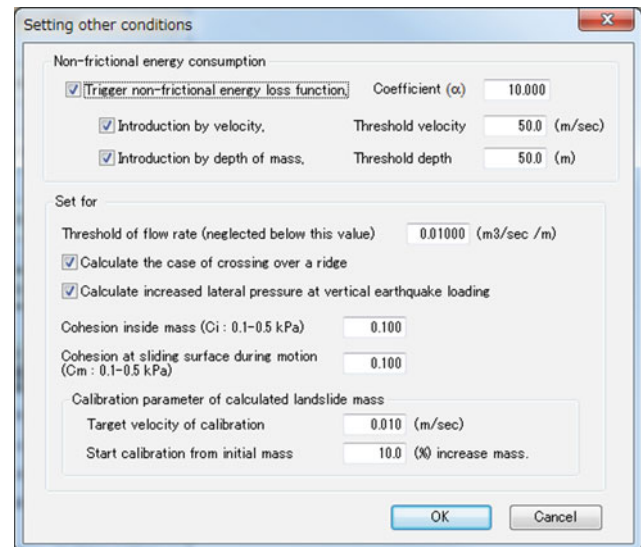


Fig. 50 Screenshot of setting other conditions window for rainfall-induced landslide simulation

Figure 60 presents the stress paths and time series data for the Atami sample. The measured steady-state shear resistance was 30 kPa. The friction angle of the peak failure line and friction during motion were 30.5° and 16.4°, respectively.

4.2.2 SLIDE Model

To simulate the landslides caused by rainfall, the pore-water pressure ratio needs to be calculated. Based on the research of Montarasio and Valentino (2008) and Liao et al. (2010), the SLIDE model can be used to calculate the pore water pressure from the rainfall intensity using Eq. 22:

$$r_u = \frac{\Delta U}{\sigma} = \frac{m H \gamma_n \cos^2 \beta}{H \gamma_s \cos^2 \beta} = \frac{m \gamma_n}{\gamma_s} \quad (22)$$

Changes in the ratio of the groundwater layer to the soil layer pressure (m) is calculated by:

$$\begin{cases} m_1 = 0 \\ O_t = K_t (\sin \beta) m_t H (\cos \beta) \Delta t \\ \Delta m_t = \frac{(I_t - O_t)}{n H (1 - S_r)} \\ m_{t+1} = m_t + \Delta m_t \end{cases} \quad (23)$$

where t is time, Δt is the time interval, m₁ is the initial value of m, m_t is calculated at each time-step, O_t represents the water outlet of a finite portion of a slope of finite length L, I_t is rainfall intensity, K_t is the significance of a global drainage

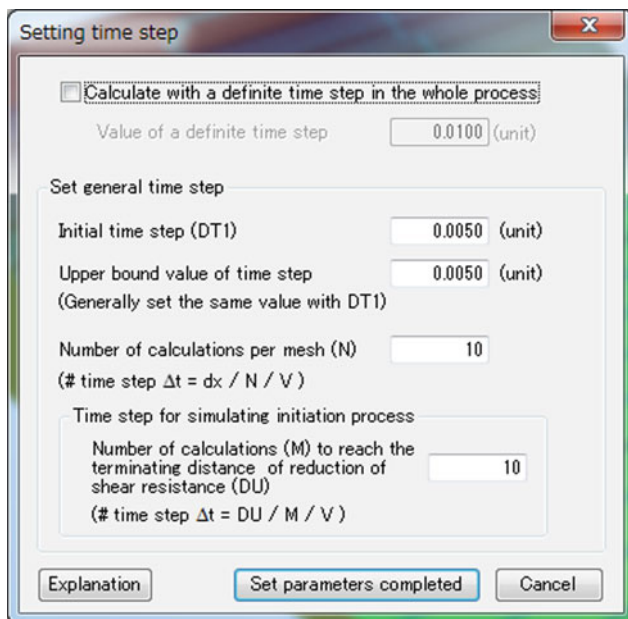
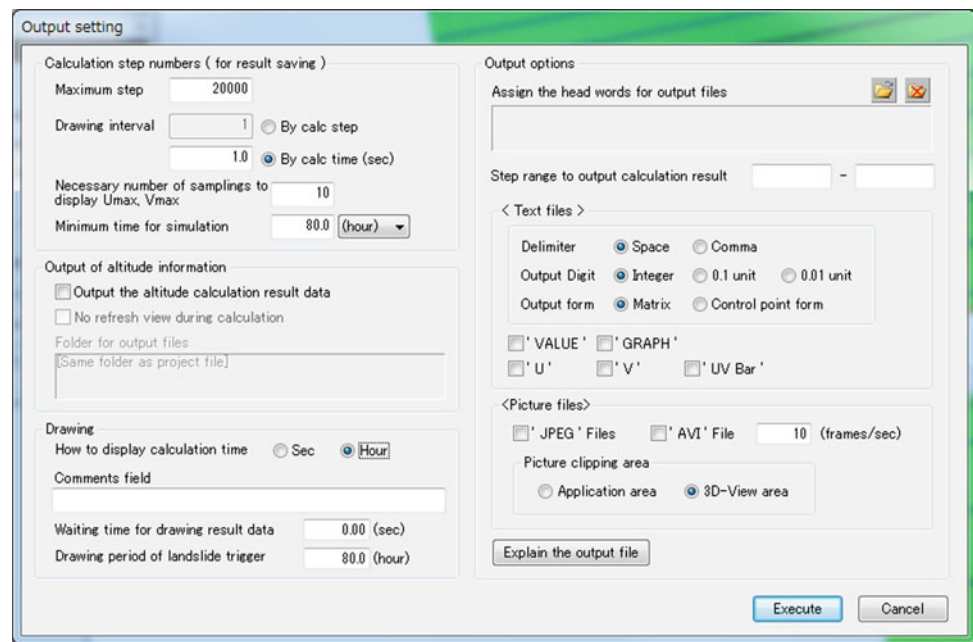


Fig. 49 Screenshot of setting time step window

Fig. 51 Output settings for rainfall-induced landslide on the simple slope



capability due to both the intrinsic soil permeability and the presence of numerous preferential down-flow ways, H is the landslide depth, n is porosity, β is the slope angle and S_r is the degree of saturation. These variables are schematically shown in Fig. 61 for the infiltration of water into an infinite slope model.

4.2.3 Application of LS-RAPID and SLIDE Model to the Atami Debris Flow

The pre-failure and post-failure digital elevation models, ortho-photos were published by Geospatial Information Authority of Japan and the Shizuoka Prefecture. The option “Slope/Sliding Elev.” is used to provide the slope surface elevation and the sliding surface elevation in this example. The steps to establish the simulation area of Atami debris flow are provided below and in the video titled, “17. Atami Debris Flow.”

Simulation Area

Click the “Simulation area” button in Section “1: Mesh” on the left side of LS-RAPID “Flow” panel, shown in Fig. 9.

The minimum and maximum values of the x- and y- coordinates associated with the calculation area as shown in Fig. 62. The pitches for both the x- and y-direction were set to 5 m. Click the “OK” button to complete the settings for the simulation area.

Editing Mesh

In this step, the pre- and post-failure digital elevation models from Shizuoka Prefecture are exported to mesh data and inputted in LS-RAPID. The details of the steps are provided below:

1. Slope Surface Elevation
 - a. Click the “Editing of mesh” button in the “Flow” panel and select the “Slope/Sliding” option in the “Selection of input-data type” section and chose the “Slope Surface Elevation” tab as illustrated in Fig. 63.
 - b. Once the pre-failure elevation data has been copied into to “Slope Surface Elevation” tab, the simulation area will be displayed in the viewing pane of LS-RAPID, as shown in Fig. 64.

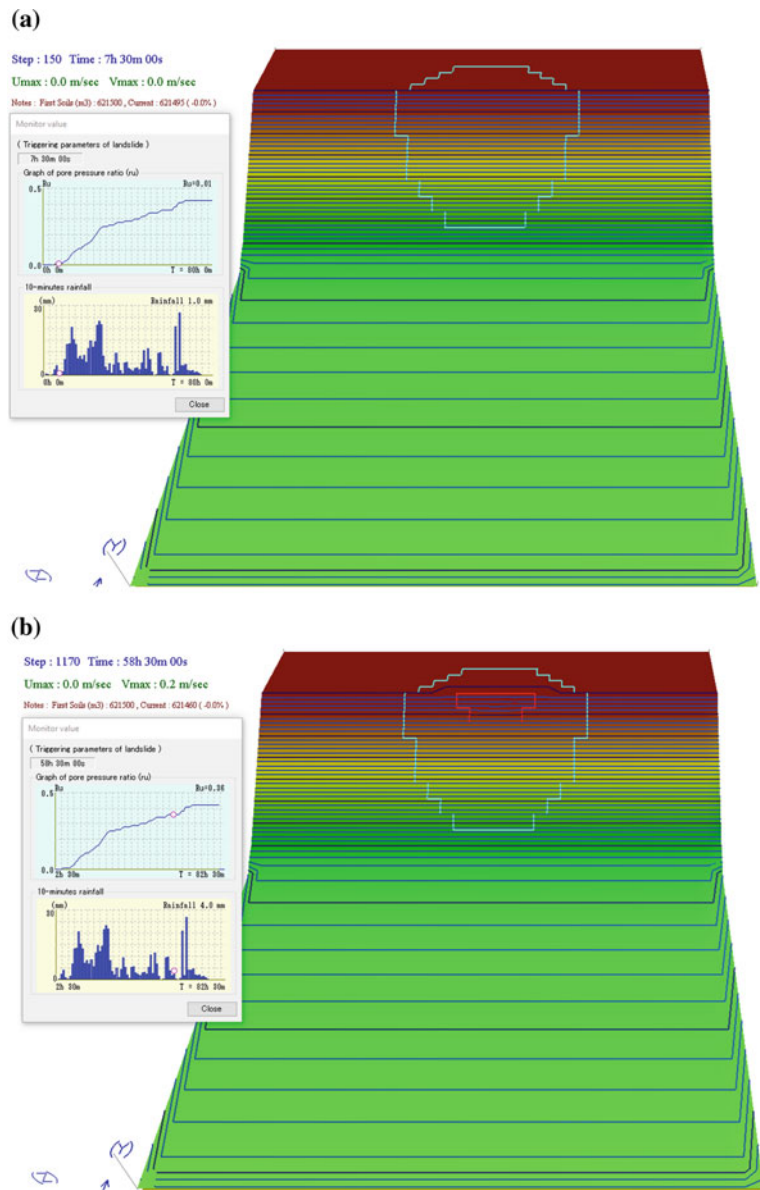


Fig. 52 Results of the simulation of the rainfall-induced landslide on the simple slope at **a** 7 h 30 m 00 s, **b** 58 h 30 m 00 s, **c** 68 h 15 m 08 s, and **d** 68 h 15 m 42 s from the start of rainfall

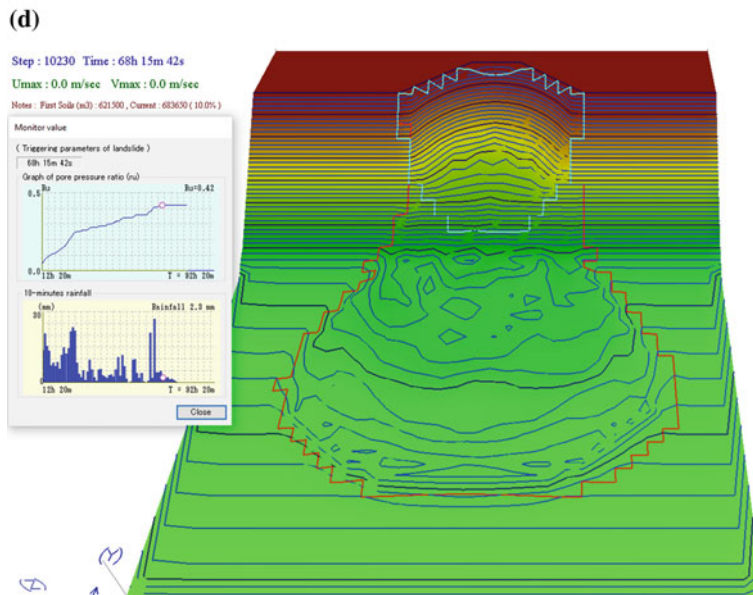
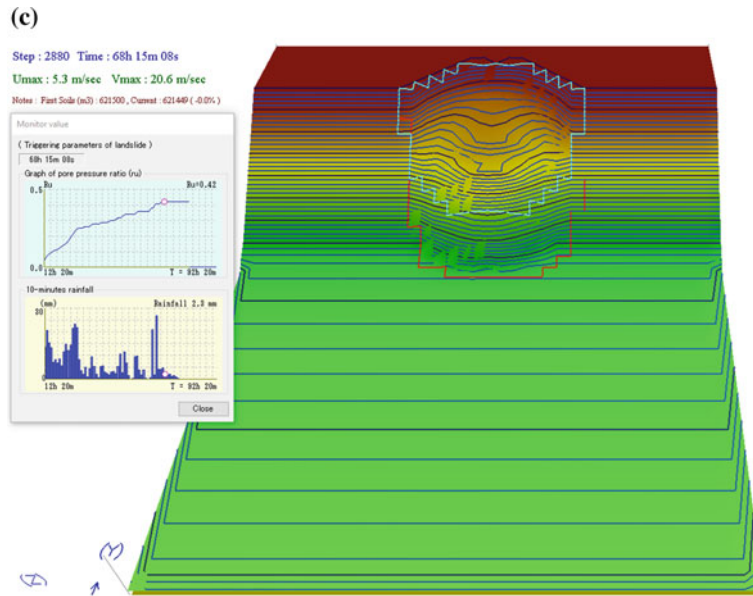


Fig. 52 (continued)

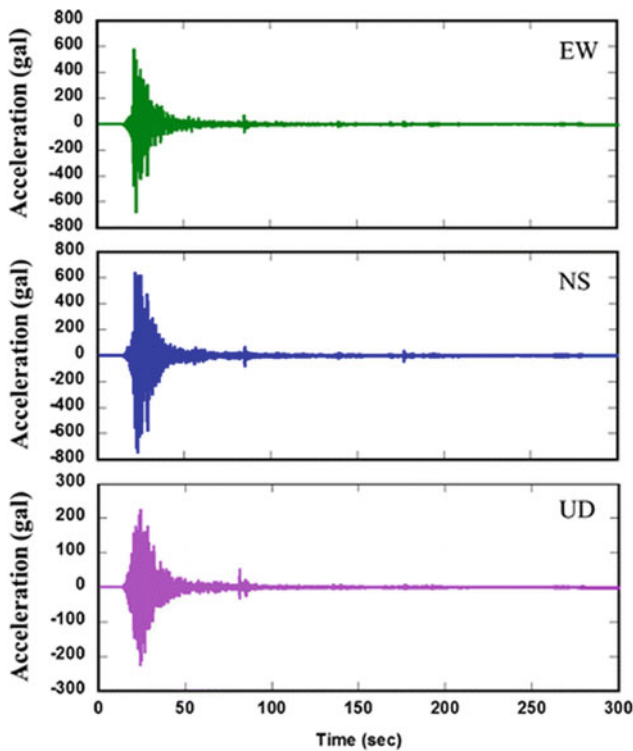


Fig. 53 2008 Iwate-Miyagi earthquake record (MYG004) used as the triggering seismic parameter

2. Sliding Surface Elevation

- a. The same steps used for the slope surface elevation are used for “Sliding Surface Elevation.” Specifically, click the “Editing of mesh” button in the “Flow” panel and chose the “Sliding Surface Elevation” tab in Fig. 65.
- b. Copy the post-failure elevation data into to “Sliding Surface Elevation” tab. The simulation area (after the landslide) will be displayed in LS-RAPID, as shown in Fig. 66.

Background Images in Simulation

To easily identify the landslide source area, an ortho-photo obtained from an unmanned aerial vehicle (UAV) is set as the background image. The steps to set this background image are presented below.

1. From the “File(F)” menu, click “Setting background image file” (Fig. 34). The “Setting background image file” window shown in the Fig. 67 will open.
2. Click the “Select file” button from the “Background image file” section to select the ortho-photo. In this example, the coordinate of ortho-photo is the same as the

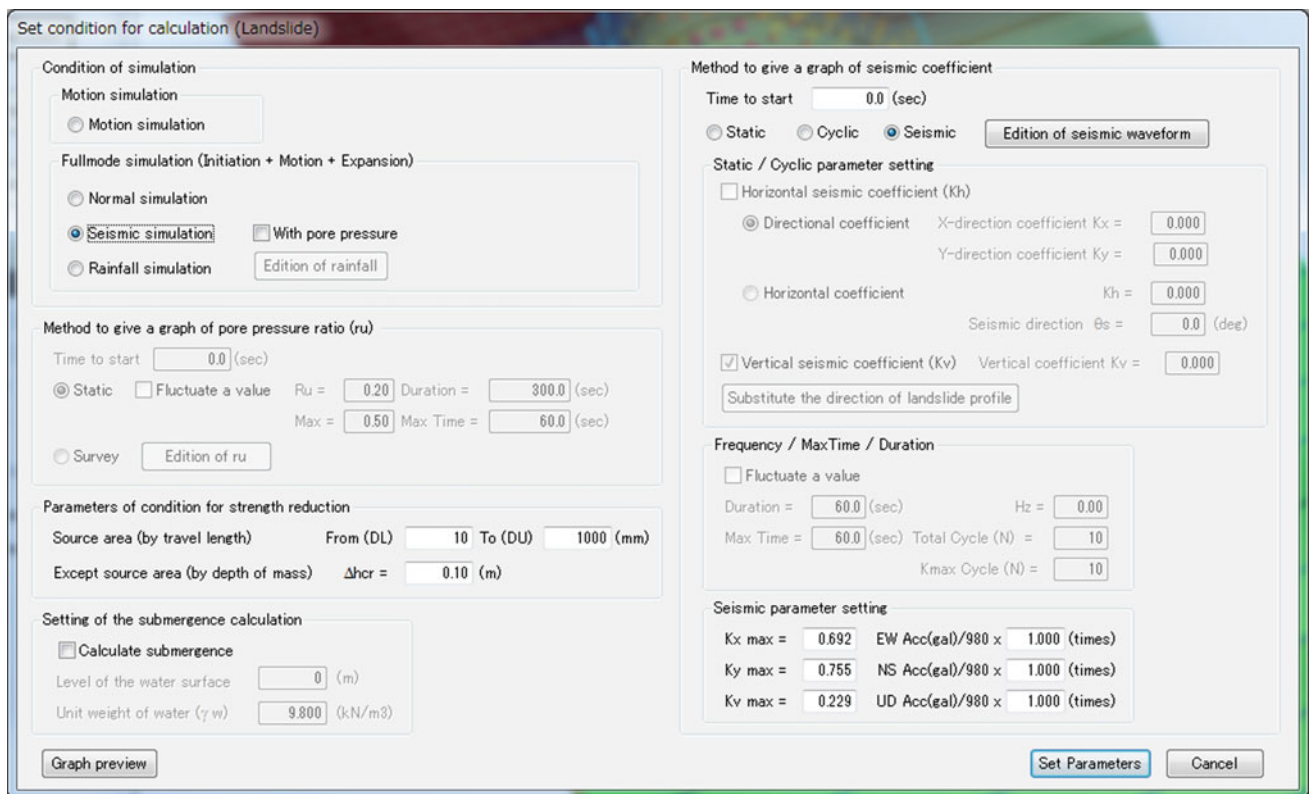


Fig. 54 Set conditions for earthquake-induced landslide simulation

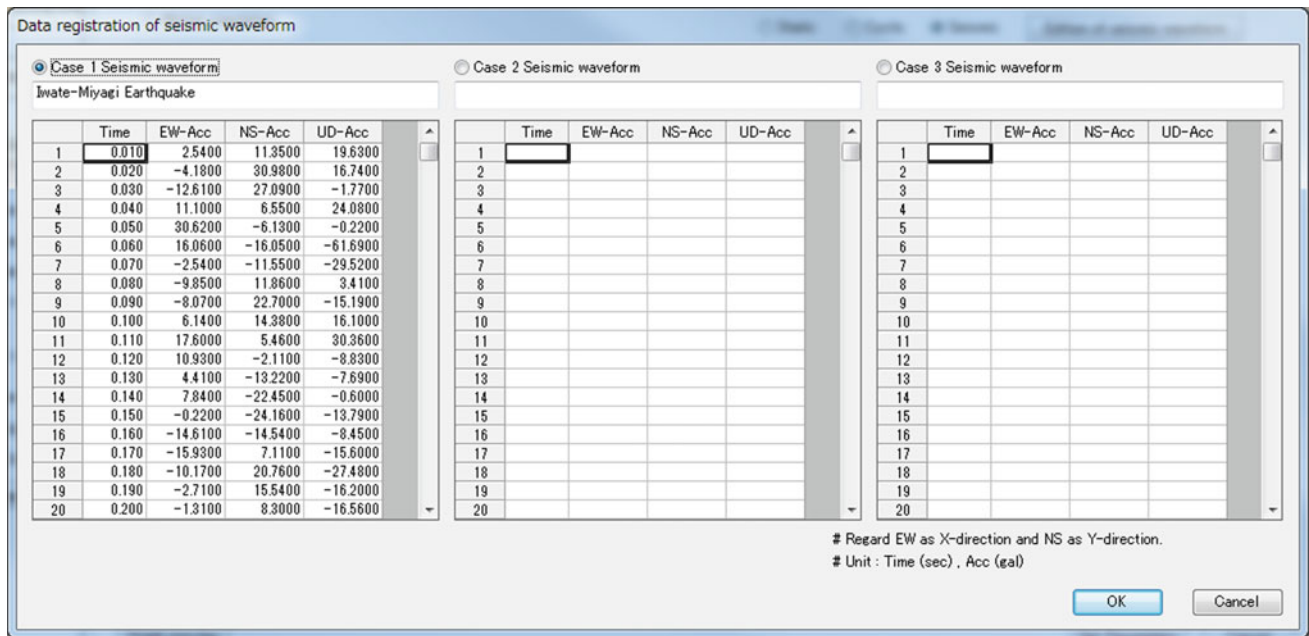


Fig. 55 Seismic data of the 2008 Iwate-Miyagi earthquake as Inputted into the “data registration of seismic waveform” window

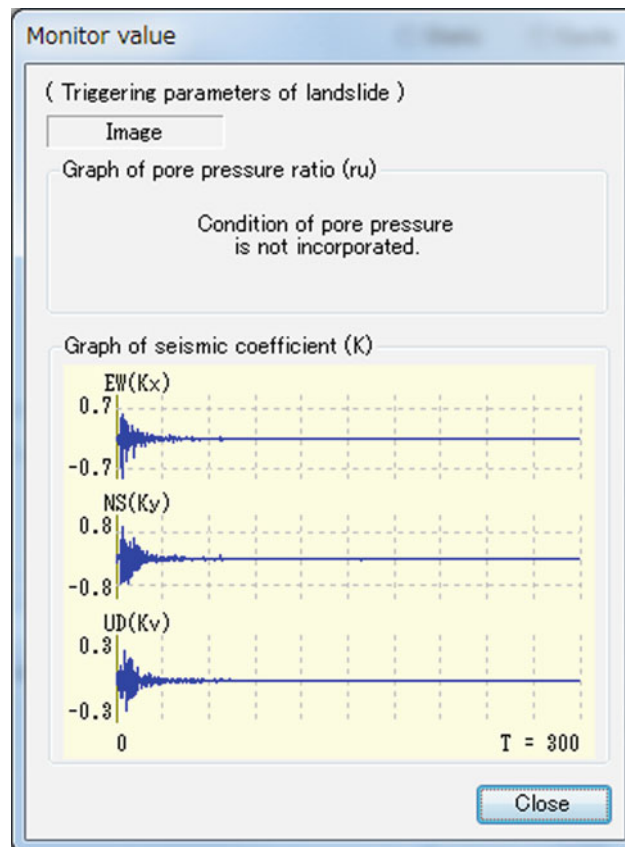
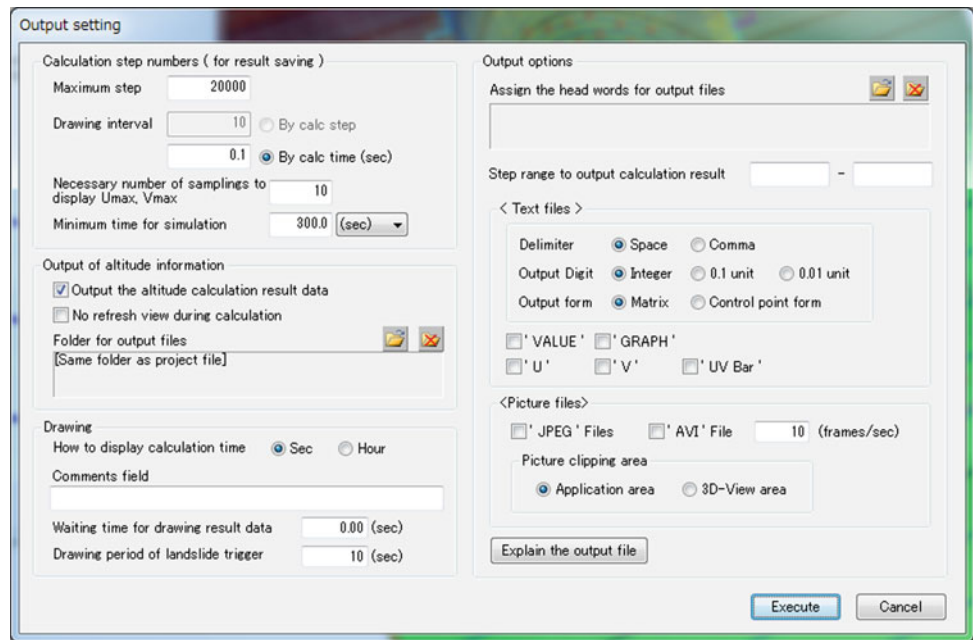


Fig. 56 Graph of seismic coefficient used as the triggering factor for earthquake-induced landslide simulation

Fig. 57 Output settings for earthquake-induced landslide on the simple slope



- simulation area. Therefore, the “Coordinates relation” are defined by Pos. A at (0,0), Pos. B at (1024,0), Pos. C at (1024,1024) and Pos. D at (0,1024) as shown in Fig. 67.
3. Click “Ok.” The result with the ortho-photo as the background in the topography is shown in Fig. 68.

Delineating Unstable Mass

Based on the elevation change, the Atami debris flow consists of a source area, an enlargement area and a flow area. The steps to set these areas are summarized below:

1. Selecting the “Delineating unstable mass” button in Section “1: Mesh” in the “Flow” panel. Click the “Polygon area” to draw the source area. The source area is shown in yellow in Fig. 69. After selecting the source area, click the “Set landslide source area (red).” This will cause the color of the cells is change to red as shown in Fig. 69.
2. Select the “Add” button to create area 2 representing the enlargement area from the toe of source area to the residential area. After selecting the enlargement area, click the “Set enlargement volume source area (blue).” The color of the cells will change to blue, as shown in Fig. 70.

3. Select the “Add” button to create area 3 for the flow area from the toe of enlargement area to the Atami Sea. This is based on the Atami flow path shown in Fig. 59.

Input Soil Parameters

The parameters used in the computer simulation are listed in Table 6. These are based on the ring shear test results when available. Otherwise, the parameters are based on assumptions by the authors.

As shown in Fig. 25, click on the “Soil parameters” button from Section “2: Calculation condition” of the “Flow” panel. The “Editing of mesh” window from Fig. 71 will be displayed. Figure 71 shows an example input for the lateral pressure ratio.

4.2.4 Triggering Factors

The amount of heavy rainfall needed to trigger the Atami debris flow was calculated using a SLIDE model. This pore-water pressure ratio was then inputted into LS-RAPID as a graph of the triggering factor. The rainfall data and pore water pressure ratio from SLIDE model is shown in Fig. 72.

In the LS-RAPID program, to open the “Set condition for calculation (Landslide)” window, click the “Conditions for

Fig. 58 Simulation results for earthquake-induced landslide on the simple slope at **a** 0.4 s, **b** 4.3 s, **c** 11.3 s, and **d** 56.4 s from the start of earthquake

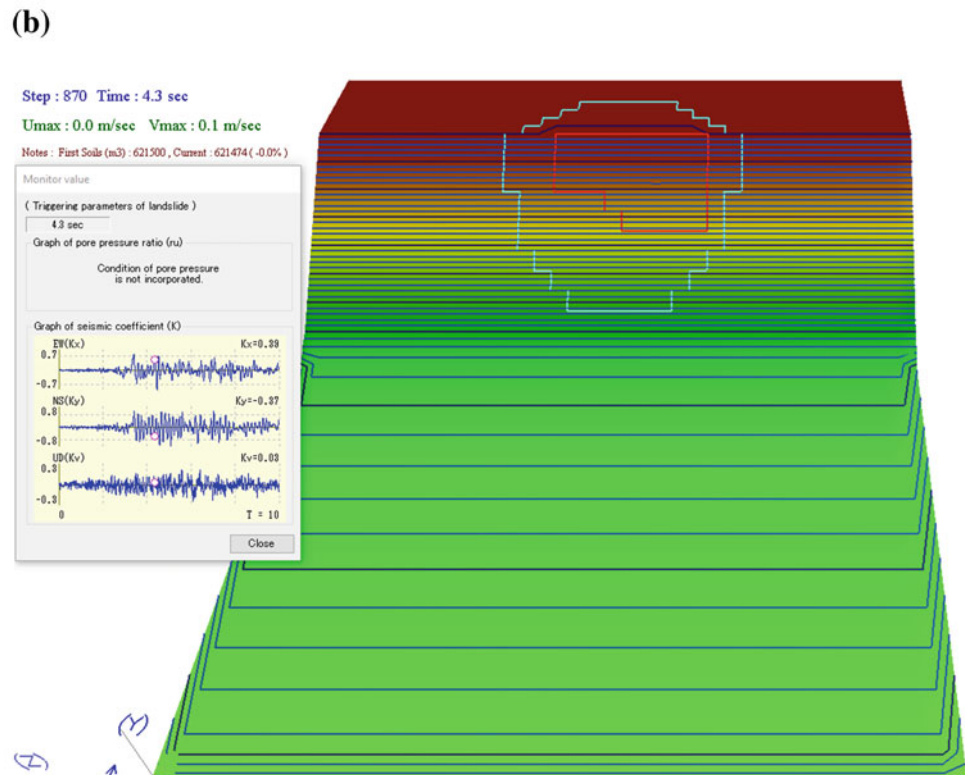
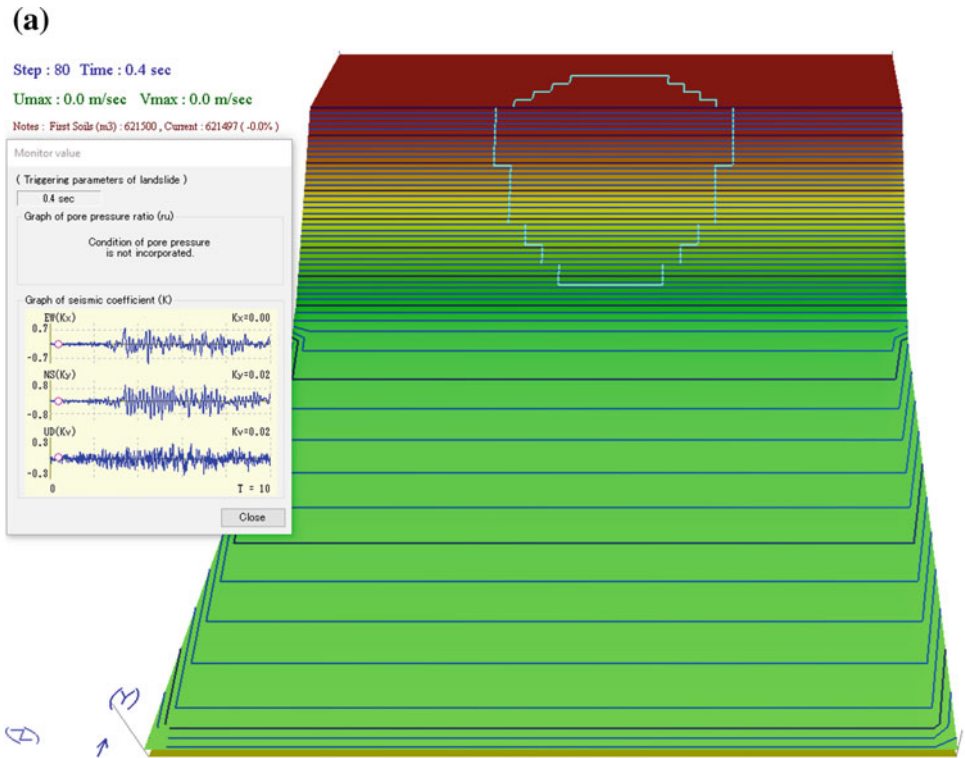
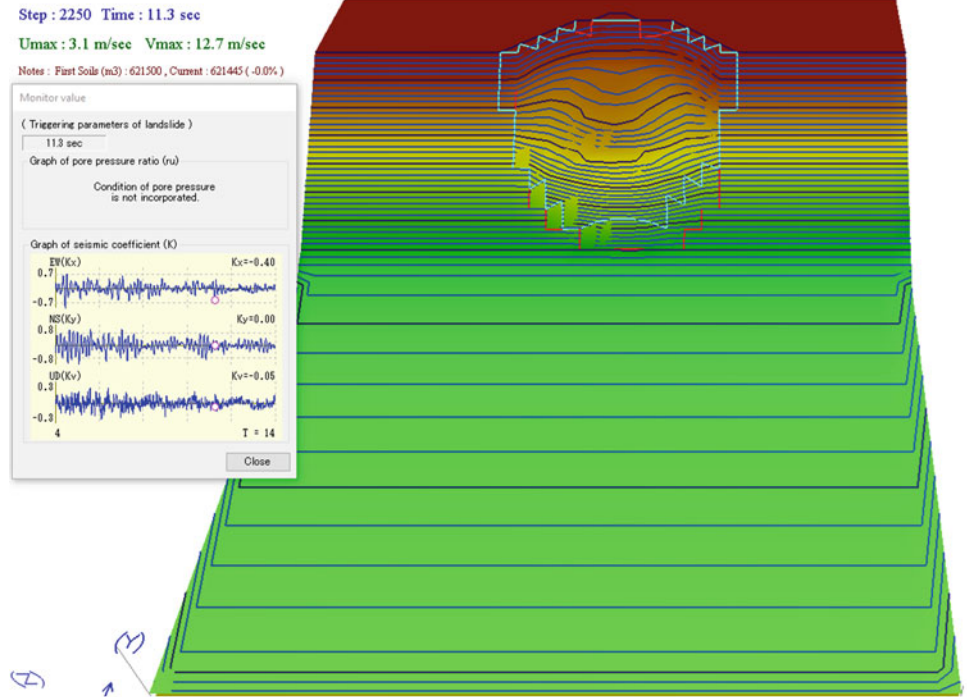
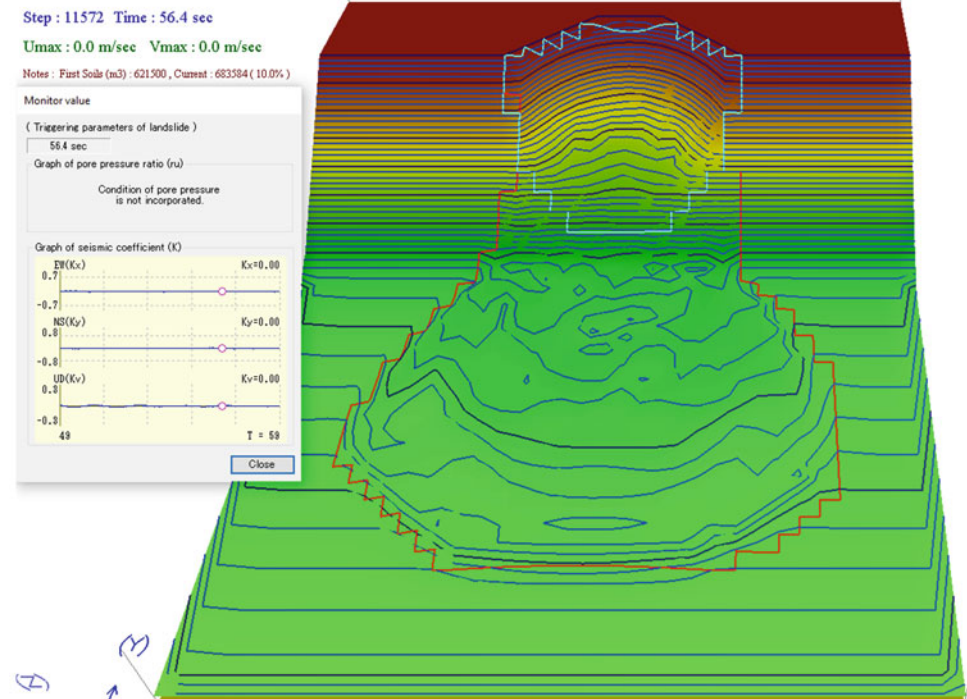


Fig. 58 (continued)

(c)



(d)



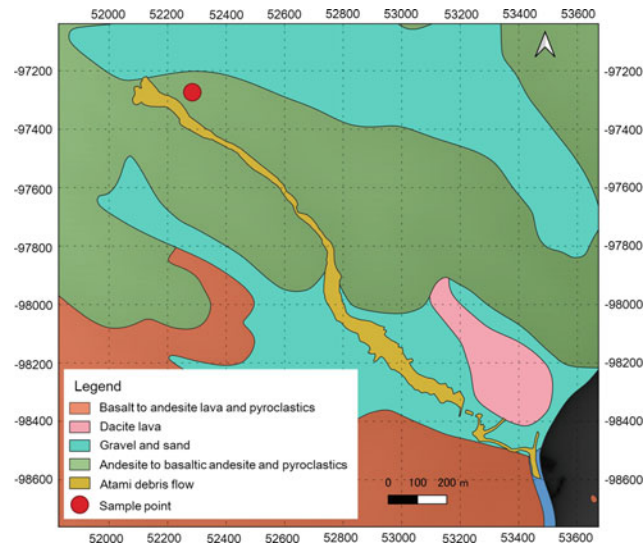


Fig. 59 Geological map of study area (this map is made based on the data from the geological survey of Japan and the geospatial information authority of Japan)

calculation” button from Section “2: Calculation condition” in the “Flow” Panel (Fig. 45). Next, select the “Rainfall simulation” radial button to conduct a rainfall-induced landslide simulation and click on the “Edition of rainfall” button to input the rainfall intensities.

The input of the rainfall intensities used in this example is shown in Fig. 73. For the “Method to give a graph of pore pressure ratio (ru),” select the “Survey” radial button and click on the “Edition of ru ” button to input the pore water pressure data in the “Pore pressure ratio” window, as depicted in Fig. 74. To reduce the computation time for the landslide simulation, the “Calculation pitch” and the “Velocity limit” are set as 120,000 times and 0.01 m/s, respectively. The pore pressure ratios from the SLIDE model are entered into the “Pore pressure ratio” window. After entering the rainfall data and pore water pressure ratios, their corresponding graphs could be previewed, as shown in Fig. 75. Click the “Set Parameters” button in the bottom right corner of the “Set condition for calculation (Landslide)” window from Fig. 45 to complete this step.

4.2.5 Setting Time Steps and Other Conditions

The settings for the time steps and other conditions are the same as those described previously in Sect. 4.1.5.

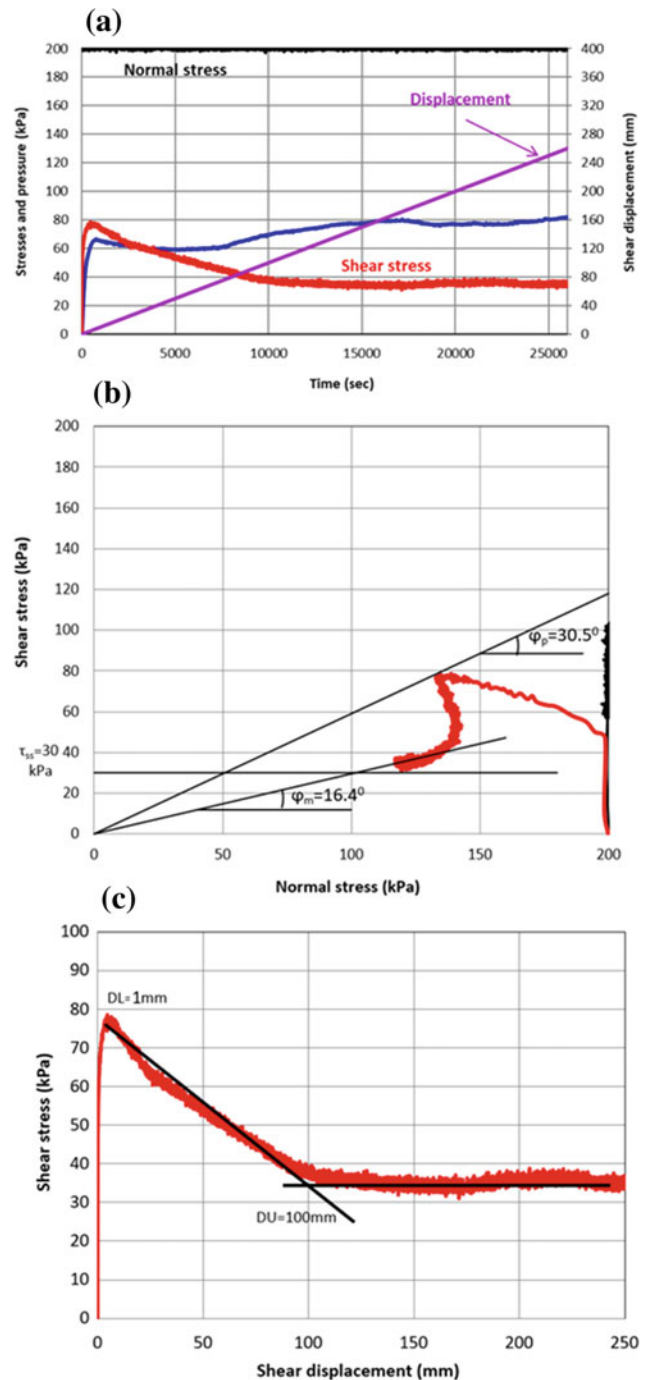


Fig. 60 Undrained speed stress-controlled test on the Atami sample: **a** time series data, **b** stress path and **c** relationship between shear stress and shear displacement

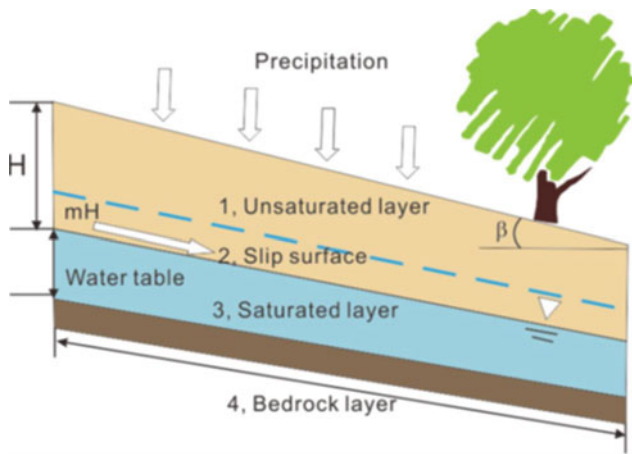


Fig. 61 Schematic illustration of water infiltration in an infinite slope (from Liao et al. 2010)

Output Settings

A long simulation containing 72 h of rainfall is conducted for this rainfall-induced landslide. Thus, the output settings are selected as those shown in Fig. 51. Specifically, the “Maximum step” is set to 1,000,000, the “Minimum time for simulation” and the “Drawing period of landslide trigger” are set to 72 h and 1 s, respectively. The calculation time is selected to display in hours. All other settings are kept at their default values.

4.2.6 Starting the Simulation and Displaying the Results

The results from simulation of the Atami debris flow from LS-RAPID are displayed in Fig. 76. The aqua polygon

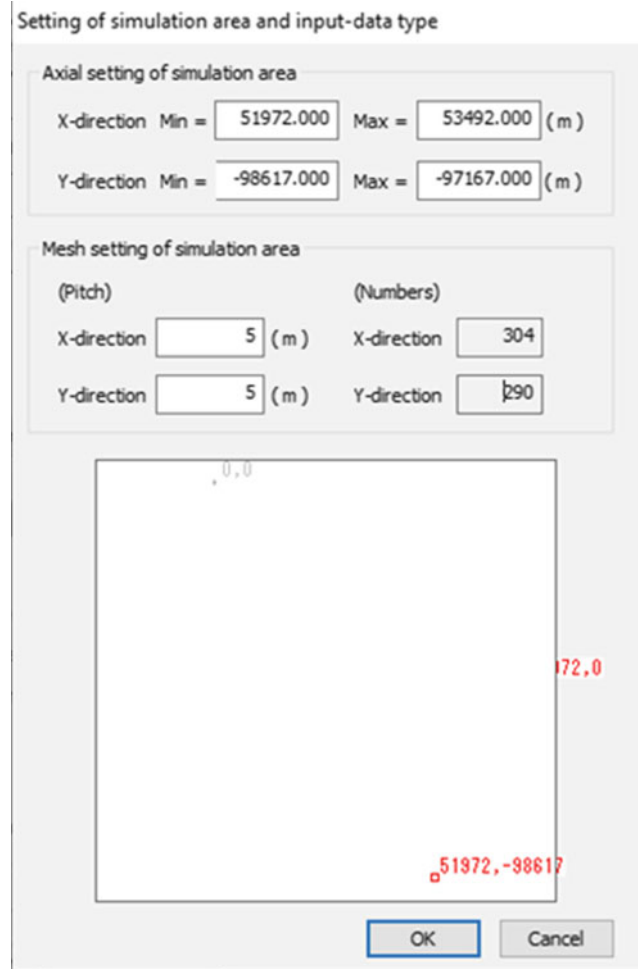


Fig. 62 Setting of simulation area for Atami debris flow

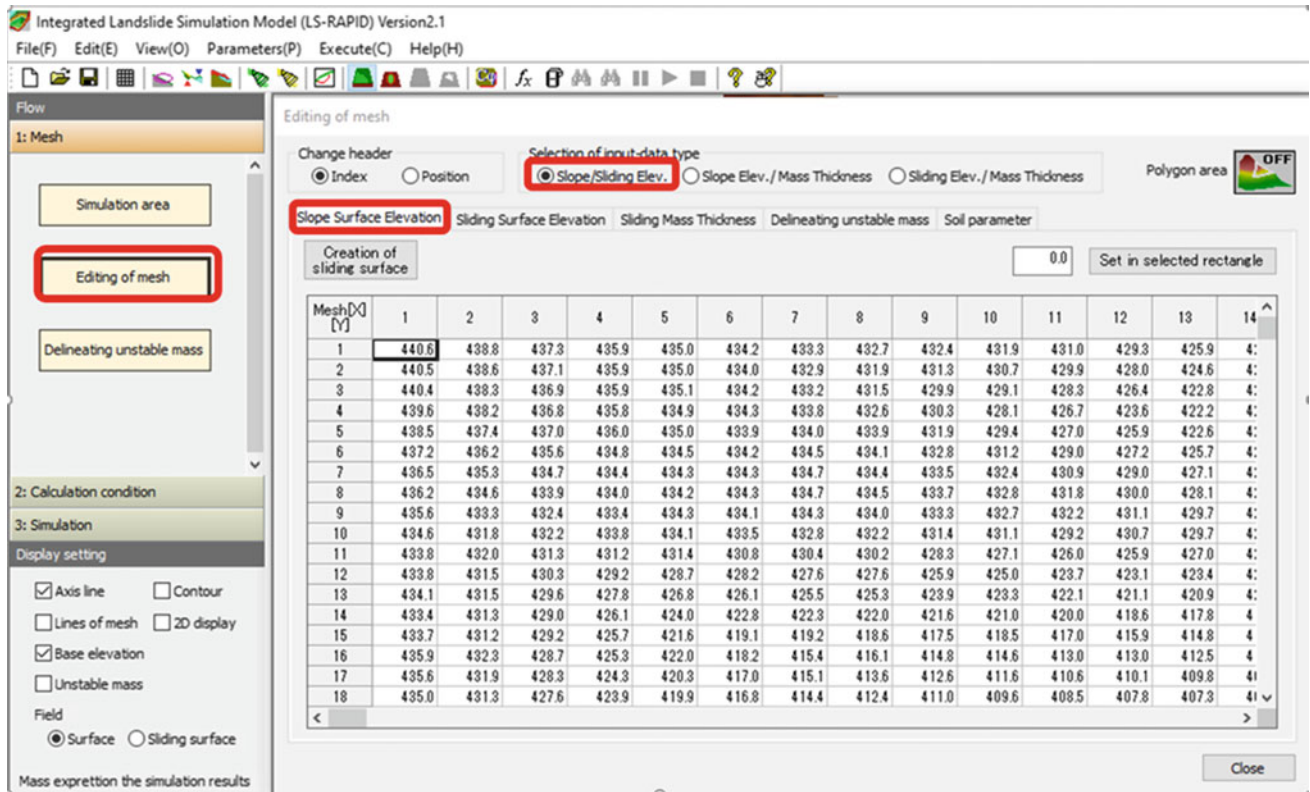


Fig. 63 Inputting pre-failure digital elevation model (slope surface elevation)

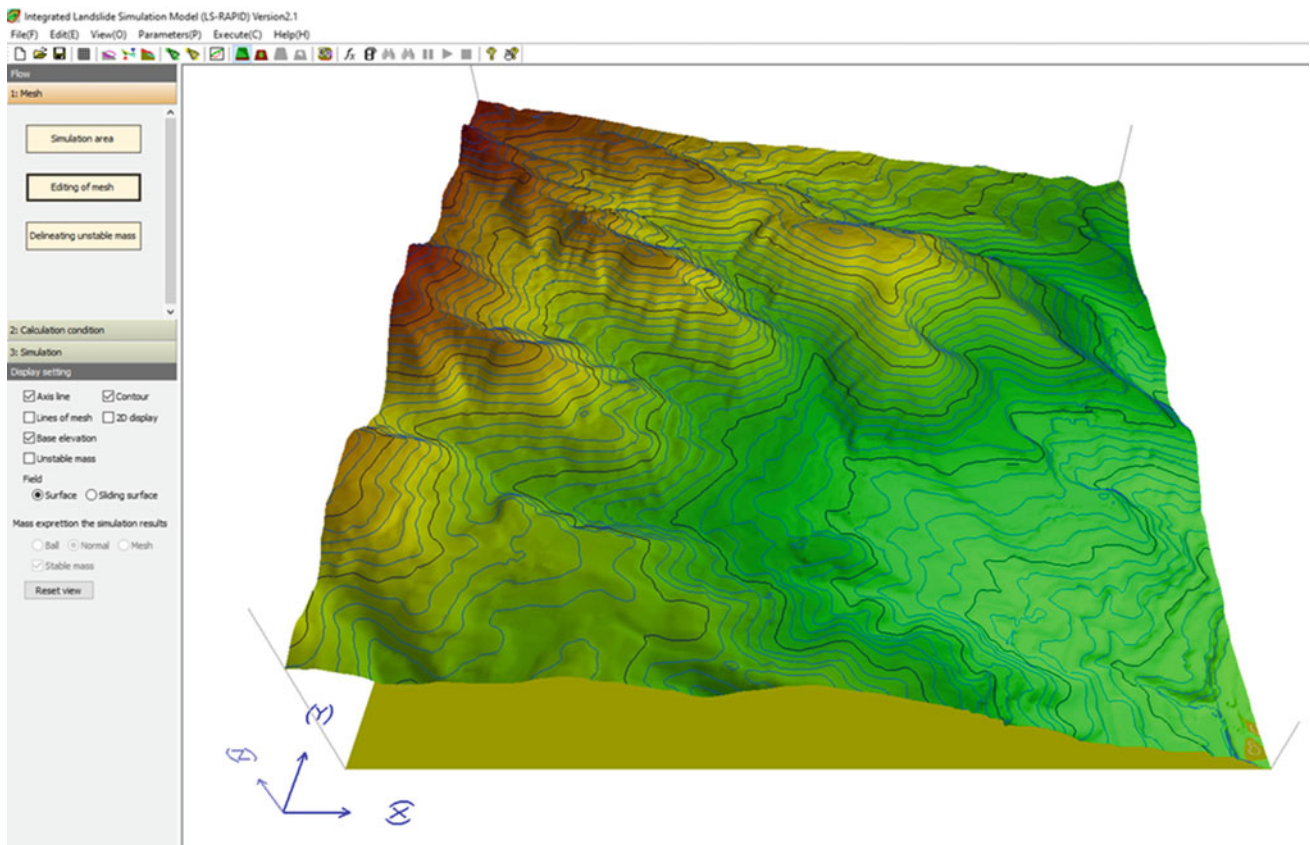


Fig. 64 Atami topography (before the landslide) with contours

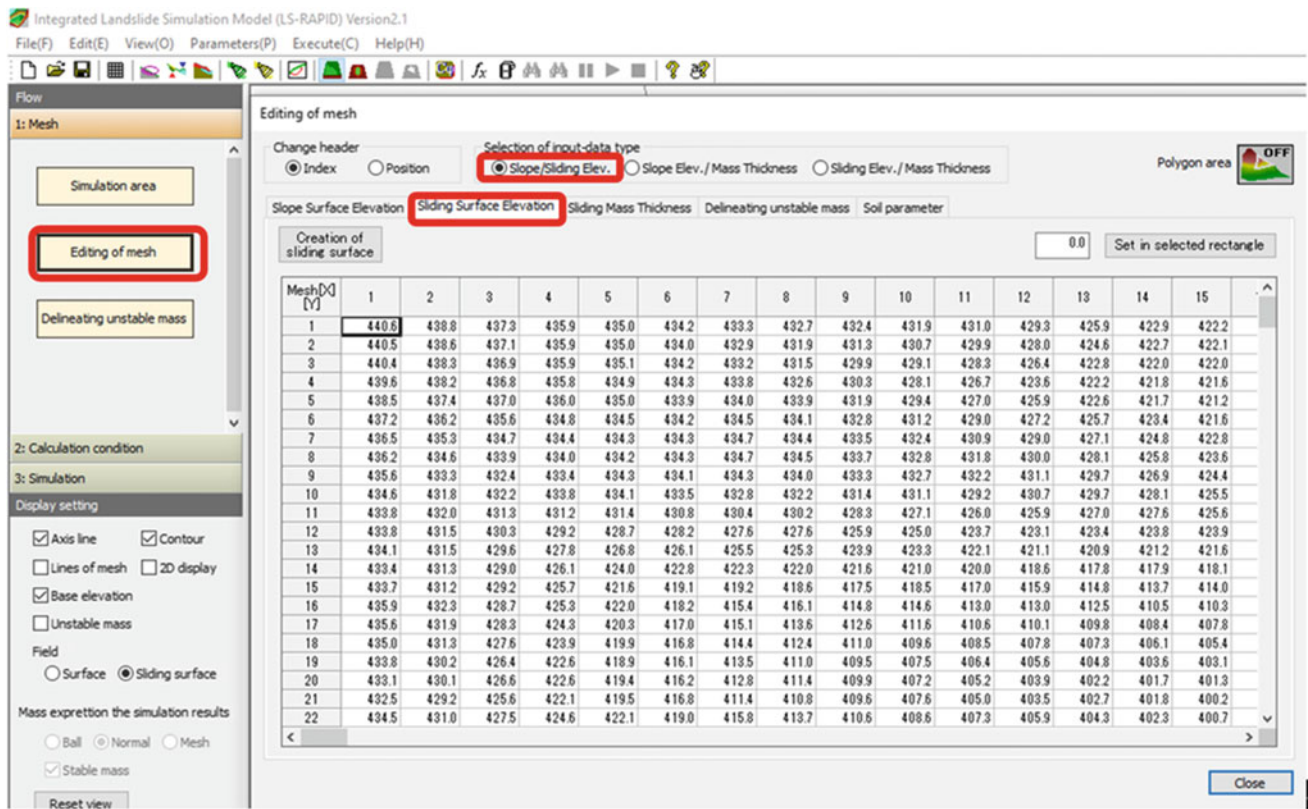


Fig. 65 Inputting post-failure digital elevation model (sliding surface elevation)

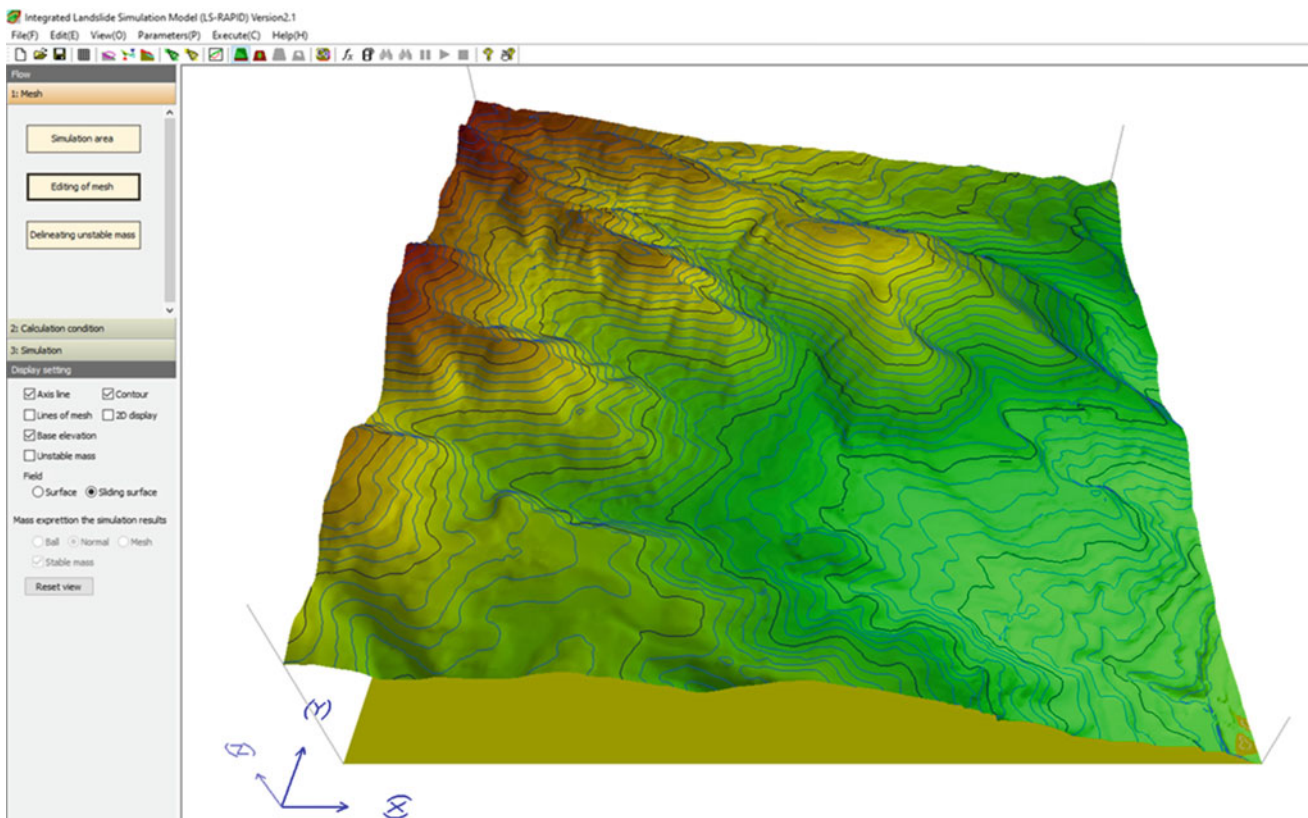


Fig. 66 Atami topography (after the landslide) with contours

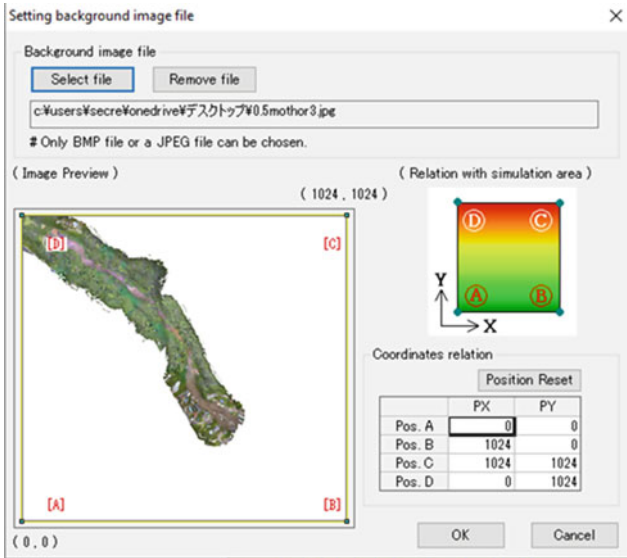


Fig. 67 Setting of an ortho-photo for the Atami debris flow

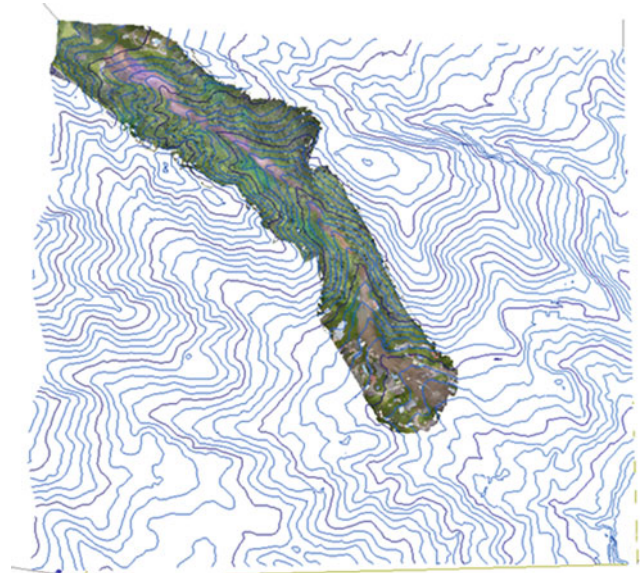


Fig. 68 Topography with background image file

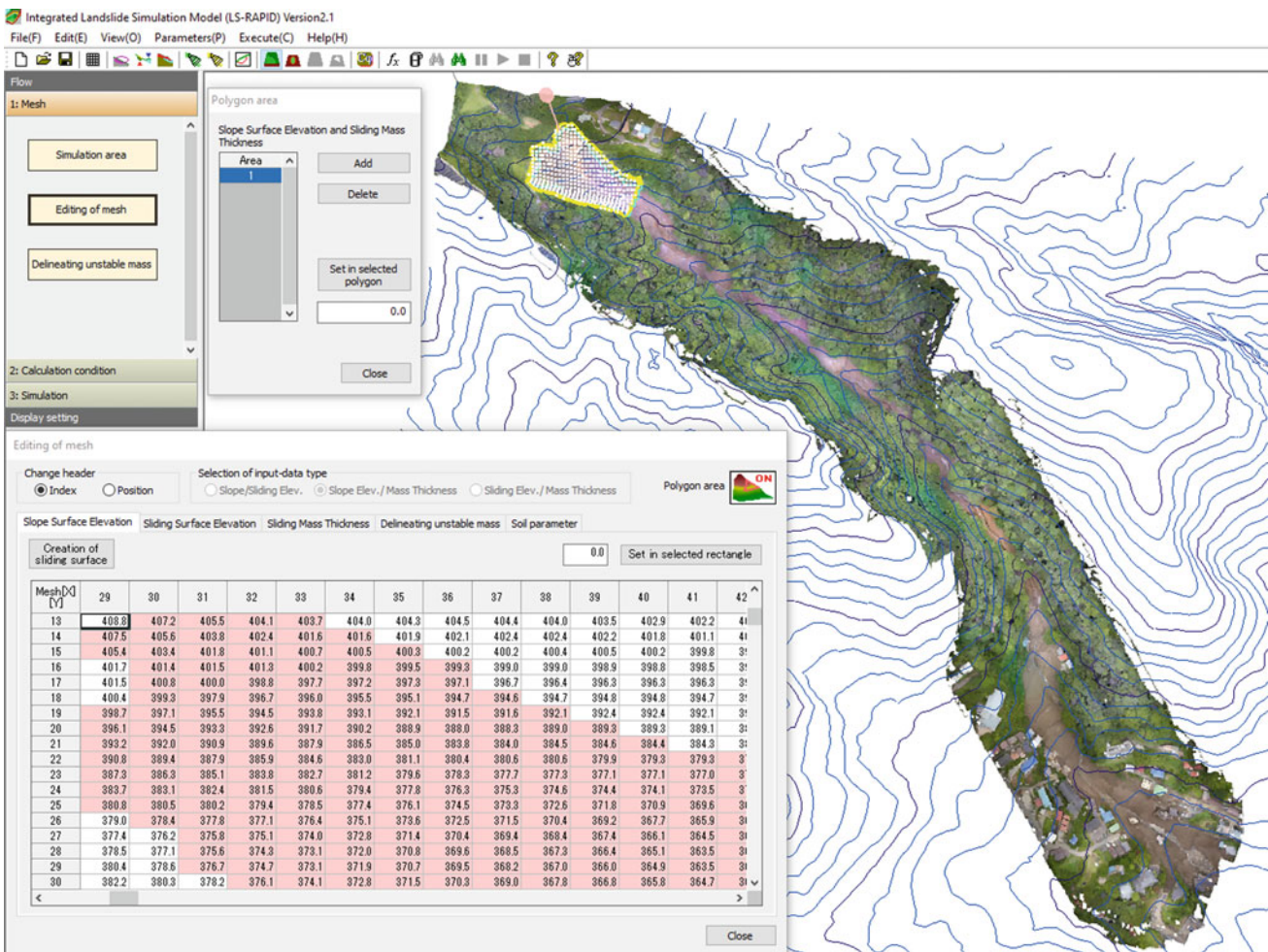


Fig. 69 Setting landslide source area

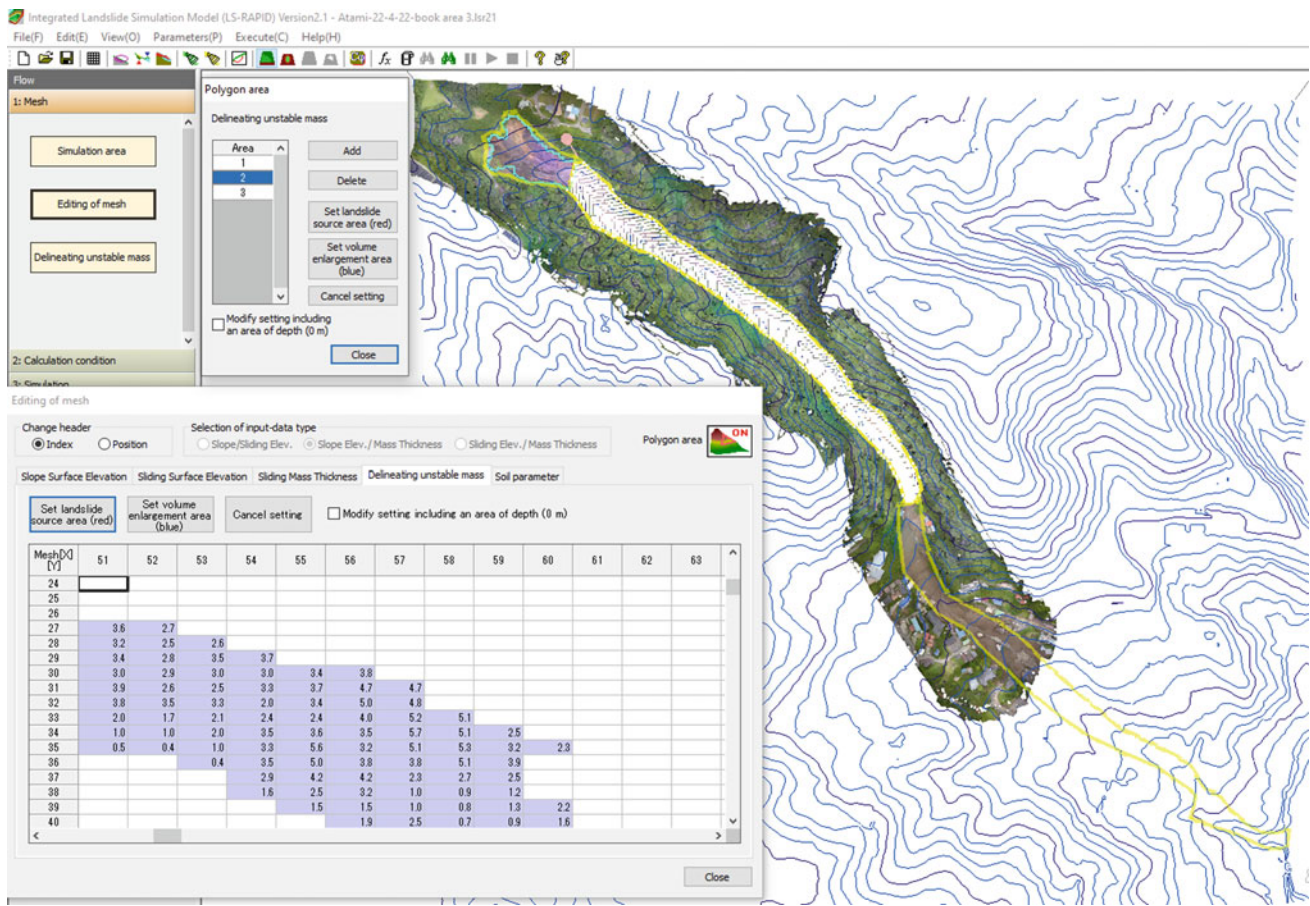


Fig. 70 Setting enlargement area


Table 6 Input soil parameters for Atami debris flow

Parameters	Value	Source
Steady-state shear resistance τ_{ss} in the source area	30 kPa	Test data
Lateral pressure ratio ($k = \sigma_h / \sigma_v$)	0.5	Assumption
Friction angle at peak (ϕ_p)	30.5°	Test data
Friction angle during motion (ϕ_m)	16.4°	Test data
Shear displacement at the start of strength reduction (D_L)	1 mm	Test data
Shear displacement at the end of strength reduction (D_U)	100 mm	Test data
Pore pressure generation rate (B_{ss})	0.85	Assumption
<i>Enlargement area</i>		
Steady state shear resistance	10 kPa	See Sassa et al. (2004)
Lateral pressure ratio ($k = \sigma_h / \sigma_v$)	0.6	Assumption
<i>Flow area</i>		
Steady state shear resistance	10 kPa	See Sassa et al. (2004)
Lateral pressure ratio ($k = \sigma_h / \sigma_v$)	0.8	Assumption

Editing of mesh

Change header
 Index Position

Selection of input-data type
 Slope/Sliding Elev. Slope Elev./ Mass Thickness Sliding Elev./ Mass Thickness

Polygon area 

Slope Surface Elevation **Sliding Surface Elevation** Sliding Mass Thickness Delineating unstable mass Soil parameter

Edit	Items	Symbols	Unit	Normal Value
1 *	Lateral pressure ratio	$k = \frac{\sigma_{Dk}}{\sigma_{Dv}}$		0.30 - 0.60
2	Friction coefficient inside landslide mass	$\tan \phi_i$		0.36 - 0.58
3	Friction coefficient during motion at sliding surface	$\tan \phi_m$		0.46 - 0.70
4	Steady state shear resistance at sliding surface	τ_{Nss}	kPa	5 - 50
5	Rate of excess pore-pressure generation	Bss		0.0 - 1.0
6	Peak friction coefficient at sliding surface	$\tan \phi_{op}$		0.65 - 0.78
7	Peak cohesion at sliding surface	C_p	kPa	10 - 100
8	Unit weight of mass	γ_A	kN/m ³	

About parameters of soil characteristics

0.000 Set in selected rectangle

Mesh [X] [Y]	39	40	41	42	43	44	45	46	47	48	49	50	51
24	0.500	0.500	0.500	0.500	0.500	0.500	0.500	0.500	0.500	0.500	0.500	0.500	0.500
25	0.500	0.500	0.500	0.500	0.500	0.500	0.500	0.500	0.500	0.500	0.500	0.500	0.600
26	0.500	0.500	0.500	0.500	0.500	0.500	0.500	0.500	0.500	0.500	0.500	0.600	0.600
27	0.500	0.500	0.500	0.500	0.500	0.500	0.500	0.500	0.500	0.500	0.500	0.600	0.600
28	0.500	0.500	0.500	0.500	0.500	0.500	0.500	0.500	0.500	0.500	0.500	0.600	0.600
29	0.500	0.500	0.500	0.500	0.500	0.500	0.500	0.500	0.500	0.500	0.500	0.600	0.600
30	0.500	0.500	0.500	0.500	0.500	0.500	0.500	0.500	0.500	0.500	0.500	0.600	0.600
31	0.500	0.500	0.500	0.500	0.500	0.500	0.500	0.500	0.500	0.500	0.500	0.600	0.600
32	0.500	0.500	0.500	0.500	0.500	0.500	0.500	0.500	0.500	0.500	0.500	0.600	0.600
33	0.500	0.500	0.500	0.500	0.500	0.500	0.500	0.500	0.500	0.500	0.500	0.600	0.600
34	0.500	0.500	0.500	0.500	0.500	0.500	0.500	0.500	0.500	0.500	0.500	0.600	0.600

Close

Fig. 71 Inputting lateral pressure ratios for Atami debris flow

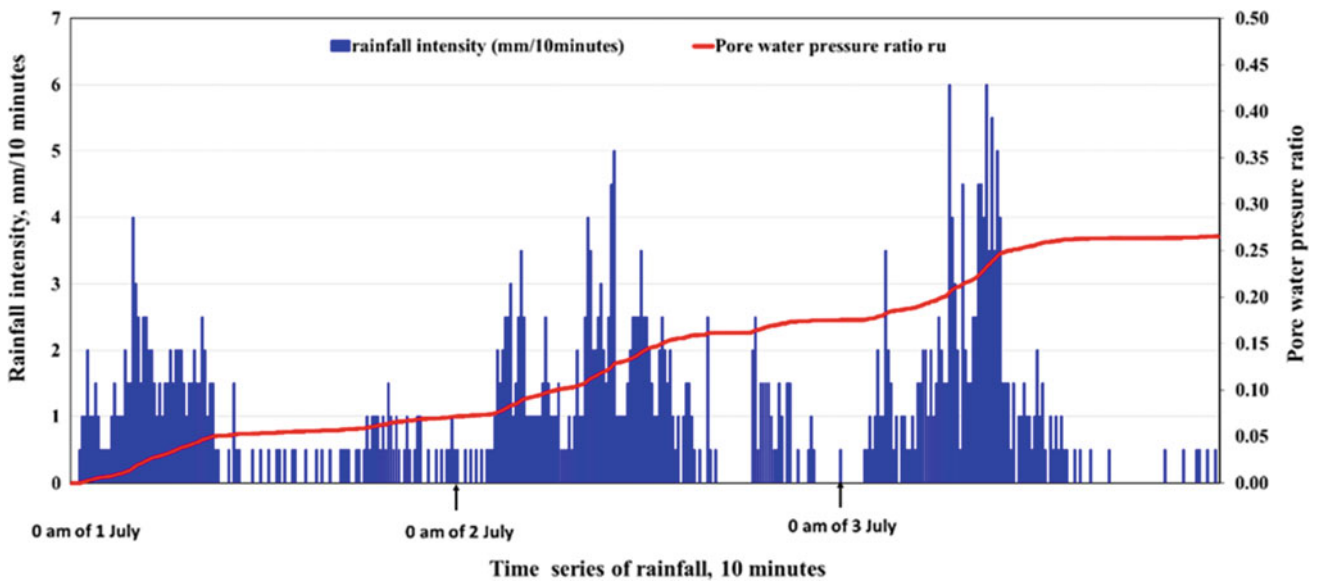


Fig. 72 Rainfall intensity and pore water pressure ratio

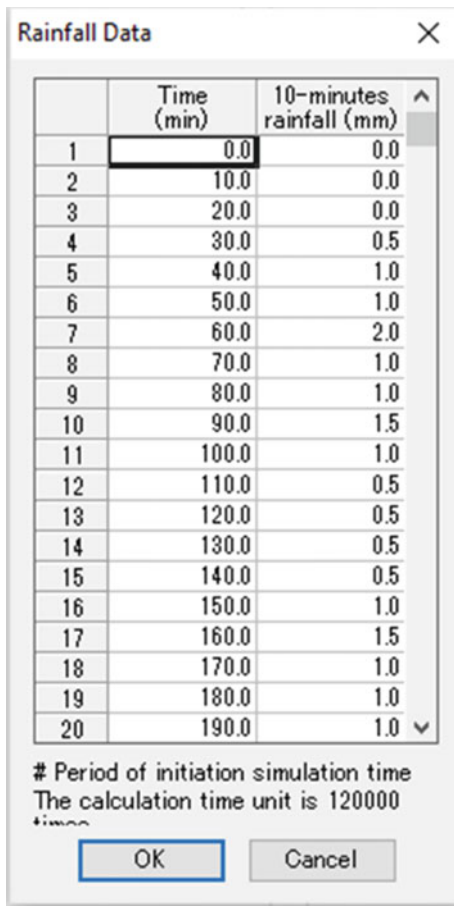


Fig. 73 Inputting rainfall data

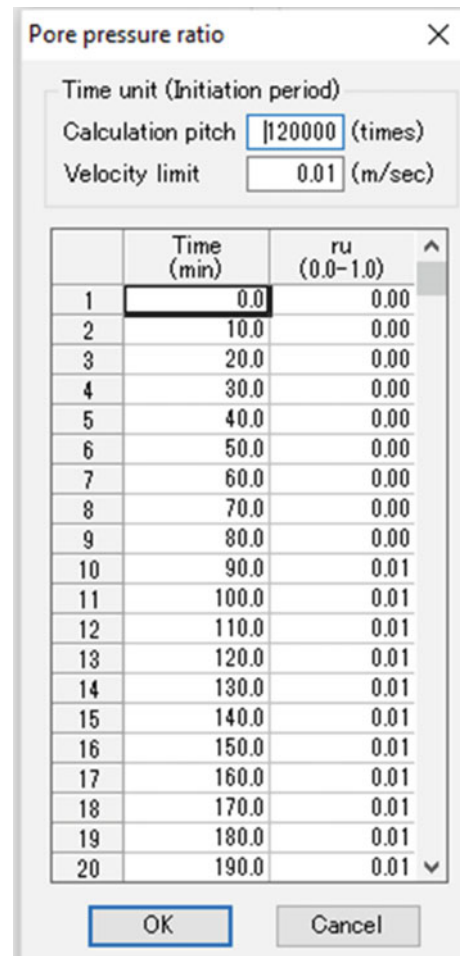


Fig. 74 Inputting pore water pressure ratio

represents the source area, while the pink area represents the moving mass. When the pore pressure ratio reaches 0.25 at 58 h 40 m 00 s (10:40:00 am on 3 July 2021), failure starts from the top of the landslide source area. After 13 s, at 58 h 40 m 13 s, the entire landslide mass is formed and starts to

move downwards towards the residential area reaching this area at 58 h 41 m 27 s. The landslide mass stops moving and is completely deposited at 58 h 43 m 00 s.

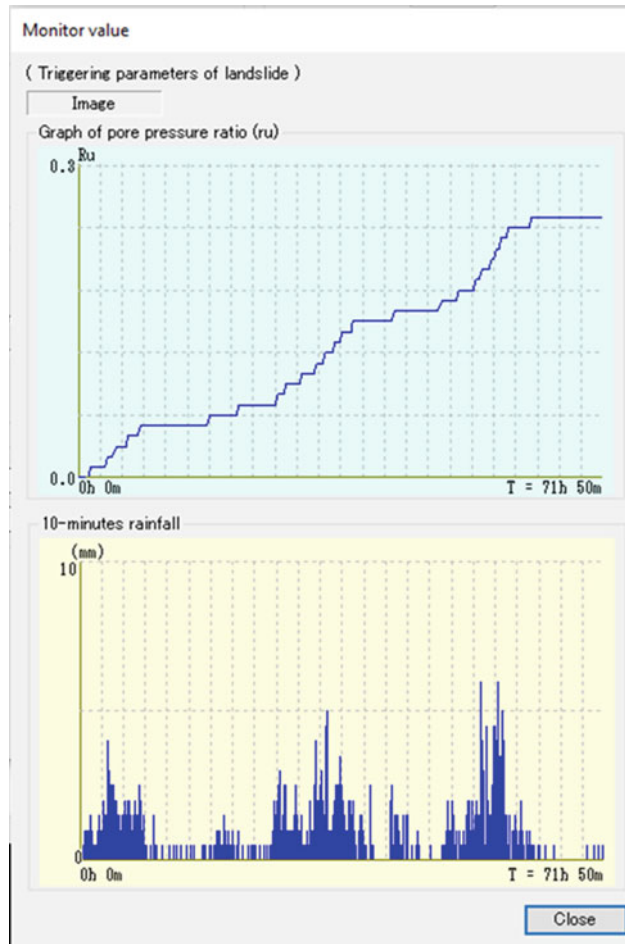


Fig. 75 Graph of rainfall data and pore water pressure in LS-RAPID for Atami debris flow simulation

Fig. 76 Simulation results of Atami debris flow at **a** 58 h 40 m 00 s, **b** 58 h 40 m 13 s, **c** 58 h 41 m 27 s, and **d** 58 h 43 m 00 s from the start of rainfall

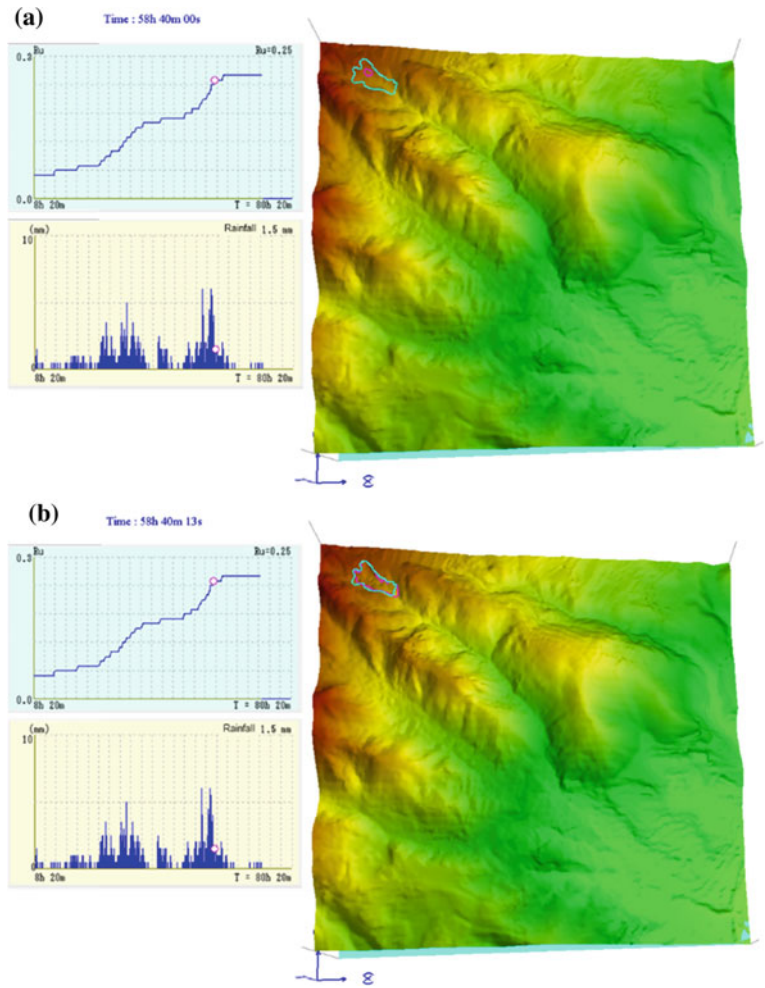
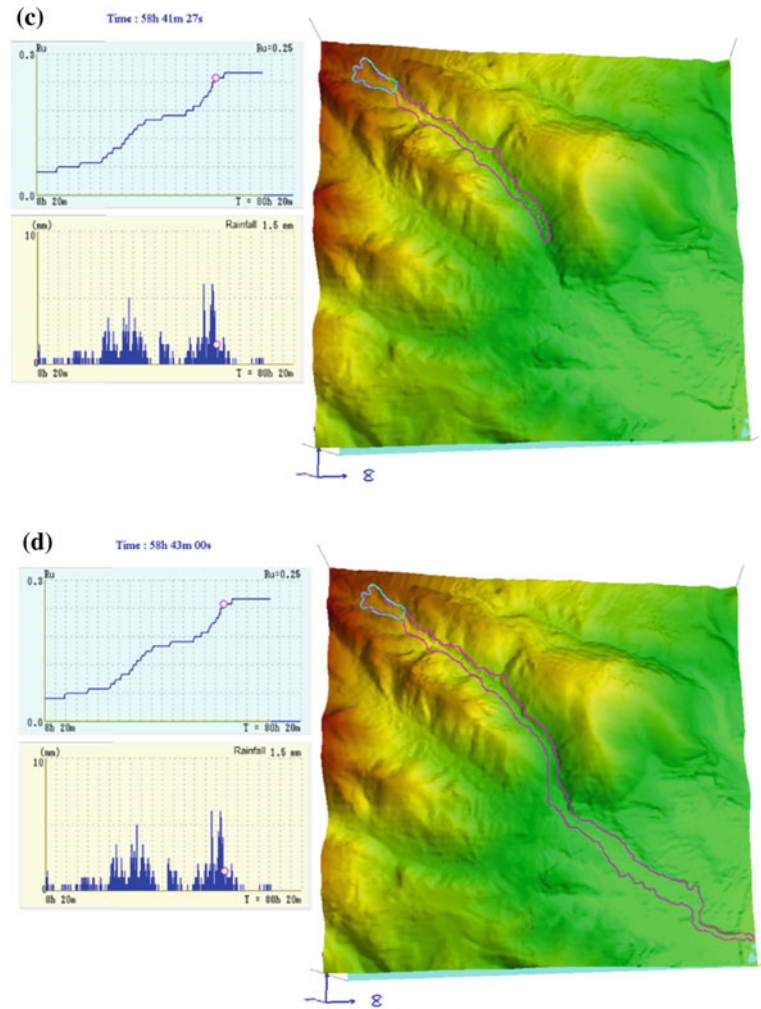


Fig. 76 (continued)

5 Conclusions

As an integrated simulation model, LS-RAPID is capable of reproducing the entirety of a landslide process of a slope from a stable condition to movement and deposition of the slope materials. The program is able to simulate both rainfall- and earthquake- induced landslides as well as landslides triggered under the influence of both factors. A review of the recent applications of LS-RAPID program showed its widespread use around the world to evaluate various case studies. This paper presented a detailed manual allowing interested users to quickly and efficiently use the program for their own case studies. The user manual provided in this paper was further supplemented by video tutorials that broke each step into quick visual representations of the process. The paper concluded with three examples and tutorials

presented in both written and visual formats. In particular, a simple slope geometry was developed. Failure of this geometry was first triggered by a rainfall time history and second, by a recorded earthquake motion. The third and final tutorial provided in this paper was for the Atami debris flow, which was a real-world example of a rainfall-induced slope failure.

Acknowledgements The authors acknowledge support from a Japan-Sri Lanka bilateral SATREPS (Science and Technology Research Partnership for Sustainable Development) project titled, "Development of early warning technology of Rain-induced Rapid and Long-travelling Landslides joint programme from 2019 to 2025." The project is implemented by the International Consortium on Landslides (ICL) and the National Building Research Organization, Sri Lanka (NBRO). Prof. Kazuo Konagai and Mr. Sanchita Sharendra are thanked for their support in the investigation of the Atami debris flow and associated testing.

References

- Borden RH, Putrich SF (1986) Drained-strength parameters from direct shear tests for slope stability analyses in overconsolidated fissured residual soils. *Transp Res Rec* 1089:102–113
- Cancelli A (1977) Residual shear strength and stability analysis of a landslide in fissured overconsolidated clays. *Bull Int Assoc Eng Geol* 16:193–197
- Collotta T, Cantoni R, Pavesi U, Ruberl E, Moretti PC (1989) A correlation between residual friction angle, gradation and the index properties of cohesive soils. *Géotechnique* 39(2):343–346
- Dang K, Sassa K, Fukuoka H et al (2016) Mechanism of two rapid and long-runout landslides in the 16 April 2016 Kumamoto earthquake using a ring-shear apparatus and computer simulation (LS-RAPID). *Landslides* 13:1525–1534. <https://doi.org/10.1007/s10346-016-0748-9>
- Dang K, Sassa K, Konagai K et al (2019) Recent rainfall-induced rapid and long-traveling landslide on 17 May 2016 in Aranayaka, Kagelle District, Sri Lanka. *Landslides* 16:155–164. <https://doi.org/10.1007/s10346-018-1089-7>
- Duc DM, Khang DQ, Duc DM et al (2020) Analysis and modeling of a landslide-induced tsunami-like wave across the Truong River in Quang Nam province, Vietnam. *Landslides* 17:2329–2341. <https://doi.org/10.1007/s10346-020-01434-2>
- Eid HT (1996) Drained shear strength of stiff clays for slope stability analyses. Ph.D. Dissertation, University of Illinois at Urbana-Champaign
- Eid HT, Rabie KH, Wijewickreme D (2016) Drained residual shear strength at effective normal stresses relevant to soil slope stability analyses. *Eng Geol* 204:94–107
- Gibo S (1985) The ring shear behavior and residual strength. In: *Proceedings of the 4th international conference and field workshop on landslides*, pp 283–288
- Geological Survey of Japan, <https://gbank.gsj.jp/geonavi/geonavi.php#13.35.10501,139.09065>. Accessed on 25 Jan 2022
- Geospatial Information Authority of Japan (<https://fgd.gsi.go.jp/download/menu.php>). Accessed on 6 Jan 2022
- Gradiški K, Sassa K, He B, Arbanas Ž, Arbanas S M, Krkač M, Kvasnička P, Oštrić M (2018) TXT-tool 3.385-1.1: application of integrated landslide simulation model LS-rapid to the Kostanjek landslide, Zagreb, Croatia. In: Sassa K et al (eds) *Landslide dynamics: ISDR-ICL landslide interactive teaching tools, vol 2, Testing, risk management and country practices*. Springer, Cham, pp 101–109. https://doi.org/10.1007/978-3-319-57777-7_3
- Ha ND, Sayama T, Sassa K et al (2020) A coupled hydrological-geotechnical framework for forecasting shallow landslide hazard—a case study in Halong City, Vietnam. *Landslides* 17:1619–1634. <https://doi.org/10.1007/s10346-020-01385-8>
- Hawkins AB, Privett KD (1985) Measurement and use of residual shear strength of cohesive soils. *Ground Eng* 22–29
- Huy LD, Sassa K, Fukuoka H, Sato Y, Takara K, Setiawan H, Tien PV, Dang K (2018) TXT-tool 3.081–1.4: initiation mechanism of rapid and long run-out landslide and simulation of Hiroshima landslide disasters using the integrated simulation model (LS-RAPID). In: Sassa K et al (eds) *Landslide dynamics: ISDR-ICL landslide interactive teaching tools, vol 2: testing, risk management and country practices*. Springer, Cham, pp 149–168. https://doi.org/10.1007/978-3-319-57777-7_6
- Jovančević SD, Nagai O, Sassa K, Arbanas Ž (2018) TXT-tool 3.385-1.2: deterministic landslide susceptibility analyses using LS-rapid software. In: Sassa K et al (eds) *Landslide dynamics: ISDR-ICL landslide interactive teaching tools, vol 2: testing, risk management and country practices*. Springer, Cham, pp 169–179. https://doi.org/10.1007/978-3-319-57777-7_7
- Kanji MA (1974) The relationship between drained friction angles and atterberg limits of natural soils. *Géotechnique* 24(4):671–674
- Kanji MA, Wolle CM (1977) Residual strength—new testing and microstructure. In: *Proceedings of the 9th international conference on soil mechanics*, vol 1, pp 153–154
- Liao ZH, Yang H, Wang J, Fukuoka H, Sassa K, Karnawati D, Fathani F (2010) Prototyping an experimental early warning system for rainfall-induced landslides in Indonesia using satellite remote sensing and geospatial datasets. *Landslides* 7(3):317–324
- Loi DH, Quang LH, Sassa K et al (2017) The 28 July 2015 rapid landslide at Ha Long City, Quang Ninh, Vietnam. *Landslides* 14:1207–1215. <https://doi.org/10.1007/s10346-017-0814-y>
- Lupini JF, Skinner AE, Vaughan PR (1981) The drained residual strength of cohesive soils. *Géotechnique* 31(2):181–213
- Mesri G, Cepeda-Diaz AF (1986) Residual shear strength of clays and shales. *Géotechnique* 36(2):269–274
- Montarasio L, Valentino R (2008) A model for triggering mechanisms of shallow landslides. *Natural Hazards Earth Sci* 8:1149–1159
- Müller-Vonmoss M, Løken T (1989) The shearing behavior of clays. *Appl Clay Sci* 4:125–141
- Prodan MV, Jovančević SD, Arbanas A (2018) TXT-tool 3.385-1.3: landslide occurrence prediction in the Rječina river valley as a base for an early warning system. In: Sassa K et al (eds) *Landslide dynamics: ISDR-ICL landslide interactive teaching tools, vol 2: testing, risk management and country practices*. Springer, Cham, pp 263–275. https://doi.org/10.1007/978-3-319-57777-7_13
- Sassa K (1988) Geotechnical model for the motion of landslides. In: *Proceedings 5th international symposium on landslides, “landslides”*. Balkema, Rotterdam, pp 37–56
- Sassa K, Fukuoka H, Wang G, Ishikawa N (2004) Undrained dynamic-loading ring-shear apparatus and its application to landslide dynamics. *Landslides* 1(1):7–19
- Sassa K, Fukuoka H, Sato Y, Takara K, Huy LD, Setiawan H, Tien PV, Khang DQ (2014a) Initiation mechanism of rapid and long runout landslide and simulation of Hiroshima landslide disasters using the integrated simulation model (LS-RAPID). In: *Proceeding of international forum “urbanization and landslide disaster”*, Kyoto, Japan, 8 October 2014a, pp 85–112
- Sassa K, He B, Miyagi T, Strasser M, Konagai K, Ostric M, Setiawan H, Takara K, Nagai O, Yamashiki Y, Tutumi S (2012) A hypothesis of the Senoumi submarine megaslide in Suruga Bay in Japan—based on the undrained dynamic-loading ring shear tests and computer simulation. *Landslides* 9:439–455. <https://doi.org/10.1007/s10346-012-0356-2>
- Sassa K, Nagai O, Solidum R, Yamazaki Y, Ohta H (2010) An integrated model simulating the initiation and motion of earthquake and rain induced rapid landslides and its application to the 2006 Leyte landslide. *Landslides* 7:219–236. <https://doi.org/10.1007/s10346-010-0230-z>
- Sassa K, Dang K, He B et al (2014b) A new high-stress undrained ring-shear apparatus and its application to the 1792 Unzen–Mayuyama megaslide in Japan. *Landslides* 11:827–842. <https://doi.org/10.1007/s10346-014-0501-1>
- Sassa K, Dang K, Yanagisawa H et al (2016) A new landslide-induced tsunami simulation model and its application to the 1792 Unzen–Mayuyama landslide-and-tsunami disaster. *Landslides* 13:1405–1419. <https://doi.org/10.1007/s10346-016-0691-9>
- Sassa K., Dang K (2018) Text Tool 0.081-1.1 Landslide dynamics for risk assessment. In: Sassa K, Tiwari B, Liu K, McSaveney M, Strom A, Setiawan H (eds) *Landslide dynamics-ISDR-ICL landslide interactive teaching tools*. Springer, pp 1–79
- Senthilkumar V, Chandrasekaran S, Maji V (2017) Geotechnical characterization and analysis of rainfall—induced 2009 landslide at Marappalam area of Nilgiris district, Tamil Nadu state, India.

- Landslides 14:1803–1814. <https://doi.org/10.1007/s10346-017-0839-2>
- Setiawan H, Fathani TF, Wilopo W, Karnawati D (2019a) Analysis of potential landslide and its motion behavior in Salem District, Brebes Regency, Central Java of Indonesia by using the LS-RAPID numerical simulation. In: Proceedings international conference on landslide and slope stability SLOPE 2019a. Bali, Indonesia, pp E3 (1–12)
- Setiawan H, Sassa K, He B (2018a) TXT-tool 3.081-1.3: a hypothesis of the Senoumi submarine megaslide in Suruga Bay in Japan—based on the undrained dynamic-loading ring shear tests and computer simulation. In: Sassa K et al (eds) *Landslide dynamics: ISDR-icl landslide interactive teaching tools, vol 2: testing, risk management and country practices*. Springer, Cham, pp 131–147. https://doi.org/10.1007/978-3-319-57777-7_5
- Setiawan H, Sassa K, Takara K, Fukuoka H (2017) Detail study of the Aratozawa large-scale landslide in Miyagi Prefecture, Japan. In: Mikoš M, Vilímek V, Yin Y, Sassa K (eds) *Advancing culture of living with landslides*. WLF2017. Springer, Cham, pp 473–480. https://doi.org/10.1007/978-3-319-53483-1_56
- Setiawan H, Sassa K, Takara K, Ostric M, Miyagi T, Fukuoka H (2018b) TXT-tool 4.081-1.2: mechanism of the Aratozawa large-scale landslide induced by the 2008 Iwate-Miyagi earthquake. In: Sassa K et al (eds) *Landslide dynamics: ISDR-icl landslide interactive teaching tools, vol 2: testing, risk management and country practices*. Springer, Cham, pp 819–831. https://doi.org/10.1007/978-3-319-57777-7_54
- Setiawan H, Wilopo W, Wiyoso T, Fathani TF, Karnawati D (2019b) Investigation and numerical simulation of the 22 February 2018 landslide-triggered long-traveling debris flow at Pasir Panjang Village, Brebes Regency of Central Java, Indonesia. *Landslides* 16 (11):2219–2232. First Online 5 August 2019b. <https://doi.org/10.1007/s10346-019-01245-0>
- Shizuoka Prefecture (2022) About the occurrence of debris flow in the Atami Izusan area. https://www.pref.shizuoka.jp/kinkyu/r3_atami_dosyasaigai.html. Accessed on 25 Apr 2022
- Skempton AW (1964) Long-term stability of clay slopes. *Géotechnique* 14(2):77–102
- Stark TD, Eid HT (1994) Drained residual strength of cohesive soils. *J Geotech Eng* 120(5):856–871
- Stark TD, Hussain M (2015) Empirical correlations: drained shear strength for slope stability analyses. *J Geotech Geoenviron Eng* 139 (6):853–862
- Tan Q, Sassa K, Dang K et al (2020) Estimation of the past and future landslide hazards in the neighboring slopes of the 2016 Aranayake landslide, Sri Lanka. *Landslides* 17:1727–1738. <https://doi.org/10.1007/s10346-020-01419-1>
- Tien P V, Sassa K, Khang D (2018a) TXT-tool 3.081-1.1: an integrated model simulating the initiation and motion of earthquake and rain induced rapid landslides and its application to the 2006 Leyte landslide. In: Sassa K et al (eds) *Landslide dynamics: ISDR-ICL landslide interactive teaching tools, vol 2: testing, risk management and country practices*. Springer, Cham, pp 83–99. https://doi.org/10.1007/978-3-319-57777-7_2
- Tika TE, Hutchinson JN (1999) Ring shear tests on soil from the Vaiont landslide slip surface. *Géotechnique* 49(1):59–74
- Tiwari B, Ajmera B (2011) A new correlation relating the shear strength of reconstituted soil to the proportions of clay minerals and plasticity characteristics. *Appl Clay Sci* 53(1):48–57
- Tiwari B, Ajmera B (2018) Soil laboratory tests. *Encyclopedia Eng Geol* 1–20. https://doi.org/10.1007/978-3-319-12127-7_304-1
- Tiwari B, Ajmera B (2020) “Keynote lecture—recent developments in the evaluation and application of residual and fully softened shear strengths for stability analyses of landslides”, understanding and reducing landslide disaster risk. WLF2020. ICL Contribution *Landslide Disaster Risk Reduction*, Kyoto, Japan 4:11–45
- Tiwari B, Marui H (2003) Estimation of residual shear strength for bentonite-kaolin-toyoura sand mixture. *J Japan Landslide Soc* 40 (2):124–133
- Toyota H, Nakamura K, Sugimoto M, Sakai N (2009) Ring shear tests to evaluate strength parameters in various remoulded soils. *Géotechnique* 59(8):649–659
- Van Tien P, Sassa K, Takara K, Fukuoka H, Dang K, Shibasaki T, Ha ND, Setiawan H, Loi DH (2018b) Formation process of two massive dams following rainfall-induced deep-seated rapid landslide failures in the Kii Peninsula of Japan. *Landslides* 15:1761–1778. <https://doi.org/10.1007/s10346-018-0988-y>
- Van Tien P, Luong LH, Sassa K, Takara K, Sumit M, Thanh Nhan T, Dang K, Minh Duc D (2021) Mechanisms and modeling of the catastrophic landslide dam at Jure Village, Nepal. *J Geotech Geoenviron Eng* 147(11):05021010. [https://doi.org/10.1061/\(ASCE\)GT.1943-5606.0002637](https://doi.org/10.1061/(ASCE)GT.1943-5606.0002637)
- Voight B (1973) Correlation between Atterberg plasticity limits and residual shear strength of natural soils. *Géotechnique* 23(2):265–267
- Yin Y, Li B, Wang W, Zhan L, Xue Q, Gao Y, Zhang N, Chen H, Liu T, Li A (2016) Mechanism of the December 2015 catastrophic landslide at the Shenzhen landfill and controlling geotechnical risks of urbanization. *Engineering* 2(2):230–249. <https://doi.org/10.1016/J.ENG.2016.02.005>

Open Access This chapter is licensed under the terms of the Creative Commons Attribution 4.0 International License (<http://creativecommons.org/licenses/by/4.0/>), which permits use, sharing, adaptation, distribution and reproduction in any medium or format, as long as you give appropriate credit to the original author(s) and the source, provide a link to the Creative Commons license and indicate if changes were made.



The images or other third party material in this chapter are included in the chapter’s Creative Commons license, unless indicated otherwise in a credit line to the material. If material is not included in the chapter’s Creative Commons license and your intended use is not permitted by statutory regulation or exceeds the permitted use, you will need to obtain permission directly from the copyright holder.

Technical Notes and Case Studies



Challenges in Defining Frequentist Rainfall Thresholds to Be Implemented in a Landslide Early Warning System in India

Stefano Luigi Gariano, Massimo Melillo, Maria Teresa Brunetti, Sumit Kumar, Rajkumar Mathiyalagan, and Silvia Peruccacci

Abstract

In India, rainfall-induced landslides cause a high toll in terms of fatalities and damages. Therefore, the adoption of tools to predict the occurrence of such phenomena is urgent. For the purpose, the LANDSLIP project aimed at developing a landslide early warning system (LEWS) to forecast the occurrence of rainfall-induced landslides in two Indian pilot areas: Darjeeling and Nilgiris. Rainfall thresholds are a widely used tool to define critical probability levels for the possible occurrence of landslides in large areas, and are particularly suitable to be implemented in LEWSs.

In this work, we exploited two catalogues of 84 and 116 rainfall conditions likely responsible for landslide triggering in Darjeeling and Nilgiris, respectively. Adopting a frequentist statistical method and using an automatic tool, we determined rainfall thresholds at different non-exceedance probabilities for the two pilot areas. Despite the daily temporal resolution of rainfall data and the spatial and temporal distribution of the documented landslides, the thresholds calculated for the two areas have acceptable uncertainties and were implemented in the LANDSLIP LEWS prototype. We expect that the new

thresholds and the whole system will contribute to mitigate the landslide risk in the study areas.

Keywords

Rainfall thresholds • Landslides • India • Darjeeling • Nilgiris • LEWS • LANDSLIP project

1 Introduction

According to the global landslide dataset published by Froude and Petley (2018), 75% of all landslide events between 2004 to 2016 occurred in Asian countries. Notably, the highest number of non-seismically triggered landslides, i.e. more than 600 records (16% of the whole catalogue), was recorded in India. Most of these landslides were triggered by rainfall, particularly during the monsoon seasons. According to the EM-DAT disaster database (Guha-Sapir et al. 2022), 4739 people lost their life due to landslides in India and more than 400,000 people have been affected by this hazard since 1950. A significant upward trend in the occurrence of fatal landslides was observed in India in the period 1995–2014 (Haque et al. 2019). Due to the significant toll in terms of human lives and damages, the adoption of reliable tools to predict the occurrence of rainfall-induced landslides in India is urgent.

The LANDSLIP (LANDSLide Multi-Hazard Risk Assessment, Preparedness and Early Warning in South Asia: Integrating Meteorology, Landscape and Society) project (www.landslip.org) aimed at reducing the impact of hydrologically related landslide multi-hazards and increasing the resilience to landslides in vulnerable, hazard-prone areas in India. One of the operational goals of the LANDSLIP project was the development of a landslide early warning system (LEWS) to forecast the occurrence of landslides induced by rainfall in two pilot areas. Recently, several regional LEWSs have been designed and implemented in various

S. L. Gariano (✉) · M. Melillo · M. T. Brunetti · S. Peruccacci
CNR IRPI, 06134 Perugia, Italy
e-mail: stefano.luigi.gariano@irpi.cnr.it

M. Melillo
e-mail: massimo.melillo@irpi.cnr.it

M. T. Brunetti
e-mail: maria.teresa.brunetti@irpi.cnr.it

S. Peruccacci
e-mail: silvia.peruccacci@irpi.cnr.it

S. Kumar · R. Mathiyalagan
Geological Survey of India, Meghalaya, Shillong, India
e-mail: sumit.kumar@gsi.gov.in

R. Mathiyalagan
e-mail: rajkumar.mathiyalagan@gsi.gov.in

countries (Piciullo et al. 2018; Guzzetti et al. 2020), and many of them rely on rainfall thresholds, often combined with a susceptibility zonation. Rainfall thresholds are the most widely used tool to define critical probability levels for the possible occurrence of landslides in wide areas. Empirical rainfall thresholds are derived from the statistical analysis of rainfall conditions that have resulted in past landslides (e.g. Guzzetti et al. 2007, 2008; Segoni et al. 2018). Establishing reliable thresholds in large areas requires the availability of a large amount of information on the occurrence of past landslides (a statistically significant sample size) and of rainfall data.

To date, only a few works have studied the relationship between rainfall and landslides in some areas or states in India, and mostly in the Indian Himalayan Region (Dikshit et al. 2020b). Analyses of rainfall conditions responsible for slope failures have been conducted for single phenomena (e.g. Sengupta et al. 2010) and for population of landslides (e.g. Sajinkumar et al. 2020) and using both rain gauges and satellite data. Examples of rainfall thresholds defined using ground-based rainfall data are found in Uttarakhand (Kanungo and Sharma 2014), Sikkim (Sengupta et al. 2010; Harilal et al. 2019), West Bengal, particularly in Darjeeling (Dikshit and Satyam 2019; Dikshit et al. 2020a) and Kalimpong (Dikshit and Satyam 2018; Teja et al. 2019; Abraham et al. 2020), Tamil Nadu (Jaiswal and van Westen 2009; Thennavan et al. 2020), and Kerala (Naidu et al. 2018; Abraham et al. 2019, 2021). Some authors have calculated rainfall thresholds over large areas in India using satellite rainfall products: e.g. in Uttarakhand, northern India, using TRMM precipitation estimates (Mathew et al. 2014) and over the Western Ghats, south-western India, using TMPA and IMERG-derived rainfall data (Thakur et al. 2020). Brunetti et al. (2021) defined rainfall thresholds for the whole Indian Peninsula using GPM and SM2RAIN-ASCAT satellite rainfall products, and their merging, at daily and hourly temporal resolution, and daily rain gauge measurements from Indian Meteorological Department. Finally, a few works have analyzed landslides affecting highways and other infrastructures (Jaiswal and van Westen 2009; Sengupta et al. 2010; Kanungo and Sharma 2014).

In this work, we describe data, procedures, analysis, and challenges faced in calculating empirical rainfall thresholds for the possible initiation of shallow landslides in two pilot areas in India, using a consolidated approach.

2 Study Area

The Indian Peninsula is bounded on the north by the Himalayas and includes the Western Ghats, a N-S mountain chain on the western edge, and the Eastern Ghats, running mostly in a NE-SW direction. The steep topography and

geological complexity produce high landslide activity, especially during the monsoon season, which dominates the climate for over one-third of the year. Neal et al. (2020) identified seven broad-scale weather regimes in India. The summer monsoon usually happens between May and September, being mostly active during July and August.

Two pilot areas were selected in the Indian territory: the Darjeeling and the Nilgiris districts (Fig. 1). Both areas have population densities up to over 600 inhabitants per km² and have experienced rainfall-induced landslides that caused fatalities and heavy socio-economic impacts. Both areas are subject to intense rainfall in the monsoon period, which affects the two regions for several months triggering numerous landslides.

The Darjeeling District is located in the Eastern Himalayas, NE India, and belongs to the state of West Bengal. It covers 3232 km² with elevations ranging 100–4500 m a.s.l. and slope inclinations ranging 0–60° (average ≈ 18°). The population of this district is approximately 1.9 million people. The area is underlain by a sequence of metamorphic rocks from the Himalayan Fold Thrust Belt (FTB). Landslide failure mechanisms encountered within this pilot area are controlled by FTB deformation of the rocks. The average annual rainfall varies between 3000 and 5000 mm·yr⁻¹, of which approximately 90% is within the active monsoon period (June to September).

The Nilgiris District, located within the state of Tamil Nadu, in the southern part of the Indian Peninsula, covers 2566 km² and hosts approximately 0.8 million persons. It includes the Nilgiris hills (1900 km²), a plateau with

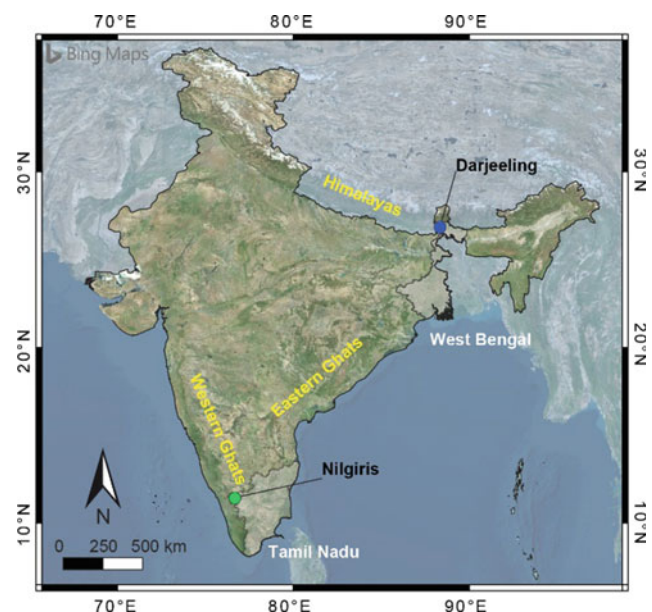


Fig. 1 Location of the two pilot areas of Darjeeling and Nilgiris in India, with indication of the boundaries of the West Bengal and Tamil Nadu states

elevation reaching 2400 m a.s.l. that is one of the most landslide-prone regions in the state. The plateau includes high peaks and rocky escarpments composed by gneiss overlain by lateritic soils. The Nilgiris is impacted by the northeast monsoon (October through December), which accounts for nearly all of the annual precipitation in the area and is responsible for the triggering of most landslides (predominantly debris/earth slides or flows).

3 Data

We used information on the occurrence of 684 landslides in the Darjeeling district from October 1968 to July 2015 and of 392 landslides in the Nilgiris district from December 1987 to January 2017. Rainfall measurements were obtained from regional rain gauge networks in the two pilot areas. In particular, we used daily rainfall data recorded by 36 rain gauges located in Darjeeling district in the period 01/Jan/1959–31/Dec/2017 and by 24 stations from 01/Jan/1987 to 31/Jul/2017 in Nilgiris district (Fig. 2).

Rain gauge selection was based on the number of time series available, and on data quality and sensor location, being these characteristics crucial to model the spatio-temporal variation of precipitations.

Using the entire rainfall data set, we estimated the distribution of monthly rainfall in the areas. In Darjeeling (Fig. 3a) the monthly rainfall has a peak in July and high values from June to September. As a result, all the 684 landslides are concentrated in the monsoon period, May through October, with nearly half of the events (327 out of 684, 48%) recorded in July (Fig. 3b). Hence, the monthly distributions of rainfall and landslides overlap, except in June and August, when the number of recorded landslides is very low if compared to the less rainy May. In Nilgiris, the distribution of monthly rainfall shows two peaks, with a significant increase, in October and November (Fig. 3c). The 392 landslides are heterogeneously distributed during the year, with more than 80% of the events (326 out of 392) between October and December (Fig. 3d), closely replicating the rainfall distribution.

4 Method

For the reconstruction of the rainfall conditions responsible for landslide initiation and for the calculation of rainfall thresholds, we adopted the procedure and the automatic tool named CTRL-T (Calculation of Thresholds for Rainfall-induced Landslides—Tool) described in Melillo et al. (2018) and successfully used in different contexts (e.g. Gariano et al. 2019; Teja et al. 2019; Jordanova et al. 2020; Melillo et al. 2020; Abraham et al. 2021).

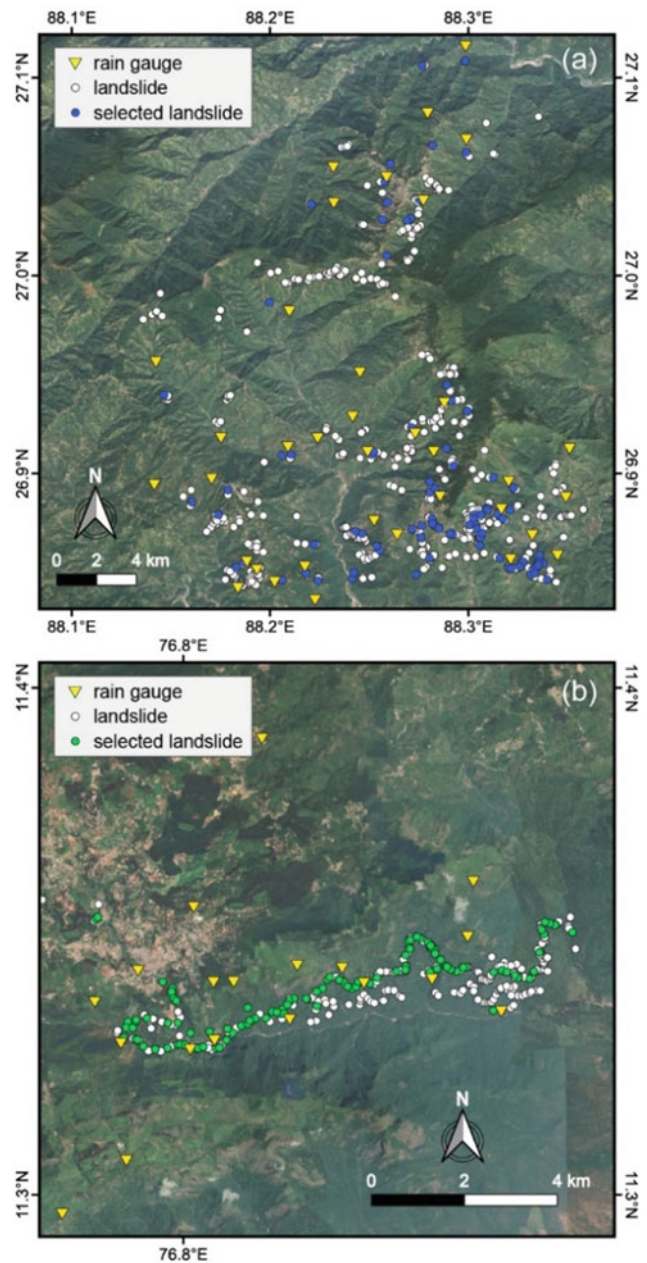


Fig. 2 Location of rain gauges and landslides selected for threshold calculation in the **a** Darjeeling and **b** Nilgiris pilot areas

CTRL-T exploits continuous rainfall measurements, and landslide information, to (1) reconstruct rainfall events; (2) select automatically the representative rain gauges; (3) identify multiple rainfall conditions responsible for the failure; (4) attribute a probability to each rainfall condition; and (5) calculate probabilistic rainfall thresholds and their associated uncertainties. Input data consists of: (i) rainfall event setting parameters, (ii) rainfall data, (iii) rain gauge locations, (iv) landslide locations, and (v) landslide occurrence times.

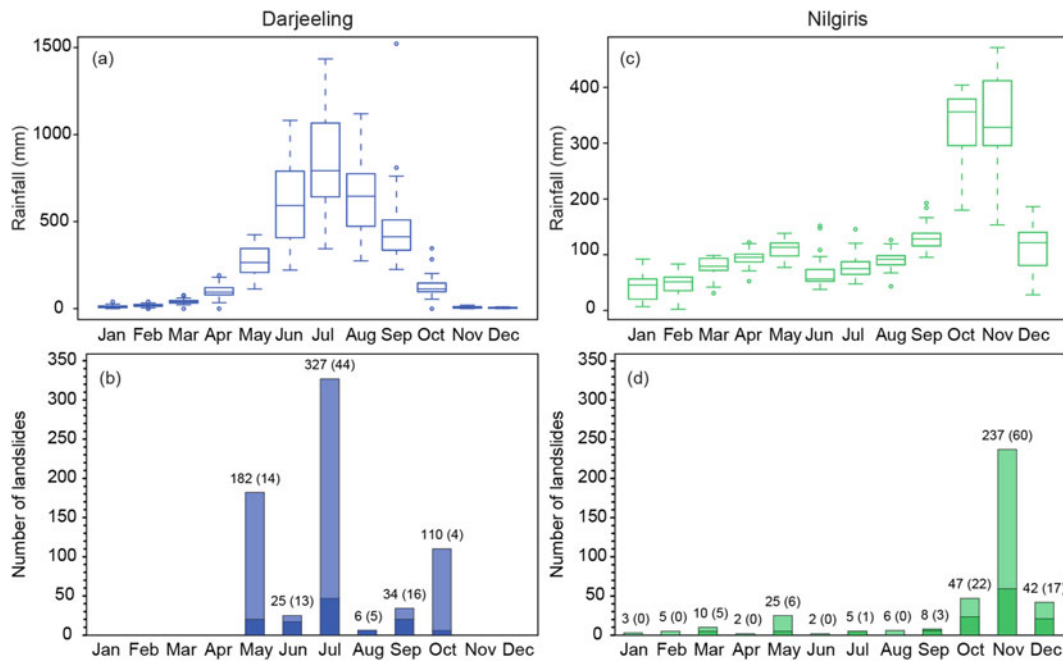


Fig. 3 Top: annual distribution of monthly rainfall in **a** Darjeeling (1959–2017) and **c** Nilgiris (1987–2017). Bottom: monthly distribution of landslides in **b** Darjeeling and **d** Nilgiris; lighter bars indicate the

total numbers of catalogued landslides in each pilot area; darker bars indicate the landslides used to calculate the thresholds (numbers in brackets)

The tool is divided into three main logical blocks. The first block executes the reconstruction of rainfall events. A rainfall event is a period of continuous rainfall separated from consecutive events by a dry (no-rain) period of two days. The second block combines rainfall events and landslide information, selects the rainfall events that have resulted in landslides and determines the rainfall duration, D , and the cumulated event rainfall, E , responsible for the landslides. Specifically, rainfall conditions were reconstructed from rainfall measurements recorded by rain gauges located within a 12-km radius circular buffer centered on the landslide. To select the representative rain gauges and the rainfall condition likely responsible for each failure, a weight function was used that considers D , E , and the distance between the rain gauge and the landslide. In the case of two or more landslides occurring in the same day and associated with the same rainfall condition, we considered the first one in order to avoid duplicates that would invalidate the frequentist method adopted to define the thresholds. The third block calculates rainfall thresholds at different non-exceedance probabilities adopting a frequentist statistical method (Brunetti et al. 2010; Peruccacci et al. 2012). The approach assumes the threshold curve is a power law that

links the cumulated event rainfall E (in mm) to the rainfall duration D (in days);

$$E = (\alpha \pm \Delta\alpha) \cdot D^{(\gamma \pm \Delta\gamma)} \quad (1)$$

where, α is a scaling constant (the intercept), γ is the shape parameter (that defines the slope of the power law curve), and $\Delta\alpha$ and $\Delta\gamma$ represent the uncertainties of α and γ , respectively. The uncertainties $\Delta\alpha$ and $\Delta\gamma$ are calculated using a “bootstrap” non-parametric statistical technique (Peruccacci et al. 2012). The uncertainties associated with the thresholds depend on the number and the distribution of the empirical data points, and reduce as the number of the empirical data increases.

For the reconstruction of the rainfall conditions likely responsible for the failures, CTRL-T outputs were checked and eventually revised by expert investigators from CNR IRPI and GSI to consider (i) the difference in local rainfall regimes at the two pilot areas (presence of monsoons), (ii) the coarse (daily) temporal resolution of rainfall measurements and (iii) the possible inaccuracy of the landslide occurrence date. For a few uncertain events, multiple investigators analyzed all available landslide and rainfall

information and agreed to revise the rainfall conditions automatically reconstructed by CTRL-T. We acknowledge that this procedure has introduced a hint of subjectivity into the reconstruction of the rainfall events responsible for failures, but we maintain that this additional check was necessary to reduce the uncertainties listed above.

5 Results and Discussion

5.1 Rainfall Conditions

Applying the above-mentioned procedure, we reduced the number of rainfall conditions associated with landslides in the two areas to 96 and 114, respectively. In addition, in the Darjeeling pilot area, the subset was further reduced to 84 landslides by discarding 12 more records for which a reliable triggering rainfall condition could not have been associated. These two landslide subsets have the same monthly distribution as the initial ones.

In the Darjeeling pilot area, the 84 rainfall conditions associated with the landslides have durations ranging between one and eight days (24–192 h) and cumulated rainfall varying between 74.0 and 10,775.0 mm (average value = 320.5 mm). In the Nilgiris pilot area, the rainfall conditions have durations ranging between one and six days (24–144 h) and cumulated rainfall varying between 45.0 and 675.5 mm (average value = 260.3 mm).

5.2 Magnitude Analysis

For civil protection purposes, it is worth mentioning that the number of landslides triggered by each rainfall condition can be assumed as a proxy for the magnitude of the event. For the purpose, we divided the ensemble of rainfall conditions responsible for the failures in the two pilot areas into two classes: those that triggered (i) from one to ten, and (ii) more than ten landslides.

We analyzed separately the D and E distributions of the rainfall conditions associated with landslides for the two magnitude classes. Figure 4 shows the box-and-whisker plots of D and E for each class for the two pilot areas (in shades of blue and green, respectively). For Darjeeling, the number of landslides associated to a single rainfall condition varies from one to 182 (event occurred on 26th May 2009). For Nilgiris, the number of landslides associated with a single rainfall event ranges from one to 138 (event occurred on 14th November 2006). Overall, median and maximum values of D remain stable for the two classes, whereas median values of E increase with the magnitude for both pilot areas.

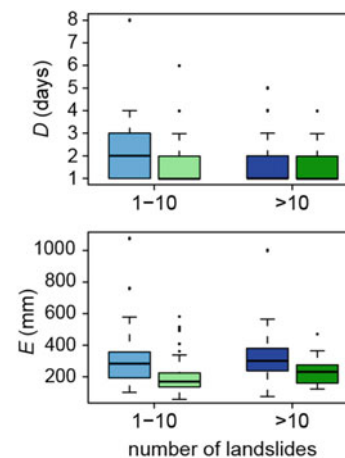


Fig. 4 Box-and-whisker plots of the duration, D (top) and cumulated event rainfall E (bottom) of the 84 and 114 rainfall conditions used to calculate rainfall thresholds in Darjeeling (in shades of blue) and Nilgiris (in shades of green) pilot areas, respectively, categorized into two classes of magnitude: (i) 1–10, and (ii) >10 landslides

5.3 Rainfall Thresholds

Using the 84 and 114 rainfall conditions, we defined frequentist rainfall thresholds for the two areas. Table 1 lists the parameter values and uncertainties for thresholds at different non-exceedance probability levels. Figure 5 shows, in a log–log plane, the rainfall conditions responsible for the failures and the rainfall thresholds at 5% non-exceedance probability levels with the associated uncertainties for Darjeeling (Fig. 5a) and Nilgiris (Fig. 5b).

The thresholds have ranges of validity equal to the range of rainfall durations D , and are defined at discrete (daily) rainfall durations D . Therefore, thresholds can be used only for the prediction of landslides for D equal to one day or multiples.

Figure 6 portrays the comparison of $T_{5,Dar}$ (blue curve) and $T_{5,Nil}$ (green curve) in logarithmic coordinates, with the shaded areas showing the uncertainty associated with the thresholds. Inspection of the figure reveals that $T_{5,Dar}$ is higher than $T_{5,Nil}$, meaning that, regardless of the rainfall duration, a larger amount of rainfall is necessary to trigger landslides in the Darjeeling pilot area. Further inspection of the figure reveals that $T_{5,Nil}$ is slightly steeper than $T_{5,Dar}$. This result agrees with the different rainfall regimes of the two pilot areas.

The relative uncertainties in the γ parameter, $\Delta\gamma/\gamma$, are equal to 14.5% and 11.5% in Darjeeling and Nilgiris, respectively. Moreover, considering the 5% non-exceedance probability level, the relative uncertainties in the α parameter, $\Delta\alpha/\alpha$, are equal to 8.9% and 4.9%, respectively. The two values are lower than 10%, considered an acceptable value for reliable thresholds, as proposed by Peruccacci et al. (2012).

Table 1 Parameters of the ED rainfall thresholds at different non-exceedance for the possible initiation of landslides in Darjeeling ($T_{1,Dar}$, $T_{5,Dar}$, $T_{10,Dar}$) and Nilgiris ($T_{1,Nil}$, $T_{5,Nil}$, $T_{10,Nil}$) pilot areas

Threshold name	Threshold parameters				Duration range (days)
	α	$\Delta\alpha$	γ	$\Delta\gamma$	
$T_{1,Dar}$	89.0	9.3	0.62	0.09	1–8
$T_{5,Dar}$	114.0	10.2	0.62	0.09	1–8
$T_{10,Dar}$	130.2	10.7	0.62	0.09	1–8
$T_{1,Nil}$	42.7	2.7	0.78	0.09	1–6
$T_{5,Nil}$	56.7	2.8	0.78	0.09	1–6
$T_{10,Nil}$	66.0	2.9	0.78	0.09	1–6

Note that the equations are defined for durations in days and cumulated event rainfall in mm

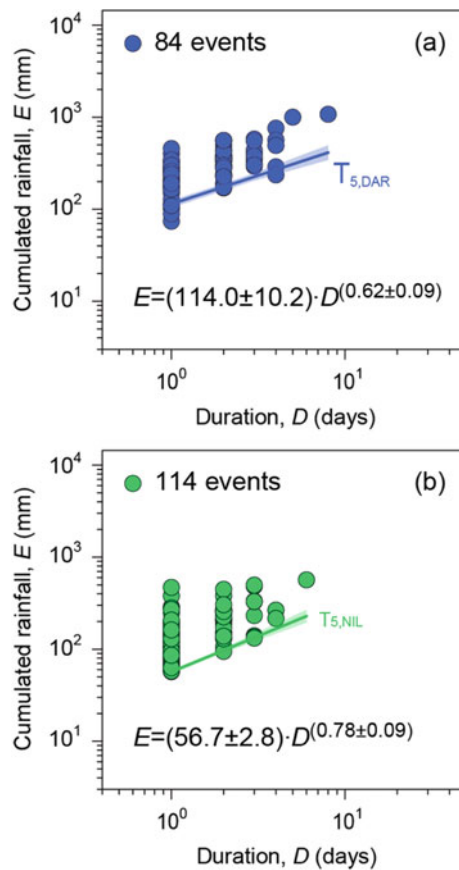


Fig. 5 DE conditions that have resulted in landslides in **a** Darjeeling and **b** Nilgiris, and corresponding threshold at 5% non-exceedance probability level. Shaded area shows uncertainty of the thresholds. Data shown in logarithmic coordinates

The thresholds defined for the two pilot areas have high values of the parameter γ , as a result of the distribution of the empirical data points in the DE plane. The uncertainties associated with thresholds are high and depend primarily on the number and distribution of the (D, E) pairs.

The daily temporal resolution of landslide and rainfall data affects the calculation of thresholds for two main

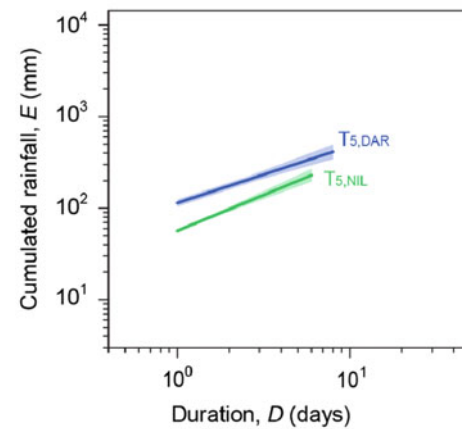


Fig. 6 Comparison between the 5% ED thresholds for Darjeeling ($T_{5,Dar}$) and for Nilgiris ($T_{5,Nil}$) pilot areas. Data shown in logarithmic coordinates

reasons. First, as mentioned above, thresholds are valid and can be used only for durations ranging 1–8 days and 1–6 days in Darjeeling and Nilgiris, respectively. Second, the daily rainfall resolution results in a large dispersion of E values, especially for the shortest events (lasting one or two days). Presumably, the cumulated rainfall recorded at one day (especially the lower cumulated values) fell over a shorter time period. According to the data point distribution, thresholds are very steep (high values of γ parameter) and the associated uncertainties are high. Marra (2019) and Gariano et al. (2020) noted that the use of daily data leads to a worse threshold predicting capability than using hourly data.

6 Conclusions

An effective landslide forecasting model is a key component of a LEWS. In this work, we described the procedures and the challenges for calculating frequentist rainfall thresholds

for the possible occurrence of shallow landslides in two Indian pilot areas. Thresholds defined for Darjeeling and Nilgiris areas were based on 84 and 114 landslide-triggering rainfall conditions, respectively. Despite some limitations, mostly due to the daily temporal resolution of rainfall data and to the spatial and temporal distribution of the reported landslides, the thresholds defined for the two pilot areas have acceptable values of uncertainties.

Frequentist rainfall thresholds obtained for different non-exceedance probabilities are particularly suitable for designing probabilistic schemes to be implemented in LEWS for the prediction of rainfall-induced landslides. In particular, the thresholds here defined were implemented in the LANDSLIP short-range prototype LEWS. Every day, the system compares measured and forecasted rainfall amounts against the rainfall thresholds, and assigns, for a given combination of cumulated rainfall and rainfall duration (i.e. for a given rainfall scenario), a possibility level of landslide occurrence, also based on the susceptibility maps of the two pilot areas. The landslide possibility level is categorized into four classes: *low*, *moderate*, *high*, and *very high* possibility of landslide occurrence—based on the number of landslides that might occur in one or many locations. The warning message is issued to each administrative area within the two pilot areas: four areas in Darjeeling and six areas in Nilgiris. The short-range landslide forecast only covers shallow landslides caused by rainfall and is valid for the successive 48 h, with different values for each day. The forecast is included in a bulletin of information for district authorities to support them in their decision-making.

The thresholds and the whole forecasting model require ongoing evaluation and refinement by assessing both forecasting and operational capabilities. The evaluation relies upon standardized landslide and rainfall data collection and management. Additional landslide data and different rainfall data inputs (e.g. hourly rainfall measurements, and/or radar and satellite rainfall estimates) will be useful to validate the thresholds and improve the forecasting model.

Acknowledgements This work was carried out as part of WP3-Task3.4 (Weather-based thresholds for short-term landslide forecasting) of the LANDSLIP (LANDSLide Multi-Hazard Risk Assessment, Preparedness and Early Warning in South Asia: Integrating Meteorology, Landscape and Society) project, which had two UK grant funders: NERC and DFID (Grant numbers: NE/P000681/1 and NE/P000649/1). More information can be found at www.landslip.org. Rainfall measurements and landslide information were gathered and provided by the Geological Survey of India. The CTRL-T software tool was written using the R open-source software and can be freely downloaded at <https://doi.org/10.5281/zenodo.4533719>.

References

- Abraham MT, Satyam N, Rosi A, Pradhan B, Segoni S (2021) Usage of antecedent soil moisture for improving the performance of rainfall thresholds for landslide early warning. *CATENA* 200:105147. <https://doi.org/10.1016/j.catena.2021.105147>
- Abraham MT, Satyam N, Kushal S, Rosi A, Pradhan B, Segoni S (2020) Rainfall threshold estimation and landslide forecasting for Kalimpong, India Using SIGMA Model *Water* 12:1195. <https://doi.org/10.3390/w12041195>
- Abraham MT, Pothuraju D, Satyam N (2019) Rainfall thresholds for prediction of landslides in Idukki, India: an empirical approach. *Water* 11:2113. <https://doi.org/10.3390/w11102113>
- Brunetti MT, Melillo M, Gariano SL, Ciabatta L, Brocca L, Amarnath G, Peruccacci S (2021) Satellite rainfall products outperform ground observations for landslide prediction in India. *Hydrol Earth Syst Sci* 25:3267–3279. <https://doi.org/10.5194/hess-25-3267-2021>
- Brunetti MT, Peruccacci S, Rossi M, Luciani S, Valigi D, Guzzetti F (2010) Rainfall thresholds for the possible occurrence of landslides in Italy. *Nat Hazards Earth Syst Sci* 10:447–458. <https://doi.org/10.5194/nhess-10-447-2010>
- Dikshit A, Satyam DN (2018) Estimation of rainfall thresholds for landslide occurrences in Kalimpong, India. *Innov Infrastruct Solut* 3:24. <https://doi.org/10.1007/s41062-018-0132-9>
- Dikshit A, Satyam N (2019) Probabilistic rainfall thresholds in Chibo, India: estimation and validation using monitoring system. *J Mt Sci* 16:870–883. <https://doi.org/10.1007/s11629-018-5189-6>
- Dikshit A, Sarkar R, Pradhan B, Segoni S, Alamri AM (2020a) Rainfall induced landslide studies in Indian Himalayan region: a critical review. *Appl Sci* 10:2466. <https://doi.org/10.3390/app10072466>
- Dikshit A, Satyam N, Pradhan B, Kushal S (2020b) Estimating rainfall threshold and temporal probability for landslide occurrences in Darjeeling Himalayas. *Geosci J* 24:225–233. <https://doi.org/10.1007/s12303-020-0001-3>
- Froude MJ, Petley DN (2018) Global fatal landslide occurrence from 2004 to 2016. *Nat Hazards Earth Syst Sci* 18:2161–2181. <https://doi.org/10.5194/nhess-18-2161-2018>
- Guha-Sapir D, Below R, Hoyois PH (2022) EM-DAT: international disaster database, Université Catholique de Louvain, Brussels, Belgium. Available at <http://www.emdat.be>. Last accessed 11 Feb 2022
- Gariano SL, Melillo M, Peruccacci S, Brunetti MT (2020) How much does the rainfall temporal resolution affect rainfall thresholds for landslide triggering? *Nat Hazards* 100:655–670. <https://doi.org/10.1007/s11069-019-03830-x>
- Gariano SL, Sarkar R, Dikshit A, Dorji K, Brunetti MT, Peruccacci S, Melillo M (2019) Automatic calculation of rainfall thresholds for landslide occurrence in Chukha Dzongkhag, Bhutan. *Bull Eng Geol Environ* 78(6):4325–4332. <https://doi.org/10.1007/s10064-018-1415-2>
- Guzzetti F, Gariano SL, Peruccacci S, Brunetti MT, Marchesini I, Rossi M, Melillo M (2020) Geographical landslide early warning systems. *Earth-Sci Rev* 200:102973. <https://doi.org/10.1016/j.earscirev.2019.102973>
- Guzzetti F, Peruccacci S, Rossi M, Stark CP (2007) Rainfall thresholds for the initiation of landslides in central and southern Europe. *Meteorol Atmos Phys* 98:239–267. <https://doi.org/10.1007/s00703-007-0262-7>

- Guzzetti F, Peruccacci S, Rossi M, Stark CP (2008) The rainfall intensity–duration control of shallow landslides and debris flows: an update. *Landslides* 5:3–17. <https://doi.org/10.1007/s10346-007-0112-1>
- Haque U, da Silva PF, Devoli G, Pilz J, Zhao B, Khaloua A, Wilopo W, Andersen P, Lu P, Lee J, Yamamoto T, Keellings D, Wu JH, Glass GE (2019) The human cost of global warming: deadly landslides and their triggers (1995–2014). *Sci Tot Environ* 682:673–684. <https://doi.org/10.1016/j.scitotenv.2019.03.415>
- Harilal GT, Madhu D, Ramesh MV, Pullarkatt D (2019) Towards establishing rainfall thresholds for a real-time landslide early warning system in Sikkim, India. *Landslides* 16:2395–2408. <https://doi.org/10.1007/s10346-019-01244-1>
- Jaiswal P, van Westen CJ (2009) Estimating temporal probability for landslide initiation along transportation routes based on rainfall thresholds. *Geomorphology* 112:96–105. <https://doi.org/10.1016/j.geomorph.2009.05.008>
- Jordanova G, Gariano SL, Melillo M, Peruccacci S, Brunetti MT, Jemec Auflič M (2020) Determination of empirical rainfall thresholds for shallow landslides in Slovenia using an automatic tool. *Water* 12:1449. <https://doi.org/10.3390/w12051449>
- Kanungo DP, Sharma S (2014) Rainfall thresholds for prediction of shallow landslides around Chamoli-Joshimath region, Garhwal Himalayas, India. *Landslides* 11:629–638. <https://doi.org/10.1007/s10346-013-0438-9>
- Marra F (2019) Rainfall thresholds for landslide occurrence: systematic underestimation using coarse temporal resolution data. *Nat Hazards* 95:83–890. <https://doi.org/10.1007/s11069-018-3508-4>
- Mathew J, Babu DG, Kundu S, Vinod Kumar K, Pant CC (2014) Integrating intensity–duration-based rainfall threshold and antecedent rainfall-based probability estimate towards generating early warning for rainfall-induced landslides in parts of the Garhwal Himalaya, India. *Landslides* 11:575–588. <https://doi.org/10.1007/s10346-013-0408-2>
- Melillo M, Gariano SL, Peruccacci S, Sarro R, Mateos RM, Brunetti MT (2020) Rainfall and rockfalls in the Canary Islands: assessing a seasonal link. *Nat Hazards Earth Syst Sci* 20:2307–2317. <https://doi.org/10.5194/nhess-20-2307-2020>
- Melillo M, Brunetti MT, Peruccacci S, Gariano SL, Roccati A, Guzzetti F (2018) A tool for the automatic calculation of rainfall thresholds for landslide occurrence. *Environ Model Softw* 105:230–243. <https://doi.org/10.1016/j.envsoft.2018.03.024>
- Naidu S, Sajinkumar KS, Oommen T, Anuja VJ, Samuel RA, Muraleedharan C (2018) Early warning system for shallow landslides using rainfall threshold and slope stability analysis. *Geosci Front* 9:1871–1882. <https://doi.org/10.1016/j.gsf.2017.10.008>
- Neal R, Robbins J, Dankers R, Mitra A, Jayakumar A, Rajagopal EN, Adamson G (2020) Deriving optimal weather pattern definitions for the representation of precipitation variability over India. *Int J Climatol* 40:342–360. <https://doi.org/10.1002/joc.6215>
- Peruccacci S, Brunetti MT, Luciani S, Vennari C, Guzzetti F (2012) Lithological and seasonal control on rainfall thresholds for the possible initiation of landslides in central Italy. *Geomorphology* 139–140:79–90. <https://doi.org/10.1016/j.geomorph.2011.10.005>
- Piciullo L, Calvello M, Cepeda JM (2018) Territorial early warning systems for rainfall-induced landslides. *Earth-Sci Rev* 179:228–247. <https://doi.org/10.1016/j.earscirev.2018.02.013>
- Sajinkumar KS, Rinu S, Oommen T, Praveen KR, Rani VR, Muraleedharan M (2020) Improved rainfall threshold for landslides in data sparse and diverse geomorphic milieu: a cluster analysis based approach. *Nat Hazards* 103:639–657. <https://doi.org/10.1007/s11069-020-04004-w>
- Segoni S, Piciullo L, Gariano SL (2018) A review of the recent literature on rainfall thresholds for landslide occurrence. *Landslides* 15:1483–1501. <https://doi.org/10.1007/s10346-018-0966-4>
- Sengupta A, Gupta S, Anbarasu K (2010) Rainfall thresholds for the initiation of landslide at Lanta Khola in north Sikkim, India. *Nat Hazards* 52:31–42. <https://doi.org/10.1007/s11069-009-9352-9>
- Teja TS, Dikshit A, Satyam N (2019) Determination of rainfall thresholds for landslide prediction using an algorithm-based approach: case study in the Darjeeling Himalayas India. *Geosciences* 9:302. <https://doi.org/10.3390/geosciences9070302>
- Thakur MK, Kumar TVL, Narayanan MS, Kundeti KR, Barbosa H (2020) Analytical study of the performance of the IMERG over the Indian landmass. *Meteorol Appl* 27:e1908. <https://doi.org/10.1002/met.1908>
- Thennavan E, Ganapathy Pattukandan G, Chandrasekaran SS, Rajawat AS (2020) Probabilistic rainfall thresholds for shallow landslides initiation—a case study from the Nilgiris District, Western Ghats, India. *Int J Disaster Risk Manag* 2:1–13. <https://doi.org/10.18485/ijdrm.2020.2.1.1>

Open Access This chapter is licensed under the terms of the Creative Commons Attribution 4.0 International License (<http://creativecommons.org/licenses/by/4.0/>), which permits use, sharing, adaptation, distribution and reproduction in any medium or format, as long as you give appropriate credit to the original author(s) and the source, provide a link to the Creative Commons license and indicate if changes were made.



The images or other third party material in this chapter are included in the chapter’s Creative Commons license, unless indicated otherwise in a credit line to the material. If material is not included in the chapter’s Creative Commons license and your intended use is not permitted by statutory regulation or exceeds the permitted use, you will need to obtain permission directly from the copyright holder.

KLC2020 Official Promoters

The Kyoto Landslide Commitment 2020 (KLC2020)

Kyoto 2020 Commitment for Global Promotion of Understanding and Reducing Landslide Disaster Risk

A Commitment to the Sendai Landslide Partnerships 2015–2025, the Sendai Framework for Disaster Risk Reduction 2015–2030, the 2030 Agenda Sustainable Development Goals, the New Urban Agenda and the Paris Climate Agreement-

KLC2020 Official promoters are public and private organizations who promote the Kyoto Landslide Commitment 2020 and provide financial support for the implementation of the KLC2020 activities including the Open Access Book Series “Progress in Landslide Research and Technology.”

Host organization

International Consortium on Landslides (ICL)/Nicola Casagli.

Public sectors: KLC2020 Official Promoters-public

International Unions/Associations, Governmental organizations, Universities and Research institutes

- The International Union of Geological Sciences (IUGS)/ John Ludden
- The International Union of Geodesy and Geophysics (IUGG)/Kathy Whaler

- The International Association for the Engineering Geology and the Environment/Rafiq Azzam
- International Geosynthetics Society (IGS)/John Kraus
- Geological Survey of Canada, Natural Resources Canada, Canada/Daniel Lebel
- Faculty of Civil and Geodetic Engineering, University of Ljubljana, Slovenia/Matjaž Mikoš
- China University of Geosciences, Wuhan, China/Huiming Tang
- Department of Civil Engineering, National Taiwan University, Chinese Taipei/Shang-Hsien Hsien
- Institute of Rock Structure and Mechanics, the Czech Academy of Sciences/Josef Stemberk
- Institute of Cold Regions Science and Engineering, Northeast Forestry University/Wei shan.

Private sectors: KLC2020 Official Promoters-private

Companies and corporation.

- Marui & Co. Ltd, Japan
- Nippon Koei Co., Ltd, Japan
- Ellegi srl, Italy
- IDS GeoRadar s.r.l., Italy
- Chuo Kaihatsu Corporation, Japan
- Godai Corporation, Japan
- Kiso-Jiban Consultants Co., Ltd, Japan
- Kokusai Kogyo Co., Ltd., Japan
- OSASI Technos, Inc., Japan.



Introduction

The International Geosynthetics Society (IGS) is a non-profit learned society founded in Paris in 1983.

We are a member of the Federation of International Geo-Engineering Societies and also hold Liaison Organization status with International Organization for Standardization (ISO) Technical Committee 221 (TC 221) on Geosynthetics. The IGS is proud to be part of a multi-agency commitment with Kyoto Landslide Commitment 2020 (KLC2020).

The IGS is dedicated to the scientific and engineering development of geotextiles, geomembranes, related products, and associated technologies. Our membership forms a global community of over 3000 including corporate, individual and student members, with a shared passion for what geosynthetics can achieve (Figs. A.1 and A.2).

Geosynthetics are durable, high-performing polymeric materials used make infrastructure more sustainable in a variety of ways, for example:

Reduced energy consumption and emissions through:

- less on-site excavation;
- reduced transport of bulky construction materials;
- extended infrastructure lifetimes and reduced maintenance.

Protection of surface and groundwater through:

- landfill lining and containment of hazardous waste

- sludge dewatering and purification
- construction of sludge and tailings lagoon capping
- grey water storage for re-use
- preservation of potable and irrigation water supplies by lining canals, dams and reservoirs.

Replacement of other construction materials:

- sand and aggregate
- concrete, lime and cement
- steel.

Environmental protection:

- nuclear waste disposal
- sustainable urban drainage systems
- green and blue roof construction
- cost effective and resilient flood defences
- coastal defence.

Geosynthetics help prevent landslides in a number of ways, for example:

- performing a barrier and/or a filter function, mitigating the effects of water seepage;
- reinforcing soil and stabilising slopes;
- holding topsoil in place, preventing slippage;
- draining excess rainwater without washing soil away;
- encouraging growth of new vegetation, stabilizing slopes through natural means.



Fig. A.1 Geosynthetics used to stabilize a slope using soil in-fill and seeding for plants



Fig. A.2 Geosynthetics used to stabilize a slope by interacting with vegetation root structures



Geological Survey of Canada, Natural Resources Canada

GSC-Pacific Division

Geological Survey of Canada—Who We Are

The Geological Survey of Canada (GSC) is part of the Earth Sciences Sector of Natural Resources Canada. The GSC is Canada's oldest scientific agency and one of its first government organizations. It was founded in 1842 to help develop a viable Canadian mineral industry by establishing the general geological base on which the industry could plan detailed investigations. Throughout its long and colourful history, the GSC has played a leading role in exploring the nation.

Today, the GSC is Canada's national organization for geoscientific information and research. Its world-class expertise focuses on the sustainable development of Canada's mineral, energy and water resources; stewardship of Canada's environment; management of natural geological and related hazards; and technology innovation (Fig. A.3).

The GSC celebrated its 175th anniversary in 2017 which coincided with Canada's 150th anniversary of Confederation.

The GSC co-leads the Canada-Nunavut Geoscience Office and works with dozens of universities and research institutes, industry organizations, other federal departments, provinces, territories and municipalities in Canada and across the world. In particular, we work closely with other geological survey organizations in Canada through the unique Intergovernmental Geoscience Accord.

Every year, we publish hundreds of maps, Open Files, peer-reviewed papers and other reports. Our scientists are recognized worldwide and sought after for their expert advice

GSC-Pacific Division 1500-605 Robson St.,
Vancouver, BC, V6B 5J3, Canada
e-mail: David.Huntley@nrcan-mrcan.gc.ca

Marui & Co. Ltd. 1-9-17,
Goryo, Daito City, Osaka 574-0064, Japan
e-mail: hp-mail@marui-group.co.jp



Fig. A.3 Paleotsunami investigations in order to understand regional earthquake cycles and submarine landslide hazards

on locating mineral, energy and groundwater resources, reducing risk from natural hazards and reviewing environmental assessments.

Strategic Priorities

The GSC has attempted to plot a course through this changing, uncertain world.

First, we identify three core areas of persistent scientific endeavour, which reflect stable, long-term needs of society:

- **Geological knowledge for Canada's onshore and offshore lands**
- **Geoscience for sustainable development**
- **Geoscience for keeping Canada safe.**

Next, we outline a new, fourth area of endeavour, Geoscience for society, which is the need to address the uncertainties of the changing world by expanding the reach and impact of geoscience knowledge in land-use decision making and in efforts to reduce the risk of disasters.

Finally, we recognize that our strength lies in a fifth area of endeavour, Our people, Our science, which we need to nurture to maintain a high-performing workforce capable of world-leading innovative geoscience for the benefit of Canada.

(a) Geological knowledge for Canada's onshore and offshore lands

Geoscientific knowledge is fundamental to managing our onshore and offshore lands and their abundant resources. With its 10 million km² of onshore land and an additional 7 million km² of ocean estate, Canada is a vast country and a core mission of the GSC is to map and understand the land and its resources. Our Geo-mapping for Energy and Minerals (GEM) program continues to advance our knowledge of the North and by 2020 will complete a first mapping of surface geology at a coarse scale.

In the offshore lands, our geoscience knowledge also serves to confirm the farthest extents of the Canadian territory. Our joint program with Global Affairs Canada and Fisheries and Oceans Canada to delineate the outer limits of the continental shelf in the Atlantic and Arctic Oceans will reach a critical milestone in 2019. The program will file its Arctic submission under the United Nations Convention on the Law of the Sea (UNCLOS) (Fig. A.4).

(b) Geoscience for sustainable development

Finding new resources remains a major challenge. Many near-surface deposits have been discovered in Canada, but significant mineral resources remain to be found in less accessible regions and at depths below the surface. Finding new resources requires systematic, intensive and innovative methods to assess the mineral potential in remote locations.



Fig. A.4 The GSC studies the sea floor of the Arctic to understand its geology and geohazards. Here a small craft surveys the bottom of Southwind Fjord (Baffin Island, N Nunavut)



Fig. A.5 GSC geologists near the Heiberg Formation in northern Ellesmere Island (NU) as part of the geo-mapping for energy and minerals program. This formation is the primary host of major gas accumulations in the Canadian High Arctic

It requires searching beneath overburden cover, imaging the 3-D structure of the earth and understanding the geological processes that lead to concentration of minerals in certain locations (Fig. A.5).

For the Energy sector, the greatest challenge is in the transition to a low-carbon economy. Although global fossil fuel use is likely to continue to grow over the foreseeable future, the trend will likely be at a decreasing rate. Canada has an abundant supply of conventional and unconventional (oil sands and shale) oil and gas, so development in frontier areas is likely to be slow. In addition, the government has placed a moratorium on exploration activity in the Arctic offshore lands.

(c) Geoscience for keeping Canada safe

The GSC will continue to work on understanding how landscapes will change, how infrastructure will be affected and how resilience to climate change can be built into new infrastructure. Climate change will likely have a significant impact on the water cycle. GSC research will shed light on the risk to potable water supplies, hydroelectric power generation, and hazards from floods and drought (Fig. A.6).

(d) Geoscience for society

The scientific knowledge required to assess cumulative effects is broad. The complex interactions between land use, water management and waste management require an integrated approach at a landscape scale. The GSC is a national provider of information on both land (surficial and solid geology) and water, including the integration of surface water and groundwater into the complete water cycle (Fig. A.7).

The GSC recognizes that this area of endeavour involves inherent complexities and that our goals in this area will be to some degree aspirational. However, we will investigate



Fig. A.6 The GSC conducts climate change studies, here documenting the effects of fast melting permafrost leading to extreme coastal erosion on Pelly Island, NT



Fig. A.7 The GSC conducts geohazard studies to reduce risks to people and infrastructure, here installing equipment to monitor landslide activity above a critical railway corridor in central BC

new ways of planning our programs, undertaking our field-work, interacting with key stakeholders, and communicating our expert knowledge in ways that contribute positively to decision making about resource development.

(e) **Our people, Our science**

As a science organization within the federal government, the GSC's mandate is to conduct world-class science to inform public decision making. The Canadian government has articulated and adopted the principle of evidence-based decision making and reaffirmed the need for government science to be objective and non-partisan.

To remain at the leading edge, our scientists need to work with a variety of partners. We need to reinforce the central role that the GSC plays in the Canadian geoscience community by building networks of collaboration, fully participating in



Fig. A.8 Among many celebratory activities for the GSC's 175th anniversary in 2017, the GSC held a Rock and Fossil Exhibit, at its site at the Bedford Institute of Oceanography (Dartmouth, NS), as part of a two-day open-house event, where more than 20,000 visitors participated

national geoscience initiatives, and advocating for Canadian geoscience at the international level (Fig. A.8).

Moving forward

Some of the objectives and goals that the GSC has set represent familiar territory for a national geoscience organization, but many others will pull us out of our comfort zone. We will take the time to better understand the challenges of delivering objective, nonpartisan science to support evidence-based decision making in Canada at a time of great technological and social change.

We will not be able to do this alone, so we look forward to strengthening our ties to other federal departments, provinces and territories, universities, Indigenous organizations, the private sector and civil society as a whole.

We ask all our stakeholders to contact us, to challenge us and, most importantly, to join with us to assure the future of Canada through thoughtful, respectful dialogue about the land we live on, its resources and its future (Fig. A.9).

Exploring Canada

Through its history, the GSC has been responsible for mapping the land mass of Canada, which supported the integration of the western provinces and northern territories into the country that we have today. The limit of Canada's offshore territory is still being extended today through surveys conducted by the GSC and the Canadian Hydrographic Service.

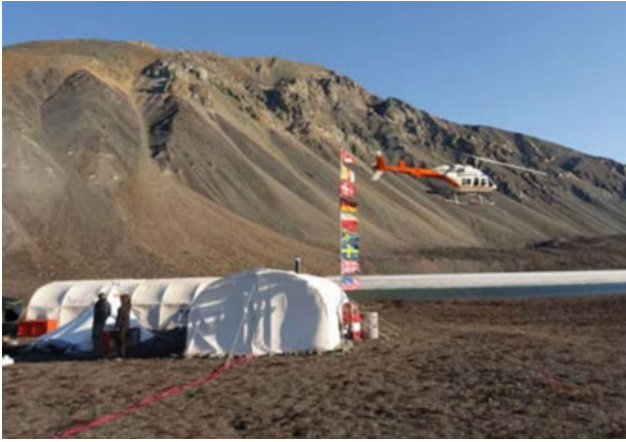


Fig. A.9 Joint Canadian/German (GSC/BGR) field mapping camp on northern Ellesmere Island, looking west as the fog covered sea ice of Yelverton Inlet, 2017

In more recent years, the GSC helped find the first economic diamond deposit in the Northwest Territories, leading to the expansion of diamond mining in Canada. These are only a few of the key GSC achievements that have built our knowledge of Canada's lands and provided the building blocks of its natural resource economy.

Today, exploration of this vast land is still reaping its natural resource rewards. The search for natural resources is difficult, akin to looking for a needle in a haystack.

The GSC's GEM program is exploring vast tracts of Canada's North, a land mass roughly equivalent to the combined areas of Quebec, Ontario and Manitoba, to find the "haystacks" with resource potential. This information is shared with the provinces and territories, as well as the private sector, so that the search for the "needles" can continue. The information is also critical to inform land-use planning.



In November 2016, the Royal Canadian Geographical Society (RCGS) awarded its prestigious Gold Medal to the GSC in recognition of the Survey's outstanding contribution to the development of Canada on the occasion of its 175th anniversary.



Matjaž Mikoš

Summary

In 2019, the Faculty of Civil and Geodetic Engineering of the University of Ljubljana (ULFGG) celebrated its centennial: The precursor of the faculty was the Technical Faculty established in 1919 as one of five founding faculties of UL.

ULFGG, covering technical disciplines of civil and geodetic engineering, as well as water science and technology, has been involved in landslide risk reduction activities at the national level in Slovenia (former Yugoslavia, until 1991) for decades (Fig. A10). In 2008, ULFGG became an ICL Full Member and has gradually developed its ICL engagement. ULFGG has been awarded the title of the World Centre of Excellence (WCoE) in Landslide Risk Reduction for 5 consecutive periods (2008–2011, 2011–2014, 2014–2017, 2017–2020, 2020–2023). Together with the Geological Survey of Slovenia, another ICL member in Slovenia, ULFGG hosted the 4th World Landslide Forum in Ljubljana, Slovenia, from May 29 to June 2, 2017. ULFGG strongly supports diverse activities of the International Consortium on Landslides, Kyoto, Japan, and thus contributes to the 2030 Agenda for Sustainable Development, as well as to the Sendai Framework for Disaster Risk Reduction 2015–2030 (SF DRR). ULFGG was a signatory of the Sendai Landslide Partnerships 2015–2030, and is a strong promoter of the Kyoto Landslide Commitment 2020, a SF DRR voluntary commitment by ICL.

In 2019, ULFGG hosted, together with the Slovenian Chamber of Engineers, the World Construction Forum 2019 (WCF 2019; www.wcf2019.org) in Ljubljana under the forum

motto “Buildings and Infrastructure Resilience.” The Forum with one of the themes on Disaster Risk Management and Governance for Resilient Communities was co-organized by the World Federation of Engineering Organizations (WFEO) in support to the implementation of the 2030 Agenda for Sustainable Development. All lectures given at the WCF2019 are available for free on the forum web page, as a contribution to Open Science efforts.

In the field of capacity building, ULFGG offers several courses for graduate and postgraduate students in landslide mechanics and dynamics, landslide stabilization and landslide risk mitigation. In this paper, a short overview of the past activities of ULFGG as ICL Full Member is shown.

World Centre of Excellence on Landslide Risk Reduction and IPL projects

WCoE activities

The title of World Centre of Excellence (WCoE) on Landslide Risk Reduction is given to a governmental or non-governmental entity, which contributes to the landslide disaster risk reduction at a regional and/or global level in a specific unique field of expertise, as well as helps promoting International Programme on Landslides (IPL) and landslide research intellectually, practically and financially (<https://www.landslides.org/ipi-info/world-centre-of-excellence/>). ULFGG was granted the title of WCoE five consecutive times: (Fig. A.10)

- WCoE 2008–2011 & 2011–2014: Mechanisms of landslides in over-consolidated clays and flysch.
- WCoE 2014–2017: Mechanisms of landslides and creep in over-consolidated clays and flysch.
- WCoE 2017–2020: Landslides in Weathered Flysch: from activation to deposition.
- WCoE 2020–2023: Landslides in Weathered Heterogeneous Sedimentary Rock Masses such as Flysch.

M. Mikoš

Faculty of Civil and Geodetic Engineering
University of Ljubljana, Jamova cesta 2, SI-1000
Ljubljana, Slovenia
e-mail: matjaz.mikos@fgg.uni-lj.si

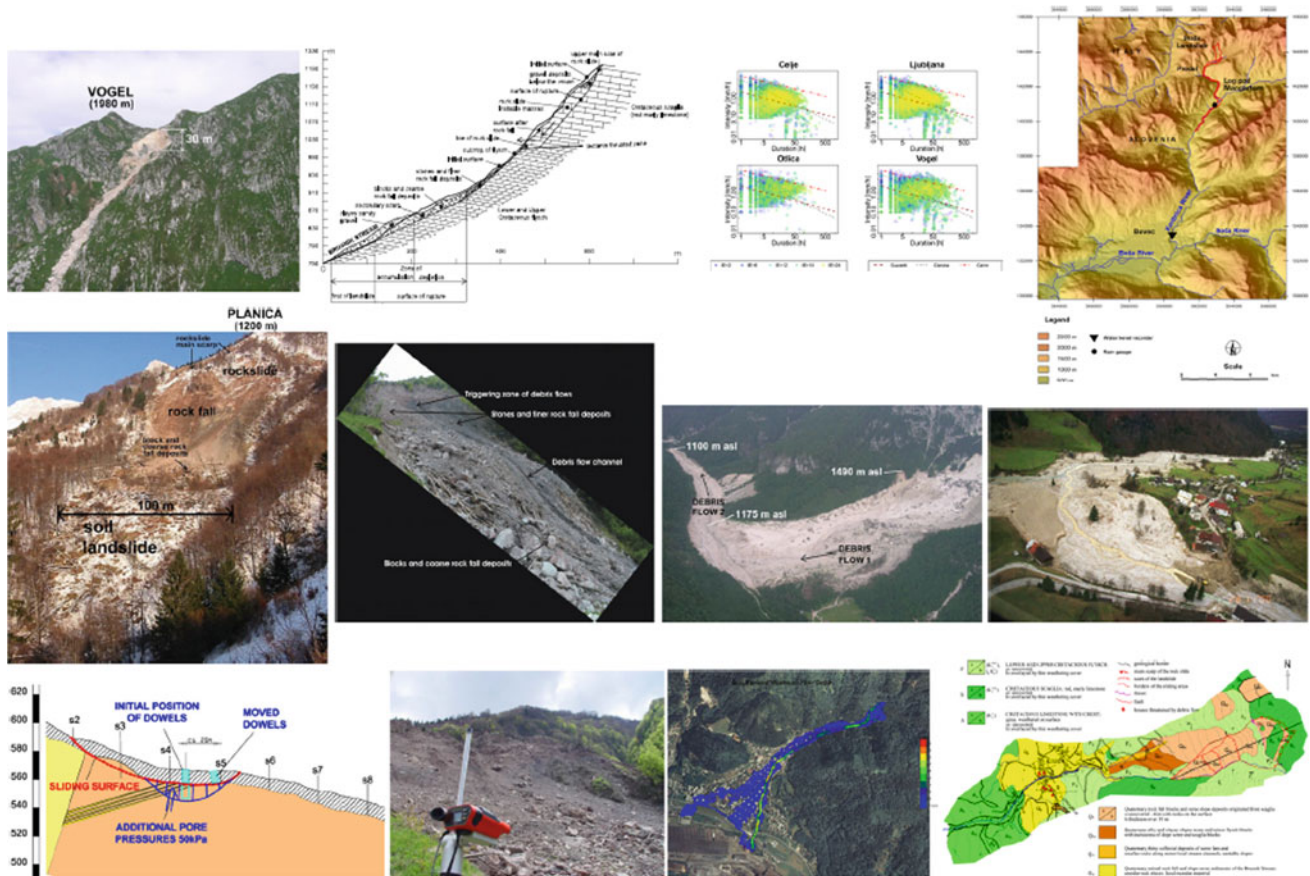


Fig. A.10 A collage of landslides in Slovenia and their investigation performed by UL FGG

The research efforts at ULFGG were focused on:

- Mechanisms of triggering such landslides (mud flows), estimation of debris-flow magnitudes triggered as shallow or deep-seated landslides (debris slides), and triggering of shallow rainfall-induced landslides using advanced statistical methods.
- Field and laboratory investigations of suction in over-consolidated clays and flysch, such as to improve the understanding of softening in stiff over-consolidated clays and marls, using soil matrix suction as an indicator for mudflow occurrence, and executing suction long-term monitoring of the Slano Blato landslide.
- Laboratory investigations of coarse debris-flow rheological parameters and soil–water characteristic curve of residual soil from a flysch rock mass.
- Mathematical modelling of debris flows (hazard assessment in deposition areas), using different numerical models and different digital terrain models.

The WCoE activities were financially supported by the Slovenian Research Agency through the Research Programme P2-0180 “Water Science and Technology, and Geotechnical Engineering: Tools and Methods for Process

Analyses and Simulations, and Development of Technologies,” as well as by several national and international (bi-lateral) research projects.

ULFGG and the Geological Survey of Slovenia jointly organized 4th World Landslide Forum (WLF4), in Ljubljana between May 29 and June 2, 2017, followed by a three-day field study tour to see the variety of landslide forms in Slovenia and in its immediate NW surroundings. With over 600 participants from 49 countries and 5 international organizations, WLF4 was promoting the culture of living with natural hazards.

IPL projects

An important ICL activity is IPL projects (<https://www.landslides.org/projects/icl-world-report-on-landslides/>). The IPL Evaluation Committee examines the submitted proposals of ICL members by carefully reading the written proposals and by listening to their presentations at annual ICL conferences. The initially accepted proposals by the IPL Evaluation Committee are discussed and then approved at the annual Board of Representatives meeting of ICL members (Annual Assembly). Finally, the IPL projects are approved annually

by the IPL Global Promotion Committee. ULFGG has successfully submitted several proposals for IPL projects and has been so far actively involved in the following ones:

- IPL-151 Soil matrix suction in active landslides in flysch—the Slano Blato landslide case (2010–2012).
- IPL-225 Recognition of potentially hazardous torrential fans using geomorphometric methods and simulating fan formation (2017–2020).
- IPL-226 Studying landslide movements from source areas to the zone of deposition using a deterministic approach (2017–2020)—coordinated by the Geological Survey of Slovenia.

ICL thematic and regional networks

Following the ICL Strategic Plan 2012–2021, several thematic networks and regional networks have been established (for an overview, see <https://www.landslides.org/projects/icl-networks/>).

Landslide Monitoring and Warning Thematic Network

In 2012, ULFGG proposed the ICL landslide monitoring and warning thematic network (abbr. LaMaWaTheN), and almost 10 ICL members joined the initiative. The general objective of the proposed network was to compare experiences in the field of landslide monitoring and installed early warning systems for active landslides in various regions of the world. A proposal for landslide monitoring techniques database was. The network was later coordinated by the Croatian Landslide Group from the Faculty of Civil Engineering, University of Rijeka, Croatia, and the Faculty of Mining, Geology and Petroleum, University of Zagreb, Croatia. Lately, we contributed to the network activities by preparing practice guidelines on monitoring and warning technology for debris flows.

The idea of the network was partially taken over by the web database ICL World Report on Landslides (<http://iplhq.org/lr-world-report-on-landslide/>), created to be a platform to share landslide case studies among the global landslide community, with monitoring and warning systems being a part of the story.

ICL Adriatic-Balkan Network

Jointly with other ICL members from Croatia and Serbia, in 2013, ULFGG proposed to establish an ICL Adriatic-Balkan Regional Network (ICL ABN; <https://www.klizista-hr.com/>

[en/organization/about-us/icl-abn/](https://www.klizista-hr.com/en/organization/about-us/icl-abn/)). Various network activities were proposed, the most active being the organization of biennial regional symposia on landslide risk reduction in the Adriatic-Balkan Region (called ReSyLAB). ULFGG supported the 1st Symposium in Zagreb (Croatia) in 2013 (March 6–9), and the 2nd in Belgrade (Serbia) in 2015 (May 14–16), and jointly organized the 3rd in Ljubljana (Slovenia) in 2017 (October 11–13) together with the Geological Survey of Slovenia (also an ICL member).

In the last decade, ULFGG has signed bilateral research projects with the ICL members in the region: “Adriatic-Balkan Regional Network: Landslide Risk Mitigation for Society and Environment” (2012–13 with University of Belgrade, Serbia), “Study of landslides in flysch deposits: sliding mechanisms and geotechnical properties for landslide modelling and landslide mitigation SoLiFlyD” (2014–15 with University of Rijeka, Croatia), and “Laboratory investigations and numerical modelling of landslides in flysch deposits in Croatia and Slovenia” (2016–17 with the University of Rijeka, Croatia). This joint research has helped strengthen regional cooperation within the ICL ABN regional network.

Other ICL-related international activities

ULFGG served the ICL by taking different leading roles in the Consortium, i.e. ULFGG member served as Chair of IPL Evaluation Committee, twice as ICL Vice President, and was elected to Co-Chair and in 2021 to Chair of the IPL-KLC (<https://www.landslides.org/ipi-info/ipi-klc-global-promotion-committee/>).

ULFGG has been strongly supporting the journal *Landslides: Journal of the International Consortium on Landslides*, published by Springer Nature (<https://link.springer.com/journal/10346>) since its launch in 2004. ULFGG works for the journal in the roles of reviewers and an associate editor, and regularly publishes its top research results in the journal, as well as disseminates information important for capacity building in landslide risk reduction in the journal.

ULFGG followed the development of the journal from its bibliometric perspective, and compared scientometric impacts of the journal with the other ICL publications (monographs, volumes from World Landslide Forums) in the field of landslide research.

ULFGG also contributed to the two-volume set of *Landslide Dynamics: ISDR-ICL Landslide Interactive Teaching Tools (LITT)*, namely to Volume 1: Fundamentals, Mapping and Monitoring by practice guidelines on monitoring and warning technology for debris flows (<https://www.springer.com/gp/book/9783319577739>), and to Volume 2: Testing, Risk Management and Country Practices (<https://www.springer.com/gp/book/9783319577760>) by a

state-of-the-art overview on landslide disaster risk reduction in Slovenia, a study on two-dimensional debris-flow modelling and topographic data, and by study on intensity-duration frequency curves for rainfall-induced shallow landslides and debris flows using copula functions.

UNESCO Chair on Water-related Disaster Risk Reduction

Experiences and knowledge accumulated in the past decades at the Chair on Hydrology and Hydraulic Engineering at ULFGG in the field of (applied) hydrology in experimental basins, landslide research, landslide risk reduction, and flood risk management, culminated in 2016 in the establishment of the UNESCO Chair on Water-related Disaster Risk Reduction (WRDRR Chair; www.unesco-floods.eu) at the University of Ljubljana. The UNESCO WRDRR Chair was positively evaluated in 2020 and prolonged for another 4 years (2020–2024). The Chair is associated to the university twinning and networking UNITWIN UNESCO—Kyoto University—ICL on “Landslide and Water-Related Disaster Risk Management”.

ULFGG supports activities of the Slovenian National Committee for UNESCO Intergovernmental Hydrological

Programme (www.ncihp.si) – focus of the activities is the development of the IHP-IX Programme (2022–2029).

Conclusions

ULFGG as one of World Centres of Excellence in Landslide Risk Reduction, hosts the UNESCO Chair on Water-related Disaster Risk Reduction. ULFGG strongly supports ISDR-ICL Sendai Partnerships 2015–2025 for global promotion of understanding and reducing landslide disaster risk, and its extension to 2030 and beyond: the Kyoto 2020 Commitment for Global Promotion of Understanding and Reducing Landslide Disaster Risk that that was signed in November 2020. ULFGG is proud to be its Official Promoter, and will specifically work for its Actions 2, 5, 6, 9 and 10.

This review contribution is intentionally written without giving references to described activities. For this purpose, listed websites and web search engines may be used.

The author wants to thank numerous colleagues from ULFGG and from the wide ICL community for a long-lasting excellent cooperation with a joint vision to reduce landslide disaster risk.



Huiming Tang, Changdong Li, and Qinwen Tan

Introduction

China University of Geosciences, Wuhan (CUG), founded in 1952, is a national key university affiliated with the Ministry of Education. It is also listed in the National “211 Project”, the “985 Innovation Platform for Advantageous Disciplines” and the “Double First-class Plan”. CUG, featuring geosciences, is a comprehensive university that also offers a variety of degree programs in science, engineering, literature, management, economics, law, education and arts. Its Geology and Geological Resources & Engineering have both been ranked as national number one disciplines.

CUG has two campuses in Wuhan. The main campus is the Nanwang Mountain Campus, located in the heart of the Wuhan East Lake National Innovation Demonstration Zone, which is popularly known as China Optics Valley. The Future City Campus is located in the east of Wuhan and is 27 km from the main campus. These two picturesque campuses cover a combined area of 1,474,353 m². They are ideal places to study, work, and enjoy life. CUG owns a 4A-Level tourist attraction—the Yifu Museum. CUG also boasts four field training centers: Zhoukoudian in Beijing, Beidaihe in Hebei Province, Zigui in Hubei Province, and Badong in Hubei Province.

CUG has established a complete education system. As of December 2020, 30,239 full-time students, including 18,080 undergraduate students, 9302 master’s students, 1916 doctoral students, and 941 international students have enrolled in its subsidiary 23 schools and 86 research institutes. CUG currently has a faculty of 1858 full-time teachers, among which there are 539 professors (11 of which are members of the Chinese Academy of Sciences) and 984 associate professors.

CUG is focused on fostering high-quality talent. Among its over 300,000 graduates, many have gone on to become scientific and technological elites, statesmen, business leaders and athletes. And they have made great contributions to the nation and society, represented by former Premier WEN Jiabao and 39 members of the Chinese Academy of Sciences and Chinese Academy of Engineering.

CUG has strengthened exchanges and cooperation with international universities. It has signed friendly cooperation agreements with more than 100 universities from the United States, France, Australia, Russia and other countries. CUG has actively carried out academic, scientific and cultural exchanges with universities around the world. There are about 1,000 international students from more than 100 countries studying at CUG. It also sponsors more than 900 teachers and students to study abroad or conduct international exchanges, and invites more than 400 international experts to visit, lecture, and teach at CUG every year. In 2012, CUG initiated and co-established the International University Consortium in Earth Science (IUCES) with 11 other world-renowned universities. IUCES is committed to promoting the common development of geosciences education and scientific research through resource sharing, exchange and cooperation among its member institutions. In addition, CUG has partnered with Bryant University from USA, Alfred University from USA, and Veliko Turnovo University from Bulgaria in establishing three Confucius institutes on their campuses (Fig. A.11).

Strategic plan of building a world-renowned research university in earth sciences—a beautiful China and a habitable earth: towards 2030

CUG reviewed and approved Strategic Plan of Building a World-Renowned Research University in Earth Sciences on December 25 of 2019.

Huiming Tang, Changdong Li, Qinwen Tan
China University of Geosciences, No. 388 Lumo Road
Wuhan, P.R. China
e-mail: tanghm@cug.edu.cn

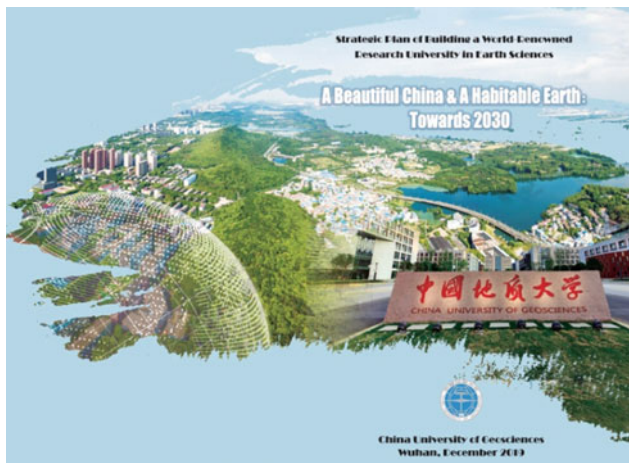


Fig. A.11 Strategic plan of building a world-renowned research university in earth science

Themed on “A Beautiful China & A Habitable Earth”, the Plan depicts the blueprint of the second goal of the “three-steps strategic goals”, which is to build a world-renowned research university in Earth Sciences by 2030 based on the attained goal of developing CUG into a “high-level university with first-class Earth Sciences and coordinated development of multi-disciplines”.

According to the Plan, our education missions are: Remaining true to CUG’s core value of “seeking harmonious development between man and nature”, we are committed to cultivating innovative talents who have lofty morality, solid foundation, and profound expertise, and who pursue the unity of knowing and doing. We should provide personnel support, and endeavor to innovate, apply and spread knowledge in order to provide theories, technologies and approaches for the construction of a Beautiful China and a Habitable Earth. We should strive to optimize governance, reform culture, and fully invigorate the vitality of running a university. We should provide our service to the construction of an innovative country and to the promotion of a harmonious co-existence between man and nature. We should provide our service to the people and the governance of China. We should provide our service to the consolidation and development of the system of socialism with Chinese characteristics. We should provide our service to the reform and opening up and to the construction of the socialist modernization.

According to the Plan, our endeavoring goals are: By 2030, we will have built a world-renowned research university in Earth Sciences, whose main indexes will have reached or nearly reached the level of other world-class universities. To upgrade CUG into a world-class university, we will endeavor to make the discipline of Earth Sciences rank top in the world and forge boldly ahead in competition to improve the quality

of other disciplines of CUG. We will assemble a contingent of teachers and researchers with international competitiveness and influences to build a university with Chinese characteristics and superiority. We will build a world-class university that will be fully engaged in international exchange and cooperation and that will achieve educational, academic, cultural, and administrative excellence.

Outstanding Recent Achievements

In recent years, CUG has achieved significant progress in the research fields of geohazards, water resource, geochemistry, paleontology, geodetic surveying and lunar exploration program, etc. To keep to the theme of KLC2020, recent achievements on geohazards researches of CUG are focused and introduced.

a. Approval of National Observation and Research Station for Geohazards in the Three Gorges Reservoir Area, Hubei

CUG was newly approved **National Observation and Research Station for Geohazards in the Three Gorges Reservoir Area, Hubei**. This station, founded and administrated by Prof. Huiming Tang, is responsible to carry out field observations and scientific research on geohazards in condition of reservoir operation.

The central site of the station is located in Badong County of the Three Gorges Reservoir area (hereinafter abbreviated as the TGR area), and a larger monitoring network of multiple sites has been established, including the geohazard field test site for the Majiagou landslide, Zigui County, and systematic geophysical monitoring station for the whole TGR area, etc.

The Badong field site (also named Badong in-situ large-scale experimental station) is located in the Huangtupo landslide area, which has been recognized the largest reservoir landslide by volume in the TGR area. The field site consists of a tunnel complex and a series of monitoring systems (Fig. A.12). The tunnel complex, built in the Huangtupo riverside sliding mass #1, consists of a main tunnel with a length of 908 m and a width of 5 m, five branch tunnels (5 m to 145 m long, 3.5 m wide), two test tunnels, and 35 observation windows. The test tunnels exposed the sliding zones of the landslide, facilitating their direct observation and the execution of scientific experiments, such as large-scale in-situ mechanical tests and deep deformation monitoring. The monitoring systems measure deformation as well as hydrologic, meteorological and hydro-chemical variables. The deformation system is

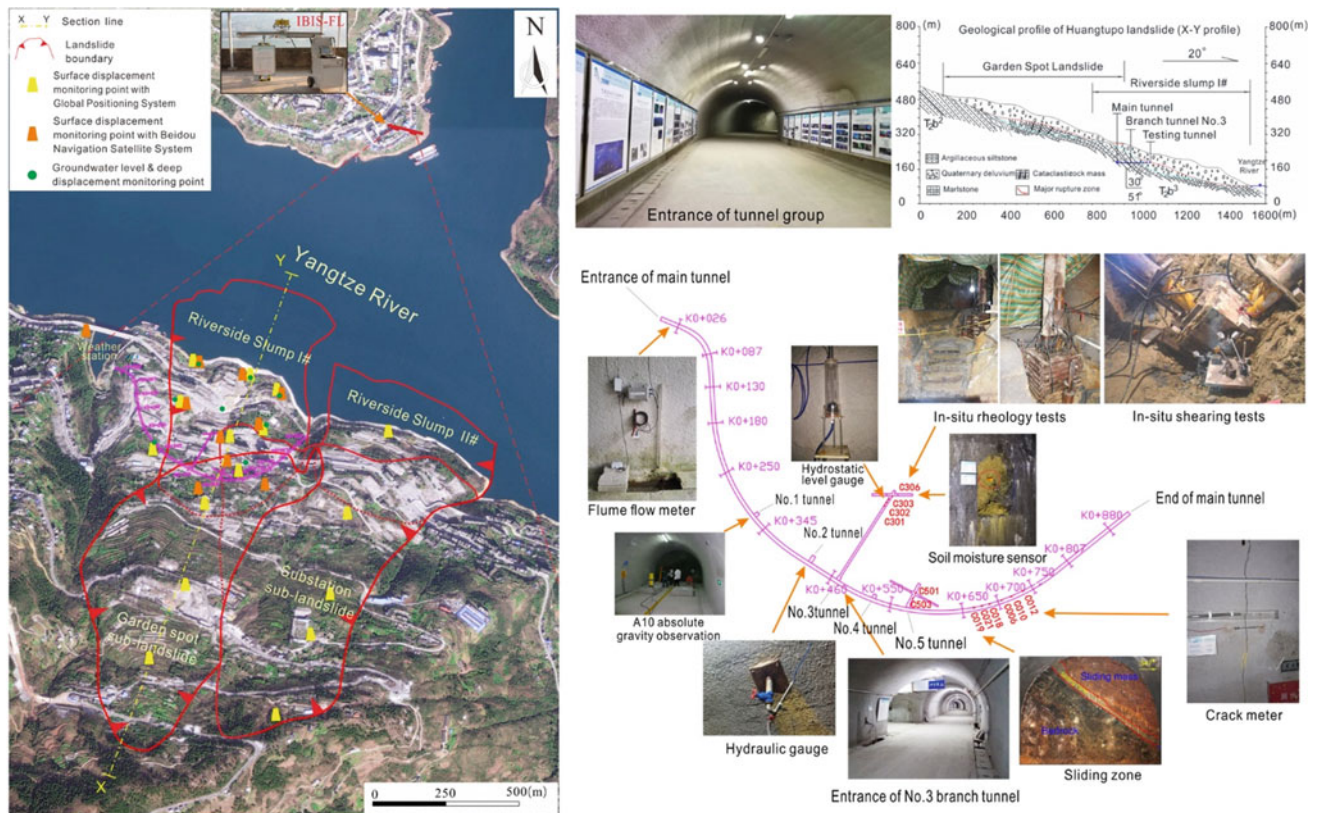


Fig. A.12 Badong in-situ large-scale experimental station of the National Observation and Research Station for Geohazards in the Three Gorges Reservoir Area, Hubei

composed of a slope surface displacement measurement unit and an underground displacement measurement unit. The slope surface displacement unit includes a number of GPS (Global Positioning System) and BDS (BeiDou Navigation Satellite System) measurement points, as well as an IBIS-FL (Interferometric Radar) monitoring system (Fig. A.12). The underground displacement unit includes nine deep inclinometer boreholes, a number of crack meters installed on the ground and the walls of tunnels, and many hydrostatic level gauges that measure the settlement of the tunnels in the sliding mass. The hydrologic system includes a number of devices that allow for observation of the water level of the Yangtze River, the ground water level and water discharge of the tunnels (Fig. A.12). A small meteorological station is located on the landslide and provides rainfall data. So far, multiple and massive data have been collected for the landslide area since the year 2012, when the field site was constructed; over 10,000 people with a variety of geology-related backgrounds from > 20 countries have visited this experimental station.

b. Approval of the Basic research on the prediction and forecasting of major landslides program supported by the Major Program of NSFC

CUG was approved the **Basic research on the prediction and forecasting of major landslides** program (2021–2025), supported by the Major Program of the National Natural Science Foundation of China. The program was designed for the prediction and forecasting of major landslides, with the concentration on the core scientific problems of landslide evolution process and physical-mechanical mechanism. Three key scientific problems, including correlation mechanism for landslide initiation, physical-mechanical mechanism for landslide initiation, and prediction and forecasting theory based on landslide evolution were proposed.

Five topics were set up to achieving those objectives. Topic 1 was proposing the initiation classification of major landslides based on large field test platform, with the adoption of field prototype test and other technical means. Topics 2-4 aimed to reveal the physical and mechanical mechanism

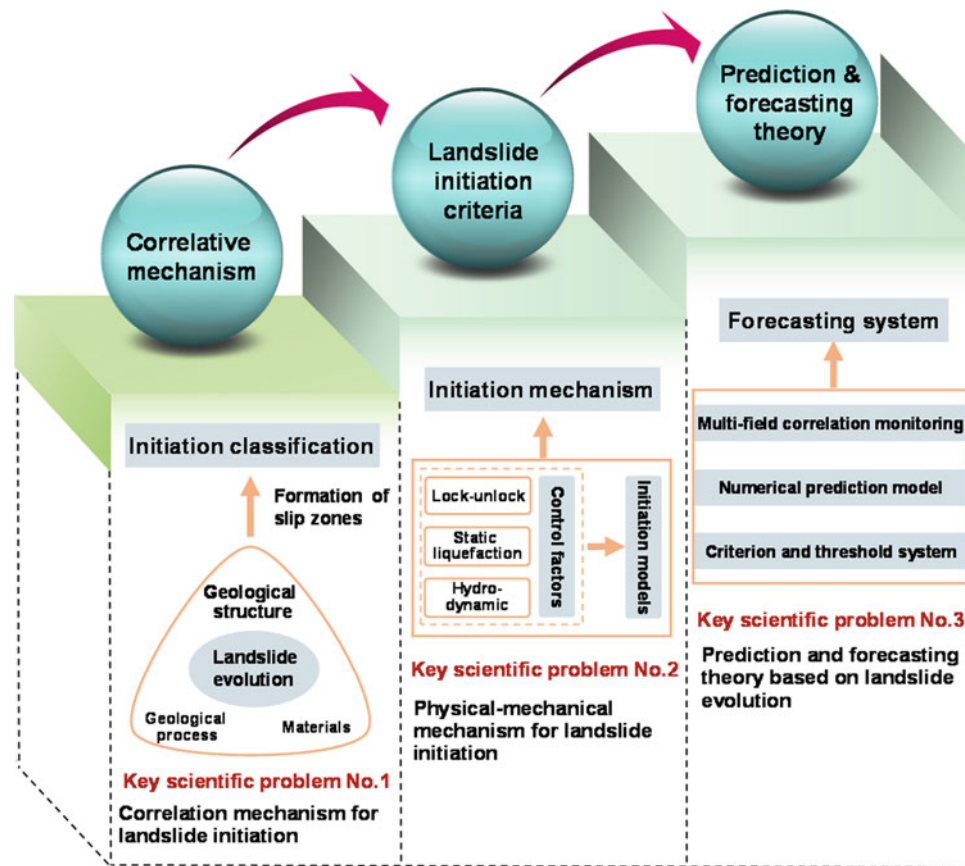


Fig. A.13 Scientific thought for the implement of research

of locked-segment dominated landslide, static liquefaction loess landslide and hydrodynamic pressure-driven landslide, and to establish the corresponding landslide initiation criteria, respectively. Topic 5 was responsible to established the prediction mode and real-time forecasting system. Ultimately, the landslide prediction and forecasting theory based on the evolution process and physical-mechanical

mechanism would be put forward. The scientific thought for the implement of research is exhibited in Fig. A.13.

The implementation of the research is respected to lay the geological, mechanical and physical foundation for the above three types of landslide prediction, and to substantially promote the research on landslide prediction.



Department of Civil Engineering, National Taiwan University

Department of Civil Engineering, National Taiwan University

Introduction

National Taiwan University (NTU) was originally established in 1928, when Taiwan was under Japanese rule, as Taihoku Imperial University. The current name dates back to 1945. As Taiwan's oldest and most prestigious university, we are also the largest comprehensive higher education institution (HEI) in the country. The academic freedom that we cherish and our excellent faculties attract both domestic and international students. Throughout our 90-year history, we have nurtured many talents, including leading academics and leaders in the public and private sectors. Our campus is vast, and spans across multiple locations, including Taipei, Yilan, Hsinchu, Yunlin, and mountainous areas in central Taiwan—accounting for nearly 1% of Taiwan's total land area. This provides teachers and students with an environment rich in biological and ecological diversity.

As the leading university in Taiwan, we are strongly committed to social responsibility as we strive to drive sustainable development and influence positive change in society. This was also reflected in the first University Impact Rankings launched in 2019 by Times Higher Education (THE), which measure the contributions of HEIs to the United Nations' Sustainable Development Goals (SDGs). We were ranked 70th in the world overall, and 1st in the world for SDG16: Peace, Justice, and Strong Institutions. Starting from creating a sustainable culture on campus, we aim awareness about sustainability throughout the university, through innovative teaching and research, environmental protection and recycling efforts, and a school administration that supports equality and wellbeing. Our sustainability

efforts extend beyond our campus through industry-academia collaborations and service teams deployed to remote areas. In the near future, we will continue to reinforce the spirit of innovation and sustainability thinking among all faculty members and students. We will also continue our efforts to address economic, environmental, and social challenges through interdisciplinary collaboration, as we create connections between the local and the international community.

The Department of Civil Engineering (Fig. A.14) can be regarded as the root of The College of Engineering. The early civil engineering education covers a wide range of professions. With the development and differentiation of various social industries, some fields have gradually separated and established specialized departments. We have also moved on, combining different fields and top-notch technology to remain as the leader of the tide.

Civil engineering is inseparable from the development of human civilization. From the beginning of civilization, all man-made structures have enmeshed and highlighted the value of civil engineering. NTU Civil Engineering is no exception. From the Department of Civil Engineering of the Imperial College of Taipei to the National Taiwan University Department of Civil Engineering today, the majority of Taiwan's significant constructions is and will always be our finest gallery.

In National Taiwan University, you will obtain high-quality guidance in and out of the classroom. Academic resources in the classroom and sports culture clubs, various student activities throughout the year, will bind you together with peers of the same dream. These friends may also be partners that can help you in future careers. If you are willing to take civil engineering as a career and take on the challenges and step forward as a team, then listen to your inner call, join us, and let us stride ahead hand in hand (Fig. A.15).

Department of Civil Engineering, National Taiwan University
No.1, Sec. 4, Roosevelt Road,
Taipei, 10,617, Taiwan
e-mail: louisge@ntu.edu.tw

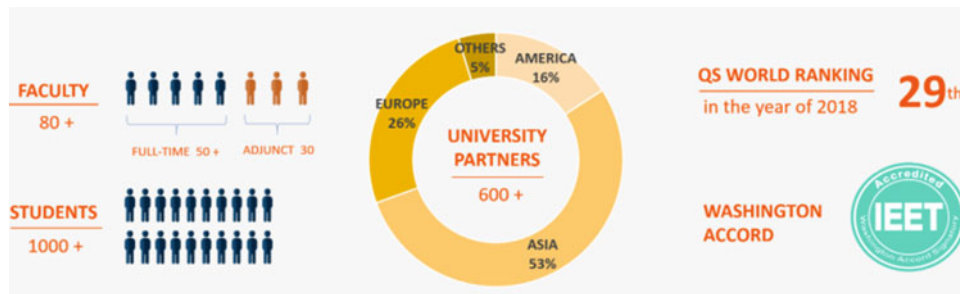


Fig. A.14 Quick facts of the Department of Civil Engineering



Fig. A.15 Life beyond Classroom

Outstanding Recent Achievements

Mitigating the Impacts of Natural Disasters via Cutting Edge Technology

Taiwan is located in the Circum-Pacific seismic belt, with many active faults and frequent typhoons. Due to the effects of climate change, extreme rainfall events that used to occur once in a century are now becoming more frequent, exacerbating the threat of landslides and debris flows. The prevention and mitigation of natural disasters such as earthquakes and flooding have therefore become a priority for the twenty-first century.

(a) Earthquake Early Warning Systems: gain valuable response time

For most natural disasters, potential losses to life and property can be mitigated through early warning and prevention. After the earthquake disaster of September 21st, 1999, building safety inspections needed to be conducted all

across Taiwan. Our faculty and students with expertise in civil engineering and geology were quick to respond to this urgency, working closely with the National Center for Research on Earthquake Engineering to help the government improve the earthquake resistance standards and test specifications. Moreover, they proposed a more elaborate system for earthquake damage and liquefaction assessment, and conducted a complete review and classification of the earthquake risk tolerance for all areas in Taiwan. The team also developed new disaster prevention technologies. One of the most significant contributions was to assist the public high (vocational) schools around Taiwan with assessments of the earthquake resistance and reinforcement needs of old buildings. In the numerous earthquakes that have since occurred, the effect of these reinforcements has become apparent. The stronger earthquake resistance of these buildings has improved safety for 2.65 million teachers and students around Taiwan (Fig. A.16).

Our school has also developed technology to monitor the status of bridges with high traffic volumes. This optical fiber monitoring system will emit a warning whenever poor conditions are recorded, prompting an early response from management that can prevent a disaster from happening. When bridges in remote areas are damaged, a lightweight bridge developed by NTU out of composite materials can be assembled by residents in short time. In this way, access to affected areas can be quickly restored, and disaster relief provided more efficiently. In the event of an earthquake, Taiwan's citizens will immediately receive an emergency alert by text message. This warning system, which was developed by Professor Wu, Yih-Min at our Department of Geosciences, analyzes the properties of a P-wave within three seconds after detecting the wave so that it can issue an alert to citizens more than 10 seconds before the S-wave, which is most likely to cause damage arrives. This early warning system is accurate and fast, giving people valuable seconds to escape to safety. Because it is also much cheaper to manufacture network of multiple sites has been established, including the geohazard



Fig. A.16 Taiwan Earthquake Loss Estimation System (TELES)

field test site for the Majiagou landslide, Zigui County, and systematic geophysical monitoring station for the whole TGR area, etc. than previous seismographs, it could be rapidly rolled out to several hundred elementary and junior high schools, ensuring better protection of our country's younger generation. Moreover, this system has been successfully introduced in other earthquake-threatened countries, such as Indonesia, India, Vietnam, Nepal, and Mexico.

(b) After the Flood: Rapid Mobilization and Improved Ability to Provide Relief

Another critical area is flood disaster prevention. Also here, our faculty and students are actively involved in key activities ranging from early warning and response during the disaster, to raising the awareness of, and capability for, disaster prevention among citizens more generally. Our Center for Weather Climate and Disaster Research comprises experts in meteorology, hydrology, bioenvironmental engineering, and geology etc. This center helped New Taipei

City and Keelung City establish an extreme weather and flood monitoring & warning system. Other projects include combining advanced deep learning with the analysis of radar data, which allows for closer monitoring of rainfall data in hydrologically sensitive areas. The improvement of flood models increases the accuracy of flood warnings and provides disaster prevention units with valuable information for them to rapidly formulate response strategies. From past experiences outside of Taiwan, we know that self-help and mutual support account for the largest share of the relief effort (90%) in the event of a disaster. In other words, even if flood warnings are effective, people in the affected area still need to be able to take own measures to protect themselves. At NTU, we actively participate in the community-level disaster relief preparations around the country, as well as in the training of disaster relief officers. Our experts provide citizens with the most up-to-date knowledge in disaster prevention, operate independent disaster relief systems, and evaluate the safety of shelters. These efforts contribute to the resilience and ability of local communities to mitigate impact, helping them recover more quickly. A plan for how to improve the disaster relief ability in the country proposed by our experts is another example of how we help make sure that the best disaster response capacity is in place. After improving the ability to respond to disasters, NTU's team also contributed to disaster prevention infrastructure around Taiwan, such as seismic isolation technology for buildings and equipment, or detention ponds in communities at risk. Our work and efforts in these areas help protect lives and property. As climate change continues to impact the world, we hope to leverage our technologies and expertise in these domains even further, and help strengthen the capacity to prevent and withstand natural disasters throughout the world.



Josef Stemberk

Introduction

The Institute of Rock Structure and Mechanics of the Czech Academy of Sciences is specializing in the study of the structure and properties of rocks and the rock environment. It is also involved in research into glass, ceramic materials for technical use, composite materials and biomaterials, their properties and application potential, and technological topics relating to the processing of inorganic as well as organic waste. Its research activities are spread across six scientific departments:

- Department of Geochemistry
- Department of Composites and Carbon Materials
- Department of Materials Structure and Properties
- Department of Neotectonics and Thermochronology
- Department of Engineering Geology
- Department of Seismotectonics.

The Department of Engineering Geology analyze and interpret the dangerous geodynamical phenomena and processes, which affect the behavior, development and stability of the rock environment in their natural deposition in the Earth's crust. These phenomena are linked with exogenous processes, such as slope deformations and weathering, as well as endogenous processes, such as tectonics, fault movements and gas emanations. Special attention is paid to the development of reliable and accurate methods of monitoring of slope and tectonic processes and predicting their development and occurrence in space and time.

J. Stemberk
Institute of Rock Structure and Mechanics
The Czech Academy of Sciences V Holešovičkách 41, 18,209
Prague, Czech Republic
e-mail: stemberk@irms.cas.cz

Global and Regional Inventories

The Global Database of Giant Landslides on Volcanic Islands summarizes statistics and knowledge about giant landslides (mainly debris avalanches) on volcanic islands that are up to hundreds of cubic kilometers in size. They are among the largest geological features on Earth and are fully comparable in size to the extra-terrestrial landslides observed on Mars. (Landslides 16, 2045–2052, 2019) (Figs. A.17, A.18 and A.19).

The regional landslide database for the territory of Czechia is built by analyzing media news and reports from the “Landslide Tracker” mobile phone app. It provides a timely overview of events and related losses while it is shared with a worldwide audience through the NASA Landslide Reporter website: https://www.nasa.gov/solve/landslide_reporter.

Landslide Monitoring

Čečniště site natural laboratory is a complex landslide in Tertiary neovolcanites of České středohoří. It is equipped with state-of-art monitoring systems including DMS multi-parametric column able to measure landslide movements in 2D, groundwater level and acceleration. The lower part of the landslide is equipped with continuous time-lapse ERT geophysical measurement, climatic station and streamflow measurement. Complementary measurements include geodetic (tachymetry and precise levelling) and geotechnical (extensometer) monitoring.

Crack meter monitoring on unstable rock slopes takes place in several parts of Czechia. It is coupled with observation of climatic variables and thermal properties inside the rock mass. As a consequence, the thermoelastic wave within the rock mass can be observed. (Geosci. Instrum. Method. Data Syst., 10, 203–218) (Figs. A.20 and A.21)



Fig. A.17 Scarp of a giant landslide—volcano collapse named El Golfo. El Hierro, Canary Islands, Spain

Landslide Research for a Safer Society

Long-term activities aiming at landslide risk reduction are part of our voluntary commitment to the Sendai Partnerships 2015–2025 for “Global Promotion of Understanding and Reducing Landslide Disaster Risk”.

The long-term collaboration with the Czech National Highway Authority resulted in several landslide hazard

studies and the implementation of improved construction technical norms.

The Czech public is being involved in collaborative citizen science projects to improve their awareness about landslide risk. Similarly, the ongoing participative research in Peru involves inhabitants of mountain villages or local experts contributing to their sustainable economic development (e.g. infrastructure safety) or improving institutional resilience by implementing new monitoring approaches (e.g. rock monitoring at the National Archeological Park of Machupicchu) (Fig. A.22)

Research Cooperation

The Institute’s research cooperation includes universities (e.g. Université de Liège, Wrocław University of Environmental and Life Sciences, University of Zurich), research institutes (e.g. Geophysical Institute of the Polish Academy of Sciences, Instituto Nacional de Investigación en Glaciares y Ecosistemas de Montaña) or private companies (e.g. Strix Engineering, RockNet, Gamma Remote Sensing).

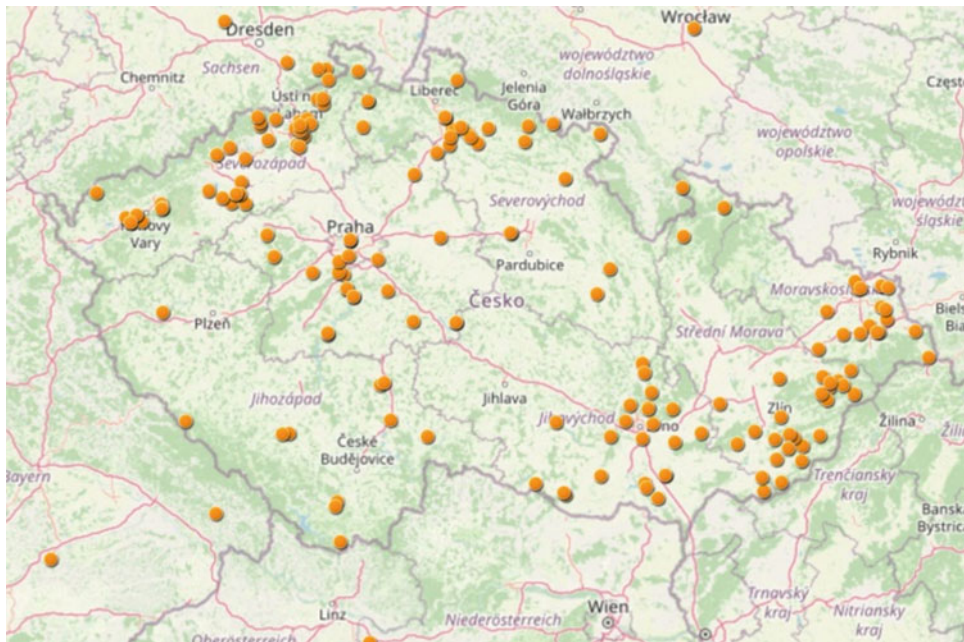


Fig. A.18 National landslide database based on media reports in Czechia as can be viewed on the NASA Landslide Viewer web page (yellow dots are reported landslides)

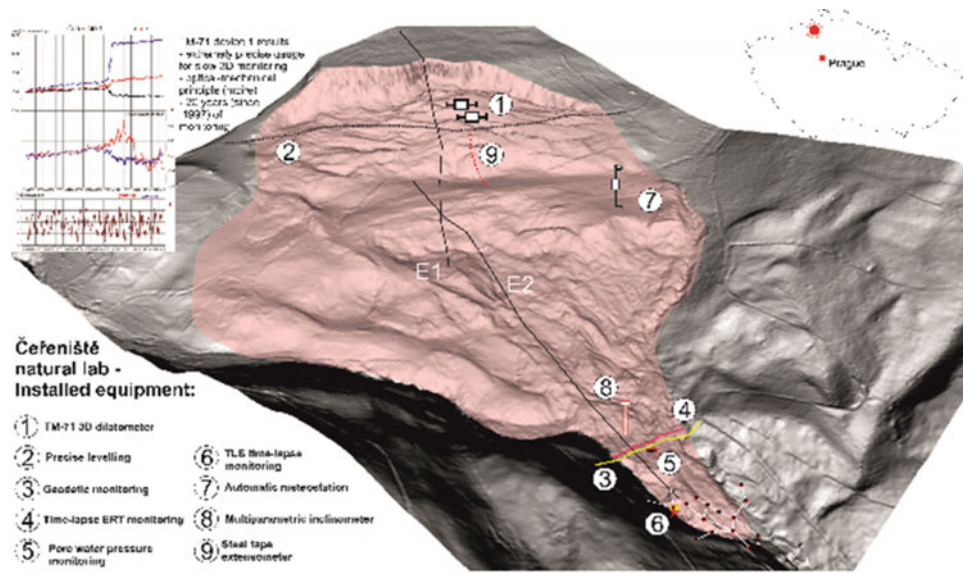


Fig. A.19 Monitoring equipment at the Čeraniště natural laboratory. Inset: results of movement monitoring

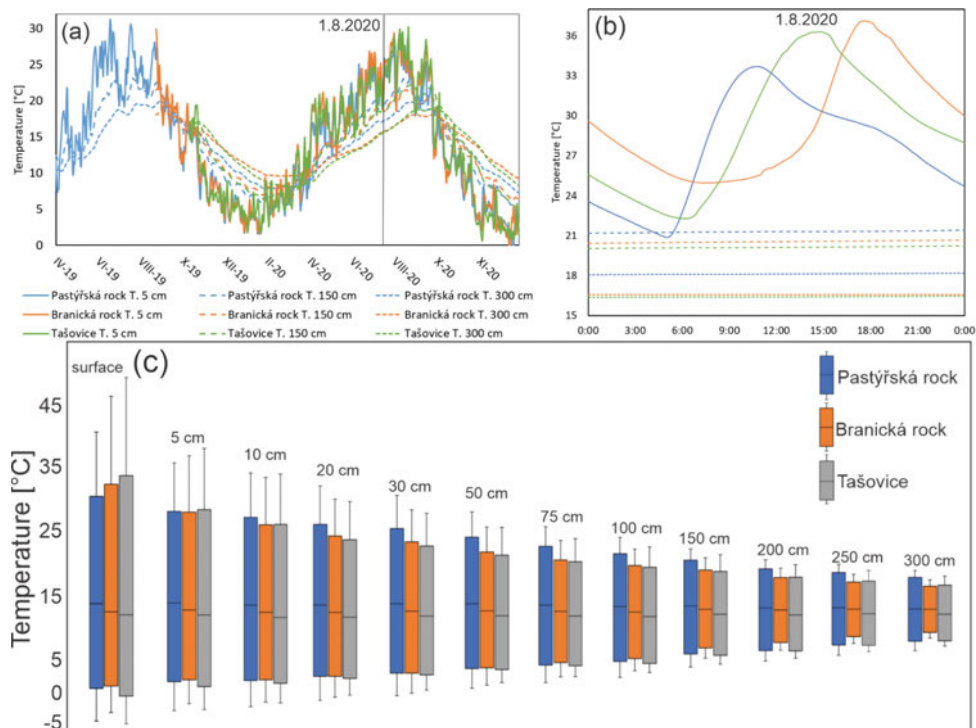


Fig. A.20 Comparison of temperatures at different rock slope depths at three different sites



Fig. A.21 Landslide (in red) in the way of the planned motorway D35 in eastern Czechia



Fig. A.22 Sharing and discussing results of landslide risk reduction project with its “recipients” empowers the community to modify the project according to their needs and allows them to become part of it. The photo shows the joint meeting of the community leaders and schoolchildren (Rampac Grande, Cordillera Negra, Peru)



Institute of Cold Regions Science and Engineering, Northeast Forestry University

Wei Shan and Ying Guo

Introduction

Institute of Cold Regions Science and Engineering of Northeast Forestry University (ICRSE-NEFU) is committed to the environmental geology and engineering geology of high latitude permafrost region and deep seasonal frozen area under the background of climate change, and attaches importance to the combination of basic research and applied research. With undergraduate, master, doctor, postdoctoral professional training system and standards, ICRSE-NEFU initiated “Geological environment risk research plan for permafrost degraded areas in Northeast China (GERRP)”. With the support of the Chinese government, “Field scientific observation and research station of the Ministry of Education—Geological environment system of permafrost area in Northeast China (FSSE-PFNEC)” was established. Its observation stations cover all kinds of permafrost areas in Northeast China. At the same time, in order to develop and transfer technologies related to environmental governance and infrastructure construction in permafrost regions, “Provincial Collaborative Innovation Centre, Environment and road construction & maintenance in permafrost area of Northeast China (PCIC-PFER)” was established. Over the years, ICRSE-NEFU have continuously established cooperation with academic institutions and organizations at home and abroad, held various academic exchanges and regularly held “Academic Seminar on Engineering Geology and

Environmental Geology in the Permafrost Along the Sino-Russian-Mongolian Economic Corridor”, edited and published research cases of geoenvironmental disasters in permafrost regions in Northeast China, and shared the research results of GERRP. At present, the research results of GERRP are gradually enriched, some of them have highly academic value, and have been put into engineering practice.

ICRSE-NEFU has gradually shown its unique research charm since it became an ICL member in 2003 2002. In 2012, ICRSE-NEFU established a landslide research network in cold regions (ICL-CRLN), and then Research Center of Cold Regions Landslide was built.

Permafrost as one of the elements of the cryosphere, the change of thermodynamic stability of permafrost will directly affect the changes of hydrosphere, biosphere and lithosphere. Under the trend of global warming, the frequency and intensity of environmental and engineering geological disasters caused by permafrost degradation are getting higher and higher (Figs. A.23 and A.24). Taking the cold area in the southern boundary of the permafrost zone in Northeast China as study area, disasters such as ground subsidence, slope icing, landslides and other disasters caused by permafrost melting were studied. At the same time, we found melting permafrost also leads to seasonally high concentrations of greenhouse gases, triggering wildfires that may further accelerate permafrost degradation and environmental changes of terrestrial ecosystems and roads.

W. Shan · Y. Guo
Institute of Cold Regions Science and Engineering
Northeast Forestry University
Harbin, China
e-mail: shanwei456@163.com

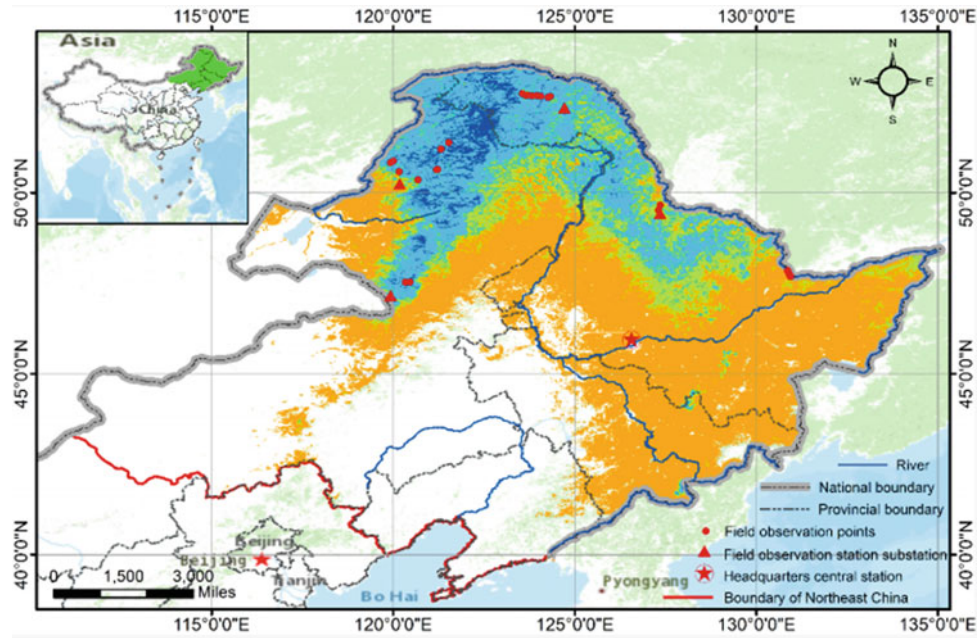


Fig. A.23 Permafrost distribution in NE of China (2014–2019)

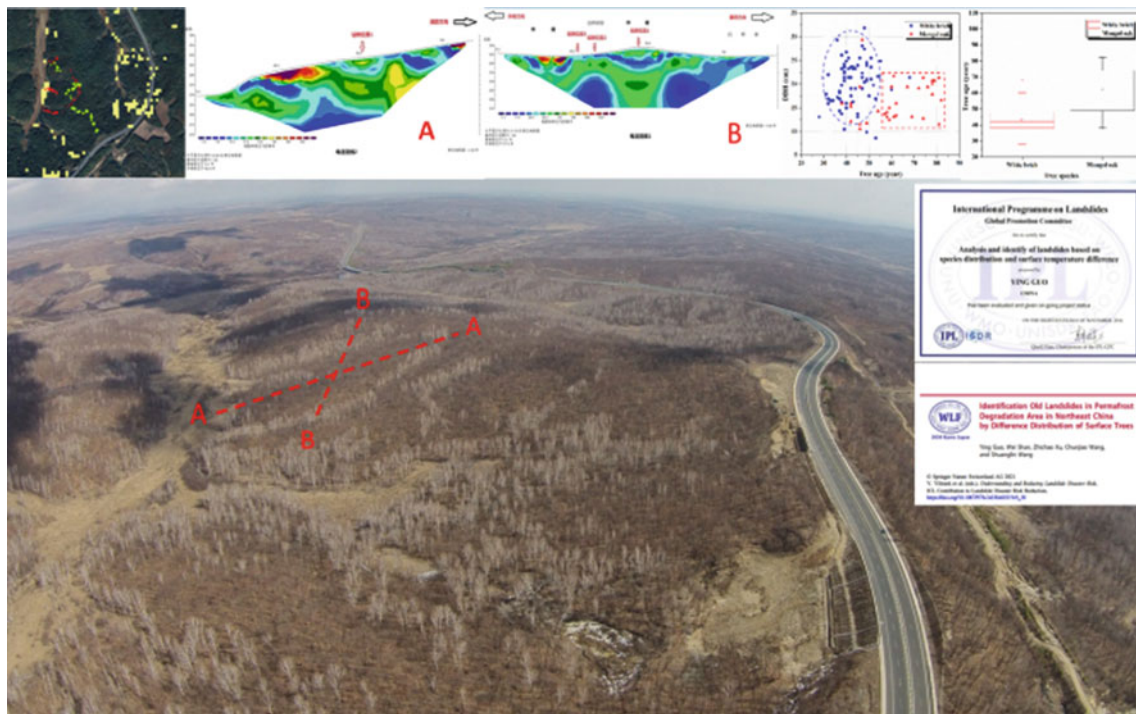


Fig. A.24 Different tree species and ages in the landslide area caused by permafrost degradation

Taketoshi Marui and Yuji Ikari

Introduction

Marui & Co. Ltd. celebrates its 100th anniversary in 2020. Marui, as one of the leading manufacturers of testing apparatuses in Japan, has been constantly striving to further improve its service since its foundation in 1920, thus contributing to the sustainable development of our nation and society. Our main products cover a wide variety of destructive and non-destructive testing apparatuses in the fields of geotechnical engineering, concrete engineering (mortar, aggregates, etc.), and ceramic engineering (Fig. A.25). Of special note is that Marui has been helping to manufacture ring-shear apparatuses (Fig. A.26) for the past half-century based on the leading-edge ideas of Dr. Kyoji Sassa, Professor Emeritus at the Kyoto University. Marui has delivered a total of seven ring-shear apparatuses to the Disaster Prevention Research Institute, Kyoto University, and two to the International Consortium on Landslides. Also, the apparatuses have been exported to the United States of America, China, Croatia and Vietnam.

Since 2002, Marui has been a supporter of the International Consortium on Landslides (ICL) and has gradually been intensifying its contribution to the ICL worldwide efforts for landslide risk reduction and international promotion of landslide research. According to NASA, more frequent and intense rainfall events due to climate change have been causing frequent landslides particularly in mountains of Asian regions including Japan where waters can be stored in various ways. Summer monsoon rains as well as snow and glacier melt waters can destabilize steep mountainsides,

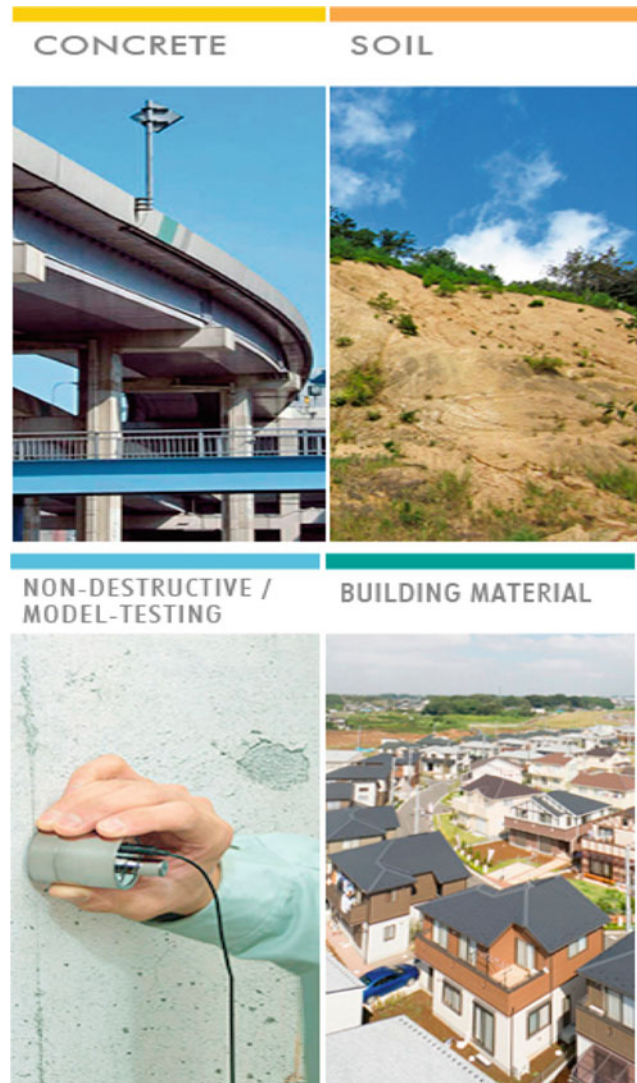
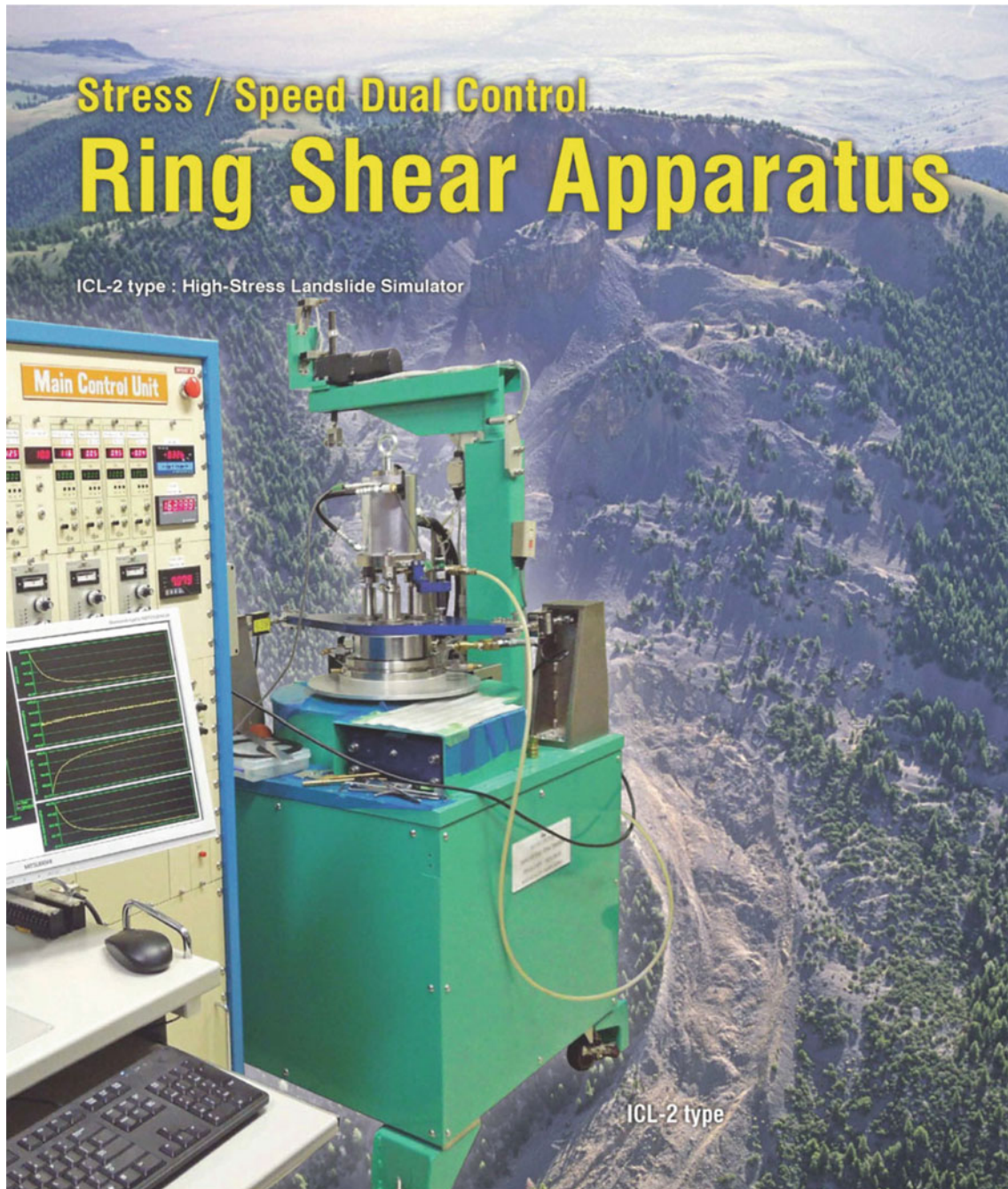


Fig. A.25 Products of testing apparatus such as non-destructive/model-testing for measuring intensity, physical property, durability, etc. for concrete, soil, building material, etc.

T. Marui · Y. Ikari
 Marui & Co. Ltd. 1-9-17 Goryo, 18,209
 Osaka 574-0064, Japan
 e-mail: hp-mail@marui-group.co.jp
 URL: <http://marui-group.co.jp/en/index.html>



Web site : <https://www.marui-group.co.jp/en/>

E-mail : hp-mail@marui-group.co.jp

Address : 1-9-17 Goryo, Daito City,
Osaka Prefecture,
574-0064, Japan

Phone : 81-72-869-3201

F a x : 81-72-869-3205

Fig. A.26 High-stress landslide simulator

triggering landslides, which are down-slope movements of rocks, soils, water, trees, etc. Marui, as an engineering supporter, commits deeply to various activities of research particularly on triggering mechanisms of landslides.

Marui & Co. Ltd. takes great pleasure in developing, manufacturing, and providing new products of high value sharing the delight of achievement with our customers, and thus contributing to the social development. The entire staff of Marui & Co. Ltd. is determined to devote ceaseless efforts to keep its organization optimized for its speedy and

high-quality services, by the motto “Creativity and Revolution”, and strive hard to take a step further, as a leading manufacturer of testing apparatuses, to answer our customer's expectations for the 22nd century to come.

Marui continuously contributes to the 2030 Agenda for Sustainable Development, as well as to the Sendai Framework for Disaster Risk Reduction 2015–2030. In line with this, Marui signed KLC 2020 in 2019 and will strongly support its actions, especially KCL2020 actions 3, 4, 5, and 9.

***NIPPON KOEI* Nippon Koei Co., Ltd., Geohazard Management Division**

Hiroaki Tauchi

For the supplemental information, please scan the QR code or visit this link: Nippon Koei Co., Ltd.—7th Asia–Pacific Climate Change Adaptation Forum (asiapacificadapt.net).



Introduction

The Nippon Koei Group (NK) has been a leading international consultant in providing engineering consulting services to over 5500 multi-disciplinary infrastructure and development projects in 160 countries all over the world. The landslide prevention specialist team (at present called Geohazard Management Division) was established in 1966 to specifically provide countermeasures against sediment disasters. Over the last 50 years, we have significantly improved the capacity of countries to respond and reduce risk from debris flows, slope instabilities, landslides, avalanches and rock falls due to torrential rains, large-scale earthquakes, and volcanic eruptions that threaten a country's vital economic infrastructure lifelines, especially the road networks. At present, approximately 160 engineers provide engineering consulting services to protect communities from a variety of disasters (Figs. A.27 and A.28). During disasters, we provide experienced professional engineers to

quickly make a risk assessment and promptly respond with a series of engineering design analyses, emergency and permanent measures based on our extensive experience and know-how. To maximize the effectiveness of infrastructures, we address efficient countermeasure plans, design and research in terms of cost reduction and cost-effectiveness using various numerical analyses such as finite element method (FEM) and discrete element method (DEM), etc.

In Japan, we have worked hard to restore and recover from sediment-related disasters caused by earthquakes and heavy rainfalls that have frequently occurred in recent years (the 2011 Great East Japan Earthquake, the Northern Kyushu Flood in 2017, etc.). We have received letters of appreciation for our efforts from the national and local governments.

Our major international projects include “The Project for Countermeasure Construction Against the Landslides on Sindhuli Road Section II, Nepal,” “The project for the rehabilitation of Sindhuli road affected by the 2015 Gorkha Earthquake, Nepal,” and “The project for landslide prevention for National Road 6 in Honduras”; all funded by the Japan International Cooperation Agency (JICA) grants-in-aid. Through these projects, we are contributing to the socioeconomic development of each country by improving vulnerable locations in road networks against sediment disasters, promoting traffic safety, and providing logistics assistance for road users. In particular, the 1st of the three NK's projects mentioned above won the “3rd JAPAN Construction International Award” from the Ministry of Land, Infrastructure, Transport and Tourism as the project that has realized “high-quality infrastructures” through its excellent know-how, technical capabilities, and project management capabilities.

NK is an ICL member and has been using its technology to reduce geohazard risk. Through various projects, NK is continuously contributing to the 2030 Agenda for Sustainable Development and the Sendai Framework for Disaster Reduction 2015–2030. Using our full capability with abundant experiences in Japan and Asia prone to natural disasters,

H. Tauchi
Geohazard Management Division, Nippon Koei Co., Ltd.
5–4 Kojimachi, Chiyoda-ku, Tokyo 102–8539, Japan
e-mail: tauchi-hr@n-koei.jp
URL: <https://www.n-koei.co.jp/english/>

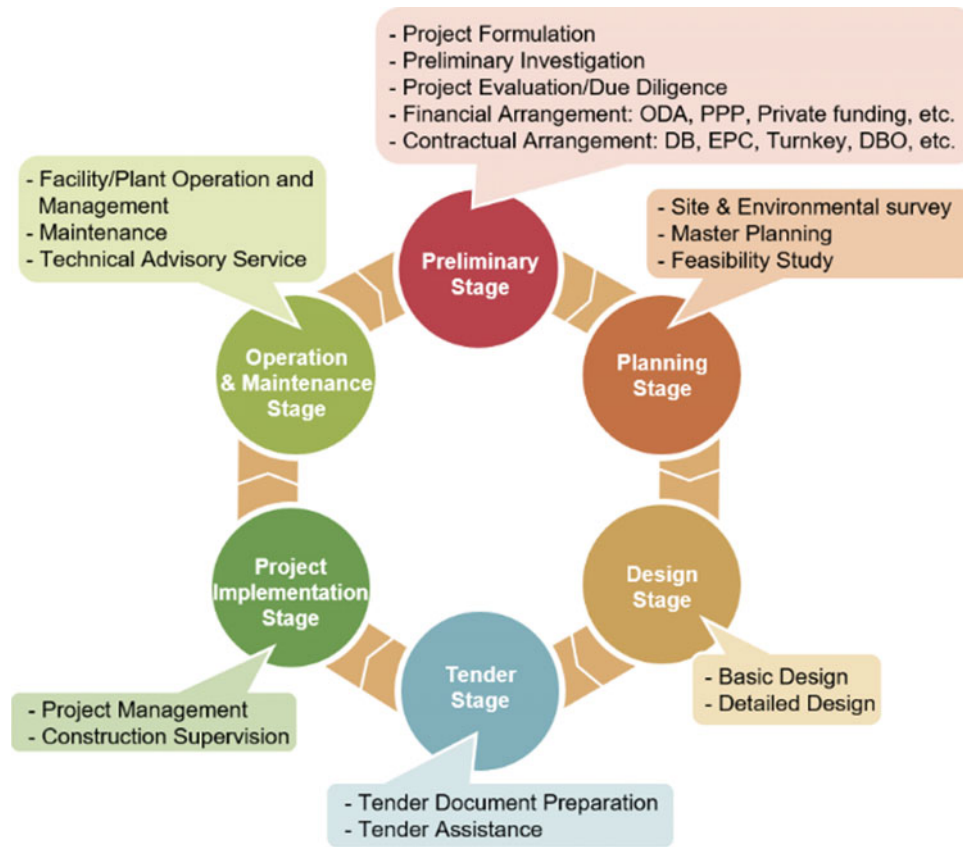


Fig. A.27 Our service for geohazard management

we hope to contribute much more to a reduction of global sediment disasters including landslides. In line with this, NK

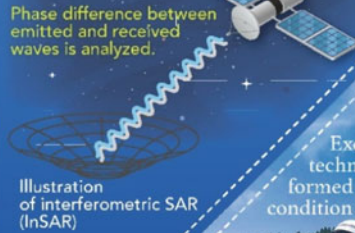
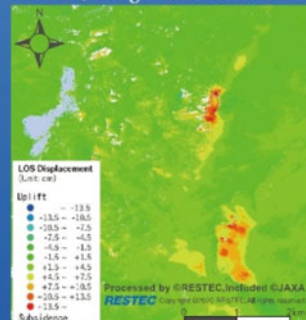
has signed the KLC 2020, and will strongly support its actions, especially KCL2020 actions 1, 2, 3, 5, 6, and 8.

Geohazard Management

Response to natural disasters with various technologies from space to the surface

Remote Sensing Technology

Potential hazards around the globe are assessed by optical remote sensing and InSAR which can detect land-resources, topographic features, and ground deformation. Example of InSAR, shown below, is a new effective way to detect deformation of slopes along infrastructures such as roads and railways.



Landslide monitoring using InSAR

Integrated technologies and engineers' Application of spaceborne, airborne, and ground-based technologies for disaster risk reduction.

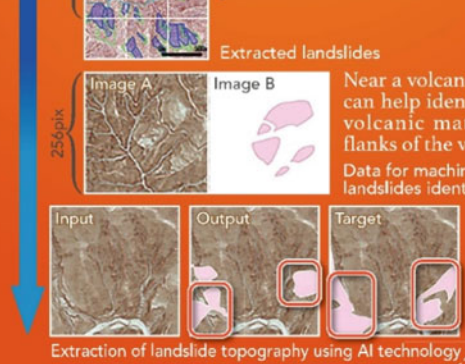
A team of 5,497 multidisciplinary experts

Excellent teams, covering advanced and wide range of technologies based on long-standing experiences, are formed to provide optimum solutions customized for each condition and needs.



AI Technology

Our AI technology helps quickly identify morphological features of past and current landslides.

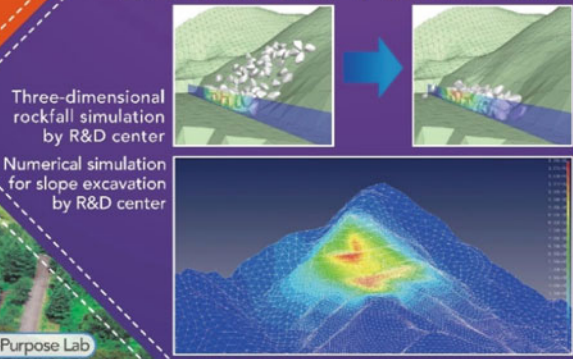


Extracted landslides

Near a volcano, our AI technology can help identify unstable masses of volcanic matters perching on the flanks of the volcano.
Data for machine learning: DEM and landslides identified by an expert

Numerical simulation

We can predict the extent of the damage in the event of a disaster and the effectiveness of countermeasure works by numerical analysis.



R&D center

State-of-the-Art Nippon Koei's R&D Center



NIPPON KOEI

Global Consulting Engineering Firm

Head Office 5-4 Kojimachi, Chiyoda-ku, Tokyo 102-8539, Japan

TEL +81-3-3238-8030

Website www.n-koei.co.jp/english



Fig. A.28 Introduction of our survey analysis technology for geohazard

Ellegi Srl

Introduction

Ellegi srl provides worldwide monitoring services and produces Ground Based synthetic aperture radar (GBInSAR) for remote measurement of displacements and deformations on natural hazards and manmade buildings using its own designed and patented LiSALab system.

Its activities started in 2003 as a spin off project to exploit commercially the Ground Based Linear Synthetic Aperture Radars technology developed by European Commission's Ispra Joint Research Centre and based on the results of more than 10 years of research. Since then, Ellegi has industrialized and developed the core technology of the LiSALab system and latest LiSAMobile system represents the 5th generation of development.

In 2003 it was the first commercial company in the world to provide GBInSAR measurements of natural hazards and structure (Figs. A.29 and A.30).

Ellegi srl offers:

- Displacement fields measurement, control and monitoring of the deformation caused by natural hazards, like landslides, rockslides, sinkhole, volcanic deformation in every operative condition, including emergencies,
- Structural strain fields measurement, control, monitoring and diagnosis of the deformation affecting buildings, bridges, viaducts, dams.
- GBInSAR monitoring systems, installation, management and maintenance in order to provide information about natural hazards or anthropic activity, that can generate or cause slopes failures or buildings instabilities.

In all the above-mentioned activities Ellegi srl uses the GBInSAR LiSALab technology that represents a real “break-through”.

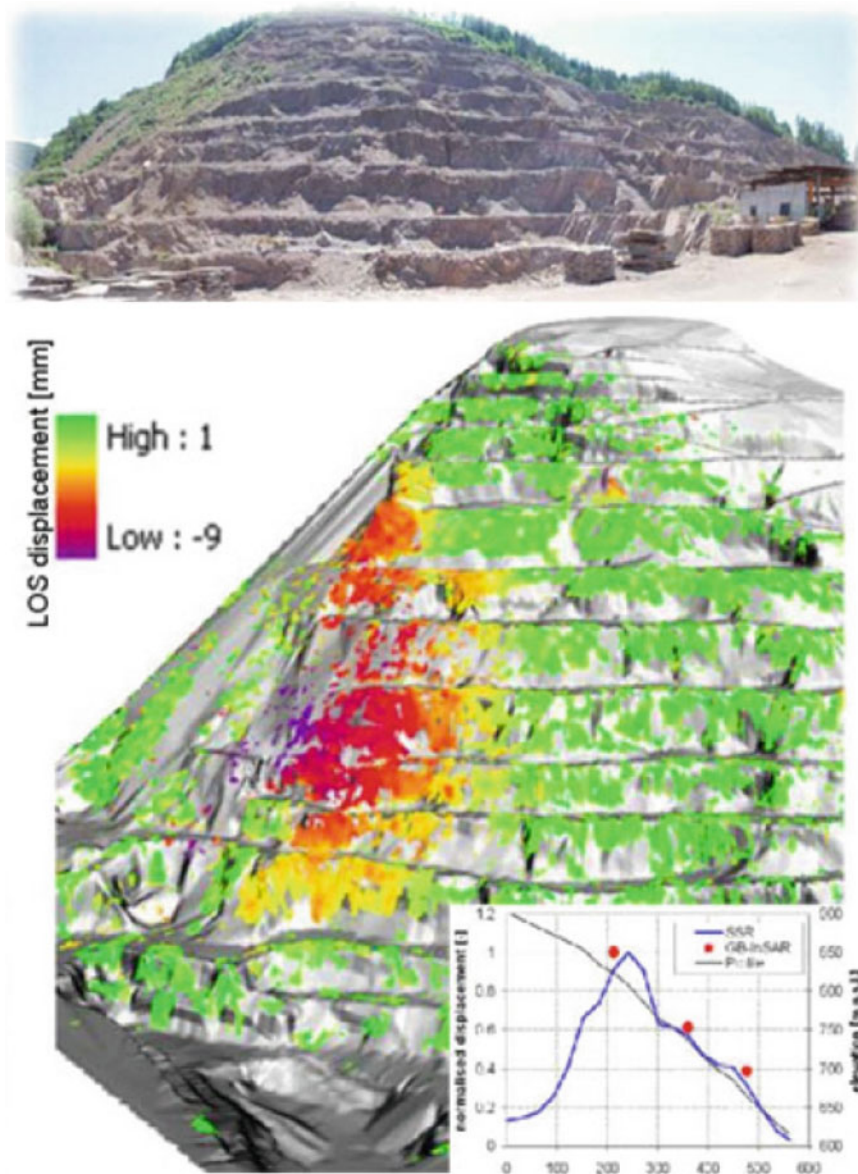


Fig. A.29 GBInSAR LiSALab technology quarry monitoring example and displacements' field comparison between the GBInSAR measurement and FEM model results

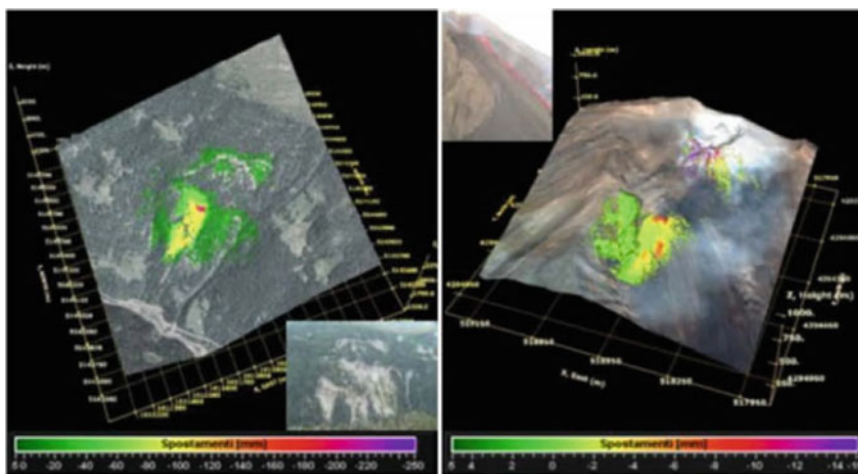


Fig. A.30 GBInSAR LiSALab technology result in monitoring a slope affected by a landslide (left) and a volcanic slope affected by deformation (right). Landslide or moving area mapping and boundaries identification is made easy by GBInSAR LiSALab technology

Introduction

IDS GeoRadar, part of Hexagon, provides products and solutions, based on radar technology, for monitoring applications including landslides, rockfalls, complex structures, mining and civil engineering. The company is a leading provider of Ground Penetrating Radar (GPR) and Interferometric Radar solutions worldwide.

IDS GeoRadar is committed to delivering best-in-class performance solutions and to the pursuit of product excellence, through the creation of application-specific, innovative and cost-efficient systems for a wide range of applications:

- Utility mapping and detection
- Civil engineering
- Railway and road engineering
- Geology and environment management
- Archaeology
- Forensics
- Landslide monitoring
- Mining safety

Natural Hazard Monitoring Solution

The use of slope monitoring radar is now the standard practice for the active monitoring of slope in open pit mines and for safety critical landslide monitoring with the aim of providing alerts in the event of progressive movements which could potentially lead to slope failure and assessing worker safety. The unique IBIS-FM EVO radar system accurately monitors multiple scales of displacements in real time, from early detection of slow movements to fast

accelerations associated with slope collapse. The great operative range, up to 5000 m, allows to safely deploying the system in comfortably accessible areas, without exposing people and equipment to hazardous zones.

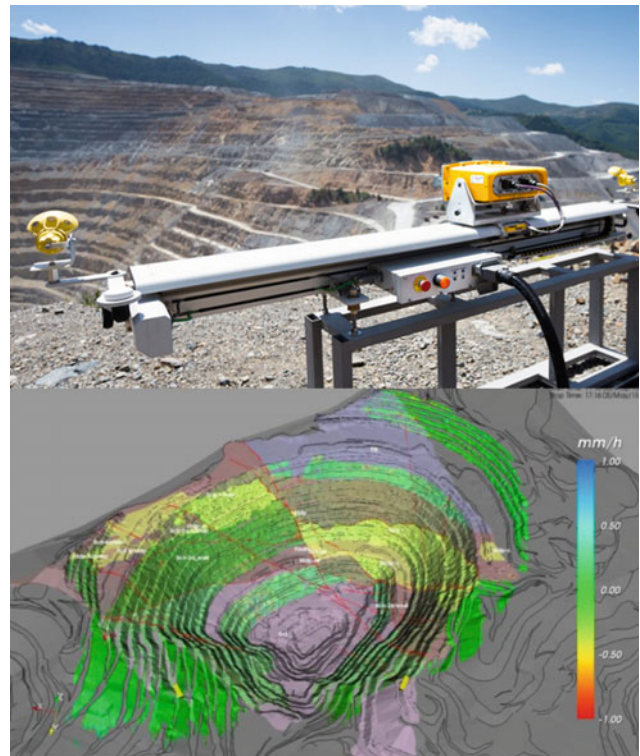


Fig. A.31 IDS GeoRadar: innovative interferometric radar for mining, environmental and civil engineering

IDS GeoRadar cooperate with TRE ALTAMIRA, the worldwide leader in ground monitoring services using satellite InSAR offer a comprehensive solution—InSAR Service—to fulfill all mine stability needs, ranging from monitoring large-scale mining operations over hundreds of square kilometers, to specific movements at the pit scale. With the large spatial coverage of satellite data, mining engineers can identify unstable areas over wide areas, also with the ability to extend the analysis of deformation back in time. All mining assets can be monitored regularly and precisely for deformation (Figs. A.31 and A.32).

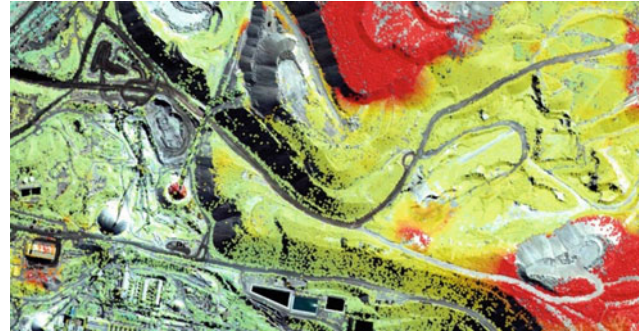


Fig. A.32 InSAR service—ground motion monitoring for mining operations



Chuo Kaihatsu Corporation

Lin Wang <https://www.ckcnet.co.jp/contactus/>

Introduction

Chuo Kaihatsu Corporation (CKC) was founded in 1946, and has been aiming to become the “Only One” consultant for our customers. We engage in the hands-on work that will “Remain with the earth, Remain in people’s hearts, and Lead to a prosperous future”. We focus on road, river and dam engineering to flesh out industrial infrastructures specifically by means of geophysical/geotechnical/geological investigations,

civil engineering surveys and project implementations. In recent years, we make significant efforts on earthquake disaster mitigation, sediment disaster prevention/mitigation and ICT information services. Many achievements of ours have already contributed to the mitigation of natural disasters such as landslides, earthquakes and slope failures in Japan, Asia and the Pacific Region. We aim to provide technological contributions so that a sustainable society will continue to develop in the future (Figs. A.33, A.34, A.35 and A.36).



Fig. A.33 Design for various structures

L. Wang
Chuo Kaihatsu Corporation, 3-13-5 Nishi-waseda, Shinjuku-ku,
Tokyo, 169-8612, Japan
e-mail: wang@ckcnet.co.jp
URL: <https://www.ckcnet.co.jp/global/https://www.ckcnet.co.jp/contactus/>

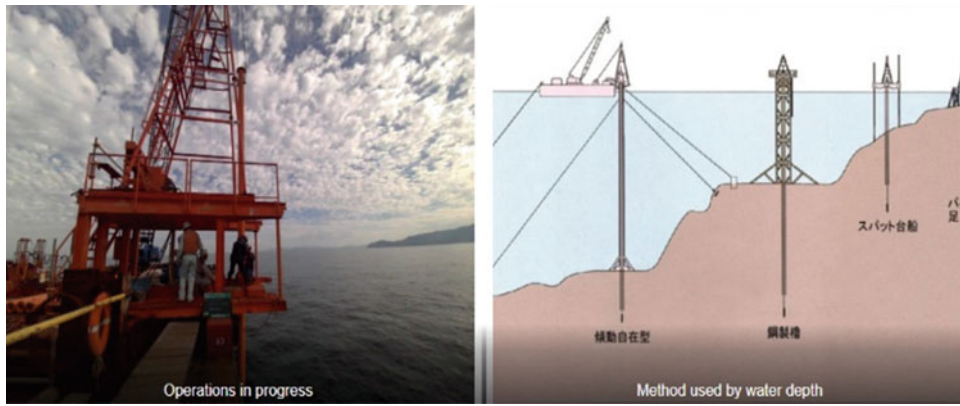


Fig. A.34 Deepwater drilling surveys

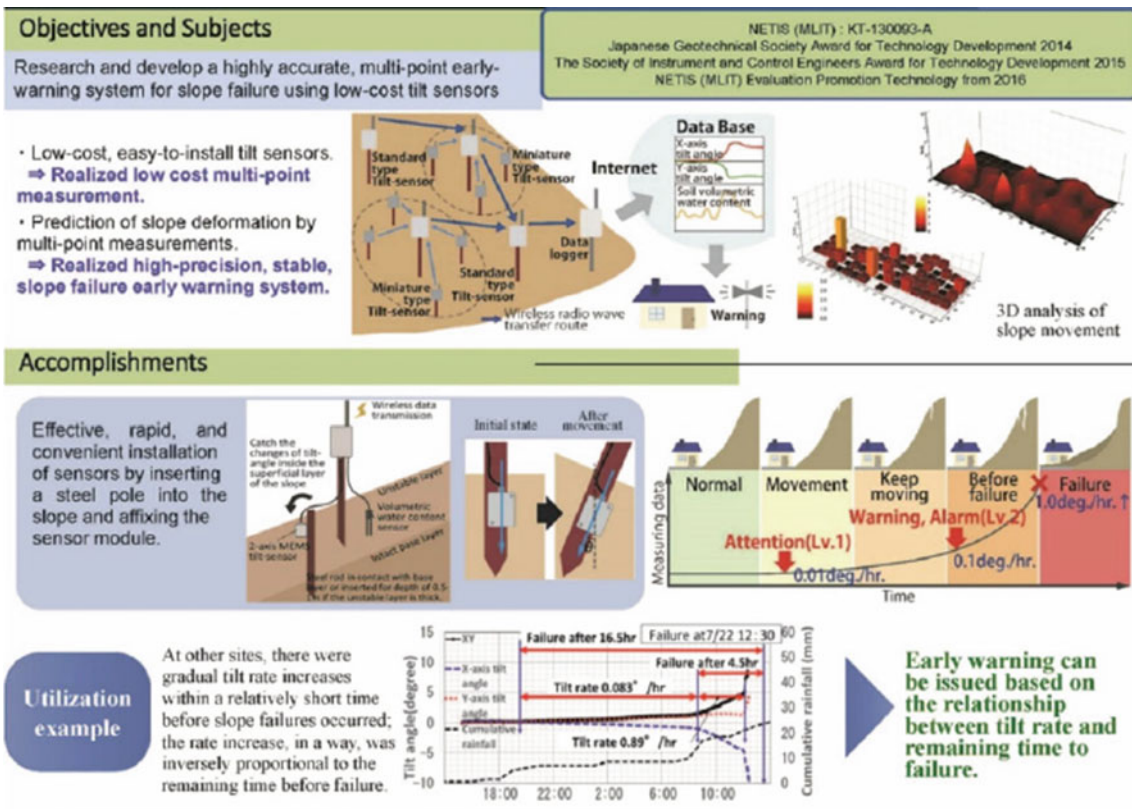


Fig. A.35 The early warning monitoring system of slope failure using multi-point tilt change and volumetric water content

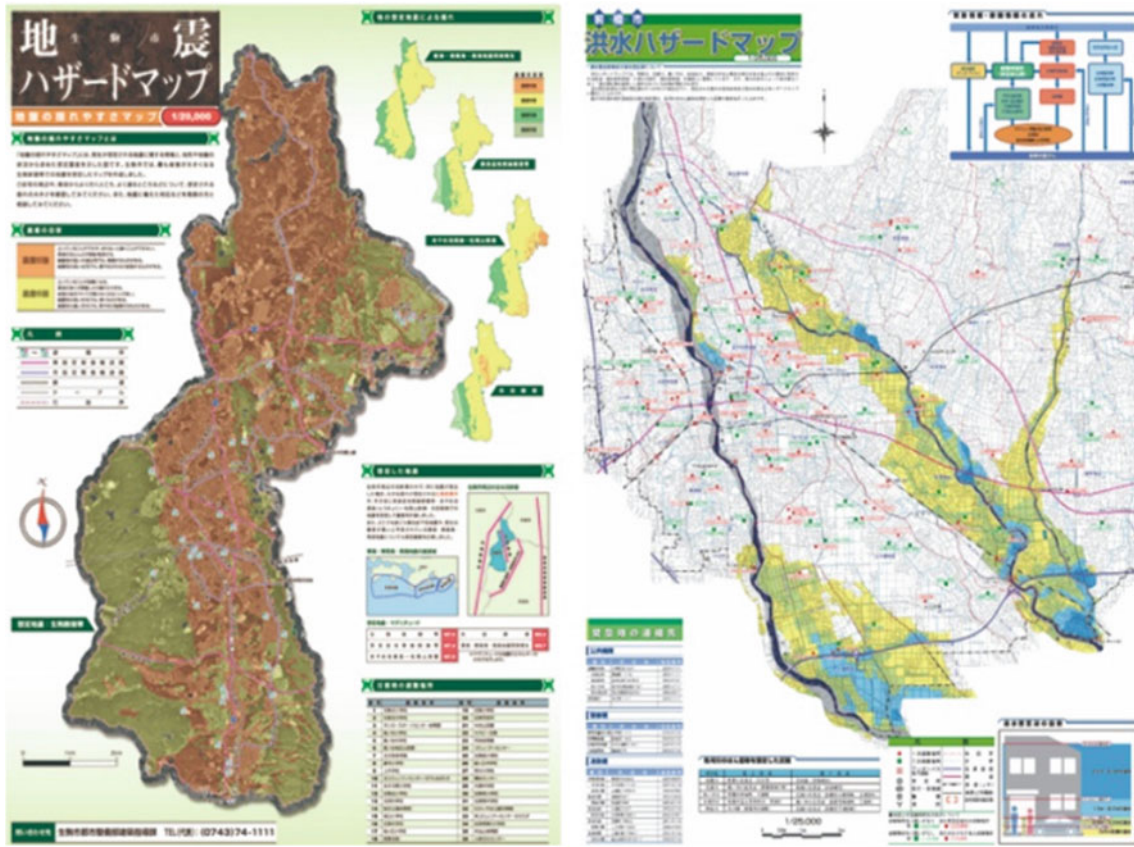


Fig. A.36 Making hazard map for sediment disaster, tsunami, flood, earthquake, liquefaction, etc....



Godai Corporation

Godai Corporation

Introduction

Ever since its foundation in 1965, Godai Kaihatsu Co. Ltd. a civil engineering consulting firm, has long been providing a variety of software and measures particularly for natural disaster mitigation. With its rich expertise in both civil

engineering and information technology (IT), the company has its primary goal to address real-world needs of disaster mitigation. All the staff of Godai Kaihatsu Co. Ltd. feels it more than happy that their cutting-edge technologies help mitigate natural disasters (Figs. A.37, A.38, A.39 and A.40).

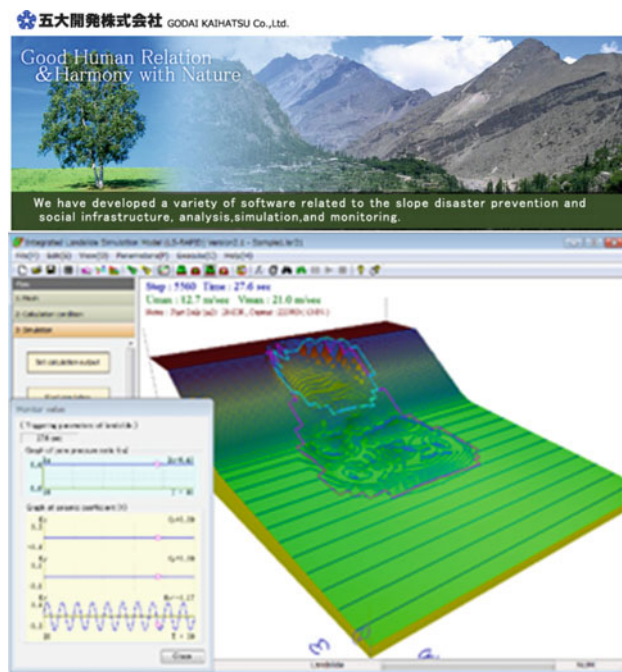


Fig. A.37 Integrated model simulating of earthquake & rain induced rapid landslides (LS-RAPID)

Godai Corporation 1-35 Kuroda, Kanazawa City, Ishikawa, Japan
e-mail: pp-sales@godai.co.jp
URL: <https://soft.godai.co.jp/soft/>

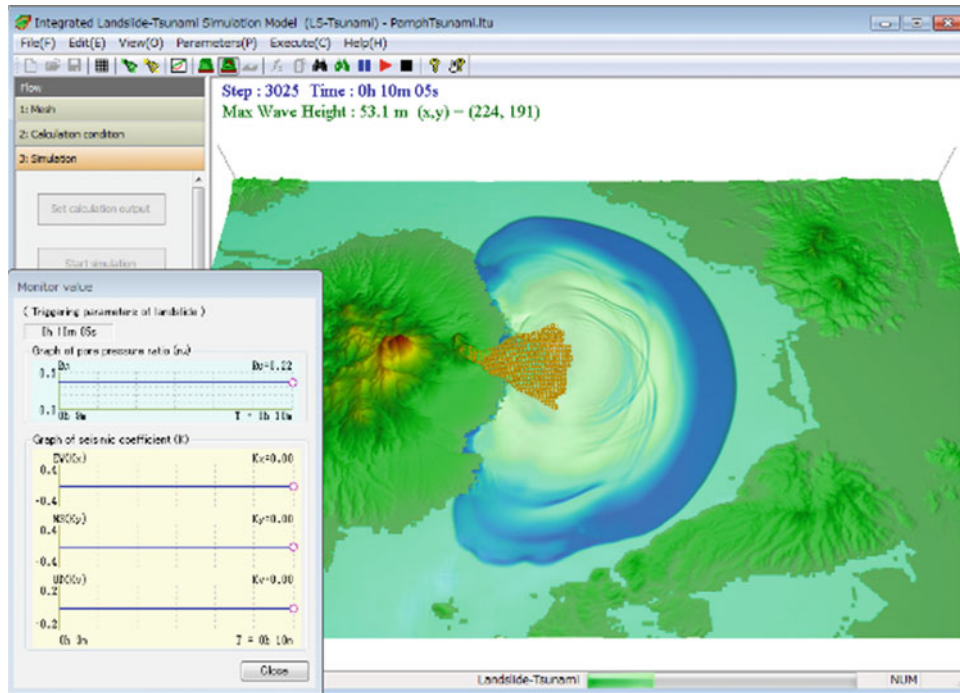


Fig. A.38 Tsunami model (LS-Tsunami)

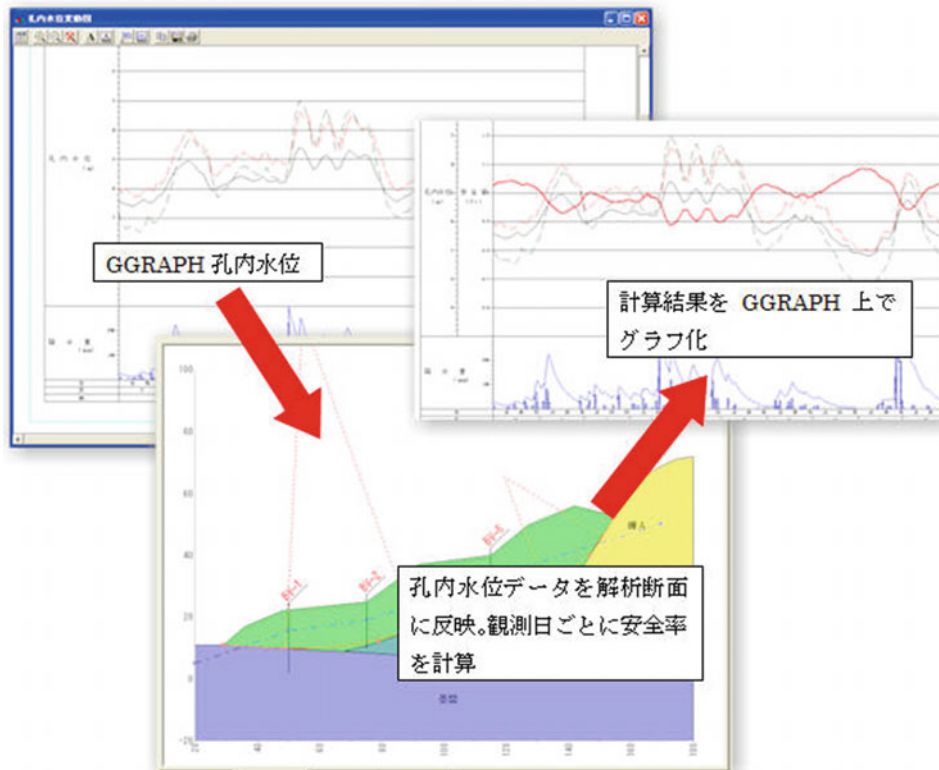


Fig. A.39 Power SSA PRO-Two-dimensional slope stability calculation of earthquake and rain induced landslide

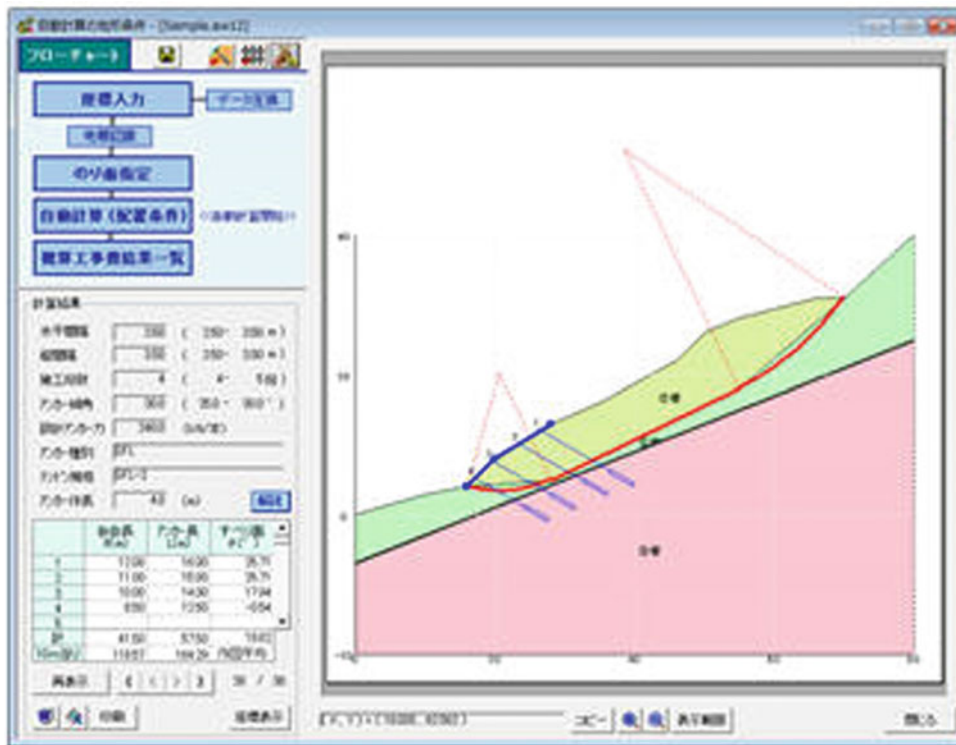
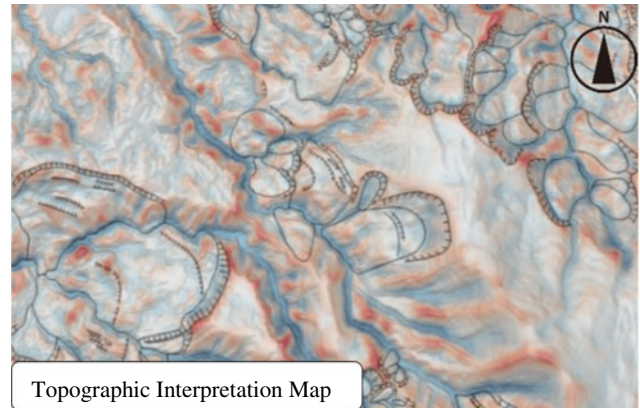


Fig. A.40 Anchor software-slope stability analysis for ground anchor

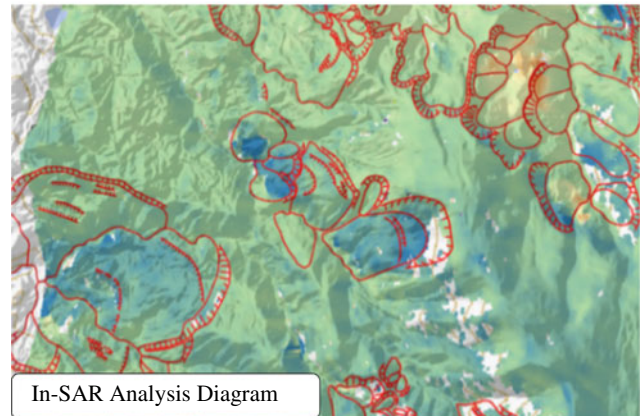
Introduction

Since its establishment in 1953, Kiso-Jiban has been contributing on the development of social infrastructure as a "comprehensive construction consultant with strong geotechnical capabilities" in various situations, such as ground investigation, laboratory testing, analysis, civil structure design, etc. Kiso-Jiban has been working on the technological development for disaster prevention and mitigation against the recent exacerbation of natural disasters.



InSAR (Interferometric Synthetic Aperture Radar)

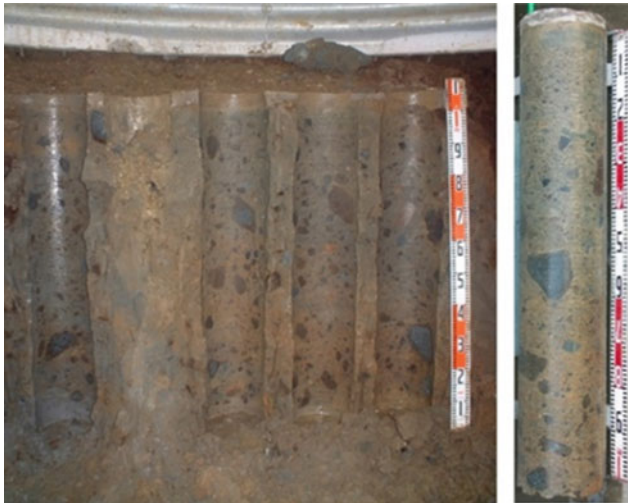
SAR is a technique that utilizes interference of radio waves for precise determination of distance. Kiso-Jiban has succeeded in estimation of both extent and rate of landslide movements by combining the topography interpretation and InSAR analysis.



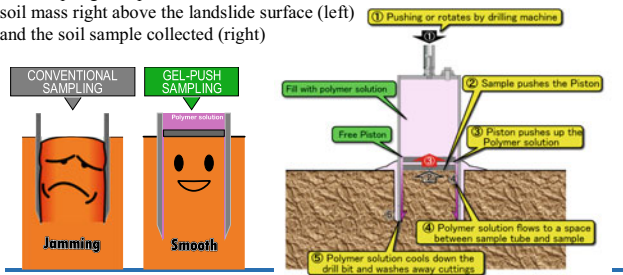
GP (Gel-Push) Sampling

GP Sampling can collect gravelly soil, etc., which is difficult to be collected by conventional samplers, by using a highly-concentrated water-soluble polymeric gel. GP Sampling was introduced in ISO 22475-1: 2021 revised in October 2021 as Category A, which provides the highest quality soil samples.

K. Hanai · J. Odaka
Kiso-Jiban Consultants Co. Ltd., Kinshicho Prime Tower 12
Floor1-5-7 Kameido, Koto-ku, Tokyo 136-8577, Japan
e-mail: kisojiban-contactus@kiso.co.jp
URL: <https://www.kisojiban.com/>

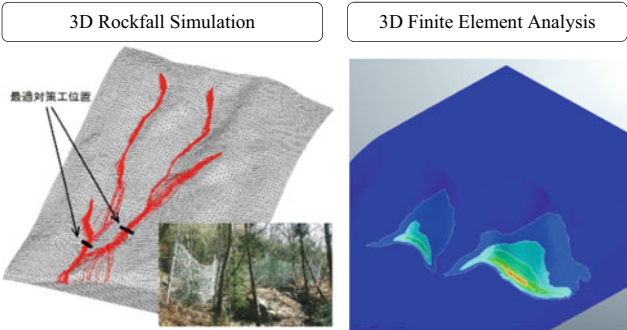


GP Sampling was performed in the disturbed soil mass right above the landslide surface (left) and the soil sample collected (right)



Slope Stability Analysis and Evaluation

Kiso-Jiban provides a wide range of numerical analyses related to slope stability evaluation. We have a wide range of analysis methods, from general two-dimensional limit equilibrium analysis to finite element analysis and analysis of rock masses with discontinuities, and we are challenging on the analysis that considers variability of ground and modelling uncertainty.





Kokusai Kogyo Co. Ltd

Kokusai Kogyo Co. Ltd.

Introduction

Kokusai Kogyo Co. Ltd. as a leading company of geospatial information technologies has long been providing public services with its comprehensive expertise to address real-world needs and cutting-edge measurement technologies. Kokusai Kogyo Co. Ltd. helps rebuild “Green Communities,” which has been of our great concern in terms of “environment and energy,” “disaster risk reduction” and “asset management”. Kokusai Kogyo Co. Ltd. offers advanced and comprehensive analyses of geospatial information for developing new government policies, maintaining and operating social

infrastructures safe and secure, and implementing low-carbon measures in cities. Influenced by the recent global climate change, extreme rainfall events have become more frequent worldwide and resultant hydro-meteorological hazards are creating more deaths and devastations particularly in many developing countries where effective advanced countermeasures are not readily available. Kokusai Kogyo Co. Ltd. is proud of its achievements in establishing resilient infrastructure systems and implementing effective monitoring/early warning systems in developing countries, which have long been helping reduce the risks from natural hazards (Figs. A.41, A.42, A.43 and A.44).



Fig. A.41 Our realtime hazard map reflects up-to-date information of soil natures and precipitations at landslide hazard sites, etc. that can constantly be changing, and evaluates area-wide hazard risk in real-time

Kokusai Kogyo Co. Ltd.
2 Rokubancho, Chiyoda-Ku, Tokyo 102-0085, Japan

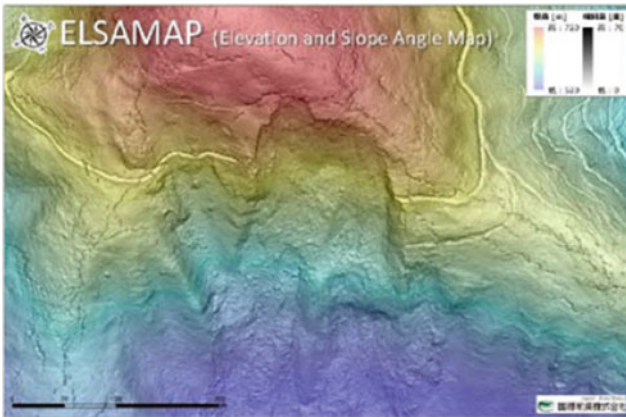


Fig. A.42 ELSAMAP is our cutting-edge 3D terrain visualization method allowing great geomorphological details to be visualized in one glance with gray-scaled slope inclinations and colored altitudes. ELSAMAP has been used to interpret micro-topographies, landslides and some other things



Fig. A.44 “Shamen-net” is a total monitoring system integrating GNSS and other monitoring device (Measurement precision: \pm mm, on a real time basis)

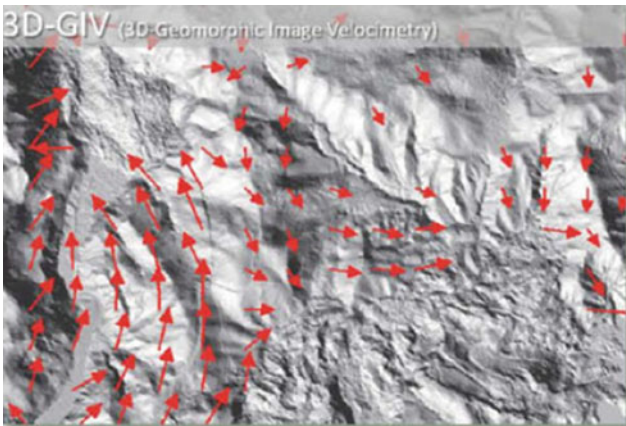


Fig. A.43 3D-GIV can help grasp the ground surface displacement caused by natural phenomena such as landslide by analyzing differences between digital geomorphic images obtained through ad hoc Airborne Laser Surveys



OSASI Technos, Inc.

OSASI Technos, Inc.

Introduction

OSASI Technos, Inc. has been making its best efforts to develop its cutting-edge technologies for landslide early warning. Its unique compact and lightweight sensors making up the Landslide Early Warning System enable long-term monitoring of unstable landslide mass movements, precipitations, porewater

pressure buildups, etc. in a remote mountainous area where commercial power is often unavailable. OSASI Technos, Inc. is also proud of its advanced technology to transfer observed data even in areas with poor telecom environments as proven in the successful implementations in South Asia. All staff members of OSASI Technos work together for mitigation of landslide disasters worldwide (Figs. A.45, A.46 and A.47).

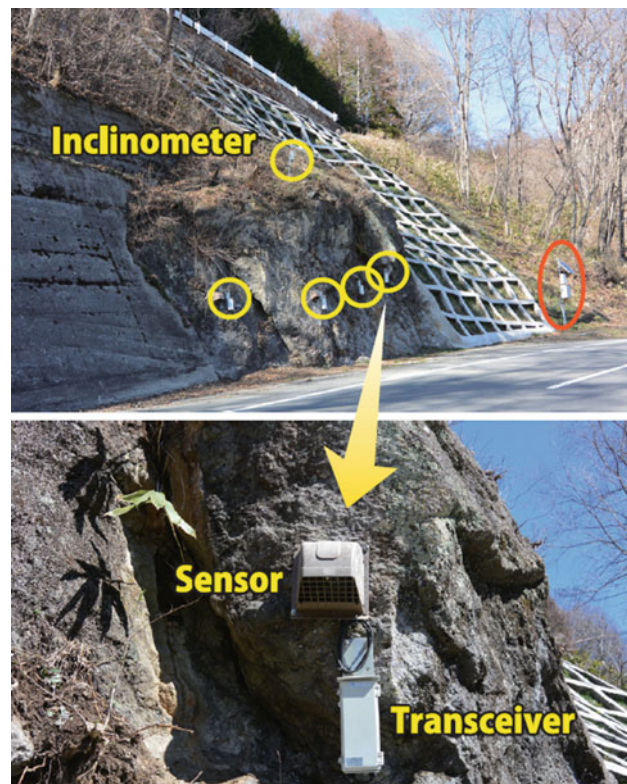


Fig. A.45 Bedrock slope monitoring (maintenance control)

OSASI Technos, Inc. 65-3 Hongu-cho, Kochi City, Kochi,
780-0945, Japan



Fig. A.46 Measurement of the dynamic state of landslide using inclinometers with a wireless function



Fig. A.47 Cut slope monitoring

List of ICL Members

International Consortium on Landslides

An international non-government and non-profit scientific organization promoting landslide research and capacity building for the benefit of society and the environment

President: Nicola Casagi (University Florence, Italy)

Vice Presidents: Peter Bobrowsky (Geological Survey of Canada, Canada), Zeljko Arbanas (University of Rijeka, Croatia), Binod Tiwari (California State University, USA), Faisal Fathani (University of Gadjah Mada, Indonesia), Veronica Tofani (University of Florence, Italy), Vit Vilimek (Charles University, Czech Republic) Executive Director: Kaoru Takara (Kyoto University, Japan), Treasurer: Kyoji Sassa (Prof. Emeritus, Kyoto University, Japan)

<i>Country/Region</i>	<i>ICL full member</i>
Bosnia and Herzegovina	The Geotechnical Society of Bosnia and Herzegovina
Brazil	Center for Scientific Support in Disasters—Federal University of Parana
Canada	Geological Survey of Canada
Canada	University of Alberta
China	Northeast Forestry University, Institute of Cold Regions Science and Engineering
	China University of Geosciences
	Chinese Academy of Sciences, Institute of Mountain Hazards and Environment
	Tongji University, College of Surveying and Geo-Informatics
	Shanghai Jiao Tong University
	Tsinghua University
	Civil Engineering and Development Department, Geotechnical Engineering Office, Hong Kong
	The Hong Kong University of Science and Technology
	The University of Hong Kong
Colombia	Universidad Nacional de Colombia
Croatia	Croatian Landslide Group from Faculty of Civil Engineering University of Rijeka and Faculty of Mining, Geology and Petroleum Engineering University of Zagreb
Czech Republic	Charles University, Faculty of Science
	Institute of Rock Structure and Mechanics, Department of Engineering Geology
	Brown Coal Research Institute
Egypt	The American University in Cairo
Germany	Technische Universität Darmstadt, Institute and Laboratory of Geotechnics
Georgia	Department of Geology of National Environmental Agency of Georgia
Honduras	Universidad Nacional Autónoma de Honduras (UNAH)
India	Amrita Vishwa Vidyapeetham, Amrita University
	National Institute of Disaster Management, New Delhi
Indonesia	Gadjah Mada University, Center for Disaster Mitigation and Technological Innovation (GAMA-InaTEK)
	Parahyangan Catholic University
	Agency for Meteorology, Climatology, and Geophysics of the Republic of Indonesia (BMKG Indonesia)

(continued)

Italy	UNESCO Chair for the prevention and the sustainable management of geo-hydrological hazards - University of Florence
	ISPRA-Italian Institute for Environmental Protection and Research
	University of Calabria, DIMES, CAMILAB
	Istituto di Ricerca per la Protezione Idrogeologica (IRPI), of the Italian National Research Council (CNR)
	Università di Torino, Department of Earth science
	Centro di Ricerca CERI—Sapienza Università di Roma
	National Institute of Oceanography and Applied Geophysics—OGS, Italy
Japan	Kyoto University, Disaster Prevention Research Institute
	Japan Landslide Society
	International Consortium on Geo-disaster Reduction
Korea	Korea Institute of Geoscience and Mineral Resources (KIGAM)
	Korean Society of Forest Engineering
	National Institute of Forest Science
	Korea Authority of Land & Infrastructure Safety
	Korea Institute of Civil Engineering and Building Technology
Malaysia	Slope Engineering Branch, Public Works Department of Malaysia
Mexico	Institute of Geography, National Autonomous University of Mexico (UNAM)
Russia	Moscow State University, Department of Engineering and Ecological Geology
	JSC “Hydroproject Institute”
Serbia	University of Belgrade, Faculty of Mining and Geology
Slovakia	Comenius University, Faculty of Natural Sciences, Department of Engineering Geology
Slovenia	University of Ljubljana, Faculty of Civil and Geodetic Engineering (ULFGG)
	Geological Survey of Slovenia
Sri Lanka	Central Engineering Consultancy Bureau (CECB)
	National Building Research Organization
Chinese Taipei	Landslide group in National Central University from Graduate Institute of Applied Geology, Department of Civil Engineering, Center for Environmental Studies
	National Taiwan University, Department of Civil Engineering
Thailand	Ministry of Agriculture and Cooperatives, Land Development Department
	Asian Disaster Preparedness Center (ADPC)
Ukraine	Institute of Telecommunication and Global Information Space
United Kingdom	British Geological Survey
USA & Nepal	California State University, Fullerton & Tribhuvan University, Institute of Engineering
Viet Nam	Institute of Transport Science and Technology
	Vietnam Institute of Geosciences and Mineral Resources (VIGMR)
<i>Country/Region</i>	<i>ICL associate member</i>
Belgium	Liege University, Georisk and Environment (G&E) group
China	State Key Laboratory of Geohazard Prevention and Geoenvironment Protection (Chengdu University of Technology)
	State Key Laboratory of Plateau Ecology and Agriculture (Qinghai University)
Czech Republic	Czech Geological Survey
Italy	Department of Earth and Environmental Sciences, University Aldo Moro, Bari
	University of Sannio, Department of Sciences and Technologies
	Geotechnical Engineering Group (GEG), University of Salerno
	Department of Earth and Environmental Sciences – University of Pavia
	University of Chieti-Pescara, Department of Engineering and Geology
	Federico II University of Naples, Department of Earth, Environmental and Resource Sciences
DIA – Università degli Studi di Parma	
University of Urbino “Carlo Bo”, Department of Pure and Applied Sciences	
Japan	Ehime University, Center for Disaster Management Informatics Research

(continued)

Macedonia	Macedonian Association for Geotechnics	
Russia	Russian State Geological Prospecting University n.a. Sergo Ordzhonikidze (MGRI-RSGPU)	
Slovenia	University of Ljubljana, Faculty of Natural Sciences and Engineering (UL NTF)	
Switzerland	Institute of Earth Sciences, Faculty of Geoscience and Environment / University of Lausanne	
USA	Iowa State University	
<i>Country/Region</i>	<i>ICL Supporter</i>	
Italy	IDS GeoRadar s.r.l	
Japan	Marui & Co., Ltd., Osaka	Okuyama Boring Co., Ltd., Yokote
	Ohta Geo-Research Co., Ltd., Nishinomiya	Japan Conservation Engineers Co., Ltd., Tokyo
	Sabo Technical Center, Tokyo	GODAI Development Corp., Kanazawa
	OYO Corporation, Tokyo	Kokusai Kogyo Co., Ltd., Tokyo
	OSASI Technos Inc., Kochi	NIPPON KOEI CO., LTD
Chinese Taipei	Sinotech Engineering Consultants, Inc	
ICL Secretariat		
Secretary General: Kyoji Sassa		
International Consortium on Landslides, 138-1 Tanaka Asukai-cho, Sakyo-ku, Kyoto, 606-8226, Japan		
Web: http://icl.iplhq.org/ , http://www.iplhq.org/ , E-mail: secretariat@iclhq.org		
Tel: + 81(75) 723 0640, Fax: + 81(75) 950 0910		

Author Index

A

Abe, Shinro, 149
Ahari, Hossein Emami, 343
Ajmera, Beena, 343
Alam, Md. Nurul, 175
AlcÁntara-Ayala, Irasema, 137
Ariyarathna, Imaya, 217
Asano, Shiho, 217
Ávila, Guillermo, 315

B

Balek, Jan, 295
Bandara, Kithsiri N., 217
Barriga Delgado, Lesly Mercedes, 209
Bezak, Nejc, 83
Bhandary, Netra Prakash, 163
Bianchini, Silvia, 267
Blahút, Jan, 295
Bobrowsky, Peter, 11, 249
Brunetti, Maria Teresa, 409

C

Canuti, Paolo, 11
Carlà, Tommaso, 267
Casagli, Nicola, 11, 267
Chambers, Jonathan, 249
Cocking, Robert, 249
Costa, Joao Pita, 83
Cui, Chen, 113
Cuomo, Sabatino, 123

D

Damians, Ivan P., 197
Dang, Khang, 343
Dewi, Anggraini, 175
Dias, A.A. Virajh, 327
Di Perna, Angela, 123
Donohue, Shane, 249

E

Elwood, David, 249
Esperancinha, Sergio, 209

F

Fanti, Riccardo, 267
Fathani, Teuku Faisal, 277
Frodella, William, 267

G

Garbarino, Matteo, 99
Gariano, Stefano Luigi, 409
Garnica-Peña, Ricardo J., 137
Gigli, Giovanni, 267
Gratchev, Ivan, 113
Grilli, Stephan T., 65
Grobelnik, Marko, 83
Gusiakov, Viacheslav K., 65

H

Han, Qunli, 45
Hayashi, Kazunori, 149
Herath, H. M. J. M. K., 327
Higaki, Daisuke, 149
Hirai, Joe, 237
Holmes, Jessica, 249
Huntley, David, 249

J

Jayakody, Sanchitha, 217
Jayasinghe, Susantha, 175
Jermol, Mitja, 83
Joseph, Jamel, 249
Joshi, Anish, 175

K

Karnawati, Dwikorita, 65, 277
Karunawardena, Asiri, 217
Kim, Dong Hyun, 113
Klimeš, Jan, 295
Kolomenskiy, Dmitry, 237
Konagai, Kazuo, 217
Kraus, John, 197
Kulathilake, L. K. N. S., 327
Kumar, Sumit, 409
KusÁk, Michal, 295

L

Loi, Doan Huy, 343
Løvholt, Finn, 65

M

MacLeod, Roger, 249
Mandrone, Giuseppe, 99
Martinelli, Mario, 123
Massri, M. Beshar, 83
Mathiyalagan, Rajkumar, 409
Meldrum, Philip, 249
Melillo, Massimo, 409
Mikoš, Matjaž, 1, 45, 83
Miyata, Yoshihisa, 197
Moncayo, Steven, 315
Moretti, Sandro, 267
Morresi, Donato, 99

N

Nam, Kounghoon, 305
Novalija, Inna, 83

O

Onishi, Ryo, 217, 237

P

Pavlova, Irina, 209
Peruccacci, Silvia, 409

R

Ravindran, Sinnappoo, 113
Rimoldi, Pietro, 197
Rotheram-Clarke, Drew, 249
Rowberry, Matt, 295

S

Sasahara, Katsuo, 217
Sassa, Kyoji, 1, 11, 45, 65, 217, 343
Sassa, Shinji, 65
Sattler, Kevin, 249
Segoni, Samuele, 267
Setiawan, Hendy, 277, 343
Strom, Alexander, 285

T

Tang, Qianhao, 113
Tappin, David R., 65
Tiwari, Binod, 185
Tiwari, Ram Chandra, 163
Tofani, Veronica, 267
Touze, Nathalie, 197
Towashiraporn, Peeranan, 175
Tran, Duc, 185

U

Uzuoka, Ryosuke, 217

V

Vacha, Damiano, 99

W

Wang, Fawu, 305
Wijaya, I Putu Krishna, 175
Wilkinson, Paul, 249
Wilopo, Wahyu, 277

Y

Yasuda, Yuki, 237
Yasukawa, Soichiro, 209